ISSN 2039-6651
Anno 2015_Numero 27

miscellanea INGV

Abstracts Volume 6th International INQUA Meeting on

Paleoseismology, Active Tectonics and Archaeoseismology

19 | 24 April 2015, Pescina, Fucino Basin, Italy

27

Istituto Nazionale di
Geofisica e Vulcanologia

REGISTRAZIONE AL TRIBUNALE DI ROMA N.178|2014, 23 LUGLIO

Sede legale: Via di Vigna Murata, 605 | Roma

ISSN 2039-6651
Anno 2015_Numero 27

Miscellanea INGV

6TH INTERNATIONAL INQUA MEETING ON
PALEOSEISMOLOGY, ACTIVE TECTONICS AND ARCHAEOSEISMOLOGY

19 | 24 APRIL 2015, PESCINA, FUCINO BASIN, ITALY

Editors Anna Maria Blumetti, Francesca Romana Cinti, Paolo Marco De Martini, Fabrizio Galadini, Luca Guerrieri
Alessandro Maria Michetti, Daniela Pantosti, Eutizio Vittori

27

The Fucino 2015 Organizing Committee

Anna Maria Blumetti (ISPRA - Istituto Superiore per la Protezione e la Ricerca Ambientale) annamaria.blumetti@isprambiente.it
Francesca Romana Cinti (INGV - Istituto Nazionale di Geofisica e Vulcanologia) francesca.cinti@ingv.it
Paolo Marco De Martini (INGV - Istituto Nazionale di Geofisica e Vulcanologia) paolomarco.demartini@ingv.it
Fabrizio Galadini (INGV - Istituto Nazionale di Geofisica e Vulcanologia) fabrizio.galadini@ingv.it
Luca Guerrieri (ISPRA - Istituto Superiore per la Protezione e la Ricerca Ambientale) luca.guerrieri@isprambiente.it
Alessandro Maria Michetti (Università degli Studi dell'Insubria) alessandro.michetti@uninsubria.it
Daniela Pantosti (INGV - Istituto Nazionale di Geofisica e Vulcanologia) daniela.pantosti@ingv.it
Eutizio Vittori (ISPRA - Istituto Superiore per la Protezione e la Ricerca Ambientale) eutizio.vittori@isprambiente.it

Scientific committee

Alfonsi L., Amit R., Audemard F., Baize S., Boncio P., Bosi C., Comerci V., Costa C., Doglioni C., Galli P., Grutzner C., Hinzen K., Karakhanian A., Kim Y.S., Livio F., Masana E., Mc Calpin J., Messina P., Okumura K., Papanikolaou I., Perez Lopez R., Piccardi L., Porfido S., Reicherter K., Roberts G., Rockwell T., Saroli M., Schwartz D., Scotti O., Serva L., Silva P.G., Smedile A., Szczucinski W., Tatevossian R. and Villani F.

Immagine di frontespizio
Logo del convegno

Normazione ortoeditoriale, Revisione testi e Impaginazione
Rossella Celi Centro Editoriale Nazionale INGV
Francesca Di Stefano Centro Editoriale Nazionale INGV

agenzia spaziale italiana

The **Italian Space Agency** programs on Earth Observation mainly deal with environmental protection, natural disaster prevention, homeland and citizens security. **COSMO-SkyMed**, a constellation of four satellites for environmental monitoring, is the largest Earth Observation space program ever undertaken by Italy. In order to increase national technological and scientific knowledge, ASI is also directing its efforts towards several missions, such as **MIOSAT** (Microsatellite–based optical light mission), for the progress and qualification in orbit of new technological products; **ROSA** (Radio Occultation Sounder for Atmosphere), aimed at studying the atmosphere; **PRISMA** (Hyperspectral Precursor of the application mission), that can determine, by hyperspectral sensors, the chemical-physical composition of objects. ASI contributes significantly to European programs such as **GOCE** (Gravity field and steady-state Ocean Circulation Explorer), for the measurement of the gravitational field and the determination of the Earth's surface and **GMES** (Global Monitoring for Environment and Security).

www.asi.it / www.asiTv.it

EPOS - EUROPEAN PLATE OBSERVING SYSTEM

Integrates national and transnational research infrastructures for solid Earth science	*for*	seamless access to pan-European data and services
Guarantees open access to multidisciplinary Research Infrastructures	*for*	cross-disciplinary and transnational research
Creates novel e-infrastructure and integrated core services	*for*	a multidisciplinary community of users
Fosters scientifi , technological and ICT innovation	*for*	successfully addressing global Grand Challenges in Earth science
Improves geo-hazard assessment, risk mitigation, and sustainable management of georesources	*for*	a safe and prosperous society

25 COUNTRIES

Austria, Belgium, Bulgaria, Czech Republic, Denmark, Finland, France, Germany, Grecee, Hungary, Iceland, Ireland, Italy, Netherland, Norway, Poland, Portugal, Romania, Slovakia, Slovenia, Spain, Sweden, Switzerland, Turkey, United Kingdom

4 INTERNATIONAL ORGANIZATIONS

Orfeus, Emsc, Euref, Intermagnet

256 NATIONAL RESEARCH INFRASTRUCTURES

4939 SEISMIC STATIONS

2272 GPS RECEIVERS

464 TB SEISMIC DATA

118 LABORATORIES

828 INSTRUMENTS

Several PetaBytes of solid Earth Science data will be available

Several thousands of **users** expected to access the infrastructure

EPOS

Integrating European Research Infrastructures for solid Earth Science

EUROPEAN PLATE OBSERVING SYSTEM phone +39 06 51860.401 / 577 / 652 / 636 | fax +39 06 51860565 | epos@ingv.it | epos.secretariat@ingv.it | www.epos-eu.org

EUROGEOSURVEYS
European Geoscience for Society
The Geological Surveys of Europe

EuroGeoSurveys knows the Earth we want

EuroGeoSurveys (EGS), The Geological Surveys of Europe, is a not-for-profit organisation representing 37 National Geological Surveys, an overall workforce of several thousand experts.

In our day-to-day activities, we promote the contribution of geosciences to **European Union affairs** and action programmes, and provide a permanent network between the Geological Surveys of Europe and a common, but not unique, gateway to each of the Members and their national networks. We promote cooperation among Geological Surveys worldwide with the vision to share and make geoscienfic information available. Over the last 15 years EGS Expert Groups have been involved in more than **250 projects addressing societal challenges** in field such as Marine Geology, Geochemistry, GeoEnergy, Earth Observation-Geohazards, Mineral Resources, Water Resources, International Cooperation & Development, Soil Resources, Spatial Information.

ISSN 2039-6651
Anno 2015_Numero 27

Table of Contents

INQUA Focus Group on Paleoseismology and Active Tectonics

Preface

Dear Participant,

we are very happy to welcome you in Pescina (Abruzzi, Italy) for the 6th INQUA International Workshop on Active Tectonics, Paleoseismology and Archaeoseismology ("6th PATA Days"). In the last six years, INQUA TERPRO Focus Group on Paleoseismology and Active Tectonics (PALACTE), supported very successful Workshops annually held in Europe and Overseas, the last in Korea in 2014. The 6th joint meeting locates in the central Apennines, one of the most tectonically active area in the Mediterranean. In fact, the scientific sessions will be attended in the Pescina village that was completely destroyed by the 1915 M7 Fucino earthquake, one of the most devastating earthquakes ever occurred in Italy. This event is also one of the first to be well documented in the Mediterranean, with surface ruptures and other effects on the environment. We will commemorate the Centenary of this event occurrence. We will be also very close to the source of the 2009 M6.3 L'Aquila event, located about 50 km to the north. The two-days field trip will be dedicated to both the earthquake areas.

We are expecting a very intense and worldwide scientific meeting with over 180 participants from 25 different countries, and about 150 studies to be presented and discussed. All this will occur in the unique historical atmosphere of the ancient Pescina village at the Centro Studi "Ignazio Silone", a cultural center devoted to the fellow citizen, world-famous writer.

During the Fucino 2015 event we will discuss the final results of the INQUA Project 1299 – EEE METRICS Parametrization of Earthquake Environmental Effects (2011-2015) that will be formally presented on July 2015 at the XIX INQUA Congress in Nagoya (Japan). This will be also the occasion to further discuss future joint research projects for the 2015-2019 intercongress period. Two major research areas have been identified in the PALACTE meeting held in Madrid last year (26-28 February 2014), i.e., 1) Minimum Magnitude Surface Rupture (MMR) and Maximum Potential Earthquake (MPE) from paleoseismic Quaternary records, and 2) Geological Earthquake Mapping of recent, historical and paleoseismic events: Quaternary Geology for Seismic Hazard Analyses. Preliminary community projects covering these areas will be discussed during the INQUA Business Meeting in Pescina.

You are also kindly invited to the workshop between the European Plate Observing System (EPOS, an integrated solid Earth Sciences research infrastructure), and EuroGeoSurveys (EGS, an organization representing 37 National Geological Surveys and some regional Surveys in Europe). During the workshop, an open debate involving the Fucino 2015 participants will be focused on the integration of geological and geophysical data for scientific research purposes, as well as on common data policies in order to access to harmonized multidisciplinary data.

We wish to acknowledge all the people who supported this event and in particular, the Mayor of Pescina Municipality Antonio Iulianella and the Comitato Pescina 2015 for their invaluable work with the organization, the members of the Scientific Committee, the Sponsors, and all the Colleagues who handled the abstracts.

We wish you a fruitful conference with constructive scientific discussion but also the discovery of history, tradition and food of the Abruzzi region in the central Italy.

"GRAZIE" for your contribution to Fucino 2015!

The Fucino 2015 Organizing Committee

Anna Maria Blumetti
Francesca Romana Cinti
Paolo Marco De Martini
Fabrizio Galadini
Luca Guerrieri
Alessandro Maria Michetti
Daniela Pantosti
Eutizio Vittori

INQUA Focus Group on Paleoseismology and Active Tectonics

paleoseismicity.org

Active tectonics in the Santa Ines basin (Venezuela): morphotectonic evidence related to blind thrusting with opposite vergences

Alarcon, E. (1,2), Audemard, F. (1,2), Singer, A. (1,2)

(1) Dept. of Geology, Central University of Venezuela Venezuela. Email: edualarcong@gmail.com
(2) Dept. of Earth Sciences, Venezuelan Foundation for Seismological Research, Venezuela

Abstract: *This paper presents a partial overview of morphotectonic evidences that describe the active deformation of growth folds associated with two different thrust-fold belts with opposite vergences. The SSE-verging Santa Ines blind thrust fault and NNW-verging Moroturo blind thrust fault articulate the northern and southern foothills of Santa Ines basin (northwestern Venezuela), respectively. Along these foothills areas, the best exposed geomorphic features of tectonic activity are fold-scarp landforms, drainage anomalies, and paleosols development on deformed sediments as young as Pleistocene age. The correct geomorphological identification of morphotectonic evidences in the landscape can be a powerful tool in the recognition of active tectonic structures linked to blind thrust faults.*

Key words: *Active tectonics, geomorphology, blind thrust faults, Santa Ines-Moroturo, fold-scarps.*

INTRODUCTION

For the last 30 years, the study of morphotectonic criteria has been used to characterize thrust belts in foothills areas of northwestern and western Venezuela. For instance, drainage anomalies show evidence of surface response due to tectonic uplift (e.g. Soulas et al., 1987; Beltran & Giraldo, 1989). Fold-scarps have been studied (Audemard, 1993; Audemard, 1999; Audemard, 2003; Ollarves et al., 2006; Alarcon, 2014; Alarcon et al., 2014) with special interest on surface response of blind faults underlying alluvial sediments in humid tropical environments of Venezuela.

Hence, this paper focuses on a summarized analysis of fold-scarps, drainage anomalies and paleosols development, related to thrust-folds in northern and southern foothills of Santa Ines basin, northwestern Venezuela (Fig. 1). The study area corresponds to two active thrust-fold systems with opposite vergences, bulging Pleistocene sediments of the Santa Ines valley (Alarcon, 2014). Both foothills are mainly composed of low-lying hills with characteristic topographic expressions of fold-scarp geometry, on the tip of active blind faults.

Figure 1: A partial shaded relief map showing the opposite-verging active faults in the center of Santa Ines basin, between the towns of Santa Ines and Moroturo. (1) Active fault; (2) inferred active fault; (3) blind thrust fault, (4) Quaternary anticline; (5) bulged alluvial sediments; (6) Quaternary fold-scarp.

FOLD-SCARP LANDFORMS

Several fold-scarp landforms grow at the front of active thrust-fold belts in northern and southern foothills of Santa Ines basin. Nonetheless, the occurrence and evolution of different shortening mechanisms of thrust-faulting induce different surface responses on the fault-related topographic features (Alarcon, 2014).

In the northern foothills of Santa Ines, a SSE-verging foreland-type thrust system induces at least two deformation fringes with different development stages (Fig. 2a). Associated with Santa Ines blind fault, cumulative flexural deformation of Miocene rocks induces fold scarps, progressively incised to form trapezoidal facets and wine-glass canyons (Fig. 2b). Likewise, active growth of Pleistocene fold-scarps in response to a younger blind fault induces asymmetrical local bulging, elevation of flats and the formation of southeast-facing convex ramps (Fig. 2c).

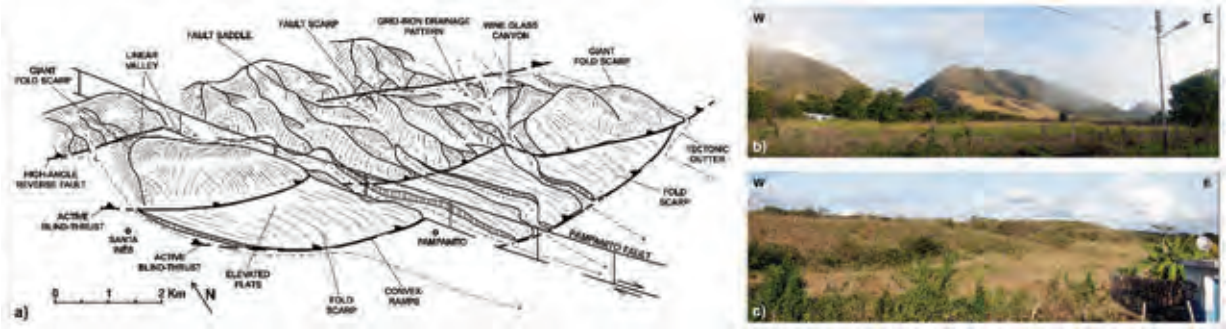

Figure 2: a) Drawing of landscape, depicting the assemblage of landforms associated with active thrust faults in the Santa Ines foothills (modified from Alarcon, 2014). b) Giant fold scarps in the Santa Ines foothills, showing heights of 500 m, incised to form trapezoidal facets and wine-glass canyons. c) Pleistocene fold scarps showing elevated flats and southeast-facing convex ramps, near the town of Santa Ines.

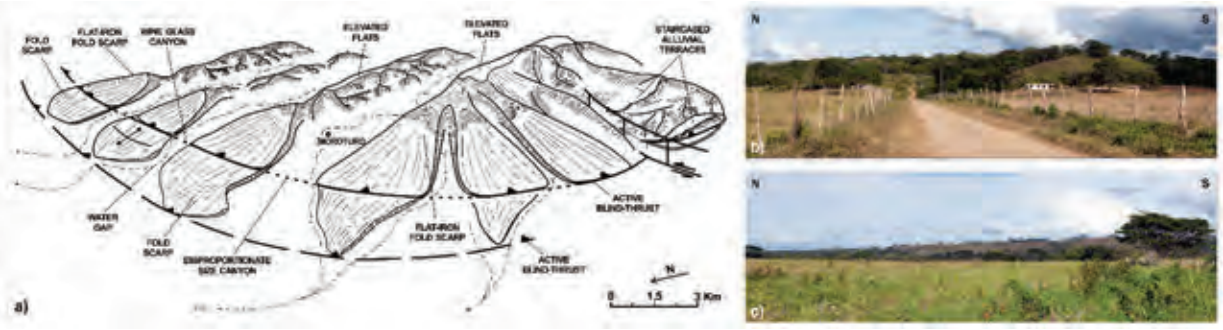

Figure 3: a) Drawing of landscape, depicting the assemblage of landforms associated with active thrust faults in the Moroturo foothills (modified from Alarcon, 2014). b) Fold scarp in the Moroturo foothills, showing heights of 200 m, incised to form flat-iron geometry and wine-glass canyons. c) A north-facing Pleistocene fold scarp showing a smooth tilted surface, near the town of Moroturo.

To the south, the Moroturo foothills are uplifted as a single unit, in a continuous NNW-verging flexural scarp associated with a fold, above the blind termination of Moroturo fault (Fig. 3a). The incision of antecedent rivers on the fold-scarp results in triangular facets or "flat-irons" (Fig. 3b), and disproportionate size between present river width and canyons (Audemard, 1999). A subsequent active front, associated with a younger blind thrust fault, emerge as a continuous fold-scarp that gentle flexes the overlying Pleistocene deposits. This fold-scarp shows positive but not prominent relief (Fig. 3c), with very smooth tilted surface and a deeply dissected topography, resulting in several longitudinal facets similar to an “arrowhead” pointing northward.

DRAINAGE PATTERN ANOMALIES

The disruption of the drainage network in response to active uplift shows different behaviors, linked to the geometry and evolution of thrust-fold deformation. The drainage system in the Santa Ines foothills is adjusted to several parallel NNE-trending active structures. Small rivers merge to form grid-iron patterns; meanwhile, rivers which could not keep up with vertical uplift result in wind gaps on the top of structures (Audemard, 1999). Some rivers at the younger flexural front reflect subtle topographic modifications due to active growth; for example, eastward diversion of a small river in the town of Arenilla induces an abandoned channel and a drainage capture by a large river (Fig. 4), suggesting a faster growth rate at the northwest of thrust-fold belt (Alarcon, 2014).

Westward of the Moroturo foothills, the Bobare River changes his morphology from high to low sinuosity when passes the Moroturo flexure (Fig. 5), in a very similar behavior to the Catatumbo River (Venezuela), reported by Ollarves et al., (2006). This change in morphology implies active uplift on the ground surface of Bobare River, associated with Moroturo blind fault. Simultaneously, the uplift of this unit allows the formation of staircased alluvial terraces in the hanging block (Fig. 5).

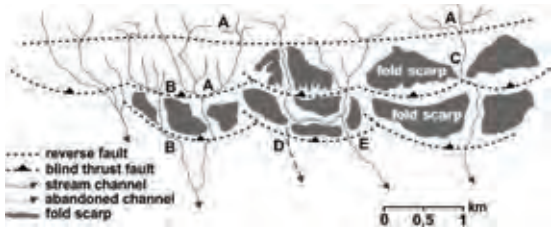

Figure 4: Patterns of thrust fault-related stream channels near the town of Arenilla, in the Santa Ines foothills. (A) Grid-iron drainage pattern; (B) drainage deflection; (C) wine-glass canyon, (D) abandoned channel; (E) drainage capture.

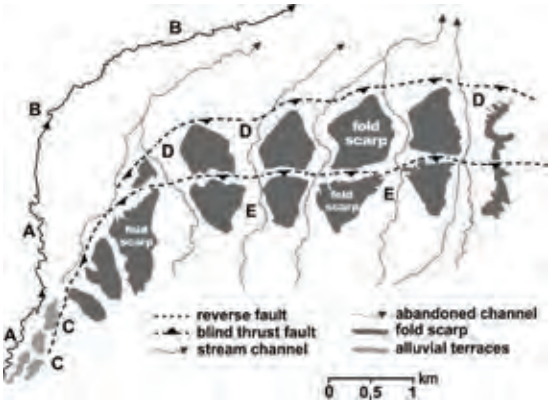

Figure 5: Patterns of thrust fault-related stream channels near the town of Moroturo, in the Moroturo foothills. (A) High sinuosity of the Bobare River; (B) low sinuosity of the Bobare River; (C) staircased alluvial terraces, (D) disproportionate size between present river width and canyons; (E) water gaps.

PALEOSOL DEVELOPMENT

The growth of folds produces changes in elevation of pre-existing surfaces (Suppe, 2014). Under this assumption, we can recognize paleosols in elevated flats, associated to high periods of exposure and pedogenetic evolution, under humid tropical climate (Zinck, 1970; 1981; 2013). Therefore, Alarcon (2014) discusses the relationship between criteria of paleosols development and the relative age of fold-scarp formation.

For example, paleosols developed on early Pleistocene elevated flats, linked with Santa Ines fold-scarp bulging, can be related to high degrees of weathering of the parental material. This process is reflected on paleosols (oxisols/ultisols) as lixiviation, disintegration of gravels, and high degree of rubification (gradual increase of red color soils) associated to weathering of the ferromagnesian minerals (Fig. 6). Likewise, loss of alkaline cations due to desaturation as a function of time, results in an increase in pH acidity of the soil solution. Similar paleosols can be found on sediments of Moroturo flexural scarp, at elevations 250 meters above the Santa Ines valley.

Acknowledgements:
We are grateful to acknowledge the gracious support of GEODINOS grant (FONACIT-2002000478) of Venezuelan Foundation for Seismological Research (FUNVISIS), the department of Earth Sciences of FUNVISIS and the department of Geology at Central University of Venezuela.

References

Alarcón, E.A., (2014*). Estudio neotectónico de la depresión de Santa Inés, estado Lara. Trabajo Especial de Grado.* Escuela de Geología, Minas y Geofísica, Universidad Central de Venezuela. 195pp.

Alarcón, E.A., Audemard, F.A. and A. Singer, (2014). Mapa neotectónico de la depresión de Santa Inés, estado Lara, Venezuela. *Jornadas de Investigación de la Facultad de Ingeniería 2014*. Universidad Central de Venezuela. 11pp.

Figure 6: a) A north-verging fold scarp, south of the town of Moroturo, showing bulged Pleistocene sediments with a paleosol development. b) A paleosol (ultisol) at the top of the fold scarp described in (a), showing evidence of high degree of rubification.

Audemard, F.A., (1993). *Néotectonique, sismotectonique et aléa sismique du Nord-Ouest du Vénézuéla (systeme de failles d'Oca-Ancón)*. Thèse PhD. Université Montpellier II, 369 pp.

Audemard, F.A., (1999). Morpho-structural expression of active thrust fault systems in the humid tropical foothills of Colombia and Venezuela. *Zeitschrift für Geomorphologie*, Vol. 118: 227-244.

Audemard, F.A., (2003). Geomorphic and geologic evidence of ongoing uplift and deformation in the Mérida Andes, Venezuela. *Quaternary International*. Vol. 101:43-65.

Beltrán, C. and C. Giraldo, (1989). *Aspectos neotectónicos de la región nororiental de Venezuela*. VII Congreso Geológico Venezolano, Barquisimeto. Vol. 3: 1000-1021.

Ollarves, R., Audemard, F.A. and M. Lopez, (2006). Morphotectonic Criteria for the Identification of Active Blind Faulting in Alluvial Environments: Case Studies from Venezuela and Colombia. *Zeitschrift für Geomorphologie*. Vol. 145: 81-103.

Soulas, J.P., Singer, A. and M. Lugo, (1987). *Tectónica cuaternaria, características sismogénicas de las fallas de Boconó, San Simón y del piedemonte occidental andino y efectos geológicos asociados a la sismicidad histórica (Proyecto Sumandes I)*. Informe FUNVISIS para MARAVEN, Caracas, 90 pp.

Suppe, J., (2014). Active folding of landscapes and sedimentary basins. In: *Proceedings 5th International INQUA Meeting on Paleoseismology, Active Tectonics and Archeoseismology (PATA)*. pp. 23-27.

Zinck, J.A., (1970). *Aplicación de la geomorfología al levantamiento de suelos en zonas aluviales*. Ministerio de Obras Públicas (MOP). Barcelona, Venezuela.

Zinck, J.A., (1981). *Definición del ambiente geomorfológico con fines de descripción de suelos*. Centro Interamericano de Desarrollo e Investigación Ambiental y Territorial, Universidad de Los Andes, Venezuela.

Zinck, J.A., (2013). *Geopedology: elements of geomorphology for soil and geohazard studies*. ITC Faculty of Geo-Information Science and Earth Observation. Enschede, The Netherlands. 135pp.

INQUA Focus Group on Paleoseismology and Active Tectonics

Liquefaction assessment by in situ testing in the Fucino plain (central Italy)

Amoroso, S. (1), Boncio, P. (2), Famiani, D. (3), Hailemikael, S. (4), Manuel, M.S. (5), Milana, G. (6), Monaco, P. (7), Vassallo, M. (8), Vessia, G. (9)

(1) Istituto Nazionale di Geofisica e Vulcanologia, L'Aquila, Italy. E-mail: sara.amoroso@ingv.it
(2) Dept. Scienze Psic. Uman. e Terr., University of Chieti - Pescara, Italy
(3) Istituto Nazionale di Geofisica e Vulcanologia, Roma, Italy
(4) Agenzia naz. nuove tecn., energia e sviluppo ec. sost., C.R. Casaccia, Roma, Italy
(5) Geo Geotecnica e Geognostica s.r.l., Arpino, Italy
(6) Istituto Nazionale di Geofisica e Vulcanologia, Roma, Italy
(7) Dept. Civil, Arch. and Env. Engineering, University of L'Aquila, Italy
(8) Istituto Nazionale di Geofisica e Vulcanologia, L'Aquila, Italy
(9) Dept. Ingegneria e Geologia, University of Chieti - Pescara, Italy

Abstract: *An extensive geological, geotechnical and geophysical investigation was undertaken for the seismic microzonation of Avezzano, the main town of Fucino plain (L'Aquila province, Italy). Here, during the 1915 Fucino earthquake evidences of liquefaction were detected. The present study focuses on the liquefaction hazard assessment based on in-situ tests like piezocone (CPTu), dynamic penetration (standard SPT and super heavy DPSH tests), and seismic dilatomer SDMT tests. Results at the test site of Pozzone area have been reported and discussed hereafter. Preliminary results of liquefaction analyses carried out using simplified methods are illustrated, compared and discussed throughout the paper. According to these first outcomes, the SDMT and CPTu investigation methods show similar values of liquefaction susceptibility.*

Key words: *Liquefaction assessment, in situ testing, seismic microzonation.*

INTRODUCTION

The Fucino plain is an alluvial basin characterized by silty and sandy soils, that can be susceptible to liquefy. In this respect an extensive geological, geotechnical and geophysical campaign was committed for the seismic microzonation of Avezzano, the main town of Fucino plain located in central Italy, where evidences of liquefaction were recorded during the 1915 Fucino earthquake (Galli 2000, Prestininzi & Romeo 2000).
This paper analyses and compares the results from tests carried out in the Pozzone area by using different in situ geotechnical and geophysical methods: seismic dilatometer (SDMT), piezocone (CPTu), dynamic super heavy penetration (DPSH) tests and seismic noise measurements.
Preliminary evaluations of safety factor against liquefaction and liquefaction potential based on SDMT, CPTu and DPSH are discussed throughout the paper.

GEOLOGICAL CONTEXT

The Pozzone site is located in the northern side of the Fucino lacustrine basin. The basin was formed during the Quaternary, due to the activity of two important systems of normal faults. The main fault system dips to the SW and borders the basin to the East. The second fault system dips to the SSE and borders the basin to the North (Cavinato et al. 2002). The main SW-dipping normal fault system is presently active and was activated by the large (M 7.0) January 13, 1915 earthquake. The Pozzone site is located close to the northern fault system.

Four main geo-lithological domains can be identified within the Fucino basin:

1. Meso-Cenozoic calcareous or siliciclastic bedrocks, cropping out at the margins of the basin and buried below a thick cover of continental Quaternary deposits within the basin;
2. Lower-to-Middle Pleistocene slope-derived breccia, fluvial and marginal lacustrine deposits cropping out mostly along the northern slopes;
3. Upper Pleistocene fluvio-glacial fans interfingering with coeval lacustrine deposits at the rims of the basin;
4. open lacustrine deposits in the most central part of the basin; the central part of the basin hosted an old lake until its complete drainage at the end of 19th century.

In particular, the Pozzone site is located in the 4th domain, close to the transition to the 3rd domain. The outcropping sediments are lacustrine deposits of latest Pleistocene-Holocene age (Lac3 in Fig. 1). Typically, the Lac3 unit is formed by grey-blue clayey silt passing upwards to light coloured silt and sandy silt, with interlayers of sand and peat. The Lac3 unit overlies a thick pile of fine-grained sediments which, according to borehole and seismic reflection data, are up to 200-250 m thick (Boncio et al. 2014, Cavinato et al. 2002). The detailed shallow subsurface stratigraphy of the Pozzone site is poorly known. Only very synthetic logs of wells drilled during '50s for hydrogeological exploration/exploitation are available (Fig. 1). The top 10-15 m depths are dominated by pelitic sediments (prevailing clay, according to borehole logs). Below 10-15 m depths, there are bodies of coarse-grained sediments the lateral continuity of which is difficult to

establish (sand, sand and clay, sand and gravel or gravel). The site is characterized by the presence of small permanent lakes interpreted as sinkholes (Nisio et al. 2007). After the 1915 earthquake, Oddone (1915) documented a number of phenomena, such as: a) ground fracturing; b) the disappearance of a small island within the largest of the Pozzone lakes; c) variations of the water level within the lakes; d) a long-lasting turbidity; and e) the tilting of a building, accompanied by the appearance of loose soil, in a site located ~1.3 km SE of Pozzone. Some of these phenomena collectively could suggest the occurrence of liquefaction processes.

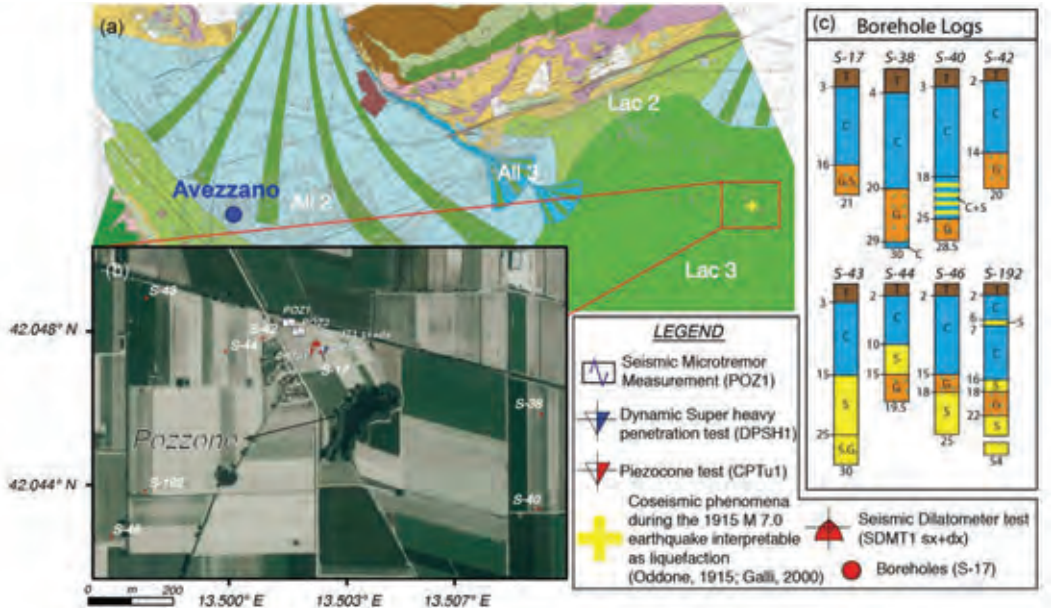

Figure 1: (a) Geological map of the Pozzone area (Boncio et al. 2014): All2, All3= alluvial and fluvio-glacial deposits (Late Pleistocene-Holocene), Lac2 e Lac3=lacustrine deposits (Late Pleistocene-Holocene); (b) location of the geotechnical and geophysical investigations; (c) boreholes logs: T = topsoil, C = clay, S = sand, G = gravel into confined aquifer , C+S = clay with levels of sand, S.G. = sand and gravel, G.S. = gravel and sand into confined cquifer.

SITE INVESTIGATIONS

At Pozzone several boreholes, 20-54 m depth (Fig. 1), were available from the seismic microzonation of Avezzano (Boncio et al. 2014), the closest city to the studied area (Fig. 1).
In this respect, the geotechnical and geophysical characterization was completed performing a seismic dilatometer test (SDMT1 sx+dx), a piezocone test (CPTu1), a dynamic super heavy penetration test (DPSH1), and seismic noise measurements (POZ1, POZ2), as shown in Fig. 1. A 20 ton light penetrometer was used to push SDMT, CPTu, and DPSH equipment. The details of the in situ testing and the noise measurements are extensively described by Amoroso et al. (2015). Pozzone site is characterized by the succession of silty clays with a consistent lens of silty sand at 12.60-14.40 m depth, as identified by SDMT1 s+dx, CPTu1 and DPSH1 tests, and approximately by the previous boreholes (i.e. S-17 in Fig. 1). The ground water level was detected at 1.70 m depth.

LIQUEFACTION ASSESSMENT

The liquefaction analysis was carried out according to the "simplified procedure" introduced by Seed & Idriss (1971), based on the comparison of the seismic demand on a soil layer generated by the earthquake (cyclic stress ratio *CSR*) and the capacity of the soil to resist liquefaction (cyclic resistance ratio *CRR*). Indeed, the liquefaction safety factor F_L was defined as the ratio between *CRR* and *CSR*. In addition, according to Iwasaki et al. (1982) the liquefaction potential index I_L was introduced to estimate the liquefaction susceptibility for the whole soil profile.

Cyclic stress ratio (CSR)
The cyclic stress ratio *CSR* was estimated by Seed & Idriss (1971) formulation, evaluating the Magnitude Scaling Factor *MSF* and the shear stress reduction coefficient r_d according to Idriss (1999) , as shown in Figs. 2 and 3 (middle plot).
For a preliminary assessment, the value of the peak ground acceleration *PGA* at the ground surface was assumed equal to 0.341 g. This value was obtained by the product of the design peak ground acceleration a_g for stiff ground (type "A") and a soil factor *S*, which depends on the subsoil stiffness, namely the stratigraphic amplification factor S_S, and on the topography, defined by the topographic amplification factor S_T, according to the Italian Building Code (NTC 2008).
At Pozzone test site a_g was assumed equal to 0.255 g; this value corresponds to a design earthquake for a return period T_R = 475 years, as reported by the Italian Seismic Hazard Maps (Gruppo di Lavoro MPS 2004). S_S was estimated equal to 1.339 considering ground type

"C", as indicated by the V_S profile (Fig.2), and S_T was evaluated equal to 1 identifying Pozzone in a flat area. A magnitude scaling factor *MSF* = 1.14 was applied for the magnitude M_w = 7.06, introduced considering the 923 seismogenetic zone, valid for Fucino plain according to Gruppo di Lavoro MPS (2004).

Cyclic resistance ratio (CRR)

The goal of this paragraph is to compare different estimations of the cyclic resistance ratio CRR, by means of V_S or K_D, as indicated in Figs. 2 and 3.

The *CRR* was estimated considering all the in situ tests performed at Pozzone test site, i.e. SDMT1 sx+dx, CPTu1, DPSH1.

In particular, the seismic dilatometer test (Marchetti 1980, Marchetti et al. 2001, Marchetti et al. 2008) provides at each depth geotechnical and geophysical parameters, including the horizontal stress index K_D (provided by current DMT interpretation) and the shear wave velocity V_S (measured), that can be used for the liquefiability assessment.

Various *CRR*-K_D correlations have been developed in the last two decades, stimulated by the recognized sensitivity of K_D to a number of factors which are known to increase liquefaction resistance, such as stress history, prestraining/aging, cementation, structure, and by its correlation with relative density and state parameter (see e.g. Monaco et al. 2005). Three recent *CRR*-K_D correlations (Monaco et al. 2005, Tsai et al. 2009, Robertson 2012) were used in this study. In addition *CRR* was evaluated from V_S using the correlation proposed by Andrus & Stokoe (2000), while for CPTu test the Robertson & Wride (1997) method was used introducing the normalised tip resistance q_{c1n}. *CRR* was also estimated from DPSH, although the method seems to be less consistent due to the introduction of a energy conversion coefficient that tries to convert DPSH into SPT data.

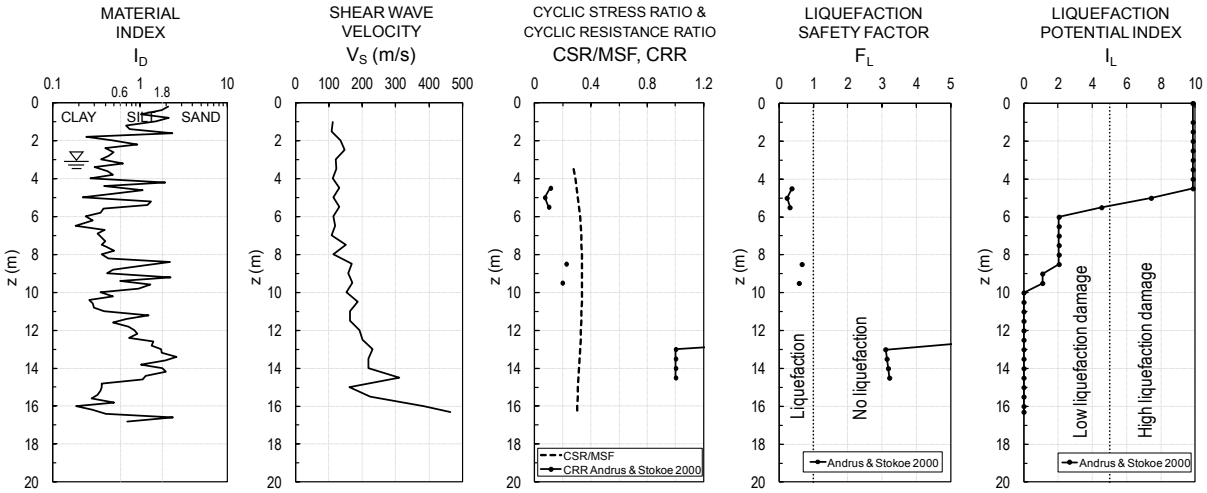

Figure 2: Results of liquefaction analysis based on the shear wave velocity V_S at Pozzone test site.

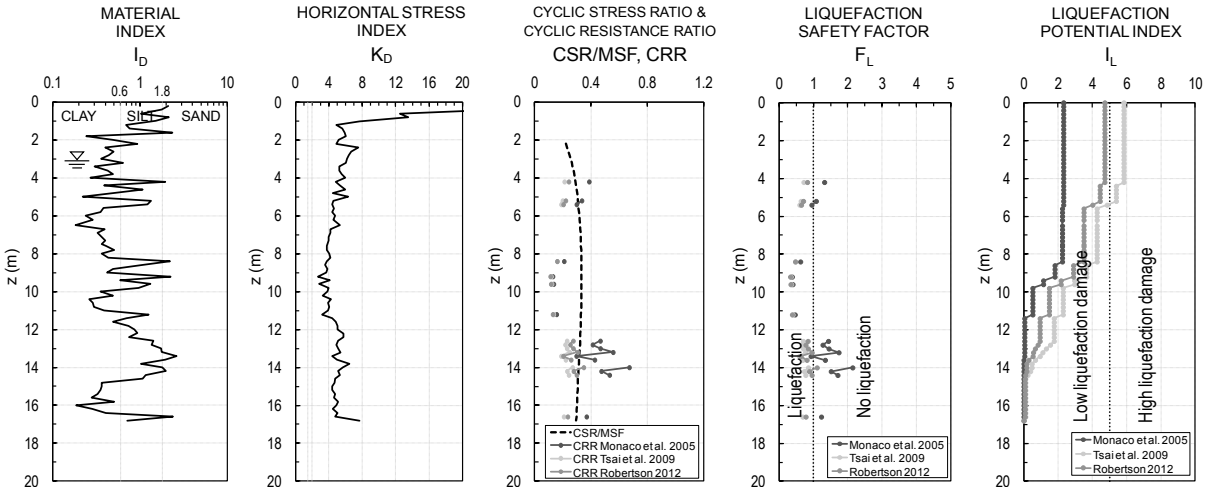

Figure 3: Results of liquefaction analysis based on the DMT horizontal stress index K_D at Pozzone test site.

The details of alle the mentioned analyses is presented by Amoroso et al. (2015). Figs 2 and 3 show the profiles with depth of: the DMT material index I_D (indicating soil type and used to filter the DMT data for $I_D > 2$ into *CRR*-K_D correlations), the parameter used for evaluating *CRR* (shear wave velocity V_S, Fig. 2, or horizontal stress index K_D, Fig. 3), the cyclic stress ratio *CSR* (divided by the magnitude scaling factor *MSF*) compared to the cyclic resistance ratio *CRR*, the liquefaction safety factor F_L, and the liquefaction potential index I_L.

The most evident feature emerging from the comparison of the profiles of F_L and I_L obtained by different methods is that *CRR*-V_S and *CRR*-K_D correlations provide different results. In particular, *CRR*-K_D methods detect the consistent lens of silty sand (12.60-14.40 m depth) as marginally liquefiable, in agreement with CPTu results, while the *CRR*-V_S method indicates liquefiability of the shallower layers. This aspect could be due to the fact that K_D is more sensitive than V_S to stress history, prestraining/aging, cementation, structure, relative density and state parameter. However, a similar discrepancy between *CRR* predicted by V_S and by K_D has been observed in several other cases investigated by SDMT (see e.g. Maugeri & Monaco 2006).

CONCLUSIONS

The large amount of data provided by the seismic microzonation of Avezzano (Italy), supplied a useful tool for a preliminary liquefaction assessment of Pozzone test site.

CPTu- and DMT-based analyses provide similar results in terms of liquefaction potential index, while the DPSH-based method seems to be less consistent due to the introduction of an energy conversion coefficient, and the V_S-based method indicates a higher liquefiability of the shallower layers.

Further investigations and analyses will be performed to increase the knowledge on liquefaction of the Fucino plain soils.

Acknowledgements: This study was founded by Geo Geotecnica e Geognostica s.r.l.

References

Amoroso, S., P. Boncio, D. Famiani, S. Hailemikael, M.S. Manuel, G. Milana, P. Monaco, M. Vassallo, (2015). Preliminary liquefaction studies for seismic microzonation of Avezzano, Italy. Accepted for publication in DMT'15, *The 3th International Conference on the Flat Dilatometer*, 15-17 June 2015, Rome, Italy.

Andrus, R.D. and K.H. Stokoe II, (2000). Liquefaction resistance of soils from shear-wave velocity. *J. Geotech. Geoenviron. Eng.*, ASCE. 126(11), 1015-1025.

Boncio, P., G. Milana, F. Cara, G. Di Giulio, D. Di Naccio, D. Famiani, M. Francescone, F. Galadini, T. Mancini, M. Nardone, G. Rosatelli, and M. Vassallo, (2014). Microzonazione Sismica di Livello 1 del Comune di Avezzano. Unpublished Report with 1:5000 maps and sections. Regione Abruzzo, 2014, in Italian.

Cavinato, G., C. Carusi, M. Dall'Asta, E. Miccadei, and T. Piacentini, (2002). Sedimentary and tectonic evolution of Plio-Pleistocene alluvial and lacustrine deposits of Fucino Basin (central Italy). *Sediment. Geol.* 148, 29–59.

Galli, P., (2000). New empirical relationships between magnitude and distance for liquefaction. *Tectonophysics*. 324, 169-187.

Gruppo di Lavoro MPS, (2004). *Redazione della mappa di pericolosità sismica prevista dall'Ordinanza PCM 3274 del 20 marzo 2003*. Rapporto Conclusivo per il Dipartimento della Protezione Civile, INGV, Milano-Roma, aprile 2004, 65 pp. + 5 appendici. http://zonesismiche.mi.ingv.it/, in Italian.

Idriss, I.M., (1999). *An update to the Seed-Idriss simplified procedure for evaluating liquefaction potential*. Proc. TRB Workshop on New Approaches to Liquefaction, Publ. No. FHWA-RD-99-165, Federal Highway Administration.

Iwasaki, T., K. Tokida, F. Tatsuoka, S. Watanabe, S. Yasuda, and H. Sato, (1982). *Microzonation for soil liquefaction potential using simplified methods*. Proc. of 3rd Int. Conf. on Microzonation, Seattle, 3, 1319–1330.

Konno, K. and T. Ohmachi, (1998). Ground motion characteristics estimated from spectral ratio between horizontal and vertical components of microtremors. *Bull. seism. Soc. Am.* 88-1, 228-241.

Marchetti, S., (1980). In Situ Tests by Flat Dilatometer. *J. Geotech. Engrg. Div., ASCE*. 106, No.GT3, 299-321.

Marchetti, S., P. Monaco, G. Totani, and M. Calabrese, (2001). *The Flat Dilatometer Test (DMT) in Soil Investigations* – A Report by the ISSMGE Committee TC16. Proc. Int. Conf. on Insitu Measurement of Soil Properties and Case Histories, Bali, 2001, official version reprinted in Flat Dilatometer Testing, Proc. 2nd Int. Conf. on the Flat Dilatometer, Washington D.C., April 2-5, 2006, 7-48, R.A.Failmezger, J.B.Anderson (eds).

Marchetti, S., P. Monaco, G. Totani, and D. Marchetti, (2008). In: Situ Tests by Seismic Dilatometer (SDMT). *From Research to Practice in Geotechnical Engineering, ASCE, Geotechnical Special Publication*, 180, 292-311, J.E. Laier, D.K. Crapps, M.H. Hussein (eds).

Maugeri, M. and P. Monaco, (2006). *Liquefaction Potential Evaluation by SDMT*. Proc. 2nd Int. Conf. on the Flat Dilatometer, Washington, D.C., 295-305.

Monaco, P., S. Marchetti, G. Totani and M. Calabrese, (2005). *Sand liquefiability assessment by Flat Dilatometer Test (DMT)*. Proc. XVI ICSMGE, Osaka, 4, 2693-2697.

Nisio, S., G. Caramanna, and G. Ciotoli, (2007). Sinkholes in Italy: first results on the inventory and analysis. *Geological Society, London*. Special Publications 2007; v. 279; p. 23-45 doi: 10.1144/SP279.4

NTC, (2008). Approvazione delle nuove norme tecniche per le costruzioni. *Gazzetta Ufficiale della Repubblica Italiana*, n. 29 del 4 febbraio 2008-Suppl. Ordinario n. 30, in Italian.

Oddone, E. (1915). Gli elementi fisici del grande terremoto Marsicano-Fucense del 13 gennaio 1915. *Bollettino della Società Sismologica Italiana*, 19, 71-217, in Italian.

Prestininzi, A. and R.W. Romeo, (2000). Earthquake-Induced Ground Failures in Italy. *Engineering Geology*. 58(3-4), 387-397.

Robertson, P. K., and C.E. Wride, (1997). *Cyclic liquefaction and its evaluation based on the SPT and CPT*. Proc. NCEER Workshop on Evaluation of Liquefaction Resistance of Soil, 41–87.

Robertson, P.K., (2012). *The James K. Mitchell Lecture: Interpretation of in-situ tests – some insights*. Proc. 4th Int. Conf. on Geotechnical and Geophysical Site Characterization – ISC'4, Porto de Galinhas, Brazil, 1, 3-24.

Seed, H.B. and I.M. Idriss, (1971). Simplified procedure for evaluating soil liquefaction potential. *J. Geotech. Engrg. Div.*, ASCE, 97(9), 1249–1273.

Tsai, P., D. Lee, G.T. Kung, and C.H. Juang, (2009). Simplified DMT-based methods for evaluating liquefaction resistance of soils. *Engineering Geology*. 103(2009), 13-22.

INQUA Focus Group on Paleoseismology and Active Tectonics

Reliability of first-hand accounts for study of past tsunami events in northeastern Venezuela (southeastern Caribbean Sea), since 1530 AD

Audemard F.A.M., Leal Guzmán A.F.

Dept. Earth Sciences, Venezuelan Foundation for Seismological Research -FUNVISIS-, Caracas, Venezuela.
Email: faudemard@funvisis.gob.ve

Abstract: *Any physical measure of tsunami height provided in eye-witness accounts in historical times (after 1492 AD in the "New World") cannot be taken for granted despite of appearing to be an accurate value. From a thorough and detailed evaluation of historical first-hand accounts reporting on Venezuelan tsunamis along the northeastern Venezuelan low-lying coasts, crosschecking of reported wave heights during several historical Venezuelan earthquake-triggered tsunami waves (particularly during the 1853, 1900 and 1929 events) against the both natural and cultural settings of the affected region has proven that reported wave heights are largely overestimated most of times. On top of that, the occurrence of tsunami waves at villages and settlements at several river mouths makes us suspect that riverbore is a significant and relevant feature during coastal lowlands inundation and sea incursion by these tsunami waves. This is a phenomenom that requires further investigation in tropical regions where river flow at river mouths seems likely to be of prime importance in tsunami wave growth when striking delta areas.*

Key words: *First-hand accounts, Historical Seismology, Tsunami, Wave Height, Caribbean, Venezuela.*

The 1983 National Inventory of Geologic Hazards (Singer et al., 1983) and the 1999 Catalog of felt/destructive Venezuelan Earthquakes (1530-1998; Grases et al., 1999) reliably report the occurrence of tsunami waves on the Caribbean eastern Venezuelan coasts, or phenomena that might be interpreted as substantial sea level modifications in the region, during 5 earthquakes: 1-IX-1530, 15-VII-1853, 29-X-1900, 17-I-1929 and 9-VII-1997. We have confirmed this through the search and evaluation of the accounts by primary sources (eye witnesses) of the tsunami inundation during these 5 events. All but the 1900 shock affected the Cumaná city, and the offshore right-lateral strike-slip El Pilar fault (EPF) has been held responsible for the 4 other events. The 1900 AD tsunami waves were reported along most of the Ensenada de Barcelona coast (W of Cumaná) and Los Roques Archipelago, being this quake attributed to the San Sebastián fault (SSF) segment running offshore Cabo Codera. The 1530 and 1853 earthquakes were produced by the Cariaco trough segment of the EPF west of Cumaná, within a restricted over-1000-m-deep marine pull-apart basin on the SSF-EPF right-lateral releasing step-over, whereas the 1929 and 1997 events occurred on the EPF segment east of Cumaná, inside the shallower Cariaco gulf. Several authors have interpreted all those four tsunamis as the result of major submarine sliding inside the steep-walled trough. First-hand accounts by locals about the abnormal waves during the Cariaco 1997 event, as well as the identification of coastal sliding at the Manzanares river mouth at Cumaná, support this thesis at least for the two latest events, because of the small size of the tsunami-affected area. In addition, recent monitoring (CARIACO Project) has recorded turbidite currents in the Cariaco trough and the Manzanares canyon during the Cariaco Mw 6.9 earthquake and a smaller Mw. 5.2 August 2008 event. However, the 1900 tsunami, and the 1530 and 1853 tsunamis by extension, appears to result from right-lateral tectonic slip along the Cariaco Trough walls.

The first striking conclusion from the historical evaluation of eye-witness accounts is that inundation for all these earthquakes are reported at river mouths or settlements on their mouths: Paparo, Río Chico, Tuy, Neverí, Manzanares. From comparison with modern analogs, such as the Valdivia 1960, Camaná 2001, Sumatra 2004, and Tohoku-Oki 2011 tsunamis, this is not surprising because inundation and wave invasion happens sooner, faster and more efficiently along rivers, through the river mouth. The explanation is obvious: there is no natural barrier blocking the inland wave progression. This also drives that maximum inundation tends to happen and occur along rivers. However, a major difference seems to pop up between the Venezuelan historical tsunami events and those above-mentioned. Venezuela lies in a tropical region where river flow is hardly negligible and appears to be significantly higher than in the other cases. This should then lead to the occurrence of riverbore when both waters (tsunami wave and river flow) encounter at river mouths, rising river level and flooding over banks. Then, this may have fundamental implications on the dynamics of the inundation process, as well as on characteristics of the tsunami waves, particularly as to wave height.

To explore the above and reliability of first-hand accounts on the description of past tsunami waves in northeastern Venezuela, we have started this assessment by looking into the most recent historical event (the January 17th, 1929 earthquake) that should logically have the largest number of accounts, which has happened to be the case. For that earthquake, the occurrence of tsunami waves at the city of Cumaná is repeatedly reported. For instance, Centeno Graü (1940) indicates: "*El mar se retiró de la playa como 200 mts y vino después a la*

costa una ola como de 6 metros de altura que barrió parte de las casas de la playa." (The sea retreated some 200 m and came back to shore as a 6 m high wave that washed down houses on the beach; Free translation by authors –FTBA-). Paige (1930) reports "A tidal wave followed the earthquake causing much damage." The front page of the Caracas newspaper La Esfera on January 19 1929 says "… *embarcaciones de caleta que se encontraba en el muelle de Puerto Sucre fueron alejados al mar; éste, embravecido, lanzó sus aguas hacia la población, en sentido inverso a una tromba de lo que envolvió completamente al "Commewynne" y otras embarcaciones, de las cuales algunas naufragaron. El mencionado vapor holandés se vio juguete de olas y sólo, gracias a la entereza de su capitán que ordenó hábiles maniobras, a posibles contingencias*. (Anchored boats at Puerto Sucre –Cumaná seaport- were pulled offshore; the sea returned with strong surfs to the village, wrapping completely the steam vessel Commewynne and other boats, of which some sunk. The Dutch steam vessel seemed like a toy and only skillful manoeuveurs of its capitain saved it; FTBA)". This is confirmed by another Caracas newspaper on the same day January 19 (El Nuevo Diario), which expresses *"….en Puerto Sucre, donde los daños fueron menores, hubo un violento mar de eleva. El vapor holandés por esta causa, tuvo que retirarse varias veces hacia alta mar, volviendo luego a la Costa. ….Los botes amarrados al costado del muelle se anegaron por completo*." (In Puerto Sucre, where damage was minor, there was a violent tidal wave. The Dutch steamboat, due to the tidal wave, had to sail to open sea several times, later returning to shore. …Boats tied to the sides of the pier were completely drowned; FTBA)". Three days later, the same newspaper writes the following: "*Dos detalles impresionantes del terremoto fueron el desbordamiento del río Manzanares, que en su curso atraviesa la ciudad, cuyas aguas arrastraron cuanto encontraron a su paso, causando enormes daños. Fue el otro la invasión del mar que, elevándose en una marejada de nueve pies sobre su nivel ordinario, se lanzó sobre "El Salado", inundándolo totalmente. Este caserío sufrió considerablemente. La mayoría de sus viviendas, todas gente pobre y trabajadora, quedaron casi destruidas.*" (Two impressive facts of the earthquake were the overflowing of the Manzanares River that crosses the city, whose waters destroyed everything, causing much damage. And the other was the sea incursion, which with an abnormal height of 9 feet struck El Salado –a small fishermen settlement on the southern bank of the Manzanares mouth; now being part of Cumaná-, flooding it completely. This settlement suffered considerably. Most of the dwellings, belonging to poor and labor people, were almost destroyed –FTBA). The same newspaper on March 03, a couple of weeks after the earthquake and tsunami, says: "*El mar por un momento se retiró para luego tornar formando una extensa marejada de gran elevación, que inundó la población situada en el puerto…. El Río hinchó violentamente sus ondas que se llevaron por delante cuanto a su paso encontraron* (The sea for a short while retreated to return later as a tidal wave of big height… The river swelled violently destroying everything at its passage –FTBA-)". The last first-hand account we could find appeared on the nationwide newspaper El Universal on March 22, 1929. It indicated "… *en el preciso momento de la catástrofe algunos pescadores cuyas barcas estaban ancladas en Puerto Sucre vieron amenazante hacia el Norte franco una negra y formidable nube que se levanta sobre las aguas del mar, y que creyendo fuera una borrasca o chubasco marino dieron la voz de alarma es decir, de amarrar o de asegurar sus embarcaciones, de la cual no tuvieron tiempo, pues al instante estalló el cataclismo y una ola colosal los arrojo con sus barcos sobre la playa*" (…right at the moment of the catastrophe, some fishermen, whose boats were anchored at Puerto Sucre, saw an amazing and black threatening cloud rising over the sea due north, and believing it was a storm, gave the alarm of tying and securing the boats, but in such a short notice and having not enough time, a colossal wave rafted the boats to shore).

These several accounts provide very useful information for the understanding of what precisely happened during the January 17th, 1929 earthquake and tsunami that struck Cumaná, and particularly at its western coast, extending between the Manzanares River mouth to the north and the city port named Puerto Sucre to the south, and affecting the fishermen village of el Salado sitting on that coast stretch. The city is well known to the first author since it is his birthplace. This allows describing the pre-event scenario rather confidently. The city of Cumaná sits on a salt-flat that had to be progressively artificially filled to be constructed and urbanized through the years. The salt-flat originally formed behind a coastal sand barrier that hardly reaches 1.7-2.0 m in elevation amsl, and the salt flat floor used to be close to a 1 m below msl. It is important to indicate that tidal range along the Venezuelan coast is less than 35 cm. It is significant to mention that fishermen in northeastern Venezuela in the first half of the XX century most frequently used "Piragua" boats that are 6 to 10 m long and have a draught between 1 and 2 m depending on the load aboard, which are still in use by present-day fishermen.

From all these accounts, the tsunami wave height retained by most scientists is the one from Centeno (1940) of 6 m. It is the most straightforward and no interpretation is needed. But we have to bear in mind that Centeno's work is in itself a catalog; in other words, a compilation and not a first-hand account. However, this value can be in some way tested and contested. As a matter of fact, another account indicates only 9 feet high waves (some 3 m; El Nuevo Diario of January 22nd, 1929). Another estimate of the wave height can be derived from the following facts: A) The anchored boats at Puerto Sucre (probably of the Piragua type) were rafted ashore by the waves; being these boats no more than 3 m deep and exhibiting draughts between 1 and 2 m, and taking into account that the coastal sand barrier is about 1.5 m high, to abandon the boats at the shore, as mentioned in the account, the tsunami waves were hardly over 3 m in height. B) The fact that the "*Commewynne*" steam-boat at Puerto Sucre could sail out to sea several times, it implies that the captain had

time to respond to arriving tsunami waves, which were not large and powerful enough to drift the ship to shore. C) Several boats tied to the pier drowned. If these boats also are of the Piragua type, a 2-3 m high wave would be largely enough to sink boat that cannot freely float. And D) The sea along the west coast of Cumaná, which is very flat, retreated some 200 m before returning and overflowing the sandy beach. If this is compared to the first author's observations collected during the 1997 event (González et al., 2004), a sea retreat in the same portion of beach of a 100 m allowed estimating a wave height in the order of a 1 m. By analogy, at constant beach and very nearshore slope gradient, the retreat of some 200 m during the 1929 tsunami would be equivalent to a wave of a couple of meters at most.

From these observations several other conclusions can be drawn: 1) Several waves seem to have happened. 2) Most eye-witnesses first report a sea retreat. 3) The tsunami wave are reported on the west coast of Cumaná, on the open sea side, opposed to the earthquake epicenter proposed by Mocquet (1996) and Audemard (1999; 2007). Therefore, it should be considered that this tsunami is necessarily related to a submarine slump or slide occurring in the Cariaco trough, and probably inside the Manzanares submarine canyon, in a similar way to the tsunami wave reported during the 1997 earthquake, which shows evidence of subaerial sliding at the Manzanres mouth (González et al., 2004), whose turbidite currents were reported by Thunell et al. (1999) and Lorenzoni et al. (2012). And 4) Two first-hand accounts (El Nuevo Diario on 1929/01/22 and 1929/03/03) report the rise of the Manzanares River waters along its final stretch, overbanking and flooding along the river course. This seems to point out to the formation of a waterbore at the river mouth.

For the October 29th, 1900 earthquake-tsunami, the first-hand accounts tell us a similar story. The newspaper la Linterna Mágica on November the 2nd says: "*En el **Puerto Tuy** el mar se separó como ocho cuadras, y luego se vino encima de la playa una gran mole de agua como de diez metros de altura que anegó los almacenes.*" (At Puerto Tuy, sea retreated like 8 "cuadras" -distance unit ranging between 100 a 150 m in length-, and then returned onto the beach as a huge wall of water of about 10 m high, which flooded the warehouses –FTBA-). Another account in the same newspaper indicates that: "*Una parte del pueblo de **Paparo** se hundió en el agua, quedando las casas sólo con la mitad afuera.*" (A portion of the village of Paparo was drowned, being only the upper half of the houses standing out –FTBA-). On la Religión of November 6th, the following note was found: "*En **San José**, población situada a menos de dos millas de Río Chico, se desbordó el río que atraviesa el pueblo en ambas márgenes, bañando las calles y luego se volvió a su cauce natural, siendo más grave este fenómeno cuanto que una de las márgenes del río San José tiene cuatro metros de altura. El mismo fenómeno se verificó en todo el curso del río, brotando a tierra un sinnúmero de peces que sirvieron de alimento a la población en aquellos instantes de pavor; y de divertimento durante todo el día a los chiquillos (...) Media hora después del cataclismo crecieron las aguas de los ríos sin que antes ni después de aquel aciago momento hubiese llovido en sus lechos.*" (In San José, village located less than 2 miles from Río Chico, the river that crosses town overbanked on both sides, flooding the streets before getting back into its natural course. This is even worse if considering than one of the river bank is 4 m higher than the river course. This was seen all along the river course, throwing on land countless fish that fed the population during those dreadful days; and used as toys by kids the day long….. Half an hour later than the cataclysm, the river waters rised without any rain before or after that terrible moment –FTBA-). To understand the relevance of these accounts, the coastal area of Barlovento, along the Ensenada de Barcelona shore, needs to be described. The Barlovento depression exhibits a flat-lying topography, bounded by a sandy beach that is usually less than 1.7 m high. It extends far inland with almost no relief for tens of kilometers, being the villages of Paparo, San José and Río Chico not far from the coast. The October 29th, 1990 earthquake strikes this region before sunrise, still at full darkness (4:45-5:00 am local time) and the tsunami, as mentioned by one of the accounts, strikes the region around half an hour later, still at dark. We actually wonder how an eye-witness could reliably see and measure anything at night time and furthermore how he could survive a 10 m high wave in an area with no elevation and vertical escape except for tall trees. If the other accounts are analyzed in detail, it would be more appropriate to believe that riverbores took place, in which case, the water elevation could reach up to 3-4 m, eventually to 5 m at most, considering that houses were half drowned and they may sit on river banks, which are 3 to 4 m above the river course in normal conditions.

Acknowledgements: This is a contribution to Project FONACIT 2013000361 (2013-2016) and past projects FONACIT-ECOS Nord PI-2003000090 and PI-2009000818.

References

Audemard, F.A., (1999). *Nueva percepción de la sismicidad histórica del segmento en tierra de la falla de El Pilar, Venezuela nororiental, a partir de primeros resultados paleosísmicos*. VI Congreso Venezolano de Sismología e Ingeniería Sísmica, Mérida, Venezuela. Edición en CD-ROM.

Audemard, F.A., (2007). Revised seismic history of El Pilar Fault, Northeastern Venezuela, after the Cariaco 1997 Earthquake and from recent preliminary paleoseismic results. *Journal of Seismology*. 11(3): 311-326.

Centeno Graü, M., (1940). *Estudios sismológicos*. Litografía del Comercio, Caracas.

Grases, J., R. Altez, M. Lugo, (1999). *Catálogo de sismos sentidos o destructores. Venezuela. 1530–1998*. Academia de Ciencias Físicas, Matemáticas y Naturales/Facultad de Ingeniería Universidad Central de Venezuela, Editorial Innovación Tecnológica.

González, J., M. Schmitz, F.A. Audemard, R. Contreras, A. Mocquet, J. Delgado, F. De Santis, (2004). Site effects of the 1997 Cariaco, Venezuela earthquake. *Engineering Geology*. 72(1-2): 143-177.

Lorenzoni, L., C. Benitez-Nelson, R. Thunell, D. Hollander, R. Varela, Y. Astor, F.A. Audemard, F. Muller-Karger, (2012). Potential role of event-driven sediment transport on sediment accumulation in the Cariaco Basin, Venezuela. *Marine Geology*. 307-310: 105-110.

Mocquet, A., C. Beltrán, M. Lugo, J.A. Rodríguez, A. Singer, (1996). *Seismological interpretation of the Historical data related to the 1929 Cumaná earthquake, Venezuela*. 3rd International Symposium on Andean Geodynamics, pp. 203-206.

Paige, S., (1930). The Earthquake at Cumaná, Venezuela. January 17, 1929. *Bull. Seismol. Soc. Am*. 20: 1-10.

Singer, A., M. Lugo, C. Rojas, (1983). *Inventario Nacional de Riesgos Geológicos. Informe preliminar*. FUNVISIS, 128 pp. + map.

Thunell, R., E. Tappa, R. Varela, M. Llano, Y. Astor, F. Müller-Karger, R. Bohrer, (1999). Increased marine sediment suspension fluxes following an earthquake. *Nature*. 398: 233.

INQUA Focus Group on Paleoseismology and Active Tectonics

Assessing seismic efficiency from scalar Moment-rates: an application to Mt. Etna volcano (Italy)

Azzaro, R., Barberi, G., Cannavò, F., Cocina, O., Palano, M., Scarfì, L.

INGV - Istituto Nazionale di Geofisica e Vulcanologia - Osservatorio Etneo, Catania, Italy. Email: raffaele.azzaro@ingv.it

Abstract: *Here we propose an improved estimation of the scalar seismic (from instrumental and historical catalogues), geodetic and geologic moment-rates for the eastern flank of Mt. Etna. The estimated moment-rates have been compared in terms of seismic efficiency. Results show that all the calculated efficiency values are lower than 40%, i.e., the geodetic moment-rate estimations are generally larger than the seismic and the geologic ones. Although a number of reasons may account for the observed discrepancy, we are confident that a large amount of the deformation affecting the eastern flank occurs aseismically.*

Key words: *Mt. Etna, moment-rates, seismic efficiency, creeping faults.*

INTRODUCTION

The comparison of seismic, geologic and geodetic moment-rates can provide crucial insights for understanding fault behaviour in tectonically active zone, with obvious implications on seismic hazard assessment (Masson et al., 2005; Pancha et al., 2006; Puskas et al., 2011; Talebian, 2012). It is well acknowledged that when the seismic moment-rate is lower than geodetic or geologic ones, the exceeding moment-rate is released in aseismic mode. In fact, the observed geological and geodetic moment-rates include both elastic and inelastic deformations, and since only the elastic component is responsible for earthquakes, the comparison of these moment-rates with the seismic one do not balance in regions affected by creeping faults or where significant amounts of deformation take place plastically (Palano et al., 2011).

It is the case of Etna, where slow aseismic slip due to fault creep is a common mode of displacement along many of the fault segments in the eastern flank (Rasà et al., 1996).

A first application of the methodology to estimate and compare the scalar seismic, geodetic and geological moment-rates was recently applied at Mt. Etna (Barberi et al., 2014) following the methodology proposed for the Southern Apennines by Palano et al. (2011) and Ferranti et al. (2014). The preliminary results have been now improved by a more precise constraints on geometric and kinematic fault parameters to reduce uncertainties on the geological moment-rate estimation. The present analysis has allowed to estimate the seismic efficiency of the faults in the eastern flank of Etna, that appears essentially low due to the relevant component of the aseismic deformation.

Seismological data

In order to define the seismotectonic features of the faults in the eastern flank of Etna, we considered both long- and short-term seismicity data.

As regards the first ones, we used the huge historical data set represented by the macroseismic catalogue of earthquakes occurring at Etna from 1832 to 2013 [CMTE Working Group, 2014]. For the analysis we selected major events located in the eastern flank, i.e. 167 shocks with epicentral intensity $I_0 \geq$ V EMS (above the damage threshold) corresponding to an equivalent magnitude $M_L \geq 3.0$ according to Azzaro et al. (2011). The above thresholds represent a portion of the catalogue statistically complete, so these earthquakes may be considered as representative of the seismic cycle in the long-term (Azzaro et al., 2012b).

Regarding the short-term, the instrumental data set covers the time interval from the 2005 to 2013. The choice of this time-span is justified by the development of a modern seismic network, equipped with digital stations and broad-band sensors, allowing the detection of small magnitude events and hence the application of advanced techniques for locating epicenters.

From the initial dataset - about 4,570 seismic events with a magnitude M_L between 1.0 and 4.8 (magnitude of completeness $M_c \geq 1.5$) - we selected about 1,600 earthquakes located in the study areas of Timpe and Pernicana faults (Fig. 1). In order to better define seismic clusters or epicentre alignments, the selected earthquakes have been relocated using the tomoDDPS algorithm (Zhang et al., 2009) and the 3D velocity model of Alparone et al. (2012). Results show that seismic events tend to cluster around active faults mainly in the depth range 3-10 km in the Timpe zone, and between -1 and 3 km along the Pernicana fault.

Geodetic data

Available GPS observations collected by the Mt. Etna permanent GPS Network, spanning the 2005.00-2013.99 time interval and covering the eastern flank of Mt. Etna (Fig. 1), have been processed using the GAMIT/GLOBK software following the method described in Gonzalez and Palano (2014). Estimated geodetic velocities were referred to the "Etn@ref" reference frame (a local reference frame computed to isolate the Mt. Etna volcanic deformation from the background regional tectonic pattern; see Palano et al. 2010 for details).

The resulting velocity field confirms the seaward motion of the eastern flank of Mt. Etna. In detail, sites close to the central sector of the unstable flank are characterized by velocities up to 35 mm/yr, while moving southward or northward the velocity field decreases to values of ca. 1-2 mm/yr.

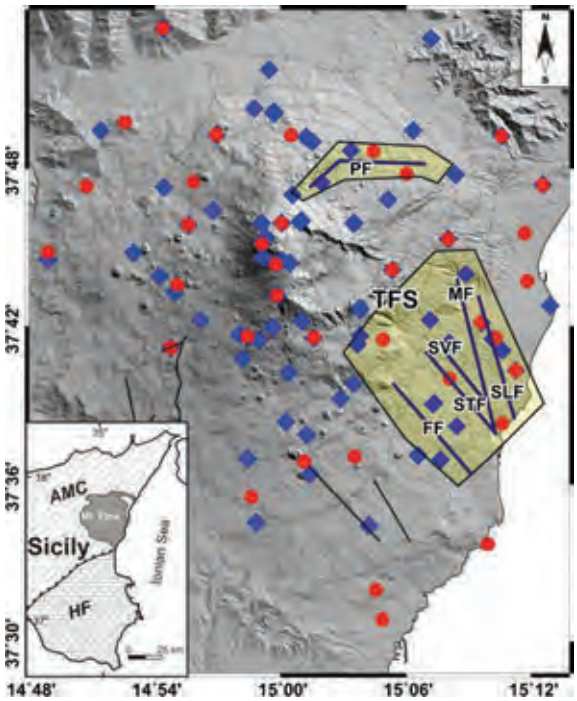

Figure 1: Sketch map of Mt. Etna. Continuous GPS stations are reported as red points, while seismic stations are reported as blue diamonds. The highlighted boxes represents the surface projection of the prismatic bodies used for the moment-rates estimations. Abbreviations: PF, Pernicana fault; FF, Fiandaca fault; SLF-MF, S. Leonardello–Moscarello fault system; STF-SVF, S. Tecla–S. Venerina fault system; TFS, Timpe fault system. The inset reports a simplified structural map of eastern Sicily; AMC: Apenninic-Maghrebian Chain; HF: Hyblean Foreland.

Geologic data

The region of Mt. Etna is characterised by intense geodynamics at the scale of the volcano, with a continuous ESE seaward sliding instability process affecting the eastern flank, which represents the result of interaction among regional stress regime, magma intrusion and basement geometry (Azzaro et al., 2013). Evidence of active tectonics is mostly distributed over the unstable sector, with a number of faults forming two main structural systems: the Timpe faults, and the Pernicana fault. The Timpe fault system crosses the central part of the eastern flank with a 20 km long and 5 km wide belt of mainly extensional structures, striking from N to NW and consisting of well-developed morphological scarps and hidden fault segments (Azzaro et al., 2012a). Their intense activity is expressed not only by seismicity but also fault creep, with geological slip-rates varying from 1.0 to 5.3 mm/yr (see Azzaro et al., 2012a for an overview). The analysis of ground deformation decennial time series (GPS, SAR) has shown that inside the Timpe system there are kinematic domains characterised by different velocity and displacements, but all showing discontinuous dynamics (Palano et al., 2008; Bonforte et al., 2011). Basically, the fairly constant mid-term (decennial) ESE seaward sliding is interrupted by sudden short-term (months to year) accelerations related to flank eruptions. Conversely, there is a general agreement on identifying the Pernicana fault system to represent the northern boundary of the unstable sector (Fig. 1). Dynamics of this important tectonic element became evident through geodetic data collected since 1997 (Azzaro et al., 2001, Palano et al., 2006), which evidenced a fairly stable slip with an average rate of about 28 mm/yr, related to the continuous long-term sliding motion of the eastern flank of the volcano toward the sea. Abrupt, even transient, increase in the seismic and geodetic strain release of the Pernicana fault has been measured during some recent flank eruptions (e.g. 2001 and 2002-03) and interpreted as a result of additional stressed induced by the magma ascent in the feeding system (Palano et al., 2008; Alparone et al., 2013; Bonaccorso et al., 2013).

In order to estimate the geologic moment-rates, we collected geometric and kinematic parameters from published and unpublished studies (see Azzaro et al., 2013 and references therein). More in detail, for each structure we considered the following parameters: length (L), strike (θ), dip (φ), down-dip width (H), and slip-rate (if available, we used both short- and long-term estimations). On the whole, the faults have length typically in the ~5-8 km range and down-dip width in the 1.6-4.5 km range. Slip-rates (long-term) range from 1 up to 5.2 mm/yr in the Timpe system while along the Pernicana fault the slip-rate obtained for the last millennium is much more higher, up to 24 mm/yr (Ferreli et al., 2002).

Computation of moment-rates

As a first step, taking into account the spatial distribution of the active faults and their seismogenic thickness Hs, we divided the investigated volume into prismatic bodies (Fig. 1). Then, by adopting relevant formulations (see Barberi et al., 2014 for details), we calculated for each prismatic body the scalar moment-rates.

The seismic moment-rate was calculated according to the Kostrov (1984) general formulation which takes into account the number of events occurred in the selected volume during the considered time interval. By considering both instrumental and historical earthquake catalogues, we performed two different computations. All magnitudes were converted into scalar moments through the relationship proposed for this area by Giampiccolo et al. (2007). The obtained seismic moment rates range in the interval $3.55 \cdot 10^{13}$ - $8.06 \cdot 10^{14}$ Nm/yr, and 2.2710^{14} - $1.96 \cdot 10^{15}$ Nm/yr, for the instrumental and historical catalogues, respectively.

The geodetic moment-rate was estimated by adopting the formulation proposed by Savage and Simpson (1997), which takes into account the average strain-rate tensor for the selected area, the volume of each

prismatic body and the shear modulus of rocks. The estimated geodetic moment-rate ranges in the interval $8.16 \cdot 10^{14}$ - $2.57 \cdot 10^{16}$ Nm/yr.

Lastly, the geological moment-rate was computed by using the Brune (1968) formulation which takes into account the shear modulus of the rocks involved in faulting, the dimensions (length and down-dip width) of the dislocation and the average geologic slip-rate. The calculated geological moment-rate ranges in the interval $2.16 \cdot 10^{14}$ - $3.81 \cdot 10^{15}$ Nm/yr. Figure 2 shows the values of the different typologies of moment-rates for the analysed faults.

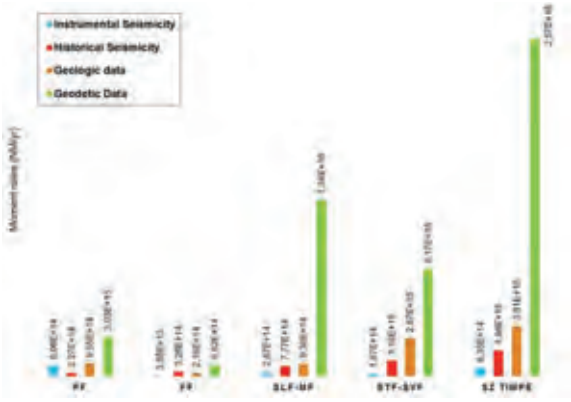

Figure 2: Seismological, geological and geodetic moment-rates obtained for the analysed structures. Abbreviations as in Figure 1.

RESULTS AND CONCLUSIONS

The comparison of moment-rates has been performed through the concept of seismic efficiency (value expressed in percentage of the seismological and geological moment-rates with respect to the geodetic one) as described in Caporali et al. (2003). The theoretical range of seismic efficiency is between 0% and 100%: the more the value close to 100%, the larger part of the deformation is released by brittle deformation, i.e. through earthquakes. Conversely, a low ratio shows an apparent seismic-moment deficit, which could indicate either a high creep component (aseismic deformation) or accumulating strain not released by seismicity. The values of seismic efficiency for the analysed fault systems are reported in Figure 3.

This result shows that, for the investigated zones, seismic efficiency values are lower than 40%, since the geodetic moment-rate estimations are generally larger than the seismic and the geologic ones. Similar results have been observed in other tectonically active areas such as the Southern Apennines in Italy (Palano et al., 2011) and the Bitlis-Zagros collisional belt in Iran (Masson et al., 2005).

In general, a number of reasons may account for the observed discrepancy among the estimated moment-rates, such as: i) uncertainties on geodetic strain rates estimations related to the station coverage, ii) uncertainties of the geologic slip-rate estimations; iii) not well constrained geometry of modelled faults, especially for down-dip width; iv) role of buried/hidden fault segments in accommodating deformation (slip-rate partitioning); v) limited length of the instrumental earthquake catalogue. Nevertheless, such a relevant difference confirms that a large amount of the deformation at Etna occurs aseismically along faults in the eastern flank, as previously suggested by field observations (Rasà et al., 1996). Although such a kind of approach is not common in volcanic areas, a relevant component of aseismic deformation has been recognised along the East African Rift System (Depréz et al., 2013), and seems to be related with the local rheological properties of the crust.

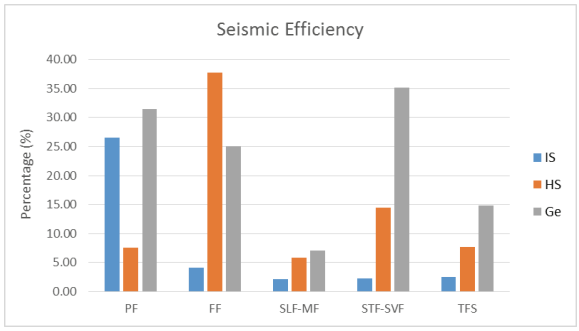

Figure 3: Values of seismic efficiency estimated for the analysed faults. Bars represent the seismological moment-rates (IS, from instrumental data; HS, from historical data) and the geological ones (Ge) expressed in terms of percentage with respect to the geodetic moment-rate.

In conclusion this study provides, for the first time, an analytical estimation of creep processes at Mt. Etna volcano by means of the deficit of seismic moment-rate calculated with respect the geodetic one. This may be viewed as a proxy of loading processes on locked fault segments prone to seismic failure, to be used with other approaches (Azzaro et al., 2013; Cannavò et al. 2014) to forecast next earthquake ruptures.

Acknowledgements: This study has benefited from funding provided by the Italian Presidenza del Consiglio dei Ministri – Dipartimento della Protezione Civile (DPC), in the frame of the 2012-14 Agreement with Istituto Nazionale di Geofisica e Vulcanologia-INGV, Project V3 "Multi-disciplinary analysis of the relationships between tectonic structures and volcanic activity". This paper does not necessarily represent DPC official opinion and policies. The authors are grateful to S. D'Amico for having provided supplementary elaborations useful for the study.

References

Alparone, S., G. Barberi, O. Cocina, E. Giampiccolo, C. Musumeci & D. Patanè, (2012). Intrusive mechanism of the 2008–2009 Mt. Etna eruption: constraints by tomographic images and stress tensor analysis. *Journal of Volcanology and Geothermal Research*. 229-230, 50-63, doi: 10.1016/j.jvolgeores.2012.04.001.

Azzaro, R., S. D'Amico & T. Tuvè, (2011). Estimating the magnitude of historical earthquakes from macroseismic intensity data: new relationships for the volcanic region of Mount Etna (Italy). *Seism. Res. Lett.* 82, 4, 533-544.

Azzaro, R., S. Branca, K. Gwinner & M. Coltelli, (2012a). The volcano-tectonic map of Etna volcano, 1:100.000 scale: an

integrated approach based on a morphotectonic analysis from high-resolution DEM constrained by geologic, active faulting and seismotectonic data. *Italian Journal of Geosciences*. 131, 153-170, doi:10.3301/IJG.2011.29.

Azzaro, R., S. D'Amico, L. Peruzza & T. Tuvè, (2012b). Earthquakes and faults at Mt. Etna (southern Italy): problems and perspectives for a time-dependent probabilistic seismic hazard assessment in a volcanic region. *Bollettino di Geofisica Teorica ed Applicata*. 53, 75-88.

Azzaro, R., A. Bonforte, S. Branca & F. Guglielmino, (2013). Geometry and kinematics of the fault systems controlling the unstable flank of Etna volcano (Sicily). *Journal of Volcanology and Geothermal Research*. 251, 5-15, doi: 10.1016/j.jvolgeores.2012.10.001.

Azzaro, R., M. Mattia & G. Puglisi, (2001). Fault creep and kinematics of the eastern segment of the Pernicana Fault (Mt. Etna, Italy) derived from geodetic observation and their tectonic significance. *Tectonophysics*. 333, 401-415, doi:10.1016/S0040-1951(01)00021-X.

Barberi, G., F. Cannavò, O. Cocina, M. Palano, L. Scarfì & R. Azzaro, (2014). *Comparing seismic, geodetic and geologic scalar moment-rates at Mt. Etna volcano (Italy): some preliminary results for seismogenic zones in the eastern flank*. Proc. XXXIII° Convegno Nazionale GNGTS, 25-27 November 2014, Bologna (Italy), p. 32-37.

Boehm, J., B. Werl & H. Schuh, (2006). Troposphere mapping functions for GPS and very long baseline interferometry from European Centre for Medium-Range Weather Forecasts operational analysis data. *Journal of Geophysical Research*. 111, B02406, doi:10.1029/2005JB003629.

Bonaccorso, A., G. Currenti & C. Del Negro, (2013). Interaction of volcano-tectonic fault with magma storage, intrusion and flank instability: a thirty years study at Mt. Etna volcano. *Journal of Volcanology and Geothermal Researches*. 251, 127-136.

Bonforte, A., F. Guglielmino, M. Coltelli, A. Ferretti & G. Puglisi, (2011). Structural assessment of Mount Etna volcano from Permanent Scatterers analysis. *Geochemistry Geophysics Geosystems*. 12, Q02002, doi: 10.1029/2010GC003213.

Brune, J.N., (1968). Seismic moment, seismicity and rate of slip along major fault zones. *Journal of Geophysical Research*. 73 (2), 777-784, doi:10.1029/JB073i002p00777.

Cannavò, F., A. Arena & C. Monaco, (2014). Local geodetic and seismic energy balance for shallow earthquake prediction. *Journal of Seismology*. 19 (1), doi: 10.1007/s10950-014-9446-z

CMTE Working Group, (2014). *Catalogo Macrosismico dei Terremoti Etnei, 1832-2013*. INGV, Catania, http://www.ct.ingv.it/macro/etna/html_index.php.

Depréz, A., C. Doubre, F. Masson & P. Ulrich, (2013). Seismic and aseismic deformation along the East African Rift System from a reanalysis of the GPS velocity field of Africa. *Geophys. J. Int*. 193 (3), 1353-1369, doi:*10.1093/gji/ggt085*.

Ferranti, L., M. Palano, F. Cannavò, M.E. Mazzella, J.S. Oldow, E. Gueguen, M. Mattia & C. Monaco, (2014). Rates of geodetic deformation across active faults in southern Italy. *Tectonophysics*. 621, 101-122, doi:10.1016/j.tecto.2014.02.007.

Ferreli, L., A.M. Michetti, L. Serva & E. Vittori, (2002). Stratigraphic evidence of coseismic faulting and aseismic fault creep from exploratory trenches at Mt. Etna volcano (Sicily, Italy). In: *Ancient Seismites* (Ettensohn, F.R., Rast, N., Brett, C.E. eds.), Geological Society of America, Special Paper, 359, 49–62.

Giampiccolo, E., S. D'Amico, D. Patanè & S. Gresta, (2007). Attenuation and source parameters of shallow microearthquakes at Mt. Etna volcano (Italy). *Bulletin of the Seismological Society of America*. 97 (1b), 184-197, doi:10.1785/0120050252.

González, P.J. & M. Palano, (2014). Mt. Etna 2001 eruption: new insights into the magmatic system feeding and the mechanical response of the western flank from geodetic data. *Journal of Volcanology and Geothermal Research*. 274, 108-121, doi:10.1016/j.jvolgeores.2014.02.001.

Gruppo Analisi Dati Sismici, (2014). *Catalogo dei terremoti della Sicilia Orientale – Calabria Meridionale (1999–2013)*. INGV-Catania (http://www.ct.ingv.it/ufs/analisti/catalogolist.php).

Herring, T.A., (2003). MATLAB Tools for viewing GPS velocities and time series. *GPS Solutions*. 7 (3), 194-199, doi:10.1007/s10291-003-0068-0.

Kostrov, B., (1974). *Seismic moment and energy of earthquakes and seismic flow of rock*. Izv. Acad. Sci. USSR, Phys. Solid Earth, 1, 23-40.

Masson, F., J. Chéry, D. Hatzfeld, J. Martinod, P. Vernant, F. Tavakoli & M. Ghafory-Ashtiani, (2005). Seismic versus aseismic deformation in Iran inferred from earthquakes and geodetic data. *Geophys. J. Int*. 160, 217-226, doi: 10.1111/j.1365-246X.2004.02465.x.

Palano, M., M. Aloisi, M. Amore, A. Bonforte, F. Calvagna, M. Cantarero, O. Consoli, S. Consoli, F. Guglielmino, M. Mattia, B. Puglisi & G. Puglisi, (2006). Kinematic and strain analyses of the eastern segment of the Pernicana fault (Mt. Etna, Italy) derived from geodetic techniques (1997–2005). *Annals of Geophysics*. 49 (4/5), 1105-1117, doi: 10.4401/ag-3103.

Palano, M., G. Puglisi & S. Gresta, (2008). Ground deformation patterns at Mt. Etna from 1993 to 2000 from joint use of InSAR and GPS techniques. *Journal of Volcanology and Geothermal Research*. 169, 99-120, doi:10.1016/j.jvolgeores.2007.08.014.

Palano, M., M. Rossi, C. Cannavò, V. Bruno, M. Aloisi, D. Pellegrino, M. Pulvirenti, G. Siligato & M. Mattia, (2010). Etn@ref, a geodetic reference frame for Mt. Etna GPS networks. *Annals of Geophysics*. 53 (4), 48-79, doi:10.4401/af-4879.

Palano, M., F. Cannavò, L. Ferranti, M. Mattia & E. Mazzella, (2011). Strain and stress fields in the Southern Apennines (Italy) constrained by geodetic, seismological and borehole data. *Geophys. J. Int.* 187 (3), 1270–1282.

Pancha, A., J.G. Anderson & C. Kreemer, (2006). Comparison of Seismic and Geodetic Scalar Moment Rates across the Basin and Range Province. *Bulletin of the Seismological Society of America*. 96, 11-32, doi: 10.1785/0120040166.

Puskas, C., R.B. Smith, W. Chang, A.Cannaday & C.B. DuRoss, (2011). *Comparison of Moment Rates from GPS observations and Late Quaternary paleoearthquakes on the Wasatch Fault, Utah*. AGU, Fall Meeting 2011, abstract #G11A-0860.

Rasà, R., R. Azzaro & O. Leonardi, (1996). Aseismic creep on faults and flank instability at Mt. Etna volcano. In: *Volcano instability on the Earth and other planets* (McGuire, W.J., Jones, A.P., Neuberg, J. eds). Geological Society, London, Special Publications, 110, 179-192, doi: 10.1144/GSL.SP.1996.110.01.14.

Saastamoinen, J., (1972). Contribution to the theory of atmospheric refraction. *Bulletin Géodésique*. 105 (1), 279-298, doi:10.1007/BF02521844.

Savage, J.C. & R.W. Simpson, (1997). Surface strain accumulation and the seismic moment tensor. *Bulletin of the Seismological Society of America*. 87, 1345-1353.

Scarfì, L., H. Langer & A. Scaltrito, (2009). Seismicity, seismotectonics and crustal velocity structure of the Messina Strait (Italy). *Phys. Earth Planet. Inter.* 177, 65–78. http://dx.doi.org/10.1016/j.pepi.2009.07.010.

Talebian, M., (2012). Comparison of seismic, geodetic and geologic moment rates in Eastern Alborz and Kopeh Dagh. *Geosciences*. 22 (86), 183-192.

Zhang H., C. Thurber & P. Bedrosian, (2009). Joint inversion for Vp, Vs, and Vp/Vs at SAFOD, Parkfield, California. *Geochemistry Geophysics Geosystems*. 10, Q110032, doi:10.1029/2009GC002709.

INQUA Focus Group on Paleoseismology and Active Tectonics

Is a geometric-kinematic approach valid for estimating the expected seismicity rates in volcano-tectonic areas? Ideas and results from seismogenic sources at Mt. Etna (Italy)

Azzaro, R. (1), D'Amico, S. (1), Pace, B. (2), Peruzza, L. (3)

(1) INGV - Istituto Nazionale di Geofisica e Vulcanologia - Osservatorio Etneo, Catania, Italy. Email: raffaele.azzaro@ingv.it
(2) Università degli Studi "G. d'Annunzio" Chieti-Pescara, DiSPUTer, Chieti, Italy
(3) OGS Istituto Nazionale di Oceanografia e di Geofisica Sperimentale, Trieste, Italy

Abstract: *At Mt. Etna (Sicily, Italy), the Timpe fault system is a structurally homogeneous domain characterized by a high seismic potential; several considerations led us to assume that faults are, on average, constantly loaded in time, supporting the idea that the faults behaviour is controlled by tectonic processes more than magma-induced, transient, stresses. The seismicity rates that have been till now assigned to the fault sources are based on macroseismic and instrumental data; they can be considered complete respectively above the damage threshold during the last two centuries, and for about ten years above M_L=2. We are now testing if these results are coherent with the seismicity rates that can be obtained using a geometric-kinematic approach, widely used if only geological and structural data are available. The characterization of a magnitude-size scaling relationship in volcanic environment is a key step for closing the loop, but the preliminary results are encouraging.*

Key words: *Mt. Etna, volcano-tectonic faults, time-dependent seismic hazard, magnitude-size scaling relationships.*

INTRODUCTION

Seismic hazard studies have been undertaken at Etna volcano in the last years with the aim of estimating the potential of local fault's activity in generating destructive earthquakes.
The methodologies applied at Mt. Etna area include probabilistic approaches based on the use of historical macroseismic data (the "site approach" by the software code SASHA, see Azzaro et al., 2008) and fault-based time-dependent models in which occurrence probabilities of major earthquakes are estimated through the Brownian Passage Time (BPT) function and the time elapsed since the last event (Azzaro et al., 2012b; 2013b). Mean return period of major earthquakes - strong to destructive events with epicentral intensity $I_0 \geq$ VIII EMS, considered as "proxies" of "characteristic" earthquakes – have been obtained by the fault seismic histories, i.e. by the associations "earthquake-seismogenic fault" derived from the historical catalogue of the Etnean earthquakes (CMTE Working Group, 2014). Inter-time statistics of major earthquakes have been applied to the Timpe tectonic system, considered as a homogeneous seismotectonic domain obtaining a mean recurrence time (Tmean) of about 70 years, and an aperiodicity factor α (σTmean/Tmean) that spans from values of 0.4-0.9, thus indicating semi-periodic to quasi-stationary processes.
In the present study we present the preliminary results of an analysis aimed at verifying the variability of the mean occurrence times of major earthquakes generated by the main tectonic systems at Etna (Pernicana and Timpe faults) by using a geological approach based on geometric-kinematic parameters (3D dimensions, slip-rates, etc.) representative of fault activity.

METHOD AND INPUT DATA

The analysis has been carried out through the software code ErrorPropagation (EP), a Matlab® routine produced in the framework of the projects DPC-INGV S2 in order to quantify the seismic activity from geometry and slip-rates of a fault (Pace et al., 2013). The adopted approach is based on the criterion of "segment seismic moment conservation" (Field et al., 1999), where the T_{mean} can be obtained by estimating the M_{max}, provided that three-dimensional geometry and slip rate of a seismogenic structure are known. In the probabilistic procedure for calculating the seismic hazard, the mean recurrence time (T_{mean}) of the maximum magnitude (M_{max}) expected on a fault, together with the quantification of its variability, are the basic ingredients to compute occurrence earthquake probabilities, both under Poissonian assumptions as well as in a time-dependent perspective. The best situation for a given fault segment is to have a long list of associated events, so that mean and variability derive directly from observations. Cases of effective repetition in Italy of characteristic events occurring on the same fault segment are definitely few, mostly represented by recent active sources along the Central Apennines (e.g., Paganica fault). More favourable conditions are present at Etna, where some ten major earthquakes (M_L 4.3-5.2) repeatedly occurred along fault segments of the Timpe system. Peruzza et al. (2010) extended the "segment seismic moment conservation" approach by introducing some errors propagation concepts in the estimated T_{mean} and α. Applying this methodology, Peruzza et al. (2011) demonstrated that the probability of occurrence of an event with M> 6 for the Paganica fault before the 6 April 2009 earthquake, considering an exposure time of 5 years, was the highest of Central Apennines (~3.5%).

The EP code uses different empirical and analytical relationships between the geometry of each input source and the characteristics of the expected earthquake, in order to quantify several values of M_{max} and associated T_{mean}. EP, therefore, formally propagates the errors of magnitude and slip-rate obtaining, for each seismogenic source, the most likely value of recurrence interval and the associated error. Finally, it uses the selected values to calculate the hazard rates, for a given exposure time, following a BPT probability density function (time-dependent) and a Poissonian distribution.

FAULT PARAMETERS AND EARTHQUAKE SCALING RELATIONSHIPS

The analysis and integration of different types of data such as tectonics, active faulting and long-term seismicity have produced a first seismotectonic model of the Etna region including information on segmentation, kinematics and seismic behaviour (Azzaro, 2004). Later, geometry and slip-rates of active faults have been constrained by geological/geomorphological field investigations (Azzaro et al., 2012a), while geodetic data modelling provided information on the extension at depth of faults as well as slip-rates and kinematics in the short-term (Azzaro et al., 2013a). Finally, the magnitude of the historical earthquakes has been calibrated by means of new ad-hoc relationships in terms of M_L and M_W (Azzaro et al., 2011).

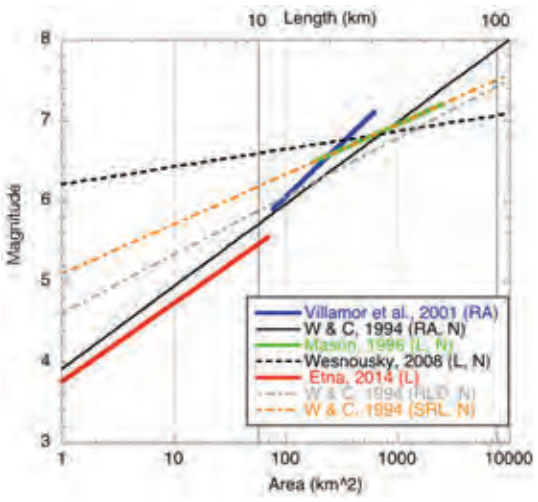

Figure 1: Plot of magnitude vs. surface rupture length equations for the Etna region (this study) and Taupo volcanic zone (Villamor et al., 2001), compared with worldwide relationships for tectonic domains (Wells and Coppersmith, 1994; Mason, 1996; Wesnousky, 2008). RA=rupture area; N=normal kinematics; L=fault length; RLD=rupture length in depth; SRL=surface rupture length.

The missing ingredient for EP calculations is a magnitude-rupture length relationship suitable for the Etnean earthquakes, since the equations derived for purely tectonic domains are proven to be inapplicable outside the domain and magnitude range they have been derived from., To this end, we derived a new empirical relationship specific for the Etna region by using the coseismic surface faulting dataset by Azzaro (1999), updated to 2013. The result is represented in Fig. 1, where our relationship is compared with the one obtained by Villamor et al. (2001) for the Taupo volcanic zone (New Zealand). Considering the different magnitude range the relationships have been calibrated from, and the adopted correlation of x-axes due to the use of different dimensional parameters (subsurface fault length for Etna, and rupture area for volcanic NZ sources), the agreement is quite satisfactory. Note analogies and discrepancies with respect to the relationships suggested by Stirling et al. (2013) for thick crust volcano-tectonic contexts (Wesnousky, 2008; Mason, 1996; normal fault), and the worldwide used relationship (Wells and Coppersmith, 1994) here given as a function of rupture area, subsurface rupture length and surface rupture length. It is important to highlight that the Wells and Coppersmith (1994) relationships are extrapolated outside its definition ranges and applied to volcano-tectonic environments, thus overestimating earthquake fault dimension. These considerations suggested us introducing the Villamor et al. (2001) relationship in the area-based computations of EP code, but leaving the Wells and Coppersmith (1994) ones.

EP, in addition to the M_{max}'s calculated by the above defined empirical scaling relationships, defines for each fault other two expected M_{max}: one from the general formula of magnitude as a function of the scalar seismic moment, starting from a constant strain drop value (here $2X10^{-5}$); and the other by using the aspect ratio relationships derived by Peruzza and Pace (2002).

PRELIMINARY RESULTS AND CONCLUSIONS

Applying the EP code to the Etna case we obtained the most likely values of characteristic expected magnitude (M_{char}) with the associated standard deviation σ, the corresponding mean recurrence times (T_{mean}) and the aperiodicity factor α, for each fault of the Timpe and Pernicana fault systems. The α values suggest fault behaviours that can potentially be modelled by a time-dependent approach. Moreover the M_{max} values calculated by the different methods are comparable to each other as well as with the observed historical earthquakes (except for a few cases).

The results of this work, still in progress, suggest that a geological approach based on geometric-kinematic parameters to estimate the expected seismicity rates can be also adopted with success on the volcanic context of Etna. A comparison between our results with scalar moment rates estimated from seismic and geodetic data will provide important constraints on the fault parameters and validate the goodness of the applied methodology.

Acknowledgements: This study has benefited from funding provided by the Italian Presidenza del Consiglio dei Ministri - Dipartimento della Protezione Civile (DPC), in the frame of the 2014-2015 Agreement with Istituto Nazionale di Geofisica e Vulcanologia - INGV, project V3: "Multi-disciplinary analysis of

the relationships between tectonic structures and volcanic activity ". This paper does not necessarily represent DPC official opinion and policies.

References

Azzaro, R., (1999). Earthquake surface faulting at Mount Etna volcano (Sicily) and implications for active tectonics. *Journal of Geodynamics*. 28, 193-213.

Azzaro, R., (2004). Seismicity and active tectonics in the Etna region: constraints for a seismotectonic model. In: *Mt. Etna: volcano laboratory* (Bonaccorso, A., Calvari, S., Coltelli, M., Del Negro, C., Falsaperla, S. eds). American Geophysical Union, Geophysical monograph, 143, 205-220.

Azzaro, R., M.S. Barbano, S. D'Amico, T. Tuvè, D. Albarello & V. D'Amico, (2008). First studies of probabilistic seismic hazard assessment in the volcanic region of Mt. Etna (Southern Italy) by means of macroseismic intensities. *Bollettino di Geofisica Teorica e Applicata*. 49, 77-91.

Azzaro, R., S. D'Amico & T. Tuvè, (2011). Estimating the magnitude of historical earthquakes from macroseismic intensity data: new relationships for the volcanic region of Mount Etna (Italy). *Seism. Res. Lett.* 82, 4, 533-544.

Azzaro, R., S. Branca, K. Gwinner & M. Coltelli, (2012a). The volcano-tectonic map of Etna volcano, 1:100.000 scale: an integrated approach based on a morphotectonic analysis from high-resolution DEM constrained by geologic, active faulting and seismotectonic data. *Italian Journal of Geosciences*. 131, 153-170.

Azzaro, R., S. D'Amico, L. Peruzza & T. Tuvè, (2012b). Earthquakes and faults at Mt. Etna (Southern Italy): problems and perspectives for a time-dependent probabilistic seismic hazard assessment in a volcanic region. *Bollettino Geofisica Teorica e Applicata*. 53, 75-88.

Azzaro, R., A. Bonforte, S. Branca & F. Guglielmino, (2013a). Geometry and kinematics of the fault systems controlling the unstable flank of Etna volcano (Sicily). *Journal of Volcanology and Geothermal Research*. 251, 5-15.

Azzaro, R., S. D'Amico, L. Peruzza & T. Tuvè, (2013b). Probabilistic seismic hazard at Mt. Etna (Italy): the contribution of local fault activity in mid-term assessment. *Journal of Volcanology and Geothermal Research*. 251, 158-169.

CMTE Working Group, (2014) *Catalogo Macrosismico dei Terremoti Etnei dal 1832 al 2013*. INGV, Catania, http://www.ct.ingv.it/macro/etna/html_index.php.

Field, E.H., D.D. Johnson & J.F. Dolan, (1999). A mutually consistent seismic-hazard source model for Southern California. *Bulletin of the Seismological Society of America*. 89, 559-578.

Pace, B., F. Visini & L. Peruzza, (2013). D5.1 Numerical simulation of earthquake recurrence time for selected fault. DPC-INGV Project S2-2102 "Constraining Observations into Seismic Hazard", https://sites.google.com/site/ingvdpc2012progettos2/deliverables/d5_1, v. 0.15 released online on 30 Aug 2013.

Peruzza, L. & B. Pace, (2002). Sensitivity analysis for seismic source characteristics to probabilistic seismica hazard assessment in Central Apennines (Abruzzo area). *Bollettino di Geofisica Teorica ed Applicata*. 43, 79-100.

Peruzza, L., B. Pace & F. Cavallini, (2010). Error propagation in time-dependent probability of occurrence for characteristic earthquakes in Italy. *Journal of Seismology*. 14,119-141.

Peruzza, L., Pace, B. & Visini, F., (2011). Fault-based earthquake rupture forecast in Central Italy: remarks after the L'Aquila Mw 6.3 event. *Bulletin of the Seismological Society of America*.101, 404-412.

Stirling, M., T. Godet, K. Berryman & N. Litchfield, (2013). Selection of earthquake scaling relationships for seismic-hazard analysis. *Bulletin of the Seismological Society of America*. 103, 2993-3011.

Villamor, P., R.K.R. Berryman, T. Webb, M. Stirling, P. McGinty, G. Downes, J. Harris & N. Litchfield, (2001). Waikato Seismic Loads: revision of Seismic Source Characterisation. GNS Client Report 2001/59.

Wells, D.L. & K.J. Coppersmith, (1994). New empirical relationships among magnitude, rupture lenght, rupture area, and surface displacement. *Bulletin of the Seismological Society of America*. 84, 974-1002.

Wesnousky, S.G., (2008). Displacement and geometrical characteristics of earthquake surface ruptures: issues and implications for seismic-hazard analysis and the process of earthquake rupture. *Bulletin of the Seismological Society of America*. 98, 1609-1632.

INQUA Focus Group on Paleoseismology and Active Tectonics

Earthquake geology and geophysical studies for assessing the seismic hazard: a synthesis for the Diablo Canyon Nuclear Power Plant (USA, California)

Baize, S.

IRSN, BP 17, 92 262 Fontenay-aux-Roses, France. Email: Stephane.baize@irsn.fr

Abstract: *The Diablo Canyon Nuclear Power Plant case is summarized and discussed in this paper because it represents an exemplary seismotectonic study that could be applied to other nuclear facilities for the seismic hazard analysis. The scientific studies, available either through publications or official websites, were performed during the last 30 years all around the power plant, in this active region of Western USA. These were produced in the framework of a Long-Term Seismic Program lead by the plant operator. The investigations cover a wide range of techniques and methodologies related to earthquake geology, involving an outstanding process of continuous data acquisition and analysis, inclusion of various defensible opinions and models, as well as of peer reviewing and public reporting. This approach is seldomly applied in the nuclear industry and it could be set up or adapted in other countries.*

Key words: *Nuclear Plants, Earthquake Geology, Exploration Geophysics, Seismic Hazard Analyses Management*.

INTRODUCTION

The Diablo Canyon Nuclear Power Plant (DCPP) is an outstanding case for which earthquake geology investigations significantly contributed to the seismic hazard assessment (SHA) and its continuous re-evaluation. This synthesis is based on published documents, in scientific journals or in technical reports available online.

Framework of the geological studies around the dcpp

The power plant is located along the south-central coast of California (USA), 80 km west of the San Andreas Fault (Figure 1) and several capable faults run through the near-regional area of DCPP. The earthquake geology investigation includes onshore and offshore studies exploring the seismic landscape, i.e. marine geophysics, coastal geology and geomorphology, onshore neotectonics, paleoseismological trenching, etc. Beyond the scientific field, the DCPP case is of great interest in the way the SHA was managed through time since the licensing process in the 1970's, with increased and enhanced geological datasets.

In spite of a seashore location, the operator did not engage offshore studies before construction permit of the Nuclear Power Plant (NPP) because, in those times, this kind of investigations was not required in regulatory guidelines. However, only a few months after construction permits were issued (1968-1970), offshore geophysical studies by an oil company revealed a previously unmapped fault, the Hosgri Fault (HF) (figure 1). The discovery of this fault, together with other safety related issues, resulted in a long and contentious licensing process. As early as 1976-1977, the DCPP was designed for a M=7.5 earthquake associated with the newly discovered HF. Thus, the peak ground acceleration of the design spectrum was upgraded from 0.4 to 0.75 g.

Finally, operating licensing was delivered in 1984-1985, but the US regulator (NRC) then imposed conditions to the licensee (PG&E) to maintain operation. These conditions cover the regular acquisition and analysis of relevant data for the periodic assessment of the seismic hazard. The operator therefore set up a perennial program of research related to seismic hazard, the so-called Long-Term Seismic Program (LTSP). In the last version of this LTSP (2011-2012), the program is managed through a structured procedure (Senior Seismic Hazard Analysis Committee; SSHAC), which provides guidance on the process to incorporate data, models and related uncertainty from the informed technical community. The "SSHAC" process insures for DCPP a significant robustness of the seismic hazard evaluation, including consideration of the range of defensible interpretations and uncertainties, continual peer review, and also guarantees transparency of the process and the results, including specific roles of participants, dialogue between the operator, the regulator and the public, independence of the involved experts from the sponsor, publication of data in peer-review journals.

To illustrate, the most recent study (PG&E, 2014), which includes high-resolution geophysical profiling to measure the offset of morphological features, was performed after recommendations by an external peer-review committee (IPRP) from 2011 onwards. The 2014 study results allowed quantifying the offset of recent morphological features crossing the closest-to-site active faults (PG&E, 2014), necessary to clarify the slip rates. However, the IPRP Report (2014) clearly emphasizes that further investigations of sediment coring and dating are required to enable the slip rate estimation.

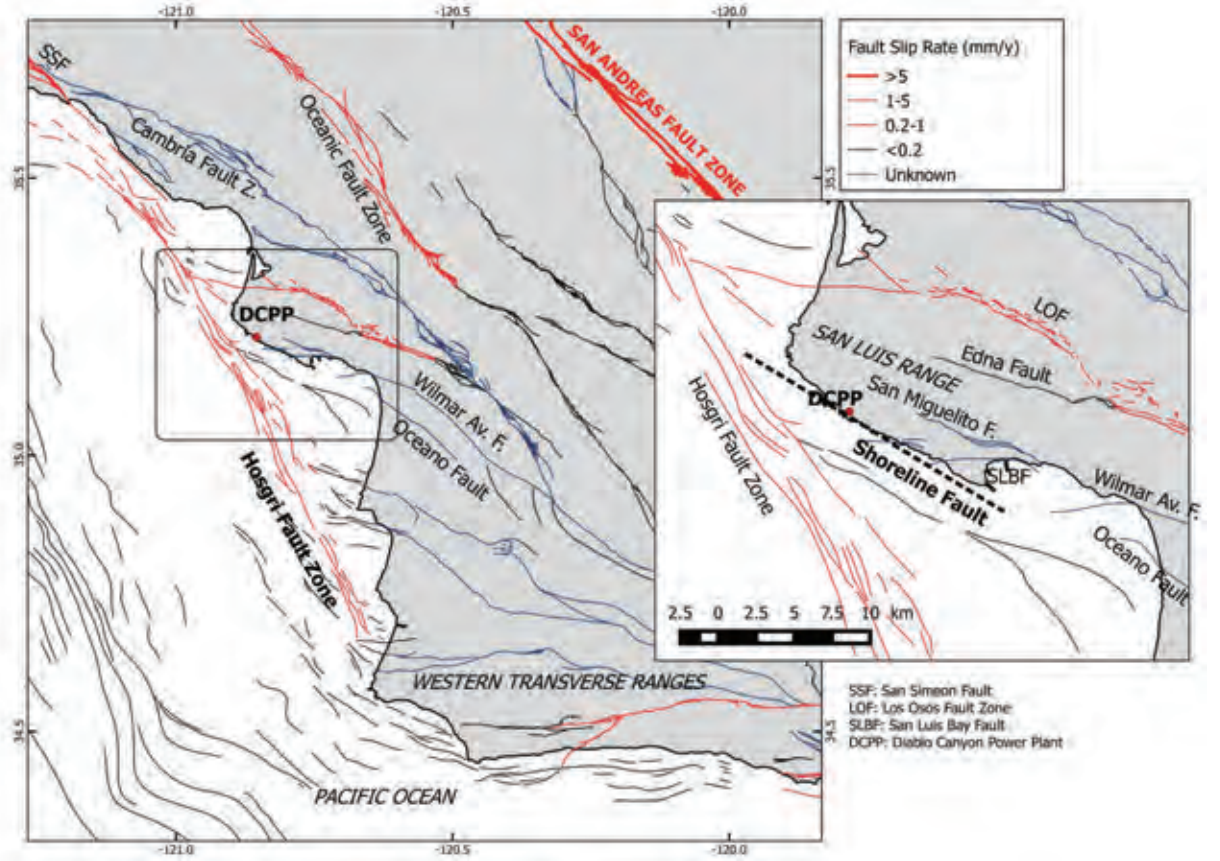

Figure 1: Capable fault map of the southern coast area of California. The fault database is from the United States Geological Survey (http://earthquake.usgs.gov/hazards/qfaults/). DCPP is the Diablo Canyon Power Plant.

Geology, active faults and related studies performed for the seismic hazard analyses

The DCPP SHA considers both deterministic and probabilistic approaches. They both include four local (i.e. in a ≈10 km-radius around DCPP) fault sources, which are simplified representations of the local fault zones among the regional network of active faults. Throughout the LTSP, a series of paleoseismological sites (26), either with natural exposure(s) or artificial trench(es), were studied along the main active faults of the region (Hall, 2011). The paleoseismological sites are spread over the San Simeon (SSF), the Los Osos (LOF), the San Luis Bay (SLBF) and Wilmar Avenue (WAF) Faults (figure 1). These 4 faults turned out to be active during the Late Pleistocene/Holocene, while the study of the Edna and San Miguelito Faults revealed no perceptible displacement during Late Pleistocene/Holocene times. Note that the LTSP includes remote sites (San Simeon sites, up to 60 km to the north of DCPP) where inland studies were carried out, aiming at constraining the paleoseismic activity and slip rate of the site-threatening San Simeon-Hosgri Fault System.

The Hosgri Fault (HF), located at only 5 km west of the plant in its closest position, is the major capable fault in the site vicinity. It is an offshore right-lateral fault, as long as ≈100 km. It is structurally connected to the SSF (Figure 1), the latter has been trenched in its inland section with outstanding evidences of multiple slips during the Holocene (Hall et al., 1994; Hall, 2011). In a general way, the Hosgri-San Simeon Fault System slip rate decreases from about 3 mm/y to the north (San Simeon), to less than 1 mm/y to the south where it dies out in the Western Transverse Ranges (figure 1). This fault has been studied through extensive high-resolution seismic surveys all along its length, validating its recent activity and its kinematics (PG&E, 2011a; Johnson and Watt, 2012). Recent marine geophysical studies have been performed in the DCPP area, to constrain the slip rate between 0.5 and 4 mm/y with preferred value around 2 mm/y (PG&E, 2014). According to this new data, the HF is now suspected to be able to generate a Mmax=7.3 earthquake instead of Mmax=7.1 one (PG&E, 2011b).

The Los Osos Fault (LOF), located at only 10 km north-northeast of DCPP, is believed to be a discontinuous 55 km-long transpressive fault zone. According to new data and interpretations, the low dip option (30°) to the SW has been discarded, in favour of high dip values 45° to 75° to the SW. Extensive studies, including detailed geologic mapping and paleoseismic trench surveys (over 7 trench sites), were conducted on this fault, evidencing an Holocene activity (e.g. Lettis and Hall, 1994). The LOF slip rate is about 0.2 to 0.5 mm/y (Lettis and Hall, 1994; Hall, 2011). This fault is thought to be capable of producing a Mmax=6.8 earthquake (PG&E, 2011a).

The San Luis Bay Fault Zone (SLBF), a segment of Southwestern Boundary Fault Zone bordering the San Luis Range to the south (figure 1), cuts a marine terrace and fluvial deposits in the San Luis Bay area, 6 km southeast of the DCPP. This fault could be as long as 10 km and it can host an Mmax=6.2 earthquake. The slip rate is low, between 0.1 and 0.2 mm/y (PG&E, 2011a).

The Shoreline Fault (SF) is an offshore fault that has been lately revealed thanks to an alignment of microseismicity (Herdebeck, 2010), running all along the seashore (figure 1). This finding triggered a series of geological and geophysical studies aiming at characterizing this capable structure because of its critical interest for the DCPP safety. Actually, the challenge therefore came out to be double because of the proximity to the site:

- ✓ Could the ground shaking caused by an earthquake on this fault exceed the current design and then threat the DCPP safety?
- ✓ Could this earthquake generate surface displacement at the site and jeopardize the reactor or other equipment relevant for the safety?

To address these two crucial points, high-resolution investigations were launched in 2008 along the coastline area: new onshore geological mapping, coastline topography (LIDAR) and bathymetry (Multibeam Echo Sounding) campaigns, magnetic surveys, reprocessing of previous gravity surveys, high-resolution seismic reflection profiling. These new dataset shows that the Shoreline fault includes several segments, defining a 45-km-continuous fault zone from the Hosgri fault (to the north) and to the Oceano fault (to the south). The overall strike is N110°E to 120°E. The fault is almost vertical and its depth (according to seismicity) reaches 10 to 15 km and it is a right-lateral strike-slip fault. Correlation of submerged paleoshorelines, paleostrandlines and buried channels across the SF indicates a possible horizontal slip rate around 0.1 mm/y, despite the scarcity of age data on the offset features (PG&E, 2014). This fault should be capable of generating a Mmax=6.7 earthquake (PG&E, 2014).

Immediately offshore of DCPP, the central segment is located only 600 m SW of the power reactors and 300 m SW of the intake structure.

Hazard impact of these findings

The SHA accounting for the 2014 geophysical results on the HF and SF will be updated in 2015.

Regarding seismic motion, the 2011 findings on the SF and LOF did not alter the previous deterministic (DSHA) and probabilistic (PSHA) assessments (NRC, 2012). First of all, the increase in southward dip values of LOF tends to lower the associated seismic motion at the site located to the south. Second, the Mmax=6.7/0.6 km-distant earthquake scenario (DSHA) on the SF produce lower acceleration levels than the one used to design the plant (i.e. the M=7.5/5 km-distant HF scenario). In addition, the updated probabilistic hazard analysis (PSHA) shows after deaggregation that the hazard is controlled by the HF, because of its higher Mmax and moreover because of its larger slip rate (one order higher).

Regarding the surface displacement hazard, the new detailed datasets show that the active fault trace is 300 to 600 m away from the intake and the reactors, respectively. A rupture on the SF is thus not directly a threat for the DCPP. However, secondary surface faulting may occur during a major event on the SF, requiring additional exploration. The operator then performed a Probabilistic Fault Displacement Hazard Analysis (PFDHA), especially for some components of the NPP, like dresser couplings along pipes. For five selected earthquake scenarios along the SF trace, the estimated annual probabilities of exceedance of a 2 cm-displacement are very low ($\approx 10^{-7}$), even for the "worst" scenario (M=6.7 at 300 m distance, with a slip rate of 0.3 mm/y). The threat is then considered to be negligible for the site safety because it is significantly lower than the seismic Core Damage Frequency ($\approx 10^{-5}$) (NRC, 2012).

CONCLUSIONS

The past three decades, with their geologic investigations and seismic hazard analyses, have substantially improved the seismotectonic knowledge in the Diablo Canyon Power Plant area. It regularly allowed upgrading the hazard evaluation and enhancing the plant safety. The process of continuous data acquisition and analysis, of inclusion of all defensible opinions and models, as well as the peer reviewing of analysis reports and public reporting, led to build robust SHA and to largely share their content.

This Californian case, in its technical approach and its management, should serve as a reference model to end up with completely risk-informed decisions about plant safety regarding seismic hazard. This approach is defended by Chapman et al. (2014) to handle the Japanese NPP that are currently under threat of permanent closure due to potential active fault hazards, and could be applied or adapted to other countries, for instance in Europe. However, for this, there is a critical need to improve and increase the database of surface ruptures on which PFDHA calculations are based (see Baize et al., 2015).

References

Baize, S., McCalpin, J., Scotti, O., Costa, C., Cinti, F. R., Michetti, A. M., Okumura, K., Dawson, T., (2015). Earthquake geology of shallow crustal faults and Seismic Hazard Assessment: Challenges ahead. 6th INQUA International Workshop on Active Tectonics Paleoseismology and Archaeoseismology, 19-24 April 2015, Pescina, Fucino Basin, Italy.

Chapman, N., K. Berryman, P. Villamor, W. Epstein, L. Cluff, & H. Kawamura, (2014). Active Faults and Nuclear Power Plants. *Eos*. Vol. 95, No. 4, PAGES 33–40.

California Public Utilities Commission, (2014). Comments on PG&E's Central Coastal California Seismic Imaging Project Report part 1: offshore seismic studies intended to reduce the uncertainty in seismic hazard at Diablo Canyon Power Plant. Independent Peer Review Panel Report No. 7. Available at www.cpuc.ca.gov/

Hall, N.T., Hunt T.D. and Vaughan P.R., (1994). Holocene behavior of the San Simeon fault zone, south-central coastal California. In: (Alterman I.B., McMullen R.B., Cluff L.S. and Slemmons D.B. eds). *Seismotectonics of the central California*

Coast Ranges: Geological Society of America Special Paper. 292, p. 167–191.

Hall, T., (2011). LTSP Trenching Investigations. DCPP SSHAC Workshop 1, December 01, 2011, 40 slides. Available at http://www.pge.com/.

Hardebeck, J.L., (2010). Seismotectonics and fault structure of the California Central Coast. *Bulletin of the Seismological Society of America*. 100, 1031–1050, doi:10.1785/0120090307.

Johnson, S.Y. and Watt J.T., (2012). Influence of fault trend, bends, and convergence on shallow structure and geomorphology of the Hosgri strike-slip fault, offshore central California. *Geosphere*. doi:10.1130/GES00830.1.

Lettis, W.R. and Hall N.T., (1994). Los Osos Fault Zone, San Luis Obispo County, California: In: (Alterman I.B., McMullen R.B., Cluff L.S. and Slemmons D.B. eds.). *Seismotectonics of the central California Coast Ranges: Geological Society of America Special Paper*. 292, p. 73–102.

Lettis, W.R., Hanson K.L., Unruh J.R., McLaren M. and Savage W.U., (1995). Quaternary Tectonic Setting of South-Central Coastal California. In: (Keller M.A. ed.). *Evolution of Sedimentary Basins/Offshore Oil and Gas Investigations-Santa Maria Province: U.S. Geological Survey Bulletin*. Chapter AA, 21 pages.

NRC, (2012). Confirmatory Analysis of Seismic Hazard at the Diablo Canyon Power Plant from the Shoreline Fault Zone. *Research Information Letter 12-01*. Available at http://a4nr.org/

PG&E, (2011a). SSHAC Studies for DCPP Seismic Hazard Update; Seismic Source Characterization; Workshop 1 Presentations; Nov 29 to Dec 1, 2011. Available at http://www.pge.com/

PG&E, (2011b). Report on the analysis of the Shoreline Fault Zone, Central Coastal California; Report to the U.S. Nuclear Regulatory Commission. Available at http://www.pge.com/

PG&E, (2012). SSHAC Studies for DCPP Seismic Hazard Update; Seismic Source Characterization; Workshop 2 Presentations; Nov 6 to Nov 8, 2012. Available at http://www.pge.com/.

PG&E, (2014). Central Coastal California Seismic Imaging Project (CCCSIP). Report available at http://www.pge.com/en/safety/systemworks/dcpp/seismicsafety/report.page

INQUA Focus Group on Paleoseismology and Active Tectonics

Earthquake geology of shallow crustal faults and Seismic Hazard Assessment: Challenges ahead

Baize, S. (1), McCalpin, J. (2), Scotti, O. (1), Costa, C. (3), Cinti, F.R. (4), Michetti, A.M. (5), Okumura, K. (6), Dawson, T. (7)

(1) Institut de Radioprotection et Sûreté Nucléaire, BP 17, 92 262 Fontenay-aux-Roses, France. Email: stephane.baize@irsn.fr
(2) GEO-HAZ Consulting, Crestone, CO, United States
(3) Departamento de Geología, Universidad Nacional de San Luis, E. de los Andes 950, 5700 San Luis, Argentina
(4) Istituto Nazionale di Geofisica e Vulcanologia, Via di Vigna Murata 605, 00143 Roma, Italy
(5) Università degli Studi dell'Insubria, Dip. Scienza e Alta Tecnologia, Via Valleggio 11, 22100 Como, Italy
(6) Hiroshima University, Japan
(7) California Geological Survey, Menlo Park, CA, United States

Abstract: *With the development of modern techniques, we are able to improve the mapping of faint coseismic or cumulative surface deformation features, potentially enabling detection of blind faults. This also opens the opportunity to improve the empirical relationships relating earthquake magnitude to coseismic surface displacement or fault length towards the moderate magnitudes. The developing use of the probabilistic approach in assessing the surface displacement will require enhanced catalogues describing both primary and distributed surface ruptures, to allow development of attenuation relationships of displacement with distance. Another key point required for seismic hazard analysis will be to include the local conditions, including surficial geology, soil parameters and crustal rheology.*

Key words: *Capable faults, surface displacement, new technologies, scaling relationships, PFDHA.*

INTRODUCTION

The catastrophic earthquakes in the last decade reminded us that Quaternary faults may cause severe damage, due to seismic shaking, tectonic surface ruptures or secondary effects. For several of these events, the source fault was unknown before the earthquake (e.g. Bhuj, India, 2001; Bam, Iran, 2003; Darfield, New Zealand, 2010) or its seismic potential was underestimated (e.g. Sichuan, China, 2008; Port-au-Prince, Haiti, 2010). Besides these large magnitude events, the past decade also showed that moderate earthquakes (Mw 5-6.5) can cause damages and casualties (e.g. L'Aquila, 2009; Christchurch, 2010; Lorca, 2011, Napa, 2014). Whatever the case, one of the shared conclusions among geoscientists is that sound "pre-historical" data should have added crucial information for seismic hazard assessment (SHA) and the preparedness of society. We will here focus on geological topics that are critical in SHA, including fault location, length and surface displacement used to estimate magnitude and slip rate.

NEW TOOLS FOR ACTIVE FAULT DETECTION

One of the future big challenges in SHA is the recognition of the earthquake faults, especially those of moderate extension, producing moderate-magnitude earthquakes and associated with slight surface deformation, as well as small cumulative offsets. Surface faulting generally occurs above a magnitude threshold. For instance, Pezzopane & Dawson (1996) state that US M6 earthquakes have a 50%-probability to reach the surface, whereas this probability relates to Mw=6.5 events in Japan (Takao et al., 2013). Based on sound observation datasets, these statements are however conditioned by the past decades' resolution of observation and the recent technological developments may question them. The tough task of detection of the moderately active faults now finds a valid support with the recent advances in remote sensing techniques, which enable mapping subtle fault morphologies (e.g. Light Detection And Ranging) and tenuous interseismic displacements (e.g. Interferometric Synthetic Aperture Radar). These technological advances certainly improve our ability to recognize surface faults, especially the ones with low amplitude ground deformation, leading to new perspectives for the geological input of SHA (fault length, segmentation, slip rate). Moreover, these developing techniques drastically increase our capacity in mapping and quantifying the distributed deformation features associated with moderate and large earthquakes (e.g. Dawson et al., 2008; Oskin et al., 2012).
On the opposite, there are cases where strong crustal earthquakes (M around 7.0 or more) occurred either without (e.g. San Juan, 1977, Argentina; Loma Prieta, USA, 1989) or with a faint morphogenic signature (Bhuj, 2001, India; Van, Turkey, 2012). These would be cases where documentation of prehistoric events becomes very critical for SHA. Lettis et al. (1997) claimed that "conventional mapping and surveying" alone are likely insufficient to recognize Quaternary blind thrusts which might rupture or deform the surface. They have also pointed out that intraplate reverse earthquakes seldom occur on faults associated with pre-existing recognizable surface deformation. We here emphasize that it is worth to revisit these considerations given that the new tools allow capturing very subtle surface deformation.
All these developments are thus promising tools for the characterization of ruptures, then 1) improving our

understanding of the relation between surface faulting parameters and magnitude, 2) questioning the existing empirical relationships used in SHA to estimate magnitudes, 3) estimating the capability of active faults to cause primary and distributed displacement and/or deformation at or near the ground surface.

IMPROVING THE SEISMIC HAZARD ASSESSMENT

Understanding the factors that control the surface faulting

Magnitude is the primary parameter that controls the capability of a fault to break the surface along a certain length/area and with a certain amount of displacement. The slip type (Wells & Coppersmith, 1994) and the plate tectonics context and crustal type (Stirling et al., 2013) are considered when selecting the relevant scaling relationship. However, several examples show that the classical regressions between surface faulting parameters and magnitude are sometimes misleading (figure 1). The large Mw7.7 reverse Bhuj earthquake in intraplate India (2001) hardly cut the ground surface (McCalpin & Thakkar, 2003). On the other hand, the intra-cratonic Mw5.4 event in Australia (2012) resulted in longer rupture and larger offset (Clark et al., 2013), as well as the Coalinga earthquake (June 11, 1983, Ml 5.2) which was responsible for 64 cm vertical offset and 20 cm dextral slip on the Nuñez Fault (Rymer et al 1990). As well, the reverse Nagano earthquake (Nov. 2014, Mw6) also led to significant surface faulting up to 0.9 m (Takemoto et al., 2014) (see table 1). This large variability of response, which is an outstanding fact for reverse earthquakes, may have several origins. For instance, Moss et al. (2013) and Stanton (2013) concluded that the likelihood of rupture propagation to the surface are controlled by superficial parameters such as nature, thickness and stiffness of soil, as well as soil rupture history. In a strike-slip environment, significant ground rupture (SRL: 8 km, Max Displacement: 40 cm) has been observed for the shallow Mw5 Pisayambo event (Ecuador), probably because of a low rigidity crust (Champenois et al., in prep.; figures 1 and 2). In further developments, we emphasize the need to account for the natural complexity and variability of surface effects, which derives from the local geology and also to value the influence of pre-existing structural heterogeneities on the spatial extent of the ground ruptures. Not only the fault kinematics must be considered, but also the focus of the earthquake and the local soil characteristics in which the rupture propagated.

Mechanism	ID	Country	Year	Mw	SRL (km)	MD (m)	A (km^2)	Reference
Reverse	Ernabella	Australia	2012	5.4	1.6	0.51	7	Clark et al. (2014)
	Emilia	Italy	2012	5.9	0.1*	0.2*	80	Bignami et al. (2012)
	Nagano	Japan	2014	6.2	11	0.9	110	Takemoto-S. et al. (2014)
	Bhuj	India	2001	7.6	0.8	0.35	1300	McCalpin & Thakkar (2003)
	Nuñez	USA	1983	5.2	3.3	0.64		Rymer et al.. 1990
Normal	Cuzco	Peru	1986	5.2	3	0.1	10	Cabrera & Sébrier (1998)
	Wells	USA	2010	6	0.1*	0.15*	100	DePolo et al. (2011)
	L'Aquila	Italy	2009	6.3	3-6	0.15	200	Cinti et al. (2011). Vittori et al. (2011)
	Borah Peak	USA	1983	7.3	33	2.7	660	Wells & Coppersmith (1994)
Strike-Slip	Imperial	USA	1966	3.6	10	0.02	15	Brune & Allen (1967)
	Pisayambo	Ecuador	2010	5	8	0.4	16	Champenois et al. (in prep.)
	Napa	USA	2014	6	15	0.5	165	Dawson et al. (2014)
	Al Hoceima	Morocco	2004	6.3	2	0.05	100	Cakir et al. (2006)
	Superstition H.	USA	1987	6.6	27	0.9	330	Wells & Coppersmith (1994)
	Landers	USA	1992	7.3	71	6	744	Wells & Coppersmith (1994)

**Value was fixed to be plotted in the diagram. Actual values are null because the faults were blind. However, INSAR analyses evidenced localized uplift/subsidence patches, suggesting a near-surface ruptures.*

Table 1: Selected earthquake data of historical and recent events.

Upgrading the surface faulting databases

In SHA, the great challenge is the recognition of faults which are capable of generating ground displacement because they pose a threat to critical facilities (Chapman et al., 2013) or infrastructures and buildings (Cohen-Waeber et al., 2014). This issue is addressed for facility design or definition of exclusion/avoidance buffers around faults. A statistical methodology has been developed in the USA (Probabilistic Fault Displacement Hazard Analysis: PFDHA) which aims at predicting the exceedance probability of a certain amount of displacement during a time frame (Youngs et al., 2003; Petersen et al., 2011). This approach is based on the same equations as the Probabilistic Seismic Hazard Analysis for seismic motion. As in PSHA, it requires empirical equations describing the attenuation of displacement with distance along and around the fault. The equations for shaking have been intensely studied and many correlations have been edited for various types of crusts and geodynamic contexts.

On-fault and off-fault data catalogues are on the contrary very sparse and displacement attenuation

equations are actually poorly constrained. Nonetheless, this probabilistic approach is used worldwide (e.g. nuclear plant design in the USA, in Slovenia). It is generally considered that off-fault distributed displacement rapidly decreases with distance, but recent Mw6 event in Napa (California), clearly evidence once again that distributed deformation could extend at least to 2 km away from the primary fault (Dawson et al., 2014; Hudnut et al., 2014), causing damages to buildings and infrastructures (figure 3) (see also the 2009 l'Aquila case in Vittori et al., 2011). Thanks to the technological evolution and rapid post-earthquake rupture reconnaissance, quantification of coseismic deformation of future events is now accessible for a wide magnitude range. And we can potentially upgrade the surface faulting datasets to consolidate the probabilistic approach.

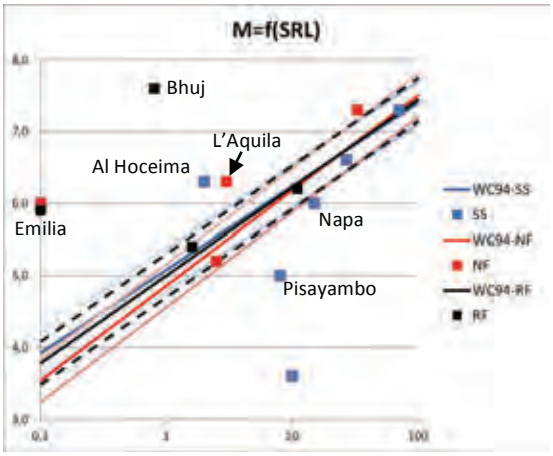

Figure 1: Selected earthquakes (Table 1) plotted on the empirical relationship relating rupture length (SRL) and magnitude (M) from Wells & Coppersmith (1994) (mean value and uncertainty M±0.3).

A COMMUNITY PROJECT

These topics will be proposed during the XIX INQUA Congress in Nagoya (27 July – 2 August 2015) by the INQUA Paleoseismological Focus Group as key issues for the next intercongress period 2015-2019. Developing a network of local Quaternary scientists and earthquake geologists is critical for increasing the databases with worldwide cases, improving the completeness of records in terms of tectonic and geological variability, and then lowering the uncertainties due to our lack of knowledge. Today, the databases are largely dominated by US, Japanese or Mediterranean area cases. Many active areas with frequent crustal earthquakes are poorly represented, like South-Eastern Asia and Himalayan regions, Iran-Caucasus area, Eastern Africa or South-America.

CONCLUSION

With increasing inclusion of earthquake geology in PSHA and PFDHA, there is a need for sound databases relating earthquake magnitude and fault parameters like surface displacement and surface length, as well as slip rate information. This task can be achieved with the development and the spread of modern and precise techniques of mapping and measurement.
Datasets would account for the variability of the phenomenon (earthquake-related deformation), which is controlled by several parameters in addition to earthquake mechanism, like soil nature and stiffness, focal depth and crustal rheology. We suggest including those new parameters to describe the future description of surface displacement evidences (see table 2).

Figure 2: Dextral surface faulting observed in Pisayambo area (Ecuador) after the Mw5 event (3/26/2010).

Figure 3: Distributed ground displacement associated with the 2014 Mw6 earthquake in the Napa valley, California. The curb is dextrally displaced of about 5-7 cm, associated with the Browns Valley strand.

Eq ID	Lat.	Long.	Mw	Depth	Focal mech.	Seismo MD/AD	Fault ID	SRL/W	Dip /Strike	Mean Vs	Mean density	Seismo thick.	PT
Point	Lat/ Long	Pr./Dis.	Dip	Strike	VD	HD	rD/AD	rD/MD	rX/SRL	X/Fault ID	Slope	Soil	Vs30
1													
N													

MD: Maximum displacement; AD: Average displacement; PT: Plate tectonics and crust type context (e.g. SCR; extended crust; orogenic; plate boundary; volcanic)
Pr./Dis.: Primary or distributed deformation; VD: dip-slip displacement; HD: along-strike displacement; X: distance; rX: relative distance along segment; rD: relative displacement

Table 2: Suggestion of database structure for the future surface faulting catalogue.

References

Bignami, C., et al., (2012). Coseismic deformation pattern of the Emilia 2012 seismic sequence imaged by Radarsat-1 interferometry. *Annals of Geophysics*. 55, 4, 789-795.

Cabrera J. & M. Sébrier, (1998). Surface rupture associated with a 5.3-mb earthquake: The 5 April 1986 Cuzco earthquake and kinematics of the Chincheros-Quoricocha faults of the High Andes, Peru. *BSSA*. 88, 1, 242-255.

Cakir, Z., et al., (2006). Surface Deformation Associated with the Mw 6.4, 24 February 2004 Al Hoceima, Morocco, Earthquake Deduced from InSAR: Implications for the Active Tectonics along North Africa. *BSSA*. 96, 1, 59-68.

Champenois, J., et al., (2015). A newly discovered active fault generating large surface displacement during M5 earthquake (Central Ecuador). *EPSL*. In preparation.

Chapman, N., et al., (2014). Active Faults and Nuclear Power Plants. *EOS, Transactions, AGU*. 95, 4, 33–40.

Cinti, F. R., et al., (2011). Evidence for surface faulting events along the Paganica fault prior to the 6 April 2009 L'Aquila earthquake (central Italy).*JGR*. 116, B07308.

Clark, D., et al., (2014). Coseismic surface deformation caused by the 23 march 2012 Mw 5.4 Ernabella (Pukatja) earthquake, Central Australia: implications for fault scaling relations in cratonic settings. *BSSA*. 104, 24-39.

Cohen-Waeber, J., et al., (2014). Effects of surface fault ruptura on infrastructure. In Geotechnical Engineering Reconnaissance of the August 24, 2014 M6 South Napa Earthquake. Report of the NSF Sponsored GEER Association Team, CGS, PEER Center, USGS. Report No. GEER-037, Section 4.

Dawson, J., et al., (2008). Shallow intraplate earthquakes in Western Australia observed by Interferometric Synthetic Aperture Radar. *JGR*. 113, B11408.

Dawson, T., et al., (2014). Surface fault rupture associated with the South Napa Earthquake of August 24, 2014. In: Geotechnical Engineering Reconnaissance of the August 24, 2014 M6 South Napa Earthquake. Report of the NSF Sponsored GEER Association Team, CGS, PEER Center, USGS. Report No. GEER-037, Section 3.

DePolo, C.M., et al., (2011). Summary of the 2008 Wells, Nevada Earthquake, Documentation Volume. Nevada Bureau of Mines and Geology Special Publication 36.

Hudnut, K. W., et al., (2014). Key recovery factors for the August 24, 2014, South Napa Earthquake. *USGS Open-File Report*. 2014-1249, 51 pages.

Lettis, W., et al., (1997). Empirical observations regarding reverse earthquakes, blind thrust faults and Quaternary deformation: Are blind thrust truly blind? *BSSA*. 87, 1171-1198.

Lienkaemper, J., et al., (2014). Surface slip associated with the 2014 South Napa, California earthquake measured on alinement arrays. AGU Fall Meeting, San Francisco, poster S33F-4898.

McCalpin, J. & M.G. Thakkar, (2003). 2001 Bhuj-Kachchh earthquake: surface faulting and its relation with neotectonics and regional structures, Gujarat, Western India. *Annals of Geophysics*. 46, 5, 937-956.

Moss, R.E., et al., (2013). The Impact of Material Stiffness on the Likelihood of Fault Rupture Propagating to the Ground Surface. *SRL*. 84, 485-488.

Oskin, M.E., et al., (2012). Near-Field Deformation from the El Mayor–Cucapah Earthquake Revealed by Differential LIDAR. *Science*. 335, 702-705.

Takemoto-Shimomura, H., et al., (2014). The evidence of the Late Quaternary fault activity in pollen fossil assemblages and the estimate of the coseismic events using pollen data, Central Japan. AGU Fall Meeting, San Francisco, poster T41C-4649.

Pezzopane, S.K., & T.E. Dawson, (1996). Fault displacement hazard: a summary of issues and information. In: *Seismotectonic Framework and Characterization of Faulting at Yucca Mountain* (Whitney, J.W. Editor). Department of Energy, Las Vegas, 9-1 – 9-160.

Rymer, M.J., K.J. Kendrick, J.J. Lienkaemper & M.M. Clark, (1990). 16. The Nunez Fault and its surface rupture during the Coalinga Earthquake Sequence. *United States Geological Survey Professional Paper*. 1487, 299-318.

Stanton, K.V., (2013). Investigation of parameters influencing reverse fault rupture propagation to the ground surface. Thesis "Master of Science in Civil and Environmental Engineering", Faculty of California Polytechnic State University, San Luis Obispo.

Stirling, M., et al., (2013). Selection of Earthquake Scaling Relationships for Seismic-Hazard Analysis. *BSSA*. 103, 6, 2993–3011, doi: 10.1785/0120130052.

Takao, M., et al., (2013). Application of Probabilistic Fault Displacement Hazard Analysis in Japan. *Japan Association for Earthquake Engineering*. 13, 1.

Vittori, E., et al., (2011). Surface faulting of the April 6, 2009, Mw 6.3 L'Aquila earthquake in Central Italy. *Bulletin of the Seismological Society of America*. 101 (4), August 2011, 1507-1530, doi: 10.1785/0120100140

Wells, D.L. & K.J. Coppersmith, (1994). New empirical relationships among magnitude, rupture length, rupture width, rupture area and surface displacement. *BSSA*. 84, 974-1002.

Youngs R.R., et al., (2003). A Methodology for Probabilistic Fault Displacement Hazard Analysis (PFDHA). *Earthquake Spectra*. 19, 1, 191–219.

INQUA Focus Group on Paleoseismology and Active Tectonics

Historical, archaeoseismic, paleoseismological and active tectonics markers in the Avola Vecchia area (southern Sicily)

Barbano, M.S., Pirrotta, C., De Guidi, G., Farina, C.

Dipartimento di Scienze Biologiche, Geologiche e Ambientali, Università di Catania, Corso Italia 57, 95129 Catania, Italy.
Email: barbano@unict.it

Abstract: *Coeval sources describe with certainty a landslide triggered by the 11 January 1693 Sicilian earthquake near Avola Vecchia. The landslide occurred west of the town, at Mt Ginisi, along the Miranda river, which was the economic and productive focus of the territory hosting five mills. The landslide destroyed three mills and dammed the river. Near Avola Vecchia, at Mt Aquilone, we have recognized several fractures in rock masses as well as in anthropogenic caves (the so-called cave houses) and oven-shaped tombs, dating back to the Byzantine period and Sicels' age respectively. The mesostructural analysis of the rock masses showed that fractures are mainly classifiable as joints and that some of them are due to the tectonic stress field confirming that in southern Sicily a WNW - ESE extensional regime is still active. Some fractures are due to seismic shaking and slope gravity effects, suggesting that several earthquakes have affected the area.*

Key words: *Earthquake-triggered landslide, joints, cave houses, 1693 earthquake.*

INTRODUCTION

Strong earthquakes can trigger several soil deformation phenomena, such as liquefaction, ground fracturing and landslides, which can often cause more damage than the seismic shaking itself. Rocks and sediments can record such effects as evidence of paleoearthquakes.
Eastern Sicily is a seismically active area in which some of the most disastrous Italian earthquakes, with Mw up to 7.4 (Rovida et al., 2011), have occurred causing damage, numerous fatalities and triggering several ground failures, as reported by historical sources. Geological evidence of liquefactions, correlated to some of the strongest earthquakes of eastern Sicily, were found in the Holocene deposits of the Mascali area and in the Catania Plain, both characterized by a continental fluviatile sedimentation environment (Guarnieri et al., 2008). Moreover, Pirrotta & Barbano (2011) reported seismically induced deformation structures along the rocky coast of Vendicari (southeastern Sicily). In this paper, we describe a seismically induced landslide along with some fractures affecting archaeological structures in the ancient site of Avola Vecchia, southwest of Syracuse (Figure 1).
Avola Vecchia is located in the eastern coastal sector of the Hyblean Plateau, which is the emerged part of a gently deformed segment of the African continental margin representing the Tertiary foreland of the Apenninic-Maghrebian Thrust Belt. NE–SW and NW–SE trending normal fault systems affect the outcropping Miocene terrain (Lentini et al., 1984). Late Pleistocene terraced deposits, consisting of yellow sands and bioclastic calcarenites, crop out discontinuously along the coastal areas (Figure 1). A study focused on joint sets and grid-lock fracture systems allows documenting, in southeastern Sicily, the existence of an extensional tectonic regime whose activity is younger than Middle Pleistocene (De Guidi et al., 2013). However, the recent activity of this tectonics has never been documented for lacking of fractured Holocene terrains.

HISTORICAL DATA

The foundation of Avola, in an area previously inhabited by the Sicans, is perhaps connected to the history of the older city of Hybla Major (Di Maria, 1745) that was invaded by the Sicels in the 13th-12th centuries BC.The Greeks colonized the city in the 8th century BC. After the Syracuse domination (4th century BC), the Romans conquered Sicily in 227 BC. Hybla disappeared in the early middle Ages, and the territory started to be repopulated during the Islamic domination of Sicily (9th-11th centuries AD). The Sicels' age is testified by numerous finds, especially pottery and dishes, found in the oven-shaped tombs resembling a beehive and characterizing Avola Vecchia and the near site of Cavagrande di Cassibile. Moreover, the cave houses are a type of dwelling cave carved into the rock that marks the ancient Avola urban centre. They date back to the Byzantine-medieval period (6th-9th century AD) and people lived there until the 1693 earthquakes (Gringeri Pantano, 1996). However, Avola Vecchia appeared only during the Norman or Hohenstaufen rule (12th-13th centuries). In 1693, two earthquakes destroyed Avola Vecchia, as well as many of the southeastern Sicily towns. The city was abandoned and rebuilt in a new location along the coast (Figure 1), following the geometrical and regular plan designed by the architect friar Angelo Italia.

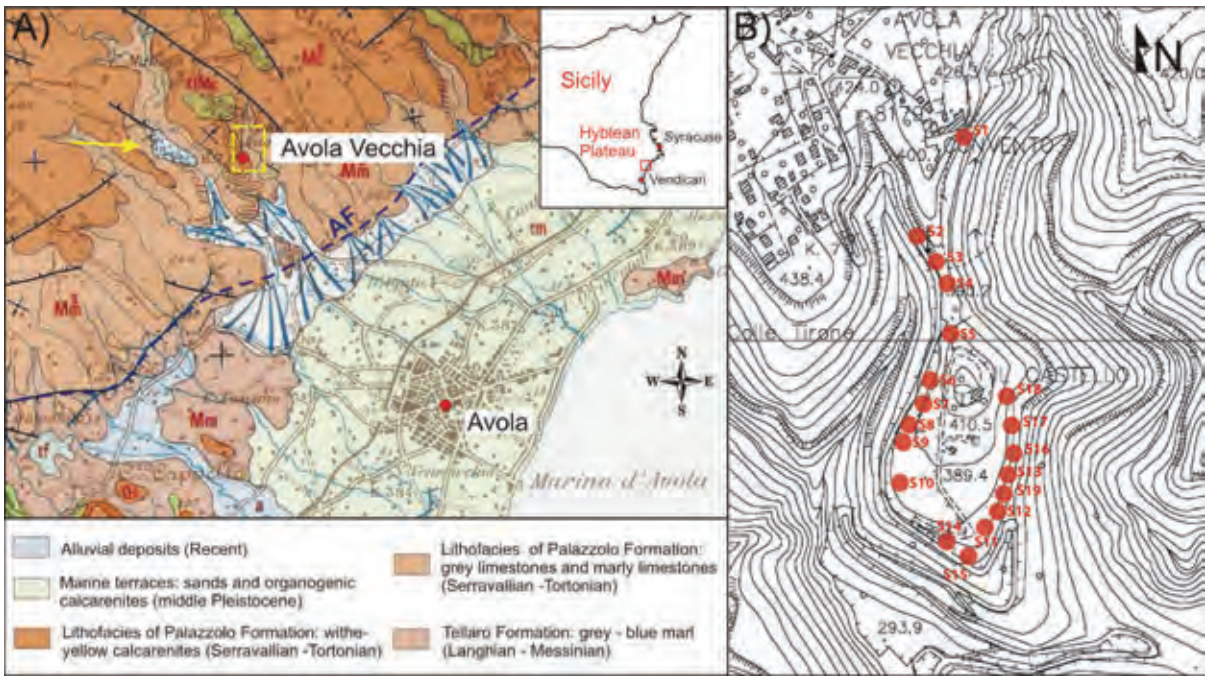

Figure 1: A) Geologic map (modified after Lentini et al., 1984) and location of the studied area; AF is the Avola Fault; the yellow arrow marks the 1693 Mt Ginisi landslide; B) Mt Aquilone, and location of the caves with the mesostructural stations.

Among the numerous historical sources, well describing the effects of the 1693 earthquakes in Avola Vecchia, we selected two witness contemporary and reliable accounts: Dell'Arte (1699) and Di Maria (1745).

"In Avola Vecchia, the January 9 at four-thirty (Italian time) in the night (~21 GMT), a strong earthquake destroyed almost the whole quarters known as *di Sopra* and *Marchi*, ruining houses since foundations with the loss of 500 citizens. 40 hours after the first shock, the 11 January at 20 hours and a quarter (~13 GMT), the earthquake was so proud and terrible that destroyed the entire city. No stone remained upon stone, including caves, and people was not able to distinguish one house from the other houses" (Dell'Arte, 1699). The earthquake "unhinged stones above Avola was located; then unhinged throughout the whole city" (Di Maria, 1745). Five hundred people died for this shock. In Avola, the whole fatalities were 1,000 out of 6,225, in minor percentage than other Sicilian cities, because most of the inhabitants, were outdoors, having felt another slight shock at 16 hours (~9 GMT). The fortified castle, located on the acropolis of Mt Aquilone, was destroyed, although it had been rebuilt a first time after the December 10 1542 earthquake, "which had ruined the castle and many houses" (Gallo, 1966).

"The Mount called Gisini split, and almost half Mount breaking away with fury sank in the bed of the Valley called Carnevale, remaining under the portentous mass three mills with many people inside them" (Di Maria 1745). The Mt Gisini landslide is further documented by the archive plan concerning the construction of a canal system (Figure 2) to bypass the occlusion and provide water to the plantations and factories (Gringeri Pantano, 1996).

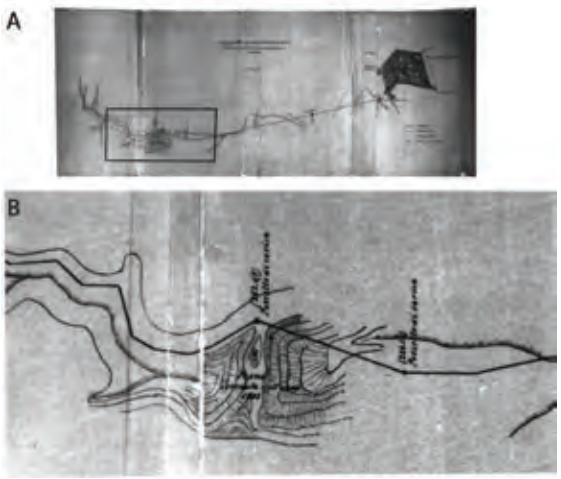

Figure 2: A) The plan of the Avola aqueduct, drawn in 1887. B) Enlarged inset showing the site of Mt. Gisini landslide, with the annotation "Frana avvenuta nell'anno 1693" (Landslide occurred in year 1693) (after Grangeri Pantano et al., 2002).

SEISMOGEOLOGICAL ANALYSIS

Aerial-photos interpretation, field survey and mesostructural analysis near Avola Vecchia allowed us to observe some devastating effects of the 1693 earthquakes still evident on the surface.

The Mt. Gisini landslide (Figure 1 and 3) occurred to the west of Avola Vecchia. It was a planar translational rockslide, with a steep slip surface, involving a volume of 2 x 10^6 m^3 of sub-horizontally bedded Tortonian and Messinian calcarenite and marly limestone (Gringeri et al., 2002). The accumulation, about 250 m wide and 370 m long, is around 60 m high above the valley bottom. Despite the high degree of fracturing, the rock stratification remains sub-horizontal. The landslide produced the obstruction of the Miranda river causing a dam belongs to type II (spanning the entire valley) according to the classification of landslide dams by Costa and Schuster (1988) (Nicoletti & Parise, 2002). Nowadays the landslide body is re-incised by the Piscitello stream that creates a V valley on it. The erosion processes on the downstream face have triggered a secondary landslide on the downstream side of the same landslide body. The Mt. Gisini landslide seems to have reached the position of minimum potential energy and, therefore, the probability of a further failure seems low (Nicoletti & Parise, 2002).

Figure 3: The Mt. Gisini landslide that dammed the River Miranda on 11 January 1693, and destroyed three mills killing people.

The calcarenites, marly limestones and limestones of Miocene age, outcropping at Mt Aquilone, are affected by mechanical discontinuities with decimetric spacing.
We performed systematic and mesostructural analyses (stereographic projections and rose diagrams) of 137 fractures affecting 19 caves of Mt Aquilone (Figure 1 B). These fractures show no, or few, evidence of shear motion, being originated as purely extensional fractures. This type of brittle features is known as "extensional joints" and they have been recognized as one of the most common deformational structures in every tectonic environment (Caputo, 2010 and references therein). They are up to several metres long, often opened from few millimetres to several centimetres (Figure 4B, C), and sometimes filled by re-crystallized calcite deposit.
The joints are grouped in two orthogonal sets with main directions N45 and N140 (Figure 4D). According to Caputo (2005), two orthogonal joint sets are due to stress swap mechanisms between σ_2 and σ_3 stress axes that occur locally causing stress field deformation. However, the prevalence of fractures with direction NE-SW indicates that the local tectonic maximum extension is almost NW-SE oriented (Figure 4E) and it is compatible with the regional stress field. This stress field is also responsible of the Avola fault (AF in Figure 1A) that lies close to the study site and, according to some Authors, may be active and could be the source of the 9 January 1693 earthquake (Monaco & Tortorici, 2000).

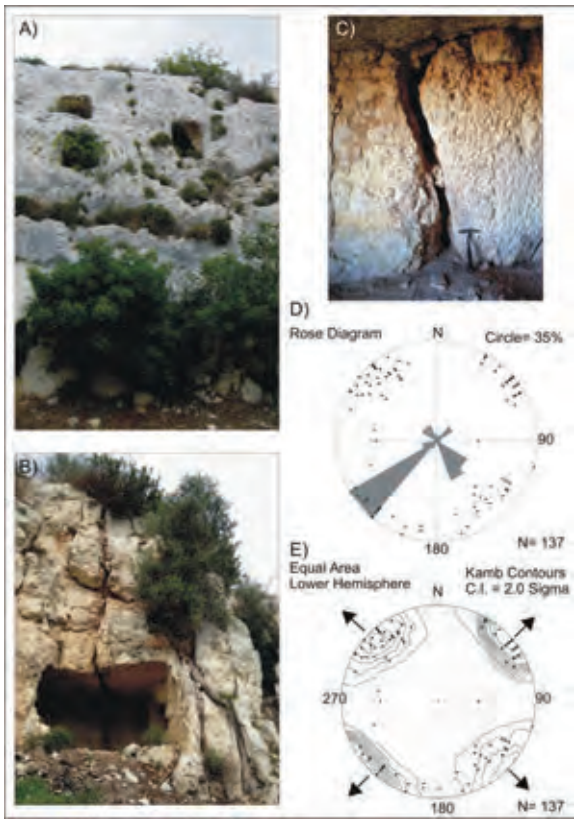

Figure 4: A) Fractures in the limestone affecting oven-shaped tombs in the Sicels' necropolis; B) and C) open fractures in the calcarenite affecting cave houses dated back to the Byzantine-medieval period (6th-9th century AD); D) Stereographic projections of the joints in the surveyed stations and rose diagram; E) stress inversion.

Nevertheless, the fractures can be triggered by other mechanisms such as seismic shacking. Indeed historical accounts describe damage in the cave houses and "unhinged stones" during the 1693 earthquakes.
We have also compared the trend of the NE-SW fractures, with that of the slope at the location of each mesostructural station. A similitude between the two directions was observed for the most of the stations indicating that the NE-SW set represents potential failure surfaces for future rockfalls. Moreover, the weakening of the rock slope, along with the enlargement of the fractures, is likely enhanced by water circulation dissolving the limestone and by the presence of the caves. Therefore, seismic shaking, which in turn can drive slope instability, can be considered a cause for the rock fracturing superimposed on tectonic stress.

Seismically induced brittle deformation on rock, usually found close to active fault zones worldwide (Montenat et al., 2008), is documented locally at Vendicari (10 km south from the study site) (Pirrotta & Barbano, 2011).

CONCLUDING REMARKS

The Avola Vecchia area shows several effects of active tectonics and earthquake shaking. We have observed brittle deformational structures and seismically induced features such as the Mt. Gisini landslide.

The occurrence of landslides and ground fracturing during strong earthquakes in eastern Sicily is also supported both by the historical accounts, reporting the observation of such phenomena in several places of this region, and by previous field works that studied similar seismically induced structures.

The large and inactive landslide occurred near Avola Vecchia is described by historical accounts as related to the 1693 earthquake. Other landslides were surveyed in the same area and in southeastern Sicily. Since this is a seismic region but commonly considered no prone to slide failure, these landslides are considered earthquake-triggered (Nicoletti & Parise, 2002). The landslides testify the occurrence of seismic events with magnitude greater than 5 and intensity greater than IX, that are the thresholds for which these seismo-induced features may develop in a site (e.g. Pirrotta & Barbano, 2011). According to empirical relationship between source parameters and epicentral distance of the site where landslides developed during historical earthquakes in eastern Sicily, the triggering earthquakes occurred at a distance lower than 20 km, considering the threshold parameters, or at a longer distance but with a higher magnitude than the threshold.

The study of joint sets and grid-lock fracture systems, allows documenting the existence of an extensional tectonic regime, that is still active since fractures affect historical and archaeological man-made structures. The obtained stress orientations are in good agreement with the regional extensional tectonic stress field and support the activity of the Avola fault located close to Mt Aquilone. Since the joints can be related and reopened either because of coseismic shaking, or for slope instability, additional surveys and analysis need to validate their connection to the actual stress field.

Therefore, we plan to perform structural and morphometric analyses of the Avola area and the possibility of dating landslides and fractures to provide new and useful information on ancient earthquakes in order to better define the seismic framework in Sicily having a strong seismic activity but poorly defined seismogenic sources.

Acknowledgements: The research was supported by University of Catania PRA grants.

References

Caputo, R., (1995). Evolution of orthogonal sets of coeval extension joints. *Terra Nova*. 7, 479–490.

Caputo, R., (2010). Why joints are more abundant than faults. A conceptual model to estimate their ratio in layered carbonate rocks. *Journal of Strucural Geol*ogy. 32, 1257–1270.

Costa, J.E. & R.L. Schuster, (1988). The formation and failure of natural dams. *Geological Society of America Bulletin*. 100, 1054–1068.

Dell'Arte, P., (1699). *Storia dell'Antica Avola e del terremoto dell'anno fatale 1693*.

De Guidi, G., R. Caputo & S. Scudero, (2013). Regional and local stress field orientation inferred from quantitative analyses of extension joints: Case study from southern Italy. *Tectonics*. 32 (2) 239–251.

Di Maria, F., (1745). *Ibla rediviva*. 1989 Reprint. Pro Loco, Avola. 160 pp.

Gallo, C., (1966). *Poblemi ed aspetti storici della ricostruzione a Noto e nella Sicilia orientale dopo il terremoto del 1693*. Archivio Storico Siciliano. serie III, 15, 89-190.

Gringeri Pantano, F., (1996). *La città esagonale. Avola: l'antico sito, lo spazio urbano ricostruito*. Sellerio, Palermo, 269 pp.

Gringeri Pantano, F., P.G. Nicoletti & M. Parise, (2002). Historical and Geological Evidence for Seismic Origin of Newly Recognized Landslides in Southeastern Sicily, and Its Significance in Terms of Hazard. *Environmental Management*. 29 (1), 116–131.

Guarnieri, P., C. Pirrotta, M.S. Barbano, P.M De Martini, D. Pantosti, F. Gerardi & A. Smedile, (2009). Paleoseismic investigation of historical liquefactions along the Ionian coast of Sicily. *Journal of Earthquake Engineering*. 13, 68–79.

Lentini, F. et al., (1984). *Carta geologica della Sicilia Sud-Orientale*. Scale 1:100.000. S.EL.CA., Florence.

Monaco, C. & L. Tortorici, (2000). Active faulting in the Calabrian arc and eastern Sicily. *Journal of Geodynamics*. 29, 407-424.

Montenat, C., P. Barrier, P. Ott d'Estevou & C. Hibsch, (2008). Seismites: an attempt at critical analysis and classification. *Sedimentary Geology*. 196, 5–30.

Nicoletti, P.G. & M. Parise, (2002). Seven landslide dams of old seismic origin in southeastern Sicily (Italy). *Geomorphology*. 46 (3–4), 203– 222.

Pirrotta, C. & M.S. Barbano, (2011). Analysis of deformation structures in Pliocene and Quaternary deposits of the Hyblean Plateaux (South-eastern Sicily). *Tectonophysics*. 499, 41-53.

Rovida, A., R. Camassi, P. Gasperini & M. Stucchi (eds.), (2011). *CPTI11, the 2011 version of the Parametric Catalogue of Italian Earthquakes.* Milano, Bologna, http://emidius.mi.ingv.it/CPTI.

INQUA Focus Group on Paleoseismology and Active Tectonics

Sedimentary impacts of recent moderate earthquakes in different settings in the Western Gulf of Corinth, Greece

Beckers, A. (1,2), Mortier, C. (1), Beck C. (2), Hubert-Ferrari, A. (1), Reyss, J.-L. (3), Albini, P. (4), Develle, A.-L. (5), Tripsanas, E. (6), Sakellariou, D. (6), Crouzet, C. (2), Rovida, A. (4) and Scotti, O. (7)

(1) Dept of Geography, University of Liège, allée du 6 août 2, 4000 Liège, Belgium. Email : abeckers@ulg.ac.be.
(2) ISTerre, CNRS UMR 5275, University of Savoie, F-73376 Le Bourget du Lac, France
(3) LSCE, CNRS UMR 8212, avenue de la Terrasse, 91198, F-91191 Gif-sur-Yvette, France
(4) Istituto Nazionale di Geofisica e Vulcanologia, Via E. Bassini, 15, 20133 Milano, Italy
(5) EDYTEM, University of Savoie/CNRS, Le Bourget du Lac, France
(6) Institute of Oceanography, Hellenic Center for Marine Research, GR-19013 Anavyssos, Greece
(7) Institut de Radioprotection et de Sûreté Nucléaire (IRSN), Fontenay-aux-Roses, France

Abstract: *11 short gravity cores retrieved in the Western Gulf of Corinth, Greece, allowed identifying event deposits whose age ranges were compared to an updated earthquakes catalogue for the area. ^{210}Pb-derived age-depth curves show that the majority of the event deposits may have been triggered by earthquakes. These results show that moderate earthquakes (M_w ~6.0-6.5) may significantly impact different marine settings, from shallow shelves (70-100 m deep) to the basin floor (330 m deep). The deepest coring sites show the best possible record, but one major earthquake is missing and the age of one event deposit does not fit with any known earthquake. More cores are needed to check the spatial extent of each deposit and to validate the absence of record of some earthquakes, like the 1995 Aigion earthquake.*

Key words: *Paleoseismology, marine sediments, event deposits, sediment density flows, turbidite.*

INTRODUCTION

Marine or lacustrine paleoseismology has several advantages in comparison with onland methods: higher potential for preservation, possible long-term record, and better spatial coverage (Goldfinger, 2009). However, most of the sedimentary processes that are considered as potential offshore indicators of earthquake (EQ) shaking (submarine landslides, turbidity currents, tsunami backwash flows) can also be triggered without any EQ. Many works have been achieved to try to discriminate earthquake-triggered from non-earthquake-triggered offshore event deposits (e. g. Adams, 1990; Shiki et al., 2000), but the existence of diagnostic criterion is still debated (Talling, 2014).

The aim of this communication is to analyze in detail the influence of moderate EQ shaking on the sedimentation

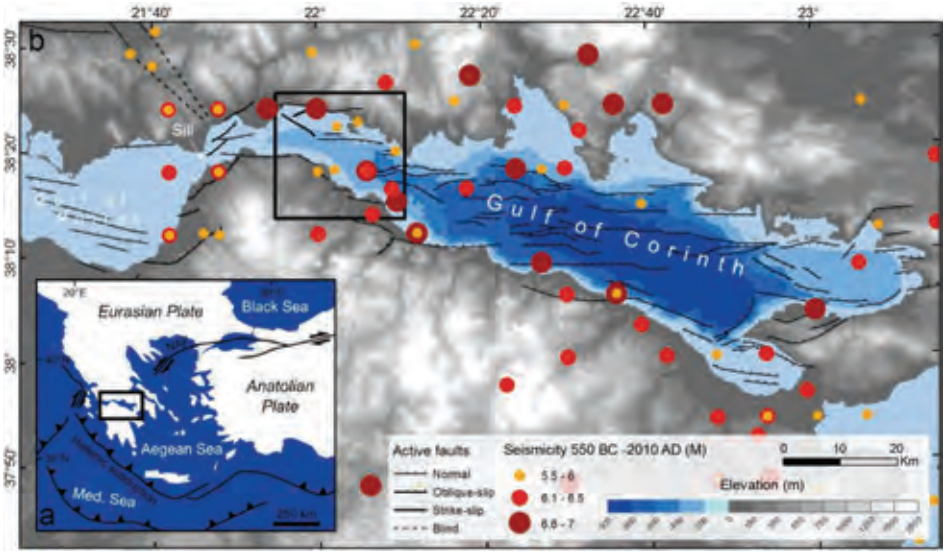

Figure 1: Physiography, active faults, and historical seismicity (550 BC – 2010 AD, M≥5.5) in the area of the Gulfs of Patras and Corinth The black box in (b) shows the study area. Location in inset a. Historical earthquakes from Papazachos et al. (2000, 2010). Active faults in the Corinth rift and in the Gulf of Patras from Beckers et al. (2015) and references therein. Bathymetry adapted from Bell et al. (2009), elevation from SRTM (http:// http://srtm.usgs.gov/).

in different marine settings, from shelves to basin floor, in order to identify which environment may provide the more complete and the less noisy EQs record.

STUDY AREA

The study area is the Gulf of Corinth, Greece. It is a 120 km long, 869 m deep depression located in central Greece (Fig. 1). This basin is connected to the Mediterranean Sea at its western tip through a 62 m deep, 2 km wide sill. Numerous damaging EQs are known in Gulf of Corinth region for at least 2000 years by historical sources (Fig. 1), with largest estimated magnitudes approaching 7 (Ambraseys & Jackson, 1997). In the western part of the Gulf, that is investigated in the present study, tsunamis and submarine landslides have been triggered by historical EQs (Schmidt, 1887; Papatheodorou & Ferentinos, 1997), but these phenomena also happened without any EQ (Heezen et al., 1966). Only one study has been dedicated to the identification of offshore historical (before 1990) earthquake-related deposits in this area (Lykousis et al., 2007). These authors investigated the basin floor of the Western Gulf with short box cores and identified a widespread 6-10 cm thick sandy deposit attributed to the 1861 earthquake. This result highlights the potential of this area for developing offshore paleoseismological methods.

METHODS

The method developed here consists in crossing estimated macroseismic intensity data series with age-estimated event deposits identified in short gravity cores. The aim is to check the completeness of the sedimentary records of EQs in different settings of the Western Gulf. An in-depth analysis of existing and newly found historical sources has been done to build an updated catalogue of past EQs in the Western Corinth Rift area, from ~1400 AD to today. 9 short gravity cores (40-85 cm long) have been retrieved in four different sites (Fig. 2) : the Aigion Shelf (~40 m deep), the Erineos Shelf (70-100 m deep); the Trizonia sub-basin (~180 m deep), and the basin floor (330 m deep). X-radiography, magnetic susceptibility, core-scanner X-ray fluorescence (XRF) measurements and high-resolution (2 mm) grain-size measurements have been carried out to highlight and characterize specific layers possibly deposited during or shortly after earthquakes, such as turbidites and tsunami back-wash flow deposits. The age control is based on unsupported ^{210}Pb and ^{137}Cs activity profiles measured on 4 cores. The average last-century sedimentation rates have been applied to the hemipelagic intervals downcore to estimate the age of deeper layers. The use of the event deposit associated to the largest EQ as an anchor point in the age-depth curve is tested. Finally, a source area has been defined for each coring site as the offshore and coastal areas where sediment failures could have occurred and could have triggered sediment-density flows recorded at this coring site. Based on the Papazachos and Papaioanou (1997)'s attenuation model for Greece and our updated EQ catalogue, intensity (Modified Mercalli Intensity scale, MMI) has been estimated for each EQ in each source area.

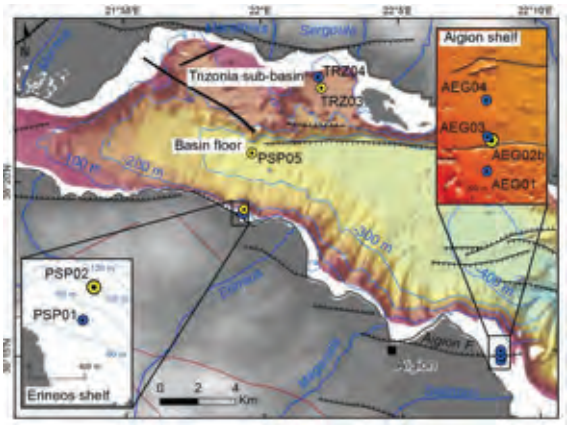

Figure 2: Location of the coring sites. Circles indicate cores location; yellow circles indicate cores where ^{210}Pb and ^{137}Cs activity profiles have been measured. Bathymetry from Hellenic Center for Marine Reasearch (unpublished data) and from Cotterill (2006). Active normal faults (black lines, bold indicates a strike-slip component) from Beckers et al. (2015) and references therein.

RESULTS AND INTERPRETATION

The first coring site is in the Aigion Shelf, a ~40 m deep shelf crossed by the Aigion fault and characterized by a field of pockmarks and sand volcanoes (Fig. 2). The 4 cores (AEG01 to 04) are visually homogenous and composed of grey-brown silt. 3 coarse-grained layers have been highlighted by the grain-size analysis and some XRF ratios. ^{210}Pb and ^{137}Cs activity profiles are very irregular and do not allow to derive valuable age control. The Erineos Shelf is a small shelf located west of the homonimous delta (Fig. 2). Two cores (PSP01 and 02) have been retrieved at -70 m (62 cm long) and -100 m (85 cm long). Four coarse-grained layers have been identified in the longest core, and two of them can be correlated with the 2 events observed in the shortest core. Events are 2-5 cm thick and are made of sandy silt, the sandy fraction being composed of plants remains and of a few terrigenous grains. Accurate age-depth curve shows that events could have been triggered by 2 EQs (i.e. in 1817 and 1861). However, the number of EQs with MMI ≥VII is larger than the number of event deposits identified in the cores during the 260-300-year sampled period.

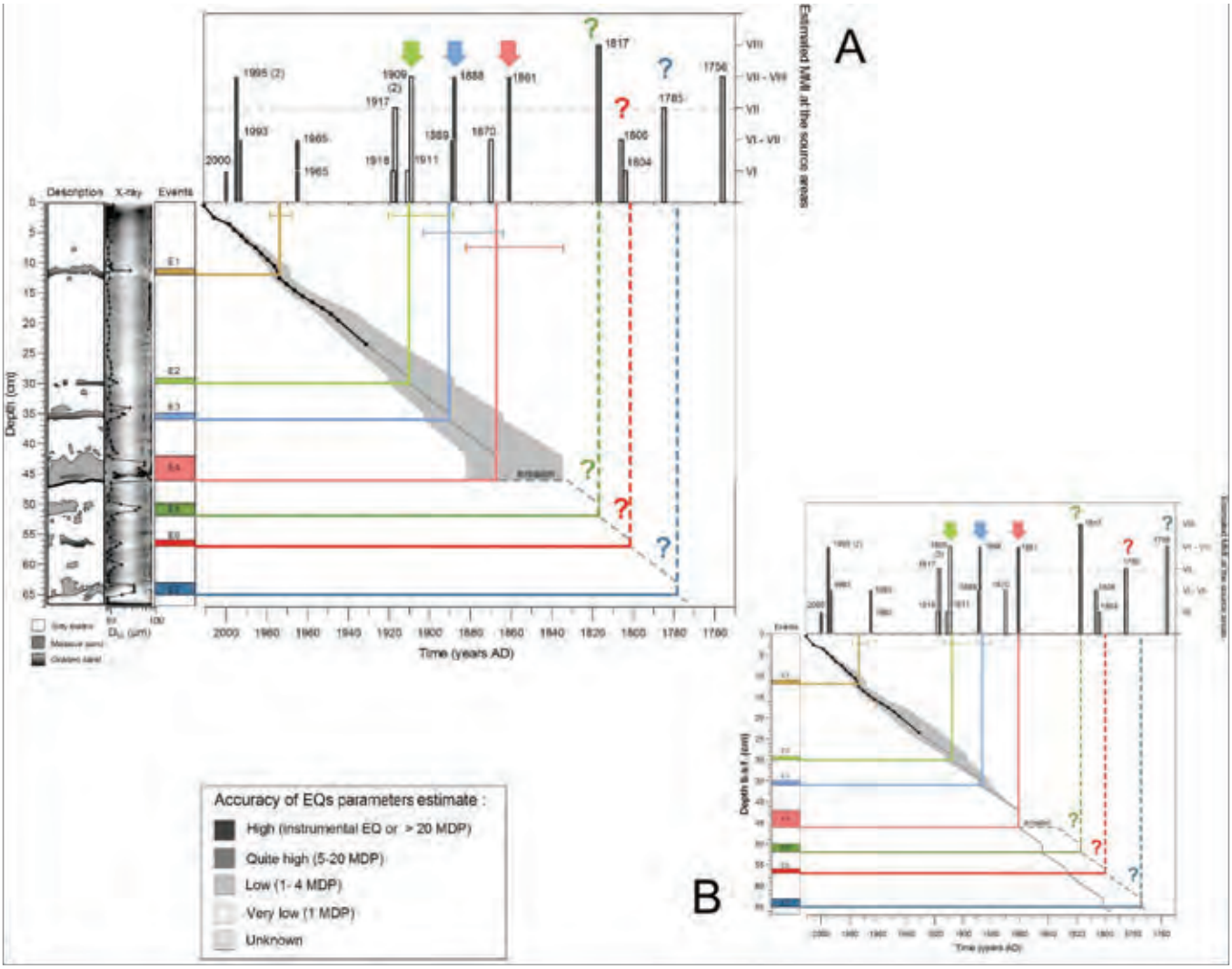

Figure 3: Example of analysis carried out for the core PSP05 (basin floor). A) to the left, core description, X-radiography, grain-size profile and event deposits; to the top, macroseismic intensities (MMI: Modified Mercalli Intensity scale) estimated for historical earthquakes; in the center, ^{210}Pb-based age-depth curve. B) same core but age-depth curve built using the likely 1861 earthquake deposit as an anchor point. Colored arrows highlight earthquakes that have probably impacted the sedimentation. Bottom left: accuracy of earthquakes parameters estimate (magnitude and location) based on available data (MDP: macroseismic intensity data point(s)).

Two cores (60 and 70 cm long) have been retrieved in the 180 m deep Trizonia Sub-basin (Fig. 2). The cores both contain 5 event deposits. They consist of thin bioturbated sandy layers, some of them having been only detected by high-resolution grain-size analyses or X-radiography. Correlation between the cores is difficult because of the absence of anchor points in the hemipelagic intervals and because of the bioturbation. Age-depth curve for TRZ03 shows that 5 event deposits in this core fit reasonably well with the 5-7 EQs of MMI ≥ VII. However, the last major EQ, the 1995 Aigion EQ, seems to be not recorded despite a local estimated MMI between VII and VIII. In addition, an event occurred between 1930 and 1950, a period without any significant EQ in this area.

The last site is in the basin floor, at 330 m below sea level (Fig. 2). The 65 cm long core retrieved there contains 7 sandy layers (Fig. 3). These event deposits are 1-4 cm thick and XRF data show that they are made of terrigenous grains. The deposits are normally graded (turbidites) or massive. Age-depth curve shows that the thickest event, E4, very likely corresponds to the 1861 EQ (Fig. 3). As in the Trizonia Sub-basin, the number of event deposits reasonably matches the number of MMI ≥ VII EQs. Using E4 as an anchor point reduces the age uncertainty for E1, E2 and E3, and reinforces the interpretation that E2 and E3 have been triggered by the 1909 and 1888 EQ (Fig. 3). However, similarly to the Trizonia Sub-basin, the 1995 Aigion EQ is missing and one event (E1) probably does not fit with any known EQ.

DISCUSSION

Our results allow discussing the interest of different marine settings for paleoseismology. The Aigion shelf appears as not appropriate because of the low contrast between possible event deposits and the background sedimentation, and the difficulty to establish an age-depth curve. The event-deposits record is clearer in the Erineos Shelf, but the two retrieved cores did not allow to find a complete record of MMI ≥ VII EQs. Either some of these EQs did not trigger any sediment density flow, or the associated deposits do not have a wide spatial extent or have been eroded. Shelf environments are characterized by a discontinuous sedimentation influenced by river floods and oceanic processes (Addington et al., 2007; Knikskern et al., 2009). When marine currents are present, erosion may occur frequently (Carlin & Dellapenna, 2014). Shelves consequently may not be the more suitable setting for off-fault paleoseismology. In deeper settings (Trizonia sub-basin and basin floor), the record seems more complete, and age-depth curves are easiest to establish. The deepest site appears to show the best record in terms of event thickness, age-depth curve, and completeness of the possible EQ records. However, based on one core, the event-deposits record does not fit perfectly with the MMI ≥ VII EQs series. More cores are needed to check the spatial extent of each deposit and to validate the absence of records for some EQs, like the 1995 Aigion EQ.

We tried to use the event deposits associated with a remarkable event (the 1861 EQ, M≈6.5) as an anchor point to improve the age-depth curves. The risk was to fall into a circular reasoning. However, this earthquake induced an estimated MMI ≥ VII in the source area of each coring site, and an event deposit has been observed in each core at a depth that could correspond to the age of this earthquake. Consequently, this hypothesis may be considered as reasonable. Fig. 3 shows that including this anchor point does not improve the possible association between event deposits and earthquakes for the period before 1861. This may be due to a change in the sedimentation rate, which is difficult to constrain for this time period. However, for the sediments deposited after 1861 in PSP05, the improved age-depth curve allows to reduce the age uncertainty for 3 events, showing that 2 of them accurately fit with two earthquakes.

CONCLUSION

A detailed sediment cores analysis associated with the development of a new, updated, earthquake catalogue shows that moderate EQs probably significantly impact different marine settings at the Western tip of the Gulf of Corinth. The event deposits record however does not perfectly match the MMI ≥ VII earthquake historical record. More work is needed to improve the spatial coverage of coring sites in order to check this mismatch.

References

Adams, J., (1990). Paleoseismicity of the Cascadia subduction zone - Evidence from turbidites off the Oregon-Washington margin, *Tectonics*. 9, 569–583.

Addington, L.D., Kuehl, S.A., McNinch, J.E., (2007). Contrasting modes of shelf sediment dispersal off a high-yield river: Waiapu River, New Zealand. *Marine Geology*. 243, 18-30.

Ambraseys, N.N., Jackson, J.A., (1997). Seismicity and strain in the Gulf Of Corinth (Greece) since 1694. *Journal of Earthquake Engineering*. 1,433-474.

Beckers, A., Hubert-Ferrari, A., Beck, C., Bodeux, S., Tripsanas, E., Sakellariou, D., De Batist, M., (2015). Active faulting at the western tip of the Gulf of Corinth, Greece, from high-resolution seismic data. *Marine Geology*. 360,55-69.

Bell, R.E., McNeill, L.C., Bull, J. M., Henstock, T.J., Collier, R.E.L., Leeder, M.R., (2009). Fault architecture, basin structure and evolution of the Gulf of Corinth Rift, central Greece. *Basin Research*. 21, 824–855.

Carlin, J.A., Dellapenna, T.M., (2014). Event-driven deltaic sedimentation on a low-gradient, low-energy shelf: The Brazos River subaqueous delta, northwestern Gulf of Mexico. *Marine Geology*. 353, 21-30.

Cotterill, C.J., (2006). A High-resolution Holocene Fault Activity History of the Aigion Shelf, Gulf of Corinth, Greece. PhD Thesis, University of Southampton.

Goldfinger, C., (2009). Sub-Aqueous Paleoseismology. In *Paleoseismology (*Mcalpin, J., ed.). Elsevier, 119-169.

Heezen, B.C., Ewing, M., Johnson, G. L., (1966). The Gulf of Corinth floor. *Deep-Sea research*. 13, 381–411.

Kniskern, T.A., Kuehl, S.A., Harris, C.K., Carter, L., (2009). Sediment accumulation patterns and fine-scale strata formation on the Waiapu River shelf, New Zealand. *Marine Geology*. 270, 188-201.

Lykousis, V., Sakellariou, D., Rousakis, G., Alexandri, S., Kaberi, H., Nomikou, P., Georgiou, P., Balas, P., (2007). Sediment Failure Processes In Active Grabens: The Western Gulf Of Corinth (Greece). In: *Submarine Mass Movements and Their Consequences* (Lykousis, V., Sakellariou, D., Locat, J., eds.). Springer, Advances in Natural and Technological Hazards Research. 27, 297 - 305.

Papatheodorou, G., Ferentinos, G., (1997). Submarine and coastal sediment failure triggered by the 1995, M_s = 6.1 R Aegion earthquake, Gulf of Corinth, Greece. *Marine Geology*. 137, 287-304.

Papazachos, B. C., Comninakis, P.E., Scordilis, E. M., Karakaisis, G. F., Papazachos, C. B., (2010). A catalogue of earthquakes in the Mediterranean and surrounding area for the period 1901 – 2010. *Publ, Geophys, Laboratory, University of Thessaloniki*.

Papazachos, B.C., Comninakis, P.E., Karakaisis, G.F., Karakostas, B. G., Papaioannou, Ch. A., Papazachos, C.B., Scordilis, E.M., (2000). A catalogue of earthquakes in Greece and surrounding area for the period 550BC-1999. *Publ, Geophys, Laboratory, University of Thessaloniki*. 1, 333 pp.

Papazachos, C., Papaioannou, C., (1997). The macroseismic field of the Balkan area. *Journal of seismology*. 1, 181-201.

Schmidt, J., (1887). Studien iiber Erdbeben. Leipzig.

Shiki, T., Kumon, F., Inouchi, Y., Kontani, Y., Sakamoto, T., Tateishi, M., Matsubara, H., Fukuyama, K., (2000). Sedimentary features of the seismo-turbidites, Lake Biwa, Japan. *Sedimentary Geology*. 135, 37-50.

Talling, P. J., (2014). On the triggers, resulting flow types and frequencies of subaqueous sediment density flows in different settings. *Marine Geology*. 352, 155-182.

INQUA Focus Group on Paleoseismology and Active Tectonics

paleoseismicity.org

Paleoseismicity data on the San Demetrio ne' Vestini fault (L'Aquila Basin, Central Italy)

Blumetti, A.M., Di Manna, P., Vittori, E., Comerci, V. & Guerrieri, L.

ISPRA, Geological Survey of Italy, Via Brancati 48, 00144 Roma, Italy. Email: annamaria.blumetti@isprambiente.it

Abstract: *The San Demetrio ne' Vestini fault is a NW-SE trending normal fault at the southeastern tip of the L'Aquila Basin fault zone. During seismic microzonation studies after the April 6, 2009, L'Aquila earthquake, this fault, which runs across the historical centre of San Demetrio ne' Vestini, was pointed out as capable, mapped in detail and portrayed by geophysical investigations. Paleoseismological trench investigations, confirming fault capability, have revealed at least 4 surface faulting events with discrete offsets from a few to several tens of centimetres. Based on radiocarbon dating, 3 surface faulting events occurred in the Holocene, respectively after 7030-6570 BC, between 5470-5220 BC and 3640-3480 BC and after 2760-2470 BC. An older surface faulting event, related to an earthquake with larger magnitude, because associated to a large gravity graben and an offset of about 80 cm, occurred between 16430-16010 BC and 7030–6570 BC.*

Key words: *Paleoseismology, capable fault, seismic microzonation, Fault Displacement Hazard.*

INTRODUCTION AND GEOLOGICAL FRAMEWORK

In the months following the April 6, 2009, Mw 6.3 L'Aquila earthquake in Central Apennines (Italy), the Geological Survey of Italy (ISPRA) carried out a seismic microzonation of the San Demetrio ne' Vestini's territory, severely damaged by the 2009 event, based on detailed geological, geomorphological and geophysical surveys. This village is within the L'Aquila intramountain basin, made of a system of northwest-southeast-trending tectonic depressions (total length about 30 kilometres) developed inside the inner sector of the Meso-Cenozoic orogenic belt of the Apennines, between the Gran Sasso and the Monti d'Ocre morphotectonic units (Fig. 1).

Active crustal extension across this part of the Apennines, marked by strong historical seismicity, is measured by GPS velocities around 3 mm/yr (D'Agostino et al., 2011). There is also wide geological evidence of active faulting (Bagnaia et al., 1992; Blumetti, 1995; Boncio et al., 2004; Galadini & Galli, 2000; Moro et al., 2002; Roberts and Michetti, 2004; Blumetti & Guerrieri 2007; Galli et al., 2010; Cinti et al., 2011; Galli et al., 2011; Giaccio et al., 2012; Blumetti et al., 2013).

San Demetrio is at the southern tip of the L'Aquila basin fault zone, an area characterized by en echelon and sub-parallel NW-SE trending fault segments. This structural setting is typical at the transition between two primary fault zones (in this case between the L'Aquila Basin F.Z. and the Subequan Basin F.Z., this last partly represented in Fig. 1A by the Fontecchio fault). The territory of the San Demetrio municipality is crossed by 4 NW-SE trending fault segments that have displaced Quaternary deposits (Fig. 1B; Bertini and Bosi, 1993). One of them, cutting across the historical centre, was pointed out as capable by the Working Group MS–AQ (2010). The San Demetrio fault, identified as possibly active by Bagnaia et al. (1992), does not crop out with an evident free-face, but it is inferred at the base of an up to 25 meters high fault scarp that displaces the flat surface of a recent alluvial terrace (Figs. 1 and 2). This note summarizes the results of the paleoseismological study carried out by ISPRA on this fault, aimed at characterizing its capability in terms of seismic and surface faulting potential.

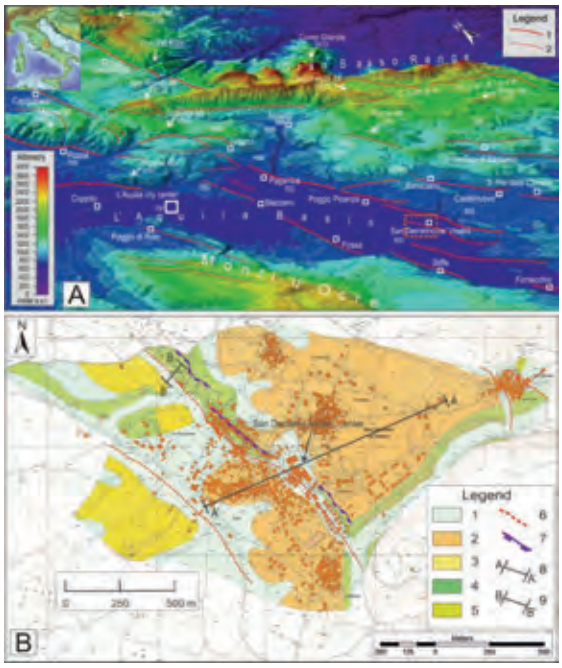

Figure 1: (A) Oblique view (based on 20 m DTM) of the L'Aquila region with the grid of capable faults. Legend: 1) Primary fault; 2) Secondary fault. (B) Geological map. Legend: 1) Colluvial and debris deposits (Holocene); 2) Alluvial fan gravel and sand (upper part of Mid Pleistocene); 3) Sand (upper part of Mid Pleistocene); 4) Fan delta conglomerates (Lower to Mid Pleistocene); 5) Whitish silty lacustrine deposits (Lower to Middle Pleistocene); 6) Capable fault (not outcropping); 7) Fault scarp edge; 8) location of the cross section shown in Fig. 2B; 9) Trace of paleoseismological trench. Modified after Working Group MS–AQ (2010).

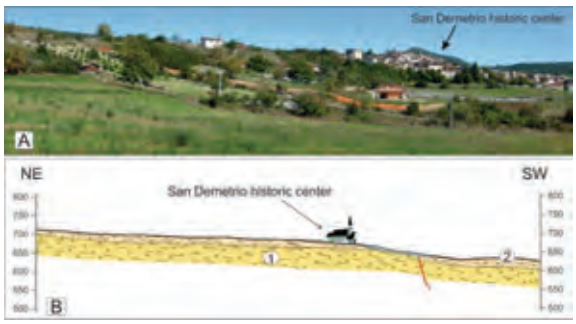

Figure 2: (A) Landscape view of the scarp related to the San Demetrio fault. The orange stripe (fence net) marks the trench site. (B) Geological profile across the fault (location in Fig. 1). Legend: 1) Fan delta conglomerates (Lower to Middle Pleistocene); 2) Gravel and sand (upper part of Middle Pleistocene). Modified, after W.G. MS–AQ (2010).

PALEOSEISMOLOGICAL ANALYSIS

The most suitable trenching site was identified NW of the historical centre of the village (Fig. 1), where morphotectonic observations and geophysical data (Electrical Resistivity Tomography and seismic refraction tomography) consistently indicated the presence of a fault cutting up to the surface.

Both trench walls were logged in detail and bulk samples, taken from both walls, were dated through the radiocarbon method, namely accelerator mass spectrometry (AMS), at the Center for Dating and Diagnostics (CEDAD) of the University of Salento. The detailed analysis of the stratigraphy exposed in the trench walls (Figs. 3 and 4) and the obtained ages (Table 1) have confirmed that the fault is capable, having produced surface ruptures during the Holocene.

A complex fault zone, about 4 m wide, with synthetic and antithetic structures, was found in the trench walls. In the eastern wall, at least two colluvial wedges can be identified, i.e., Levels 4 and 10 in Fig. 3B. Level 4 is ca. 25 cm thick, bounded downslope by a small antithetic fault. Moreover, it is slightly displaced (just a few centimetres) by a tiny fracture that is linked downwards to a major fault. The radiocarbon age of a bulk sample taken in this level (SD 65 in fig. 3B, Table 1) is 3640-3480 BC.

ID	Radiocarbon Age (BP)	δ13C (‰)	Calibrated ages (BC) (Range 2σ)
SD61	4070±45	-25.6±0.5	2,760-2,470 (81.3%)
SD62	18944±80	-20.8±0.8	21,100-20,550 (95.4%)
SD64	7858±60	-38.3±0.7	7,030-6,570 (95.4%)
SD63	6359±60	-29.3±0.6	5,470-5,220 (95.4%)
SD65	4717±45	-38.4±0.5	3,640-3,480 (53.8%)
SD43	14960±65	-31.3±0.5	16,430-16,010 (95.4%)
SD50	38344±400	-31.4±0.7	41,100-39,900 (95.4%)

Table 1: Calibrated C^{14} ages of samples (location in Figs. 3-5). All datings (AMS) carried out at Center for Dating and Diagnostics (CEDAD) of the University of Salento.

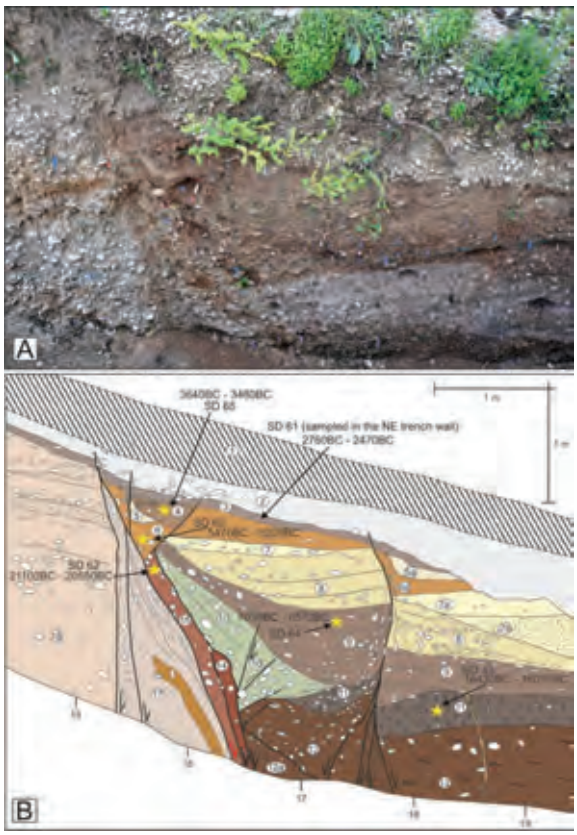

Figure 3: (A) View of the fault zone exposed in the eastern trench wall. (B) Stratigraphic sketch of the fault zone exposed in the eastern wall of the San Demetrio trench. Levels 4 and 10 are colluvial wedges.

Figure 4: Detail of west trench wall. A brown colluvium (level 3, where SD 61 was taken) is involved in the deformation, alongside the bottom layer of the gravel (level 2).

The faulted colluvial wedge dated back to 3640-3480 BC testifies to two surface faulting events, one slightly before this age and the other younger. Just above level 4, a thin colluvial layer (level 3), partly making the matrix of imbricated gravels (bottom of level 2), is also deformed, and displaced by a few centimetres (Figs. 3 and 4). Its calibrated age (2,760-2,470 BC, Table 1) is the *terminus post quem* the most recent surface faulting event registered in the trench.

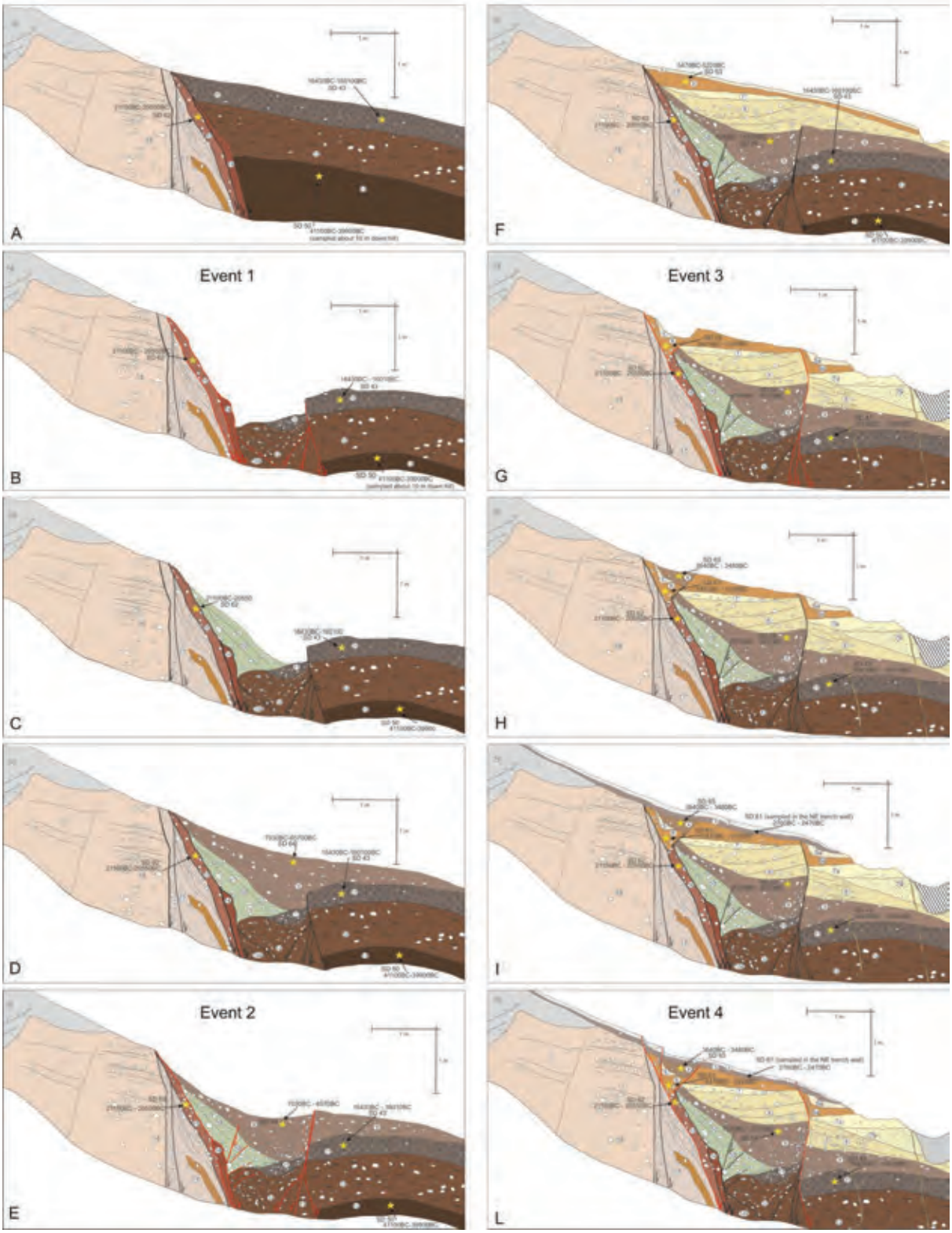

Figure 5: Reconstruction of the whole sequence of depositional and surface faulting events. In red the activated fault planes.

Other two surface faulting events can be inferred observing the bottom part of the sequence exposed in the eastern trench wall. Here, an about 1 meter thick colluvial wedge, constituted of coarse gravels (Level 10) is clearly visible (Fig 3). It is characterised by a very steep attitude of the stratification and it is downthrown by a

small synthetic fault, linked in depth to the major fault. This small fault does not cut layers younger than level 9, whose upper part was dated back to 7,030-6,570 BC (Table 1). This geometry should indicate the occurrence of two additional older events.

DISCUSSION

The following sequence of depositional and surface faulting events can be inferred from the stratigraphy exposed in the eastern trench wall (Fig. 5):

In the Latest Pleistocene, the stratigraphy was that shown in cartoon A of Fig. 5. Faulting had already affected the slope, but the first evidence of a paleoearthquake is that provided by level 15, dated 21,100-20,550 BC, which coated the fault zone already before Event 1.

A strong earthquake (Event 1, cartoon B of Fig. 5) caused a gravity graben to open; levels 12 and 11 (this last dated back to 16,430-16,010 BC) were down faulted of about 80 cm.

Subsequently, a very thick (1 m) colluvial wedge formed (level 10, cartoon C of Fig. 5), demonstrating a strong magnitude of the correlated surface faulting event.

The gravel deposition of level 9 completed the filling of the gravity graben and smoothed the fault scarp caused by Event 1 (cartoon D of Fig. 5). The age of Event 1 is also constrained by the age of the upper part of this level, dated back to 7,030-6,570 BC.

A second strong event occurred (Event 2, Cartoon E of Fig. 5). Also during this event a gravity graben formed, as demonstrated by the clear dragging of the gravel of the upper part of Level 9 along the antithetic fault that limits the graben downslope. The height of the fault scarp associated to Event 2 was about 10-20 cm.

During this event, the colluvial wedge 10 was faulted by minor faults. The ages of levels 9 (7,030- 6,570 BC) and 6 (5,470-5,220 BC) are respectively terminus post quem and ante quem for Event 2.

The gravel deposition of levels 8, 7, 6, and 5 filled the gravity graben and smoothed the fault scarp related to Event 2 (Cartoon F of Fig. 5).

A moderate earthquake displaced the sequence (Event 3, Cartoon G of Fig. 5), causing a few centimetres high, down dip throw and a small trench, about 25 centimetres deep. A small colluvial wedge formed (Level 4), filling the trench (Cartoon H of Fig. 5). This colluvial wedge dates back to 3,640-3,480 BC.

During the last part of the Holocene *optimum climaticum* (ca. 5000 cal BP, Kalis et al., 2003; Giraudi et al., 2011), thin colluvial deposits characterised the slope (level 3, Cartoon I of Fig. 5).

Sampled in the western trench wall (Fig. 4), they date back to 2,760–2,470 BC. This colluvial layer partly makes the matrix of the imbricated gravel (bottom of level 2).

One more moderate event occurred (Event 4, Cartoon L of Fig. 5) that displaced for a few centimetres levels 4 and 3. Also the bottom of level 2 was plainly involved in the deformation (see Figs. 3 and 4). The age of Event 4 is constrained by the age of level 3. However, since the gravel sealing the faults (upper part of level 2, Fig. 3) is most likely historical, because correlating with nearby layers with Roman pottery (I century AD), the age of this last event is likely much younger than the age of level 3.

In conclusion, a number of surface faulting events took place during the Holocene along the San Demetrio Fault, with variable offsets from few centimetres to about 80 cm. The latter would imply a magnitude sensibly larger than that of the 2009 L'Aquila earthquake, likely >6.5. Further trench investigations along this fault would be useful to confirm and hopefully improve the present picture of the local seismic hazard. However, the now knowledge already confirms the key role of this fault in the recent evolution of the eastern edge of the L'Aquila tectonic depression.

Acknowledgements: We thank Valeria Eulilli, Fernando Ferri and Luca M. Puzzilli for the geophysical investigations.

References

Bagnaia, R., A. D'Epifanio and S. Sylos Labini, (1992). Aquila and subaequan basins: an example of Quaternary evolution in Central Apennines, Italy. *Quaternaria Nova.* II, 187-209 (preprint spec. number 1, 1-23- 1989).

Bertini, T. and C. Bosi, (1993). La tettonica quaternaria nella conca di Fossa (L'Aquila). *Il Quaternario.* 6, 293-314.

Blumetti, A.M., (1995). Neotectonic investigations and evidence of paleoseismicity in the epicentral area of the January-February 1703 Central Italy earthquakes. In: (Leonello Serva Editor). *Perspectives in Paleoseismology*. Bulletin of the American Association of Engineering Geologists, Special Volume n. 6, Boston, 83-100.

Blumetti, A.M. and L. Guerrieri, (2007). Fault-generated mountain fronts and the identification of fault segments: implications for seismic hazard assessment, *Boll. Soc. Geol. It.* (Ital. J. Geosci.), 126 (2) 307-322.

Blumetti, A.M., L. Guerrieri, and E. Vittori, (2013). The primary role of the Paganica-San Demetrio fault system in the seismic landscape of the Middle Aterno Valley basin (central Apennines). *Quaternary International.* http://dx.doi.org/10.1016/j.quaint.2012.04.040.

Boncio, P., G. Lavecchia, and B. Pace, (2004). Defining a model of 3D seismogenic sources for Seismic Hazard Assessment applications: the case of central Apennines (Italy). *Journal of Seismology*. 8 407-425.

Cinti, F.R., D. Pantosti, P.M. De Martini, S. Pucci, R. Civico, S. Pierdominici, L. Cucci, C.A. Brunori, S. Pinzi, and A. Patera, (2011). Evidence for surface faulting events along the Paganica fault prior to the April 6, 2009 L'Aquila earthquake (Central Italy). *Journal of Geophysical Research*. 116, B07308.

D'Agostino, N., S. Mantenuto, E. D'Anastasio, R. Giuliani, M. Mattone, S. Calcaterra, P. Gambino, and L. Bonci, (2011). Evidence for localized active extension in the central Apennines (Italy) from global positioning system observations. *Geology*. 39, 291-294.

Galadini, F. and P. Galli, (2000). Active tectonics in the central Apennines (Italy) e input data for seismic hazard assessment. *Natural Hazard.* 22, 225-270.

Galli, P., B. Giaccio and P. Messina, (2010). The 2009 central Italy earthquake seen through 0.5 Myr-long tectonic history of the L'Aquila faults system. *Quaternary Science Reviews.* 29, 3768-3789.

Galli, P.A.C., B. Giaccio, P. Messina, E. Peronace, and G.M. Zuppi, (2011). Palaeoseismology of the L'Aquila faults (Central Italy, 2009, Mw 6.3 earthquake): implications for active fault linkage. *Geophysical Journal International*. 187, 1119-1134.

Giaccio, B., P. Galli, P. Messina, E. Peronace, G. Scardia, G. Sottili, A. Sposato, E. Chiarini, B. Jicha and S. Silvestri, (2012). Fault

and basin depocentre migration over the last 2 Ma in the L'Aquila 2009 earthquake region, central Italian Apennines. *Quaternary Science Reviews.* 56, 69-88.

Giraudi C., M. Magny, G. Zanchetta and R.N. Drysdale (2011). The Holocene climatic evolution of Mediterranean Italy: A review of the continental geological data. *The Holocene*. 21, 105-115.

Kalis, A.J., J. Merkt and J. Wunderlich, (2003). Environmental changes during the Holocene climatic optimum in central Europe-human impact and natural causes. *Quaternary Science Reviews*. 22, 33–79.

Moro, M., V. Bosi, F. Galadini, P. Galli, B. Giaccio, P. Messina and A. Sposato, (2002). Analisi paleosismologiche lungo la faglia del M. Marine (alta valle dell"Aterno): risultati preliminari. *Il Quaternario*. 15, 267–278.

Roberts, G.P. and A.M. Michetti, (2004). Spatial and temporal variations in growth rates along active normal fault systems: An example from the Lazio-Abruzzo Apennines, Central Italy. *J. Struct. Geol*. 26, 339–376.

Working Group MS–AQ, (2010). *Microzonazione sismica per la ricostruzione dell'area aquilana*. Regione Abruzzo. Dipartimento della Protezione Civile, L'Aquila, 3 vol. + Cd-rom.

INQUA Focus Group on Paleoseismology and Active Tectonics

Local seismic hazard from detailed geologic investigations: the Avezzano town in the epicentral area of the M7, 1915 earthquake (Fucino basin, central Italy)

Boncio, P. (1), Milana, G. (2), Cara, F. (2), Di Giulio, G. (3), Di Naccio, D. (3), Famiani, D. (2), Galadini, F. (2), Rosatelli, G. (1), Vassallo, M. (3)

(1) Dip. DiSPUTer, G. D'Annunzio University, Chieti, Italy. Email: pboncio@unich.it
(2) Istituto Nazionale di Geofisica e Vulcanologia, Rome, Italy
(3) Istituto Nazionale di Geofisica e Vulcanologia, L'Aquila, Italy

Abstract: *We present the results of a study on the local seismic hazard of the Avezzano town, located in the epicentral area of the large 1915 central Italy earthquake. The study consists of a "Level 1" seismic microzonation, obtained by detailed geological investigations and numerous HVSR analyses. The area is susceptible to almost all the site effects that we could expect after a large earthquake, such as slope instabilities (mostly rock falls), soil liquefaction, coseismic surface faulting and, stratigraphic amplifications of the ground motion, including 2D effects.*

Key words: *Central Italy, local seismic hazard, seismic microzonation, site effect, subsurface geological model.*

INTRODUCTION

The town of Avezzano was completely destroyed by the January 13, 1915 M7.0 earthquake (Intensity XI on the MCS scale). The severity of the damage was certainly due to the vicinity of the town to the seimogenic source, as the town is located nearly in the hanging wall of the SW-dipping Fucino normal fault, activated by the 1915 earthquake (see Fig. 1 for location). Nevertheless, there are reasons to believe that the ground shaking was significantly amplified by local geologic conditions. In fact, Avezzano is located within the Fucino basin, a continental basin formed during Quaternary times due to the activity of the Fucino normal fault system (Fig. 1).
The local seismic hazard of the Avezzano town is studied within a project of Seismic Microzonation (SM). In this work we present the Level 1 of SM, which is the first step of an in-depth SM study according to the Italian guidelines for SM (Level 3 is the maximum level of investigation and includes the numerical quantification of the ground motion; Working Group SM, 2008).

GEOLOGICAL SETTING

The Fucino basin is a Quaternary graben located in the core of the central Apennines of Italy. Its evolution is related to the activity of two main fault systems. The first system strikes NW-SE and dips to the SW (Fucino normal fault system); the second system strikes WSW-ENE and dips to the SSE (Tre Monti fault system). Though the SSE-dipping Tre Monti system had an important role during the early evolution of the basin, the master fault of the graben is the SW-dipping Fucino fault system (Galadini and Messina, 1994). Seismic reflection data show a typical half-graben sedimentary infill in the hanging wall of the Fucino fault, with a maximum thickness of the Quaternary sediments up to ~1000 m (Cavinato et al., 2002). In the central part of the basin the stratigraphy is dominated by fine-grained lacustrine sediments (silt and clay). Along the perimeter of the basin, medium-to-coarse-grained fluvial, alluvial fan, and slope-derived deposits are interfingered with lacustrine sediments. The graben hosted a large lake, which was drained at the end of the XIX century. The Quaternary continental deposits cover unconformably a bedrock formed by Mesozoic-to-Middle Miocene carbonates, cropping out in the Mt. Salviano and Tre Monti ridges, and by Late Miocene siliciclastic turbidites, mostly buried by the Quaternary sediments. The Avezzano town is located in the north-western corner of the Fucino basin. Its reconstruction after the 1915 earthquake took place mostly along the marginal part of the basin, at the piedmont of the Mt. Salviano and Tre Monti ridges. In more recent times the urbanization expanded also towards the central part of the basin, even though the most depressed, flat area of the basin is devoted to agricultural activity (i.e., most of Lac3 in Fig. 1b), and ordinary urbanization is not allowed.

METHODS AND DATA

The Level 1 of SM is an indispensable step for a SM activity. All the basic geologic constraints are collected in this phase. The main aim of the Level 1 SM is the detailed reconstruction of the shallow subsurface geology by using original field mapping data, pre-existing subsurface data, and new geophysical data from recordings of ambient seismic noise. The Level 1 SM of Avezzano was organised in 4 phases:
1) collection, quality-selection and georeferencing of all the pre-existing geological, geognostic and geophysical investigations. Overall, we collected 435 data points, including 160 wells (geognostic or for water exploration/exploitation) 35 of which drilled up to the geologic bedrock (maximum well depth 270 m; Fig. 1a).
2) 1:5,000-scale geologic and geomorphologic mapping and construction of detailed geologic sections (Figs. 1, 2).

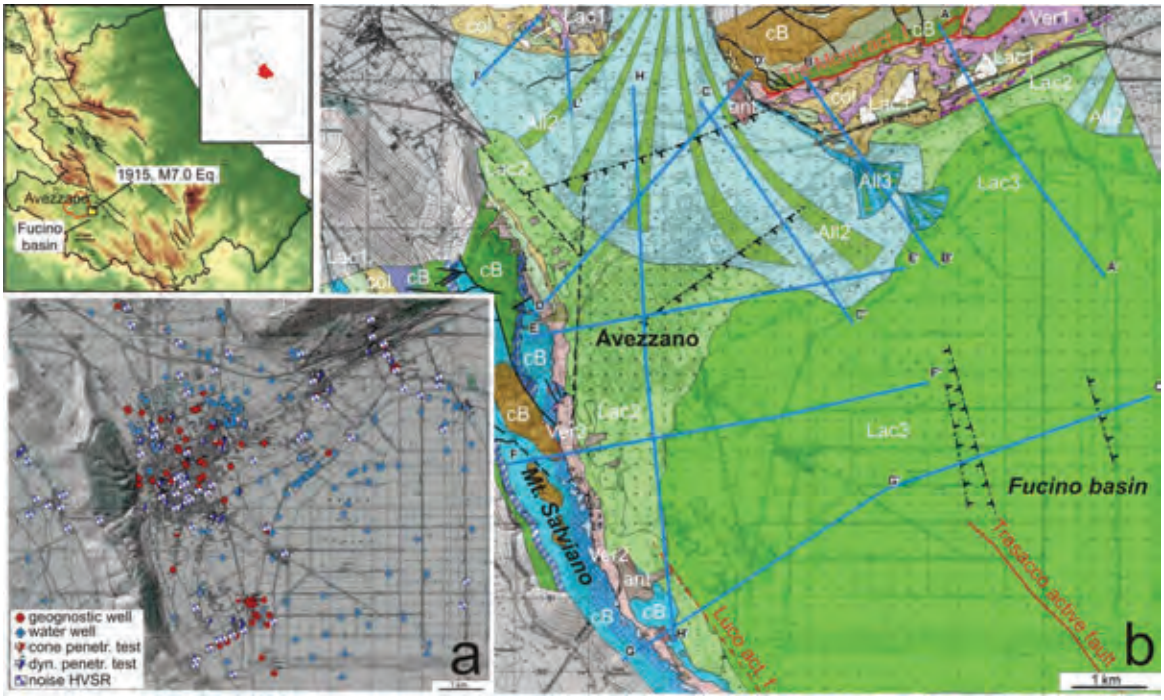

Figure 1: Location of the Avezzano town in the Fucino basin. a) Pre-existing sub-surface data collected for Level 1 SM (HVSR include pre-existing and new data); b) geological-technical map obtained from 1:5,000 field survey. Lac: lacustrine deposits (1 = Early-Middle Pleistocene; 2 = Late Pleistocene; 3 = Latest Pleistocene-Holocene); All: alluvial deposits (numbers as for Lac); Ver: slope-derived deposits (numbers as for Lac): col: colluvium; ant: anthropic infill; cB: carbonate bedrock (pre-Quaternary).

3) Single-station recording of ambient seismic noise (65 new recordings) and analysis with the Horizontal-to-Vertical Spectral Ratio technique (HVSR), in order to identify: i) the zones likely unaffected by amplification of the ground motion (flat H/V); ii) the zones characterized by site amplification; iii) the likely resonance frequency (F0) for the amplifying sites, and iv) the relationships between Fo and the local stratigraphy. The last point has important implications on how HVSR data can be used to infer the depth to the seismic bedrock in areas where other geologic-geophysical data are lacking (Fig. 2).
4) Synthesis of the data in a map of homogeneous microzones (Fig. 3).

RESULTS

The shallow subsurface geology of the Avezzano area can be synthetically divided in three typologies:
A) Simple basin-edge geometry; B) Sharp basin termination due to boundary normal fault; and C) B-type geometry covered by a thick layer of fan gravels (zone north of Avezzano, covered by the large Valle Majelama alluvial fan).
A) The simple basin-edge geometry is shown by section G of figure 2. It characterizes the western edge of the Fucino basin. Section G is constrained by a number of deep geognostic wells, some of which drilled up to the carbonate bedrock. East of the geognostic wells the depth of the bedrock is constrained by seismic reflection data (Cavinato et al., 2002). The western part of the section is characterized by a nearly-horizontal surface on the carbonate bedrock carved by the water of the Fucino Lake during the last glaciation, when the lake level was at a maximum height (~18-20 ka ago; Giraudi, 1988). To the east, the continental infill shows a progressive thickening towards the centre of the basin (~200 m below point G', further thickening eastwards). We performed a number of noise recordings along the section in order to calibrate the HVSR analyses with independent geologic data. We observed clear peaks in the H/V curves at fundamental frequencies (F0) well-correlated to the thickness of the Quaternary lacustrine infill. The F0 decreases to the east, varying from 1.7 to 1.0 to 0.7 Hz as the bedrock deepens (0.4 Hz ~3 km NE of point G', not shown in fig. 2). These results have two significant implications, showing i) the value of HVSR data for discovering the stratigraphic amplifications and their lateral variations also in short horizontal distances; and ii) the potential of F0 from HVSR for constraining the bedrock depth.
B) The sharp basin termination due to a boundary normal fault is shown by section A, representative of the northern edge of the basin. The basin deepens sharply (~150 m) in the hanging wall of a boundary normal fault located at the base of the Tre Monti ridge. The interpretation of the HVSR data is less straightforward. In fact, the H/V curves show two peaks. The first peak occurs at low frequency (0.5 Hz), and is probably related to the deep bedrock. The second peak is at higher frequency (~1 Hz), and is perhaps generated by contrasts of impedance within the Quaternary stratigraphic sequence. Often the two peaks coexist (F0 and F1). This might be related to a more heterogeneous stratigraphy, probably due to the sedimentation

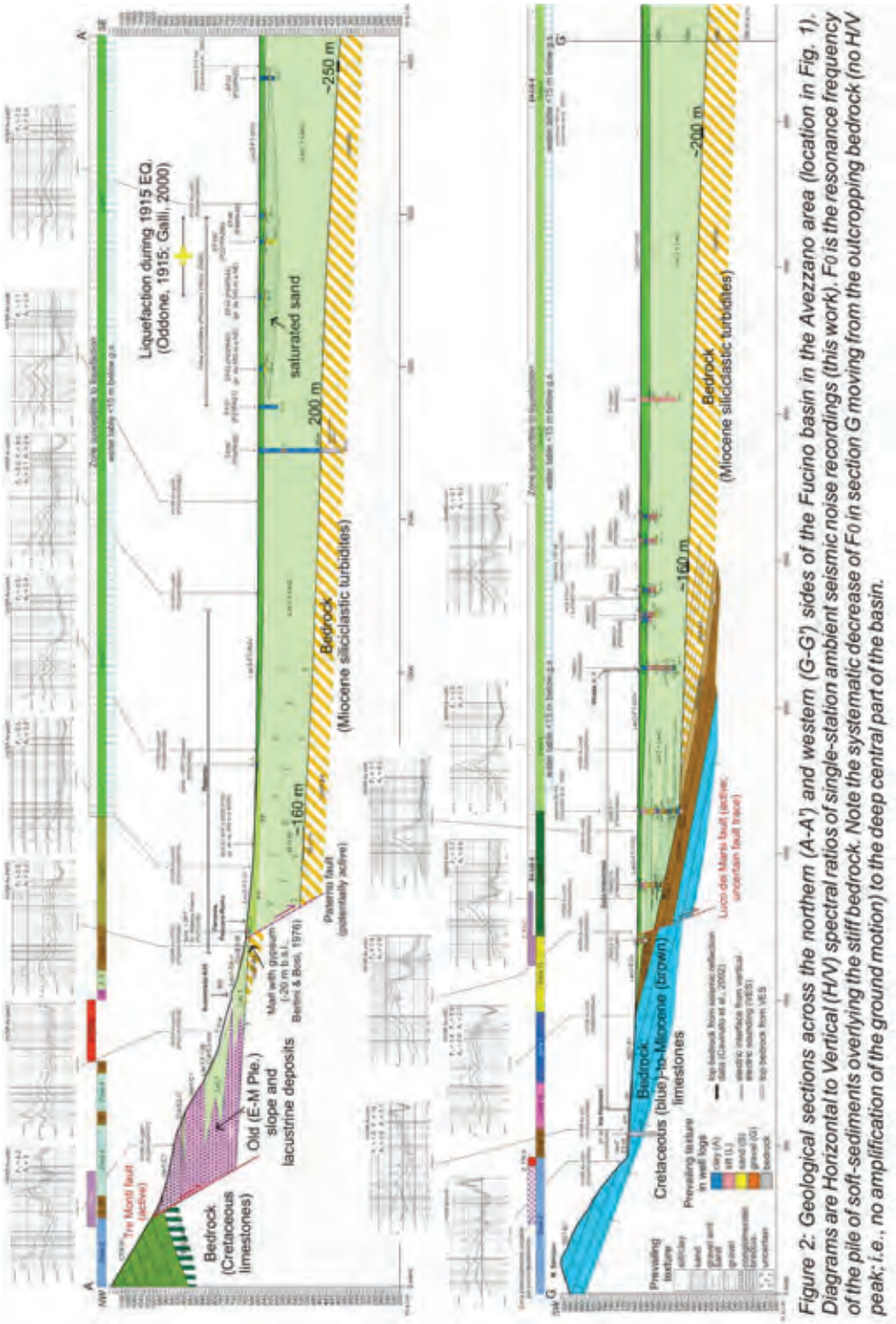

Figure 2: Geological sections across the northern (A-A') and western (G-G') sides of the Fucino basin in the Avezzano area (location in Fig. 1). Diagrams are Horizontal to Vertical (H/V) spectral ratios of single-station ambient seismic noise recordings (this work). F0 is the resonance frequency of the pile of soft-sediments overlying the stiff bedrock. Note the systematic decrease of F0 in section G moving from the outcropping bedrock (no H/V peak; i.e., no amplification of the ground motion) to the deep central part of the basin.

within the basin of large volumes of coarse-grained sediments feed by the footwall of the normal fault. Unfortunately, the subsurface data are not sufficient to provide additional constraints.

In Figure 3 we show a map that synthesizes all the geologic and geophysical (HVSR) data into zones that can be considered homogeneous from a seismic response perspective. The map indicates zones without appreciable amplifications (dark blue; i.e., stiff bedrock in nearly horizontal topography) and zones susceptible to amplification due to topographic (light blue) or stratigraphic (other colours) conditions. The HVSR analyses indicate significant amplifications at F0 that is decreasing towards the centre of the basin. The F0 is higher (> 1 Hz up to 2.5-5.0 Hz) along the perimeter of the basin. Towards the centre of the basin, F0 is <1 Hz, down to values as low as 0.4 Hz.

The map also indicates zones susceptible to coseismic permanent deformation, including: 1) zones susceptible to slope instability, particularly rock falls along the steep slopes of fractured rocks bordering the basin; 2) soil liquefaction, both along the urbanized perimeter of the basin and within the youngest, central part of the basin; and 3) coseismic surface faulting along normal faults. All the phenomena were documented during the 1915 earthquake (Oddone, 1915; Galli, 2000; Castenetto and Galadini, 1999 and references therein). The active normal faults near Avezzano are secondary structures compared to the main Fucino normal fault, which borders the eastern side of the basin. In fact, the Luco and Trasacco faults are antithetic and synthetic splays, respectively, while the Tre Monti fault is a hanging wall structure nearly orthogonal to the main fault. Nevertheless, paleoseismological data suggest that all of them can be activated contemporaneously with the main fault during earthquakes as large as the 1915 one (Castenetto and Galadini, 1999).

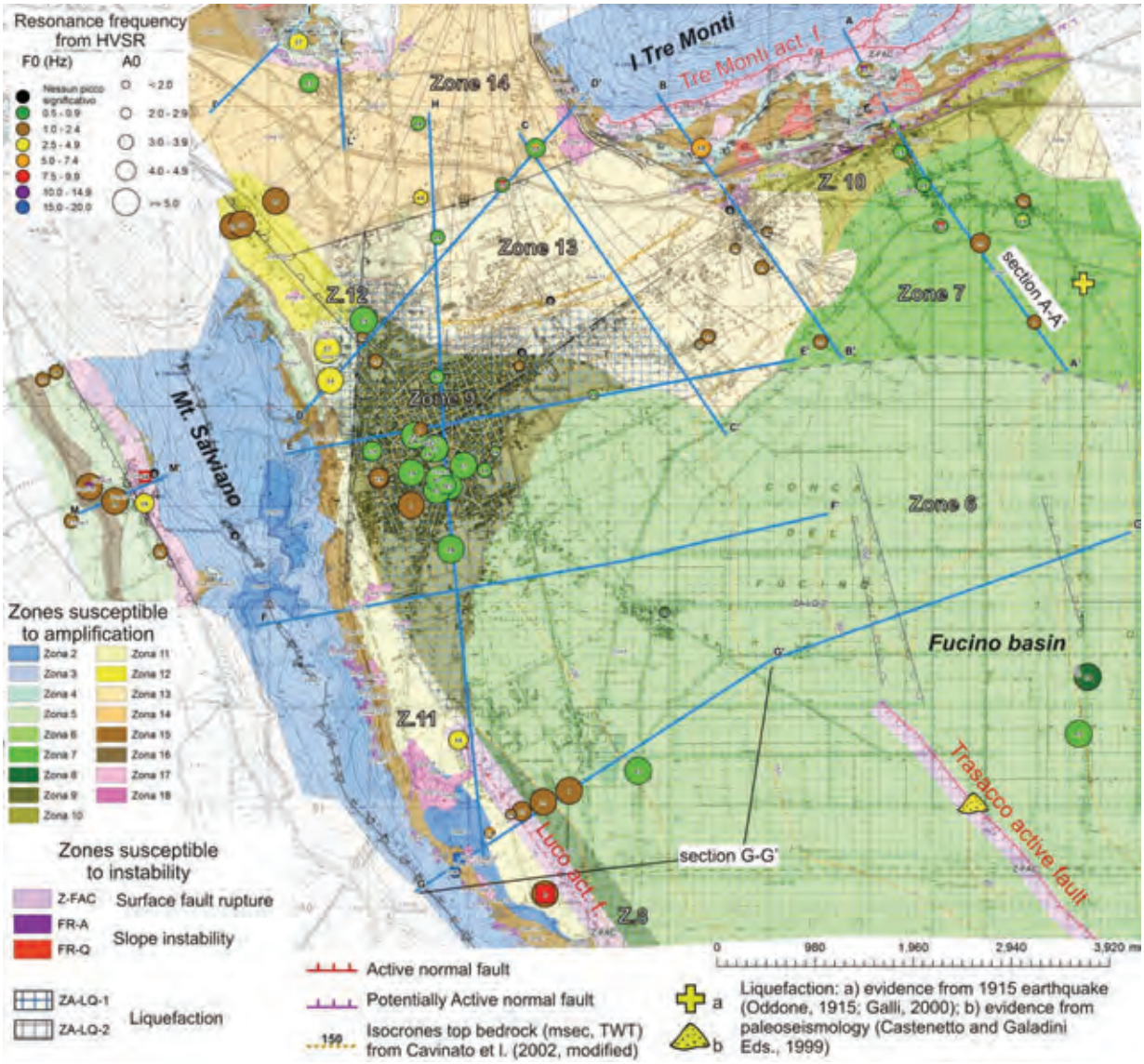

Figure 3: Level 1 seismic microzonation map of the Avezzano area with resonance frequencies from noise HVSR analyses (symbol size is proportional to the amplitude of the H/V peak, A0). Dark blue areas (Zone 1) are zones without amplification of the ground motion (stiff bedrock in nearly horizontal topography). Other zones are susceptible to site amplification of the ground motion. Zones susceptible to liquefaction (ZA-LQ) are characterized by saturated sand bodies within the first 20 m depths; ZA-LQ-2 (corresponding to Lac3 unit of Fig. 1) is characterized by larger uncertainties (less data) than ZA-LQ-1. ZA-FAC are 150 m-wide in the hanging wall of the fault and 30 m-wide in the footwall, according to Boncio et al. (2012). A larger ZA-FAC is shaped for the Luco fault due to uncertainties in fault trace location. Zones susceptible to slope instability (FR; A= active, Q= dormant) include susceptibility to rock fall (eastern side of Mt. Salviano ridge) and reactivation of active or dormant soil landslides (S of Tre Monti).

Acknowledgements: The project is funded by the Regione Abruzzo local authority (POR-FESR, IV, 3.1.c) and the Italian National Department of Civil Protection (art. 11 del DL 39/2009).

References

Boncio, P., P. Galli, G. Naso & A. Pizzi, (2012). Zoning Surface Rupture Hazard along Normal Faults: Insight from the 2009 Mw 6.3 L'Aquila, Central Italy, Earthquake and Other Global Earthquakes. *Bull. Seism. Soc. Am.*, 102, 918-935.

Castanetto, S., F. Galadini, Eds. (1999). *13 Gennaio 1915. Il terremoto della Marsica.* Servizio Sismico Nazionale e C.N.R. Istituto di Ricerca sulla Tettonica, Roma, 788 pp.

Cavinato, G., C. Carusi, M. Dall'Asta, E. Miccadei, & T. Piacentini, (2002). Sedimentary and tectonic evolution of Plio-Pleistocene alluvial and lacustrine deposits of Fucino Basin (central Italy). *Sediment. Geol.*, 148, 29–59.

Galli, P., (2000). New empirical relationships between magnitude and distance for liquefaction. *Tectonophysics*, 324, 169-187.

Giraudi, C., (1988). Evoluzione geologica della piana del Fucino (Abruzzo) negli ultimi 30.000 anni. *Il Quaternario*, 1(2), 131-159.

Oddone, E., (1915). Gli elementi fisici del grande terremoto marsicano fucense del 13 gennaio 1915. *Boll. Soc. Sismol. It.,* 19, 71-216.

Working Group SM, (2008). *Indirizzi e Criteri per la Microzonazione Sismica*. Conferenza delle Regioni e delle Province autonome, Dipartimento della Protezione Civile, Roma, 3 vol. e Cd-rom.

INQUA Focus Group on Paleoseismology and Active Tectonics

Evidence of paleoseismicity within the West Quebec Seismic Zone, eastern Canada, from the age and morphology of sensitive clay landslides

Brooks, G.R.

Natural Resources Canada, Geological Survey of Canada, 601 Booth Street, Ottawa, ON, Canada. Email: Greg.Brooks@NRCan-RNCan.gc.ca

Abstract: *Two groups of 13 and 12 sensitive clay landslides aged between 5000-5400 and 980-1060 cal BP, respectively, are present within a dataset of 50 dated landslides from the Ottawa Valley, eastern Canada. The landslides within these groups include side-scarp failures, failures involving the simultaneous collapse of deposits along both sides of a stream course, and failures located along the sides of a confined valley. Both landslide groups are interpreted to have been triggered by paleoearthquakes, based on the setting and morphology of the landslides, and an assessment of other possible mechanisms. The estimated magnitudes are M_w 6.4 (5000-5400 cal BP event) and M_w 6.1 (980-1060 cal BP event). Side-scarp landslides with intact debris fields are the most promising morphology to date for identifying groups of commonly-aged sensitive clay landslides.*

Key words: *Paleoearthquakes, sensitive clay, landslides, radiocarbon chronology, Champlain Sea.*

INTRODUCTION

Historically, regional seismicity in eastern Canada has been concentrated primarily within southern and western Quebec and eastern Ontario, along a reactivated Iapetan rift system and along a Cretaceous hotspot trace (Adams and Basham, 1991). Major Canadian urban centres in this region that are vulnerable to earthquake hazards are Montreal, Quebec City and Ottawa, Canada's national capital. One of the seismically active areas is the West Quebec Seismic Zone (WQSZ) that encompasses parts of western Quebec, eastern Ontario, and northern New York State (Fig. 1). Significant historic seismic events in the WQSZ include the AD 1732 Montreal (M 5.8), 1935 Temiscaming (M 6.1), and 1944 Cornwall (M 5.8) earthquakes (Lamontagne, 2010); however, no evidence of historical or prehistorical fault displacement has been recognized within the WQSZ.

Large areas of the St. Lawrence and Ottawa valleys in southern-southwestern Quebec and southeastern Ontario are underlain by glaciomarine silty-clay and clayey-silt sediment that accumulated within the Champlain Sea during the late Pleistocene-early Holocene, following the local retreat of the Laurentide Ice Sheet. In many locations, these sediments are geotechnically sensitive and prone to large (>1 ha) earth flows and earth spreads that can retrogress rapidly many hundreds of metres or more into a slope. (Torrance, 2012). In the Ottawa Valley, approximately 250 sensitive clay landslides are delineated on surficial geology maps. Most of these failures occurred prehistorically and are of unknown age. Historically, sensitive clay landslides occur every few years, most often in the spring, and at widely-dispersed locations throughout the St. Lawrence-Ottawa valleys region (Demers et al., 2014). There are also recent examples in the region where landslides have been triggered by seismic shaking, as occurred during the AD 2010 Val-des-Bois (M_w 5.0) and AD 1988 Saguenay (M_w 5.9) (Lefebvre et al, 1992; Locat, 2011).

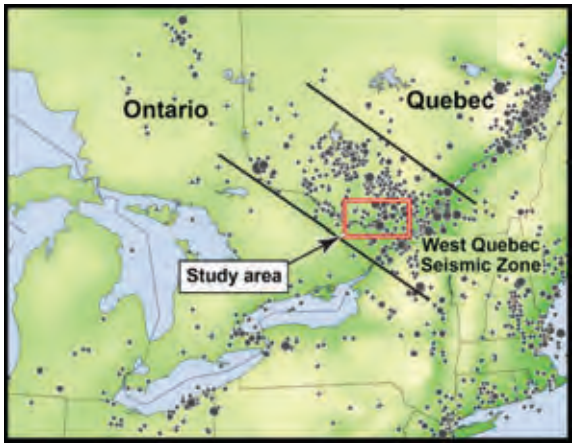

Figure 1: Map showing the seismicity (>M3) in southern Quebec and southern Ontario, eastern Canada, and the Ottawa Valley study area within the West Quebec Seismic Zone.

This paper summarizes chronologic and geomorphic evidence that two groups of similarly-aged sensitive clay landslides are the product of two paleoearthquakes within the WGSZ. New data are presented that augments previously presented results. The paper also identifies the morphology of sensitive clay landslides that are most likely to be earthquake-triggered and represents the most promising landslide target for paleoseismic investigations in the St. Lawrence and Ottawa valleys.

Methods and data

Fifty sensitive clay landslides in the Ottawa Valley (Fig. 2) have been dated by the radiocarbon analysis of woody organic materials buried within or beneath landslide debris, or sampled from the base of ponds or wetlands that developed in depressions on a landslide surface (Brooks et al., 2013; Brooks, unpublished data). Several landslides were dated from wood acquired opportunistically from construction sites. Landslides east

of Ottawa were dated primarily from an investigation of landslide ages along paleochannels of the proto-Ottawa River, while those west and north of Ottawa were dated as part of a paleoseismic investigation of the WQSZ. The ages of 21 landslides are represented by single radiocarbon dates, while those of 29 failures are interpreted from between two and 17 radiocarbon ages.

RESULTS AND DISCUSSION

The calibrated ages of the sensitive landslides span about 8000 years (Fig. 3), which extends back to the time of the recession of the Champlain Sea from the Ottawa Valley. The ages occur reasonably regularly over this timespan, but there are two distinct age groupings between approximately 5000-5400 and 980-1060 cal BP consisting of 13 and 12 landslides, respectively. The greater range of the ages in the older group is the product of uncertainty produced by the calibration of the radiocarbon ages to sidereal years and not from large analytical uncertainties with the radiocarbon dates. Eleven of the landslides forming the 5000-5400 cal BP age group were first reported by Aylsworth et al. (2000); all are located east of Ottawa (Fig. 2). Each is the product of a failure that retrogressed into the steep back margin of a paleochannel or terrace. (This setting of failure is hereafter referred to as a "side-scarp" landslide.) The source areas within three sub-groups of two, three and two landslides are spaced less than a kilometre apart. The debris fields of all 11 landslides are splayed onto the adjacent paleochannel or terrace surface and remain well-preserved in the landscape (Fig. 4).

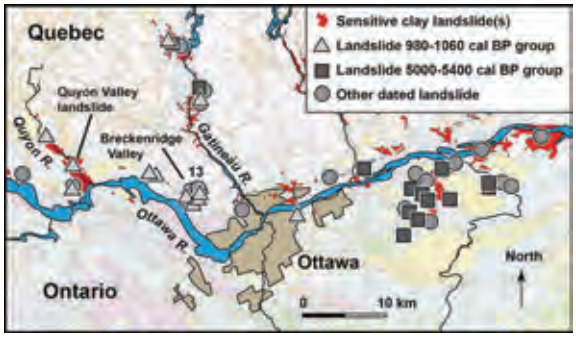

Figure 2: Map showing the locations of the 50 dated sensitive clay landslides in the Ottawa Valley study area (data from Aylsworth et al. 2000; Brooks, 2013; Brooks et al., 2013; Brooks unpublished). The landslides within the 980-1060 and 5000-5400 cal BP age groups are each represented by distinct symbols. The "13" denotes thirteen closely-spaced landslides dated within Breckenridge Valley.

The other two landslides within the 5000-5400 cal BP group are located north of Ottawa within tributary valleys of the Gatineau River (Fig. 2). Both landslide source areas are large (~7.2 and 2.4 km^2) and both landslides are the product of the simultaneous collapse of glaciomarine deposits along both sides of the respective valley bottom. These two landslides were dated following field work in 2013 and augment the 11 side-scarp landslides located east of Ottawa. The two most-distant landslides in the 5000-5400 cal BP group are located ~90 km apart.

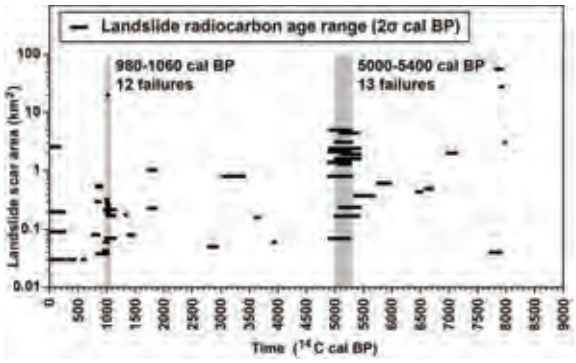

Figure 3: Plot of landslide scar/feature area versus the interpreted calibrated radiocarbon age for each of the 50 dated landslides in the Ottawa Valley study area. Light grey zones highlight the two groups of similarly-aged landslides, as discussed in the text (data from Aylsworth et al., 2000; Brooks, 2013; Brooks et al., 2013; Brooks, 2014; Brooks, unpublished).

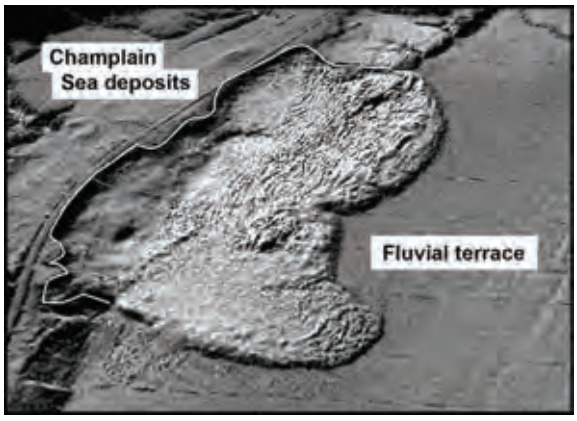

Figure 4: Lidar DEM showing an example of a side-scarp sensitive clay landslide that has retrogressed into the back-slope of a fluvial terrace (© Government of Quebec). The failed debris forms a well-preserved lobe splayed onto the terrace.

The landslides forming the 980-1060 cal BP group are located within, west or north of Ottawa (Fig. 2) and consist of a range of morphologies. Four are side-scarp landslides situated along the back-slopes of proto-Ottawa River terraces (Fig. 4). The debris fields are splayed onto the respective terrace surfaces and are well preserved, analogous to the side-scarp landslides in the 5000-5400 cal BP group located east of Ottawa. Four of the failures are a subset of 13 dated landslides within a cluster of 31 landslides along Breckenridge Valley (Fig. 2). Two landslides are located along Quyon River valley, including the Quyon Valley landslide scar covering ~28 km^2 and one of the largest sensitive clay landslides in eastern Canada (Brooks, 2013). The second is located about one kilometer upstream of the Quyon Valley

landslide and flowed into the valley bottom. The remaining two landslides are located along tributaries of the Gatineau River and were dated from field work in 2013 (Fig. 2). Both of these originated from the margin of older large landslide scars, one of which is the most northerly landslide in the 5000-5400 cal BP group. The two most-distant landslides in the 980-1060 cal BP group are located ~64 km apart.

The interpreted radiocarbon ages for each of the landslides within the two age groups are ranges of tens to several hundred years rather than being specific to-the-year age determinations. Nevertheless, the occurrences of two groups of 13 and 12 landslides with similar age ranges provide compelling circumstantial evidence that each group is the product of a common triggering mechanism. Mechanisms usually attributed to the inferred synchronous occurrence of landslides are severe rainstorms and earthquakes (Jibson, 2009), but for sensitive clay landslides the scenario of a wet spring following a winter of high snow accumulation is an additional meteorological consideration.

A commonly recognized trigger for sensitive clay landslides is fluvial erosion along the toe of a valley-side slope in combination with saturated soil conditions (Torrance, 2012), suggesting that a meteorological mechanism may be a reasonable cause for either landslide age group. Severe rainstorms unquestionably have occurred in eastern Canada, however, there are no examples of large (>1 ha) sensitive clay landslides having been triggered by a historical severe rainstorm, despite the well-documented occurrences of widespread small-scale landslides and significant bank erosion within sensitive clay areas (Brooks, 2013). There are numerous examples of large (>1 ha) historical sensitive clay landslides in the St, Lawrence and Ottawa valleys occurring during April and May following a high snowfall winter-wet spring, but no examples of a cluster of large sensitive clay landslides being triggered. Instead, landslides triggered in the spring occur irregularly every few years at widely dispersed locations regionally within the glaciomarine areas of southern Quebec-southeastern Ontario.

As recognized by Aylsworth et al. (2000), an important consideration for assessing the meteorological mechanisms is the setting of the side-scarp landslides with preserved debris lobes, which are located on paleochannel and terrace surfaces of the proto-Ottawa River. The lack of truncation of the debris lobes indicates that the paleochannels or terraces surfaces had been abandoned by the river prior to the occurrence of the landslides. Thus the initiating failures at these sites were not the product of over-steepening of the slope from river erosion, negating a major flood, whether rainstorm- or snowmelt-driven, as a triggering mechanism. Eleven and four of the landslides within the 5000-5400 and 980-1060 cal BP age groups, respectively, are side-scarp failures with intact debris lobes. Although the two meteorological mechanisms cannot be ruled out definitely, neither seem likely to have generated either group of similarly-aged landslides (Aylsworth et al., 2000; Brooks, 2013).

Several factors are supportive of an earthquake-triggering mechanism. The occurrence of the side-scarp landslides with preserved debris lobes in both landslide age groups is readily attributable to an earthquake mechanism, as is the close proximity of 2 to 4 landslides within three subgroups in each of the 5000-5400 and 980-1060 cal BP age groups. An earthquake trigger also seems the most plausible mechanism that could trigger large-scale failures concurrently on both sides of the Quyon Valley during the large Quyon Valley landslide (980-1060 cal BP group) and at the sites of the two large landslides along the Gatineau tributary valleys (5000-5400 cal BP group). Finally, multiple, large sensitive clay landslides are known to have been triggered by a significant historical earthquake in eastern Canada, as exemplified by the AD 1663 M_w 7.2±0.2 Charlevoix earthquake (Locat, 2011). Overall, the occurrences of the sensitive clay landslides within the 5000-5400 and 980-1060 cal BP age groups are best explained by paleoearthquakes in the WQSZ, as was interpreted by Aylsworth et al. (2000) and Brooks (2013).

Estimates of the paleoearthquake magnitudes are M_w 6.4 and M_w 6.1 for the 5000-5400 and 980-1060 cal BP groups, respectively, based an empirical relationship between area of landsliding and earthquake magnitude (Keefer, 1984; Rodríguez et al., 1999). Uncertainties associated with applying this relationship to the distribution of sensitive clay landslides are discussed by Brooks (2013). On balance, the two estimates are considered to be minimum magnitudes, primarily because the distribution of dated landslides almost certainly underestimates the overall distribution of landslides triggered by the paleoearthquakes, which was considered to be more important than the factors that may overestimate the magnitude.

Brooks (2014) examined the earthquake-interpreted landslides within the two age groups to identify morphological consistencies of landslides more likely to be earthquake triggered, to improve the targeting of undated sensitive clay landslides for paleoseismic investigations. As a general trend, larger (>1 km^2) sensitive clay landslides are more likely to be earthquake triggered than smaller ones. Side-scarp landslides with intact debris fields splayed onto a fluvial surface are the dominant morphology within the two age groups, especially within the 5000-5400 cal BP group, where they represent 11 of 13 landslides. In the Ottawa Valley, however, six dated side-scarp landslides with preserved debris fields have ages that fall outside of the two age groups and occur in isolation temporally or coincide with only a single other landslide. The variation in ages exhibited by these landslides indicates that single dated side-scarp landslide cannot be inferred to be paleoearthquake-triggered without significant supporting evidence. Regardless, side-scarp sensitive clay landslides with intact debris fields represent the most promising landslide morphology to target for dating landslides to identify possible paleoearthquakes (Brooks, 2014).

Sensitive clay landslides that are the product of simultaneous failures along both sides of a valley bottom

also are a promising target for paleoseismic investigations, although the sample size is small (three landslides). This morphology of landslides typically is large (>1 km^2) so they are obvious targets from the size perspective, especially when greater than 10 km^2 (e.g., Quyon Valley landslide).

Based on the ages of failures within the Ottawa Valley and elsewhere in southern Quebec (Brooks, 2014), sensitive clay landslides along confined valleys can have substantial variations in age. This at least partly reflects the triggering of landslides from active lateral stream erosion at the toe of the valley side slopes (Torrance, 2012). A relatively large number of landslides thus may need to be dated before a meaningful pattern of similar landslide ages becomes apparent in this setting relative to the other two morphologies.

CONCLUSIONS

Of the 50 dated sensitive clay landslides within the Ottawa Valley, 13 and 12 landslides fall within two age groupings of 5000-5400 and 980-1060 cal BP, respectively. Both landslide groups are interpreted to have been triggered by paleoearthquakes in the WQSZ, based on: the close proximity of two to four landslides to each other that form subgroups within each age group; the occurrence of multiple side-scarp landslides with preserved debris lobes in settings that are difficult to explain by a meteorological mechanism; and the known occurrence of multiple, large sensitive clay landslides by a significant historical earthquake in eastern Canada.

The estimated paleoearthquake magnitudes are M_w 6.4 and M_w 6.1 for the 5000-5400 and 980-1060 cal BP events, respectively.

In the Ottawa and St. Lawrence valleys of eastern Canada, side-scarp landslides with intact debris fields represent the most promising sensitive clay landslide morphology to date for identifying groups of commonly-aged landslides in paleoseismic studies.

Acknowledgements: Comments on the paper by J. Hunter are appreciated. Research on sensitive clay landslides in the Ottawa Valley has benefited greatly from the work of now-retired GSC colleagues J. Aylsworth and T. Lawrence. This research was supported by the Public Safety Geoscience Program, Earth Sciences Sector, Natural Resources Canada. This paper represents ESS Contribution 20140369.

References

Adams., J. & P. Basham, (1991). The seismicity and seismotectonics of eastern Canada. In: (Slemmons, D.B., Engdahl, E.R., Zoback, M.D., Blackwell, D.D., eds.). *Neotectonics of North America*. Geological Society of America, Decade Map. v. 1, 261-276.

Aylsworth, J.M., D.E. Lawrence & J. Guertin, (2000). Did two massive earthquakes in the Holocene induce widespread landsliding and near-surface deformation in part of the Ottawa Valley, Canada?. *Geology*. 28, 903-906.

Brooks, G.R., (2013). A massive sensitive clay landslide, Quyon Valley, southwestern Québec, Canada, and evidence for a paleoearthquake triggering mechanism. *Quaternary Research*. 80, 425-434.

Brooks, G.R., B.E. Medioli, J.M. Aylsworth & D.E. Lawrence, (2004). A compilation of radiocarbon dates relating to the age of sensitive clay landslides in the Ottawa Valley, Ontario-Québec. *Geological Survey of Canada.* Open File 7432, 58 p.

Brooks, G.R., (2014). Prehistoric sensitive clay landslides and paleoseismicity in the Ottawa Valley, Canada. In: *Landslides in Sensitive Clays: from Geosciences to Risk Management* (L'Heureux, J.-S., Locat, A., Leroueil, S. Demers, D. and Locat, J. eds.). Advances in Natural and Technological Hazards Research, v. 36, Springer, Dordrecht, 119-131.

Demers, D. and others, (2014). Inventory of large landslides in sensitive clay in the Province of Québec, Canada: preliminary analysis. In: (L'Heureux, J.-S., Locat, A., Leroueil, S. Demers, D. and Locat, J., eds.). *Landslides in Sensitive Clays: from Geosciences to Risk Management.* Advances in Natural and Technological Hazards Research, v. 36, Springer, Dordrecht, 77-89.

Jibson, R.W., (2009). Using landslides for paleoseismic analysis. In: *Paleoseismology* (McCalpin, J.P. ed.). International Geophysics. 95, 565-601.

Keefer, D.K., (1984). Landslides caused by earthquakes. *Geological Society of America Bulletin*. 95, 406-421.

Lamontagne, M., (2010). Historical earthquake damage in the Ottawa-Gatineau region, Canada. *Seismological Research Letters*. 81, 129-139.

Lefebvre, G., D. Leboeuf & P. Hornych, (1992). Slope failure associated with the 1988 Saguenay earthquake, Quebec, Canada. *Canadian Geotechical Journal.* 29, 117-130.

Locat, J., (2011). La localisation et la magnitude du séisme du 5 février 1663 (Charlevoix) revues à l'aide des mouvements de terrain. *Canadian Geotechical Journal.* 48, 1266-1286.

Rodríguez, C.E., J.J. Bommer & R.J. Chandler, (1999). Earthquake-induced landslides: 1980–1997. *Soil Dynamics and Earthquake Engineering*. 18, 325–346.

Torrance, J.K., (2012). Landslides in quick clay. In: *Landslides: Types, Mechanisms and Modeling* (Clague, J.J., Stead, D. eds). Cambridge University Press, Cambridge, 83-94.

INQUA Focus Group on Paleoseismology and Active Tectonics

paleoseismicity.org

Active faulting, earthquakes and geomorphological changes: effects on the urban evolution of the Roman town of Sybaris, Ionian sea (southern Italy)

Brunori, C.A., Alfonsi, L., Cinti, F.R.

Istituto Nazionale di Geofisica e Vulcanologia, via di Vigna Murata, 605 – 00143 Roma, Italy. Email: carloalberto.brunori@ingv.it

Abstract: *Using an 1m pixel LiDAR DEM we analyse morphological features in order to recognize the presence of an hidden fault responsible of morpho-tectonic evolution in the Sibari coastal plain (Calabria, southern Italy). In the SIbari plain is located the archaeological site of Sybaris, founded by the Greeks in 720 B.C its life went on up to the late Roman time (V-VI A.D.). The town was located within the Sibari Plain near the Crati River mouth (Ionian northern Calabria, southern Italy). Sybaris occurs in area repeatedly affected by natural damaging phenomena, as frequent flooding, high local subsidence, marine storms, and earthquakes. The 2700 long record of history of Sybaris stores the traces of these natural events and their influence on the human ancient environment through time.Among the natural disaster, we recognize two Roman age earthquakes striking the town.*

Key words: *LiDAR, high resolution DTM, Archaeo-seismology, hidden fault.*

THE RECOGNITION OF THE SYBARIS FAULT

The archaeological site of Sybaris is located in the coastal Sibari plain (CS, Calabria region, southern Italy – Figure 1). Archaeoseismic data collected at the ancient Roman town of Sybaris define a fault zone, about 1 km long, along which vertical and right lateral movements occur. The fault zone was previously unknown and is here named "Sybaris fault zone" During its life the archaeological site was destroyed by two earthquakes: one occurring at the first half of the II century A.D, and another after the VI century A.D. and possibly before the VIII century A.D. This latter event produced widespread liquefaction phenomena and surface rupture along the Sybaris fault zone (*Figure 2*). The fault has an oblique normal-dextral mechanism, compatible with the present-day E-W to ENE-WSW compressional deformation active in the Ionian offshore. We used high-resolution topographic profiles to find evidence of the Sybaris fault out of the archaeological site (Cinti et al. 2014). The band of deformations is confirmed to extend toward west and east on the base of the topographic setting across the inferred fault zone and of the riverbeds migration within the Sibari plain through time. The Sybaris fault zone reaches a length of about 10 km and has a N50°-60° strike. The archaeoseismic study of the archaeological site constitutes a unique means to deepen our knowledge of the seismotectonic of the area (Cinti et al., 2015). The recognition and characterization of the coseismic deformation affecting the structures of the Sybaris archaeological site is the objective of the present study. To identify past coseismic deformation events at Sybaris, we proceeded with (1) a systematic survey of the deformed structures, (2) an analysis of the tectonic deformation, (3) the formulation of a hypothesis for tectonics and earthquakes inferences, and (4) constraints on the timing of the deformation based on archaeological stratigraphy and absolute dating.

Figure 1: Location of the archaeological site of Sybaris (black rectangle in satellite image and upper left inset). Instrumental seismicity larger than M 4 is shown as gray stars, scaled by magnitude (Italian Seismological Instrumental and Parametric Data-Base [ISIDe], 2010). Historical earthquakes are shown as gray boxes (size-scaled by intensity degree), with the dates of occurrence. Dashed white box is the possible epicentral area of the paleoearthquake inferred in the area of the town of Castrovillari and near the Pollino range. The schematic outline of the faults (white lines) in the study area is also shown. In the upper right inset is an aerial view of the present-day setting of the archaeological study site. Satellite image from Google Earth.

Archaeoseimic Data Analisys

Coseismic features are consistently oriented fractures (see rose diagrams of figure 2), tilting, warping and clockwise horizontal rotation of walls, liquefaction and collapses (photos marked in # blue at Parco del Cavallo, and photo # green at Casa Bianca) (Figures 3-4).

The fractures cross artefacts and soft terrain with a strike ranging N50-60°. The fractures have a high-angle dip, an opening of max. 5 cm and show a prevalent right lateral displacement of 20-30 cm.

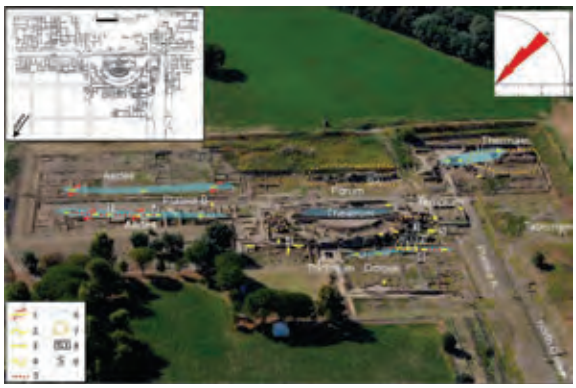

Figure 2: Locations of the coseismic features at Parco del Cavallo. The upper left inset is the plan of the site (based on a plan from Soprintendenza per i Beni Archeologici della Calabria, Copyright 2007). The background image is available at www.ilgiornaledellarte.com (last accessed October 2014). In the upper right corner, a rose diagram shows the strikes of fractures.

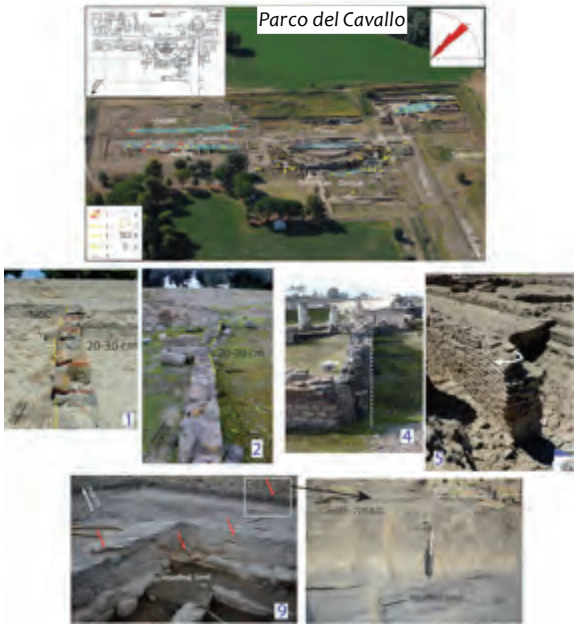

Figure 3: Parco del Cavallo Site: 1- open fracture and sense of movement; 2- collapse direction; 3- sense of rotation; 4- lateral movement; 5- fracture location as described in deformed section; 6- zone with archaeological report (Marino2012) 7- sampling for 14C dating; homogeneous characteristics of; 8- position of photos the deformation (# green).

The consistency of the orientation of the fractures along with their continuity define the presence of a brittle deformation zone within the site of Sybaris with a strike of N50-60°.

Figure 4: Casa Bianca Site: Legend of the panoramic view. 1- open fracture and sense of lateral movement; 2- warping; 3- direction of tilting; 4- sense of rotation; 5- interpolation of closely spaced fractures; 6- zone of consistent characteristics of the deformaion; 7- vast collapses; 8- TL sampling; 9- position of photos (bluesampling).

High Resolution Topography Data Analisys

The Figure 5 shows the orography of the Ionian coast and of the Sibari plain represented by the color-coded DSM (1m pixel size). DSM is the result of the raw airborne LIDAR acquisition processed data (Italian Ministry of Environment Territory and Sea Protection). LIDAR data were elaborated using QGis/ARCGis LAStools plugins.

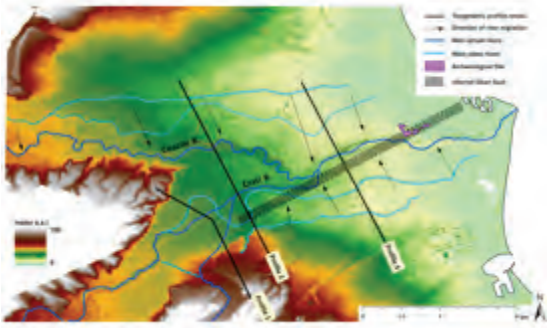

Figure 5: Shows the orography of the Ionian coast and of the Sibari plain represented by the DSM (1m pixel size). DSM is the result of the raw airborne LIDAR acquisition processed data (Italian Ministry of Environment Territory and Sea Protection).

The positions of the main actual rivers, i.e. Crati and Coscile, and of the paleorivers recognized from the analysis of the DSM and of the aerial photographs, are shown. The black arrows indicate the migration of the river courses to their actual positions. The paleoriver beds have been drawn toward the central part of the Sibari plain. This general trend is interpreted as the direct effect of the tectonic control caused by the long term activity of the Sybaris fault zone.

Three topographic profiles traced in in Figure 5 allow the recognition of morphological features describing the evolution of Sibari plain river network in relation with the activity of Sibari Fault Plane.

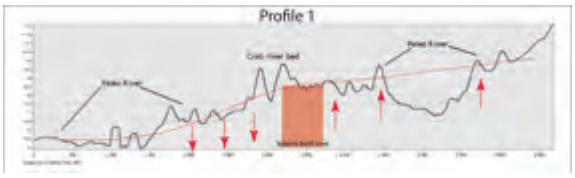

Profile 1 (Fig. 5) This is the closest to the archaeological site, where direct evidence of the fault movements are observed, it is orthogonal to the inferred fault trace and to the actual and paleo rivers beds. The profile defines an elevation difference of the topographic surface of the plain across the fault zone (see also the red line as smoothed profile). The watercourses tend to joint and are presently flowing in the hangingwall of the Sybaris fault.

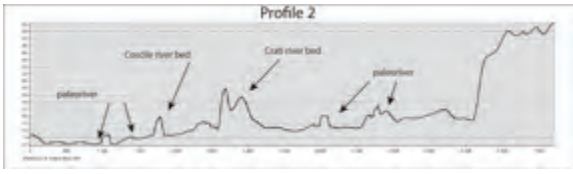

Profiles 2 (Fig. 5) This profile crosses the western tip of the Sybaris fault zone. It is still visible the elevation difference in the topographic profile across the fault zone. The hangingwall of the fault zone is the preferential area where the Crati river and its affluent are presently flowing.

Profile 3 (Fig. 5) is traced across the Crati valley very close to the end of the inferred Sybaris fault zone. It reveals the presence of well developed fluvial terraces on the right hand side of the valley. The resulting valley asymmetry is the reflex of the activity of the Sybaris fault: the Crati river tends to migrate toward the centre of the valley to reach the lower topographic level created by the tectonic.

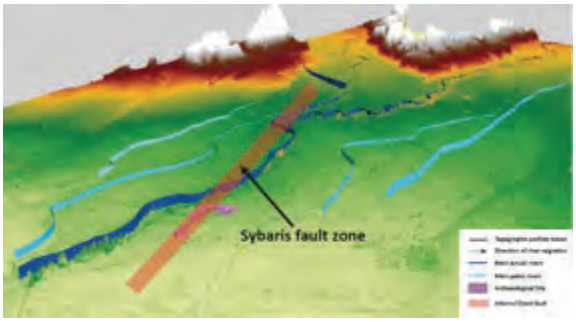

Figure 6 Birds-eye view of the same area of figure 3 from east. Elevations are exaggerated 10 times with respect to distance.

SUMMARY

This study revealed the great potential of the archaeological Sybaris site to contribute information concerning the reconstruction of the earthquake history of this sector of southern Italy and to provide new knowledge about the active tectonics of the coastal Ionian sector of the northern Calabria region. The brittle zone mapped at ancient Sybaris represents the first direct evidence for surface faulting in Holocene times in this portion of the Ionian territory. We mapped the effects of earthquakes affecting an ancient site for which no other records of earthquakes have been available up to now. Moreover, Holocene activity of the fault (the Sybaris fault) is controlling the local morphology and the present Crati river course, and the availability of LIDAR derived 1m DTM allows mapping of morphostructures with low gradient in the wide area, revealing tectonic control by the Sabari fault of the Sabari plain river network (*Figures 5 and 6*).

Acknowledgements: LiDAR data are provided by Ialian Ministry of the Environment, Land and Sea (National Geoportal project - http://www.pcn.minambiente.it/GN/index.php?lan=en)

References

Cinti, F.R., L. Alfonsi, D. Alessio, S. Marino & C.A. Brunori, (2015). Faulting and Ancient Earthquakes at Sybaris Archaeological Site, 86(1), 245–254. doi:10.1785/02201401071

Alfonsi, L., C.A. Brunori, F.R. Cinti, (2014). Active Faulting, Earthquakes and Geomorphological Changes from Archaeoseismic Data and High-Resolution Topography: Effects on the Urban Evolution of the Roman Town of Sybaris, Ionian Sea (Southern Italy). *American Geophysical Union Fall Meeting*. December 15-19, 2014 San Francisco (CA, USA).

INQUA Focus Group on Paleoseismology and Active Tectonics

Inferring surface uplift from longitudinal stream profiles in the Mt. Alpi area, southern Apennines, Italy

Buscher, J. (1), Ascione, A. (1), Valente, E. (2), Mazzoli, S. (1)

(1) Dipartimento di Scienze della Terra, dell'Ambiente e delle Risorse, University of Naples Federico II, Largo San Marcellino 10, 80138 Naples, Italy. Email: jamie.buscher@unina.it
(2) Dipartimento di Scienze Umanistiche, Sociali e della Formazione, Università del Molise, Campobasso, Italy

Abstract: *The tectonic framework of extensional mountain belts typically results from low-angle detachments and/or high-angle normal faults, with the potential for each end-member to generate signature landscape features that can be inferred from topographic analyses. The Mt. Alpi region in the southern Apennines has experienced recent extension in two phases---exhumation along detachment faults (late Pliocene) and uplift along high-angle normal faults (middle Pleistocene) (e.g., Mazzoli et al., 2014). Low-temperature thermochronometry data from the Mt. Alpi area suggest that rapid exhumation was focused during the first extensional phase along detachment faults but apparently decreased when extension initiated along high-angle normal faults (e.g., Mazzoli et al., 2014). To help elucidate the role of extensional tectonics on the topographic development of the Mt. Alpi area, longitudinal stream profiles were generated from DEM data using ArcGIS, with first-order results suggesting that stream profile convexities from the Mt. Alpi area may reflect recent surface uplift.*

Key words: *Geomorphology, tectonics, longitudinal stream profiles, ArcGIS, DEM.*

INTRODUCTION

The growth of rugged mountain belts is controlled by the impact of tectonics and erosion (e.g. England & Molnar, 1990; Ring et al., 1999, Whipple, 2004), but unraveling the role that each process plays on generating tectonically active landscapes is yet to be fully constrained. In extensional settings, exhumation is controlled by both tectonic denudation and erosion, creating a challenge for determining how each process contributes to the development of an extensional landscape. The Mt. Alpi region in the southern Apennines is currently in the extensional stage of a tectonic background believed to have involved both thin- and thick-skinned deformation, with a transition from a compressional setting in the late Miocene to an extensional setting in the late Pliocene (e.g. Cello et al., 1982; Sgrosso, 1988; Cinque et al., 1993; Cello & Mazzoli, 1999; Butler et al., 2004, Ascione et al., 2012, Mazzoli et al., 2014). The extensional tectonic history is thought to have occurred in two stages: (1) thin-skinned extension along low-angle detachment faults that formed in response to upper-crustal collapse of allochthonous units above folded Apulian Platform carbonates (e.g. Cello & Mazzoli, 1999), and (2) thick-skinned extension starting in the middle Pleistocene along high-angle normal faults that bisect structures throughout the rock record, including the detachment faults (Cello et al., 1982; Cinque et al., 1993). Since this region is the end result of a complex extensional tectonic history, various approaches are needed to highlight how long-term upper crustal deformation and short-term surface processes have shaped the present-day Mt. Alpi landscape.

For constraints at the Myr time scale, bedrock samples from Mt. Alpi and adjacent areas have been analyzed using low-temperature thermochronometry (Corrado et al., 2005; Mazzoli et al., 2006, 2008, 2014; Iannace et al., 2007; Invernizzi et al., 2008). Apatite (U-Th)/He (AHe) and apatite fission track (AFT) ages are relatively young in the region (<10 Ma) but the youngest ages (≤3 Ma) are found in the footwall of the Cogliandrino detachment fault at Mt. Alpi and at Mt. Sirino (Figure 1). Because Mt. Alpi and Mt. Sirino consist of rock units typically found at several km depth elsewhere in the area (Mazzoli et al., 2001; Aldega et al., 2003; Corrado et al., 2005), the young cooling ages suggest that rapid exhumation was focused at Mt. Alpi and the immediate surroundings starting in the late Pliocene (Mazzoli et al., 2014). Interestingly, models of AHe and AFT data indicate that exhumation rates in the Mt. Alpi and Mt. Sirino area decreased from 1 mm/yr to <0.6 mm/yr at 1.5 Ma, while samples found outside this area had similar low rates of <0.6 mm/yr over the last 4 Ma or longer (Mazzoli et al., 2014).

Extension of the Mt. Alpi region has generated a variable topographic ruggedness, with four distinct peaks (Mt. Alpi = 1900 m, Mt. Sirino = 2005 m, Mt. Raparo = 1761 m and Mt. La Spina = 1652 m) separated from each other by relatively wide valleys and bound elsewhere by relatively high-standing but low-slope highland features, possibly representing a common paleosurface (Valente, 2009) (Figure 1). An east-west swath profile from the region shows that wide valleys located between Mt. Sirino and Mt. Alpi are elevated relative to adjacent topography and that elevation decreases gradually to the east of this high peak area and more abruptly to the west (Valente, 2009; Mazzoli et al., 2014). Swath profiles trending approximately north-south along the major peaks in the area show a more abrupt decrease in elevation from Mt. Alpi, Mt. Raparo, Mt. La Spina and the southern flank of Mt. Sirino, while elevation decreases more progressively north of Mt. Sirino (Mazzoli et al., 2014).

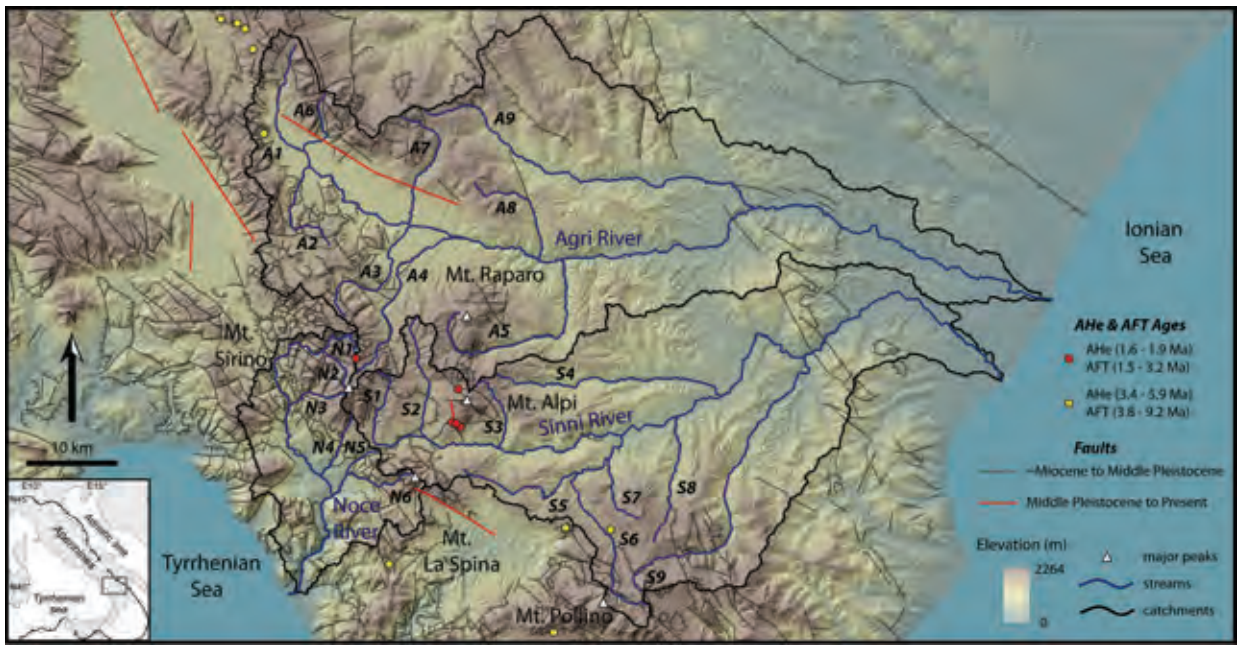

Figure 1: Shaded relief map of the Mt. Alpi region using 10 m DEM data from the Istituto Nazionale di Geofisica e Vulcanologia (INGV) (Tarquini et al., 2007, 2012), showing streams analyzed in this study. Stream numbers on map correspond to respective stream profiles in Figure 2. AHe and AFT data from Corrado et al. (2005) and Mazzoli et al. (2006, 2008, 2014). Fault data modified from Bonardi et al. (1988).

These gross topographic features and the location of very young cooling ages at Mt. Alpi and Mt. Sirino (Corrado et al., 2005; Mazzoli et al., 2006, 2008, 2014) suggest that recent rapid exhumation may have been followed by surface uplift of the area, warranting better constrains from topographic analyses.

To complement existing cooling age and topographic data and to help elucidate the role of surface processes on landscape development, a digital elevation model (DEM) of the Mt. Alpi region was analyzed using ArcGIS software to qualify how recent surface uplift may have affected stream profiles. ArcGIS tools were applied to a mosaic of 10 m DEMs downloaded from the Istituto Nazionale di Geofisica e Vulcanologia (INGV) (Tarquini et al., 2007, 2012) to trace the path of the digital thalweg for analysis of longitudinal stream profiles. The primary goal of this first-order stream analysis is to determine if the DEM stream profiles exhibit convex shapes (i.e. knickzones), possibly reflective of surface processes including tectonic uplift (e.g. Whipple, 2004; Wobus et al., 2006; Kirby & Whipple, 2012), or more typical concave profiles with steep upper reaches transitioning to flat lowlands.

DISCUSSION

The geometry of drainage networks can be used to help differentiate relatively short-term fluctuations in topographic development from long-term incision. Analyzing geomorphological features from drainages in the Apennines can be particularly insightful (e.g., Molin et al., 2004; Whittaker et al., 2008; Cyr et al., 2010) because variations in tectonic activity and rock type have played a dominant role in shaping the Apennine mountain belt (Ascione & Cinque, 1999). Unlike the northern and central Apennine chain where many of the highest peaks are found east of the drainage divide (e.g., Galli et al., 2002), several of the highest peaks in the southern Apennines are located west of the divide (e.g., Amato et al., 1995), possibly reflecting a change in subduction rate due to slab rollback (e.g., Calcagnile et al., 1982; Doglioni et al., 1996; Galli et al., 2002) or slab detachment (e.g., Spakman & Wortel, 2004; Ascione et al., 2012), or possibly the difference in lithology from resistant Apennine Platform carbonates in the west to more erodible sedimentary rocks in the east. Because stream profiles can be affected by both localized and regional-scale surface changes, stream analyses can be an important tool for deciphering how tectonics and erosion control landscape development.

Profiles of major streams and tributaries from the Agri, Sinni, and Noce catchments reveal that the location of convexities varies between individual profiles (Figures 2 & 3). In the Agri catchment area, knickzones are primarily found in the upper to middle reaches of the profiles for streams located south of the Agri River (A2-A5), while convexities are less apparent in profiles to the north (with the exception of A9). The most distinct knickzones in the Sinni catchment profiles are from streams located adjacent to Mt. Sirino, Mt. Alpi and Mt. La Spina (S1, S2, S3, S5), with streams to the east exhibiting more of a concave profile (S4). Profiles for the Noce catchment area are relatively steep (e.g. N2-N4) due to the steep western and southern flanks of Mt. Sirino, with convexities primarily found in the upper and middle stream reaches.

Although numerous convexities are observed in profiles throughout the area, an important factor must be taken into consideration. The lithology of the Mt. Alpi region consists primarily of erosionally resistant carbonates in the western part of the area (Mt. Alpi---Apulian Platform carbonates; Mtns. Raparo/La Spina---Apennine Platform carbonates; Mt. Sirino peak---Lagonegro carbonates) and more easily erodible sedimentary rocks in the east (~Miocene to Present), thus being a possible control on stream network development (Figure 3).

The possible influence of lithology on stream profile shape seems to vary throughout the region. In the Agri catchment area, rock type appears to play more of a primary role on controlling stream profiles north of the Agri River (convex reach of A6 correlates well with location of Lagonegro carbonates and profiles A7 & A8 exhibit concave profiles along stream paths on weaker lithologies), while those to the south display convexities in both resistant and erodible rock (Figure 3). In the Sinni catchment area, the streams predominantly flow on more erodible substrate, yet exhibit distinct convexities, especially adjacent to Mt. Sirino, Mt. Alpi and Mt. La Spina (S1, S2, S3, S5). In the Noce catchment area, convexities of streams north and west of Mt. Sirino correlate closely with changes in lithology (N1-N3), while this is less clear for streams to the south, with N4 having a convexity along a path in basin strata and a concave shape in carbonates, and N6 having a pronounced convexity in Apennine carbonates and Miocene deposits.

Considering both the longitudinal stream profile data and regional lithology, it would appear that convexities observed in streams adjacent to Mt. Sirino, Mt. Alpi and Mt. La Spina may reflect recent surface uplift. The presence of well-exposed high-angle normal faults in the area (e.g. western flank of Mt. Alpi) also lends support to this finding. However, it is important to note that landslides dominate the Mt. Alpi area (e.g., Santangelo et al., 2013) and karst landforms can sometimes obscure the interpretation of features thought to be generated from tectonic and/or surface processes, thus a thorough topographic and stream analysis is required to better constrain the surface uplift in this area.

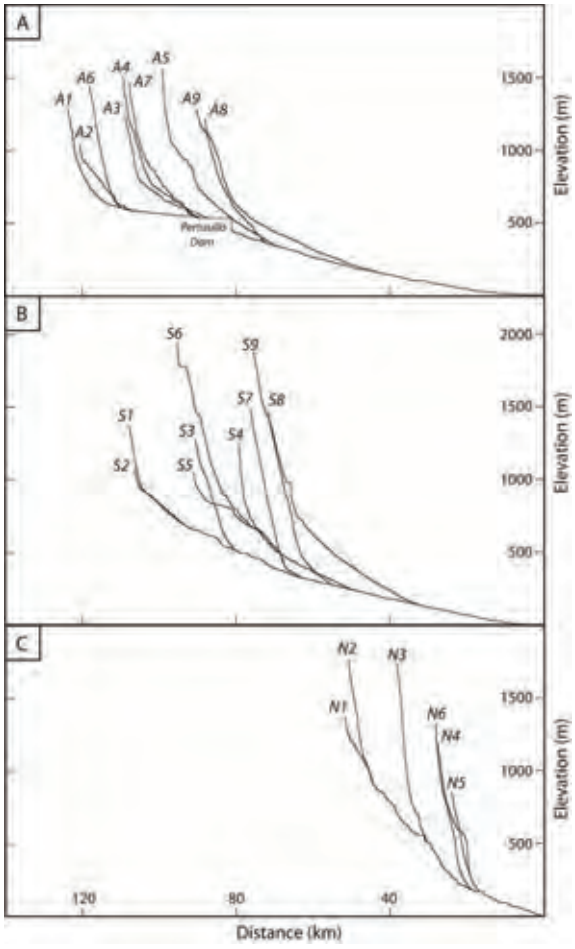

Figure 2: Longitudinal profiles of trunk streams and tributaries from the Agri (A), Sinni (B), and Noce (C) catchments.

INQUA Focus Group on Paleoseismology and Active Tectonics

paleoseismicity.org

Figure 3: Lithologic map of the Mt. Alpi area. Geologic data compiled and modified from Bonardi et al. (1988), Ascione et al. (2012) and Mazzoli et al. (2012). Lithologic units are broadly classified as either more (+R) or less (-R) resistant to weathering.

References

Aldega, L., G. Cello, S. Corrado, J. Cuadros, P. Di Leo, C. Giampaolo, C. Invernizzi, C. Martino, S. Mazzoli, M. Schiattarella, M. Zattin, & G. Zuffa, (2003). Tectono-sedimentary evolution of the Southern Apennines (Italy): Thermal constraints and modelling. *Atti Ticinensi Scienze della Terra*, *Serie Speciale*. 9, 135-140.

Amato, A., A. Cinque & N. Santangelo, (1995). Il controllo della struttura e della tettonica plio-quaternaria sull'evoluzione del reticolo idrografico dell'Appennino meridionale. *Studi Geologici Camerti*. 2, 23-30.

Ascione, A. & A. Cinque, (1999). Tectonics and erosion in the long-term relief history of Southern Apennines (Italy). *Zeitschrift für Geomorphologie*. 118, 1-16.

Ascione, A., S. Ciarcia, V. Di Donato, S. Mazzoli & S. Vitale, (2012). The Pliocene-Quaternary wedge-top basins of southern Italy: an expression of propagating lateral slab tear beneath the Apennines. *Basin Research*. 24, 456–474, doi:10.1111/j.1365-2117.2011.00534.x

Bonardi, G., B. D'Argenio & V. Perrone, (1988). Carta geologica dell'Appennino meridionale. *Memorie Società Geologica Italiana*. 41, p. 1341.

Butler, R.W.H., S. Mazzoli, S. Corrado, M. De Donatis, D. Di Bucci, R. Gambini, G. Naso, C. Nicolai, D. Scrocca, P. Shiner & V. Zucconi, (2004). Applying thick-skinned tectonic models to the Apennine thrust belt of Italy: Limitations and implications, in Thrust Tectonics and Petroleum Systems (K.R. McClay ed.). *American Association of Petroleum Geologists Memoir*. 82, 647-667.

Calcagnile, G., F. D'Ingeo, P. Farrugia & G.F. Panza, (1982). The lithosphere in the central-eastern Mediterranean area. *Pure and Applied Geophysics*. 120, 389-406.

Cello, G. & S. Mazzoli, (1999). Apennine tectonics in southern Italy: a review. *Journal of Geodynamics*. 27, 191-211.

Cello, G., I. Guerra, L. Tortorici, E. Turco & R. Scarpa, (1982). Geometry of the neotectonic stress field in southern Italy: geological and seismological evidence. *Journal of Structural Geology*. 4, 385-393.

Cinque, A., E. Patacca, P. Scandone & M. Tozzi, (1993). Quaternary kinematic evolution of the Southern Apennines. Relationships between surface geological features and deep lithospheric structures. *Annali di Geofisica*. 36, 249-260.

Corrado, S., L. Aldega, P. Di Leo, C. Giampaolo, C. Invernizzi, S. Mazzoli & M. Zattin, (2005). Thermal maturity of the axial zone of the southern Apennines fold-and thrust-belt (Italy) from multiple organic and inorganic indicators. *Terra Nova*. 17, 56-65.

Cyr, A.J., D.E. Granger, V. Olivetti & P. Molin, (2010). Quantifying rock uplift rates using channel steepness and cosmogenic nuclide-determined erosion rates: Examples from northern and southern Italy. *Lithosphere*. 2, 188-198.

Doglioni, C., M. Tropeano, F. Mongelli & P. Pieri, (1996). Middle-Late Pleistocene uplift of Puglia: An "anomaly" in the Apenninic foreland. *Memorie Società Geologica Italiana*. 51, 101-117.

England, P. & P. Molnar, (1990). Surface uplift, uplift of rocks, and exhumation of rocks. *Geology*. 18, 1173-1177.

Galli, S., A. Torrini, C. Doglioni & D. Scrocca, (2002). Divide and highest mountains versus subduction in the Apennines. *Studi Geologici Camerti*. 1, 143-153.

Iannace, A., S. Vitale, M. D'Errico, S. Mazzoli, A. Di Staso, E. Macaione, A. Messina, S. M. Reddy, R. Somma, V. Zamparelli, M. Zattin & G. Bonardi, (2007). The carbonate tectonic units of northern Calabria (Italy): a record of Apulian paleomargin evolution and Miocene convergence, continental crust subduction, and exhumation of HP–LT rocks. *Journal of the Geological Society, London*. 164, 1165–1186.

Invernizzi, C., G. Bigazzi, S. Corrado, P. Di Leo, M. Schiattarella & M. Zattin, (2008). New thermobaric constraints on the exhumation history of the Liguride accretionary wedge, southern Italy. *Ofioliti*. 33, 21–32.

Kirby, E. & K.X. Whipple, (2012). Expression of active tectonics in erosional landscapes. *Journal of Structural Geology*. 44, 54-75.

Mazzoli, S., S. Barkham, G. Cello, R. Gambini, L. Mattioni, P. Shiner & E. Tondi, (2001). Reconstruction of continental margin architecture deformed by the contraction of the

Lagonegro Basin, Southern Apennines, Italy. *Journal of the Geological Society, London*. 158, 309-319.

Mazzoli, S., L. Aldega, S. Corrado, C. Invernizzi & M. Zattin, (2006). Pliocene-Quaternary thrusting, syn-orogenic extension and tectonic exhumation in the Southern Apennines (Italy): Insights from the Monte Alpi area. In: *Styles of Continental Contraction* (Mazzoli, S. & Butler, R.W.H. eds.). *Geological Society of America, Special Paper*. 414, 55-77, doi: 10.1130/2006.2414(04).

Mazzoli, S., M. D'Errico, L. Aldega, S. Corrado, C. Invernizzi, P. Shiner & M. Zattin, (2008). Tectonic burial and 'young' (< 10 Ma) exhumation in the southern Apennines fold and thrust belt (Italy). *Geology*. 36, 243–246, doi: 10.1130/G24344A.

Mazzoli, S., A. Ascione, J.T. Buscher, A. Pignalosa, E. Valente & M. Zattin, (2014). Low-angle normal faulting and focused exhumation associated with late Pliocene change in tectonic style in the southern Aapennines (Italy). *Tectonics*. 33, 1802-1818, doi: 10.1002/2014TC003608.

Molin, P., F.J. Pazzaglia & F. Dramis, (2004). Geomorphic expression of active tectonics in a rapidly-deforming forearc, Sila Massif, Calabria, southern Italy. *American Journal of Science*. 304, 559-589.

Ring, U., M.T. Brandon, S.D. Willett & G.S. Lister, (1999). Exhumation processes. In: *Exhumation Processes: Normal Faulting, Ductile Flow, and Erosion* (Ring, U., Brandon, M.T., Lister, G.S. & Willett, S.D. eds.). *Geological Society, London, Special Publications*. 154, 1-27.

Santangelo, M., D. Gioia, M. Cardinali, F. Guzzetti & M. Schiattarella, (2013). *Geomorphology*. 188, 54-67.

Sgrosso, I., (1988). Nuovi dati biostratigrafici sul Miocene del Monte Alpi (Lucania) e conseguenti ipotesi paleogeografiche. *Memorie Società Geologica Italiana*. 41, 343-351.

Spakman, W. & M.J.R. Wortel, (2004). A tomographic view on western Mediterranean geodynamics. In: *The TRANSMED Atlas, The Mediterranean Region from Crust to Mantle* (Cavazza, W., Roure, F., Spakman, W., Stampfli, G.M. & Ziegler, P.A. eds.). SpringerVerlag, Berlin, 31-52.

Tarquini, S., I. Isola, M. Favalli, F. Mazzarini, M. Bisson, M.T. Pareschi & E. Boschi, (2007). TINITALY/01: a new Triangular Irregular Network of Italy. *Annals of Geophysics*. 50, 407-425.

Tarquini, S., S. Vinci, M. Favalli, F. Doumaz, A. Fornaciai & L. Nannipieri, (2012). Release of a 10-m-resolution DEM for the Italian territory: Comparison with global-coverage DEMs and anaglyph-mode exploration via the web. *Computers & Geosciences*. 38, 168-170, doi:10.1016/j.cageo.2011.04.018.

Valente, E., (2009). Long-term morphotectonic evolution of the southern Apennines, Ph.D. Thesis, Università di Napoli "Federico II", Napoli, 235 p.

Whipple, K.X., (2004). Bedrock rivers and the geomorphology of active orogens. *Annual Review of Earth & Planetary Sciences*. 32, 151-185.

Whittaker, A.C., M. Attal, P.A. Cowie, G.E. Tucker & G. Roberts, (2008). Decoding temporal and spatial patterns of fault uplift using transient river long profiles. *Geomorphology*. 100, 506-526.

Wobus, C., K.X. Whipple, E. Kirby, N. Snyder, J. Johnson, K. Spyropolou, B. Crosby & D. Sheehan, (2006). Tectonics from topography: Procedures, promise, and pitfalls. In: *Tectonics, Climate, and Landscape Evolution* (Willett, S.D., Hovius, N., Brandon, M.T. & Fisher, D.M. eds.). *Geological Society of America Special Paper*. 398, 55-74, doi: 10.1130/2006.2398(04).

INQUA Focus Group on Paleoseismology and Active Tectonics

The Greek Database of Seismogenic Sources (GreDaSS): A compilation of potential seismogenic sources (Mw>5.5) in the Aegean Region

Caputo, R. (1,3), Pavlides, S. (2,3), GreDaSS Woking Group (4)

(1) Dept. of Physics & Earth Sciences, Ferrara University, via Saragat 1, 44122 Ferrara, Italy. Email: rcaputo@unife.it
(2) Dept. of Geology, Aristotle University of Thessaloniki, Thessaloniki, Greece
(3) Research and Teaching Center for Earthquake Geology, Tyrnavos, Greece
(4) Principal scientific contributors are: Chatzipetros A., Koukouvelas I., Michailidou A., Sboras S., Tarabusi G., Valkaniotis S.

Abstract: *The Greek Database of Seismogenic Sources (GreDaSS) is a repository of geological, tectonic and active fault data for the Greek territory and its surroundings including sectors of western Anatolia, southern Bulgaria, FYR of Macedonia and Albania. The principal aim of this international project is to create a homogenized framework of all data relevant to the seismotectonics, and especially the seismic hazard assessment, of Greece and its surroundings as well as a common research platform for performing seismic hazard analyses, modelling and scenarios from specific seismogenic structures.The released version 2.0 of the database contains more than 300 composite seismogenic sources (CSS) and ca. 110 individual seismogenic sources (ISS).They are documented by more than 3000 references (papers , reports, maps, etc.) and 1000 figures including maps, graphs, photos, diagrams, etc. The database follows and openfile philosophy and hence should be continuously considered as in progress.*

Key words: *Earthquake Geology, Seismotectonics, Seismic Hazard.*

INTRODUCTION

The broader Aegean Region is among the most tectonically active areas of the Mediterranean realm. The tectonic regime is rather complex producing earthquakes with many different orientations of nodal planes and a large variety of fault types both in terms of dimension and kinematics. Three are the dominating large-scale tectonic structures in the area. i) The Hellenic subduction zone, where the African plate is subducted underneath the Aegean; it is associated with a compressive stress field all along the arc. ii) The Inner Aegean region characterized by widespread, mainly N-S trending, crustal extension. iii) The North Aegean Trough (NAT) which represents a transtensional stress regime due to overlapping contribution of the western propagation of the purely strike-slip North Anatolian Fault and the Aegean extension. The combination of all previous tectonic processes produces an intense lithospheric fracturing and the formation of a large number of active faults.

The same region is also characterized by the highest seismicity of the Mediterranean real both in terms of frequency of events and magnitudes. As a matter of fact, it is not always straightforward to correlate seismicity with the causative fault(s). This is mainly due to two reasons: firstly, several crustal sectors of the Aegean, where historical or instrumental epicentres are located, are affected by a dense fault population bearing evidences of recent activity, but with poorly defined seismotectonic behaviour. Secondly, large sectors of the broader Aegean Region are covered by the sea, therefore lacking crucial field and direct observations. In the latter case, the typical geological approaches are generally replaced with geophysical and seismological investigations (detailed bathymetry, seismic profiles, microseismicity, focal mechanisms, *etc.*), which can be proved very useful though the uncertainties in some cases remain not negligeable (Pavlides *et al.*, 2010; Caputo *et al.*, 2012; Sboras *et al.*, 2013).

The database

GreDaSS represents an on-going project based on the results of decades of investigations by the GreDaSS Working Group and by numerous other researchers working on the active tectonics of the broader Aegean Region.

Members of the WG have contributed in several national and European projects like FAUST (Faults as a seismological tool, 1998-2000; FAUST, 2001) and SHARE (Seismic Hazard and Armonization in Europe, 2009-2012; Basili *et al.*, 2013).

As a major difference from the above mentioned databases (FAUST and EDSF), GreDaSS is continuously updated by the WG, with the aim of improving its completeness in terms of seismogenic sources analysed and included time to time, but also of enriching and better defining all parametric and the ancillary information of each source.

GreDaSS is based on the DISS software (version 3.2) provided by the DISS WG of the INGV (Basili *et al.*, 2008) which is warmly acknowledged.

At present, both Composite Seismogenic Sources (CSSs) and Individual Seismogenic Sources (ISSs) have been included in the database by following a critical review of all available information relative to the specific tectonic structure. At this regard, literature data, either published papers and unpublished reports, have been taken into account together with our decades-long field-work experience on many active faults of the Aegean Region. This systematic work allowed to define most of the seismotectonic parameters required to fullfill the form of

every source. Some of the parameters have been obtained based on commonly used empirical relationships (Wells and Coppersmith, 1994; Pavlides and Caputo, 2003). In any case, the main source of information used by the compiler(s) is clearly specified for each numerical entry of the database.

At present, the database contains more than 300 CSSs and about 110 ISSs (Figure 1) associated with more than 3000 citations and ca. 1000 among figures, maps, photos and graphs.

Version 2.0 of GreDaSS has been recently released and it is available on the web (*gredass.unife.it*; Caputo and Pavlides, 2013). Once uploaded in GoogleEarth the kmz file, all seismogenic sources could be examined by clicking on them. An html page is thus created containing the full parametric information on the specific tectonic structure. For many of the sources included in GreDaSS, additional information, like open questions, the summaries of the relevant literature, figures, maps, photos, graphs and references are also provided as html pages (Figure 2).

The database is continuously updated by the WG, with the aim of improving its completeness in terms of seismogenic sources analysed and already included, but also of enriching and better defining all parametric and ancillary information on each source.

Any additional (and/or critical) contribution by the broader Scientific Community is welcome and will be fully acknowledged in the database. Please, contact the authors at this concern.

Figure 1: The Greek Database of Seismogenic Sources (GreDaSS, version 2.0) plotted on a GoogleEarth satellite background. By clicking on a specific source, end-users can generate an html page containing full parametric information of the tectonic structure.

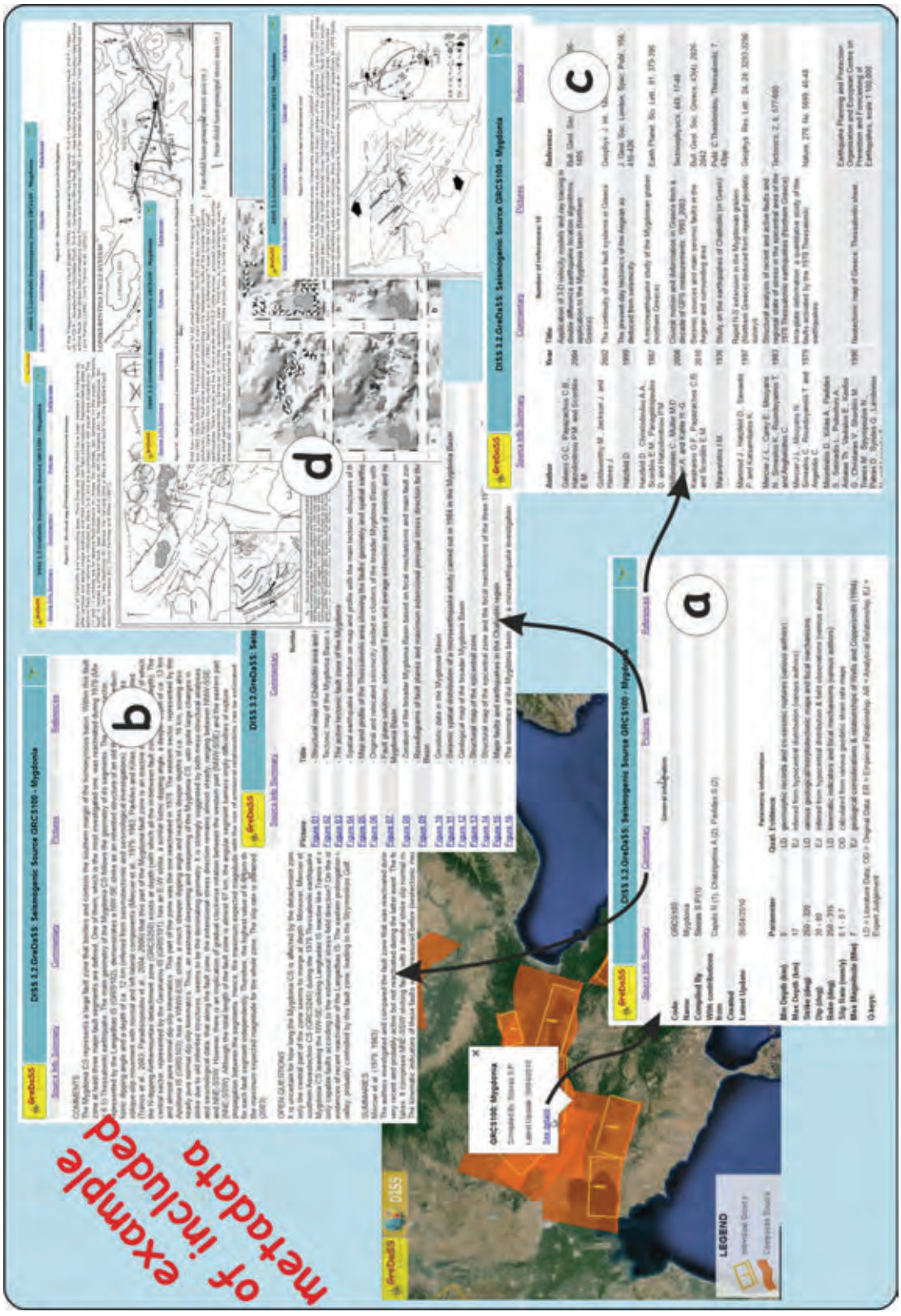

Figure 2: Example of metadata associated to a Composite Seismogenic Source (GRCS100 - Mygdonia). Additional information is displayed as html pages. The different pages provide (a)full parametric information on the source; (b) comments, open questions and summaries; (c) full references list; (d) maps, photos, diagrams and graphical information.

References

Basili, R., G. Valensise, P. Vannoli, P. Burrato, U. Fracassi, S. Mariano, M.M. Tiberti and E. Boschi, (2008). The Database of Individual Seismogenic Sources (DISS), version 3: Summarizing 20 years of research on Italy's earthquake geology. *Tectonophysics*. 453(1-4), 20-43, doi:10.1016/j.tecto.2007.04.014.

Basili, R., V. Kastelic, M.B. Demircioglu, D. Garcia Moreno, E.S. Nemser, P. Petricca, S.P. Sboras, G.M. Besana-Ostman, J. Cabral, T. Camelbeeck, R. Caputo, L. Danciu, H. Domac, J. Fonseca, J. García-Mayordomo, D. Giardini, B. Glavatovic, L. Gulen, Y. Ince, S. Pavlides, K. Sesetyan, G. Tarabusi, M.M. Tiberti, M. Utkucu, G. Valensise, K. Vanneste, S. Vilanova and J. Wössner, (2013). *The European Database of Seismogenic Faults (EDSF) compiled in the framework of the Project SHARE*. http://diss.rm.ingv.it/share-edsf/, doi: 10.6092/INGV.IT-SHARE-EDSF.

Caputo, R. and S. Pavlides, (2013). T*he Greek Database of Seismogenic Sources (GreDaSS), version 2.0.0: A compilation of potential seismogenic sources (Mw>5.5) in the Aegean Region*. http://gredass.unife.it, doi: 10.15160/unife/gredass/0200.

Caputo, R., A. Chatzipetros, Pavlides S. and S. Sboras, (2012). The Greek Database of Seismogenic Sources (GreDaSS): state-of-the-art for northern Greece. *Annals of Geophysics*. 55(5), 859-894, doi: 10.4401/ag-5168.

FAUST, (2001). *FAUlts as a Seismological Tool, European Union Environment project.* Final Report, http://www.ingv.it/~roma/banche/catalogo_europeo/index.html (ENV4-CT97-0528).

Pavlides, S.B. and R. Caputo, (2004). Magnitude versus faults' surface parameters: quantitative relationships from the Aegean. *Tectonophysics*. 380, 3-4, 159-188.

Pavlides, S., R. Caputo, S. Sboras, A. Chatzipetros, G. Papathanasiou and S. Valkaniotis, (2010). The Greek catalogue of active faults and database of seismogenic sources. *Bulletin of the Geological Society of Greece*. 43(1), 486-494.

Sboras, S., S. Pavlides, R. Caputo, A. Chatzipetros, A. Michailidou, S. Valkaniotis and G. Papathanasiou, (2013). Improving the resolution of seismic hazard estimates for critical facilities: the Database of Greek crustal seismogenic sources in the frame of the SHARE project. *Bollettino di Geofisica Teorica ed Applicata*. 55(1), 55-67, doi: 10.4430/bgta0101.

Wells, D.L. and J.K. Coppersmith, (1994). New empirical Relationships among Magnitude, Rupture Length, Rupture Width, Rupture Area, and Surface Displacement. *Bulletin of the Seismological Society of America*. 84, 974-1002.

INQUA Focus Group on Paleoseismology and Active Tectonics

Large thrust faulting earthquakes in Eastern Kazakhstan – first results from paleoseismic trenching

Carson, E. (1), Grützner, C. (2), Mackenzie, D. (1), Walker, R. (1), Mukambayev, A. (3), Moldobaev, A. (4), Abdrakhmatov, K. (4)

(1) Department of Earth Sciences, University of Oxford, South Parks Road, OX1 3AN Oxford, UK
(2) Department of Earth Sciences, University of Cambridge, Madingley Rise, Madingley Road, CB3 0EZ Cambridge, UK. Email: chg39@cam.ac.uk
(3) Kazakhstan National Data Center, Chaikinoy str. 4, 050020 Almaty, Kazakhstan
(4) Kyrgyz Seismological Institute, Academy of Sciences of the Kyrgyz Republic, Asanbay str. 52/1, 720060 Bishkek, Kyrgyz Republic

Abstract: *Large faults in Eastern Kazakhstan accommodate a significant portion of the India-Eurasia convergence and appear to have long recurrence intervals. They may rupture in rare, but strong events that pose a hazard to cities like Almaty. In order to evaluate the seismic history of one of these structures, we investigated an E-W striking, 50 km long active thrust fault using remote sensing, mapping, and paleoseismological trenching. Here, we present the trenching data. We found evidence for two surface rupturing events in the late Quaternary, probably in the Holocene. Fault length and observed offsets indicate that the Bartogay Fault is capable of earthquakes with magnitudes in the order of M7.0.*

Key words: *Kazakhstan, thrust fault, trenching, alluvial fan.*

INTRODUCTION

The Tien Shan and Dzhungarian Ala-tau mountains of Eastern Kazakhstan are active ranges that take up about 25% of the overall collisional movement between India and Eurasia (Zubovich et al., 2010). This N-S convergence is accommodated by numerous E-W thrust faults, NW(E)-SE(W) strike-slip faults, and large-scaled folding in growing E-W striking anticlines (cf., Tapponier & Molnar, 1979). Most of the thrust faults are large active structures of up to several hundreds of kilometres in length, probably capable of very large earthquakes. Historical data prove that major events occurred in the broader study area, like the 1887 Verny earthquake (M7.3), the 1889 Chilik earthquake (M8.3), or the 1911 Kemin earthquake (M8.2; see Campbell et al., 2013, and references therein). However, many of the main thrust structures have not generated a large earthquake in historical times. Little is known about slip rates, last earthquake events, maximum possible magnitudes, and recurrence intervals at these faults and paleoseismic studies are rare. One of the problems arising from this situation is that the seismic hazard for cities like Almaty cannot be well constrained. Another issue is that we lack knowledge on how the overall deformation is distributed among the different active structures (cf. Thompson et al., 2002, who worked on a similar problem in Kyrgyzstan).

In this study we report on our work at the Bartogay Fault, east of Almaty. We performed remote sensing analyses, geomorphological investigations, and paleoseismological trenching in order to contribute to solving the problems mentioned above.

We present first outcomes of our field work and concentrate on the results obtained from paleoseismological trenching.

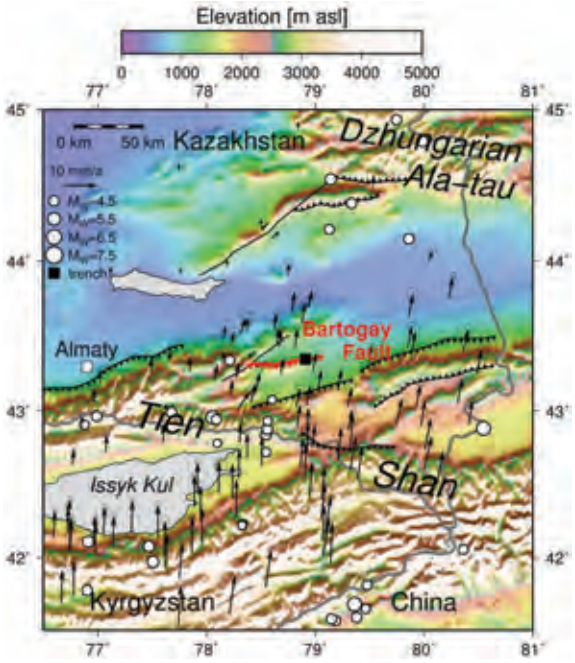

Figure 1: The Bartogay Fault in Eastern Kazakhstan. GPS velocities relative to stable Eurasia with 95 % confidence interval ellipses are from Zubovich et al. (2010), instrumental seismicity >M4.5 is from the catalogue of Engdahl et al. (1998).

STUDY SITE

The Bartogay Fault is a more than 50 km long, E-W striking thrust fault, about 150 km east of Almaty (Fig. 1). The fault crops out at ~1400 m altitude. It dips to the S and separates a large plain in the north from an up to 2400 m high mountain range in its south. A fault scarp

offsetting alluvial fans which formed at the base of the mountains is visible in SPOT and Kompsat satellite imagery (Fig. 2). The scarp is discontinuous and varies in height as different generations of terraces are offset. The feature can be observed for ~25 km. Such offsets are commonly ascribed to Late Quaternary or even Holocene age, as it is assumed that they would have been erased during periods of higher precipitation and subsequent erosion and sedimentation during the glacials.

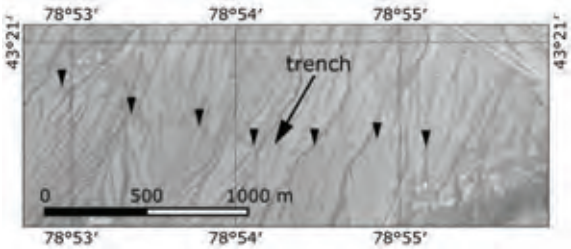

Figure 2: Kompsat imagery of the Bartogay Fault, the scarp is marked with black triangles.

METHODS

We mapped the entire fault and measured the height of the fault scarp. Differential GPS (DGPS) was used to precisely measure the offset of alluvial fans with vertical errors of less than 0.15 m. A helium balloon was used to collect thousands of aerial images with a digital camera. We surveyed the entire length of the scarp and produced a high-resolution digital elevation model (DEM) from overlapping imagery using the structure-from-motion technique (SFM). The DEM then allowed for the extraction of heights and offsets. Prominent offset alluvial fans were sampled for OSL dating in order to calculate slip rates.

Paleoseismic trenching was performed in the eastern section of the Bartogay Fault at N43.34628°, E078.90904°. The scarp height of around 1.3 m at this location (lowest terrace) lead us to assume that probably one single (Holocene?) earthquake event was responsible for the observed offset.

We opened a trench which was 2 m wide, 18 m long and up to 2 m deep. The trenched was oriented N-S and crossed the scarp perpendicularly. After cleaning the eastern trench wall we installed a 1x1 m grid and flagged the lithological contacts. A trench log was documented noting lithology, grain size, colour, evidence for bedding, deformation, fracturing, and gravel orientation. Photographs were taken, and using the SFM technique a 3D model and orthophoto of the trench was produced. DGPS profiles were also taken around the trench and across the terrace perpendicular to the fault trace.

We took two samples for radiocarbon dating and four samples for OSL dating from the trench. The dating is still in progress and we expect first results in late spring 2015.

RESULTS

The balloon survey and the DGPS measurements show that the height of the fault scarp varies from 1.3 m at the trench site to 13 m in the centre of the fault. We assume that the scarps in the centre of the fault represent cumulative offset of several surface rupturing seismic events.

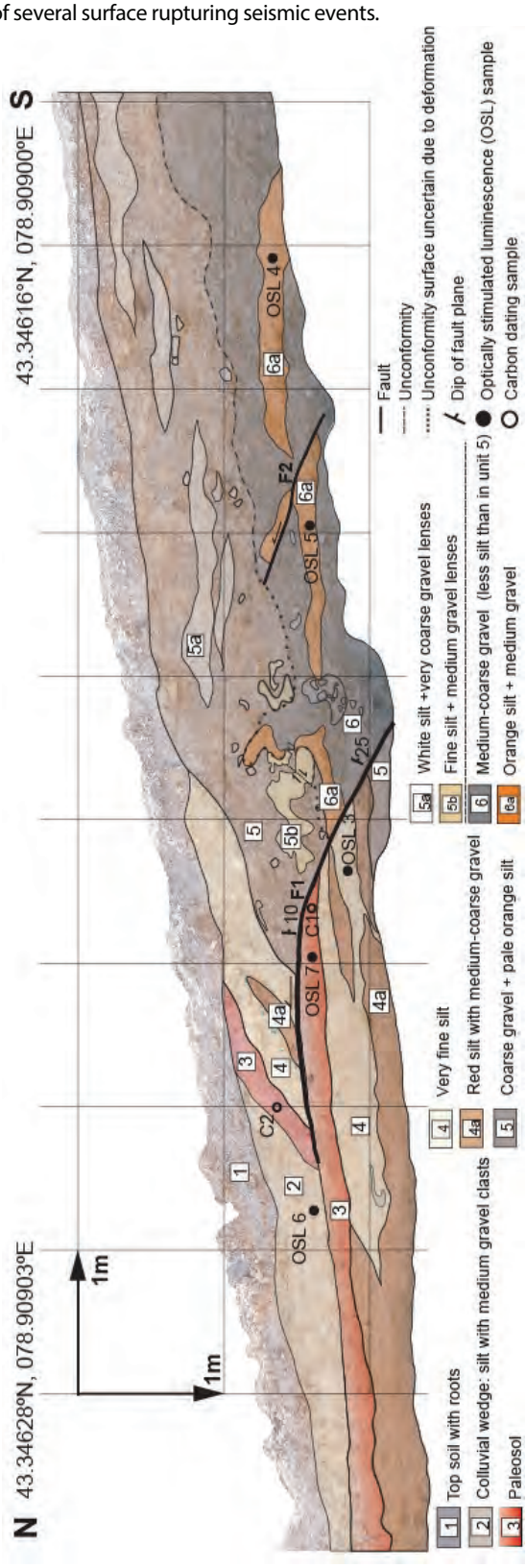

Figure 3: Log of the eastern wall of the trench with the main lithological units.

Our trenching revealed evidence for two surface rupturing earthquakes at two fault zones F1 and F2 (Fig. 2). The trench exposes coarse alluvial deposits which interfinger with channelized silt and sand lenses. At fault zone F1 the stratigraphy can be divided into three distinct units which have been offset.

The lowermost unit (5) is a coarse, poorly sorted alluvial gravel deposit with silty lenses. Above we encountered a massive (~0.8 m thick) loess deposit (4), which is discontinuous where it interfingers with coarse gravel. This loess-gravel horizon probably represents a time of active channel migration, with the fine silt deposited on the channel banks and levees, and the coarse gravel where transport energy was high. A red tinted paleosol lies stratigraphically above (unit 3). Its offset and truncation at the fault plane presents evidence for surface rupturing during the most recent earthquake event.

Units 5-3 can be traced across the fault into the hanging-wall, where they have been offset and tilted. The stratigraphy in the hanging-wall is complex, because the coseismic deformation has severely warped and distorted most units (see gravel and silt lenses of units 5a,b). At the base of unit 5 there is an erosional unconformity, most clearly visible in the southern section of the trench, where there is a transition from well sorted medium gravels to coarse, poorly sorted, and comparatively silt-rich material. Close to the fault plane this surface is harder to discern.

Deformation and structure

In order to quantify the horizontal and vertical offset which resulted from the last event, a retrodeformation was performed. Results indicate that this event was associated with ~1.8 m of displacement along the fault plane. Using a fault dip of 25°, we calculate ~1.6 m of horizontal shortening and a vertical displacement of ~0.8 m.

This event also resulted in deformation of the lenses within unit 5. In particular 5b has been sheared in a back thrust-style and units 5 and 6 have been warped in the vicinity of the fault. The northward dip of units 3 and 4 in the hanging wall suggests the existence of a broad anticline, the hinge of which probably lies further to the south and is not visible in this trenched section. Both warping and larger-scaled folding would accommodate additional shortening, which fits well with the observations from DGPS profiling, see below.

In the southern section of the trench there is evidence for a penultimate event. Unit 6a is truncated, and a wedge of material has been displaced vertically at an angle of ~18° along the fault plane F2. Assuming that the wedge of material is from unit 6a, restoring the section indicates a horizontal offset of ~0.6 m and a vertical offset of ~0.2 m, resulting in a total slip of ~0.63 m. This is a minimum estimate for displacement during the penultimate event, as the wedge could in fact have come from a similar unit stratigraphically below unit 6a.

A penultimate event on F2 can also explain the unconformity surface between units 5 and 6. A sequence of events is proposed in figure 3, beginning with the F2 event. Uplift which occurred during event F2 then lead to scarp degradation and erosion which formed the unconformity. After a period of time stability was reached and units 4 and 5 were deposited. Fan surface stability then ensued and a soil layer began to develop. However, this surface was broken and displaced when the most recent earthquake occurred along F1.

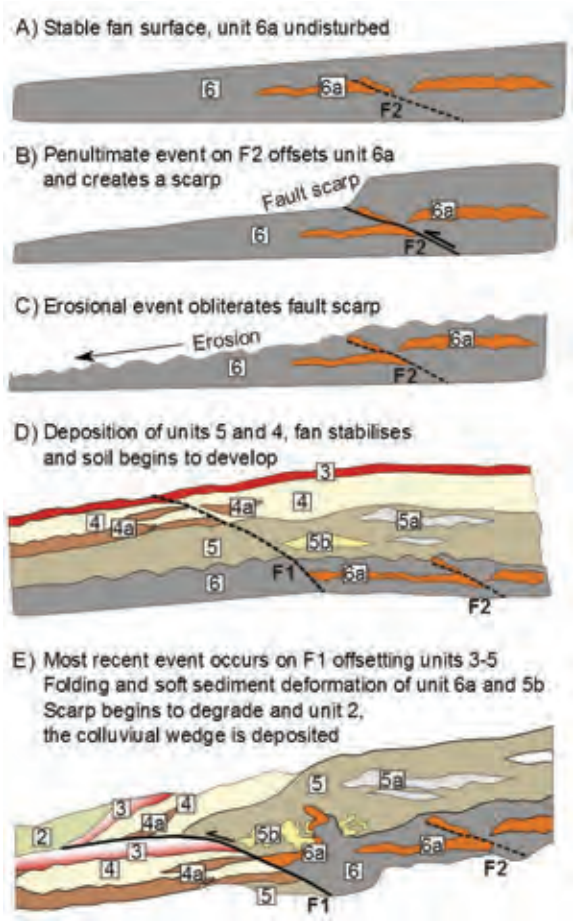

Figure 4: A possible retrodeformation of the present day trench.

DISCUSSION

We calculated possible magnitude values based on empirical relationships and varying input parameters (Table 1). According to the Wells & Coppersmith (1994) relationships, a 50 km long fault could cause an earthquake of magnitude ~M7.1. If we used the length of the visible scarp (~25 km) for the calculation, an earthquake of M6.7 is reasonable. The total offset of 1.8 m caused by the last event as derived from the trench would correspond to a magnitude of M6.6-M6.9 if this was the maximum displacement and to M6.7-M7.1 if it was the average displacement. Magnitude-area relationships indicate M6.9-M7.2, assuming an average dip angle of 45° and a seismogenic thickness of 20 km.

DGPS profiling shows that the fan surface has been offset by 1.3 m in the area surrounding the trench. As this is the vertical offset only, the overall slip would be

higher and probably in the order of 3 m if the fault dip is 25° close to the surface. The abovementioned scaling relationships would then point to a magnitude of M6.7-M7.0 (max displacement) or M6.7-M7.3 (average displacement). Further towards the centre of the fault, the vertical offset of the scarp reaches its maximum with up to ~2.5 m, indicating ~5.5-6 m total slip (corresponding to M6.9-7.3). The average vertical offset along the entire scarp is ~1.6 m, indicating a total slip of 3.8 m and possible magnitudes of M6.7-7.4.

Probably not all of the deformation and uplift is accommodated by slip along the fault plane itself. Previous paleoseismological studies of thrust faults have shown that deformation and uplift is accommodated at the surface by folding, in addition to movement along the fault plane (Lee et al., 2001; Salomon et al., 2013). The rotation of units 3 and 4 in the hanging wall and the folding of the lenses of material within unit 5 suggest that some of this additional uplift recorded in the DGPS can be explained by folding, in particular by the development of an anticline in the hanging-wall.

Table 1: Wells & Coppersmith (1994) empirical relationships for the last surface rupturing earthquake.

Wells & Coppersmith (1994) relationship used	Input value	Magnitude
Fault length, mapped	50 km	7.1
Fault length, visible scarp	25 km	6.7
Offset from trench, maximum	1.8 m	6.6-6.9
Offset from trench, average	1.8 m	6.7-7.1
Area, 45° dip, 20 km seismogenic thickness, 25 km length	700 km^2	6.9
Area, 45° dip, 20 km seismogenic thickness, 50 km length	1400 km^2	7.2
Offset from DGPS, at trench	3 m	6.7-7.3
Offset from DGPS, maximum	6 m	6.9-7.3
Offset from DGPS, average	3.8 m	6.7-7.4

A magnitude estimate can be calculated for the penultimate event, based on the offset visible in the trench (Table 2). A slip of 0.63 m would require a magnitude of at least M6.4-M6.5 (max displacement) or M6.6-M6.8 (average displacement). However, due to the unknown erosion history and the limited insight that the trench could provide, we emphasize that these are minimum values only.

Table 2: Wells & Coppersmith (1994) empirical relationships for the penultimate event.

Wells & Coppersmith (1994) relationship used	Input value	Magnitude
Offset from trench, maximum	0.63 m	6.4-6.5
Offset from trench, average	0.63 m	6.6-6.8

Our trench is located close to the eastern tip of the fault and not in the centre, where the slip per event might be higher (Fig. 1). We therefore regard the magnitude values calculated with the equation for maximum displacement as lower boundaries only.

CONCLUSION

Our study shows that the Bartogay Fault is capable of large, probably Holocene, earthquakes with magnitudes of up to M7, probably even larger. Dating results will allow us to determine a slip rate and to date the last major event. This fault seems to be similar to other faults in the area in the sense that it ruptures in rare, but large events. Such long recurrence intervals and short observation periods by means of historical information illustrate the need for paleoseismological studies of these structures.

Our study also illustrates the problems of paleo-magnitude estimation based on trenching data only.

Acknowledgements: CG, DM, and RW are part of COMET+: http://comet.nerc.ac.uk/. This study was conducted in the framework of the Earthquakes without Frontiers project: http://ewf.nerc.ac.uk/.

References

Campbell, G. E., Walker, R. T., Abdrakhmatov, K., Schwenninger, J.L., Jackson, J., Elliott, J.R. & Copley, A. (2013). The Dzhungarian fault: Late Quaternary tectonics and slip rate of a major right-lateral strike-slip fault in the northern Tien Shan region. *JGR: Solid Earth*. 118(10), 5681-5698.

Engdahl, E.R., van der Hilst, R. & Buland, R. (1998). Global teleseismic earthquake relocation with improved travel times and procedures for depth determination. *BSSA*. 88(3), 722-743.

Lee, J. (2004). A Vertical Exposure of the 1999 Surface Rupture of the Chelungpu Fault at Wufeng, Western Taiwan: Structural and Paleoseismic Implications for an Active Thrust Fault. *BSSA*. 91(5), 914-929.

Salomon, E., Schmidt, S., Hetzel, R., Mingorance, F. & Hampel, A., (2013). Repeated Folding during Late Holocene Earthquakes on the La Cal Thrust Fault near Mendoza City (Argentina). *BSSA*. 103(2), 936-949.

Tapponnier, P. & Molnar, P. (1979). Active faulting and Cenozoic tectonics of the Tien Shan, Mongolia, and Baykal regions. *JGR: Solid Earth (1978–2012)*. 84(B7), 3425-3459.

Thompson, S.C., Weldon, R.J., Rubin, C.M., Abdrakhmatov, K., Molnar, P. & Berger, G.W., (2002). Late Quaternary slip rates across the central Tien Shan, Kyrgyzstan, central Asia. *JGR: Solid Earth (1978–2012)*. 107(B9), ETG-7.

Wells, D.L. & K.J. Coppersmith, (1994). New empirical relationships among magnitude, rupture length, rupture width, rupture area, and surface displacement. *BSSA*. 84, 974–1002.

Zubovich, A.V., and many others, (2010). GPS velocity field for the Tien Shan and surrounding regions. *Tectonics*. 29(6).

INQUA Focus Group on Paleoseismology and Active Tectonics

Radon distribution as shallow evidence of buried fault geometry in the Fucino plain (Central Italy)

Ciotoli, G. (1), Bigi, S. (2), Cavinato, G.P. (1)

(1) IGAG-CNR Istituto di Geologia Ambientale e Geoingegneria, Consiglio Nazionale delle Ricerche, Area della Ricerca Roma 1, Via Salaria km 29.300, 00016 Monterotondo Stazione (Roma), Italy Email: giancarlo.ciotoli@igag.cnr.it
(2) Dipartimento di Scienze della Terra, Sapienza Università di Roma, P.le A. Moro, 5 – 00183 Roma, Italy

Abstract: *The Fucino plain is characterised by a network of buried and known faults activated during the Avezzano earthquake in 1915. Since radon in soil gas is used as an effective fault tracer, radon anomalies in the eastern sector of the plain has been re-interpreted according to new seismic data and new techniques of geospatial analysis to reconstruct the shallow geometry of these buried and known faults. E-W radon profiles was calculated using the radon distribution map, and the spatial distribution of radon peaks was mapped. Spatial location of the radon peaks highlights eastward sharp deviations along the NW-SE oriented Trasacco, Ortucchio Faults, as well as along the San Benedetto dei Marsi fault that borders the eastern side of the plain. These deviations can be inferred as fractured zones (e.g., relay ramps) or real transfer faults causing moving back of these structures towards the mountain.*

Key words: *Soil gas radon, fault geometry, fluid migration.*

INTRODUCTION

Soil gas measurement has received much attention as an effective method to trace hidden faults (e.g., Baubron et al., 2002; Fu et al., 2005; Ciotoli et al., 2007; Walia et al., 2009; Ciotoli et al., 2014; Bigi et al., 2014). The stress/strain changes related to seismic activity may force crustal fluid to migrate up, especially along faults (King, 1986), thereby altering the geochemical characteristics of the faults (Annunziatellis et al., 2008). Therefore, active faults, and surrounding zones composed of highly fractured rock materials, gouge and fluid, may favour gas leaks from the solid earth (Baubron et al., 2002).

Among the soil gases, ^{222}Rn, a radioactive inert gas with a half life of 3.82 days, is considered a convenient fault tracer in geosciences. Due to the ubiquity of its parent nuclides (^{226}Ra and ^{238}U), the release of ^{222}Rn, takes place in every geological environment. The increase of ^{222}Rn activity in the soil gas related to active fault zones at different sites has been reported in Ciotoli et al., 2014; Bigi et al., 2014; Lombardi and Voltattorni, 2010; Ciotoli et al., 2007; Baubron et al., 2002; Font et al., 2007; King et al., 1996; Seminsky and Bobrov, 2009; Swakon et al., 2005; and is a subject of interest for researchers in risk analysis and mapping of active fault areas (Burton et al., 2004).

Numerous soil gas measurements were performed at different scales across known and inferred structural discontinuities in the Fucino Basin and are reported in Ciotoli et al., 2007 and Ciotoli et al., 1998. Results clearly highlight the shallow pattern of buried faults in the plain. In particular, the distribution of radon anomalies differentiates the relatively simple dip-slip geometry of the San Benedetto dei Marsi-Gioia dei Marsi (SBGMF) and the Ortucchio (OF) faults (activated during the 1915 Avezzano earthquake, M = 7.0) in the eastern sector of the plain, from the inferred more complex geometry of the faults of the western sector of the plain (Trasacco Fault, TF). In this work, the radon results in Ciotoli et al., 2007 has been re-interpreted and discussed in the light of new seismic data reported in recent works (Cara et al., 2011; Saroli et al., 2008), and also thanks to the facilities provided by the new GIS and geospatial analyses.

DISCUSSION

The Fucino plain (Central Italy) is an intramontane basin formed by the extensional tectonics that affected the central-western Apennine range during Late Pliocene. This tectonic depression was filled by Upper Pliocene-Holocene lacustrine and alluvial sediments (Giraudi, 1988; Bosi et al., 1995) that unconformably overlie Meso-Cenozoic carbonate and Neogene terrigenous sequences (Cara et al., 2011). The maximum thickness of the lacustrine sequence is about ~1000 m in the north-eastern sector of the plain (Cavinato et al., 2002).

The plain is bordered and crossed by a complex network of buried and/or known faults and fractures characterized by seismic activity (Oddone, 1915). The activity of these faults is testified by the terraced Middle-Upper Pleistocene alluvial fan and fluvial-lacustrine deposits hanging for hundreds of meters above the present valley floor in the north and north-eastern borders of the basin (Cavinato et al., 2002; Galadini et al., 1997; Michetti et al., 1996).

The main faults recognized in the Fucino basin are (1) the Avezzano-Celano (ACF-inferred) faults (ENE trending, SE dipping) in the northern sector; (2) the San Benedetto–Gioia dei Marsi fault (SBGMF), reactivated during the 1915 Avezzano earthquake and the Statale Marsicana (SSMF) faults in the eastern sector; (3) the Ortucchio fault (OF-inferred) near the center of the basin; and (4) the Trasacco (TF) and Luco dei Marsi (LF) faults (NW trending, SW dipping) in the southwestern sector (Cavinato et al., 2002; Galadini et al., 1997; Michetti et al., 1996) (Fig. 1).

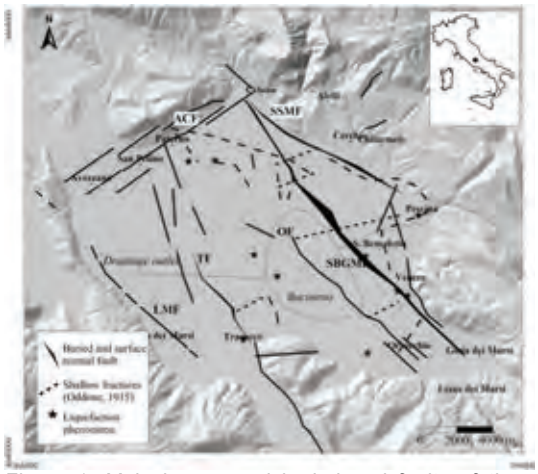

Figure 1: Main known and buried and faults of the Fucino plain. ACF, Avezzano-Celano fault; SSMF, Statale Marsicana fault; SBGMS, San Benedetto-Gioia dei Marsi fault; OF, Ortucchio fault, TF, Trasacco fault; LMF, Luco dei Marsi fault. The thickness of the line indicates the fault offset as reported in Cara et al., 2011. Map limits are in WGS84 UTM33 projection.

The vertical offset across the SBGMF in the Middle and Late Pleistocene very likely exceeds 300 m, providing a slip rate of about 1 mm yr^{-1} (Cara et al, 2011; Michetti et al., 1996; Galadini et al., 1997). Along the SBGMF, up to 0.9 m of vertical coseismic offset was measured after the magnitude 7.0 Avezzano earthquake of 13 January 1915 (Ward and Valensise, 1989; Oddone, 1915). During the earthquake, other seismo-induced geological phenomena, such as liquefaction, spring anomalies, and gas and water emissions, were observed inside the plain (Oddone, 1915) (Fig.1). Furthermore, paleoseismological studies carried out at along the SBGMF demonstrated that coseismic displacement of magnitudes comparable to 1915 earthquake occurred at least once and possibly twice during the Middle Ages (Michetti et al., 1996; Galadini et al., 1997).

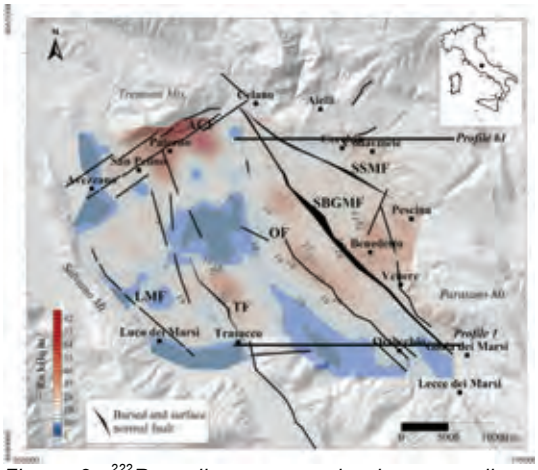

Figure 2: ^{222}Rn soil gas map showing anomalies characterised by an anisotropy along the direction of the main faults of the plain. To simplify the reading of the map, figure shows only the first and the last profiles (1 and 61).

A large number of soil gas samples (more than 1000) were collected in the plain and analysed for different gas species (Rn, CO_2, He and CH_4). Results, discussed in Ciotoli et al., 2007, highlight the presence of linear gas anomalies both in correspondence of known and visible faults of the eastern border of the plain (SBGMF), as well as provided clear indication of the presence of buried faults (OF and TF) in the middle of the plain.
Furthermore, geostatistical analysis conducted on radon data provided a clear correlation between the shape and orientation of the radon anomalies, and the different gas-bearing properties and geometry of the faults recognized both in the western and eastern sectors of the plain. This behaviour implies a broader distribution of radon anomalies and lower values along the TF linked to a wider and highly fractured zone. Whereas, higher values and more sharp anomalies occur along the OF and SBGMF in the eastern side of the plain.

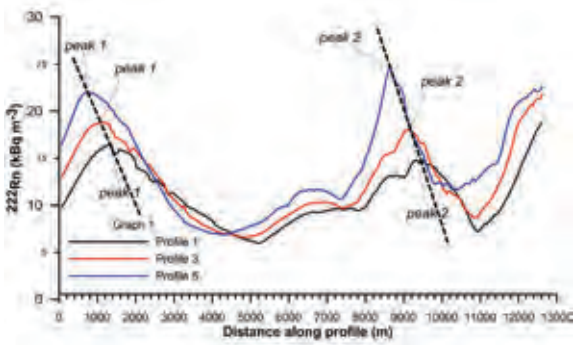

Figure 3: Three radon profiles where two shifted radon peaks are recognised. The distances of the peaks along the profiles was used to locate the peaks on the map.

In this work a re-interpretation of the radon data discussed in Ciotoli et al., 2007 has been conducted in the light of the recent seismic lines, geological data and well stratigraphy reported in Cara et al., 2011 that better define the fault network of the Fucino plain. In particular, the radon map distribution elaborated in Ciotoli et al., 2007 has been sliced to extract 61 E-W radon profiles (see profile1 and profile 61 in fig. 2), 200m spaced in the north direction (Fig. 2). As an example three profiles that shows the shifting of the radon peaks are reported in figure 3. The locations of the sharp radon peaks was then reported in a post-map to study their spatial distribution (Fig. 4).

In general the highest radon values of each profile well delineate the shallow trace of the known SBGMF and TF, as well as also highlight the presence of the inferred OF. Furthermore, the locations of the radon peaks also show sharp deviations toward east at some sectors of the faults, thus indicating the presence of junction zones probably related to fractured zones with geometry e.g., relay ramps or real transfer faults causing the moving back of these structures towards the mountain range. These particular types of geometry are typical of dip-slip structures as those bordered the eastern side of the Fucino plain.

As reported in Ciotoli et al., 2007, radon at equilibrium with its parent nuclide, ^{226}Ra, was calculated by using the Akerblom formula (Akerblom, 1993) from ^{226}Ra content measured in some soil samples; ^{222}Rn at equilibrium yields a value of 26 $kBqm^{-3}$. Thus radon concentrations greater than this value was considered as the anomaly threshold and can be linked to an upward radon migration along enhanced permeability pathways (i.e., faults).

The classed-post map of the radon peaks highlights that values decrease below the anomaly threshold in correspondence of the displacement zones (Fig. 5). It shoud be noted that in the western sector of the plain (in correspondence of TF) radon anomaly threshold is a little bit lower with respect to the eastern sector. are lower.

Figure 4: Post-map of ^{222}Rn soil gas peak (black cross). Radon peaks also show sharp deviations toward east (dotted lines) at some points of the faults, thus indicating the presence of junction zones probably related to fractured zones (e.g., relay ramps) or real transfer faults.

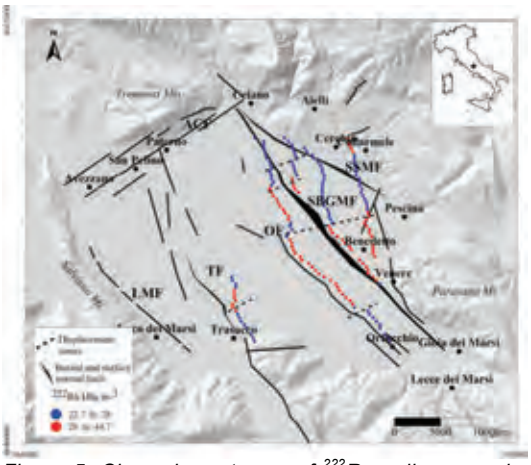

Figure 5: Classed- post map of ^{222}Rn soil gas peak (blue/red circles). Radon values below the anomaly threshold occur in correspondence of the displacement zones along the radon peak alignments.

Two mechanisms can be invoked to explain this phenomenon. The high fracturing of these sectors of the faults may facilitate the penetration of atmospheric air at the sampling depth thus decreasing radon concentrations in the soil pores by dilution. Otherwise, relay ramp structure can also control the stratigraphic nature of the substratum. In this case in the north the presence of lower radon values can be caused by the presence of impermeable siliciclastic sequence interposed between the carbonates and the lacustrine deposits, whereas in the south this latter covers uncorformably the calcareous substratum.

References

Akerblom, G., (1993). Ground radon: Monitoring procedure in Sweden, paper presented at the ''JAG'' Disc. Meeting on Radon Workshop, Geology, Environment, Technology, R. Astron. Soc., London, 12 Feb.

Annunziatellis, A., S.E. Beaubien, S. Bigi, G. Ciotoli, M. Coltella, S. Lombardi, (2008). Gas migration along fault systems and through the vadose zone in the Latera caldera (central Italy): implications for CO2 geological storage. *Int. J. Greenhouse Gas Control*. 2, 353–372.

Baubron, J.C., A. Rigo and J. P. Toutain, (2002). Soil gas profiles as a tool to characterise active tectonic areas: The Jaut Pass example (Pyrenees, France). *Earth Planet. Sci. Lett*., 196, 69–81.

Bigi, S., S.E. Beaubien, G. Ciotoli, C. D'Ambrogi, C. Doglioni, V. Ferrante, S. Lombardi, S. Milli, L. Orlando, L. Ruggiero, M.C. Tartarello, P. Sacco, (2014). Mantle derived CO2 migration along active faults within an extensional basin margin (Fiumicino, Rome, Italy). *Tectonophysics*. 637, 137-149.

Bosi, C., F. Galadini and P. Messina, (1995). Stratigrafia plio-pleistocenica della Conca del Fucino. *Quaternario*, 8(1), 83-94.

Burton, M., Neri, M., Condorelli, D., (2004). High spatial resolution radon measurements reveal hidden active faults on Mt. Etna. *Geophys. Res. Lett.*. 31, L07618.

Cara F., Di Giulio G., Cavinato G.P., Damiani F., Milana G., (2011). Seismic characterization and monitoring of Fucino Basin (Central Italy). *Bull. Eartquake Eng*.. 9, 1961-1985.

Cavinato, G.P., C. Carusi, M. Dall'Asta, E. Miccadei, and T. Piacentini, (2002). Sedimentary and tectonic evolution of

Plio-Pleistocene alluvial lacustrine deposits of Fucino basin (central Italy). *Sediment. Geol.*. 148, 29–59.

Ciotoli G., A. Ascione, S. Bigi, S. Lombardi, S. Mazzoli, (2014). Soil gas distribution in the main coseismic surface rupture zone of the 1980, Ms=6.9, Irpinia earthquake (southern Italy). *J. Geophys. Res. Solid Earth*,. 119, 2440–2461, doi:10.1002/2013JB010508.

Ciotoli, G., S. Lombardi, A. Annunziatellis, (2007). Geostatistical analysis of soil gas data in a high seismic intermontane basin: Fucino Plain, central Italy. *J. Geophys. Res*. 112, B05407. http://dx.doi.org/10.1029/2005JB004044.

Font, Ll., Baixeras, V. Moreno, J. Bach, (2007). Soil radon levels across the Amer fault. *Radiat. Meas.*, doi: 10.1016/j.radmeas.2008.04.072

Fu, C.C., T.F. Yang, V. Walia, and C.-H. Cheng, (2005). Reconnaissance of soil gas composition over the buried fault and fracture zone in southern Taiwan. *Geochem. J.*. 39, 427–439.

King, C.Y., B.S. King, W.C. Evans, and W. Zang, (1996). Spatial radon anomalies on active faults in California. *Appl. Geochem*.. 11, 497–510.

Galadini, F., P. Galli and C. Giraudi (1997). Geological investigations of Italian earthquakes: New paleoseismological data from the Fucino Plain (central Italy). *J. Geodyn*.. 24(1) – (4), 87– 103.

Giraudi, C., (1988). Evoluzione geologica della Piana del Fucino (abruzzo) negli ultimi 30000 anni. *Il Quaternario*. 1(2), 131-159.

Lombardi, S., and N. Voltattorni, (2010). Rn, He and CO2 soil gas geochemistry for the study of active and inactive faults. *Appl. Geochem*.. 25(8), 1206–1220

Michetti, A.M., F. Brunamonte, L. Serva, and E. Vittori, (1996). Trench investigations of the 1915 Fucino earthquake fault scarps (Abruzzo, central Italy): Geological evidence of large historical events. *J. Geophys. Res*.. 101, 5921–5936.

Oddone, G., (1915). Gli elementi fisici del grande terremoto marsicanofucense del 13 gennaio 1915. *Boll. Soc. Sismol. Ital*.. 19, 71– 215

Saroli, M., M. Moro, H. Borghesi, D. Dell'Acqua, F. Galadini, P. Galli, (2008). Nuovi dati paleosismologici dal settore orientale del bacino del Fucino (Italia centrale). *Il Quaternario*. 21(1B), 383-394.

Seminsky, K.Zh., A.A. Bobrov, (2009). Radon activity of faults (western Baikal and southern Angara areas). *Russian Geology and Geophysics*. 50 (8), 682-692. http://dx.doi.org/10.1016/j.rgg.2008.12.010

Swakon, J., K. Kozak, M. Paszkowski, R. Gradzinski, J. Loskiewicz, J. Mazur, M. Janik, J. Bogacz, T. Horwacik, P. Olko, (2005). Radon concentration in soil gas around local disjunctive tectonic zones in the Krakow area. *J. Environ Radioact*. 78, 137–149.

Walia, V., T.F. Yang, W.L. Hong, S.J. Lin, C.C. Fu, K.J. Wen, and C.H. Chen, (2009). Geochemical variation of soil–gas composition for fault trace and earthquake precursory studies along the Hsincheng fault in NW Taiwan. *Appl. Radiat. Isot*.. 67, 1855-1863

Ward, S.N., and G. Valensise, (1989). Fault parameters and slip distribution of the 1915 Avezzano, Italy, earthquake derived from geodetic observations. *Bull. Seismol. Soc. Am*.. 79, 690–710.

INQUA Focus Group on Paleoseismology and Active Tectonics

Imaging the three-dimensional architecture of the Middle Aterno basin (2009 L'Aquila earthquake, Central Italy) using ground TDEM and seismic noise surveys: preliminary results

Civico, R. (1), Sapia, V. (1), Di Giulio, G. (2), Villani, F. (2), Pucci, S. (1), Vassallo, M. (2), Baccheschi, P. (2), De Martini, P.M. (1), Amoroso, S. (2), Cantore, L. (2), Di Naccio, D. (2), Smedile, A. (2), Orefice, S. (1,3), Pinzi, S. (1), Pantosti, D. (1), Marchetti, M. (1)

(1) Istituto Nazionale di Geofisica e Vulcanologia, via di Vigna Murata 605, 00143 Roma, Italia. Email: riccardo.civico@ingv.it
(2) Istituto Nazionale di Geofisica e Vulcanologia, via dell'Arcivescovado 8, 67100 L'Aquila, Italia
(3) Università degli Studi Roma 3, Largo S. Leonardo Murialdo, Roma, Italia

Abstract: *We present preliminary results from a multidisciplinary geophysical approach applied to the imaging of the three-dimensional architecture of the Middle Aterno basin, close to the epicentral area of the 2009 L'Aquila earthquake (central Italy). We collected several time domain electromagnetic soundings (TDEM) coupled with seismic noise measurements focusing on the characterization of the bedrock/infill interface. Our preliminary results agree with existing geophysical data collected in the area, and show that the southeastern portion of the basin is characterized by a deepening of the Mesozoic-Tertiary bedrock down to a depth of more than 450 m. We found that a joint use of electromagnetic and seismic methods significantly contributes in obtaining new insights on the 3D geometry of the Middle Aterno basin. Moreover, we believe that our combined approach based on TDEM and noise measurements can be adopted to investigate similar geological settings elsewhere.*

Key words: *Central Apennines, extensional basin, TDEM, ambient noise.*

INTRODUCTION

The Mw 6.1 April 6, 2009 L'Aquila earthquake and related sequence (Herrmann et al., 2011) struck a densely populated area in central Italy causing heavy damage in the town of L'Aquila and surrounding villages, with 309 fatalities and thousands of injured. The mainshock was related to a 12 to 19 km-long, NW-SE oriented, SW-dipping causative normal fault (Chiaraluce, 2012 and references therein), which caused coseismic surface breaks and noticeable hangingwall subsidence (Atzori et al., 2009; Emergeo Working Group, 2010 and references therein). This fault belongs to the Paganica - San Demetrio fault system (PSDFS, according to Galli et al., 2010 and Civico et al., 2014). The latter consists of a ~20 km long network of Quaternary normal faults that originated a wide intermontane continental basin (Middle Aterno basin; Pucci et al., 2014).

The PSDFS belongs to a wider system of Pliocene-Quaternary, NW-SE and NNW-SSE striking normal faults affecting the whole inner central Apennines and responsible for the generation of several intermontane continental basins (Cavinato & De Celles, 1999; Ghisetti & Vezzani, 1999).

The Middle Aterno basin is characterized by the presence of an extensive cover of lacustrine and fluvial/alluvial deposits accumulated upon a Meso-Cenozoic carbonatic and siliciclastic bedrock, and generally separated by unconformities and/or displaced by the PSDFS (Pucci et al., 2014).

The 2009 L'Aquila earthquake triggered several studies aimed at defining the subsurface geometry of the Middle Aterno basin (among the others: MS-AQ Working Group, 2010; Balasco et al., 2011; Improta et al., 2012; Santo et al., 2013).

Balasco et al., (2011) investigated the large-scale structure of the northeast part of the basin by means of a ~8 km-long, Electric Resistivity Tomography (ERT) that complemented a magnetotelluric profile (~1000 m investigation depth). Their resistivity section highlights the existence of complex lateral and vertical resistivity changes in the NE sector (between Mt. Bazzano and Paganica), that can be related to the presence of a shallow conductive alluvial filling (~200 m-thick) above a rugged carbonate substratum. In the same area, Improta et al., (2012) performed a high-resolution seismic survey over an 8 km long section. Their tomographic images define the basin structure down to a depth of ~350 m, highlighting the presence of a complex topography of the pre-Quaternary substratum, with a ~350 m deep depocenter in the Bazzano sub-basin. They evidence strong lateral heterogeneities and steps in the substratum (NE of Mt. Bazzano), suggesting the presence of buried synthetic and antithetic fault splays involving bedrock and basin infill deposits within the Paganica sub-basin.

Santo et al., (2013) present the subsurface setting of the south-easternmost portion of the basin obtained by merging existing geophysical data from microzoning activity and some old vertical electrical soundings reported by Bosi & Bertini (1970).

Although the abovementioned results provided new information of the subsurface basin geometry, they still suffer from limited areal extension and/or investigation depth, moreover the long-term reconstruction of the fault system and basin evolution is hampered by few reliable subsurface constraints covering the whole basin.

To contribute to fill this gap of knowledge, we performed extensive surveys in the Middle Aterno basin by using a combined geophysical approach based on

Time-Domain Electromagnetic Method (TDEM) and ambient noise vibrations measurements. The main aim of our approach is to map the buried interface between the continental infilling deposits and the Mesozoic-Tertiary marine substratum. TDEM and noise measurements resulted a suitable strategy for defining the geometry of the Middle Aterno basin to more than 450 m in depth.
The work is still in progress, anyway we can present the areal extent of the already collected data and a preliminary reconstruction of a limited portion of the Middle Aterno basin at depth.

METHODS AND DATA ACQUISITION

Time-domain electromagnetic method (TDEM) is based on the induction of a time-varying secondary magnetic field produced by decay current in the ground. This secondary magnetic field is measured by an induction receiver coil, generally placed at the centre of a transmitter loop. As the current diffuses deeper into the ground (at later time), the signal measurements provide information on the conductivity of the lower layers. TDEM is sensitive to subsurface resistivity: the latter for near-surface earth materials can vary by several orders of magnitude, being thousands of Ωm for carbonates or crystalline rocks and few Ωm for clay and/or saturated alluvium (e.g. Palacky 1987). Although it is not possible to establish a 1:1 correlation between resistivity values and heterogeneous infill materials, TDEM soundings can offer a cheap alternative to drilling several wells in defining the depth of a gently dipping bedrock (Hobza et al. 2012; Bedrosian et al., 2013).
We used a three-component receiver coil, in conjunction with a transmitter square loop of 50 m and 100 m size, respectively. TDEM measurements were performed both in central-loop and offset receiver configuration. We adopted standards from Geonics Ltd. (Rob Harris, personal communication) for the determination of the input current, gain setting and number of stacks.
We performed our TDEM surveys taking into account local issues in order to avoid high-noise sites (related to infrastructures/lifelines). Indeed, for each site we performed initial noise tests, showing that the signal-noise level was generally low in the study area. However, since the surveys span a large geographic area, we repeated the initial noise tests for each site. It helped us in discarding some unreliable TDEM measurements due to anthropogenic noise. In addition, unreliable data distorted by 2D or 3D structure (i.e. fault) were also removed prior to inversion (Newman et al., 1986). Data processing was made with the SiTEM software, and the resistivity data were inverted with the SEMDI program (Effersø et al., 1999) to obtain 1-D resistivity model of the subsurface.
We coupled TDEM measurements with recordings of ambient seismic vibrations, in order to better constrain the depth of the seismic basement. We used the classical H/V method (Nakamura, 1989) based on the spectral ratio between the horizontal and the vertical components of ambient noise data. The resonance frequency (f0) was obtained from the peak of the H/V curves. The value of f0, for 1-D structures, is closely linked to the mean properties (thickness and shear-wave velocity Vs) of the soft soil (Bonnefoy-Claudet et al., 2006). Assuming the 1-D quarter wavelength approximation, we derived the bedrock depth (in terms of a range of possible values) from the f0 values. This implies that a reliable Vs profile of the sedimentary filling was first assumed in the valley. Indeed Vs values were provided by surveys carried out in the L'Aquila surroundings and in the Middle Aterno after the microzoning activity. Typical estimated Vs values of the sedimentary filling within the basin are 600-700 m/s (MS-AQ Working Group, 2010; Di Giulio et al., 2014). Ambient noise was recorded using 24-bit Reftek130 data loggers

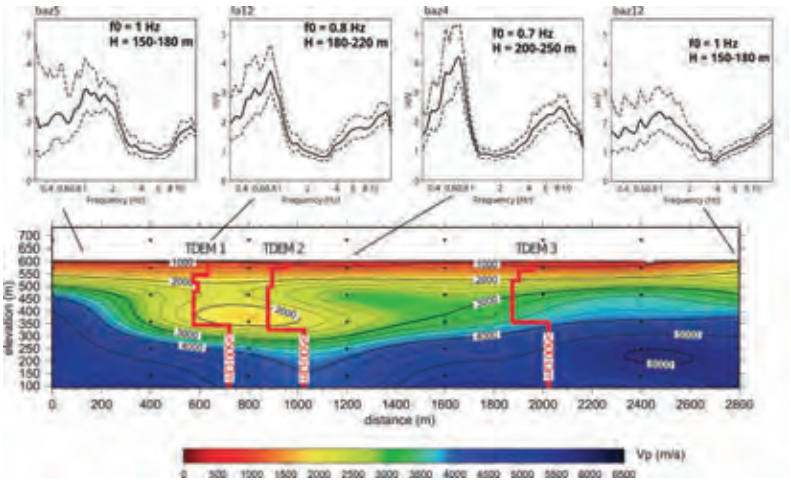

Figure 1: Vp tomogram of two merged high-resolution seismic lines across the Bazzano basin (B1 and B2, modified after: Improta et al., 2012). Three 1-D resistivity models derived from the inversion of TDEM data (solid red lines), and four H/V curves computed from noise measurements (upper panel), are also projected along the Vp model. The infill/bedrock interface displays high resistivity (> 500 Ωm) in the 1-D models, and high Vp (>3500 m/s) in the tomogram. The values of f0 and H (where H indicates a possible range for the depth of the bedrock) are also shown in the inset of the H/V curves. The blue line at 650 m distance along the tomgram indicates a 150 m deep borehole (Porreca et al., 2013) conducted as part of the FIRB Abruzzo Project.

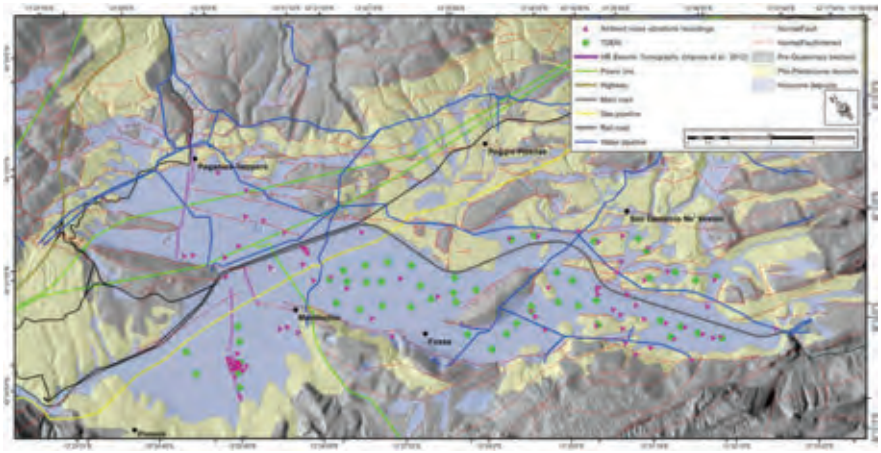

Figure 2: Location map of TDEM and seismic noise surveyed sites, showing the main infrastructures and lifelines in the Middle Aterno basin, and the trace of the seismic lines and Deep ERT. Simplified geology and main faults of the area redrawn after Pucci et al., (2014).

coupled to Lennartz LE-3D5s velocimeters with eigenfrequency of 0.2 Hz. The sampling rate was fixed at 250 Hz with recording duration of at least 50 minutes. Data processing for computing the H/V curves was performed with the Geopsy code (http://www.geopsy.org).

We successfully calibrated TDEM and ambient seismic noise data against: available wells information (MS-AQ Working Group, 2010; Porreca et al., 2013), existing geophysical investigations (Improta et al., 2012) and Deep ERT profiles (Delcher et al., in prep.). As an example, in Figure 1 we show the results of three TDEM soundings and four noise measurements collected along the high-resolution seismic tomography profile. In particular, we observe at ~230 m depth in the 1-D models a high resistivity contrast, with values larger than 500 Ωm, that we interpreted as the interface between the Quaternary infill and the Mesozoic-Tertiary bedrock.

The recovered 1-D resistivity models show a good agreement with the seismic section both in the near surface and in the deeper part of the two models. The f0 trend resulting from H/V curves is also fairly in agreement with the bedrock depth shown by the seismic section.

We then expanded our survey performing TDEM and microtremor measurements at regularly spaced intervals (about 500 m spacing between adjacent stations) and collecting so far a total of 51 TDEM and 103 seismic noise measurements respectively (Figure 2). We eventually interpolated a raster surface from depth to bedrock data points using a two-dimensional minimum curvature spline technique. The spline tool uses an interpolation method that estimates values using a mathematical function that minimizes overall surface curvature and the resulting smooth surface passes exactly through the input depth to bedrock points. As primary boundary conditions, we obviously imposed the bedrock depth to be zero along the perimeter of all the bedrock outcrops within the basin and along its margins.

PRELIMINARY RESULTS AND DISCUSSION

Despite logistical difficulties, the geophysical survey by means of TDEM and noise methods is in progress along the whole Middle Aterno basin. Here, we present a preliminary interpolation of the recovered depth of the pre-Quaternary bedrock top-surface of the southern portion of the basin, in order to reconstruct its subsurface geometry (Figure 3).

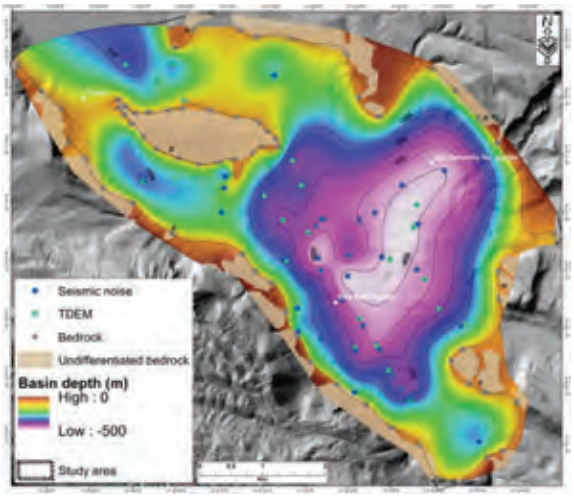

Figure 3: Interpolated top-bedrock surface in the south-eastern sector of the Middle Aterno basin (contour interval: 100 m).

Notwithstanding it might be difficult to discriminate among Meso-Cenozoic carbonate bedrock and Early Quaternary cemented carbonatic breccias (Megabrecce Fm Auct. - mainly found in the northwestern portion of the basin), our result highlights the presence of a complex basin structure formed by thresholds separating some 100-200 m-deep depocenters, with a maximum depth >450 m located between the villages of San Demetrio Ne' Vestini and Villa Sant'Angelo, at the southern end of the Middle Aterno basin (Figure 3). This

deepest part of the basin has a rough triangular shape with a side paralleling the western slope of the valley and a vertex close to the San Demetrio Ne' Vestini village. As a consequence, the SE side of the depocenter is characterized by a strong topographic gradient, in coincidence with the tip of the Quaternary basin. Notably, the shape of this maximum depocenter is not coherent with the NW-trending, Quaternary normal faults affecting the eastern side of the basin. This evidence suggests that the onset of the Middle Aterno Quaternary basin was controlled by the long-term activity of a differently oriented fault system that could have played a key role before or together with the PSDFS segments through time.

This buried deep depocenter of the basin is also confirmed by a 2-D deep ERT (Delcher et al., in prep.) as well as by a low-resolution map of gravimetric anomalies (Di Filippo et al., in: MS-AQ Working Group, 2010) performed independently in the same area.

The data of the present work yield new insight to reconstruct the 3D image of the Middle Aterno basin. Indeed, our study emphasizes the utility and flexibility of combining two different methods (TDEM and ambient noise) in reconstructing the 3D geometry of the Middle Aterno Basin bottom.

The reconstruction of the physiography of the tectonic-related Quaternary basin bottom represents a critical contribution to the estimation of the fault system evolution and thus to the evaluation of the seismogenic potential of the active structures.

Acknowledgements: The measurements were collected in the Abruzzo project, "High-resolution analyses for assessing the seismic hazard and risk of the areas affected by the 6 April 2009 earthquake" (http://progettoabruzzo.rm.ingv.it/en; funding codes: RBAP10ZC8K_005, RBAP10ZC8K_003, RBAP10ZC8K_007), and from available measurements resulting from the activity connected to the microzoning activity of the area. We are grateful to Rob Harris and Antonio Menghini for their technical support in data acquisition. We also thank Aarhus Geophysics Aps for their precious help in TDEM data modeling.

References

Atzori, S., I. Hunstad, M. Chini, S. Salvi, C. Tolomei, C. Bignami, S. Stramondo, E. Trasatti, A. Antonioli & E. Boschi, (2009). Finite fault inversion of DInSAR coseismic displacement of the 2009 L'Aquila earthquake (central Italy), *Geophys. Res. Lett.*. 36, L15305, doi:10.1029/2009GL039293.

Balasco, M., P. Galli, A. Giocoli, E. Gueguen, V. Lapenna, A. Perrone, S. Piscitelli, E. Rizzo, G. Romano, A. Siniscalchi & M. Votta, (2011). Deep geophysical electromagnetic section across the middle Aterno Valley (central Italy): preliminary results after the April 6, 2009 L'Aquila earthquake. *Boll. Geofis. Teor. Appl.*. doi: 10.4430/bgta0028

Bedrosian, P.A., M.K. Burgess & T. Nishikawa, (2013). Faulting and groundwater in a desert environment: constraining hydrogeology using time-domain electromagnetic data. *Near Surface Geophysics*. 11, (5), 545-555.

Bergamaschi, F., G. Cultrera, L. Luzi, R.M. Azzara, G. Ameri, P. Augliera, P. Bordoni, F. Cara, R. Cogliano, E. D'Alema, D. Di Giacomo, G. Di Giulio, A. Fodarella, G. Franceschina, F. Galadini, M.R. Gallipoli, S. Gori, P. Harabaglia, C. Ladina, S. Lovati, S. Marzorati, M. Massa, G. Milana, M. Mucciarelli, F. Pacora, S. Parolai, M. Picozzi, M. Pilz, S. Pucillo, R. Puglia, G. Riccio, M. Sobiesiak, (2011). Evaluation of site effects in the Aterno river valley (Central Italy) from aftershocks of the 2009 L'Aquila earthquake. *Bulletin Earthquake Engineering*. 9, 697-715.

Bonnefoy-Claudet, S., C. Cécile, B. Pierre-Yves, C. Fabrice, M. Peter, K. Jozef & D. Fäh, (2006). H/V ratio: a tool for site effects evaluation. Results from 1-D noise simulations. *Geophysical Journal International*. 167, (2), 827-837.

Bosi, C. & T. Bertini, (1970). Geologia della media valle dell'Aterno. *Mem. Soc. Geol. It.*. 9, 719 - 777

Cavinato, G.P. & P.G. De Celles, (1999). Extensional basins in the tectonically bimodal central Apennines fold-thrust belt, Italy: response to corner flow above a subducting slab in retrograde motion. *Geology*, 27. (10), 955-958.

Chiaraluce, L., (2012). Unraveling the complexity of Apenninic extensional fault systems: A review of the 2009 L'Aquila earthquake (Central Apennines, Italy). *Journal of Structural Geology*. 42, 2-18.

Civico, R., S. Pucci, D. Pantosti & P.M. De Martini, (2014). Morphotectonic analysis of the long-term surface expression of the 2009 L'Aquila earthquake fault (Central Italy) using airborne LiDAR data. In press. *Tectonophysics*. doi:10.1016/j.tecto.2014.12.024.

Di Giulio, G., I. Gaudiosi, F. Cara, G. Milana & M. Tallini, (2014). Shear-wave velocity profile and seismic input derived from ambient vibration array measurements: the case study of downtown L'Aquila. *Geophysical Journal International*. 198, (2), 848-866.

Effersø, F., E. Auken, K.I. Sørensen, (1999). Inversion of band-limited TEM responses. *Geophysical Prospecting*. 47, 551–564.

Emergeo Working Group, (2010). Evidence for surface rupture associated with the Mw 6.3 L'Aquila earthquake sequence of April 2009 (central Italy). *Terra Nova*. 22: 43–51, doi: 10.1111/j.1365-3121.2009.00915.x

Fäh, D., F. Kind & D. Giardini, (2001). A theoretical investigation of average h/v ratios. *Geophysical Journal International*. 145, 535-549.

Galli, P., B. Giaccio & P. Messina, (2010). The 2009 central Italy earthquake seen through 0.5 Myr-long tectonic history of the L'Aquila faults system. *Quaternary Science Reviews*. 29, 3768-3789.

Ghisetti, F., & L. Vezzani, (1999). Depths and modes of Pliocene-Pleistocene crustal extension of the Apennines (Italy). *Terra Nova*, 11, 67-72.

Herrmann, R.B., L. Malagnini, and I. Munafò, (2011). Regional Moment Tensors of the 2009 L'Aquila Earthquake Sequence. *Bulletin of the Seismological Society of America*. 101, (3), 975-993.

Hobza, C.M., P.A. Bedrosian and B.R. Bloss, (2012). Hydrostratigraphic interpretation of test-hole and surface geophysical data, Elkhorn and Loup River Basins, Nebraska, 2008 to 2011. *U.S. Geological Survey Open-File Report 2012–1227*.1-95.

Improta, L., F. Villani, P.P. Bruno, A. Castiello, D. De Rosa, F. Varriale, M. Punzo, C.A. Brunori, R. Civico, S. Pierdominici, A. Berlusconi, G. Giacomuzzi, (2012). High-resolution controlled-source seismic tomography across the Middle Aterno basin in the epicentral area of the 2009, Mw 6.3, L'Aquila earthquake (central Apennines, Italy). *Italian Journal of Geosciences*. 131, (3), 373-388.

MS-AQ Working Group, (2010). Microzonazione sismica per la ricostruzione dell'area aquilana. In: *Regione Abruzzo-Dipartimento della Protezione Civile*. 3, 1–796.

Nakamura, Y., (1989). A method for dynamic characteristics estimation of subsurface using microtremor on the ground surface. *Railway Technical Research Institute, Quarterly Reports*. 30, (1), 25-33.

Newman G.A., G.W. Hohmann & W.A. Anderson, (1986). Transient electromagnetic response of a three-dimensional body in a layered earth. *Geophysics*. 51, 1608–1627.

Palacky, G.J., (1987). Resistivity characteristics of geologic targets. In: (M.N. Nabighian ed.). *Electromagnetic Methods in Applied Geophysics*. 1, 53 –129.

Porreca, M., T. Mochales Lopez, A. Smedile, P. Macrì, A. Di Chiara, I. Nicolosi, F. D'Ajello Caracciolo, R. Carluccio, G. Di Giulio, M. Vassallo, S. Amoroso, F. Villani, L. Sagnotti, F. Speranza, (2013). LAqui-core, a 150 m deep borehole into the depocenter of the basin controlled by the 2009 Mw=6.1. L'Aquila earthquake fault. *AGU Fall Meeting 2013*. San Francisco, 9-13 December, 2013

Pucci, S., F. Villani, R. Civico, D. Pantosti, P. Del Carlo, A. Smedile, P.M. De Martini, E. Pons-Branchu, A. Gueli, (2014). Quaternary geology map of the Middle Aterno Valley, 2009 L'Aquila earthquake area (Abruzzi Apennines, Italy). *Journal of Maps*. doi: 10.1080/17445647.2014.927128.

Santo, A., A. Ascione, G. Di Crescenzo, E. Miccadei, T. Piacentini & E. Valente, (2013). Tectonic-geomorphological map of the middle Aterno River valley (Abruzzo, Central Italy). *Journal of Maps*. doi: 10.1080/17445647.2013.867545

INQUA Focus Group on Paleoseismology and Active Tectonics

Tectonic evidence in the Palaeolithic site of Lademagne (San Giovanni Incarico – FR, Southern Latium, Italy)

Comerci, V.(1), Biddittu, I. (2), Di Manna, P. (1), Germani, M. (2), Piccardi, L. (3), Ventura, G. (1), Vittori, E. (1)

(1) ISPRA, Geological Survey of Italy, Via Vitaliano Brancati, 48, Roma, Italy. Email: valerio.comerci@isprambiente.it
(2) Italian Istitute of Human Paleontology, Piazza Ruggero Bonghi, 2, Anagni (FR), Italy
(3) CNR, Institute of Geosciences and Earth Resources, Via La Pira, 4, Firenze, Italy

Abstract: *Within the project for the construction of a photovoltaic power plant in the territory of San Giovanni Incarico (Frosinone, Southern Latium, Italy), the Palaeolithic site of Lademagne has undergone archaeological preventive investigations by the Superintendence for Archaeological Heritage of Latium. During the excavation of trenches along the eastern border of the northwest – southeast oriented fault-bounded Lademagne relief, a series of tectonic structures were brought to light. In particular, fault planes (reaching the topographic surface) and a liquefaction evidence were found, affecting sediments possibly belonging to Middle-Late Pleistocene, according to a tentative stratigraphic correlation based also on content of archaeological artefacts and bones. The preliminary analysis of this neotectonic evidence are presented here. More studies are underway to verify the potential paleoseismological relevance of the area.*

Key words: *Surface faulting, Liquefaction, Palaeolithic, Lademagne, Southern Latium.*

INTRODUCTION

The Paleolithic site of Lademagne (San Giovanni Incarico - Frosinone), discovered and investigated by Biddittu since 1965, is located just over a kilometre to the east of San Giovanni Incarico lake and just over two kilometres northwest of the confluence of the Melfa River in the Liri River (Fig. 1).
Surface investigations carried out by the Italian Institute of Human Paleontology in the last decades allowed to identify two archaeological levels (separated by about 5 meters of sediment) attributed to the Lower Paleolithic (Acheulean facies with bifacial, bone and flake industry and fossil fauna; Biddittu & Celletti, 2003).
Within the project for the construction of a grounded photovoltaic power system, the site has undergone prior archaeological investigations by the Superintendence for Archaeological Heritage of Latium. Between 120 and 100 m a.s.l., 20 trenches oriented northwest - southeast and north-south have been excavated. The length of each segment of the trenches ranged from 5 to 45 meters, the average width was about 1.40 m and the average depth was 1.30 m.
Along the eastern edge of the investigated area, the trench 18A oriented north-south has brought to light a tectonic element, in addition to archaeological material and macrofossil fauna.

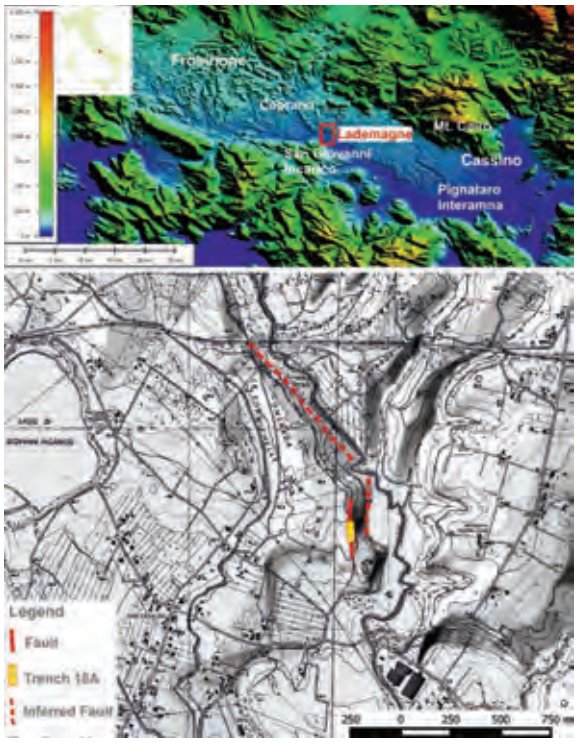

Figure 1: Location of the Lademagne site, trench 18A and inferred faults.

GEOLOGY AND TECTONICS OF THE SITE

The Lademagne site is located at the northwestern edge of the sedimentary basin called Lake Lirino (Ferrero, 1879; Devoto, 1965) that, in the Middle Pleistocene, stretched for at least 30 km in length, from Ceprano to Cassino - Pignataro Interamna (Fig. 1), and on average 10 km in width. In the study area, the lacustrine deposits show thickness ranging from 70 to 100 meters: in the lower portion, they are prevalently represented by white and yellow silt and silty clay with interbedded tuffs levels, while, in the upper portion, grey silty clay, yellow sands and travertine are present. These deposits are dissected by apenninic and antiapenninic normal faults and show diffuse evidence of extensional active

tectonics during the Lower-Middle Pleistocene. In this sector, the major fault mapped as active in the Pliocene-Quaternary time is the Mt Cairo fault, bordering the north-eastern flank of the Lirino basin (Ambrosetti et al., 1987). The same fault is mapped as inactive by Roberts and Michetti (2004).

On the site, in particular, emerge terraced alluvial deposits, predominantly gravelly-sandy, attributed, according to Centamore et al. (in press) to the *Sintema di Ceprano* (II order terraces), Middle-Late Pleistocene in age.

A stratigraphic section in Lademagne was already proposed by Segre (1984), with an indication of findings of Acheulean lithic industry within sediments that appear to correspond to the deposits of the terraces of III order described by Carrara (1991).

Acheulean industry was also found in a layer of a geological section excavated near the northeastern shore of the San Giovanni Incarico lake, in 1999, during the construction of the *TAV* high speed railway line (Leonardi et al., 1999; Biddittu & Celletti, 2003).

Datings made by the method of racemization on a molar of *Bos primigenius* Bojanus, found in a level possibly attributable to the same layer, have provided an age of about 174 kyr (Belluomini & Vessica, 1999).

A few metres north of the trench 18A an excavation reached a depth of -3.1 metres, starting from the elevation of 105 m a.s.l.. Figure 2 shows the stratigraphic sequence. The gastropods found in level c (*Planorbis sp.*, *Valvata cristata*, *Pisidium sp.*) indicate a quiet (lacustrine) freshwater habitat. These fossils are known in the Plio-Pleistocene sediments of Central Italy (Settepassi & Verdel, 1965; Ciangherotti & Esu, 2000); in particular, *Valvata cristata* is reported in the levels of typical and late lacustrine facies.

During the digging of the trench 18A, a fault throw of 10-15 cm was found in the carbonate silts outcropping on the bottom of the excavation. This extensional tectonic element is oriented approximately north-south (N10° E) and dips toward east of 70-80 degrees. The fault step has been observed for a length of more than 13 metres (Figure 3). The fault also displaces the gravelly-sandy sequence overlying the white carbonate silts.

Figure 4 shows the downthrow of about 15 cm in sands and gravels outcropping in the southern wall of trench 18 (III), which is perpendicular to the trench 18A. The fault is highlighted by whitish calcium carbonate precipitated from fluids of interstitial circulation along the tectonic discontinuity. The faulted sediments presumably belongs to the upper part of Middle Pleistocene, according to the archaeological artefacts and bones found in the gravelly and sandy layers (for description see Biddittu et al., 2012). Moreover, it is evident that the fault has reached the surface topography, dislocating it. The fault, indeed, ends only against the ploughed soil.

In the north wall of trench 18A is also observed a "seismite", i.e. evidence of liquefaction of the ground due to seismic shaking (Figure 5). Because of the latter, the pore water pressure has exceeded the effective

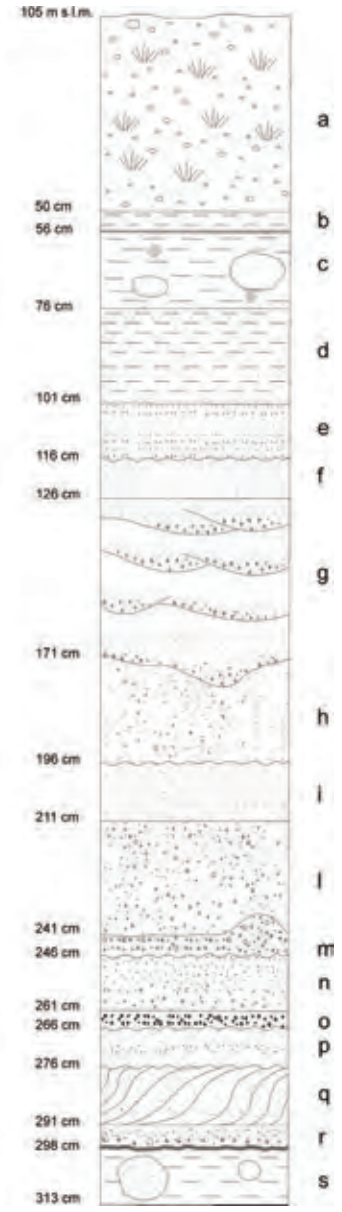

*Figure 2: Stratigraphic log of Lademagne site. a: ploughed soil; b: sandy silt with, at the base, a gray pyroclastic fine-grained level, 1 cm thick; c: light brown clayey silts with the presence of gastropods (*Planorbis sp., Valvata cristata, Pisidium sp.*) and decimetric carbonate findings; d: brown sandy silt with oxidation and altered volcanic minerals; e: sand and gravel up to 1 centimeter, with interbedded fine sands; f: yellowish fine sands with a reddish oxidation level on top; g: alternations of cross-bedded gravels and sands; h: thin gravels with oxidations; i: sands rich in volcanic minerals; l: centimetric gravels in sandy matrix with interbedded sands rich in volcanic minerals; m: rounded carbonate gravels with an oxidated level on top; n: thin gravels with interbedded sands, oxidation levels and films; o: centimetric oxidated gravels; p: Sands with interbedded gravels; q: cross-bedded millimetric sandy gravels with foreset laminae; r: upward fining rounded carbonate gravels, up to centimeters. On the bottom and at the top of the layer, centimetric patinas of oxidation; s: yellowish silt with included decimetric rounded sandy findings, and decimetric carbonate deposits.*

stress of silty-sandy sediments, liquefying them. The sediments stratification is, indeed, interrupted by the seismite (marked in black in Figure 5).
This evidence of liquefaction was found in correspondence of the fault, exactly where the step downthrowing the carbonate silts intersects the northern wall of the trench (Figure 3). In the trenches adjacent to the 18A, other evidence of faulting were found.

Figure 3: The fault step outcropping in the trench 18A, downthrowing eastward the carbonate silts. On the northern wall of the trench is visible a liquefaction feature (see Figure 5).

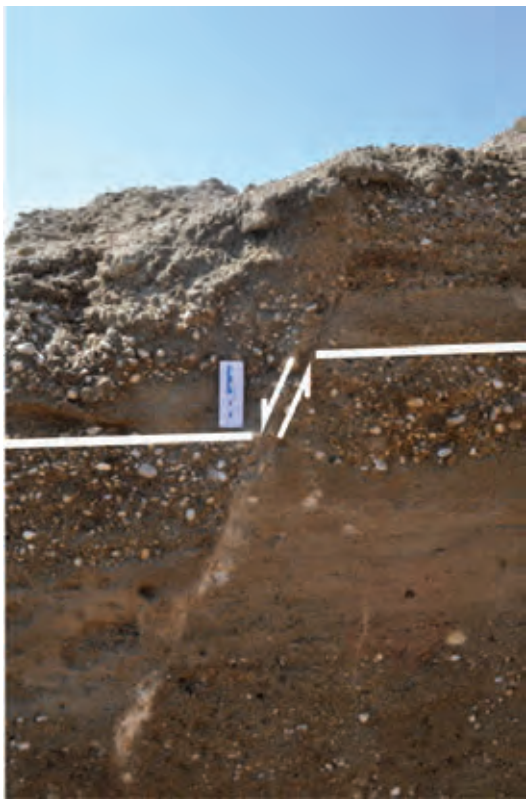

Figure 4: The extensional fault that displaces all the sediments of the trench 18 (III) (southern wall) up to the surface. The downthrow is about 15 cm.

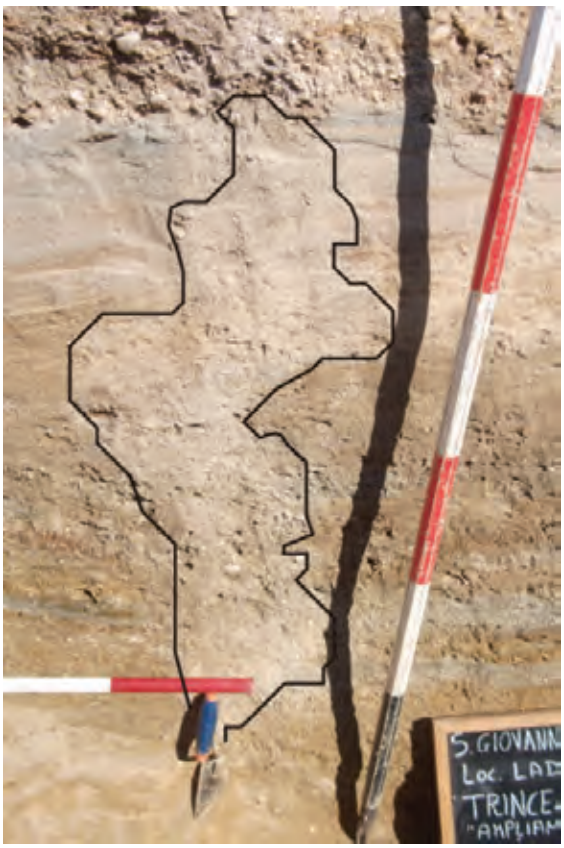

Figure 5: Evidence of liquefaction along the northern wall of the trench 18A, located in correspondence of the fault (see Figure 3).

The south wall of the trench 18 (II) is shown in Figure 6. It is possible to see, also in this case, a fault trace coming up to the topographic surface. This fault has the same direction and dipping of the one displacing the white carbonate silts (found in trench 18A) and is located some metres upstream. Also the degree of downthrow is comparable. It is worth noting that the stratification is tilted westward, consistently with the kinematics of the described extensional fault system.

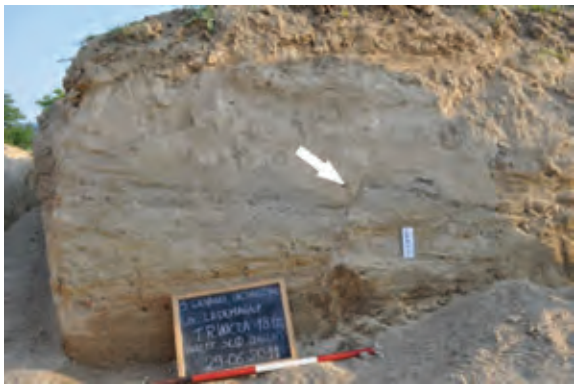

Figure 6: Southern wall of trench 18 (II). The arrow indicates an extensional east-dipping fault, synthetic to the fault found in the trench 18A and with similar downthrow.

CONCLUSIONS

The preliminary results presented here are a clear indication of the Pleistocene extensional tectonics that affected the area. Further studies are needed to frame the discovered evidence in the context of regional tectonics, and better constrain the neotectonic activity.
The faults here described can represent secondary structures, synthetic to the main lineament presumably bordering eastward the Lademagne relief. Supplementary investigation is needed to confirm (or reject) this hypothesis, define the role played by the tectonic evolution on the stratigraphy and geomorphology, and, possibly, assess the current seismic hazard, both in terms of seismic shaking and surface faulting, considering that the area has a modest seismic history, but it is bordered (just north and east) by the Sora-Arpino and Cassino highly seismic zones.

References

Ambrosetti, P., C. Bartolini, C. Bosi, F. Carraro, N. Ciaranfi, M. Panizza, G. Papani, L. Vezzani, A. Zanferrari, (1987). Neotectonic Map of Italy (Scale 1:500.000). *C.N.R., P.F. Geodinamica*.

Belluomini, G., P. Vessica, (1999). Aminocronologia. In: (Zarattini A., ed.) *Isoletta (Arce), indagine geoarcheologica e paleoambientale*. Inedited.

Bidditu, I., P. Celletti, (2003). Età della pietra. Uomini ed elefanti nella preistoria del Lazio meridionale. *Quaderni Fregellani*. Museo Archeologico di Fregellae. 160 p.

Bidditu, I., E. Canetri, V. Comerci, M. Germani, G. Picchi, (2012). Nuove ricerche nel giacimento del Paleolitico inferiore di Lademagne, S. Giovanni Incarico (Frosinone). In: (Ghini, G., Mari, Z., eds). *Lazio e Sabina*. Edizioni Quasar, 9, 437-443.

Carrara, C., (1991). Travertine deposits of the middle Liri Valley (Central Italy): geomorphological, sedimentological and geochemical study. Palaeoenvironmental and paleoclimatic implications. *Il Quaternario*. 4, 1a, 55-84.

Centamore, E., F. Dramis, P. Di Manna, D. Rossi, M.R. Palombo, (in press). Depositi continentali plio-quaternari - Note illustrative della Carta Geologica d'Italia alla scala 1:50.000 – Foglio 402-Ceccano. ISPRA-Servizio Geologico d'Italia.

Ciangherotti, A., D. Esu, (2000). Paleoecologic and biochronologic meaning of Early Pleistocene molluscan fauna from the Anghiari Basin (Tiber River Upper Valley, Central Italy). *Boll. Soc. Paleont. It.*. 39 (2), 217-224.

Devoto, G., (1965). Lacustrine Pleistocene in the Lower Liri Valley (Southern Latium). *Geologica Romana*. 4, 291-368.

Ferrero, L.O., (1879). Le terre della Provincia di Lavoro. Profili sopra la costituzione del suolo della provincia, con attinenze della Geologia collo studio del suolo agrario. *Per l'esposizione regionale di Caserta*. Caserta.

Leonardi, R., V. Pisano, C. Villani, P. Zambianchi, (1999). Ricostruzione paleoambientale e stratigrafia. In: *Isoletta (Arce), indagine geoarcheologica e paleo ambientale* (Zarattini, A. ed.). Inedited. 2-74.

Roberts, G.P., A.M. Michetti, (2004). Spatial and temporal variations in growth rates along active normal fault Systems: an example from the Lazio-Abruzzo Apennines, Central Italy. *Journal of Structural Geology*. 26 (2004), 339–376.

Segre, A.G., (1984). Scheda 85. Lademagne, Lazio. In: *I primi abitanti d'Europa*. Museo Nazionale Preistorico Etnografico "Luigi Pigorini", Roma, 167-168.

Settepassi, F., U. Verdel, (1965). Continental Quaternary mollusca of Lower Liri Valley (Southern Latium). *Geologica Romana*. 4, 369-452.

INQUA Focus Group on Paleoseismology and Active Tectonics

Morphogenic paleoearthquakes in the Andean broken-foreland (Pampean Ranges, Argentina): How large?, how often?

Costa, C.

Departamento de Geología, Universidad Nacional de San Luis, E. de los Andes 950, 5700 San Luis, Argentina. Email: costa@unsl.edu.ar

Abstract: *The Pampean Ranges are Neogene uplifted blocks bounded by reverse faults, where Quaternary faulting has been extensively documented, but no historic surface ruptures were reported. This contribution discusses on some characteristics and challenges posed by paleoearthquake evidences, regarding their significance in terms of seismogenic sources. Examples of two fault systems suggest that the threshold magnitude for morphogenic earthquakes in this crustal setting should be close to M 7.5, whereas recurrence intervals seems to have been quite variable.*

Key words: *Pampean Ranges, Argentina, morphogenic earthquakes, paleoseismology.*

INTRODUCTION

The most prominent geologic provinces related to Neogene mountain building at the southern Pampean flat-slab in Argentina (31°S and 33°S) (Fig. 1), are from West to East: the Andean orogeny and the Pampean Ranges (Sierras Pampeanas). These ranges constitute a distinctive characteristic related to the sub- horizontal subducting geometry of the Nazca plate (Jordan et al., 1983, Ramos et al. 2002), which widely crop-out at Central Western Argentina. The Pampean uplifts are bounded by West-verging reverse faults dipping 30°-55°E, where Quaternary deformations are concentrated.
The current active orogenic front is located between the Eastern foothills of the Precordillera and the western boundary of the Sierras Pampeanas. Such a dynamic interaction is highligthed by a clustered crustal seismicity and by the occurrence of the most destructive earthquakes in the country of the 20th century (Alvarado et al., 2007). It concentrates also the most striking Quaternary deformation in Argentina.

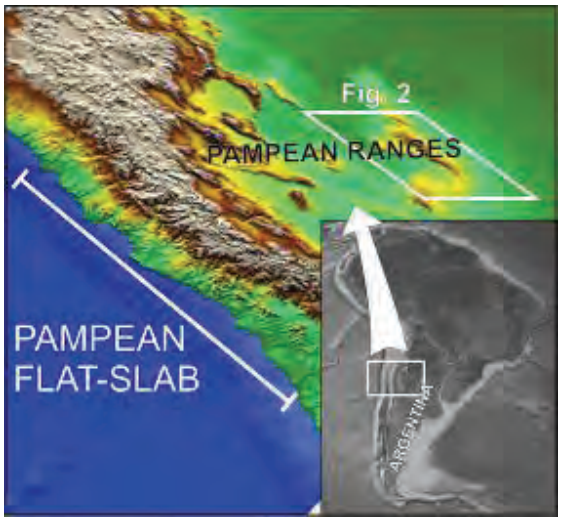

Figure 1: Location of the Pampean Ranges.

Only moderate shallow crustal earthquakes (≤ M 6.5) have shocked the Pampean Ranges region during historical times. Accordingly, based on the seismic catalog, the seismogenic potential of this region, has traditionally been envisaged as considerably lower than the Andean belt. However, many earthquake-related evidences have been found during the last years along several neotectonic structures in the Pampean Ranges, such as primary surface ruptures, large rock-avalanches and paleoliquefaction phenomena (Costa et al., 2014 among others). These evidences have no historical analogs, but they testify for the occurrence of large earthquakes since the Late Pleistocene.
There are no too many "neotectonic analogs" worldwide of this kind of compressive crustal intraplate setting, for comparing how large the threshold morphogenic earthquake might be. Besides, other issues usually turn challenging or preclude a reliable use of the empirical relationships for estimating paleoearthquake magnitudes, such as: the lack of preserved primary geomorphic evidences, for determining unitary rupture lengths and the lack of preservation of stratigraphic markers at both fault walls for estimating coseismic slip.
This contribution focuses on some characteristics and challenges posed by the Quaternary faulting at the Pampean Ranges, regarding the characterization of these structures as seismogenic sources. It also aims to provide a paleoseismological perspective in order to contribute with more realistic estimation on the seismic hazard of this region.

EXAMPLES OF QUATERNARY ACTIVE STRUCTURES IN THE PAMPEAN RANGES

The Sierras Pampeanas (Pampean Ranges) of Argentina are characterized by mountain blocks bounded by reverse faults, whose last stage of uplift has been attributed to the shallowing of the Nazca plate (< 11Ma) (Ramos et al., 2002). These faulted blocks constitute a prominent surface feature of the Pampean flat-slab in

the Central Andes (27°-33°S), as well as a modern analog of the Rocky Mountains Laramide uplifts in North America. Evidence of Quaternary activity has been reported along main bounding structures (Massabie 1987, Costa, 1996, Costa et al., 2000, 2001, 2014, among many others). However, the scarcity of suitable conditions for paleoseismological analysis has hampered in many cases successful attempts to address key questions regarding the seismogenic potential of these intraplate faults.

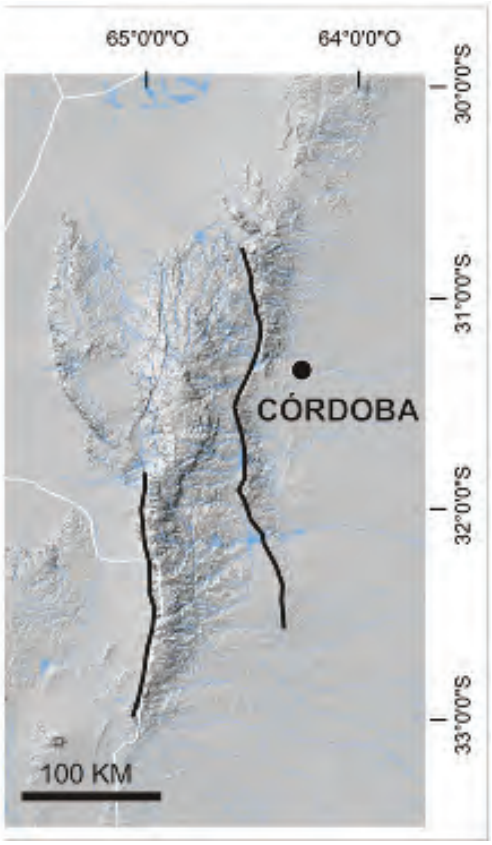

Figure 2: Digital elevation model of the Cordoba ranges, indicating from West to East the Comechingones and the Sierra Chica fault systems (with bold lines).

Some data and insights are here provided from the Comechingones and the Sierra Chica Fault Systems (Fig. 2). These thick-skinned thrust systems constitute the neotectonic uplift front of these faulted blocks, located at the steep western slope of these ranges.
In both cases, most recent deformations are not located at the main slope break defined by the range-piedmont junction. They are related instead to foot-wall shortcuts of the main thrust surface, cored by crystalline rocks, suggesting a down-to-the-basin migration of the tectonic activity during the Quaternary. This tectonic activity is expressed at surface as a piedmont foreland, whose geomorphic imprint in the piedmont environment varies from well imposed to very subtle (Costa, 1996, Costa et al., 2014).

The Comechingones Fault System
This thrust system runs along 160 km partly bounding the Córdoba ranges (Figs. 2), although just a couple of natural exposures have been reported so far along this structure (Costa et al., 2014).
Trenches across the thrust Quaternary-active short-cut bounding the piedmont foreland at the El Molino section of this structure (32°21'30,75"S - 64°58'57,77"W), have exposed two opposing-verging thrusts at the outcrop scale (Costa & Vita Finzi, 1996, Costa et al., 2001, 2010) (Fig. 3). These structures exhibit a complex interaction and propagate into the Holocene cover. The eastern branch or main fault emplaces Precambrian basement over proximal scarp-derived deposits, whereas the western thrust results in an east-directed fault-propagation fold that deforms wash-slope and fluvio-aeolian deposits. The ages of the fault-related deposits have been reasonably defined through radiocarbon and OSL methods which provide ages ranging from 7.1+0.4 ka to 350+40 cal yr BP.
Evidences of surface deformation are related to multiple-events with colluvial wedges and filling wedges derived from bending-moment ruptures at the fold hinge zone (Fig. 3). Discriminating discrete coseismic displacements is very challenging because fault-related Quaternary stratigraphy is only preserved at the fault downthrown side. However, the basement boulder pointed out in Fig. 3, with an exposed long axis of 0.62m, is thought to have been derived from a coseismic scarp with at least that height (0.62 m). From the fault slip component analysis derived from slickenlines measured in the main fault surface, turns out that the vertical slip contributes with 15% to 36% of the total slip vector. Therefore a single coseismic slip ranging from 1.30 to 2.13 m could be interpreted for one of those events.
It has not been possible to unravel whether these structures slipped in simultaneous or separated events. Accordingly, a minimum of four and a maximum of nine surface ruptures younger than 7.1+0.4 ka can be preliminarily interpreted.
Estimated recurrence intervals vary according to different approaches from 0.8 to 3.0 ka (preferred 1.0-2.5 ka), whereas by retrodeforming the total shortening exposed in the trenches, a maximum slip rate of 1.13 mm/a was obtained.

The Sierra Chica Fault System
This structure constitutes the easternmost surface expression of Quaternary faulting at the Pampean flat-slab of the Andes, 700 km away of the ocean trench (Figs. 1 & 2). It exhibits a general NNE trend, although at a local scale several sections with different directions and geometries stand out (Massabie, 1987, Martino et al., 2012, Costa et al., 2014).
The piedmont foreland, at whose western margin evidences of most recent evidences of tectonic activity have been described, is variable in terms of geomorphic expression and geometry along the fault system.

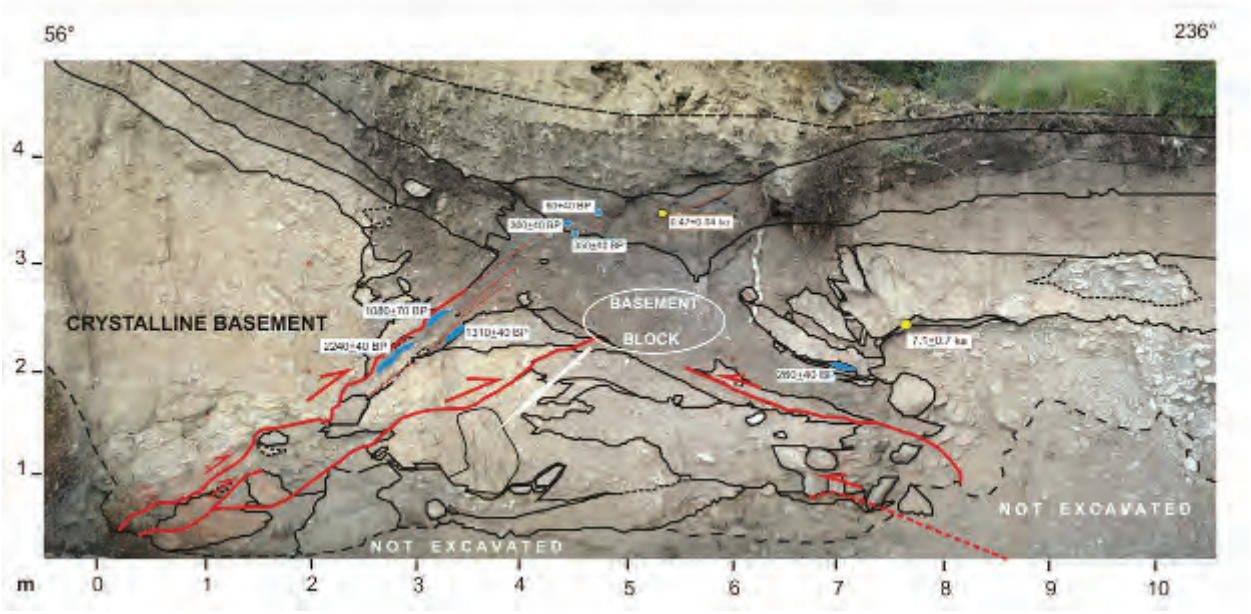

Figure 3: Simplified trench log of the El Molino fault trench site, after Costa et al (2010). The Precambrian crystalline basement (sheared migmatites) overrides alluvial and scarp-derived deposits, whereas a transposed fault propagation fold in alluvial gravels and wash slope deposits defines the expression of a opposite thrust.Blue dots correspond to radiocarbon samples and yellow dots to OSL samples with the corresponding ages.See text for explanation.

Figure 4: Exposure of the Sierra Chica Fault System at Villa Carlos Paz, near Córdoba city. Arrows point out the tectonic contact between Precambrian gneisses (above) and Late Pleistocene sediments, where OSL ages vary from 57,9 ± 3,6 ka to ≥ 70 ka (Costa, 2010). No scarp-related morphologies at the ellipse zone. A geologist within white circle for scale.

At the Villa Carlos Paz site (31° 26' 45,0"S - 64° 30'01,1"W), the Precambrian basement overrides Late Pleistocene sediments through a thrust surface dipping 12° E (average) with an exposed apparent slip of 45.8 m and a cumulative displacement of the basement erosion surface of 117,22m. (Costa, 2010, Costa et al., 2014) (Fig. 4). Despite the significant slip of this structure during the Late Pleistocene, there is no noticeable scarp-related morphology. However, colluvial wedges-like deposits, preserved in the uppermost units (Holocene?), suggest prehistorical surface ruptures, although without chances for estimating individual coseismic slip.

DISCUSSION

There are no historic reports of primary fault-related ruptures in the Pampean Ranges. Therefore paleoearthquake evidences cannot be properly linked to local empirical data, regarding key seismogenic parameters. This information is crucial for successfully incorporating the paleoseismological data into seismic hazard assessment models.

Main questions arising are: which is the threshold magnitude for shallow crustal earthquakes to leave imprints in the landscape and/or in the stratigraphic record?, and, how well the empirical relationships fit with the available paleoseismological data?.

Probable paleomagnitudes for the Maximum Credible Earthquake in the study sites were derived from common parameters such as rupture length; rupture area and coseismic slip (e.g. Stirling et al., 2013), resulting in magnitudes ranging from M 4.69 to M 7.44.

Historic crustal earthquakes ($M \leq 6.5$) left no evidence of neither primary nor secondary surface deformation. Deformation related to the 1977 Mw 7.4 (19 km depth) Caucete earthquake, located at the westernmost Pampean range, resulted in sub-metric discontinuous scarps without geometric and kinematic connection with the main source. Accordingly, it is suspected that most empirical relationship, tend to underestimate the threshold paleoearthquake magnitude capable for producing surface rupture and deformation. This mainly concerns to the rupture length and rupture area criteria, which in many cases resulted in magnitudes $M < 5$, even if historic earthquakes larger than this magnitude did no leave evidences in the stratigraphic/morphologic record.

Based on the records of historic seismicity; the regional seismotectonic setting as well as on comparisons with thresholds magnitudes of earthquakes for rupturing at surface in other regions, it is considered that the threshold earthquake magnitude for producing primary deformation at surface is $M \geq 7.0$ and more probably closer to M 7.5.

As for the recurrence of rupturing events, slip rates estimated at the Comechingones Fault System are almost one order of magnitude higher than those estimated at other master bounding faults along neighboring Pampean blocks. It also appears to be high for an intraplate region with much lower strain rates than the frontal deformation zone of the Andes. The data collected suggest that there has been a peak in fault activity with associated surface deformation during the past 7 ka at the study site, resulting in a clustering of crustal earthquakes ($M > 7.0$). If so, current knowledge suggests that recurrence intervals of these faults could be highly variable.

Acknowledgements: Financial support from UNSL Project 340303 and data derived from consulting activities are acknowledged.

References

Alvarado, P., S. Beck & G. Zandt, (2007). Crustal structure of the south-central Andes Cordillera and Backarc region from regional waveform modeling. *Geophys. J. Int. Tectonics and Geodynamics*. doi: 10.1111/j.1365-246X.2007.03452.x.

Costa, C., (1996). *Análisis neotectónico en las Sierras de San Luis y Comechingones: Problemas y métodos*. 13° Congreso Geológico Argentino, Actas 2: 285-300. Buenos Aires.

Costa, C., (2010). *Proyecto Central Nuclear Embalse.* Project Report N°8: Summary & Conclusions. Private Report, 58p., San Luis.

Costa, C. & C. Vita-Finzi, (1996). Late Holocene faulting in the Southeast Sierras Pampeanas of Argentina. *Geology*. 24 (12): 1127-1130.

Costa, C., M. Machette, R. Dart, H. Bastías, J. Paredes, L. Perucca, G. Tello, & K. Haller, (2000). Map and database of Quaternary faults and folds in Argentina. *U.S.G.S Open-file report 00-0108*. 76p., one map.

Costa, C., V. Murillo, G. Sagripanti & C. Gardini, (2001). Quaternary intrapalate deformation in the southearstern Sierras Pampeanas, Argentina. *Journal of Seismology*. 5: 399-409.

Costa, C., W. Ricci, L. Owen, W. Johnson, A. Halperin & E. Ahumada, (2010). *Holocene paleoearthquake clustering along a Sierras Pampeanas (Argentina) bounding fault?*. American Geophysical Union Fall Meeting, San Francisco. T42A-05.

Costa, C., A. Massabie, G. Sagripanti, E. Brunetto, y M. Coppolecchia, (2014). Neotectónica de la provincia de Córdoba. In: *Relatorio del XIX Congreso Geológico Argentino* (Martino, R., Guereschi, A. eds,) Asoc. Geol. Arg., 725-748.

Jordan, T., B. Isacks, R. Allmendinger, J. Brewer, V. Ramos & C. Ando, (1983). Andean tectonics related to geometry of subducted Nazca plate. *Geological Society of America Bulletin*. 94 (3): 341-361.

Massabie, A., (1987). *Neotectónica y Sismicidad en la región de las Sierras Pampeanas Orientales, Sierras de Córdoba, Argentina.* 10º Congreso Geológico Argentino, Actas 1: 271-274.

Ramos, V., E. Cristallini & D. Pérez, (2002). The Pampean flat-slab of the Central Andes. *Journal of South American Sciences.* 15: 59-78.

Stirling, M., T. Goded, K. Berryman & N. Lichtfield, (2013). Selection of earthquake scaling relationships for Seismic-Hazard Analysis. *Bulletin Seismological Society America*. 103 : 2993-3011, doi: 10.1785/0120130052.

INQUA Focus Group on Paleoseismology and Active Tectonics

paleoseismicity.org

Active tectonics at the frontal Potwar Plateau, NW Himalaya of Pakistan: Insights from 10Be ages in fluvial terraces at the Mahesian Anticline and seismic hazard implications

Cortés-Aranda, J. (1), Mugnier, J-L., (1), Vassallo, R. (1), Jouanne, F. (1), Carcaillet, J. (2), Adnan, A. (3)

(1) Institut des Sciences de la Terre (ISTerre), Université de Savoie, 73376 Le Bourget du Lac cedex. Email: cortesaj@univ-savoie.fr
(2) Institut des Sciences de la Terre (ISTerre), Université Joseph Fourier, rue de la Piscine, 38400 Saint-Martin d'Hères
(3) Geological Survey of Pakistan 84, St.03, H-8/1, Islamabad, Pakistan

Abstract: *We quantify Holocene deformation rates of the Mahesian Anticline, located in the frontal part of the Potwar Plateau, NW Himalaya of Pakistan. Fluvial terraces have been hanged and preserved at the SE flank of this anticline, which we dated by employing 10Be cosmogenic measurements. Two generations of terraces were properly dated at ca. 6.5 ka and ca. 3.3 ka (maximum ages). This allowed the estimation of uplift rates of ca. 9 m/ka and shortening rates of ca. 13 m/ka. These values are significantly higher than those reported by geodesy in that area. We interpret that this recent decrease is due to the loss of thickness of the salt detachment underneath the Mahesian Anticline. This would enhance the locking of this detachment and may propitiate the triggering of moderate to large earthquakes. We hypothesize that these earthquakes may propagate to shallow levels along thrusts leading active structures as the Mahesian Anticline.*

Key words: *Mahesian Anticline, shortening rates, 10Be ages, fluvial terraces, seismic hazard.*

INTRODUCTION

The Potwar Plateau is the biggest plateau at the frontal NW Himalaya of Pakistan, which corresponds to a fold-and-thrust belt at the western flank of the Hazara-Kashmir Syntax (e.g. Jaume and Lillie, 1988; Figure 1a-b). This plateau propagates southwards over the Indian Plate, due to the occurrence of a late Precambrian-Early Cambrian salt deposits, acting as a detachment layer (e.g. Crawford, 1974) that mostly precludes the generation of earthquakes in the area; this differs from what occurs in most of the frontal zones along the Himalaya (e.g. Gahalaut and Arora, 2012). GPS velocity fields indicate that the Potwar Plateau slips to the S-SE at rates ranging between 3 mm/y and 5 mm/y in its central part (Figure 1b; e.g. Jouanne et al., 2014). On the contrary, propagation velocities (slip rates) are almost null at their east and west borders (Figure 1b; e.g. Jouanne et al., 2014). In general, GPS velocities are much slower than those estimated from geological evidence for the long term, which are of around 8 mm/y since the last 12 - 2 My (e.g. McDougall and Khan, 1990; Figure 2a). No propagation velocities at the thousands of years' time-scale have been still estimated for the Potwar Plateau, which is a main obstacle to discuss the significance of the Present-day slow slip rate values in terms of how strain is being conducted along the active structures in the area, as for example those at the frontal Himalaya of Pakistan. There, the structural pattern is represented by a set of parallel fault propagation folds related to blind faults (e.g. Leathers, 1987; Figure 1a-b; Figure 2b). Among these, the most clearly expressed active structure is the Mahesian Anticline (e.g. Nakata et al., 1991; Figure 1a-b; 2b; 3a), located in a zone where the salt thickness is 0.5 to 1 km (Leathers, 1987; Figure 1b) and where GPS velocities show almost null slip magnitudes (Jouanne et al., 2014; Figure 1b).

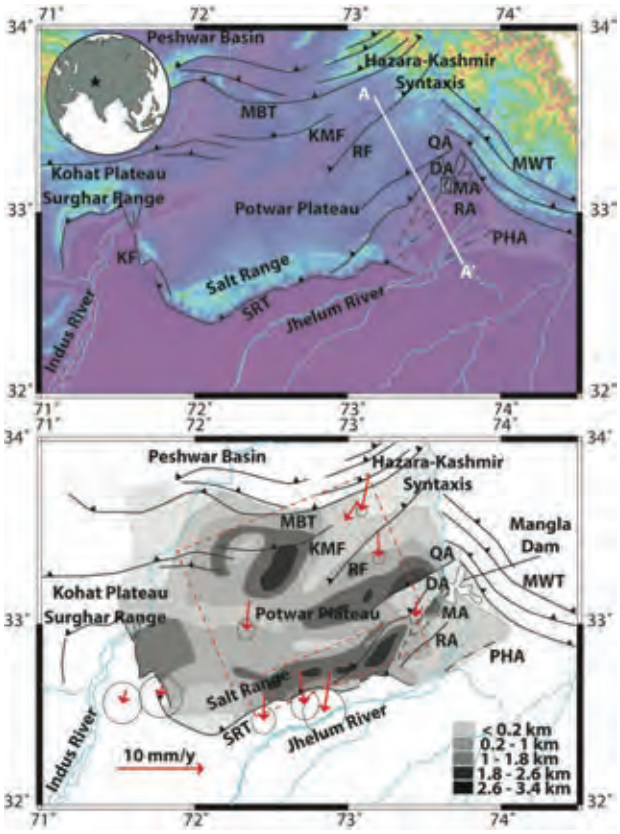

Figure 1: a) Location of the study area; b) Isopach map of the salt deposits according to Leathers (1987). GPS velocities of Jouanne et al. (2014) are depicted by red arrows; segmented red rectangle is the dislocation used in their model. KF= Kalabagh Fault; SRT= Salt Range Thrust; MBT= Main Boundary Thrust; DA= Domeli Anticline; MA= Mahesian Anticline, RA= Rhodas Anticline; PHA= Pabbi Hills Anticline, RF= Riwat Fault, KMF= Khairi-Murat Fault, QA=Qazian Anticline. AA' is the profile of figure 2b.

Herein, we present the results of a neotectonic survey oriented to quantify the Holocene deformation along the Mahesian Anticline. We have mapped three generations of fluvial terraces hanging at the S-E flank of this anticline; quartz clasts were collected from the two youngest groups of terraces for ^{10}Be analysis in order to obtain their exposure ages. From these data, cumulative uplift rates were estimated. By applying simple geometrical relations (e.g. Mosar & Suppe, 1991), we derived cumulative shortening rates (slip rates) for the time spans encompassing since the terrace abandonment to the Present. We compare these intermediate time-scale slip rates with those obtained from geodetic methods in the area (e.g. Jouanne et al., 2014) and discuss the significance of their difference in terms of the thickness of the salt detachment. Our results and interpretations attempt to indirectly evaluate the seismic potential in a region where earthquakes must be considered as an important threat. There, the 9th largest dam in the world (Mangla Dam), which is more than 137 m high, is built at the intersection of the Jhelum River and the Mahesian Anticline (Figure 1b; Adams and Asghar, 1969).

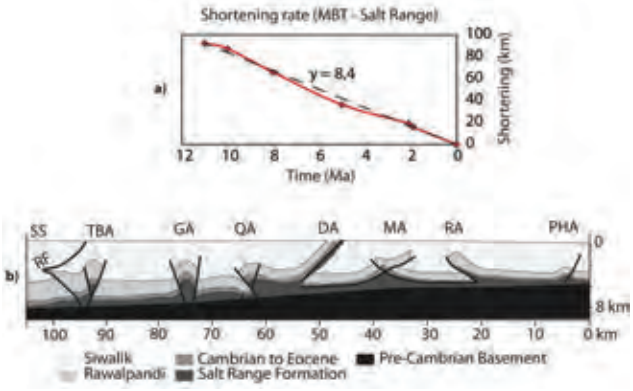

Figure 2: a) Long term shortening rate diagram for the area between the MBT and the Salt Range (e.g. Singh et al., 2008); b) Structural profile of the main structures at the Potwar Plateau – Salt Range tectonic domain. SS= Soan Syncline; RF= Riwat Fault; TBA= Tanwin Basin; GA= Gungril Anticline, QA= Qazian Anticline; DT= Domeli Anticline; MA= Mahesian Anticline; RA= Rothas Anticline; PHA= Pabbi Hills Anticline.

DISCUSSION

Three generations of fluvial terraces have been distinguished atop of the S-E flank of this anticline (Figure 3a). We have named these terraces from older to younger as terraces T1 to T3; these are located at 241-290 m, ~270 m, and 220 -255 m, respectively, with respect to the surface of the geoid of the WGS 84 reference system (Figure 3a). On the other hand, the elevation of the river bed is ~ 208 m.

Among these terraces, the most developed generation is the group of terrace T2; terraces of groups T1 and T3 exist only locally (Figure 3a). We performed topographic profiles across the Jhelum River from the periphery of the Mahesian Anticline to around 15 km southward and observed that this terrace configuration exists only in the study area, close to the Mangla Dam (Figure 1b). Only there, where profile C1 was performed, there is an altitudinal difference of around 70 m between the terrace T1 and the river bed (Profile C1, Figure 3a,b). Further south along the Jhelum River there is not such an altitudinal difference (Profile C2, Figure 3a,c). Assuming that the incision rate has not changed since the formation of the oldest terrace, we interpret that most of the Present-day elevation of fluvial terraces in the study area is due to the development of the Mahesian Anticline (tectonic effect) and just secondarily consequence of the river incision. With this evidence, we think that these fluvial terraces can be considered as markers to quantify uplift rates and further derive shortening rates for the Mahesian Anticline.

By using 10Be measurements, we were able to estimate the age of the two youngest generations of terraces, T2 and T3. To determine the exposure ages, we have collected boulders and pebbles of quartz both atop of these terraces and along vertical profiles. Following the strategy of Anderson et al. (1996), vertical samples were gathered to around 2.5 m depth in order to estimate the

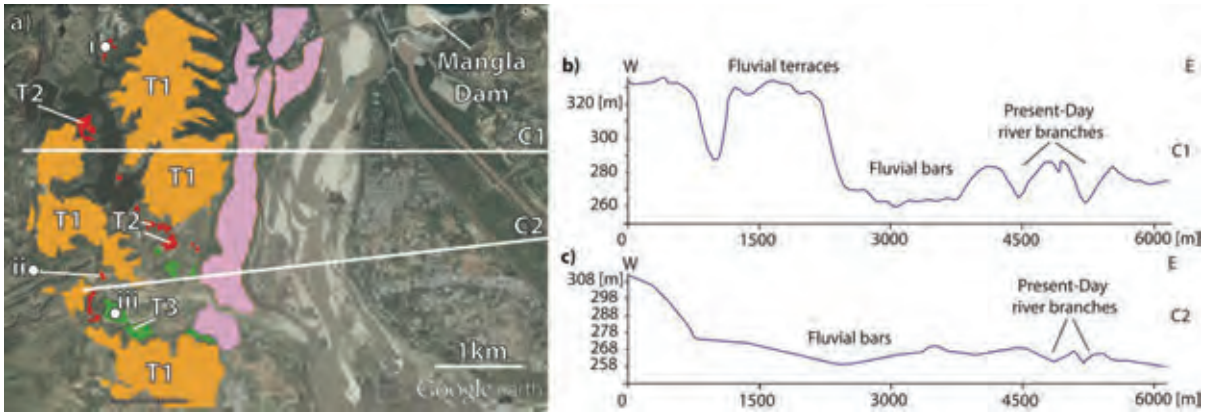

Figure 3: a) Fluvial terraces at the S-E flank of the Mahesian Anticline. T1, T2 and T3 are represented by red, orange and green areas, respectively. Pink zones are the youngest terraces of the Jhelum River. i, ii and iii are the 10Be sample sites. C1 and C2 are the topographic profiles shown in b and c, respectively. Note that fluvial terraces are only preserved in C1 (Figure 3b).

amount of inherited 10Be in clasts due to prior exposure processes. Samples are supposed to have not been remobilized after their deposition since they are partially or completely buried in the terrace deposit. Cosmogenic ages for similar fluvial terraces along the Himalayan Front have resulted in ca. 10 ka or younger (Boohagen et al., 2006), so even though erosion may have acted on terraces at the Mahesian Anticline, this would not affect significantly our 10Be results. Further, the aspect of terraces T2 and T3 is dominantly flat, which led us to suppose that erosion is negligible for age calculations. 13 samples were obtained from terrace T2 at ~62 m (Figure 3a and 4a) over the river bed and 7 from terrace T3 at ~30 m (Figure 3a and 4b) over the river bed.

Samples obtained both at surface and at depth for terrace T2 show a significant scattering in terms of the 10Be concentration (Figure 4a). These barely fit with the theoretical curve of 10Be concentration at depth, thus suggesting a potential inherited amount of this isotope (Figure 4a). If this is correct, the samples less affected by inheritance are those with the lowest concentration of 10Be both at surface and depth. Since we assumed zero erosion for our calculations, we developed a least square inversion -that is function of the exposure age and inheritance- to generate a model that verifies the production rate attenuation law of Lal (1991), considering these two samples with their uncertainties (curve in figure 4a). In diagrams of figure 4a-b, the samples positioned to the right of the model (curve) contain higher inheritance than those that may be located to the left. All the solutions to the left of the model are possible; therefore, the model represents the maximal age with the minimum inheritance. In this sense, the maximal age of terrace T2 would be of ca. 6.5 ka. This age roughly correlates with a cool and dry climate period in NW Himalaya reported at ca. 7.7 to 6.1 ka (Trivedi and Chauhan, 2009), favorable to promote the construction of fluvial terraces (*sensu* Boohagen et al., 2006).

If we follow the same reasoning that for terrace T2, for terrace T3 we may suggest that the samples with the less concentration of 10Be both at surface and depth can be employed to estimate its maximal exposure age (Figure 4b). This concentration is consistent with a maximal age of ca. 3.3 ka for terrace T3, coherently younger than the maximal age of terrace T2. The estimated maximal age for terrace T3 can be correlated with other Holocene terraces in the Himalaya and with a cool and dry climate stage that took place in NW Himalaya at ca. 4 ka to 2 ka (Trivedi and Chauhan, 2009).

Since we interpret that the current terrace configuration in the study area is due to the fold construction and just marginally consequence of the river incision, we can estimate uplift rates locally induced by the Mahesian Thrust, the fault leading our targeted anticline.

Considering the estimated ages for T2 and T3, and their elevation with respect to the river bed, we calculated uplift rates of ca. 9.5 m/ka and ca. 9.1 m/ka for the last ca. 6. 5 ka and ca. 3.3 ka., respectively. The geometry of the Mahesian Anticline is compatible with a blind fault dipping to the east with around 30° – 45°, although west

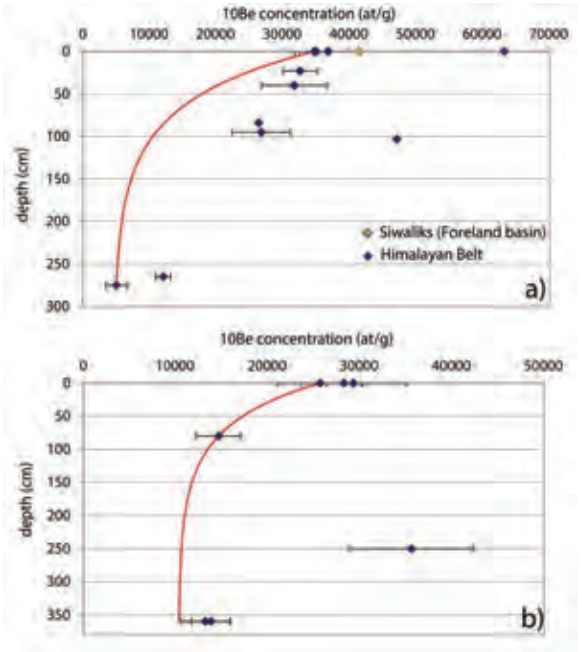

Figure 4: 10Be concentration versus depth diagrams for samples from T2 (a) and T3 (b). Red curves in both graphics are the inversion model.

dipping faults may be also present (Yeats and Lillie, 1991; Figure 2b). According to the geometrical relations proposed by Mosar & Suppe (1991) for fold related faults, uplift rates can be converted into shortening rates according to the formula V= U/Sin α. In this formula, V is the shortening rate, U is the uplift rate, and α is the dip angle of the causative fault. By considering this relation, the derived shortening rates for the Mahesian Thrust are ca. 13.6 m/ka and ca. 13 m/ka for the last ca. 6.5 ka and ca. 3.3 ka, respectively. These values are larger than the regional estimations for the Potwar Plateau for the last 12-2 Ma (e.g. Jaume and Lillie, 1988) and roughly consistent with those obtained by Baker et al. (1988) for the last ca. 2 Ma west of the Mahesian Anticline, at the frontal Salt Range. On the other hand, our results are significantly faster than the reduced GPS velocities constrained in the periphery of the Mahesian Anticline by Jouanne et al., 2014 (Figure 1b). The logical deduction of the shortening rate decrease for the Mahesian Anticline area is that it occurred recently at some time after ca. 3.3 ka. A similar rate diminution has occurred in the Kohat Plateau (Figure 1a-b), for which strong differences between long term and geodetic slip rates have been documented (Satyabala et al., 2012). This change has been related to the thinning of the salt detachment in the area. Also, this reduction has been associated to a Mw 6 earthquake that in 1992 struck the Kohat Plateau area, a region formerly supposed of low seismic risk; the occurrence of this event insinuates that the mechanical behavior along the salt detachment has been evolving, at least partially, from creeping to stick slip behavior (Satyabala et al 2012). Interestingly, the eastern termination of the Potwar Plateau at the periphery of the Mahesian Anticline, where the slowest

geodetic slip rates have been determined (Figure 1b; Jouanne et al., 2014), is also positioned over a zone where the salt bed thickness is reduced (no more than 500 m thick, Leathers, 1987). Contrary, the highest GPS velocities are observed at the central zones of the Potwar Plateau, as the Salt Range, where the salt thickness is thicker than 1.8 km (Figure 1b). Because of this, we interpret that the reduction of the slip rate after ca. 3.3 ka in the study area is linked to a thinning of the underlying salt detachment (Figure 1b). Although no historical earthquakes have been reported in the area, we hypothesize that the main detachment beneath the eastern termination of the Potwar Plateau may be partially locked. If so, that region may be struck by moderate to large earthquakes in the future, which can be able to propagate to shallow levels along thrusts leading active structures as the Mahesian Anticline. Shallow depth earthquakes have been reported beneath similar anticlines in California (the 1983 Mw 6.5 Coalinga Earthquake, the 1985 M 6.1 Kettleman Hills Earthquake and the 1987 M 6.0 Whittier Narrows Earthquake) without producing any surficial rupture (e.g. Lin and Stein, 1989). In those cases, geodetic surveys have revealed that anticlines were suddenly uplifted as consequence of the mainshocks. This suggests that the construction of these anticlines is the result of repeated moderate earthquakes over a period of around 200 years (e.g. Lin & Stein, 1989). Based on these antecedents, we propose that the Mahesian Anticline may be the result of successive moderate earthquakes shallowly beneath it without surficial expression. This may represent a source of significant seismic risk for a densely inhabited zone located in the periphery of the 9th biggest dam in the world, the Mangla Dam.

Acknowledgements: Joaquin Cortés-Aranda is a postdoc researcher granted by BecasChile. We thank the ANR Project Pakistan-France that financed 10Be analysis and field trips.

References

Adams, R.D. & A. Aaghar, (1969). Seismic effects at Mangla Dam, Pakistan. *Nature. 222*, 1153-1155.

Anderson, R., J.L. Repka & G.S. Dick, (1996). Explicit treatment of inheritance in dating depositional surfaces using in situ 10Be and 26Al. *Geology*. 24.1, p. 47-51.

Baker, D.M., R.J. Lillie, R.S. Yeats, G.D. Johnson, M. Yousuf & A.S.H. Zamin, (1988). Development of the Himalayan frontal thrust zone: Salt Range, Pakistan. *Geology*. *16*(1), 3-7.

Bookhagen, B., D. Fleitmann, K. Nishiizumi, M.R., Strecker & R.C. Thiede, (2006). Holocene monsoonal dynamics and fluvial terrace formation in the northwest Himalaya, India. *Geology*. *34*(7), 601-604.

Crawford, A.R., (1974). The Salt Range, the Kashmir syntaxis and the Pamir arc. *Earth and Planetary Science Letters*. *22*, 371-379.

Gahalaut, V.K. & B.R. Arora, (2012). Segmentation of seismicity along the Himalayan Arc due to structural heterogeneities in the under-thrusting Indian plate and overriding Himalayan wedge. *Episodes*. *35*(4), 493-500.

Jaume, S.C. & R.J. Lillie, (1988). Mechanics of the Salt Range-Potwar Plateau, Pakistan: A fold-and-thrust belt underlain by evaporates. *Tectonics*. *7*(1), 57-71.

Jouanne, F., A. Awan, A. Pêcher, A. Kausar, L. Mugnier, I. Khan, N.A. Khan & J. Van Melle, (2014). Present-day deformation of northern Pakistan from Salt Ranges to Karakorum Ranges. *J. Geophys. Res. Solid Earth*. 119, 2487–2503, doi:10.1002/2013JB010776.

Lal, D., (1991). Cosmic ray labeling of erosion surfaces: in situ nuclide production rates and erosion models. *Earth and Planetary Science Letters*. *104*(2), 424-439.

Leathers, M., (1987). *Balanced structural cross section of the Salt Range and western Potwar Plateau, Pakistan: Deformation near the strike-slip terminus of an overthrust sheet* [M.S. thesis]: Corvallis, Oregon State University, 228 p.

Lin, J. & R.S. Stein, (1989). Coseismic folding, earthquake recurrence, and the 1987 source mechanism at Whittier Narrows, Los Angeles Basin, California. *Journal of Geophysical Research: Solid Earth (1978–2012)*. *94*(B7), 9614-9632.

McDougall, J.W. & S.H. Khan, (1990). Strike-slip faulting in a foreland fold-thrust belt: The Kalabagh Fault and Western Salt Range, Pakistan. *Tectonics*. *9*(5), 1061-1075.

Mosar, J. & J. Suppe, (1991). Role of shear in fault-propagation folding. In: (McClay, K.R., ed.). *Thrust tectonics*. London, Chapman & Hall, 123–132.

Nakata, T., H. Tsutsumi, S.H. Khan & R.D. Lawrence, (1991). Active faults of Pakistan. *Hiroshima University Research Center for Regional Geography Special Publication*. 21, 141 p.

Satyabala, S.P., Z. Yang & R. Bilham, (2012). Stick-slip advance of the Kohat Plateau in Pakistan. *Nat. Geosc*. *5*(2), 147-150.

Trivedi, A. & M.S. Chauhan, (2009). Holocene vegetation and climate fluctuations in northwest Himalaya, based on pollen evidence from Surinsar Lake, Jammu region, India. *Journal of the Geological Society of India*. *74*(3), 402-412.

INQUA Focus Group on Paleoseismology and Active Tectonics

Implications of slip rate variability along extensional faults in the central Apennines for geodynamic interpretations and earthquake hazard assessment

Cowie, P.A. (1), Roberts, G.P. (2), Phillips, R.J. (3), McCaffrey, K. (4), Gregory, L.C. (3), Faure Walker, J. (5), Zijerveld, L.J.J. (1), Dunai, T.J. (6), Binnie, S.A. (6), Freeman, S. (7), Wilcken, K. (7), Wedmore, L. (5), Watson, Z. (5), Papanikolaou, I. (8)

(1) University of Bergen, Bergen, Norway. (Previous address: University of Edinburgh, UK). Email: Patience.cowie@geo.uib.no
(2) Birkbeck College, University of London, London, United Kingdom
(3) University of Leeds, Leeds, United Kingdom
(4) University of Durham, United Kingdom
(5) University College London, London, United Kingdom
(6) University of Cologne, Cologne, Germany
(7) Scottish Universities Environmental Research Centre, AMS Laboratory, East Kilbride, United Kingdom
(8) Agricultural University of Athens, Athens, Greece

Abstract: *Over long spatial and temporal scales (10^5 m and 10^4 years) extensional deformation across the Italian Apennines can be characterised by a viscous flow law. This result was obtained by analysing the relationship between mean elevation and Holocene-averaged fault strain rates. Geodetic data in this area, which reflect interseismic strain accumulation, are also consistent with such a flow law. Viscous deformation can be modelled using continuum mechanics but it implies that fault slip rates measured at the surface are set by the rate of viscous flow at depth and thus approximately uniform over the Holocene. Here we use measurements of cosmogenic ^{36}Cl, collected along bedrock fault scarps in Abruzzo, to estimate fault Slip Rate Variability (SRV) to evaluate the influence of deep viscous flow versus upper-crustal elastic interaction in controlling Holocene activity of individual faults and thus the limitations of continuum mechanics in seismic hazard assessment over centennial to millennial timescales.*

Key words: *Active tectonics, Extensional faulting, Slip rates, Geodynamic models, Earthquake hazard.*

INTRODUCTION

Slip rate measurements on faults are a fundamental component of our understanding of geodynamic processes and earthquake recurrence in a region. Specifically, spatial and temporal variations in slip rate can be used to evaluate the underlying rheological controls on deformation and in particular strain localisation (e.g., Cowie et al., 2005).

Field evidence for slip rate variations over time periods of several 100 thousand to several millions of years have been widely documented in extensional fault systems, including the fault system developed in the Italian Apennines (see Cowie et al., 2007 for a review). These variations have been interpreted in terms of interaction between growing and linking fault segments, primarily elastic interactions that arise from perturbations to the upper crustal stress field (e.g., Cowie et al., 2012). Over shorter timescales (10^4 to 10^5 years), other studies (e.g., Nicol et al., 2006) have demonstrated that fault slip rate variations relate directly to changes in the spatial-temporal distribution of earthquake ruptures. In fact, Nicol et al., argue in their 2006 paper that 'all faults interact and their earthquake histories are interdependent' and that 'each fault is a component of a kinematically coherent system'.

In contrast, when it comes to geodetic observations of crustal deformation, measured over a few years to decades, it is often argued that the kinematics of active upper crustal faults and earthquake moment release rates may be interpreted in terms of deformation of a continuum (e.g., Floyd et al., 2010). In a continuum mechanics interpretation upper crustal faults respond passively to flow at depth and fault slip rates at the surface are set by the rate of viscous deformation in deeper ductile layers. Temporal variations in fault slip rate in this case require instabilities to be invoked such as those that can arise during deformation of highly non-linear viscous fluids.

The extensional fault system in the Italian Apennines (Fig. 1) offers us the opportunity to test these two competing/contradictory hypotheses. We have shown previously (Cowie et al., 2013) that over long spatial and temporal scales (10^5 m and 10^4 years), the Holocene-averaged extensional deformation, when summed across *several* seismogenic faults in the upper crust, can be characterised by a well-defined viscous flow law (Fig. 1b). Geodetic data in this area are also consistent with such a flow law even though the resolution of these data does not permit the inferred flow law to be constrained. Thus, when averaged over long/large temporal and spatial scales brittle deformation, at least across the central Apennines, does indeed appear to be consistent with the continuum mechanics interpretation derived from geodetic measurements of interseismic strain accumulation (D'Agostino et al., 2014). However, the key question is whether Holocene slip rates on *individual faults* (e.g., those shown in Fig. 1c) are consistent with a passive response to this flow and, if not, what does control fault slip rate? Furthermore, do the slip rates vary over time during the Holocene and if so by how much and over what time scale can the slip rate change from

one rate to another? Answering these questions will give us a fundamentally better understanding of the underlying controls on fault activity and ultimately seismic hazard.

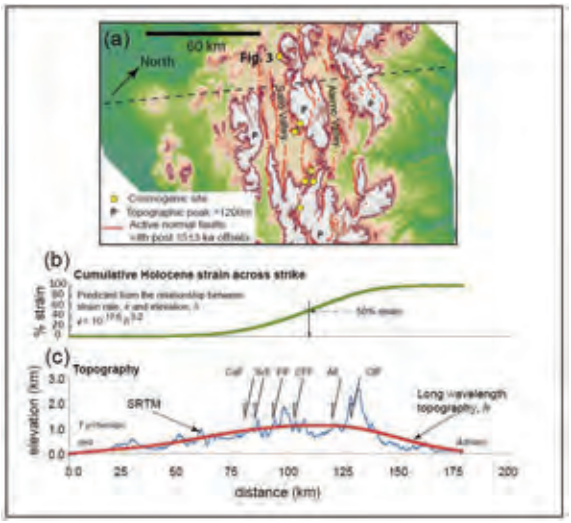

Figure 1: (a) Location map, (b) across strike cumulative fault strain predicted from the viscous flow law inferred from the relationship between Holocene-averaged strain rates and mean elevation (Cowie et al., 2013), (c) topographic cross-section from SRTM data across Abruzzo with major faults indicated; thick red line is the long wavelength topography from D'Agostino et al. (2011) (location of topographic profile shown by dashed line in Fig. 1a). AF = L'Aquila fault, CIF = Campo Imperatore fault, CaF = Carsoli fault, ScF = Scurcola fault; FiF = Fiamignano fault and CFF = Campo Felice fault. See Discussion for more details.

Here we consider two possible end-members: (i) surface strain rates and thus slip rates on individual faults are set entirely by the rate of viscous flow at depth, i.e., the faults are 'passive' (this is what we call the 'continuum mechanics' model in Fig. 2), and (ii) fault slip rates are primarily controlled instead by elastic interactions between adjacent structures so that regional loading rates can only be deduced by considering the entire fault array over long time periods because each fault is only intermittently active.

In case (i) we expect little or no variation in fault slip rates and any variations that we do see should be gradual in space and in time whereas in case (ii) we predict significant temporal variations in slip rate on individual faults that are controlled by the spatial geometry of the fault network, i.e., interaction between neighbouring structures in particular those across strike (see Fig. 2). To quantify changes in slip rate over time we use the measure Slip Rate Variability (SRV) which was defined by Cowie et al. (2012) as:

$$SRV = \sigma_{SR}/SR_{mean} \qquad \text{Equation 1}$$

where σ_{SR} is the standard deviation of short term slip rates over a sliding time window of fixed length and SR_{mean} is the long term average slip rate.

As the lithosphere consists of both brittle-elastic and viscous (or visco-elastic) layers, it is likely that neither end-member explains everything that we observe but it is important to establish if there is a dominant control on fault behaviour and how this may vary over different spatial and temporal scales.

Figure 2 shows that measuring SR_{mean} and SRV for individual faults in Abruzzo might be one way to address this challenge. For example, if continuous deformation at depth controls fault slip rates measured at the surface then we expect SR_{mean} to vary spatially but SRV ≈ 0. However, if fault interaction is the dominant control, then we expect SRV > 0 and it should vary systematically according to the percentage of across strike deformation that each fault or fault segment accommodates (e.g., see red and blue symbols and regressions shown in Fig. 2).

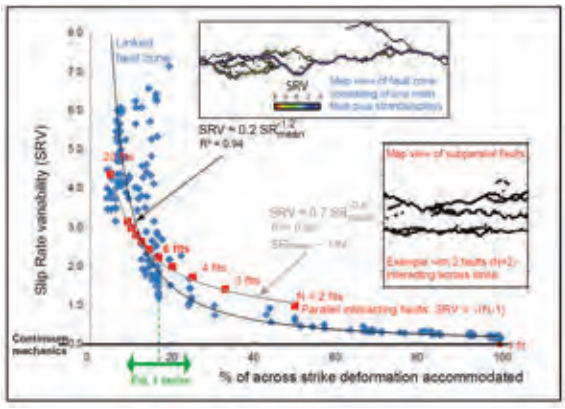

Figure 2: Slip Rate Variability (SRV) versus the percentage of across strike deformation accommodated by each fault or fault strand. Blue diamonds show output from a numerical fault growth model (Cowie et al., 2012) where the deformation is mainly taken up by one main through-going fault with subsidiary strands and splays that accommodate less deformation. This model includes elastic interaction that results in 0 < SRV < 1 on the main fault but SRV > 1 on the strands/splays. The red squares show an alternative relationship given by an analytical expression SRV = √(N - 1), which refers to the case where deformation is shared equally by N separate subparallel faults across strike but, at any given time, only one of the faults is active and takes up all of the deformation while the other faults are inactive followed by the activity shifting to a different fault across strike and so on. Two empirical fits are also shown (black and grey lines) obtained by regression through the blue and red symbols respectively. The green arrow and green dashed line indicate the likely range of across strike deformation accommodated by the six faults shown in Figure 1(a&c) (see Discussion for details). SRV = 0 is the expected behaviour of faults in a continuum mechanics interpretation.

APPROACH

Our approach is to estimate SRV (Eqn 1) along active normal faults in Abruzzo using measurements of the concentration of cosmogenic ^{36}Cl that accumulates in

bedrock scarps during the process of gradual tectonic exhumation by fault slip over the Holocene.

The selection of sample sites, characterisation of the site geometry, sample collection and preparation are described in other contributions to this volume (Gregory et al., and McCaffrey et al.). We show an example of one of our sites in Fig. 3. A novel feature of our sampling strategy is that we systematically sample both the exhumed fault scarp and the subsurface fault plane via trenching at each site. The concentration of cosmogenic ^{36}Cl at the top of the trench as well as the variation in concentration going from the subaerial to subsurface parts of the fault plane improve our ability to constrain the modelling of these data. We also utilize fault surface roughness information obtained from LiDAR.

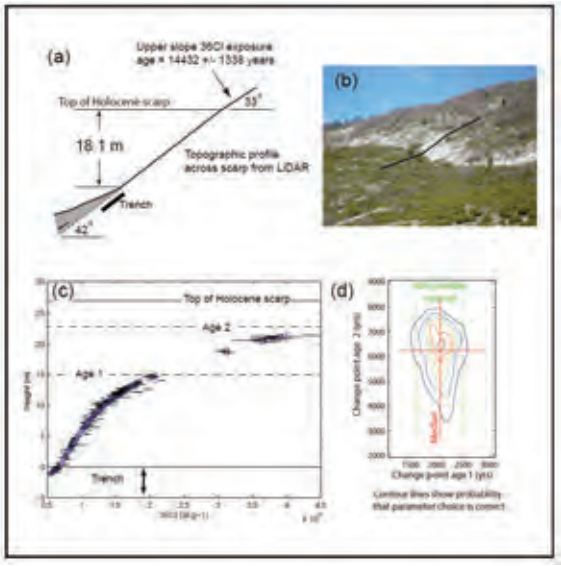

Figure 3: Example of ^{36}Cl samples collected at a site along the Fiamignano fault (located in Fig. 1) illustrating how a Bayesian inference approach can be used to determine when the fault slip rate changes and thus calculate SRV (Eqn. 1). (a) Bedrock scarp topographic profile obtained from LiDAR data showing the site geometry, (b) photograph showing the sample site, (c) measured ^{36}Cl concentrations both in the trench and up the fault plane (black dots) and best-fit model (lowest RMSw, see blue circles), and (d) results of Bayesian parameter estimation using an MCMC approach to determine when the fault slip rate changes as well as the 90% credible interval on these ages. See Approach for more details.

We use the Matlab code developed by Schlagenhauf et al. (2010) to model the measured ^{36}Cl variations (e.g., see small blue circles in Fig 3c). Gregory et al. (this volume) describe in more detail how the modelling of each site is constrained. In this work we use the Matlab code of Schlagenhauf et al. in combination with both optimisation and Bayesian Inference Markov Chain Monte Carlo (MCMC) modelling approaches to obtain the best fit model as well as to estimate the uncertainties on our values for SR_{mean} and SRV for each site.

DISCUSSION

The site shown in Fig. 3 is on the Fiamignano fault located in the cross section in Fig. 1c. According to the predicted distribution of strain shown in Fig 1(b), the L'Aquila fault and the Campo Imperatore fault together accommodate approximately 50% of the total extension (~25% each) whereas the other 4 faults (Carsoli, Scurcola, Fiamignano and Campo Felice faults) accommodate the remaining 50% (~12% each). This partitioning of strain is indicated by the large green arrow in Fig. 2. The topographic profile (SRTM) shown in Fig. 1(c) suggests that the L'Aquila fault may accommodate more deformation than the Campo Imperatore fault over long timescales and thus may accommodate the bulk of the extension in this cross section, (as suggested by D'Agostino et al., 2011), perhaps as much as 30-40%. In this case the green arrow could extend further along the x-axis to the right in Fig. 2. Alternatively the Holocene strain may be distributed more uniformly between all of these six faults in which case they might each accommodate about ~17% of the strain (see vertical dashed green line in Fig 2). According to the relationships show in Figure 2, SRV values between about 1.5 and 3.0 are anticipated if fault interaction is significant. Using the variations in cosmogenic ^{36}Cl along each fault that we have sampled we evaluate whether, to first order, SRV is ≈ 0 or not. Then for sites where SRV is > 0 we investigate how SRV and SR_{mean} vary as a function of the percentage of Holocene deformation that each fault accommodates and if they co-vary or not (cf. Fig. 2).

CONCLUSIONS

Profiles of cosmogenic ^{36}Cl collected along bedrock scarps can be used to infer both Holocene-averaged slip rates and Holocene Slip Rate Variability (SRV; Eqn. 1). SRV can be used to evaluate how the rheological structure of the lithosphere controls fault behaviour from centennial to millennial timescales. We will present estimates of SRV for faults in Abruzzo and discuss how these values can be interpreted in terms of geodynamic processes.

Acknowledgements: N. D'Agostino supplied the data defining the long wavelength topography shown in Fig. 1c. This work was supported by NERC grants: NER/S/A/2006/14042, NE/E01545X/1 and NE/I024127/1. This project was initiated while P.A.C. was employed by the University of Edinburgh. Financial support was also provided to P.A.C. by the Statoil-University of Bergen Akademia agreement.

References

Cowie, P.A., C.H. Scholz, G.P. Roberts, J.P.F. Walker, P. Steer, (2013). Viscous roots of active seismogenic faults revealed by geologic slip rate variations. *Nature Geosc.*. 6 (12), 1036-1040.

Cowie, P.A., G.P. Roberts, J. Bull & F. Visini, (2012). Relationships between fault geometry, slip rate variability and earthquake recurrence in extensional settings. *Geophys. J. Int.*. 189, 143-160, doi:10.1111/j.1365-246X.2012.05378.x.

Cowie, P.A., G. Roberts and E. Mortimer, (2007). Strain localisation within fault arrays over timescales of 10**0 to 10**7 years - Observations, explanations and debates. In: *Handy, M.R., G. Hirth, and N. Hovius, eds. Tectonic Faults: Agents*

of Change on a Dynamic Earth. Dahlem Workshop Report 95. Cambridge, MA: MIT Press, (p.47-77).

Cowie, P.A., J.R. Underhill, M.D. Behn, J. Lin and C. Gill, (2005). Spatio-temporal evolution of strain accumulation derived from multi-scale observations of Late Jurassic rifting in the northern North Sea: A critical evaluation of models for lithospheric extension. *Earth Planet. Sci. Lett.*. 234, 401-419.

D'Agostino, N., P. England, I. Hunstad, G. Selvaggi, (2014). Gravitational potential energy and active deformation in the Apennines. *Earth Planet. Sci. Lett.*. 397, 121-132.

D'Agostino, N., S. Mantenuto, E. D'Anastasio, R. Giuliani, M. Mattone, M. Calcaterra, P. Gambino, and L. Bonci, (2011). Evidence for localized active extension in the central Apennines (Italy) from global positioning system observations. *Geology*. 39, 291–294, doi: 10.1130/G31796.1.

Floyd, M.A., H. Billiris, D. Paradissis, G. Veis, A. Avallone, P. Briole, S. Clusky, J.-M. Nocquet, K. Palamartchouk, B. Parsons, P.C. England. (2010). A new velocity field for Greece: Implications for the kinematics and dynamics of the Aegean. *J. Geophys. Res.*. doi:10.1029/2009JB007040.

Nicol, A., J. Walsh, K. Berryman, P. Villamor, (2006). Interdependence of fault displacement rates and paleoearthquakes in an active rift. *Geology*. 34 (10), 865e868. doi:10.1130/G22335.1.

Schlagenhauf, A., Y. Gaudemer, L. Benedetti, I. Manighetti, L Palumbo, I. Schimmelpfennig, R. Finkel & K. Pou, (2010). Using in situ Chlorine-36 cosmonuclide to recover past earthquake histories on limestone normal fault scarps: a reappraisal of methodology and interpretations, *Geophys. J. Int.*. 182, 36-72, doi: 10.1111/j.1365-246X.2010.04622.x.

Earthquake recurrence in the central-southern Apennines: a comparison from geodesy and historical earthquake catalogue

D'Agostino, N.

Centro Nazionale Terremoti, Istituto Nazionale Geofisica Vulcanologia, Via Vigna Murata 605, 00143 Roma, Italy.
Email: nicola.dagostino@ingv.it

Abstract: *Here I compare estimates of tectonic strain rates from dense Global Positioning System measurements with the seismicity released in the last ~500 years in the Apennines (Italy). The rates of seismic moment accumulation from geodesy and of historical seismic release by earthquakes agree within the uncertainties, ruling out significant aseismic deformation. Within the considered 400 km-long section of the Apennines, this balance yields an average recurrence interval of 30–75 years for Mw ≥ 6.5 events without requiring a future earthquake larger than those observed historically (Mw ~7).*

Key words: *Strain rate, Earthquake recurrence, GPS, Apennines.*

INTRODUCTION

Assessment of seismic hazard is, in most places, mainly based on historical seismicity. Short-term fluctuations, at temporal scales similar to the historical record, are an inevitable consequence of the episodic earthquake release. It is thus of primary importance to evaluate whether the sampled seismicity is representative of the effective rate of tectonic deformation, i.e. stationary relative to the steady state tectonic loading (Main, 1996). The elastic rebound theory (Reid, 1910) offers a conceptual framework to link the rate of tectonic loading and the intermittent earthquake release, but the successful application of quasi-periodic, deterministic models of recurrence has been challenging (Scholz, 2002). The constrain that, given enough time, the rate of strain released by earthquakes should mirror the rate of tectonic deformation provides a powerful tool for the assessment of seismic hazard. Measurements of crustal deformation can, under simple assumptions, be translated in estimates of the average frequency and magnitude of the largest events (Molnar, 1979; Kagan, 2002). Further advances in this field are thus likely to come from regions combining a long historical record of earthquakes and accurately measurable geodetic strain rates. The Apennines are an actively extending mountain belt running for ~700 km in a NW-SE direction along the Italian peninsula. Active deformation is well documented by the instrumental and historical seismic catalogues (Selvaggi, 1998; Rovida et al., 2011; Chiarabba et al., 2005) and by geological (Galli et al., 2008; Roberts and Michetti, 2004) and geodetic data (Hunstad et al., 2003; D'Agostino et al., 2011). NE-SW extension overprints previous contractional structures, now active in the Northern Adriatic Sea and in the Po Plain. Active extension (Figure 1) now appears to be driven by a combination of relative NE-SW motion between the Adriatic and Tyrrhenian domains and by gradients of gravitational potential energy localizing strain along the crest of the Apennines (D'Agostino et al., 2011). Here I compare estimates of tectonic strain from dense (average station spacing < 50 km) Global Positioning System (GPS) measurements with the seismicity released in the last ~500 years in the Apennines.

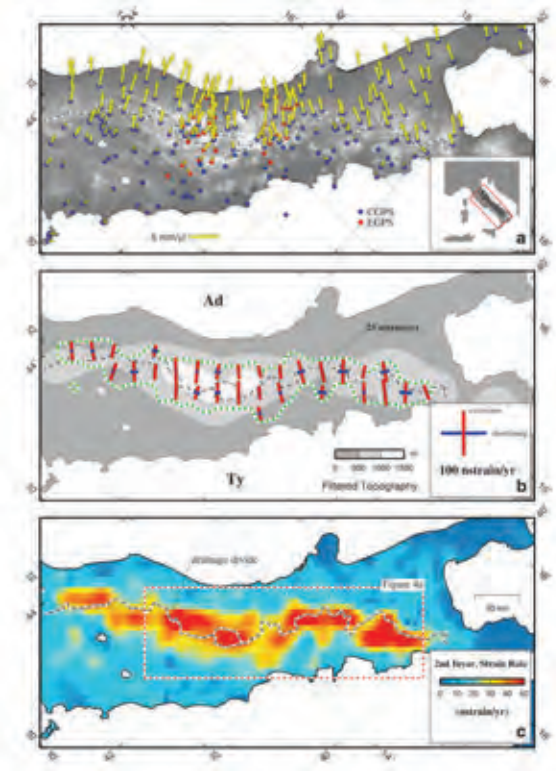

Figure 1. (a) Horizontal velocities of continuous (blue circles) and survey (red) sites in a Tyrrhenian reference frame. (b) Extensional (red bars) and contractional (blue) principal axes of the model strain rate field plotted for values of the second invariant > 25 nstrain/yr (green dashed contour). Also shown is the regionally filtered topography (wavelength > 100 km), and the drainage divide (dashed line) between the Tyrrhenian (Ty) and Adriatic (Ad) Sea. (c) Second invariant of the strain rate tensor. Maps are displayed in an oblique Mercator projection with the equator azimuth parallel to the trend of the Apennines (N135).

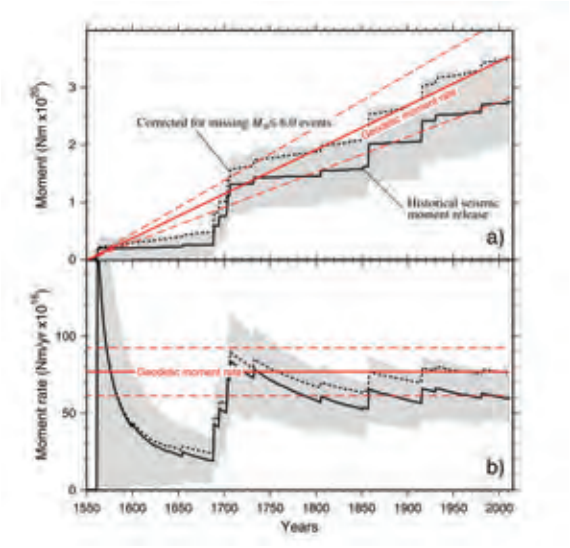

Figure 2. (a) Cumulative seismic moment (black line) released by earthquakes (±1 sigma uncertainty) in the area shown (red dashed line) in Figure 1b. The rate of seismic moment buildup from GPS is shown with a red line (dashed lines are ±1 sigma uncertainty). (b) Rate of seismic moment release calculated in progressively increasing time windows.

ANALYSIS OF GPS STRAIN RATE

I estimate the rate of seismic moment accumulation from geodesy using the strain rate field in a 400 × 130 km^2 area parallel to the Apennines (Figure 1c). The relationship between the strain rate tensor and scalar moment rate is not unique (Savage and Simpson, 1997). Various relationships between the strain rate tensor and the scalar seismic moment, listed in Pancha et al. (2006), have been proposed. In the case of a dominant uniaxial strain, as in the Apennines, these methods provide very similar results, and I use the scalar version of Kostrov's formula (Kostrov, 1974) proposed by Ward (1998). Details of the analysis and methods used to calculate the GPS velocity and the strain rate fields are given in D'Agostino (2014). This calculation furnishes an estimate for the rate of seismic moment accumulation of 76.9 ± 15.6 × 10^{16} Nm/yr. A constant value of 10±2.5 km which includes the ipocentral depths of instrumentally recorded M> 5 earthquakes (Chiarabba et al., 2005) is used as a value for the thickness of the seismogenetic upper crust.

Historical seismicity

Seismic events with Mw ≥ 5.0 in the time interval 1550–2010 have been extracted from the CPTI11 catalogue of Italian earthquakes (Rovida et al., 2011). Each event in the CPTI11 catalogue has an estimate of equivalent moment magnitude obtained from all available intensities and equated to Mw using regression coefficients calibrated with intensity data available for instrumentally recorded earthquakes (Rovida et al., 2011). Assessments of catalogue completeness (Stucchi et al., 2011) suggest that in the axial belt of the Apennines, the catalogue is complete for Mw ≥ 6 events starting approximately from the beginning of the sixteenth century. The largest selected event (1857 Val D'Agri Mw 7.0) contributes for 14% to the total seismic moment, whereas the contribution of the three biggest events (1857, 1915, and 1688) amounts to 39%. My estimate of seismic moment release is thus unlikely to be critically affected by a few, large events in the catalogue. Since the instrumentally recorded earthquakes and the pattern of geodetic deformation consistently indicate uniaxial extension in a NE-SW direction, I assume that all seismic events have released NE-SW extension by slip on 45°-dipping NW-SE trending normal faults. Using this approximation, the eigenvectors of the seismic moment tensors are horizontal or vertical and the rate of seismic moment release can be obtained simply by summing the scalar moments of each individual event. There are two sources of errors which affect estimates of long-term rates of seismic moment release. The first is the error of scalar moment of individual earthquakes, whereas the second is the spatiotemporal randomness of earthquake occurrence. Considering earthquake occurrence as a random, Poisson-like process, I assign an uncertainty equal to its seismic moment to each event. Assuming stationary seismicity, independent events and absence of aseismic deformation the seismic moment rate can be viewed as a random variable which, for a sufficiently large time interval, tends asymptotically to the value of the long-term tectonic loading moment rate. The cumulative seismic moment since 1550 (Figure 2a) agrees within the uncertainties with the seismic moment predicted by the geodetic accumulation rate assumed to be stable in the last centuries. This is most clearly shown by the evolution of the seismic moment rate (Figure 2b) calculated in progressively longer intervals, displaying large initial fluctuations but converging asymptotically toward a stable value in agreement with the rate of tectonic loading.

Earthquake recurrence

Empirical observations show that small earthquakes occur more frequently than large ones following a distribution (G-R, Gutenberg and Richter, 1944) that relates the cumulative number of earthquakes N above a given magnitude M, by log(N) = a – bM where a is a constant and the b value is generally approximately 1. I verify the hypothesis that the total seismic moment accumulation distributes into earthquake sizes following a G-R distribution that conserves (Kagan, 2002) the rate of tectonic loading without requiring events larger than those observed historically (Mmax ~7.0). In other words I test the hypothesis that the historical earthquakes (1) released an amount of seismic moment comparable to that provided by tectonic forcing while (2) distributing following a G-R relationship. By truncating the cumulative G-R distribution above magnitudes corresponding to moment Mmax (the seismic moment of the Mmax event), the frequency distribution of earthquakes of moment ≥ M0 can be calculated using the relationship from Molnar (1979). Figure 3 shows the

frequency distribution calculated using the geodetic moment rate and Mmax from the largest event in the catalogue, and a b value of 1 (as suggested by recent analyses of the instrumental catalogue, Gasperini et al., 2013). The G-R distribution so obtained (Figure 3) agrees within uncertainties with the observed seismicity for Mw > 6. At lower magnitudes, observed frequencies are systematically lower than the G-R model consistently with the completeness analysis of the CPTI11 catalogue (Stucchi et al., 2011). The G-R model predicts that (1) a Mw ≥ 6.5 event must occur, on average, every 30–75 years (95% confidence range) to seismically balance the rate of tectonic deformation and (2) that the fraction of seismic moment released by Mw ≤ 6 events is ~30% of the total.

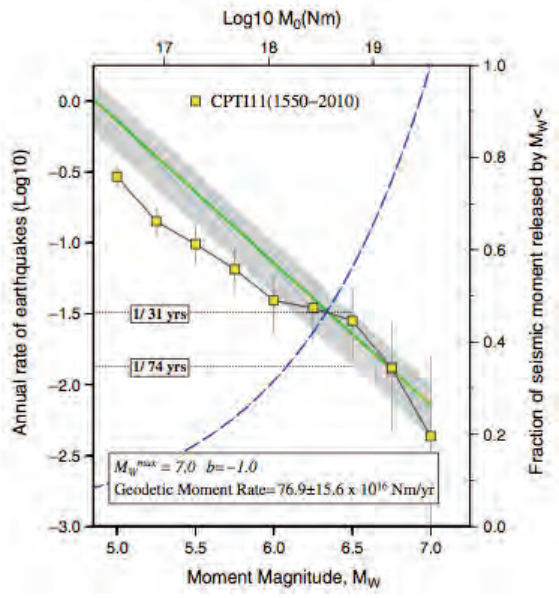

Figure 3. Observed 1550–2010 seismicity distribution (yellow squares with 95% Poisson confidence intervals) compared with a G-R model (green line and associated 95% confidence interval) whose total seismic moment rate matches the geodetic estimate. The two values agree for events Mw ≥ 6.0 that, overall, release ~ 70% of the total seismic moment (blue dashed line).

DISCUSSION

It is of interest to characterize the average recurrence for the smallest possible dimension, namely, for an area large enough to contain the fault length associated with the Mmax event (i.e., ~50 km for a M ~7 event). Since the rate of extension is relatively constant along strike, I simply estimate the recurrence of Mw ≥6.5 events by scaling by a factor 8 (400/50) the recurrence in the total 400 km long section. Balancing the tectonic loading by earthquakes thus requires a Mw ≥ 6.5 event to locally strike, on average, every 240–600 years. Elapsed times in regions of unreleased strain have a comparable duration, possibly pointing to heightened seismic hazard in these regions. Two major sources of uncertainty affect estimates of seismic hazard based on seismic moment deficit. The first arises from the poorly known seismic history and uncertain level of strain prior to 1550. The second source comes from the intrinsic uncertainty of earthquake recurrence. In particular, it is not clear if the distribution of recurrence intervals is best described by a renewal model with a strong central tendency (Matthews et al., 2002), by the view that repeated large earthquakes can happen in rapid succession without requiring time for stress regeneration (Jackson and Kagan, 2006) or that strain is released by clustered events in a time span considerably shorter than their mean recurrence interval (Wallace, 1987).

In summary, the convincing evidence of complete seismic release of tectonic deformation in the Apennines argues for a stationary response of seismicity to tectonic loading at the timescale of ~500 years. Previously reported discrepancies (Hunstad et al., 2003) are thus likely to originate from the limited temporal (126 years) and spatial dimensions used for comparison of seismic and geodetic strain rates. Although starting from a similar cumulative value of historical seismic moment release, Selvaggi (1998) obtained an average extension rate (~1.6 mm/yr) across the central-southern Apennines a factor of 2 smaller than the one measured geodetically (~3 mm/yr). The adoption of a longer time interval (700 years), likely to be significantly incomplete before the sixteenth century, is probably the reason for the observed discrepancy. These comparisons emphasize the need for an accurate selection of appropriate spatial and temporal dimensions when comparing geodetic and seismic deformation data (Ward, 1998; Pancha et al., 2006).

The results of this work provide the basis (1) to evaluate the completeness of the seismic catalogue, (2) to guide the spatial design of the seismogenetic zoning in probabilistic seismic hazard assessments, (3) to improve the definition of frequency and magnitude of the largest events, and (4) to motivate a wider integration of geodetic data in seismic hazard practices.

References

Chiarabba, C., L. Jovane, and R. Di Stefano (2005). A new view of Italian seismicity using 20 years of instrumental recordings. *Tectonophysics*. 395, 251–268, doi: 10.1016/j.tecto.2004.09.013.

D'Agostino, N., et al., (2011). Evidence for localized active extension in the central Apennines (Italy) from global positioning system observations. *Geology*. 39, 291–294, doi:10.1130/G31796.1.

D'Agostino, N. (2014). Complete seismic release of tectonic strain and earthquake recurrence in the Apennines (Italy). *Geophys. Res. Lett*. 10.1002/2014GL059230.

Galli, P., et al., (2008). Twenty years of paleoseismology in Italy. *EarthSci.Rev. 88*, 89–117, doi:10.1016/j.earscirev.2008.01.001.

Gasperini, P., B. Lolli, and G. Vannucci (2013). Empirical calibration of local magnitude data sets versus moment magnitude in Italy. *Bull. Seismol. Soc. Am.* 69, 2227–2246, doi:10.1785/0120120356.

Gutenberg, B., and C.F. Richter, (1944). Frequency of earthquakes in California. *Bull. Seismol. Soc. Am. 4*, 185–188.

Hanks, T.C., and H. Kanamori, (1979). A moment magnitude scale. *J. Geophys. Res. 84*, 2348-2350.

Hunstad, I., et al., (2003). Geodetic strain in peninsular Italy between 1875 and 2001. *Geophys. Res. Lett.* 30(4), 1181, doi:10.1029/2002GL016447.

Jackson, D.D., and Y.Y. Kagan, (2006). The 2004 Parkfield earthquake, the 1985 prediction, and characteristic earthquakes: Lessons for the future. *Bull. Seismol. Soc. Am.* 96(4B), 397–409, doi:10.1785/0120050821.

Kagan, Y.Y., (2002). Seismic moment distribution revisited: II. Moment conservation principle. *Geophys. J. Int.* 149(3), 731-754, doi:10.1046/j.1365-246X.2002.01671.x.

Kostrov, V.V., (1974). Seismic moment and energy of earthquakes, and seismic flow of rock. *Phys. Solid Earth*. 1, 23–44.

Main, I., (1996). Statistical physics, seismogenesis, and seismic hazard. *Rev. Geophys.* 34(4), 433–462, doi:10.1029/96RG02808.

Matthews, M.V., W.L. Ellsworth, and P.A. Reasenberg, (2002). A Brownian model for recurrent earthquakes. *Bull. Seismol. Soc. Am.* 92, 2233–2250.

Molnar, P., (1979). Earthquake recurrence intervals and plate tectonics. *Bull. Seismol. Soc. Am.* 69, 115–133.

Pancha, A., et al., (2006). Comparison of seismic and geodetic scalar moment rates across the Basin and Range Province. *Bull. Seismol. Soc. Am.* 96(1), 11–32, doi:10.1785/0120040166.

Reid, H.F., (1910). *The California Earthquake of April 18, 1906. Volume II. The Mechanics of the Earthquake*. Carnegie Institution of Washington, Washington, D.C.

Roberts, G.P., and A.M. Michetti, (2004). Spatial and temporal variations in growth rates along active normal fault systems: an example from The Lazio–Abruzzo Apennines, central Italy. *Journ. Struct. Geol.* 26 (2), 339-376.

Rovida, A., R. Camassi, P. Gasperini, and M. Stucchi (Eds.), (2011). *CPTI11, the 2011 version of the parametric catalogue of Italian earthquakes.* Milano, Bologna. http://emidius.mi.ingv.it/CPTI.

Savage, J.C., and R.W. Simpson, (1997). Surface strain accumulation and the seismic moment tensor. *Bull. Seismol. Soc. Am.* 87, 1345–1353.

Scholz, C.H., (2002). *The Mechanics of Earthquakes and Faulting,* 2nd ed., Cambridge Univ. Press, Cambridge, New York, Melbourne.

Selvaggi, G., (1998). Spatial distribution of horizontal seismic strain in the Apennines from historical earthquakes. *Ann. Geofis.* 41(2), 241–251.

Stucchi, M., et al., (2011). Seismic hazard assessment (2003–2009) for the Italian building code. *Bull. Seismol. Soc. Am.* 101, 1885–1911,doi:10.1785/0120100130.

Wallace, R., (1987). Grouping and migration of surface faulting and variations in slip rates on faults in the Great Basin province. *Bull. Seismol. Soc. Am. 77*(3), 868–876.

Ward, S.N., (1998). On the consistency of earthquake moment release and space geodetic strain rates: The United States. *Geophys. J. Int.* 134(1), 172–186.

INQUA Focus Group on Paleoseismology and Active Tectonics

paleoseismicity.org

New preliminary data on the Late Quaternary evolution of Magliano dei Marsi area (Abruzzo, Central Italy)

De Caterini, G. (1), Blumetti, A.M. (2), Coen, G. (3), Della Ventura, G. (4), Eulilli, V. (2), Ferri, F. (2), Guerrieri, L. (2), Leoni, G. (2), Lucci, F. (4), Mariani, M. (5), Puzzilli, L. (2), Santoponte, A. (6), Vittori, E. (2), Zaffiro, P. (1)

(1) ENGEO Praxis S.r.l., Via di Donna Olimpia, 166, 00152 Roma, Italy. Email: giovanni.de.caterini@gmail.com
(2) ISPRA Istituto Superiore per la Protezione e la Ricerca Ambientale - Dip. Difesa del Suolo. Via V. Brancati 60, 00144 Roma, Italy
(3) E&G S.r.l. Via dell'Amba Aradam, 24, 00184, Roma, Italy
(4) Dipartimento Scienze - Università Roma Tre. L.go S. Leonardo Murialdo, 1, 00146, Roma, Italy
(5) Magliano dei Marsi Municipality, (AQ), Italy
(6) Magliano dei Marsi Municipality Consultant. – Largo Bacone, 13, 00137, Roma, Italy

Abstract: *Within a seismic micro-zonation study in the district of Magliano dei Marsi (Abruzzo) recent geological investigations have provided new data regarding the Late Quaternary evolution of this area which is located a few kilometers West of the Fucino Plain. Stratigraphic and geophysical data have identified a new tectonic element (Colle Lucciano structure) that seems to have controlled the recent local landscape evolution. This fault could have triggered the strong 1905 earthquake, possibly causing surface faulting. The coseismic reactivation of this tectonic element could have produced surface faulting: this assumption needs to be confirmed by paleoseismological surveys.*

Key words: *Seismic microzonation, capable fault.*

INTRODUCTION

The Magliano dei Marsi village (Abruzzo Central Apennines) is located in the upper Salto River valley, a few kilometers west of the Fucino Plain. This area has been continuously struck by earthquakes, e.g. that of 1905 (Mw= 5.7), with epicenter located near Rosciolo.

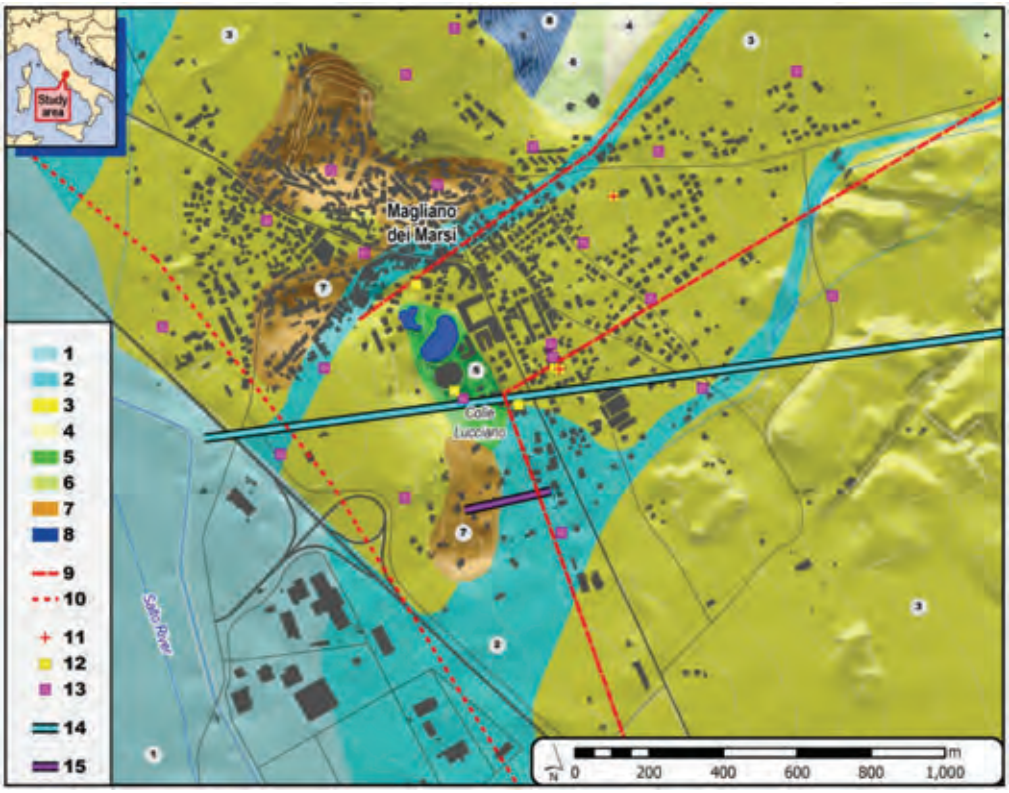

Figure 1: (1) sands and silts of alluvial deposits (Holocene), (2) gravels of alluvial and fluvioglacial deposits (Holocene),(3) cemented breccias of alluvial and fluvioglacial deposits (S. Valle Majelama, Upper Pleistocene), (4) gravels of slope deposits (S. Valle Majelama, Upper Pleistocene), (5) lacustrine clays (S. Aielli-Pescina, Lower Pleistocene), (6) gravels of slope deposits (S. Aielli-Pescina, Lower Pleistocene), (7) limestone (Miocene), (8) limestone (Cretacic), (9) buried active fault (proposed), (10) buried fault, (11) downhole test, (12) borehole, (13) HVSR and SASW test, (14) geologic section, (15) SRT section.

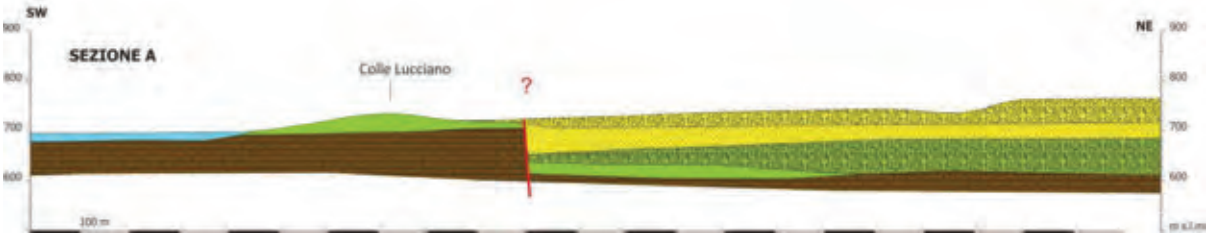

Figure 2: Geologic section (see trace in Fig. 1).

Considering the high level of seismicity, geological constrains about the area were really poor comparing to the surrounding areas. The micro-zonation study of Magliano dei Marsi municipality, together with other professionals researches have given the opportunity to get new information about the Late Quaternary evolution of this area, and in particular about a new, potentially seismogenic and capable, tectonic lineament.

Geological and seismic framework

The stratigraphy of the Magliano Plain (Figure 1) consists of fluvio-glacial fan deposits which are mainly made of gravel and sand of the "Sintema di Valle Majelama" and lay over lacustrine, sandy-loam deposits of the "Supersintema di Aielli-Pescina" which date back to the Middle Pleistocene (Nijman W., 1971; Giraudi, 1988; Frezzotti & Giraudi, 1992; Galadini et al., 1997; APAT, 2006; Centamore et al., 2006).

The alluvial fan, well exposed both on the field and in several quarry cuts, shows a high degree of cementation (geophysical surveys recorded Vs >900 m/s) and an increasing thickness towards NE (De Caterini et al., 2013). The conglomerates thin right under the village of Magliano dei Marsi and they lay on lacustrine deposits outcropping at Colle Lucciano. These deposits have been used for the production of clay for bricks and the former quarries have been now filled with water.

The historical seismicity of the area has been very relevant especially in the last century: one earthquake occurred in 1904 (local MCS intensity IX) and another one in 1915 (local MCS intensity X; Oddone, 1915; Ward & Valensise, 1989; Rovida et al., 2011).

New geological investigations

The Magliano dei Marsi Municipality has carried out new geological investigations (position in Figure 1) regarding the study of seismic micro-zonation (MZS).

These surveys, at 1:5,000 scale, have been undertaken in susceptible and urbanized areas simultaneously with recordings of seismic noise, Spectral Analysis of Surface Waves (SASW) investigations for each measuring station and systematic gathering of geognostic and geophysical data. Thanks to recent local seismic response surveys for the construction of a school, it has been possible to reach the geological bedrock through continuous logging drilling to a depth of 56 meters from ground level. The related Down-Hole investigation has led to a very detailed characterization of geotechnical and physical properties of filling deposits.

Considering the last data acquired and the previous geoelectrical surveys (1954), it has been possible to build a geotechnical model that has divided the stratigraphy into lithotechnical units with different physical characteristics. The results of the Horizontal to Vertical Spectral Ratios (HVSR) tests, together with the geognostic surveys have brought to the reconstruction of a schematic evolution of this sector.

DISCUSSION

During the survey at the primary school of Magliano, new materials of pyroclastic origin have been found, located below Upper Pleistocene conglomerates. This pyroclastic deposit is about 20 m thick, and it is divided in two different levels by a thin layer of gravel. This relevant thickness has been considered atypical because much higher than similar deposits found in the Fucino area (Zarlenga, 1987; Narcisi, 1995). For this reason, the Roma Tre University is carrying out mineralogical and sedimentological analysis to clarify if this is due to an in

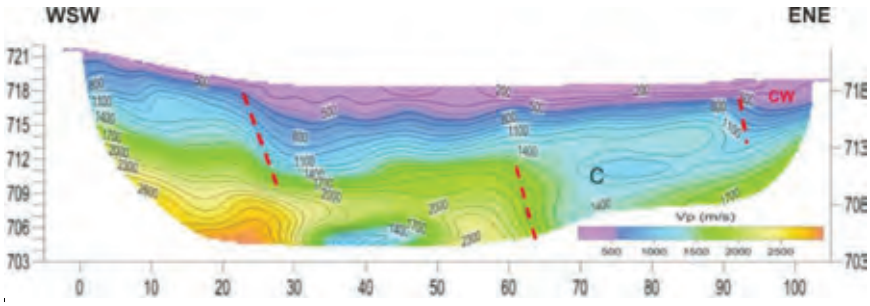

Figure 3: SRT image with the main seismic discontinuities (in red); C= inferred colluvial wedge. Elevation and distance scale in meters.

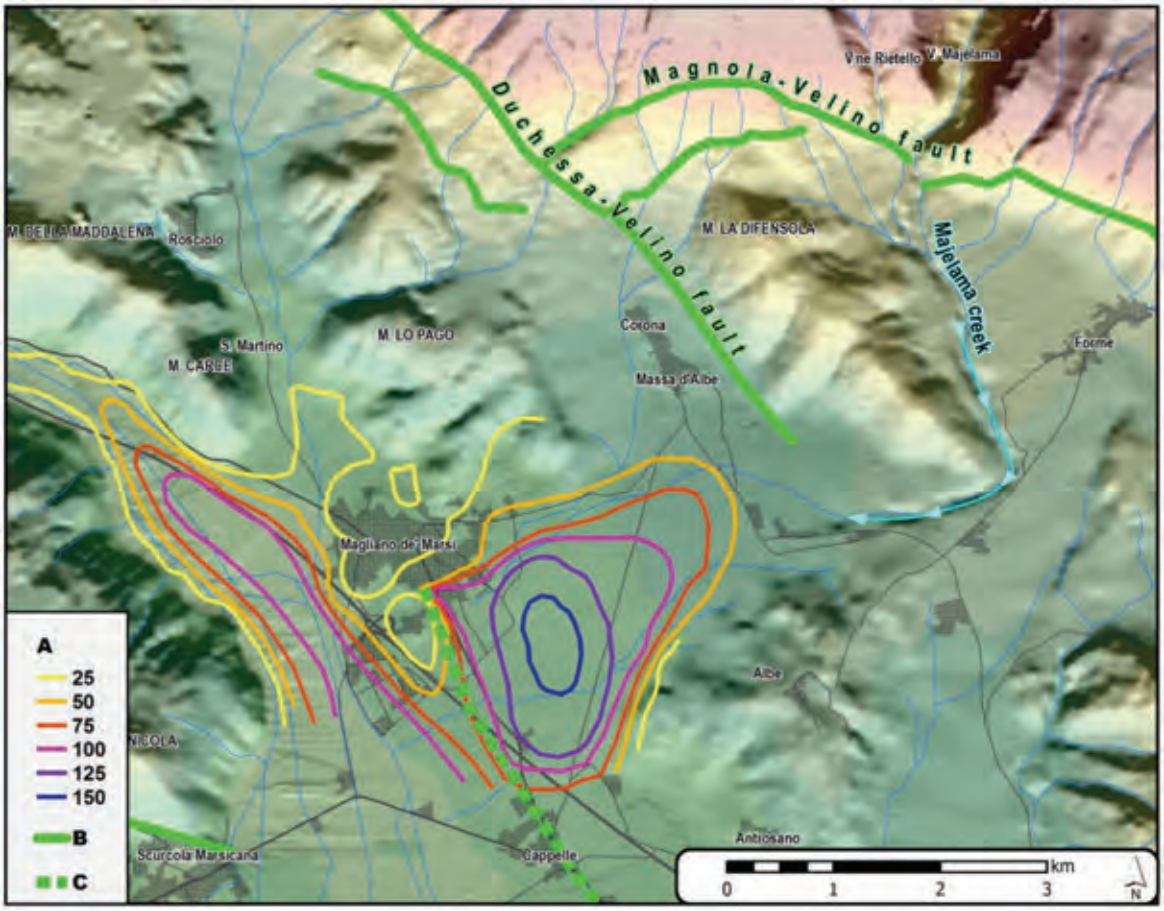

Figure 4: Geological bedrock model: (A) bedrock isobath (depth in meters), (B) ITHACA active and capable faults, (C) new hypothetical fault.

situ pyroclastic deposit or, more probably, to altered deposits. In addition thin colluvial deposits have been found widespread at the Colle Lucciano foothill (C in Figure 3).

Another new element is the outcropping of Miocene limestones in the area of Colle Lucciano (Figure 1). This outcrop is already documented in the Regione Abruzzo Geological Map (Vezzani & Ghisetti, 1997) but not on the official CARG geological map (scale 1:50,000, APAT, 2006) where it has been indicated as Quaternary conglomerate. This outcrop plays an important role in the definition of the geological layout of the Magliano Plain. As a matter of fact the geological bedrock deepens in the centre of the alluvial fan (see Figure 2 and Figure 4) with a lowering constrained between 50 and 150 m, probably because of a fault responsible for the dislocation of the deposits dating back to Middle Pleistocene.

Geoelectrical, seismic and radar surveys made by ISPRA and Regione Abruzzo along the hypothetic faults, confirmed the presence of a tectonic break in the Upper Pleistocene conglomerate deposits (Figure 3).

This hypothesis suggests that the evolution of the area since Middle Pleistocene was characterized by the deepening of the Magliano alluvial fan under the influence of a tectonic element following the main NW-SE typical trend. Such a tectonic element could have been responsible of the Valle Majelama creek capture, south of Forme village, which deflected towards SW the water course, previously directed to Avezzano.

FINAL REMARKS

The Colle Lucciano structure represents a Late Quaternary NW-SE trending fault, consistent with other seismogenic and capable faults of the area, like the Velino-Magnola fault, located 3 km to the northeast.

From a structural point of view it seems to be continuous with the Rosciolo structure, 3 km to the northwest, and the buried Cappelle structure to the southeast, for a total length of about 3 km (Figure 3). This structure could have been reactivated during the 1905 earthquake, with epicenter in Rosciolo (Molin et al. 1999).

Moreover it is important to remark that the isoseismal trend and cosesismic ruptures pointed by Oddone (1915) fit very well with a buried structure joining Magliano and Avezzano, passing through Cappelle, and able to produce shallow faulting.

In this case, the seismic and fault displacement hazard associated to the Colle Lucciano tectonic element should

be relevant. Nevertheless, this hypothesis needs to be confirmed by further detailed paleoseismological investigations, that could point out (or not) the occurrence of surface faulting during Late Pleistocene to Holocene strong earthquakes along the Colle Lucciano structure.

Acknowledgements: We would like to thank Dr. Ing. Stefano Bernardinetti and Dr. Giuseppe Cocchiararo for their support in geophysical field survey, and Dr. Anna Maria Bilotta for the translation.

References

APAT, (2006). *Carta Geologica d'Italia alla scala 1:50.000. Foglio 368 Avezzano*. SELCA, Firenze.

Centamore, E., U. Crescenti & F. Dramis (a cura di), (2006). *Note illustrative della Carta Geologica d'Italia alla scala 1:50.000, Foglio 368, Avezzano*. SELCA, Firenze.

De Caterini, G., G. Leoni, A. Santoponte, P. Zaffiro, G. Pezzo, (2013). *Studio di Microzonazione Sismica - Livello 1 – Comune di Magliani de' Marsi* (ai sensi della O.P.C.M. 29 febbraio 2012, n. 4007 e della D.G.R. 10 settembre 2012, n. 577). Unpublished report.

Galadini, F., P. Galli C. & Giraudi, (1997). Paleosismologia della Piana del Fucino (Italia Centrale). *Il Quaternario*. 10 (1): 27-64.

Galli, P., P. Messina, B. Giaccio, E. Peronace & B. Quadrio, (2011). Early Pleistocene to late Holocene activity of the Magnola fault (Fucino fault system, central Italy). *Bollettino di Geofisica Teorica ed Applicata*. Vol. 53, n. 4, pp. 435-458; December 2012.

Giraudi, C. (1988). Evoluzione geologica della Piana del Fucino (Abruzzo) negli utlimi 30.000 anni. *Il Quaternario*. 1(2), 131-159.

Frezzotti, M. & C. Giraudi, (1992). Evoluzione goelogica tardopleistocenica ed olocenica del conoide complesso di Valle Majelama (Massiccio del Velino - Abruzzo). *Il Quaternario*. 5(1), 33-50.

Molin, D., F. Galadini, P. Galli, L. Mucci & A. Rossi, (1999). Terremoto del Fucino del 13 gennaio 1915. Studio Macrosismico. In: (Castanetto S., Galadini F. Rebuffat M. & Sebastiano M. a cura di) *13 gennaio 1915. Il terremoto nella marsica*. Servizio sismico Nazionale – Agenzia di Protezione Civile. CNR - IRTR Istituto di Ricerca sulla Tettonica Recente. Istituto Poligrafico e Zecca dello Stato, 788 pp.

Narcisi, B., (1995). Caratteristiche sedimentologiche, mineralogiche e geochimiche di un livello tufitico del Pleistocene medio nei sedimenti della piana del Fucino, Italia centrale. *Il Quaternario*. 8(1): 235-238.

Nijman, W., (1971). *Tectonics of the Velino - Sirente area, Abruzzi, Central Italy*. Koninkl. Nederl. Akademie van Wetenshappen, Proceedings, B, 74 (2): 156-184.

Oddone, E., (1915). Elementi fisici del grande terremoto Marsicano-Fucense del 13 gennaio 1915. *Boll. Soc. Sismologica Italiana*. n.19, p. 71, Roma 1915.

Rovida, A., R. Camassi, P. Gasperini and M. Stucchi (eds.), (2011). *CPTI11, the 2011 version of the Parametric Catalogue of Italian Earthquakes*. Milano, Bologna, http://emidius.mi.ingv.it/CPTI, doi: 10.6092/INGV.IT-CPTI11

Servizio Geologico d'Italia, (1934). *Foglio 145 "Avezzano" della Carta Geologica d'Italia alla scala 1:100.000*. A cura di C. Crema. Poligrafico dello Stato, Roma.

Vezzani, L. & F. Ghisetti, (1997). *Carta geologica dell'Abruzzo*. SELCA, Firenze.

Ward, S.N. and G. Valensise, (1989). Fault parameters and slip distribution of the 1915, Avezzano, Italy earthquake derived from geodetic observations. *Bull. Seism. Soc. Am.* 79:690-710.

Zarlenga, F., (1987). I depositi continentali del Bacino del Fucino (L'Aquila, Italia Centrale). *Geologica Romana* 01/1987; 26.

INQUA Focus Group on Paleoseismology and Active Tectonics

paleoseismicity.org

Characterizing Active Faults in the Urban Area of Vienna

Decker, K. (1), Grupe, S. (2), Hintersberger, E. (1)

(1) Department of Geodynamics and Sedimentology, University Vienna, Althanstrasse 14, A-1090 Vienna, Austria.
Email: kurt.decker@univie.ac.at
(2) Wiener Gewässer Management Gesellschaft mbH, Wilhelminenstrasse 93/1, A-1160 Vienna, Austria

Abstract: *The identification of active faults that lie beneath a city is of key importance for seismic hazard assessment. Fault mapping and characterization in built-up areas with strong anthropogenic overprint is, however, a challenging task. Our study of Quaternary faults in the city of Vienna starts from the re-assessment of a borehole database of the municipality and geological descriptions of historical outcrops. The latter were found to be particularly valuable by providing unprejudiced descriptions of Quaternary faults. Data provides evidence for several active normal faults that are part of a fault system compensating fault-normal extension at a releasing bend of the Vienna Basin Transfer Fault. Slip rates estimated for the urban faults are in the range of several hundredths of millimetres per year matching the slip rates of normal faults that were trenched outside the city. Fault dimensions of the faults suggest that they are capable of producing earthquakes with M>6.*

Key words: *Active fault, fault slip rate, paleoseismology, seismic hazard, Vienna.*

INTRODUCTION

The city of Vienna is located about 20 km NW of the Vienna Basin Transfer Fault (VBTF), an active sinistral strike-slip fault which moves with a velocity of about 1 to 2 mm/a (Decker et al., 2005). It has been shown that the strike-slip fault is kinematically linked to a series of active normal faults that accommodate fault-normal extension at two large-scale releasing bends (Figure 1). These faults branch from the strike-slip fault at knickpoints where the fault strike changes by angles of 20°–35°. The normal faults merge with the strike-slip fault at a common detachment which is thought to coincide with the Alpine-Karpathian floor thrust at about 8 to 12 km depth (Beidinger & Decker, 2012). The detachment dips with about 5-10° to SE. This topography results in a strong asymmetry of the normal faults with respect to the strike slip fault. All major branch faults extend to the N and NW of the strike-slip fault, i.e., towards and into the city of Vienna.

Historical seismicity (Imax/Mmax = 8/5.2) in the Vienna Basin is moderate and exclusively focused along the NNE-SSW striking left-lateral strike-slip VBTF that delimits the basin towards the east. The normal splay faults seem to have been seismically inactive during historic times (the oldest earthquake records from the Vienna Basin date to the 18th century; Nasir et al., 2013). Paleoseismological data, however, proves that both types of faults, the strike-slip system and the normal branch faults are capable of releasing strong earthquakes with magnitudes up to M~7 (Hintersberger et al., in press; Hintersberger et al., 2013). In spite of the apparent seismic potential of the normal faults and the importance of fault parameters for seismic hazard analyses an attempt to identify and characterize active faults in the built-up area of Vienna has so far not been undertaken.

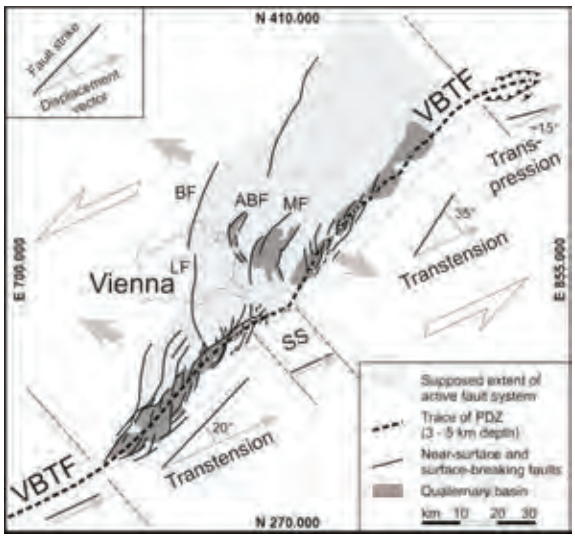

Figure 1: Active faults in the Vienna Basin. VBTF: sinistral strike-slip faults of the Vienna Basin Transfer Fault System; note the two transtensional releasing bends. Normal branch faults: LF: Leopoldsdorf fault; BF: Bisamberg fault; ABF: Aderklaa-Bockfließ fault; MF: Markgrafneusiedl fault. SS: non-transtensive strike-slip segment.

Database

Our approach to map Quaternary faults in an urban area uses the following data: (1) Miocene fault maps based on drillings and geophysical data that were collected for deep ground water and hydrocarbon exploration. (2) A database of several tens of thousands of shallow boreholes maintained by the City of Vienna. These data proved extremely valuable for mapping the base of the Pleistocene river terraces of the Danube and establishing isopach maps of Quaternary sediment thickness. Data allows identifying Quaternary faults by the offset of

terraces or the existence of Quaternary growth strata. (3) Historical outcrop documentations of sandpits and construction pits that were excavated in the 19th and 20th century in today's built area. (4) Digital elevation data including Lidar. (5) Vertical ground displacement measured by two radar interferometry campaigns (ERS 1995-2000 and ENVISAT 2002-2010). The random noise in the data and strong anthropogenic effects, however, did not allow for a tectonic interpretation of this data.

Quaternary faults in the urban area

The Quaternary faults extending into the city limits of Vienna are part of the E-dipping Leopoldsdorf normal fault system that branches from the VBTF 20 km south of Vienna (Figure 1). The fault formed as a Miocene growth fault and has a maximum cumulative vertical offset of about 3 km. It terminates towards N where extension is transferred via a left fault step to the Bisamberg normal fault system, another Miocene fault with c. 1 km throw. The stepover between the two systems is located within the urban area of Vienna.

Quaternary normal faulting at the Leopoldsdorf fault system is evident from the displacement of Late Pleistocene terraces of the Danube SE of Vienna and the tilting of the terraces by hangingwall rollover. The tilted terrace dips against the flow direction of the Danube.

Quaternary faulting is further proved by the displacement of late Middle Pleistocene loess and Late Pleistocene (Holocene?) gravels of the Danube, which were exposed in historical sandpits and construction pits in Vienna. Kümmel (1935) described E-directed normal faults with dip-slip slickenlines from such an historical outcrop in great detail noting the orientation of the fault plane, striation, and the alignment of elongated pebbles that parallel the fault plane and slickenline (location 1 in Figure 2). His description and biostratigraphic data by Frank & Rabeder (1997) prove that the exposed fault offsets late Middle Pleistocene loess (older than about 120 ky) for several meters suggesting a slip rate of a few hundredths of one millimetre per year for the formerly exposed normal fault.

Wiener Gewässermanagement (2011, 2014) published geological cross sections constructed from a dense network of shallow boreholes. The profiles show E-dipping normal faults offsetting Late Miocene sediments. Some of these faults coincide with terrace boundaries of two Pleistocene terraces in the South of Vienna (Figure 3). The ages of the terraces are not constrained by physical age data. The interpretation of fault controlled rather than erosional terrace boundaries is corroborated by the increase of the thickness of Quaternary sediments towards the faults which is indicative for rollover or flanking fold formation and growth strata deposition.

E-dipping normal faults offsetting the fluvial gravels of the lowermost terrace of the Danube have further been exposed by drilling and excavation close to the Danube (Plachy, 1981; location 4 in Figure 2). A temporary construction pit exposed a normal fault that offsets the gravel of the terrace. The base of the Pleistocene sediments is described to be offset for about 2 m indicating a Late Pleistocene to (?) Holocene growth fault. Assuming a Wuermian age for the terrace gravel leads to an estimated normal displacement rate of a few hundredths of one millimetre per year which is comparable to the estimate derived from the observations described by Kümmel (1935).

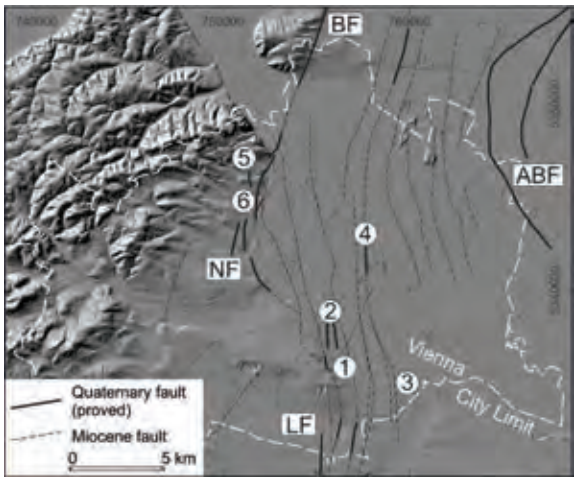

Figure 2: Quaternary faults in the city of Vienna. Evidence for Quaternary faulting at locations 1 to 6 is described in the text. LF: Leopoldsdorf fault; BF: Bisamberg fault; NF: Nussdorf fault; ABF: Aderklaa-Bockfließ fault.

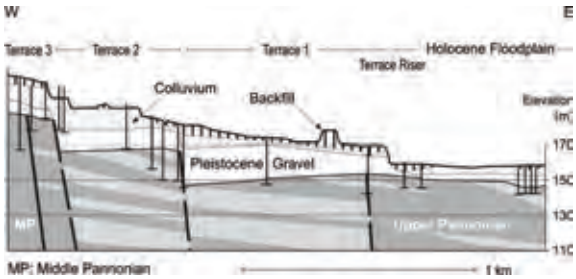

Figure 3: Splay faults of the Leopoldsdorf fault forming the boundaries of the undated Pleistocene terraces 1 to 3 in the South of the city of Vienna. Redrawn from Wiener Gewässermanagement (2014). Location 2 in Figure 2.

The Bisamberg and Nussdorf normal fault system forms the western boundary of the Vienna Basin within the city of Vienna and north of it. Quaternary normal faulting is indicated by the tilt of the Middle Pleistocene Gaenserndorf terrace E of Vienna which has been dated to 300 to 200 ky by OSL/IRSL age dating (Fig. 4; Hintersberger et al., in press). The terrace dips westwards towards the Bisamberg and Aderklaa-Bockfließ fault with a slope of about 0.005°. Tilting of the terrace against the gradient of the Danube must have occurred in the last 200 ky after the abandonment of the terrace. The amount of normal offset at the faults W of the terrace is estimated from a reconstruction of the paleo-surface. Restoring the original surface by back fitting the Quaternary fault offsets by a move-on-fault approach and back-tilting of the paleo-surface to the river gradient

of the Danube suggests about 29 m cumulative normal offset at the Bisamberg and Aderklaa-Bockfließ fault which corresponds to a cumulative average slip rate of these faults of about 0.15 mm/y for the last 200 ky.

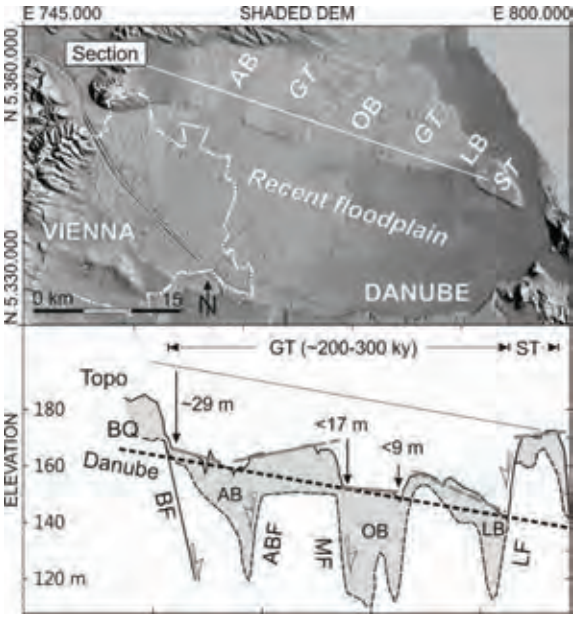

Figure 4: DEM of the floodplain of the Danube and the Middle Pleistocene Gänserndorf-Schlosshof terrace. The terrace is displaced by faults and tilted against the flow direction of the Danube. BF: Bisamberg fault; ABF: Aderklaa-Bockfließ fault; MF: Markgrafneusiedl fault; LF: Lassee fault; BQ: base of Quaternary; Quaternary basins: AB: Aderklaa basin; OB: Obersiebenbrunn basin; LB: Lassee basin. Redrawn from Decker et al. (2005).

The Nussdorf fault forms the southern continuation of the Bisamberg fault (Figure 2). It follows a morphological scarp between the lowermost Pleistocene terrace of the Danube and the foothills of the Wienerwald range. The Quaternary activity of several of its branch faults has been proved by historical outcrops in construction pits and sandpits which were exploited in the late 19th and 20th century. Faulted Quaternary sediments have been mapped by Fink et al. (1958; offset Pleistocene gravel and loess, Wien-Hohe Warte; location 5, Figure 2), Küpper et al. (1951), and Toula (1906; E-dipping normal faults in loess, Wien-Heiligenstadt; location 6, Figure 2). Toula (1906) provided an extensive description of E-directed normal faults offsetting a succession of "older" loess, which pre-date the deposition of a "younger" succession of loess and colluvial gravel suggesting a Pleistocene event horizon. Additional faults with smaller offsets are described to cut the youngest loess deposits. The southern continuation of the Nussdorf fault shown in Figure 2 is drawn according to data by Küpper (1951) who interpreted Quaternary growth faults in gravels of the Prater terrace from shallow boreholes. In addition, Plachy (1981) described E-dipping normal faults from Late Pleistocene terrace gravels which were exposed in construction pits close to the center of the city.

DISCUSSION AND CONCLUSIONS

The continuation and architecture of both, the Leopoldsdorf and Nussdorf-Bisamberg faults outside the city is well constrained by deep hydrocarbon exploration wells and reflection seismic. Data shows that both faults consist of a series of near-surface splay faults that merge downwards into a master fault. The surface breaking Quaternary faults identified in Vienna are regarded as parts of these splay faults. Data further constrains the fault length and fault areas of the master faults (Table 1).

Fault	Slip	Slip rate (mm/y)	Length (km)	Area (km²)	Mwmax
Bisamberg	normal	< 0.1 **	33	438	6.6-6.7
Leopoldsdorf	normal	< 0.05 *	33	685	6.7-6.8
Aderklaa-Bockfließ	normal	< 0.1 **	16	175	6.2
Markgrafneusiedl	normal	0.015-0.085	36	620	6.7-6.8

*Table 1: Fault parameters of active faults in Vienna. Slip rates: *estimates for single splay faults; **estimated cumulative rate of Bisamberg and Aderklaa-Bockfließ fault: 0.15 mm/y. Mwmax: maximum magnitude estimated from fault parameters according to Wells & Coppersmith (1994).*

Due to the location of the faults in the city investigations by trenching are not feasible. A preliminary and speculative assessment of their seismotectonic characteristics may be obtained from a comparison to the Aderklaa-Bockfließ and the Markrafneusiedl normal fault (Figure 1). Both faults were investigated by trenching (Hintersberger et al., in press). Analogies exist with respect to fault orientation, kinematics, fault dimensions, age, kinematic linkage to the releasing bends of the VBTF, wall rock rheology, fault history, and slip rates. For the Markrafneusiedl fault, trenching revealed five Late Pleistocene surface-breaking paleoearthquakes with magnitudes between M=6.3 and M=7.0 and an average recurrence time of 20 to 25 ky. The magnitudes and recurrence intervals are in line with the fault dimensions and the average fault slip rate of about 0.015 to 0.085 mm/y which were established from geomorphic data and trenching. The latest events at the Markrafneusiedl and Aderklaa-Bockfließ fault occurred between 13-14 ky and after about 15-16 ky, respectively.
Our data from the urban area of Vienna and the comparison of the identified Quaternary faults clearly indicates that both, the Bisamberg-Nussdorf and Leopoldsdorf fault system have significant seismic potential and may release earthquakes with M>6 at large recurrence intervals. Both faults may therefore not be disregarded in seismic hazard assessment.

Acknowledgements: The research projects on active faults in the Vienna Basin and the city of Vienna was funded by OMV, Land Niederösterreich and Stadt Wien / Ma 31.

References

Beidinger, A. & K. Decker, (2011). 3D geometry and kinematics of the Lassee flower structure: Implications for segmentation and seismotectonics of the Vienna Basin strike-slip fault, Austria. *Tectonophysics*. 499, 22-40.

Decker, K., H. Peresson & R. Hinsch, (2005). Active tectonics and Quaternary basin formation along the Vienna Basin Transform fault. *Quaternary Science Reviews*. 24, 305-320.

Fink, J., R. Grill, K. Kollmann & H. Küpper, (1958). Beiträge zur Kenntnis des Wiener Beckens zwischen Grinzig und Nußdorf (Wien XIX). *Jb. Geol. B.-A.* 101, 117-138.

Frank, C. & G. Rabeder, (1997). Laaerberg. In: *Pliozäne und pleistozäne Faunen Österreichs* (Döppes, D., Rabeder, G. eds.). Mitteilungen der Kommission für Quartärforschung der österreichischen Akademie der Wissenschaften, 10, 88-92, Wien (Österr. Akad. Wiss.)

Hintersberger, E., K. Decker, J. Lomax, M. Fiebig & C. Lüthgens, (2013). *Active tectonics and the earthquake cycle*. Geophysical Research Abstracts, EGU2013-12755

Hintersberger, E., K. Decker & J. Lomoax, (in press). Evidence of a M~7 paleoearthquake in the Vienna Basin. *Terra Nova*.

Kümmel, F., (1935). Der Löß des Laaerberges bei Wien. *Verhandlungen Geol. B.-A.* 1935, 132-135.

Küpper, H., (1951). Zur Kenntnis des Alpenabbruches am Westrand des Wiener Beckens. *Jb. geol. B.-A.* 94, 41-92.

Nasir, A., W. Lenhardt, E. Hintersberger & K. Decker, (2013). Assessing the completeness of historical and instrumental earthquake date in Austria and the surrounding areas. *AJES*. 106, 90-102.

Plachy, H., (1981). Neue Erkenntnisse zur Tektoink im Wiener Raum. *Mitt. Österr. Geol. Ges*. 74/75, 231-243.

Toula, F., (1906). Die Kreindelsche Ziegelei in Heiligenstadt-Wien (XIX. Bez.) und das Vorkommen von Congerienschichten. *Jahrbuch der k. u. k. geol. R.-A.* 56, 170-196.

Wells, D.L. & K.J. Coppersmith, (1994). New empirical relationships among magnitude, rupture length, rupture width, rupture area, and surface displacement. *Bulletin of the Seismological Society of America*. 84, 974-1002.

Wiener Gewässermanagement [S. Grupe & T. Payer], (2011). Angewandte Hydrogeologische Forschung - Stadtgebiet Wien. Wissenschaftsbericht der Stadt Wien 2010, 292-295.

Wiener Gewässer Management (MA 45), (2014). Angewandte Hydrogeologische Forschung Stadtgebiet Wien, Teilgebiet 2014. Hydrogeologischer Längenschnitt WNW-OSO Science Center / A23-Südosttangente etc.; Hydrogeologischer Längenschnitt West-Ost A23 bis Simmeringer Haide.

INQUA Focus Group on Paleoseismology and Active Tectonics

paleoseismicity.org

Neotectonic activity along the Culoz fault, southern Jura – Alps junction (France): Implications for seismic hazard analyses

De La Taille, C. (1,2), Jouanne, F. (1), Crouzet, C. (1), Beck, C. (1), Jomard, H. (2)

(1) Université de Savoie Mont Blanc, ISTerre, CNRS, 73376 Le Bourget-du-Lac, France. Email: delataic@univ-savoie.fr
(2) Institut de Radioprotection et Sureté Nucléaire, BERSSIN, 92260 Fontenay-aux-Roses, France

Abstract: *This manuscript aims to study the geometry of the strike-slip Culoz fault (CF) in the Southern Jura (France) for constraining its seismic hazard potential.Therefore, the fault has been studied using different methods and predominantly high-resolution seismic reflection offshore in Lake Le Bourget and electrical resistivity tomography. The CF was recognized in land during field investigations. Seismological data were acquired to determine the possibility of the fault to be rooted in the basement as it develops through a fold and thrust mountain belt. Overall, a minimum 25 km fault length has been estimated.In addition the foci minimum depth (4 km) indicates that the top of the crystalline basement is involved. Based on these informations, and the observation of deformed quaternary deposits, we propose that a Mw 6 – 6.8 magnitude earthquake can occur on the CF.*

Key words: *Jura, Alps, seismic hazard, active tectonic, Lake Le Bourget.*

INTRODUCTION

This work is a contribution for a better knowledge of active faults in the Jura-Alps junction, through a specific study along the Culoz Fault (CF) system, providing a offshore prolongation within a large and deep natural lake. This fault has a long recurrence interval (of a couple or thousand of years). That is significantly larger that the period covered by the historical record. Therefore, a fault-specific approach is rather than an historical record approach. This is particularly true in France for sensitive and classified facilities (nuclear power plants, dams, etc...).
In the studied area, most of the Pliocene-Pleistocene markers of deformation have been eroded by successive glaciations. Therefore possible markers are usually recent mostly as post-Würmian lake sediments which may register recent deformations and enrich their characterization. To image these markers, we used different geophysical methods from high resolution seismic reflection, high resolution electrical resistivity tomography, seismicity recording, and fieldwork mapping.

GEOLOGICAL SETTINGS

The Pre-Quaternary Substratum
The Jura fold and thrust belt (Figure 1) represents the most external part of the Alpine chain in its northwestern sector (Laubscher, 1961; Guellec, 1989; Philippe, 1995; Burkhard and Sommaruga, 1998; Willett and Schlunegger, 2010). Horizontal shortening in the Jura took place above a basal décollement horizon within Triassic evaporites, mostly during Middle-Late Miocene and Pliocene.
In its southern part, the Jura Mountains present a virgation (an arch form) (Figure 1) related to the disappearance of Triassic evaporites levels in the Chambéry area. The width of the décollement level affected by displacements has been estimated to 65 km between Neuchâtel and Besançon (Sommaruga, 1997) and 20 km around the southern, latitude of Chambéry. As the total shortening is the same (i.e. ca 20 km), this difference is mainly due to displacement above the décollement level, no deformation recorded in the central Jura (formation of plateaus) whereas in the southern Jura the deformation is accommodated by a set of narrow anticlines.

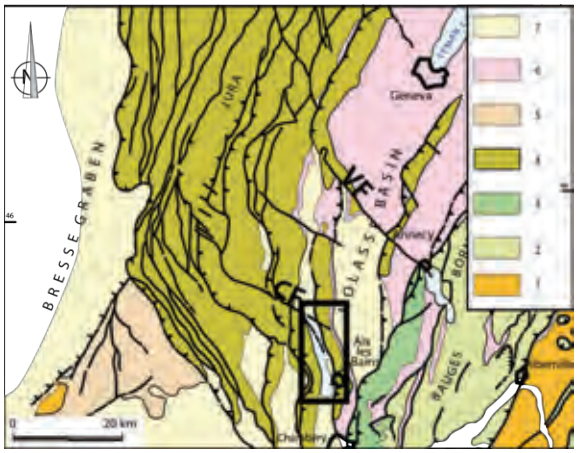

Figure 1: Geological and structural sketch map of northwestern Outer Alps and Jura foreland. 1. Crystalline basement; 2 to 4: Outer Alps Mesozoic series (2, Dauphinois z.; 3, Pre-subalpine z.; 4, Jurassian z.); 5. Autochthon Mesozoic series; 6. Oligocene-Lower Miocene siliclastics; 7. Middle-Upper Miocene and Pliocene silicilastics. V.F.: Vuache Fault; C.F.: Culoz Fault.

The disappearance of the low-friction detachment level also induces the disappearance of the perialpine Molasse basin, which separated the Jura Mountains from the Subalpines massifs. This change between the southern and central Jura Mountains is also accommodated by a

set of strike-slip transfer faults (Vuache, Culoz, and Col du Chat faults; Figures 1 et 2) that allow the existence of differential deformation on both sides of the faults.
It has to be noted, that the occurrence of earthquakes localized in the crystalline basement as well as the observations of thrusts in deep seismic profiles suggest that the recent and present day deformation is partly localized in the basement. However, the existence of a mechanical coupling between the detached Mesozoic sedimentary cover and the underlying basement still remains unclear.

Regional neotectonic setting
This area is characterized by moderate seismicityas shown by the observation of neotectonic index such as Saint Etienne de Crossey (Grellet et al., 1993; Baize et al., 2002), the anomalous direction of horizontal stress (Becker and Werner, 1995; Becker, 2000) in the southern Jura and significant historical seismicity (Thouvenot et al., 1990).
At the eastern tip of the Culoz fault, Lake Le Bourget is recognized as a tectonically active region by structural investigations, seismo-tectonics, historical seismicity (Vogt and Godefroy, 1979) and occurrence of lacustrine seismically induced destructurations (Beck, 2009).
The current stress/strain map pattern is quite similar to the Mio-Pliocene situation (Becker, 2000) and mountain building still appears active in the southern Jura, mainly within the internal zones (Philippe, 1995). However, the origin of these boundary conditions as to whether they derive from tectonic forces and/or body forces is debated (Delacou et al., 2004; Delacou et al., 2008).
In the southern Jura, the tectonic activity appears concentrated along NW-SE (N120 and N140) left lateral strike slip faults, such as the Culoz Fault and the Vuache Fault (CF and VF on Figure 1). The Culoz Fault extends from the Jura to the Chautagne swamp, north of Lake Le Bourget (Savoie). Historical earthquakes are known in the vicinity of this fault, in particular of the most significant of which was the 19th February 1822, which had an epicentral intensity of VII - VIII (Vogt and Godefroy, 1979). From the analysis of the spatial distribution of macro-seismic intensities, the 1822 earthquake most probably initiated in the basement (9-10 km depth, SISMALP catalog, http://sismalp.obs.ujf-grenoble.fr) indicating that present deformation is not only localized in the sedimentary cover, but also in the basement. On 2 March 2014, an earthquake of ML -magnitude 2.7 occurred to the NE of Lake Bourget (near Chindrieux), attributed to the Culoz fault. While the "onshore" sections of this fault which extends below the Lake Le Bourget is precisely mapped, its eastern termination remain to be determined. Previous "offshore" lake investigations (seismic and side scan sonar) indicated the possible impact of the recent tectonic activity on the basin fill (Chapron et al., 1996; Beck, 2009).

METHODS

A seismic survey was designed specifically to image the suspected subaqueous ("offshore") prolongation of the Culoz Fault, previously mapped onshore and analyzed by different authors. The navigation plan was carried out based on land data, electrical resistivity tomography (ERT performed previously) as well as published works on Lake Bourget (Chapron et al., 1996; Van Rensbergen et al., 1999). Seismic profiles were performed parallel and perpendicular to the faults. In addition, seismological stations were installed around Lake Le Bourget for six months.

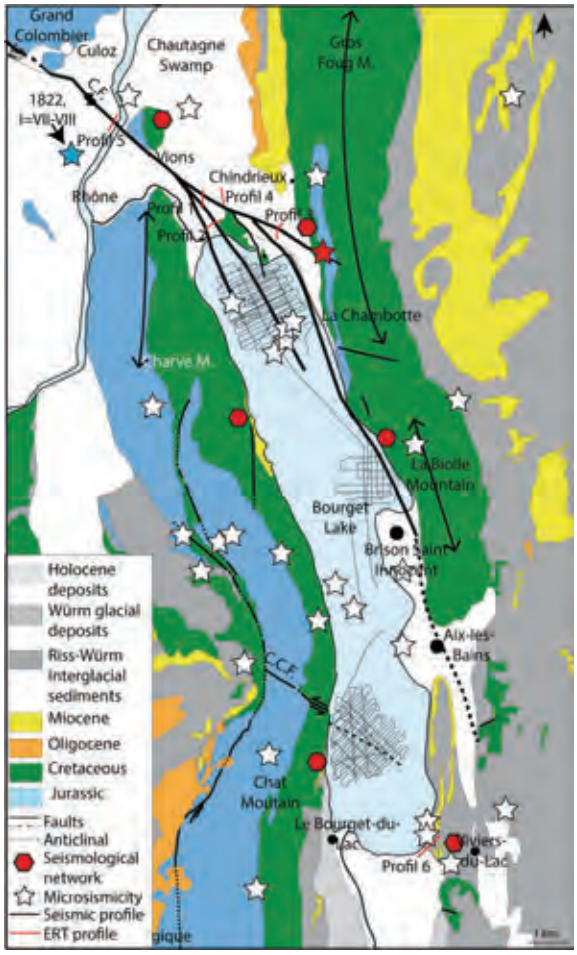

Figure 2: Geological map of the Lake Le Bourget (black rectangle on Figure 1).

RESULTS

High resolution seismic reflection
The reflection seismic survey conducted in 2013 on Lake Bourget (Figure 2) allowed the imaging of the Culoz fault within lacustrine sediments (Figure 3), highlighting different fault strands. The on-land part of the Culoz Fault has a N140° direction. One segment ends in Lake Le Bourget with a N155° trending, which corresponds to the direction of the faults affecting the pre-Quaternary substratum and Late glacial sediments (direction between N150° and N160°). Surprisingly, coseismic deformations affecting Late Glacial to Holocene sediments show different directions between N100° and

N140. De La Taille et al. (in revision) propose that the deformation of the Quaternary infill is the response of an unconsolidated medium to a coseismic displacement along a well localized active strike-slip fault in the substratum. As an analogue, the Cloos model (1932) considers the deformation of a wet clay layer in response to lateral displacement between two rigid plates. Small circular depressions have been evidenced by side-scan sonar and multibeam data (Chapron et al., 1996). These depressions are interpreted as the trademarks of fluids expulsions tentatively related to (1) large gravity sliding processes (Chapron et al., 2004); (2) The Culoz fault motion and/or (3) liquefaction induced by earthquakes.

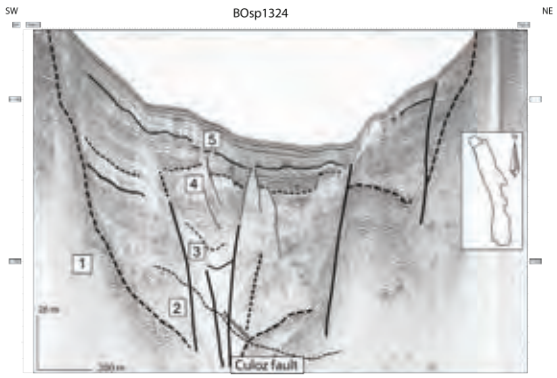

Figure 3: High resolution seismic stratigraphy of northern Lake Le Bourget. 1: Pre-Quaternary bedrock (limestone, sandstone, etc.); 2: Early stage, still in contact with glaciers, small sub-glacial glacier front, in situ reworked tills;3: absent on this profile; 4: Progressive warming and appearance of thermal summertime stratification; partly prograding sedimentation (here Rhodanian feeding) and gradual onset of constituents related to biological activity; 5: Holocene to Present situation - typical "drape" configuration indicates a mainly bio-induced sedimentation.

In the deepest central part of the lake, the top of unit 5 is dominated by an up to 30 ms twt thick chaotic and transparent lense that Chapron et al. (1996) named "the Hautecombe Disturbed Unit" (HDU, 11.500 years). Located at the distal end of the Rhône river fan and covering about 8 km^2, the HDU may resulted from a large seismic event. During the period of Rhodanian sedimentation (terrigenous flux, unit 4), there was stronger potential instability which explains the many mass-transport deposits in the lake. Some pre-Holocene MTD (Mass transport deposit) may be synchronous with the HDU (Hautecombe disturbed unit).

Electrical resistivity tomography (ERT)

Electrical resistivity tomography profiles acquired in the Chautagne swamp (North Lake Bourget, Figure 2) helped us to precisely locate the Culoz fault. This method proved to be efficient in this swampy area, revealing significant resistivity contrasts in the quaternary basin infill (Figure 4), by connecting these discrepancies, we obtain a precise fault trace.

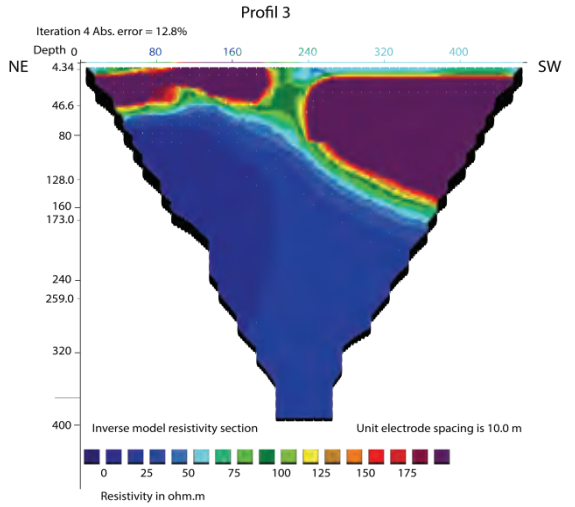

Figure 4: ERT profile. Profile 3 on Figure 2.

Geological investigations

Field investigations conducted in an open quarry in Brison Saint Innocent (East Lake, Figure 2) allowed us to observe quaternary deformations along the Culoz fault (Figure 5). Dating of samples taken at this locality are in process. Meanwhile, we propose an interglacial age of the affected deposits, according to regional stratigraphic correlation.

Figure 5: Interpreted picture of Brison Saint Innocent outcrop.

Seismological data

The current activity of the Culoz fault is also illustrated by seismological data from SISMALP and a temporary seismological network deployed in 2013 (Table 1).

Most of the detected earthquakes show more than 3 km-deep epicenters (between 4 and 14 km – Table 1). As the décollement level is located at 3 km below the surface, one can speculate that the Culoz fault system is deeply rooted in the basement.

Date	Magnitude ML	Depth (km)
5/ 1/ 1993	1.45	8.1
22/ 10/ 1994	1.58	6.94
27/ 10/ 1994	1.61	8.73
6/ 3/ 1995	1.38	-2.09
14/ 3/ 1995	1.35	6.83
3/ 10/ 1996	0.95	10.09
25/ 5/ 1997	0.85	5.8
9/ 7/ 1997	0.11	11.99
3/ 3/ 1998	2.31	8.7
9/ 4/ 2000	0.69	9.98
16/ 10/ 2004	1.39	14.19
19/ 9/ 2005	1.27	13.15
24/ 3/ 2006	1.19	16.82
2/ 3/ 2014	3.1	4.11
8/ 9/ 2014	1.8	6 to 10

Table 1: Seismic catalog from SISMALP.

CONCLUSION

A multidisciplinary approach has been followed in order to locate the Eastern part of the Culoz fault and constraint its length (minimum 25 km to a maximum estimated around 40 km). Also, this study confirms the continuity of the fault between the sedimentary cover and the basement.

Taking into account (1) the length of this fault (25 to 40 km) and (2) the depth of recorded earthquakes between 4 and 14 km, the potentially ruptured surface could range from 100 to 560km^2. The latter implies a Moment Magnitude range from M=6.0 to M=6.8 based on worldwide empirical scaling relationships (Wells and Coppersmith 1994).

Acknowledgements: The authors thank the Assemblée des Pays de Savoie and the Institut de Radioprotection et de Sûreté Nucléaire. This work was also supported by LABEX OSUG@2020 and ISTerre. The authors thank Marc De Batist for giving us the possibility to use the Renard Centre of Marine Geology (Ghent University) seismic facilities to image lake sediments. Kingdom Suite seismic interpretation software was provided by IHS, Inc. through their University Grant Program. The authors thank Thomas Lebourg for giving us the possibility to use the Geoazur (Nice University) electrical devices to image Culoz fault.

References

Baize, S., E.M. Cushing, F. Lemeille, T. Granier, B. Grellet, D. Carbon, P. Combes and C. Hibsch, (2002). Inventaire des indices de rupture affectant le Quaternaire en relation avec les grandes structures connues, en France métropolitaine et dans les régions limitrophes. *Mém. h.s. Soc. géol.* Fr., 175, 142 p.

Beck, C., (2009). Late Quaternary lacustrine paleo-seismic archives. In north-western Alps: Examples of earthquake-origin assessment of sedimentary disturbances. *Earth-Sciences Reviews*. 99,327-344.

Becker, A. and D. Werner, (1995). Neotectonic state of stress in the Jura Mountains. *Geodinamica Acta*. 8(2), 99-111.

Becker, A., (2000). The Jura Mountains —an active foreland fold-and-thrust belt? *Tectonophysics*. 321, 381-406.

Burkhard, M. and A. Sommaruga, (1998). Evolution of the western Swiss molasse basin: structural relations with the Alps and the Jura belt. In: Cenozoic foreland basins of western Europe. *Geol. Soc. Spec. Publ*. 143, 279-298.

Chapron, E., P. Van Rensbergen, C. Beck, M. De Batist, and A. Paillet, (1996). Lacustrine sedimentary records of brutal events in Lake Le Bourget (Northwestern Alps-Southern Jura). *Quaternaire*. 1, (2-3), 155-168.

Chapron, E., P. Van Rensbergen, M. De Batist, C. Beck, and J.P. Henriet, (2004). Fluid-escape features as a precursor of a large sublacustrine sediment slide in Lake Le Bourget, NW Alps, France. *Terra Nova*. 16, 305–311.

Cloos, E., (1932). "Feather joints" as indicators of movements in faults, thrusts, joints and magmatic contacts. *Proc. Nat. Acad. Sci*., USA. 18, 387-395.

De La Taille, C., F. Jouanne, C. Crouzet, C. Beck, H. Jomard, K. de Rycker, M. Van Daele, Impact of active faulting on the Post LGM infill of Lake Le Bourget (western Alps, France). *Tectonophysics*. (in revision).

Delacou, B., C. Sue, J.-D. Champagnac, and M. Burkhard, (2004). Present-day geodynamics in the bend of the western and central Alps as constrained by earthquake analysis. *Geophys. J. Int.* 158,753-774.

Delacou, B., C. Sue, J.-M. Nocquet, J.-D. Champagnac, C. Allanic, M. Burkhard, (2008). Quantification of strain rate in the Western Alps using geodesy: comparisons with seismotectonics. *Swiss Journal of Geosciences*. 101, (2), 377-385.

Grellet, B., Ph. Combes, Th. Granier, H. Philip, (1993). Sismotectonique de la France métropolitaine, *Mém. H.S. Soc. Géol. Fr.* 164, (1), 76.

Guellec, S., M. Tardy, F. Roure, and J.-L. Mugnier, (1989). New interpretation of the Bornes massif (western french Alps) - constraint with deep geophysical and geological data. *Comptes Rendus de l'Académie des Sciences. Série 2. Mécanique, physique, chimie, astronomie*. 309, (9),913-920.

Laubscher, H., (1961). Die fernschubhypothese der jurafaltung. *Eclogae Geologicae Helvetiae*. 54, 222-282.

Philippe, Y., (1995). *Rampes latérales et zone de transfert dans les chaines plissées: géométrie, conditions de formation et pièges structuraux associés*. PhD thesis, Université de Savoie, France.

Sommaruga, A., (1997). Geology of the central Jura and the molasse basin: New insight into an evaporite-based foreland fold and thrust belt. *Mémoire de la société Neuchâteloise des sciences naturelles*. Tome XII.

Thouvenot, F., J. Frechet, F. Guyoton, R. Guiguet, L. Jenatton, (1990). SISMALP: an automatic phone-interrogated seismic network for the western Alps. *Cahier du centre Européen de Géodynamique et de Séismologie*. 1, 1-10.

Van Rensbergen, P., M. De Batist, C. Beck, and E. Chapron, (1999). High-resolution seismic stratigraphy of glacial to interglacial fill of a deep glacigenic lake: Lake le Bourget, northwestern alps, France. *Sedimentary Geology*. 128, 99-129.

Vogt, J. and P. Godefroy, (1979). Le tremblement de terre du 19 février 1822 (Bugey-Savoie). Eléments de discussion. *Technical report, BRGM*.

Wells, D., and K. Coppersmith, (1994). New Empirical Relationships among Magnitude, Rupture Length, Rupture Width, Rupture Area, and Surface Displacement. *Bulletin of the Seismological Society of America*. 84, (4), 974-1002.

Willett, S.D. and F. Schlunegger, (2010). The last phase of deposition in the Swiss molasse basin: from foredeep to negative-alpha basin. *Basin Research*. 22, 623-639.

INQUA Focus Group on Paleoseismology and Active Tectonics

Fault Specific Seismic Hazard Maps for the Attica Region

Deligiannakis, G. (1), Papanikolaou, I.D. (1,2), Roberts, G. (2)

(1) Mineralogy-Geology Laboratory, Department of Natural Resources Development and Agricultural Engineering, Agricultural University of Athens, Iera Odos 75, 118-55, Athens, Greece. Email: gdeligian@aua.gr
(2) Department of Earth Sciences Birkbeck College and University College London, WC 1E 6BT, London UK

Abstract: *Nearly half of the Greek population resides in Athens and its surrounding areas, in Attica Region, which has been shaken by damaging earthquakes for several times in the past. As the historical seismic record is incomplete even for strong events, high spatial resolution seismic hazard maps that incorporate several seismic cycles and geologic conditions are of decisive importance for risk assessment and land-use planning of the Attica Region. We modelled 22 active faults, creating 4 high spatial resolution seismic hazard maps, one for each of the intensities VII – X (MM). These maps offer a locality specific shaking recurrence record, which represents the long-term shaking record in a more complete way, since they incorporate several seismic cycles of the active faults that could affect Attica. Each one of these high resolution seismic hazard maps displays both the spatial distribution and the recurrence, over 15kyrs, of the relevant intensity.*

Key words: *Athens, Attica region, active faults, slip rates.*

INTRODUCTION

Greece is prone to various geohazards, such as floods, landslides and earthquakes, due to the geotectonic setting in plate tectonic boundaries. Seismic is the predominant risk, in terms of damages and casualties in the Greek territory. The historical record of earthquakes in Greece has been published from various researchers, providing useful data in seismic hazard assessment of Greece (e.g. Galanopoulos, 1961, Papazachos and Papazachou, 2003). However, the completeness of the historical record in Greece, despite being one of the longest worldwide, reaches only 500 years for M ≥ 7.3 and less than 200 years for M ≥ 6.5 (Papazachos and Papazachou, 2003). Considering that active faults in the area have recurrence intervals of a few 100s to several 1000s of years, it is clear that many active faults have not been activated during the completeness period covered by the historical records.

New Seismic Hazard Assessment methodologies tend to follow fault specific approaches where seismic sources are geologically constrained active faults, in order to address problems related to the incompleteness of the historical records, obtain higher spatial resolution and calculate realistic source locality distances, since seismic sources are very accurately located (e.g. Ganas and Papoulia, 2000; Roberts et al., 2004; WGCEP 2007; Pace et al., 2010; Stein et al., 2012; Papanikolaou et al., 2013). For land-use planning and critical facilities or insurance risk evaluation purposes, a higher spatial resolution is also desirable (Grutzner et al., 2014). Fault specific approaches provide quantitative assessments as they measure fault slip rates from geological data, providing a more reliable estimate of seismic hazard (e.g. Yeats and Prentice, 1996; Michetti et al., 2005).

The extended urban region of Athens and its surroundings in the region of Attica are inhabited by nearly half of the Greek population. High spatial resolution seismic hazard maps for the region of Attica are of decisive importance, as they indicate areas at high risk and also act as input for earthquake catastrophe models for the insurance industry.

METHODOLOGY

We used a fault specific seismic hazard assessment approach for the region of Attica. The method of seismic hazard mapping from geological fault throw-rate data combined four major factors (Papanikolaou, 2003; Roberts, et al. 2004):

1. Compilation of a fault database (seismic sources identification, fault lengths, kinematics and slip rates determination). Simulation of earthquake events during the last 15,000 years, thus incorporating several seismic cycles.
2. Empirical data which combine fault rupture lengths, earthquake magnitudes and coseismic slip relationships.
3. The radiuses of VI, VII, VIII and IX isoseismals on the Modified Mercalli (MM) intensity scale.
4. Attenuation - amplification functions for seismic shaking on bedrock compared to basin filling sediments.

We modelled 22 active faults (Fig. 1 and Fig. 2) that could affect the region of Attica, including Athens, using detailed data derived from published papers, neotectonic maps and fieldwork observations. The modelled intensity coverages were attenuated / amplified according to the bedrock geology.

In the case of the Attica Region, the Quaternary deposits increase the intensity by a single value. The flysch/foredeep deposits will cause no alterations, while the bedrock (mostly Mesozoic or Tertiary limestone) will decrease the intensity by one value. The input data for the surface geology came from the EPPO detailed

geotechnical map for the Athens Metropolitan Area and 1:50.000 geological maps of IGME for the rest of the Attica Region (Fig. 3).

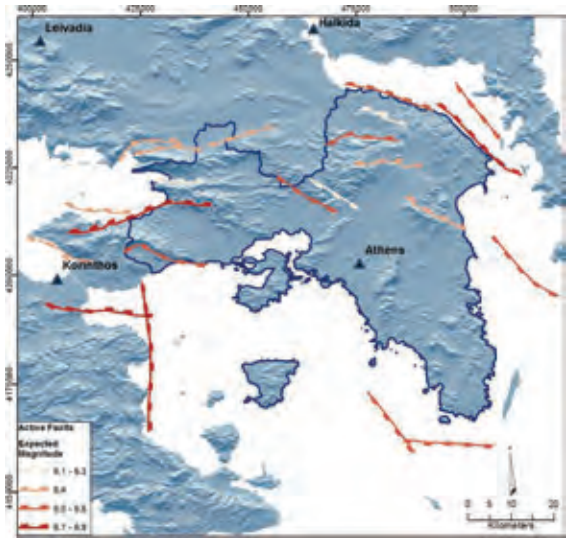

Figure 1: Map of active faults that can sustain damage within the region of Attica. Different colours represent the maximum expected magnitude that these faults can generate.

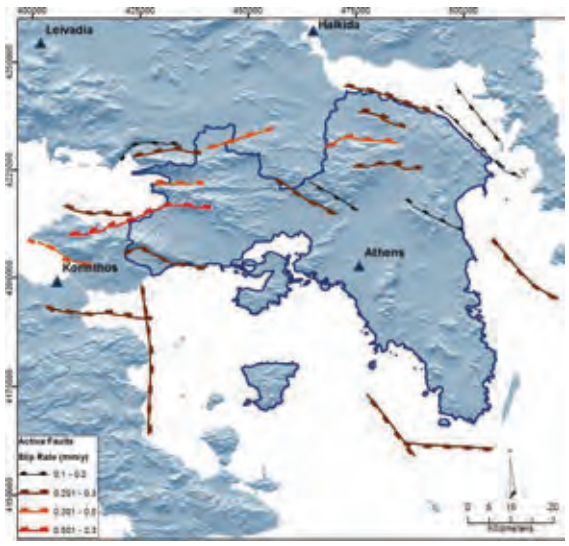

Figure 2: Map of active faults and their slip-rates. Different colours represent different slip-rate groups.

Assumptions made in key methodology aspects are connected to: a) fault lengths, b) fault slip rates, c) surface geology and d) intensity attenuation relationships. Depending on the active faults characteristics, we expect a maximum error of ± 15% on fault lengths and ± 20% variation on slip rate values. Following the standard error in geological maps, we expect a maximum deviation of ±400m on geological boundaries, which is considerably reduced on bedrock formations. Regarding the intensity values, Papanikolaou (2011) showed that they can outreach the aforementioned 20% error of the fault slip rates. As the uncertainty increases for lower intensities and further depends on the background seismicity, intensities below VII are not displayed.

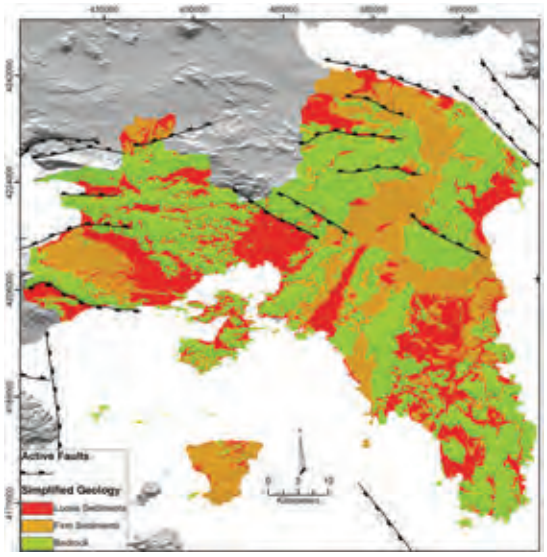

Figure 3: Simplified geological map of the area of Attica, based on 1:50.000 maps of IGME and the EPPO detailed geotechnical map for the Athens Metropolitan Area.

RESULTS

Since fault length is used to determine the expected earthquake magnitude (Fig. 1), detailed GIS mapping was carried out for each one of the active faults that could affect Attica region in case of earthquake rupture. Fault lengths vary from 9 up to 35km and modelled magnitudes from 6.1 to 6.65±0.15.

The majority of the active faults that affect the region of Attica do not exceed the relatively low slip-rate values of 0.3mm/yr. However, the faults activated during the 1981 earthquakes events (South Alkyonides Fault segments) reach or exceed slip-rate values of 2mm/yr, the mean slip-rate value of the faults that affect Attica is ~0.38mm/y.

Fault slip-rates are firstly converted into earthquake frequencies, assuming that each fault ruptures in "floating" earthquakes, which are distributed around a mean magnitude of fixed size. Then, this information is turned into a hazard map after using: i) empirical relationships between coseismic slip values, rupture lengths and earthquake magnitudes, ii) empirical relationships between earthquake magnitudes and intensity distributions, and iii) attenuation/amplification functions for seismic shaking on bedrock compared to flysch and basin filling sediments (see Papanikolaou, 2003; Roberts et al., 2004).

We created 4 high spatial resolution seismic hazard maps for the region of Attica, one for each of the intensities VII – X (MM). These maps offer a locality specific shaking recurrence record, which represents the

long-term shaking record in a more complete way, since they incorporate several seismic cycles of the active faults that could affect Attica. Each one of these high resolution seismic hazard maps displays both the spatial distribution and the recurrence of the relevant intensity over 15 kyrs, or the corresponding return periods (see Fig. 4 – Fig. 7).

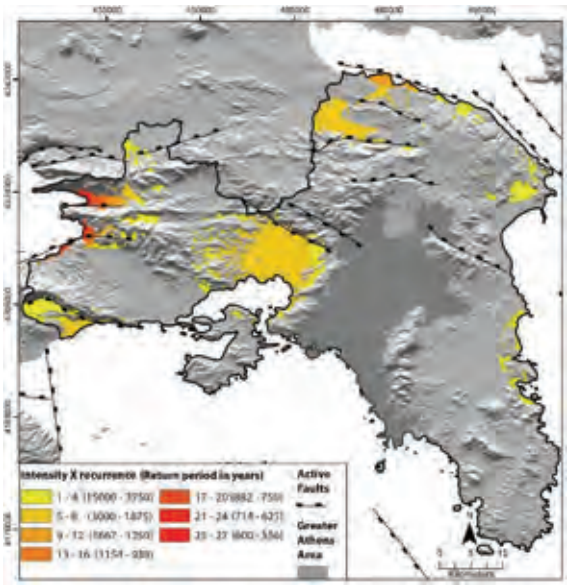

Figure 4: Seismic hazard map of Attica, showing the estimated site specific recurrence for intensities X (MM) over the past 15kyrs.

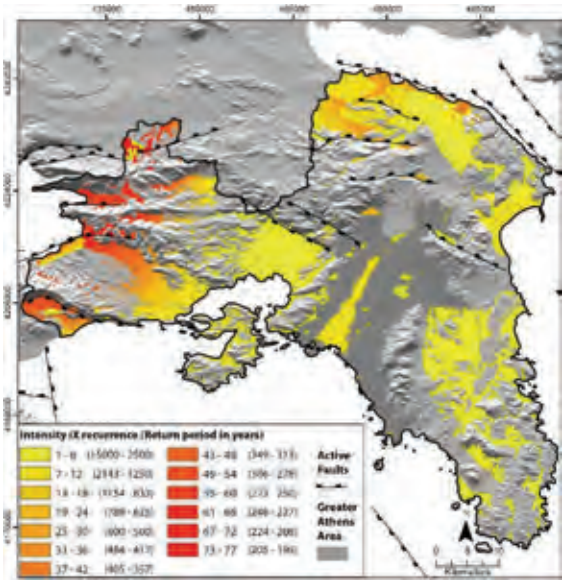

Figure 5: Seismic hazard map of Attica, showing the estimated site specific recurrence for intensities IX (MM) over the past 15kyrs.

Probabilities can be extracted based on these average recurrence intervals, using the stationary Poisson model (Papanikolaou et al., 2013). This model is usually applied when no information other than the mean rate of earthquake production is known. Overall, the best feature of the Poisson probability is that a forecast can be made without having the information about the time of the last seismic event, so according to this model odds do not change with time (Stein, 2003).

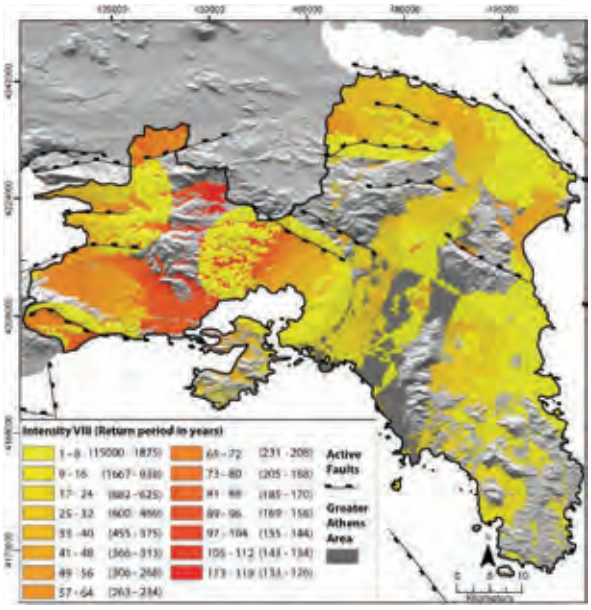

Figure 6: Seismic hazard map of Attica, showing the estimated site specific recurrence for intensities VIII (MM) over the past 15kyrs.

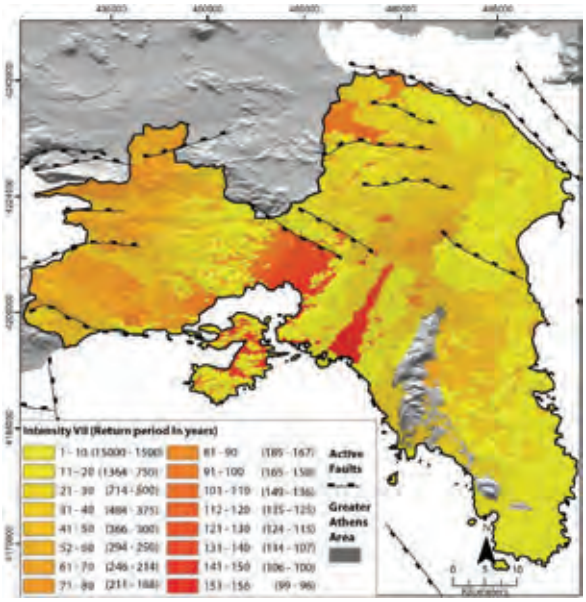

Figure 7: Seismic hazard map of Attica, showing the estimated site specific recurrence for intensities VII (MM) over the past 15kyrs.

The high spatial resolution of the maps allows an assignment of the Poisson "λ" value for every map pixel (45x45m) (Fig. 8).

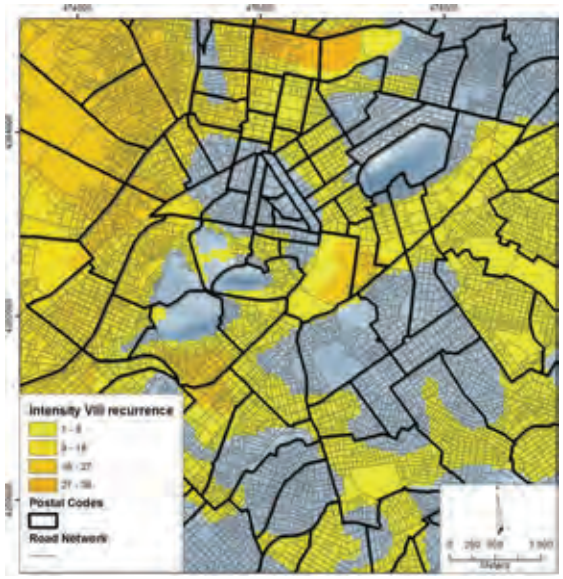

Figure 8: Fault Specific Seismic hazard map of the centre of Athens. Colour variations show how many times these localities have received enough energy to shake at intensity VIII over the past 15kyrs. This map offers a high spatial resolution of the intensities' distribution and recurrence, therefore it allows a detailed calculation of Poisson "λ" values.

DISCUSSION

Fault specific seismic hazard maps incorporate several seismic cycles of the active faults that can affect any area of interest. The detailed mapping of the active faults is of decisive importance, for modelling earthquake events of M=6R or above. However, intensities resulting to building damages can be produced during earthquake events of smaller magnitude, caused by blind faults with no surface rupture. For that reason, a combination of fault specific with background seismicity modelling should be developed.

The fault specific seismic hazard maps of the greater Athens area and its surroundings can be used as an input to loss reserves and capital requirements calculation for the insurance industry. The high spatial analysis of the modelled earthquake events allows a detailed simulation of the damages of each event, which can be transformed to economical loss for each construction. Moreover, the produced seismic hazard maps can be used as a damage ratio factor for each Postal Code.

The implementation of the Environmental Seismic Intensity scale (ESI 2007) can be a future prospect, in order to overcome the subjectivity of the traditional structural damage – based intensity scales (MMI, EMS-98, etc.).

CONCLUSIONS

We created 4 high spatial resolution fault specific seismic hazard maps for the greater Athens area and its surroundings. Each map shows the estimated site specific recurrence for intensities VII – X of the Modified Mercalli Intensity Scale. They are based on the detailed analysis of 22 active faults that can affect the study area and incorporate several seismic cycles, along with the surface geology conditions. Time independent probabilities for each intensity can be extracted for every pixel of the maps using the Poisson model.

Acknowledgements: The National and Kapodistrian University of Athens, Antonios Papadakis Legacy Postgraduate Scholar and the Bank of Greece are thanked for the support.

References

Galanopoulos, A., (1961). *A Catalogue of Shocks with Io ≥VII for the Years Prior to 1800*. National Observatory of Athens, Athens.

Ganas, A. and I. Papoulia, (2000). High-resolution, Digital Mapping of the Seismic Hazard within the Gulf of Evia Rift, Central Greece using normal fault segments as line sources. *Natural Hazards*. 22, pp. 203–223.

Grützner, Ch., S. Barba, I. Papanikolaou, R. Perez-Lopez, (2014). Earthquake Geology: science, society and critical facilities. *Annals of Geophysics*. 56 (6), S0683, doi:10.4401/ag-6503.

Michetti, A.M., F.A. Audemard, and S. Marco, (2005). Future trends in paleoseismology: Integrated study of the seismic landscape as a vital tool in seismic hazard analyses. *Tectonophysics*. 408, pp. 3-21.

Pace, B., L. Peruzza, and F. Visini, (2010). LASSCI2009.2: layered earthquake rupture forecast model for central Italy, submitted to the CSEP project. *Annals of Geophysics*. 3, pp.85-97.

Papanikolaou, I.D., (2003). *Generation of high resolution seismic hazard maps through integration of earthquake geology, fault mechanics theory and GIS techniques in extensional tectonic settings*. Unpublished Ph.D thesis, University of London, 437pp.

Papanikolaou, I.D., (2011). Uncertainty in intensity assignment and attenuation relationships: How seismic hazard maps can benefit from the implementation of the Environmental Seismic Intensity scale (ESI 2007). *Quaternary International*. 242, pp. 42-51.

Papanikolaou, I.D., G. Roberts, G. Deligiannakis, A. Sakellariou, and E. Vassilakis, (2013). The Sparta Fault, Southern Greece: From segmentation and tectonic geomorphology to seismic hazard mapping and time dependent probabilities, *Tectonophysics*. 597-598, pp. 85-105.

Papazachos B.C. and C. Papazachou, (2003). *The earthquakes of Greece*. 3rd ed. Thessaloniki: Ziti Publications.

Roberts, G.P., P. Cowie, I. Papanikolaou, and A.M. Michetti, (2004). Fault scaling relationships, deformation rates and seismic hazards: An example from the Lazio-Abruzzo Apennines, central Italy. *Journal of Structural Geology*. 26, pp. 377-398.

Stein, R.S., (2003). Earthquake conversations. *Scientific American*. 60–67.

Stein, S., R.J. Geller, M. Liu, (2012). Why earthquake hazard maps often fail and what to do about it. *Tectonophysics*. 562-563, 1-25.

Working Group on California Earthquake Probabilities (WGCEP), (2007). *Uniform California Earthquake Rupture Forecast 2 Final Report*.

Yeats, R.S., and C.S. Prentice, (1996). Introduction to special section: Paleoseismology. *Journal of Geophysical Research*. 101, pp. 5847-5853.

Graviquakes

Doglioni, C. (1,2), Carminati, E. (1,2), Petricca, P. (1,3), Riguzzi, F. (4)

(1) Dipartimento di Scienze della Terra, Università Sapienza, Roma. Email: carlo.doglioni@uniroma1.it
(2) CNR-IGAG, Roma
(3) GFZ Helmholtz-Zentrum Potsdam
(4) Istituto Nazionale Geofisica Vulcanologia, Via Vigna Murata 605, 00143 Roma, Italy

Abstract: *When the hangingwall of normal faults falls, the primary energy is gravity. The dip and friction of faults control the amount of energy accumulation and type of dissipation; the steeper the normal fault, the higher the vertical displacement and the static friction and the larger the seismic energy released. Statistically, the maximum length of faults along strike associated with extensional earthquakes is about three times the hypocentre depth. Our calculations show a deficit of Mw>1.5 between the available gravitational potential energy and the radiated seismic energy by a normal fault. The difference implies a dissipation of hundreds times larger energy in shear heating and cataclastic deformation. Foreshocks in the inferred conjugate dilated band, InSAR data and fluids discharge anomalies may become precursors of a seismic event. Therefore, unlike earthquakes generated in contractional settings controlled by elastic storage of energy, extensional settings could rather be distinguished as graviquakes.*

Key words: *Graviquakes, normal fault, fault dip, friction, precursors.*

INTRODUCTION AND GEOLOGICAL MODEL

Earthquakes are energy dissipation due to pressure gradients wherever they occur at plate boundaries. Normal faulting is widespread in several geodynamic environments, such as continental rifts, backarc basins, mid-ocean ridges, orogens and strike-slip settings. The usual assumption is that seismicity represents the dissipation of elastic energy accumulated during the interseismic period (Scholz, 1990). This is likely true for contractional tectonic settings, but in tensional environments, the influence of the gravitational force may rather be dominant (Doglioni et al., 2011; Dempsey et al., 2012). In this paper we discuss some fundamental parameters that control the energy dissipation in shallow crustal extensional settings, such as the involved volume, the dip of the normal fault and the static friction (Marone, 1998). Natural examples will be used from the Apennines belt and other geodynamic settings characterized by widespread extensional fault activity and related earthquakes. In addition we address the energy partitioning of earthquakes (Kanamori and Rivera, 2006) comparing the potential energy stored by the volume involved during the coseismic collapse (Doglioni et al., 2014) with that inferred from earthquake magnitude. The results show that potential energy is far greater, indicating that, in the energy budget, most of the potential energy is dissipated by other geological phenomena (heat flow and fracturing above all), consistent with previous works (e.g., Pittarello et al., 2008).

In a simplified two-layers crust, within the brittle upper crust, the faults are generally locked or slowly creeping, and the deformation is mostly assumed to be stick-slip (Fig. 1). During the secular interseismic period of lithospheric stretching, the ductile lower crust is permanently shearing and thinning by viscous flow and

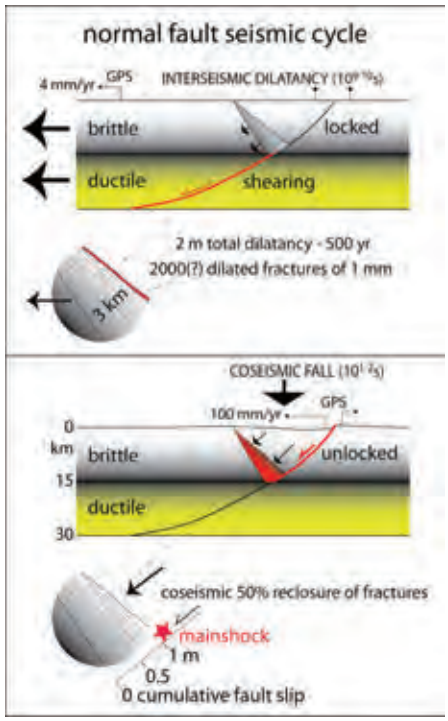

Figure 1: During the interseismic period, while the lower crust is shearing in a steady state, the brittle upper crust is locked and a dilating band is inferred. The open fractures allow the fall of the hangingwall at the coseismic stage, when the fault plane and the dilated band cannot sustain anymore the upper suspended block. Note that the mainshock is located along the fault at the upper tip of the dilated band, consistently with the seismological observations showing that the mainshock is located slightly above the rupture zone (e.g., like in the L'Aquila, 6 April 6.3 Mw earthquake).

deformation is inferred as a continuous process. The brittle-ductile transition (BDT) is in average located in the middle Earth's crust. When a brittle fault merges into a ductile shear zone cross-cutting the whole crust, the BDT is characterized by a pressure gradient because the brittle upper crust is mostly locked, whereas the viscous-plastic lower crust is sheared steadily.

The collapse of a normal fault hangingwall dissipates mostly gravitational potential energy (Doglioni et al., 2011; 2014; Dempsey et al., 2012), being the elastic component a minor effect of the fall. Since the steady deformation of the ductile lower crust has to be transferred upward, Doglioni et al. (2011) proposed that the stretching could be accommodated in the brittle realm by dilation in a band conjugate to the episodically active normal fault (Fig. 1). This dilated band is inferred due to the strain partitioning and the pressure gradient between the ductile lower crust and the brittle upper crust. The occurrence of the dilated band from the geological model is also supported by the fact that the hangingwall of a normal fault could not collapse without a corresponding vacuity at the base of the activated fault segment (Fig. 1).

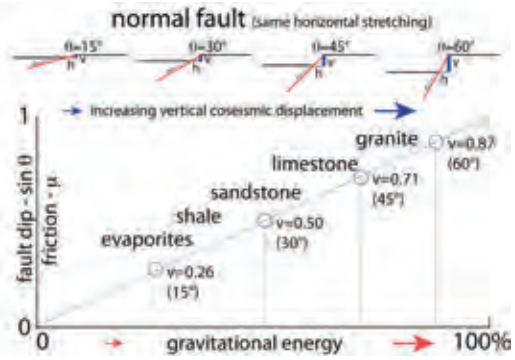

Figure 2: For a given amount of crustal extension, which is represented by the horizontal component of the normal fault displacement (h), the dip of the normal fault (ϑ) controls the vertical displacement (v). The shallower the dip, the smaller the vertical displacement. Therefore, steeper faults release larger amounts of gravitational potential energy at the earthquake. This is consistent with the absence of energetic earthquakes associated with low-angle normal faults. It is observed that low-angle normal faults develop in rocks having low friction and vice-versa steep normal faults form in high friction rocks.

The opening of fractures and the fluids permeating them, gradually weaken the dilated band that should gradually loose strength during the interseismic stage. Therefore, the suspended hangingwall is lying on the fault on one side, and is bounded on the other side by the dilated band. When the fault and the conjugate band will not be any more sufficiently strong to support the hangingwall, the sudden collapse will generate the earthquake (Fig. 1). The mass of the hangingwall wedge will be given by the volume times its density and the hangingwall will collapse when the weight of this volume will overtake the strength of the fault plane and of the dilated band. At the coseismic stage the band will partly recover, by fracture closure, the dilation occurred during the interseismic period (Fig. 1). This is proposed to be accompanied by expulsion of fluids that permeated the fractured rocks (Di Luccio et al., 2010; Doglioni et al., 2014).

The Mw 6.3 2009 April 6th L'Aquila earthquake (Chiarabba et al., 2009) can be taken as a case history for this model. During 4-5 months before the quake, a series of foreshocks occurred in the volume of the hangingwall and along the inferred dilated band (Doglioni et al., 2011). This is consistent with the initial fall of the hangingwall in the same period as detected by InSAR data (Luo et al., 2014).

Fault rupture length increases with earthquake magnitude and depends also on the tectonic setting (Leonard, 2010). Based on the deformed volume constrained by seismic sequences in Italy, regional studies of surface ruptures and InSAR and GPS data, normal fault-related seismicity is usually associated with rupture fault length about three times the hypocentre depth (Fig. 2).

NORMAL FAULT DIP AND FRICTION

Along a normal fault, the hangingwall moves downward (falls) at the coseismic stage. As a consequence, gravity contributes to the generation of the motion, thus the larger the vertical movement, the larger will be the gravitational energy released. Following the Mohr-Coulomb criteria, a normal fault ideally nucleates at about 60° (Sibson, 1977). However, normal faults develop at variable angles as a function of the static friction m (Fig. 2). The higher the friction of rocks, the steeper is the fault; vice versa, the lower the friction, the shallower the fault dip. With a constant extension, the shallower the dip, the lower is the vertical component of the fault slip. Therefore low-angle normal faults deliver lower energy than steeper normal faults (Fig. 2). This inference is consistent with the small number and the low magnitude of earthquakes nucleated along low-angle normal faults (Jackson and White, 1989). Low-angle normal faults (LANF) may creep in case of low friction fault rocks. A decrease in friction (e.g., moving from granites to evaporites) induces a decrease of the vertical component of displacement and a lowering of the gravitational potential energy. Normal friction (m=0.6-0.8) rocks (e.g., platform carbonates) need higher energy to break and slip than low friction (m=0.2) rocks. Since low friction rocks may easily slip with lower energy, in active tectonic settings they tend to be associated with higher strain rates (Fig. 3). Therefore, in the brittle domain, normal faults cross-cutting low friction rocks creep faster than normal faults in high friction rocks, which may be activated only with higher amount of stored energy, thus providing larger magnitude earthquakes (Fig. 3). The variability of strain rate in active tectonic zones may be related either to the relaxation after past earthquakes or to lateral variation of the average friction of a given crustal volume. Moving along both strike and dip of the Apennines belt, variations in

velocities and consequently in strain rate are observed (Riguzzi et al., 2012). These may be related to rock friction gradients generated by the alternance of abundant low-friction shaly or evaporitic layers, enhancing creep, and of high-friction carbonatic rocks. Aseismic creep is frequent along active faults and may be related to low friction lithologies in the upper brittle crust. In addition to friction, other factors control seismicity. It is well known that fluids may further deeply control rock mechanics.

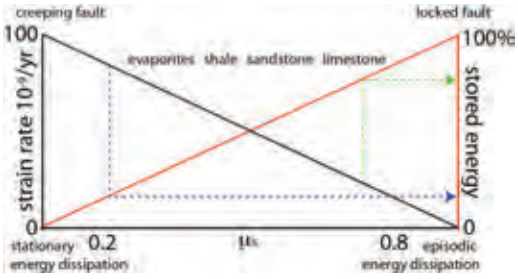

Figure 3: The strain rate decreases with friction. In fact the most energetic earthquakes occur in active tectonic zones where the strain rate is relatively lower. This implies that low friction allows creeping and more continuous dissipation of energy, whereas high friction determines locked faults and higher storage of energy during the interseismic period.

ENERGY DISSIPATION

As we aim to define the maximum seismic potential given by a volume of rock, the starting point is to define the three-dimensional geometry of the system. Each type of tectonic setting has its own involved volumes, i.e., determining the maximum expected magnitude. The maximum volumes are computed assuming L=a*z where L is the fault length, z the hypocentre depth and a is a parameter that varies as a function of the tectonic setting. A shape ratio of L=3z (with L and z lateral extent and height of the brittle volume respectively) is consistent with literature data in extensional tectonics. The larger the involved volume, the higher the expected magnitude.

Therefore, defining the brittle volume depends on fault dip, brittle-ductile transition depth, rupture length and tectonic setting. In order to quantify the energy along a normal fault, we first compute the volume in the hangingwall of the normal fault (e.g., assuming the BDT as the hypocenter depth, the fault dip, the conjugate band dip). In order to compute the mass, the volume is then multiplied by the density (e.g., 2.5-2.7 g/cm3). Then from the mass we can quantify the gravitational potential energy in joule assuming a given vertical component of the fault throw (kg*m2/s2), which can be transformed into the available energy at the coseismic collapse. The resulting magnitude is far larger than the observed one and the computation of the real magnitude from the volume potential energy can only occur with a correction radiation coefficient of 0.02.

We can calculate the energy released for example by two prismatic volumes above hypocentres respectively at 7 and 15 km depth. Italian examples can be the Northern Apennines 1997-1998 seismic sequence with the Mw 5.7-6 1997 September 26th two mainshocks at about 7 km depth (Stramondo et al., 1999), and the 15 km deep Irpinia Mw 6.9-7, 1980 November 23th (Bernard and Zollo, 1993). If the faults dip 45° and ruptures cross-cut the entire overlying rocks, assuming a conjugate band at about 70°, emerging at the surface at a distance of 10 and 20 km from the seismogenic faults respectively, the involved volumes amount to ca. 735 and 6750 km3. With 0.5 m displacement that corresponds to 0.35 m of vertical motion, with an average density of 2600 kg/m3, the gravitational energy delivered is around 6.6 x 1015J for the shallower earthquake (nucleated at 7 km depth). This amount of energy would correspond to an Mw 7.6 earthquake, far greater than what is observed in nature along faults having such parameters, i.e., Mw 5.8-6.1 (Fig. 6). This means that gravity alone is far more than enough to generate normal faults earthquakes. Assuming a hypocentre at 15 km depth and a coseismic displacement of 1 m (0.7 m of vertical component), the gravitational energy delivered is instead around 1.2 x 1017J. This would mean an event of Mw 8.5, far greater than the observed earthquakes (e.g., Irpinia Mw 6.9-7, 1980; Bernard and Zollo, 1989) that usually are about Mw 6.7-6.9 (Fig. 6). We highlight the following observations: the doubling of the hypocentre depth makes the volume about 9 times bigger; the available gravitational energy is at least 15-20 times larger for the deeper earthquake; in both cases, the observed magnitude is far lower than the dissipated energy. Since the expected magnitude is about 1.5 larger than the real earthquake, this allows us to infer that the difference is dissipated in fracturing and shear heat. It has been demonstrated that gravitational energy variations associated with earthquakes are partly radiated out of the source and in part accommodated by fracturing and frictional dissipation. Fulton et al. (2011) showed that most of the energy dissipated by the earthquake is transformed into heat. Pittarello et al. (2008), studying pseudotachylites concluded that 97–99% of the energy was dissipated as heat during seismic slip.

Low magnitude earthquakes in the dilated conjugated band of a normal fault may be precursors of the instability of the hangingwall (Doglioni et al., 2011), which will eventually fall. Combining seismicity with InSAR data (Lou et al., 2014) and monitoring of fluids anomalies (Doglioni et al., 2014) may become important signals of a developing seismic sequence.

CONCLUSIONS

Crustal normal fault-related earthquakes release a seismic energy that is at least Mw 1.5 lower than the available gravitational potential energy (Fig. 4). Given the observation that the energy of a volume collapsing during an extensional earthquake is far bigger than the radiated seismic energy, we suggest that 1) the gravitational fall of the hangingwall volume of a normal

fault is the cause of extensional earthquakes and that 2) most of the energy is dissipated into shear heating and deformation. The energy released during an earthquake generated by a normal fault increases with the involved collapsing volume, the dip of the fault (Fig. 2) and the static friction of involved rocks (Fig. 3). Moreover, the larger the volume, the bigger is the coseismic displacement. The gravitational potential energy dissipated by the collapse of the hangingwall of a normal fault is about 100 times larger than the observed magnitude (Fig. 4). This model of earthquake is different from the ideal elastic-rebound model and it could rather be defined as a "graviquake". Since its mechanism is different, we may expect different evolution and peculiar precursors from the typical thrust-related earthquakes where the accumulated energy is mostly elastic (elastoquake). Low magnitude earthquakes along the conjugated band and within the volume in the hangingwall of an active normal fault may be the indication that the dilated band, formed during the interseismic period (Fig. 1), is going to loose the strength required to sustain the hangingwall, allowing the activation of the fault, the consequent collapse of the volume and the generation of the graviquake.

The phenomenology associated to the coseismic stage of graviquakes may be summarized into a number of possible precursors such as foreshocks, subsidence and increase of fluids release indicating the initiation of the instability that will eventually culminate into the collapse of the volume in the hangingwall of a normal fault and the closure on the conjugate dilated band formed during the interseismic period.

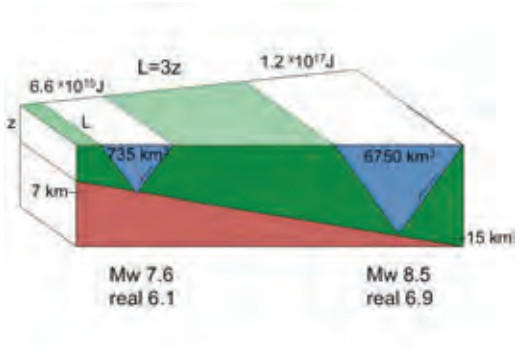

Figure 4: The potential energy in joule of a suspended volume above a normal fault having the brittle-ductile transition at 7 km is about 15 times smaller than the potential energy of an hangingwall above a BDT at 15 km. The volume is computed assuming that the length (L) of the activated fault along strike is three times the hypocenter depth (z). Since the deeper hypocentre determines a longer fault, it is considered a displacement of 0.5 m for the shallow earthquake and 1 m for the deeper one. Note that the energy dissipated during the hangingwall gravitational fall is far greater than the observed magnitude (Mw 7.3 and 8.1).

References

Bernard, P., and A. Zollo, (1989). The Irpinia (Italy) 1980 earthquake: detailed analysis of a complex normal faulting. *Journal of Geophysical Research.* 94, B2, 1631-1647.

Chiarabba, C., and 28 others, (2009). The 2009 L'Aquila (central Italy) MW6.3 earthquake: main shock and aftershocks. *Geophysical Research Letters.* 36, L18308, doi:10.1029/2009GL039627.

Collettini, C. & R.H. Sibson, (2001). Normal faults, normal friction? *Geology*. 29, 927–930.

Dempsey, D., S. Ellis, R. Archer, J. Rowland, (2012). Energetics of normal earthquakes on dip-slip faults. *Geology*. 40, 279-282.

Di Luccio, F., G. Ventura, R. Di Giovambattista, A. Piscini, F.R. Cinti, (2010). Normal faults and thrusts re-activated by deep fluids: the 6 April 2009 Mw 6.3 L'Aquila earthquake, central Italy. *Journal of Geophysical Research.* 115, B06315, 15, doi:10.1029/2009JB007190.

Doglioni, C., S. Barba, E. Carminati, F. Riguzzi, (2011). Role of the brittle-ductile transition on fault activation. Physics of the *Earth and Planetary Interiors.* 184, 160-171. doi:10.1016/j.pepi.2010.11.005

Doglioni, C., S. Barba, E. Carminati, F. Riguzzi, (2014). Fault on-off versus coseismic fluids reaction. *Geoscience Frontiers*. 5, 767-780, doi.org/ 10.1016/j.gsf.2013.08.004

Doglioni C., S. Barba, E. Carminati, F. Riguzzi, (2014). Fault on-off versus strain rate and earthquakes energy. *Geoscience Frontiers*. doi: http://dx.doi.org/10.1016/j.gsf.2013.12.007

Fulton, P.M. & A.P. Rathbun, (2011). Experimental constraints on energy partitioning during stick–slip and stable sliding within analog fault gouge. *Earth and Planetary Science Letters*. 308(1), 185-192.

Jackson, J.A., N.J. White, (1989). Normal faulting in the upper continental crust: observations from regions of active extension. *Journal of Structural Geology*. 11, 15--36.

Kanamori, H., and L. Rivera, (2006) Energy Partitioning During an Earthquake, in Earthquakes: Radiated Energy and the Physics of Faulting (eds. R. Abercrombie, A. McGarr, G. Di Toro and H. Kanamori). *American Geophysical Union*, Washington, D.C.. doi: 10.1029/170GM03

Luo, S., X. Meng, W. Bo, S. Zhu, L. Fu, (2014). *Ground Surface Deformation of L'Aquila Earthquake Revealed by InSAR Time Series*. FIG Congress 2014 Engaging the Challenges – Enhancing the Relevance, 16-21 June 2014 Kuala Lumpur, Malaysia, pp 1-14.

Marone, C., (1998). Laboratory-derived friction laws and their application to seismic faulting. Annual Review of *Earth Planetary Science*. 26, 643–696.

Pittarello, L., G. Di Toro, A. Bizzarri, G. Pennacchioni, J. Hadizadeh, M. Cocco, (2008). Energy partitioning during seismic slip in pseudotachylyte-bearing faults (Gole Larghe Fault, Adamello, Italy). *Earth and Planetary Science Letters*. 269, 131-139.

Riguzzi, F., M. Crespi, R. Devoti, C. Doglioni, G. Pietrantonio, A.R. Pisani, (2012). Geodetic strain rate and earthquake size: New clues for seismic hazard studies. *Physics of the Earth and Planetary Interiors*. 206-207, 67–75.

Scholz, C.H., (1990). *The Mechanics of Earthquakes and Faulting.* Cambridge, New York, Cambridge University Press, Ref. QE534.2.S37.

Sibson, R.H., (1977). Faults rocks and fault mechanisms. *J. Geol. Soc. London*. 133, 191-213.

Stramondo, S., M. Tesauro, P. Briole, E. Sansosti, S. Salvi, R. Lanari, M. Anzidei, P. Baldi, G. Fornaro, A. Avallone, M.F. Buongiorno, G. Franceschetti, and E. Boschi, (1999). The September 26, 1997, Colfiorito, Italy, earthquakes: modelled coseismic surface displacement from SAR interferometry and GPS. *Geophys. Res. Lett*. 26, 883–886.

INQUA Focus Group on Paleoseismology and Active Tectonics

paleoseismicity.org

Seismic monitoring and ground motion amplification of Monteluco Hill and Roio Plain (L'Aquila)

Durante, F. (1), Di Giulio, G. (2), Tallini, M. (1), Milana, G. (3), Del Monaco, F. (1)

(1) Dipartimento di Ingegneria Civile, Edile-Architettura e Ambientale, Università degli Studi di L'Aquila, L'Aquila, Italy. Email: geol.durante.federica@gmail.com
(2) Istituto Nazionale di Geofisica e Vulcanologia (INGV) L'Aquila, Italy
(3) Istituto Nazionale di Geofisica e Vulcanologia (INGV) Roma, Italy

Abstract: *The topography and the subsoil model, the stratigraphic variations as well as the physical and mechanical soil properties, and their changing with depth, may determine ground motions amplification, which control the uneven distribution of damages sometimes in spite of a relatively short distances. We present a study of the Monteluco Hill and the nearby Roio Plain (L'Aquila Municipality) using seismic noise and aftershock measurements, which were accurately elaborated and interpreted through the integration of borehole logs and outcropping data. The aim of the study was to investigate the seismic local effects due to topography and stratigraphy.*

Key words: *Seismic noise, Aftershock, Stratigraphic effect, Topographic effect, L'Aquila Municipality.*

INTRODUCTION

We present a study of high-density sampled seismic noise data acquisition and long-term aftershock measurements integrated with borehole logs and outcropping data of the Monteluco-Roio area (L'Aquila Municipality). The goal was to analyse in depth the seismic local effects due to topography (Monteluco Hill) and stratigraphy (Roio Plain), whose understanding is useful for seismic microzonation planning of the April 6th 2009 L'Aquila earthquake epicentral area.

From the geological point of view, the Monteluco-Roio area (Fig. 1) should be considered a "key sector" to understand the Plio-Quaternary evolution of the "middle Aterno River Valley basins", because of its central location between the Scoppito-L'Aquila basin and the Fossa-S.Demetrio one (Demangeot, 1965).

In the study area, four lithological Pleistocenic units have been recognized. Two of them can be referred to lacustrine/alluvial environment (S. Rufina unit, which outcrops broadly in the Roio Plain and the Via Mausonia unit); one of them can be referred to as debris-flow like deposits (Malepasso unit); the last one can be interpreted as a hill-slope deposit (Canetre unit). The pre-Quaternary substratum is referred to Upper Cretaceous, Paleogene and Miocene limestones, which were, at times, strongly jointed and faulted (Blumetti et al., 1996; Gruppo di lavoro MS-AQ, 2010; Hailemikael et al., 2010; 2015).

Monteluco Hill has an NW-SE trending elliptical shape and it is formed by a monocline of thick-bedded Miocene calcarenites. Roio Plain is a semi-graben basin bordered north-eastward by a normal fault and is surrounded by carbonate reliefs.

It is filled up by about 100 m thick Quaternary alluvial-lacustrine clay laying upon the calcareous bedrock (Blumetti et al., 1996; Gruppo di lavoro MS-AQ, 2010; Hailemikael et al., 2010; 2015).

These Quaternary deposits are formed by alternating clay, clayey silt and sandy silt with an increasing of consistency to depth, which lie beneath a 20 m thick sandy deposit (S. Rufina unit) (Gruppo di lavoro MS-AQ, 2010; Hailemikael et al., 2010).

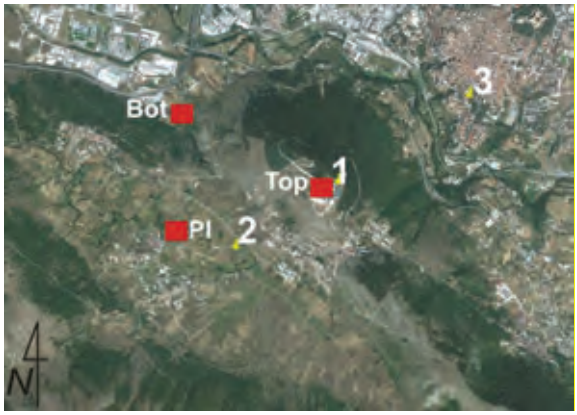

Figure 1: The study area of Monteluco Hill (1) and Roio Plain (2); L'Aquila downtown (3); red squares: location of the aftershock long-term measurements stations (Pl: Roio Plain; bottom (Bot) and top (Top) of Monteluco Hill.

Seismic noise measurements

More than 100 seismic noise measurements were collected between December 2011 and March 2012 using two types of three-component seismometers (Tromino Micromed and SR04 Sara Electronic Instruments s.r.l.). More precisely, we acquired 35 and 73 HVSR measurements in the Roio Plain and Monteluco Hill respectively.

Microtremors data were collected during a short time window (20-30 minutes). Signals were cut into short duration windows of 30 seconds and processed through

a detrigger algorithm to remove those affected by strong transient disturbs (SESAME, 2004). Fourier spectra were smoothed using the method proposed by Konno & Ohmachi (1998). Finally, the average HVSR spectral curve, along with the standard deviation, was evaluated computing the ratio of the horizontal over the vertical components (HVSR). The characteristic peak in the HVSR curves was assumed to be the site predominant frequency (F_0). The high density of measuring sites allowed to define with a good detail the lateral changing of F_0, and to detect zones with homogeneous seismic behaviour.

The variations of F_0 in the Monteluco Hill and Roio Plain are shown in Figure 2.

In the Monteluco Hill, the majority of the HVSR curves show high frequency values of F_0, with values ranging from 15 Hz to 20 Hz, due to a shallow jointed zone of limestones, or no resonance peaks, because of massive outcropping limestone. On the top of Monteluco Hill, on the contrary, the HVSR curves evidence F_0 of about 3-5 Hz, suggesting a topographic effect.

In the Roio Plain, HVSR curves show F_0 from 1 to 3 Hz, likely related to a seismic impedance contrast of the Quaternary soft deposits laying on the carbonatic bedrock.

Bedrock depth estimation and 1D numerical modelling (Roio Plain)

The bedrock depth H within the Roio Plain was firstly estimated using the 1-D quarter wavelength approximation F_0= Vs/4H, where Vs is the shearwave velocity estimated from down-hole tests (Gruppo di lavoro MS-AQ, 2010), F_0 is the resonance frequency measured from HVSR curves. Under this assumption, F_0 is caused by the 1-D resonance of soft deposits overlaying the carbonatic bedrock.

We reconstructed also the 1-D subsoil models of seven sites in the Roio Plain by using down-hole tests, stratigraphic borehole logs and gravimetric data (Gruppo di lavoro MS-AQ, 2010; Hailemikael et al., 2010) (Fig. 3). Then, 1-D numerical response was calculated in these sites through STRATA software (Kottke & Rathje, 2008) to strengthen the subsoil model of Roio Plain.

This software assumes an equivalent-linear approach to compute the seismic response in the frequency domain, using time domain input motions, for 1-D soil column, characterized by Vs velocity, damping ratio, total unit weight and thickness. For linear elastic 1-D wave propagation, the soft soil is assumed as a Kelvin-Voigt solid. The amplitudes of the 1-D transfer functions are controlled by the soil damping ratio.

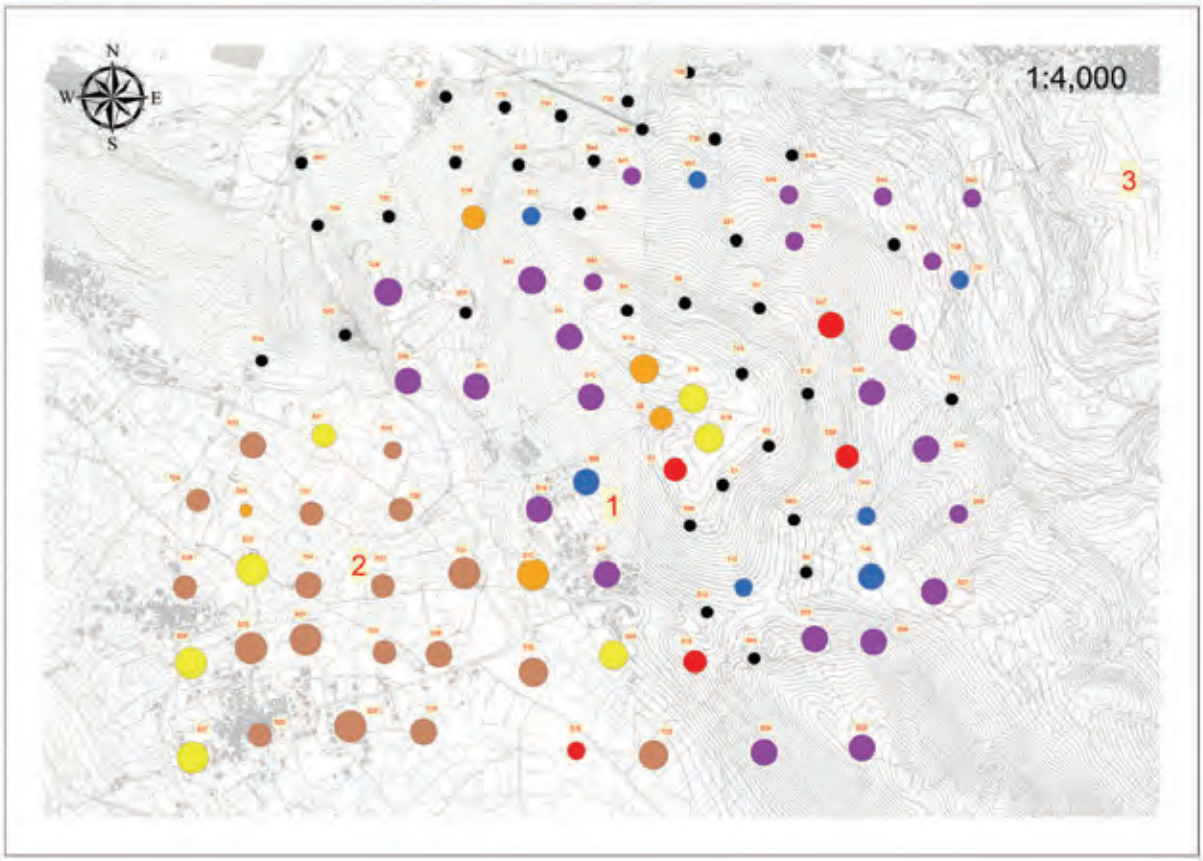

Figure 2: Map of the resonance frequencies (F_0); Monteluco Hill (1), Roio Plain (2), L'Aquila (3). Black: no pick; Brown: 1.0-2.4 Hz; Yellow: 2.5-4.9 Hz; Orange: 5.0-7.4 Hz; Red: 7.5-9.9 Hz; Violet: 10-14.9 Hz and Blue: 15.0-20 Hz.

The comparison between 1-D STRATA modelling and the experimental HVSR spectral curves shows same frequencies (about 1 and 3 Hz) evidencing the reliability of the Roio Plain subsoil model. In Figure 3, the case site of S. Rufina is reported as an example.
To summarize, the main result of the modeling shows an average depth of the carbonatic bedrock of about 90-100 m which in agreement with previous studies (Gruppo di lavoro MS-AQ, 2010; Hailemikael et al., 2010).

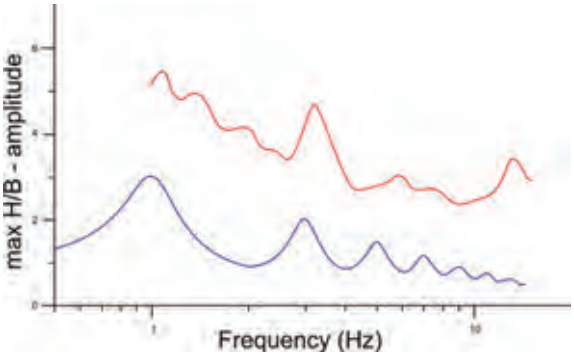

Figure 3: Comparison between 1-D STRATA modeling (blue line) and HVSR curve (red line) of S. Rufina site located in PI in Figure 1.

Analysis of the topographic amplification (Monteluco Hill) using earthquake data
The earthquake monitoring took place during January-April 2013 in three sites (top and bottom of Monteluco Hill, and Roio Plain). During the monitoring period, the seismic stations acquired about twenty local earthquakes (Ml ranging from 1.1 to3.6) and a far-field one (Mw 4.8, epicentral area Sora, time of occurence 02/13/2013) (Fig. 4). The earthquakes data allowed to analyse the topographic and stratigraphic effects of Monteluco Hill and Roio Plain, respectively. The analysis was performed according to the SSR technique (Borcherdt, 1970). SSR consists in computing the ratio of the Fourier spectrum of the earthquake recordings at the studied site, with respect to a reference nearby rocky site for the same seismic event. We computed also the HVSR spectral ratios using earthquakes.
The HVSR curves computed on earthquakes show a F_0 of about 3-5 Hz at the top of Monteluco Hill, which is in agreement with microtremor data (Figs. 2 and 4).
SSR analysis evidences the same resonance frequency at about 3 Hz, indicating that the horizontal component measured at the top of Monteluco Hill (Htop) is about five times larger than the horizontal component measured at the bottom of the hill (Hbot) (Fig. 5). In addition, the peak ground velocity (PGV) trend shows consistently the PGV values at the top of Monteluco Hill are 2-3 times larger than the one as at the bottom (Fig. 6).

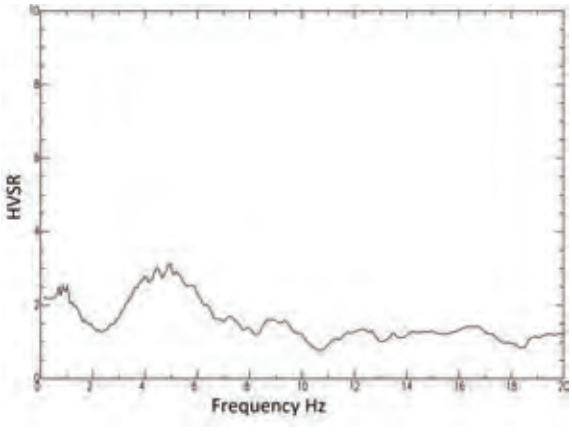

Figure 4: HVSR average curve computed on different local earthquakes (acquisition period: January-April 2013) recorded at the top of Monteluco Hill.

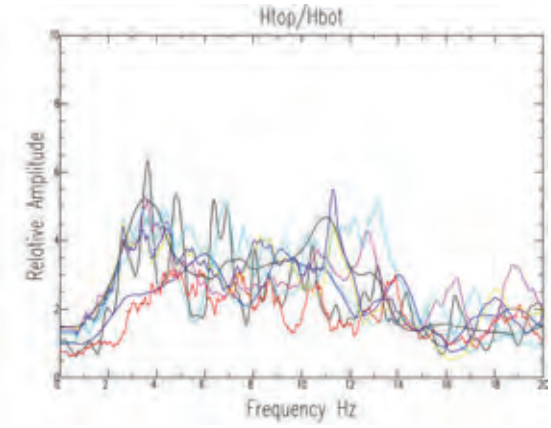

Figure 5: SSR analysis (Htop/Hbot) using different local earthquakes. Htop and Hbot are the horizontal components measured at the top and at the bottom of Monteluco Hill.

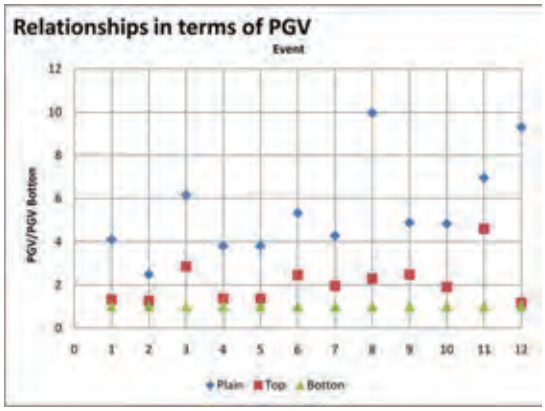

Figure 6: PGV trend. On the x- axis the number refers to different earthquakes, on the y- axis the PGV ratio is reported at three sites (Roio Plain, top and bottom of Monteluco Hill) using as reference the PGV value recorded at the bottom site (Roio Plain, top and bottom of Monteluco Hill).

CONCLUSIONS

Integrated seismic data (microtremor and earthquake monitoring, geological and geophysical data and 1D numerical modelling) permitted to investigate the seismic response of two adjoining areas located in L'Aquila Municipality (Roio Plain and Monteluco Hill) (Fig. 1).

For the Roio Plain, we elaborated the subsoil model through down-hole tests, borehole logs and with the 1-D numerical modelling by using the STRATA software, whose results are comparable with the experimental microtremor data (Fig. 3). At Roio Plain, seismic local response is mainly controlled by a stratigraphic effect (i.e. soft sediment upon carbonate bedrock), as already outlined by previous authors (Bertrand et al., 2011; Gruppo di lavoro MS-AQ, 2010; Hailemikael et al., 2010; 2015).

As regards the seismic behaviour of Monteluco Hill, seismic noise (Fig. 2) and earthquake data (Figs. 4, 5 and 6) evidence a possible topographic amplification in the range of 3-5 Hz. In this case, our working in progress will involve also a 2-D numerical modelling, which can furnish further additional information on the conceivable topographic effect of Monteluco Hill.

References

Bertrand, E., A.M. Duval, J. Régnier, R.M. Azzara, F. Bergamaschi, P. Bordoni, F. Cara, G. Cultera, G. Di Giulio, G. Milana & J. Salichon, (2011). Site effects of the Roio basin, L'Aquila. *Bull. Earthquake Eng.* 9, 809-823.

Blumetti, A.M., G.P. Cavinato & M. Tallini, (1996). Evoluzione Plio-Quaternaria della conca di L'Aquila-Scoppito: Studio Preliminare. *Il Quaternario*. 9, 281-286.

Borcherdt, R.D., (1970). Effects of local geology on ground motion near San Francisco Bay. *Bull. Seism. Soc. Am*. 60, 29-61.

Demangeot, J., (1965). Géomorphologie des Abruzzes Adriatiques. *Mém. et Doc. du C.N.R.S.*, Paris.

Gruppo di Lavoro MS–AQ, (2010*). Microzonazione sismica per la ricostruzione dell'area aquilana*. Regione Abruzzo – Dipartimento della Protezione Civile, L'Aquila, 3 vol. e Cd-rom.

Hailemikael, S., L. Lenti, S. Martino, A. Paciello & G. Scarascia Mugnozza, (2010). *2D numerical modelling of observed amplification effects on a carbonate ridge: the Colle di Roio (Italy) case-history*. In: Proceedings of the 14th European conference on earthquake engineering, 14ECEE, Ohrid, Macedonia.

Hailemikael, S., L. Lenti, S. Martino, A. Paciello & G. Scarascia Mugnozza, (2015). Parametric numerical study of observed amplification effects on the Colle di Roio limestone ridge (Central Italy). *Engineering Geology for Society and Territory*. 5, 1133-1136.

Konno, K. & T. Ohmachi, (1998). Ground-motion characteristics estimated from spectral ratio between horizontal and vertical components of microtremor. *Bull. Seism. Soc. Am*. 88, 228-241.

Kottke, A.R. & E.M. Rathje, (2008). *STRATA*, University of Texas at Austin, Version alpha, Revision 381.

Nakamura, Y., (1989). A method for dynamic characteristics estimation of subsurface using microtremor on the ground surface. *QR of RTRI* 30, 25-33.

SESAME, (2004). *Guidelines for the implementation of the h/v spectral ratio technique on ambient vibrations-measurements, processing and interpretations*. SESAME European research project EVG1-CT-2000-00026, deliverable D23.12. (http://sesame.geopsy.org/index.htm).

INQUA Focus Group on Paleoseismology and Active Tectonics

ESI-07 ShakeMaps for Instrumental and historical events in the Betic Cordillera (SE Spain): a preliminary approach applied to seismic hazard based on geological data

Elez, J. (1), Silva, P.G. (1), Giner-Robles, J.L. (2), Rodríguez-Pascua, M.A (3), Pérez-López, R. (3), Roquero, E. (4), Bardají, T. (5), Huerta, P. (1), Mártinez-Graña, A. (1)

(1) Dpto. de Geología, Universidad de Salamanca, Escuela Politécnica Superior. AvilaSpain. Email: jelez@usal.es
(2) Dpto. de Geología y Geoquímica, Universidad Autónoma de Madrid, Cantoblanco (Madrid), Spain
(3) Instituto Geológico y Minero de España, IGME. Madrid, Spain
(4) Dpto. de Edafología. E.T.S.I. Agrónomos. Universidad Politécnica de Madrid. Madrid, Spain
(5) U.D. Geología. Universidad de Alcalá. Alcalá de Henares (Madrid), Spain

Abstract: *This work presents shake scenarios for two earthquakes occurred in the Betic Cordillera (SE Spain) such as the AD 2011 Lorca event (VIII ESI07; 5.2 Mw) and AD 1863 Huércal-Overa event (VIII ESI07; 4.9 Mw). The Lorca event presents instrumental measures, allowing comparison of the distribution and magnitude of the modelled PGA values, as well as a detailed field based characterization and mapping of the related geological effects. To explain the wide variety of slope movements and other geological effects recorded along the studied earthquakes, obtained PGA models must include a topographic amplification factor, normally not considered instandard Shake models. Additionally, V_s^{30}models derived from topography resulted in overestimations of the PGA values in flat terrains, such as, pediments or flat erosion surfaces, carved in resistant materials. This was corrected applying a factor related to the thickness of the Quaternary deposits. The incorporation of those basic amplification factors upgraded the resulting macroseismic scenarios, clearly identifying zones prone to record environmental damage.*

Key words: *ShakeMaps, ESI-07 Scale, PGA, Seismic Hazard, Betic Cordillera, Spain.*

INTRODUCTION

This work presents shake scenarios for two earthquakes occurred in the Betic Cordillera (SE Spain). The AD 2011 Lorca event (VIII ESI07; 5.2 Mw) and the AD 1863 Huercal-Overa event (VIII ESI07; 4.9 Mw). The Lorca event presents a significant range of instrumental measures, allowing the cross-cheking of the distribution and size of the obtained Peak Ground Acceleration (PGA)valuesand models. For both events there is a detailed field based characterization and mapping of the related earthquake environmental effects (EEEs) provided by the recently published Spanish EEE Catalogue (Silva et al., 2014a).

METHODOLOGY

From the methodological standpoint, the modelling of the spatial distribution of the PGA values (shakemaps) has required a workflow based on the integration of the diverse spatial models in a Geographic Information System (GIS) environment. Here, field EEE-data have been incorporated together with other levels of information (DTMs, slope models and ground-motion prediction models among others) for comparison purposes. In this environment, modelling results have been iterated many times to estimate how the different adjustments introduced in the workflow modified the results at different scales.
For the elaboration of earthquake models, 5 m and 25 m pixel Lidar DTMs, obtained from the IGN online database, wereused as the base-maps for the calculation of the different derived models and final ShakeMap

Figure 1: Location of the two earthquakes analyzed in this work (stars) in the framework of the fault system of the Eastern Betic Shear Zone (EBSZ). Black circles are locations cited in the text.

scenarios. There is an important amount of Ground-motion prediction equations in the literature, (e.g. Ambraseys et al., 2005; Chiou& Young, 2008; Boore& Atkinson, 2008; etc.), but some of them are quite difficult to implement in a GIS environment. This complicated the election of only one fitting the requirements of this work. Among the different proposals, the selected one should be relatively simple in its application(due to the necessary iteration-related workflow), not much time consuming and yet reliable and well tested. Eventually, for the preliminary approaches presented here, the

method developed by Boore et al., (1997), widely used in the USGS Earthquake Hazards Program, fulfilled all those requirements.

A number of data and models are needed to design a proper PGA model of an earthquake from the Boore et al., (1997) ground-motion prediction equations. Those are: the location of the epicentre, fault type, dimensions and shape of the fault rupture, Mw, site condition map (V_s^{30}) and Joyner-Boore distance. In a first step we proceed to model the 2011 Lorca event in order to cross-check the results with the significant amount of instrumental (Morales et al., 2014) and field data (Alfaro et al., 2011; Silva et al., 2014b) existing for this event. In a second step, the obtained methodology was applied to a historical example from which sufficient ESI data areavailable, as is the case of the AD 1863 Huercal-Overa event (Silva et al., 2014c).

Shake map for the 2011 lorca event

For the 2011Lorca earthquake, the epicentre location, fault parameters and Mw were obtained from Morales et al., (2014). The fault plane geometrywas estimated as the envelope to the main set of deeper events of the aftershock seriesdescribed by these authors.Due to the absence of Vs_{30} measures in the study area, the site condition map is obtained applying the empirical approach used in the USGS ShakeMap program (Wald & Allen, 2007), in which the terrain slope is considered as proxy for seismic site conditions and amplification. Finally Joiner-Boore distance algorithm predicts the PGA spatial distribution and propagation from the modelled seismic source, otherwise easy to implement in the GIS environment from the theoretical fault geometry and kinematics (strike-slip, reverse, etc.).

Preliminary models obtained from the application of theBoore et al. (1997) equations fitted rather well with instrumental measures. However, some disagreement arose mainly related to the distribution and features of the mapped geological effects (Silva et al., 2014b). Those discrepancies are threefold:

1) There is a lack of correlation concerning the wide variety of slope movements recorded in the Lorca event and the calculated PGA values for those zones widely affected by EEEs. This typically occurs in places with steep slopes. Here, lithologies are usually hard and hence account for high V_s^{30} values. This implies that PGA values obtained from the preliminary model are systematically underestimated in steep areas. The conversion of inverted values of slope in progressively higher V_s^{30} values underestimate apparent topographic amplification occurred in these areas during the 2011 Lorca event (Rodríguez-Peces et al., 2011).
2) V_s^{30} models derived from terrain slope models resulted in overestimations of the PGA values in flat terrains, such as thin alluvial fan deposits, pediments, flat erosion surfaces or structural reliefs, carved in resistant Neogene materials. These models assume that flat terrains widely correspond to thick Quaternary fillings, but this is not the case for the aforementioned cases. Therefore a binary factor has been introduced in the terrain model in order to weight the complete or partial application of the slope as proxy of site conditions in relation to the occurrence / absence of thick Quaternary sequences at least 20-30 m thick.
3) The USGS ShakeMap program use the large scale 900 m/pixel DTMs from the global coverage SRTM30 data-base (Shuttle Radar Topography Mission), since some studies indicate that the use of more detailed terrain models do not significantly improve the results (Allen &Wald, 2009). However, in the cases explored here,maximum damage is restricted to areas around 100 km^2. Consequently, the use of SRTM30 base-maps result in limited coverage zones of about only 100 pixels, where mean slopes of these large-sized (900m) pixels diffuse the analysis. For these pixel scales the results are mainly controlled by the Joyner-Booreparameter (distance-dependent), blurring the slope component in the macroseismic areas. For the kind of moderate events studied here (c. 5.0 Mw) the small areas affected by EEEs are far for the resolution analysis offered by the SRTM30 terrain models. Higher-resolution DTMs (25 and 5 m/pixel) were used in order to identify areas affected by secondary earthquake effects of moderate-size, linked to intensities≥ VII ESI-07.

In order to correct the problems detected with the topographic amplification and the use of the terrain slope as an "inverse proxy" for site conditions (V_s^{30}), several improvements have been included in the calculation of the ESI07 ShakeMaps developed in this work:

(a) To explain the wide variety of slope movements and other geological effects recorded during the Lorca earthquake, PGA models must include a Topographic Amplification factor (T_S^0). Based on the works of Rodríguez (2006) and García Rodríguez &Malpica(2010), we scaled the slope-based topographic amplification intervals proposed these authors by means of the calculation of the best-fit 2nd Order Polynomial function, resulting in the following equation:

$$T_s^0 = -9\times10^{-5}s^2 + 0.0167s + 0.9864$$

where(s) is the terrain slope in degrees. This roughly means that for flat areas the amplification factor is 1 and for steeper areas (≥5º) is smoothly increasing up to 1.5 at slopes of 40^0 with maximum amplification of 1.8 for near-vertical locations (≥ 70º). This factor related to the slope amplification effect has not been considered in most available shake-models.However its use seems essential to fit instrumental PGA records, since the sole use of slope-derived V_s^{30} valuesdo not consider, and even minimize, the triggered topographic amplification.

(b) The significant impact of slope-derived V_s^{30} values in flat terrains without Quaternary cover has been corrected by applying a factor related to the known thickness of Quaternary deposits.Those places were the total thickness of Quaternary deposits is clearly less than 30 metres the applied correction factor is $Q_T^{30} = (Y_{Vs^{30}}*0.8)$ in order to prevent overestimations in flat terrains without a significant Quaternary cover.

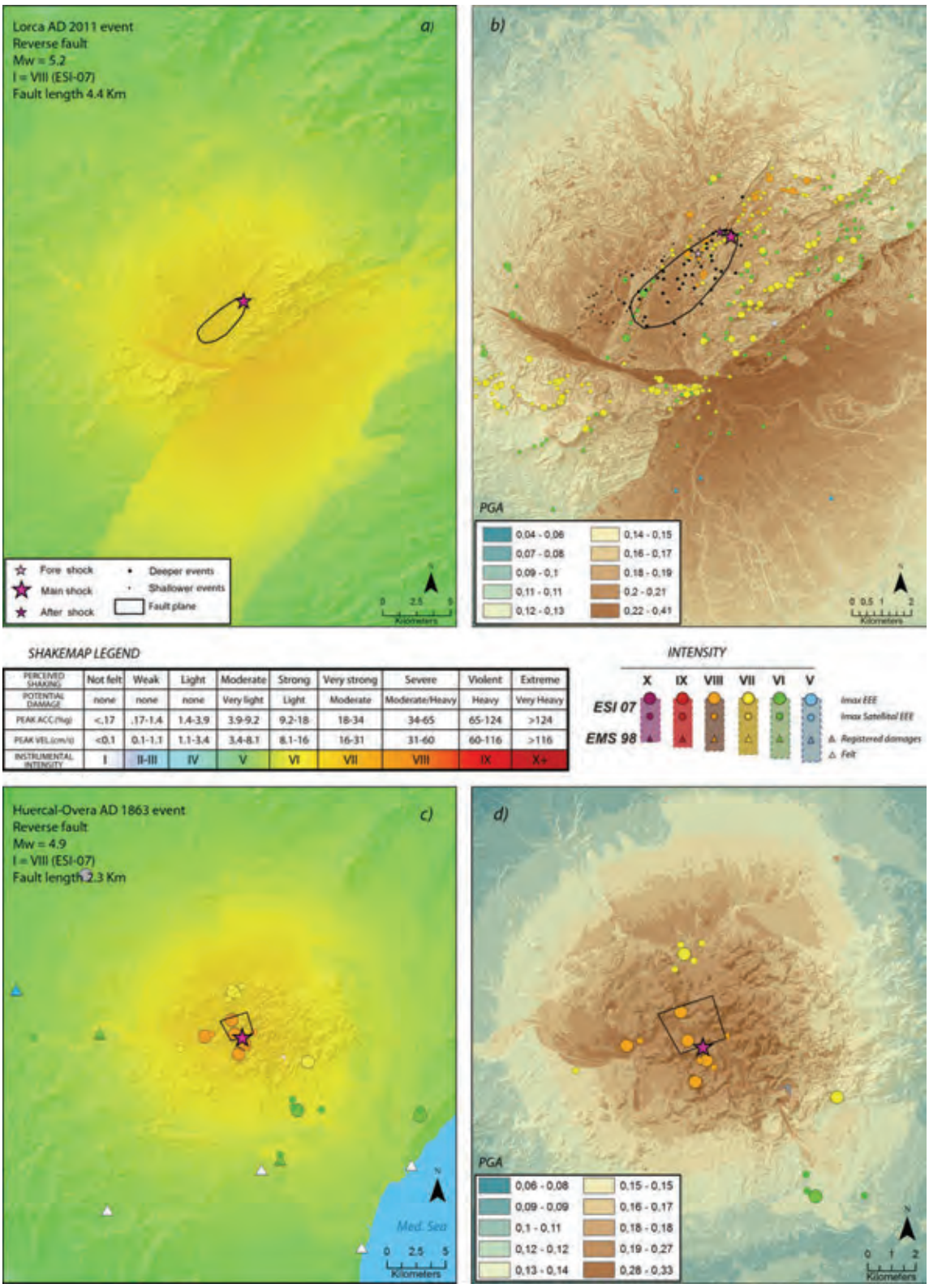

Figure 2: (a)&(c) are the USGS-style ShakeMaps for the 2011 Lorca (a) and 1863 Huércal-Overa (b) earthquakes produced from 5 m/pixel (a) and 50 m/pixel (c) digital terrain models from ESI-07 (circles) andEMS-98 (triangles) data. The Lorca map (a) was produced by the implementation of existing instrumental data. The Huércal-Overa map (c) fault-parameters were estimated by empirical approaches and existing seismic data for the zone. (b) & (d) are detailed shake-models of the respective macroseismic areas for both earthquakes. Note different colour scales to enhance those zones where topographic amplification occurred.

The value of this correction parameter has been estimated from successive logic trial approaches to fit calculated PGA values to those instrumentally recorded for the entire affected area at 90% confidence level.
The Quaternary Thickness factor (Q_T^{30}), completes the function proposed here to calculate shakemap models in those zones where the thickness of Quaternary deposits is no significant:

$$PGA_{ESI} = Q_T^{30} \times T_S^0 \times Y_{Vs^{30}}$$

where $Y_{Vs^{30}}$ is the obtained PGA from the Boore et al. (1997) ground motion prediction equations. In those zones, where the Quaternary thickness is significant (Guadalentin Depression and Guadalentin river valley) the Q_T^{30} correctionfactor was not applied since site conditions predicted by slope-derived V_s^{30}values are reliable, matching to the instrumental records with errors down to ± 10%.
In this way PGA values recorded in the city of Lorca (4 km away from the epicentre) was of 0.365g and those predicted by the Shake model are of 0.326g. For more distant localities, such as Alhama de Murcia (30 km away) recorded values were of 0.043g and those predicted by the model are of 0.050g. In the epicentral area, north of Lorca, maximum predicted PGA are in the range of 0.38 – 0.41g for a zone of about 10 km^2, matching with PGA ranges of intensity VIII MM of the USGS (0.34 -0.65g) and with ESI-intensity evaluations of the zone (Silva et al., 2014b).The comparison of instrumental data and calculated PGA models result in an uncertainty of c. ±10%,for the studied area. Faintly low calculated values result for the epicentral area (10 km radius) and faintly high ones for more distant areas when compared with the instrumental records. This fact indicates that the corrections introduced in this work for the production of PGA models are still conservatives for the epicentral zone where most EEEs were produced.
The obtained values fit better enough shake-models elaborated after the Lorca earthquake, which resulted in predicted PGA values for Lorca of about 0.250g (Benito et al., 2012). These authors used different ground motion prediction functions, but considering homogeneous ultraconservative hard rock-like Vs_{30} unreliable values (1100 m/s) for the entire Murcia region. Consequently all the models elaborated by these authors resulted in significant underestimations (c. 33%) of the computed values, otherwise similar to those resulting for the application of the existing Spanish Seismic Building Codes (NCSE-02) before the 2011 earthquake.
On the contrary, the shake model calculated in this work results in a good correlation between the modelled distribution of the PGA and the diverse geological data (251 data-points), the spatial distribution of the resulting ESI-07 intensities (Silva et al., 2014b) and the instrumental measures of the Lorca earthquake (10 data-points). Consequently, the incorporation of the basic correction factors considered here upgrades the resulting macroseismic scenario, clearly identifying those zones prone to record environmental damage.

SHAKEMAP FOR THE AD 1863 HUERCAL-OVERA EVENT: Historical Seismic Scenarios.

For thishistorical event, fault parameters and earthquake size were calculated from the set of available EMS and ESI data points (n = 40) and intensity distribution proposed by Silva et al. (2014c). This approach results in different seismic parameters (location and size) that those considered in the IGN Catalogue (Martínez Solares & Mezcua, 2002) or other recent re-evaluations (Mezcua et al., 2013).
The epicentre location is estimated from the spatial distribution of the ≥ VII ESI07 data-points, matching with the location of the Almanzora Tectonic Corridor blind-thrust zone and with the 3D distribution of recent seismicity recorded in the area (Pedrera et al. 2009). A focal depth of 5 km was assumed considering the geophysical models of blind thrusting and surface folding proposed for the area by the same authors. Mw was calculated by means of the intensity-derived functions used in Spain (Mezcua et al., 2013) resulting in a magnitude of 4.9 Mw. Fault dimension parameters has been estimated from standard empirical approaches (i.e. Wells and Coppersmith, 1994) adjusting the fault plane geometry to a simplified rectangular form resulting from the projection of the northwards blind-thrust at surface. The subsequent procedures have been the same ones that those checked for the calculation of the Lorca ShakeMap.
The resulting shake model clearly identifies the areas affected by environmental damage during the 1863 event within the Almanzora canyon-valley and the old depopulated areas of Los Oribes and the Ancient Obera. In all these zones VIII ESI07 intensities were recorded, by significant rock-falls, Apparition and relevant changes of flow-rate and position of springs, the river stopped to flow during several minutes and a small lake-basin completely disappeared by the occurrence of hectometric-length ground-cracks (Silva et al., 2014c). The model also match with the intensity ranges VI – VII assigned to different localities (EMS: Huercal-Overa, Cuevas, Vera, Albox, Arboleas, etc.) or natural locations (ESI: Alboraija lake, TresPacos, El Retablo, El Portillo, Almagrera mines, etc.).
The obtained shake model for the Huercál-Overa event provides a reliable seismic scenario for a historical event largely based on geological data derived from the application of the ESI07 Scale (Michetti et al., 2007). Other seismic scenarios, resulting for other parametric proposals of the event have been checked (Martínez Solares & Mezcua, 2002; Mezcua et al., 2013), but resulting in unreliable PGA distributions with respect to the existing ESI-07 and EMS-98 data-points.
The proposal of the IGN Catalogue (4.2 Mw event, close to Huercal-Overa; Martínez Solares & Mezcua, 2002) resulted in lower PGA values no matching with the intensity levels (≥ VI) in the affected area. Other proposal relating the earthquake with the Albox Fault, 7 km north of Huercal-overa (4.6 Mw; Mezcua et al., 2013), resulted in shake scenarios unable to explain the set of geological effects recorded in the Almanzora Canyon (Silva et al.,

2014c) and predict significant intensities (VI – VIII) for localities in which the 1863 earthquakewas only slightly felt (≤IV) or there are no intensity data.

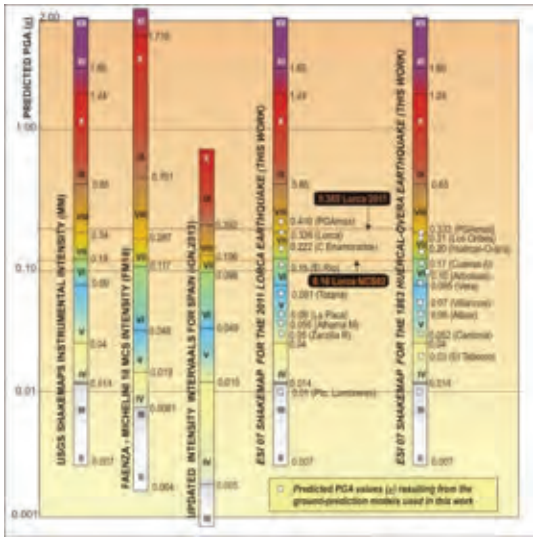

Figure 3: PGA values (g) obtained by the Shake-models elaborated in this work within the USGS MM intensity ranges (right) compared with PGA ranges for different intensity scales. Note the lower PGA EMS-intensity ranges of the updated values for Spain (IGN, 2013) when compared with MM and MCS intensity scales.

DISCUSSION

Shake models produced in this work are fully applicable to understand seismic hazard from instrumental and historical earthquakes. The two earthquakes explored here were no-surface faulting events, with moderate magnitudes of about 5.0 Mw, but produced a large number of earthquake environmental effects (EEEs). The use of these geological intensity data-points, by means the application of the ESI-07 scale improve the assessment of intensity distribution, providing upgraded frameworks to produce slope-derived Shake models similar to those developed by the USGS ShakeMap program (Fig. 2). However, the direct application of simple ground motion prediction models based on the slope as proxy for site conditions (i.e. Boore et al., 1997; Wald & Allen, 2007): (a) ignore the occurrence of topographic amplification; and (b) overestimate site conditions for flat terrains in rock-resistant materials.Correction factors introduced in this work upgrade the correlation of predicted and observed PGA values with an uncertainty of c. 10% improving previous proposed models (Benito et al., 2012).

Ground shaking prediction models presented here introduce correction factors to discriminate and solve these problems for detailed DTM scales down to 30 and 5m/pixel (Fig. 2). Larger scales used in the USGS program (900 m/pixel) are clearly applicable to stronger surface-faulting events with magnitudes above 6.5 -7.0 Mw which minimize these problems due to the larger affected areas. On the contrary, for regions in which moderate events (< 7.0 Mw) dominate the seismic records, seismic hazard can be clearly investigated from secondary EEEsthrough the application of the ESI-07 Scale. ShakeMaps developed in this work, have been generated with the aim to be simple to apply to historical or ancient events for which a representative number of EEE assessments might be merged with existing damage-based intensity dataas recommended in the ESI-07 Scale guidelines (Michetti et al., 2007).

Regarding to the state of the art in Spain, results from this work indicate that PGA assessments considered in the old and updated seismic hazard programs for the development of Seismic Building codes are clearly underestimated (Fig. 3). In detail, for the case of Lorca the obtained PGA values are close to those recorded instrumentally (IGN, 2012) being unnecessary appeal to suspect over-amplifications triggered by directivity effects along the fault trace as suggested by other authors (Benito et al., 2012). For the Huercál-Overa historicalcase, routines learned during the production of the 2011Lorca Shake Maps were applied. In this case we explored the different seismic sources and earthquake sizes cited in the literature, resulting in unreliable seismic scenarios, difficult to explain the variety and distribution of EEEs catalogued for this event (Silva et al., 2014).

PreliminaryShake models presented in this work are the first shake maps available for instrumental and historical earthquakes in Spain, but also the first ones world-wide produced from detailed digital terrain models. They represent a preliminary approach to the final products of the 1299 INQUA Project: EEE Metrics. Presently, we are checking and evaluating the application of second-generation ground prediction models (i.e. NGAE) in order to refine the resulting seismic scenarios and validate the use of geological data (EEEs) in the eventual production reliable tools for seismic hazard assessments. In this first approach we choose the USGS MMI intensity-PGA conversion since the ones proposed for Spain (IGN, 2013) or other Mediterranean regions (Faenza & Michelini, 2010) don`t correlate well the observed intensity levels with the corresponding bracketed PGA values (Fig. 3).

Shake models presented in this work use the 2011 Lorca earthquake as the only "calibration event", since it is the only significant event (≥ 5.0 Mw) recorded during the instrumental period in Spain with representative instrumental and intensity data (ESI-07 plus EMS-98) to be compared. In spite of this limitation, its application to the historical case of Huercal-Overa is appropriate since, both events are located in close areas within the Eastern Betic Cordillera subject to similar seismotectonic features and fault slip rates (IGN, 2012). However future approaches will consider to calibrate the intensity levels using a sample of other representative and stronger earthquakes occurred in the Mediterranean region.

Acknowledgements: This work has been funded by the Spanish research projects CGL2012-37281-C02.01: QTECTBETICA (USAL) and CATESI-07 (IGME). This is a contribution of the INQUA TERPRO Project 1299 EEE Metrics and the Working Group QTECT-AEQUA.

INQUA Focus Group on Paleoseismology and Active Tectonics

References

Alfaro, P., J. Delgado, F.J. García-Tortosa, L. Lenti, J.A. López, C. López-Casado, S. Martino, (2012). Widespread landslides induced by the Mw 5.1 earthquake of 11 May 2011 in Lorca, SE Spain. *Eng. Geology*. 137-138, 40-52.

Allen, T., D. Wald, (2009). On the Use of High-Resolution Topographic Data as a Proxy for Seismic SiteConditions (Vs30). *Bull. Seism. Soc. Am*. 99, 935-943.

Allen, T., D. Wald, A. Hotovec, P. Earle, K. Marano, (2008). An Atlas of ShakeMaps for Selected Global Earthquakes. *USGS Open-File Report*. 2008-1236, 35 p.

Ambraseys N.N., J. Douglas, S.K. Sarma & P.M. Smit, (2005). Equations for the Estimation of Strong Ground Motions from Shallow Crustal Earthquakes Using Data from Europe and the Middle East: Horizontal Peak Ground Acceleration and Spectral Acceleration. *Bulleting of Earthquake Engineering*. 3, 1-53.

Benito, B., Rivas, A., Gaspar-Escribano, M., Murphy, P. (2012). El terremoto de Lorca (2011) en el contexto de la peligrosidad y el riesgo sísmico en Murcia. *Física de la Tierra.* 24, 255-287.

Boore, D.M., G. Atkinson, (2008). Ground-Motion Prediction Equations for the Average Horizontal Component of PGA, PGV, and 5%-Damped PSA at Spectral Periods Between 0.01 s and 10.0 s. *Earthquake Spectra.* 24, 99-138.

Boore, D.M., W. Joyner, T. Fumal, (1997). Equations for estimating horizontal response spectra and peak acceleration from Western North American earthquakes: A Summary of recent Work. *Seismological Research Letters.* 68 (1), 128-153.

Chiou, B.S., R. Youngs, (2008). An NGA model for the average horizontal component of peak ground motion and response spectra. *Earthquake Spectra*. 24 (1), 173-215.

Faenza, L., F. Michellini, (2010). Regression analysis of MCS intensity and ground motion parameters in Italy and its application in ShakeMaps. *Geophysical Journal International*. 180 (3), 1138-1152.

García Rodríguez, M.J., J.A. Malpica, (2010). Assessment of earthquake-triggered landslide susceptibility in El Salvador based on Artificial Neural Network model. *Nat. Hazards Earth Syst. Sci*. 10, 1307-1315.

IGN, (2012). *Informe del sismo de Lorca del 11 de mayo de 2011*. IGN. Madrid, Spain, 129 pp.

IGN, (2013). *Actualización de Mapas de Peligrosidad Sísmica en España 2012*. IGN. Madrid. 267 pp.

Martínez Solares, J.M., J. Mezcua, (2002). Catálogo Sísmico de la Península Ibérica (880 a.C. - 1900). *Monografías IGN*. 18. IGN. Madrid (Spain). 253 pp.

Michetti, A.M., E. Esposito, L. Guerrieri, et al., (2007). Environmental Seismic Intensity scale – ESI 2007. In: *Intensity Scale ESI-07* (Guerrieri, L., Vittori, E. Eds.). Mem. Descr. Carta Geologica d'Italia 74. APAT, Rome. Italy. 41 pp.

Mezcua, J., J. Rueda, R.M. García Blanco, (2013). Re-evaluation of historic earthquakes in Spain. *Seismological Research Letter*. 75, 75-81.

Morales, J., J.V. Cantavella, FdL. Mancilla, L. Lozano, D. Stich, E. Herráiz, J.B. Martín, J.A. López-Comino & J.M. Martínez-Solares (2014). The 2011 Lorca seismic series: Temporal evolution, faulting parameters and hypocentral relocation. *Bulletin of Earthquake Engineering*. 12 (5), 1871-1888.

NCSE-02, Norma de la construcción sismorresistente española (2002). Real Decreto 997/2002, de 27 de septiembre. *Boletín Oficial del Estado*. Vol. 244, 35898-35967.

Pedrera, A., J. Galindo-Zaldívar, A. Ruíz-Constán, C. Duque, D. Martín-Lechado, I. Serrano, (2009). Recent large fold nucleation in the upper crust: Insight from gravity, magnetic, magnetotelluric and seismicity data (Sierra de Los Filabres–Sierra de Las Estancias, Internal Zones, Betic Cordillera). *Tectonophysics*. 463, 145-160.

Rodriguez, C.E. (2006). Earthquake-induced landslides. In: *Central America, Geology, Resources and hazards* (Bundschuh & Alvarado, Eds.). Balkema.

Rodríguez-Peces, M.J., J. García-Mayordomo, J.M. Azañón and A. Jabaloy, (2011). Regional Hazard Assessment of Earthquake-Triggered Slope Instabilities Considering Site Effects and Seismic Scenarios in Lorca Basin (Spain). *Environmental & Engineering Geoscience*. 17, 183-196.

Silva, P.G., M.A. Rodríguez-Pascua, J.L. Giner-Robles, R. Pérez-López, J. Lario, M.A. Perucha, T. Bardají, P. Huerta, E. Roquero, M.B. Bautista Davila, (2014a). Catálogo de los efectos geológicos de losterremotos de España. PG Silva y M.A. Rodríguez-Pascua (eds). IGME-AEQUA. *Riesgos Geológicos / Geotecnia*. nº4. 352 pp. Madrid.

Silva, P.G., R. Pérez-López, M.A. Rodríguez-Pascua, E. Roquero, J.L. Giner Robles, P. Huerta, A. Martínez-Graña, T. Bardají, (2014b). Macroseismic analysis of slope movements triggered by the 2011 Lorca Earthquake (Mw 5.1): Application of the ESI-07 scale. *Geogaeta*. 55.

Silva, P.G., M.A. Rodríguez-Pascua, J.L. Giner Robles, E. Roquero, R. Pérez-López, P. Huerta, T. Bardají, (2014c). Anatomy of an earthquake: Geological analysis of the Huércal-Oera AD 1863 event (Almería, SE Spain). In: *IBERFAULT II*. IGME. Madrid. pp.153-156.

Wald, D.J., T.I. Allen, (2007). Topographic slope as a proxy for seismic site conditions and amplification. *Bulletin of the Seismological Society of America.* 97, 1379-1395.

Wells, D.L., K.J. Coppersmith, (1994). New empirical relationships among magnitude, rupture length, rupture width, rupture area, and surface displacement. *Bulletin of the Seismological Society of America*. 84, 974-1002.

INQUA Focus Group on Paleoseismology and Active Tectonics

Field characterization of the most recent great earthquake on the eastern Altyn Tagh fault: A rupture between two fault bends

Elliott, A.J. (1), Oskin, M.E. (1), Liu-Zeng, J. (2)*

(1) Dept. of Earth and Planetary Sciences, University of California Davis, Davis, CA 95616. Email: ajelliott@ucdavis.edu
(2) Institute of Geology, China Earthquake Administration, Beijing, China
*Presently at Department of Earth Sciences, University of Oxford, Oxford, UK OX1 3AN

Abstract: *We map the trace, extent, and distribution of preserved offsets along a relatively fresh surface rupture of the eastern Altyn Tagh fault in Gansu Province, China. These metrics indicate the size of this paleoearthquake, which is likely the 1270-1775 AD event identified in paleoseismic investigations of Washburn et al. (2001). Importantly, we constrain the eastern extent of this rupture, which corresponds with the most highly misoriented reach of the fault, at the Aksay restraining double-bend (RDB). From there the rupture extends continuously 365 km westward, where it apparently terminates at the Akato Tagh RDB. Rupture termini at bent reaches of the fault suggest strong geometric segmentation of the Altyn Tagh during earthquakes, supporting the inference that ruptures along this major strike-slip fault may be impeded only by major changes in strike.*

Key words: *Surface rupture, rupture extent, earthquake barrier, Altyn Tagh fault, paleoearthquake, fault bend.*

INTRODUCTION

Coseismic rupture extent along a fault dictates the magnitude of an earthquake. Thus, forecasting plausible rupture lengths along strike-slip faults permits an assessment of the suite of possible earthquake sizes. To determine possible rupture lengths, we must constrain the fault properties that serve to halt propagating ruptures and map out their positions along a fault.

In this paper we compare observed rupture extent to mapped fault geometry along the eastern Altyn Tagh fault in Gansu Province, western China, in order to examine the relationship between fault geometry and coseismic rupture propagation. We map the extent and slip distribution of the most recent surface rupture along the reach of the fault within Gansu province (east of 92.8°E longitude; Fig. 1). We document the eastern terminus of this rupture where the fault attains its most highly misoriented strike, 25° clockwise from regional strike. To the west our mapping is continuous with that of prior studies, which show the rupture terminating at another restraining double-bend on its western end. Together these observations suggest that rupture along the highly linear Altyn Tagh fault may only be impeded by its widely separated double-bends, producing quasi-characteristic-type earthquakes controlled by geometry.

BACKGROUND

Rupture Termination at Steps and Bends

Modelling and field evidence have suggested that fault geometry plays a dominant role in controlling earthquake size, with the majority of historic continental strike-slip ruptures having stopped at discontinuous stepovers (Wesnousky, 2006), and numerical modelling repeatedly showing that stepovers are indeed theoretically expected to physically impede rupture propagation (King and Náblek, 1985; Harris and Day, 1993; Duan and Oglesby, 2006).

Even continuous fault stepovers, otherwise known as fault double-bends, have been implicated as barriers to rupture, due to the increased Coulomb failure stresses resolved from a regional stress field onto the bent fault segment (Duan and Oglesby, 2005; Kase and Day, 2006; Lozos et al., 2011). In the case of fault double-bends, fault strike becomes an important factor in whether or not ruptures propagate through (Lozos et al., 2011). In these models the navigability of a bend by a rupture is controlled by both the angle and length of the bent portion of the fault, with bends of over 18° reliably halting ruptures along bent segments of >5 km length. These modelling results merit calibration and verification with natural observations.

Figure 1: Location and setting of the study, showing Altyn Tagh fault and surrounding structures. Faults from HimaTibet fault database (Styron et al., 2010). Note different elevation scales in main figure and inset index figure.

Geometry and Setting of the Altyn Tagh Fault

The Altyn Tagh fault (ATF) forms the northwestern boundary of the Tibet-Qinghai Plateau, juxtaposing the plateau against the Tarim basin. This mature, sinistral fault extends for ~1800 km and exhibits cumulative slip of 350-450 km (Ritts and Biffi, 2000; Yue et al., 2001; Cowgill et al., 2003; Yue et al., 2005). Estimates of its slip rate from geology and geodesy are converging on ~1 cm/yr (e.g., Searle et al., 2011 and references therein). Its exceptionally linear trace is punctuated by restraining double-bends (Fig. 1). Many workers have postulated that the long straight segments may support unimpeded supershear rupture (Bouchon et al., 2010; Molnar and Dayem, 2010; Robinson et al., 2010). Investigating where and how such earthquakes stop is critical to forecasting possible earthquake magnitudes.

Molnar et al. (1987) recognized relatively fresh rupture on the Altyn Tagh fault to the west of Aksay bend. Paleoseismic investigations reported in Washburn et al. (2001) and Washburn et al. (2003) revealed the most recent surface rupture here to have occurred between 1215 and 1775, with overlapping event ages from three different trenches suggesting a tighter age window of 1456-1500 AD. Wang et al., (2002) and Meriaux et al., (2005) confirmed the presence of similar relatively fresh scarps within the Aksay bend. We have investigated these features in the context of coseismic rupture parameters and fault geometry.

METHODS

Mapping the Fault Rupture

Using basemaps of 60-cm resolution DigitalGlobe Quickbird satellite imagery and field surveys with differential GPS, we mapped out the fresh scarp array that characterizes the fault along this reach, identifying preserved lateral offsets of geomorphic features.

Measuring Offsets

We identified and measured small offsets along the fault in order to construct a coseismic slip distribution. Magnitudes of offset were measured along the strike of the fault between linear projections of the upstream and downstream thalwegs of small gullies. These values represent the "preferred" offset measurement, incorporating no additional assumptions about the geomorphic history or prior course of the offset channels. Minimum and maximum permissible offsets were then measured as the distance between inner and outer channel margins, respectively (Fig. 2). The difference between these and the preferred values supplied our conservative negative and positive uncertainties.

OBSERVATIONS

Coseismic Rupture Extent

The southern Altyn Tagh fault through this reach is characterized by small, relatively steep scarps and irregular moletracks (narrow, hummocky disruption of the ground resulting from local alternation between

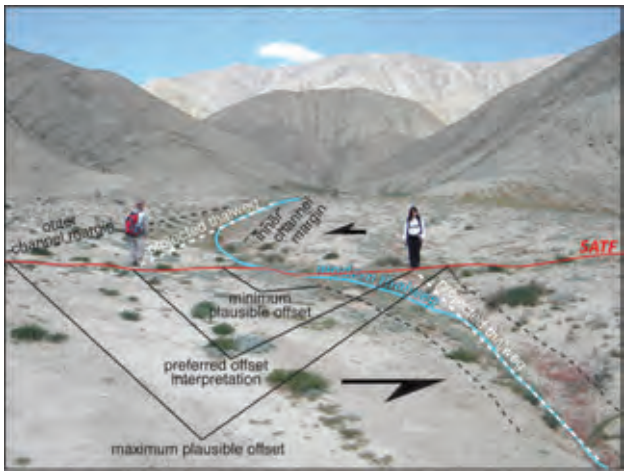

Figure 2: Illustration of offset measurement method on representative feature, including graphical representation of key parameters: minimum, preferred, and maximum measured offset.

transpression and transtension at a small scale within a strike-slip fault zone), which offset, disrupt, and cut across all geomorphic surfaces except for the bedload of modern channels. Above an elevation of 3500 m, the fault trace is distinctly characterized by wide, en echelon fissures, representing tension gashes within rigid permafrost (Fig. 3). Similar morphology is present along other high-altitude strike-slip faults in Tibet as reported by Cowgill et al. (2004) and Lin et al., (2004).

To the east, this continuous surface rupture can be traced as far as 93.52°E, beyond which the fault is not expressed in Holocene alluvial surfaces (Fig. 4). At this reach the fault strikes 100°, 25° clockwise (more transpressional) from the strike of 75° exhibited by the segments immediately outside of the Aksay bend. 5 km

Figure 3: Characteristic rupture trace morphology at high elevations, where frozen ground fractures into large rotating blocks separated by deep en-echelon fissures. 30 cm x 40 cm map-board for scale, circled at center left.

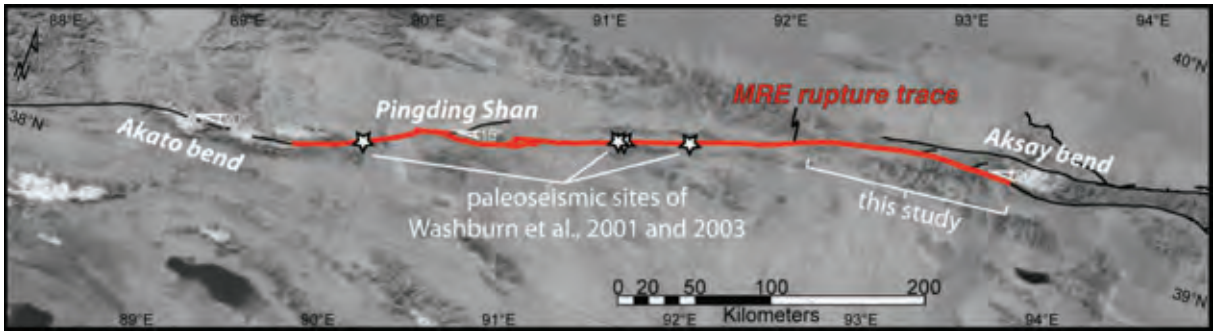

Figure 4: Mapped rupture extent of most recent event on the eastern Altyn Tagh fault. Figure represents a synthesis of mapping from this study and prior work by Washburn et al. (2001) and Washburn et al. (2003). Bend angles where rupture terminates (or doesn't) indicated on map.

east of the last evident small scarp, an alluvial fan extends across the projection of the fault undeformed. Evidence for a latest Pleistocene age of this feature is presented in Elliott et al. (2014) and Elliott et al. (in review).

From its terminus in the Aksay bend, the continuous rupture trace extends at least 95 km, to the border of Xinjiang Province, where it connects with fresh rupture as reported by Washburn et al. (2001).

Coseismic Offsets

Along this 95 km reach of fault we identify and measure 117 offsets of <15 m, a value taken to represent the maximum credible coseismic slip in a strike-slip earthquake based on historical observations. From these measurements an average coseismic slip of 5.6 m is derived.

DISCUSSION

Westward Rupture Extent

At the border between Gansu and Xinjiang provinces, the scarps we have mapped are continuous with those reported in Washburn et al. (2001), which extend westward a further 270 km to the Akato Tagh bend. In total this represents a strike-length of 365 km. A rupture of this length may be expected from such a mature, linear continental strike-slip fault, consistent with observed historic ruptures on the Kunlun, Denali, and San Andreas faults. Notably, the western terminus of the rupture as reported by this prior work also coincides with a large restraining double-bend (Fig. 5). Washburn et al. (2003) propose the alternative interpretation that the fresh scarps along this reach actually represent two distinct ruptures, separated along strike by the smaller Pingding Shan double-bend. In this case the total rupture length would be 250-300 km, but would still terminate at a restraining bend.

Inferred Earthquake Magnitude

Based on empirical scaling relationships derived in Wells and Coppersmith (1994), the average slip we observe implies an earthquake in excess of M7.5. A rupture length of 250-365 km places the magnitude between 7.8 and 8.0, again consistent with more recent ruptures along the planet's major strike-slip faults.

CONCLUSIONS

We document the length, average slip, and termini of the most recent rupture on the eastern Altyn Tagh fault. Our remotely sensed and field-verified measurements reveal a 365 km long rupture with an average slip of 5.6 m, suggesting a M>7.8 earthquake that likely corresponds to the event dated at 1215-1775 AD by Washburn et al. (2001) and Washburn et al. (2003). Importantly, both ends of this rupture coincide with major restraining double-bends, suggesting geometric control on rupture extent along this fault. Our observations confirm the predictions of numerical models that ruptures are halted by restraining bends of >18°, and support the inferences of Bouchon et al. (2010), Molnar and Dayem (2010), and Robinson, Das, and Searle (2010) that ruptures along this exceptionally straight, mature strike-slip fault may be impeded only by large changes in strike.

Acknowledgements: This work was supported by U.S. National Science Foundation (NSF) grant EAR-1050060 as well as an NSF graduate student fellowship. This abstract summarizes work presented as Chapter 2 of Elliott's PhD dissertation and submitted for publication in early 2015 (Elliott et al., in review).

References

Bouchon, M., H. Karabulut, M.P. Bouin, J. Schmittbuhl, M. Vallée, R. Archuleta, S. Das, F. Renard, and D. Marsan, (2010). Faulting characteristics of supershear earthquakes. *Tectonophysics*. 493(3-4), 244–253, doi:10.1016/j.tecto.2010.06.011.

Cowgill, E., A. Yin, T.M. Harrison, and X.F. Wang, (2003). Reconstruction of the Altyn Tagh fault based on U-Pb geochronology: Role of back thrusts, mantle sutures, and heterogeneous crustal strength in forming the Tibetan Plateau. *Journal of Geophysical Research*. 108(B7), doi:10.1029/2002jb002080.

Cowgill, E., A. Yin, J.R. Arrowsmith, W.X. Feng, S.H. Zhang, W. Xiao Feng, and Z. Shuanhong, (2004). The Akato Tagh bend along the Altyn Tagh fault, northwest Tibet 1: Smoothing by vertical-axis rotation and the effect of topographic stresses on bend-flanking faults. *Geological Society of America Bulletin*. 116(11), 1423, doi: 10.1130/B25359.1.

Duan, B., and D.D. Oglesby, (2005). Multicycle dynamics of nonplanar strike-slip faults. *Journal of Geophysical Research*. 110(B3), doi:10.1029/2004JB003298.

Duan, B., and D.D. Oglesby, (2006). Heterogeneous fault stresses from previous earthquakes and the effect on dynamics of

parallel strike-slip faults, *Journal of Geophysical Research*. 111(B5), doi:10.1029/2005JB004138.

Elliott, A.J., M.E. Oskin, J. Liu, Y. Shao, (2014). *Slip rate gradients along parallel strands of the eastern Altyn Tagh fault confirm modeled rupture behavior at a transpressional bend* [conference abstract]. American Geophysical Union Fall Meeting 2014, San Francisco, USA.

Elliott, A.J., M.E. Oskin, J. Liu, Y. Shao (in press). Rupture termination at restraining bends: the last great earthquake on the Altyn Tagh fault. *Geophysical Research Letters*.

Harris, R.A., and S.M. Day, (1993). Dynamics of Fault Interaction - Parallel Strike-Slip Faults. *Journal of Geophysical Research-Solid Earth*. 98 (B3), 4461–4472, 1993.

Kase, Y. and S.M. Day, (2006). Spontaneous rupture processes on a bending fault. *Geophysical Research Letters*. 33(10). doi: 10.1029/2006GL025870.

King, G., & J. Nábělek, (1985). Role of Fault Bends in the Initiation and Termination of Earthquake Rupture. *Science*. 228(4702), 984–987.

Lin, A., J. Guo, and B. Fu, (2004). Co-seismic mole track structures produced by the 2001 Ms8.1 Central Kunlun earthquake, China. *Journal of Structural Geology*. 26, 1511–1519, doi:10.1016/j.jsg.2004.01.005.

Lozos, J.C., D.D. Oglesby, B. Duan, and S.G. Wesnousky, (2011). The Effects of Double Fault Bends on Rupture Propagation: A Geometrical Parameter Study. *Bulletin of the Seismological Society of America*. 101(1), 385–398, doi:10.1785/0120100029.

Mériaux, A.S., P. Tapponnier, F.J. Ryerson, X. Xu, G. King, J. Van der Woerd, R.C. Finkel, H. Li, M.W. Caffee, Z.Q. Xu, and W.B. Chen, (2005). The Aksay segment of the northern Altyn Tagh fault: Tectonic geomorphology, landscape evolution, and Holocene slip rate. *Journal of Geophysical Research*. 110(B4), B04,404, doi:10.1029/2004JB003210.

Molnar, P., B. Burchfiel, L. K'uangyi, and Z. Ziyun, (1987). Geomorphic evidence for active faulting in the Altyn Tagh and northern Tibet and qualitative estimates of its contribution to the convergence of India and Eurasia. *Geology*. 15(3), 249–253, doi: 10.1130/0091-7613(1987)15¡249.

Molnar, P., and K.E. Dayem, (2010). Major intracontinental strike-slip faults and contrasts in lithospheric strength. *Geosphere*. 6 (4), 444–467, doi:10.1130/GES00519.1.

Ritts, B.D., and U. Biffi, (2000), Magnitude of post-Middle Jurassic (Bajocian) displace- ment on the central Altyn Tagh fault system, northwest China, *Geological Society of America Bulletin*. 112(1), 61–74.

Robinson, D., S. Das, and M. Searle, (2010). Earthquake fault superhighways. *Tectonophysics*. 493(3-4), 236–243, doi:10.1016/j.tecto.2010.01.010.

Searle, M., J.R. Elliott, R.J. Phillips, and S.L. Chung, (2011). Crustal lithospheric structure and continental extrusion of Tibet. *Journal of the Geological Society, London*. 168, 633–672, doi:10.1144/0016-76492010-139.

Styron, R., M.H. Taylor, and K. Okoronkwo, (2010), Database of Active Structures From the Indo-Asian Collision. *Eos*. 91(20), 0–1. doi:10.1130/GES00217.1.Wessel

Wang, F., X. Xu, R. Zheng, W. Chen, P. Tapponnier, (2002). Segmentation of surface ruptures on the eastern segment of the Altyn Tagh fault zone [Chinese with English abstract]. *Seismology and Geology*. 24(2), 145–158.

Washburn, Z., J.R. Arrowsmith, S.L. Forman, E. Cowgill, X.F. Wang, Y.Q. Zhang, Z.L. Chen, W. Xiaofeng, Z. Yueqiao, and C. Zhengle, (2001). Late Holocene earth- quake history of the central Altyn Tagh fault. China, *Geology*. 29(11), 1051–1054, doi:10.1130/0091-7613.

Washburn, Z., and J.R. Arrowsmith, (2003). Paleoseismology of the Xorxol segment of the central Altyn Tagh fault, Xinjiang, China. *Annals of Geophysics*. 46 (5).

Wells, D., and K. Coppersmith, (1994). New empirical relationships among magnitude, rupture length, rupture width, rupture area, and surface displacement. *Bulletin of the Seismological Society of America*. 84(4), 974–1002.

Wesnousky, S.G., (2006). Predicting the endpoints of earthquake ruptures. *Nature*. 444(7117), 358–360, doi: 10.1038/Nature05275.

Yue, Y.J., B.D. Ritts, and S.A. Graham, (2001). Initiation and long-term slip history of the Altyn Tagh fault. *International Geology Review*. 43 (12), 1087–1093.

Yue, Y.J., S.A. Graham, B.D. Ritts, and J.L. Wooden, (2005). Detrital zircon provenance evidence for large-scale extrusion along the Altyn Tagh fault. *Tectonophysics*. 406 (3-4), 165–178, doi: 10.1016/J.Tecto.2005.05.023.

INQUA Focus Group on Paleoseismology and Active Tectonics

Integrated geophysical surveys supporting shallow subsurface faults detection and characterization : two case studies in the Central Appennines

Eulilli, V. (1), Ferri, F. (1), Puzzilli, L.M. (1)

(1) ISPRA – Geological Survey of Italy, via Vitaliano Brancati 60, 00144 Roma, Italy. Email: valeria.eulilli@isprambiente.it

Abstract: *This paper focuses on the joint application of high resolution near-surface geophysical methods, including electric resistivity tomography (ERT), seismic refraction tomography (SRT) and ground penetrating radar (GPR), to successfully support paleo-seismological studies concerning the San Demetrio Fault System characterization in San Demetrio ne' Vestini (AQ) municipality and to investigate a newly identified fault-zone in the framework of Seismic Microzonation Studies (MZS) of Magliano de' Marsi (AQ) municipality.*

Key words: *Applied geophysics, fault detection, Abruzzo.*

INTRODUCTION

After the 2009 (Mw 6.3) L'Aquila earthquake, the identification and characterization of active and capable faults represented more and more a priority issue in the framework of Seismic Microzonation Studies (MZS) still ongoing at present and financially supported for the whole Country by the Italian Government (art. 11 Law n. 77/2009). Near surface applications of geophysics often support the detection of shallow subsurface faults, especially when the standard approach based on the interpretation of aerial photos, morphotectonic investigations, geological field surveys, etc. is hampered by geomorphological processes or man-made activities.
This paper deals with the joint application of geophysical methods used to support the characterization of the San Demetrio Fault System inside San Demetrio ne' Vestini (AQ) (placed within the 2009 earthquake's most damaged area) and to investigate a newly identified fault-zone in Magliano dei Marsi (AQ), town affected by catastrophic earthquakes in 1904 (Mw 5.7) and in 1915 (Fucino, Mw 7.0). In both cases, integrated geophysical methods provided detailed and valuable information on the subsurface setting of the investigated areas, confirming the existence of some faults.

GEOLOGICAL AND TECTONIC SETTING

San Demetrio ne 'Vestini is placed within the Middle Aterno Valley basin, in the Abruzzi Apennines. The area is located within a complex tectonic depression which includes the Aquilan basin and extends to a length of about 30 km, striking NW-SE, between the structural units of the Gran Sasso, to the North, and Velino-Sirente-Mounts d'Ocre, to the South. An important NW-SE trending fault system with Quaternary activity limits this depression at NE (Paganica - San Demetrio Fault System SDFS), (Working Group MS AQ, (2010).
In particular, the municipality of San Demetrio ne' Vestini is interested by one specific fault, part of the SDFS, classified as active and capable (Working Group MS Aquila, 2010).

Magliano dei Marsi (AQ) is located at the left flank of the Salto river valley, on the southern foothills of Velino mount and about 10 kms NW of the Fucino plain.
Two active faults in this area have been recently inferred through field geological studies and borehole data during the MZS of the municipality (De Caterini et al., 2013; 2015).
The Quaternary geology of both sites is characterized by fluvial, lacustrine and alluvial sediments covered by Holocene colluvia and detrital deposits (APAT, 2006a, 2006b).

INTEGRATED GEOPHYSICAL SURVEYS

A multimethod approach to the geophysical characterisation of active faults is increasingly recognized as the most promising investigation strategy (Improta et al., 2010). In this paper we present a successful joint application of electrical resistivity tomography (ERT), seismic refraction tomography (SRT) and ground penetrating radar (GPR) using specific data acquisition and processing techniques for high resolution imaging of shallow faults. Over the last decades many authors have demonstrated the ERT method usefulness in locating tectonic structures and in the reconstruction of their characteristics as the amplitude of the fractured area, deformation style, and presence of fluid circulation (Giocoli et al., 2011, Siniscalchi et al., 2010). The SRT method, within the well known limitations of refraction seismics, allows the detection of velocity anomalies in subsurface deposits and can provide accurate information about the location and geometry of discontinuities of associated colluvial deposits of appropriate size (Atre & Carpenter, 2010). The GPR is considered a powerful tool for the definition of the geometry of sedimentary and tectonic structures associated with shallow faults (Salvi et al., 2003). In both surveys the ERT 2D models were obtained by an inversion routine based on the smoothness-constrained least-squares method proposed by De Groot-Hedlin and Constable (1990) with further improvement by Loke & Barker (1996), while the SRT velocity models were

obtained using a WET Wavepath Eikonal Traveltime tomographic inversion (Schuster & Quintus-Bosz, 1993). The GPR radargrams were obtained applying standard 1D signal processing and using a time-depth conversion velocity of 0,1 m/nsec (Roberts et al., 2010).

GEOPHYSICAL SURVEY ACROSS THE SAN DEMETRIO FAULT SYSTEM

The main geophysical survey performed across SDFS inside San Demetrio ne' Vestini (AQ) is located at the NW bound of the settlement (*Figure 1a)*. We investigated a NE-SW section, first through ERT followed by SRT and GPR surveys overlapping most of the geoelectrical profile. The positioning of this profile was decided on the basis of ISPRA field geomorphological investigations that inferred the presence of a normal fault in the area (Working Group MS Aquila, 2010) and provided a detailed geological map. The ERT image (*Figure 1b)* shows within a framework of high resistivity (max > 1000 Ωm) due to the presence of coarse deposits, two shallow conductive bodies, attributable to sandy-loam deposits ten meters thick, separated by an area of medium-high resistivity (95-200 Ωm). The marked lateral variation present at 63 m (black arrow in *Figure 1b)* represents the more interesting discontinuity, being a clear indication of a possible fault reaching the surface.

The SRT image (*Figure 1c*) shows an upper velocity layer, 2 to 4 meters thick, with prevailing Vp values ≤ 600 m/s. At 23 m a lateral gradient marks the lowering of this velocity layer towards SW: the shape of this Vp low zone is consistent with the effect of the colluvial wedge of a normal fault. The intermediate depth section of the velocity model reveals the presence of velocity inversions and is bounded in depth by a strong Vp gradient (Vp 1000 – 1500 m/s). These isovelocities also show a step like feature that could be the deeper effect of the normal fault but the further continuation of the discontinuity is unclear, probably due to the greater uncertainties in this part of the Vp inversion model.
The GPR image (*Figure 1d*) shows the higher resolution of the GPR compared to the ERT and SRT. In particular, across the shallow fault zone imaged by ERT and SRT, it highlights the presence of a very complex buried architecture with at least two fault traces seeming to reach the surface.
The overall consistency between geophysical models and local geology has been supported by stratigraphy data from a nearby shallow borehole. The subsequent paleoseismological trench (*Figure 1*e) dug by ISPRA (Blumetti et al., 2015) has led to the identification of a normal fault affecting the Holocene deposits, validating the fault location pinpointed by the geophysical surveys. It is worth to note that the detected fault is not positioned on a topographic slope break, moreover no other surface evidence is present.

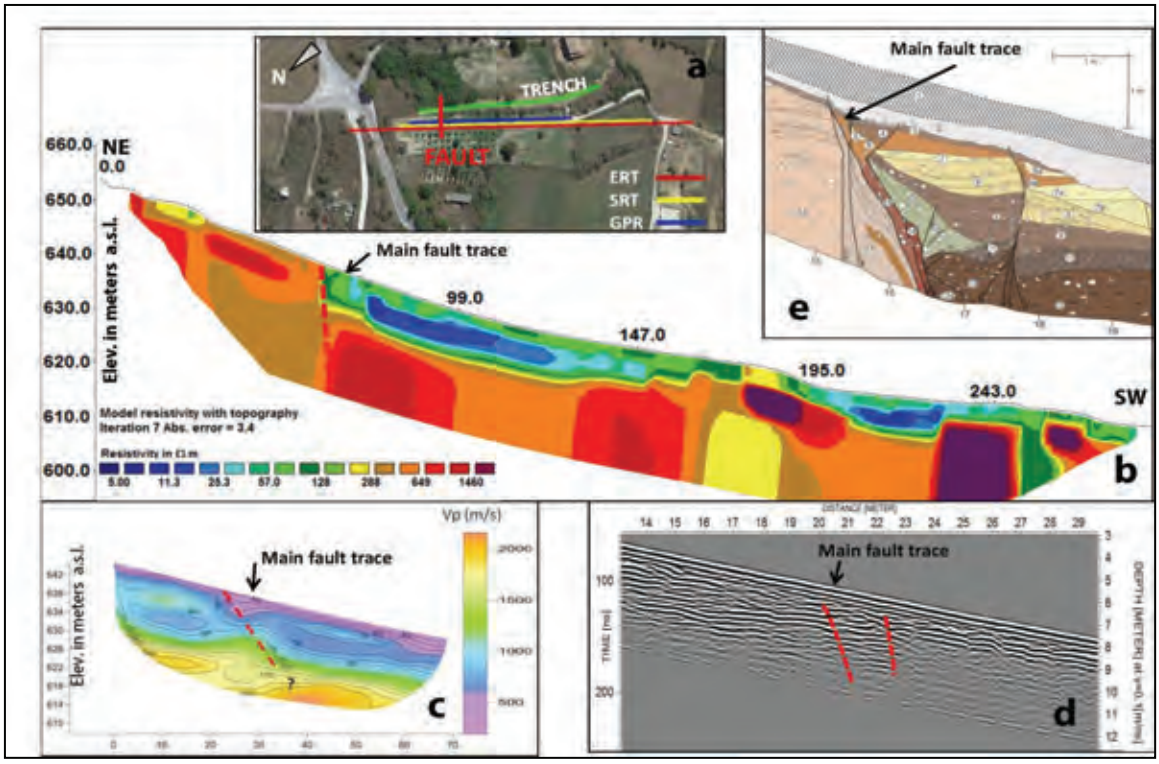

Figure 1: (a) map view of the geophysical profiles and trench in San Demetrio ne' Vestini area; (b) ERT model; (c) SRT model; (d) GPR radargram; (e) portion of the trench log with main fault (modified from Blumetti et al., 2015). Main geophysical discontinuities shown by red dashed lines.

GEOPHYSICAL SURVEY IN MAGLIANO DE' MARSI (AQ) AREA

The geophysical investigation has been performed along a WNW - ESE section starting from the western flank of the Cotecorno hill where Miocene calcarenites outcrop (*Figure 2a*), SRT and GPR surveys overlap most of the geoelectrical profile. The final ERT model (*Figure 2b*) shows a distribution of the resistivity characterized by very high values (up to 1500 Ωm) from the surface to about 15 m in depth and by a deeper conductive layer reaching the bottom of the geoelectrical model (~ 20 m). The first clear conductive anomaly along the ERT is visible at 120 m - 130 m and provides evidence of a normal fault juxtaposing the calcarenitic Miocenic bedrock and the Pleistocenic gravel deposits. The latter are characterized by a gradually increasing thickness eastward, according to the expected geological model of this area. At 175 m the gravel body is interrupted by a sharp discontinuity revealed by a conductive anomaly and a clear lowering of the top of the gravels to East, allowing to correlate this anomaly with the presence of a normal fault. The SRT Vp image (*Figure 2d*) shows an upper layer with Vp values ≤ 500 m/s with a variable thickness between 1.5 and 3.5 m. At 25 m the isovelocity contours clearly show a fault lowering the calcarenites and define a possible colluvial wedge-like geometry.

Starting from 30 m the Vp image shows, at the depth of ~ 8 m, a sharp vertical inflection of the contours caused by an abrupt deepening of the bedrock along a deeper discontinuity that does not appear to affect the shallow deposits. Near 90 m (*Figure 2d*) a sharp gradient marks the presence of a possble colluvial wedge of the normal fault imaged by ERT and GPR. The GPR image (*Figure 2c*) shows a remarkable overall consistency with the ERT and SRT models: it complements them mostly for the first 4-6 meters from surface. The presence of many faults affecting the shallow layers are clearly indicated (*Figure 2d)* by abrupt changes of continuity and/or dipping of reflectors along the whole GPR section. The integrated survey thus improved the knowledge of the local geology along the profile, revealing a number of previously unknown shallow discontinuities (by ERT and mainly by GPR) and also a deeper normal fault (mainly by SRT). Moreover, on the basis of the age attributed by Frezzotti & Giraudi (1992) to the Pleistocenic coarse deposits, at least some faults inferred by geophysical evidences must be considered as active and further investigations are highly recommended.

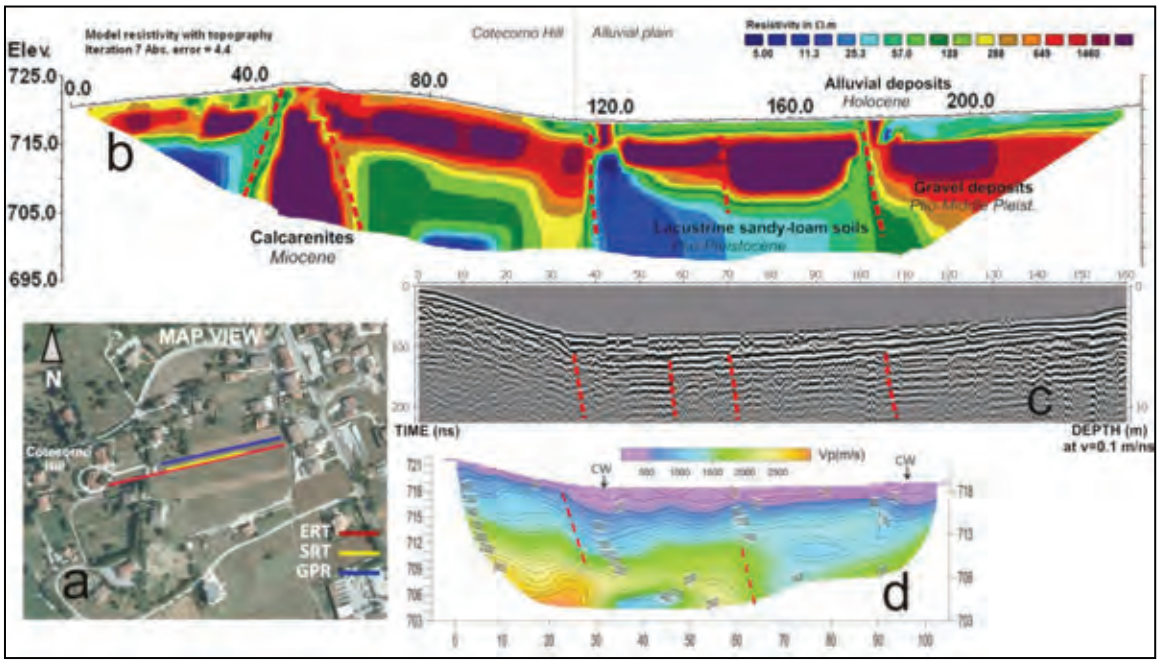

Figure 2: Geophysical profiles in Magliano de Marsi area: (a) map view of the their location; (b) ERT model; (c) GPR radargram; (d) SRT model. Main geophysical discontinuities shown by red dashed lines.

CONCLUSIONS

The joint application of geophysical methods in high resolution mode allowed a meaningful reduction of ambiguities, normally arising from the use of each single indirect method. The careful survey design and data processing has been effective to improve the sub-surface geological model of the investigated areas, providing valuable information for: 1) the accurate location of the faults, particularly of those with poor or null exposure at the ground surface; 2) fault characterization in terms of geometry and last activity

age; 3) the best positioning for paleoseismological trenches; 4) the extension at depth of the observations made in existing trench walls.

On the basis of the results described above and of previous experiences by many authors, we recommend a standardized use of integrated geophysical surveys in Level 1 of MZS.

Acknowledgements: We would like to thank for their support during field operations Dr. B. Porfidia, D. Matarazzo, C. Quadrozzi, D. Pompili, E. Mariani, C. Tugliozzi of ISPRA Geophysical Service. We also thank the San Demetrio ne' Vestini and Magliano de' Marsi Municipalities; Dr. G. De Caterini and Dr. G. Leoni for providing geological data of the Magliano de' Marsi area.

References

APAT, (2006a). *Carta Geologica d'Italia alla scala 1:50.000. Foglio 359 L'Aquila*. SELCA, Firenze.

APAT, (2006b). *Carta Geologica d'Italia alla scala 1:50.000. Foglio 368 Avezzano*. SELCA, Firenze.

Atre, S.R., P.J. Carpenter, (2010). Identification of cross-valley faults in the Maynardville Limestone Oak Ridge Reservation, Tennessee, using seismic refraction tomography. *Environ Earth Sci*. 60, 1245–1256.

Blumetti, A.M., P. Di Manna, E. Vittori, V. Comerci. L. Guerrieri, (2013). Facing fault displacement hazard in Italy through palaeoseismic investigations: the San Demetrio ne' Vestini (AQ) example. In: *Proceedings of 4th International INQUA Meeting on Paleoseismology, Active Tectonics and Archeoseismology (PATA)*. 9-14 October 2013, Aachen, Germany.

Blumetti, A.M., P. Di Manna, E. Vittori, V. Comerci & L. Guerrieri, (2015). Paleoseismicity data on the San Demetrio ne' Vestini fault (L'Aquila Basin, Central Italy). This issue.

De Caterini, G., G. Leoni, A. Santoponte, P. Zaffiro, G. Pezzo, (2013). Studio di Microzonazione Sismica – Livello 1 - Comune di Maglano de' Marsi (AQ). Unpublished report.

De Caterini, G., A.M. Blumetti, G. Coen, G. Della Ventura, V. Eulilli, F. Ferri, L. Guerrieri, G. Leoni, F. Lucci, M. Mariani, L.M. Puzzilli, A. Santoponte, E. Vittori, P. Zaffiro, (2015). New preliminary data on Late Quaternary evolution of Magliano dei Marsi area (Abruzzo, Central Italy). This issue.

De Groot-Hedlin, C., S. Constable, (1990). Occam's inversion to generate smooth, two-dimensional models form magnetotelluric data. *Geophysics*. 5.

Frezzotti, M., C. Giraudi, (1992). Evoluzione geologica tardo-pleistocenica ed olocenica del conoide complesso di Valle Majelama (Massiccio del Velino, Abruzzo). *Il Quaternario*. 5(1), pp 33-50.

Giocoli, A., P. Galli, B. Giaccio, V. Lapenna, P. Messina, E. Peronace, G. Romano, S. Piscitelli, (2011). Electrical Resistivity Tomography across the Paganica-San Demetrio fault system (L'Aquila 2009 earthquake). *Bollettino di Geofisica Teorica ed Applicata*. Vol. 52, n. 3, pp. 457-469; September 2011.

Improta, L., L. Ferranti, P.M. De Martini, S. Piscitelli, P. Bruno, P. Burrato, R. Civico, A. Giocoli, M. Iorio, G. D'Addezio, L. Maschio, (2010). Detecting young, slow-slipping active faults by geologic and multidisciplinary high-resolution geophysical investigations: A case study from the Apennine seismic belt, Italy. *J. Geophys.Res*. 115, B11307.

Loke, M.H., R.D. Barker, (1996). Rapid least-squares inversion of apparent resistivity pseudosections using a quasi-Newton method. *Geoph. Prosp*. 44, 131-152.

Roberts, G.P., B. Raithatha, G. Sileo, A. Pizzi, S. Pucci, J.F. Walker, M. Wilkinson, K. McCaffrey, R.J. Phillips, A.M. Michetti, L. Guerrieri, A.M. Blumetti, E. Vittori, P. Cowie, P. Sammonds, P. Galli, P. Boncio, C. Bristow & R. Walters, (2010). Shallow subsurface structure of the 2009 April 6 Mw 6.3 L'Aquila earthquake surface rupture at Paganica, investigated with ground-penetrating radar. *Geophysical Journal International*. 183, 774–790.

Salvi, S., F.R. Cinti, L. Colini, G. D'Addezio, F. Doumaz and E. Pettinelli, (2003). Investigation of the active Celano-L'Aquila fault system, Abruzzi (central Apennines, Italy) with combined ground-penetrating radar and palaeoseismic trenching. *Geophys. J. Int*. 155, 805-818.

Schuster, G, A. Quintus-Bosz, (1993). Wavepath eikonal traveltime inversion: Theory. *Geophysics*. 58(9), 1314-1323.

Siniscalchi, A., S. Tripaldi, M. Neri, S. Giammanco, S. Piscitelli, M. Balasco, B. Behncke, C. Magri, V. Naudet, E. Rizzo, (2010). Insights into fluid circulation across the Pernicana Fault (Mt. Etna, Italy) and implications for flank instability. *Journal of Volcanology and Geothermal Research*. 193, 137-142.

Working Group MS AQ, (2010). Microzonazione sismica per la ricostruzione dell'area aquilana. *Regione Abruzzo - Dipartimento della Protezione Civile*, *L'Aquila*, 3 vol. e 1 DVD.

INQUA Focus Group on Paleoseismology and Active Tectonics

paleoseismicity.org

Earthquake- induced Geomorphology: A Neotectonic Study at the Front of the Alps (Lake Thun & Aare Valley, Switzerland)

Fabbri, S.C. (1), Herwegh M. (1), Schlunegger, F. (1), Volken, S. (2), Möri, A. (2), Anselmetti, F.S. (3)

(1) Institute of Geological Sciences, University of Bern, Baltzerstrasse 1+3, 3012 Bern, Switzerland.
Email: stefano.fabbri@geo.unibe.ch
(2) Bundesamt für Landestopografie swisstopo, Seftigenstrasse 264, CH-3084 Wabern
(3) Institute of Geological Sciences and Oeschger Centre of Climate Change Research, University of Bern, Baltzerstrasse 1+3, 3012 Bern, Switzerland

Abstract: *We present a multi-disciplinary two-step approach to assess the potential for seismic hazard of the Aare valley and perialpine Lake Thun (Switzerland). High-resolution seismic images and multibeam-bathymetric data, complemented by field observations represent the tools to identify potentially active seismogenic fault structures. Several second-order earthquake effects such as subaqueous mass movements, seismites and liquefaction structures have been observed in Lake Thun and ultimately document the seismic activity of the study area. A first investigation of possibly first-order active structures is presented in the scope of this study.*
Recently acquired bathymetric data in Lake Thun reveal significant morphologic depressions aligning with an observed lineament on land. Furthermore, high-resolution seismic images indicate potential fault structures in Lake Thun. However, their continuation with depth has to be verified with a multichannel seismic campaign, scheduled for March 2015.

Key words: *Paleoseismology, Seismic survey, Bathymetry, Geomorphology, Lake Thun.*

INTRODUCTION

To understand the hazard of future earthquakes and their associated damage, a thorough analysis of geological evidences of past events is absolutely vital. This study aims to find such evidences in the form of surface expressions related to recently active tectonic fault structures in terrestrial as well offshore areas.
A compilation of paleoseismic data over several lakes along the northern margin of the Central Swiss Alps showed that earthquake-triggered subaquatic mass movements occur with a return period of roughly 1'000 - 2'000 years (Strasser et al., 2013). Strong earthquakes (i.e. intensities >VI-VII) are considered as main triggers of subaquatic slope failures and reflect recent tectonic activity in the Alpine region. Only spontaneously collapsing shorelines and deltas are exceptions to this rule due to their often quickly accumulated sediment load. The larger of these events (i.e. Magnitude >6) are expected to produce surface ruptures due to the size and displacement of the slipping surface. However, such first-order evidence as, for instance, offset moraine crests and fluvial terrace risers, deflected river courses and fault scarps, are rare-to-absent in the field. Likewise, only a few studies successfully showed the existence of active faults cutting through Alpine nappe stacks (Sue et al., 2007; Ustaszewski et al., 2007).
The expected high preservation potential of a lake makes it the ideal environment to find earthquake-caused topographic offsets. This contrasts to onland conditions, where terrestrial erosional surface processes complicate their preservation.
The study area covers the upper Aare valley between Interlaken and Bern and crosses the North Alpine nappe front (see figure 1). The overdeepened basin of Lake Thun, located in the easternmost part of the study area, is surrounded by steep flanks of the Helvetic and Penninic thrust nappes. Farther to the west, the topography descends to the subalpine Molasse which, in turn, builds the transition to the Alpine foreland. The valley is, based on instrumental earthquake solutions, dominated by a strike-slip stress regime with steeply dipping fault planes (Kastrup et al., 2004).

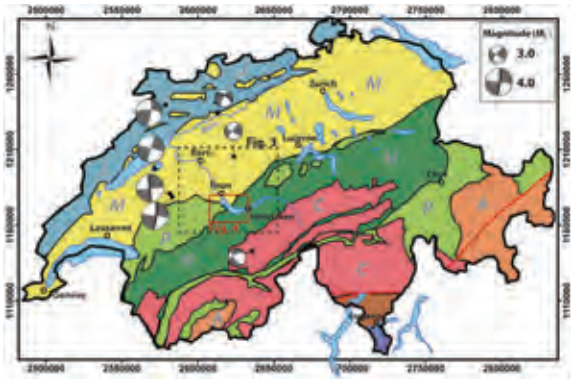

Figure 1: Principal tectonic units in Switzerland. J: Jura mountains; M: Molasse basin, H: Helvetic nappes, P: Penninic nappes, C: Crystalline basement, A: Austroalpine nappes. The six fault plane solutions are based on earthquakes occurring between 1979 and 1995. Thick black lines mark the orientation of known active fault planes (Kastrup et al., 2004).The coordinate system is given in meters (Swiss grid CH1903+).

INQUA Focus Group on Paleoseismology and Active Tectonics

APPROACH & METHOD

The perimeter lines up with the Lake Lucerne and Lake Zurich areas, which proved to show significant paleoseismological activity along the Alpine arc and its foreland (Strasser et al., 2006). In addition to the earthquake catalogue of Switzerland ECOS-09 (Fäh et al., 2011) covering the time span between AD 250 till the end of 2008, small-scale deformation structures (seismites), turbidite deposits and liquefaction structures ultimately prove the recent tectonic activity, and have all been observed in Lake Thun as shown in figure 2 (Wirth et al., 2011). In addition, different phases of neotectonic activity are recorded by damaged speleothems and broken soda straws as it has been reported from the nearby St. Beatus cave and the Siebenhengste-Hohgant cave system (Becker et al., 2012).

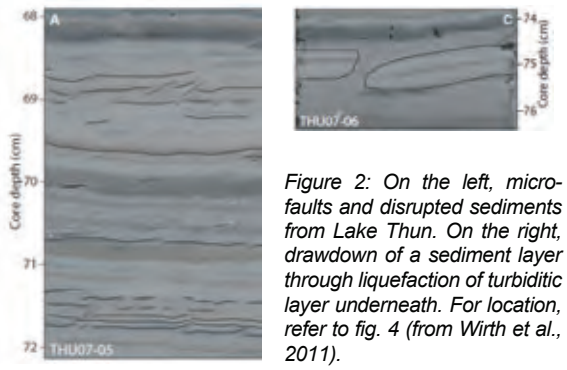

Figure 2: On the left, micro-faults and disrupted sediments from Lake Thun. On the right, drawdown of a sediment layer through liquefaction of turbiditic layer underneath. For location, refer to fig. 4 (from Wirth et al., 2011).

In this study, we present a multi-disciplinary two step-approach to characterize potentially active faults in the Aare valley.

Step 1: Offshore methods
In a first step, we focused our investigation on Lake Thun starting with a review of high-resolution seismic data (3.5 kHz pinger, zero-offset) of Lake Thun showing potential faults at the lake bottom (Wirth et al., 2011). This data is complemented by a multibeam bathymetric survey using a Kongsberg EM2040 multibeam echo sounder (Kongsberg Maritime, Horten, Norway), carried out in September 2014. The positioning system being used for the bathymetric campaign was a Leica GX1230 GNSS receiver (Leica Geosystems, Heerbrugg, Switzerland) in combination with the swispos GIS/ GEO real-time kinematic positioning service (Swiss Federal Office of Topography, Wabern, Switzerland). This allows a real time correction of the data which yields in an improved accuracy of the positioning from a few meters to 2-3 centimeters and, finally, in a lake-bottom resolution of a few decimeters. An overview of the bathymetric map is given in figure 4.

Step 2: Onshore methods
At a second stage, we extended our investigation to terrestrial areas inspecting LiDAR data and orthophotographs (courtesy of swisstopo), correlating lake observations with those on land. Promising identification of such features will be compared to the distribution of epicenters provided by ECOS-09 (Fäh et al., 2011).

DISCUSSION

In the last 300 years, there were six earthquakes with moment magnitudes Mw ≥4.3 and intensities I_0 ≥VI in the area of the upper Aare valley (see table 1).

Table 1: List of recent earthquakes in the vicinity of Lake Thun (Fäh et al., 2011).

Year	Mw	I_0	Location	Epicentral Distance to Lake Thun [km]
1898	4.8	VI	Kandersteg	ca. 10
1885	4.9	VII	Zweisimmen	ca. 30
1881	4.8	VII	Bern	ca. 20
1827	4.3	V-VI	Wengen	ca. 10
1774	4.7	VI	Bern	ca. 30
1729	5.2	VI	Frutigen	ca. 10

ECOS-09 documents 338 single events in the time span between AD 1569 and 2008 within the applied rectangular perimeter (Aarberg [2'587'589/ 1'210'279] till Finsteraahorn [2'652'743/ 1'154'232]) as indicated in figure 1. No events between 250 and 1569 are documented by ECOS-09 in the study area.

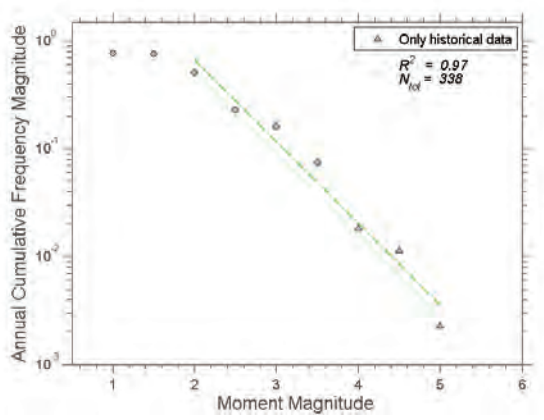

Figure 3: Annual cumulative frequency of earthquakes as function of moment magnitude in the area of the upper Aare valley between Bern and Interlaken. The used perimeter is indicated in figure 1.

From figure 3, we would expect one Mw= 3 earthquake about every 10 years and an Mw= 4 event every 100 years. The cut-off magnitude is difficult to estimate, but magnitudes smaller than 2 or even 2.5 are likely to be incomplete for the time span of about 440 years. Events documented in the vicinity of Lake Thun are illustrated in figure 4, including the larger event close to Frutigen with a moment magnitude Mw =5.2. A recently recorded earthquake swarm, initiated on April 2014 with more than 260 events till December 2014, reveals the seismic activity of the region (Swiss Seismological Service, 2015). Its relation to the Frutigen earthquake (AD 1729) cannot

be entirely ruled out. However, a first analysis of relocated hypocenters suggests an ENE dipping plane, being in agreement with the regional stress field (pers. comm., Swiss Seismological Service).

Seismic survey

The visual evaluation of the 3.5 kHz high-resolution seismic data and its structural interpretation was complicated by several artefacts such as diffraction hyperbola, multiples, bow-ties and acoustic blanking due to gas-rich sediments. Nevertheless, we observed a few structures, which deserve further specification. Their penetration and continuation into the bedrock will be investigated during a multichannel seismic campaign scheduled for March 2015, since, at this stage, we cannot entirely rule out the possible effect of the bedrock topography causing similar structures.

Bathymetric survey

The bathymetric map in figure 4 reveals several distinct subaqueous mass movements and the deposits of at least two rockfalls are clearly identifiable ("Ralligen" and "Därligen" rockfalls). However, the number of mass-movement deposits seismically and bathymetrically imaged is so large that other trigger mechanisms than solely earthquakes are very likely. The artificial deviation of the Kander river course in 1714, shortcutting it into Lake Thun, created a sudden huge increase in sediment input resulting in rapid sediment accumulation and the subsequent destabilization of slope sediments, and therefore increasing the sensitivity dramatically to subaquatic slope failure (Girardclos et al., 2007; Nakajima and Kanai, 2000; Wirth et al., 2011). The doubling or even tripling of the sediment input since the Kander redirection (Sturm and Matter, 1972; Wirth et al., 2011) complicates the identification of offset lake-bottom structures. However, other evidences such as cone-like morphologic depressions line up with geomorphologic findings on land.

Field studies

An observed lineament on LiDAR data crosses a gravel pit at site A (see figure 4 for location). The lineament cuts through a large moraine crest and leads into two morphologic depression in Lake Thun revealed by bathymetric data. The alluvial deposits of the gravel pit at site A are made of unconsolidated gravels with a significant amount of sand. The larger clasts of the gravel deposits reveal generally a horizontal bedding. We found, however, a distinctive offset by ~0.5 m with steeply dipping clast in the center of the section. An apparent dip analysis carried out along the steepened clasts revealed in the centered section significantly higher dips than the surrounding clast.

The unconsolidated state and the absence of overburden deformation indicate that the deposits have not been overprinted by a glacier and hence can be assumed to be post-LGM deposits. This would indicate that the structure could be caused by subrecent tectonic movements along a steeply dipping plane.

At site B in figure 5, the 'Untere Süsswasser Molasse' (USM - Lower Freshwater Molasse) reveals an overturned anticline with a steeply dipping limb in direct contact

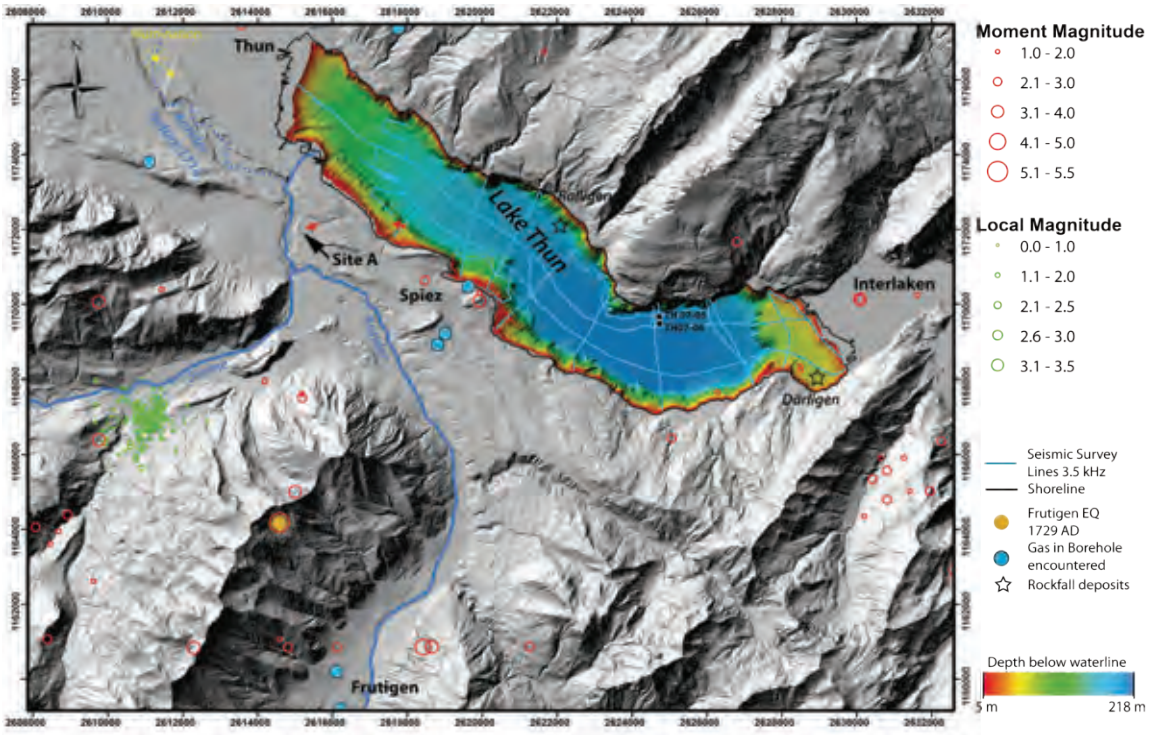

Figure 4: LiDAR data (courtesy of swisstopo) with recently acquired bathymetric data of Lake Thun. Historic earthquakes are illustrated as red circles. Green circles reflect an earthquake swarm initiated on April 2014 with more than 260 events (Swiss Seismological Service, 2015). Bright blue dots show encountered gas escapes while drilling and probing (Office for water and waste, canton Bern). The Kander course before and after its redirection in 1714 is indicated. Red arrows mark an observed lineament. Refer to the red polygon in figure 1 for location.

with the horizontally oriented beds of the 'Obere Meeres Molasse' (OMM - Upper Marine Molasse). The 'Noflen'-fault is nicely exposed at site B and the sandstone of the USM is strongly fractured. Four earthquakes are located very close by the fault and are likely to be associated with it. The larger one occurred in 1770 and showed a moment magnitude of 3.9. The three smaller ones were recorded in April and December 1990 with moment magnitudes between 2.1 and 2.6 in roughly 10 km depth and hence might be an indication of ongoing activity along this or neighboring faults.

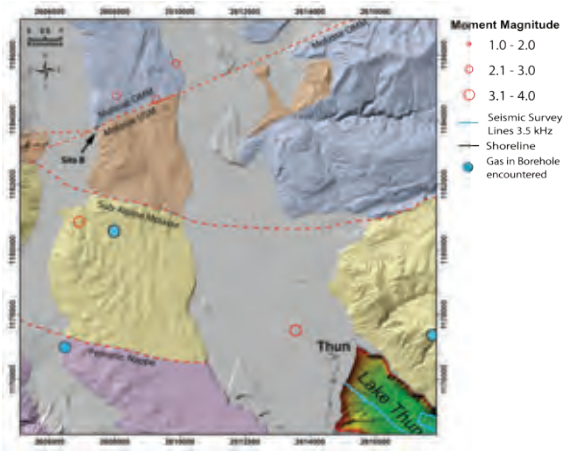

Figure 5: Site B marks the outcrop where USM and OMM are in direct contact. Interpretation of geologic units according to GeoCover and tectonic map (courtesy of swisstopo).

CONCLUDING REMARKS

The annual cumulative frequency-magnitude of the upper Aare valley indicates little activity regarding strong earthquakes. This is very likely related to the short time span of roughly 1800 years being covered by the earthquake catalogue and therefore may lead to an underestimation of the seismic hazard in the area.

There are several geomorphologic features in the Lake Thun area suggesting the occurrence of potentially active structures. At site A, a potentially young fault structure disrupts gravel beds. Likewise, we found a few structures offset sediment in Lake Thun. The latter will be further investigated in the frame of a multichannel seismic campaign using an airgun source of 50 cubic inch chamber size in order to ensure sediment and bedrock penetration. The equipment will be able to overcome the drawbacks (limited penetration, high sensitivity to gas-rich sediments, unmigrated images) of the high-resolution pinger, and the results will enable us to trace the origin of faults observed in the sediment cover down to the bedrock and finalize the investigation of the lake bottom.

This multidisciplinary approach concerning the data acquisition is of great importance to improve our understanding of future earthquakes, their recurrence time and their associated damage potential.

Acknowledgements: The bathymetric field campaign was financially supported by the building insurance of the Kanton Bern (GVB) what we are very thankful for. The comments of L. Guerrieri helped to improve the manuscript and are gratefully acknowledged.

References

Becker, A., P. Hauselmann, J. Eikenberg and E. Gilli, (2012). Active tectonics and earthquake destructions in caves of northern and central Switzerland. *International Journal of Speleology*. 41 (1), p. 35-49.

Fäh, D., D. Giardini, P. Kästli, N. Deichmann, M. Gisler, G. Schwarz-Zanetti, S. Alvarez-Rubio, S. Sellami, B. Edwards and B. Allmann, (2011). ECOS-09 earthquake catalogue of Switzerland release 2011 report and database. Public catalogue, 17. 4. 2011. *Swiss Seismological Service. ETH Zurich. Report SED/RISK.*

Girardclos, S., O.T. Schmidt, M. Sturm, D. Ariztegui, A. Pugin and F.S. Anselmetti, (2007). The 1996 AD delta collapse and large turbidite in Lake Brienz. *Marine Geology*. 241 (1-4), p. 137-154.

Kastrup, U., M.L. Zoback, N. Deichmann, K.F. Evans, D. Giardini and A.J. Michael, (2004). Stress field variations in the Swiss Alps and the northern Alpine foreland derived from inversion of fault plane solutions. *Journal of Geophysical Research, Solid Earth*. 109 (B1).

Nakajima, T. and Y. Kanai, (2000). Sedimentary features of seismoturbidites triggered by the 1983 and older historical earthquakes in the eastern margin of the Japan Sea. *Sedimentary Geology*. 135 (1-4), p. 1-19.

Swiss Seismological Service, SED, (2015). Swiss Earthquakes in 2014: A Review. *Press Release.* p. 1-2.

Strasser, M., F.S. Anselmetti, D. Fah, D. Giardini and M. Schnellmann, (2006). Magnitudes and source areas of large prehistoric northern Alpine earthquakes revealed by slope failures in lakes. *Geology*. 34 (12), p. 1005-1008.

Strasser, M., K. Monecke, M. Schnellmann and F.S. Anselmetti, (2013). Lake sediments as natural seismographs: A compiled record of Late Quaternary earthquakes in Central Switzerland and its implication for Alpine deformation. *Sedimentology*. 60 (1), p. 319-341.

Sturm, M. and A. Matter, (1972). Sedimente und Sedimentationsvorgänge im Thunersee. *Eclogae Geologicae Helvetiae*. 65 (3), p. 563-590.

Sue, C., B. Delacou, J.D. Champagnac, C. Allanic, P. Tricart, and M. Burkhard, (2007). Extensional neotectonics around the bend of the Western/Central Alps: an overview. *International Journal of Earth Sciences*. 96 (6), p. 1101-1129.

Ustaszewski, M., M. Herwegh, A.F. McClymont, O.A. Pfiffner, R. Pickering and F. Preusser, (2007). Unravelling the evolution of an Alpine to post-glacially active fault in the Swiss Alps. *Journal of Structural Geology*. 29 (12), p. 1943-1959.

Wirth, S.B., S. Girardclos, C. Rellstab and F.S. Anselmetti, (2011). The sedimentary response to a pioneer geo-engineering project: Tracking the Kander River deviation in the sediments of Lake Thun (Switzerland). *Sedimentology*. 58 (7), p. 1737-1761.

INQUA Focus Group on Paleoseismology and Active Tectonics

paleoseismicity.org

Noise measurements along fault zones in central Appenines

Famiani, D. (1), Amoroso, S. (2), Boncio, P. (3), Bordoni, P. (1), Cantore, L. (2), Cara, F. (1), Di Giulio, G. (2), Di Naccio, D. (2), Hailemikael, S. (4), Mercuri, A. (1), Milana, G. (1), Vassallo, M. (2)

(1) Istituto Nazionale di Geofisica e Vulcanologia, Roma, Italy. E-mail: daniela.famiani@ingv.it
(2) Istituto Nazionale di Geofisica e Vulcanologia, L'Aquila, Italy
(3) Dept. Scienze Psic. Uman. e Terr., University of Chieti - Pescara, Italy
(4) Agenzia Naz. Eff. Energetica, Centro Ricerche Casaccia, Roma, Italy

Abstract: *Normal fault systems, outcropping or hidden below Quaternary covers in intermountain basins, are the expression of the Neogene-Quaternary evolution of central Italy, characterized by an extensional tectonic regime following the fold and thrust structuring of the Appenninic orogen. The presence of these features plays an important role in seismic risk evaluation of an area. In this work we deal with the use of single-station seismic noise measurements to detect sudden lateral variations of the geometries and/or properties of subsoil connected to the presence of tectonic elements (fault zones). Ambient noise data were collected along transects perpendicular to the strike of hypothetical fault lines for 3 test sites within the Abruzzi Region. The proposed approach is suitable for detecting in a fast and simple way local lateral changes in the subsoil characteristics close to geological structures and can be very effective to properly address more expensive and time consuming classical geophysical and paleoseismological approaches.*

Key words: *Ambient noise, fault trace.*

INTRODUCTION

In the paper we analyse single station ambient noise H/V spectral ratios (HVNSR) (Konno and Ohmachi, 1998) to detect the presence of buried tectonic discontinuities in three case studies characterized by a different a priori knowledge of the presence of an outcropping fault. All the test sites (Figure 1) are located in the central part of Abruzzi region (Central Italy).

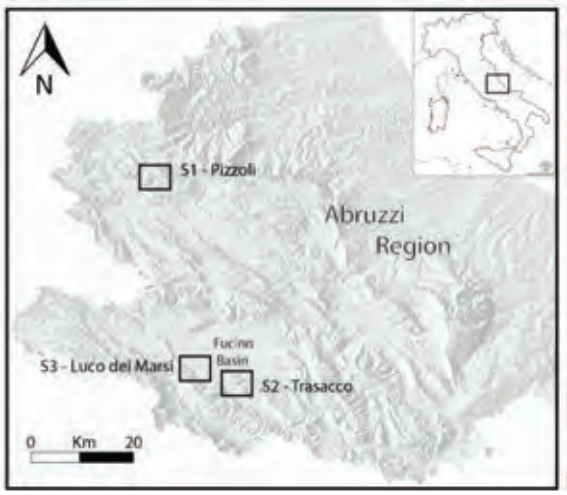

Figure 1: Geographical setting of the study area.

DISCUSSION

The first HVNSR analysis was performed in a site close to the Pizzoli village were a paleoseismological trench pointed out the presence of a dislocation in the very shallow sedimentary layers, probably correlated to an active and capable fault. The trench is located on recent slope sediments at the base of a NW-SE trending mountainside characterized by an important normal fault system recognized as active by several authors (Moro et al., 2002, Gori et al., this meeting).

Four HVNSR measurements were performed along a N20 trending transect deployed on a gentle slope parallel to the paleoseismological trench.

The inter-station distance was of about 20 meters. Two of the measuring points were located North of the dislocation found in the trench, on the hypothetical footwall (TRC1 – TRC2), while the two remaining on the hangingwall.

The HVNSR results are shown in Figure 2 were the rotate H/V ratio (Spudich et al., 1996) is presented. For all the analyzed stations spectral ratios detect a clear resonance peak with amplitude ranging from 3 to 5. Despite to the short station distance the resonance frequency present a quick and regular variation from North to South with f_0 values shifting from 7.0 to 4.1 Hz. The shape of resonance peak is quite sharp at the two sites located close to the edges of the trench (TRC1 and TRC4), while for the other two sites (TRC2 and TRC3) the peaks are broader with lower amplitude.

An important difference can be found also in terms of signals polarization with the polarization angle moving from about 0-20° for TRC1 and TRC2 to 45-50° for TRC3 and TRC4. In conclusion we can sustain that for this case study HVNSR results clearly show significative variations passing across the discontinuity revealed by the trench.

The step forward was, then, to verify if this approach could be applied in different areas with similar geological characteristics.

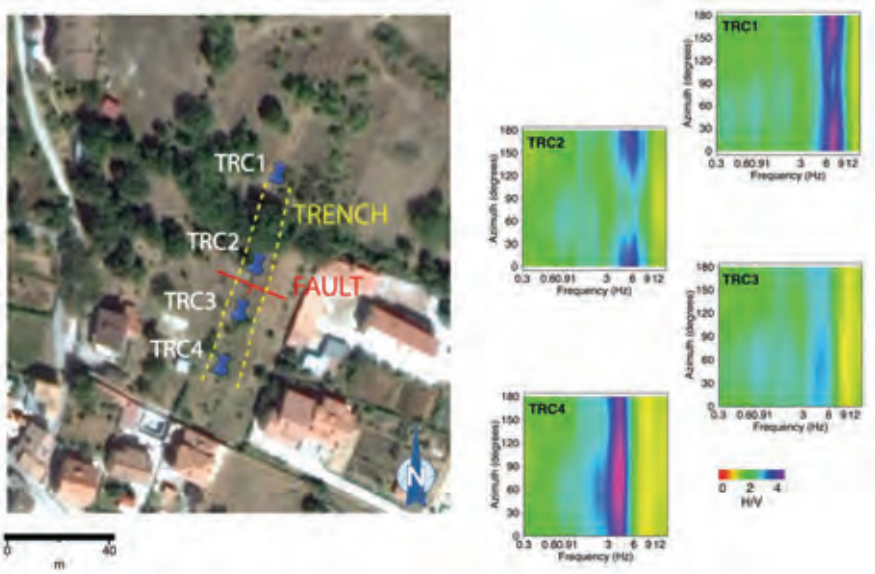

Figure 2: S1 Pizzoli test site.

The second test site is located in the Trasacco municipality, in the NW-SE trending Vallelonga valley that merges into the southern edge of Fucino Basin. It is characterized by fluvio-glacial deposits (gravels) that progressively thickens moving away from the foot of a rocky slope. Previous works (Galadini and Messina, 1999) defined this area as a tectonic valley due to the presence of the Vallelonga fault system that seem to have played an important role in the depositional history of the southern portion of the Fucino basin.

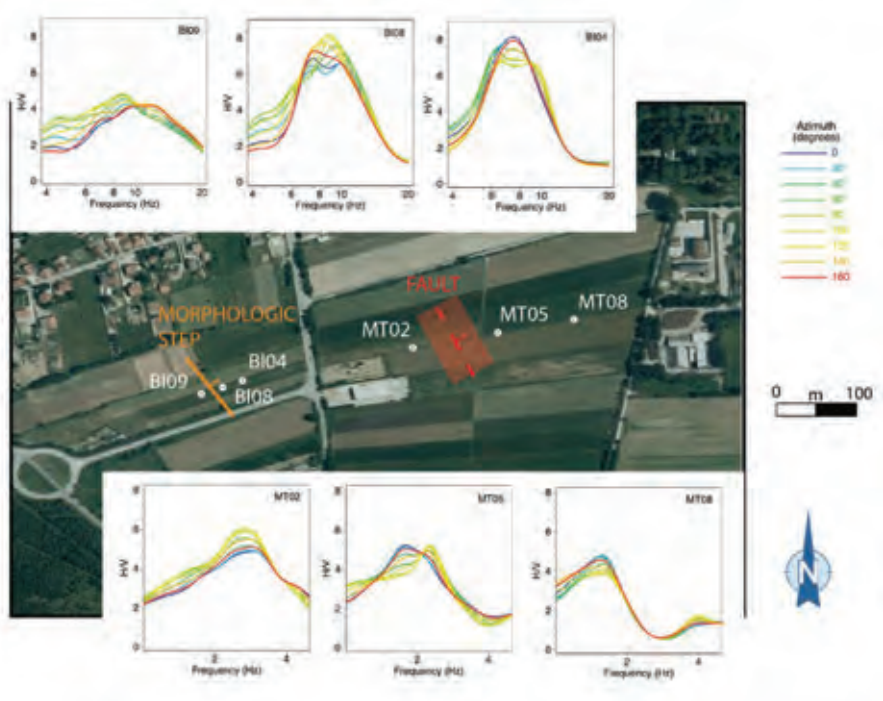

Figure 3: S2 Trasacco test site.

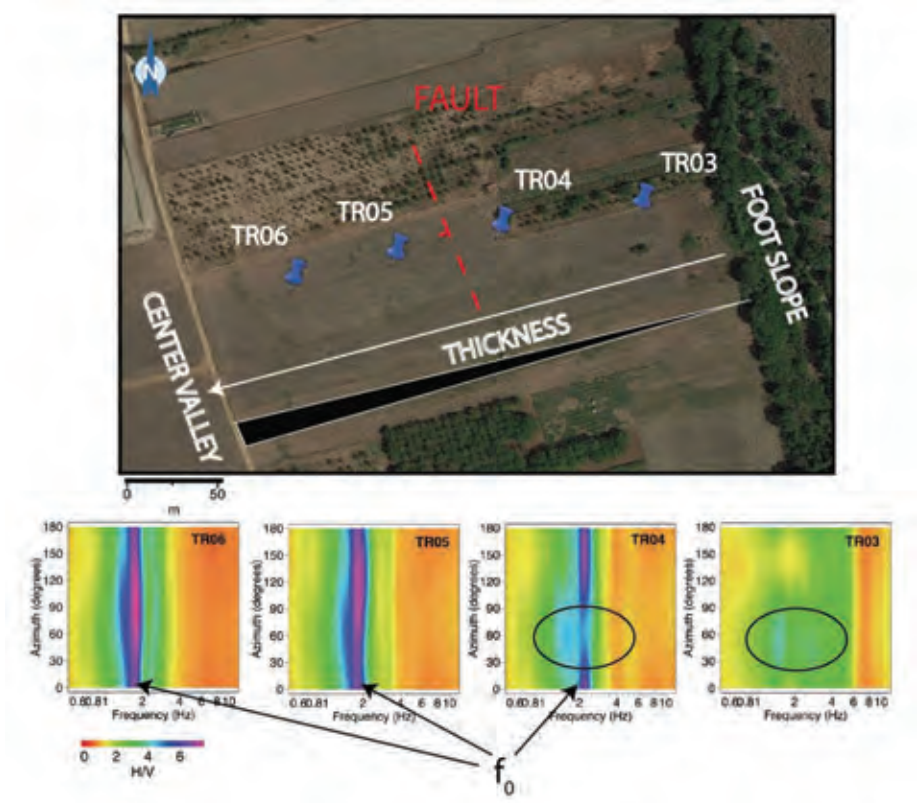

Figure 4: S3 Incile test site.

Single-station ambient noise measurements have been performed along a N75 trending transect, perpendicular to the elongation of the valley.

The inter-station distance in this case is of about 50-60 meters. Along this transect, spectral ratios results, shown in Figure 3, highlight the presence of a clear shift of resonance peak related to the quick variation of gravels thickness. In this case it is possible to notice a 60 degrees polarized energy at about 1.5Hz at stations close to the slope (TR03 - TR04) where HVNSR reaches amplitude values of 4-4.5.

Moving towards the center of the valley (TR05 and TR06), it disappears because is merged with the fundamental resonance peak. This complexity in HVNSR results can be ascribed to some 2D effect.

The third case study is located in the Incile hamlet, in the South-western margin of Avezzano municipality. The selection of this site has been addressed by the presence of the Luco dei Marsi fault together with the availability of a huge amount of previous multidisciplinary studies and investigations (Oddone 1915, Galadini et al., 1997, Giraudi 1988, Cavinato et al., 2002, Boncio et al., 2014). Besides the general knowledge of the geological and tectonic setting, previous investigations available for the area have to be considered in order to plan the geophysical survey. In fact, the interpretation of commercial seismic lines, evidences of superficial effects after the M 7.0 1915 Fucino earthquake and results of a paleoseismological trench has been useful to better locate the fault trace. Luco dei Marsi fault is a tectonic element buried by Quaternary deposits of Fucino basin, with NNW-SSE trend that borders the foot of Monte Salviano, dipping towards the central part of the basin. In this site we have deployed a transect of seismic stations, with minimum inter-station distance of 30 meters and a total length of 700 meters, perpendicularly to the hypothetical fault trace on a gently dipping sandy gravels slope. Once performed the noise spectral ratios analysis, some parts of the seismic station alignment showed-up features similar to S1 and S2 sites. In this case, to better show the polarization effect and the shift in frequency, we have plotted together spectral ratios curves calculated from 0 to 180 degrees with a step of 20 degrees.

For both the "BI" and "MT" measurements (Figure 4), spectral ratios curves show for some stations a shift in frequency of the resonance peak as result of rotational analysis. By looking into further detail, for BI stations an electrical resistance tomography has been performed in order to detect and localize any possible lateral resistivity contrast. Results of this geophysical survey highlighted the presence of a high resistivity contrast related to a morphological step on shallow sediments generated by erosional process related to the fluctuations of the level of the Fucino lake (Giraudi et al., 1988, Boncio et al., 2014). Spectral ratios curves obtained show, for BI stations close to this geomorphologic element, a split of the frequency peak moving from a parallel to a perpendicular direction respect to its azimuth. Furthermore, we have observed that for parallel directions, the frequency values of the peak are compatible with the monodimensional response of the

site (BI09 with lower and BI08 with higher thickness of the gravelly layer), while, moving to the perpendicular polarizations, the peak represents more a 2D effect due to the sudden variation of the shallow layer. BI09 station in fact, for perpendicular azimuths, shows a lowering of the frequency peak (from 11 to 8.5 Hz), while BI08, located on the other side of the step, highlights the opposite behavior. BI04 station (located few tens of meters away from BI08) confirms the general deepening trend of the area: the spectral ratios curve shows a double peak of resonance for perpendicular azimuths, reflecting the influence of the very rapid lateral thickness variation of the superficial layer. MT measurements have been deployed in order to better reconstruct the trend of subsoil geometries towards the center of the basin detecting a quick lateral variation connected to the presence of the Luco dei Marsi fault. For this part of the seismic station transect, thicker sandy silts characterize the superficial layer; therefore, the analyzed frequency range is lower. MT02 and MT08 show a sharp single resonance peak on the HVNSR curves (2.7 Hz for MT02 and 1.6 Hz for MT08) for almost all the azimuth considered in the rotational analysis, with a small variation only in amplitude values (from 5 to 6 for MT02 and from 3.5 to 5 for MT08). MT05 conversely, highlights a double frequency peak: the low frequency one (1.7 Hz) is obtained for NNW-SSE azimuths, while the other one (2.3 Hz) becomes clear for perpendicular directions. In conclusion, between MT02 and MT05 stations a lateral variation of the seismic response is clearly visible. In the light of the observations aforementioned, we can infer the presence of a hidden geologic feature is present close to them, which interrupts the normal progressive deepening of the basin eastward due to the gentle dipping of Monte Salviano buried slopes.
Electrical resistance tomography investigations are going to be deployed for this portion of the basin in order to better define the geometry of shallow deposits. To definitely assess the presence of Luco dei Marsi fault, further direct investigations (e.g. paleoseismological trench) are needed.

CONCLUSIONS

The use of HVNSR analysis become quite common in microzonation studies since it is quick, easy to perform and cost effective. The technique is very robust in simple 1D cases and for sites characterized by important impedance contrasts in the shallow sedimentary layers. In 2D geometrical situations H/V spectral ratios exhibit more complex features with broader amplification peaks. Some of these complexities can be explained, as suggested by other author (Matsushima et al., 2014), taking into account the signal polarization characteristics. The results shown in this paper confirm this hypothesis even if, in our opinion, some other case studies must be analyzed and some numerical models must be performed to fully support the proposed thesis.

Acknowledgements: This work was financially supported by INGV FIRB-Abruzzo project, research unit UR7.

References

Boncio, P., G. Milana, F. Cara, G. Di Giulio, D. Di Naccio, D. Famiani, M. Francescone, F. Galadini, T. Mancini, M. Nardone, G. Rosatelli and M. Vassallo, (2014). Microzonazione Sismica di Livello 1 del Comune di Avezzano. Unpublished Report with 1:5000 maps and sections. *Regione Abruzzo*. 2014. (in Italian).

Cavinato, G., C. Carusi, M. Dall'Asta, E. Miccadei and T. Piacentini, (2002). Sedimentary and tectonic evolution of Plio-Pleistocene alluvial and lacustrine deposits of Fucino Basin (central Italy). *Sediment. Geol.* 148, 29-59.

Galadini, F., P. Galli and C. Giraudi, (1997). Paleosismologia della Piana del Fucino (Italia Centrale). *Il Quaternario, Italian Journal of Quaternary Sciences*. 10 (1), 27-64. 1997.

Galadini, F. and P. Messina, (1999). *13 gennaio 1915: Il terremoto nella Marsica. chapter 9 - Neotettonica della piana del Fucino*. Agenzia di Protezione Civile e Servizio Sismico Nazionale. Roma. 1999.

Giraudi, C., (1988). Evoluzione geologica della Piana del Fucino (Abruzzo) degli ultimi 30.000 anni. *Il Quaternario*. 1 (2), 131-159. 1988.

Gori, S., E. Falcucci, M. Moro, M. Saroli, G. Fubelli, C. Chiarabba, F. Galadini, (2015). Recent advances in the comprehension of the central Apennine seismotectonics, by cross-checking Quaternary geology, paleoseismological and seismological data. (This meeting).

Konno, K., and T. Ohmachi, (1998). Ground motion characteristics estimated from spectral ratio between horizontal and vertical components of microtremors. *Bull. seism. Soc. Am.* 88-1, 228-241.

Matsushima, S., T. Hirokawa, F. De Martin, H. Kawase, F.J. Sánchez-Sesma, (2014). The effect of lateral heterogeneity on horizontal-to-vertical spectral ratio of microtremor inferred from observation and synthetics. *Bull. Seism. Soc. Am*. 104 (1) 381-393.

Moro, M., V. Bosi, F. Galadini, P. Galli, B. Giaccio, P. Messina, A. Sposato, (2002). Analisi paleosismologiche lungo la faglia del Monte Marine (Alta valle dell'Aterno): risultati preliminari. *Il Quaternario, Italian Journal of Quaternary Sciences*. 15 (2), 267-278.

Oddone, E., (1915). Gli elementi fisici del grande terremoto Marsicano-Fucense del 13 gennaio 1915. *Bollettino della Società Sismologica Italiana*. 19, 71-217. (in Italian).

Spudich, P., M. Hellweg, H.K. Lee, (1996). Directional topographic site response at Tarzana observed in aftershocks of the 1994 Northridge, California, earthquake: implications for mainshock motions. *Bull. Seism. Soc. Am*. 86, S193-S208.

INQUA Focus Group on Paleoseismology and Active Tectonics

Long-term strain rates as a tool for understanding the mechanics of continental extension and the importance of local 3D fault geometry for local throw-rates across faults

Faure Walker, J.P. (1), Roberts, G.P. (2), Cowie, P.A. (3), McCaffrey, K. (4), Wedmore, L. (1), Watson, Z. (1), Gregory, L.C. (5)

(1) University College London, London, United Kingdom. Email: j.faure-walker@ucl.ac.uk
(2) Birkbeck College, University of London, London, United Kingdom
(3) University of Bergen, Bergen, Norway
(4) University of Durham, United Kingdom
(5) University of Leeds, Leeds, United Kingdom

Abstract: *Strain-rates have been measured in the central Italian Apennines in a regular 5km and 20km square grids using field measurements of fault geometry, slip vectors and throw-rates measured across offset Late Pleistocene-Holocene landforms and sediments. Comparisons of these strain-rates with rates derived from historical seismicity and geodesy show that strain-rates vary over different timescales (order 10^4, 10^2 and 10^1 yrs), demonstrating that short time periods (10^1-2 yrs) are of insufficient length to capture the long-term deformation. Long-term strain-rates across individual faults can be used as a benchmark for studying shorter-term earthquake histories and stress interactions. Strain-rates measured at higher resolutions (2-3km) across selected individual faults demonstrate the interdependence of local strike, dip and slip-vectors and are used as evidence for a geometry-dependent throw-rate theory across active normal faults.*

Key words: *Strain-rates, long-term, fault, breach, Apennines.*

INTRODUCTION

Long-term rates of deformation are needed to understand the mechanics of continental extension and to provide a benchmark against which short-term deformation rates, changes in stress, fault interactions and the timing of earthquakes can be measured. Since recurrence intervals in the Italian Apennines vary from a few hundred to several thousand years, strain-rates measured over 15±3 kyrs cover multiple seismic cycles, capturing the long-term stress-loading across the faults and hence the signal of long-term mechanisms causing extension. Comparisons of strain-rates measured over different length-scales and timescales allow the importance of the governing forces of the extension and fault interactions to be investigated over these different length-scales and timescales. Strain-rates measured at higher resolutions (2-3 km) across selected individual faults demonstrate the interdependence of local strike, dip and slip-vectors and are used as evidence for a geometry-dependent throw-rate theory across active normal faults. This theory suggests that local throw-rates will vary systematically with the local 3d geometry (strike and dip) and slip vector so as to keep strain-rates concomitant with their position along a fault. This highlights the importance of knowing the local 3d geometry when extrapolating point data along a fault.
This paper aims to bring together the results of selected papers investigating 15±3 kyrs strain-rates in the central Apennines, highlighting their significance for studies of the mechanics of extension in the Apennines and paleoseismic investigations, with particular reference to time-scales, length-scales, and the use of long-term strain-rates for earthquake recurrence and Coulomb Stress Transfer investigations. The discussion will provide an overview of (1) Strain-rates calculated at a resolution higher than that of individual faults (5km) and a lower resolution comparable to the length of individual faults (20km), (2) Comparisons of strain-rates measured using long-term and short-term rates of deformation and the need for long-term strain-rates for understanding the mechanics of continental extension, and as a benchmark for understanding the significance of the timing of historical earthquakes with reference to Coulomb Stress Transfer and (3) Relationships between local 15±3 kyr throw-rates, local 3d geometry and strain-rates at high-resolution and how this relates to extrapolating throw-rate data along strike of a fault.

METHODS

The following provides a summary of the methods used in Faure Walker et al. (2009, 2010).
Faults have been mapped using a combination of published geological maps (e.g. Vezzani and Ghisetti, 1998), Google Earth imagery (Roberts, 2008), SRTM topographic data, field mapping and have been supplemented by paleoseismic trench investigation (e.g. Galli et al. 2008 and references therein) studies and macro-seismic earthquake data (see Faure Walker et al., 2010). Where fault scarps occur at the surface or offsets have been constrained in paleoseismic trench investigations, the fault trace can be constrained within a few metres. Faults scarps have formed through repeated fault slip since the demise of the Last Glacial Maximum when Late Pleistocene-Holocene slopes stabilised and erosion rates slowed allowing fault slip to outpace erosion of the scarps. Fault throw-rates

averaged over the last 15±3 kyrs were calculated from scarp profiles constructed at multiple locations along each fault from topographic profiles with 1m resolutions using a metre rule or hand-held laser. Topographic profiles locations were chosen so as to ensure the throw was the total throw since the slope formation and therefore experienced negligible erosion or sedimentation down the slopes, negligible along-strike lateral erosion of the slopes due to transport of material along the scarp base and the offset was not influenced by local water or debris channel erosion. The data collected was supplemented by data from terrestrial LiDAR and InSAR-DEM such that the offsets are constrained at over 100 locations in the central Apennines. Where data is lacking, estimates were made based on simplified fault length and slip-rates (see Faure Walker et al., 2010 for details). Slip vectors were measured from striations and corrugations on the limestone fault scarps at over 150 sites (2-102 measurements at each site) in the central Apennines. These measurements are consistent with converging patterns of slip-vectors previously identified (Roberts, 2007) and hence where data is missing on a couple of faults, a converging pattern of slip was assumed. Strain-rates were calculated using the field measurements (fault strike, dip, slip trend, slip plunge, throw and length) as input into strain-rate tensor equations that have been adapted from Kostrov (1997) so as to be applied to field measurements. These methods follow the work of Holt and Haines (1995) and England and Molnar (1997) and are explained in detail in Faure Walker et al. (2010) (Eq. 1).

Strain-rates were calculated within regular grid squares of a 5km x 5km (Figure 1) and 20km x 20km grid orientated with axes NE-SW and NW-SE so as to align with the regional principal strain orientation. In order to compare the 15±3 kyr strain-rates with strain-rates calculated from moment tensors of earthquakes using the historical earthquake catalogue over 700yrs (Selvaggi, 1998) and geodesy (126yrs (Hunstad et al., 2003), 11yrs and 5yrs) the 5km x 5km grid squares were combined into polygons so as to match the shape and area of polygons created in these shorter-term studies. Strain-rates were also calculated at smaller sizes for investigating at a high spatial resolution how strain-rates vary along particular fault examples. In order to investigate the interdependence of the local 3d geometry and throw-rates, the strain-rate equations were simplified to the case of individual fault segments within an area.

$$principal\ strain\ rate = \left(\frac{1}{2at}\right)\Sigma_{k=1}^{K}\{L^k T^k cotp^k[\sin(\phi^k - \Phi^k) + \sin(\phi^k + \Phi^k + \arctan(\Sigma_{k=1}^{K}\{L^k T^k cotp^k \cos(\phi^k + \Phi^k)\} / \Sigma_{k=1}^{K}\{L^k T^k cotp^k \sin(\phi^k + \Phi^k)))]\}$$

Equation 1: a=area of grid square, t=time, L = fault length, T=throw, p=plunge, ϕ^k= slip vector azimuth, Φ^k=fault strike, for each fault segment.

DISCUSSION

Comparing the strain-rate fields measured at a length-scale less than that of individual faults (5km) with that at the scale of individual faults (20km) shows that at shorter length scales strain-rates are complex and governed by the orientations and offsets across individual faults, but at larger length scales form a regular regional field, suggesting local strain-rates are influenced by fault geometry and interactions, whereas at a larger scale regional forces are governing the long-term strain-rates.

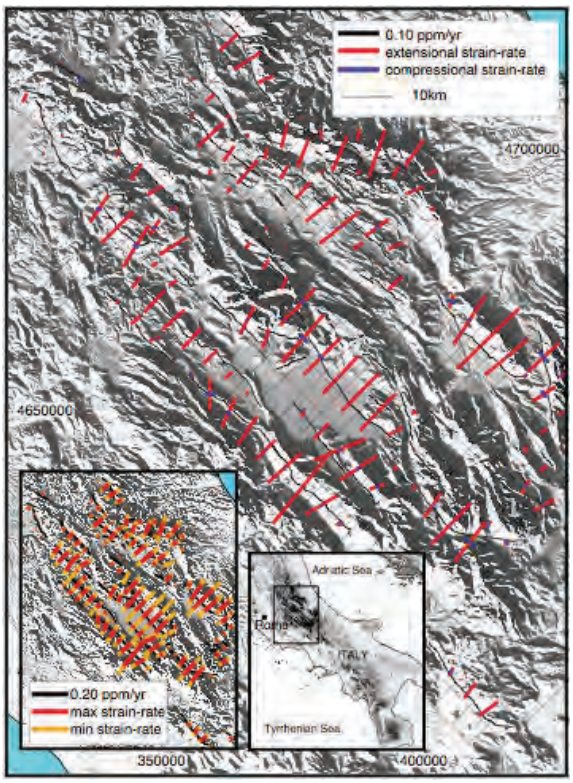

Figure 1: Principal strain-rates calculated in the central Apennines in a regular 5km x 5km grid. The insert shows the maximum and minimum principal strain-rates in the principal strain-rate direction, taking account of errors in the input values.

The comparison of long-term (15±3 kyrs) strain-rates measured over multiple seismic cycles with short term rates inferred from historical records of shaking (700 yrs) and geodesy (126 yrs) show the discrepancies in deformation rates over these timescales. The discrepancy in strain-rates measured from historical seismicity and geological rates (Figure 2) highlights that the historical record is of insufficient length to measure long-term average deformation rates and hence the mechanics of extension over long-term timescales.

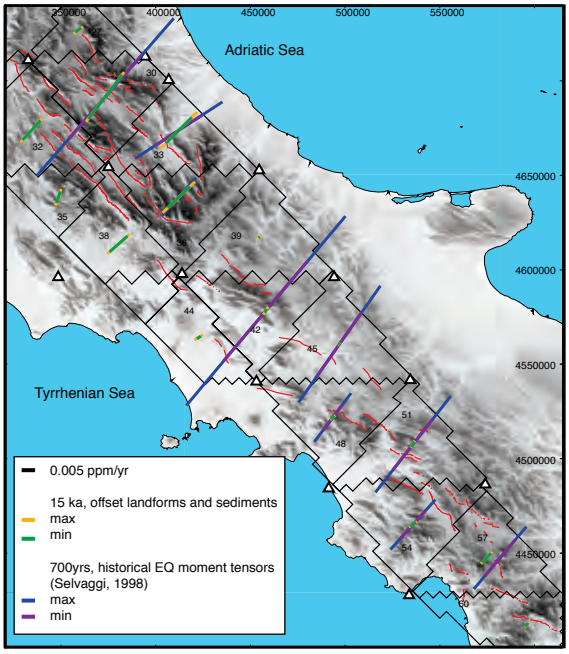

Figure 2: Comparisons of long-term (15ka) strain rates calculated from offset landforms and sediments (yellow-green) with those calculated from summation of moment tensors derived from the historical record of earthquake shaking over 700yrs (blue-purple) (Selvaggi, 1998). Maximum and minimum values include errors associated with the input data.

This is because there is natural variability in recurrence intervals due to temporal earthquake clustering and because in the Italian Apennines, average recurrence intervals for large magnitude events vary between different faults from a few hundred to several thousand years (Pace et al., 2006) and hence strain-rates measured over this timescale are not equal to those measured over 15±3 yrs that represent deformation over multiple seismic cycles. The discrepancies between strain-rates measured from geodesy over 126yrs and long-term geologic measurements show that strain accumulation rates during inter seismic periods are not equal to the average long-term rates and thus cannot be used to estimate the long-term average rates. These results highlight that seismic hazard assessments based on the historical record of shaking or geodetic records are of insufficient time length to capture the magnitude and spatial distribution of seismic hazard, this is especially problematic in areas which have not had an earthquake in historical time but are in close proximity of active faults and high population centres.

Therefore, long-term strain-rates are needed to act as a benchmark against which shorter-term earthquake histories can be investigated. Historical records of shaking, supplemented by data on elapsed time from paleoseismic trench investigations and cosmogenic exposure dating can provide an earthquake history on the active faults in the Italian Apennines that can be used to study stress transfer in earthquakes. However, in order to obtain a cumulative stress history that does not start the clock at the beginning of the historical record and hence assume that there were neutral stresses on the faults at this time, a longer-term history of the stress loading is required. Cowie et al. (2013) described the quantitative relationship between the long-term strain rates across the Apennines and the long wavelength topography and used this to infer that the faults are slipping on narrow shear zones at a depth of about 15km. This allows the calculation of the average rate stress loading history on the faults that covers multiple seismic cycles, to which we can add the stress transfers that have occurred during the historical records. This extends the record over a time-period long enough to identify which faults have current stress states conducive to earthquake rupture and investigate which parameters have constrained the timing and geography of earthquake rupture and the role of recent events in this. Therefore, the long-term strain-rate map at a spatial resolution higher than that of individual faults can be used to infer the individual average loading histories across the faults in the Apennines and hence provide a benchmark against which to investigate stress-loading through the historical record.

In addition to the importance of long-term strain-rates, this paper also addresses the need for measurements of fault displacement, slip direction and 3d geometry at multiple sites along each fault.

Faure Walker et al. (2009) proposed a theory that relates the evolution of commonly observed displacement or throw minima across breach faults (where two outer fault have been linked) and the local 3D fault geometry and hence demonstrates the importance of local 3D fault geometry for fault growth and linkage and the evolution of geomorphology across such a system. This theory suggests that whether a displacement minimum across a breach fault is preserved or diminished through time is dependent on the relative 3D geometry (strike and dip), slip trend, slip plunge and throw rate of the breach fault relative to the outer fault segments it connects. Specifically, it suggests that if strain-rates are to remain concomitant with their position along a fault, a higher throw rate is required across a breach fault that has either a steeper dip than the outer faults it connects or a more oblique slip vector. A lower throw-rate is required across a breach fault with a relatively low dip and more dip-slip slip vector. The theory has been tested using a strain-rate investigation across the Parasano-Pescina active normal fault in the central Italian Apennines displaying a normal breach fault at its centre, which is younger than the outer fault segments it connects (Faure Walker et al., 2009). In this example, the breach fault has a higher dip and strike obliquity to the slip-vector than the outer faults and, consistent with the theory, a higher throw-rate across the breach fault than across the outer faults such that strain-rates remain concomitant with their position along the whole fault (outer segments and breach fault). For this breach fault, it is thus proposed that the displacement minimum across the breach fault will decrease with time.

We currently lack sufficient field examples in the literature to answer whether it is typical for breach faults

to display this type to geometry and hence whether it is typical for displacement minima across them to diminish through time. It is proposed herein that, if the slip vector is preserved across the relay zone, there are no pre-existing planes of weakness and the breach fault grows at a more oblique strike angle to the slip trend than the outer faults it connects, it should be typical for the breach fault to have a higher dip than the outer faults and hence for the displacement minimum to diminish over time. This is due to the Anderson theory of faulting that demonstrates the optimal dip angles for faults to form in terms of energy are approximately 55-60° for normal faults and 90° for strike-slip faults. Therefore, a breach fault that is characterized by normal fault slip with a strike-slip component (due to its oblique strike) would be expected to form at an angle between 55deg and 90deg and steeper than the dominantly pure-dip slip faults in connects. If sites of fault linkage occur where the slip vector is oblique then a breach fault could develop with a higher or lower dip angle depending on the relative orientations of the slip vectors and strikes of the fault segments it connects.

The relationship between the local 3D orientation of the fault and the strain-rate has also been investigated across a single fault segment (Campo Felice Fault) in the central Italian Apennines (Wilkinson et al., 2014). In this example, despite significant variations in strike and throw, the strain-rate displays a linear decrease from the centre towards the tip of the fault, as would be expected for a planar fault without small-scale orientation changes. High precision terrestrial LiDAR data and detailed structural mapping demonstrate local offsets across faults can vary significantly over short length-scales. We therefore propose the "geometry-dependent throw-rate theory" that generalizes the results for the breach fault in Faure Walker et al. (2009) to the general case of active normal faults (Figure 3).

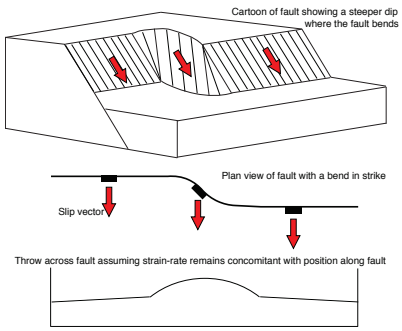

Figure 3: Cartoon showing the "geometry-dependent throw-rate theory" which suggests a higher throw-rate across a fault segment that has more oblique strike and higher dip than the outer segments it connects.

This theory suggests that throw-rates may be higher or lower than expected given the position along the fault if there are sites of fault linkage or sites with altering 3D orientation and hence normal faults have local throw-rates governed by regional-scale external forces, displacement gradients along the fault and the local 3D geometry of the fault. The effect of the local 3D geometry on local throw-rates and displacement-rates could be used to explain some of the variations in shape and the scatter in measurements of fault displacement profiles seen along the length of faults (e.g. Manighetti et al., 2005). This theory demonstrates that the local 3D geometry needs to be taken into account when extrapolating fault offset and slip vector data measured at particular sites along a fault, particularly across bends and at sites of former fault linkage and therefore needs to be considered in paleoseismic studies.

CONCLUSIONS

Long-term strain-rates calculated using detailed fault throw-rates that cover multiple seismic cycles vary along individual faults, at length-scales of individual faults and at the regional length-scale. These strain-rates can be used to make inferences about the mechanics of extension in the Italian Apennines. Comparisons between long-term and short-term strain rates show that deformation rates measured over short time periods are not representative of long-term rates and hence long-term rates are needed to provide a benchmark for seismic hazard assessments and calculations of the evolution of stress on individual faults. Therefore, seismic hazard assessments based on short-term rates such as from the historical record of shaking or from geodesic measurements are of insufficient length to capture the geography of future seismic hazard. The 3D geometry of faults, fault throw-rates and kinematics vary along individual faults and are interdependent such that the strain-rate remains concomitant with the position along the fault. The interdependence of these values demonstrates the need for caution when interpreting and extrapolating point data along a fault.

Acknowledgements: The work was funded by NER/S/A/2006/14042, NERC GR9/02995, NERC NE/B504165/1, NE/E01545X and NE/I024127/1

References

Faure Walker, J.P., G.P., Roberts, P.A. Cowie, I. Papanikolaou, A.M. Michetti, P. Sammonds and R. Phillips, (2009). Horizontal strain-rates and throw-rates for breached relay-zones: an example from active normal faults in the Apennines, Italy. *Journal of Structural Geology*. 31, 1145-1160.

Faure Walker, J.P., G.P. Roberts, P. Sammonds, P.A. Cowie, (2010). Comparison of earthquakes strains over 102 and 104 year timescales: insights into variability in the seismic cycle in the central Apennines, Italy. *Journal of Geophysical Research, Solid Earth*. Vol. 115, B10418, 26 pp., 2010 doi: 10.1029/2009JB006462.

Vezzani, L. and F. Ghisetti, (1998). *Carta Geologica dell' Abruzzo, 1:100000*. SELCA SPA. Florence. Italy.

Roberts, G.P., (2007). Fault orientation variations along the strike of active normal fault systems in Italy and Greece: Implications for predicting the orientations of subseismic-resolution faults in hydrocarbon reservoirs. *AAPG Bull.* 91 (1), 1-20.

Roberts, G.P., (2008). Visualisation of active normal fault scarps in the Apennines, Italy: A key to assessment of tectonic strain

release and earth- quake rupture. *Google Earth Sci. J. Virtual Explorer*. 29, paper 4. doi: 10.3809/jvirtex.2008.00197.

Kostrov, V.V., (1974). Seismic moment and energy of earthquakes, and seismic flow of rock, Izv. *Earth Phys.* 1, 23-40. (Engl. Transl. UDC 550.341, 13-21).

Holt, W.E. and A.J. Haines, (1995). The kinematics of northern South Island, New Zealand, determined from geologic strain-rates. *J. Geophys. Res.* 100 (B9), 17,991-18,010.

England, P. and P. Molnar, (1997). The field of crustal velocity in Asia calculated from Quaternary rates of slip on faults. *Geophys. J. Int.* 130, 551-582.

Selvaggi, G., (1998). Spatial distribution of horizontal seismic strain in the Apennines from historical earthquakes. *Ann. Geofis.* 41 (2), 241-251.

Hunstad, I., G. Selvaggi, N. D'Agostino, P. England, P. Clarke and M. Pierozzi, (2003). Geodetic strain in peninsular Italy between 1875 and 2001. *Geophys. Res. Lett*. 30 (4), 1181. doi: 10.1029/2002GL016447.

Pace, B., L. Peruzza, G. Lavecchia and P. Boncio, (2006). Layered Seismogenic Source Model and Probabilistic Seismic-Hazard Analyses in Central Italy. *Bulletin of the Seismological Society of America.* v. 96, no. 1, p. 107-132, doi: 10.1785/0120040231.

Cowie, P., C. Scholz, G. Roberts, J.P. Faure Walker, P. Sheer, (2013). Viscous roots of active seismogenic faults revealed by geologic slip rate variations. *Nature Geoscience*. 6, 1036-1040.

Wilkinson, M., G.P. Roberts, K. McCaffrey, P. Cowie, J.P. Faure Walker, I. Papanikolaou, R.J. Phillips, A. Michetti, E. Vittori, (2014). Slip distributions on active normal faults measured from LiDAR and field mapping of geomorphic offsets: an example from L'Aquila, Italy, and implications for modelling seismic moment release. *Geomorphology*. doi: 10.1016/j.geomorph.2014.04.026.

Manighetti, I., M. Campillo, C. Sammis, P.M. Mai and G. King, (2005). Evidence of self-similar, triangular slip distributions on earthquakes: Implications for earthquakes and fault mechanics. *Journal of Geophysical Research*. 110, B05302.

INQUA Focus Group on Paleoseismology and Active Tectonics

Evaluation of the seismogenic potential in key areas of the central and southern Apennines through analysis of speleothem vulnerability

Ferranti, L. (1), Pace, B. (2), Vasta, M. (3), Colella, A. (1), Ramondini, M. (4), Calcaterra, D. (1), Di Bianco, S. (1), Valentini, A. (2), De Massis, J. (2), Teodoro, P. (2), Berardi, D. (5), La Rocca, N. (6)

(1) Dipartimento di Scienze della Terra, dell'Ambiente, e delle Risorse, Università degli Studi Federico II, Napoli, Italy. Email: lferrant@unina.it
(2) DiSPUTer, Università degli Studi G. d'Annunzio, Chieti, Italy
(3) Dipartimento INGEO, Università degli Studi G. d'Annunzio, Chieti, Italy
(4) Dipartimento di Ingegneria Civile, Edile ed Ambientale, Università degli Studi Federico II, Napoli, Italy
(5) Associazione Geonaturalistica Gaia Montesilvano, Pescara, Italy
(6) Gruppo Speleologico Sparviere, Alessandria del Carretto, Cosenza, Italy

Abstract: *We used speleothem vulnerability for assessing the seismic ground shaking threshold probably experienced or not in caves located within Apennines seismogenic areas. On the southern flank of the Pollino Range, which is considered a current seismic gap, cave observations suggest the lack of significant earthquake-related deformation in the last ~5-7 ka, but the widespread occurrence of creep. In the central Apennines, homogenously-trending collapses within the Grotta Cola (Petrella Liri, AQ) evidence a significant co-seismic deformation event radiometrically bracketed at ~4-5 ka. We supplemented the cave observations with numerical modeling and static test analysis of the speleothem mechanical behaviour to stipulate probability density functions for the bending stress leading to rupture, and established different vulnerability curves for speleothems according to their shapes. Model results are consistent with the co-seismic deformation at Grotta Cola as being caused by the Liri or by the Velino fault. On the other hand, unbroken speleothems in the Pollino area were used to define an upper limit of the "strength" for earthquakes that could have occurred during the speleothems' lifetime.*

Key words: *Seismic Hazard, Speleothem vulnerability, Seismic ground motion threshold, central and southern Apennines.*

INTRODUCTION

Earthquake forecast and seismic hazard models are generally based on historical and instrumental seismicity. However, in regions characterized by moderate strain rates and by strong earthquakes with recurrence longer than the time span covered by historical catalogues, such as in many parts of the Apennines, different approaches are desirable to provide an independent test of seismologically-based models.

We used non-conventional methods, such as the so-called "Fragile Geological Features" (FGFs), and in particular cave speleothems, for assessing and improving existing paleoseismological databases and seismic hazard models for selected areas of the Apennines.

The analysis of speleothem deformation (breakage or offset) is part of speleoseismological studies, which seek for evidence of past earthquake within the cave archive (Forti, 2001; Becker et al., 2006). Radiometric dating of the deformation events can be performed with relative ease and thus "speleoseismic" events can be compared to historical seismicity catalogues (e. g. Forti & Postpischl, 1984), or be used to extend back in time the paleoseismological record (e. g. Delaby, 2001; Becker et al., 2005; Kagan et al., 2005).

The underlying idea is based on the stalactite-stalagmite oscillatory system which represents the vertical datum. Provided that other sources are excluded (e. g. landslide, flooding, animal or men passage), the deviation from the vertical of the growth axis, and the speleothem breakage, is evidence for shaking of the cave walls (Forti & Postpischl, 1984; Kagan et al., 2005). However, the difficulty in quantitative modeling of the observed deformation, and its direct attribution to a geometrically-constrained seismogenic source is a major issue (Lacave et al., 2004; Becker et al., 2006).

Lacave et al. (2000) investigated the range of fundamental natural frequencies and the damping of speleothems, and established that most of the broken speleothems are a direct indicator of the peak ground acceleration (PGA) during past earthquakes. Based on the analysis of the mechanical behaviour of speleothems through static tests, Lacave et al. (2004) stipulated the PDF (probability density functions) for the bending stress leading to rupture, and established different vulnerability curves (probability of breaking as a function of PGA) for speleothems according to their shapes. On the other hand, unbroken speleothems may be used to define an upper limit of the "strength" for earthquakes that could have ever occurred during the speleothems' lifetime. This approach was applied by Lacave et al. (2012) to two pilot caves in Lebanon.

Based on these results, we started developing speleothem-based vulnerability curves for selected areas within the axial seismogenic belt of the Apennines. The study area in southern Italy is in northern Calabria (Pollino Range), and represents a gap in the belt of active faults and current seismicity, but, based on paleoseismological data, it is thought to host seismogenic faults (Cinti et al., 2002). Our previous work on broken speleothems from caves distributed around suspect active faults established past episodes of speleothem deformation, tentatively related to

earthquakes (Ferranti et al., 1997; Ferranti and Maschio, 2007), but no investigation on vulnerability was carried.
The study area in central Apennines is located ~10 km west of the Fucino Plain, one of the largest tectonic basin of the Apennines, affected by the large 1915 earthquake (M=7). In detail, the cave is located close to the Liri fault, a ~42 km long and southwest dipping normal fault, considered by some authors (e.g. Roberts & Michetti, 2004) active and seismogenic.

RESEARCH STRATEGY

The starting step of the research was to select within the target areas the caves with required features (concretions within near-surface rooms, wide range of speleothem shapes, easy access, and so on). We visited four caves scattered on a ~20 km stretch on the southern flank of the Pollino Range, and one cave in Abruzzi. In both settings, caves are in the immediate footwall of suspect active normal faults (Pollino-Castrovillari, and Liri faults, respectively). The shape of speleothems was recorded by measuring length and diameter of intact and deformed speleothems. Care was taken in distinguishing within the speleothem data the subset related to non-seismogenic deformation (e. g. creep, manifested in quasi-continuous change of the growth axis), and to seismic processes (speleothem breakage and fall, discrete change of growth axis), respectively. Vulnerability analysis of the speleothem population based on the length and diameter ratio was initially carried according to published curves (Lacave et al., 2012).
In a following step, we performed static tests on a representative speleothem population from the different settings in order to correctly define the speleothem vulnerability curves (in terms of probability to be broken), and thus past PGA thresholds, for each investigated area.
In addition, we performed theoretical and numerical modelling in order to estimate the values of the horizontal ground acceleration required to failure the speleothems. In particular we used a finite element method (FEM), with the SAP200 software, starting from the detailed geometry of the speleothems and their mechanical properties.
Laboratory analysis included radiometric dating of the speleothem deformation events in order to define, for each area, the paleoseismological frame. For unbroken speleothems, dating of the most recent speleothem layer was used to define the time interval of the limited PGA threshold experienced by speleothems.
The speleothem-based estimate was then compared with the acceleration predicted by the national seismic hazard model (MPS04, 2004).

DISCUSSION

In the Pollino area, we found a good chronological correlation between deformation events recorded by single speleothems of comparable size from an individual cave. At a larger scale, type and age correlation of events among different caves located along a ~20 km stretch of the southern flank of the range led to identification of a well-constrained, regional collapse event at ~5-7 ka, and a previous similar event at ~23 ka. Because these events are recorded by speleothem with moderate vulnerability, we regard them as related to strong, but infrequent earthquakes. Conversely, we did not found evidence of significant seismic shacking between ~40-23 ka, ~23-7 ka, and after~5-7 ka, for this latter time frame even for more vulnerable speleothems. Instead, we observed the widespread existence of "slow" deformation events that we relate to creeping.
Laboratory tests on a representative Pollino speleothem population documented P-wave velocities ranging from 3 to (mostly) 5-6 km/s and an inverse correlation between velocity and porosity. Preliminary results of static uniaxial tests show instead a more complex relation between deviatoric stress and deformation. Broadly, samples with higher P-wave velocity and lower porosity show a higher deviatoric stress reached at a lower deformation amount when compared to slower and more porous samples. Although not yet completed, these tests are being used to build dedicated vulnerability curves for the Pollino caves.
Within the Grotta Cola in central Italy, on the other hand, we found evidence of significant co-seismic deformation, represented by near similar-sized speleothem concretions on collapsed speleothems. This deformation event, which is recorded in several rooms of the cave, is characterized by a consistent direction of stalagmite collapse toward N330°±10°. Such collapse direction is expected for seismic wave propagation along a NNW-SSE striking causative fault, consistent with the strike of either the Liri fault, mapped at the foot of the range hosting Grotta Cola (Roberts & Michetti, 2004), and of the Velino fault, located further northeast and having the Grotta Cola in its hanging-wall (Schlagenhauf et al., 2011). We dated the deformation at between ~4.2-5.8 cal ka. Taking into account an up to 20% correction to account for the age contamination due to water circulation into the Mesozoic carbonate reservoir (Alessio et al., 1991), an ~4-5 ka age for this event is estimated. Although we do not provide dates, observations are consistent with more than a single event recorded in the cave.
Laboratory measurements were performed on Grotta Cola speleothem samples in order to characterize their mechanical properties. The obtained values of density, Young's modulus and tensile failure stress, both from broken and unbroken speleothems, have been used as input data for theoretical calculations and numerical modelling of the main collapsed speleothem. The horizontal ground acceleration resulting in failure and the natural frequency of the speleothem were assessed by the FEM modelling. The results suggest either the Liri or the Velino fault as the most probable causative fault of the cave speleothem collapses recorded ~4-5 ka ago. Noteworthy, the time range bracketed for the speleothem deformation is well consistent with a period of clustered slip recorded by cosmogenic dating of the Velino-Magnola fault scarp (Schlagenhauf et al., 2011).

In summary, our research contributes to assess the existence or lack of past earthquakes within the axial seismogenic belt of the Apennines. As a matter of fact, the Grotta Cola lies just west of the Fucino plain, where historical and modern seismic deformation of the central Apennines seismic belt has concentrated. Similarly, the Pollino region is at the transition between southern Apennines and Calabria seismogenic provinces, where a marked decrease in seismic and geodetic deformation occurs (Totaro et al., 2013; Ferranti et al., 2014). Definition of the upper threshold for seismic shaking, as in the case for the recent behaviour of the Pollino region, can help reducing overestimated risks and calls for a fault-based revision of seismic hazard maps.

References

Alessio, M., L. Allegri, F. Antonioli., G. Belluomini, L. Ferranti, S. Improta, L. Manfra & A. Proposito, (1992). Risultati preliminari relativi alla datazione di speleotemi sommersi nelle fasce costiere del Tirreno Centrale. *Giornale di Geologia*. 54 (2), 165-193.

Becker, A., M. Ferry & K. Monecke, (2005). Multiarchive paleoseismic record of late Pleistocene and Holocene strong earthquakes in Switzerland. *Tectonophysics*. 400, 153-177.

Becker, A., C.A. Davenport, U. Eichenberger, E. Gilli, P.Y. Jeannin & C. Lacave, (2006). Speleoseismology: A critical perspective. *J. Seismol.*10, 371-388.

Cinti, F.R., M. Moro, D. Pantosti, L. Cucci & G. D'Addezio, (2002). New constraints on the seismic history of the Castrovillari fault in the Pollino gap (Calabria, southern Italy). *J. Seismol*. 6, 199-217.

Delaby, S., (2001). Palaeoseismic investigations in Belgian caves. *Netherlands J. Geosciences*. 80 (3-4), 323-332.

Ferranti L., S. Improta, L. Maschio & E. Vittori, (1997). Attività tettonica recente nel massiccio del Pollino suggerita dallo studio di speleotemi fratturati. *Il Quaternario*. 10 (2), 501-504.

Ferranti, L. & L. Maschio, (2007). Ricerche speleosismologiche nel massiccio del Pollino, Appennino Meridionale. *Atti I Convegno Regionale di Speleologia "Campania Speleologica"*. 1-3 Giugno. Oliveto Citra (SA). 201-215.

Ferranti, L., M. Palano, F. Cannavò, M.E. Mazzella, J.S. Oldow, E. Gueguen, M. Mattia & C. Monaco, (2014). Rates of geodetic deformation across active faults in southern Italy. *Tectonophysics*. 621, 101-122.

Forti, P., (2001). Seismotectonic and paleoseismic studies from speleothems: The state of the art. *Netherlands J Geosciences,* 80 (3-4), 175-185.

Forti, P. & D. Postpischl, (1984). Seismotectonic and paleoseismic analyses using karst sediments. *Mar. Geol.* 55, 145-161.

Kagan, E.J., A. Agnon, M. Bar-Matthews & A. Ayalon, (2005). Dating large infrequent earthquakes by damaged cave deposits. *Geology*. 33 (4), 261-264.

Lacave, C., A. Levret & M. Koller, (2000). Measurements of natural frequencies and damping of speleothems. *Proc. of the 12th World Conference on Earthquake Engineering.* Auckland. New-Zealand. paper 2118.

Lacave, C., M.G. Koller & J.J. Egozcue, (2004). What can be concluded about seismic history from broken and unbroken speleothems? *J. Earthquake Engineering.* vol. 8 (3), pp. 431-455.

Lacave, C., B. Sadier, J.J. Delannoy, C. Nehme & J.J. Egozcue, (2012). The use of speleothems to better constrain long return period seismic hazard in Lebanon. *Proc. of the 15th World Conference on Earthquake Engineering*. Lisbon. Portugal.

Roberts, G.P. & A.M. Michetti, (2004). Spatial and temporal variations in growth rates along active normal fault Systems: an example from Lazio-Abruzzo, central Italy. *J. Struct. Geol*. 26, 339-376.

MPS Working Group, (2004). Redazione della mappa di pericolosità sismica prevista dall'Ordinanza PCM 3274 del 20 marzo 2003. *Rapporto Conclusivo per il Dipartimento della Protezione Civile*. INGV, Milano- Roma. 2004 april. 65 p.

Schlagenhauf, A., I. Manighetti, L. Benedetti, Y. Gaudemer, R. Finkel, J. Malavieille & K. Pou, (2011). Earthquake supercycles in Central Italy, inferred from 36Cl exposure dating. *Earth Plan. Scie. Letters*. 307, 487-500.

Totaro, C., D. Presti, A. Billi, A. Gervasi, B. Orecchio, I. Guerra & G. Neri, (2013). The ongoing seismic sequence at the Pollino Mountains, Italy. *Seismol. Res. Lett.* 84, no. 6, doi: 10.1785/0220120194.

INQUA Focus Group on Paleoseismology and Active Tectonics

Archaeoseismology and paleoseismology in the area of Tiberias city, Sea of Galilee – preliminary results

Ferrario, M.F. (1), Katz, O. (2), Livio, F. (1), Michetti, A.M.(1), Amit, R. (2)

(1) Università degli Studi dell'Insubria, via Valleggio 11, 22100, Como, Italy. Email: Francesca.ferrario@uninsubria.it
(2) Geological Survey of Israel, 30 Malkhe Israel Street, 95501 Jerusalem, Israel

Abstract: *The city of Tiberias (Israel) is sited on the shores of the Sea of Galilee, a pull-apart basin located along the Dead Sea Transform. This paper aims to present the first results of a cross-disciplinary investigation focused on the evaluation of earthquake hazard for the city: aerial photo interpretation and field surveys were combined with shallow seismic surveys and paleoseismic analyses. An archaeoseismic survey has been performed on two different structures on the Berniki hill, a Roman theatre and the remains of a byzantine church. Further work has to be done for a complete seismic hazard characterization, but our study highlights several deformation features that might be earthquake-related; specifically, a previously unknown fault trace has been constrained both on natural sediments and archaeological structures.*

Key words: *Archaeoseismology; Dead Sea Transform; Sea of Galilee; Active tectonics.*

INTRODUCTION

The Dead Sea Transform (DST) is the tectonic boundary between the Arabia and Sinai (Africa) plates, extending from the Red Sea, to the south, to the Eurasian Plate, to the north. The DST is a continental transform, with a post-Miocene 105 km left-lateral displacement (e.g., Garfunkel, 1981; Fig. 1a). The Sea of Galilee is a N-S extended pull-apart basin, bounded by the Jordan Valley Fault (JVF) to the east and by the Western Marginal Fault (WMF) to the west (Fig. 1b).
Several historical large destructive (M > 6.5) earthquakes struck the area; among them, the AD 749 event (M 7.0 - 7.5; Marco *et al.*, 2003) is attributed to the JVF and caused heavy damage to the cities of Tiberias and Susita, on the western and eastern shores of the lake, respectively. The abundance of archaeological sites and well-dated man-made structures along the DST enabled to find direct evidences of coseismic surface rupture related to historical earthquakes (e.g., Ellenblum *et al.*, 1998; Marco *et al.*, 2003). Instrumental seismicity is also present; in 2013, a seismic swarm (M = 3.5) hit the area, with epicenters located in the northern part of the Lake. However, the long term prehistorical record of earthquake behavior, including determination of recurrence time intervals of large events is yet missing in this highly populated area.
This study is aimed at reconstructing the late-Pleistocene -Holocene seismic history of the western area of the Sea of Galilee by means of cross-disciplinary investigations, encompassing geology, geophysics, palaeo- and archaeo- seismology. Results will be later integrated with paleoseismic and seismic data available for the eastern area of the Sea of Galilee and surroundings regions (e.g., Marco *et al.*, 2003; Yagoda-Biran *et al.*, 2010; Katz *et al.*, 2012) to give a complete picture of the seismic hazard around the Lake.

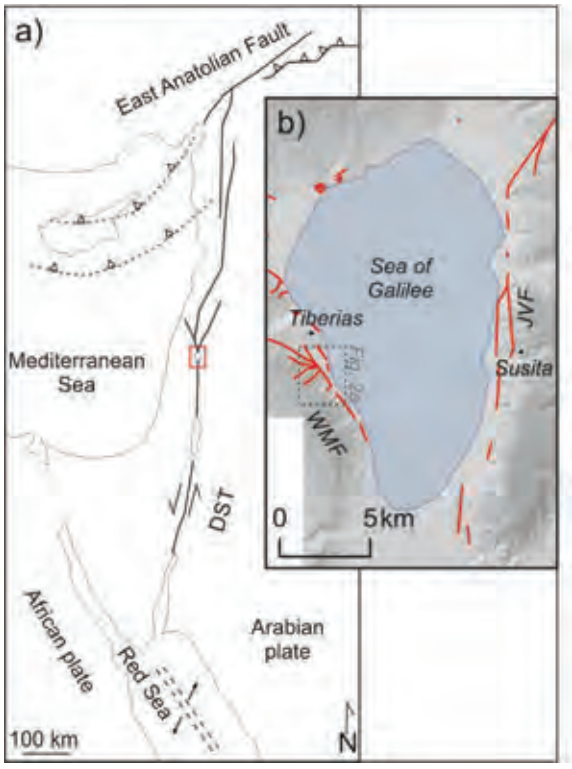

Figure 1: a) General tectonic setting of the Dead Sea Transform (DST), modified after Garfunkel (1981); the Sea of Galilee is marked in red. b) Digital elevation model and main active faults around the Sea of Galilee.

The study area is located ca. 1 km south of the center of the city of Tiberias at the western coast of the Sea of Galilee. The geological setting is dominated by Miocene-Pliocene sedimentary rocks, mainly limestone and conglomerates, and interbedded basalts (Fig. 2a). Several short watercourses flow to the NE in steep

slopes. The Lake and the top of the slopes are ca. 1.5 km apart, and the difference in their elevation is of 400 m.
Several faults which have a clear geomorphic expression at the surface were mapped: part of the faults and lineaments are crossing a Roman byzantine archeological site named "Berniki". In addition several lineaments are crossing the distal part of landslides more to the south.
Three achaeological sites were studied: (i) a theatre ("Berniki theatre") built in the I century AD, where dislocations and tilting, possibly related to palaeo-earthquakes, were analyzed; (ii) a byzantine church built in VI century AD on the top of Mt. Berniki; this site was presumably destroyed by the AD 749 earthquake and then rebuilt and used up to the Crusader period (end of XII century AD); (iii) an archeological site including city walls, a drainage system and two defensive towers.

METHODS

The study is based on a multidisciplinary approach that integrates different investigative techniques. Firstly, a preliminary field reconnaissance was performed on the study area and a morphotectonic map was drawn based on the interpretation of stereoscopic aerial photos (two coverages imaging the area at 1945 and 1982) and their subsequent georeferentiation and processing by GIS software. We also used high resolution seismic reflection, a paleoseismological analysis by trenching the faults detected and identified in the field and in the seismic lines, as well as archaeoseismic analyses. Further research will include opening additional trenches, a survey by airborne Lidar and a detailed field survey in order to crosscheck features mapped through photointerpretation. The lineaments will be mapped, and possibly suitable outcrops will be sampled for OSL dating. At a second stage of the project, a study based on quantitative tectonic geomorphology will be performed on the mountain front south of the city.

RESULTS AND DISCUSSION

Aerial photo interpretation
Features and anomalies of the drainage network, possibly related to tectonic activity, have been mapped. About 20 NNW-SSE oriented lineaments were identified, most of them interpreted as normal faults dipping to the ENE. Four landslides and several alluvial fans were recognized due to their clear morphological expression; the former are also crossed by some of the mapped lineaments. The streams show several anomalies, in particular fluvial elbows and piracy events, testified by abrupt changes in the flow direction and by beheaded valleys in the downstream sectors (Fig. 2b).

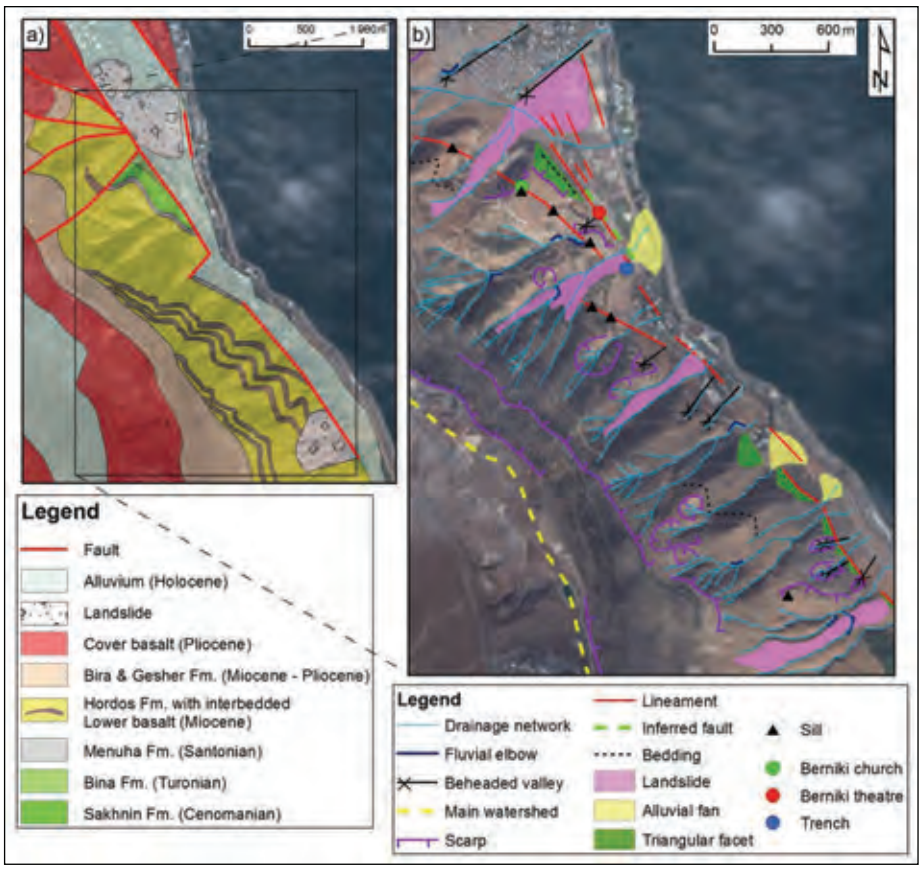

Figure 2: a) Geologic map of the study area and fault traces (after Bogoch and Sneh, 2008 and Sneh, 2008). b) Morphotectonic.map based on aerial photo interpretation and field surveys.

Paleoseismic trench

A trench was opened across an inferred lineament, NNE-SSW oriented and inferred as crossing the Berniki theatre (see Fig. 2b for location). The trench position was chosen based on (i) field evidence, i.e. where a clear scarp is present and (ii) discontinuities recorded by seismic survey interpreted as a fault. The trench is ca. 2.5 m deep, 15 m long and 1 m wide. A manual log at 1:20 scale was drawn for the entire southern wall length and for part of the northern wall, in correspondence with stratigraphic deformation. Five stratigraphic units, mainly made up of alluvial or anthropogenic sediments, were described based on grain size, texture, color, type of boundaries and presence of artifacts. Several archaeological remains were found, as well as human bones, at the base of the trench. Oldest uncovered findings are dated approximately at the Islamic period (XI century AD).

No unquestionable evidence of faulting has been found, however, some minor deformations are present: layers generally dip a few degrees to the east except between 12 and 14 meters, where a back-tilting is clearly visible. Obtained results are not compelling and other triggering mechanism, beside earthquake, cannot be ruled out.

Archeoseismic survey

An archaeoseismic survey has been performed on two different archaeological structures, the Berniki theatre and the remains of a church on top of Mt. Berniki. Here we present the results obtained at Berniki theatre only, where at least 12 different points reveal deformation features that might be earthquake-related (Fig. 3). In particular, they include tilting and open fractures of the walls; lateral displacements on the order of few cm, still not clearly associated to fault activity, can be seen at some points.

Some of the observed damage can be explained only with the occurrence of an external event (e.g., earthquake, landslide, geotechnical failure). The archaeoseismic survey at Berniki theatre highlight that earthquake seems the most likely triggering mechanism, because features A, B, C, D, L, G and K are all aligned along a N140° direction (see Fig. 3c), that we interpret as a fault trace. This interpretation is also supported by (i) the alignment of the inferred fault with the mountain front to the NW, (ii) the coherence with the regional geologic setting and the morphotectonic map and (iii) the alignment with the House of the Bronzes (Fig. 4), where archaeological excavations suggest that the destruction of the site is due to an earthquake (Hirschfeld & Gutfeld, 2008).

Landslide processes are common in the Sea of Galilee area and are spatially associated with normal faults (e.g., Katz *et al.*, 2010; Yagoda-Biran *et al.*, 2010); however, deformations recorded at Berniki theatre are unlikely triggered by landslides: stratigraphic layers on the morphological scarp are continuous and any landslide body has been mapped upslope the theatre, nor by field surveys, nor by photointerpretation.

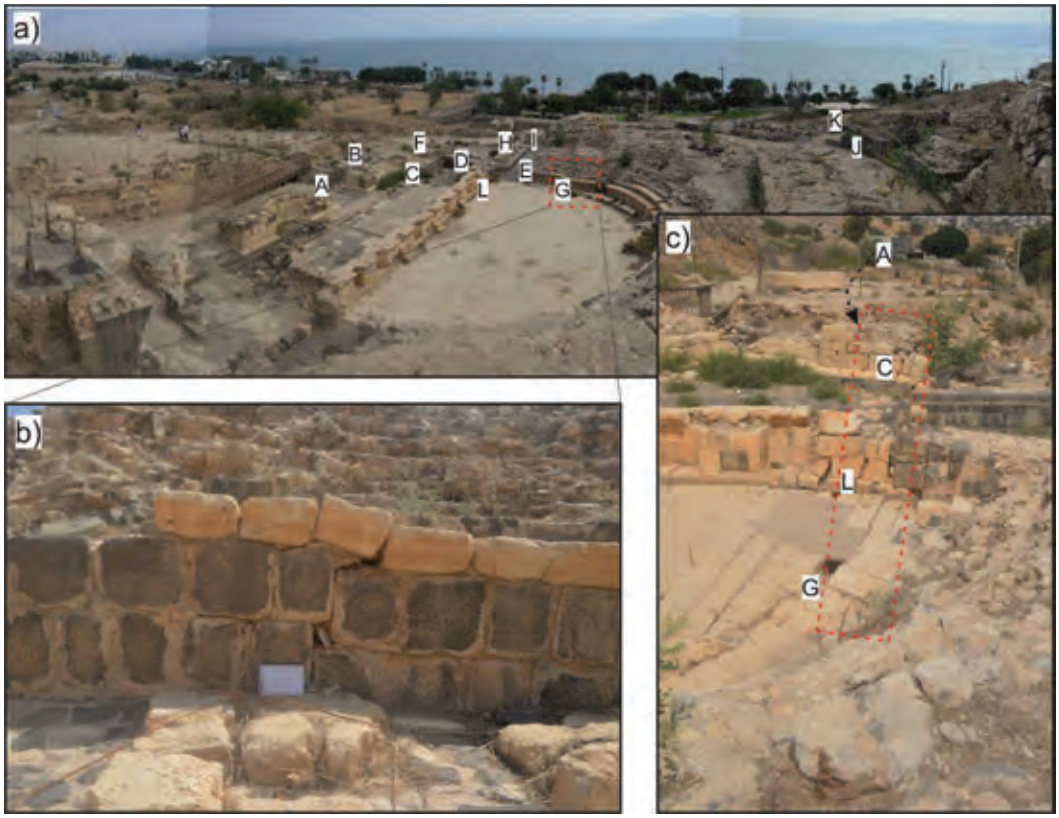

Figure 3: a) General view of the Berniki theatre (looking NE); the letters show locations of main features. b) Detail of an observed deformation. c) Alignment of deformations along a N140° direction.

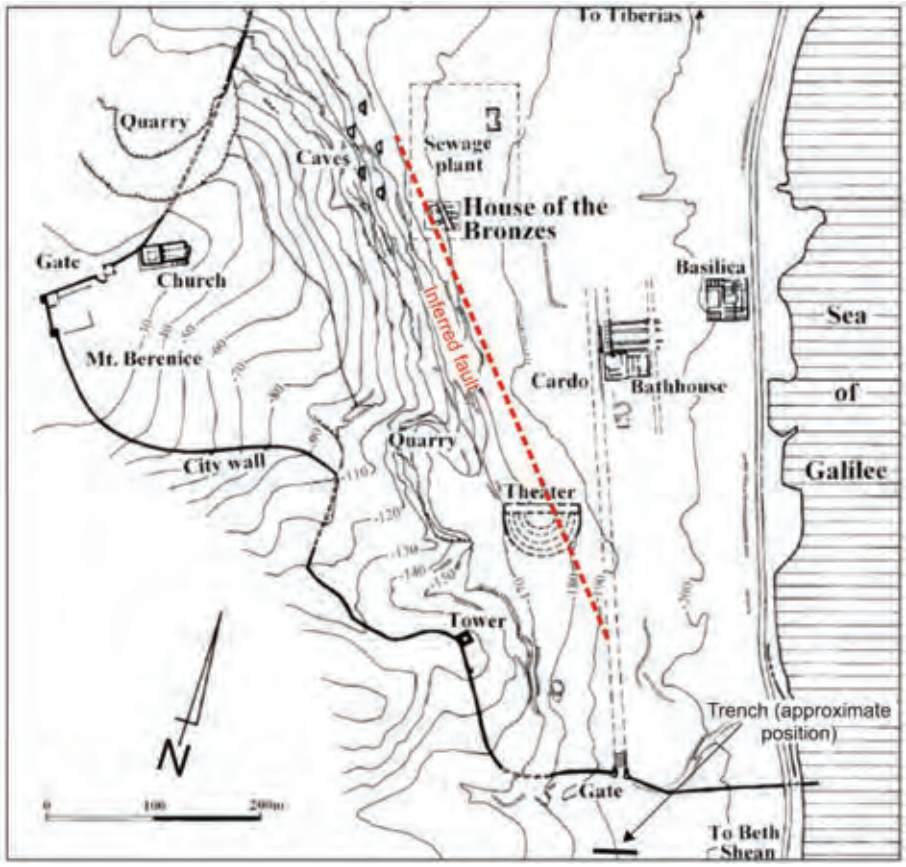

Figure 4: Map of ancient Tiberias (modified after Hirschfeld & Gutfeld, 2008) with indication of the inferred lineament and trench position.

CONCLUSIONS

In the study area we found deformations recorded by natural and archaeological features that might be related to historical earthquakes. The integration between stratigraphy, palaeoseismology and archaeology allowed us to gain a more accurate estimate of the geological landscape and the possible risks for Tiberias.

Data here discussed represent the preliminary results of this project; research is still ongoing and further investigations has been already planned, including the opening of new trenches, a detailed field survey at the periphery of the archaeological site, analysis of the fluvial network and analysis of slope instability and landslides related to fault lines. The completion of activities should shed light on some open issues and should give more conclusive results.

Acknowledgements: MFF benefited from a grant provided by Fondazione della Banca del Monte di Lombardia; we are grateful to an anonymous reviewer which helped us to improve the text. We would like to thank the Geophysical Institute for seismic lines, Yoav, Yakov and Rami for field assistance and the Israel Antiquities Authority. This study was partially supported by Tiberias municipality.

References

Bogoch, R., A. Sneh, (2008). *Geological Map of Israel, 1:50,000, Sheet 4-I Arbel*. Geological Survey of Israel. Jerusalem.

Garfunkel, Z., (1981). Internal structure of the Dead Sea leaky transform (rift) in relation to plate kinematics. *Tectonophysics.* 80, 81-108.

Ellenblum, R., S. Marco, A. Agnon, T. Rockwell, A. Boas, (1998). Crusader castle torn apart by earthquake at dawn, 20 May 1202. *Geology*. 26 (4), 303-306.

Hirschfeld, Y., O. Gutfeld, (2008). Tiberias excavations in the House of the Bronzes. Final Report, vol. I. QEDEM - *Monographs of the Institute of Archaeology*.

Katz, O., R. Amit, G. Yagoda-Biran, Y.H. Hatzor, (2012). Quaternary earthquakes and landslides in the Sea of Galilee area, the Dead Sea Transform; paleoseismic analysis and evaluation of current hazard. *Isr. J. Earth Sci*. 58, 275-294.

Marco, S., M. Hartal, N. Hazan, L. Lev, M. Stein, (2003). Archaeology, history, and geology of the A.D. 749 earthquake, Dead Sea Transform. *Geology*. 31 (8) 665-668.

Sneh, A., (2008). *Geological Map of Israel, 1:50,000, Sheet 4-II Teverya*. Geological Survey of Israel. Jerusalem.

Yagoda-Biran, G., Y.H. Hatzor, R. Amit, O. Katz, (2010). Constraining regional paleo peak ground acceleration from back analysis of prehistoric landslides: example from Sea of Galilee, Dead Sea transform. *Tectonophysics.* 490, 81-91.

INQUA Focus Group on Paleoseismology and Active Tectonics

First lateral slip-rates along the left-lateral strike-slip Alhama de Murcia fault obtained with 3D trenching (SE Iberian Peninsula)

Ferrater, M. (1), Ortuño, M. (1), Masana, E. (1), Perea, H. (2), Baize, S. (3), Pallàs, R. (1), García-Meléndez, E. (5), Echeverría, A. (1), Martínez-Díaz, J.J. (4), Rockwell, T. (6)

(1) RISKNAT Group. GEOMODELS. Departament de Geodinàmica i Geofísica, Facultat de Geologia, Universitat de Barcelona, c/ Martí i Franquès, s/n, 08028 Barcelona, Spain. Email: marta.ferrater@ub.edu
(2) Barcelona Center for Subsurface Imaging (B-CSI), Departament de Geociències Marines - Institut de Ciències del Mar - CSIC, 08003 Barcelona, Spain
(3) Institut de Radioprotection et Sûreté Nucléaire - Seismic Hazard Division (BERSSIN), BP 17, 92262 Fontenay-aux-Roses, France
(4) Departamento de Geodinamica, Universidad Complutense, Instituto de Geociencias IGEO (UCM, CSIC), 28040 Madrid, Spain
(5) Área de Geodinámica Externa, Facultad de CC. Ambientales, Universidad de León, Campus de Vegazana s/n 24071 León, Spain
(6) Department of Geological Sciences, San Diego State University, San Diego, CA 92182, USA

Abstract: *Seismic hazard scales with the slip rate of a fault. The left-lateral strike-slip Alhama de Murcia fault (AMF; SE Iberian Peninsula) is proven to be seismogenic, but there have been large uncertainties as to its strike slip rate up until now. We use 3D trenching with morphotectonic analysis to establish the far-field trend of channels that are offset by the fault to obtain contrained lateral slip-rate for the AMF. We excavated ten trenches and identified a channel correlated on both sides of the fault. This channel: a) shows mean lateral offsets of 15.9 m (and median and 2σ bounds of 15.5 +2.6/-0.7 m), and b) is younger than cal. 25228-25832 a cal BP. The derived mean minimum left-lateral slip-rate is 0.62 mm/yr (0.61 +0.10/-0.03 mm/yr). These values are larger than those givern in prior studies for the AMF and therefore will likely increase the seismic hazard estimates for the area.*

Key words: *Left-lateral strike-slip fault, lateral slip-rate, 3D trenches, Alhama de Murcia fault, Iberian Peninsula.*

INTRODUCTION

The seismic potential of an active fault scales with its slip rate as fast moving faults are more prone to produce larger or more frequent earthquakes than slow faults. The most common methods to assess the slip-rate along a strike slip fault are: a) three-dimensional trenching studies (Liu et al., 2006; McCalpin et al., 2009; Rockwell et al., 2009), or b) morphotectonic analyses of offset features (Salisbury et al., 2012; Scharer et al., 2014; Zielke et al., 2012). These two approaches follow different criteria when measuring offset features. 3D trenching consists of excavating a trench on both sides of the fault and cutting them back to follow a buried lineal feature into and across the fault. The morphotectonic analysis aims to detect a linear surface feature, such as a channel, and to measure the distance between the two piercing points obtained by projecting the trend of the feature into the fault.

The Alhama de Murcia fault (AMF) is a seismogenic left-lateral slow to moderate rate strike-slip fault whose lateral component is uncertain (Martínez-Díaz et al., 2003; Masana et al., 2004; Ortuño et al., 2012). Our new work provides a new and better-constrained lateral slip-rate value for the fault based on a 3D paleoseismic trenching data. In addition to using 3D trenching to locate buried piercing lines, we combined the morphotectonic approach that determinates the trend of the piercing lines (channels) and projects them into the fault to obtain the offset. We did, thus, a three-dimensional trenching analysis applying the criteria that belongs to morphotectonic analysis.

GEOLOGICAL SETTING

The AMF is a N45E – N65E left-lateral strike-slip fault with a reverse component and is one of the main faults composing the Eastern Betics Shear Zone (EBSZ; Fig. 1). This shear system absorbs part of the convergence between the Eurasian and African plates (Masana et al., 2004) that ranges 4-5 mm/yr (Nocquet, 2012).

Several earthquakes have been produced by the AMF (IGN, 2012). Previous paleoseismic studies suggest that the vertical component of its slip-rate along the transpressional parts of the fault ranges between 0.04 and 0.35 mm/yr (Martínez-Díaz et al., 2003; Masana et al., 2004). A very rough lateral slip rate estimate of 0.21 mm/yr was proposed from the analysis of morphological features on the surface of the El Saltador Alluvial fan (Martínez-Díaz et al., 2003). Ortuño et al. (2012) estimate the net rate of individual fault branches at the SW termination of the AMF to be between 0.45 and 1.33 mm/yr. However, all these values have a high uncertainty due to the high degree of anthropogenic alteration of the original morphology.

In this work, we focused on the El Saltador site, located on the southern branch of the AMF along the Lorca-Totana segment of the fault (6 km NE of Lorca, Fig. 1). A previous paleoseismological analysis at the site suggested the occurrence of two paleoearthquakes (Martínez-Díaz et al., 2003; Masana et al., 2004). Ten new trenches were excavated, six of them parallel to the fault (Fig. 2). The main objective of these new trenches was to better constrain the left-lateral slip-rate for the AMF by exposing linear features (i.e. paleochannels) that are offset by the fault.

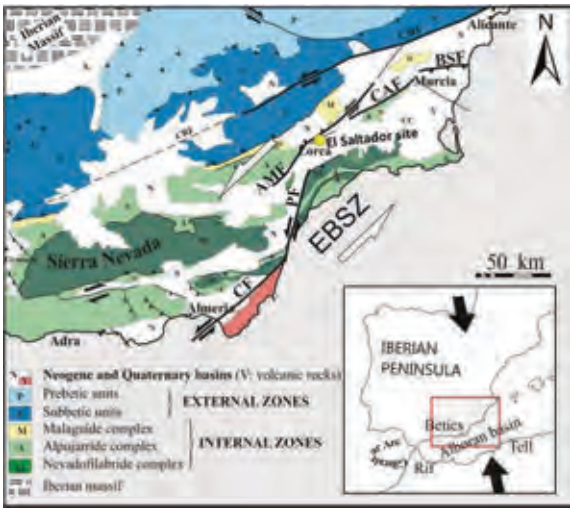

Figure 1: Geological map of Eastern Betics Shear Zone (EBSZ). Legend: AMF, Alhama de Murcia fault; CAF, Carrascoy fault; CF, Carboneras fault; CRF, Crevillente fault; PF, Palomares fault; (Masana et al., 2004).

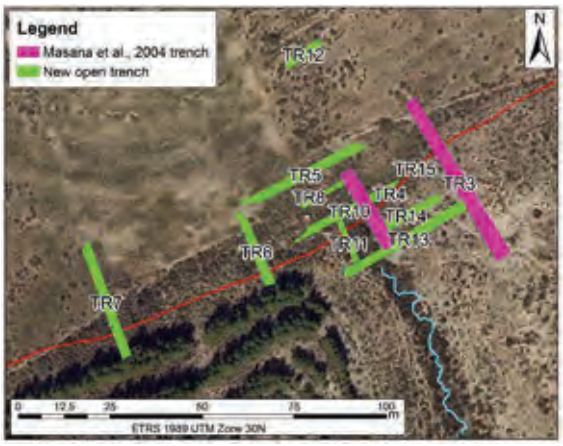

Figure 2: Aerial photo of the El Saltador site.

METHODOLOGY

Three-dimensional trenching studies and morphotectonic analysis of laterally offset features use slightly different criteria to obtain the lateral offsets. In the first case, several trenches are excavated progressively towards the fault in each block in order to measure the offset directly next to the fault, whereas in the other case the precise morphology next to the fault of the considered feature is not important, and the measurement takes into account the far-field tendency of a channel and projects it to the fault. In this study we measure the offset of buried units by a 3D analysis, determining the far-field trend of the linear features in these units, i.e. a three-dimensional trenching analysis with morphotectonic criteria.

In a simplified way or at a very large scale, a channel is a linear feature, but at a more detailed scale, its base is a surface composed by infinite lines. To reduce the uncertainty, it is important to select a specific line within the channel. This can be done for example by following some morphological bends along the channel shape in a vertical section such as the banks or the bottom if the incision is sharp, or by identifying sediment units that fill the channel and use them as piercing lines defined by the points where they intersect the trench wall (Fig. 3). In the trenches, we selected reference points in these channels that correspond to the intersection of these piercing lines with the trench wall (Fig. 3). For at least two trenches on both sides of the fault, we identified the same reference points. The position of the reference points was recorded in the field with a GPS (Leica Zeno 5). The best three-dimensional fit line (piercing line in Figure 3), the intersection of this with the fault plane (piercing point in Figure 3) and their associated errors were calculated with Matlab scripts. We applied the probability density calculation functions proposed by Zechar and Frankel (2009) in order to resolve the final estimates of lateral slip.

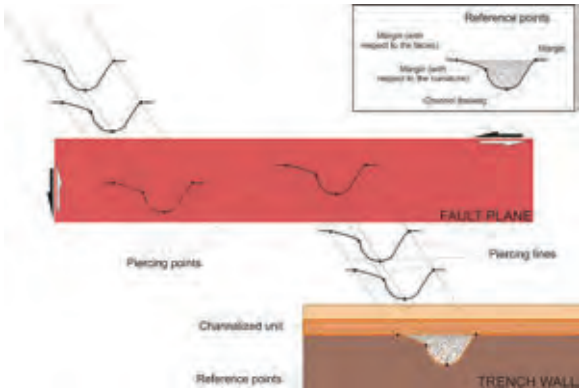

Figure 3: Diagram showing the methodology used to calculate buried paleochannel tendency in order to obtain piercing points in the fault plane.

This approach is useful when present-day analogues have constant channel trends in the modern landscape. This is the assumption we make and that prevents us to calculate smaller or larger offsets due to a change of channel trend next to the fault.

RESULTS AND DISCUSSION

We analysed channelized unit D in the El Saltador trenches (Fig. 4). Offset and slip-rate estimates are expressed by a mean (and by median and 2σ bounds).

Offset measurements

The total net offsets calculated for different piercing lines identified on the channelized unit D range between 15.06 ± 0.15 m and 17.25 ± 0.60 m (Fig. 4), whereas the lateral components of slip are in the range of 15.00 ± 0.15 m and 17.19 ± 0.60 m. For mean for net offsets is 15.95 m (15.55 +2.59/-0.71 m; Fig. 4), whereas the mean component of the lateral displacement is 15.89 m (15.49 +2.59/-0.71 m; Fig. 4). Vertical displacements were much smaller, indicating that the AMF at El Saltador is predominantly a strike slip fault.

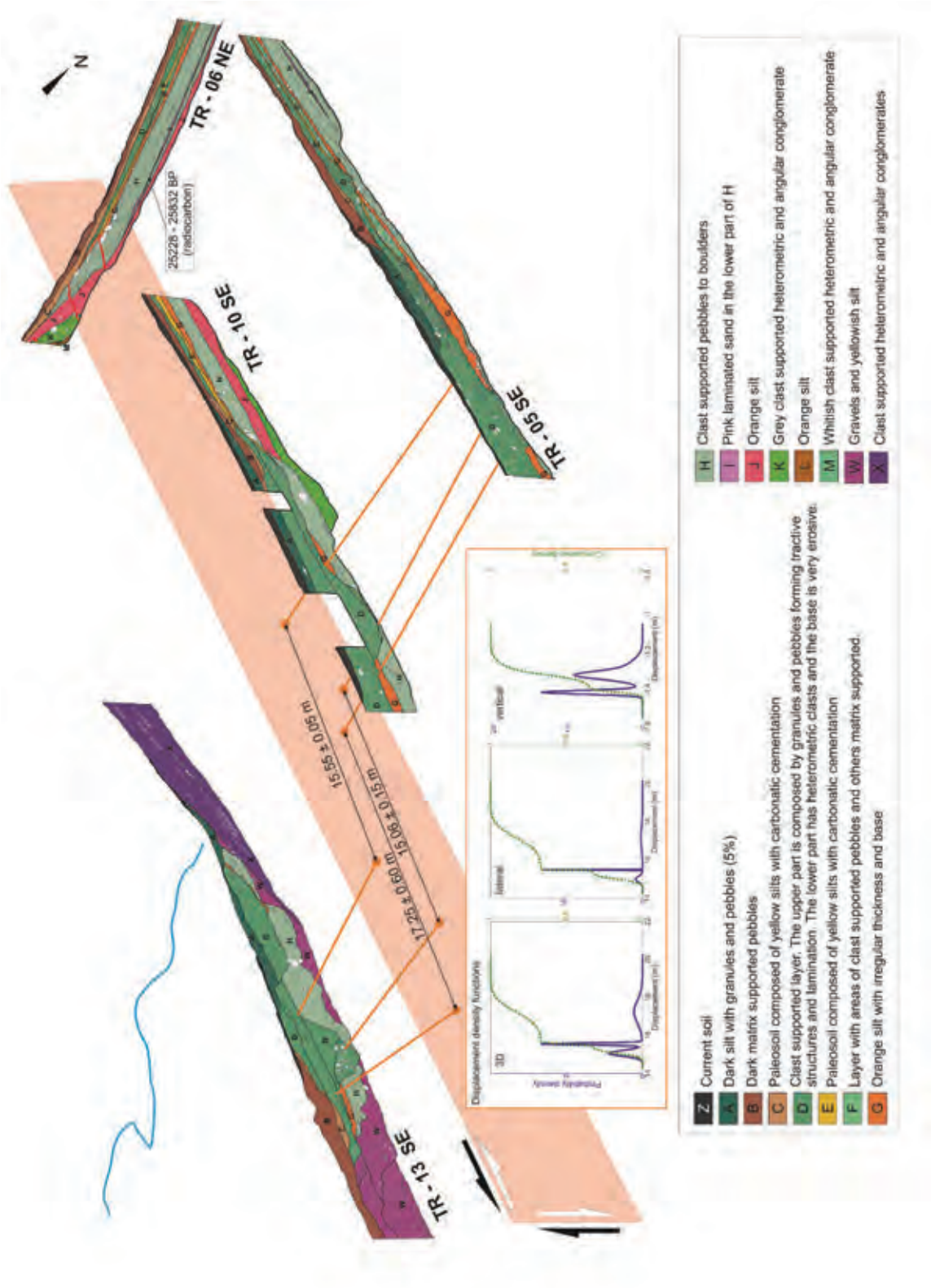

Figure 4: Three-dimensional model of the El Saltador trenches. Piercing lines, 3D offset measurements and ^{14}C dating are shown.

Dating

Dating of the units described in El Saltador site are in progress. We gathered samples to be dated using ^{14}C, OSL (Optically Stimulated Luminescence), AAR (Amino-acid racemization) and U-series applied to pedogenic carbonate. A Radiocarbon-dated charcoal sample taken

from the underlying unit H yields a calibrated age of 25228-25832 a cal BP (2σ interval). Unit H is stratigraphically much lower than unit D (Fig. 4), thus making unit D potentially significantly younger than 25228-25832 a cal BP.

Lateral slip-rate calculation

We obtained a minimum slip-rate, as we used a maximum age for unit D. The mean minimum lateral slip-rate is 0.62 mm/yr (0.61 +0.10/-0.03 mm/yr). This value only refers to the southern branch of the AMF. Even being a minimum, these values are larger than those suggested for the vertical slip-rate (0.04-0.35 mm/yr; Martínez-Díaz et al., 2003; Masana et al., 2004). This supports the interpretation that the predominant component of slip for the Alhama de Murcia fault is left-lateral (Bousquet, 1979; Martínez-Díaz, 1998). GPS results in the area (Echeverría et al., 2013) relative to stations located W from the AMF and E of the Palomares fault suggest even higher velocities. Thus, all evidence in consistent with these slip rates being minimum values.

CONCLUSIONS

After the analysis of ten new trenches at the El Saltador site, we identified one buried channel on both sides of the fault in the sedimentologic record. This channel shows a clear offset in its projection into the fault. The offset measurements for the channel was done applying a new 3D paleoseismic approach that mixes morphotectonic criteria with 3D trenching analysis. We suggest a preliminary mean minimum left-lateral slip-rate of 0.62 mm/yr. These results complement the vertical slip-rate obtained by previous authors and suggest that the AMF might have more frequent of larger earthquakes than considered to date. This should be taken into account in the seismogenic hazard assessment in the area.

Acknowledgements: The authors were supported by research projects: CGL2011-30005-C02-02 SHAKE and Project LE311A12-2. Fundings for the postdoctoral and doctoral fellowships are: Juan de la Cierva fellowship for H. Perea; FPU fellowship for M. Ferrater; and APIF fellowship for A. Echeverria. We are very grateful to Manuel Jesús Royán.

References

Bousquet, J., (1979). Quaternary strike-slip faults in southeastern Spain. *Tectonophysics*. 52, 277-286.

Echeverría, A., G. Khazaradze, E. Asensio, J. Gárate, J. Martín Dávila & E. Suriñach, (2013). Crustal deformation in eastern Betics from CuaTeNeo GPS network. *Tectonophysics*. 608, 600-612.

Instituto Geográfico Nacional, IGN, (2012). *Catálogo de terremotos*. Available in: http://www.01.ign.es/ign/layoutIn/sismoFormularioCatalogo.do

Liu-Zeng, J., Y. Klinger, K. Sieh, C. Rubin & G. Seitz, (2006). Serial ruptures of the San Andreas fault, Carrizo Plain, California, revealed by three-dimensional excavations. *Journal of Geophysical Research*. 111 (B2), B02306. doi: 10.1029/2004JB003601

Martínez-Díaz, J.J., (1998). *Neotectónica y Tectónica Activa del Sector Centro-Occidental de la Región de Murcia y Sur de Almería (Cordillera Bética - España)*. Universidad Complutense de Madrid.

Martínez-Díaz, J.J., E. Masana, J.L. Hernández-Enrile & P. Santanach, (2003). Effects of repeated paleoearthquakes on the Alhama de Murcia Fault (Betic Cordillera, Spain) on the Quaternary evolution of an alluvial fan system. *Annals of Geophysics*. 46 (5), 775-791.

Masana, E., J.J. Martínez-Díaz, J.L. Hernández-Enrile, & P. Santanach, (2004). The Alhama de Murcia fault (SE Spain), a seismogenic fault in a diffuse plate boundary: Seismotectonic implications for the Ibero-Magrebian region. *Journal of Geophysical Research*. 109, 1-17. doi: 10.1029/2002JB002359

McCalpin, J.P., T.K. Rockwell, & R.J. Weldon, (2009). Paleoseismology of Strike-Slip Tectonic Environments. In: (McCalpin, J.P., eds.). *Paleoseismology*. International Geophysics. Academic Press. 613 p.

Nocquet, J.M., (2012). Present-day kinematics of the Mediterranean: A comprehensive overview of GPS results. *Tectonophysics*. 579, 220-242.

Ortuño, M., E. Masana, E. Garcia-Melendez, J. Martinez-Diaz, P. Stepancikova, P.P. Cunha, & A.S. Murray, (2012). An exceptionally long paleoseismic record of a slow-moving fault: The Alhama de Murcia fault (Eastern Betic shear zone, Spain). *Geological Society of America Bulletin*. 124 (9-10), 1474-1494. doi: 10.1130/B30558.1.

Rockwell, T., D. Ragona, G. Seitz, R. Langridge, M.E. Aksoy, G. Ucarkus & B. Akbalik, (2009). Palaeoseismology of the North Anatolian Fault near the Marmara Sea: implications for fault segmentation and seismic hazard. *Geological Society London. Special Publications*. 316 (1), 31-54. doi: 10.1144/SP316.3.

Salisbury, J.B., T.K. Rockwell, T.J. Middleton & K.W. Hudnut, (2012). LiDAR and Field Observations of Slip Distribution for the Most Recent Surface Ruptures along the Central San Jacinto Fault. *Bulletin of the Seismological Society of America*. 102 (2), 598-619. doi: 10.1785/0120110068.

Scharer, K.M., J.B. Salisbury, J.R. Arrowsmith & T.K. Rockwell, (2014). Southern San Andreas Fault Evaluation Field Activity: Approaches to Measuring Small Geomorphic Offsets-Challenges and Recommendations for Active Fault Studies. *Seismological Research Letters*. 85 (1), 68-76. doi: 10.1785/0220130108.

Walker, F. & M.B. Allen, (2012). Offset rivers, drainage spacing and the record of strike-slip faulting: The Kuh Banan Fault, Iran. *Tectonophysics*. 530-531, 251-263. doi: 10.1016/j.tecto.2012.01.001

Zechar, J.D., & K.L. Frankel, (2009). Incorporating and reporting uncertainties in fault slip rates. *Journal of Geophysical Research*. 114 (B12), B12407. doi:10.1029/2009JB006325.

Zielke, O., J.R. Arrowsmith, L. Grant Ludwig & S.O. Akciz, (2012). High-Resolution Topography-Derived Offsets along the 1857 Fort Tejon Earthquake Rupture Trace, San Andreas Fault. *Bulletin of the Seismological Society of America*. 102 (3), 1135-1154. doi: 10.1785/0120110230.

INQUA Focus Group on Paleoseismology and Active Tectonics

paleoseismicity.org

ArMedEa project: archaeology of medieval earthquakes in Europe (1000-1550 AD). First research activities

Forlin, P. (1), Gerrard, C. (1), Petley, D. (2)

(1) Department of Archaeology, Durham University, South Road, Durham, DH1 3LE, UK. Email: paolo.forlin@durham.ac.uk
(2) School of Environmental Science, University of East Anglia, Norwich Research Park, Norwich, NR4 7TJ, UK

Abstract: *This paper introduces the research of the Armedea project. Armedea (Archaeology of medieval earthquakes in Europe, 1000-1550 AD) is a medieval archaeology project undertaken at the Department of Archaeology of Durham University which analyses archaeological evidence related to late medieval seismic-affected contexts at a European scale. This project is therefore focused on both earthquake effects on archaeological sites, their standing buildings and environment, and the archaeological evidence that reveals the response of medieval societies in terms of risk reduction, protection and resilience. A first preview of GIS analysis of seismic activity impact on medieval societies and fieldwork activities carried out in Italy, Cyprus and Azores (Portugal) is presented here. This research is supported by a Marie Curie Intra European Fellowship within the 7th European Community Framework Programme.*

Key words: *Medieval Archaeology, Medieval Europe, historical seismicity, GIS, fieldwork.*

INTRODUCTION

Seismic catalogues of historic events play a significant role in hazard mitigation across the European Union. These projects are based mainly on documentary surveys or driven from an earth-science perspective but the archaeological verification for seismic activity remains under-researched. The aim of ArMedEa project (April 2014 - March 2016) is to develop more fully the analysis of the physical impacts of and human reaction to earthquakes, tsunamis and seismic-induced landslide during the later Middle Ages (Gerrard and Petley, 2013). Our work is at a European scale and adopts a specifically archaeological approach to collate and integrate information from a wide range of sources including standing buildings, buried stratigraphical sequences and palaeoenvironmental data.

The main objectives of the ArMedEa project are fourfold:

1 - To develop a geographical database (GIS) able to collect, organise and interrogate archaeological and environmental evidence related to seismic events in the Middle Ages, drawing on existing catalogues, publications and untapped 'grey literature';

2 - to create maps which appropriately quantify exposure to seismic risk in the later medieval period, taking into account changing medieval population densities through time against actual seismic hazards maps. A similar analysis will be carried out to understand the impact of known earthquakes on medieval societies through a comparison of the same population density maps with the isoseismal maps of the most significant medieval earthquakes;

3 - To investigate a sample of well-documented episodes using a combination of remote sensing and fieldwork. These case-studies will be located in different European countries, such as Spain, Portugal, Italy, Greece and Austria, for instance;

4 - To understand the 'risk-sensitive tactics' adopted by medieval societies in different regions, particularly their resilience and hazard reduction strategies from an archaeological perspective.

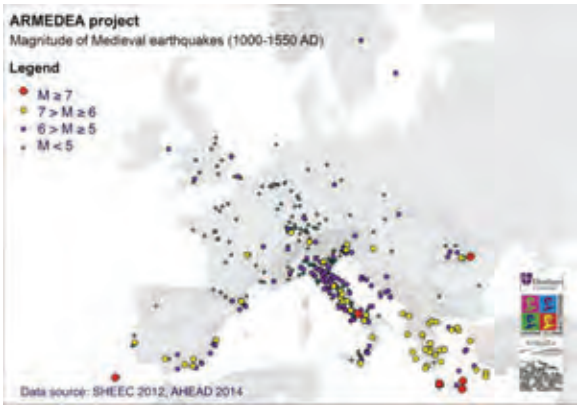

Figure 1: Epicentres of catalogued late medieval earthquakes (Data source: SHEEC and AHEAD projects, Stucchi et al. 2013; Locati et al. 2014).

ARMEDEA GIS DATABASE

The Armedea GIS database has been defined in order to collate archaeological evidence relating to medieval seismic activity (fig. 1), such as data from excavations, architectural evidence preserved on standing buildings, and earthquake environmental effects (EEE) such as tsunamis and landslides. The database therefore presents a tree structure on three different levels that, for each event, allows the organisation of general information relating to the earthquake (*level 1*: name, date, epicentre, magnitude, intensity, sources, references, etc.), the related affected places (*level 2*: name of the locality, intensity, type of information, etc.), shown as Macroseismic Data Points (MDPs data source: AHEAD archive: Locati et al., 2014; Stucchi et al., 2013), and the archaeological effects (or the documentary

sources that recorded them) within each MDP (*level 3*: data from excavations, architectural evidence, tsunami, landslide, with details). This catalogue will allow us to implement queries about the quality and geographical distribution of information, the nature of the damage and strategy of response relating to the medieval earthquakes in Europe during the period 1000-1550 AD from an archaeological perspective.
Earthquakes occurring up to the beginning of the 13th century have been recorded so far. Figure 2 shows an output map from the Veronese earthquake (1117 AD, highest intensity = IX) file, indicating buildings and archaeological excavations with seismic-related evidence in the Dome's area of Padua (after Brogiolo, 2011, p. 62, fig. 38).

Figure 2: Padua, Piazza del Duomo. Gis map showing catalogued buildings and excavations with earthquake archaeological evidence.

EARTHQUAKES IMPACT ON MEDIEVAL SOCIETIES AND ECONOMIC ACTIVITIES

By virtue of national and international historical seismic catalogues, we already know with a reasonable accuracy where earthquakes occurred during the late Middle Ages in Europe. The real unknown is to gauge how great the impact of these seismic events was on societies and their economies. GIS data management allows us to run a crude analysis to quantify the effects of catalogued earthquakes on people and economic activity in medieval Europe. To do this, a set of preliminary maps was created showing the medieval population density for every century in 1000-1550 time-window (fig. 3). These data were obtained from pre-existing studies of medieval demography (for instance, Malanima, 2010) which illustrate, for example, regions of Europe with the highest population density during the Middle Ages (Italy and Flanders), and fluctuations in European medieval population, characterised by progressive growth up to 1348 followed by a profound contraction and a weak recovery. The creation of those maps is still in progress, and a greater refinement of regional-scale outputs is currently underway.

The next step is to overlay these population and urban density maps with raster maps displaying the macro-seismic effects (isoseismal maps) of each single medieval earthquake with an equivalent calculated magnitude ≥ 5. The end result, therefore, will be a set of maps showing the degree of seismic impact in terms of population affected by the catalogued seismic activity.

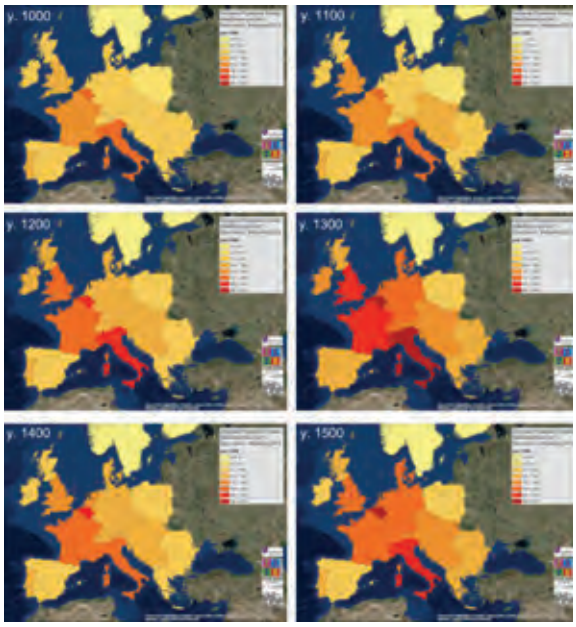

Figure 3: Mosaic of European population density maps in 1000-1500 AD time-window.

Nevertheless, we need to take into account that population density and seismic recording represent two parameters that may provide a false positive when correlated (the denser the population and the higher the economic activity, the greater the accuracy of the historical information). To avoid this, actual seismic hazard maps will be compared against both medieval population density maps and medieval seismic activity maps. Only then we can identify regions in which exposure to seismic activity has been underestimated because of a lack of relevant information.
In addition, one outcome of this analysis will be therefore an archaeological predictive 'risk' map that infers the distribution of seismic-related sites in medieval Europe, but within a contemporary social and economic context.

ARMEDEA CASE STUDIES AND FIELDWORK

Armedea aims to develop fieldwork on several European areas affected by seismic activity during the Middle Ages (fig. 4). So far, five case studies have been selected.
They are:

- Azores (earthquake and landslide in 1522);

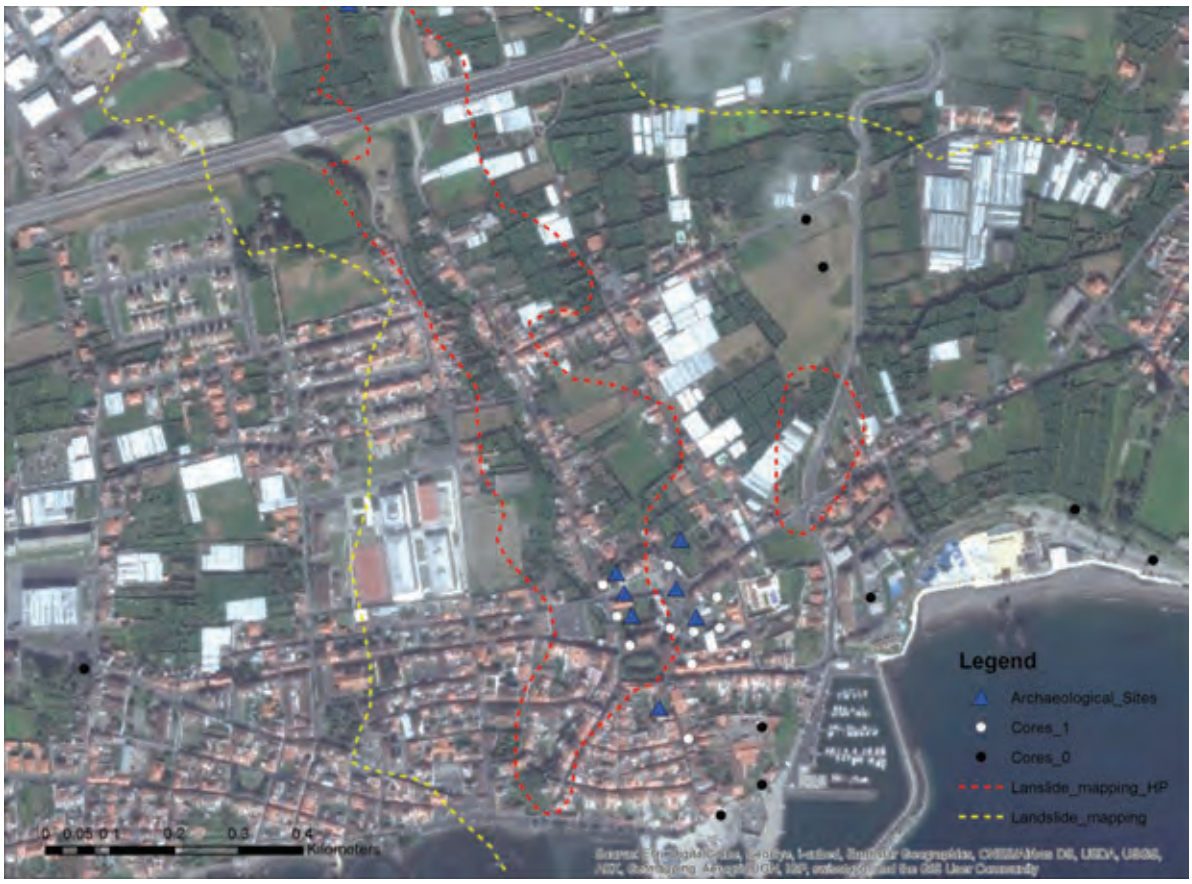

Figure 5: Map showing the distribution of the archaeological sites found by Oliveira (Bento 1989) in relationship with the landslide that buried the old Vila Franca do Campo in 1522 (after Marques et al. 2009).

- Andalusia (earthquakes during the 12th and 13th century);
- Northern Italy and Carinthia, Austria (earthquakes and landslides in 1117, 1222 and 1348);
- Crete (earthquake 1303);
- Cyprus (earthquakes, tsunamis and landslides in 1222 and 1491).

By the end of 2014, preliminary fieldworks have been carried out in Cyprus and in the Azores.

In Saõ Miguel, the largest Azorean island, a preliminary evaluation of the archaeological potential of the ancient Vial da Franca do Campo site was undertaken (fig. 5).

On October 22nd, 1522, a Mw 5.0-5.9 earthquake triggered several landslides on the island of Saõ Miguel. The largest one was activated by an active fault identified east of the Fogo volcano on the Achada das Furnas plateau (Carmo et al., 2013). This mass movement, the volume of which has been calculated as 6.75×106 m3 with an extension of 4.5 km2 (Marques et Al. 2009), buried most of the settlement of Vila Franca do Campo, then-capital of Portuguese Azores, killing ca. 5000 people according to contemporary sources (Frutuoso, 1981).

Archaeological investigations carried out during the 1960s and '70s by a local archaeologist, Sousa d'Oliveira (Bento, 1989), identified several remains of the buried settlement at a depth of between 2 and 5 m underneath the actual surface. However, the quality of the archaeological documentation was not detailed; only very approximate plans and sections were produced. Nevertheless, the site presents a very high archaeological potential, as most of the ancient Vila Franca do Campo possibly lies preserved beneath this mass movement deposit.

Preliminary fieldwork conducted in November gave us the opportunity to cross-reference available archaeological and palaeoenvironmental information, as shown by the attached GIS map. A first evaluation of the archaeological deposit distribution has therefore been assessed in order to consider possible future research. This case study allows us to open an exceptional window on the effects of the seismic event, but also on the reaction activated by the local population. Since the 'new' Vila Franca do Campo was founded along the western side of the landslide (for instance, the convent of São Francisco was built immediately after the earthquake in 1522), this context can be seen as an extraordinary example of resilience of that community, who again faced another destructive earthquake in 1536.

In Cyprus, research has focused on sites affected by earthquakes in 1222 and 1491. At Saranda Kolones, Paphos, a Crusader castle completely destroyed by 1222 earthquake (fig. 6), and at churches in Nicosia and Famagusta severely damage by 1491 seismic event, preliminary EAE (earthquake archaeological effects) analysis allowed to recognise several structural damages such as detached walls, penetrative fractures in walls, displaced masonry blocks, collapsed vaults, deformed arches and columns. Consultation of local archives under the supervision of the Department of Antiquities of Cyprus has begun, and unpublished evidence about the destruction of Saranda Kolones site, for instance, has been identified. Moreover, a preliminary mapping of landslides possibly related with the aforementioned events has been carried out in the surroundings of Satvrovouni and Chrysoroiatissa monasteries. Archaeological contexts in Cyprus are of primary interest as they show different strategies of response to medieval seismic effects, ranging from complete site abandonment to articulated efforts in reconstructing, reshaping and restoring the damaged buildings.

Figure 6: Paphos, Cyprus. Saranda Kolones Crusader castle. Internal pilaster with penetrative fractures.

In northern Italy, fieldwork is mainly focused on those medieval cities that suffered during the 1117 AD earthquake. A reassessment of some urban archaeological sequences and architectural remains is currently in progress, above all in Veneto's cities such as Verona, Vicenza and Padua. Here, new data on 1117 earthquake effects are emerging with data crossing of published and unpublished researches with recent fieldwork and excavation. This event appears crucial in terms of medieval response to seismic risk analysis since it affected a large portion of what was one of the most densely inhabited and economically significant European region. Again, archaeological evidence allows us to open a new window on 12th century northern Italian societies and on their effort to react to one of the most destructive seismic events that this region has suffered during the last 2000 years.

Acknowledgements: We would like to thank the Department of Antiquities of Cyprus, the Soprintendenza per i Beni Archeologici del Veneto, prof. Gian Pietro Brogiolo (University of Padua), prof. Massimiliano Stucchi, dr. Mario Locati (INGV) and José Bettencourt (University of Lisbon) for their support.

References

Bento, C.M., (1989). *Escavações Arqueológicas em Vila Franca do Campo 1967-1982*. São Miguel. Associação Arqueológica do Arquipélago dos Açores.

Brogiolo, G.P., (2011). Architetture religiose a Padova, In: Padova, architetture medievali. *Progetto ARMEP* (2008-2010) (Chavarria Arnau, A., ed.), Mantova, 35-74.

Carmo, R., J. Madeira, A. Hipólito, T. Ferreira, (2013). Paleoseismological evidence for historical surface faulting in São Miguel island (Azores). *Annals of Geophysics*. 56, 6, 2013, S0671. doi: 10.4401/ag-6221.

Frutuoso, G., (1522-1591†). Livro Quarto das Saudades da Terra, In: *Saudades da Terra*. (Frutuoso, G., ed.), 2a ed. Ponta Delgada. Instituto Cultural de Ponta Delgada. II, 1981.

Gerrard, C.M. and D. Petley, (2013). A risk society? Environmental hazards, risk and resilience in the later Middle Ages in Europe. *Natural Hazards*. June 2013. doi: 10.1007/s11069-013-0750-7.

Locati, M., A. Rovida, P. Albini and M. Stucchi, (2014). *The AHEAD Portal: A Gateway to European Historical Earthquake Data*. doi: 10.1785/0220130113

Malanima, P., (2010). *Pre-modern European economy. One thousand years (10th-19th centuries)*. Leiden-Boston, Bril.

Marques, R., J.L. Zêzere, J.L. Gaspar, P. Amaral, (2009). Reconstituição e modelação probabilística da escoada detrítica de Vila Franca do Campo desencadeada pelo sismo de 22 de Outubro de 1522 (S. Miguel, Açores*). Publicações da Associação Portuguesa de Geomorfólogos*. Volume VI, APGEOM. Braga. 2009. p. 175-182.

Stucchi M., A. Rovida, A.A. Gomez Capera, P. Alexandre, T. Camelbeeck, M.B. Demircioglu, P. Gasperini, V. Kouskouna, R.M.W. Musson, M. Radulian, K. Sesetyan, S. Vilanova, D. Baumont, H. Bungum, D. Fäh, W. Lenhardt, K. Makropoulos, J.M. Martinez Solares, O. Scotti, M. Živcic, P. Albini, J. Batllo, C. Papaioannou, R. Tatevossian, M. Locati, C. Meletti, D. Viganò, and D. Giardini, (2013). The SHARE European Earthquake Catalogue (SHEEC) 1000-1899. *Journal of Seismology*. doi: 10.1007/s10950-012-9335-2.

Reconstruction of the subsurface geology aimed at identifying areas susceptible to liquefaction in the epicentral area of the M7, 1915 earthquake (Fucino Basin, central Italy)

Francescone, M. (1), Nardone, M. (1), Boncio, P. (1), Vessia, G. (2), Amoroso, S. (3)

(1) Dept. DiSPUTer, G.D'Annunzio University, Chieti, Italy. Email: mib87@hotmail.it
(2) Dept. INGEO, G. D'Annunzio Universtity, Chieti, Italy
(3) Istituto Nazionale di Geofisica e Vulcanologia, L'Aquila, Italy

Abstract: *The present study deals with co-seismic liquefaction due to strong earthquakes (Ml>5) where the water table is near the ground surface and sandy-to-silty soils (e.g., lacustrine sediments) characterize the first ~20 m of stratigraphy. This is the case of the Fucino Basin area in central Italy, which was struck by the large 1915 earthquake. Historical reports of the geological effects of the earthquake documented evidence of severe ground deformation referable to near-surface liquefaction. In order to develop a liquefaction hazard map, we performed a detailed reconstruction of the shallow subsurface geology of the Fucino basin. We demonstrate that large areas, including urbanized areas, are susceptible to liquefaction.*

Key words: *Coseismic effect, liquefaction, local seismic hazard, microzonation, subsurface geology.*

INTRODUCTION

Coseismic ground liquefaction might be the cause of severe damage during strong-to-large earthquakes. In spite of the very large number of cases documented in modern, historical and pre-historical times (e.g., see Galli, 2000 for Italy), there are areas where the urban development pays very little attention to liquefaction hazard. This occurs also in areas where past earthquakes triggered liquefaction phenomena. This is the case of the Fucino basin in central Italy, struck by the January 13, 1915, M 7.0 earthquake.

The Fucino basin is a long-lived half-graben controlled by a large, still active SW-dipping normal fault which activated during the 1915 earthquake (see Castenetto and Galadini, 1999 with references therein). The graben hosted a large lake, which was drained at the end of the XIX century. The graben is filled by a thick sequence (up to ~1000 m) of Lower Pleistocene-to-Holocene continental deposits. In the central basin the stratigraphy is dominated by fine-grained lacustrine sediments, while in the perimetrical areas medium-to-coarse-grained fluvial and alluvial fan deposits interfinger with lacustrine sediments.

In the epicentral area of the 1915 earthquake, Oddone (1915) documented a number of geological coseismic effects referable to liquefaction. The statement that urbanization policies (and practice) pay very little attention to liquefaction hazard is motivated by a crude examination of the geologic, geognostic, geophysic and geotechnic data performed in the past in the urbanised perimeter of the Fucino basin. Detailed geologic investigations aimed at quantifying the potential of ground liquefaction are very rare. In most of the cases, the geologic and geognostic investigations are not adequate to quantify the susceptibility to liquefaction, or the investigated depths are not sufficient.

Therefore, it seems extremely important to define the areas susceptible to coseismic ground liquefaction. This is the aim of this work, which is based mostly on geological data. Our work and results are important in projects of systematic assessment of local seismic hazard, such as seismic microzonation studies.

DATA AND METHODOLOGY

In order to reconstruct the subsurface geology of the area we collected a large number of well and geognostic data in the entire Fucino area. Overall, we collected 427 stratigraphies of wells drilled since '50 for hydrogeologic exploration/exploitation, the results of 3 geophysical investigations (mostly Vertical Electric Soundings) for hydrogeologic investigations performed between '50 and '80, and several *in situ* geognostic investigations made available by professional geologists or published by research institutes. These data include 69 stratigraphies from geognostic wells, 133 dynamic penetration tests, 8 static penetration tests, and 6 seismic and flat dilatometer tests.

From the collected data we extracted the information useful for defining the susceptibility to liquefaction, such as the depth of the water table and the depth and thickness of layers characterized by prevailing sandy texture (sand, silty sand, clayey sand, gravelly sand). The information on the water table was obtained directly from the analysed geognostic data and/or from the hydrogeologic map of the Fucino basin (Petitta et al., 2005).

By combining subsurface data with surface geological data (geologic maps from Carta Geologica d'Italia, 2005; original geological maps from an ongoing project of seismic microzonation of the Avezzano Municipality), we constructed a number of detailed geological sections in order to define the geometry and lateral continuity of sedimentary bodies susceptible to liquefaction. In particular, we concentrated our attention in the northern part of the Fucino basin, where we drew 11 geologic sections (vertical scale 1:1000; Fig. 1). The reconstructed

2D geometries allowed us to identify the areas characterized by water-saturated sandy bodies within the first 20 m depths. From a geologic point of view, these areas can be considered potentially susceptible to liquefaction.

town. Moreover, all the Fucino plain (light blue in Fig. 1) is potentially susceptible to liquefaction.

The preliminary estimates from penetrometer tests indicate LPI within the geology-defined zones mostly varying from moderate to high. On the other hand, in the

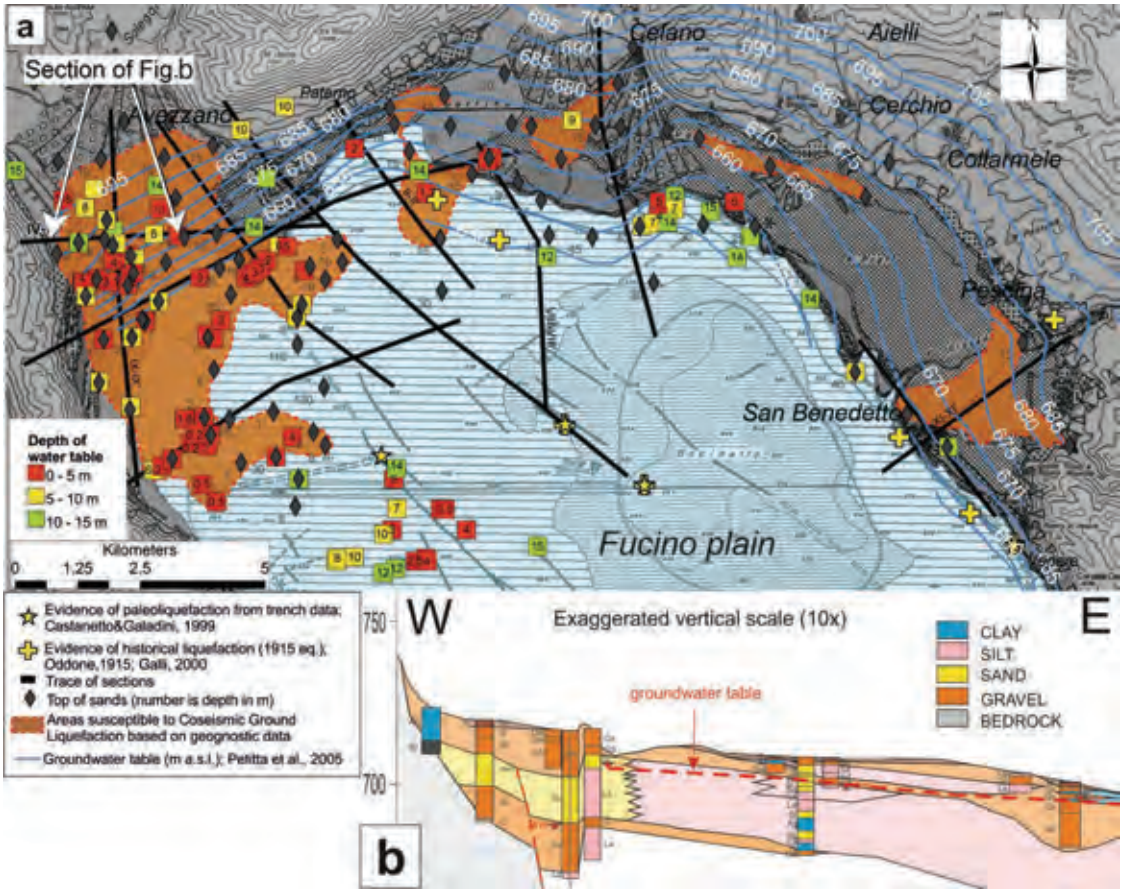

Figure 1: a) Map of zones potentially susceptible to liquefaction based on geologic and geognostic data, and location of historical (1915) and paleo- liquefactions. Note that the entire Fucino plain (light blue) might be susceptible to liquefaction but a more detailed zonation is not possible due to the lack of subsurface data. This may explain why historical and paleo-liquefactions apparently do not correlate with hazard (orange) areas. b) Example of section across the Avezzano town.

Finally, we preliminary tested the geology-based results by estimating the Liquefaction Safety Factor (LSF) and the Liquefaction Potential Index (LPI) by applying simplified methods (e.g., Idriss and Boulanger, 2004) to the pre-existing dynamic penetration tests and cone (a few) penetration tests.

RESULTS

The detailed reconstruction of the shallow subsurface geology in the Fucino basin allowed us to define a number of zones potentially susceptible to liquefaction. The zones correspond to areas with significantly thick, laterally continuous sandy bodies within the first 20m depths, and below the water table (orange areas in Fig. 1) These zones affect a large part of the urbanized perimeter of the Fucino basin, including the Avezzano

same geology-defined zones the same analyses indicate low or null LPI, due to high resistance to penetration of sandy layers. Therefore, it is clear that the geological approach is not sufficient and the whole area deserves a greater number of *in situ* geognostic/geotechnic investigations. But it is also clear that the geological approach is necessary in order to adequately address the analyses for a robust quantification of the hazard. We concluded that this aspect was seriously underestimated during the development of the Fucino area, despite the severe effects left by the 1915 earthquake.

References

Carta Geologica d'Italia, (2005). Foglio 368 Avezzano, scala 1:50.000. *APAT. Servizio Geologico d'Italia and Regione Abruzzo.*

Castanetto S. & F. Galadini, eds. (1999). 13 Gennaio 1915. Il terremoto della Marsica. *Servizio Sismico Nazionale e C.N.R. Istituto di Ricerca sulla Tettonica.* Roma, 788 pp.

Galli, P., (2000). New empirical relationships between magnitude and distance for liquefaction. *Tectonophysics*. 324, 169-187.

Oddone, E., (1915). Gli elementi fisici del grande terremoto marsicano fucense del 13 gennaio 1915. *Boll. Soc. Sismol. It.* 19, 71-216.

Petitta M., E. Burri, A. Del Bon & A. Marchetti, (2005). *Carta idrogeologica del Fucino, scala 1/50.000. Atlante tematico del Fucino*, foglio 1. ARSSA Abruzzo. SELCA Firenze.

Idriss, I.M. & R.W. Boulanger, (2004). Semi-empirical procedures for evaluating liquefaction potential during earthquakes. *11th International Conference on Soil Dynamics & Earthquake Engineering. Proceedings of the 11th ICSDEE & 3rd ICEGE*, Berkeley. January. 7-9, 2004, 2004-01.

INQUA Focus Group on Paleoseismology and Active Tectonics

Geochronology, pedostratigraphy, and late Quaternary landscape evolution in the western Po Plain (northern Italy)

Frigerio, C. (1), Zerboni, A. (2), Livio, F. (1), Bonadeo, L. (1), Michetti, A.M. (1), Brunamonte, F. (1), Fioraso, G. (3), Amit, R. (4), Porat, N. (4)

(1) Dipartimento di Scienza e Alta Tecnologia, Università degli Studi dell'Insubria, Via Valleggio n. 11, 22100 Como, Italy. Email: cfrigerio@uninsubria.it
(2) Dipartimento di Scienze della Terra "A. Desio", Università degli Studi di Milano, Via L. Mangiagalli 34, I-20133 Milano, Italy
(3) CNR, Istituto di Geoscienze e Georisorse, Torino, Italy
(4) Geological Survey of Israel, 30 Malkhe Israel St., Jerusalem, Israel

Abstract: *Deciphering the Late Quaternary evolution of the landscape is the key to understand the dynamics of the territory, to reconstruct its recent evolution and hypothesize its future trend. With this in mind, in the recent years a number of tectonic and morphostratigraphic studies were performed in the Piedmont sector of the Western Po Plain, with the intention to reconstruct its landscape evolution since the Plio-Pleistocene. In particular, new seismotectonic models have been defined to characterize the state of activity of the fold and thrust belt along the Torino Hill – Monferrato Arc, and the related seismic potential. In fact, according to the available historical and instrumental information the local seismicity level should be considered very low. This hypothesis was questioned after the 2012 Modena sequence, which raised the concern that earthquake hazards in the Po Plain have been largely overlooked until now. The detailed analysis of Quaternary landscapes is the key for attacking this issue. The evolutionary framework obtained so far, however, lacks a robust radiometric time reference, which would give a more precise definition of the Pleistocene fault slip-rates and their variability in time and space along the different segments of the Monferrato Arc. This opens a new research perspective, aimed to a detailed geochronological characterization of the western part of the Po river basin, through the use of innovative dating techniques, such as cosmogenic nuclide and OSL dating. The widespread presence of well preserved flights of terraces sealed by sequences of loess deposits makes the study area a unique natural laboratory for this kind of research.*

Key words: *Western Po Plain, Quaternary evolution, pedostratigraphy, radiometric dating, active tectonics*.

INTRODUCTION

At the western Po Plain (Northern Italy), close to the Asti and Torino Hills, flights of terraces composed by Quaternary sediments have been shaped during the evolution of the mid-southern Piedmont region drainage network. These sediments and the related landforms record the deformations induced by a belt of buried compressional tectonic structures linked to the Monferrato Arc structural front. Recent studies provide evidence of Late Pleistocene to Holocene tectonic displacement along some segment of this structural front (e.g., Michetti et al., 2012; Giraudi, 2014). This is of vital interest for seismic hazard assessment, due to the lack of historical and instrumental data in the available seismic catalogues. Indeed, the earthquake potential in this area can only be evaluated through geological investigations.

Tectonic setting

The Monferrato Arc in the Italian scientific literature has often been defined as the "Padanian Thrust Front" (PTF). It structurally belongs to the northernmost sector of the Apennines and it is bounded to the west and to the north by the western Alps and to the south by the Ligurian Alps (Figs. 1 and 2). The metamorphic Penninic Units of the western Ligurian Alps are tectonically juxtaposed against the non-metamorphic Ligurian Units of the Apennines, along an E-W trending regional fault zone, just south of the Torino–Monferrato hills.

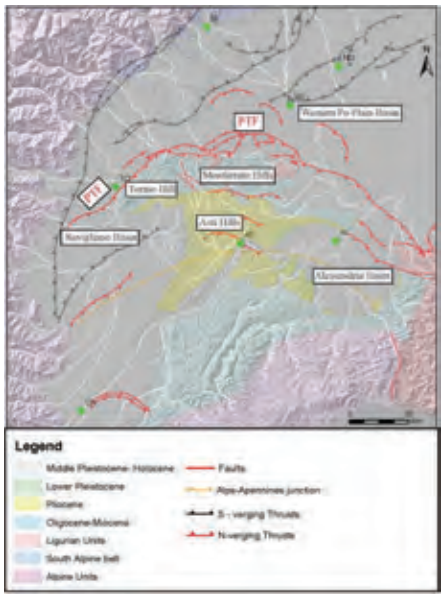

Figure 1: Monferrato Arc. The north-verging Padanian Thrust Front (PTF) is buried beneath the alluvial surface of the Po Plain, bounding the northern slope of the Torino and Monferrato Hills (modified after Bonadeo, 2014).

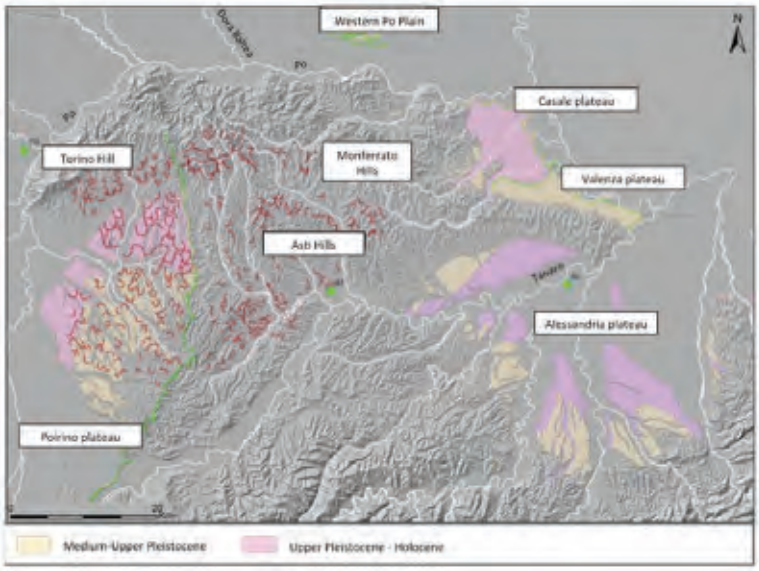

Figure 2: Geological and geomorphological map showing deposits and Quaternary evolution forms linked to regional drainage network (modified after Bonadeo, 2014).

The Monferrato area exposes a sequence of Late Eocene to Messinian deposits, which lie on a substratum of Ligurian Units (e.g., Bonsignore et al. 1969), which extensively outcrop along the Torino Hill.
The latter lies on the hangingwall anticline of an out-of-sequence, north-verging, breakthrough thrust. Conversely, beneath the Monferrato hills, an important imbricate and north-verging thrust sheet is present. The Rio Freddo Deformation Zone, a north-west striking transpressive fault zone (Piana & Polino, 1995), separates the Torino Hill and Monferrato domains.
The available seismic lines highlight a considerable lowering of the tectonic activity along the junction between the Alps and the Apennines since the Oligocene, and a contemporary progressive activation of out-of-sequence, north-verging thrusts from the west to the east (e.g., Falletti et al. 1995, Mosca et al. 2009). These latter structures typically cut off older alpine thrusts along the so-called 'Torino Hill structural belt' (Mosca, 2006). The data made available by CARG (CARtografia Geologica, isprambiente.gov.it) geological mapping project (Dela Pierre et al. 2003a, Dela Pierre et al. 2003b, Festa et al. 2009a, Festa et al. 2009b) clearly document the progressive offset of stratigraphic units and geomorphic paleosurfaces across the PTF during the Pliocene and Quaternary. In the Monferrato area, the tectonic evolution is also revealed by the particularly emphasized morphological evolution. Dramatic changes in the drainage network occurred during the mid-to-late Pleistocene in response to the growth of the Torino Hill and the Monferrato frontal thrusts. A complex rearrangement of fluvial drainage affected the Po, Dora Baltea and Tanaro Rivers (e.g. Forno 1982, Carraro et al. 1995), and it testifies the important recent tectonic activity of the PTF. In particular, until probably the late Pleistocene, the Po River drained eastward, south of the Torino and Monferrato Hills. This is suggested by: (a) the age of the oldest fluvial deposits, related to the Po River, north of Torino Hill, and (b) the clear traces of a huge meandering river that are preserved on the Poirino Plateau and in the Asti Hills (e.g., Forno 1982; Carraro & Valpreda, 1991). Moreover the tectonic deformation caused a change in the Tanaro River course that was flowing from south to north and abruptly diverted to the east just south of the Poirino plateau; the Tanaro River flows into the course of an ancient paleo river just southeast of the Asti hills.
In the Torino Hill and Monferrato area, therefore, unequivocal geologic and geomorphic evidence points out surface deformation and/or faulting at rates higher than those of the local depositional/erosional morphogenic processes (Barbero et al., 2007; Festa et al., 2009b). This implies that the late Quaternary - and especially Holocene - history of deformation and the local seismic landscape are far more valuable tools in estimating the local seismic hazard than has generally been appreciated until now. As shown by the earthquake sequence of Modena 2012 (Michetti et al., 2012), strong earthquakes with Mw 6 to 6.5, though very rare, must be considered credible events along all the Quaternary faults throughout the whole Po Plain foredeep, and in particular along the Monferrato Arc. The detailed analysis of Quaternary landscapes is the key for attacking this issue.

Geomorphic setting

The present-day configuration of the physical environment of this area of the Po Plain is characterized by undulating and plain landscapes, with low topographic gradients and marked by the presence of extensive shallow soil horizons formed on relatively recent sedimentary units. Within the study area, it is possible to separate to different landscape units: the Western Po Plain, the Torino - Monferrato Hills, the Poirino and Alessandria Plateau and the Asti Hills (Fig. 2).
The Western Po Plain is surrounded by fluvioglacial fans that extend from the outer border of the Ivrea and Rivoli-Avigliana end-moraine systems to the base of the hills,

where the rivers drain to the Po River. The entire drainage network of this area, is currently incised several meters deep within the fans that, at the distal sectors, are eroded by the Po River. The present riverbeds are related to the highest surface of the plain through flight of terraces.

The Torino and Monferrato Hills are the two morphological domains that constitute the hilly belt with arched trending emerging from the Western Po Plain. They differ from each other by their lithostratigraphic characteristics and structural pattern of the substrate.

The Poirino and Alessandria Plateaux, are sub-plain areas characterized by gentle inclinations, with variable directions between one area and another. They mostly consist of alluvial deposits related to the past fluvial activity of rivers now extinct.

The Asti Hills are carved in the Pliocene formations that, because of their physical-mechanical characteristics, greatly influence the morphology of the reliefs and the valley: the landscape is characterized by gentle hills and broad valleys.

All these landscapes are generally related to Plio-Pleistocene time intervals. However, there is a lack of radiometric constraints for the Quaternary deposits that compose the infill of the plain areas, the covers of the plateaux, and the surfaces present along the hillsides. Today this is the main obstacle to a more precise definition of the Quaternary dynamics and in particular to the characterization of the degree of activity of the tectonic structures.

The distribution and facies of Quaternary deposits, and in particular of the fluvial sediments, are controlled by major recent changes in the regional drainage network. These events are relatively dated based essentially on the intensity of weathering and on the degree of soil development (e.g., Arduino et al., 1984). The literature relating to pedogenetic characterization of Quaternary deposits in this area was mainly published during the '80s and has not been subject to recent review and geochronological calibration using updated dating methods. Therefore, there is a need to improve the radiometric age constraints, in geochronological terms, in regard to previous studies.

A new research project

This is a new research perspective; we intend to obtain a geochronological characterization of the entire area, through the use of innovative methods of absolute dating, as Optically Stimulated Luminescence (OSL) and the Cosmogenic Nuclide Dating on sediments. This approach has been recently applied at key sections of the central Po Plain (e.g., Livio et al., 2014).

For this purpose, we are looking for new outcrops and new pedosedimentary sequences, to apply these dating methods in order to better define the complex dynamics that characterized this area of the Po Plain. Eolian Loess deposits mark the last sedimentological event that cover and preserve the elevated terrain. The fluvial terraces accumulate the wind-blown sediments loess. Each of these terraces presents a different time period. The oldest loess deposits discovered, date back to the Middle Pleistocene and are identified in limited areas, at the Alpine edge. Since the end of the Middle Pleistocene, throughout the late Pleistocene and the LGM, the eolian sediments have interested large areas, the Alps and Apennine edges and the isolated terraces of the Po Plain. (Cremaschi, 1990).

Previous studies of sedimentary sequences from middle Pleistocene to LGM, reconstructed the palaeoenvironment history of this area. However, it is necessary to re-analyze these sediments using new methodologies such as those presented in the INQUA-AEOMED report (Amit & Zerboni, 2013). The present project will try to correlate different sequences of loess deposited on similar geomorphological units, located at the western part of the Po basin. It aims to evaluate the origin and the sources of these sediments. Besides, we will evaluate the rate of loess deposition and its weathering in the context of the late Quaternary paleoclimatic reconstruction. We will consider well known and freshly discovered sections in the region and

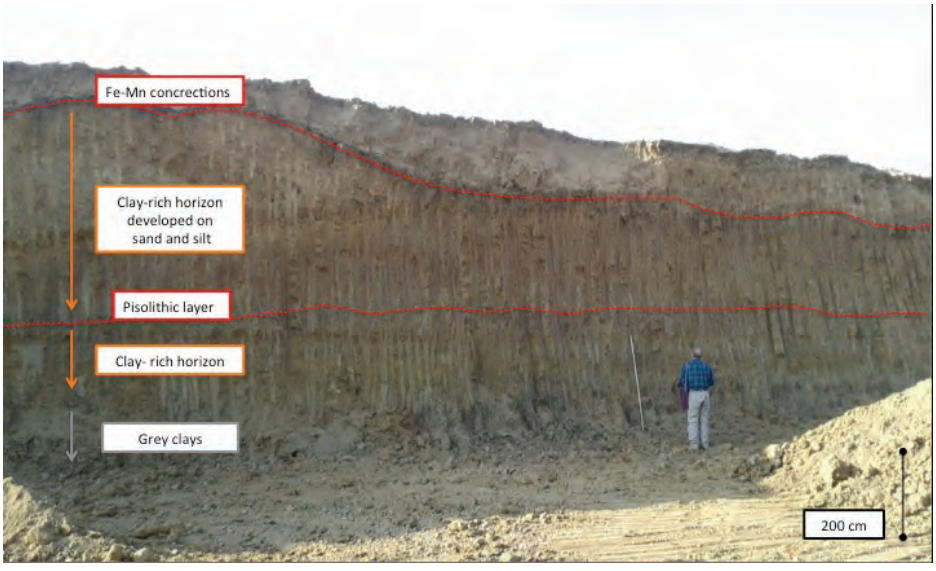

Figure 3: The studied section at Alessandria Plateau. Note the marked horizons.

in adjoining areas with the purpose of correlate them. As an example of suitable sites, Sassone et al. (2015) describe evidence of recent surface reverse faulting observed during excavation works conducted on the Casale plateau.

Moreover, the study of soils and paleosols will contribute to the reconstruction of the history of this landscape. The soil system, in fact, is one of the paleoenvironmental archives that preserve the historical memory of climate events (Cremaschi & Rodolfi, 1991).

A preliminary survey of the lowest terrace at the Alessandria Plateau has already been accomplished, in order to identify deposits that could be interpreted as primary or secondary aeolian sediments.

A first type section has been identified (Fig. 3); it is truncated at its top, marked by a pedogenetic horizon rich with Fe-Mn concretions; several B horizons below rich in clay- developed on silty to sandy-silty parent materials. Subsequent B horizons are generally separated by pisolithic layers, due to standing perched groundwater. At the base of the section, a massive clay deposit has been observed, which possibly deposited in a water body (decantation). The section was sampled for pedostratigraphic analyses and OSL dating; moreover, some undisturbed samples for the micromorphological analysis have been extracted. The study of thin sections will be an additional tool for decipher the nature and the complexity of the pedostratigraphic sections, aim to understand each evolutionary phase.

The detailed study and the analysis relating to this first sequence, together with other new sections that will be studied, will enable the reconstruction of the morphodynamics of the entire area. The precise radiometric time references from these study, could give useful information about the fault-slip-rate in the Pleistocene and their variability in time and space along the different segments of the entire area.

References

Alessio, M., L. Allegri, P. Ambrosetti, G. Bartolomei, F. Bella, G. Belluomini, G. Calderoni, F. Carraro, G. Charrier, C. Cortesi, D. Esu, M.G. Forno, S. Improta, L. Manfra and V. Petrone, (1982). Il giacimento fossilifero pleistocenico superiore di Moncucco Torinese. *Geogr. Fis. Dinam. Quat*. 5, 219-239.

Amit, R., A. Zerboni, (2013). Report on the INQUA-AEOMED field-trip workshop 'Reconsidering Loess in Northern Italy' (Po Plain, 1-3 July 2013). *Alpine and Mediterranean Quaternary*. 26 (2).

Arduino, E., E. Barberis, F. Carraro & M.G. Forno, (1984). Estimating relative ages from iron- oxide/total-iron ratios of soils in the western Po Valley, Italy. *Geoderma*. 33 (1), 39-52.

Barbero, D., P. Boano, M.T. Colla & M.G. Forno, (2007). Pleistocene terraced succession, northern slope of Torino hill. *Quaternary International*. 171-172, 64-71.

Boano, P., G.M. Forno and S. Lucchesi, (2004). Pleistocene deformation of the Collina di Torino inferred from the modelling of their fluvial succession. *Il Quaternario*. 17 (2/1), 145-150.

Bonadeo, L., (2014). *Studio sismotettonico del settore della Pianura Padana occidentale compreso tra il Tortonese ed il fronte della Collina di Torino*. Università dell'Insubria. Ph.D. pp. 178.

Bonsignore, G., G.C. Bortolami, G. Elter, A. Montrasio, F. Petrucci, U. Ragni, R. Sacchi, C. Sturani and E. Zanella, (1969). *Note Illustrative della Carta Geologica d'Italia alla scala 1:100.000, Fogli 56 e 57*. Torino/Vercelli. 2nd ed. Serv. Geol. It. Roma. 96.

Carraro, F. & E. Valpreda, (1991). The middle-upper Quaternary of the "Asti Basin". *Il Quaternario*. 4 (1°), 1991. 151-172.

Carraro, F., G. Collo, M.G. Forno, M. Giardino, F. Maraga, A. Perotto and D. Tropeano, (1995). L'evoluzione del reticolato idrografico del Piemonte centrale in relazione alla mobilità quaternaria. In: (Polino, R., and Sacchi, R., eds.). *Atti del Convegno "Rapporti Alpi-Appennino" e guida alle escursioni* (May 31-June 1st 1994, Peveragno, CN, Italy). Acc. Naz. Sc. Roma. 14, 445-461.

Cremaschi, M., (1990). The loess in Northern and Central Italy: a Loess Basin between the Alps and the Mediterranean Region. *Quaderni di Geodinamica Alpina e Quaternaria*. 1. Centro di Studio per la Stratigrafia e Petrografia delle Alpi Centrali. Milano. 187 pp.

Cremaschi, M. & G. Rodolfi, (1991). *Il Suolo*. Nuova Italia Scientifica.

Dela Pierre, F., F. Piana, P. Boano, G. Fioraso, M.G. Forno, R. Polino and P. Clari (2003a). Carta Geologica d'Italia alla scala 1:50.000, Foglio 157 "Trino". *APAT, Agenzia per la Protezione dell'Ambiente e per i Servizi Tecnici*. Dipartimento Difesa del Suolo. Roma.

Dela Pierre, F., F. Piana, G. Fioraso, P. Boano, E. Bicchi, M.G. Forno, D. Violanti, P. Clari, and R. Polino, (2003b). Note illustrative della Carta Geologica d'Italia alla scala 1:50.000, Foglio 157 "Trino". *APAT, Agenzia per la Protezione dell'Ambiente e per i Servizi Tecnici*. Dipartimento Difesa del Suolo. Roma. 147 pp.

Falletti, P., R. Gelati and S. Rogledi, (1995). Oligocene-Miocene evolution of the Monferrato-Langhe, related to deep structures. In: (Polino, R., and Sacchi, R., eds.). *Rapporti Alpi-Appennino*. Accad. Naz. Scienze. 14, 1-20.

Festa, A., P. Boano, A. Irace, S. Lucchesi, M.G. Forno, F. Dela Pierre, G. Fioraso and F. Piana (2009a). Carta Geologica d'Italia alla scala 1:50.000, Foglio 156 "Torino Est". *ISPRA*. Roma.

Festa, A., F. Dela Pierre, A. Irace, F. Piana, G. Fioraso, S. Lucchesi, P. Boano and M.G. Forno, (2009b). Note illustrative della Carta Geologica d'Italia alla scala 1:50.000, Foglio 156 "Torino Est". *ISPRA*. 143 pp.

Forno, M.G., (1982). Studio Geologico dell'altopiano di Poirino (Torino). *Geogr. Fis. e Dinam. Quat*. 5, 129-162.

Irace, A., P. Clemente, M. Natalicchio, L. Ossella, S. Trenkwalder, D.A. De Luca, P. Mosca, F. Piana, R. Polino & D. Violanti, (2009). *Geologia e Idrostratigrafia Profonda della Pianura Padana Occidentale*. Regione Piemonte. 111 p., 61 tables. La Nuova Lito. Firenze. 2009.

Livio, F., A. Berlusconi, A. Zerboni, L. Trombino, G. Sileo, A.M. Michetti, H. Rodnight and C. Spotl, (2014). Progressive offset and surface deformation along a sesimogenic blind thrust in the Po Plain foredeep (Southern Alps, Northern Italy). *Journal of Geophysical Research, Solid Earth*. 199 (10) 7701-7721, 10-2014.

Michetti, A.M., F. Giardina, F. Livio, K. Mueller, L. Serva, G. Sileo, E. Vittori, R. Devoti, F. Riguzzi, C. Carcano, S. Rogledi, L. Bonadeo, F. Brunamonte and G. Fioraso, (2012). Active compressional tectonics, Quaternary capable faults, and the seismic landscape of the Po Plain (N Italy). *Annals of Geophyisics*. 55, 5, 2012.

Mosca, P., (2006). *Neogene basin evolution in the Northern Po Plain (NW Italy). Insights from seismic interpretation, subsidence analysis and low temperature (U-Th)/He thermocronology*. PhD Thesis. VU University Amsterdam. 190 pp.

Mosca, P., R. Polino, S. Rogledi and M. Rossi, (2009). New data for the kinematic interpretation of the Alps-Apennines junction (Northwestern Italy). *Int. J. Earth. Sci*. 99, 833-849.

Piana, F. and R. Polino, (1995). Tertiary structural relationships between Alps and Apennines: the critical Torino hill and Monferrato area, Northwestern Italy. *Terra Nova*. 7, 138-143.

Sassone, P., R. Gamba and L. Navone, (2015). Strutture recenti nordvergenti a basso angolo in Val Cerrina (Monferrato Casalese): nuove segnalazioni. *AIQUA Congress* 2015. Torino, 24-26 February 2015. Abstract Volume 26. pp. 41-42.

INQUA Focus Group on Paleoseismology and Active Tectonics

A proposed scale of intensity scale for historical, based on the symbolism of the codex Tellariano Remensis, Mexico

Garduño-Monroy, V.H.

Instituto de Investigaciones en Ciencias de la Tierra, Edificio U. Ciudad Universitaria. Universidad Michoacana de San Nicolás de Hidalgo. 58060, Mexico. Email: vhgardunom@gmail.com

Abstract: *In this paper a possible interpretation of the various symbols used in the codex Tellariano Remensis that may represent seismic events. These symbols are a combination of the words Tlalli and Ollin. By analyzing the drawings in the codex and by using the philosophy of the Maya numbering, a scale of intensities is proposed that might help to understand these historical events.*

Key words: *Sismos históricos, intensidades, escala.*

INTRODUCTION

In Mexico there are a number of historical documents, "codices" that can be used to understanding the past earthquakes. In these codices various symbols relate the occurrence of earthquakes. However, until now these symbols have been used by specialists (only to interpret an event in generic form, i.e. without more precise data on the quake, its intensity or effects, etc.
In the codex Telleriano Remensis there is a wealth of drawings that represent seismic events that affected the center of Mexico. The symbol usually used is the *tlalollin* that in the Nahuatl language is composed by two glyphs, one is the *tlalli* or earth (coffee bar with points) and the second is *ollin* or movement (propeller) (Kovach 2004), both have been translated as earth movement or well as earthquake, Pérez et al., (1986), García-Acosta y Suárez-Reynoso (1996) (Fig. 1). When used separately the two symbols do not have the meaning of earthquake since Ollin means movement of any kind. *Tlalli* is earth, so their combination means motion of the earth. In the international geological congress of 1906 held in Mexico, some symbols to express the presence of past seismic events such as the 1495 (Fig. 1) were already indicated, in the libretto trips to Oaxaca.
This paper proposes a possible interpretation of the different symbols of earthquakes from the Telleriano Remensis codex, which when combined with the philosophy of the Mayan numbering, could represent a scale of intensities, older that the Mercalli's scale.

El Codice Teleriano Remensis
The Telleriano-Remensis Codex, produced in the sixteenth century in Mexico and printed on European publication is one of the finest surviving examples of the Aztec manuscript painting. Its Latinized name comes from Charles-Maurice Le Tellier, archbishop of Reims, who possessed the manuscript in the late 17th century. The Codex Telleriano-Remensis is divided into three sections, the first section, spanning the first seven pages, describes the 365-day solar calendar, called the *xiuhpohualli*. The second section, spanning pages 8 to 24, is a *tonalamatl*, describing the 260-day *tonalpohualli* calendar. It is in the last section that described ascensions and deaths of rulers, battles, earthquakes, and eclipses, from the 14th century to the 16th century, including events occurred during the early Colonial period in Mexico.

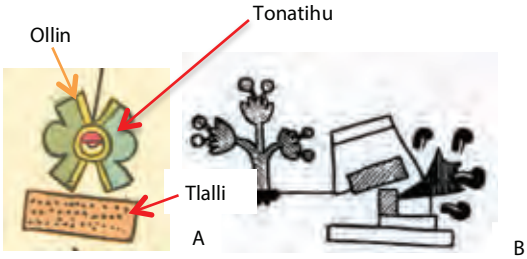

Figure 1: A. Representation of earthquake with Tlalli and Ollin. B. Representation of 1495 earthquake from 1906 field trip international Geological Congress.

The Tlalollin
Garcia-Acosta et al (2001) relate the tlalollin and seismic intensities, mentioning that this association is probably due to the way of defining the intensity of earthquakes.
In the codex Telleriano Remensis 12 seismic events (see Table I), with *tlalollin* arrangements could be grouped into four classes: A. Earthquakes where the *Ollin* is positioned on the first bar of the Earth, B. seismic events where one half of the *Ollin* is within the first bar Earth, C. Earthquakes where the *Ollin* are completely inside the bars 1 and 2 of the Earth. D. Earthquakes where *Ollin* is among the layers 2 and 5.
Colors and a central circle (eye) are also observed. When the eye (*Tonatihu*, sun) is open the quake had occurred during the day (Kovach, 2004) (Fig. 1 and table 1).

Intensity (ESI, 2009) –Tlalollin
If these representations in the codex are due to all earthquakes that were felt by ancestors, it means that within the modified Mercalli scale, these events should have an intensity of at least V, i.e. strong earthquakes.

Given the scale of ESI 2007, these earthquakes must be cataloged as having intensity ≥ VI.
Considering the four designated groups and observing the *tlalli* relationship and *Ollin* in the codex Telleriano Remensis, we could not ignore that *tlalli* bars could be related to the bars of the Maya numeration, where each bar would have a value of 5, if we consider the actual value of each bars in the Mayan numeration (fig. 2); however if we consider them as units, then each bar would have a value of 1 (Fig. 3).

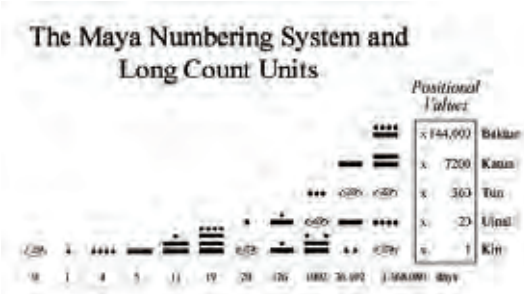

Figure 2: Numerical Mayan Numbering, where the bars have a value of 5.

On the other hand, there is the *ollin* position in the *tlalli* bars to be also considered. This representation may indicated the effects of the earthquake on earth, the "ollines" with very internal positions on the bars, would correspond to high intensity earthquake events, i.e. more cracks and landslides have occurred. Considering this argument, the 1542 earthquake (12, see Table I) would be the strongest earthquake in the scale of Tellariano Remensis. However, the effects described in the codex do not help substantiate their possible intensity.

Figure 3: Relation between tlalli (earth) and intensity (bars).

An earthquake with *ollin* placed on the surface, has produced little effects on the ground, with ESI-2007 corresponding intensity of VI. An earthquake, represented with two bars, is equivalent to 2 and then equivalent to an earthquake of VI-VII in the ESI 2007 scale. Considering also the entire context of the codex, i.e. all the drawings of events occurred on the day of the earthquake it is possible to derive additional information on the earthquake effects., Figure 4 a great earthquake occurred during a solar eclipse in year two cane (1507), when 2000 warriors drowned. The latter information suggested us to consider that the 1507 earthquake caused a landslide in the Tuzac River in the Mixteca region; and possibly means the warriors were caught by flood wave created by the landslide (Escalante-Gonzalbo, 2010), stone and mud (a lahar deposit) are also depicted in the codex for the 1507 earthquake event (Fig.4). If we now combine the symbol of tlalollin (4) and the related effects, in the ESI scale, the intensity of the earthquake would result between VI and VII.

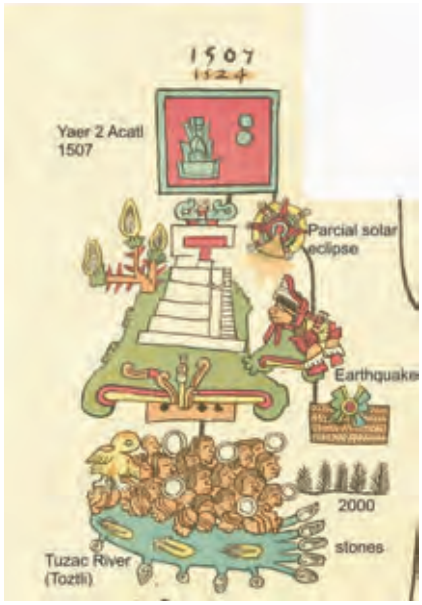

Figure 4: Telleriano Remensis codex with the 1507 earthquake representation. The water flow with stones, causing the death of the 2000 warriors.

Considering this interpretation of intensities as possible, the 1542 earthquake a very strong event with a value in bars 4. However the symbolism of what happened in the ninth rabbit year, considering the landslide, gives an ESI 2009 scale VII-VIII.
Table 1 describes the 12 seismic events of the Telleriano-Remensis Codex with two columns where their intensities interpreted with the Tlalollin scale and with the corresponding Esi-2007 scale are proposed. In the codex, the number of bars corresponds to a specific intensity, with the highest intensity being the one with six bars (e.g. the 1542 event). Sometime the effects of the events are drawn in the paintings, as for the earthquakes of 1512 and 1513. The 1512 earthquake happened along with hydrometeorologic events that caused death among the population while the one of 1513 had effects like strong movement of trees recorder in the paintings. In the ESI 2007 scale, this latter event would be classified with an intensity of V-VI.

Number	Tlalcilin	Symbol associated	Years	ESI 2007 scalle	Tellariano Remensis scalle	Observation
12				V-VI	VI tlalli	
11				V-VI	II tlalli	stellar activity
10				V-VI	II tlalli	stellar activity
9				V-VI	II tlalli	
8				V-VI	III tlalli	trees sway
7				VII	II tlalli	stellar activity snow and mortality
6				VII-VIII	IV tlalli	stellar activity partial eclipse, 2000 warrior killed by a lahar in the river Tuzac
5				V-VI	II tlalli	mortality
4				V-VI	I tlalli	
3				V-VI	I tlalli	
2				V-VI	II tlalli	
1				V-VI	II tlalli	

Table 1: In this there are the 12 earthquakes from Telleriano Remensis codex. Here are the earthquake symbols with representations of side events and an intensity suggested through the bars of the codex and its corresponding intensity in the ESI 2007 scale.

CONCLUSIONS

According to the above data, it seems that earthquakes represented in the Aztec codices, through symbols or *Tlalollin* are events corresponding at least to intensity VI, in the ESI 2007 scale. Using *Tlalollin* forms and the philosophy of the Maya numbering, we propose a possible intensity for the earthquakes sometimes corroborated by drawings showing the side effects of the historical events. In this paper, we propose Azteca-Mixteca intensity scale based on the philosophy of the Maya numbering and on the codices drawn effects. It is worth noticing the great knowledge that these cultures had on natural phenomena, as shown in this case the profound knowledge of the side effects associated to major earthquakes.

References

Escalante Gonzalbo, P., (2010). *Los códices Mesoamericanos antes y después de la conquista Española*. Fondo de Cultura Económica. 413 p.

García-Acosta, V., G. Suárez-Reynoso, (1996). *Los sismos en la historia de México*. Tomos I. 718 p.

Kovach, R., (2004). *Early Earthquakes of the Americas*. Cambridge University Press. First publication. 268 p.

Pérez, Z.J.M., V. García-Acosta, T. Rojas Rabiela, (1986). *Y volvió a temblar: cronología de los sismos en México (de 1 pedernal a 1821)*. Cuadernos de la Casa Chata. 135. 204 p.

INQUA Focus Group on Paleoseismology and Active Tectonics

paleoseismicity.org

Paleoseismology of the North Panamá Deformed Belt from Uplifted Coral Platforms at Moín and Limón, Caribbean Coast of Costa Rica

Gath, E. (1), Gonzalez, T. (1), Madugo, C.(1), Montero W. (2)

(1) Earth Consultants International, 1642 E. 4th St., Santa Ana, CA 92701, USA;. Email: gath@earthconsultants.com
(2) Geological Research Center, San Jose, 11501, Costa Rica

Abstract: *In 1991, the Caribbean coastal area between Moín and Limón was coseismically uplifted up to 1.8 m by a M_s 7.6 earthquake on the western segment of the North Panamá Deformed Belt (NPDB), resulting in the emergence of a broad coral reef platform. Review of historical accounts showed that multiple large earthquakes have been felt in the region during its ~270 year historical record, with an event in 1822 described somewhat similarly to the 1991 event. Geologic reconnaissance revealed multiple older platforms that provided an opportunity to quantify the timing and rate of 1991-like uplift earthquakes on the Limón section of the NPDB. Mapping and hand surveying identified 7 pre-1991 coral platforms and wave cut notches preserved on the coastal-facing slope beneath a set of higher marine terraces that cap the coast between Moín and Limón. 48 coral samples were obtained but only 12 were suitable for U-series dating due to diagenetic alteration of the original aragonite to calcite. Assuming that these coral die offs were caused by coseismic uplift events, and using additional dated corals from published sources and one radiocarbon-dated shell, we have interpreted and temporally constrained as many as 12 events in the past ~7,000 years. Our preliminary work indicates that the penultimate earthquake did occur in 1822, but was smaller than 1991. We calculate an average slip rate of 3.8±0.3 mm/yr on the NPDB using a geophysically determined fault dip of 27°, and an average earthquake recurrence of ~600 years, but return periods are irregular and clustered, suggesting that the region experiences two types of events: large events with ~1400-year return periods that could reflect multi-segment ruptures of the NPDB, and smaller events with recurrence intervals in the 100s of years.*

Key words: *Paleoseismology, Costa Rica, Panama, corals, PSHA.*

INTRODUCTION

As part of a Probabilistic Seismic Hazard Analysis (PSHA) for a new port facility in Moín, Costa Rica, we completed a field reconnaissance of uplifted coral reef platforms of the Caribbean Coast in the Moín-Limón area (ECI, 2012). The purpose of our study was to determine the geologic recurrence of past coseismic uplift events on the offshore North Panama Deformed Belt (NPDB) similar to the M_s7.6 Limon earthquake of April 22, 1991 that resulted in up to 1.8 m of coastal uplift within the project area (Denyer et al., 1994; Plafker and Ward, 1992).

Figure 1: Fault map of eastern Costa Rica and western Panama showing the North Panama Deformed Belt off their northern Caribbean coasts, and the fault rupture (in red) that occurred in 1991 (inset). Figure modified from (Montero et al. (1998).

The NPDB is a large thrust fault accommodating the northward push of the Cocos-Nazca plates against the Isthmus of Panama. While the majority of the ~90 mm/yr convergence (DeMets, 2001) is consumed by subduction along the Pacific Margin, attempted subduction of the Cocos Ridge and a string of submarine volcanoes (inset in Fig. 2), is acting as a plow, shoving the isthmus onto the Caribbean plate at an estimated 7 mm/yr (Trenkamp et al., 2002). The strain that is partitioned northward forms a large and poorly studied thrust system that reaches from Moín, Costa Rica eastward for 800 km along the entire northern Panama coastline. This fault is assumed to have generated the ~M_s7.9 1882 earthquake off the San Blas Archipelago, Panama (Camacho and Víquez, 1993), but no other confirmed large historical events are known prior to 1991, when the westernmost 80 km of the fault ruptured from Bocas del Toro, Panama to Moin, Costa Rica.

Figure 2: Map of the Moín and Limón harbor areas, showing the location of the proposed new harbor site, and the topographic uplift associated with the left bend of the NPDB as it turns ashore.

The NPDB steps ashore just west of Moín (Figs. 1 & 2), and continues ~50 km westward as the Siquirres-Matina fault (Montero et al., 1998), forming a prominent escarpment. Where the NPDB steps ashore, it has formed a 7.5 km long left-lateral tear fault, the Río Blanco, that experienced up to 1.4 m of lateral displacement and 0.5 m of vertical surface offset in 1991 (Fig. 1; Denyer et al. 1994). Consistent left-laterally deflected streams along the Río Blanco fault show strong evidence for multiple Holocene events. Between Moín and Limón, an elevated headland has been formed by the leftward bend of the NPDB (Fig. 2). It is this localized uplift that has preserved the coral platforms that formed the basis for our investigation.

Review of historical accounts show that an earthquake reported in 1822 had similar descriptive effects at Moín-Limón as the 1991 event (Ambraseys et al., 2001; Boschini & Montero, 1994); & Camacho & Víquez, 1993), suggesting a recurrence interval of 170 years between uplift events. To confirm this, and to potentially extend this event record paleoseismically for an offshore fault, we mapped and sampled a suite of uplifted coral platforms along about 8 km of the Limón coast (Figures 3, 4 & 5).

Figure 3: Photo showing the coral platform uplifted by the 1991 earthquake (right), the penultimate platform (grassy area lower left) and pre-penultimate platform (upper left, somewhat obscured in the vegetation).

Figure 4: Older uplifted coral platforms uphill from Fig. 3.

Seven discrete coral platforms were recognizable on the shoreward-facing coastal slope in the Playa Bonita area between Moín and Limón (Fig. 4). Capping the slope is a marine terrace, with other marine terraces occurring at higher elevations inland. We concentrated on the coral platforms, which could be dated using U-Th dating, and did not map the marine terraces. If they could be dated, or at least correlated to the eustatic marine sea level curve, these uplifted marine terraces would provide an excellent length to the Holocene uplift rate that we determined from the coral platforms.

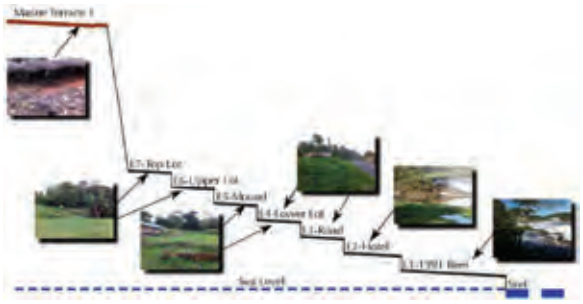

Figure 5: The suite of seven coral platforms identified during the initial reconnaissance at the Playa Bonita site, capped by the marine terrace platform from Punta Portete (Fig. 2). Because each bench was vertically separated by 1-2 meters, our preliminary working hypothesis was that each bench recorded an earthquake. Diagram not to scale.

INVESTIGATION

Because of the urban environment, and the short duration of the project, we did not prepare a comprehensive map of all of the coral platforms, but concentrated our efforts at three locations where they were particularly well expressed and preserved. To measure lateral distances we used a hand-held 100-meter tape, and to measure the vertical separation between platforms, we used a hand-made stadia rod and an iPhone-based "Theodolite" application (Theodolite© by Hunter Research & Technology LLC) (Fig. 6). We estimate that our vertical error could be as much as 0.5 meters for long traverses, but less than 0.2 meters for most measurements.

Figure 6: Example shot of the theodolite surveying of the relative vertical separation between the coral platforms.

To provide age control, we obtained 48 coral samples from a wide range of vertical and spatial locations for U-Th age dating. We sampled some obvious 1991-killed corals to check the accuracy of the dating technique (Fig. 6). We then sampled at least one coral from each identified platform at each location along the coast. Unfortunately, 75% of our coral samples were not suitable for U-series dating due to diagenetic alteration of the original aragonite to calcite.
In addition to the corals, we also collected two shells, one from its growth position at the base of a bench. These corals were dated using 14C.

Figure 7: One of the corals uplifted by the 1991 earthquake.

Figure 8: Sampling drill used for the older coral platforms.

RESULTS

Despite the difficulties with the U-Th dating of the corals, the study did generate important results concerning the paleoseismic history of the NPDB that were useful to the PSHA for the project. Before those results could be understood however, the coral ages needed to be put into context of their vertical positioning with respect to the many mapped platforms (Fig. 9). Not all paleo-events might be preserved everywhere along the coast due to dissolution or erosional removal.
In Fig. 9 we correlate the various sea level indicators and platforms that we mapped at the three principal study locations (vertical transects) from west to east along the coast. Within the error limits of our mapping results, there are definite correlations of platform elevations across the 5 km coastline. But there are also platforms that are recognizable at only one or two locations. Additional mapping along the coastline between the three principal locations should result in better resolution of the platform correlations.

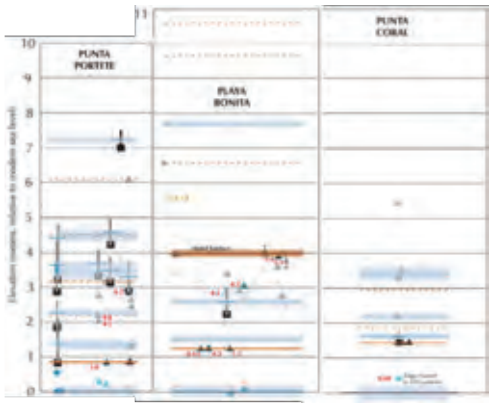

Figure 9: Composite plot of the coral platform (brown) and notch (light blue) elevations that were mapped at three principal localities, west to east (left to right) along the Limón coast. Elevation in meters on the left; horizontal distance is about 5 km. The line widths represent the uncertainties in the elevation measurements.

After correlating the coral samples across the various platforms, we needed to correct their current elevations with the sea level elevation that was present at their determined age (Fig. 10). The 6.2 ka coral sample was obtained from the fourth highest platform on Punta Portete (Fig. 9) at a modern elevation +2.9 m. Absent better information on coral water depth ranges, we assumed an original water depth of 2 m for all stony coral samples and 0.5 m for others. As illustrated on Fig. 9, at 6.2 kya the sea level was at -6 m, resulting in an uplift of 10.9 m (2.9+2+6) in 6.2 ka (uplift rate = 1.8 mm/yr). Similar results were calculated for all of the other datable samples and they were placed into context on Fig. 11 to show their true positioning with both age and lateral correlation.

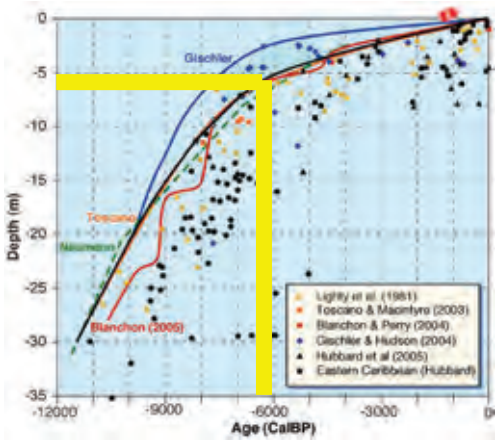

Figure 10: Composite plot of the various Caribbean sea level results developed by six different researchers. The black line from Hubbard et al. (2005) represents an approximate mean value that we used in our analysis to correct for paleo sea level elevation. The yellow bars illustrate that the 6.2 ka coral sample corresponds to a -6 m sea level.

Figure 11 shows how the various events were counted across the study area, and how often they correlate to other dated locations laterally, west to east. Unless we are missing events, which is possible, the pattern of earthquakes strongly indicates that they are irregular, with several events clustered between longer quiescent intervals.

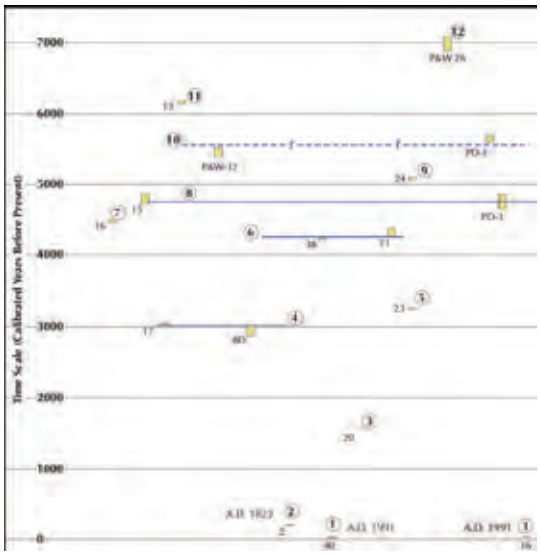

Figure 11: A twelve event earthquake chronology that was determined after correcting and correlating the dated coral sample elevations for the 7.5 m sea level rise in the last 7 ka, as measured from Fig. 10. The interpreted event number is circled, starting with 1991 and 1882 AD near the bottom. Age in years on the left, distance west to east (left to right) across the bottom (Fig. 9), but not to scale.

Our limited data set allows only speculation about event magnitude, but the two most recent events (1822 and 1991) resulted in ~1 m and 1.8 m uplift events respectively, clearly implying that they were of different magnitudes. From Figure 11, before the 1822-1991 cluster, it was almost 1500 years to the pre-penultimate event (#3), and another 1500 years to the one before that (#4), closely preceded by an event (#5). Then it was over 1000 years before a series of temporally clustered events (#6-11) followed by an 800 year hiatus to event #12.

With 12 events recognized in 7 ka, the average recurrence interval would be ~600 years. But based on events 2, 5 & 7, we conclude that the recurrence between uplift events can be as short as ~200 years, while the recurrence between larger events can be as long as 1400 years. These rates are in good agreement with those determined by Plafker and Ward (1992) but provide a much higher degree of resolution to be able to interpret the temporal variability.

To calculate the uplift rate we calculated each dated sample's uplift rate (1.6–2.7 mm/yr, strongly clustered between 1.6 and 2.1 mm/yr, and averaged them. To calculate the fault's slip rate, we used the geophysically-imaged 27° of the offshore fault (Brandes et al., 2008) and resolved the rate trigonometrically from the uplift rate, resulting in 3.8±0.3 mm/yr, or about 50% of the Trenkamp et al. (2002) rate for Caribbean convergence.

CONCLUSIONS

- 75% of the coral samples were too degraded to date (aragonite to calcite transformation).
- Those samples dated ranged from 1991 to ~7,000 years BP.
- Interpreted 12 events on the NPDB, assuming the coral deaths were all earthquake-induced.
- Holocene uplift rate of 1.9 ± 0.2 mm/yr.
- Slip rate on NPDB of 3.8 ± 0.3 mm/yr.
- Irregular earthquake recurrence with larger events ~1400 years and smaller events ~200+ years.
- Most recent event was April 22, 1991 (M_s7.6).
- Penultimate event was in 1822, while the pre-penultimate event was 1.6 ka.
- There is a huge opportunity for more work.

Acknowledgements: This project was done under contract to CH2M Hill and we appreciate their permission to present this work. Warren Sharp of the Berkeley Chronology Center processed our coral samples for U-Th dates. Our paleoseismic results were incorporated into the project's PSHA, and while those results are not included in this short paper, we also thank Dario Rosidi, Nason McCullough, and Ken Campbell for their contributions.

References

Ambraseys, N.N. and R.D. Adams, (2001). The Seismicity of Central America: A Descriptive Catalogue 1898-1995. *Imperial College Press*. London, 309 p.

Boschini, I. and W. Montero, (1994). Sismicidad histórica e instrumental, Volumen Especial Terremoto de Limón 22 de abril de 1991. *Revista Geológica América Central*. pp. 65-82.

Brandes, C., A. Astorga, R. Littke and J. Winsermann, (2008). Basin modelling of the Limón Back-arc Basin (Costa Rica): burial history and temperature evolution of an island arc-related basin-system. *Basin Research*. v. 20, pp. 119-142.

Camacho, E. and V. Víquez, (1993). Historical seismicity of the North Panama Deformed Belt. *Revista Geológica de América Central*. Vol. 15, pp. 49-64.

Denyer, P., O. Arias, and S. Personius, (1994). Efecto tectónico del terremoto de Limón. *Revista Geológica de América Central*. Volumen Especial del Terremoto de Limón. pp. 39-52.

Earth Consultants International, (2012). *Seismic Hazard Assessment for a Proposed Harbor Facility in Moín, Costa Rica*. unpublished consulting report to CH2M Hill. Feb. 21, 2012. ECI PN 3312. 68 p.

Hubbard, D.K., H. Zankl, I. van Heerden and I.P. Gill, (2005). Holocene reef development along the northeastern St. Croix shelf, U.S. Virgin Islands. *Journal of Sedimentological Research*. Vol. 75, pp. 97-113.

Montero, W., P. Denyer, R. Barquero, G.E. Alvarado, H. Cowan, M.N. Machette, K.M. Haller, and R.L. Dart, (1998). Map and Database of Quaternary Faults and Folds in Costa Rica and its Offshore Regions. *USGS Open-File Report*. 98-481, 63 p. map scale 1: 500,000.

Plafker, G. and S.N. Ward, (1992). Backarc thrust faulting and tectonic uplift along the Caribbean sea coast during the April 22, 1991 Costa Rica earthquake. *Tectonics*. Vol. 11, No. 4, pp. 709-718.

Trenkamp, R., J.N. Kellogg, J.T. Freymueller and H.P. Mora, (2002). Wide plate margin deformation, southern Central America and northwestern South America. CASA GPS observations. *Journal of South American Earth Sciences*. Vol. 15, pp. 157-171.

INQUA Focus Group on Paleoseismology and Active Tectonics

Relationships between the ESI-07 scale and expected PGA values from the analysis of two historical earthquakes (≥ VIII EMS) in East Spain: Tavernes 1396 AD and Estubeny 1748 AD events

Giner-Robles, J.L. (1), Silva, P.G. (2), Elez, J. (2), Rodríguez-Pascua, M.A. (3), Pérez-López, R. (3), Rodríguez-Escudero, E. (1)

(1) Dpto. de Geología y Geoquímica, Universidad Autónoma de Madrid, Cantoblanco 28040 (Madrid), Spain. Email: jorge.giner@uam.es
(2) Dpto. de Geología, Universidad de Salamanca, Escuela Politécnica Superior. Avila Spain
(3) Instituto Geológico y Minero de España, IGME. Madrid 28003, Spain

Abstract: *The application of the ESI-07 macroseismic scale to two historical strong earthquakes in eastern Spain (Tavernes, 1396 AD and Estubeny, 1748 AD) allows a detailed analysis of intensity distributions. In both cases the affected zones exceeding intensity VI ESI-07 covered areas up to 1000 km^2. Accelerations intervals have been assigned to each of the obtained intensity zones following intensity-PGA relationships used for the USGS Instrumental Intensity ShakeMap program. The comparison of PGA_{475} values of the recently updated seismic hazard maps for Spain (IGN, 2013) with the theoretical PGA ranges for the different intensity levels in the different localities affected by both seismic events indicate that updated PGA_{475} are underestimated. Theoretical PGA values recorded in the zone for periods less to c. 360 years largely surpass those predicted for the new Spanish seismic hazard maps for 475 years (PGA_{475}), especially for areas affected by intensity ≥ VIII during both seismic events.*

Key words: *ESI-07 intensity scale, Tavernes earthquake (1396 AD), Estubeny earthquake (1748 AD), PGA, Eastern Spain.*

INTRODUCTION

The recent moderate earthquakes in Spain triggered peak ground accelerations that have exceeded the maximum PGA values considered in both, Spanish Seismic Building Code (NCSE-02) and the newly revised seismic hazard maps updated after the 2011, Lorca 5.1 Mw event (IGN, 2013). This is the case of the 2011 Lorca earthquake (Fig. 1), during which maximum PGA values recorded in the city of Lorca were of 0.365 g, nearly tripling the basic PGA values (0.16 – 0.19 g) considered in the documents for 475 years return periods. Another similar case occurred during the 2007, Escopete earthquake in Guadalajara (4.2mb_{Lg}; Central Spain), whose epicenter was located close to the José Cabrera NPP. This area of Central Spain, out of the application of Seismic Building Code (NCSE-02), recorded a PGA of 0.07 g (Carreño et al., 2008), nearly duplicating the minimum values considered in the NCSE-02 (< 0.04 g).

These two examples illustrate that old (NCSE-02) and updated basic PGA values in Spain (based in recorded seismicity) are clearly underestimated. Even with the application of amplification factors considered in the NCS-02 for "maximum scenarios" the obtained values are nearly two times lower. The best way to solve this problem is the improvement of seismic records by the incorporation of geological information of past historical events through the application of the ESI-07 Macroseismic Scale (Michetti et al., 2007). The newly published Catalogue of Earthquake Geological Effects in Spain (Silva et al., 2014a) clearly indicate that the use of macroseismic information derived from earthquake environmental effects (EEE) allow a better understanding on the spatial distribution of intensities and parameterization, especially when combined with data derived from classical macroseismic scales. This is significancat in Spain, where the use of the EMS-98 scale do not consider EEEs for the intensity value assessment.

Figure 1: Location of the two historical earthquakes analyzed: Tavernes (1396 AD) and Estubeny (1748 AD). Are also illustrated the 2011 Lorca and 2007 Escopete earthquakes (see text for explanation).

In this work two strong historical earthquakes (6.2 – 6.5 Mw) occurred in the Valencia zone (East Spain) and affected similar areas are analyzed: Tavernes de la Valldigna (AD 1396) and Estubeny (AD 1748). We have selected these two events due to: (a) their temporal spacing (352 years apart) are within the standard recurrence periods used in the Spanish seismic hazard maps (475 years); (b) the large amount of existing EEE and EMS data (Giner-Robles et al., 2014; Silva et al., 2014); and (c) their effects overlap a common area of about 1000 km^2 with comparable intensities. The final objective of this contribution is to compare the obtained ESI-07 intensity values for different affected areas with standard

PGA values according to MM USGS and EMS in order to establish the reliability of the PGA values considered in Spain for the development of seismic hazard maps and seismic building codes (IGN, 2013).

EARTHQUAKE ANALISYS

The AD 1396 Tavernes Earthquake (VIII-IX EMS; IX MSK; 6.2 Mw; Martínez Solares & Mezcua, 2002) produced extensive damage on buildings, churches and castles, triggering the almost total destruction of the localities of Alzira and Tavernes, (Galbis, 1932). Extensive damage in all types of buildings was documented in Simat, Cullera, Sueca and Riola. Damaged buildings were also recorded in Gandia, Valencia and Lliria. No casualties are reported for this earthquake.

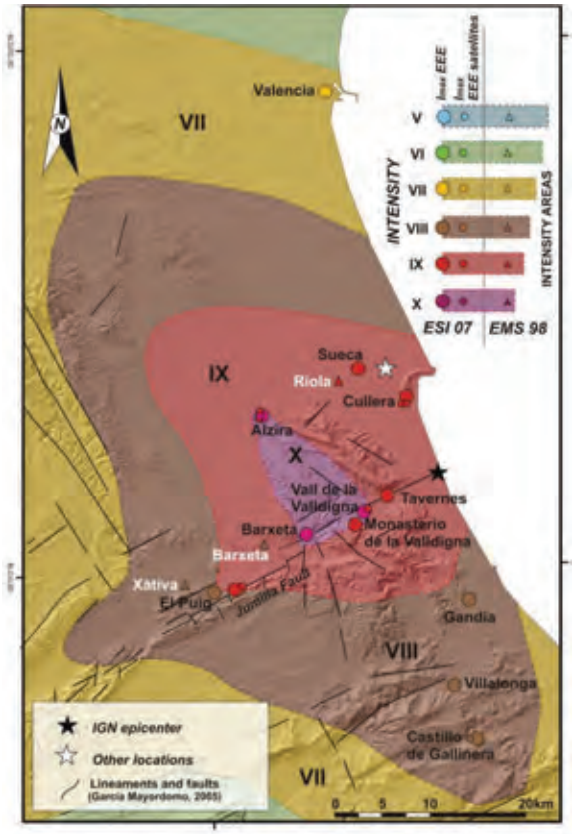

Figure 2: Map of ESI-07 intensities for the Tavernes Earthquake (1396 AD) (Valencia, Spain) (Imax ESI-07: X).

The main event (VIII-IX EMS / IX MSK), occurred on December 18th, 1396, was preceded by two events of smaller intensity. The main earthquake was felt with intensity IX MSK (VIII-IX EMS), in sites located less than 20 km away from the epicenter considered by the IGN Catalogue, such as Alzira, Tavernes de la Valldigna, Sueca, Cullera and Riola (Fig. 2). Other localities at epicentral distances of 20-30 km where shacked with VIII MSK intensity, such as Gandia (VI-VII EMS), Xàtiva, Villalonga and Barxeta (VII EMS). According to the chronicles this event was felt in towns such as Valencia (45 km away, V-VI EMS), Lliria (68 km, VI-VII EMS) and even in Tortosa (Tarragona; Ebro Delta; IV EMS) located about 200 km away from the epicenter.

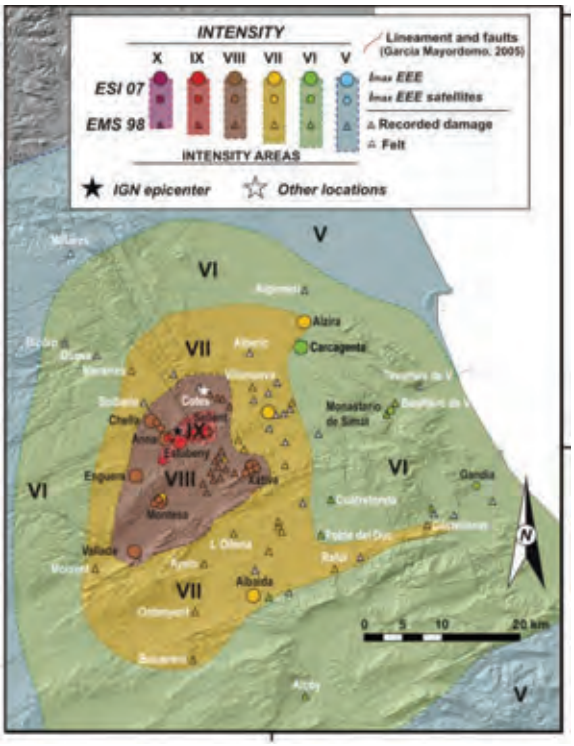

Figure 3: Map of ESI-07 intensities for the Estubeny Earthquake (1478 AD) (Valencia, Spain) (Imax ESI-07: IX) (modified from Giner-Robles et al., 2014; Silva et al., 2014).

Re-evaluation of intensities for the ESI-based EEE catalogue developed in Spain (Silva et al., 2014) indicate that maximum intensity was of X ESI-07 covering an area of about 25 km^2 in the Valldigna Valley and Murta Valley, between the towns of Alzira, Tavernes de la Valldigna and Barxeta (Fig. 2) (primary effects absent). The epicentral location of IGN is located about 6 km east of the area defined as intensity X. Documented EEEs for this event cover a large area of 1200 km^2 included within the intensity zone VIII ESI-07 (Silva et al., 2014; Fig. 2). However, most significant secondary EEEs (ground cracks, slope movements, liquefaction processes) are included in an area of 350 km^2, where ESI-07 intensities ≥ IX were evaluated.

The AD 1748 Estubeny earthquake (6.2 Mw; IX EMS) produced extensive damage to buildings, churches and castles, with almost total destruction of the locality of Montesa and other towns located in the epicentral area, such as Estubeny and Sellent (Galbis, 1932; Martínez Solares & Mezcua, 2002). Extensive damage in all types of buildings in the localities located less than 10 km away (Anna, Enguera, Xàtiva and Vallada), producing 38 causalities (Fig. 3). The event was part of a seismic series that lasted more than 9 months including major aftershocks. The main event occurred on 23th March, 1748 was felt with intensity IX EMS at Estubeny, Sellent and Montesa; VIII EMS in Anna, Enguera, Chella, Anahuir, Cerdá and Llaneras; VII-VIII EMS in Vallés, Rotgla i

Corberá, Novetlé, Navarrés, Xàtiva, among other locations. It was felt in distant locations between 40 - 75 km away with intensity V EMS (Jalance, Almansa, Valencia and Alicante), even in other localities more than 100 km away, with intensity IV, such as Orihuela (109 km) and Cartagena (159 km). A total amount of 73 EMS data are available for this earthquake (Giner-Robles et al., 2014).

Environmental damage by secondary effects (EEEs) (ground cracks, slope movements, liquefaction processes) occurred over an area of 1000 km^2 included within the isoseismal zone VII ESI-07, affecting to the localities of Estubeny, Sellent, Anna, Chella, Enguera, Montesa and Xàtiva (Fig. 3). Although most of the catalogued secondary EEEs (primary effects absent) (≥ VIII ESI-07) are included in an area of 350 km^2. More severe geological effects indicate an intensity XI ESI-07 covering an area of about 10 km^2 in the valley between the towns of Estubeny and Sellent, encircling the epicenter inventoried by IGN. 21 EEEs plus 16 Archaeo-seismological effects (EAEs) are available for this earthquake, completing a total amount of 110 EMS and ESI data from which the intensity maps have been produced (Giner-Robles et al., 2014, Silva et al., 2014a).

The affected area with intensities above VI ESI-07 during both earthquakes exceeds 1000 km^2 (Fig. 4). As displayed in Fig. 4, three intensity areas can be defined according to the minimum ESI intensity values recorded during the two events: (a) ≥ VI ESI-07 (green area); ≥ VII ESI-07 (yellow area); ≥ VIII ESI-07 (brown area). It is not heworthy that in the green area (≥ VI ESI-07), there are populations that recorded high intensity values (IX-X) during the AD 1396 Tavernes earthquake.

To establish the probable PGA intervals induced by these earthquakes, we applied the scaling of PGA values data used for the production of the USGS Instrumental Intensity Maps according MM Scale (Allen et al., 2008). These authors propose the following PGA ranges for the different intensities levels: VI (0.09-0.18 g), VII (0.18-0.34 g), VIII (0.34-0.65 g), IX (0.65-1.24 g) and ≥ X (1.24 g). The expected PGA data for each of the affected localities has been extracted from the updated seismic hazard maps published in Spain applicable to the seismic building code NCSE-02 (PGA_{475}; IGN, 2013). In spite of the recorded intensities evaluated for the studied historical events, all the analyzed localities are in areas with a maximum expected intensity IV EMS-98 (IGN, 2013) for a return period of 475 years and respective PGA values down to 0.18 g (Fig. 5).

To establish a comparative framework we have used instrumental data recorded in the city of Lorca during the May 2011 earthquake (5.1 Mw; VII EMS). This locality recorded a PGA of 0.365 g (IGN, 2012), while previous (0.16 g) and updated (0.19 g) official PGA_{475} are noticeably lower. Moreover, after considering "site effect" equations provided in the NCSE-02, the resulting old (0.23 g) and updated (0.28 g) PGA values are still clearly underestimated (Fig. 5). In this way, the ESI-07 intensity established for the city of Lorca is VII (Silva et al., 2014), although in the epicentral area (4 km away) was VIII. Calculated PGA values for this earthquake according to USGS methodology (Elez et al., 2015) is 0.33 g in Lorca and 0.38 g in the epicentral area, being more consistent with the obtained instrumental data.

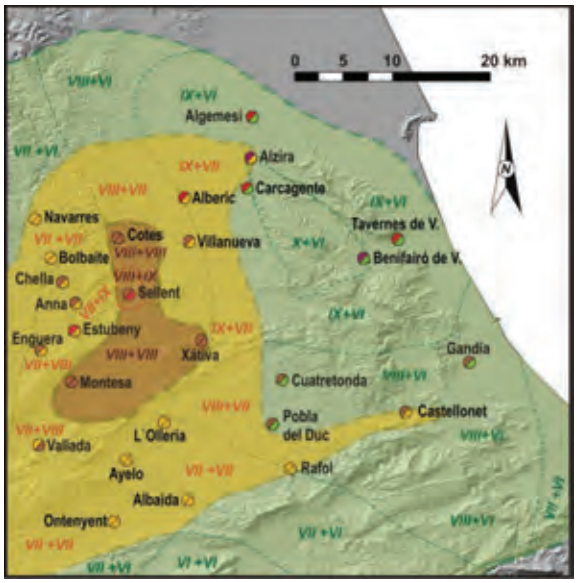

Figure 4: Common areas for the two earthquakes analyzed with intensity ESI-07 equal to or greater than VI. The colors of the data points (circles) represent the ESI-07 intensities of the two considered historical earthquakes (see caption Figure 2).

DISCUSSION

Figure 5 displays the obtained ESI-07 intensities for each of the analyzed localities during both earthquakes (Tavernes and Estubeny) in the framework of the scaling of PGA values used in the USGS Shake Map (Allen et al., 2008). When comparing these data with those recently defined for Spain by the IGN (2013) important discordances arise (Fig. 5). In our opinion, the dates of these two events, occurred in the last 600 years, are comparable with the return period of 475 years considered in Spain (IGN, 2013), since the elapsed time between both events is of c. 350 years, and the last one (Estubeny) occurred 265 years ago.

To make a direct comparison the PGA intensity-ranges used by the USGS, we can define a minimum historical PGA (PGAHmin) and a maximum historical PGA (PGAHmax), values produced by the historical seismicity in each of the studied localities (Fig. 5), and therefore to be expected in the future for the activity of the causative seismic sources. The results are grouped according to the location of the cities with respect to the three areas of minimum intensity ESI-07 (Fig. 4). The group of intensity ESI-07 ≥VI, the IGN PGA_{457} values for the localities in the area, are consistent with the data of PGA_{Hmin} defined in these towns (data from Estubeny earthquake). However, in some of these localities (eg. Carcagente, Tavernes or Benifairó) can be assigned much higher acceleration ranges than those defined by

the IGN (2013). In this area the relationship between the different accelerations is: $PGA_{Hmin} < PGA_{475} << PGA_{Hmax}$.

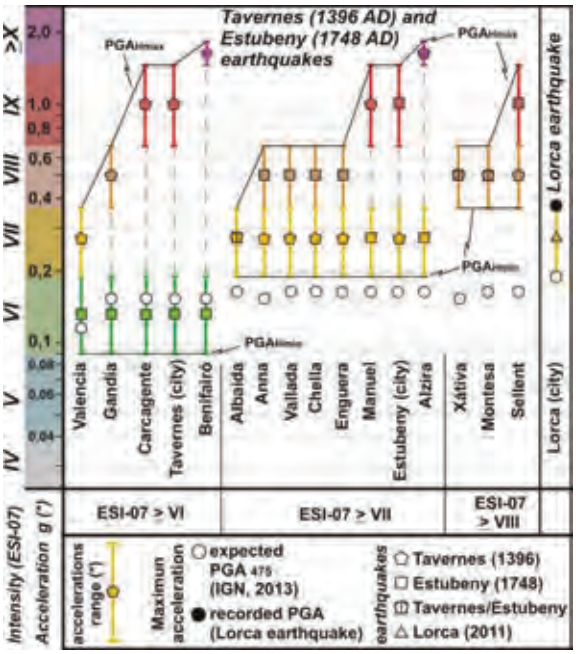

Figure 5: Preliminary accelerations from ESI-07 intensity data for some of the localities affected by both historical earthquakes (Tavernes 1396 and Estubeny 1748). The expected maximum accelerations (PGA_{475}; IGN, 2013) are included for each. (*) Allen et al. (2008) (see text for explanation).

In the rest of the groups for intensities ESI ≥ VII (Fig. 5), PGA_{475} values defined by the IGN (2013) are always clearly below than those defined by their respective ESI-07 intensity intervals, specially in the case of the area affected by intensity ≥VIII (Fig. 4), where deduced PGA values in this study can triplicate those considered in the Spanish seismic hazard maps (IGN, 2013). In these areas the relationship between the different accelerations is: $PGA_{475} < PGA_{Hmin} << PGA_{Hmax}$.

The results of this study, clearly indicate that the recently updated PGA_{475} values for Spain are noticeably underestimated, especially in areas with intensity ESI-07≥ VII. This fact is also evident for the 2011 Lorca earthquake (Fig. 5) where instrumental PGA measurements (0.365 g) duplicated the previous (0.16 g) and updated (0.19 g) expected PGA_{475} values. The study evidence that PGA_{475} proposed by the IGN (2013) are too conservative since PGA_{min} y PGA_{max} resulting for intensity-PGA relationships used in classical intensity scales MM (Allen et al., 2008) are significantly above the ESI-07/EMS-98 combined set of intensity data used for the development of the maps displayed in this study. Consequently updated PGA values in Spain come from really conservative approaches, based only on intensity assessments from a macroseismic scale (EMS-98), which no consider the earthquake environmental effects. For historical events, EEEs commonly occur out of the populated areas, an their use clearly improve the definition and parameterization of seismic intensities.

Acknowledgements: This work has been funded by the Spanish research projects CGL2012-37281-C02.01: QTECTBETICA (USAL) and CATESI-07 (IGME). This is a contribution of the INQUA TERPRO Project 1299 and the Working Group QTECT-AEQUA.

References

Allen, T., D. Wald, A. Hotovec, P. Earle, K. Marano, (2008). An Atlas of ShakeMaps for Selected Global Earthquakes. *USGS Open-File Report.* 2008-1236, 35 p.

Benito, B., A. Rivas, M. Gaspar-Escribano, P. Murphy, (2012). El terremoto de Lorca (2011) en el contexto de la peligrosidad y el riesgo sísmico en Murcia. *Física de la Tierra.* 24, 255-287.

Carreño, E., B. Benito, J.M. Martínez Solares, L. Cabañas, J.L. Giner, P. Murphy, et al., (2008). The 7 June 2007 mbLg 4.2 Escopete Earthquake: An Event with Significant Ground Motion in a Stable Zone (Central Iberian Peninsula). *Seismological Research Letters.* 79 (6), 664-673.

Elez, J., P.G. Silva, J.L. Giner-Robles, M.A. Rodríguez-Pascua, R. Pérez-López, E. Roquero, T. Bardají, et al., (2015). ESI-07 *ShakeMaps for Instrumental and historical events in the Betic Cordillera (SE Spain): a preliminary approach applied to seismic hazard based on geological data*. This volume.

Galbis Rodríguez, J., (1932). Catálogo Sísmico de la zona comprendida entre los meridianos 5ºE y 20ºW de Greenwich y los paralelos 45º y 25º N.D.G. *Instituto Geográfico, Catastral y de Estadística.* Tomo I.

García-Mayordomo, J., (2005). *Caracterización y análisis de la peligrosidad sísmica en el sureste de España.* Tesis doctoral, Universidad Complutense de Madrid. 373 pp.

Giner-Robles, J.L., P.G. Silva, M.A. Rodríguez-Pascua, R. Pérez-López, A. Alberola Romá, (2014). *Geological and archaeological effects of the AD 1748 Estubeny Earthquake (SE Spain).* IBERFAULT II. IGME. Madrid. pp.149-152.

IGN, (2012). *Informe del sismo de Lorca del 11 de mayo de 2011*. IGN. Madrid. Spain. 129 pp.

IGN, (2013). *Actualización de Mapas de Peligrosidad Sísmica en España 2012*. IGN. Madrid. 267 pp.

Martínez Solares, J.M., J. Mezcua, (2002). *Catálogo Sísmico de la Península Ibérica (880 a.C. - 1900).* Monografías IGN. 18. IGN. Madrid. Spain. 253 pp.

Michetti, A.M., E. Esposito, L. Guerrieri, et al., (2007). Environmental Seismic Intensity scale - ESI 2007. Intensity Scale ESI-07 (Guerrieri, L., Vittori, E. Eds.). *Mem. Descr. Carta Geologica d'Italia 74*. APAT. Rome. Italy. 41 pp.

NCSE-02, Norma de la construcción sismorresistente española (2002). Real Decreto 997/2002, de 27 de septiembre. *Boletín Oficial del Estado.* vol. 244, 35898-35967.

Silva, P.G., M.A. Rodríguez-Pascua, J.L. Giner-Robles, R. Pérez-López, J. Lario, M.A. Perucha, T. Bardají, P. Huerta, E. Roquero, M.B. Bautista Davila, (2014a). Catálogo de los efectos geológicos de los terremotos de España. (Silva, P.G. y Rodríguez-Pascua, M.A. eds.). *IGME-AEQUA. Riesgos Geológicos/Geotecnia.* nº 4. 352 pp. Madrid.

Silva, P.G., R. Pérez-López, M.A. Rodríguez-Pascua, E. Roquero, J.L. Giner Robles, et al., (2014b). Macroseismic analysis of slope movements triggered by the 2011 Lorca Earthquake (Mw 5.1): Application of the ESI-07 scale. *Geogaeta.* 55.

INQUA Focus Group on Paleoseismology and Active Tectonics

Recent advances in the comprehension of the central Apennine seismotectonics, by cross-checking Quaternary geology, paleoseismological and seismological data

Gori, S. (1), Falcucci, E. (1), Moro, M. (1), Saroli, M. (1,2), Fubelli, G. (3), Chiarabba, C. (1), Galadini, F. (1)

(1) Istituto Nazionale di Geofisica e Vulcanologia, Via di Vigna Murata 605, 00143, Roma, Italy. Email: stefano.gori@ingv.it
(2) DiMSAT, Università di Cassino, Viale dell'Università (Campus Universitario), Loc. Folcara, 03043, Cassino, Italy
(3) Dipartimento di Scienze, Università degli Studi Roma Tre, Largo San Leonardo Murialdo 1, 00146 Roma, Italy

Abstract: *Here we present the results of Quaternary geological field investigations, paleoseismological and seismological analyses performed over the past five years, aimed at obtaining an updated view of the seismotectonic features of the central Apennines. We investigated some of the major extensional tectonic structures of central Italy, and that are potentially responsible for large magnitude seismic events (M 6.5-7), namely the Fucino, the Middle Aterno Valley-Subequana Valley, the Mt. Marine and the Assergi faults. Moreover, the analysis of the 2009 L'Aquila earthquake sequence enabled to decrypt the complex structural setting of the area comprised between the Gran Sasso Range and the Middle Aterno Valley-Subequana Valley fault, where a high density of short (few km in plan view), closely spaced Quaternary normal faults occur.*

Key words: *Quaternary geological survey; paleoseismology; capable faulting; vertically restricted faults; structural interference.*

INTRODUCTION

Major active normal fault systems of the central Apennines are organised in chain parallel, NW-SE trending tectonic "corridors". The systems are composed by segments, often *en-echelon* arranged (Fig. 1a). Many of these segments were the object of geological and paleoseismological investigations in the past decades (e.g. Galadini and Galli, 2000; Galli et al., 2008; Falcucci et al., 2011); these studies permitted the association of fault activation episodes to large magnitude earthquakes (M of up to about 7) that struck central Italy over the past millennium. These studies, therefore, allowed to relate most of the central Apennine active fault strands to seismogenic sources potentially responsible for destructive earthquakes (e.g. Vannoli et al., 2012). In the past five years, we performed Quaternary geological field analyses and paleoseismological investigations (Fig. 1a) along some of the active faults for which information about the recent kinematic behaviour was incomplete or completely lacking.

DATA ANALYSIS AND CONCLUSIONS

We obtained new data on the slip history of the Fucino fault, responsible for the 1915 Avezzano earthquake (M 7) (Michetti et al., 1996; Galadini and Galli, 1999), and of the Mt. Marine strand of the Upper Aterno fault system, that activated during the Feb. 2 shock of the 1703 seismic sequence (Moro et al., 2002). As for the former, excavations made for the realisation of a photovoltaic plant near Pescina exposed several fault planes, parallel to the Marsicana Highway fault segment, that brought into contact Early Pleistocene lacustrine silt and alluvial/colluvial sediments (Fig. 1b) containing Bronze Age and Roman artefacts and pottery fragments. The present soil was also involved in the tectonic deformation, confirming the activation of the Marsicana Highway strand during the 1915 earthquake, as hypothesised by Galadini and Galli (1999).

As for the Mt. Marine fault, paleoseismological trenching revealed the displacement of colluvial sediments containing Roman pottery fragment,; confirming the activation of the structure during historical times. Presently ongoing radiocarbon dating will provide further chronological data to strictly constrain the record of Holocene faulting events, and to help confirming fault activation during the 1703 seismic shock (Moro et al., 2002).

Geological investigations performed along the Middle Aterno Valley fault system defined a long term slip rate on the order of 0.3 mm/yr, based on the displacement of Early Pleistocene breccias along the main strand of the tectonic structure (Gori et al., 2014). Paleoseismological investigations defined the occurrence of two Holocene faulting episodes, the last of which occurred during the 1st century B.C. These data confirm that the Middle Aterno Valley fault is part of a 30-km-long system with the Subequana Valley fault - based on geological and structural data (Falcucci et al., 2011) -, that is capable and potentially responsible for M 6.8 seismic events, and whose last activation took place about 2000 years BP. This is confirmed by a trench dug across the Subequana Valley fault, into a small debris fan that seals the structure; radiocarbon dating indicates that the fan was deposited at least (the excavation did not reach the fan base) since the last thousand years (Gori et al., 2014).

Field analyses allowed mapping in detail the surface expression of the about 10-km-long Assergi fault, considered as part of a longer fault system with the Campo Imperatore fault segments (Galadini and Galli, 2000), affecting the SW slope of the Gran Sasso Range. Geomorphic analyses performed along the southern sector of the Assergi fault permitted the identification of an about 1-m-high scarp at the base of the western flank of the Fossa di Paganica depression, antithetic to the

main fault plane. Paleoseismological trenches dug across this landform revealed that it coincides with an antithetic fault plane. It placed in contact colluvial sediments, at the fault footwall, with lake and colluvial sediments, at the hanging wall (Fig. 1c). The fault displaced the whole sequence exposed by the trench, up to the base of the present soil. In particular, a horseshoe nail, archaeologically dated at the Middle Age, was found within one of the uppermost faulted layers. Such an evidence indicates that the Assergi fault was activated during (or after) the Middle Age; ongoing radiocarbon dating will help to define the association between this activation episode and known large magnitude seismic events that affected this part of the central Apennines during the past centuries.

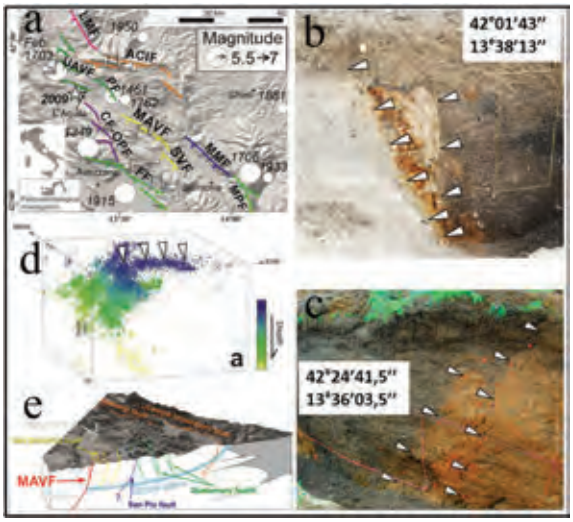

Figure 1: a) Seismotectonic framework of the central Apennines (modified from Falcucci et a., 2011); b) Paleoseismological trench across the Marsicana Highway segment of the Fucino fault and (c) across the Assergi fault (white triangles, fault planes); d) 3-D aftershock distribution of the 2009 seismic sequence (white triangles, low angle seismo-structural discontinuity); e) Proposed structural scheme of the area comprised between the Aterno valley and the Gran Sasso Range.

Joint seismological and geological observations also reveals the existence of an almost flat mechanical discontinuity, located at 1-to-3 km depth in the area comprised between the northern sector of the Middle Aterno Valley-Subequana Valley fault system and the Gran Sasso Range (Gori et al., 2014) (Fig. 1d). We interpret this feature as a splay of the Gran Sasso Range thrust front. This plane probably acts as structural/rheological barrier, leading to the formation of vertically restricted extensional structures, in the area comprised between the Gran Sasso Range and the Middle Aterno Valley-Subequana Valley fault (Fig. 1e). According to our interpretation, these minor faults, even if possibly capable, are not the surface expression of seismogenic sources able to rupture during large earthquakes, being their seismic potential "limited" for the shallow decollement (Fig. 1e).

Our results give the grounds for an updated view of the seismotectonic characteristics of a large portion of the central Apennines, and of the central Italy earthquake occurrence probability.

References

Falcucci, E., S. Gori, M. Moro, A.R. Pisani, D. Melini, F. Galadini, & P. Fredi, (2011). The 2009 L"Aquila earthquake (Italy): what next in the region? Hints from stress diffusion analysis and normal fault activity. *Earth Planet. Sci. Lett*. 305, 350-358.

Galadini, F., P. Galli, (1999). The Holocene paleoearthquakes on the 1915 Avezzano earthquake faults (central Italy): implications for active tectonics in the central Apennines. *Tectonophysics*. 308, 143-170.

Galadini, F., P. Galli, (2000). Active tectonics in the central Apennines (Italy) - Input data for seismic hazard assessment. *Nat Haz*. 22, 225-270.

Galli, P., F. Galadini, & D. Pantosti, (2008). Twenty years of paleoseismology in Italy. *Earth-Science Rev*. 88, 89-117.

Gori S., E. Falcucci, M. Moro, G. Fubelli, M. Saroli, C. Chiarabba, F. Galadini, (2014). Deep reaching versus vertically restricted Quaternary normal faults: implications on seismic potential assessment in tectonically active regions. Lessons from the middle Aterno valley fault system, central Italy. *GNGTS congress*. Bologna. November 2014. 25-27.

Michetti, A.M., F. Brunamonte, L. Serva, & E. Vittori, (1996). Trench investigations of the 1915 Fucino earthquake fault scarps (Abruzzo, Central Italy): geological evidence of large historical events. *J. Geophys. Res*. 101, 5921-5936.

Moro, M., V. Bosi, F. Galadini, B. Giaccio, P. Messina, & A. Sposato, (2002). Analisi paleosismologiche lungo la faglia del M. Marine (Alta Valle dell'Aterno): risultati preliminari. *Il Quaternario (Italian Journal of Quaternary Sciences)*. 15, 259-270.

Vannoli, P., P. Burrato, U. Fracassi, & G. Valensise, (2012). A fresh look at the seismotectonics of the Abruzzi (Central Apennines) following the 6 April 2009 L'Aquila earthquake (Mw 6.3). *Boll. Soc. Geol. It. (Int. J. Geosci.)*. 131 (3), 309-329.

KEY-NOTES:

(1) Major active normal fault systems of the central Apennines are analysed.

(2) Quaternary geological field investigations defined the long term faults slip history.

(3) We identified displacement events of the investigated faults during earthquakes occurred during the past two millennia.

(4) Joint geological and seismological analyses defined the role of pre-existing tectonic structures in the development and evolution of active normal fault segments.

INQUA Focus Group on Paleoseismology and Active Tectonics

Detailed fault slip-histories based on cosmogenic ^{36}Cl analyses from Abruzzo, Italy, reveal fault behaviour over multiple earthquake cycles

Gregory, L.C. (1), Phillips, R.J. (1), Roberts, G.P. (2), Cowie, P.A. (3), Shanks, R.P. (4), McCaffrey, K. (5), Wedmore, L.N.J. (6), Papanikolaou, I. (7), Faure Walker, J. (6), Watson, Z.K. (6)

(1) University of Leeds, Leeds, United Kingdom. Email: l.c.gregory@leeds.ac.uk
(2) Birkbeck College, University of London, London, United Kingdom
(3) University of Bergen, Bergen, Norway
(4) Scottish Universities Environmental Research Centre, AMS Laboratory, East Kilbride, United Kingdom
(5) University of Durham, United Kingdom
(6) University College London, London, United Kingdom
(7) Agricultural University of Athens, Athens, Greece

Abstract: *Analysis of variations in cosmogenic nuclide concentration along active bedrock fault scarps provides unique insight into past fault slip over several thousand years and multiple earthquake cycles. Variations in slip-rate and fault interaction on hundred- to thousand- year time scales across networks of faults can be inferred based on datasets of ^{36}Cl concentration measured systematically up the scarps. In this presentation, we will use a new, unpublished, and extensive ^{36}Cl dataset to document Pleisto-Holocene activity across the complicated network of normal faults in Abruzzo, Italy, which includes data processed within the last year at the new University of Leeds Cosmogenic Isotope Lab. We discuss the importance of well-documented cosmogenic sampling sites and careful characterisation of local geomorphology. We highlight ^{36}Cl data from some faults that can be modeled with highly variable fault slip through time, such that faults may have experienced periods of intense seismicity separated by more quiescent intervals.*

Key words: *Chlorine-36, cosmogenic nuclides, slip rate variability, Abruzzo, tectonic geomorphology.*

INTRODUCTION

Typical earthquake hazard assessments rely heavily on the recent or historical earthquake record combined with geodetic data. This reliance may significantly underestimate the hazard along faults with slip-rates lower than can be resolved by geodetic methods or that have not experienced a notable earthquake during the last few hundred years. Irregular earthquake recurrence complicates hazard assessment even further, particularly when estimating long-term average slip rate. In order to fully assess earthquake hazard and fault behaviour, faulting must be investigated on timescales long enough to incorporate multiple earthquake cycles, particularly in continental regions where deformation is distributed across a complicated network of faults.

We use chlorine-36 cosmogenic nuclide exposure techniques to measure active faulting since the Late Pleistocene (Zreda and Noller, 1998; Schlagenhauf et al., 2010). ^{36}Cl is only produced at and just below the Earth's surface. The concentration of ^{36}Cl on bedrock faults scarps is directly related to the history of exposure of the scarp due to past earthquakes, elucidating the behaviour of faults over multiple earthquake cycles and 10^3-10^4 years.

The climate history, slope geomorphology, and bedrock geology in Abruzzo is such that bedrock fault scarps are abundantly well preserved, providing an ideal setting for ^{36}Cl cosmogenic nuclide analyses. The region has a long historical earthquake record and rich geodetic and palaeoseismic datasets available for comparison of recent earthquake and modern-day strain patterns to long-term (10^3-10^4 years) fault activity (e.g. D'Agostino et al., 2011; Galli et al., 2002). There is also a wealth of data on longer term, Pleistocene-Holocene strain (e.g. Roberts and Michetti, 2004), providing a framework for more the detailed fault-slip histories revealed by cosmogenic exposure techniques. The complicated network of parallel normal faults in Abruzzo is also ideal for gaining an understanding of fault interaction on timescales greater than one earthquake cycle.

Fault Geomorphology

NE-SW directed extension in the Italian Apennines since 2-3 Ma is localised on NW-SE trending normal faults. Faulting since the demise of last glacial maximum (LGM) has displaced slopes preserved since the LGM (~12-18 kyr in Abruzzo), creating scarps of exposed bedrock limestone that have throws between 2-20 metres (Figure 1). During the last glacial maximum, erosion rates generally exceeded fault slip rates and the potential for preservation of fault scarps at this time was low. The timing of the LGM is evidenced by several studies, for example changes in sedimentation rates through the demise of the LGM as a proxy for slope stability in Zolitschka and Negendank (1996), as well as our results from exposure age dating of bedrock in the footwall slope of sampling sites.

The geomorphology of sampling sites must be carefully constrained to ensure that exposure of the fault is only due to seismic activity and not the result of mass transport

or erosional processes. We quantify the geomorphology of each site using ground penetrating radar (GPR) and LiDAR (terrestrial and airborne, Figure 1b).

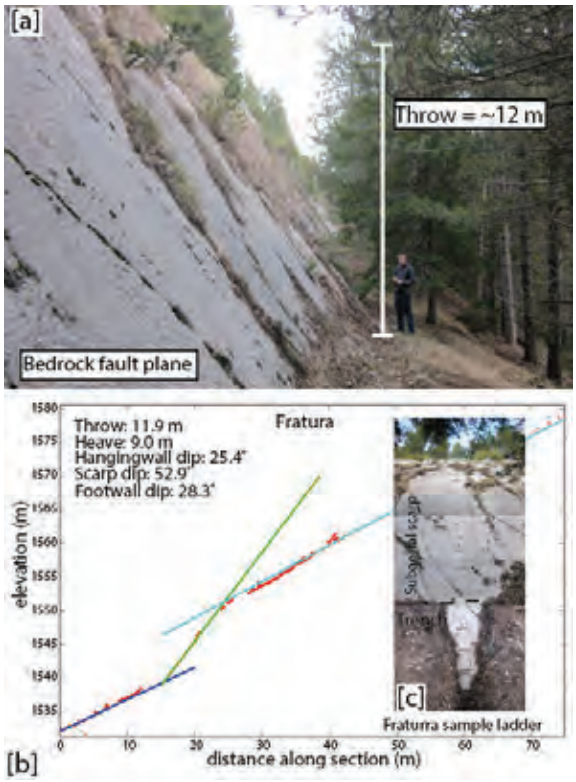

Figure 1: (a) Photo of the Fraturra fault scarp. (b) Throw profile derived from LiDAR dataset. Lines are fit to the data to calculate site characteristics and total faulted displacement of the LGM slope. (c) Sampling ladder at the Fraturra fault, showing the fault surface sampled above and below the fault plane intersection with the ground.

^{36}Cl Methods and Modelling

Chlorine-36 is produced *in-situ* at the Earth's surface and down to a few metres depth, primarily due to interactions between calcium and high energy cosmogenic radiation (see review from Gosse and Phillips, 2001). Cosmogenic production rates decrease exponentially with depth, decaying to very low muonic production rates below ~2 metres depth in gravelly soils. ^{36}Cl accumulates in bedrock fault scarps as the plane is progressively exhumed by earthquakes.

Samples of fault planes were collected using a hand-held angle grinder with an average spacing of 20-100 cm up the fault plane and below the ground surface down to ~2 meters (generally at a greater sampling density near the ground surface, see Figure 1c). Samples are cleaned and secondary material is removed prior to crushing to a 250-500 µm size fraction. Preparation basically follows methods outlined by Stone et al. (1996). Briefly, samples are dissolved and spiked with an isotopically enriched $^{35/37}$Cl carrier, and AgCl is precipitated and cleaned for measurement on the SUERC AMS. The SUERC AMS is tuned for low ^{36}Cl concentrations, and is the optimal machine for our samples. AMS measurements follow procedures outlined in Wilcken et al. (2013, and references within). We measure bulk elemental chemistry on dissolved aliquots of each sample on ICP-OES and ICP-MS, in order to correct for the effect of chemical variations on production rate, particularly of Ca and K.

We also colleced samples for cosmogenic exposure dating of bedrock in the planar foot wall of each sample locality, in order to improve constraints on Holocene slip rates and to better understand erosional processes acting on the fault-displaced slopes. Samples standing slightly proud above the footwall slope were carefully selected to avoid small gullies in the footwall or other slope processes. Samples were prepared in the same manner as fault plane samples for measurement on the AMS.

We use the Matlab code developed by Schlagenhauf et al. (2010) to model fault slip histories based on ^{36}Cl data from above and below the ground surface. Model parameters for the sample site geometry and total scarp height are obtained from our LiDAR and GPR datasets collected at each locality (e.g. Figure 1b). Our approach is to model the full height of the scarp (measured from our LiDAR data), including the section above the point at which samples are collected and where the scarp is degraded, in order to fully interpret data from the part of the fault that we have sampled. A constant slip rate is achieved in the model by inputting equal recurrence of earthquakes with magnitudes that are typical of Abuzzo (M 5.8-6.9), and with appropriately scaled displacements based on Wells and Coppersmith (1994) empirical scaling relationships. We vary the slip rate by increasing the number of earthquakes (keeping magnitude approximately constant) for different time intervals, depending on how well the models fit the data. We are currently developing methods for more automated modelling techniques (see presentation by Cowie et al. in this abstract volume).

In addition to fitting models to the measured ^{36}Cl concentration, we also compare the measured concentration to the ^{36}Cl expected if the fault scarps are preserved since the demise of the LGM (15 ± 3) and have slipped at a uniform rate during the whole of the Holocene. This provides a basis for identifying variations in fault behaviour between sites on adjacent faults.

RESULTS

Across Abruzzo (Figure 2) average fault slip rates based on cosmogenic profiles vary between approximately 2.0 to 0.2 mm/yr, which is in agreement with average strain rates predicted by methods in Roberts and Michetti (2004). Data from some faults can be fit by straightforward constant rate slip models using the code developed by Schlagenhauf et al. (2010). Other faults can be modelled with periods of intense slip separated by more quiescent intervals, and some models involve a change in slip rate that persists for several thousand years.

INQUA Focus Group on Paleoseismology and Active Tectonics

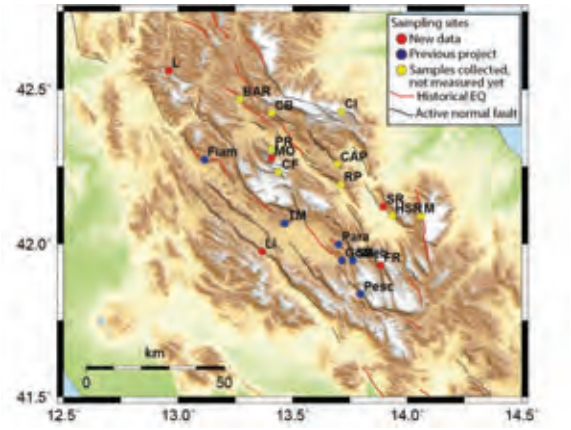

Figure 2: ASTER GDEM map of sampling localities for chlorine-36 analyses on bedrock faults in Abruzzo, central Apennines. Historical earthquakes are mapped based on shaking records.

INTERPRETATION

Significant time-varying fault slip variability is often predicted by numerical models of interacting fault networks (e.g. Cowie et al., 1998; 2012), but is rarely observed due to the timescales over which it occurs. We will present evidence for this behaviour on several faults across Abruzzo, and discuss whether it potentially occurs on the majority of faults, but in a manner such that it is beyond the resolution of our data. We do not attempt to resolve individual earthquakes in our data. Our aim is to investigate the variation of slip rate on large scales in time and space (10^4 years and 10^5 meters) in order to reveal potential across strike interactions between faults. Slip-rate variability occurring over multiple earthquake cycles suggests that slip may be transient across a network of faults over multiple earthquake cycles, and recent seismicity on any one fault strand may be variable compared to what is expected from average slip rate estimates. This concept will be further explored in other presentations within this abstract book (Cowie et al., Roberts et al.).

CONCLUSIONS

Our data confirm that displacement on bedrock faults of LGM slopes formed during the Late Pleistocene-Holocene, and that the profiles of ^{36}Cl concentration are not the result of single erosional events such as landslides. We demonstrate the importance of site selection and characterisation for obtaining robust fault slip datasets. This study highlights the need to characterise and compare fault behaviour over multiple timescales in order to anticipate future seismicity.

Acknowledgements: This study was funded by NERC Standard Grants NE/E01545/1 and NE/I024127/1. A World Universities Network Research Mobility Grant to Gregory and Phillips facilitated collaboration between the University of Leeds and the University of Bergen.

References

Cowie, P.A., (1998). A healing-reloading feedback control on the growth rate of seismogenic faults. *Journal of Structural Geology*. 20, 1075-1087.

Cowie, P.A., G.P. Roberts, J.M. Bull, & F. Visini, (2012). Relationships between fault geometry, slip rate variability and earthquake recurrence in extensional settings. *Geophysical Journal International*. Volume 189, Issue 1, pages 143-160.

D'Agostino, N., S. Mantenuto, E. D'Anastasio, R. Giuliani, M. Mattone, S. Calcaterra, P. Gambino, L. Bonci, (2011). Evidence for localized active extension in the central Apennines (Italy) from global positioning system observations. *Geology*. 39, 291-294.

Galli, P., F. Galadini, M. Moro, C. Giraudi, (2002). New paleoseismological data from the Gran Sasso d'Italia area (central Apennines). *Geophysical Research Letters*. 29.

Gosse, J.C. & F.M. Phillips, (2001). Terrestrial in situ cosmogenic nuclides: theory and application. *Quaternary Science Reviews*. 20, 1475-1560.

Roberts, G.P., A.M. Michetti, (2004). Spatial and temporal variations in growth rates along active normal fault systems: an example from Lazio-Abruzzo, central Italy. *Journal of Structural Geology*. 26, 339-376.

Schlagenhauf, A., Y. Gaudemer, L. Benedetti, I. Manighetti, L. Palumbo, I. Schimmelpennig, R. Finkel & K. Pou, (2010). Using *in situ* Chlorine-36 cosmonuclide to recover past earthquake histories on limestone normal fault scarps: a reappraisal of methodology and interpretations. *Geophysical Journal International*. doi: 10.1111/J.1365-246X.2010.04622.X

Stone, J.O., G.L. Allan, L.K. Fifield, & R.G. Cresswell, (1996). Cosmogenic chlorine-36 from calcium spallation. *Geochemica et Cosmochimica Acta*. 60**,** 679-692.

Wilcken, K., S.P.H. Freeman, C. Schnabel, S.A. Binnie, S. Xu, R.J. Phillips, (2013). ^{36}Cl accelerator mass spectrometry with a bespoke instrument. *Nuclear Instruments and Methods in Physics Research Section B: Beam Interactions with Materials and Atoms*. 294, 107-114.

Zolitschka, B., J.F.W. Negendank, (1996). Sedimentology, dating and palaeoclimatic interpretation of a 76.3 ka record from Lago Grande di Monticchio, Southern Italy. *Quaternary Science Reviews*. 15, 101-112.

Zreda, M., & J.S. Noller, (1998). Ages of prehistoric earthquakes revealed by cosmogenic chlorine-36 in a bedrock fault scarp at Hebgen Lake. *Science*. 282, 1097-1099.

INQUA Focus Group on Paleoseismology and Active Tectonics

The Italian Catalogue of Earthquake Environmental Effects: a contribute to seismic hazard assessment through the ESI intensity scale

Guerrieri, L. (1), Baiocco, F. (1), Blumetti, A.M. (1), Brustia, E. (1), Comerci, V. (1), Lucarini, M. (1), Porfido, S. (2), Scaramella, A. (1), Vittori, E. (1)

(1) ISPRA, Geological Survey of Italy, Via Vitaliano Brancati, 48, Roma, Italy. Email: luca.guerrieri@isprambiente.it
(2) Institute for coastal marine environment, National Research Council of Italy, Calata Porta di Massa, Napoli, Italy

Abstract: *Earthquake, environmental effects (EEEs) are a component of seismic hazard in addition to vibratory ground motion. Their primary role in the scenario of damage has been clearly pointed out by recent strong seismic events.*
The scientific interest of EEEs has increased in the last twenty years, in the frame of the INQUA TERPRO "Paleoseismology and Active Tectonics" Focus Group: i) in 2007 it was published the ESI intensity scale, that evaluates epicentral and local intensity based only on EEEs; ii) in 2011 it was launched the infrastructure of the EEE Catalogue, a free accessible database designed to collect the characteristics of EEEs worldwide occurred.
This note is focused on the Italian Catalogue of EEEs, which collects information about EEEs induced by 39 strong earthquakes (modern, historical and paleo) occurred in the Italian territory. These data allow to identify the areas more exposed to the occurrence of EEEs and to evaluate the seismic intensity through the ESI scale.

Key words: *Earthquake environmental effects, EEE Catalogue, ESI intensity scale, Italy.*

INTRODUCTION

Earthquake Environmental Effects (EEEs) are all the phenomena generated in the natural environment by a seismic event.
EEEs are classified into two main types:

- primary effects, that include any surface expression of the seismogenic tectonic source, (e.g. surface faulting, surface tectonic uplift/ subsidence);
- secondary effects, that include a wide range of natural phenomena generally induced by the ground shaking.

These phenomena represent a significant source of hazard, especially (but not exclusively) during large earthquakes, substantially contributing damage our increasingly vulnerable towns.
This result has been recently confirmed by seismic events occurred in very different parts of the world (e.g. 2011 March 11, Mw 8.9 Tohoku, Japan earthquake; 2011 February 22, Mw 6.3 Christchurch, New Zealand earthquake; 2008 May 12, Mw 7.9 Wenchuan, China, earthquake). Earthquake Environmental Effects can be a major source of hazard, in addition to vibratory ground motion: therefore, a comprehensive assessment of potential seismic damage and, consequently, a more effective seismic hazard assessment has to include the whole set of earthquake-related effects, both the structural and the environmental ones.
In this note we present the Italian Catalogue of Earthquake Environmental Effects. This catalogue has been developed in the frame of INQUA (International Union for Quaternary Research).

THE INQUA PROJECTS ON ESI SCALE AND EEE CATALOGUE

In the last twenty years the scientific interest on EEEs has increased, especially in the frame of INQUA TERPRO "Paleoseismology and Active Tectonics" Focus Group.
In 2007, it has been published the ESI (Environmental Seismic Intensity; Michetti et al., 2007) intensity scale, a new scale based only on the characteristics, size and areal distribution of EEEs.
The ESI scale can provide a better estimation for intensity assessments than the traditional intensity scales because earthquake environmental effects are independent from time (modern, historical or paleo) and do not depend on the socio-economic development of the damaged zones. This new scale complements and/or replaces traditional macroseismic scales i) for earthquake intensity degrees $\geq$X, when damage-based assessments are extremely difficult because the built environment is practically totally destroyed; ii) in sparsely populated areas, where man-made structures are absent or rare, so that only the environmental effects allow intensity estimates; iii) in paleoseismic analyses, where traditional macroseismic scales are not applicable. The scale has been already applied to many cases around the world (Fokaefs and Papadopoulos (2007), Guerrieri et al. (2007), Lalinde et al. (2007), Papathanassiou et al. (2007), Papathanassiou and Pavlides (2007), Porfido et al. (2007), Serva et al. (2007), Tatevossian (2007), Guerrieri et al. (2008), Alì et al. (2009), Mosquera-Machado et al. (2009), Ota et al. (2009), Papanikolaou et al. (2009), Berzhinskii et al. (2010), Lekkas (2010), Papanikolau (2011), Gosar (2012), Fontoulis and Mavroulis (2013), Mavroulis et al., (2013), Silva et al. (2013), Velazquez Bucio et al. (2013), Bashir et al. (2014).
The EEE Catalogue, freely accessible,is designed to collect worldwide standardized information about the

characteristics, size and spatial distribution of Earthquake Environmental Effects from modern, historical and paleo-earthquakes. This information about EEEs gathered in a single database, greatly facilitates its use for seismic hazard studies. The database implementation has been endorsed by the INQUA TERPRO Project #0811 ("A global catalogue and mapping of earthquake environmental effects"; 2008 – 2011), through a Working Group coordinated by ISPRA - Geological Survey of Italy. The first official release of the EEE Catalogue was done under the framework of the XVIII INQUA Congress, held in Bern in July 2011.

THE ITALIAN CATALOGUE OF EARTHQUAKE ENVIRONMENTAL EFFECTS

At present (January 2015) 39 Italian earthquakes are included in the EEE Catalogue. For each event, the information is collected at three levels of increasing detail: Earthquake, Locality and Site. Also available imagery documentation (photographs, videos, sketch maps, stratigraphic logs) can be stored in the database. Moreover, within the EEE Catalogue the epicentral and local intensity values based on the ESI scale are recorded. This allows an objective comparison of earthquake effects and intensity for events that have occurred in different areas and/or in different periods.
Data can be explored from the following public interface: http://www.eeecatalog.sinanet.apat.it/italy/earthquake/index.php.
More details in Figure 1.
The major added value of this catalogue for seismic risk assessment is the possibility to explore the scenarios of environmental effects induced by past earthquakes and therefore to identify the areas where the human settlements and infrastructures are more exposed to this hazard.
The content of the Italian EEE Catalogue is summarized in Table 1.

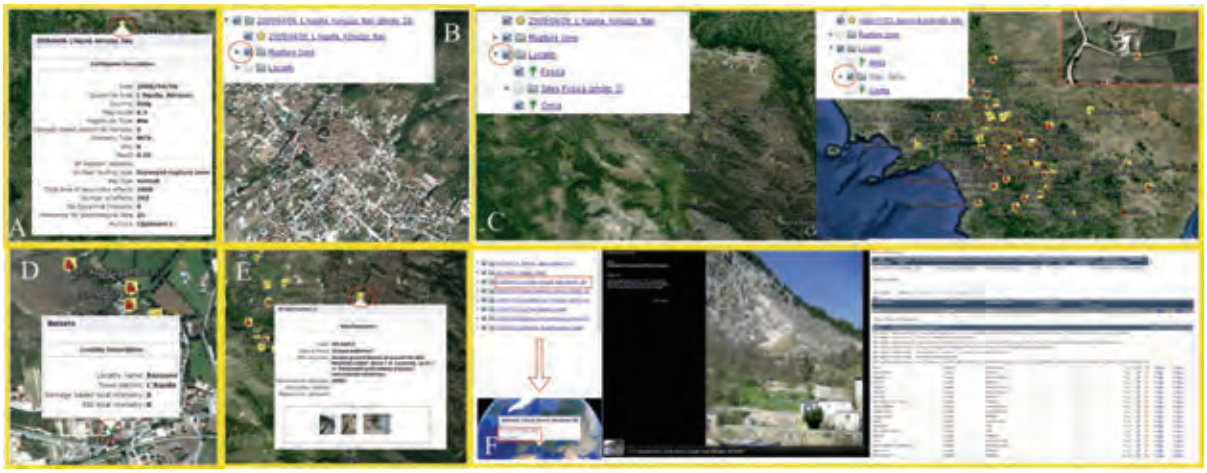

Figure 1: Types of information stored into the EEE Catalogue. From the URL http://www.eeecatalog.sinanet.apat.it/italy/earthquake/index.php it is possible to view some general information about the earthquakes located on a Google Baloon, by clicking on each epicentre (yellow star, frame A), including the pattern of coseismic ruptures (primary or secondary), surveyed or interpreted, by clicking on the gray triangle indicated in frame B, which activates the box Rupture Zone. The geographic distribution of localities (green drops) and sites (classified in 7 EEE categories), can be viewed by clicking on the gray triangle of the Locality level (frame C). Each Locality and Site can be zoomed to better locate each individual element (red box in frame C).
Some general information about the Locality (e.g. local intensity) and Site (e.g., EEE Classification, Description, Reference and photographs) are visible on a Google Baloon, by clicking on the Locality (frame D) and Site (frame E). The entire database and photogallery (including maps, video, and other pdf documents) related to a specific earthquake, can be consulted by clicking on the earthquake string in the table of contents (frame F).

Modern earthquakes
For six modern earthquakes, data on EEEs have been surveyed in a systematic way and therefore the reliability, completeness and resolution of location are very high. It is the case of the 2012 Emilia earthquake (Mw=5.9) characterized by a widespread presence of liquefactions that strongly amplified the local impact of this moderate event (Di Manna et al., 2012). EEE data for the 2009 L'Aquila earthquake (Mw=6.3), including a detailed pattern of surface faulting along the Paganica fault (Vittori et al., 2011), are the result of the integration of field surveys conducted by different research groups.
Also for the 1997 Colfiorito earthquake (Mw=6.0) the EEE dataset is quite complete, due to the integration of surveys from several teams, allowing to compare the ESI and MCS intensity scenarios (Guerrieri et al., 2008).
Concerning the 1980 Irpinia (Ms=6.9) and the 1976 Friuli (Mw=6.6) earthquakes, the EEE scenario has been built on data collected from contemporary reports and maps. The amount of information and the areal distribution of EEE is outstanding. The accuracy of the description and the precision in the location was good for most of the cases.

INQUA Focus Group on Paleoseismology and Active Tectonics

Year	Month	Day	Epicentral Area	Magnitude (Mw)	SRL (km)	MaxD (cm)	Total area (km2)	Number of effects	ESI	Damage based Intensity (MCS)
Modern Earthquakes										
2012	5	20	Finale Emilia	5.9	-	-	370	210	8	8
2012	5	29	Medolla, Emilia Romagna	5.8	-	-	360	103	8	8
2009	4	6	L'Aquila, Abruzzo	6.3	6	15	1000	192	9	9
1997	9	26	Colfiorito	6.0	12	8	1400	275	9	9
1980	11	23	Irpinia	6.9	40	90	7400	346	10	10
1976	5	6	Friuli	6.4	18	50	400	35		10
Historical Earthquakes										
1930	7	23	Vulture, Southern Apennines	6.6	38	40	3900	132	10	10
1919	6	29	Mugello, Northern Apennines	6.1	-	-	900	17	9	9
1915	1	13	Fucino	7.0	24	100	400	18	10	11
1908	12	28	Messina Straits	7.2	?	?	20000	486	11	11
1905	9	8	Southern Calabria	7.0	?	?	15000	212	11	11
1857	12	16	Basilicata	7.0	45	250	13200	104	10	11
1805	7	26	Bojano	6.9	40	150	5300	106	10	10
1783	2	5	Cittanova, Calabria	7.0	35	>80	3500	68	10	11
1703	1	14	Norcia, Umbria	6.8	10	?	700	5	10	11
1703	2	2	L'Aquila, Abruzzo	6.6	10	60	1000	19	10	10
1694	9	5	Irpinia	6.9	38	-	6300	16	10	10
1688	6	5	Sannio	6.7	32	-	1700	21	10	11
Paleo Earthquakes										
745±145			Pollino, Italy	6.6	-	160	-	-	10	-
700±200			Fucino	7.0	-	1	-	5	10	-
590±100			Eastern Cagno Basin, Calabria	6.8	-	120	-	2	10	-
372±2			Cittanova, Calabria	6.9	26	80	-	-	10	-
-241±1095			Campo Imperatore	7.0	-	38	-	1	10	-
-580±470			Aremogna- 5 Miglia Plain	6.3	-	100	-	-	10	-
-828±1389			M.Vettore Fault (Central Ap.)	6.5	-	45	-	1	10	-
-1050±100			Northern Cagno Basin, Calabria	6.8	-	120	-	-	10	-
-1500±100			Fucino	7.0	-	150	-	-	10	-
-1550±4500			Campotosto area (Laga Mts.)	6.6	-	-	-	-	10	-
-1875±2130			Cittanova, Calabria	6.9	26	-	-	-	10	-
-2050±100			Cagno basin (northern sector)	6.8	-	120	-	1	10	-
-2050±100			M. Vettore (Central Ap.)	6.5	-	-	-	-	10	-
-3338±398			Aremogna- 5 Miglia Plain	6.3	-	30	-	-	10	-
-3813±3227			Pollino, Italy	6.6	-	160	-	-	10	-
-4074±549			Campo Imperatore	7.0	38	-	-	-_	10	_-

-4700±1200	Fucino	7.0	-	200	-	2	10	-
-6415±60	Campotosto area (Laga Mts.)	6.6	-	-	-	-	10	-
-8100± 2600	Fucino	7.2	-	300	-	3	11	-
-10050±	Cittanova, Calabria	6.9	-	-	-	-	10	-
-12550±	Campo Imperatore	7.0	38	-	-	-	10	-

Table 1: List of the 40 italian earthquakes catalogued, with information on the content of the database. See text for details.

Historical earthquakes

Back in time, 12 earthquakes are named "historical", since EEE data result from the retrieving of contemporary historical documents, reporting information collected sometimes for different purposes. The degree of completeness and resolution in the location may be very different.

For example, for the 1908 Messina earthquake (Mw=7.1) the wealth of information is huge and the location of effects is often very precise (Comerci et al., 2015). Conversely, for the 1915 Fucino earthquake (Ms=7.0), although a large amount of EEE could be expected, the contemporary documentation is mainly focused on surface faulting (Oddone, 1915), and the information on secondary effects is missed or not yet well catalogues. Consequently, the total area of secondary effects is underestimated and cannot be used for ESI intensity assessment.

As regard the seismic sequence occurred in Calabria (Southern Italy) in 1783 (started with a main shock on 5th February, Mw 7.2), the scenario of EEE is particularly well documented and complete. The impressive EEE were so carefully described and mapped by the contemporary reports (e.g. Sarconi, 1784; De Dolomieu, 1784; Vivenzio,1788), that Cotecchia et al. (1986) allow, after more than 200 years, to characterize the "geomorphological crisis" induced by the earthquakes and to map the coseismic landslides.

For other events occurred in the last three centuries (1930, 1919, 1805, 1703, 1694 and 1688), the scenario of EEE is incomplete (cfr. Serva et al., 2007). Sometimes, it is possible to estimate the length of fault rupture but not the maximum displacement. Nevertheless, it is important to outline that the EEEs preserved in the historical reports are typically the most impressive, i.e. the most evident effects: therefore, the application of the ESI scale to these data provides an evaluation of the maximum local intensity produced by the earthquake.

Paleoearthquakes

The catalogue includes also 21 paleoearthquakes resulting from paleoseismic investigations mostly in the Central-Southern Apennines. For these events, the most common information is the coseismic fault displacement measured in the paleoseismic trench. If the evidence of a fault is visible in more than one trench it is possible to estimate also its length (of course a minimum value).

By applying the empirical relationships by Wells and Coppersmith (1994) it has been possible to estimate a minimum magnitude of such paleoearthquakes. Of course, this is a very preliminary assessment since it is based only on one or a few pieces of evidence, but it is sometimes very important for updating the seismic hazard assessment of specific areas. Concerning the epicentre location assignment, in absence of other information, it coincides with the trench site (if one) or with the baricenter among the trench sites (if many).

CONCLUSIONS

The compilation of the Italian Catalogue of Earthquake Environmental Effects is still in progress. A web infrastructure is available to upload data from a remote position at the URL:

http://www.eeecatalog.sinanet.apat.it/login.php

In the meanwhile, this infrastructure will be available also for the collection in a standard format and almost in real time of EEE induced by earthquakes in the next future.

Acknowledgements: For the support in the compilation of the Italian Catalogue of Earthquake Environmental Effects are acknowledged Davide Campagnolo, Pio Di Manna, Eliana Esposito, Anna Maria Giordano, Gabriele Leoni, Letizia Lippmann, Alessandro Michetti, and Giancanio Sileo.

References

Ali, Z., M. Qaisar, T. Mahmood, M.A. Shah, T. Iqbal, L. Serva, A.M. Michetti, and P.W. Burton, (2009). The Muzzaffarabad, Pakistan, earthquake of 8 October 2005: Surface faulting, environmental effects and macroseismic intensity. *Geol. Soc. London.* Spec. Publ. 316 155-172. doi:10.1144/SP316.9.

Bashir, A., S. Hamid, A. Akhtar, (2014). Macroseismic intensity assessment of 1885 Baramulla Earthquake of northwestern Kashmir Himalaya, using the Environmental Seismic Intensity scale (ESI 2007). *Quaternary International*. 321, 13 February 2014, 59-64.

Berzhinskii, Yu. A., A.P. Ordynskaya, A.S. Gladkov, O.V. Lunina, L.P. Berzhinskaya, N.A. Radziminovich, Ya. B. Radziminovich, V.S. Imayev, A.V. Chipizubov, and O.P. Smekalin, (2010). Application of the ESI_2007 Scale for Estimating the Intensity of the Kultuk Earthquake, August 27, 2008 (South Baikal). *Seismic Instruments.* 46 (4) 307-324. Allerton Press Inc., ISSN 0747_9239.

Comerci, V., E. Vittori, A.M. Blumetti, E. Brustia, P. Di Manna, L. Guerrieri, M. Lucarini and L. Serva, (2015). Environmental effects of the December 28, 1908, Southern Calabria-Messina (Southern Italy) earthquake. *Natural Hazards*. Vol. 75, doi: 10.1007/s11069-014-1573-x.

Cotecchia, V., A. Guerricchio, and G. Melidoro, (1986). The geomorphogenetic crisis triggered by the 1783 earthquake in Calabria (southern Italy), paper presented at the

International Symposium on Engineering Geology Problems in Seismic Areas. Int. Assoc. of Eng. Geol. Bari. Italy. 1986.

De Dolomieu, D., (1784). Mèmoire sur le tremblemants de terre de la Calabre Ulterieure pendant l'anné 1783. *Fulgoni Ed.* Roma.

Di Manna, P., L. Guerrieri, L. Piccardi, E. Vittori, D. Castaldini, A. Berlusconi & A.M. Michetti, (2013). Ground effects induced by the 2012 seismic sequence in Emilia: implications for seismic hazard assessment in the Po Plain. *Annals of Geophysics*. 55 (4), ISSN 2037-416x. 727-733.

Fokaefs, A. and G. Papadopoulos, (2007). Testing the new INQUA intensity scale in Greek earthquakes. *Quaternary International*. 173-174 15-22.

Fountoulis, I.G. and S.D. Mavroulis, (2013). Application of the Environmental Seismic Intensity scale (ESI 2007) and the European Macroseismic Scale (EMS-98) to the Kalamata (SW Peloponnese, Greece) earthquake (Ms=6.2, September 13, 1986) and correlation with neotectonic structures and active faults. *Annals of Geophysics*. 56, 6, 2013, S0675; doi: 10.4401/ag-6237.

Gosar, A., (2012). Application of Environmental Seismic Intensity scale (ESI 2007) to Krn Mountains 1998 Mw = 5.6 earthquake (NW Slovenia) with emphasis on rockfalls. *Nat. Hazards Earth Syst. Sci.* 12 1659-1670, doi: 10.5194/nhess-12-1659-2012.

Guerrieri, L., A.M. Blumetti, E. Esposito, A.M. Michetti, S. Porfido, L. Serva, E. Tondi and E. Vittori, (2008). Capable faulting, environmental effects and seismic landscape in the area affected by the 1997 Umbria-Marche (Central Italy) seismic sequence. *Tectonophysics*. 476 (1-2) 269-281, doi: 10.1016/j.tecto.2008.10.034.

Guerrieri, L., R. Tatevossian, E. Vittori, V. Comerci, E. Esposito, A.M. Michetti, S. Porfido and L. Serva, (2007). Earthquake environmental effects (EEE) and intensity assessment: the INQUA scale project. *Boll. Soc. Geol. It. (Ital. J. Geosci.)*. Special Section "Tectonic Geomorphology". (Dramis, F., Galadini, F., Galli, P., Vittori, E., editors) 126 (2) 375-386.

Lalinde, C.P. and J.A. Sanchez, (2007). Earthquake and environmental effects in Colombia in the last 35 years. INQUA Scale Project. *Bull. Seism. Soc. Am*. 97 (2) 646-654.

Lekkas, E.L., (2010). The 12 May 2008 Mw 7.9 Wenchuan, China, Earthquake: MacroseismicIntensity Assessment Using the EMS-98 and ESI 2007 Scales and Their Correlation with the Geological Structure. *Bull. Seism. Soc. Am.* 100 (5B) 2791-2804, doi: 10.1785/0120090244.

Mavroulis, S., I. Fountoulis and E. Lekkas, (2010). Environmental effects caused by the Andravida (08-06-2008, ML=6.5, NW Peloponnese, Greece) earthquake, In: (Williams, A., Pinches, G., Chin, C., Mc-Morran, T. and Massey C., eds.), *Geologically Active: 11th IAEG Congress*. Taylor & Francis Group. Auckland, New Zealand. 451-459.

Michetti, A.M., E. Esposito, L. Guerrieri, S. Porfido, L. Serva, R. Tatevossian, E. Vittori, F. Audemard, T. Azuma, J. Clague, V. Comerci, A. Gürpinar, J. Mc Calpin, B. Mohammadioun, N.A. Mörner, Y. Ota, and E. Roghozin, (2007). Intensity Scale ESI 2007. In: *Mem. Descr. Carta Geologica d'Italia* (Guerrieri, L. and Vittori, E. editors), Servizio Geologico d'Italia. Dipartimento Difesa del Suolo. APAT. Rome. Italy. 74.

Mosquera-Machado, S., C. Lalinde-Pulido, E. Salcedo-Hurtado, A.M. Michetti, (2009). Ground effects of the October 18, 1992, Murindo Earthquake (NW Colombia), using the Environmental Seismic Intensity Scale (ESI 2007) for the assessment of the intensity. *Geol. Soc. London.* Spec. Publ. 316123-144. doi: 10.1144/SP316.7.

Oddone, E., (1915). Gli elementi fisici del grande terremoto marsicano-fucense del 13 gennaio 1915. *Boll. Soc. Sism. It*. 19, 71-215.

Ota, Y., T. Azuma and N. Lin, (2009). Application of INQUA Environmental Seismic Intensity Scale to recent earthquakes in Japan and Taiwan. *Geol. Soc. London.* Spec. Publ. 316 55-71.

Papanikolaou, I.D., D.I. Papanikolaou, E.L. Lekkas. (2009). Advances and limitations of the Environmental Seismic Intensity scale (ESI 2007) regarding near-field and farfield effects from recent earthquakes in Greece: implications for the seismic hazard assessment. In *Palaeoseismology: Historical and Prehistorical Records of Earthquake Ground Effects for Seismic Hazard Assessment*. (Reicherter, K., Michetti, A.M., Silva Barroso, P.G. editors). Geol. Soc. London. Spec. Publ. 316, 11-30.

Papanikolaou, I.D., (2011). Uncertainty in intensity assignment and attenuation relationships: How seismic hazard maps can benefit from the implementation of the Environmental Seismic Intensity scale (ESI 2007). *Quaternary International*. 242, 42-51.

Porfido, S., E. Esposito, L. Guerrieri, E. Vittori, G. Tranfaglia, and R. Pece, (2007). Seismically induced ground effects of the 1805, 1930 and 1980 earthquakes in the Southern Apennines, Italy, *Ital. J. Geosci.* (Boll. Soc. Geol. It.). 126, 333-346.

Sarconi, M., (1784). Istoria de' Fenomeni del Tremoto Avvenuto nelle Calabrie, e nel Valdemone nell'Anno 1783 e sulla Geografia fisica di quelle regioni. *R. Acc. Sc. e Belle Lett. Di Napoli*. Naples. Giuseppe Campo.

Serva, L., E. Esposito, L. Guerrieri, S. Porfido, E. Vittori and V. Comerci, (2007). Environmental Effects from some historical earthquakes in Southern Apennines (Italy) and macroseismic intensity assessment. Contribution to INQUA EEE scale project. *Quaternary International.* 173-174, 30-44.

Silva, P.G., R. Pérez-López, M.A. Rodríguez-Pascua, J.L. Giner, P. Huerta, T. Bardají, and F. Martín-González, (2013). Earthquake Environmental Effects (EEEs) triggered by the 2011 Lorca earthquake (Mw 5.2, Betic Cordillera, SE Spain): Application of the ESI-07 Macroseismic Scale. *Proceedings of the 4th International INQUA Meeting on Paleoseismology, Active Tectonics and Archeoseismology* (PATA). 9-14 October 2013. Aachen. Germany. 237-240. ISBN: 978-3-00-042796-1.

Tatevossian, R.E., (2007). The Verny, 1887, Earthquake in Central Asia: Application of the INQUA Scale based on Coseismic Environmental Effects. Dark Nature: rapid environmental change and human response. *Quaternary International.* 173-17423-29.

Velázquez-Bucio, M.M., A.M. Michetti, L. Benente, G. Groppelli, V.H. Garduño-Monroy, S. Filonzi, M.A. Rodríguez-Pascua, R. Pérez-López, K. Chunga, (2013). ESI2007 assessment of paleoseismic features in the Acambay and Ixtlahuaca graben, Mexico: evidence for capability along the Perales Fault. *Proceedings of the 4th International INQUA Meeting on Paleoseismology, Active Tectonics and Archeoseismology* (PATA). 9-14 October 2013. Aachen. Germany. 285-289. ISBN: 978-3-00-042796-1.

Vittori E., P. Di Manna, A.M. Blumetti, V. Comerci, L. Guerrieri, E. Esposito, A.M. Michetti, S. Porfido, L. Piccardi, G. Roberts, A. Berlusconi, F. Livio, G. Sileo, M. Wilkinson, K. McCaffrey, R. Phillips, P.A. Cowie, (2011). Surface faulting of the April 6, 2009, Mw 6.3 L'Aquila earthquake in Central Italy. *Bulletin of the Seismological Society of America.* August 2011. 101:1507-1530. doi: 10.1785/0120100140.

Vivenzio, G., (1788). Istoria de' tremuoti avvenuti nella Provincia della Calabria Ulteriore, e nella Città di Messina nell'anno 1783. E di quanto nella Calabria fu fatto per lo suo risorgimento fino al 1787. Preceduta da una teoria ed istoria generale dei tremuoti. *Istoria Gen. de' Tremuoti*. Stamperia Reale. 2 vols. Naples.

INQUA Focus Group on Paleoseismology and Active Tectonics

The Contribution of Paleoseismology to Seismic Hazard Assessment in Site Evaluation for Nuclear Installations

Guerrieri, L. (1), Vittori, E. (1), Blumetti, A.M. (1), Michetti, A.M. (2), Reicherter, K. (3), Serva, L. (4), Silva, P.G. (5), Fukushima, Y. (6)

(1) ISPRA, Geological Survey of Italy, Via Vitaliano Brancati, 48, Roma, Italy. Email: luca.guerrieri@isprambiente.it
(2) Dipartimento di Scienza e Alta Tecnologia Università dell'Insubria Via Valleggio, 11, 22100 Como, Italy
(3) RWTH Aachen University Lochnerstr. 4-20 52056 Aachen, Germany
(4) Independent Consultant, Via della Resistenza, 171 – 02014, Cantalice, Rieti, Italy
(5) Departamento de Geología, Universidad de Salamanca, Escuela Politécnica Superior de Ávila, 05003 Avila, Spain
(6) IAEA, International Seismic Safety Center, Vienna

Abstract: *In the frame of site evaluation/re-evaluation procedures for nuclear installations, paleoseismology is essential for both Fault Displacement Hazard Assessment (FDHA) and Seismic Hazard Assessment (SHA), as recommended in the reference IAEA Safety Guide SSG-9.*
After the accident at the Fukushima Daiichi nuclear power plant caused by the disastrous Tohoku earthquake and tsunami in 2011, the IAEA International Seismic Safety Centre has promoted a technical document (IAEA-TECDOC DD1084), aimed at highlighting the value of earthquake geology studies and paleoseismology for site safety and providing standard methodologies to perform such investigations. This technical document developed by several experts from academic and research institutes as well as from regulatory bodies, is being published by IAEA in 2015. This note aims at summarizing the most relevant issues to consider in the use of paleoseismology for site evaluation of nuclear installations.

Key words: *Paleoseismology, seismic hazard assessment, site evaluation, nuclear installation, IAEA.*

INTRODUCTION

Paleoseismology is the discipline devoted to the study of paleoseismicity. According to IAEA SSG-9, "paleoseismicity" is the evidence of a prehistoric or historical earthquake revealed by displacement on a fault or by secondary effects such as ground deformation (i.e., liquefaction, tsunami, landslides). Actually, the geological effects of earthquakes can be preserved in the geological record and therefore discovered by specific investigations. They are among the environmental effects of earthquake (EEE) that are the basis of the ESI-07 Scale (Michetti et al., 2007).
Within the site evaluation/re-evaluation procedures for nuclear installations (NI), paleoseismology plays an essential role for both Fault Displacement Hazard Assessment (FDHA) and Seismic Hazard Assessment (SHA). The relevance of paleoseismology, recommended in the reference IAEA Safety Guide SSG-9, has been recently dramatically confirmed after the accident at the Fukushima Daiichi NPP caused by the disastrous Great Tohoku, Japan earthquake and tsunami of 11 March 2011.
After that event, the IAEA International Seismic Safety Centre (ISSC) has promoted a technical document aimed at encouraging and supporting Member States, especially from newcomer countries, to include paleoseismic investigations into their geologic database, highlighting the value of earthquake geology studies and paleoseismology for site safety and providing standard methodologies to perform such investigations.
This technical document (IAEA-TECDOC DD1084), developed by several experts from academic and research institutes as well as from regulatory bodies, is being published by IAEA in 2015. The detailed guidelines and practical tools in the TECDOC integrate classical handbooks on paleoseismology (e.g. Mc Calpin, 2009) with the aim to improve seismic hazard evaluation of nuclear installations, resulting of potential great importance in support of the post Fukushima hazard assessments.
In the following, the most relevant issues to consider in the use of paleoseismology for site evaluation of nuclear installations are summarized.

OBJECTIVES OF PALEOSEISMIC RESEARCH FOR NI SITING

Objectives
In the site evaluation of nuclear installations, paleoseismic investigations have the next main objectives:
i) identification of seismogenic structures based on the recognition of effects of past earthquakes in the regional area; ii) improvement of the completeness of earthquake catalogues, by identifying and dating the traces preserved in the geologic record of ancient moderate to large earthquakes, iii) estimation of the maximum seismic potential of an identified seismogenic structure/source, typically based on the extent of displacement per event (as measured in fault-trenching analyses), as well of the geomorphic and stratigraphic features representing the cumulative effect of repeated large seismic events (concept of "seismic landscape"); iv) approximate calibration of probabilistic seismic hazard assessment (PSHA), taking advantage of the recurrence

interval of large earthquakes detected through paleoseismic investigations, and providing a "truth check" based on direct observations of earthquake environmental effects.

Limitations

The paleoseismic data used as input into SHA models have intrinsic weaknesses, such as:

1) Assessment of uncertainties: the problem is particularly evident when evaluating recurrence intervals and slip rates based on dating of samples and offsets measured with paleoseismic methods. Every attempt should be carried out to get the most complete and robust database to minimize the epistemic uncertainties.

2) Historical data show the common occurrence of clustered earthquakes. However, paleoseismic investigations cannot always reveal such behavior: in fact, along a fault a paleoseismic history is rarely wide enough to demonstrate if events are temporally clustered, or simply have a large variability around a single-mode recurrence type.

3) Empirical relationships between magnitude (e.g. Mw) and surface faulting parameters allow evaluating the magnitude range expected along a seismogenic fault. However, the obtained magnitude might be deceptive being sometimes the paleoseismic interpretation not univocal: for example, the same paleoseismic feature can result from a single large paleoearthquake as well as from several smaller paleoearthquakes closely spaced in time (see above). To overcome such uncertainties in the assessment of maximum magnitude, the "seismic landscape" concept may prove greatly beneficial.

4) The stratigraphic record seen in a natural of artificial section across a potential capable fault often provides an incomplete paleoseismic characterization, mainly because of erosional processes or lack of sedimentation. Moreover, pedogenesis and root penetration can disrupt or blur the original stratigraphy. These effects cause an underestimation or overestimation of the paleoseismic history. Furthermore, even when the stratigraphic record is complete and clearly exposed, the lack of datable material or landforms can inhibit a full paleoseismic characterization.

SPATIAL SCALES FOR PALEOSEISMIC ANALYSES

According to SSG-9 (3.6–3.19), geologic and geophysical investigations for NPP siting are to be conducted at four spatial scales with increasing detail: regional (typical radial extent 300 km), near regional (25 km), site vicinity (5 km) and site area.

Regional scale analysis should achieve the best knowledge of the geodynamic setting and current tectonic regime of the region surrounding the site, in order to identify and characterize the most significant geologic features for the seismic hazard.

The near regional studies aim to: i) define the seismotectonic features of the area; (ii) recognize the latest fault movements; and (iii) determine the extent and nature of displacements, rates of activity and evidence related to fault segmentation.

Site vicinity research must define at the best achievable resolution the neotectonic history of the faults, especially to assess the current potential for and rate of fault displacement around and across the site (fault capability), and to identify other potential geologic instabilities within the site area.

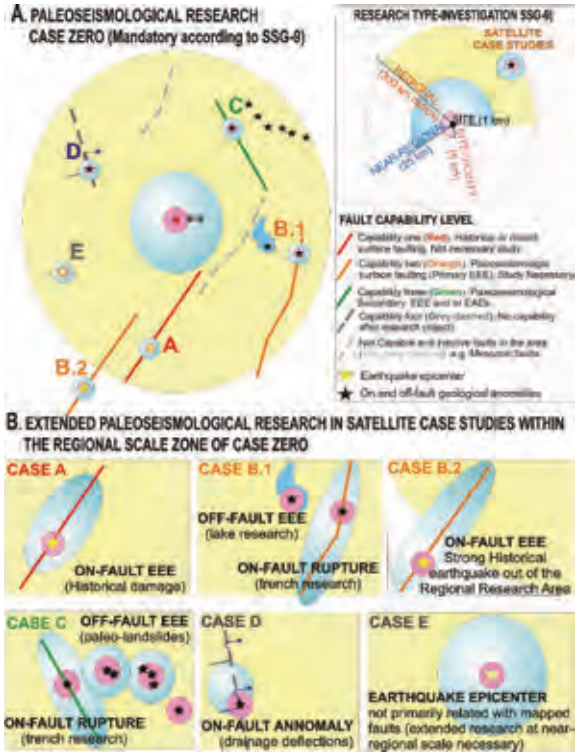

Figure 1: A) Paleoseismic research type-investigations according to the SSG-9 (Case Zero). The figure illustrates the typical cases of fault capability expected in the entire regional area (and adjacent zones) linked to satellite study-cases requiring complementary investigation at near-regional and site-vicinity scales. B) According to the type of evidence it is possible to distinguish six cases in which complementary investigation is necessary to establish the fault capability level. Blue and pink circles show respectively the near-regional and site vicinity research scale areas centered on the faults, tectonic structures and/or identified geological anomalies under investigation (radius not in scale). Source: IAEA-TECDOC DD 1084.

Paleoseismic investigations are mandatory in the site vicinity area and shall be conducted at the site vicinity scale. Within the site vicinity area (typically 5 km radius), paleoseismic trenching is applied with the purpose of characterizing the potential for surface faulting at the site. However, as clearly stated in the IAEA SSG-9, these analyses are by no means limited to the site vicinity area. In fact, site vicinity type and scales investigations might be of critical value also for assessing the seismic hazard at the site, by identifying and characterizing the relevant seismogenic structures located in the near regional and regional area. This point is illustrated in Figure 1. This

figure schematically illustrates several cases of fault capability that are typically expected in the regional area (300 km) and outside of it, for a site under investigation (advised from SSG-9 guidelines; Case Zero in Fig. 1).
According to the type of evidence, six cases are possible. As a consequence, near regional and site vicinity type-research scale zones might be identified along different structural elements within the regional area (300 km) or even have to be extended to the surrounding zone under investigation. In coastal areas located in subduction zone margins, hazardous seismotectonic structures can be located far away (>300 km), but they must be subject to detailed investigation at site vicinity and site type-research scales, since dangerous secondary earthquake environmental effects (e.g., tsunamis, liquefaction, landslides) can be triggered.

THE CONCEPT OF SEISMIC LANDSCAPE

Michetti et al. (2005) defines the seismic landscape as *"the cumulative geomorphic and stratigraphic effect of the signs left on an area's physical environment by its past earthquakes over a geologically recent time interval"*. The notion of "seismic landscape" is based on the observed correlation between i) the erosional and depositional processes, the landforms, and the late Quaternary geological record in an area, and ii) the earthquake magnitude assessed from the earthquake ground effects, for instance from a colluvial wedge along a fault scarp exposed by means of exploratory trenching.
If the rates of surface displacement are much higher than the local rates of sedimentation and erosion, it is possible to infer paleoearthquake magnitudes coherent with the near regional geologic and geomorphic environment. In fact, in this case the cumulative effect of repeated strong surface faulting events produces characteristic morphologies and stratigraphic features that will continue to grow over a geological time interval. In other words, the local morphology evolves basically through the repetition of coseismic environmental phenomena (such as landslides, liquefaction, fault scarps, coastline uplift or subsidence) of similar size over a long time period.
The Quaternary geological evidence strongly suggests that significant earthquakes (typically Mw ≥ 5.5 – 6.0) repeat along a specific seismic source (Allen, 1975; Slemmons & de Polo, 1986; Michetti & Hancock, 1997). Thus, from the paleoseismological viewpoint, strong earthquakes are far from "random" phenomena. Thus, over a certain time-interval, a set of earthquake-related features will control the local morphology and stratigraphy, imprinting a typical seismic landscape. The study of these features should enable to assess the source parameters (including magnitude, style of faulting, slip-rates) of the reference seismic event for the investigated region.
Figure 2 illustrates an example of seismic landscape, in a region where tectonic rates exceeds erosional and depositional rates, resulting in a characteristic geomorphic signature (the classic intermountain basins of the Central Apennines).

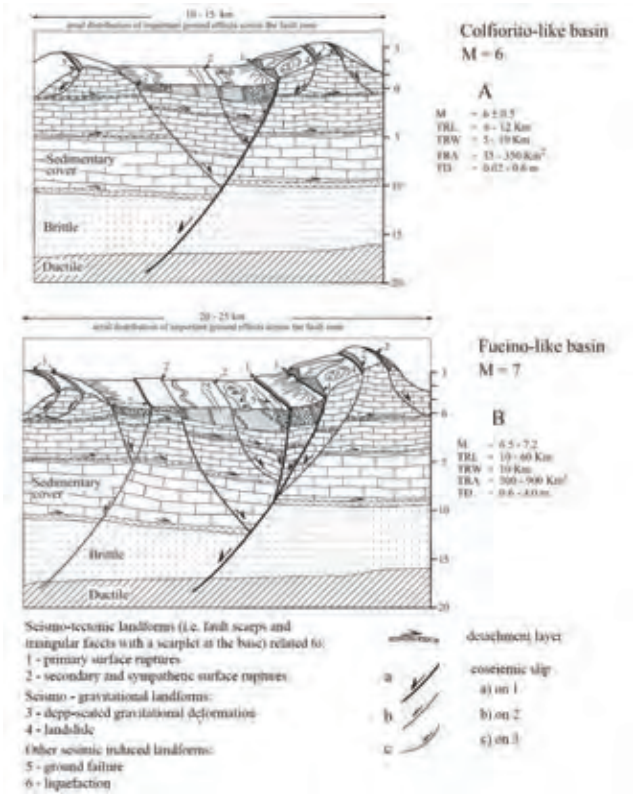

Figure 2: Seismic landscape of two intermountain basins in Central Italy, A) the Colfiorito basin, affected by the September 26, 1997, M 5.6 and 6.0 earthquakes (Vittori et al., 2000) and B) the Fucino basin, affected by the January 13, 1915, MS 7.0 earthquake (Michetti et al., 1996). M) magnitude; TRL) typical rupture length; TRW) typical rupture width; TRA) typical rupture area; TD) typical displacement; INT) epicentral macroseismic intensity.
The differences in the geomorphology and geologic structure of the two basins are consistent with the repeated occurrence of similar earthquakes of different magnitude and rupture length over the Quaternary, so that it is possible, within the extensional setting of the Apennines, to define A) as an M6-type seismic landscape, and B) as an M7-type seismic landscape. This figure is reproduced with the permission from Serva et al. (2002).

The dimensions and structures of each intermountain basin show a clear relation with the earthquake magnitude of the local causative normal faults (Serva et al., 2002). By this approach, the assessed magnitude and recurrence intervals would be consistent with the geologic, geomorphic and paleoseismic features around the causative earthquake source(s). In summary, the role of the seismic landscape, if well defined, should be to calibrate the paleoseismic data coming from detailed geological analysis, such as fault-trenching (on-fault data) and/or cataloguing of earthquake environmental effects (EEE off-fault data) by means the use of the ESI-07 Macroseismic Scale.

PALEOSEISMIC CHARACTERIZATION OF DIFFUSE SEISMICITY

Seismicity that cannot be attributed to specific faults or seismogenic structures is referred to as "diffuse seismicity". By this definition, its characterization can only come from paleoseismic evidence provided by off-fault geologic environmental earthquake effects (secondary EEE), sometimes labelled as "seismites". The more significant indicators are:

I. Paleo-liquefaction features, mostly recorded in past lacustrine, flood plain and coastal plain environments.
II. Disturbance in cave environments (speleo-seismites).
III. Paleo-landslides (only when other paleoseismic data converge to prove coseismic origin).
IV. Paleo-tsunami deposits (tsunamites).

Such environments are never spatially continuous and often absent in many settings. Moreover, lack of evidence is not always evidence of no past seismic activity, but possibly of the absence of suitable conditions for occurrence / preservation of seismites.
The best approaches to characterize diffuse seismicity come for the availability of multi-archive paleoseismic records, in terms of type of earthquake effects (EEE), geographic distribution and repeated events. Multiple paleoseismic events evidenced in the geologic record can derive from the same seismogenic source or from different sources affecting the same area (Becker et al., 2005). The ESI-07 scale allows evaluating intensities, from which the minimum size of the causative event(s) can be estimated (Michetti et al., 2007). The main limit of this approach is the uncertainty on the seismic source location and actual size of the event(s), which otherwise improves with the increasing number of intensity data points derived from geological research.

CONCLUSIONS

In the frame of site evaluation of nuclear installation, paleoseismology plays a critical role, as it improves seismic hazard assessment based on a geological time window.
In areas where surface faulting occurs, a combination of primary and secondary earthquake effect analyses offers the best scenario for improving the seismic history and the evaluation of the potential seismic hazard. In areas of diffuse seismicity, paleoseismic evidence from off-fault (secondary) effects may be used as diagnostic element for intensity assessment through the application of the ESI-07 scale.
More details, including several case studies, will be provided in the TEC-DOC DD1084, under publication by IAEA.

Acknowledgements: The Authors wish to thank all the members of the IAEA-ISSC Working Group on Paleoseismology and co-authors of the IAEA TEC-DOC DD1084 and in particular Stephan Baize, Carlos Costa, Marc Cushing, Kurt Decker, Ester Hintersperger, Kazuo Hirata, Goro Itoh, Bruce Jaffe, Jack Mason, Steve Mc Duffie, Yuichi Nishimura, Raul Perez-Lopez, Kalid Pervaiz, Roberto Romeo, Marzio Roncoroni, Josè Sanchez-Cabanero, Jorge Schlittenhardt, Thomas Spies, Martitia Tuttle and Junichi Uchida. This work is a contribution of the collaboration between IAEA-ISSC and the INQUA 1299 EEE Metrics Project.

References

Allen, C.R., (1975). Geologic criteria for evaluating seismicity, *Geological Society of America Bulletin*. 86, 1041-1056.
Becker, A., M. Ferry, K. Monecke, M. Schnellman, D. Giardini, (2005). Multiarchive paleoseismic record of late Pleistocene and Holocene strong earthquakes in Switzerland. *Tectonophysics*. 400 4, 153-177.
IAEA, (2010). Seismic Hazards in Site Evaluation for Nuclear Installations, *IAEA Safety Standards Series.* No. SSG-9, IAEA. Vienna.
IAEA, (in publication). *The Contribution of Paleoseismology to Seismic Hazard Assessment in Site Evaluation for Nuclear Installations.* TEC-DOC DD1084. Vienna.
Mc Calpin, J.P., (2009). Paleoseismology. *Elsevier*. 2nd edition, 613 pp.
Michetti, A.M., P.L. Hancock, (1997). Paleoseismology: Understanding past earthquakes using Quaternary geology. *Journal of Geodynamics*. 24, 4 3-10.
Michetti, A.M., F.A.M. Audemard, S. Marco, (2005). Future trends in paleoseismology: Integrated study of the seismic landscape as a vital tool in seismic hazard analyses. *Tectonophysics*. 408, 4 (2005) 3-21.
Michetti, A.M., E. Esposito, L. Guerrieri, S. Porfido, L. Serva, R. Tatevossian, E. Vittori, F. Audemard, T. Azuma, J. Clague, V.Comerci, A. Gürpinar, J. Mc Calpin, B. Mohammadioun, N.A. Mörner, Y. Ota, and E. Roghozin, (2007). Intensity Scale ESI 2007. In: Mem. Descr. Carta Geologica d'Italia (Guerrieri, L. and Vittori, E. editors). *Servizio Geologico d'Italia*. Dipartimento Difesa del Suolo. APAT. Rome. Italy. 74.
Serva, L., A.M. Blumetti, L. Guerrieri, A.M. Michetti, (2002). The Apennine intermountain basins: the result of repeated strong earthquakes over a geological time interval, *Boll. Soc. Geol. It.* 121 (2002) 939-946.
Slemmons, D.B., C.M. de Polo, (1986). Evaluation of active faulting and associated hazard. *Active Tectonics*. Wallace, R.E. (Panel Chairman). National Academy Press. Washington D.C. (1986) 45-62.

INQUA Focus Group on Paleoseismology and Active Tectonics

Review of May 21, 2003 Boumerdes (Algeria) earthquake (Mw 6.8): Application of the ESI2007 Scale

Heddar, A. (1), Si Bachir, R. (1), Beldjoudi, H. (1), Boudiaf, A. (2), Yelles, K. (1)

(1) CRAAG, Centre de Recherche.en Astronomie Astrophysique et Géophysique, Algiers, Algeria. Email: a.heddar@hotmail.fr
(2) Consultant Géologue, 42 rue du Moulin à vent 34200 Sète, France

Abstract: *We intend to apply the Environmental Seismic Intensity (ESI 2007) scale to Algerian earthquakes in the purpose to introduce this scale, which proves to be useful for assessing the seismic hazard. In this paper, we review Boumerdes (Mw: 6.8, 2003) earthquake which occurred in the North of Algeria along the boundary between African and Eurasian plates. The main shock located on the coastline was associated to an unknown submarine structure. No surface faulting was associated to this event on land, but many earthquake environmental effects (EEE) have been observed in the epicentral area in land, also turbidity currents underwater responsible for 29 submarine cable breaks have been reported. These coseismic environmental effects were catalogued including, coastal uplifts, liquefaction phenomena, tsunami waves, turbidity currents, cracks, rock falls, slope movements and Hydrological anomalies. The distribution of ground effects suggests Intensity IX that appears below intensity X calculated traditionally with EMS 98 scale.*

Key words: *Boumerdes earthquake, Algeria, ground effects, turbidity currents, ESI2007, seismic hazard.*

INTRODUCTION

In this note we attempt to review the earthquake environmental effects (EEE) of the seismic sequence that struck Boumerdes and the eastern part of Algiers (capital of Algeria), using the ESI 2007 macroseismic intensity scale (Michetti and al., 2007). On May 21, 2003, a strong earthquake (Mw 6.8) hit the Boumerdes province fifty kilometers east to Algiers. It is the most significant earthquake recorded in Algeria since the 1980 El Asnam earthquake (Ms=7.3). It affected a heavily developed and urbanized area (Boumerdes and the eastern Algiers province), and was widely felt within ~ 400 km across the country, causing considerable damage and more than 3,000 victims. The main shock was located on coastline (Yelles-Chaouche et al., 2003, Bounif et al., 2004). The focal mechanism calculated (Delouis et al., 2004) is represented by a reverse fault striking NE–SW and dipping SE. This shallow event did not produce surface ruptures on solid area but triggered coastal uplift, liquefaction features and other environmental earthquake effects. It also triggered large turbidity currents responsible for 29 submarine cable breaks (Harbi et al., 2007, Cattaneo et al., 2012). Tsunami waves up to 1.5 m height (Alasset et al., 2006) were recorded along the Spanish coast. The macroseismic intensity attributed to this event (Harbi et al., 2007) is X on EMS98 scale.

Seismotectonic Setting

The Tell Atlas (North of Algeria) is an orogenic area wide ~ 200 km. It forms a part of the perimediterranean Alpine system characterized by folds and thrust faults trending NE-SW to E-W (Morel and Meghraoui, 1996).The region of interest lies within the central part of this active tectonic domain characterized by permanent seismicity, associated to identified active faults on land (Meghraoui et al., 1986) and offshore (Deverchère et al., 2005). The 21 may, 2003 earthquake occurred in the Northeastern part of Mitidja basin (Figure 1), a coastal intermountain Quaternary basin, exhibiting a morphological shape stretched E-W as Cheliff basin due to the N-S to NW-SSE shortening movements (Meghraoui and Doumaz, 1996). The basin whose NNE extremity is drowning in the Mediterranean Sea through the Bay of Algiers (Figure 1) is bounded by two active structures belonging to distinct domains. At the North, the Sahel ridge runs along the coast and links the Chenoua and Algiers-Bouzareah massifs that are relics belonging to Internal Zones (Durant-Delga, 1969). This structure is a north-west dipping blind thrust fault (Meghraoui, 1991) 60 km long, which is assumed being the main source of seismic hazard for the region of Algiers (Meghraoui, 1991, Harbi et al., 2004, Maouche et al., 2011, Heddar et al., 2013). At the other side, the south of the basin is limited by the NE-SW trending Blida thrust-and-fold system where Mesozoic and Cenozoic formations over thrust Neogene and Quaternary layers.

The seismic monitoring prior to 2003 indicated few earthquakes and seismic hazard was considered relatively low (Yelles-et al., 2003). Nevertheless, the region of Algiers and its vicinities have experienced several events in the past. For example, the 1365 earthquake that triggered sea waves in the lower parts of Algiers city, or the 1716 one, which claimed about 20000 human lives (Mokrane et al 1994), or else the Blida 1825 earthquake that struck the southern side of the Mitidja basin (Ambraseys and Vogt, 1988, Mokrane et al., 1994). Moreover, according to archaeologist and historian, Dellys an ancient city founded in Roman times, actually situated 50km east to Boumerdes on the coast was destroyed by an earthquake during the Roman period at about 42 A.D. (Harbi et al., 2007).

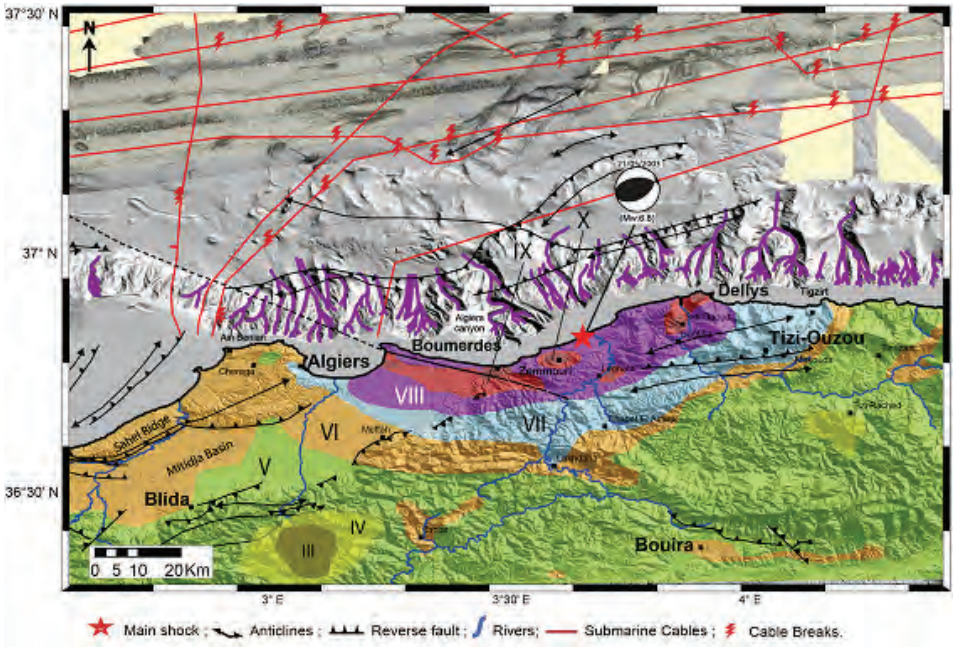

Figure 1: Seismotectonic map of the Boumerdes (Algeria) region and surrounding wrapped with EMS98 Macro seismic intensities (Harbi et al., 2007), main shock (Bounif et al., 2004), focal mechanism (Delouis et al., 2004) and cable breaks (Cattaneo et al., 2012).

According to Bounif et al., (2004) aftershocks dissemination on land and offshore suggests the offshore extension of the continental Blida thrust fault system that showed no significant seismic activity since the 1825 earthquake (Meghraoui et al., 2004).

Spatial distribution and description of earthquake environmental effects

The Boumerdes earthquake did not produce surface ruptures in land, but investigations carried out allowed us to map different ground effects. We classify them according to Audemard and Michetti, (2011) into three types A, B and C. Six categories of earthquake environmental effects have been catalogued, mainly uplift, liquefaction phenomena, mass movement, ground cracks, hydrological anomalies and tsunami waves. The first tree ground effects are located in the epicentral area (Fig.1). Other secondary effects are equally important to point out; these are underwater instabilities that damaged cables on 150 km between Algiers and Azzefoun (Fig.1) inducing a break in communications that lasted few days.

Type A:

In this sub-class are gathered secondary effects including soft sediments deformation such as soil liquefaction, cracks, mass movements and fallen precarious rocks generated by seismic shaking. These effects are mainly concentrated into the area (Fig. 1) corresponding to the isoseists X to VIII in the EMS98 scale (Harbi et al., 2007).

<u>Slope movements and ground cracks</u>: This type of ground effects were mostly observed between Dellys and Bordj el Bahri (Fig. 2). They also affect the road system and may reach 120 m of length and show uplift from 4 to 10 cm

<u>*Liquefaction:*</u> This phenomenon was observed in the epicental area, along Oued Isser and Oued Sebaou riverbanks (Fig. 3), and along the beach between Boumerdes and Dellys. Also liquefaction features vary from few centimeters to 1 m in diameter, sometimes liquefied sand may spread through cracks of several meters long.

<u>*Rock falls:*</u> affected precarious rocks of Chiffa and Lakhdaria gorges (Fig. 3).

Figure 2: Ground effects observed after 2003 Boumerdes (Algeria) earthquake. a: cracks, b: slope movements, c: volcano crater of liquefaction, d: coastal uplift.

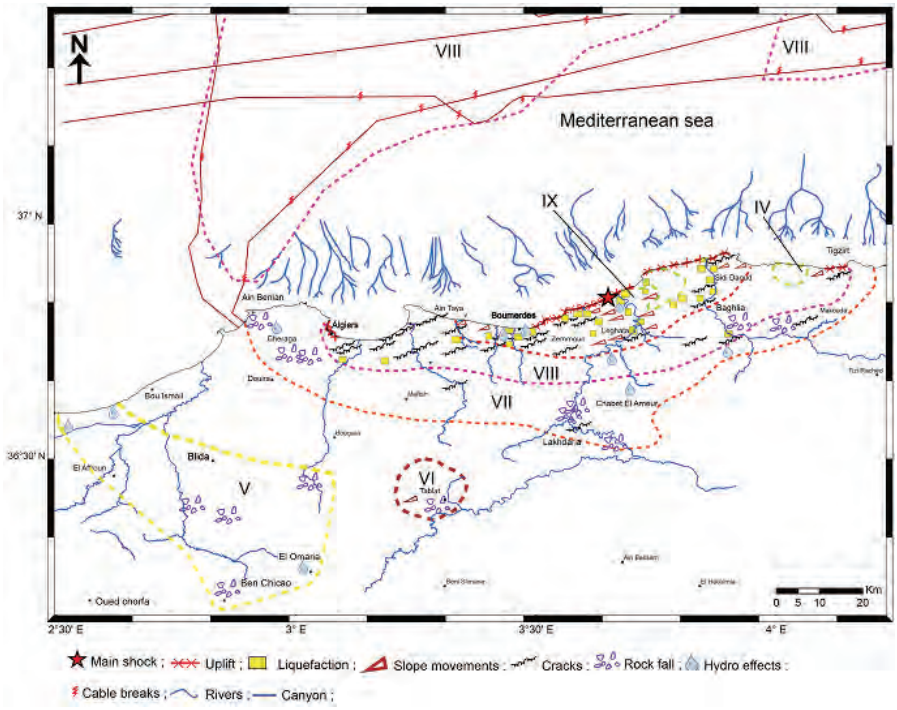

Figure 3: The 2003 Boumerdes earthquake isoseismal map based on the ESI2007 scale (based on the surveyed ground effects).

Type B:
This category of effects consists of remobilized and redeposited sediments (e.g. turbidites) and transported rock fragments. During the Boumerdes earthquake, the main shock caused 29 breakpoints in the submarine cables over a distance of 150 km long (Fig. 1). The cable breaks occurred between 36 min and 3 h and 48 min after the earthquake as far as 70 km away from the coastline (Cattaneo et al., 2012). The same phenomenon was observed off Ténès following the Orléansville (Algeria) earthquake (1954, Ms 6.7) (Heezen and Ewing, 1955).

Type C:
In this category, tectonic deformation, like uplift or subsidence related to the causative fault itself, can range from local to regional scale (Audemard and Michetti, 2011). Boumerdes earthquake recorded a coastal uplift (Fig.2) estimated around 0.55m (Meghraoui et al. 2004) on a distance of 40 km between Dellys and Boumerdes (Fig.3). This tectonic effect catalogued as primary effect according to the ESI 2007 (Micheti et al.,2007) was the most spectacular phenomenon generated by the earthquake. Other EEE generated by the seismic shaking of Boumerdes earthquake, are mentioned here after:

Tsunami waves
Witnesses observed a withdrawing of sea estimated at 100m along 50 km from Corso to Dellys (Harbi et al., 2007). In addition, the Balearic Islands recorded tsunami waves that reached approximately 2 m and damaged the harbors of the region. This phenomenon was recorded by tide-gauges of the western Mediterranean (Alasset et al., 2006) and an intensity of 3 is attributed to this event in the (EMTC) Euro-Mediterranean Tsunami Catalogue (Maramai et al., 2014). Another observation was reported by local fishermen it concerns disappearance of fish in the Zemmouri El Bahri zone (epicentral area) few days before the earthquake (Harbi et al., 2007).

Hydrological Anomalies
This anomaly exceeds the epicentral area of Boumerdes earthquake. The testimonies indicate several anomalies particularly at water sources and well levels in many provinces such as Algiers, Médeéa, and Tizi-Ouzou province (Fig. 3). In the epicentral area, spring dried up south to Zemmouri, Boumerdes, Corso and Djamaa N'sharidj, while a new hot spring appeared in Chaabet village and flow springs increased in Cheraga (Algiers province).

ESI Intensity Assessment
Note that this is the first time that ESI 2007 is applied to assess the intensity of an Algerian earthquake. Therefore, it is quite possible that EEE mapping lacks some details, given the significance of Boumerdes earthquake magnitude, however, almost all EEE are represented and allow establishing a preliminary map
using the ESI 2007 scale. Considering the rate of the uplift estimated to few decimeters, the tsunami waves that reached 2m in Balearic Islands and evaluating the total area affected by the most significant EEE on shore and offshore to 4455 Km^2, we assess the ESI epicentral intensity of the main shock to IX (Fig. 3) in the localities of Boumerdes, Zemmouri. and Dellys. If we compare this intensity value with macroseismic intensity evaluation

(EMS98, Harbi et al., 2007), it appears one degree lower than EMS98 intensity based on the pattern of damages to buildings. This result is consistent with the recommendations of the ESI 2007.

CONCLUSION

Boumerdes earthquake triggered earthquake environmental effects in land and offshore. The most important effects are uplift along the coast, and turbidity currents that cause damages in submarine cables off Algiers region. Most ground effects are concentrated at the West of the epicental area and show a NE-SW trending in agreement with the fault striking NE–SW and dipping SE that would have caused the earthquake. Even if the ESI2007 intensity calculated is comparable to the macroseismic EMS98 one, the distribution of ground effects appeared important in seismic hazard assessment, and using Earthquake Environmental Effects is a valuable tool for land-use planning and critical facilities for areas such as Algiers.

Therefore reviewing Boumerdes earthquake through ground effects solely and evaluating intensities using ESI2007 scale, is also a tool to study other events that historical archives do not mention or because the areas that they affected were uninhabited.That would be a solution to complete the historical Algeria catalogue that is poor. Since the oldest event recorded in the catalogue is the earthquake that hit Algiers in 1365.

References

Alasset, P.J., H. Hébert, S. Maouche, V. Calbini, and M. Meghraoui, (2006). The tsunami induced by the 2003 Zemmouri earthquake (M w =6.9, Algeria): Modelling and results. *Geophys. J. Int*. 166, 213-226.

Ambraseys, N., J. Vogtt, (1988). Material for the investigation of the seismicity of the region of Algiers. *European Earthquake Engineering*. 3, 198.

Audemard, F. and A.M. Michetti, (2011). Geological criteria for evaluating seismicity revisited: Forty years of paleoseismic investigations and the natural record of past earthquakes. *Geological Society of America*. Special Papers. 479, 1-21.

Ayadi, A., et al., (2003). Strong Algerian earthquake strikes near capital city. *Eos Transactions*. AGU. 84 (50), 561-568.

Bounif, A., C. Dorbath, A. Ayadi, M. Meghraoui, H. Beldjoudi, N. Laouami, M. Frogneux, A. Slimani, J.P. Alasset, A. Kharroubi, F. Oussadou, M. Chikh, A. Harbi, S. Larbes, & S. Maouche, (2004). The 21 May 2003. (Mw 6.8) Zemmouri (Algeria) earthquake relocation and aftershock sequence analysis. *Geophysical Research Letters*. 31, L19606. doi.org/10.1029/2004GL020586.

Cattaneo, A., N. Babonneau, G. Ratzov, G. Dan-Unterseh, K. Yelles, R. Bracène, B. Mercier de L´epinay, A. Boudiaf & J. Deverchère, (2012). Searching for the seafloor signature of the 21 May 2003 Boumerdes earthquake offshore central Algeria. *Nat. Hazards Earth Syst. Sci.* 12, 2159-2172, 2012. doi: 10.5194/nhess-12-2159-2012.

Delouis, B., M. Vallée, M. Meghraoui, E. Calais, S. Maouche, K. Lammali, A. Mahsas, P. Briole, F. Benhamouda & K. Yelles, (2004). Slip distribution of the 2003 Boumerdes-Zemmouri earthquake, Algeria, from teleseismic, GPS, and coastal uplift data. *Geophysical Research Letters*. Vol. 31, L18607. doi: 10.1029/2004GL020687.

Deverchère, J., K. Yelles, A. Domzig, B. Mercier de Lépinay, J.P. Bouillin, V. Gaullier, R. Bracène, E. Calais, B. Savoye, A. Kherroubi, P. Le Roy, H. Pauc, & G. Dan, (2005). Active thrust faulting offshore Boumerdes Algeria, and its relations to the 2003 Mw 6.9 earthquake. *Geophys. Res. Lett.* 32,L04311. doi: 10.1029/2004GL021646, 2005

Durand-Delga, M., (1969). Mise au point sur la structure du Nord-Est de la Berberie. *Bulletin of Geological Algeria Card Service*. 39, 89-131.

Harbi, A., S. Maouche, A. Ayadi, D. Benouar, G.F. Panza, H. Benhallou, (2004). Seismicity and tectonics structures in the site of Algiers and its surroundings: a step towards microzonation. *Pure and Applied Geophysics*. 161, 949-967.

Harbi, A., S. Maouche, F. Ousadou, Y. Rouchiche, A. Yelles-Chaouche, M. Merahi, A. Heddar, O. Nouar, A. Kherroubi, H. Beldjoudi, A. Ayadi, & D. Benouar, (2007). Macroseismic study of the Zemmouri earthquake 21 May 2003 (Mw 6.8, Algeria). *Earthquake Spectra*. 23 (2), 315-332.

Heddar, A., C. Authemayou, H. Djellit, A.K. Yelles, J. Déverchère, S. Gharbi, A. Boudiaf, B. Van Vliet Lanoe, (2013). Preliminary results of a paleoseismological analysis along the Sahel fault (Algeria): new evidence for historical seismic events. *Quaternary International*. 302, 210-223. doi: 10.1016/j.quaint.2012.09.007.

Heezen, B.C. and M. Ewing, (1955). Orléansville earthquake and turbidity currents. *AAPG Bulletin*. 39, 2505-2514.

Maouche, S., M. Meghraoui, C. Morhange, S. Belabbes, Y. Bouhadad, H. Haddoum, (2011). Active coastal thrusting and folding, and uplift rate of the Sahel Anticline and Zemmouri earthquake area (Tell Atlas, Algeria). *Tectonophysics*. 509 (1-2), 69-80.

Maramai, A., B. Brizuela, and L. Graziani, (2014). The Euro-Mediterranean Tsunami Catalogue. *Annals of Geophysics*. *57* 4, 2014, s0435. doi: 10.4401/ag-6437.

Meghraoui, M., A. Cisternas and H. Philip, (1986). Seismotectonics of the lower Cheliff basin: structural background of the El-Asnam (Algeria) earthquake. *Tectonics*. 6, 1-17.

Meghraoui, M., (1991). Blind reverse faulting system associated with the Mont Chenoua-Tipasa earthquake of 29 October 1989 (north-central Algeria). *Terra Nova*. 3, 84-93.

Meghraoui, M. & F. Doumaz, (1996). Earthquake-induced flooding and paleoseismicity of the El Asnam (Algeria) fault related fold. *J. Geophys. Res.* 101, 17617-17644.

Meghraoui, M., S. Maouche, B. Chemaa, Z. Cakir, A. Aoudia, A. Harbi, P.J. Alasset, A. Ayadi, Y. Bouhadad, and F. Benhamouda, (2004). Coastal uplift and thrust faulting associated with the Mw=6.8 Zemmouri (Algeria) earthquake of 21 May, 2003. *Geophys. Res. Lett.* 31, L19605.

Michetti, A.M., E. Esposito, L. Guerrieri, S. Porfido L. Serva, R. Tatevossian, E. Vittori, F. Audemard, T. Azuma, J. Clague, V. Comerci, A. Gürpinar, J. Mc.Calpin, B. Mohammadioun, N.A. Mörner, Y. Ota, & E. Roghozin, (2007). Environmental Seismic Intensity Scale 2007 - ESI 2007, In: (Guerrieri, L. and Vittori. E. eds.). *Intensity Scale ESI 2007, Memorie descritive della Carta Geologica d'Italia*. 74, 7-54.

Mokrane, A., A. Ait Messaoud, A. Sebaï, A. Ayadi, M. Bezzeghoud & H. Benhallou, (1994). Les séismes en Algérie de 1365 à 1992. Publication du *Centre de Recherche en Astronomie, Astrophysique et Géophysique (C.R.A.A.G)*. Algiers. Algeria. 277 pp.

Morel, J.L. and M. Meghraoui, (1996). The Goringe-Alboran-Tell (Galtel) tectonic zone: A transpression system along the Africa-Eurasia plate boundary. *Geology*. 24, 755-758.

Yelles, K., H. Djellit, and M. Hamdache, (2003). The Boumerdes-Algiers (Algeria) earthquake of May 21, 2003 (Mw = 6.8), *CSEM/EMSC Newsl*. 20, 3-5.

INQUA Focus Group on Paleoseismology and Active Tectonics

Estimating magnitudes of paleo-earthquakes from multiple observations

Hintersberger, E. (1), Decker, K. (2)

(1) Dep. of Geodynamics and Sedimentology, University of Vienna, Althanstrasse 14, Vienna, 1090, Austria.
Email: esther.hintersberger@univie.ac.at
(2) Dep. of Geodynamics and Sedimentology, University of Vienna, Althanstrasse 14, Vienna, 1090, Austria

Abstract: *We present a method to estimate magnitudes of paleoearthquakes combining several observations. The method is a further development of a probabilistic approach by Biasi and Weldon (2006). Testing for earthquakes with known magnitudes show good results for the respective magnitudes derived by our method. Furthermore, 4 to 6 observation points per fault seem to be sufficient to significantly reduce the uncertainties related to magnitude estimates based on surface-displacement observations.*

Key words: *Paleo-earthquakes, paleomagnitudes, multiple observations, method development.*

INTRODUCTION

One of the major contributions of paleoseismology to seismic hazard assessment are paleoearthquake magnitudes. Especially in regions with low or moderate seismicity, such as Central Europe north of the Alps, paleomagnitudes are normally much larger than those of historical earthquakes (e.g., Camelbeeck et al., 2007) and therefore provide essential information about seismic potential and expected maximum magnitudes of a certain region. In general, these paleo-earthquake magnitudes are based on surface displacement observed at trenching sites. Several well-established correlations provide the possibility to link the observed surface displacement to a certain magnitude (e.g., Wells and Coppersmith, 1994). However, the combination of more than one observation is still rare and not well established. We present here a method based on a probabilistic approach proposed by Biasi and Weldon (2006) to combine several observations to better constrain the possible magnitude range of a paleo-earthquake. In addition, we evaluate the optimum number of observations to reduce significantly the uncertainties for paleomagnitude estimates.

METHODOLOGY

Biasi & Weldon (2006) proposed a probabilistic magnitude estimate given one observed displacement, taking into account the natural variability of surface displacement along a fault. However, in case of more observation points (i.e. trench sites) per fault, single-event displacements at different locations can be correlated and result in a larger set of observed displacements for each earthquake. This can be used to narrow down the possible magnitude range associated with the generating earthquake. Extrapolating the approach of Biasi and Weldon (2006), the single-observation probability density functions (PDF) are assumed to be independent of each other, since observations of each trench do not depend on the findings of other trenches. Following this line, the common PDF for all observed surface displacements generated by one earthquake is the product of all single-displacement PDFs.

TESTING RESULTS

In order to test our method, we use surface displacement data for modern earthquakes, where magnitudes have been determined by instrumental records. We divided the surface displacement into 100 equidistant sections in order to simulate observations made at various trench sites. For each run (see Fig. 1), we selected randomly 15 "observations" and calculated the associated PDFs for each "observation point". We then combined the PDFs into one common PDF for an increasing number of "observations". In Fig. 1, the most probable magnitudes are plotted (i.e. the highest peaks of the PDFs) against the number of combined "observations". As shown by the example of the 1944 "Bolu-Gerede" Earthquake (Ms=7.3), the resultant range of most probable magnitudes is very close to the magnitude derived by instrumental methods.

APPLICATION TO PALEOSEISMOLOGICAL DATA

To test our method with real trenching observations, we used the results of a paleoseismological investigation within the Vienna Pull-Apart Basin (Austria), where three trenches were opened along the normal Markgrafneusiedl Fault (MGNSF). Even if the Vienna Basin is characterized by low to medium seismicity (Mmax = 5.3/Imax = 8), there is no historical seismicity recorded along the MGNSF. However, our studies provide evidence for at least 5 major earthquakes with M > 6.0 along the MGNSF during the last ~ 100 ka (Hintersberger et al., 2015). Using events that are observed within all three trench sites, we derived common magnitude PDFs for each set of observed displacements related to a single event.

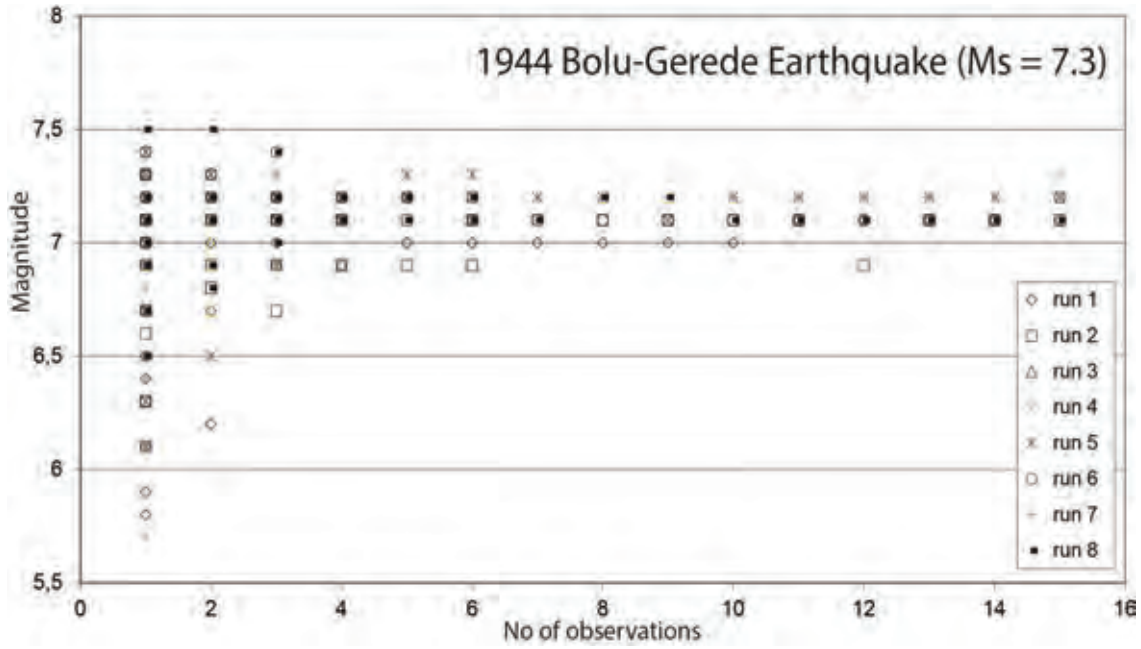

Figure 1: Resultant magnitudes for the 1944 Bolu-Gerede Earthquake (Ms=7.3) based on increasing number of observations. Each run consists of 15 single "observations" that were combined randomly.

As expected, the final magnitude PDFs are narrower than those of the single-event magnitude PDFs. In addition, they are dominated by the largest observed displacement, especially with respect to the lowest magnitude that could have generated all observed displacements.

CONCLUSIONS

In total, we can show here that by combining several surface-displacement observations, the associated uncertainties for the magnitude of a paleoearthquake decreases rapidly. As shown in Fig. 1, it seems that a combination of 4 to 6 observations is sufficient to reduce uncertainties significantly.

Using data from earthquakes with known magnitude and surface displacement, the reproduced magnitudes based on our method are promisingly close to the instrumentally determined magnitude. Therefore, this approach seems to be a suitable method to combine observations from different locations to one magnitude value accounting for the natural variances of observed along-strike surface displacement.

References

Biasi, G.P. & R.J. Weldon, (2006). Estimating surface rupture length and magnitude of paleoearthquakes from point measurements of rupture displacement. *Bulletin of the Seismological Society of America.* 96, 1612-1623.

Camelbeeck, T., K. Vanneste, P. Alexandre, K. Verbeeck, T. Petermans, P. Rosset, M. Everaerts, R. Warnant, & M. van Camp, (2007). Relevance of active faulting and seismicity studies to assessments of long-term earthquake activity and maximum magnitude in intraplate northwest Europe between the Lower Rhine Embayment and the North Sea. *Geological Society of America. Special Paper.* 425, 193-224.

Hintersberger, E., K. Decker, & J. Lomax (2015). Evidence of a M~7 paleo-earthquake in the Vienna Basin. *Terra Nova.* in review.

Wells, D.L., & K.J. Coppersmith, (1994). New empirical relationships among magnitude, rupture length, rupture width, rupture area, and surface displacement. *Bulletin of the Seismological Society of America* 94. 974-1002.

INQUA Focus Group on Paleoseismology and Active Tectonics

paleoseismicity.org

Analysis of potential earthquake damage in the Via dei Pilastri, Alba Fucens, Central Italy

Hinzen, K.G. (1), Galadini, F. (2), Kehmeier, H. (1), Schwellenbach, I. (1), Reamer, S.K. (1)

(1) Cologne University, Vinzenz-Pallotti-Str. 26, 51429 Bergisch Gladbach. Germany. Email: hinzen@uni-koeln.de
(2) Istituto Nazionale di Geofisica e Vulcanologia, Roma, Italy

Abstract: *Alba Fucens was one of Rome's earliest colonies, located strategically between the capital and the Adriatic Sea. A thriving city in the 1st century BCE and CE, Alba Fucens declined in Late Antiquity. During excavations in the last century several damaged structures were uncovered. Among these are a row of shops in the Via dei Pilastri. We use a 3D laser scan and a discrete element model of four pilasters which were found in original toppling position to study their dynamic behaviour. As Alba Fucens sits above the seismogenic source of the 1915 Avezzano earthquake and only 15-20 km west of its surficial emergence, we use synthetic strong ground motions of this event to test whether a similar earthquake can have caused the damage probably in 5th-6th century CE.*

Key words: *Archaeoseismology, Alba Fucens, Via dei Pilastri, Discrete Element model, Avezzano Earthquake.*

ALBA FUCENS and FUCINO PLAIN

Alba Fucens (Fig. 1) is an early Roman outpost founded in the 4th century BCE (e.g. Mertens, 1969). It is located on a hill formation 950-1000 m a.s.l. and roughly 300 m above the surroundings in the Abruzzi Mountains. It was placed at a strategically important point of the *Via Valeria* which connects Rome with the Adriatic Sea. With 6000 inhabitants sent out from Rome, it was among the largest early cities in the colonies. The actual population was probably at least double the initial figure. The colony suffered destruction from war in the 1st century BCE; however it was rebuilt and modernized. Similarly to other Roman towns, the decline began during the Late Antiquity. A last historic note mentions that *Byzantine troops* camped there in winter 537 CE.

Figure 1: Alba Fucens seen from the south. Dash-dotted, dashed and continuous lines indicate the decumanus maximus, cardo maximus, and the Via dei Pilastri. The zoom window shows the anastylosis of three pilasters. The village around the castle of medieval Albe (background) was destroyed during the 1915 earthquake. (Photo H. Kehmeier)

The orientation of the main roads was not strict EW but the *decumanus maximus* followed the valley trend NW-SE. The *Via dei Pilastri* runs parallel east of the *decumanus maximus*. Along this road 18 *tabernae* were located, i.e. shops and workshops, with similar floor plans found along the eastern side of the *via*. The 5.1 to 5.5 m wide and 9 to 12 m long shops were divided into 2-3 separate rooms and backed by a heavy polygonal wall which functions as a retaining wall for the slope to the hill of medieval *Albe*.

The *Fucino Plain* (Fig. 2) belongs to one of the seismically most active regions in the Mediterranean (Blumetti et al., 2004). The basin genesis is the result of numerous coseismic movements at the border faults of the basin. Palaeoseismic studies identified such movements back to the Pleistocene-Holocene transition (Galadini and Galli, 2000). Displacements of lacustrine sediments from the historic Fucino Lake indicate one earthquake between 426 and 782 CE (Galadini et al., 2010). Blumetti et al. (2004) report a 0.15 m displacement in the western part of the historic lake dated to 500-1500 CE and a 0.15-1.0 m coseismic displacement between 500 and 885 CE.

Historical earthquake catalogs (Guidoboni, 1994) list 23 earthquakes within a distance of 100 km between 303 BCE and 537 CE.The most recent damaging earthquake in the area was the 06 April 2009 M_W 6.3 L'Aquila earthquake with its epicenter about 40 km northeast of *Alba Fucens*.

In 1915 the so called Avezzano earthquake hit the Fucino Plain directly. The earthquake caused some 30,000 casualties, 10,000 in the city of Avezzano. With widespread damage in the surrounding villages this event is the strongest earthquake in Central Italy in the last centuries (Galadini and Galli, 1999; 2000). Galadini and Galli (1999) documented vertical displacements up to 1 m and assumed that four fault sections were activated (Fig. 2). Ward and Valensise (1989) estimated a maximum vertical displacement of 0.83 m and a seismic moment of M_0 9.7 10^{18} Nm and M_S 6.9. The more recent seismic

catalog, by Rovida et al. (2011), reports a moment magnitude M_W 7.0, corresponding to M_0 3.94x10^{19} Nm. Based on the structural damage, Beal (1915) assumed the epicenter was not more than 5 km from Avezzano. Current interpretations locate the epicenter close to Gioia dei Marsi and Ortucchio, 20 km ESE from Avezzano. Instrumental records are sparse; the closest instrument in Napoli clipped (Beal, 1915). For M_S>7 Galadini and Galli (1999) and Blumetti et al. (1993) suggest a return period longer than 1000 years.

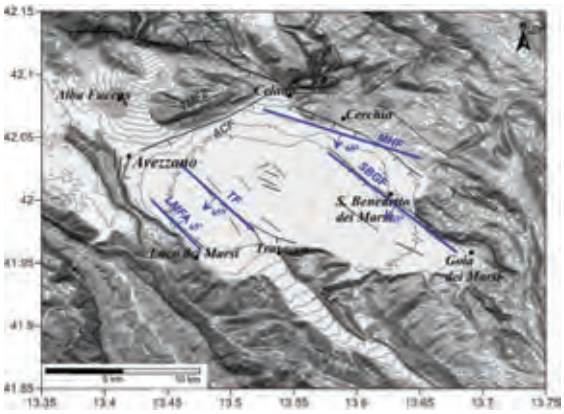

Figure 2: Digital elevation model of the Fucino Basin. Fault lines are: LMF=Luco-dei-Marsi-Fault, TF=Trasacco-Fault, SBGF=San Benedetto-dei-Marsi-Goia-dei-Marsi-Fault, MHF=Marsicana-Highway-Fault. Straight (blue) lines indicate fault segments used for the generation of synthetic seismograms for Alba Fucens site.

Archaeoseismological Model

Figure 3 shows the corner of *cardo maximus* and *Via dei Pilastri* during excavation. Of the northernmost four pilasters only three remained partially in situ after they toppled towards southwest, almost perfectly perpendicular to the trend of the *via*. The base of two pilasters remained on the sidewalk of the colonnade while the other blocks rest on sediments covering the pavement blocks of the road.

Based on a laser scan (Fig. 4) of the current archaeological site with the anastylosis of three pilasters, a discrete element was constructed (Fig. 5).

Figure 3: View from the cardo maximus along the Via dei Pilastri after its excavation (Mertens, 1969). Color shading indicates fallen and still standing pilaster blocks. (excavation photo after Galadini et al., 2010)

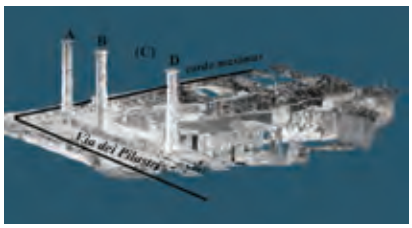

Figure 4: Perspective view of the laser scan model of the Via dei Pilastri.

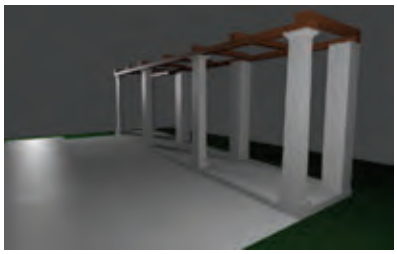

Figure 5: Perspective view from S of the DEM of four pillars in the Via dei Pilastri, Alba Fucens.

All measures were taken from the laser scan model. In order to simulate a connection of the pilaster top to the building in the back, we used a simple wood beam construction on top of the capitals (Fig. 5). The exact superstructure remains unknown and the model of the pilasters can only be used to test the vulnerability of the arcade in front of the shops. Due to the 2.2° SE dipping ground, the pilasters are modelled with increasing height from N to S from 5.07 m to 5.72 m, respectively. On top of the base, each pillar has four shaft blocks and a capital. Details of the modelling procedure can be found at Hinzen (2008).

Calculations and results

Ground motions (GM) with the form of a Morelt-wavelet were used to examine the dynamic behaviour of the model. Most vulnerable is the structure in the direction perpendicular to the *Via dei Pilastri*. Results of a series of dynamic calculations, with horizontal GM, 0.3 < f < 5 Hz, in this direction are shown in Fig. 6. Representing the strength of the GM by the peak ground acceleration (PGA) indicates a clear increase of vulnerability with decreasing frequency. While at the lower frequencies f < ~1 Hz, the pilasters tend to move as a whole in a rocking motion with the turning points on the base plate, at higher frequencies rocking of the individual pilaster blocks starts. As this internal pilaster rocking costs energy, the overall motion becomes less destructive with increasing frequency. This result is similar to previous observations with round columns (Psycharis, 2007; Hinzen, 2008).

Simulating effects of an Avezzano 1915 type earthquake

Following Rovida *et al*. (2011) the 1915 Avezzano earthquake (Fig. 2) had a M_W of 7.0. We used a 1D velocity model based on the work by Di Luzio *et al*. (2009) for the upper 40 km of the lithosphere and PREM below this depth for the calculation of Green's functions following *the method given by Wang (1999).*

Several source scenarios were used to generate strong GM for *Alba Fucens*. The total seismic moment of M_0= 3.94x10^{19} Nm was distributed to the fault segments shown

in Figure 2. The hypocentre was placed at 8 km depth at the southern edge of the first segment of SBGF.

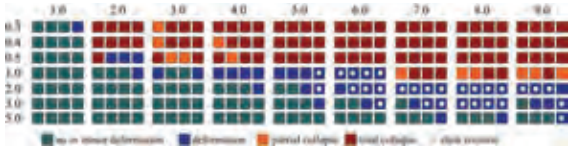

Figure 6: Results of DEM tests with Morlet-wavelet excitation in the horizontal direction perpendicular to the via. Each row of four squares represents the four pilasters of the model, starting at left with the northernmost pilaster. Numbers above columns give the PGA in m/s², numbers in front of rows give frequency in Hz. Colors indicate the status at the end of a 10 s time window.

A rupture velocity of 2.0 km/s was used. For the scenario with the GM shown in Fig. 7 a normal faulting mechanism was assumed with a possible deviation of the rake of ±10° from the vertical and fault dip of 65°±5°. HVSR spectra recorded at the site did not indicate strong resonances in the building-relevant frequency range, so no local site effects were added to the simulated GMs.

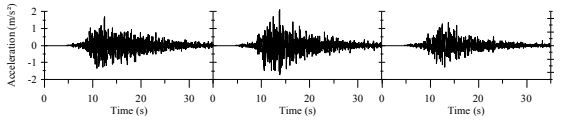

Figure 7: Synthetic seismograms for Alba Fucens during an earthquake of the Avezzano 1915 type.

Figure 8: Pilasters before (left) and after (right) their impact on the Via dei Pilastri.

CONCLUSIONS

Archaeological findings from the Roman *Alba Fucens* indicate that the site was affected by destructive earthquake GMs in the 5th-6th century CE (Galadini et al., 2010). The most striking feature at the heritage site today is the anastylosic reconstruction of three pilasters of the *Via dei Pilastri*. A laser scan-based DEM of the pilasters shows high vulnerability to horizontal GMs at low frequencies (f < 1 Hz). Though the model presented here is not a full reconstruction of the *tabernae,* as the exact constructions are unknown, the dynamic tests provide insight into the toppling mechanisms of pilasters during earthquake loading. At frequencies 0.3 < f < 0.5 Hz, one or more of the pilasters ended in a toppling position similar to that discovered during excavation (example shown in Figure 8).

The effects of the 1915 Avezzano earthquake in the mesoseismal zone are well described in the literature (*e.g.* Molin et al., 1999). Applying synthetic GMs for an earthquake similar to the 1915 event to the pilaster model indicates that the ground shaking would have been sufficient to collapse the row of pilasters. This result does not exclude the possibility that different faults in the vicinity of *Alba Fucens* were activated during the damaging earthquake, but a source in the Fucino basin is plausible. The palaeoseismically recorded earthquake between 426 and 782 CE that Galadini et al. (2010) archaeoseismologically dated to 484 or 508 CE could well be a candidate.

Acknowledgements: We thank C. Fleischer, S. Rosellen, A. Pagliaroli, E. Falcucci and S. Gori for the help with the field work including laser scanning and seismic measurements.

References

Beal, C.H., (1915). The Avezzano earthquake of January 13, 1915. *Bulletin of the Seismological Society of America*. 5 (1), 1-4.

Blumetti, A.M., F. Dramis, & A.M. Michetti, (1993). Fault generated mountain fronts in the central Apennines (Central Italy): Geomorphological features and seismotectonic implycations. *Earth Surface Processes and Landforms*. *18 (3),* 203-223.

Blumetti, A.M., A.M. Michetti, F. Dramis, L. Guerrieri, B. Gentili, & E. Tondi, (2004). Basin and Range in the central and southern Apennines. *Fiel Trip Guide Book. P65*. 32nd International Geological Congress.

Di Luzio, E., G. Mele, M.M. Tiberti, G.P. Cavinato, & M. Parotto, (2009). Moho deepening and shallow upper crustal delamination beneath the central Apennines. *Earth and Planetary Science Letters*. *280* (1), 1-12.

Galadini, F., P. Galli, (1999). The Holocene paleoearthquakes on the 1915 Avezzano earthquake faults (central Italy): implications for active tectonics in the central Apennines. *Tectonophysics*. *308* (1), 143-170.

Galadini, F., P. Galli, (2000). Active tectonics in the central Apennines (Italy) - input data for seismic hazard assessment. *Natural Hazards*. *22* (3), 225-268.

Galadini, F., E. Ceccaroni, & E. Falcucci, (2010). Archaeoseismological evidence of a disruptive Late Antique earthquake at *Alba Fucens* (central Italy). *Bollettino di Geofisica Teorica ed Applicata*. *51* (2-3), 143- 161.

Guidoboni, E., A. Comastri, & G. Traina, (1994). Catalogue of ancient earthquakes in the Mediterranean area up to the 10th century. *Instituto Nazionale di Geofisica*, *Editrice Compositori srl*. Bologna.

Hinzen, K.G., (2008). Simulation of toppling columns in archaeoseismology. *Bull. Seism. Soc. Am*. 99 (5), 2855-2875.

Mertens, J., (1969). *Alba Fucens* - Rapports et études. Études de Philologie, d'Archéologie et d'Histoire Anciennnes. *L'institut historique Belge de Rome.* Tome XII. Roma.

Molin, D., F. Galadini, P. Galli, L. Mucci, & A. Rossi, (1999). Terremoto del Fucino del 13 gennaio 1915. Studio macrosismico. In: *Il terremoto nella Marsica 13 gennaio 1915*. (Castenetto, S. and Galadini, F., eds.), Roma, pp. 321-340 and 631-661.

Psycharis, I.N., (2007). A probe into the seismic history of Athens, Greece, from the current state of a classical monument. *Earthquake Spectra.* 23, 393-415.

Rovida, A., R. Camassi, P. Gasperini, & M. Stucchi, (eds.), (2011). *CPTI11, The 2011 version of the Parametric Catalogue of Italian Earthquakes*. Milano, Bologna, http://emidius. mi.ingv.it/CPTI

Wang, R., (1999). A simple orthonormalization method for stable and efficient computation of Green's functions. *Bulletin of the Seismological Society of America*. *89* (3), 733-741.

Ward, S.N. & G. Valensise, (1989). Fault parameters and slip distribution of the 1915 Avezzano, Italy, earthquake derived from geodetic observations. *Bulletin of the Seismological Society of America*. *79* (3), 690-710.

INQUA Focus Group on Paleoseismology and Active Tectonics

Active tectonics and the link to evolutionary processes: The Lake Ohrid Basin

Hoffmann, A. (1), Reicherter, K. (2)

(1) Marine Geoarcheology & Micropaleontology Lab, Leon Charney School of Marine Sciences, University of Haifa, 199 Aba Khoushy Ave., Haifa 3498838, Israel. Email: na-hoffmann@web.de
(2) Neotectonics and Natural Hazards Group, RWTH Aachen University, Lochnerstr. 4-20, 52064 Aachen, Germany

Abstract: *The Lake Ohrid Basin is a research laboratory for studies linking the biological evolution of species to the geological features and the tectonic evolution within the basin. It is shown that these landforming processes had a significant effect on the biological evolution leading to an extraordinary amount of endemic species even when compared to other lakes with larger surface areas. The key question asked here is: is the seismic activity together with the unique geological character of Lake Ohrid capable of triggering speciation events in the lake?*
An interdisciplinary study was carried out to determine the palaeostress fields which controlled the evolution of the area; to gain information on fault orientation, geometry and spatial distribution of fault scarps; to finally define active/less active areas and to characterize the small scale morphology which can create various habitats for different species. We were able to reveal major shifts in the geodynamic setting, to provide insight into the Holocene coastal evolution and to connect the morphological expression of the lake to the formation of an extraordinary amount of endemic species populations.

Key words: *Lake Ohrid, neotectonics, basin development.*

INTRODUCTION

The Ohrid Basin (40°54'-41°10'N, 20°38'-20°48'E) hosts a cross-boundary lake called Lake Ohrid which is shared by the Republic of Macedonia and the Republic of Albania.
The fresh-water lake is the deepest lake of the Balkans with a maximum depth of almost 290m and covers an area of 358km^2. Lake Ohrid belongs to a group of intramontane basins that originated from back-arc extension during the Late Tertiary in the Dinaric-Albanide Alps. The age of the formation of the "ancient lake" is estimated around 2 - 5Ma ago. Ancient lakes have long been recognised as hot spots of biodiversity and the oligotrophic Lake Ohrid preserves an outstanding variety of more than 200 endemic species (Stankovic 1960). Considering the small surface area, this makes it the lake with the highest concentration of endemic diversity in the world. (e.g. compare to Lake Baikal with 982 described endemic species and a surface area of 31,722km^2 Albrecht 2009).
The reasons for the formation of such a high concentration of endemic species are not well known. But factors such as geology and climate issues, composition of water chemistry etc. are likely factors to influence the speciation.
The geological structures separating the basin in two large geological domains (see figure 1), together with major changes due to several phases of deformation since Tertiary and the recent seismic activity with moderate earthquakes leads to the expression of a wealth of morphological features in the landscape.

Figure 1: Lithological map of the Lake Ohrid area.

The key question asked here is: is the seismic activity together with the geological character of Lake Ohrid capable of triggering speciation events in the lake?

METHODS

In order to assess the active tectonic features and seismicity of the region, the implementation of a combination of different methods is necessary. To analyse the structures affected by brittle deformation, to provide a (neo-) tectonic history of the lake and to show how the basin initially evolved a combination of field mapping of geological structures, palaeostress analysis and study of the historical and instrumental seismicity of the area was performed.
The lake-shore and deltaic deposits of the major inflows were studied using sediment cores and shallow geophysics (ground penetrating radar and electric resistivity) in order to obtain information on Holocene lake level changes and tectonically induced coastline modifications (see Reicherter 2011, Hoffmann 2010). Grain size and geochemical analyses as well as micropalaeontological investigations supplement the results.
A tectonic geomorphology study using satellite images, digital elevation models, terrestrial laser scanning is used to classify the seismic activity of an area and to map the diverse seismic landscape.
In total our investigations of the palaeostress regime, the sedimentary mechanisms and of the geomorphological evidence, provided information on fault geometries, long-term slip rates, landscape evolution, the grade of activity of faults, etc. The data from these studies were used to determine how the landscape has evolved with respect to seismicity and how this can have an effect on speciation.

DISCUSSION

The evolution of the palaeostress field over time revealed five successive periods of basin development *Orogenic Phase:*

- *Cretaceous-Paleogene*: NE-SW compression.
- *Late Eocene-Oligocene*: NE-SW extension.
- *Oligocene-Miocene*: NE-SW shortening and strike-slip movement accompanied by oblique movements.
- *Mid-Miocene*: Transtensional phase with NW-SE extension and strike-slip movement. The opening of the basin nucleated along a mirrored "s"-shaped releasing bend, in a dextral strike-slip mode. This led to the development of an extensional duplex and the evolution of a pull apart basin.
- *Late Miocene to recent*: Change of the stress field to pure E-W extension.

The various changes of stress fields have left their imprints as highly fractured rocks with reactivations and overprinting of old joint and fault systems.
This is also reflected in the differences in deformation at different scales.

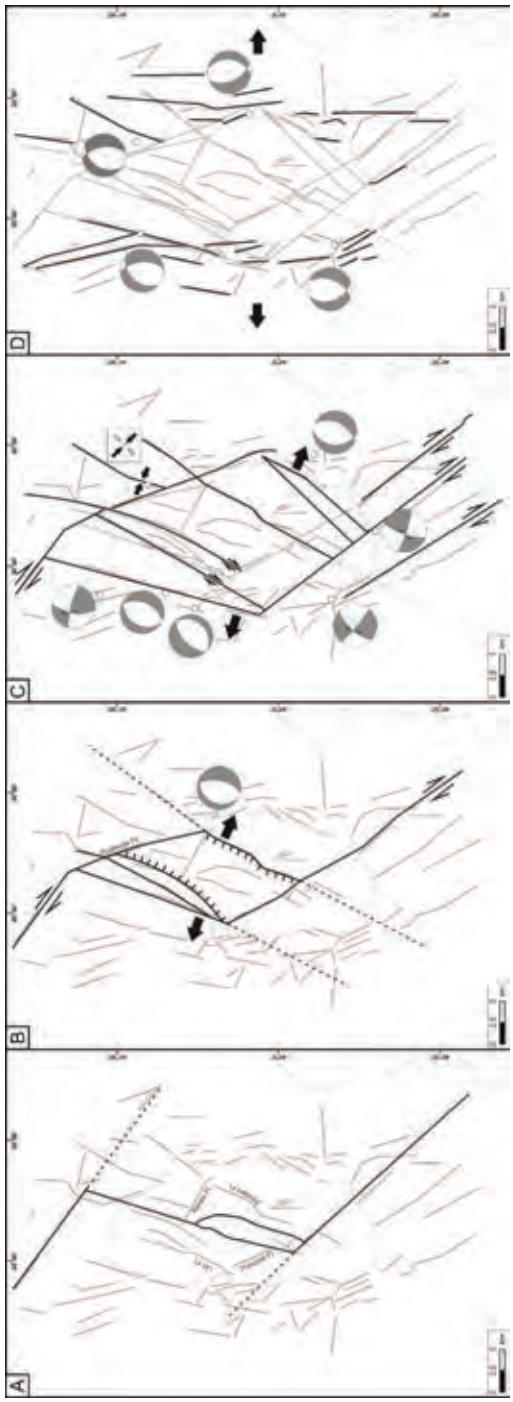

Figure 2: Schematic development of the Lake Ohrid Basin. Red lines mark faults derived from field data and maps, fault lines in the lake are adopted from Lindhorst et al. (in press). Black lines indicate the active faults at the stage of each figure. All fault plane solutions are derived from palaeostress data. A: Possible trace of the initial fault in the beginning of the transtensional period. B: The bends along the generally NW-SE trending dextral strike-slip fault lead to the transtensional opening of the basin in an extensional duplex. C: Further development of the pull apart basin with exemplary fault plane solutions. D: Shift from the transtensional regime to a pure extensional regime.

While on a large scale, the major N-S oriented faults give the basin its straight shorelines and its N-S stretched appearance, on a smaller scale the coastline is highly segmented. In contrast to the general trend, the smaller faults strike NW-SE or NE-SW which results in the zigzag line of the coast. The strong segmentation can also be seen in the lake, where several smaller faults take up the stress.

The fault orientation is mainly N-S with variations concerning the youngest deformational phase. But there are two types of fault geometry. Faults with a staircase-like appearance, and faults which have been rotated resulting in back tilting.

The spatial occurrence of fault scarps is highly connected to the influence of lithology, which is dominated by the two major units: the Mirdita Ophiolite Zone with weak resistance to weathering processes and less pronounced fault scarps; and the Korabi Zone, where the lithologies create the typical staircase-like morphology. This lithological zonation creates an inhomogeneous fault distribution with high variations in morphological expression for fault scarps produced by the same stress field.

Calculated slip rates with values ranging between 0.28mm/a and 3.25mm/a. These values exceed by far well defined slip rates in comparable conditions and are very high compared to other authors (e.g. 0.2 mm/a Benedetti 2003). The strong variability of scarp heights and therefore slip rates in the research area would mean that either the postulated age of the higher scarps is simply too young, or the higher the scarp is, the faster the movement on the fault plane must be (for further reading see Hoffmann (2013a). Therefore the concept of gravitational driven displacement by "stop and go" faults is proposed where a fault would slip every time a younger fault evolves and by doing this it generates a higher slip rate.

Thus, lithology, erosion mechanisms, climate, vegetation cover, human modifications, etc. control the expression of the fault scarps and other morphological features (e.g. triangular facets). Also, two modes of listric faulting were observed in the basin creating a mixture of faulting along rotated blocks and sets of parallel listric faults.

In general, no pattern could be assigned according to the spatial distribution, geometry or faulting mode of fault scarps. Therefore, also gravitational forces must play a major role in scarp displacement.

There are several systems of alluvial fans and delta complexes around Lake Ohrid.

The northern plain around Struga hosts large, but very shallow, alluvial fans, which are today mainly inactive. Other alluvial fans were detected along the eastern coast but their lobe shaped structure is cut by normal faults.

River deltas were investigated at the Cerava and the Daljan River in the northern and the southern part of Lake Ohrid respectively. Their meandering fluvial systems have been active at least during Holocene and seem to have been stable over a long period. The areas have been drained in the last decades for agricultural use, which partly led to depletion of the streams.

The landscape evolution is, therefore, driven by two morphological systems: the plains to the north and south dominated by sedimentary input and climatically driven alluvial fans and deltas, and the eastern and western hillslopes with a strong influence from active normal faulting.

The recent deformation regime has affected the whole basin and is seen in various morphological features all over the area creating a seismic landscape. Not only normal faulting, but also other mechanisms connected to highly fractured rocks lead to a general unstable western slope and play a major role in the basin evolution.

The shape of fault scarps, triangular facets and other features connected to the seismic activity is strongly influenced by external factors such as the lithology. What can be seen is a difference of activity between the east/west coast in contrast to the northern and southern areas. The reason is probably that most of the stress is accommodated by N-S trending faults. Thus, the Galicica, the Mali i Thate and the Mokra Mountain ranges (see figure 1) are dominated by normal faulting, and the plains of Struga and Pogradec are dominated by clastic input although indications for tectonic activity were observed here. The east coast is highly segmented with tilted blocks of basement rock, the west coast is dominated by mass wasting processes.

The fault lengths, which vary between 10 and 20km, determine the grade of activity in the basin. These large faults are considered of being capable of producing earthquakes with magnitudes between 6.0 and 7.0 and associated displacements of 0.6 to 2m per event. The historical seismic record shows severe earthquakes occur in the region, which support this estimation (e.g. the magnitude 6.7 earthquake in 1911). Frequent shallow and low magnitude earthquakes are recorded by seismic stations (e.g. June 8th 2012, M_b4.4; 41.24°N, 20.90°E; focal depth 10km, normal faulting; EMSC 2012, NEIC 2012). Seismic features and dating results (see Hoffmann 2013b) testify to an active seismic landscape in Holocene times.

The small-scale morphology creates a large variety of habitats, which can be occupied by various species.

Vast flat plains contrast the steep slopes with blocks creating small basins and niches. The step like morphology creates vertically separated and varying environmental conditions (by means of light, temperature, etc.).

Moreover, events with magnitudes larger than 6.0 can cause a large input of material into the lake (e.g. by landslides, rockfalls, etc.). These events then change the living conditions over a longer period of time e.g. by the input of small particles. Suspended particles stay within the water column with long retention times and therefore change the input of light, availability of nutritional sources, the pH-value, etc. This can add extra stress to a population and cause a speciation event. Available earthquake data only date back to historical times and data from short cores and OSL dating suggest events around 4,500 a cal. BP and at 11,000 a BP respectively. Older records possibly contain more events

and can then be correlated with molecular clock analyses to find concordant events. This might give an idea about tectonic-related speciation in Lake Ohrid. Possible triggering mechanisms driving speciation can be mass wasting processes, change of the location of rivers and streams, earthquakes and secondary seismic effects, morphological segmentation connected to tectonic activity associated with rapid changes of habitats, and the high variability of habitats linked to these processes.

Acknowledgements: Thanks to the Deutsche Forschungsgemeinschaft (grant Re 1361/10) and the RWTH Aachen University for financial support. This study was carried out in the frame of the SCOPSCO (Scientific Collaboration On Past Speciation Conditions in Ohrid) ICDP project. Thanks are extended to our partners of Macedonia, especially to Dr. Zoran Spirkovski, and of Albania, Prof. Andon Grazhdani (Univ. of Tirana).

References

Albrecht, C., T. Wilke, (2009). Ancient Lake Ohrid: biodiversity and evolution. *Hydrobiologia*. 615, 103-140.

Benedetti, L., R. Finkel, G. King, R. Armijo, D. Papanastassiou, F. Ryerson, F. Flerit, D. Farber, G. Stavrakakis, (2003). Motion on the Kaparelli fault (Greece) prior to the 1981 earthquake sequence determined from 36Cl cosmogenic dating. *Terra Nova*. 15,118-124.

Hoffmann, N., K. Reicherter, T. Fernandez-Steeger, C. Grützner, (2010). Evolution of ancient Lake Ohrid: a tectonic perspective. *Biogeosciences*. 7, 3377-3386.

Hoffmann, N., (2013a). Tectonic evolution of the Lake Ohrid Basin (Macedonia/Albania). *Logos*. Verlag. Berlin. ISBN 978-3-8325-3586-5.

Hoffmann, N., (2013b). The active tectonic landscape of Lake Ohrid (FYR of Macedonia/Albania). *Annals of Geophysics*. 56, 6, doi: 10.4401/ag-6254.

Lindhorst, K., S. Krastel, K. Reicherter, M. Stipp, B. Wagner, T. Schwenk, (in press): Sedimentary and tectonic evolution of Lake Ohrid (Macedonia/Albania). *Basin Research*.

Muco, B., (1998). Catalogue of ML 3.0 earthquakes in Albania from 1976 to 1995 and distribution of seismic energy released. *Tectonophysics*. 292, 311-319.

Reicherter, K., N. Hoffmann, K. Lindhorst, S. Krastel-Gudegast, T. Fernandez-Steeger, T. Wiatr, (2011). Active basins and neotectonics. Morphotectonics of the Lake Ohrid Basin (FYROM/Albania). *Z. dt. Ges. Geowiss*. 162/2, 217-234.

Stankovic, S., (1960). The Balkan Lake Ohrid and Its Living World. *Monographiae Biologicae*. IX, Uitgeverij Dr. W. Junk b.v. Publishers. The Hague. p. 357 pp.

INQUA Focus Group on Paleoseismology and Active Tectonics

The Southern Upper Rhine Graben - A paleoseismological pre-site survey in the Freiburg area

Hürtgen, J. (1), Jomard, H. (2), Thomas, J. (1), Reicherter, K. (1), Baize, S. (2), Röth, J. (1), Cushing, M. (2), Cinti, F.R. (3)

(1) Neotectonics and Natural Hazards Group, RWTH Aachen, Lochnerstr. 4-20, 52056 Aachen, Germany. Email: j.huertgen@nug.rwth-aachen.de
(2) Institut de Radioprotection et de Sûreté Nucléaire, BP 6, 92262 Fontenay-aux-Roses, France
(3) Istituto Nazionale di Geofisica e Vulcanologia, Via di Vigna Murata 605, 00143 Roma, Italy

Abstract: *The Upper Rhine Graben (URG) belongs to the European Cenozoic Rift System (ECRIS), which comprises several smaller graben systems in Central Europe. It is flanked by normal faults which are, especially at the eastern border of the graben, suspected to be still active. Some paleoseismological studies have been carried out in the north-western and very southern part of the URG. Our area of interest, the Freiburg area, located on the eastern border, is not covered by paleoseismic studies yet. Our aim is to find an appropriate trenching site to add paleoseismological data and extend the sparse seismic record of the eastern URG. We present insights into the geophysical part of the pre-trenching survey. The presentation of shallow ground penetrating radar profiles and electrical resistivity tomography shows promising results indicating that one of the eastern boundary faults, the Rhine River Fault, was active in the relatively recent geological past.*

Key words: *Paleoseismology, geophysics, pre-trench survey, Upper Rhine Graben, active faults.*

INTRODUCTION

This short publication presents our recent paleoseismological work in one of the most tectonically active regions in Central Europe. The region belongs to the highly segmented European Cenozoic Rift System (ECRIS), which comprises, amongst others, the Bresse Graben (BG), the Upper Rhine Graben (URG) and the Lower Rhine Graben (LRG), and extends from the Alps to the North Sea (see Fig. 1A). Our work is focussed in the area around Freiburg (southern URG, Germany). Despite relatively long earthquake recurrence periods (several thousands of years) in Central Europe, seismic activity is still a major threat to the population and economies of this highly industrialized and densely populated region. People and infrastructure (roads, buildings, dams,

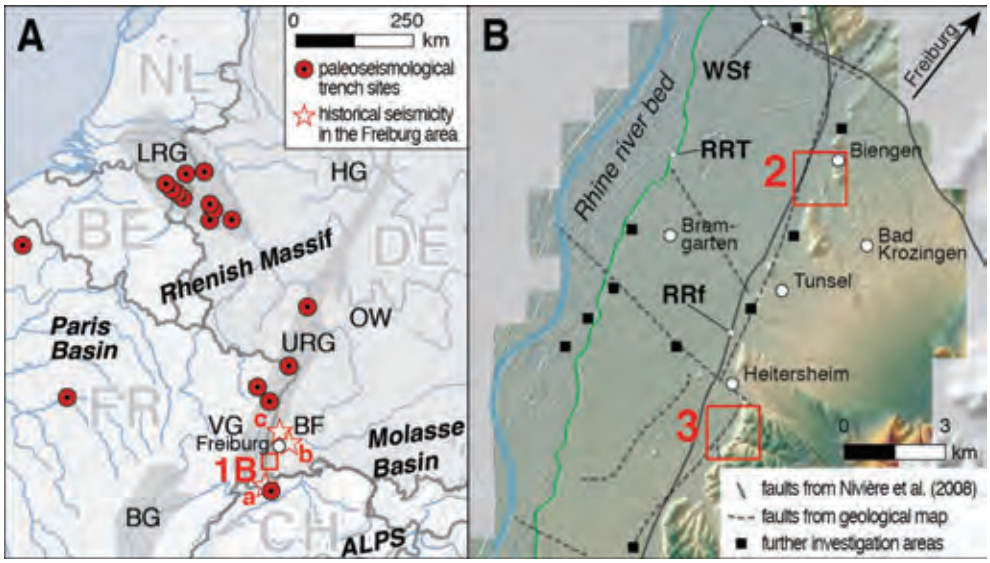

Figure 1: A: Overview of the broader region of the European Cenozoic Rift System (ECRIS), comprising, amongst others, the Lower Rhine Graben (LRG), the Hessen Graben (HG), the Upper Rhine Graben (URG), and the Bresse Graben (BG). The URG is situated in between two uplifted areas, in the west the Vosges Mountains (VG) and in the east the Black Forest (BF) and the Odenwald (OW). Additionally, the map shows the location of paleoseismological trench sites previously undertaken by various workers and some major seismic events in historical times (a: 1356 Basel; b: 1523 Freiburg; c: 1823, 1899, 1926 Kaiserstuhl). B: Extent of the study area south of Freiburg (extent indicated in 1A with red square). In this publication, we present the first results from geophysical and morphological investigations at two sites (red squares), Biengen (see Fig. 2) and Heitersheim (see Fig. 3). The black filled squares are other investigated sites but are not described in detail. RRf: Rhine River Fault, WSf: Weinstetten Fault, RRT: Rhine River terrace. DEM from LiDAR data (green/red) and SRTM data (gray) in the background.

industry) as well as critical infrastructures (supply lines, airports, telecommunication, nuclear power plants, etc.) are always at risk from earthquakes generated along the tectonically active graben system of the URG. In this region recent or instrumental seismicity has recorded earthquake magnitudes no larger than 6.0; yet, stronger historical and prehistorical earthquakes have occurred on some of the region's larger faults. The hazard assessment for the area, however, has been achieved using only a short time interval of observation (<100 years) as is typical in seismological studies. Using paleoseismological methods the lack of events in the earthquake catalog can be compensated for by trenching faults and dating the sediments associated with the fault movement. Our final aim in this study is to carry out a paleoseismological trench at a promising site with a prior evaluation of paleoseismic, neotectonic, geomorphological and high-resolution geophysical data. We give here some first insights into the geophysical data we have already obtained at several sites in the area around Freiburg.

Tectonics and seismicity

The causes of earthquakes in Central Europe are diverse: the predominant tectonic crustal stresses are caused by the ongoing Alpine collision of the Adriatic plate with Eurasia in the south, the ridge push force of the Mid-Atlantic Ridge to the west, and the post-glacial isostatic adjustment of Scandinavia's movement in the north. In this setting, a 300 km long elongated and on average 40 km wide rift flanked by uplifted plateaus (Vosges Mountains to the west and Black Forest to the east) has developed. It is bounded by major normal faults striking NNE-SSW with vertical displacements of up to 5 km. Although most faults are normal, horizontal striations on fault planes as well as earthquake focal mechanisms are frequently observed, indicating sinistral displacement. The present-day activity of the graben system is concentrated along its eastern side, which has been identified by the offset of alluvial deposits in the Freiburg area (Nivière et al., 2008).

The whole region between Basel and Karlsruhe, including the Upper Rhine Graben, has a lack of significant large events in the instrumental catalogues. However, faults such as the Rhine River Fault have the potential to generate large magnitude earthquakes (based on the fault length and empirical relationships). The present-day distribution of seismicity in the southern URG area is moderate with several intermediate magnitude events that occurred in the last 500 years (1523, 1823, 1899, 1926; see Fig. 1A and Fracassi et al., 2005 for location and details). Historical and paleoseismicity extends these records, but not in the area of Freiburg. Paleoseismological studies were carried out in the past years in the north-western and southernmost parts of the URG. In the entire area of the URG, 14 paleoseismological trench studies (Fig. 1A) have been carried out (e.g., Baize et al., 2002; Meghraoui et al., 2001; Peters et al., 2005). Thus, Pleistocene to Holocene slip along the Western Border Fault, a normal fault in the northern part of the URG, has been evidenced by trenching and geomorphological studies (Peters et al., 2005; Cushing et al., 2000). The epicentre of the major West-European earthquake in 1356 was located south of Basel (Fig. 1A), approximately where the Eastern Border Fault of the URG meets the front of the folded Jura of the

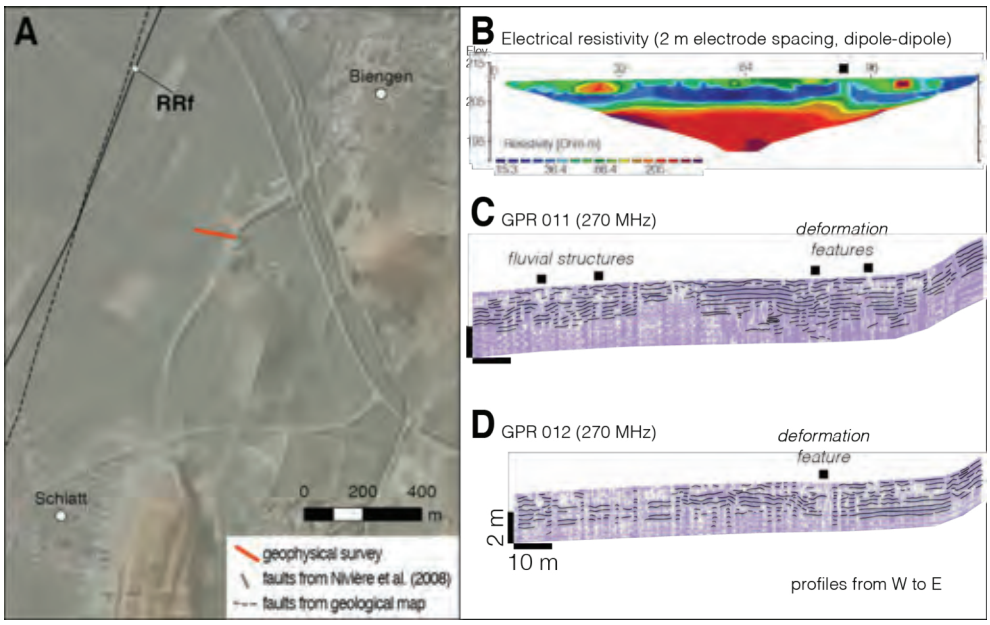

Figure 2: A: Overview of the Biengen site showing the location of faults (RRf: Rhine River Fault) provided by the geological map and Nivière et al. (2008). The red line indicates the location of the geophysical profiles shown in B, C, D. See Figure 1B for an overview of the site location. B: Electrical resistivity (ERT) profile with a 2 m electrode spacing and a dipole-dipole configuration. C and D: Ground penetrating radar (GPR) profiles parallel to the ERT profile. Black lines are highlighted main reflectors and indicate some relevant structures. The profiles are topographically corrected with 5 m LiDAR data and have been recorded from W to E. Black squares indicate where anomalies or deformation of subsurface structures are present. These probably point to seismically induced features, such as faulted strata, colluvial wedges or tilted beds.

Alps. The trenching study carried out by Meghraoui et al. (2001) evidenced the Basel earthquake and several previous paleoearthquakes.
In contrast, there are no paleoseismological studies at the eastern border of the URG (e.g., Main Border Fault and Rhine River Fault). Some geophysical, morphological and sedimentological studies have been undertaken (Nivière et al., 2008; Lämmermann-Barthel et al., 2009), which suggest that a Pleistocene reactivation of the Rhine River Fault led to the offset of young, near-surface sedimentary deposits. The long term slip rates of faults in the Freiburg area are estimated to range between 0.04 and 0.1 mm/a (Nivière et al., 2008). Lämmermann-Barthel et al. (2009) suppose a SSW-NNE striking fault in the area which forms a morphological step observed in an outcrop in the vicinity of Bremgarten village. The presence of this fault would strongly indicate a tectonic origin and reflects very recent neotectonic movements in the southern URG.

Methods

We use a variety of methods to achieve the most reliable site to excavate a paleoseismic trench. Firstly, we use high-resolution remote sensing data (5 m LiDAR data) to analyze the tectonic imprints in the morphology (e.g., morphotectonic indices, mapping of morphotectonic features). We also take different data into account to accomplish a high level of information; comprising data such as geological maps, fault data from papers and other projects (e.g. GeORG; LGRB, 2012), and seismic survey lines. We have already chosen some promising sites in the broader area of Freiburg to obtain high-resolution geophysical data of the near-subsurface. This includes ground penetrating radar (GPR) and electrical resistivity tomography (ERT) profiles. In the near future we want to validate and correlate our recorded geophysical data with sedimentological information from percussion drill cores.

RESULTS

The study area is situated just a few kilometres to the southwest of Freiburg in the graben fillings of the URG (Fig. 1B) and is characterized by agricultural land use (e.g. vineyards at topographic highs and farming at the plain areas). Strong morphological boundaries follow the general strike of the graben system (NNE-SSW). These morphological features have formed through erosional and tectonic processes. The Rhine River terrace (RRT, green line in Fig. 1B) separates the recent Rhine River bed from the older terrace plain. In the LiDAR data the present and ancient river beds are visible. The Rhine River Fault (RRf) separates the older terrace plain from topographic highs which are tilted ESE towards the Black Forest. The area along the RRf comprises mainly Quaternary sediments (sands, gravels, clays and loess) and is the target area for our recent pre-trenching study. Within the agricultural fields, a scarplet striking NE-NNE is visible in the LiDAR data, extending from south of Heitersheim to the north of Biengen. It is interpreted as a possible topographic expression of the active RRf.
We have obtained our geophysical surveys (GPR and ERT) across this scarplet. Two examples are presented here: south of Biengen (Fig. 2) and south of Heitersheim

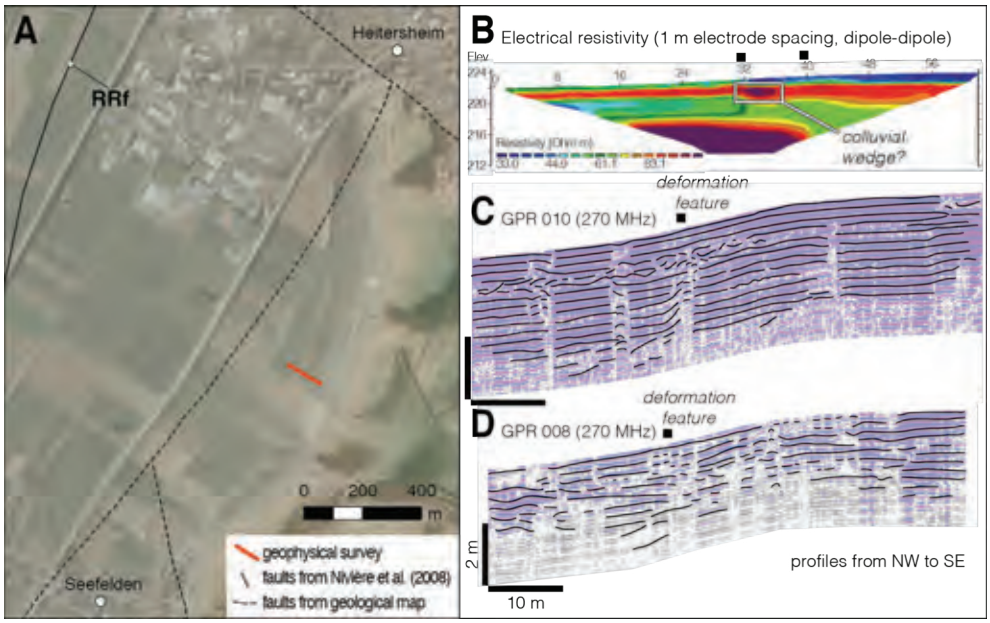

Figure 3: A: Overview of the Heitersheim site showing the rough location of faults (RRf: Rhine River Fault) provided by the geological map and Nivière et al. (2008). The red line shows the location of the geophysical profiles shown in B, C, D. See Figure 1B for an overview of the site location. B: Electrical resistivity (ERT) profile with a 1 m electrode spacing and a dipole-dipole configuration. C and D: Ground penetrating radar (GPR) profiles parallel to the ERT profile. Black lines are highlighted main reflectors and indicate some relevant structures. The profiles are topographically corrected with 5 m LiDAR data and have been recorded from NW to SE. Black squares indicate where anomalies or deformation of subsurface structures are present. These probably point to seismically induced features, such as faulted strata, colluvial wedges or tilted beds.

(Fig. 3). At both locations the ERT profiles show lateral variations in resistivity and also a strong vertical resistivity contrast that represents either two different materials in contact or a variation in water content due to a barrier structure or material. The lateral variations are mostly visible in the shallow parts of the sections due to a resolution decrease in depth in the ERT profiles. The GPR sections show a higher level of resolution to identify features of tectonic origin.

The most promising areas for fault displacement indicators are visible in the Biengen profile between 80 and 95 m (Fig. 2B) and in the Heitersheim profile at about 32 to 40 m (Fig. 3B, black square above profile). The GPR profiles of both areas indicate several structures which can be interpreted as originating from tectonic activity and fluvial processes. In the Biengen profiles (Fig. 2C/D), some major reflectors dip with higher angles than the surface (see black squares at 20-30 m and 90-100 m) and groups of reflectors end abruptly along a line. Additionally, these parts of the profiles show a more chaotic pattern. Similar features can be found in the Heitersheim profiles (Fig. 3C/D). Between 10-32 m along the profile, dipping reflectors occur at a depth of about 2 m. In some parts, the geometry of the reflectors builds wedge-like shapes. Offset and partly ending reflectors are visible between 60 and 64 m. These are just a few of the undertaken profiles and others show similar features.

DISCUSSION & OUTLOOK

We present here a small amount of the already obtained data; in total several kilometers of ERT and GPR surveys have been carried out. The observed features in the ERT and in GPR profiles indicate a tectonic origin at several chosen sites. Most promising areas in the sections (ERT and GPR) are in the Biengen area in the range about 80 to 100 m and in the Heitersheim area in the range about 20 to 40 m. The high resistivity anomaly in the Biengen ERT section could be interpreted as a colluvial wedge with regard to the structures observed in the GPR section (GPR 8, at 25 m).

However, these features may also be of another origin (e.g. erosional). To determine this, further detailed investigations have to be carried out; for example a denser coverage in GPR and ERT profiling will be undertaken to laterally map the features. The strongly modified landscape and subsurface due to agricultural use makes the interpretation of geophysical profiles often very difficult. Support by shallow percussion drillings can identify and validate the features observed in the geophysics. These are future steps in the process of finding a reliable site for a detailed paleoseismological trench study. As the historical earthquake data, the stratigraphy and the morphology of the area of interest indicates recent tectonic activity (Nivière et al., 2008; Lämmermann-Barthel et al., 2009), we must extend the knowledge into the past with paleoseismological data. In other parts of the Upper Rhine Graben, a few paleoseismological studies (e.g. Baize et al., 2002; Cushing et al., 2000; Meghraoui et al., 2001; Peters et al., 2005) have shown that paleoearthquakes can be detected. However, they are sparse and spatially distributed throughout Central Europe and even throughout the URG (see Fig. 1A). Additionally, the previous studies do not cover the eastern part of the graben system. Therefore, our ongoing study can help to characterize the eastern faults as seismogenic sources of significant earthquake events.

References

Baize, S., M. Cushing, F. Lemeille, B. Granier, B. Grellet, D. Carbon, P. Combes, C. Hibsch, (2002). Inventaire des indices de rupture affectant le Quaternaire, en relation avec les grandes structures connues, en France métropolitaine et dans les régions limitrophes. *Mémoires de la Société Géologique de France*. 175.

Cushing, M., F. Lemeille, F. Cotton, B. Grellet, J.C. Audru, F. Renardy, (2000). Paleo-earthquakes investigations in the Upper Rhine Graben (URG) in the framework of the PALEOSIS project. *Paleosis project.* (ENV4-CT97-0578 EC Environment and Climate Research Programme). 1-9.

Fracassi, U., B. Nivière, T. Winter, (2005). First appraisal to define prospective seismogenic sources from historical earthquake damages in southern Upper Rhine Graben. *Quaternary Science Review*. 389, 1-33.

Lämmermann-Barthel, J., I. Neeb, M. Hinderer, & M. Frechen, (2009). Last Glacial to Holocene fluvial aggradation and incision in the southern Upper Rhine Graben: Climatic and Neotectonic controls. *Quaternaire*. 20, 1, 25-34.

LGRB (Landesamt für Geologie, Rohstoffe und Bergbau), (2012). Regierungspräsidium Freiburg, Interreg IV Oberrhein, Projekt GeORG. Last checked: 13th January 2014 http://geo.geopotenziale.eu/geonetwork/srv/de/main.home

Meghraoui, M., B. Delouis, M. Ferry, D. Giardini, P. Huggenberger, I. Spottke, M. Granet, (2001). Active normal faulting in the upper Rhine Graben and Paleoseismic Identification of the 1356 Basel earthquake. *Science*. 293, 2070-2073.

Nivière, B., A., Bruestle, G. Bertrand, S. Carretier, J. Behrmann & J.C. Gourry, (2008). Active tectonics of the southeastern Upper Rhine Graben, Freiburg area (Germany). *Quaternary Science Reviews*. 27, 541-555.

Peters, G., T. Buchmann, P. Connolly, R. van Balen, F. Wenzel, S. Cloetingh, (2005). Interplay between tectonic, fluvial and erosional processes along the Western Border Fault of the northern Upper Rhine Graben, Germany. *Tectonophysics*. 406, 1-2, 39-66.

INQUA Focus Group on Paleoseismology and Active Tectonics

PalSeisDB v1.0 – Paleoseismic Database of Germany and Adjacent Regions

Hürtgen, J. (1), Spies, T. (2), Schlittenhardt, J (2), Reicherter, K. (1)

(1) Neotectonics and Natural Hazards Group, RWTH Aachen, Lochnerstr. 4-20, 52056 Aachen, Germany. Email: j.huertgen@nug.rwth-aachen.de
(2) BGR, Unit 'Seismic Hazard Assessment', Stilleweg 2, 30655 Hannover

Abstract: *Central Europe is an intraplate domain which is characterized by low to moderate seismicity with records of larger seismic events occurring in historical and recent times. These records of seismicity are restricted to just over one thousand years. This does not reflect the long seismic cycles in Central Europe which are expected to be in the order of tens of thousands of years. Therefore, we have developed a paleoseismic database (PalSeisDB v1.0) that documents the records of paleoseismic evidence (trenches, soft-sediment deformation, mass movements, etc.) and extends the earthquake record to at least one seismic cycle. It is intended to serve as one important basis for future seismic hazard assessments. In the compilation of PalSeisDB, paleoseismic evidence features are documented at 95 different locations in the area of Germany and adjacent regions.*

Key words: *Paleoseismology, Paleoearthquakes, Database, Germany, Central Europe.*

INTRODUCTION

We present the Paleoseismic Database of Germany and Adjacent Regions (PalSeisDB v1.0). Paleoseismic evidence from published and partly from unpublished studies in Central Europe has been collected and systematically parameterized. This is an extension of historical and instrumental earthquake catalogs that only date back approximately 1200 years (e.g. Leydecker, 2011; AHEAD, 2013). The events in these published catalogs do not have the needed temporal and spatial distribution for seismic hazard assessments. This is because they do not cover the seismic cycle of tectonically active structures which can be thousands or tens of thousands of years (Ahorner, 2001; Vanneste et al., 2013). Therefore, paleoearthquakes identified in paleoseismic investigations must be taken into account. In this regard, PalSeisDB v1.0 comes into play. It serves as one reference basis for future seismic hazard assessments.

PROJECT CONTEXT

Similar projects around the world, mostly on a national basis, have been undertaken or are in progress. These projects, however, do not collect paleoseismic data directly; they mostly compile data on active faults, including their long-term behavior. These faults are responsible for the generation of recent, ancient and paleoearthquakes. Examples of active fault and seismogenic source databases are provided by Italy's Database of Individual Seismic Sources (DISS version 3; Basili et al., 2008) and ITaly HAzards from CApable faults (ITHACA, 2012), the Quaternary Active Faults Database of Iberia (QAFI v.2.0; García-Mayordomo et al., 2012), and the Central and Eastern United States Seismic Source Characterization for Nuclear Facilities (CEUS-SSC, 2012). For Europe another project has been developed known as the SHARE Database 3.2 (Seismic Hazard Harmonization in Europe, SHARE, 2013). This includes seismogenic sources (mainly active fault data) and an earthquake catalog (historical and instrumental) for the wider European area. Their fault data is partly incorporated in our database.

Up to now no comprehensive compilation of all paleoseismic evidence exists in Central Europe. Therefore, we have started a project to collect paleoseismic and active fault data in a database structure similar to those in the aforementioned projects. PalSeisDB v1.0 will serve to fulfill the requirements of the updated German Nuclear Safety Standard, called KTA 2201.1 (Design of Nuclear Power Plants against Seismic Events). The revised version of this standard (KTA, 2011) explicitly demands the use of paleoseismic studies whose results should be considered in the estimation of the maximum historical or prehistorical reference earthquake. The new standard should include the assessment of paleoseismicity up to a distance of 200 km (radius) around the specific site. The collected information in PalSeisDB v1.0 is useful in the context of nuclear safety, but also for building regulations in a more general context (e.g. emergency facilities or infrastructure).

GEOLOGICAL FRAMEWORK OF CENTRAL EUROPE

Central Europe is an intraplate domain and is characterized by records of low to moderate seismicity. This is mainly caused by compressional stress from the NW-ward drift of the African plate relatively to Europe and the ridge-push from the North Atlantic Ridge. In this setting, a large segmented rift system formed, known as the European Cenozoic Rift System (ECRIS), which comprises, amongst others, the Bresse Graben (BG), the Upper Rhine Graben (URG) and the Lower Rhine Graben (LRG), and extends from west of the Alps to the North Sea (see Fig. 1). The historical and instrumental record indicates that the areas of the ECRIS, especially the URG

and the LRG, are able to produce larger earthquakes than magnitude 5.5, such as the 1386 Basel earthquake (M 6.0-6.5), or the 1992 Roermond earthquake (M 5.9), see Leydecker (2011). The neotectonic and recent activity in regions of the Alps, the Molasse Basin, the Vienna Basin (VB), and the Eger Graben (EG) are also of interest. In agreement with the requirements of the Nuclear Safety Standard KTA 2201.1 (KTA, 2011), we, therefore, focused our study in areas prone to larger earthquakes in Germany and also in adjacent, tectonically active regions (see Figure 1).

Figure 1: Study area for PalSeisDB v1.0 (including Germany and adjacent regions) and main geological structures. BF: Black Forest, BG: Bresse Graben, EG: Eger Graben, FP: Franconian Platform, GG: Glückstadt Graben, HG: Hessian Grabens, LRG: Lower Rhine Graben, OW: Odenwald, URG: Upper Rhine Graben, VG: Vogesen, VB: Vienna Basin. Compiled from Dèzes et al. (2004), Kaiser et al. (2005), Reicherter et al. (2008), and using Natural Earth (Free vector and raster map data @ naturalearthdata.com).

PALEOSEISMIC EVIDENCE

Evidence for paleoearthquakes can be found in different tectonic settings and can have different appearances related to the source of the earthquake. For example, to find evidence of a surface rupture in the geologic record, the magnitude of the paleoearthquake must be Mw > 5.0 (Wells and Coppersmith, 1994). Preservation in the geologic record is strongly determined by erosion and deposition rates versus the deformation rates. After McCalpin (2009), we distinguish between effects found in the vicinity of a fault (on-fault) and effects found at a distance from a fault (off-fault). PalSeisDB v1.0 includes paleoseismic studies from trenching sites which provide the most reliable evidence for paleoearthquakes (e.g. surface faulting). At a distance from the fault, secondary effects can be observed, such as earthquake-induced soft-sediment deformation (e.g. liquefaction) and mass movement features. The extent and distribution of these effects are also strongly dependent on the earthquake's size and magnitude, hypocentral depth, surface and subsurface characteristics. These types of evidence, and others, can be used to identify paleoearthquakes and tectonically active structures and to determine their seismic hazard potential.

STRUCTURE OF PALSEISDB v1.0

The aforementioned types of evidence are the central part of our database. The database itself was developed in Microsoft Access 2010 and ESRI ArcGIS 10.1. Microsoft Access has been used to build the main structure of the database and to input the data. In ArcGIS, the geospatial information has been collected. The records of spatial information are saved in the geodetic datum ETRS 1989 (European Terrestrial Reference System).
The general structure of the database is presented in Figure 2. We distinguish between the paleoseismic source, event and evidence. Observations from paleoseismic trenches give the most reliable information on the occurrence of paleoseismic events. A data table for the available trenches in the study area was implemented. From the paleoseismic evidence, information on paleoearthquakes and paleoseismic-related faults (paleoseismic source) is extracted and then added to the corresponding individual data tables. The record of paleoearthquakes comprises the location, the date of event, the intensity and magnitude when provided. The structure of the data table describing the paleoseismic-related faults is adopted from Italy's Database of Individual Seismic Sources (DISS version 3; Basili et al., 2008), the Quaternary Active Faults Database of Iberia (QAFI v.2.0; García-Mayordomo et al., 2012), and the SHARE Database 3.2 (SHARE, 2013).

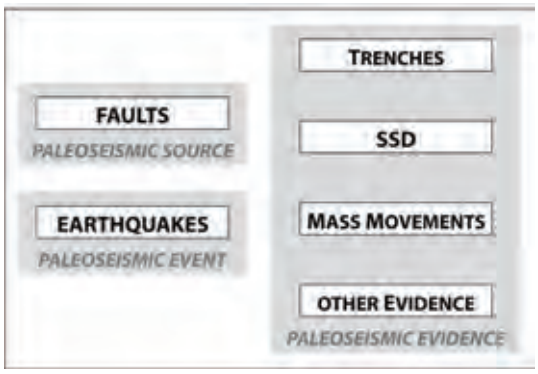

Figure 2: Conceptual scheme of PalSeisDB v1.0.

There are two further paleoseismic evidence types that are documented in our database: earthquake-induced soft-sediment deformation (SSD) and mass movement features. In Central Europe, only a few of these features

have been documented until now, but studies in other areas (e.g. CEUS, 2013) indicate that these are useful to evaluate the seismic potential in areas with low to moderate seismicity. For the documentation of soft-sediment deformation features, we adopted properties mainly based on the CEUS project (Paleoliquefaction Database, CEUS, 2013). Other, more specialized paleoseismic evidence, such as speleothem ruptures, have also been taken into account and are recorded in a separate table.

In the ideal case, one or more records of paleoseismic evidence can be related to one paleoseismic event which can be attributed to a paleoseismic source. In some cases, the conditions of the ideal case do not fit and a relation between event and source, or source and evidence, cannot be established due to complexity of the geologic record, or due to lack of information.

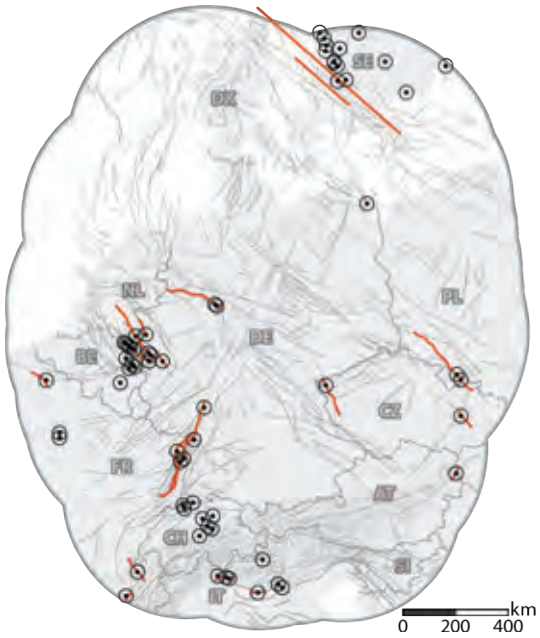

Figure 3: Comprehensive overview of the study area of the paleoseismic database of Germany and adjacent regions (PalSeisDB v1.0) including 95 locations of documented paleoseismic evidence (black dotted circles) and 26 fault traces associated with paleoseismic evidence (thick red lines). Additionally, fault traces of the main structural framework of Central Europe (thin gray lines) are shown combined with topographic imprint (hillshade of SRTM 90-m-data). Coordinate System: WGS 1984 World Mercator.

RESULTS

The compilation of PalSeisDB v1.0 shows that paleoseismic evidence is documented at 95 different locations which are unequally distributed in the area of Germany and adjacent regions (see Fig. 3). Of these, 15 locations are from investigations in Germany. In total, 86 paleoearthquakes have been determined, mostly from paleoseismic trench studies, but also from other paleoseismic studies regarding soft-sediment deformation and mass movements, as well as other paleoseismic evidence (e.g. tsunamigenic deposits, broken speleothems, etc.). Evidence for most of the paleoearthquakes (70 events) have been dated within a time period between 25,000 years BP and historical times. The nine oldest earthquakes even date back to a time period between Eemian and Mid-Pleistocene times. 75 earthquakes have values of magnitudes higher than M_w 5.7 and 53 earthquakes higher than M_w 6.5. The magnitudes have been mostly determined by relationships with rupture length or surface displacement (Wells and Coppersmith, 1994).

Paleoseismic data from 49 trenching studies have been documented and implemented in PalSeisDB v1.0. These give the most reliable information on the determination of seismic rupturing on a fault and on the occurrence of paleoseismic events. The areas with the most paleoseismic trenches are the Lower and Upper Rhine Graben systems. Furthermore, 96 seismically induced soft-sediment deformation features, 47 mass movement features, and 12 other paleoseismic evidence features have been documented. A seismogenic source could not be determined for each paleoseismic evidence feature. But in total, 26 faults are related to paleoseismic evidence and have been parameterized in PalSeisDB v1.0.

DISCUSSION

The area with the most available paleoseismic evidence is the European Cenozoic Rift System, especially the LRG and URG. The LRG has been intensively investigated by paleoseismologists over the last two decades (e.g. Skupin et al., 2008; Vanneste et al., 2013). The most investigated fault is the Feldbiss fault zone, which builds up the south-eastern border of the LRG. Distributed on its segments, nine paleoseismic trenches have been excavated. In the URG area, 14 paleoseismic trench investigations have been undertaken, e.g. at the Western Border fault (Peters et al., 2005) and at the Basel-Reinach fault (Ferry et al., 2005). Several other paleoseismic trenches have been carried out in other regions, for example in the Vienna Basin, the Eger Graben or in the Alpine area of Northern Italy. Other paleoseismic evidence related to secondary effects has been documented in Central Europe: soft-sediment deformations and landslides in Alpine lake deposits (e.g. Strasser et al., 2013), and in endokarstic cave deposits (e.g. fluvial sediments) and ruptures of speleothems in Belgium (Delaby, 2001).

The records of paleoseismic features are, however, sparse and spatially distributed throughout Central Europe (see Fig. 3). Up to now the number of paleoseismic studies characterizing potential active faults as seismogenic sources of significant earthquake events is still not sufficient. This is reflected in the missing parameterization of faults and it is a major lack of knowledge. The few existing studies have acquired paleoseismic evidence in Central Europe, mainly on a national basis. Their results were used in the present project to collect information on paleoearthquakes in a

systematic manner, but it should be mandatory to enforce future paleoseismic studies in Germany and adjacent regions to understand the complete seismic cycle of active faults and to assess their seismic hazard. Nevertheless, PalSeisDB v1.0 provides a tool useful for seismic hazard assessment in combination with local or regional earthquake catalogs in this region which is characterized by low to moderate seismicity.

OUTLOOK

Further steps in supplementing the current database are planned in near future. We propose three targets: (1) the combination of historical earthquake data and paleoearthquake field data, including environmental effects of historical events (e.g. hydrological anomalies); (2) the maintenance of the database; and (3) looking forward to future projects such as the generation of an "Active Fault Map of Germany and Adjacent Regions" using all the available geoscientific data. The database will be published in full detail, maintained and extended in the future along these purposes.

Acknowledgements: We would like to thank all the scientific experts in Paleoseismology (Stéphane Baize, Marc Cushing, Kurt Decker, Matthieu Ferry, Gottfried Grünthal, Christoph Grützner, Luca Guerrieri, Esther Hintersberger, Gösta Hoffmann, Hervé Jomard, Simon Kübler, Klaus Lehmann, Günter Leydecker, Franz Livio, Mustapha Meghraoui, Nils-Axel Mörner, Luigi Palumbo, Pablo Silva, Petr Spaček, Petra Stepančíková, Michael Strasser, Roland van Balen, Kris Vanneste) supporting us and our project with information and advice to develop and fill the current database.

References

AHEAD, (2014). European Archive of Historical EArthquake Data, http://www.emidius.eu/AHEAD/main/, last accessed December 2014.

Ahorner, L., (2001). Abschätzung der statistischen Wiederkehrperiode von starken Erdbeben im Gebiet von Köln auf Grund von geologisch-tektonischen Beobachtungen an aktiven Störungen. *Deutsche Geophysikalische Gesellschaft e.V.. Mitteilungen.* 2001, 2.

Basili, R., G. Valensise, P. Vannoli, P. Burrato, U. Fracassi, S. Mariano, M.M. Tiberti, E. Boschi, (2008). The Database of Individual Seismogenic Sources (DISS), version 3: Summarizing 20 years of research on Italy's earthquake geology. *Tectonophysics.* 453, 20-43.

CEUS-SSC, (2012). Central and Eastern United States Seismic Source Characterization for Nuclear Facilities http://www.ceus-ssc.com/, last accessed December 2014.

Delaby, S., (2001). Palaeoseismic investigations in Belgian caves. *Netherlands Journal of Geosciences.* 80, 323-332.

Dèzes, P., S.M. Schmid, P.A. Ziegler, (2004). Evolution of the European Cenozoic Rift System: interaction of the Alpine and Pyrenean orogens with their foreland lithosphere. *Tectonophysics.* 389, 1-33.

Ferry, M., M. Meghraoui, B. Delouis, D. Giardini, (2005). Evidence for Holocene palaeoseismicity along the Basel-Reinach active normal fault (Switzerland): a seismic source for the 1356 earthquake in the Upper Rhine graben. *Geophysical Journal International.* 160, 554-572.

García-Mayordomo, J., J.M. Insua-Arévalo, J.J. Martínez-Díaz, A. Jimenez-Díaz, R. Martín-Banda, S. Martín-Alfageme, J.A. Álvarez-Gómez, M. Rodríguez-Peces, R. Pérez-López, M.A. Rodriguez-Pascua, E. Masana, H. Perea, F. Martín-González, J. Giner-Robles, E.S. Nemser, J. Cabral, QAFI Compilers, (2012). The Quaternary Active Faults Database of Iberia (QAFI v. 2.0). *Journal of Iberian Geology.* 38, 285-302.

ITHACA, (2012). ITaly HAzards from CApable faults. http://sgi.isprambiente.it/GMV2/index.html, last accessed February 2015.

Kaiser, A., K. Reicherter, C. Hübscher, D. Gajewski, (2005). Variation of the present-day stress field within the North German Basin-insights from thin shell FE modeling based on residual GPS velocities. *Tectonophysics.* 397, 55-72.

KTA, (2011). Kerntechnischer Ausschuss 2201.1. Auslegung von Kernkraftwerken gegen seismische Einwirkungen Teil 1: Grundsätze. Fassung 2011-11. http://www.kta-gs.de/d/regeln/2200/2201_1_2011_11.pdf

Leydecker, G., (2011). Erdbebenkatalog für Deutschland mit Randgebieten für die Jahre 800 bis 2008. *Geologisches Jahrbuch*. Reihe E. Heft 59. Hannover.

McCalpin, J.P., (ed.), (2009). *Paleoseismology*. 2nd ed., Academic Press. San Diego.

Peters, G., T.J. Buchmann, P. Connolly, R.T. van Balen, F. Wenzel, S.A.P.L. Cloetingh, (2005). Interplay between tectonic, fluvial and erosional processes along the Western Border Fault of the northern Upper Rhine Graben, Germany. *Tectonophysics.* 406, 39-66.

Reicherter, K., N. Froitzheim, M. Jarosiński, J. Badura, H.J. Franzke, M. Hansen, C. Hübscher, R. Müller, P. Poprowa, J. Reinecker, Stackebrandt, W., Voigt, T., H. von Eynatten, W. Zuchiewicz, (2008). Alpine tectonics II - Central Europe north of the Alps. In: *Geology of Central Europe* (McCann, T., ed.). Geological Society of London.

SHARE, (2013): http://www.share-eu.org/, last accessed December 2014.

Skupin, K., K. Buschhüter, H. Hopp, K. Lehmann, R. Pelzing, J. Prüfert, M. Salamon, G. Schollmayer, A. Techmer, V. Wrede, (2008). Paläoseismische Untersuchungen im Bereich der Niederrheinischen Bucht. *Scriptum - Arbeitsergebnisse aus dem Geologischen Dienst Nordrhein-Westfalen.* 17.

Strasser, M., K. Monecke, M. Schnellmann, F.S. Anselmetti, (2013). Lake sediments as natural seismographs: A compiled record of Late Quaternary earthquakes in Central Switzerland and its implication for Alpine deformation. *Sedimentology.* 60, 319-341.

Vanneste, K., T. Camelbeeck, K. Verbeeck, (2013). A Model of Composite Seismic Sources for the Lower Rhine Graben, Northwest Europe. *Bulletin of the Seismological Society of America.* 103, 984-1007.

Wells, D.L., K.J. Coppersmith, (1994). New empirical relationships among magnitude, rupture length, rupture width, rupture area, and surface displacement. *Bulletin of the Seismological Society of America*. 84, 974-1002.

6th International INQUA Meeting on Paleoseismology, Active Tectonics and Archaeoseismology,
19-24 April 2015, Pescina, Fucino Basin, Italy

INQUA Focus Group on Paleoseismology and Active Tectonics

paleoseismicity.org

Pleistocene-Holocene extreme events in the lakes of central Mexico recorded from diatomites and detritic sediments

Israde-Alcántara, I. (1), Garduño-Monroy, V.H. (1), Rodriguez-Pascua, M.A. (2)

(1) Instituto de Investigaciones en Ciencias de la Tierra, Edificio U. Ciudad Universitaria. Universidad Michoacana de San Nicolás de Hidalgo. 58060, Mexico. Email: isaisrade@gmail.com
(2) Instituto Geológico Minero de España (IGME), Spain

Abstract: *Major morphostructural features delimit the lacustrine basins in central western Mexico. These features conform the east branch of a 6,000 km long triple junction, characterized by a numerous suite of large and small shallow lakes beginning in Lake Chapala and ending in the extreme east in the ancient Acambay lakes.*
Geophysical and stratigraphical analyses indicate that large and deep freshwater lakes alternating with fluviolacustrine deposits have been functioning from the Neogene and until Quaternary times, some of which, conserve their water columns.
Central Mexican lacustrine basins record several geological events changing the normal sedimentation regime. We present a review of the main events occurred along the Neogene-Holocene in the main lakes of central western Mexico.
The aim of this work is the analysis of fossil diatoms as indicators of extreme events in the sedimentary record. Being siliceous fossils are well preserved in the lacustrine record.

Key words: *Mexican lacustrine basins, deformation, diatomites.*

INTRODUCTION

Lacustrine basins are among the best records of the geological history of the world. Particularly in Mesoamerica, in Pleistocene-Holocene times a long history of human occupation including big mammals witnessed acute environmental events as a product of earthquakes and volcanic activity (Israde et al., 2010).
In the last decades, results of different research groups have challenged the stability of Mexican lakes (Metcalfe and Davies, 2007). Lakes in central Mexico are continuously influenced by the oblique subduction of the Pacific under the North American plate forming the Trans Mexican Volcanic Belt (TMVB) and the Chapala Acambay Graben, which include several lakes and paleolakes (fig 1a and 1b).
Fossil diatoms are excellent proxies to integrate the paleoenvironment information and the associated deformations at the time they were deposited and together with other clastic facies, they record extreme events in the central west Mexico lacustrine basins.

Methodology
Diatoms represent the most abundant taxa in outcrops and boreholes from late Miocene through Holocene times in central Mexico.
Several stratigraphic sections with tephra, and/or organic materials have provided radiometric ages from various localities along the lacustrine basins with long-lived lakes. Stratigraphy of lacustrine and fluviolacustrine deposits was sampled every 10 cm in cores and in outcrops. We detail the strata with occurrence of deformation structures (faults, slumps or changes in sedimentary regime).
Permanent diatom slides were prepared using HCl and H2O2 to eliminate carbonate and organic residue respectively in the sample. Successively the sample was rinsed for several times until reach a pH neutral. Were settle 2µl of residue in a cover slip with nafrax (N01.7) as a mounting medium.
Were observed and counted 250 valves for each sample at magnifications of 1000 X.

Study area
Miocene-Pliocene central west Mexican lakes are part of the nearly flat morphologies produced along the tectonic east-west to northeast-southwest trending- trans-tensional depressions product of an intra-arc setting.. Located between 19 ° 32' to 20° 16' north latitude, the limits of the depressions integrate several volcanic structures and faults along the Chapala- Acambay -Ixtlahuaca system (Szynkaruk et al., 2004) that continue to be seismically active. Main facies of the region consist of Volcanic ash and volcaniclastic sediments, as well as fluviolacustrine deposits.

Figure 1: a. Tectonic sketch and distribution of the main central western E-W lacustrine basins in Mexico; b. Distribution of main lakes and paleolakes in central western Mexico. Studied outcrops and drilled sites.

Lake Patzcuaro

The present Lake Pátzcuaro occupies 130 km^2 within a 928 km^2 basin at 2,035 m a.s.l., surrounded by a steeply sloped volcanic terrain. A landslide of the southern El Estribo and Tariaqueri volcanoes caused at least two huge influxes of vulcanoclastic sediments into the paleolake. A paleosoil located between the last landslides and lacustrine sequences was dated in 28,110 ±260 yr BP (Israde et al., 2005). Successively a magmatic event in the south margin of Patzcuaro lake occurred at 8,430±330 yr BP (Luhr and Simkin,1993), generating over 40 m deep uplifted and metamorphosed diatomite deposits. All these events, and others recorded in the trenches (landslides, faults, and volcanic process), deeply deformed the lacustrine sequences until at least the middle Holocene (Garduño-Monroy et al., 2004) (Fig. 2a).

Planktonic diatoms (mainly *Stephanodiscus niagarae* and other Stephanodiscus sp.) are observed in the outcrops uplifted over 40 m above the modern lake. The same diatoms are observed on the faulted edge of the lake basin, in these strata diatoms are very reworked in coincidence with faults (fig. 2b).

The last event in this lacustrine basin was a seism in 1845 having Lake Patzcuaro as its depocenter (Figueroa, 1974). The IX degrees intensity earthquake caused a 5 m sudden rise of the lake (Garduño-Monroy et al, 2011).

Lake Chapala

Lake Chapala is the largest freshwater lake of Mexico with 1,100 km^2. It is located at 1,524 m a.s.l., and is limited by grabens

Deformed diatomite deposits intruded by a laccolite dated in 7 Myr BP are observed in the wall of the northern border (Israde et al, 2010). In the same outcrops, slumps capped the Neogene deposits (fig. 3a and 3b) Diatomite records show that Lake Chapala maintained a deep lake level in Quaternary times, indicating wet climatic conditions.

In the late Holocene, in the core extruded in the depocenter of the lake evidence of deformation is observed. Diatoms show high fragmentation successive to this episode (Zárate et al., 2014).

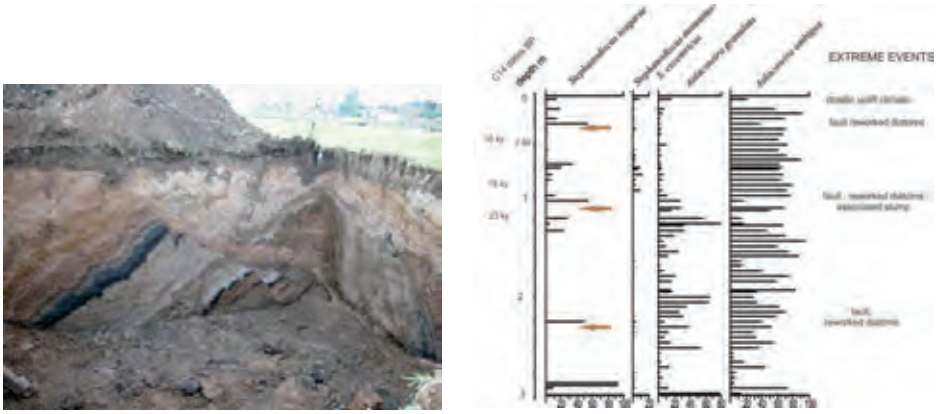

Figure 2: a. Deformation in Late Pleistocene-Holocene lacustrine sediments in south Pátzcuaro lake. b. Jaracuaro Trench, selected planktonic diatoms and changes in the diatom percents and fragmentation.

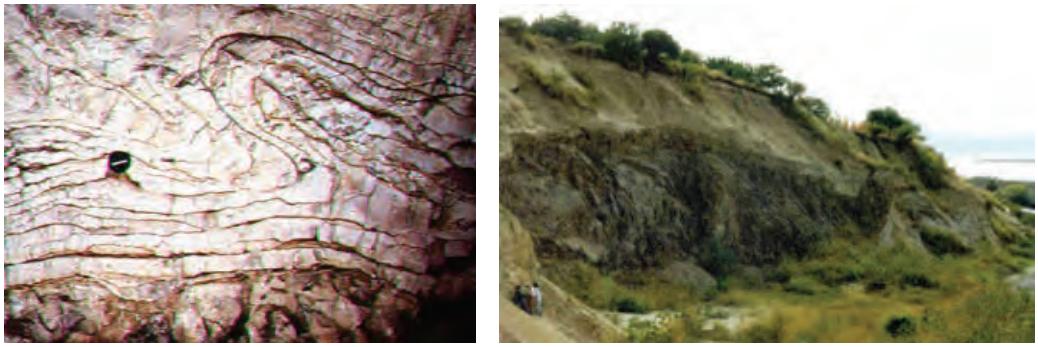

Figure 3: Deformation in northern border of lake Chapala.a. Slumps in diatomites; b. laccolite intruding the lacustrine sediments.

Lake Cuitzeo

Besides the Cuenca de Mexico Basin, Lake Cuitzeo is one of the better studied sites in the country. Lake Cuitzeo (420 km^2) is the second largest lake of Mexico, located along this E-W branch at 1,820 m a.s.l. The lake records Neogene lacustrine sediments that developed 25 km further to the south of the modern lake as a product of faulting and tilting in Quaternary times. Sedimentation interruptions between late Pleistocene early Holocene are very common in this tectonic basins (Israde et al., 2010).

Evidences of more recent faulting are recorded in trenches (Israde et al., 2010) and in normal faults in the north river of the lake having over 3 m of uplifted lacustrine deposits, which are interlayered with charcoal from burned archaeological artifacts dated at 1580 ±40 yr BP (Aguilar-Reyes et al., 2013).

Paleolake Acambay

Plio-Quaternary lacustrine sediment outcrop inside the Acambay-Tixmadejé and Pastores Fault system, comprising two ancient lacustrine areas: the Tierras Blancas with Plio-Pleistocene outcrops) and the northern Valle de los Espejos (representing the Holocene) paleolake.

The Plio-Pleistocene Tierras Blancas strata mainly consist of diatomites (Israde et al., 2010), capped by fall deposits dated at 1.2±0.13 Myr BP (Mercer, et al. 2014).

The base of the paleolake succession contains megaslump structures that are likely due to a combination of soft sediment deformation and earthquakes (Rodríguez-Pascua et al., 2010). and probably by effect of large underwater landslides. (Mercer et al., 2014). Several seismites have been recorded at the top of the Plio-Quaternary lacustrine sedimentation, i.e., sand and silt dike injections (Rodríguez-Pascua et al., 2010). Diatomite with fragmentation being more characteristic during and immediately after deformed strata.

The last 20 meters of deposition of the historic Lake Acambay are observed further east in the Valle de los Espejos paleolake, where evidence of microfaulting is recorded between 16,296 ±517 yr BP and 27,142 ±1949 yr BP. We inferred that the microfaulting observed in the cores is associated to seismicity (Carranza-Rivera et al., 2012).

Paleolake Zacapu

The dry floor of the historic Lake Zacapu occupies an extension of 260 km^2. The lake is bordered by ENE-WSW oriented extensional fault escarpments with vertical displacements observed both in outcrops and in human-made wells at different altitudes.

Inside a 27 m-deep well are observed several faults and synsedimentary structures associated to seismic activity induced by tectonic and volcanic movements of the Brinco del Diablo volcano and, successively, of the last eruption of the Alberca de los Espinos volcano occurred around 25 kyr BP (Siebe et al., 2012). Both eruptions uplifted the ancient lake several meters above the floor basin

The historic lakes Zacapu, North Cuitzeo and Acambay were both occupied by extensive marshlands that, based in diatoms observed in the sediments, and historical records, were drained to build channels systems for the expansion of farmlands

CONCLUSIONS

Modifications in the topography of basin floors, mainly caused by tectonic and volcanic activity in late Pleistocene Early Holocene, are observed in several tectonic basins along an E-W trend in central Mexico.

Diatomites record the associated deformations and, together with the stratigraphic analyses, help to discern between the influence of tectovolcanic and or climatic factors that mainly controlled the lake stability in these tectonically active basins.

References

Aguilar Reyes B., A. Goguitchaichvili, J. Morales, V.H. Garduño, M. Pineda, C. Carvallo, T. González Moran, I. Israde, and M. Calvo Rathert, (2013). An Integrated Archeomagnetic and C14 Study on Pre-Columbian Potsherds and Associated Charcoals Intercalated Between Holocene Lacustrine Sediments in Western Mexico. Geomagnetic Implications. *Journal of Geophysical Research*, *Solid Earth*. 118 (6), 2753-2763.

Carranza-Rivera AG., I. Israde-Alcántara, B.O. Aguilar-Reyes, A. Gogichiasvilli, V.H. Garduño-Monroy, (2012). Stratigraphy and paleoenviroments from Acambay paleo lake based in a 21.5 m core from the depocenter of the basin. *Paleoseismology and Archaeosesimology meeting*. 3rd INQUA-IGCP-567. 91-94.

Figueroa, J., (1974). Isosistas de macrosismos mexicanos. *Ingeniería, México.* 33 (1), 45-67.

Garduño Monroy, V.H., M.A. Rodriguez-Pascua, I. Israde-Alcántara, (2004). Evidencias paleosísmicas en fallas activas y sedimentos deformados del Lago de Pátzcuaro. Jarácuaro, Michoacán, México. *VI Congreso Geológico de España*. Geotemas. 6 (3): 151-154.

Garduño-Monroy, V.H., D.C Soria-Caballero, V.M. Hernández Madrigal, A. Rodríguez-Ramírez, I. Israde-Alcántara, M. Ostrooumov, M.A. Rodríguez-Pascua and J.C. Mora-Chaparro, (2011). Evidence of Tsunami Events Observed in the Paleolimnological Record, Lake Patzcuaro, Michoacán, México. *Geofísica Internacional*. (2011) 50-2,147-161.

Israde-Alcantara I., V.H. Garduño-Monroy, H.P. Fisher Pollard, (2005). Lake level change, climate, and the impact of natural events: the role of seismic and volcanic events in the formation of the Lake Patzcuaro Basin, Michoacan, México. *Quaternary International*. Vol. 135. 35-46.

Israde Alcántara, I., R. Velázquez Durán, S. Lozano García, V.H. Garduño Monroy. J. Bischoff, G. Domínguez Vázquez, (2010). Evolución paleolimnologica del lago de Cuitzeo, Michoacán. *Boletín de la Sociedad Geologica Mexicana*. 62 (3), 345-357.

Israde-Alcántara, I., W.E Miller, V.H. Garduño-Monroy, J. Barron, M.A. Rodriguez-Pascua, (2010). Palaeoenvironmental significance of Diatom and Vertebrate fossils from Late Cenozoic Tectonic Basins in west-central México: A review. *Quaternary International*. 219, 79-94.

Luhr, F., T. Simkin, (1993). Parìcutin, the Volcano born in a Mexican Cornfield. *Geoscience Press*. Phoenix, Arizona. 427pp.

Mercer, L., J.B. Kowallis, E.H. Christiansen, W.E. Miller, O. Carranza-Castañeda, I. Israde-Alcantara, (2014), Geology of the Tierras Blancas area in the southeastern part of the Acambay graben, central Mexico. *The Geological Society of America*. Digital Map and Chart 18. pag 1-46.

Metcalfe S. and S. Davies, (2007). Deciphering recent climate change in central Mexican lake records. *Climatic Change*. 83, 169-186.

Ortega, B., G. Vazquez, M. Caballero, I. Israde, S. Lozano-Garcıa, P. Schaaf, E. Torres, (2010). Late Pleistocene: Holocene record of environmental changes in Lake Zirahuen, Central Mexico. *Journal of Paleolimnology*. 44, 745-760.

Rodrıguez-Pascua, M.A, V.H. Garduno-Monroy, I. Israde-Alcántara, R. Pérez-López, (2010). Estimation of the paleoepicentral area from the spatial gradient of deformation in lacustrine seismites (Tierras Blancas Basin, Mexico). *Quaternary International*. 219, 66-78.

Siebe, C, M.N. Guilbaud, S. Salinas, and C. Chédeville-Monzo, (2012). Eruption of Alberca de los Espinos tuff cone causes transgression of Zacapu lake ca. 25,000 yr BP in Michoacán, México. *IAVCEI – CMV/CVS – IAS 4IMC Conference*, p 74-75.

Zarate del Valle, P. Dörfler, C. Albrechts, O. Nelle, I. Israde-Alcántara, (2014). CHAPHOLO: Paleolimnological Evaluation of Lake Chapala (Western Mexico) During the Past 10,000 Years (CONACYT CB2011, Grant 168685, In Progress). PHASE I: Drilling Campaign. *AGU Fall Meeting*. 2014.

Szynkaruk, E., V.H. Garduño-Monroy, G. Bocco, (2004). Active fault systems and tectono topographic configuration of the Central Trans Mexican Belt. *Geomorphology*. 61,111-126.

INQUA Focus Group on Paleoseismology and Active Tectonics

Tsunami Waveform Inversion of the 2007 Peru (Mw 8.1) Earthquake

Jimenez, C. (1,2), Moggiano, N. (1,2), Mas, E. (3), Adriano, B. (3), Yushiro, F. (4), Koshimura, S. (3)

(1) Faculty of Physical Sciences, National University of San Marcos, Av. Venezuela S/N, Lima-Peru. Email: cjimenezt@unmsm.edu.pe
(2) Directorate of Hydrography and Navigation, Chucuito-Callao, Peru
(3) International Research Institute of Disaster Science, Tohoku University, Sendai, Japan
(4) International Institute of Seismology and Earthquake Engineering, Building Research Institute, Ibaraki, Japan

Abstract: *An earthquake shook the central-southern coast of Peru on August 15, 2007, as a coseismic effect a tsunami was generated, which flooded some villages and beach resorts and killed 3 people. From the analysis and signal processing of 10 tidal records, we obtained the slip distribution of the seismic source and the initial coseismic deformation through an inversion modelling, in which the synthetic signals are compared with the observed signals by a non-negative least square method. The maximum slip located on the southern part of the rupture geometry is 7.0 m. The calculated scalar seismic moment is M0 = 1.99×10^{21} Nm, equivalent to a magnitude of M_w8.1. As a result, a heterogeneous seismic source model is obtained, which was the initial condition for simulating tsunami propagation and inundation.*

Key words: *Earthquake, seismic source, inversion, numerical simulation.*

INTRODUCTION

The Pisco (Peru) earthquake of 2007 (Mw 8.1) was generated at the boundary between the Nazca and South America tectonic plates. These two plates converge at a rate of 7-8 cm per year (Norabuena et al., 1999). The earthquake occurred at the interface between the two plates, the Nazca plate moving beneath the South American plate, a process known as subduction. The dominant seismic activity along the coast of Peru is a direct consequence of subduction of the Nazca plate beneath the South American plate, so that the coast of Peru has a history of great earthquakes. Over the past five centuries have been many destructive earthquakes of magnitude greater than Mw 8.0 in some place of Peru (Silgado, 1978).
As coseismic effect of the earthquake, a tsunami was generated, which originated the greatest run-up south of the Paracas Peninsula, this corresponds to the greater asperity (Ocola, 2008; Fritz et al.,2008). The focal mechanism for these earthquakes generally corresponds to a thrust fault with the nodal plane oriented in the NNW-SSE and dipping nearly horizontal plane (Tavera & Bernal 2008).

Data

Firstly, we used 12 digital tidal stations as shown in Figure 1 with red triangles. Eleven tide gauges located along the coast of Chile and Peru (IOC, http://www.ioc-sealevelmonitoring.org), and one buoy DART (Deep-ocean Assessment and Reporting of Tsunamis) of the National Data Buoy Center (NOAA website) located at deep sea. A good azimuthal geometric distribution of stations with respect to the epicentre is obtained with additional stations to the north; however, it is not the case for this event because the missing of tidal recordings of good quality, free of noise from stations located in the near and regional field to avoid dispersion effects.

Each tidal gauge signals are composed of a wide range of frequencies with 3 main components: oceanic tides (of astronomical origin), waves or surge (of atmospheric origin) and tsunami (of tectonic origin, mainly). To analyse the tidal gauge records of tsunami we applied the same algorithms of digital signal processing as in *Jimenez* (2007). For computational purposes of the inversion process, all records are synchronized in order to the arrival time of the first wave corresponds around 20th minute, i.e., close to the lower arrival time corresponding to Marcona station (Table 1).

N	Station	Lat. (°)	Lon. (°)	TA
1	Callao	-12.071	-77.174	55
2	Marcona	-15.343	-75.157	21
3	Arica	-18.476	-70.323	80
4	DART32401	-19.287	-74.731	51
5	Iquique	-20.205	-70.148	82
6	Antofagasta	-23.653	-70.404	110
7	Caldera	-27.065	-70.825	133
8	Coquimbo	-29.950	-71.335	164
9	Valparaiso	-33.027	-71.626	187
10	San Antonio	-33.580	-71.630	197
11	Juan Fernandez	-33.620	-78.830	181
12	Talcahuano	-36.695	-73.106	254

Table 1: The tidal stations are in order from north to south. The arrival times (TA) in minutes are in reference with the origin time of the earthquake.

The arrival time for Marcona station is less than the arrival time of Callao station; this is due to the bathymetry and directivity of the propagation of tsunami waves.

INQUA Focus Group on Paleoseismology and Active Tectonics

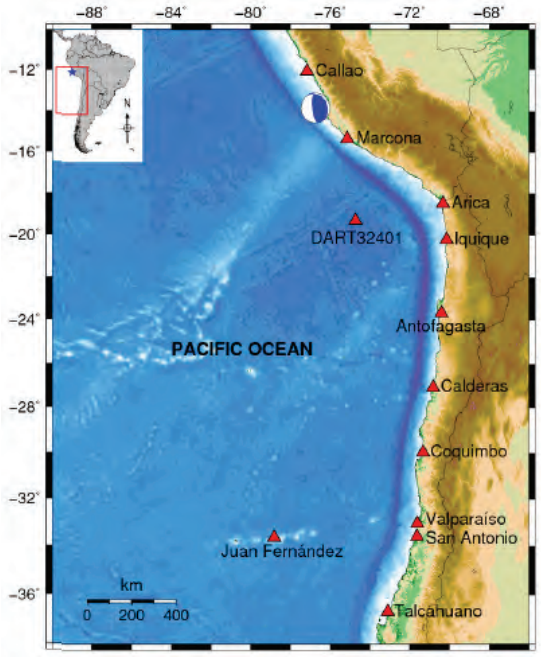

Figure 1: Distribution of tidal wave stations.

The global bathymetry model is taken from GEBCO 30 [10], with grid resolution of 30 arc sec (~927 m). For Callao station the bathymetry resolution was 3 arc sec (~92 m), corresponding to marine soundings. However, for other stations we used coarse bathymetry.

Methodology

If we know the parameters that characterize a system and its initial (and boundary) conditions, then we can predict the behaviour of the system at any instant of time. This type of problem, to predict future behaviour, is called the *direct problem*. The *inverse problem* is to use the results of certain observations to infer the values of the parameters characterizing the system (Tarantola, 2002). In this research, the tidal gauge records of tsunami will be used to infer the seismic source parameters and slip distribution which has been obtained in Table 2 as result of inversion waveform.

The process will be considered as a *Linear and Time-Invariant System*, which has two important properties:

a) Linearity, which allows using the superposition principle for Green's functions and for unitary deformations and *b)* invariance in time, that allows a shift in the time of the observed signals and their corresponding Green functions, synchronizing signals observed so that the tsunami arrival time corresponds to 20th minute, only for calculation purposes. This last point makes possible the use of tidal stations regardless of their distance from the epicentre. The solution of the inverse problem is not unique, but the set of values that provide the best correlation between observed and simulated data is chosen.

To obtain the source parameters and slip distribution of the seismic source, the inversion method for 12 tsunami waveform of good quality was used following *Satake and Kanamori (1991)* methodology. The rupture geometry was divided into 8 sub-sources (subfaults) of identical dimensions such as: length L = 45 km and width W=45 km, located at a depth Hj with respect to the upper side (in the vertical coordinate) of each sub-source (Figure 2). The coseismic deformation is calculated for each sub-source with a unitary slip using Okada (1985) formulation and focal mechanism data taken from Global CMT (http://www.globalcmt.org; Ekstrom et al., 2003) such as strike=325º, dip angle= 18º, rake angle=63º which are equal for each sub-source.

$$H_j = h + \frac{W}{2} sin\delta \; x \; [1 - mod(j,2), j = 1, \ldots, 8] \quad (1)$$

$$h = h_e - [(x_e - x_o)cos\theta - (y_e - y_o)sin\theta]tan\delta \quad (2)$$

Where h is the depth of the upper side of the rupture area, $x0$ and $y0$ are the coordinates of the lower left corner, j represents the position of the j^{th} sub-source, δ is the dip angle, $mod\ (j,2)$ represents the module or rest of j with respect to 2, (xe, ye,he) are the coordinates of the hypocentre and θ is the azimuthal angle. It should be noted that Hj is not the focal depth, but is related by Eq. (2).

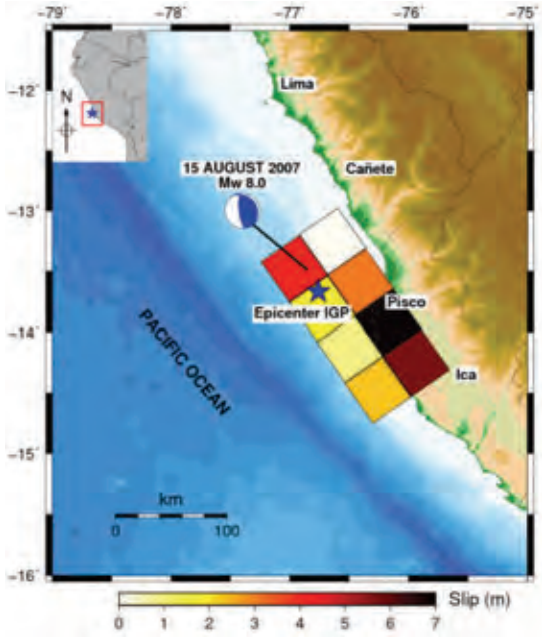

Figure 2: Slip distribution of unitary seismic sources.

The Green's functions, from the physical point of view represents the response of the system (simulated signal in the i^{th} station) when the system is disturbed by a unit impulse (deformation due to a unitary slip in the j^{th} sub-source). Using this deformation field as initial condition, the waveforms (or Green's functions) are calculated at each station simulating the propagation of tsunami waves by a finite difference method for each of the sub-sources, using an actual bathymetry. The tsunami waveforms observed are expressed as a linear

combination of the tsunami waveforms calculated, in tensor notation:

$$G_{ij}(t)\, x\, m_j = d_i(t) \qquad (3)$$

Where: $G_{ij}(t)$ is the Green function in the i[th] station generated by the j[th] sub-source, m_j is the value of slip at the j[th] sub-source, di(t) is the observed signal at the i[th] station. The linear tsunami propagation model TUNAMI in spherical coordinates was used (Imamura, 1996), with a single rectangular grid to obtain the Green's functions corresponding to the tidal stations of Chile and the DART buoy.

The inversion technique is performed by the method of non-negative least squares (Lawson & Hanson, 1974). This method compares the simulated signals with the observed signals and minimizes the squared residual:

$$|G_{ij}m_j - d_i|^2 \to 0 \qquad (4)$$

with the condition: *mj > 0*. We must take only the part of the signal corresponding to the first period of the wave to avoid contamination problems such as signal reflection effects and local resonance due to bathymetry and morphology of the coast around each station. In this case, it was taken the time window from the 20[th] minute to 60[th] minute, for purposes of calculating the inversion. The results of the inversion process are shown in Table 2.

Nº	Lat. (º)	Lon. (º)	Hj (km)	Slip(m)
1	-14.750	-76.300	14.00	2.25
2	-14.533	-75.983	27.91	5.65
3	-14.417	-76.533	14.00	0.84
4	-14.200	-76.217	27.91	6.96
5	-14.083	-76.767	14.00	1.70
6	-13.867	-76.450	27.91	3.07
7	-13.758	-77.000	14.00	4.06
8	-13.533	-76.683	27.91	0.05

Table 2: Slip distribution for each of the 8 sub-sources. The coordinates correspond to the lower left corner and the depth corresponds to the upper side (on the vertical axis) of the respective source.

RESULTS

From the slip distribution (Table 2), the vertical deformation field is obtained as a linear combination of unitary deformations, which will be used as initial condition for tsunami propagation (Figure 3). The maximum slip located at the southern part of the rupture geometry in the sub-source Nº 04 is 7.0 m. This maximum slip explains the fact that the Lagunillas bay area is the one that suffered the greatest impact due to inundation (Figure 5) because it lies within the sub-source 04. Additionally, according to geodetic data taken by the Geophysical Institute of Peru after the earthquake, a geodetic point in Punta Paracas (located 17 km SW of Pisco) moved up 0.50 m and 1.60 m to the west (Ocola, 2007). The maximum value of the vertical component of the initial coseismic deformation is 1.53 m, located SW from Paracas, on the sea.

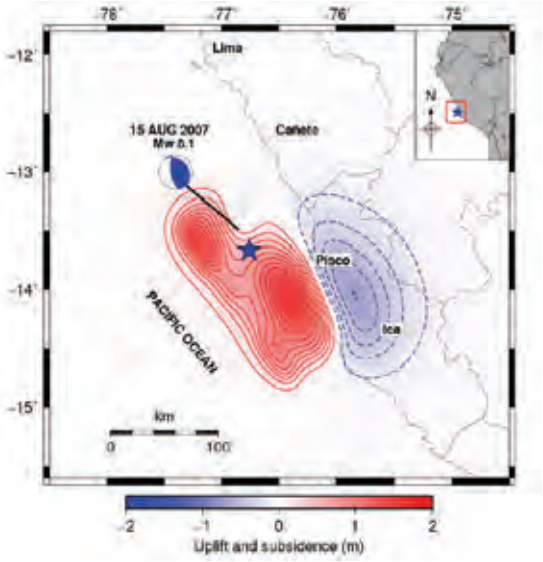

Figure 3: Vertical component of the initial coseismic deformation.

Taking the slip distribution and dimensions of each sub-source, it can be calculated the scalar seismic moment, defined as: $Mo = \mu LWD$ where: *M0* = seismic moment (Nm), μ = 4.0×10^{10} N/m^2 average rigidity of elastic medium, *L* = 180 km total length of the source, *W* =90 km total width of the source, *D* = 3.07 m, slip average. The scalar seismic moment is $M0 = 1.99\times10^{21}$ Nm and according to relation Mw = (2/3)Mo – 6.07 we obtained a moment magnitude scale of Mw 8.1.

Figure 4 shows the results of the inversion by comparing simulated and observed waveforms. We noticed that observed and simulated waves are well correlated as shown in Table 3. The stations of Coquimbo, Arica and Calderas have the best correlation. These correlations would improve if additional DART buoys (located at deep sea) were included in the inversion process, because there not would be problems of reflection and coastal resonance. However, the lack of coverage of these buoys in the western South Pacific and the large epicentral distance from the rest of these buoys would cause computing problems when working on far field simulation. For example, the dispersion effects are appreciable for far field simulation and this is a nonlinear problem. We have bypassed stations of Marcona and Juan Fernandez because they have a low correlation between simulated and observed signals. We notice that this model doesn't fit to near field tsunami.

With the seismic source obtained, the inundation was performed using non lineal model TUNAMI-N2 (Koshimura, 2009); the bathymetry and topography in this simulation has resolution of 30 m. As result the most remarkable horizontal inundation was 1 963 m in Caleta Lagunillas (south of the Paracas Peninsula), this result is very close (error 1.8%) obtained of field survey: 2000 m (DHN, 2007; Fritz et al., 2008). Figure 5 shows the comparison of the simulation results versus field survey observations from DHN (Moggiano, 2013).

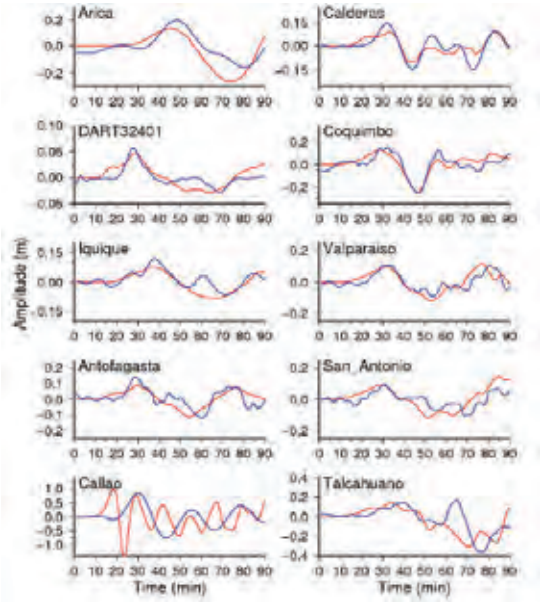

Figure 4: Comparison of tide gauge records. In blue: observed signals, in red: simulated signals. Height (m) vs. Time (min). The time is synchronized for all records with respect to arrival time on 20th minute.

N	Station	Correlation
1	Arica	0.82
2	DART 32401	0.79
3	Iquique	0.78
4	Antofagasta	0.70
5	Callao	0.01
6	Calderas	0.82
7	Coquimbo	0.85
8	Valparaiso	0.80
9	San Antonio	0.70
10	Talcahuano	0.56

Table 3: Correlation coefficient between observed and simulated signals.

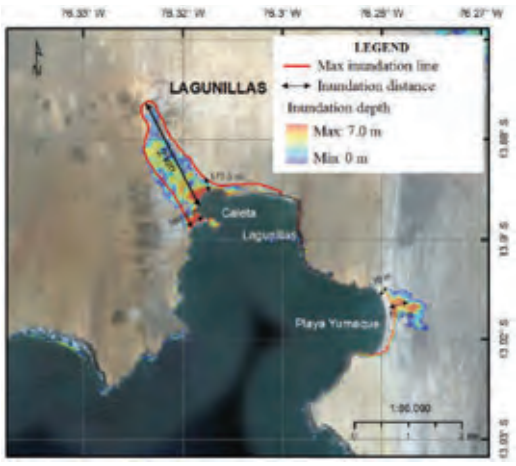

Figure 5: Tsunami inundation map for Caleta Lagunillas (southern part of Paracas). In red: maximum inundation line (DHN tsunami surve, 2007).

CONCLUSIONS

The solution of the inverse problem is not unique, but we used slip values that provide the best correlation between observed and simulated tsunami waveforms.

The maximum amplitude of the initial coseismic deformation model is 1.53 m. The maximum slip is 7.0 m and it is located in the southern part of the rupture area, specifically, south of the Paracas Peninsula.

It is important to have good azimuthal distribution of tide gauge stations around the seismic source geometry. Furthermore, the result will depend on the quality of the tide gauge data and quality of the local bathymetry around each station. The rupture process, whose beginning was at the epicentre, presented a unidirectional directivity along the azimuth from north-west to south-east. There are two principal asperities; the greater one is concentrated on southern of the Paracas Peninsula. This fact and the horizontal slope topography in Caleta Lagunillas explain the great horizontal inundation of 2 km.

The scalar seismic moment calculated is M0 = 1.99×10^{21} Nm and the magnitude of the earthquake inferred from tide gauge records is Mw 8.1.

One way to verify the seismic source model proposed is by comparing the observed and simulated tsunami waveform. The tidal stations in Coquimbo, Arica, Calderas and Valparaiso have the highest correlation values, while Callao, Marcona, Juan Fernandez and Talcahuano have a low correlation value.

The proposed model is not good in the near field region because the correlation values are low in Callao and Marcona. So, additional studies are required to improve the seismic source model and bathymetry data for tsunami inversion in near-field region.

The most remarkable horizontal inundation took place at Caleta Lagunillas and was around 2 km. Comparing with the field survey observation, there is an error of 1.8%, so, the seismic source model works very well.

Acknowledgements: The authors acknowledge support to JICA project, Directorate of Hydrography and Navigation and FENLAB Laboratory - National University of San Marcos, Peru.

References

DHN, (2007). Informe Post Tsunami Pisco 2007, Ministerio de Defensa, Marina de Guerra del Perú, Dirección de Hidrografía y Navegación. http://www.dhn.mil.pe. (Accessed Dec 2007).

Ekstrom, G., A.M. Dziewonski, N.N. Maternovskaya & M. Nettles, (2005). Global seismicity of 2003: centroid-moment-tensor solutions for 1087 earthquakes. P*hys. Earth planet. Inter.* 148 (1-2), 327-351.

Fritz, H.M., N. Kalligeris, J.C. Borrero, P. Broncano, and E. Ortega, (2008). The 15 August 2007 Peru tsunami runup observations and modeling. *Geophysical Research Letters*. 35, L10604, doi: 10.1029/2008GL033494.

Imamura, F., (1996). Review of Tsunami Simulation with a Finite Difference Method Long Waves Runup Models. *World Scientific Publishing Co. Pte. Ltd. Singapore*.

IOC, Sea Level Station Monitoring Facility, Web: http://www.ioc-sealevelmonitoring.org (Accessed Dec. 2012).

Jimenez, C., (2007). Procesamiento digital de señales sismicas con Matlab. *Revista de Investigacion de Fisica-UNMSM*. 10, (2), 23-28.

Koshimura, S., (2009) *TUNAMI-CODE, Tohoku University's Numerical Analysis Model for Investigation of Tsunami*. JST-JICA Perú Project. Disaster Control Research Center. Tohoku University.

Lawson, C. & R. Hanson, (1974). Solving Least Squares Problems. *Prentice-Hall*.

Moggiano, N., (2013). *Modelado Numerico del Maremoto de Pisco 2007*. Thesis disertation. UNMSM-FCF.

NOAA, National Data Buoy Center. Web: http://www.ndbc.noaa.gov/dart.shtml (Accessed Dec. 2012).

Norabuena, E., T. Dixon, S. Stein & C. Harrison, (1999). Deceleration and Nazca-Pacific plate motions. *Geophysical Research Letters*. Vol. 26, 3405-3408.

Ocola, L., (2007). Aspectos fisicos del maremoto de Pisco del 15 de agosto de 2007 y las inundaciones maximas. In: *El terremoto de Pisco del 15 de agosto de 2007*. Direccion de sismología CNDG/Instituto Geofisico del Peru. 395-420.

Okada, Y., (1985). Surface deformation due to shear and tensile faults in a half space. *Bulletin of Seismological Society of America.* 75, (4). 1135-1154.

Satake, K. & H. Kanamori, (1991). Use of tsunami waveform for earthquake source study. *Natural Hazards.* 4, 193-208.

Silgado, E., (1978). Historia de los Sismos mas notables ocurridos en el Peru (1513-1974). *Instituto de Geologia y Mineria*. Boletin No 3.

Tarantola, A., (2002). Inverse problem theory and methods for model parameter estimation. *Society for Industrial and Applied Mathematics.* Philadelfia.

Tavera, H. & I. Bernal, (2008). The Pisco (Peru) Earthquake of 15 August 2007. *Seismological Research Letters.* 79 (4), 510-515.

INQUA Focus Group on Paleoseismology and Active Tectonics

paleoseismicity.org

Speleoseismology in Northern Calabria: a tool for unravelling the paleoseismic history

Kagan, E. (1), Cinti, F.R. (2), Alfonsi, L. (2), Civico, R. (2), Bar-Matthews, M. (3)

(1) Department of Geo-Sciences, Tel Aviv University, 69978, Israel. Email: elisa.kagan@mail.huji.ac.il
(2) Istituto Nazionale di Geofisica e Vulcanologia, Roma, Italy
(3) Geological Survey of Israel, 30 Malkhe Israel St., Jerusalem, 95501, Israel

Abstract: *Three underground cavities in the northern Calabria region have been selected for speleoseismic analysis. Deformed speleothems as well as collapsed stalagmites were observed and sampled in the Romito and the S. Paolo caves in the Pollino Range area, and in the Monaca cave in the Catena Costiera. Deformed carbonate speleothems were sampled and dated by the U/Th method in order to constrain paleoearthquakes which shocked the cave sites and the surrounding area. Medium to large earthquakes have been recognized in the study area by paleoseismic and archaeoseismic studies. Moreover, frequent instrumental small to moderate seismicity occurs in the area. In 2010 a three year seismic sequence struck the area very close to the Romito and San Paolo caves.*

Key words: *Speleothems, Speleoseismology, Paleoearthquakes, Paleoseismicity, U/Th dating.*

INTRODUCTION

Paleoseismic data provide a long-term record of earthquake activity, crucial for hazard assessment. To make this record effective for hazard studies assessment, it is necessary to establish a high-resolution chronology of paleoearthquake events. The paleoseismic records can help to define the seismic history of an area locating past earthquake sources as well as giving constraints on magnitude and on the level of seismic shaking that affected an area. Speleothems damaged by earthquakes (speleoseismites) can provide an off-fault archive in addition to other seismic and paleoseismic data (Kagan et. al, 2005; Braun et al., 2011). Damaged speleothems can provide information on the timing of shaking and collapse in caves. Speleothems can potentially give insight into local intensity, magnitude, and source location when various caves are studied and in combination with other paleoseismic archives.

In the following we summarize the results obtained in the course of a speleoseismological study carried out at the Romito and the San Paolo caves located south of the Pollino Range, and the Monaca Cave in the Catena Costiera (Northern Calabria, Southern Italy; Fig. 1). Trenching and archaeoseismological data (Cinti et al., 2002, 2015; Michetti et al., 1997) recognize individual events larger than M>6.0 which have occurred in the area, defining a series of destructive events through time that are missing in the historical catalogue. Thus these data reveal our incomplete knowledge of the earthquake history. Other than on-fault investigation, off-fault studies such as the study of seismically deformed speleothems, can be effective in analysing a wider area and longer time period. This method can also provide chronological constraints on strong shaking events, contributing to the reconstruction of earthquake scenarios in time.

We documented damaged carbonate cave deposits which include collapsed and broken stalactites, in-situ but severed stalagmites and stalactites, and collapsed bedrock ceilings. In many cases, the damaged formations were covered by a speleothem regrowth. The caves showed no evidence of damage to speleothems by non-seismic sources, such as animals, slope instability, glacial movement, nor river flow. This and the fact that it is a seismically active area led to our working hypothesis that the damage was earthquake induced.

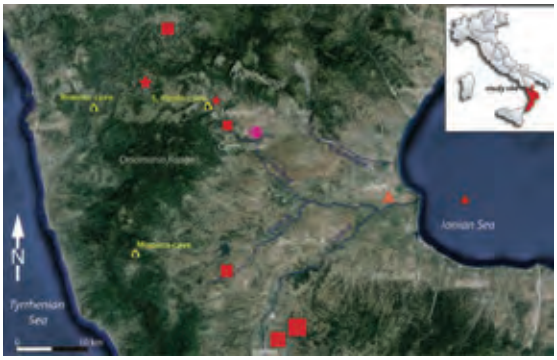

Figure 1: Location of the studied caves in Northern Calabria. The map also shows: the instrumental seismicity larger than M4, scaled by magnitude (stars); the historical earthquakes (I>VI MCS), *size-scaled by intensity degree (squares); the possible epicentral area of the paleoearthquakes succession inferred from on-fault trenching investigations (circle) and from off-fault archaeseismological studies (triangle). Satellite image from Google Earth © Map.*

SPELEOSEISMITE SAMPLING

Six speleoseismite field samples were taken from the Romito Cave (Figs. 2, 3, 4), four from the San Paolo Cave (Fig. 5), and four from the Monaca Cave. One sample of charcoal was taken from the Romito Cave, from within

an archaeological layer below (i.e. older) the cave room floor where three of the speleoseismites were sampled.

Figure 2: Sampling in the Romito Cave.

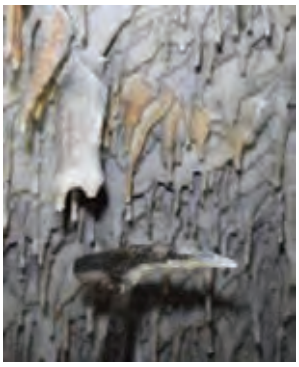

a

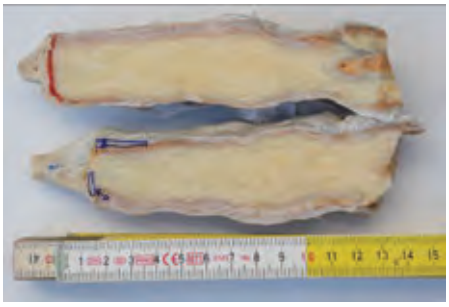

b

Figure 3: a. Sampling of a stalactite with broken tip and regrowth, hanging from the ceiling of the Romito cave; b. same stalactite after sawing, exposing the contact (thick line) between the broken lamina (pre) and the regrowth lamina (post).

The samples collected were sawed in half in order to expose breakages and contacts (Figs. 3b, 4b, 5b). The sawed samples were analysed at the INGV in Rome. The contact between the damaged speleothem and the post-damage regrowth was marked (i.e. the *paleoseismic contact*). The last lamina to grow before the damage (the *pre-contact* lamina) and the first lamina to grow after the damage (the *post-contact* lamina) were designated for sampling (Figs. 3b, 4b, 5b).

a

b

Figure 4: a. Two fallen stalactites with stalagmite regrowth, on the Romito Cave floor; b. same sample after sawing, exposing the contact (dotted line) between the stalactite and the regrowth stalagmite. The pre-contact lamina and post-contact lamina are indicated by arrows.

We recognized five couples of pre and post event laminae in the Romito Cave samples, and one post- only sample (regrowth on collapsed bedrock). From the San Paolo Cave speleoseismites, we recognized three couples of pre and post event laminae. From the Monaca Cave we recognized two couples of pre and post event laminae and two post-only samples (regrowth on collapsed bedrock).
Five speleoseismite events from the Romito Cave were chosen for the pilot dating study. The pre and post recognized laminae were then drilled at the INGV of Rome using 2 mm diameter drill bits. The powdered material obtained was sent to the Geochemistry Dept. of the Geological Survey of Israel for U/Th dating.

DATING METHODOLOGY

Speleothem calcite was dated by the U-Th disequilibrium technique. The U and Th of the carbonate fraction of the speleothems were chemically separated using chromatography and then measured by a Multi-Collector Inductively Coupled Plasma Mass Spectrometer (MC-ICP-MS) Nu Instruments Ltd (UK) equipped with twelve Faraday cups and three ion counters at the Geological Survey of Israel, methodology developed by Bar-Matthews et al. (1999) and described in Grant et al. (2012).

a

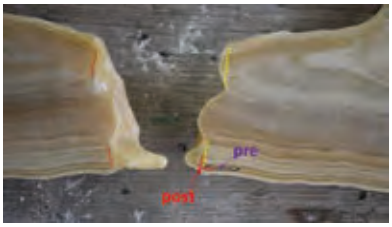

b

Figure 5: a. Broken stalactite, hanging from ceiling, with regrowth, San Paolo Cave, b. same sample after sawing, exposing the contact (dotted line) between the broken lamina (pre) and the regrowth lamina (post).

PRELIMINARY RESULTS AND DISCUSSION

The calibrated radiocarbon age of the charcoal from the Romito Cave (~8.2 ka cal BP; Beta Analytic Lab, Florida) constrains one of the U-Th dated speleoseismites to be younger than that, based on its position relative to the speleoseismite samples. This may assist in defining the detrital Th correction factor.

Field work, stratigraphy, and preliminary chronological results indicate that one or more cave-damaging events, dated by three collapses, occurred during the first two millennia of the Holocene, and another collapse took place during the Late Pleistocene. No earthquakes large enough to cause damage in the cave have occurred since. Based on this latter preliminary result, several questions arise: Does the lack of evidence for damaging earthquakes in the cave during the Late Holocene, indicate that there were no large earthquakes or that they were not close enough to damage the Romito Cave? Are the recognized effects in the cave induced by only extremely large events that occur less frequently, or only by events that are very close? Further dating in the Romito Cave, as well as ages from the other caves, will provide a stronger constraint on the timing of the events striking the study area. Moreover, we may provide further indication for long periods of quiescence of large earthquakes in the region.

The available data from paleoseismology and archaeoseismology on nearby faults, ca. 30 km from of the Romito Cave, show the occurrence of surface faulting earthquakes at a younger time, Late Holocene. Are these events too distant to deform speleothems in the study cave or did the cave conditions prevent their recording? We intend to investigate these questions further.

The ages of the recognized events, based on the above methodologies, will be compared to the dating of the surface faulting paleoevents available for the nearby faults, such as the Pollino and Castrovillari faults, and possibly allow a correlation of the seismicity occurrence. This may provide a further indication that a long period of quiescence of large earthquakes occurred in the region.

Acknowledgements: Special thanks to Dr. Felice Larocca for his precious contribution during sample collection in the caves and for fruitful discussions. This study has benefited from funding provided by the Italian Presidenza del Consiglio dei Ministri - Dipartimento della Protezione Civile (DPC). This paper does not necessarily represent DPC official opinion and policies.

References

Bar-Matthews, M., A. Ayalon, A. Kaufman & G.J. Wasserburg, (1999). The Eastern Mediterranean paleoclimate as a reflection of regional events: Soreq cave, Israel. *Earth and Planetary Science Letters*. 166, 1-2, 85.

Braun, Y., E. Kagan, M. Bar-Matthews, A. Ayalon & A. Agnon, (2009/2010). Dating speleoseismites near the Dead Sea Transform and the Carmel Fault: Clues to coupling of a plate boundary and its branch. *Israel Journal of Earth Sciences*. 58, 257-273.

Cinti, F.R., M. Moro, D. Pantosti, L. Cucci & G. D'Addezio, (2002). New constraints on the seismic history of the Castrovillari fault in the Pollino gap (Calabria, southern Italy). *J. Seismology*. 6, 199-217.

Cinti, F.R., L. Alfonsi, A. D'Alessio, S. Mariano, & C.B. Brunori, (2015). Faulting and Ancient Earthquakes at Sybaris archaeological site, Ionian Calabria, Southern Italy, *Seismological Research Letters*. 89, 1, 245-254.

Grant, K., E. Rohling, M. Bar-Matthews, A. Ayalon, M. Medina-Elizalde, C.B. Ramsey, C. Satow & A. Roberts, (2012). Rapid coupling between ice volume and polar temperature over the past 150,000 years. *Nature*. 491, 7426, 744-747.

Kagan, E., A. Agnon, M. Bar-Matthews, & A. Ayalon, (2005). Dating large infrequent earthquakes by damaged cave deposits - Testing Seismogenic and Anthropogenic Damage Scenarios. *Geology*. 33, 4, 261-264.

Michetti A.M., L. Ferreli, L. Serva & E. Vittori, (1997). Geological evidence for strong historical earthquakes in an "aseismic" region: the Pollino case (Southern Italy). *J. Geodynamics*. 24, 1-4, 61-86.

INQUA Focus Group on Paleoseismology and Active Tectonics

On-land & Offshore Evidence for Holocene Earthquakes in the Northern Gulf of Aqaba-Elat, Israel/Jordan

Kanari, M. (1,2), Ben-Avraham, Z. (1,3), Tibor, G. (2), Bookman, R. (3), Goodman-Tchernov, B.N. (3), Niemi, T.M. (4), Wechsler, N. (1), Ash, A. (3), Nimer, T. (3), Marco, S. (1)

(1) The Department of Geosciences, Tel-Aviv University, Tel-Aviv, Israel. Email: kanarimo@tau.ac.il
(2) Israel Oceanographic & Limnological Research Ltd., Tel-Shikmona, P.O.Box 8030, Haifa 31080, Israel
(3) Dept. of Marine Geosciences, Leon H.Charney School of Marine Sciences, Haifa University, Mt. Carmel, Haifa 31905, Israel
(4) Dept. of Geosciences, University of Missouri-Kansas City, MO 64110, U.S.A.

Abstract: *Located at the Northern tip of the Gulf of Aqaba-Elat, the on-land continuation of the submarine Avrona Fault underlies the Hotels District of Elat, where seismic deformation was documented after the 1995 Nuweiba (Sinai) earthquake (7.2 Mw). This active segment of the Dead Sea Fault is the transition between the deep marine basin of the Gulf and the shallow continental basin of the Arava Valley. Paleoseismic trenching revealed the fault, based on surface rupture and liquefaction features. Radiocarbon dating of the offset strata and liquefaction suggest that it ruptured in the historical earthquakes of 1068 and 1458 AD, yielding a vertical slip rate of ~1.1 mm/yr. Independent dating of anomalous coarse grain events in core sediments from offshore nearby suggests these earthquakes triggered marine sediment mass-flow. Using this pattern, we analyze anomalous coarse grain events in several cores to compile a paleoseismic record dating back to the late Pleistocene.*

Key words: *Dead Sea Fault, Avrona Fault, Paleoseismic trenching, Gulf of Aqaba-Elat, Cores.*

INTRODUCTION

At the north tip of The Gulf of Aqaba-Elat (the northeast extension of the Red Sea; *Fig. 1*), reside the cities of Elat (Israel) and Aqaba (Jordan): major economic, cultural, and recreational centers of southern Israel and Jordan, and vital aerial and naval ports. It so happens that they are both also built on active faults, which have ruptured in the past. Aqaba was completely destroyed in the 1068 AD earthquake (Ambraseys et al., 1994; Avner, 1993), and significant damage to structures in both Elat and Aqaba was inflicted by the Nuweiba (Sinai) earthquake (22.11.1995; Mw 7.2) even though the epicenter was located 70 km to the south (Klinger et al., 1999). The estimation of seismic hazard to these neighboring cities is therefore vital. The peaceful hotels and beaches of Aqaba and Elat are located on a tectonic plate boundary, which is also a transition zone between two crustal realms of the Dead Sea Fault system (DSF): the deep en-echelon submarine basins of the Red Sea (Ben-Avraham, 1985) and the shallow continental basins of the Arava (Frieslander, 2000), localizing into a single fault strand heading northward.

Previous studies of the submarine structure of the Northern Gulf of Aqaba-Elat (NGAE) suggest slip on the east and west boundary faults is predominantly normal and recently active (Ben-Avraham, 1985; Ben-Avraham et al., 1979; Ben-Avraham and Tibor, 1993). However, recent high-resolution seismic and bathymetric data (Tibor et al., 2010; Hartman, 2012; Hartman, 2015) revealed a complex fault system across the shelf of the NGAE with varying degrees of recent seismic activity. Hartman et al. (2015) conclude that during the Holocene, the submarine Avrona Fault (Evrona Fault in some papers) accommodates most of the strike-slip faulting in this transform plate boundary, between the Sinai sub-plate and the Arabian plate, with an average sinistral slip-rate of 0.7±0.3 mm/yr through the Late Pleistocene and 2.3-3.5 mm/yr during the Holocene. *(Fig. 2)*, and a Holocene vertical slip rate of 1.0 ±0.2 mm/yr, suggesting that its seismic activity has increased through recent time.

On-shore, several works estimated the location of the Avrona Fault at the border of the Elat Sabkha (Garfunkel et al., 1981) and in the vicinity of the Elat hotel district (Wachs and Zilberman, 1994). Using seismic imaging, Rotstein et al. (1994) suggested a vertical deformation band of several hundred meters wide below the eastern part of the Elat Hotel District. Further seismic data was used by Frieslander (2000) to suggest a distinct sub-vertical discontinuity in the sediments in the same area in Elat. Active surface faulting was observed following the Nuweiba (Sinai) earthquake in 1995 (epicenter 70 km south to Elat), when an offset street was reported in the same hotels area (Wust, 1997). Some 15 km farther north, Paleoseismic trenching in the Avrona Playa revealed late Pleistocene earthquake ruptures displaced 1-1.5m with estimated magnitudes M6.7-M7, and Holocene earthquakes displacing 0.2-1.3m with estimated magnitudes M5.9-M6.7 (Amit et al., 2002). Zilberman et al. (2005) had extensively detailed the surface rupture of the fault in the Avrona Playa, relating observed surface rupture to the two historical earthquakes affecting the southern Arava valley and the ancient city of Aila: the 1068 AD and the 1212 AD earthquakes. They suggest an earthquake recurrence interval of 1.2±0.3 ka for this fault zone. However, the location and the paleoseismic record of the on-land continuation of the marine Avrona Fault, as it emerges from submarine to terrestrial domain, was

not known, and surface rupture from the 1068 AD earthquake south of the Avrona playa was not observed so far. Zilberman et al. (2005) report that there was no way to determine the length of the surface rupture in the Avrona Playa due to obscuring by erosion, younger deposits and incision of alluvial fans.

OBJECTIVE AND METHODOLOGY

We aim to locate the on-land continuation of the active submarine Avrona Fault, which underlies the Hotels District at the northern beach of Elat (Israel) and recover its seismic record. Additionally, we try to augment the paleoseismic record of the region, using field evidence for past earthquakes on- and off-shore. We integrated newly suggested offshore fault location (Hartman, 2012), analysis of aerial photos from 1945, and Ground Penetrating Radar (GPR) survey to hypothesize the fault location for paleoseismic trenching site selection. Trenching revealed the fault and associated liquefaction features. Trench strata were dated using 14C radiocarbon. Submarine sediments from piston cores were logged, analyzed for grain size, and dated using 14C radiocarbon of foraminifera, pristine bivalves and gastropods.

Figure 1: Regional tectonic overview of the Dead Sea Fault. The study area, the Northern Gulf of Aqaba-Elat (NGAE) marked in black rectangle; red arrows note relative tectonic plate motion (modified after Ben-Avraham et al., 2008).

RESULTS AND DISCUSSION

Analysis of aerial photos from 1945, GPR data and previous seismic data interpretation lead to excavating of 3 paleoseismic trenches (T1-T3). Trench T1 revealed liquefaction features but no surface rupture. Trench T3 revealed both large liquefaction sand-blows (up to several meters in width) and clear evidence for surface rupture (Fig 3). We suggest that the interpolated trace (red line; *Fig. 3 right*) between this rupture area in T3 and the edge of the submarine fault (white line; *Fig. 3 left*) is the on-land continuation of the submarine Avrona fault. Seven distinct units in trench T3 were offset, with a maximum vertical offset of ~43 cm. Two other partially visible units at the top-left of the log were offset. Five of these strata demonstrated a sequence, while the other 2 pairs of layers appeared to be overlaid in unconformity, leading to suggest that they were offset by another event, other than the one that had offset the first five. Radiocarbon dating the offset strata and the sand-blow structures of the trench, using OxCal v4.2.4 and integrating two faulting events, lead to suggest that these are evidence for the faulting of two historically documented earthquakes of 1068 AD (the destruction of Aqaba) and the 1458 AD earthquake. Vertical slip rate on the on-land Avrona Fault, as calculated from the offset segments caused by the two earthquakes, is ~1.1 mm/year, which conforms to the previously calculated slip rate of the submarine Avrona Fault by Hartman et al. (2015), but overpasses the vertical slip rate reported by Amit et al. (2002) for different segments of the entire Elat fault zone (0.1-0.35 mm/yr) and the Avrona Playa segment (0.3 mm/yr). This supports the suggestion by Hartman et al. (2015) that the Avrona fault takes most of the faulting during the Holocene, and has increased its activity in that period.

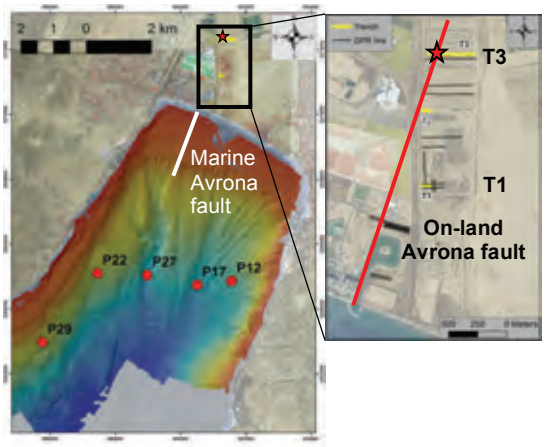

Figure 2: Map of marine and continental data presented here: the submarine Avrona Fault mapped by Hartman (2015) in white line, paleoseismic trench locations (yellow lines), piston cores in red circles; Inset: blow-up of land survey data collections (trenches in yellow and GPR lines in black; GPR data not presented here); red star: the location of the fault observed in trench T3 (Fig. 3); red line: the suggested fault trace of the on-land Avrona Fault, traced between the edge of the submarine fault and the surface rupture of the 1068 AD and 1458 AD earthquakes observed in T3.

In an independent analysis of the submarine core P27 (*Fig. 4*; see *Fig. 2* for core location) - several anomalous

coarse grain (>2mm, up to several cm maximum) events were observed, while most of the core is of typical pelagic deposition of <250 um in grain size. Radiocarbon dating of the anomalous events in the core resulted in a good match between the estimated ages of two anomalous events from the top of the core and the 1068 and 1458 AD earthquakes *(Fig. 4)*. We therefore suggest that the anomalous events in the submarine core P27 correspond to the earthquakes of 1068 AD and 1458 AD, which were also observed independently in T1 and T3 trenches on-land, just several km away to the north.

Following this similar pattern of dating anomalous events in core P27 (validated by historical and on-land observations), several other piston cores were analyzed, and their coarse grain anomalous events ages were determined using radiocarbon dating of foraminifera, gastropod and bivalves: P12, P17, P22 and P29 (460, 540, 320 and 280 mbsl). For some events, more than one anomalous events appear to coincide in time in different cores. We suggest that where anomalous events in different cores coincide in their age constraints – it is most likely evidence for mass flow triggered by earthquake events, driving coarse material from the shallower shelf edge into the deep basin (as opposed to sporadic slumping, or mass flow triggered by flashfloods). These anomalous events, observed in several cores from across the NGAE *(Fig. 5)*, serve as basis for the compilation of an earthquake record dating back to late Pleistocene. We discriminate between events validated in more than one core (high confidence level) and events that appear in one core (low level of confidence). In total, we count seven earthquake events (excluding the 1068 AD and the 1458 AD historically validated core events) of which four are of high-confidence level; one event is dated to ca 40ka, but could be of less confidence to to the limitations of the 14C dating method. Zilberman et al. (2005) suggest that 5 earthquakes ruptured the Avrona Playa between 14.2±0.3 and 3.7±0.3 ka, which conform with our marine core sediment dated events, as we identify an event ca 2.5 ka, and event ca 40 ka, and five events in a similar time range.

To conclude, we suggest that by correlating on-land and offshore paleoseismic observations, we have evidence for past earthquakes of the late Pleistocene and Holocene around 2.5, 3-3.3, 4.0-4.2, 5.8-6.3, 7.5, 14-14.5 and possibly an event around 40 ka BP. Some of these events may support evidence for past earthquakes suggested by previous authors.

Figure 3: (opposite) Trench T3 (north wall) log at the fault zone (E-W section). Seven distinct units demonstrate a maximum normal offset of ~43 cm; yellow hexagons mark 14C dating samples.

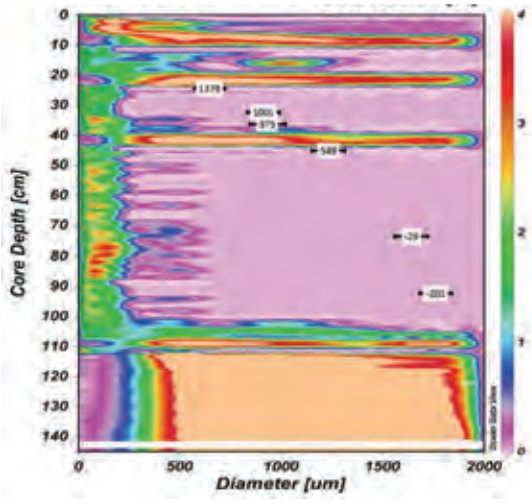

Figure 4: Grain size distribution (downcore spectrum of % volume per grain diameter) and 14C age determinations (cal BC/AD) of core P27 from the northern Gulf of Aqaba-Elat. 14C age calibrated using Calib 7.0 (Stuiver and Reimer, 1993) and Marine13 calibration curve (Reimer et al, 2013).

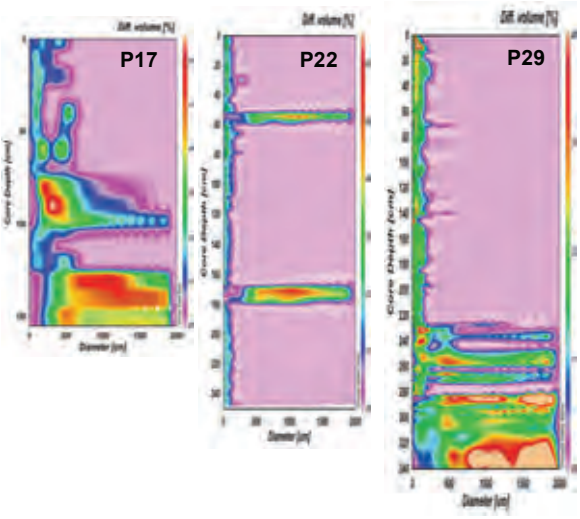

Figure 5: Grain size distribution spectra (downcore spectrum of % volume per grain diameter) of cores P17 (540 mbsl), P22 (316 mbsl) and P29 (282 mbsl) from the Northern Gulf of Aqaba-Elat; see Fig. 2 for core locations.

Acknowledgements: The project was funded by USAID-MERC project TA-MOU-08-M29-036. We wish to thank the people of the farming and plants staff of Kibbutz Eilot (Israel), and especially Rafi Saar, for their good will and kind assistance during trenching excavations in their farm lands. We thank many students from the University of Haifa for aiding in trenching field work and lab analysis.

References

Ambraseys, N.N., C.P. Melville and R.D. Adams, (1994). *The Seismicity of Egypt, Arabia and the Red Sea.* Cambridge University Press. 181 p.

Amit, R., E. Zilberman, Y. Enzel and N. Porat, (2002). Paleoseismic evidence for time dependency of seismic response on a fault system in the southern Arava Valley, Dead Sea rift, Israel. *Geological Society of America Bulletin*. v. 114, 192-206.

Avner, U., (1993). The history of the southern Negev and Elat in the light of new studies. In: *Elat-Man, Sea and Desert* (Cohen, M. and Shiler, E. eds). Ariel Press. Israel. 113-184.

Ben-Avraham, Z., (1985). Structural Framework of the Gulf of Elat (AQABA), Northern Red Sea. *J. Geophys. Res.* v. 90, 703-726.

Ben-Avraham, Z., G. Almagor, and Z. Garfunkel, (1979). Sediments and structure of the Gulf of Elat (Aqaba)-Northern Red Sea. *Sedimentary Geology*. v. 23, 239-267.

Ben-Avraham, Z., and G. Tibor, (1993). The northern edge of the Gulf of Elat. *Tectonophysics*. v. 226, 319-331.

Ben-Avraham Z., Z. Garfunkel and M. Lazar, (2008). Geology and Evolution of the Southern Dead Sea Fault with Emphasis on Subsurface Structure. *Annual Review of Earth and Planetary Sciences*. 36, 357-387.

Frieslander, U., (2000). The structure of the Dead Sea transform emphasizing the Arava, using new geophysical data. Ph.D. thesis. Hebrew University. Jerusalem.

Garfunkel, Z., I. Zak and R. Freund, (1981). Active faulting in the Dead Sea Rift. *Tectonophysics*. v. 80, 1-26.

Hartman, G., T.M. Niemi, G. Tibor, Z. Ben-Avraham, A. Al-Zoubi, Y. Makovsky, E. Akawwi, A.R. Abueladas and R. Al-Ruzouq, (2015). Quaternary tectonic evolution of the Northern Gulf of Aqaba/Elat along the Dead Sea Transform. *J. Geophys. Res. Solid Earth*. (in press).

Hartman, G., (2012). *Quaternary Evolution of a Transform Basin: The northern Gulf of Elat/Aqaba.* Ph.D. thesis. Tel Aviv University. Tel Aviv.

Klinger, Y., L. Rivera, H. Haessler and J.C. Maurin, (1999). Active faulting in the Gulf of Aqaba: New knowledge from the MW 7.3 earthquake of 22 November 1995. *Bulletin of the Seismological Society of America*. v. 89, 1025-1036.

Rotstein, Y., U. Frieslander and Y. Bartov, (1994). Detailed seismic imaging of the Dead Sea Transform. In: *Elat: Inst. Pet. Geophys.* 11.

Tibor, G., T.M. Niemi, Z. Ben-Avraham, A. Al-Zoubi, R. Sade, J.K. Hall, G. Hartman, E. Akawi, A. Abueladas and R. Al-Ruzouq, (2010). Active tectonic morphology and submarine deformation of the northern Gulf of Eilat/Aqaba from analyses of multibeam data. *Geo-Marine Letters. 30 (6), 561-573.*

Wachs, D. and E. Zilberman, (1994). Preliminary evaluation of the seismic hazard in the Elat area. *Geol. Surv. Israel Report 13/94*. 53 p. (Hebrew, English abstract).

Wust, H., (1997). The November 22, 1995 Nuweiba earthquake, Gulf of Elat (Aqaba): postseismic analysis of failure features and seismic hazard implications. *Geol. Surv. Israel.* Report GSI/3/1997.

Zilberman, E., R. Amit, N. Porat, Y. Enzel, and U. Avner, (2005). Surface ruptures induced by the devastating 1068 AD earthquake in the southern Arava valley, Dead Sea Rift, Israel. *Tectonophysics*. v. 408, no. 1-4, p. 79-99.

INQUA Focus Group on Paleoseismology and Active Tectonics

Off-fault damages to masonry buildings – a classification

Kázmér, M.

Department of Palaeontology, Eötvös University, Pázmány sétány 1/c, H-1117 Budapest, Hungary. E-mail: mkazmer@gmail.com

Abstract: *Rodríguez-Pascua and his team (2011, Quaternary International 242, 20-30) established a genetic classification of earthquake archaeological effects, of which building damages form the most significant part. A simple, descriptive system of earthquake-induced damages on masonry buildings is offered here, based on the shape of the damage and on whether it involves a single block, multiple blocks, a single wall, adjacent walls, or a whole building.*

Key words: *Archaeoseismology, buildings, masonry, classification.*

INTRODUCTION

Ever since man-made structures have been erected, earthquakes have left their marks on these constructions. The study of earthquake damage can contribute to multidisciplinary efforts to assess parameters of ancient earthquakes from archaeological evidence (archaeoseismology). Initially these studies were aimed at enriching earthquake catalogs; however, recent interest has been targeted to provide quantitative information on earthquake parameters and describe site effects (Galadini et al., 2006; Sintubin, 2011).

The fabric of the building (masonry, brick, rubble infill between retaining walls, built with or without mortar) needs to be thoroughly understood before any analysis of the archaeoseismological datum is undertaken (Rodríguez-Pascua et al., 2011). Each building material behaves differently under seismic loading; for example, dressed stone walls tend to be rather rigid, while rubble walls have limited elastic properties.

Following the seminal works of Karcz and Kafri (1978) and Stiros (1996), a multitude of studies have listed and illustrated supposed seismic-induced damage of ancient buildings, mostly from the Mediterranean. Korjenkov and Mazor (2003) and Marco (2008) discussed proven or supposed seismic origin of a rich variety of damage features, arranging them in groups of sliding and shifting blocks, fallen columns, chipped block corners, and fractured and deformed walls and floors.

Rodríguez-Pascua and his team (2011) established a comprehensive classification of earthquake archaeological effects, of which building damages form the most significant part. However, in-depth analysis, including physical or numerical modeling, is only available for just a few types of structural damage (shifted blocks: Vasconcelos et al., 2006; dropped keystone: Kamai and Hatzor, 2008; toppled columns: Hinzen, 2009; Yagoda-Biran and Hatzor, 2010; for a review, see Hinzen et al., 2011). Here a simple, descriptive system is used based on the shape of the damage and on whether it involves a single block, multiple blocks, a single wall, adjacent walls, or a whole building. This study views damaged masonry buildings from the engineer's perpective (Kázmér, 2014) and gives some relationships between the damages observed and the direction of the acting seismic load.

Damage affecting a single or multiple blocks

The vertical component of a seismic wave moves masonry blocks (ashlars or columns) rapidly up and down. The hammering effect of the upper block on the lower one yields cracks in either or both blocks (Fig. 1a). Penetrating cracks allow a chip, corner, or edge to be separated from the block (Fig. 1b). The direction of the crack is influenced by the lithology of the rock and shape of the block and by direction of hammering.

Fractures cutting through two or more blocks are often oriented close to vertical, this being the weakest plane to resist bending forces (Fig. 1c). Fractures through individual blocks are more or less connected to each other.

Damage affecting a single wall

Where blocks are arranged as walls, two categories of failure occur: *in-plane failures*, where loads act in the plane of the wall, and *out-of-plane failures*, where loads act at an angle to the wall's face.

The most common in-plane failures are *gaps* between shifted blocks (Fig. 1d), produced by lasting vibrations acting parallel to the wall. Cracks can develop across single or multiple blocks, even across whole walls. Brick walls display *diagonal cracks* near doors and windows. Masonry walls – dressed stones being significantly larger than bricks – generally do not display this feature.

Dropped keystones in arches are widely held to be the most reliable evidence of earthquake damage (Kamai and Hatzor, 2008) (Fig. 1e). These are formed during horizontal shaking, if there is no significant vertical load (i.e., when higher parts of the building have already collapsed). In multistory buildings, arches in upper floors get damaged, while lower floors do not exhibit damaged arches. Significant vertical loading tends to hold masonry blocks together through high friction at interfaces.

Figure 1: Typology of earthquake-induced damages in ancient buildings. ***A.*** *Cracks / fractures within a block (2nd century AD Palmyra theatre, Syria). Photo Kázmér #4281.* ***B.*** *Chipped edges of column and capital in the sixth-century Eufrasius cathedral, (Poreč, Croatia), damaged by the 1440 earthquake. #0080.* ***C.*** *Through-cutting fractures (repaired) in the 8-9th century Brahma temple of the Prambanan complex, Yogyakarta, Indonesia, caused by the 2006 earthquake. #6488.* ***D.*** *Horizontal shift of large ashlars; vertical joints opened up between them. Shiva temple, Prambanan complex, Yogyakarta, Indonesia. Tape measure extended 20 cm. #6498.* ***E.*** *Dropped ashlars in a Roman arch (Damascus, Syria). #2017.* ***F.*** *Broken lintels in 12th century al-Marqab citadel, coastal Syria. #4663.* ***G.*** *Clockwise rotated blocks in 12th century al-Marqab citadel, coastal Syria. #5168.* ***H.*** *Displaced drums of masonry columns of the 5th century BC Hephaisteion temple, Athens, Greece. #1132.* ***I.*** *Extruded portion of house wall. Bosra, Syria. #4183.*

Broken lintels (Fig. 1f) and *thresholds* occur widely. These features are not firm evidence for seismic shaking; similar effects can be produced also by differential deformation of walls due to inadequate foundation.

Common out-of-plane failures are rotated blocks (Fig. 1g), whose angle or rotation (clockwise or counter clockwise) reflects the direction of strong motion and the amount of friction between adjacent blocks.

Displaced drums in rows of masonry columns (Fig. 1h) are products of either in-plane or out-of plane seismic loads. Both shifting and rotation of drums occur. Historically, the observation of aligned, fallen monolithic columns has been used to infer the direction of ground movements during earthquakes. However, this interpretation can be misleading, since column alignment in fallen structures can also be produced by by other causes (Ambraseys, 2006); in particular several studies showed that the relation among the direction of fallen columns is not straightforward to deduce a reliable seismic source location (Hinzen, 2009).

Extruded blocks (Fig. 1i) indicate loads at a high angle to a wall. Displacement occurs along a more-or-less irregular pattern of masonry blocks (mostly without through going fractures), reflecting the failure of the wall core. Masonry maintains coherence during displacement, indicating that not the mortar between blocks but mortar between wall and core maintains wall integrity.

Figure 2: ***A.*** *Arcuate out-of-plane collapse in the market, Pompeii, Italy, repaired before the 79 AD eruption of Vesuvius, which buried the city. Photo: Kázmér #9266.* ***B.*** *Warped northern side of the Valens aqueduct (Istanbul, Turkey). Completed in 368 AD, several subsequent earthquakes left their traces on the massive construction #0340.* ***C.*** *V-shaped damage on the SW wall of the twelfth-century donjon of al-Marqab citadel, coastal Syria. The damage was inflicted by the 1202 earthquake (Kázmér and Major, 2010) #4589.* ***D.*** *Fallen masonry fence in the Roman city of Carnuntum (Deutsch-Altenburg, Austria) #5496.* ***E.*** *Triangular missing parts in corners of walls (al-Marqab citadel, coastal Syria) #4671.* ***F.*** *Deformed circular dome of fourth- to eleventh-century Samtavro cathedral, Mtskheta, Georgia #1633.* ***G.*** *Tilted Buddhist stupa (approximately fifteenth century) in Chiang Mai, Thailand. While a single tilted building does not indicate seismic origin, this stupa is one of 21 sites displaying tilting in the city (Kázmér et al. 2011) #3411.* ***H.*** *Buttresses support the pillars of the Valens aqueduct in Istanbul, Turkey, completed in 368 AD #0335. I. Valens aqueduct in Istanbul, completed in 368 AD. A brick arch was built to support the weakened stone arch after one of the frequent earthquakes in the region (Istanbul, Turkey) #0335.*

The *arcuate collapse* of walls (Fig. 2a) is sign of loads acting at high angle to a wall that is confined (fixed) at both ends. Wall terminations (usually supported by cross walls) maintain their full elevation, while the free-standing middle part loses coherence and collapses during heavy vibration.

A *warped wall* is produced by out-of-plane loads acting at high angle to the wall (Fig. 2b). Warping can be to one or both sides. Thick walls made of Roman concrete can behave this way, while thin walls collapse in arcuate form (Fig. 2a). Generally, there is no change of wall geometry at foundation level.

A *V-shaped extrusion* near the top of a cylindrical building (Fig. 2c) indicates strong motion in the direction of extrusion.

Fallen walls lying on the ground are more-or-less preserving original coherence (Fig. 2d). A seismic load

acting at a high angle to a wall can cause simultaneous collapse along the full length of the structure.

DAMAGE AFFECTING ADJACENT WALLS

Triangular collapses in the corners of walls (Fig. 2e) are due to differential loading of perpendicular walls. Shaking in different directions at the same time shears off the masonry joints, allowing collapse of the weakened corner.

Simple *deformed geometrical structures* (rectangular to parallelogram, circular to elliptical, etc.) (Fig. 2f). These features are hard to recognize, since deformations are subtle: parallels and right angles deviate a few degrees only (higher deformation would yield total collapse).

WHOLE BUILDINGS

Tilted buildings are signs of uneven loading of subsoil (Fig. 2g). When seismic vibrations act on water-saturated soil, it loses coherence and behaves like a fluid. Building foundations - losing support during liquefaction events - suffer differential settlement, tilting, and collapse. Traces of total failure are mostly removed, but minor tilting - not affecting the use of the building - is often left unrepaired.

Very rarely a building - if built across an active fault - is sheared by fault movement. The displaced walls indicate the sense and cumulative offset of the fault since construction time. Walls are either displaced along a single fault (i.e., Vadum Iacob crusader tower, Israel: Ellenblum et al., 1998) or along a splay of faults, where the building maintains integrity, but the floor plan gets deformed (i.e., St. Simeon monastery, Syria: Karakhanian et al., 2008).

REPAIRS

Ruins of completely collapsed buildings are usually removed after an earthquake. Moderate damages are repaired on the spot, and additions, new walls, *buttresses* (Fig. 2h), *reinforced arches* (Fig. 2i), and other *supporting structures* can be identified as evidence of past earthquakes. Repairs are often built of different, often inferior material (Fig. 2i: brick arc supporting a stone arch), poorly fitted to masonry patterns, obstructing windows - these are features of repair following structural damage.

Study of damaged ancient buildings is a major source of evidence for past earthquakes: various seismic parameters (e.g., date, intensity, strong motion direction) can be assessed from a careful, critical study.

SUMMARY

Features to aid in the identification of seismic damage to ancient masonry buildings are briefly described and arranged in a simple, descriptive system. Deformations are arranged into groups affecting single and multiple blocks of dressed masonry, single walls, adjacent walls, and whole buildings. Their recognition and distinction from other types of damage (by aging, warfare, poor construction, etc.) need thorough and systematic study but provide much needed data on past earthquakes.

References

Ambraseys, N.N., (2006). Earthquakes and archaeology. *Journal of Archaeological Science*. 33, 1008-1016.

Ellenblum, R., S. Marco, A. Agnon, T. Rockwell, A. Boas, (1998). Crusader castle torn apart by earthquake at dawn, 20 May 1202. *Geology*. 26, 303-306.

Galadini, F., K.G. Hinzen, S. Stiros, (2006). Archaeoseismology: methodological issues and procedure. *Journal of Seismology*. 10, 395-414.

Hinzen, K.G., (2009). Simulation of toppling columns in archaeoseismology. *Bulletin of the Seismological Society of America*. 99, 2855-2875.

Hinzen, K.G., C. Fleischer, S.K. Reamer, S. Schreiber, S. Schütte, B. Yerli, (2011). Quantitative methods in archaeoseismology. *Quaternary International*. 242, 31-41.

Kamai, R., Y.H. Hatzor, (2008). Numerical analysis of block stone displacements in ancient masonry structures: a new method to estimate historic ground motions. *Int. J. Numerical and Analytical Methods in Geomechanics*. 32, 1321-1340.

Karakhanian, A.S., V.G. Trifonov, T.P. Ivanova, A. Avagyan, M. Rukieh, H. Minini, A.E. Dodonov, D.M. Bachmanov, (2008). Seismic deformation in the St. Simeon monasteries (Qal'at Sim'an), northwestern Syria. *Tectonophysics*. 453, 122-147.

Karcz, I., U. Kafri, (1978). Evaluation of supposed archaeoseismic damage in Israel. *Journal of Archaeological Science*. 5, 237-253.

Kázmér, M., (2014). Damages to ancient buildings from earthquakes. In: (Beer, M., Patelli, E., Kouigioumtzoglou, I., Au, I.S.K., eds). *Encyclopedia of Earthquake Engineering*. Springer. Berlin. 7 p., 18 figs. doi: 10.1007/978-3-642-36197-5_30-1.

Kázmér, M., B. Major, (2010). Distinguishing damages of two earthquakes – archeoseismology of a Crusader castle (Al-Marqab citadel, Syria). In: (Stewart, I., Sintubin, M., Niemi, T., Altunel, E. eds). *Ancient Earthquakes*. GSA Special Paper. 471. Geological Society of America. pp. 186-199.

Kázmér, M., K. Sanittham, P. Charusiri, S. Pailoplee, (2011). Archaeoseismology of the AD 1545 earthquake in Chiang Mai, Thailand. In: *Earthquake geology and archaeology: science, society and critical facilities. 2nd INQUA-IGCP 567 international workshop on active tectonics, earthquake geology, archaeology and engineering*. Corinth. 19-24 Sept. 2011. *Proceedings vol 2*. pp 102-105.

Korjenkov, A.M., E. Mazor, (2003). Archeoseismology in Mamshit (Southern Israel): cracking a millennium-old code of earthquakes preserved in ancient ruins. *Archaeologischer Anzeiger*. 2003, (2), 51-82.

Marco, S., (2008). Recognition of earthquake-related damage in archaeological sites: examples from the Dead Sea fault zone. *Tectonophysics*. 453, 148-156.

Rodríguez-Pascua, M.A., R. Pérez-López, J.L. Giner-Robles, V.H. Garduño-Monroy, (2011). A comprehensive classification of Earthquake Archaeological Effects (EAE) in archaeoseismology: application to ancient remains of Roman and Mesoamerican cultures. *Quat. Int.* 242, 20-30.

Sintubin, M. (2011). Archaeoseismology: past, present and future. *Quaternary International.* 242, 4-10.

Vasconcelos, G., P.B. Lourenço, H. Mouzakis, L. Karapitta, (2006). Experimental investigations on dry stone masonry walls. In: *1st international conference on restoration of heritage masonry structures*. Cairo, 24-27 Apr 2006, pp P31-1/P31-10.

Yagoda-Biran G., Y.H. Hatzor, (2010). Constraining paleo-PGA values by numerical analysis of overturned columns. *Earthquake Engineering and Structural Dynamics.* 39, 463-472.

INQUA Focus Group on Paleoseismology and Active Tectonics

Earthquake-induced deformations at the Lion Gate, Mycenae, Greece

Kázmér, M. (1), Kolaiti, E. (2)

(1) Department of Palaeontology, Eötvös University, Pázmány sétány 1/c, H-1117 Budapest, Hungary. E-mail: mkazmer@gmail.com
(2) Athens, 16-18, Kefallinias str., Gr-11521 Chalandri, Athens, Greece. E-mail: kolaitieleni@gmail.com

Abstract: *One of the most famous monuments of Mediterranean antiquity, the Lion Gate of the citadel in Mycenae, Argolis, Greece, shows damage, including shifted, rotated, broken, and fallen masonry, and also fractures in the famous lion relief which might be of seismogenic origin. The damage occurred after the peak of Mycenaen rule (after the middle of the 13th century BC). In case of seismic origin, the damage corresponds to intensity VIII. Local faults are potential sources of damaging erathquakes and further research is necessary to test the hypothesis.*

Key words: *Antiquity, archaeoseismology, Mycenae, Greece.*

INTRODUCTION

Mycenae is a mountain citadel that commands the broad Argolis basin, part of the Peloponnesos Peninsula in southern Greece. Homer tells us that Agamemnon set out from here to lead the Greeks to the Trojan war (Korfmann, 2004).

Elisabeth French (1996) was the first to consider the possibility of seismic damage in the destruction of the citadel of Mycenae. However, the Lion Gate, thought to be built shortly before the calamity described by her, was considered as counter-evidence for an earthquake, surviving the collapse event intact (French, 1996: 54). For a historical overview of the development of opposing ideas see Nur & Cline (2000) and Nur & Burgess (2008).

Archaeological excavations discovered houses with skeletons covered with fallen stones (Shear, 1987, Mylonas 1975a & b). In these buildings and elsewhere in the citadel a horizon of destruction was identified and dated to the middle of the LH IIIB period (Taylour, 1981). Interpretation derived from recent excavations directed by Maggidis (2011) operates with the role of seismic activity in the destruction of Mycenae.

There is a planar rock surface next to the entrance to the citadel, at the Lion Gate. It has suffered only minor erosion, indicating it is an active, i.e. Holocene fault (Stewart & Hancock, 1988). There are further active fault planes within a few hundred metres distance. Solid, cyclopean walls are built on top of the fault; these are symbols of inactivity since the time of construction (Sintubin, 2011, his fig. 5a). However, a serious contradiction remains: the citadel has been damaged repeatedly (e.g. Nur & Burgess, 2008, 11-20, 26, his fig. 1.2), while the Lion Gate and surroundings – built shortly before the destructive events – apparently do not show any seismic record.

In this paper we put the hypothesis that at least one strong earthquake damaged the Lion Gate and the adjoining wall.

This paper is an effort to inventory and catalogue specific earthquake archaeological effects as suggested by Rodríguez-Pascua et al. (2011).

Figure 1: Mycenae, the Lion Gate before excavations and restoration (Tsountas 1893, fig. 3). The famous fault plane – which did not move for at least 3000 years – is on the lower left. Note the missing two ashlars right of the lion relief. The dressed exterior and rubble interior of the western wall on the right was still visible at that time.

During repeated field trips we identified and surveyed structural failures visible in the forecourt of the Lion Gate. Those attributable to earthquakes are described, illustrated, and explained here. Measuring tape, clinometer, and a laser distance meter were used for the survey. In absence of direct access, high-resolution photographs were used for detailed observation of the lion relief.

RESULTS

Masonry. The walls of the forecourt are made of well-dressed ashlars of Pliocene conglomerate. Size is up to 80 cm high and longer than 1 m. Thickness of ashlars cannot be seen.

Inner structure of the western wall cannot be observed today. However, a photo of Tsountas (1893, 1897, his fig. 3, our Fig. 1) exposes the inner structure: there is a mantle of elaborately carved ashlars surrounding

irregular blocks of the core. There is no mortar between the dressed stones.

Figure 2: The western wall in the forecourt of the Lion Gate. There are eight rows of well-dressed ashlars, obviously not in the same plane. Top of the long wall is 6.85 m above ground level. People for scale. Photo Kázmér, #1097.

Shifted and/or rotated ashlars. The western wall certainly has been built planar: the Lion Gate was the main access road to the citadel of Mycenae, of high royal and religious significance. Today the wall is not planar anymore. Its well-dressed ashlars are not parallel with the surface of the wall (Fig. 2): some are rotated, both clockwise and counterclockwise, up to 10° around a vertical axis relative to each other. Several centimetres of relative displacement between blocks can be easily measured (Fig. 3). There is no obvious pattern among the direction and amount of displacements, except that blocks on top suffered more shift than blocks in the bottom row.
Rodriguez-Pascua et al. (2011) ranges similar blocks among clear evidences of earthquake shaking.

Fallen ashlars. Schliemann (1878) recorded a less complete Lion Gate than it is today. His Plate III shows random fallen ashlars, partly blocking the road. One missing ashlar to the left of the relief is not a window but place of a fallen block (Wace, 1949: 52). Those two ashlars, which are obviously missing to the right of the relief, are lying on the road (Fig. 1). All three have been restored to their original position by the Athens Archaeological Society in 1950 (Mylonas, 1957: 25).
Further ashlars on the road (as variously illustrated on an etching by Schliemann, 1878, his plate III) and by Tsountas (1893, 1897) on a photo are probably from the top rows of the western wall on the left. The single ashlar in row A on the top of the western wall is witness of a wall higher than today.

Repairs. There are small, irregular pieces of light-coloured limestone, stuffed in the wide gaps between the rotated ashlars. These pieces are undressed without exception.

Fractured lion relief. Above the lintel of the gate there is a monolithic block: two lions and a column are sculpted on the external surface. The lion heads – made of different material – are missing (Mylonas, 1957: 25). The dowel holes of the fixtures are still visible. The front of the relief is clean and the texture is obvious; it has been cleaned probably not later than the restoration work in 1950 (Fig. 4).
The front is criss-crossed by narrow, open fractures, directed from upper right to lower left (Fig. 4). Some of the fractures do not extend from margin to margin; they tend to terminate within the relief block.
There are two missing blocks to the right of the relief (Schliemann, 1878). We hypothesize that while still shaking on top of the wall or when falling from the top – possibly due to an earthquake – either or both of them hit the triangular block of the relief. This sudden (probably repeated) collision initiated the fractures within the block. The fracture pattern is typical of shearing stress, exerted by the blocks hitting the relief at their respective elevation.

Figure 3: Displaced ashlars as seen from below. Blocks of rows 6 and 7 suffered opposite rotation. Blocks on the right suffered 6 cm right-lateral displacement. There are undressed limestone pieces stuffed in the wide gap between adjacent blocks. #1103.

Subsoil. Most of the subsoil below the Lion Gate is soft rock – which, among others, allowed the digging of the famous royal Shaft Graves where most of the treasures of Mycenae have been found. An exception is the portion under the eastern wall, where the foundation rests on hard Mesozoic limestone (Wace, 1950: 204), of which most of the Citadel is composed. The surface separating them is an active fault plane (Stewart & Hancock, 1988).
It is common that buildings and other constructions erected upon softer soil suffer greater damage than those built upon hard rock. (Mention the well-known example of the Colosseum in Rome: Funiciello et al., 1995.) Here we see more damage in the western wall built on soft subsoil than on the eastern wall built on hard Mesozoic limestone.

Constraints on dating. The construction of the Lion Gate and the cyclopean walls to the south and west occurred in Late Helladic IIIB times, i.e. between 1300 and 1200 B.C, and late rather than early within these limits (Mylonas, 1957: 34). The other cyclopean walls to the east can be contemporary, later or earlier than the Lion Gate.
The damage certainly occurred after the peak of the Mycenaean rule by one or more earthquakes. Surface of the shifted blocks could have been carved flat again with minimal cost. Instead, rotated blocks were left unchanged, and the gaps opened during the earthquake were filled by poorly concealed limestone rubble at some later time.

DISCUSSION

In this paper we put the hypothesis that at least one strong earthquake damaged the Lion Gate and the adjoining wall.
Rotated and displaced masonry blocks (Figs 2-3) are often taken as telling records of earthquake shaking (Rodriguez-Pascua et al., 2011). Pervasive fractures (Fig. 4) are also clear records of major stress exerted on the monolith. The relief block is cross-cut by oblique fractures, never from margin to margin, but often terminating inside the block (Fig. 4). A transient shear stress, exercised by the hit of the upper two blocks while falling from the wall into the forecourt, is suggested to produce the fractures within the stressed relief block.
What we can assess is the intensity, characterizing the maximum shaking at this place during the last three millennia (Sintubin, 2011).

Earthquake parameters - Date. Direct dating of this earthquake is not possible at the moment. However, more than a century of archaeological excavation in the citadel of Mycenae established a detailed chronology of construction and destruction.
At Mycenae, successive repairs and modifications define at least two major LH IIIB destruction horizons: one in the transition of LH IIIB1/B2 (ca. 1240 BC) and another one towards the end of LH IIIB2 (ca. 1200/1180 BC). The former, which is defined by a number of contemporary destruction layers all linked by qualitative and quantitative association (i.e. containing groups of identical vases), was apparently caused by severe earthquakes, as indicated by the type and extent of structural damage (collapsed buildings, walls curved or shifted off from their foundations), by the spatial distribution of partial and total damage inside and outside the citadel, cases of human victims buried under collapsed debris (Panagia I, Plakes), abandonment and repairs (Maggidis, 2011).

Intensity. Rapp (1986) assigned an intensity of VIII to 'considerable damage in ordinary substantial buildings' - 'some masonry walls fall'. His intensity IX is described as 'buildings shifted off foundations'.
Modified Mercalli intensity VII is widely held as the damage threshold for many archaeological sites (Kovach and Nur, 2006). Bilham et al. (2010) described displacement of heavy masonry blocks in the Pandrethan Shiva temple, related to a minimum intensity of VII and maximum intensity of IX on the MSK scale. We suggest a minimum intensity VIII for the Lion Gate earthquake.

Figure 4: The lion relief. The monolith is 3.9 m wide, 3.3 m high and up to 0.7 m thick. A network of open fractures (marked by thin lines) across the relief is interpreted as caused by the hit of the two ashlars on the upper right side during seismic shaking. These two blocks fell to the ground and were still there in the 19th century as shown in Fig. 1. Apparent lack of continuity of the fracture on both sides of the half-column is due to thin, dark crust produced by blue-green algae. #1095.

Whether the damage observed on the Lion Gate complex is related in any way to the suspect active normal fault of Mycenaean age E and SE of the citadel (Maroukian et al. 1996) cannot be answered at this moment. A proposed seismological revision of the destruction horizons in the citadel will bring us closer to the right answer to this question.
This is a first attempt for an interpretation of probably Mycenaean seismic activity in terms of earthquake parameters. A detailed study of the Lion Gate, involving modelling, a thorough revision of destruction horizons within the citadel is a matter of future research. Quantitatively assessing the site-specific effects on any archaeological site (e.g. Kamai & Hatzor, 2008) we can narrow down earthquake parameters associated to the maximum credible earthquake in the region, irrespective to the time of occurrence (Sintubin, 2011).

CONCLUSIONS

We put the hypothesis that the Lion Gate in the citadel of Mycaneae, Greece, suffered damage from an earthquake. Shifted, rotated, fractured, and fallen ashlars, and open fractures within the lion relief are possible indicators of seismic shaking. In case of seismic origin, the damage corresponds to intensity VIII. The famous active fault underlying the gate did not move, but another fault nearby probably did. Further research is suggested to test this hypothesis.

Acknowledgements: Thanks for permission to study the site to the General Direction of Antiquities of the Ministry of Culture, Greece, and to the Ephorate of Prehistorical and Classical Antiquities, Nauplion. Our thanks are due to the staff of the library of the British School of Archaeology in Athens. Financial help from Hungarian National Science Foundation (OTKA) grant K 67.583 and an IGCP 567 travel grant are sincerely acknowledged here. Advices of P. Figueiredo, A Hipólito, K. Reicherter in the field and comments of an anonymous reviewer greatly improved the manuscript.

References

Bilham, R., B.S. Bali, M.I. Bhat, S. Hough, (2010). Historical earthquakes in Srinagar, Kashmir: clues from the Shiva temple at Pandrethan. In: (Stewart, I., Sintubin, M., Niemi, T. & Altunel, E., eds). *Ancient Earthquakes*. Geological Society of America. Special Paper. 471, 107-117.

French, E.B., (1996). Evidence for an earthquake at Mycenae. In: (Stiros, S. & Jones, R.E., eds). *Archaeoseismology*. Fitch Laboratory. Occasional Paper. 7, 51-54. Athens.

Funiciello, R., L. Lombardi, F. Marra, M. Parotto, (1995). Seismic damage and geological heterogeneity in Rome's Solosseum area: are the related? *Annali di Geofisica.* 38, 927-937.

Kamai, R., Y.H. Hatzor, (2008). Numerical analysis of block stone displacements in ancient masonry structures: a new method to estimate historic ground motions. *Journal of Numerical and Analytical Methods in Geomechanics.* 32, 1321-1340.

Korfmann, M., (2004). Was there a Trojan War? *Archaeology.* 57 (3), www.archaeology.org/0405/etc/troy.html. Accessed 23 October 2011.

Kovach, R.L., A. Nur, (2006). Earthquakes and archeology: Neocatastrophism or science? *Eos (Transactions, American Geophysical Union).* 87 (32), 317. doi: 10.1029/2006EO320003.

Maggidis, Ch., (2011). *Citadel excavation. Building K (2002-2008).* http://mycenae-excavations.org/citadel.html. (23-10-2011).

Maroukian, H., K. Gaki-Papanastassiou & D. Papanastassiou, (1996). Geomophologic-seismotectonic observations in relation to the catastrophes at Mycenae. In: (Stiros, S. & Jones, R.E., eds). *Archaeoseismology*. Fitch Laboratory. Occasional Paper. 7, 189-194. Athens.

Mylonas, G.E., (1957). *Ancient Mycenae. The Capital City of Agamemnon.* Routledge & Kegan Paul, London, vii + 231 p.

Mylonas, G.E., (1975a). Mycenae. In: *Ergo Archaiologikis Etairias.* 95-111. (in Greek).

Mylonas, G.E., (1975b). Excavations at Mycenae. *Praktika Archaiologikis Etairias*. pp. 158-161. (in Greek).

Nur, A. & D. Burgess, (2008). *Apocalypse. Earthquakes, Archaeology, and the Wrath of God.* Princeton University Press. Princeton. xii + 304 p.

Nur, A., E.H. Cline, (2000). Poseidon's horses: plate tectonics and earthquake storms in the Late Bronze Age Aegean and Eastern Mediterranean. *Journal of Archaeological Science.* 27, 43-63.

Rapp, G. Jr., (1986). Assessing archeological evidence for seismic catastrophies. *Geoarchaeology*.1 (4), 365-379.

Rodríguez-Pascua, M.A., R. Pérez-López, J.L. Giner-Robles, P.G. Silva, V.H. Garduño-Monroy, K. Reicherter, (2011). A comprehensive classification of Earthquake Archaeological Effects (EAE) in archaeoseismology: Application to ancient remains of Roman and Mesoamerican cultures. *Quaternary International.* 242, 20-30.

Schliemann, H., (1878). *Mycenae*. Murray, London.

Shear, I.M., (1987). *The Panagia Houses at Mycenae*. Philadelphia University. Museum Monograph 68. University of Pennsylvania. Philadelphia.

Sintubin, M., (2011). Archaeoseismology: past, present and future. *Quaternary International.* 242, 4-10.

Stewart, I.S., P.L. Hancock, (1988). Normal fault zone evolution and fault scarp degradation in the Aegean region. *Basin Research*. 1, 139-153.

Taylour, W.D., (1981). *Well Built Mycenae. The Helleno-British Excavations within the Citadel at Mycenae 1959-1969*. Fascicule 1. The Excavations. Aris & Phillips. Warminster.

Tsountas, Ch., (1893). *Mykenai, kai mykinaios politismos*. The Estias. Athinai. 264 p. (in Greek).

Tsountas, Ch., (1897). *The Mycenean Age*. Boston. 417 p.

Wace, A.J.B., (1949). *Mycenae. An Archaeological History and Guide.* Princeton University Press. Princeton, New Jersey. xviii + 150 p. + 111 photographic plates.

Wace, A.J.B., (1950). Excavations at Mycenae, 1939. *The Annual of the British School at Athens*. 45, 203-228.

INQUA Focus Group on Paleoseismology and Active Tectonics

Identification of the Quaternary Geundeok Fault based on a sequence of Paleoseismological investigations in Samcheok, Korea

Kim, Y.S. (1), Choi, J.H. (2)

(1) Dept. of Earth & Environmental Sciences, Pukyong National University, Busan 608-737, South Korea. Email: ysk7909@pknu.ac.kr
(2) Institut de Physique de Globe de Paris, 75005 Paris, France

Abstract: *The eastern part of the Korean Peninsula is one of the hard-to-work-in regions for paleoseismological study due to fundamental reasons, such as low slip-rate faults and long recurrence interval of large earthquake, as well as climatic factors, such as high erosion-rate and dense vegetation cover. Nevertheless, a Quaternary Geundeok Fault has been recently identified based on a sequence of paleoseismic investigations in Samcheok, Korea. This paper displays each investigation in a variety of scales: 1) a short review of regional-scale active tectonics, 2) local-scale investigations such as geomorphic analysis and field observations, and 3) detailed geometric and kinematic characteristics of the fault as well as its Quaternary slip events based on trench survey. The results indicate that the Geundeok Fault has been evolved over different tectonic settings and up to the current stress regime, and hence a series of our investigations may provide a good case study emphasing the importance of careful recognition and interpretation of paleoseismic features.*

Key words: *Fault identification, Paleoseismology, Geomorphic marker, Lineament, Quaternary fault.*

INTRODUCTION

The most obvious evidence of past earthquakes is the geomorphic and stratigraphic expressions of paleo-seismic displacement, and these generally include prehistoric large earthquakes as well as historical and instrumental records of seismicity (e.g., McCalpin, 2009). In some regions, however, it is still a big challenge to conduct paleo-seismological study with sufficient geomorphic data because of tectonic and/or climatic factors; e.g., low slip-late of active faults and high erosion-rate. Note that one of the critical ingredients of geomorphic markers is the high preservation potential with respect to the time scale of tectonic process being studied.

The above-mentioned limits of the paleo-seismological approach apply in the Korean Peninsula (Fig.1). Although the Korean Peninsula is commonly considered to be an intraplate region with low seismicity, there have been many reports for the potential of large earthquake such as historical records (240 earthquake events with seismic intensity greater than or equal to Mercalli intensity (MMI) VI during AD 2-1904) and instrumental seismicity (6 earthquake events with magnitude greater than or equal to 5.0 in the last 40 years) (e.g., Lee and Yang, 2006; Houng and Hong, 2013). Therefore, it is more necessary to advance in the study of active faults and related earthquake hazards based on a well-built research process and database of past large earthquakes.

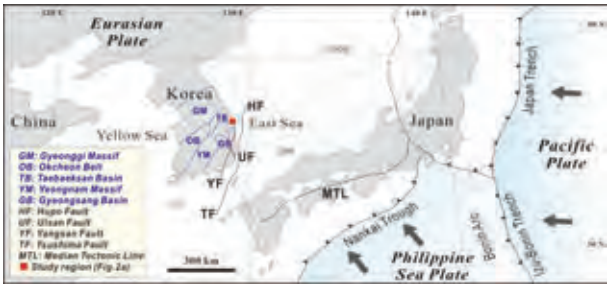

Figure 1: Simplified tectonic map around the study eastern Korea (modified from Kim and Park, 2006).

In this study, a Quaternary fault is newly identified based on an ideal sequence of paleoseismic investigations in Samcheok, Korea. This study provides not only the quantitative data useful for further discussion of active tectonics in Korean Peninsula but also the importance of recognition the direct and indirect evidences of paleoearthquakes.

STUDY REGION & LINEAMENT ANALYSIS (REGIONAL-SCALE)

Study region is the northeastern part of the Precambrian Yeongnam Massif which is mainly composed of metamorphic rocks. Recent studies of the active tectonics in the eastern coastal region indicate that 1) Cenozoic tectonic deformation is mainly associated with the NNE-SSW trending faults which have been slipped during opening and closing of the East Sea (e.g., Yoon and Chough, 1995; Kim and Park, 2006), and 2) since the Pliocene, stress field changed to E-W or ENE-WSW compression (e.g., Jun and Jeon, 2010) and the prevailing kinematic on pre-existing faults with dominant strike-slip and minor reverse-slip component. A main structural feature in the study region is the Osipcheon Fault showing NNE-SSW trending strike (Fig. 2a), and the study of its fault history imply that it has underwent at least three different movement stages; normal, thrust and strike-slip kinematics, according to relative chronological age (Kim et al., 2000).

Figure 2a shows the distribution of lineaments around the study area in regional-scale, which is mapped based on a satellite image available in Google Earth and DEM. One of the most interesting points is that a major

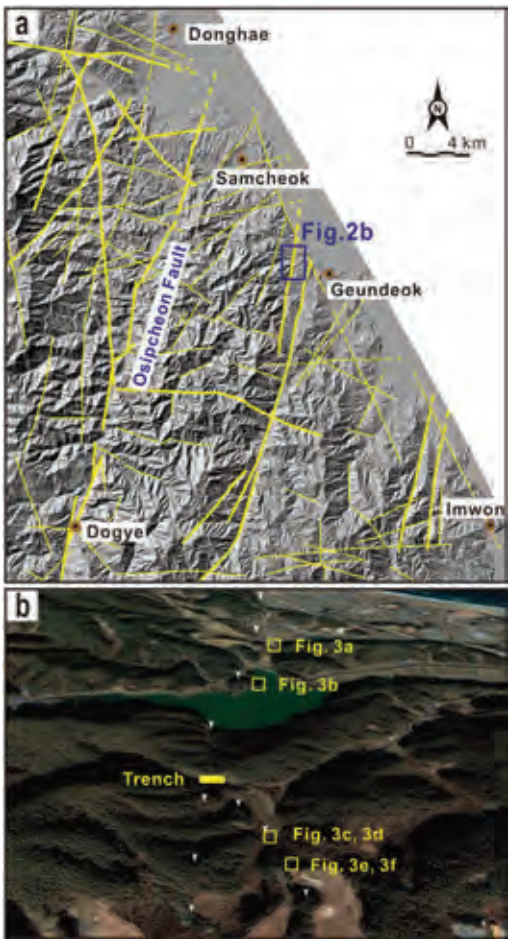

Figure 2: (a) A regional-scale lineament map around the study area. (b) A satellite image of the inferred fault trace.

lineament related to the Osipcheon Fault shows geometrically a zigzag pattern, whereas some of the NNE-SSW trending lineaments are characterized by more straight and sharp pattern which could reflect more young tectonic deformation and/or recent fault activity. Such two vivid lineaments are obviously detected at the western part of Geundeok area, and also there are Quaternary sediment deposits around their northern parts. In this study, therefore, we focused on these two inferred structures.

GEOMORPHIC EVIDENCES & FIELD INSPECTION (LOCAL-SCALE)

To confirm the existence of a fault, topographic features are investigated in field around the northern part of the inferred fault trace (Fig. 3). The collected geomorphic and hydrologic features strongly indicate the general characteristics of fault zones. Firstly, minor fault gouges with a few millimeters of width are observed in densely fractured and highly weathered rocks along the lineament (Fig. 3a). This may indicate a fault damage

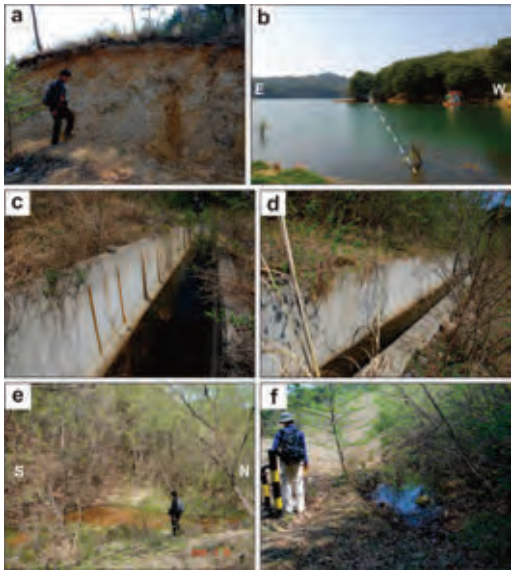

Figure 3: Fault-related topographic features along the inferred fault trace based on the filed observations. (a) Fault damage zones composed of minor slip surfaces and dense fractures. (b) Turtle-neck-shaped morphology. (c, d) Different water seepages along the fault-cross artificial drainage map. (e, f) A series of sag ponds formed by elongate depressions along the inferred fault trace.

zone composed of subsidiary structures, which is commonly developed around the fault core, characterized by a high permeability (e.g., Caine et al., 1996). The fault trace is also supported by a series of disturbed E-W trending minor streams and mountain ridges (Fig. 2b). These linear features are terminated and/or curved at the intersection points with the lineament. An excellent example in this area is a small island at the northern part of the reservoir (Fig. 3b), where the turtle-neck-shape is clearly matched with the trace of the inferred fault. One of the other interesting features is a gourd shape of the reservoir, where the neck is located at the intersection between the E-W trending valley and the lineament (Fig. 2b). This morphological feature results from differential permeability and/or erosion rate between fault zone (lineament) and undeformed basement-rock. Another interesting feature along the fault trace is water leakage pattern observed along an artificial drainage, which shows clear difference of fluid flow characteristics across the lineament (Fig. 3c, 3d). The whitish walls of the drainage were partly discolored by water leakage at only a section where it traverses the lineament. Moreover, a series of sag ponds are continuously aligned along the lineament, even in mountainous hillsides (Fig. 3e, 3f). Each sag pond is characterized by an elongate depression with nearly N-S trending long axis, which is a well-known main feature along faults (e.g., McCalpin, 2009; Zielke et al., 2015).

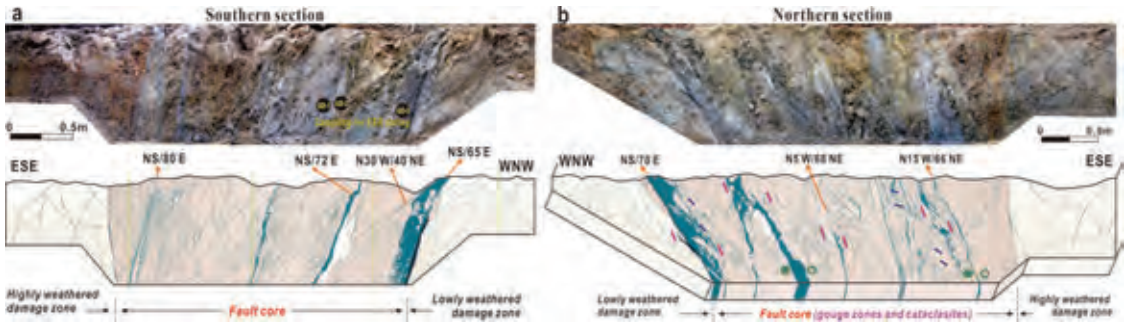

Figure 4: The identification of the Geundeok Fault in the first trench excavation. The geometric and kinematic analyses indicate that the fault underwent multiple slip events with various slip senses.

TRENCH SURVEY (SITE-SCALE)

In general, the site-investigation can be performed by drilling, geophysical prospecting, and trench survey. The latest one is a key process to examine fault activity in paleoseismological researches because recent fault history can be examined on the basis of offsets and ages of young sediments. In this study, the trench survey was carried out at the southern part of the reservoir where fluvial sediments were deposited across the inferred fault (Fig. 2b).

1st excavation: identifying fault

About 10 m long trench was excavated, perpendicular to the inferred fault, to confirm the existence of the fault. About 2.5 m wide fault core and surrounding damage zones are exposed from the trench, and herein the fault is named as Geundeok Fault (Fig. 4). The fault core is composed of multiple slip surfaces, which are generally characterized by N-S trending strike and high angle east-dipping.

On the southern wall (Fig. 4a), the fault core is composed of numerous fault gouge zones and cataclastic rocks, which display various colors and thicknesses. The whitish (or light) gouge zones show relatively irregular geometry whereas grey (or dark) ones are characterized by sharp boundaries. In the westernmost part of the fault core, the thickest grey gouge zone includes numerous fractured rock pebbles, and also a blackish gouge zone is sharply developed at the boundary between the fault core and footwall damage zone. The variations in color, thickness, and geometry of each gouge zone imply that the fault underwent multiple slip events.

The above mentioned geometric characteristics are also visible on the northern wall and floor surface in trench (Fig. 4b). Also, there are several kinematic indicators such as slip lineations and shear fabrics. In the vertical section, slickenlines with sub-vertical rake (or pitch) and shear fabrics, showing dominantly normal slip but partly reverse slip senses, imply that this fault underwent multiple dip-slip events. On the other hand, in the floor surface, sub-horizontal slickenlines and shear fabrics indicate right-lateral movement along the fault. Two different sets of slickenlines are an obvious evidence of different deformation stages, and these geometric and

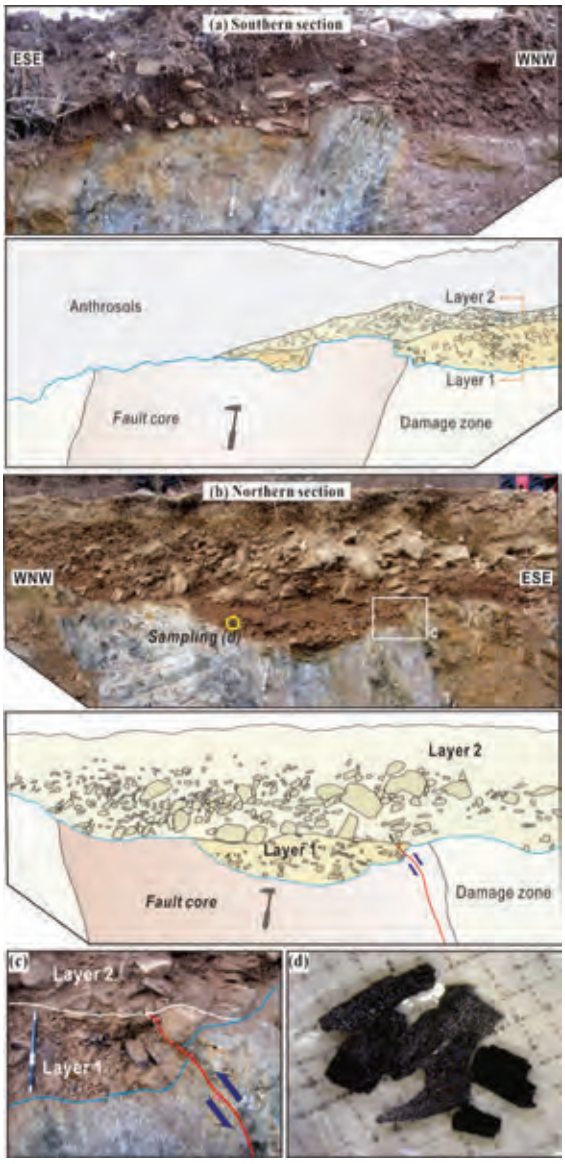

Figure 5: (a, b) Photos and sketches of the both trench walls. (c) A detailed view of the fault contact showing reverse separation. (d) Charcoals for radiocarbon dating analysis sampled in the lower layer-1, and the result indicates AD 165 (± 30).

kinematic complexities may be largely attributed to the multiple slip events under different stress regimes.

2nd excavation: paleoseismological approaches

The first excavation of about 3m width was extended to observe the contact between the fault core and its above young sediments (Fig. 5). In the trench, fluvial deposits with two separated layers cover the fault zone on both trench walls: the older layer (L-1) and the younger layer (L-2) are divided by the erosional surface between them. Here, we mainly describe contact relations between slip surfaces within the fault core and the L-1 sediment.

On the southern wall (Fig. 5a), the L-1 is mainly observed at the western part (footwall side) of the fault zone and partly observed as a wedge-shaped pocket above the fault core. Wedge-shaped sediments around slip surfaces have commonly been considered as a key evidence of surface rupture associated with paleoearthquakes. However, there are no visible secondary structures related with earthquake slip in the sediments. Therefore, the possible origin of the wedge-shaped sediments could be interpreted as a result of differential erosion around the fault zone.

Contact relationships between the fault zone and the young sediments are more clearly observed on the northern wall (Fig. 5b). The L-1 is characterized by a dish-shaped deposition, which is commonly considered as a frontal section of paleo-channels, and only developed at the eastern part of the fault core. The upper boundary of the L-1 layer is sub-horizontal and its altitude is almost similar with the unconformity between basement rock and L-2 layer. Thus, we argue that the dish-shaped L-1 layer is controlled by differential erosion associated with the L-1 layer deposition as well as by an erosional surface associated with the L-2 layer deposition. One of the interesting points on the northern trench wall is a high-angle contact relationship between the L-1 layer and the basement-rock at the easternmost part of the fault core (Fig. 5c). This contact is observed at the extension of a subsidiary slip surface, and some pebbles seem to be rotated at footwall side and their long axes are parallel to the slip surface. We argue that the eastern block apparently thrusts over the L-1 layer with only a few centimeters of vertical separation. In contrast, there is no visible deformation around the slip surface in the L-2 layer. Therefore, our observations imply that at least one Quaternary slip event has occurred between depositions of the L-1 layer and L-2 layer along the subsidiary slip surface in the fault core.

For the Geundeok Fault, we carried out two different methods: radiocarbon and ESR (Eletronic-Spin-Resonance) dating. Radiocarbon dating is carried out with charcoals in the L-1 layer, which is collected from the northern trench wall (Fig. 5d). The result shows that conventional radiocarbon age is 1,850 ± 30 BP, and this is indicative of the minimum depositional age of the L-1 layer. Thus, the surficial deformation associated with the inferred slip event has occurred after AD 165 (± 30). On the other hand, the ESR dating through quartz signal measurement was carried out for the three different fault gouge zones (Fig. 4a), but the results show no recent resets of the ESR signals. Note that this may result from a saturated fault gouge with water and a small effective confining pressure, or a mixing of recent fault gouge with older ones during its moving up to the surface (Lee and Schwarcz, 1994).

CONCLUSIONS

The results of our investigations in various scales indicate that the Geundeok Fault has been evolved under different stress regimes and up to the Quaternary. The variations in geometric and kinematic markers within the fault core indicate multiple slip events along the fault. In consideration of the current stress regime and the fault attitude, that is the NNE-SSW trending vertical fault under the ENE-WSW trending maximum horizontal compression, the inferred Quaternary slip event is probably related with a right-lateral faulting with subsidiary reverse-slip component. Thus more paleoseismic studies are necessary around the study area. This kind of process for paleoseismic investigation must be very useful to identify active faults and to make the active fault map of Korea.

Acknowledgements: This work was funded by the Korea Meteorological Administration Research and Development Program under grant CATER-2014-8010.

References

Caine, J.S., J.P. Evans, C.B. Forster, (1996). Fault zone architecture and permeability. *Journal of Structural Geology.* 24, 1025-1028.

Houng, S.E. & T.K. Hong, (2013). Probabilistic analysis of the Korean historical earthquake records. *Bulletin of the Seismological Society of America.* 103, 2782-2796.

Jun, M.S., & J.S. Jeon, (2010). Focal Mechanism in and around the Korean Peninsula. *Jigu-Mulli-wa-Mulli-Tamsa*. 13, 198-202.

Kim, J.H., W.S. Yoon, J.W. Choi, H.S. Kwon, G.H. Bae, S.W. Cheong, (2000). Geological structures in the Tongri-Dogye and Sangdeog areas in the eastern part of the Samcheog Coalfield, Korea. *Geosciences Journal.* 4, 153-163.

Kim, Y.S. & J.Y. Park, (2006). Cenozoic deformation history of the area around Yangnam-Yangbuk, SE Korea and its tectonic significance. *Journal of Asian Earth Sciences.* 26, 1-20.

Lee, H.K. & H.P. Schwarcz, (1994). Criteria for complete zeroing of ESR signals during faulting of the San Gabriel fault zone, southern California. *Tectonophysics.* 235, 317-337.

Lee, K. & W.S. Yang, (2006). Historical seismicity of Korea. *Bulletin of the Seismological Society of America.* 96, 846-855.

McCalpin, J., (2009). *Paleoseismology*. 2nd edition. Academic Press. San Diego, CA.

Yoon, S.H. & S.K. Chough, (1995). Regional strike slip in the eastern continental margin of Korea and its tectonic implications for the evolution of Ulleung Basin, East Sea (Sea of Japan*). Geological Society of America Bulletin.* 107, 83-97.

Zielke, O., Y. Klinger, J.R. Arrowsmith, (2015). Fault slip and earthquake recurrence along strike-slip faults - Contributions of high-resolution geomorphic data. *Tectonophysics.* 638, 43-62.

INQUA Focus Group on Paleoseismology and Active Tectonics

A 3000 yr history of earthquakes recorded in Hazar Lake potentially related to ruptures along the East Anatolian Fault (Turkey)

Lamair, L. (1), Hage, S. (1), Hubert-Ferrari, A. (1), Avsar, U. (2), El Ouahabi, M. (1,3), Çağatay, M.N. (4), Boulvain, F. (5)

(1) University of Liège, Department of Geography, Liège, Belgium. Email: Laura.Lamair@ulg.ac.be
(2) King Abdullah University of Science and Technology (KAUST), Thuwal, Saudi Arabia
(3) Institute of Geography, Cologne, Germany
(4) Istanbul Teknik Universitesi, EMCOL, Faculty of Mines, Istanbul, Turkey
(5) University of Liège, Department of Geology, Liège, Belgium

Abstract: *In this study, we focus on the paleoseismicity of the East Anatolian Fault (EAF). We investigated Hazar Lake, a pull-apart basin located on the EAF. During the campaign of 2007, short and long cores were taken from the bottom of the lake. Several thin earthquake-triggered sedimentary events (less than 2 cm) were detected in the cores. Radiometric dating (^{14}C, ^{210}Pb, ^{137}Cs) revealed the correlation between the youngest four events and historical earthquakes in 1874-75, 1779-1789, 1513-1514 and 1285. Thin sections showed that the sedimentary events are composed of several thin turbidites, characterized by bioturbated coarse basal sand layers. The bioturbation indicates the time elapsed between two sub-events. We inferred that Hazar Lake is extremely sensitive to earthquake shaking, and its sedimentary sequence may contain a complete record of large M>6.5 paleoearthquakes along the EAF.*

Key words: *Hazar Lake, Paleoseismology, East Anatolian Fault, Thin turbidites.*

INTRODUCTION

The East Anatolian Fault (EAF) is a major left-lateral strike-slip fault accommodating, with the conjugate North Anatolian Fault, the westward extrusion of the Anatolian Plate away from the Arabia-Eurasia collision zone. The East Anatolian Fault ruptured over most of its length during the 19th century in a series of magnitude ~7 earthquakes. During the 20th century this fault was less active with only two events of magnitude greater than 6. This absence of large earthquakes has resulted in relatively little attention being paid to the East Anatolian Fault compared to the North Anatolian Fault, which has ruptured during the last century in several earthquakes of Ms~7. To constrain the seismic history of the East Anatolian Fault at its central part, we focus on the sedimentary sequence of Hazar Lake, which occupies a 20 km long pull-apart basin. Historical earthquakes in this region are well documented (Ambraseys, 1989; 2009; Guidoboni et al., 1994; Cetin et al., 2003). We inferred that Hazar Lake is an ideal location to study the paleoseismicity of the EAF, specially the linkage between earthquakes and turbidites.

GEOLOGICAL AND TECTONIC SETTINGS

Hazar Lake (1248 m above sea level) is located in the Taurus Mountains, in the Eastern Anatolia (Turkey). It is a depression 25 km long, 7 km wide and up to 216 m deep. It is a hardwater lake characterized by a pH around 9.3 (Sen et al., 2012). The basin has been interpreted as an active pull-apart (Arpat & Saroglu, 1972; Hempton & Dunne, 1984; Sengör et al., 1985; Çetin et al., 2003). However, based on a dense grid of reflection-seismic profiles, Garcia Moreno et al. (2010) showed that a continuous left-lateral strike-slip fault runs in fact across Hazar Lake from its northeastern to its southwestern corner. Secondary oblique faults were also mapped (Garcia Moreno et al., 2010) which comprise in particular the Northwestern Sivrice Fault at the WSW extremity of the Lake and the Southern Gezin Fault bounding the steep slopes of the southern margin of the basin.

The Kurk River discharges into the southwestern part of Hazar Basin forming a wide delta. Its large catchment area is composed of the Senomamian Yüksekova Melange (andesites, basalts, gabbros, dacites dykes) and of the Middle Eocene Maden Melange (sedimentary and volcanic formations) (Sengor and Yilmaz, 1981).

The bedrock of the southern margin is mainly made of Late Jurassic magmatic rocks and Middle Eocene limestones, whereas the northern margin is composed of Late Cretaceous sedimentary rocks and ophiolite.

MATERIALS AND METHODS

Short and long sedimentary cores were collected during the 2007 field campaign in order to retrieve a paleoseismic record. Using a platform, the short cores were taken by a UWITEC gravity corer, whereas the long cores were collected using a piston hammering system of ITU-EMCOL. We obtained short cores of 1 to 1.3 m in length at six sites, and 5 m long cores at two sites (Fig. 1). The cores were split and studied at the University of Liège. The sedimentary records were analyzed by combining X-ray imagery, magnetic susceptibility, grain-size distribution, loss-on-ignition and XRF measurements. We investigated the nature and microstructure of the sedimentary events with thin sections analysis. The sources of event deposits were estimated by heavy minerals provenance analysis.

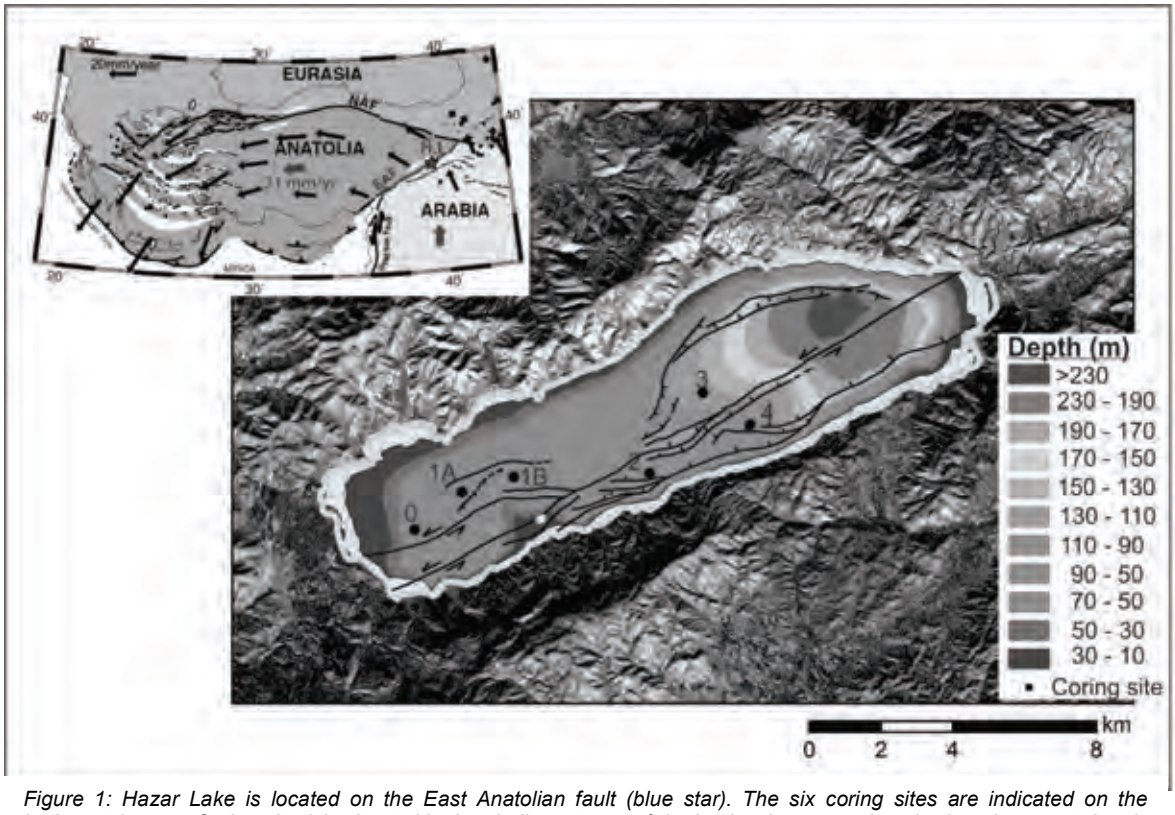

Figure 1: Hazar Lake is located on the East Anatolian fault (blue star). The six coring sites are indicated on the bathymetric map. Coring site 0 is situated in the shallowest part of the basin whereas coring site 3 and 4 were taken in the deep basin.

Identified sedimentary events were dated by radiometric dating (^{14}C, ^{137}Cs and ^{210}Pb) and compared to the historical earthquake record (Ambraseys, 1989; Ambraseys and Finkel, 1995; Ambraseys, 2009). We computed shake maps for the individual historical earthquakes in order to decipher the ones that potentially have triggered turbidites in Hazar Lake and be recorded there.

RESULTS AND DISCUSSION

All cores were correlated based on obvious along-core anomalies in the magnetic susceptibility (MS) and Ti or Ca-content profiles. These variations were related to lake level changes.

At least 4 sedimentary events characterized by MS peaks were identified in the short cores, and more in the long cores. The events are inferred to be earthquake-triggered based on (1) their occurrence at different sites, which is an indication of multiple coeval turbiditic flows; (2) their large-scale basin-wide impact on the lake sediments even at sites where no turbiditic deposit occurred. According to the radionuclide dating, the youngest four events would correspond to the historical earthquakes occurred in 1874-75, 1779-1789, 1513-1514 and 1285.

The individual events showed distinct signatures at the different sites. In particular, the magnitude of the terrigenous signal varies significantly. We thus conclude that each site has a specific sensitivity to earthquake shaking, with site 2 revealed as the most sensitive. It is located in a flat area near the base of the steep subaqueous slopes overhung by the steep subaerial southern slopes of the Hazar Mountains. The rivers draining the Hazar Mountains are ephemeral and provide restricted sedimentary supply; hence the subaqueous slopes do not accumulate significant sedimentary load. However, these steep slopes are extremely sensitive to earthquake shaking and an earthquake with an intensity of 6 or potentially less would trigger a turbiditic flow. Sites1a and 1b, located in the flat basin east of the Kürk Delta, are slightly less sensitive. Sites 0, 3 and 4, located in different dipping parts of the basin, do not record any terrigenous events. Nevertheless, Ca enrichments after these events are recorded at all sites. This means that the terrigenous events recorded at sites 1 and 2 affected the chemistry of the entire water column. We attributed Ca enrichments to indirect effects of strong earthquake shaking, which supplied nutrients in Hazar Basin by water-column mixing and triggered a benthic bloom. In these particular conditions, calcite is precipitated by phytoplankton, creating peaks of Ca. This was confirmed by SEM investigations that revealed the presence of calcite biomineralization.

Thin section analyses provided further information regarding the sedimentary arrangement of individual event deposits. In fact, it is seen that event deposits are composed of series of individual thin turbidites

characterized by a basal coarse grained sand, grading upward to a clayey layer. The thicknesses of the sub-events are less than 0.4 mm on average. We observed the presence of bioturbation caused by oligochaetes and chironomids in each sub-event. Each layer with a coarse-grained base is thus a separated turbiditic flow. The thin section study allows us to conclude that an individual event can be composed of several coarse-grained sub-events of different magnitude, with a time lapse in between longer than a week.

Individual thin turbidites are inferred to have a seismic trigger because the largest ones are recorded simultaneously at sites 1 and 2, which cannot be formed by a unique turbiditic flow. The different earthquake triggered turbiditic sub-events contained in a given sedimentary event can be interpreted in two different ways. They may be the expression of a complete earthquake sequence (i.e main-shock, foreshocks and aftershocks) or of a burst of earthquakes of M>6.5 rupturing the East Anatolian Fault in a pattern similar to the 20th century sequence of the North Anatolian Fault (Stein et al., 1997). A comparison between the computed shake maps based on historical data and the dated turbiditic record will be used to decipher between the two options.

References

Ambraseys, N.N., (1989). Temporary seismic quiescence: SE Turkey. *Geophysical Journal*. 96, 311 -331.

Ambraseys, N., (2009). *Earthquakes in the Mediterranean and Middle East - A Multidisciplinary Study of Seismicity up to 1900*. Cambridge University Press. 968 p.

Arpat, E., F. Saroglu, (1972). The East Anatolian Fault System; thoughts on its development. *Mineral Research and Exploration Institute of Turkey*. 78, 33-39.

Aksoy, E., M. Inceöz, A. Koçyigit, (2007). Lake Hazar basin: a negative flower struc- ture on the east Anatolian fault system (EAFS), SE Turkey. *Turkish Journal of Earth Science*. 16, 319-338.

Çetin, H., H. Güneyli, L. Mayer, (2003). Palaeoseismology of the Palu-Lake Hazar segment of the East Anatolian Fault Zone, Turkey. *Tectonophysics*. 374, 163-197.

Guidoboni, E., A. Comastri, G. Traina, (1994). *Catalogue of Ancient Earthquakes in the Mediterranean Area up to the 10th Century*. Istituto Naz. di Geofisica. Rome.

Hempton, M.R., L.A. Dunne, (1984). Sedimentation in pull-apart basins: active examples in eastern Turkey. *Journal of Geology*. 92, 513-530.

Garcia Moreno, D., A. Hubert-Ferrari, J.G. Moernaut, X. Boes, M. Van Daele, U. Avsar, N. Çagatay, M. De Batist, (2011). Structure and recent evolution of the Hazar Basin: strike-slip basin on the East Anatolian Fault, Eastern Turkey. *Basin Research*. 23, 2, 191-207.

Sengor, A.M.C., Y. Yilmaz, (1981).Tethyan evolution of Turkey: a plate tectonic approach. *Tectonophysics*. 75, 181-241.

Sen, B., M.A.T. Koçer, M.T. Alp, (2002). Physical and chemical properties of rivers drained into Lake Hazar. *Journal of Engineering Science*. 14, (1), 241-248.

Sengör, A.M.C., N. Görür, F. Saroglu, (1985). Strike-slip faulting and related basin formation in zones of tectonic escape: Turkey as a case study. In: *Strike-Slip Faulting and Basin Formation*. (Biddle, T., Christie-Blick, N. eds.). Society of Economic Paleontologists and Mineralogists. Special Publication. 17, 227-267.

Stein, R.S., J.H. Dieterich, A.A. Barka, (1997). Progressive failure on the North Anatolian fault since 1939 by earthquake stress triggering. *Geophysical Journal International*. 128, 3, 594-604.

INQUA Focus Group on Paleoseismology and Active Tectonics

Characteristic and timing of Quaternary faulting along the Yangsan fault

Lee, J.-H., Rezaei, S. and Kim, Y.-S.

Dept. of Earth Environmental Sciences, Pukyong National University, Busan 608-737, Korea, South Korea. Email:godgocogo@gmail.com

ABSTRACT: *Yangsan Fault system underwent at least three times of strike-slip faulting and two times of dip-slip faulting. Yangsan fault can be divided into northern and southern parts by the junction zone between Yangsan Fault and Ulsan Fault around Gyeongju city. The northern part of the Yangsan fault shows good evidences to show the characteristics of fault interaction and evolution. Yugye fault is one of the known youngest Quaternary faults located in the northern part of the Yangsan fault. The last movement of Yugye fault is around 1314yr BP, as estimated from C^{14} age data, which was the youngest fault reported in Korea until recently. However, we found a pottery bearing sediment offset by a set of fault in Danguri, located in the northern part of Yangsan fault. We requested pottery to archeologist and the pottery is presumed to be 14th ~15th Century based on its style. A modeling study for the Yangsan and Ulsan fault system based on Coulomb stress shows high stress change in the eastern block of the Ulsan Fault. Under the current stress regime with ENE-WSW maximum compressive stress axis, the Ulsan fault and the northen Yangsan fault can reactivated as a λ-fault system. This interpretation is well consistent with the occurrence of young faults in and around the northern Yangsan Fault and the eastern Ulsan Fault. Therefore, some more detailed paleoseismological researches should be conducted in this area.*

Key words: *Yangsan fault, Ulsan fault, Yugye, Danguri, Trench.*

INTRODUCTION

Since Quaternary faults were first discovered in the early 20thcentury, the Korean peninsula, many Quaternary faults have been studied in detail. Most Quaternary faults have been reported around the Yangsan and Ulsan Fault system.
The Yangsan Fault system underwent at least three strike-slip faulting and two dip-slip faulting episodes (Chae et al., 1994). Radiometric dating of volcanics rocks along the northern part of the fault indicates initial movement on the Yangsan Fault probably occurred after 45Ma (Eocene) (Chang et al., 1990). Paleo-stress analysis (Chae and Chang, 1994; Chang and Chang, 1998; Chang, 2001) indicates that movement on the Yangsan fault has been right-lateral strike-slip caused by NE-SW compression since Eocene time, including its most active period in the late Miocene. Later, the sense of movement changed to left-lateral under a NW-SW compressional stress regime at the end of the Miocene. In the Pliocene, N-S compression affected the fault, and in the Quaternary, the fault was reactivated by a right-lateral strike-slip movement under an E-W to ENE-WSW (now stress regime in the Korean Peninsula) compression. The general trend of the fault is NNE-SSW. Several Quaternary faults have been reported around the Yangsan fault system, apparently showing reverse fault geometry in general. Fault plane slickensides, however, show right-lateral strike slip with striations at a low angle. The Yangsan fault can be divided into north and south part In Gyeongju City (Yang, 2006). The junction between the Yangsan Fault and the Ulsan Fault is located around Gyeongju City. The northern part of the Yangsan fault shows good evidences indicating the characteristics of fault interaction and evolution.

Figure 1: Distribution of Quaternary faults in the southeast Korean peninsula. Youngest OSL or C^{14} ages of the sediments offset by the faults at each site (marked with numbers within white boxes) are presented in black boxes.The Yugye, Byeokgye brach is marked in the site of No. 3, 5 and The Danguri site, this study area is marked beside in the site of No. 5. (modified, Yang, 2006).

The purpose of this study is to locate and identify the most recently active faults ever found in the Korean Peninsula and to understand the recent fault activity around the Yangsan-Ulsan fault system.

LATE QUATERNARY MOVEMENT OF THE YANGSAN FAULT

Figure 1 shows the result of the age dating of Quaternary faults. The Yugye fault cut the Quaternary sediment with the age of the around 1,314yr BP. Therefore, we can presume the time of the last movement of the fault to be later than around 1314yr BP, which was the youngest faulting ever found in the Korean Peninsula.

The Yugye Fault is located in the northern part of the Yangsan Fault (Fig. 1). The characteristic of the last movement of the Yugye Fault was understood by the trench log (Fig. 2; Kim and Jin, 2006). Cretaceous sedimentary bedrock abutting to a set of reactivated fault gouge zone is crushed by repeated fault activity. The previous fault gouge is developed under the Quaternary alluvial fan deposit, reactivated gouges thrust over Quaternary alluvial fan deposits, roundness of the Cretaceous pebbles, the direction of the long axis of the Cretaceous sedimentary cobble and several stages of fault foliation development. In trench section analysis, Cretaceous rock were found be thrust over the Quaternary alluvial fan deposit. Also, the movement analysis for the gouge sample indicates reverse slip. The maximum principal stress direction for the last fault movement is NW-SE or WNW-ESE (Kim and Jin, 2006). Based on C^{14} dating of humic silt material on the upper floor of the trench section, the last movement of the fault is estimated as about around 1314yr BP (Kyung, 2003).

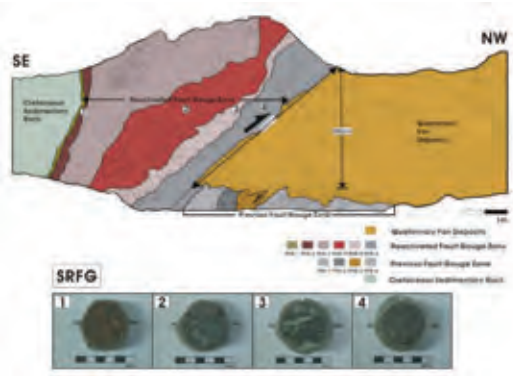

Figure 2: Yugye-ri trench. The fault gouge zone can be divided into ten bands depending on color and material property. The fault gouges are mainly divided into previous fault gouges and reactivated fault gouges (Kim et al, 2006).

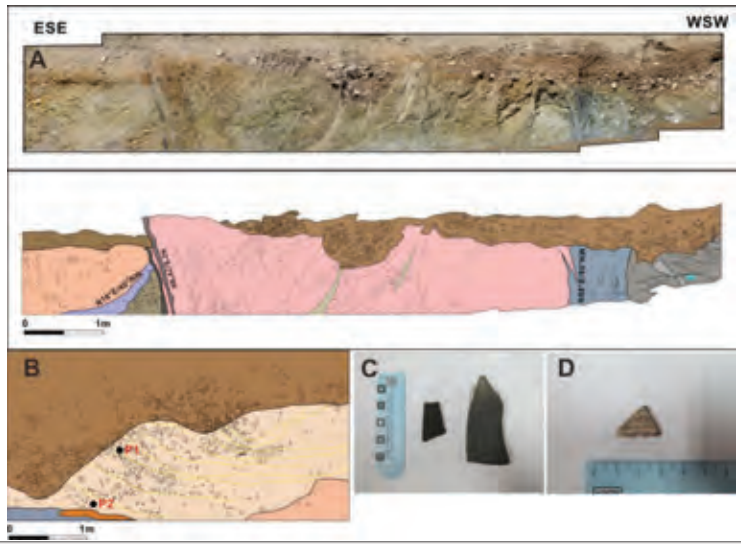

Figure 3: Danguri trench. (A) Northern wall of the first trench. The west sidewall of the fault is Quaternary deposits and the east side wall is granite. There are two types of fault gouge. (B) The west side of the first trench. P1, P2 were collected pottery

The Danguri site (36°3'35.96"N, 129°15'14.66"E) is located close to Byeokgye fault (Fig. 1) and it has very similar kinematic properties. The strike of the Byeokgye fault is N11°E/80°SE ~ 90° and it is a right-lateral strike-slip fault (Ki *et al*, 2009). East side of Byeokgye fault is composed of Cretaceous andesite and west side is Quaternary sediments (Ryu *et al*, 1999). The width of the fault zone is approximately 4m, and the gouge zone is up to 15 ~ 30cm. Slickensides indicate 011°/08°, which indicates almost pure strike-slip movement.

We excavated the two trench in Danguri and Second trench is located about 2m to the north wall the first

trench. In the first trench, we found fault and pottery. In the first, second trench, some important points were discovered. Firstly, the fault cuts Quaternary channel deposits and it is strike-slip fault with some vertical component (Fig. 3A, 4). The strike and dip of the fault is N02°E/79°SE (First Danguri trench) ~ N20°E/75°SE (Second Danguri trench). In the second trench, the fault affected the subsurface up to just 10 cm below the rice paddy (Fig. 4). Therefore, the last age of faulting is estimated very young. Secondly, several pottery was found in the first trench west wall but only in the first trench (Fig. 3B). Although it is not clear, the crosscutting relationship shows that the channel with pottery was cut by the fault in the first trench and affect up to the rice paddy in the second trench. The pottery age is estimated as early-middle Joseon Dynasty period (15th Century) based on the ceramic style. Thirdly, based on gouge type, the number of faulting event is at least two (Fig. 3A). OSL age dating, C^{14} age dating and ESR (Electron Spin Resonance) dating are still in progress.

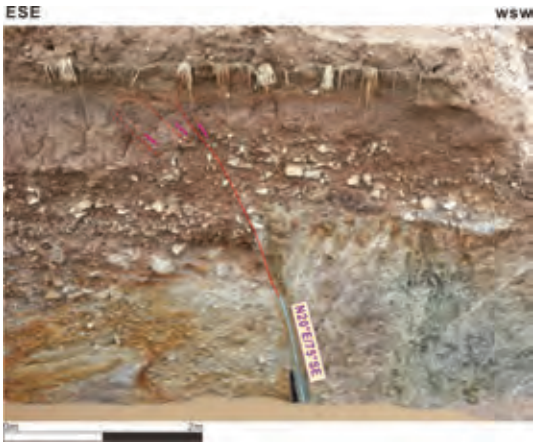

Figure 4: The northern side of the second trench. The section shows two gouges and vertical component of displacement.

DISCUSSION

We compiled information on the age of recent fault motion in Eastern Korea (Fig. 1). South of Yangsan Fault, all ages were determined using the ESR technique. Additional, the age data for the northern part of the Yangsan fault, such as the Yugye fault and the Byeokgye fault, were collected. The last event of the Danguri fault is likely very young. The Yougye, Byeokgye, Danguri faults are younger than other Quaternary faults in the study area. These faults are located in the northern part of the Yangsan Fault which must be consider to be the most active area in Korea.

A numerical modeling result for the stress change in the southeastern part of the Korean Peninsula shows high Coulomb stress change in the eastern block of the Ulsan Fault (Fig. 5). ENE-WSW compression indicates the high possibility of reactivation (Han *et al*., 2009). The eastern block of the Ulsan fault and the northern part of the Yangsan fault have high Coulomb stress change indicating higher activity. Therefore, more detailed studies should be conducted for the areas.

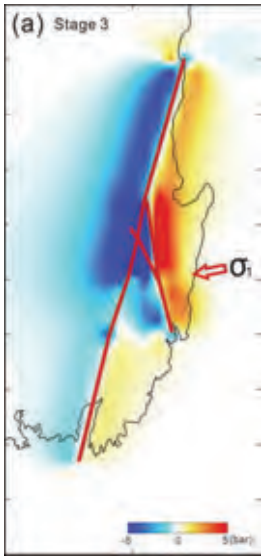

Figure 5: Coulomb stress changes are concentrated in the eastern and southeastern region of the Yangsan faultand eastern region of the Ulsan fault (Han et al., 2009).

CONCLUSION

Yangsan Fault is divided into northern and southern parts around Gyeongju. The junction point of the Yangsan Fault and the Ulsan Fault is Gyeongju, and the Yangsan Fault extends to the north.

In the northern Yangsan Fault zone, several young Quaternary faults are developed, such as the Yugye fault and the Danguri fault.

A modeling study for the Yangsan and Ulsan fault system based on Coulomb stress shows high stress change in the eastern block of the Ulsan Fault and the northern part of the Yangsan Fault.

Under the current stress regime with ENE-WSW maximum compressive stress axis, the Ulsan fault and the northern Yangsan fault can be reactivated as a λ-fault system. This interpretation is well consistent with the occurrence of young faults in and around the northern Yangsan Fault and the eastern Ulsan Fault.

References

Chae, B.G. and T.W. Chang, (1994). Movement history of Yangsan fault and its related fractures at Chongha-Yongdok area, Korea. *Jour. Geol. Soc. Korea*. 30, 4, 379-394

Chang, K.H., B.G. Woo, J.H. Lee, S.O. Park, and A. Yao, (1990). Cretaceous and early Cenozoic stratigraphy and history of eastern Kyoungsang Basin, S. Korea. *Jour. Geol. Korea*. 26, 471-487.

Chang, K.H., and T.W. Chang, (1998). Movement history of the Yangsan fault based on paleo-stress analysis. *Jour. Eng. Geology*. 8, 1, 161-171.

Chang, C.J., (2001). *Structural characteristics and evolution of the Yangsan fault.* Ph.D. thesis. Kyongbuk University. 259 pp (in Korean).

Han, S.R., J.Y. Park, S.G. Kim, (2009). Evolution modeling of the Yangsan-Ulsan fault system with stress changes. *Journal of the Geological Society of Korea.* v. 45, no. 4, p. 361-377.

Ki, W.S., Y.H. Kim, H.J. Lee, D.G. Jo, B.C. Kim, G.T. Song, H.J. Go, (2009). South eastern fault variable research and DB Construction. *KIGAM*. South Korea, 1- 327.

Kim, Y.G., K.M. Jin, (2006). Estimated earthquake magnitude from the Yugye Fault displacement on a trench section in Pohang, SE Korea. *Journal of the Geological Society of Korea*. v. 42, no. 1, p.79-94.

Kyung, J.B., K.H. Lee, (2006). Active Fault Study of the Yangsan Fault System and Ulsan Fault System, Southeastern Part of the Korean Peninsula. *J Korean Geophysical Soc.* Vol. 9, No 3, Special Volume, pp. 210-230.

Ryu, C.R., B.J. Lee, D.Y. Jo, W.C. Chol, S.J. Choi, J.Y. Kim, (1999). *Danguri: byeokgye fault.* Society of Economic and Environmental Geology / Geological Society of Korea / Korea. Institute geophysical Spring Joint Conference. Abstract 334.

Yang, J.S., (2006). *Quaternary fault in southeastern peninsula*. PhD graduation thesis. Gangwon University.

INQUA Focus Group on Paleoseismology and Active Tectonics

From sandbox modeling to paleoseismology: preliminary results on bending-moment faults modeling

Livio, F. (1), Reicherter, K. (2), Urai, J. (3)

(1) Dipartimento di Scienza ed Alta Tecnologia, Università dell'Insubria, Via Valleggio 11, Como. Email: franz.livio@uninsubria.it
(2) Lehr- und Forschungsgebiet Neotektonik und Georisiken, Geowissenschaften, RWTH Aachen, Lochnerstr. 4-20, D-52064 Aachen, Germany
(3) Geologie-Endogene Dynamik, RWTH Aachen, Lochnerstrasse 4-20, D-52056, Germany

Abstract: *Are bending-moment fault a good proxy to assess the timing of movement of underlying deeper structures? We made use of a series of sand-box experiments in order to model bending-moment faults generation and growth during progressive folding. Syn-growth sedimentation was included into the model. Our results indicated that displacement, at surface, is cumulating regularly along these structures, even when lateral propagation is inhibited, thus assuring a good reliability for the cross-section analysis of these structures (i.e. paleoseismological studies) and implying that bending-moment fault growth and associated folding could be put in relation through kinematic modelling.*

Key words: *Fold-related faults, bending-moment faults, analogue modelling.*

INTRODUCTION

Bending-moment faults are the typical brittle surface expression of shallow folding due to blind thrusting and can represent the only available feature feasible to paleoseismological investigations (e.g., Yeats, 1986, Champion et al. 2001; Heddar et al. 2013; Livio et al. 2014). Nevertheless some questions arise concerning the reliability of these structural features in paleoseismology: can these be considered a reliable indicator of deeper thrust movements? Is there a strain threshold for bending-moment faults inception, during folding? What is the mode of fault growth (i.e. self-similar vs constant length)? The completeness of a paleoseismological record solely based on these features can be questionable and these and other issues need to be solved basing on a consistent structural model.
We made use of a series of sand-box experiments in order to model bending-moment faults generation and growth during progressive folding. Syn-growth sedimentation was included into the model.

Experimental setup
We built a sand-box model (100 x 50 cm) with a base-plate made of a two lateral rigid panels and a flexible part in between. Two fulcra were placed in the middle of the rigid plates and these ones were pulled down at the sides in order to induce tilting and, therefore, a cylindrical folding in the flexible part. The box is lateral confined at the sides and two glass panels were put in front and at the rear (Fig. 2a). Considering the dimensions of the used box we expect a typical dimensional ration with the modelled features of 10-2 – 10-3. The material used is a stirred mixture of quartz sand and gypsum powder in order to obtain a good analogue for stiff soils, typically involved into the modelled deformations and characterized by a not negligible cohesion, even if down-scaled according at the model dimensional ratio.

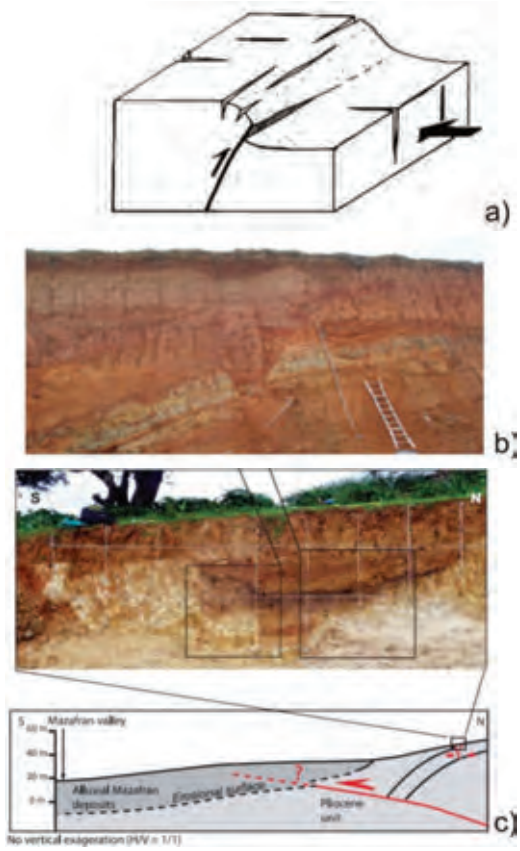

Figure 1: schematic diagram and field examples for typical bending-moment faults: a) coseismic hangingwall anticline deformation observed soon after the Mw 7.3 El-Asnam earthquake (modified after Philip & Meghraoui, 1983); outcropping bending-moment normal faults caused by blind thrusting and fault-propagation folding in b) N Italy (Livio et al. 2014) and c) in Algeria (Heddar et al., 2013).

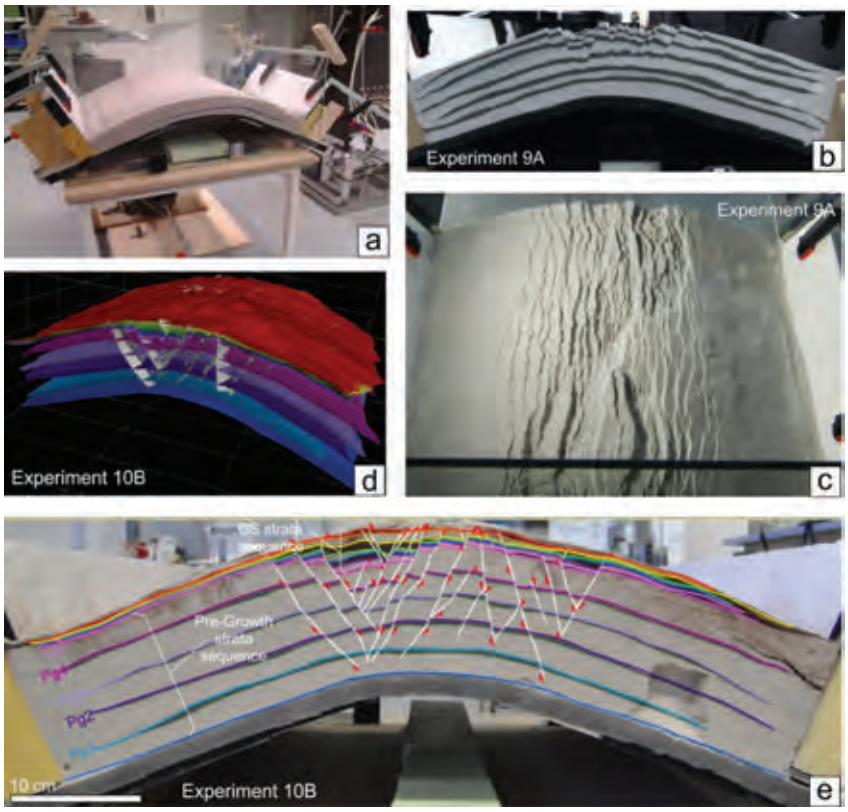

Figure 2: a) experimental setup built at the RWTH laboratories, in Aachen; b) front view and c) plane view of the run model: here only pre-growth strata were deformed during running; d) 3D digital model of the experiment; e) detail on the front view of an experiment run adding growth strata during folding.

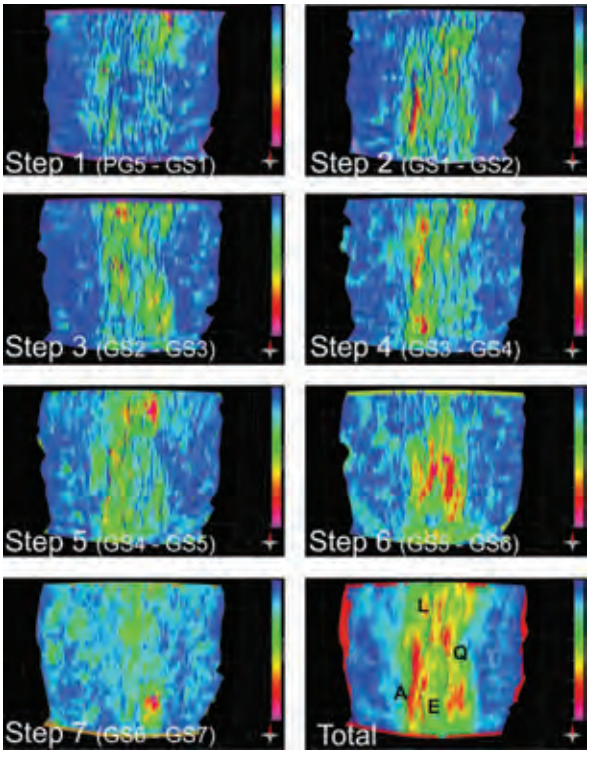

Figure 3: plant view map showing the step-by-step and total thickness of growth strata. We calculated the cumulative displacement along strike of four selected faults (labelled A,E,Q and L) illustrative of the overall observed growth style of these structures (cfr. Fig. 4).

The initial model is made up of a 10 cm-thick layer of pre-growth strata (from the bottom: PG 1 to 5) evenly coloured in grey and green; then the model run and progressive cylindrical folding is induced. During folding several bending-moment faults begin to grow and, at arbitrary time, we stop the model and add a growth layer (from the bottom: GS 1 to 7) levelling all the visible faults and thus according to a fill-to-the-top model. Then we run again the model and iterated these steps until the final stage.

We took a complete series of photos of the front panel for each incremental step and, after the final stage was reached, we wetted the model, cut it into slices every 2 cm and each section was imaged in HR photos. Finally we created a 3D vector model of the final stage, by digitizing all the slices into the 3D-MOVE platform by Midland Valley and creating mesh surfaces of every feature. Thanks to this procedure we were able to investigate not only the 3D geometry of every single fault in the model but also their growth, through the thickness-analysis of growth strata.

Results

It is clear that the brittle accommodation of strain is limited, as expected, to the central sector of the fold. The obtained typical fault architecture is composed by two symmetrical graben pinned at the base to the tips of the flexible plate (Fig. 2d). As expected, faults show maximum displacement at the surface whereas it dies

out downward. The faults run parallel the fold axis, with minor trend changes, and show relay ramps along accommodation zones and where brittle accommodation of strain switches from one graben to the other. (Fig. 2c). Breached relay zones are rare.

In Figure 3 the results of the thickness analysis are presented. Each step corresponds to an increase in fold amplitude in the model and to a subsequent growth of accommodating bending-moment faults. At each step different structures activate in order to accommodate strain and normal faults activate in adjacent sectors (i.e., STEP2 vs STEP3 and STEP5 vs STEP6; Fig. 3) suggesting that stress transfers to surround sectors following local discrete deformation.

The distribution total thickness of growth strata cumulated during folding allows to easily map location of main normal faults in plant view. Here we present preliminary results for 4 selected structures, illustrative of the overall observed growth of these structures (Fig. 4). Typical fault growth at the initial stages is ascribable to a self-similar style passing progressively to a constant length one, where slip per event remains constant while along-strike propagation of fault considerably slows down (Fig. 4b) between 140 and 170 mm (that is 1.4 – 1.7 times the model thickness or ca. 1.2 times the average fault width).

DISCUSSION AND CONCLUSIONS

The observed results suggest that bending-moment faults can be considered a good proxy for determining the timing of movements along growing folds. In fact, displacement at surface is cumulating regularly along these structures even when lateral propagation is inhibited. Conversely, the same normal fault and/or system fails at reacting every time to a folding event, thus implying that fold activity investigation, based on a single trenching analysis, would pose significant uncertainties to the record completeness.

Moreover, the definition of a reliable kinematic model linking fold amplification with bending-moment faults inception and growth could ideally allow to infer the

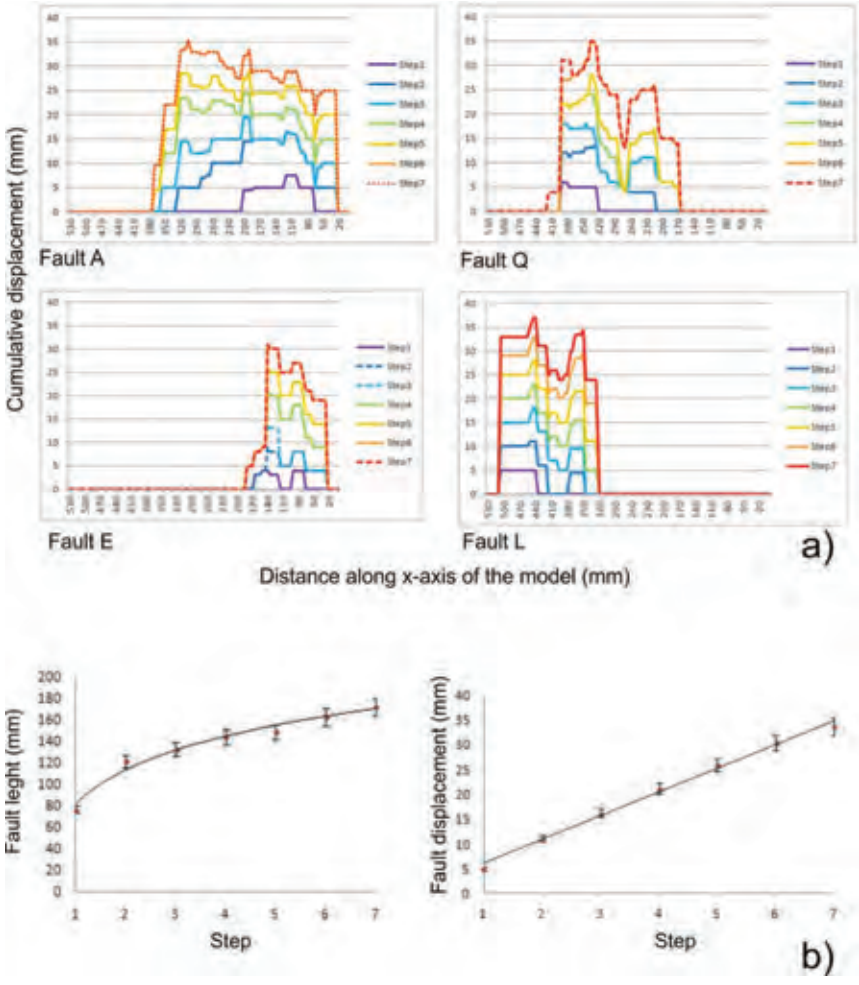

Figure 4: a) cumulative displacement profiles for a set of four select faults (see Fig. 3 for fault location). X-axis distance is progressively increasing away from the from panel; b) regression of fault length and cumulative fault maximum displacement, measured at each deformation step: data distribution indicate an overall tendency for the fault dataset to switch from self-similar to constant-length growing. These regressions were calculated on the entire preliminary dataset (N = 20).

amount and timing of progressive bending and, in turn, displacement of underlying deeper driving structures, from the paleoseismological analysis of these normal faults and associated colluvial wedge.

Acknowledgements: Sohrab Noorsalehi-Garakani and Michael Kettermann at the GED laboratories of the RWTH Aachen University are specially thanked for their helpful assistance and fruitful discussions. Samuele Pesciaioli, B.Sc. student at the Università dell'Insubria, is specially thanked for his precious and good work. An Academic License of MOVE® suite software was provided by Midland Valley and was used for faults/fold 3D modeling.

References

Champion, J., K. Mueller, A. Tate & M. Guccione, (2001). Geometry, numerical models and revised slip rate for the Reelfoot fault and trishear fault-propagation fold, New Madrid seismic zone. *Engineering Geology*. 62 (1), 31-49.

Heddar, A., C. Authemayou, H. Djellit, A.K. Yelles, J. Déverchère, S. Gharbi, A. Boudiaf & B. Van Vliet Lanoe, (2013). Preliminary results of a paleoseismological analysis along the Sahel fault (Algeria): New evidence for historical seismic events. *Quaternary International*. 302, 210-223.

Livio, F.A., A. Berlusconi, A. Zerboni, L. Trombino, G. Sileo, A.M. Michetti, H. Rodnight & C. Spötl, (2014). Progressive offset and surface deformation along a seismogenic blind thrust in the Po Plain foredeep (Southern Alps, Northern Italy). *Journal of Geophysical Research: Solid Earth*. 119 (10), 7701-7721.

Philip, H. & M. Meghraoui, (1983). Structural analysis and interpretation of the surface deformations of the El Asnam earthquake of October 10, 1980. *Tectonics*. 2(1), 17-49.

Yeats, R.S., (1986). Active faults related to folding. *Active Tectonics*. 63-79.

INQUA Focus Group on Paleoseismology and Active Tectonics

paleoseismicity.org

Ancient settlements in central Italy and capable faults: consequences for urban planning in the L'Aquila region

Lo Sardo, L. (1), Pezzo, G. (2), Moro, M. (2), Saroli, M. (1), Fubelli, G. (3), Lancia M. (1), Galadini, F. (2,4)

(1) Dipartimento di Ingegneria Civile e Meccanica, Università di Cassino e del Lazio Meridionale, V. Di Biasio 43, 03043 Cassino, Italy. Email: l.losardo@unicas.it
(2) Istituto Nazionale di Geofisica e Vulcanologia (INGV), Via di Vigna Murata 605, 00143 Roma, Italy
(3) Dipartimento di Scienze, Università Roma Tre, Largo S. L. Murialdo 1, 00146 Roma, Italy
(4) Istituto Nazionale di Geofisica e Vulcanologia (INGV), Via dell'Arcivescovado 8, 67100, L'Aquila, Italy

Abstract: *Active and capable faults (FAC) represent one of the most important risk for human activities in seismically active areas. The scientific and civil communities are constantly increasing their attention about this matter. In the Italian context, the post seismic reconstruction after the 2009 April 6th L'Aquila earthquake clearly highlighted the need of criteria for the old settlement rebuilding and/or the choice of new sites suitable for new villages. We focused our study on the identification of FACs in a sector of the central Apennines characterized by a high density of Quaternary faults and by a high density distribution of ancient urban settlements. Using classical geological, geomorphological and paleoseismological approaches, together with a temporal criteria and bibliographic analysis, we evaluate the activity and capability of the recognized faults. Then, we propose some analysis and reflections about the regulation concerning the FAC in Italy, taking into account the huge number and high density of FACs that involves the Italian urban settlements.*

Key words: *Active Tectonics, Capable Fault, Surface Faulting, Earthquake, Italian Settlement.*

INTRODUCTION

A fault can be defined active when shows "*offsets during geologically recent time, association with earthquake, and probability or potential for recurrence of these events*" (Slemmons and McKinney, 1977).
IAEA (2003) defines a capable fault as an active fault able to produce significant surface ruptures or deformations in the next future. Even if the concept of active fault and the concept of fault capability are still scarcely perceived among people living in some seismically active areas, a debate on the criteria for defining the active and capable faults is taking place, especially for slow deforming areas (Bosi and Galadini, 1995, Tondi, 2000; Guerrieri *et al.* 2009, Galadini *et al.,* 2012 and the references therein).
The scientific interest for capable faults is historically related to the identification of safety sites for building nuclear power plants (Slemmond and McKinney; 1977; Serva, 1992). In the recent period, several earthquakes hurt Italian peninsula (1980 Irpinia earthquake; 1997 Umbria-Marche seismic sequence and 2009 L'Aquila seismic event). As a consequence, the number of engineering studies dealing with interaction between the permanent soil deformations and the infrastructures are also increasing (Faccioli *et al.*, 2008; Paolucci *et al.*, 2010). The interest of the community is also testified from the recent studies published in *Linee guida per la gestione del territorio in aree interessate da faglie attive e capaci* (in preparation) that underline the criteria for a correct urban development planning, in areas affected by active and capable faults (FAC).
Aim of this paper is to identify the presence of FAC in a portion of the central Apennine characterized by a high density of Quaternary faults. Moreover these faults are located in a high density distribution of ancient urban settlements. This settlements are also currently involved in the post-seismic phase of rebuilding after the 2009 April 6 earthquake (Mw 6.1), occurred along the Paganica fault (Atzori *et al.*, 2009).
The investigated area (fig. 1) includes a large portion of the Middle Aterno Valley (MVA), located between Paganica and San Demetrio ne' Vestini villages. The study area also includes a northern portion located between the village of Pescomaggiore and Arischia, characterized by a huge density of deep seated gravitational slope deformations (DSGSD).

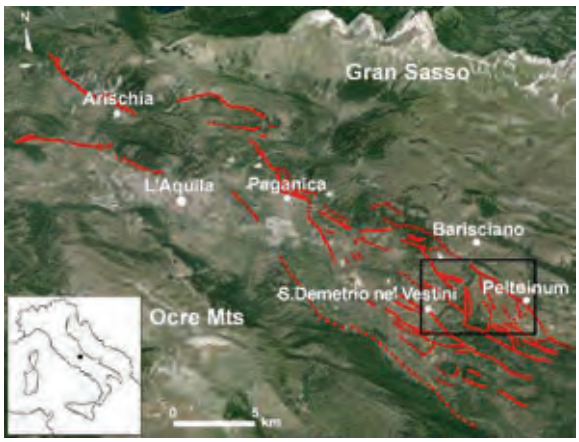

Figure 1: The Quaternary faults (red lines), located between Peltuinum archaeological area and Arischia village. The black square indicates the limits of Fig. 2. Images modified from Google Earth.

METHODOLOGIES AND RESULTS

To assess the capability of the faults situated on the study area, we applied a classical geological and geomorphological approach, based on different operative phases: the consultation of the available literature, the interpretation of the aerial photographs, the field work and a classical paleoseismological approach, integrated with a methodology based on the extrapolation of the data with LIDAR DEM technology. All collected data have been integrated with the aerial photograph interpretation and analyzed using a shaded reliefs, extrapolated from a LIDAR DEM (1m resolution). First we mapped as probably active the faults that can be considered the continuation of well-known active ones or characterized kinematic and geometric behaviours compatible with the current tectonic regime. Then, following the Galadini *et al.* (2012) sentence (*"a normal fault should be considered active and capable if it displays evidence of activation in the last 0.8 Ma, unless it is sealed by deposits or landforms not younger than the Last Glacial Maximum (LGM)"),* field work has been carried out to screen the activity and capability of the inferred faults. Therefore the field work focused on: i) the analysis of deposits across the fault plain; ii) check of paleosurface displacements across the fault planes (previously identified in the aerial photographs interpretation); iii) stratigraphic analysis of fault related deposits. Where it was not possible to establish the origin of the landforms because of the lack of data, we performed further analysis by paleoseismological trench work.

Figure 2: Map of the Quaternary faults. 1) location of Colle Cicogna - Peltuinum fault (Fig. 3); 2) Colle Separa area (Fig. 4); 3) San Demetrio ne' Vestini fault (Fig. 5); 4) San Giovanni fault (Fig. 6). Legend: a) active and capable fault; b) inferred active and capable fault; c) inactive fault; d) inferred inactive fault; e) location of the paleosismological trench (Fig. 7).

Below we show some explanatory examples among the investigated faults. The Colle Cicogna - *Peltuinum* fault plane keeps in contact with the carbonate substratum the late Pleistocene - Holocene slope deposits (Fig. 3). Moreover we observe as the paleosurface of "Valle Daria", formed between 0.6 and 0.2 Ma (Bertini and Bosi, 1993), is dislocated by the same fault close to the *Peltuinum* archaeological area. There is no trace of deposits older than 0.2 Ma that seal the fault along its whole length (5.6 km); and it allows to consider this segment as active and capable.

Figure 3: View of Colle Cicogna - Peltuinum fault (red line), corresponding to n° 1 in Fig. 2. The white arrow indicates the Peltuinum archaeological site.

Northward the Colle Cicogna - *Peltuinum* fault is interrupted by the NE-SW oriented Valle dell'Inferno, which cuts the Valle Daria paleosurface. On the Northern side of the valley, we observe the presence of two N-S oriented normal faults, as suggested by Bertini and Bosi, (1993): these faults do not dislocate the Valle Daria surface as highlights in Fig. 4, suggesting that they are inactive since the Valle Daria surface formation.

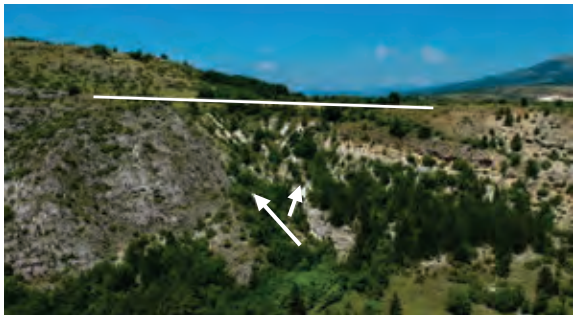

Figure 4: The faults of Colle Separa area (n° 2 in Fig. 2). The white arrows indicate the inactive faults and the sub-horizontal white line represents the Valle Daria paleosurface. View from S to N.

We also performed a field analysis of the deposits outcropping along the fault plains, interpreted by aerial photos. Following the above mentioned criteria, we consider the San Demetrio ne' Vestini fault as an active fault because it shows a continuous fault scarp (Fig. 5) that involves the carbonate substratum and the Middle Pleistocene Valle dell'Inferno deposits (Bertini and Bosi, 1993). Moreover the fault dislocates the San Giovanni surface, an erosional paleosurface formed between 0,18 and 0,27 Ma, that interests the above-quoted deposits (Bertini and Bosi, 1993).

Figure 5: Fault scarp along the San Demetrio fault (n°3 in Figure 2).

On the contrary, we consider as inactive another fault segment running parallel to the San Demetrio fault, namely the San Giovanni fault. In fact, even if this fault cuts the same unit of the San Demetrio one, the San Giovanni fault is sealed by LGM deposits (Fig. 6).

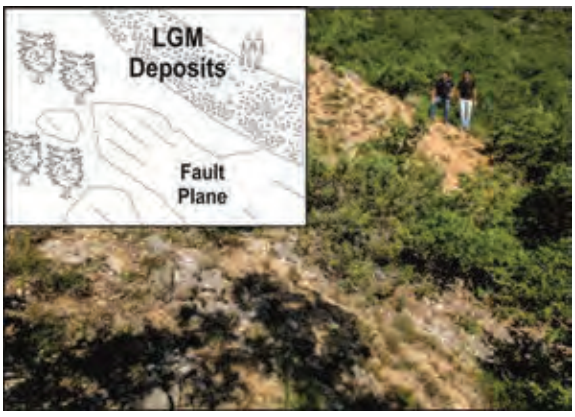

Figure 6: Detail of the LGM deposits sealing the San Giovanni fault (n° 4 in Fig. 2).

Where the lack of data makes difficult the identification of the origin of the landforms, the excavation of paleoseismological trenches permitted to evaluate the state of fault activity.
For example the Valle Daria paleosurface is characterized by a large number of convex-concave profiles forming some flat-bottom depressions; these are roughly N-S oriented and filled by eluvium-colluvial materials. Bagnaia *at al.* (1989) interpreted these features as paleodrainages; on the contrary Bertini and Bosi (1993) favoured for a tectonic origin. In fact they considered this paleodrainage "oversized" compared to the current erosional/depositional capability of the water streams. Thus, to better understand the origin of these geomorphologic features, we achieved a paleoseismological trench across one of these escarpments, boarding the valleys.
Pezzo *et al.* (in preparation) identify a wide deformation zone (more than two metres) and at least two seismic events, one of which involves all the units identified in the trench, excluding the current soil (Fig. 7). For this reasons we can hypothesize a tectonic origin of the escarpment: this can be considered as a fault escarpment and the associated fault can be considered as an active and capable fault.

Figure 7: Detail of the paleoseismological trench (Pezzo et al., in preparation), (black star in fig. 2). A wide tectonic deformation zone involving the late Pleistocene - Holocene deposits can be recognized along the trench.

DISCUSSION

In this study, we assess the capability of a large number of faults in a territory characterized by a high density of Quaternary faults and also characterized by a high density of urban settlements involved in the phase of post-seismic rebuilding. Even if a regional or national law about urban development and fault capability does not exist, some new criteria have been recently proposed by Boncio *et al.* (2012) and subsequently accepted in different temporary versions of *Linee guida per la gestione del territorio in aree interessate da faglie attive e capaci (FAC)* (in preparation).
These criteria concern the land use in areas affected by active and capable faults and are mainly based on the Californian law *Alquist - Priolo Fault Zoning Act* (APFZA, Bryan and Hart, 2007), on the *Planning for the development of land on or close to active fault* (Ministry for the Environent, New Zeland, 2003) and on the criteria regarding the minimum standards for the surface rupture faulting risk established by Batatian (2002).
However some important differences between Italian and Californian context have to be considered, both from cultural and seismological point of view.
Density of population and villages built up close to alleged active faults, coupled with their low rate of surface faulting and frequency of occurrence, would induce us to consider the APFZA not applicable in its original form to the Italian context.
Comparing the Californian earthquake records with respect to the Italian ones [for example with the review of 20 years of paleoseismological studies in Italy provided by Galli *et al.* (2008)], we observe that the

average recurrence time of the main earthquakes is in the order of thousands of years: an order of magnitude longer than the Californian one.

On the other hand, the Alquist Priolo Fault Zoning Act was born in a completely different cultural and political context with respect to the Italian one. More specifically, it was born in response to the necessity to find suitable sites for building nuclear power plants. Starting from this observation, it is necessary to point out some other differences, like the greater density of ancient and modern urban settlements in the Italian peninsula and the lower ages of California human settlements.

In this work we show that many ancient settlements of the Middle Aterno Valley are affected by the presence of capable faults (e.g. Prata D'Ansidonia, Poggio Picenze, San Demetrio ne' Vestini, etc.). Consequently, the main focus should be the identification of rational criteria regulating the post seismic rebuilding and, only secondly, the new buildings or settlements.

In the Italian context, the identification of suitable sites where rebuild settlements destroyed during earthquakes, involves many other problems. In fact, we have seen that the high density of capable faults, as identified in this work, make difficult the site choice, in a territory showing widespread different geological hazards. Indeed, the 2009 L'Aquila earthquake showed that the most damaged areas are not located along capable fault traces; on the contrary the majority of damages has been related to site effects due to the propagation of the seismic waves from the substratum to the Quaternary continental deposits. Consequently, the reconstruction of destroyed settlements in new sites, where no capable faults are recognized, not necessarily decrease the total risk. In this case, it could be useful to introduce the concept of admissible minimum risk related to the localization of a new site: the criteria to localize suitable sites must consider a synoptic overview of all geological hazards, where the risk associated to the surface faulting could be less than the risk due to the local seismic response. Moreover, the relocation of urban settlements in an area characterized by an ancient history of urbanization may bring the loss of the cultural identity of this territory, the progressive abandonment of the settlement, and any certainty of the seismic-related risk mitigation.

References

Atzori, S., I. Hunstad, M. Chini, S. Salvi, C.Tolomei, C. Bignami, S. Stramondo, E. Trasatti, A. Antonioli & E. Boschi, (2009). Finite fault inversion of DInSAR coseismic displacement of the 2009 L'Aquila earthquake (central Italy). *Geophys. Res. Lett.* 36, L15305, doi:10.1029/2009GL039293.

Bagnaia, R., A. D'Epifanio & S. Sylos Labini, (1989). Aquila and Subequan basins: an example of quaternary evolution in the Central Apennines, Italy. *Quat. Nova*. 1: 1-23.

Batatian, D., (2002). *Minimum standards for surface fault rupture hazard studies, in Salt Lake County Geologic Hazards Ordinance*. available at www.pwpds.slco.org/zoning/pdf/geologichazards/AppAfaultReportMinStds.pdf.

Bertini, T., C. Bosi, (1993). La tettonica quaternaria della conca di Fossa (L'Aquila). *Il Quaternario*. 6, 293–314.

Boncio, P., P. Galli, G. Naso & A. Pizzi, (2012). Zoning surface rupture hazard along normal faults: insight from the 2009 Mw 6.3 L'Aquila, central Italy, earthquake and other global earthquakes. *Bulletin of the Seismological Society of America*. 102 (3).

Bosi, C., F. Galadini, (1995). La fagliazione di superficie come elemento di fragilità delterritorio. *Geologia Applicata e Idrogeologia*. 30, 29-43.

Bryant, W.A., E.W. Hart, (2007). Fault-rupture hazard zones in California. Alquist–Priolo Earthquake Fault Zoning Act with Index to Earthquake Fault Zones Maps. *California Geological Survey, Spec. Publ*. 42, 42 pp.

Faccioli, E., I. Anastasopoulos, G. Gazetas, A. Callerio & R. Paolucci, (2008). Fault rupture-foundation interaction: selected case histories. *Bulletin of Earthquake Engineering*, 6, 557–583.

Galadini F., E. Falcucci, P. Galli, B. Giaccio, S. Gori, P. Messina, M. Moro, M. Saroli, G. Scardia & A. Sposato, (2012). Time intervals to assess active and capable faults for engineering practices in Italy. *Eng. Geology*. 139-140, 50-65, DOI: 10.1016/j.enggeo.2012.03.012

Galli, P., F. Galadini & D. Pantosti, (2008). Twenty years of paleoseismology in Italy. *Earth-Science Reviews*, 88, 89-117.

Gruppo di Lavoro MS, (2008). *Indirizzi e criteri per la microzonazione sismica*. Conferenza delle Regioni delle Province autonome - Dipartimento della protezione civile. Presidenza del Consiglio dei Ministri, Dipartimento della Protezione Civile, Roma, 3 vol.

Guerrieri, L., A.M. Blumetti, P. Dimanna, L. Serva, E. Vittori, (2009). The exposure of urban areas to surface faulting hazard in Italy; a quantitative analysis. Italian *Journal of Geosciences* (Bollettino della Società Geologica Italiana). 128, 179-189.

IAEA, (2003) - Evaluation of Seismic Hazards for Nuclear Power plants. *Safety Standards Series*. No. NS-G-3.3, 40 pp.

Ministry for the Environment New Zealand, (2003). *Planning for the development of land on or close to active faults. A guideline to assist resource management planners in New Zealand.* http://www.mfe.govt.nz/publications/rma/ planning-development-active-faults-dec04/index.html

NTC Norme Tecniche per le Costruzioni, (2008). DM 14 gennaio 2008, *Gazzetta Ufficiale*, n. 29 del 4 febbraio 2008, Supplemento Ordinario n. 30, www.cslp.it, Istituto Poligrafico e Zecca dello Stato, Roma.

Paolucci, R., S. Mariani & S. Griffini, (2010). Simplified modelling of continuous buried pipelines subject to earthquake fault rupture. *Earthquake and Structures*. 1, 253-267.

Pezzo G., M. Moro, M. Saroli, L. Lo Sardo, G. Fubelli, M. Lancia & F. Galadini, (in preparation). *Ancient settlements in central Italy and capable faults: (Italy)*.

Serva, L., (1992). *An analysis of the world major regulatory guides for NPP seismicdesign. A guideline for high risk facilities*. Report ENEA RT/DISP/92/03. 44 pp.

Slemmons, D.B., R. McKinney, (1977). *Definition of "active fault"*. Miscellaneous paper, S-77-8. U.S. Army Engineer Waterways Experiment Station. Soils and Pavements Laboratory, Vicksburg, Miss., 23 pp.

Tondi, E., 2000. Geological analysis and seismic hazard in the central Apennines (Italy). *Journal of Geodynamics*. 29, 517-533.

INQUA Focus Group on Paleoseismology and Active Tectonics

A transect of quaternary geological slip rates in the Kazakh Tien Shan

Mackenzie, D. (1), Abdrakhmatov, K. (2), Campbell, G. (3), Grützner, C. (3), Carson, E. (1), Moldobaev, A. (4), Mukambayev, A. (4), Walker, R.T. (1)

(1) Dept. of Earth Sciences, University of Oxford, South Parks Rd, Oxford, OX 1 4AR, UK. Email: david.mackenzie@earth.ox.ac.uk
(2) Kyrgyz Institute of Seismology, Bishkek, Kyrgyzstan
(3) Bullard Laboratories, Department of Earth Sciences, University of Cambridge, Cambridge, UK
(4) Kazakhstan National Data Center, Chaikinoy str. 4, 050020 Almaty, Kazakhstan

Abstract: *Large faults in the Tien Shan give rise to significant seismic hazard for cities in Kazakhstan, Kyrgyzstan and China, but as yet little is known about fault slip rates and the relative importance of the various structures in the region, so seismic hazard is poorly constrained. We present here a systematic approach to constrain fault slip rates throughout the region through dating of quaternary geomorphic features offset by fault motion. We apply this to a N-S transect of seven faults in eastern Kazakhstan, linking in several places to the most recent surface-ruptures on the faults also. These slip rates provide an estimate of the distribution of tectonic shortening across the region beyond the resolution limit of geodetic methods.*

Key words: *Kazakhstan, Tien Shan, Slip rate, Shortening.*

INTRODUCTION

The mountain ranges of central Asia (Pamir, Tien Shan, Borohoro Shan, Dzungarian Alatau, and the Kazakh and Mongolian Altai) represent the northernmost expression of the India-Eurasia collision zone (*Molnar and Tapponnier*, 1975; *Tapponnier and Molnar*, 1979; *Bullen and Burbank*, 2001). The intense deformation in the Himalaya has concealed or destroyed much of the evidence from the early stages of continental collision. Mountain building in the far-field regime (with less cumulative deformation) can however provide a sensitive measure of processes going on at the collision front.

Central Asia is also an under-studied area of potentially high seismic risk, with low strain rates, poor historical records and rare but damaging high magnitude earthquakes. In the past couple of centuries there have been a number of large (M_W >7) destructive earthquakes in the region (*Bogdanovich et al.*, 1914; *Ghose and Mellors*, 1997) but only a small fraction of the known active faults have failed in recorded history. Few mapped faults have known slip-rates and many more faults are still unmapped. Due to a lack of slip-rate data and incomplete mapping, current seismic hazard assessments are based entirely on instrumental seismicity and geodetic observations. However, with earthquake recurrence intervals of typically several thousand years and fault strain rates below the geodetic resolution limit, the instrumental record only samples a very small fraction of the seismic cycle.

In Kazakhstan, the compressional mountain building is separated into two discrete bands, the high Tien Shan and the Dzungarian Alatau, between them accommodating a significant fraction (around one quarter) of the ~35 mm/yr India-Eurasia convergence (*Abdrakhmatov et al.*, 1996). This tectonic shortening is accommodated by a series of E-W oriented thrust faults and conjugate strike slip faulting. Identifying the fastest moving and most important faults can give us an insight into seismic hazard assessment and, in combination with thermochronology data, the initiation, growth and propagation of mountain building.

Here we construct a transect of geological shortening rates across the Kazakh and Kyrgyz Tien Shan and the Dzungarian Alatau (shown by the line A-A" in figure 1). In this slowly deforming region (< 8 mm/yr across at least 8-10 faults), we aim to compare the rates of geological shortening with those indicated by geodetic data through the region. This will also allow us to determine which faults are likely to be the most seismically active and, in combination with palaeoseismology, estimate possible earthquake magnitudes and recurrence intervals on the faults.

Two similar studies have previously been carried out further to the west, in Kyrgyzstan, by *Thompson* (2002) and in an unpublished thesis (Ray Weldon, *pers. comms.)*. Older studies completed before modern dating techniques were available were based on estimated alluvial fan ages from climate records – these include *Avouac and Tapponnier* (1993), further east in the Borohoro Shan, China.

METHODS

The main aim of this work is to constrain a series of slip rates and shortening rates on the E-W striking thrust faults in a N-S profile. Initial reconnaissance by remote sensing is used to map the active faults and identify well situated sites for field studies. To that end we choose sites on each fault which display clearly displaced geomorphological markers in Quaternary material.

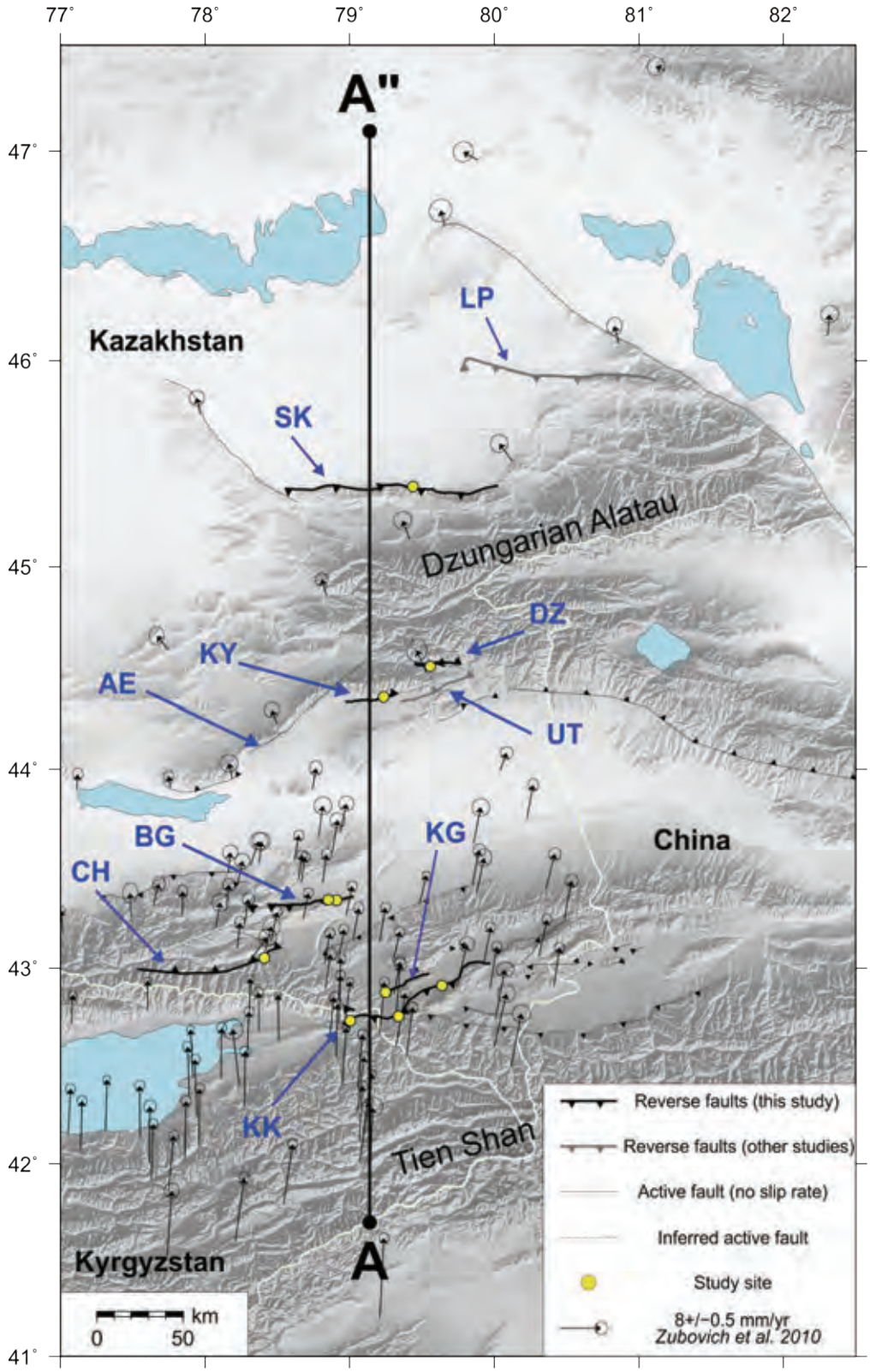

Figure 1: An overview of the Kazakh Tien Shan and Dzungarian Alatau in shaded relief from SRTM elevation data. Faults shown in bold are those we have performed slip-rate studies on, with the individual field sites shown in yellow. Other known active faults are also marked, with inferred faults shown as dotted lines. The Zubovich et al. (2010) regional GPS vectors (relative to fixed Eurasia) are shown with 95% confidence ellipses and the line A-A" is the profile onto which the GPS is projected in figure 2. Labels: KK-Karkara Fault, CH-Chilik Fault, BG-Bartogay Fault, KY-Konyrolen Fault, AE-Altyn Emel, UT-Usek Thrust, DZ-Dzungarian southern rangefront fault, SK-Sarkand Fault, LP-Lepsy Fault.

INQUA Focus Group on Paleoseismology and Active Tectonics

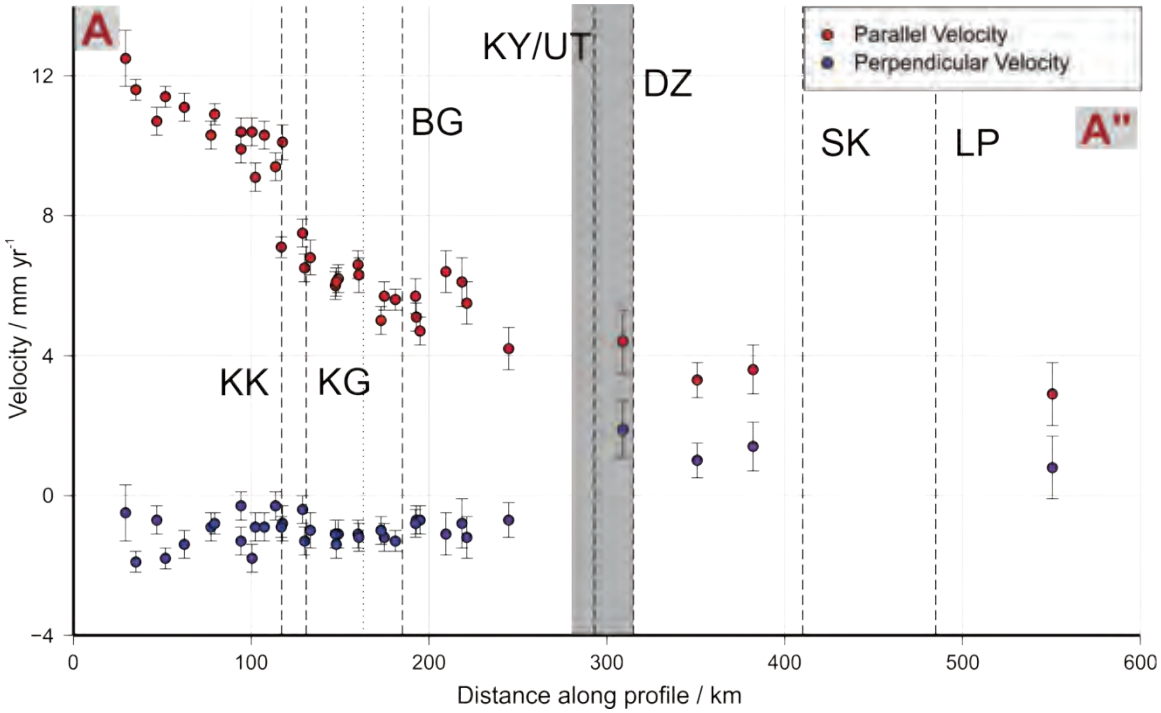

Figure 2: Regional GPS data from Zubovich et al. (2010) projected onto the line A-A", resolved into profile-parallel (red) and profile-perpendicular components. Stations from within 40 km either side of the profile are shown. Faults mapped in figure 1 are shown as dashed lines (see figure 1 caption for fault labels). Shown as a shaded region is the approximate projection of the sub-perpendicular Altyn Emel (AE) strike slip fault. We see a significant drop of ~3-4 mm/yr in the northwards (parallel) velocity across the Karkara rangefront, but the majority of the faults are unresolved. The Altyn Emel fault (AE in figure 1) may be responsible for the change in perpendicular velocity at 250-300 km. The dotted line represents a prominent fault (marked in figure 1), on which we were unable to measure a slip-rate due to poor expression in Quaternary materials – geomorphic expression does however suggest that the fault is active.

These include displaced alluvial fans, fluvial river terraces and archaeological features etc. In order to accurately quantify the morphological offsets, we use aerial photos acquired from a helium balloon to reconstruct a digital elevation model (DEM) by structure from motion (SfM) based photogrammetry (*Johnson et al.*, 2014). We further use these DEMs to quantify earthquake surface slip distributions along strike.

For the majority of our sites, we date the displaced markers by a combination of radiocarbon dating and quartz/feldspar optically/infrared stimulated luminescence (OSL/IRSL). For surfaces beyond the limit for radiocarbon, or without material for radiocarbon/OSL dating, we turn to cosmogenic dating. In some limited locations, we can also perform Uranium-Thorium dating on well stratified carbonate cements on the undersides of pebbles within the surface to be dated. Wherever possible, we use a combination of these methods.

FAULTS

We select 8 faults of interest in the region of this transect, as shown in figure 1, of which two have slip-rates published already (the Lepsy fault, (*Campbell et al. In Rev.)* and the Usek Thrust, (*Cording et al.*, 2014), LP and UT in grey in figure 1). At each of these faults, we have 1-3 field sites. Below are described a selection of these faults:

Karkara Rangefront (KK)

This fault is the only one resolvable in the GPS (figure 2), which suggests that is likely to be a significant fault. Our study site here focuses on a flight of fluvial river terraces progressively offset by fault motion, by up to 60 m. Through radiocarbon dating, we find a preliminary slip rate of 1.6-3.5mm/yr, though further dating is in progress (see *Mackenzie et al. this Volume* for more details).

Bartogay Fault (BG)

At this fault a large offset of ~12m in an alluvial fan surface provides a linear marker. With a granitic catchment, this fan is a good target for dating with a cosmogenic beryllium-10 depth profile, and OSL. We have also performed trenching at this site, on a lower section of scarp to study the most recent earthquake(s) on the fault. This fault therefore provides us with an important link between the long term fault behaviour in the region and the behaviour in individual earthquakes (see *Carson et al, this volume)* for more details).

Dzungarian Southern Rangefront (DZ)

One of two significant faults on the southern rangefront of the Dzungarian Alatau, this fault has in most places broken the surface in two parallel strands. Thus we choose to date a large fan surface in which we can clearly measure a total offset of ~30 m. With such large

offsets it is likely that the fans are beyond the range of radiocarbon dating, but we find well-developed U-Th rinds on the undersides of boulders embedded at depths of ~0.6 m within the fan. In conjunction with an OSL sample this should give us a reliable age for the fan deposits, and hence slip-rate on the fault.

Sarkand Fault (SK)

The major northern rangefront of the Dzungarian Alatau (with exception of the Dzungarian Fault to the NE, (*Campbell et al.*, 2013)), this fault appears to be moving more slowly than those further south. In the few locations that scarps are visible, they are heavily degraded. Again we date a fan surface displaced by the fault, and perform an aerial survey to study the slip distribution along strike. However, the smaller scarp of ~6 m, suggests that this represents only a 2-3 earthquakes, so any slip rate estimate here will be poorly constrained. We have also sampled from several fans which are undisturbed by the fault in attempt to constrain the minimum age of the most recent event on the fault.

CONCLUSIONS

We have identified and mapped numerous faults which displace quaternary deposits across the region of SE Kazakhstan, showing that active deformation is clearly distributed across the whole region. We have also demonstrated the utility of structure-from-motion photogrammetry both in measuring individual geomorphic marker offsets and in assessing the distribution of slip along strike. Much of the dating work is still in progress, but we aim to form a relatively comprehensive study across the majority of the identifiably active structures in the region.

Acknowledgements: We thank the members of the Oxford Radiocarbon Accelerator Unit (ORAU) and Beta Analytics for their work and advice on radiocarbon samples. DM, GC, CG, and RW are part of COMET+: http://comet.nerc.ac.uk/. This study was conducted in the framework of the Earthquakes without Frontiers project: http://ewf.nerc.ac.uk/.

References

Abdrakhmatov, K.Y., S.A. Aldazhanov, B.H. Hager, M.W. Hamburger, T.A. Herring, K.B. Kalabaev, V.I. Makarov and P. Molnar, (1996). Relatively recent construction of the Tien Shan inferred from GPS measurements of present-day crustal deformation rates. *Lett. to Nat. 384*.

Avouac, J. and P. Tapponnier, (1993). Active thrusting and folding along the northern Tien Shan and late Cenozoic rotation of the Tarim relative to Dzungaria and Kazakhstan. *J. Geophys. Res. 98* (B4), 6755-6804.

Bogdanovich, K.I., I.M. Kark, B.Y. Korol'kov and D.I. Mushketov, (1914). Earthquake in northern district of Tien Shan, 22 December 1911 (4 January 1911). Paper presented at Geology Committee. *New series,* 89. St. Petersburg (in Russian, extended abstract in French).

Bullen, M. and D. Burbank, (2001). Late Cenozoic tectonic evolution of the northwestern Tien Shan: New age estimates for the initiation of mountain building. *Geol. Soc. Am. Bull. 113* (12), 1544-1559, doi:10.1130/0016-7606.

Campbell, G.E., R.T. Walker, K. Abdrakhmatov, J. Schwenninger, J. Jackson, J.R. Elliott and A. Copley, (2013). The Dzhungarian fault: Late Quaternary tectonics and slip rate of a major right-lateral strike-slip fault in the northern Tien Shan region. *J. Geophys. Res. Solid Earth*. *118*, 5681-5698, doi:10.1002/jgrb.50367.

Cording, A., R. Hetzel, M. Kober and J. Kley, (2014). 10Be exposure dating of river terraces at the southern mountain front of the Dzungarian Alatau (SE Kazakhstan) reveals rate of thrust faulting over the past ~400ka. *Quat. Res. 81* (1), 168-178, doi:10.1016/j.yqres.2013.10.016.

Ghose, S. and R. Mellors (1997). The Ms = 7.3 1992 Suusamyr, Kyrgyzstan, earthquake in the Tien Shan: 2. Aftershock focal mechanisms and surface deformation. *Bull. Seismol. Soc. Am. 87* (1), 23-38.

Johnson, K., E. Nissen, S. Saripalli, J. R. Arrowsmith, P. Mcgarey, P. Williams and K. Blisniuk, (2014). Rapid mapping of ultrafine fault zone topography with structure from motion. *Geosphere*. *10* (5), 969-986, doi:10.1130/GES01017.1.

Molnar, P. and P. Tapponnier, (1975). Cenozoic tectonics of Asia: Effects of a continental collision, *Science*. *189* (4201), 419-426.

Tapponnier, P. and P. Molnar, (1979). Active faulting and Cenozoic tectonics of the Tien Shan, Mongolia, and Baykal regions. *J. Geophys. Res. Solid Earth*. *84* (B7).

Thompson, S.C., (2002). Late Quaternary slip rates across the central Tien Shan, Kyrgyzstan, central Asia. *J. Geophys. Res. 107* (B9), 2203, doi:10.1029/2001JB000596.

INQUA Focus Group on Paleoseismology and Active Tectonics

A fault slip-rate on the northern front of the High Tien Shan, Kazakhstan

Mackenzie, D. (1), Walker, R.T. (1), Abdrakhmatov, K. (2), Campbell, G. (3), Grützner, C. (3), Moldobaev, A. (4), Mukambayev, A. (4)

(1) Dept. of Earth Sciences, University of Oxford, South Parks Rd, Oxford, OX 1 4AR, UK. Email: david.mackenzie@earth.ox.ac.uk
(2) Kyrgyz Institute of Seismology, Bishkek, Kyrgyzstan
(3) Bullard Laboratories, Department of Earth Sciences, University of Cambridge, Cambridge, UK
(4) Kazakhstan National Data Center, Chaikinoy str. 4, 050020 Almaty, Kazakhstan

Abstract: *Large faults in the Tien Shan give rise to significant seismic hazard for cities in Kazakhstan, Kyrgyzstan and China, but as yet little is known about slip rates and the relative importance of faults in the region, so seismic hazard is poorly constrained. We present a slip-rate study on the northern rangefront of the Khan Tengri Massif in the Kazakh and Kyrgyz Tien Shan, based on dating of fluvial river terraces offset by fault motion by up to 60 m. We demonstrate the utility of structure-from-motion based photogrammetry and satellite stereo photogrammetry in generating digital elevation models for the quantitative assessment of geomorphic offsets over a variety of scales. We find a preliminary slip rate of 1.6-3.5 mm/yr.*

Key words: *Tien Shan, structure-from-motion, slip-rate, Kazakhstan.*

INTRODUCTION

Establishing the spatial distribution of shortening within continental interiors is important both in the assessment of seismic hazard and to investigate the active tectonics of the initiation, growth and propagation of mountain ranges. In the Tien Shan and Dzungarian Alatau of Kazakhstan, tectonic shortening is driven by the India-Eurasia collision, with approximately 10 mm/yr (around one quarter) of the total plate convergence is taken up across this region. This shortening is accommodated by a series of E-W oriented thrust faults and conjugate strike slip faulting, with faults extending up to several hundred kilometres in length (*Tapponnier and Molnar*, 1979; *Thompson*, 2002; *Selander et al.*, 2012).

Identifying the fastest moving and most important faults can give us an insight into the processes forming the mountains, but also holds important conclusions for earthquake hazard assessment - for example, in the past couple of centuries there have been a number of large (M_w >7) destructive earthquakes in the region (*Campbell et al.*, 2013 and references therein). However, only a small fraction of the known active faults have failed in recorded history and recurrence intervals may be in the order of thousands of years. Thus current seismic hazard assessments based on instrumental records covering the last ~100 yrs are incomplete.

STUDY SITE

We present here a case study of the northern rangefront fault of the Khan Tengri Massif (figure 1) which, according to regional GPS (*Zubovich et al.*, 2010), accommodates a significant portion of the regional convergence. This study aims to determine a geological slip-rate on the rangefront to determine its relative importance in the region. In the regional GPS velocity field, the majority of the faults in the region are not well resolved. However the rangefront at Karkara coincides with a drop of ~3-4 mm/yr in northwards velocity (see *Mackenzie et al., this volume*).

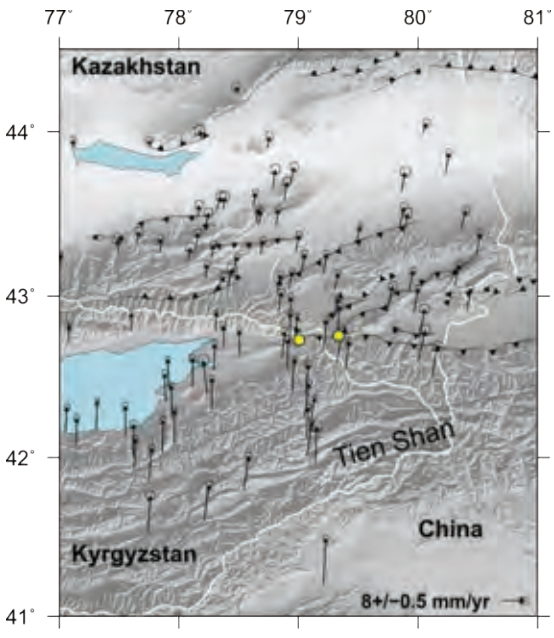

Figure 1: An overview of the Ili, Issyk and Narynkol basins of SE Kazakhstan. Study sites on the karkara fault are shown in yellow. GPS velocity vectors are from Zubovich et al., 2010 and ellipses indicate the 95% confidence interval. A significant amount of shortening is accommodated by the reverse faults in the region.

The fault is situated at an altitude of ~2300 m, rising to ~4000 m in the hanging wall of the fault, though the larger massif reaches altitudes up to ~7000 m further south. The fault strikes E-W, dips to the south, and

extends around 60 km, though it is part of the much larger rangefront of the massif which extends over 500 km into Kyrgyzstan and China and forms the boundary of the Issyk and Narynkol Basins. It is unclear how far ruptures could propagate. The range is cored with Palaeozoic bedrock, but the surface expression of the fault has propagated ~2-3 km north from the Palaeozoic contact and tertiary basin deposits are uplifted in the hanging wall.

Near the town of Karkara, the uplift associated with the rangefront fault has resulted in a series of fluvial terraces, formed as a response to past climate conditions, in each river valley crossing the fault. The terraces are cut into Neogene sediments and are capped with fluvial gravels, with a thick soil development on top. These terraces provide a geomorphic marker, with each terrace being progressively uplifted by movement on the fault (figure 2). By dating the terrace formation and measuring the offset on the terraces, we constrain the vertical displacement rate.

DISCUSSION

In order to accurately establish the terrace offsets and correlate terraces over the scale of the river valley (~1x4 km), it is necessary to construct a digital elevation model (DEM) of the valley.

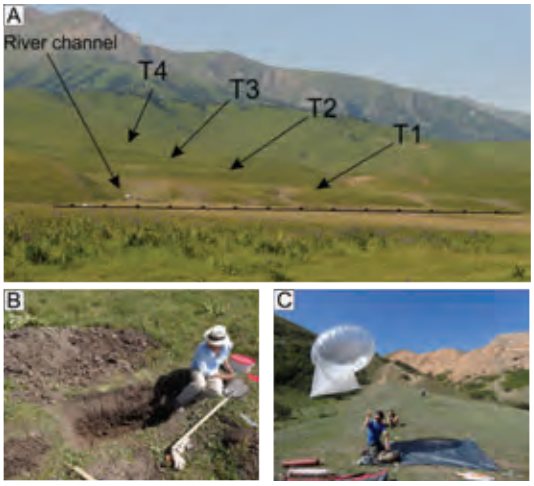

Figure 2: (A) An overview of the stepped terraces, T1-4, with the fault in the foreground. (B) We sampled for radiocarbon dating of sediments from each of the four terraces. (C) The Helikite used to obtain aerial photos for photogrammetric reconstruction to produce an elevation model of the river valley.

To achieve a DEM of sufficient resolution, we implement a workflow using photogrammetric reconstruction, by structure-from-motion (SfM) based on methods by *James and Robson* (2012) and *Johnson et al.* (2014). We use a compact digital camera (Ricoh GR Digital II) suspended from a helium filled Helikite (Allsopp Helikite Ltd.) to collect the aerial photographs for the reconstruction. The resulting DEM has a resolution of ~0.3 m (figure 3), with a scale accuracy of ~1%, demonstrating the utility of this method in assessing geomorphic structures.

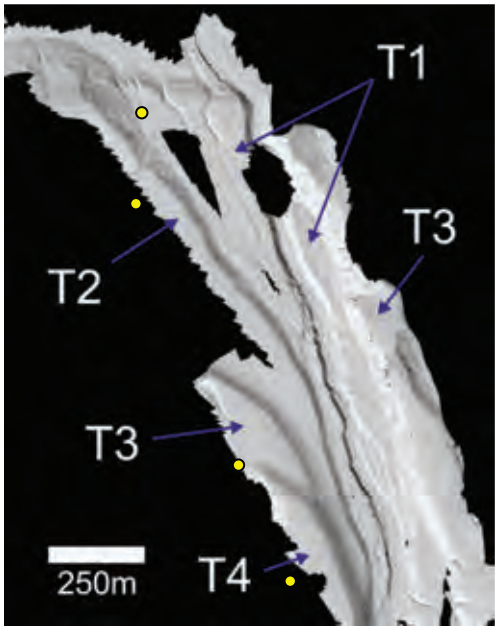

Figure 3: Shaded relief of the 0.3 m-resolution DEM produced by structure-from-motion photogrammetry. Yellow dots represent sampling locations.

In addition to the SfM DEM for the field site, we use 0.5 m Pleiades satellite stereo imagery to generate a wider area DEM at a resolution of ~1 m over a 30 km stretch along the rangefront in order to correlate the river terraces between valleys along a larger portion of the fault. Both of these methods also generate a high resolution orthoimage which is extremely useful for detailed mapping.

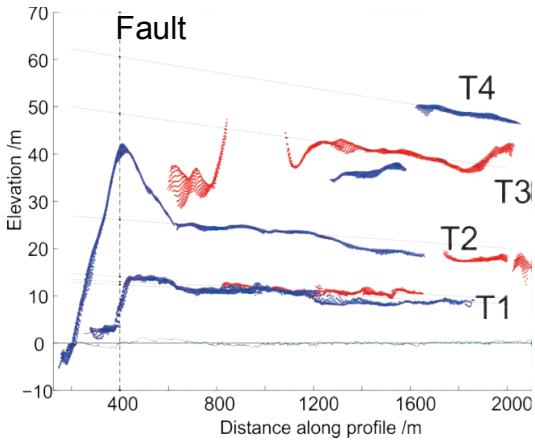

Figure 4: Terrace profiles for the fluvial terraces at Karkara, extracted from SfM elevation point cloud. Red and blue show the sections to the East and West of the river channel respectively. A linear river gradient has been removed to aid visualisation. Residuals in the river fit are shown as a faint line and are less than 1 m.

The DEM of the river valley (figure 3) and kinematic differential GPS (DGPS) profiles reveal that the terraces T1, T2, T3, T4 are offset vertically by ~10, ~22, ~45 and ~57 metres respectively (figure 4). We also note the back-tilting of T1 and T2 near the scarp (within ~100m) and attribute this to a steepening in the fault dip towards the surface in the uppermost 50-100 m of sediments.

Figure 5: (left) Sampling pit in T4, generally poorly defined stratigraphy, with a soil unit overlying soft red/brown clay interspersed with some gravel. (right) Sampling pit in T1. ~0.45 m Soil thickness, overlying fluvial gravels.

Radiocarbon dating of the material retrieved (figures 2 and 5) from the terraces is ongoing and preliminary results show a spread in ages, but suggest a lower bound on the uplift rate of ~1-1.5 mm/yr.

Estimating a slip-rate and shortening rate for the fault remains difficult however, as were unable to find fault plane exposures from which to estimate the dip. The relatively sinuous fault trace suggests a low dip in the shallow sediments, though this may be higher at depth (c.f. basement faults are often found to be >45° at depth (*Avouac and Tapponnier*, 1993)). So taking a conservative dip range of 25-40°, this would result in a slip-rate of 1.6-3.5 mm/yr, making this fault likely to be the most significant in the region.

In order to constrain the fault dip and provide further constraint on the fault activity, we carried out a second study on a site ~30 km further east, in Kyrgyzstan. A hammer seismic survey was carried out across a 14 m terrace offset, along with further collection of material for dating. These data are still being processed, but the shallow stratigraphy should provide a constraint on the shallow fault dip.

CONCLUSIONS

We find a lower bound on the slip rate of the Karkara Fault, the northern rangefront of the Khan Tengri Massif of the Tien Shan, of 1.6-3.5 mm/yr. This is the fastest known slip-rate in the northern Tien Shan. We also demonstrate the utility of structure-from-motion photogrammetry in creating digital elevation models, especially in extremely remote locations, with resolution of better than 0.3 m. These elevation models allow us to accurately quantify offsets in features displaced by faults at a variety of scales. This study forms part of a larger study to quantify fault slip rates across the Kazakh Tien Shan and Dzungarian Alatau (*Mackenzie et al., This volume)*.

Acknowledgements: DM, RW, GC, and CG are part of COMET+: http://comet.nerc.ac.uk/. This study was conducted in the framework of the Earthquakes without Frontiers project: http://ewf.nerc.ac.uk/.

References

Avouac, J. and P. Tapponnier, (1993). Active thrusting and folding along the northern Tien Shan and late Cenozoic rotation of the Tarim relative to Dzungaria and Kazakhstan. *J. Geophys. Res. 98* (B4), 6755-6804.

Campbell, G.E., R.T. Walker, K. Abdrakhmatov, J. Schwenninger, J. Jackson, J.R. Elliott and A. Copley, (2013). The Dzhungarian fault: Late Quaternary tectonics and slip rate of a major right-lateral strike-slip fault in the northern Tien Shan region. *J. Geophys. Res. Solid Earth*. *118*, 5681-5698, doi:10.1002/jgrb.50367.

James, M.R. and S. Robson, (2012). Straightforward reconstruction of 3D surfaces and topography with a camera: Accuracy and geoscience application. *J. Geophys. Res. 117* (F3), F03017, doi:10.1029/2011JF002289.

Johnson, K., E. Nissen, S. Saripalli, J.R. Arrowsmith, P. Mcgarey, P. Williams and K. Blisniuk, (2014). Rapid mapping of ultrafine fault zone topography with structure from motion. *Geosphere*. *10* (5), 969-986, doi:10.1130/GES01017.1.

Selander, J., M. Oskin, C. Ormukov and K. Abdrakhmatov, (2012). Inherited strike-slip faults as an origin for basement-cored uplifts: Example of the Kungey and Zailiskey ranges, northern Tian Shan. *Tectonics*. *31*(4), doi:10.1029/2011TC003002.

Tapponnier, P. and P. Molnar, (1979). Active faulting and Cenozoic tectonics of the Tien Shan, Mongolia, and Baykal regions. *J. Geophys. Res. Solid Earth*. *84* (B7).

Thompson, S.C., (2002). Late Quaternary slip rates across the central Tien Shan, Kyrgyzstan, central Asia. *J. Geophys. Res. 107* (B9), 2203, doi:10.1029/2001JB000596.

Zubovich, A.V. et al., (2010). GPS velocity field for the Tien Shan and surrounding regions. *Tectonics*. *29* (6), TC6014, doi:10.1029/2010TC002772.

INQUA Focus Group on Paleoseismology and Active Tectonics

Seismic Microzonation using Microtremor in Denpasar City, Bali, Indonesia

Marjiyono and Kamawan

(1) Geological Survey Institute, Geology Agency, Energy and Mineral Resources Ministry of Republic of Indonesia, Jl. Diponegoro No. 57 Bandung 40122, Indonesia. Email: marjiyono@emailcorner.net

Abstract: *The understanding of surface geological condition is a fundamental interest in seismic microzonation due to amplify incidence seismic wave. In order to characterizing near-surface material in Denpasar City and surrounding area, we applying combination of array and single station microtremor to obtain subsurface model. The two most important parameters that define the response of surface soft rock layers to shaking are layer thickness and shear wave velocity structure. Spacial autocorelation (SPAC) method was applied to obtain shear wave velocity profile in 19 sites. In this paper, the response to shaking is expressed by means of a SH-transfer function. This function shows the relative amplification of shaking as a function frequency.The result of the calculation mean amplification of Denpasar City and surounding area are 1.2-2.1.Seismic microzonation map which shows outline zones of different potential shaking intensities was compiled based on these parameter. The high amplification zone is associate to alluvial deposit in the southern part of study area.*

Key words: *Microtremor, mean amplification, seismic microzonation, SH transfer function.*

INTRODUCTION

Bali Island is the famous international tourist destination, morfologically in the northern part are volcanic range while the southern part, including the capital city of Denpasar are low lying plain where the piroclastic and fluvial processes sedimented around this area. Therefore, Denpasar City have potential risk of ground shaking due to soft sediment/soil amplification. In other hand, tectonically Bali Island also close to active seismic sources i.e. Indo-Australia oceanic plate subduction in the south, back arc thrust in the north and some local structures in the land. Two historical earthquakes in northern part of Bali Island: 1976 Seririt and 1979 Culik Earthquake with magnitude respectivelly 6.1 mb and 5,8 (Kertapati and Putranto, 2004) were associate to local geological structures caused partially destroyed around the epicenters.

As the capital city of the Bali province, Denpasar city is rapidly growth, various tourism facility have been constructed. In order to mitigate impact of ground shaking disaster which may occurred in the future, surface geological characterizing was conducted. Ideally, subsurface model are inferred from drilling other geotechnical data, however for wide area its costly and time consuming. An alternative fast method for soft surface sediment/soil characterizing is microtremor measurements (Bour, et.al., 1998, Mirzaoglu and Dykmen, 2003). In this investigation, we apply combination of array and single station microtremor for subsurface modelling.

Application of microtremors for soil characterizing was initially proposed by Kanai and Tanaka (1961). They explained that microtremors as multiple reflection of SH waves in parallel subsoil layer, while Akamatsu (1961) considered microtremor mainly the combination of Love and Rayleigh waves. In site response analysis, shear wave velocity is the most parameter as indicator of stiffness (Aki and Richard, 1980). In this paper, shear wave velocity profile was inverted from array measurements. Based on the subsurface model, site amplification was calculated as basic of seismic microzonation.

Geological Setting

Denpasar City is located on the southern part of Bali Island. The urban area of Denpasar plain mainly formed by quaternary deposits of the Buyan-Bratan-Batur volcanic group dominantly by lahar and tuff, while around the coast southern part of investigation area are covered by alluvial. The southern tip of Bali Island are formed by Miocene coral reef and in some sites founded clastic limestone of the Selatan Formation (Figure 1).

Figure 1: Geological map of investigation area (compiled from Hadiwidjojo, et.al.,1998).

Microtremor Measurements

In this study we conducted array microtremor measurement in 19 sites, while single station microtremor in 298 sites around the Denpasar City (Figure 2). SPAC method was applied to invert shear wave velocity profiles for each array microtremor site, and then interpolated to obtain velocity structure throughout investigation area. At each site, triangle-nested configuration with fourth station at the center were used to record ambient noise. In order to cover shallow layer, station separation was started from small distance: 2, 5, 10, 20, 50 m. The duration of recording was 30 minutes to one hour dependent to station separation. The instrument used for the field campaign was accelerometer OYO 1134 with A/D converter 32 bit.

The computation of the cross correlation coefficients was done for all pairs of simultaneous recordings of ambient noise and the average cross correlation determined for any given station separation. Mathematically, the average cross correlation can be expressed as :

$$\rho(r,\omega_0) = J_0\left(\frac{\omega_0}{c(\omega_0)}r\right)$$

in which J_0 is first kind of Bessel function, ω_0 is angular frequency and $c(\omega_0)$ is shear wave phase velocity (as function of ω_0.

This equation states that, if we have $\rho(r,\omega_0)$ from microtremor measurements, so we can invert the shear wave velocity.

Single station microtremor have proved to be effective in estimating fundamental period of surface sediment/soil (Field and Jacob, 1993). The method was popularized by Nakamura (1989) which well known as HVSR (horizontal to vertical spectral ratio). In this study, data collecting was done by Lennartz seismometer with natural frequency 0.2 Hz. The ambient noise was recorded by Sara data logger with sampling rate 100 Hz. The duration of the recording was 15 to 30 minutes for each site.

Figure 2: Distribution of single station (circle) and array (triangle) microtremor measurement sites in Denpasar City and surounding area.

H/V spectrum calculation for each site was done by Geopsy software. The fundamental resonant frequency (f0) for sedimentary/soil structure was estimated from main peak of H/V spectrum. If the surface sediment/soil damping is neglected and sedimentary cover has a high enough mechanical contrast with the underlying materials, therefore the thickness of surface layer (h):

$$h = \frac{c}{4f_0}$$

which c is shear wave velocity in surface layer. We have estimation of shear wave velocity for each single station microtremor site from interpolation of 19 array data, therefore the thickness of surface sediment throughout study area can be calculated.

DISCUSSION

The northern part of study area, surface lithology generally covered by volcanic product as tuff and lahar. Based on shear wave velocity profile of A001 site (located in the northern part area) the thickness of surface sediment is 9 m with shear wave velocity 212 m/s while second layer is 917 m/s. The second layer supposed massif tuff which expose in Ayung River, Denpasar. Figure 3 present shear wave velocity profile of A001 site.

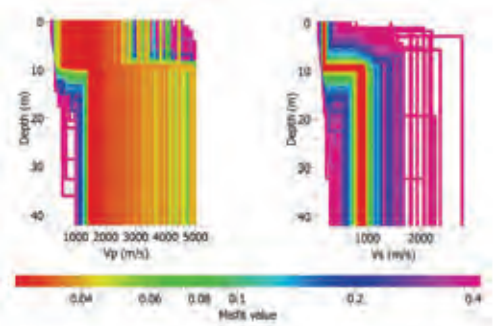

Figure 3: Compressional wave (left) and shear wave (right) velocity profile of A001 site.

In alluvial plain (southern part study area), the shear wave velocity drastically change, in A031 site the surface sediment is 83 m/s while the second layer is 305 m/s. The surface sediment shear wave velocity the result of interpolation is presented in Figure 4.

The distribution of surface shear wave shows relative high velocity area are in the northern part around the volcanic product area, while to southward which covered by alluvial tend to low velocity.

Generally the single station microtremor data are good indicated from clear peak of H/V spectrum, hence its make easier to pick resonant frequency. Based on the surface shear velocity data (Figure 4) and resonant frequency for each single station microtremor site, therefore its can calculate the surface layer thickness throughout study area (Figure 5). From the such layer

thickness can be observed that there are some small basin beneath alluvial plain.

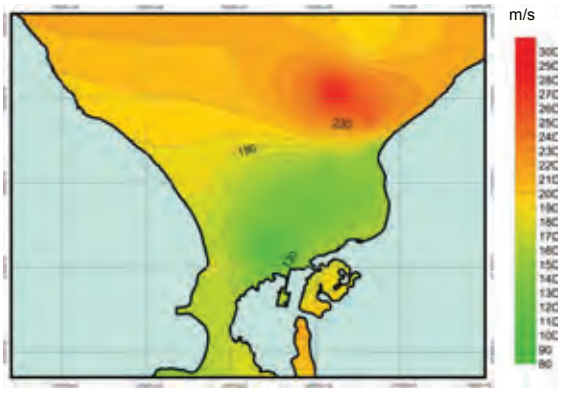

Figure 4: Distribution shear wave velocity of study area.

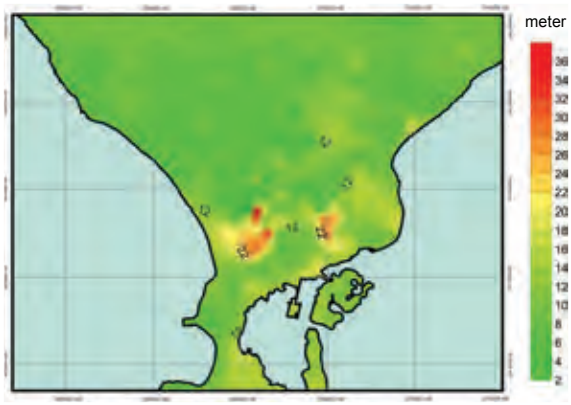

Figure 5: Distribution of surface sediment layer thickness of study area.

The subsurface model obtained above (thickness dan shear wave velocity) then were used for calculation the site amplification. In this study the surface geological response is expressed by SH-transfer function. This function shows the relative amplification of shaking as a function of shaking frequency for a specific subsurface structure (layer thickness and Vs). Because the amplification is frequency dependen, hence the maximum amplification is only valid for narrow band frequency, therefore it is required to derive a certain mean value of amplification from the frequency dependen amplifications.

The calculation of mean amplification was done by HV-explorer software. The result of calculation, mean amplification value are in the range of 1.2 to 2.1. These such range then divided into three class to show the level of relative vulnerability. Low vulnerability zone were with mean amplification below 1.5, medium vulnerability zone were 1.5 - 1.75 and high vulnerability zone were more than 1.75. Figure 6 shows microzonation map of study area based on mean amplification parameter. This microzonation map is an outline zone of different potential shaking intensity, addressed for planner (not engineer) for spatial planning.

Figure 6: Microzonation map of Denpasar City and surounding area, blue color is low vulnerability, yellow color is medium andred color is high vulnerability.

The high amplification in the southern part of Denpasar city tend associate to the soft alluvial deposits in this area. The alluvial deposits also indicated as low shear velocity zone. The volcanic product area in the northern part study area generally have low amplification.

CONCLUSSION

Site amplification in Denpasar City and surrounding area by surface sediment show the high amplification pattern correlated to alluvial deposits in the southern part of Denpasar. The value of mean amplification are in the range of 1.2 to 2.1. This value be a basic for zoning of relative vulnerability in this area.

Acknowledgements: We gratefully acknowledge to Dr. Malte Ib-von Seht for providing the microzonation software and for helpful discussion.

References

Akamatsu, K., (1961). On microseisms in frequency range from 1 /s to 200 c/s. *Bull. Earthq. Res. Inst.* Tokyo University, Vol. 39, pp. 23-75.

Aki, K., (1957). Space and time spectra of stationary stochastic wave with special reference to microtremors. *Bull. Earthq. Res. Inst.* Tokyo University, Vol. 35, pp. 415-17.

Aki, K. and P.G. Richards, (1980). *Quantitative seismology*. Freeman, San Francisco.

Bour, M., D. Fouissac, P. Dominique, C. Martin, (1998). On the use of microtremor recordings in seismic microzonation. *Soil Dyn. and Earthq. Eng.* Vol. 17, pp. 465- 474.

Field, E.H., K.H. Jacob, (1993). The theoretical response of sedimentary layers to ambient seismic noise. *Geophys. Res. Lett.* 20, 2925-2928.

Hadiwidjojo, M.M.P., H. Samodra and T.C. Amin, (1998). *Geological Map of Bali sheet, Nusa Tenggara*. Geological Research and Development Centre, Bandung, Indonesia.

Kanai, K. and T. Tanaka, (1961). On Microtremor VIII. *Bull. Earthq. Res. Inst.* Tokyo University, Vol. 39, pp. 97-114.

Kertapati K. and E.T. Putranto, (2004). *Katalog of Damaged Earthquake of Indonesia*. Geological Research and Development Centre, Bandung, Indonesia.

Mirzaogu M. and U. Dykmen, (2003). Application of Microtremors to Seismic Microzoning Procedure, *Journal of the Balkan Geophysical Society*. Vol. 6, No. 3, August, 2003, p. 143 – 156.

Nakamura, Y., (1989). A method for dynamic characteristics estimation of subsurface using microtremor on the ground surface. *QR of RTR*. 130, 25-33.

INQUA Focus Group on Paleoseismology and Active Tectonics

Planned palaeo-tsunami research in western Crete, Greece

Mason, J. (1), Schneiderwind, S. (1), Mathes-Schmidt, M. (1), Fischer, P. (2), Werner, V. (2), Vu, T. (1), Papanikolaou. I. (3), Vött. A. (2), Reicherter, K. (1)

(1) Institute of Neotectonics and Natural Hazards, RWTH Aachen University, Lochnerstr. 4-20, 52064 Aachen, Germany. Email: j.mason@nug.rwth-aachen.de
(2) Institute of Geography, University of Mainz, Johann-Joachim-Becher-Weg 21, 55099 Mainz, Germany
(3) Laboratory of Mineralogy & Geology, Department of Natural Resources Development and Agricultural Engineering, Agricultural University of Athens, 75 Iera Odos Str., 11855 Athens, Greece

Abstract: *We plan to carry out a multi-method palaeo-tsunami investigation on western Crete. The research will focus on the western part of the island where around 9 m of uplift occurred during the AD 365 earthquake. This uplift has exposed sediment traps such as ancient lagoons and harbours where tsunamigenic deposits from previous events are likely to be preserved. The proposed methods will combine drilling, geophysics, remote sensing, microplaeontology, geochemistry and absolute dating techniques. This will allow us to determine the variability of tsunami deposits (tsunamites) in space and time.*

Key words: *Crete, tsunami deposits, multi-method approach.*

INTRODUCTION

The western part of Crete was uplifted by approximately 9 m during the 21st July AD 365 earthquake and was then hit by the associated tsunami (Stiros, 2001, 2010; Shaw et al. 2008). This earthquake is probably the strongest European event to have occurred in historical times with an estimated magnitude of 8.5 (Shaw et al. 2008). Due to the strong seismic and highly tsunamigenic activity of the nearby Hellenic Trench (*Fig. 1*), it is suggested that numerous earlier tsunamis have also struck the island (Scheffers & Scheffers, 2007). To date there has been relatively little research undertaken on tsunami events prior to the AD 365 event. The main reason for this is that, although traces of high energy dislocated boulders have been described in the littoral zone (Scheffers & Scheffers, 2007), sedimentary traps where tsunami deposits may be located and identified, such as coastal plains, ancient lagoons and harbours (*Fig. 2a,b*) and river valleys, are quite rare on the island. Therefore, to date most publications focus on the coastal uplift, which is clearly shown in the landscape in the form of notches, algal rims (*Fig. 2c*) ancient shorelines and coastal caves, which are all now at varying elevations above sea level (e.g. Stiros, 2010; Tiberti et al. 2014). These features are good evidence for neotectonic activity and with accurate dating uplift rates can be determined (Tiberti et al. 2014).

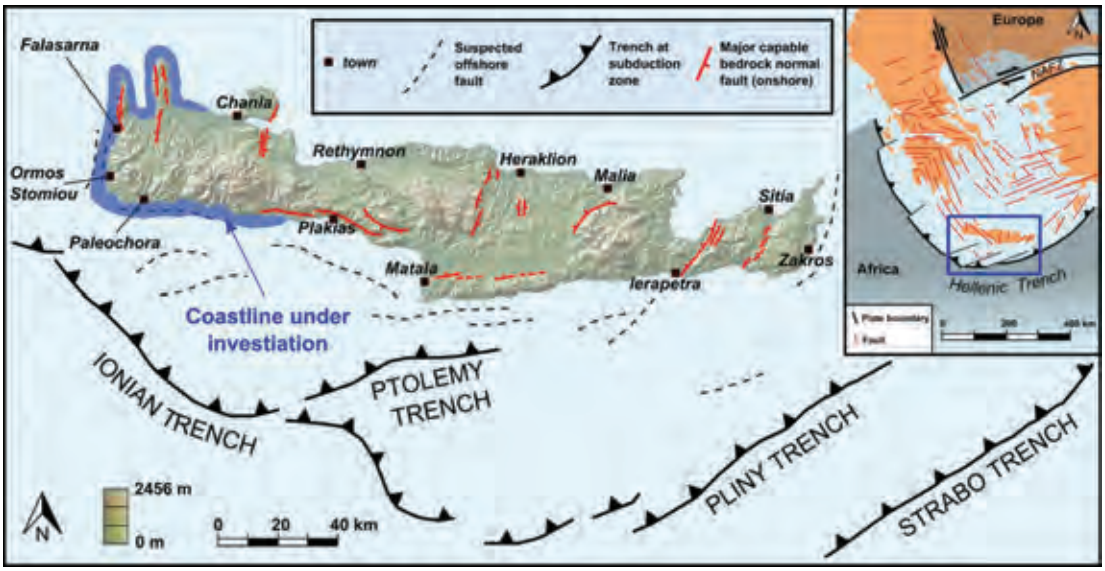

Figure 1: Topographic map of Crete showing the locations of the trenches at the Hellenic subduction zone, suspected offshore faults, bedrock faults throughout the island and the coastline under investigation highlighted in blue (fault locations from Caputo et al. 2010) - inset simplified tectonic map of the Aegean showing plate boundaries and faults, Crete is located within the blue box, NAFZ = North Anatolian Fault Zone (modified after Papanikoloau et al. 2007).

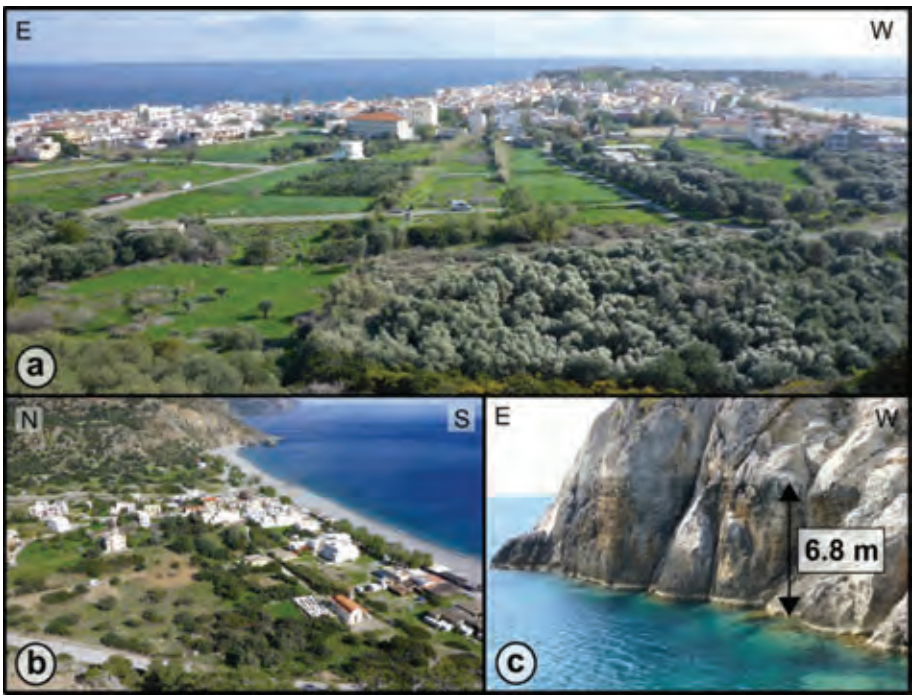

Figure 2: Promising investigation locations at Paleochora (a) and Sougia village (b) on the south west coast of Crete where there are pristine areas with flat morphology representing ancient harbours prior to the AD 365 uplift; c) uplifted algal rims in the cliffs at Sougia - the maximum uplift (between sea level and uppermost rim) was measured using dGPS.

It is highly likely that tsunami impacts were associated with the larger uplift events. However, evidence for these tsunamis has to a large extent not been identified. Only two tsunamis have been identified prior to AD 365, both of which are on the west coast (*Fig. 1*): one tsunami in AD 66 was identified in a trench in Falasarna (Dominey-Howes et al. 1999), and the other tsunami dated 3710 BC was identified from a shell bed in a dune cliff in Ormos Stomiou (Scheffers & Scheffers, 2007).

Our project will continue the works of Dominey-Howes et al. (1999) and Scheffers & Scheffers (2007) by determining the variability of tsunami deposits (tsunamites) both temporally and spatially focussing on sedimentary traps in western part of the island (*e.g. Fig. 2a, 2b*). The coastline of western Crete prior to the AD 365 event was characterised by rocky steep cliffs with bio-erosive notches. Now due to ~9m of uplift there are some areas of coastal lowlands and some ancient sedimentary traps are now exposed at the surface. We plan to identify tsunami deposits prior to the AD 365 event in various locations and determine their extent. We then hope to determine recurrence intervals for tsunami impacts. The high uplift rates also cause high erosion rates evidenced by deeply incised gorges throughout the island. These erosion rates make the process of finding remnant sediments even more difficult. Therefore, a multi-method approach will be used combining geophysics, drilling, remote sensing, microfaunal analyses, geochemistry and absolute dating techniques. We also aim to reconstruct the palaeogeography of the area in relation to seismic events and tsunami impacts.

Tsunamigenic sediments

The coastal topography and sediment regime can be significantly changed by one high-energy tsunami event due to sedimentation and erosion processes that occur during the event (forewash and backwash effects). The sedimentary structures associated with high-energy events include fining-up sequences, rip-up clasts, basal erosional contacts, bi- to multi-modal grain size distribution, lamination, and co-existence of both well rounded and angular, sharply edged components (Vött et al., 2011). Changes in micro- and macro-fauna assemblages, as well as geochemical indicators also help identify sediments as tsunamigenic. How and whether tsunamigenic deposits are located in the stratigraphy is dependent on coastal morphology, the on- and off-shore conditions, geomorphological processes and climatic conditions (Dawson et al., 2004; Tappin, 2007).

METHODS

There are various methods which can be used to determine how coastlines have been affected by palaeo-events such as tsunamis and earthquakes. We use historical, archaeological and geological data in order to describe and reconstruct the extent to which coastlines have been affected (e.g. Koster et al. 2014). The historical and archaeological period is, however, often too short to determine recurrence intervals for large tsunami events. Here we briefly describe the methods relating to geological data acquisition and analyses that we will be undertaking in Crete.

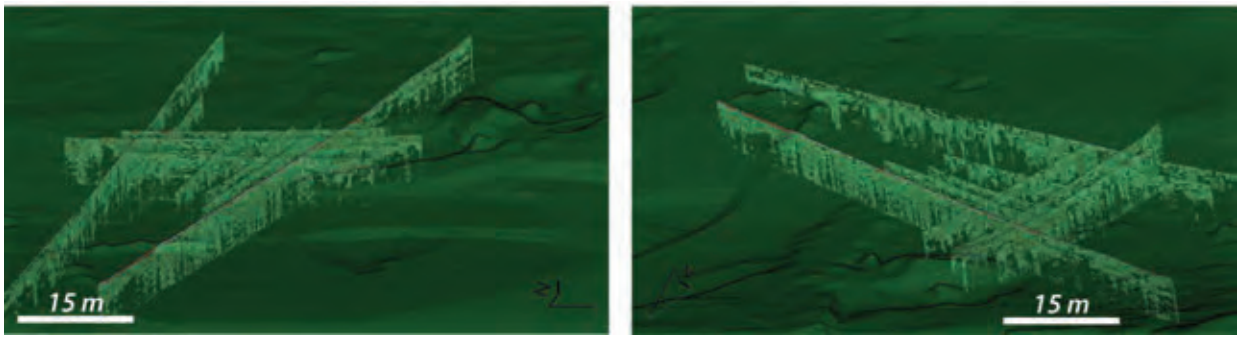

Figure 3: An example of how to combine dGPS measurements and geophysical profiles. A 2 m resolution DEM was generated by multiple dGPS measurements. Locations of GPR profiles were also measured with dGPS to enhance 3D interpretations of sedimentological features within the shallow subsurface (c. 4 m).

Vibracoring

Vibracores are drilled in order to identify tsunamigenic deposits in the sedimentary traps like uplifted lagoons and harbours. Tsunami deposits prior to the AD 365 event will be buried within fine grained sediments which were being deposited in the former bay, all of which are now uplifted to several meters above sea level. To determine the spatial extent of tsunamigenic sedimentary structures many vibracores need to be undertaken as interpolation between cores which are far apart can lead to inaccurate results due to the often high variability in sediment characteristics (Goff et al., 1998). However, when drilling is used in combination with high resolution geophysics and differential dGPS measurements (see subsequent text), fast and accurate interpolations can be carried out (Koster et al. 2014).

Geophysics

ERT (electrical/earth resistivity tomography) measurements allow us to visualise the coastal stratigraphy along profiles. ERT can achieve reasonable depths and can be easily calibrated with nearby cores. GPR (ground-penetrating radar) surveys can accurately determine the spatial distribution of tsunamigenic sediments. Using the subsurface information from GPR in combination with remote sensing and/or dGPS data we are able to build up complex 3D models that are used to visualise subsurface tsunami evidence (*Fig. 3*).

dGPS

To correlate the previously mentioned methods dGPS (differential Global Positioning System) measurements offer the highest spatial accuracy (*Fig. 3*). Furthermore, measuring the sea-level enables a reconstruction of coastal elevation and tidal differences. In cases where t-LiDAR measurements are not possible (e.g. due to the absence of an elevated scanning location) multiple dGPS measurements can be used to generate a high-resolution DEM.

Remote sensing

Long-range t-LiDAR (terrestrial light detection and ranging) scanning can be undertaken from elevated area surrounding the study site to produce a high resolution digital elevation model (DEM) of the study area. Closer-range t-LiDAR scanning (10s of metres) can identify the backscatter properties of scanned objects. *Figure 2c* shows series of uplifted calcareous algal rims located in the cliffs on Crete's south coast. Research suggests that the large amount of uplift in the area may not have occurred only from one large event (i.e. the AD 365 event) but from smaller events with interseismic subsidence culminating in the AD 365 event (Scheffers & Scheffers, 2007). This allows for many rims to form at varying heights. We plan to scan these rims with high resolution t-LiDAR and analyse the backscatter signal of each rim to help determine the relative exposure time.
We have recently acquired a hexacopter UAV (Unmanned Aerial Vehicle) which we plan to take to Crete this year. Using photogrammetric techniques we will be able to obtain DEMs with unparalleled resolution for subsequent analyses.

Macro- and micro-faunal analyses

The composition of faunal associations and the taphonomy of both micro- and macro-fauna is a strong tool to be used in palaeogeographic, palaeoecological and stratigraphic investigations. Numerous publications show how the study of faunal and foraminiferal associations can help to identify tsunamigenic sediments (e.g. Chagué-Goff et al. 2011; Mamo et al. 2009; Pilarcyzk et al. 2012; Smedile et al. 2011). Former investigations by Dominey-Howes et al. (1999) describe a rich assemblage of foraminifera at Falarsana (see Fig 1) indicating tsunami-deposited sediments. Our main focus is on both benthic and planktonic foraminifera in order to reconstruct the palaeoenvironment and identify sudden changes to it. Analysis of diatoms and ostracods will also be included. Initial findings from Limeniskos (3 km south of Falasarna) show a rich association of benthic foraminifera.

Geochemistry

Geochemical analyses of Fe, S, Sr, Ba, Na, Ca, Cl and Br are another method to identify ancient tsunamigenic deposits (Minoura, et al. 1994, Chagué-Goff 2010). This is because a tsunami often has a chemical impact in the

sedimentary sequence and can leave indicators of marine inundation (Cuven et al. 2013; Vött et al. 2011).

Magnetic susceptibility

MS (magnetic susceptibility) is a measure of the ability of a material to become magnetised in the presence of a magnetic field. Anthropocene layers and event layers can have significantly different values in both terrestrial and marine environments. When used in conjunction with palaeontological and geochemical investigations, MS measurements can help identify and trace tsunami deposits (Chagué-Goff et al., 2011).

CONCLUDING REMARKS

The western part of Crete clearly shows the effects of previous seismic events and associated tsunamis. The focus of our field campaigns in 2015 will mainly be on west coast localities (*Fig. 1*) which are sediment traps, like uplifted ancient harbours (*Fig. 2a, 2b*). The proposed multi-method approach has not been used before to study tsunami deposits on Crete; previous studies have mainly focussed on the evidence of coastal uplift, in particular from the AD 365 event. We hope to identify evidence for tsunamis prior to the AD 365 event and determine recurrence periods for these devastating events. With the data obtained from coring, geophysics and remote sensing we hope to be able to model palaeotsunami landfall and backwash dynamics. This will also allow inundation models to be developed in order to identify areas of high hazard. Crete has a long history of human habitation and there are many archaeological and protected sites around the island's coasts. Most of the planned methods (t-LiDAR, ERT, GPR, UAV) are non-invasive and non-destructive allowing tsunami research to be undertaken at these ancient sites.

Acknowledgements: The authors would like to thank Tobias Baumeister, and Lauretta Kearger for the help in the field. We also thank Dr. Kalliopi Baika for her assistance in acquiring permits and permissions.

References

Caputo, R., S. Catalano, C. Monaco, R. Romagnoli, G. Tortorici & L. Tortorici, (2010). Active faulting on the island of Crete (Greece). *Geophysical Journal International*. 183, 111-126.

Chagué-Goff, C., (2010). Chemical signatures of palaeotsunamis: A forgotten proxy? *Marine Geology*. 271(1-2), 67-71.

Chagué-Goff, C., J.L. Schneider, J.R. Goff, D. Dominey-Howes & L. Strotz, (2011). Expanding the proxy toolkit to help identify past events - Lessons from the 2004 Indian Ocean Tsunami and the 2009 South Pacific Tsunami. *Earth-Science Reviews*. 107, 107-122.

Cuven, S., R. Paris, S. Falvard, E. Miot-Noirault, M. Benbakkar, J.L. Schneider & I. Billy, (2013). High-resolution analysis of a tsunami deposit: Case-study from the 1755 Lisbon tsunami in southwestern Spain. *Marine Geology*. 337, 98-111.

Dawson, A.G., P. Lockett, S. Shi, (2004). Tsunami hazards in Europe. *Environment International*. 30, 577-585.

Dominey-Howes, D., A. Dawson, D. Smith, (1999). Late Holocene coastal tectonics at Falarsana, western Crete: a sedimentary study. In: (Stewart, I.S. & Vita-Finzi, C. eds): *Coastal Tectonics, Geological Society, Spec. Publ*. 146, 343-352.

Goff, J.R., M. Crozier, V. Sutherland, U. Cochran & P. Shane, (1998). Possible tsunami deposits from the 1855 earthquake, North Island, New Zealand. *Geological Society*, *London*, *Special Publications*. 146 (1), 353-374.

Koster, B., G. Hoffmann, C. Grützner & K. Reicherter, (2014). Ground penetrating radar facies of inferred tsunami deposits on the shores of the Arabian Sea (Northern Indian Ocean). *Marine Geology*. 351, 13-24.

Minoura, K., S. Nakaya & M. Uchida, (1994). Tsunami deposits in a lacustrine sequence of the Sanriku coast, northeast Japan. *Sedimentary Geology*. 89(1-2), 25-31.

Papanikolaou, D., I. Fountoulis & C. Metaxas, (2007). Active faults, deformation rates and Quaternary paleogeography at Kyparissiakos Gulf (SW Greece) deduced from onshore and offshore data. *Quaternary International*. Vol. 171-172, 14-30.

Pilarczyk, J.E., B.P. Horton, R.C. Witter, Ch.H. Vane, C. Chagué-Goff & J. Goff, (2012). Sedimentary and foraminiferal evidence of the 2011 Tōhoku-oki tsunami on the Sendai coastal plain, Japan. *Sedimentary Geology*. 282, 78-89.

Scheffers, A. & S. Scheffers, (2007). Tsunami deposits on the coastline of west Crete (Greece). *Earth and Planetary Science Letters*. 259, 613-624.

Shaw, B., N.N. Ambrayses, P.C. England, M.A. Floyd, G.J. Gorman, T.F.G. Highham, J.A. Jackson, J.M. Nocquet, C.C. Pain, M.D. Piggott, (2008). Eastern Mediterranean tectonics and tsunami hazard inferred from the AD 365 earthquake. *Nature Geoscience*. 1, 268-276.

Smedile, A., P.M. de Martini, D. Pantosti, L. Bellucci, P. Del Carlo, L. Gasperini, C. Pirrotta, A. Polonia & E. Boschi, (2011). Possible tsunami signatures from an integrated study in the Augusta Bay offshore (Eastern Sicily-Italy). *Marine Geology*. 281, S. 1-13.

Stiros, S.C., (2001). The AD 365 Crete Earthquake and possible seismic clustering during the fourth to sixth centuries AD in the Eastern Mediterranean: a review of historical and archaeological data. *Journal of Structural Geology*. 23, 545-562.

Stiros, S.C., (2010). The 8.5+ magnitude, AD365 earthquake in Crete: Coastal uplift, topography changes, archaeological and historical signature. *Quaternary International*. 216, 54-63.

Tappin, D.R., (2007). Sedimentary features of tsunami deposits - Their origin, recognition and discrimination: An introduction. *Sedimentary Geology*. 200 (3-4), 151-154.

Tiberti, M., R. Basili & P. Vannoli, (2014). Ups and downs in western Crete (Hellenic subduction zone). *Scientific Reports* 4. Article no. 5677.

Vött, A., G. Bareth, H. Brückner, F. Lang, D. Sakellariou, H. Hadler, K. Ntageretzis & T. Willershäuser, (2011). Olympia's Harbour Site Pheia (Elis, Western Peloponnese, Greece) Destroyed by Tsunami Impact. *Die Erde*. 142 (3), 259-288.

INQUA Focus Group on Paleoseismology and Active Tectonics

paleoseismicity.org

The Lastros-Sfaka Graben, Crete: preliminary results from a multi-method investigation

Mason, J. (1), Schneiderwind, S. (1), Pallikarakis, A. (2), Wiatr, T. (1), Mechernich, S. (3), Papanikoloau, I. (2), Reicherter, K. (1)

(1) Institute of Neotectonics and Natural Hazards, RWTH Aachen University, Lochnerstr. 4-20, 52064 Aachen, Germany. Email: j.mason@nug.rwth-aachen.de
(2) Laboratory of Mineralogy & Geology, Department of Natural Resources Development and Agricultural Engineering, Agricultural University of Athens, 75 Iera Odos Str., 11855 Athens, Greece
(3) Institut für Geologie und Mineralogie, Universität zu Köln, Greinstraße 4, 50939 Köln, Germany

Abstract: *We present the preliminary results from a multi-method investigation on the Lastros-Sfaka Graben located in the Ierapetra Fault Zone in eastern Crete. We scanned c. 1.2 km of the Lastros Fault with t-LiDAR and identified areas for throw rate calculations at locations with no external influences (anthropogenic or erosional). Preliminary maximum throw rates are 0.7 mm/yr, which is significantly less than stated in the literature. Cemented colluvium is located on the Lastros Fault, forming hanging-wall talus lobes and sheets of varying thickness attached to the fault plane. The cement is formed of calcite and further laboratory analyses are underway to determine its formation processes. GPR has been undertaken at the Lastros Fault and cemented colluvium is also present within the hanging-wall subsurface. Road cut (trenching) investigations on the Sfaka Fault identified fill material most likely deposited soon after the last paleoearthquake(s) that occurred on the fault;* ^{14}*C dating is currently being carried out to date this fill material.*

Key words: *Bedrock fault scarps, t-LiDAR, cemented colluvium, GPR, fissure fill.*

INTRODUCTION

The island of Crete is located within the active extensional regime of the Aegean. Many of the associated normal faults throughout the island have bedrock scarps which form prominent features within the mountainous landscape. These normal faults comprise footwall limestone bedrock scarps which are mainly juxtaposed against hanging-wall Quaternary colluvial and/or marine sediments. The preserved fault scarps are most likely postglacial (Benedetti et al. 2002; Papanikolaou et al. 2005) and result from cumulative earthquake events on the individual fault. These faults are considered to be capable; a capable fault is defined as a fault that has significant potential to cause displacement at or near the ground surface (IAEA, 2010). There are over 20 known bedrock normal faults/fault segments (Caputo et al. 2010) located throughout Crete (Fig. 1) which are considered to be capable and have large exposed bedrock fault scarps.

Figure 1: Topographic map of Crete showing the locations of the major capable bedrock faults throughout the island (fault locations from Caputo et al. 2010).

This extended abstract presents the preliminary results of a multi-method investigation at the Lastros-Sfaka Graben located within the Ierapetra Fault Zone (IFZ), eastern Crete (Fig. 1). The Graben is approximately 2 km wide and consists of two opposing faults, the Lastros Fault and the Sfaka Fault (Figs. 1 and 2), both of which strike approximately NNE – SSW and have prominent fault scarps. Various methods including geological mapping, trenching (road cuts), terrestrial Light Detection And Ranging (t-LiDAR), and ground penetrating radar (GPR) were used on the footwalls and hanging-walls of these faults. Laboratory analyses such as thin section analyses, and ^{14}C dating are ongoing.

The Quaternary hanging-wall colluvium of these faults mainly comprises unconsolidated material that has fallen from the footwall mountain above the scarp; in various locations this colluvium has become cemented. To date there have been no investigations into this phenomenon.

There has been anthropogenic activity on Crete dating back to Minoan times. An example is the ancient fishing village of Mochlos located at the northern end of the IFZ; potential earthquake archaeological effects have been described there (Jusseret et al. 2013). Throughout history the hanging-walls of Cretan faults have often been used for agricultural purposes and care must be taken to identify these areas in the field as anthropogenic activity can significantly influence fault scarp heights.

SEISMOTECTONIC SETTING

Crete is located in one of the most seismically active parts of Europe due to its location close to the Hellenic Arc and Trench System (LePichon and Angelier, 1979; Armijo et al. 1992; Jolivet et al. 2013). Crete has been designated as

having a high seismic risk and the island has a long record of destructive earthquakes. Throughout the Aegean, crustal back arc extension is also occurring interpreted as a response to the southward slab-rollback of the Hellenic margin, the southwestward expulsion of the Aegean microplate and the anticlockwise rotation of the African lithosphere relative to Eurasia (Meulenkamp et al., 1988; Papadopoulos, 2011). The extension is occurring orientated both arc-perpendicular and arc-parallel, which has led to a complex pattern of normal faulting throughout the region and Crete has normal faults roughly oriented both NNE – SSW and ESE– WNW (Fig. 1).

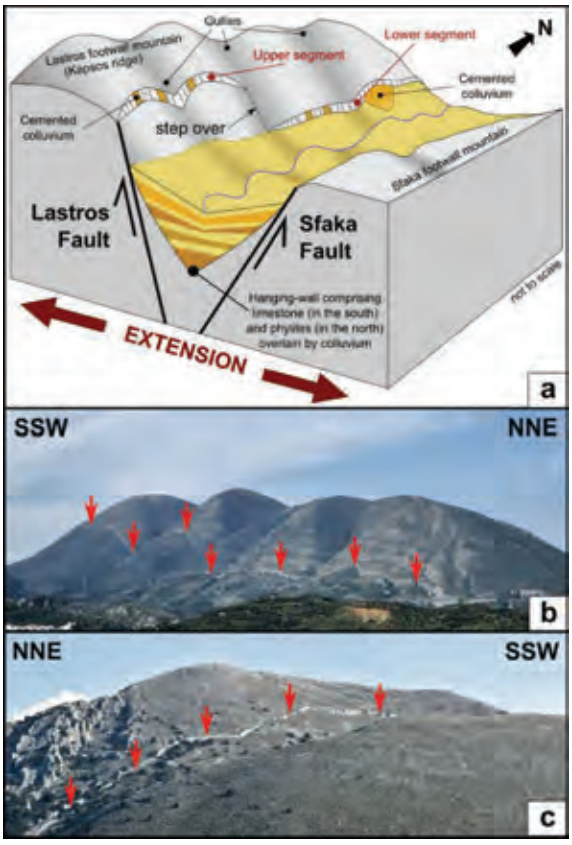

Figure 2: a) Schematic diagram of the Lastros-Sfaka Graben; b) View of the Lastros Fault; c) View of the upper segment of the Sfaka Fault.

THE LASTROS FAULT

The Lastros fault is located on the western side of the Lastros-Sfaka Graben and strikes at 020° - 200°. The fault was mapped for approximately 5 km and comprises two segments separated by a step over; in the south the fault steps back into the footwall by around 150 m (Fig. 2a, b). Manual measurements show that the upper segment in the south has an average dip angle of 65° and the lower northern segment has an average dip angle of 70°.

Figure 3: a) View of the Lastros Fault showing the Lobe of cemented colluvium; b) sheets of cemented colluvium up to 80 cm thick; c) close up of calcite cement; d) and e) 20 cm thick sheets of cemented colluvium; f) View of the Sfaka fault; g) close up of the Sfaka fault scarp showing thin sheets of cemented colluvium.

The hanging-wall colluvium is mostly unconsolidated material that has fallen from the footwall mountain above the scarp and settled on the hanging-wall; however, in many places along strike the colluvium has become cemented (Fig. 3). This cemented colluvium can be described as a breccia/conglomerate with subrounded/dissolved clasts (implying short transport distances) in a relatively hard, carbonate matrix. The cemented colluvium forms different structures: a large talus lobe is located towards the northern end of the fault (Figs. 2a, 3a, 4) which is c. 100 m in length and 140 m wide, and at many locations along strike the cemented colluvium forms sheets or slices orientated parallel to the fault plane. These sheets are attached to the fault plane and range in thickness from decimetres to several metres (Fig. 3b - e).

INQUA Focus Group on Paleoseismology and Active Tectonics

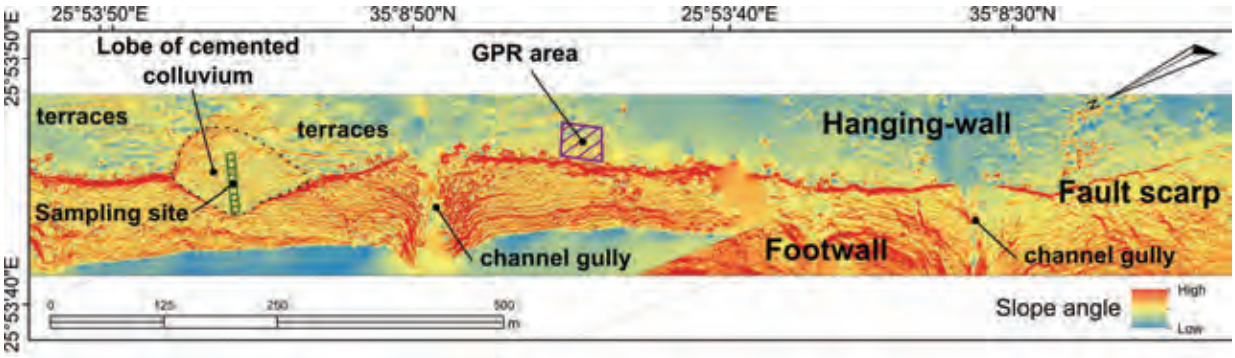

Figure 4: t-LiDAR scan of 1.2 km of the lower segment of the Lastros Fault showing slope angle. Note the gullies and the terraces in the hanging-wall; long term throw rate calculation should not be undertaken at or near these locations.

Methods and Results

The Lastros fault was mapped to determine areas for subsequent investigations. Approximately 1.2 km of the lower segment was scanned using t-LiDAR for subsequent throw rate calculations; the scanned 1.2 km was considered representative because the scarp heights of both segments are comparable as determined through manual measurements. The point cloud was georeferenced using GPS data taken in the field and converted into a raster format in GIS. Figure 4 shows the t-LiDAR derived digital elevation model (DEM) showing slope angle. The DEM clearly shows man made terraces within the hanging-wall and large catchment gullies cutting the fault. Throw rate calculations are still in progress and are being undertaken in areas away from anthropogenic influences and erosional effects. Preliminary results show maximum projected throws (Papanikolaou et al. 2005) of around 9 m at these uninfluenced locations.

GPR was also carried out on the hanging-wall to determine whether the cemented colluvium was present in the subsurface. Profiles were carried out perpendicular to strike in an area not heavily influenced by erosion or anthropogenic activity. The profiles (not presented in this abstract due to space constraints) show a number different radar facies (Neal, 2004) within the hanging-wall subsurface; one of these radar facies has very low reflectance properties compared to the surrounding material. Due to this low reflectance, its geometry and its continuity in multiple profiles, this radar facies is interpreted as cemented colluvium.

The cemented colluvial lobe at the northern end of the fault was sampled every 5 m from the fault scarp (see Fig. 4 for location). This was done to determine the composition of the cement and also whether the cemented colluvium changes with distance from the scarp. In the laboratory the samples were cut and stained with Alizarin red S and potassium ferricyanide dissolved in a dilute hydrochloric acid solution (Evamy, 1963; Dickson, 1965). Results show that the cement stained red and is therefore calcitic. Thin samples are currently being made of the cement to help determine how the calcite precipitated. We are also planning to date the cement using U-Th to determine if the cementation occurred during glacial or postglacial times.

THE SFAKA FAULT

The Sfaka Fault is located on the eastern side of the Lastros-Sfaka Graben and has an average strike of 020° - 200°. The Sfaka fault was mapped for approx. 5 km and is also comprised of two segments separated by a step over; in the south the fault steps to the west by approx. 500 m shortening the hanging-wall. The footwall of the whole fault is comprised of crystalline limestone. The hanging-wall also comprises this limestone and it is often overlain by colluvium; only in the north of the upper segment are phylites present in the hanging-wall, which are again overlain by colluvium. The average dip of the Sfaka fault plane is 63° (Fig. 3 f, g).

During mapping of the northern part of the upper segment, we followed the Sfaka Fault along a narrow valley in which a dirt road has been constructed to access nearby olive groves. Here the dirt road cuts the fault plane at two locations, one approximately 40 m from the other. These two road cuts are essentially acting like vertical shallow angle trenches opened approximately 30° from the fault's strike. Here we briefly present some preliminary results from the upper road cut, herein referred to as Trench 1.

Methods and Results

At Trench 1 the exposure was cleaned of vegetation and the outermost 10 – 15 cm of soil and gravel. Furthermore, the trench was deepened by 0.6 m using hand tools. In accordance with McCalpin (2009) the trench was logged and photographed and samples were taken from identified displaced layers and other horizons for subsequent classification analyses. Trench 1 shows fissure fill material located between the fault gouge and the colluvial layers. The fissure fill material has both a high amount of fines and gravel; some larger clasts are present within the fill and minor changes in colour could represent groundwater staining and/or different episodes of fill deposition. The fill is most likely not scarp derived but from palaeosols that developed on the surface of the hanging-wall. Orientated clasts at the boundary between the fill and the fault gouge are further evidence for a tectonic origin; however, at this preliminary stage a depositional origin cannot be ruled out. The fissure fill material has been sampled for ^{14}C

dating which is ongoing. Within the hanging-wall there are a number of small displacement antithetic faults that have developed within the colluvial gravels, which are typical of extension in unconsolidated sediments. Cemented colluvium is also present in the trench beginning c. 5m from the fault scarp.

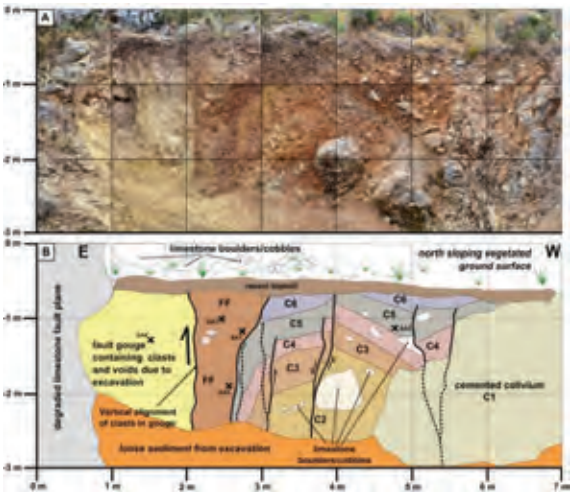

Figure 5: a) Photomosaic of Trench 1 at the Sfaka Fault; b) Trench 1 preliminary log interpretation, FF indicates fissure fill material, C2 – C6 represent uncemented colluvial layers.

CONCLUSIONS

Previous work has been carried out on the Lastros and Sfaka faults by Caputo et al. (2006, 2010). The authors calculated long-term throw rates for both the Lastros and Sfaka Faults based on scarp heights and a 13 ka (post glacial) date for first exhumation. The authors estimated a throw rate of 1.3 mm/yr for the Lastros fault using a maximum throws of 15 m. However, our preliminary t-LiDAR results show that the maximum throw is around 9 m when measurements are undertaken in areas not influenced by anthropogenic activity and erosion. When using a 13 ka post exhumation date the estimated throw rate is 0.7 mm/yr for a scarp with 9 m of throw. Further work on the DEM will determine whether more representative areas can be found for throw rate calculations. Work will also continue on the Sfaka Fault to determine if the throw rate of 1.0 mm/yr (Caputo et al. (2010) is accurate. This was calculated using a 12 m scarp height, and from initial observations in the field scarps of this height are heavily influenced by erosion.

The cemented colluvium needs further work to determine its formation process and the calcite cement's precipitation date. During fieldwork in 2013 cemented colluvium was observed on many faults throughout Crete including the Asomatos Fault, Spili Fault and Zou Fault (Sitia Fault Zone – see Fig 1). The presence of this material hampers fault scarp exposure dating on the island.

The ancient Minoan fishing village of Mochlos located on the coast at the northern end of the IFZ has potential earthquake archaeological effects (Jusseret et al. 2013). The Sfaka road cut trenches should provide earthquake dates for this fault and with continued work on the IFZ faults we hope to link the observed archaeological damage with individual earthquakes.

Acknowledgements: The authors would like to thank Alex Woywode, Tobias Baumeister, and Lauretta Kearger for the help in the field. We also thank Manolis from the Zorbas Taverna in Pachia Ammos for the loan of the generator and his great hospitality.

References

Armijo, R., H. Lyoncaen and D. Papanastassiou, (1992). East-west extension and Holocene normal-fault scarps in the Hellenic arc. *Geology*. 20, 491-494.

Benedetti, L., R. Finkel, D. Papanastassiou, G. King, R. Armijo, F. Ryerson, D. Farber & F. Flerit, (2002). Post-glacial slip history of the Sparta fault (Greece) determined by 36Cl cosmogenic dating: Evidence for non-periodic earthquakes, *Geophys. Res. Lett*. 29, 1246.

Caputo, R., C. Monaco & L. Tortorici, (2006). Multiseismic cycle deformation rates from Holocene normal fault scarps on Crete (Greece). *Terra Nova*. 18, (3), 181-190.

Caputo, R., S. Catalano, C. Monaco, R. Romagnoli, G. Tortorici & L. Tortorici, (2010). Active faulting on the island of Crete (Greece). *Geophys. J. Int*. 183, 111-126.

Dickson, J., (1965). A modified technique for carbonates in thin section. *Nature*, 205, (4971), 587.

Evamy, B., (1963). The application of a chemical staining technique to a study of dedolomitisation. *Sedimentology*. 2, 164-170.

Fountoulis, I. & I. Mariolakos, (2008). Neotectonic folds in the central-western Peloponnese, Greece. *Zeitschrift der Deutschen Gesellschaft fur Geowissenschaften*. 159/3 485-494.

International Atomic Energy Agency (IAEA), (2010). Seismic Hazards in Site Evaluation for Nuclear Installations. *Specific Safety Guide*. No. SSG-9.

Jolivet. L., C. Faccenna, B. Huet, L. Labrousse, L. Le Pourhiet, (2013). Aegean tectonics: Strain localisation, slab tearing and trench retreat. *Tectonophysics*. Elsevier, 2013, 597-598.

Jusseret, S., C. Langohr & M. Sintubin, (2013). Tracking Earthquake Archaeological Evidence in Late Minoan IIIB (~1300-1200 B.C.) Crete (Greece): A Proof of Concept. *Bulletin of the Seismological Society of America*. 103, (6), 1-18.

LePichon, X. & J. Angelier, (1979). The Hellenic Arch and Trench System: A key to the neotectonic evolution of the Eastern Mediterranean area. *Tectonophysics*. 60, 1-42.

McCalpin, J.P., (2009). *Paleoseismology*. Elsevier, 2nd edition, 613 pp.

Meulenkamp, J.E., M.J.R. Wortel, W.A. van Wamel, W. Spakman & E. Hoogerduyn Strating, (1988). On the Hellenic subduction zone and the geodynamic evolution of Crete since the late Middle Miocene. *Tectonophysics*. 146, 203-215.

Neal, A., (2004). Ground-penetrating radar and its use in sedimentology: principles, problems and progress. *Earth Science Reviews*. 66, 261-330.

Papadopoulos, G., (2011). *A Seismic History of Crete. The Hellenic Arc and Trench. Earthquake and Tsunamis: 2000 BC – 2011 AD.* Ocelots Publications. 415 pp.

Papanikolaou, I., G. Roberts & A. Michetti, (2005). Fault scarps and deformation rates in Lazio-Abruzzo, Central Italy: comparison between geological fault slip-rate and GPS data. *Tectonophysics*. 408, 147-176.

INQUA Focus Group on Paleoseismology and Active Tectonics

paleoseismicity.org

The importance of robust site characterisation for ^{36}Cl cosmogenic dating of active normal faults

McCaffrey, K. (1), Roberts, G. (2), Wedmore, L. (3), Gregory, L. (4), Cowie, P. (5), Faure Walker, J. (3), Watson, Z. (3), Wilkinson, M. (6), Bandugula, V. (6)

(1) Dept. of Earth Sciences, Durham University, UK DH1 3LE. Email: k.j.w.mccaffrey@durham.ac.uk
(2) School of Earth Sciences, Birkbeck College, University of London, UK
(3) Institute for Risk and Disaster Reduction, University College London, Gower Street, London
(4) Institute of Geophysics and Tectonics, School of Earth and Environment, The University of Leeds, UK
(5) Dept of Earth Sciences, University of Bergen, Norway
(6) Geospatial Research Ltd, Office Suite 7, Harrison House, 1 Hawthorn Terrace, Durham, DH1 4EL

Abstract: *High resolution topographic mapping has been used to create an extensive site characterisation database for normal faults in central Abruzzo, Italy. A combination of airborne and terrestrial laser scanning (lidar,) and ground penetrating radar provide constraints for ^{36}Cl cosmogenic sample site integrity and key inputs for the processing and modelling of the results obtained. The ongoing campaign to data for exposed faults in the region provides a baseline database for future large earthquakes in the region.*

Key words: *Lidar, normal faults, Abruzzo, Cosmogenic dating.*

INTRODUCTION

Fault scarps in the central Italian Apennines (Abruzzo) exhibit striated fault planes, offset dated Holocene sediments and geomorphic surfaces, and are the surface expression of a network of active normal faults formed over the past 2-3 Myrs. As part of an ongoing program to determine the spatial and temporal distribution of strain accumulation in the region and reconcile long term (10^5 yr) slip rates to historical and geodetic records (10^3-10^1 yrs), we are carrying out a programme of cosmogenic dating to establish slip-rate variability and elapsed times since the last major slip event. A key input to the project is characterisation of each sample site using high resolution terrestrial (TLS) (Fig. 1), airborne LiDAR scanning (ALS) and ground penetrating radar (GPR). This in turn has created a new understanding of the geomorphic and near surface expression of the bedrock scarps and their offsets at centimetre scales.

Figure 1: Terrestrial Laser scanning of the Velino-Magnola Fault, Abruzzo using a Riegl LMS420i.

A key assumption for the cosmogenic programme, is that the sampled scarp is created purely by tectonic uplift of the footwall. Geomorphic processes can cause a range of effects to the scarp exposures from complete removal to burial by Holocene sediments. Bubeck et al. (2014) showed that the surface expression of bedrock scarps results from the interaction between footwall incision, hangingwall sedimentation, channel incision and landsliding as well as fault slip and fault linkage. The goal of the site characterisation programme is therefore to ensure that the sample sites are an intact record of the earthquake history on each fault (Fig. 2, 3a, b).

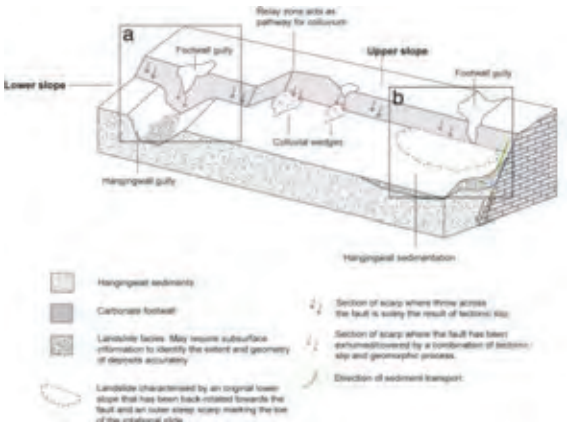

Figure 2: Illustration of geomorphic processes that can modify a fault scarp (after Bubeck et al 2014).

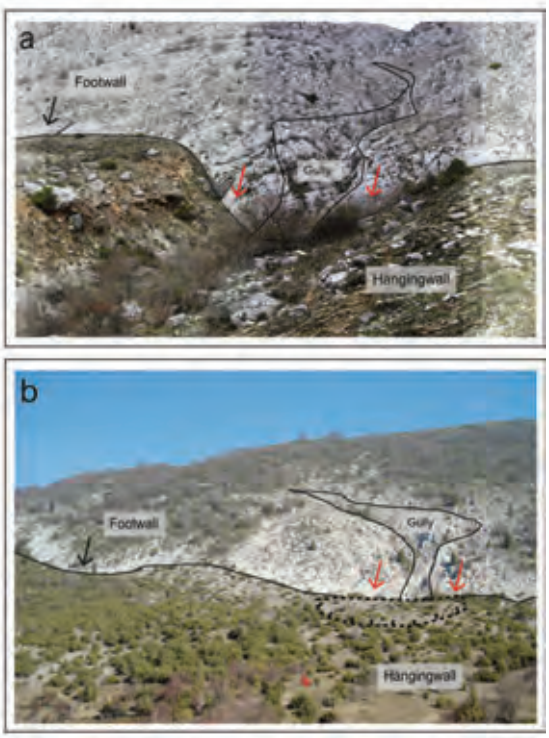

Figure 3: Examples of the geomorphic processes shown in Fig. 2 (after Bubeck et al 2014). Black arrow indicates a good sampling site, red arrow indicates a poor site.

TLS and GPR data for >20 active normal faults have been acquired in the central Apennines region since 2008 (Fig. 4). In addition, Airborne LiDAR (ALS) data was flown in two sorties (September 2011 & May 2013) across a number of the active faults. All data sets are georeferenced to UTM coordinates using campaign differential GNSS data that are tied to local permanent GPS recording stations (e.g., Rete Regionale GNSS for Abruzzo). The GNSS data is collected on reference reflectors that are placed in each laser scan view. These reflectors are used to co-register individual laser scans at each site into a single coherent dataset.

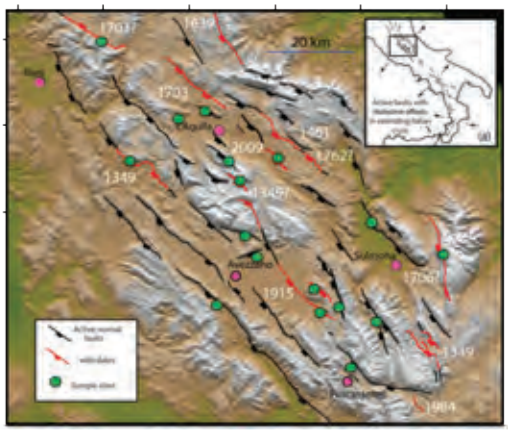

Figure 4: Sample sites in Abruzzo with TLS data.

Our standard workflow is to firstly produce a 'bare earth' digital terrain/elevation model (DTM/DEM) that can be viewed as hillshade model (Fig. 5). This requires the removal of any vegetation that gets captured in the scene and is done by a combination of data filtering and manual editing, followed by a surface interpolation.

Following DEM construction, we produce a series of terrain profiles parallel to the mapped slip vector to quantify the throw across the structure. Here, we use a modified version of a throw profile tool developed by Wilkinson et al (2014).

For example, the Fiamignano fault (Fig 3b) is one of our key ^{36}Cl sites and has been targeted in both ALS campaigns, with different flight parameters (elevation, flight directions). The same fault has also been scanned using Terrestrial Laser Scanning (TLS) methods with two different instruments, the longer range Riegl LMS z420i and the shorter range Leica Scanstation C10. 4 GPR profiles have also been captured in the fault hangingwall to study any disturbances in the sediments at this site. For Fiamignano, our data show that there are very limited places were we can be confident that the scarp has been created by tectonic processes alone (see Bubeck et al 2014) (Fig. 5).

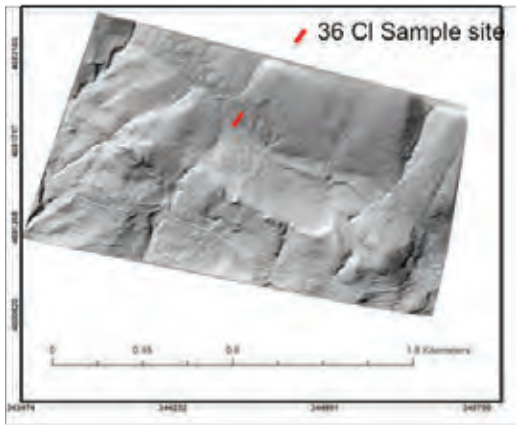

Figure 5: Hillshade image of DEM for Fiamignano fault with sample site shown.

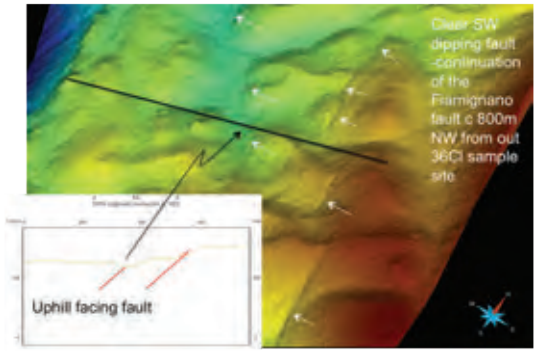

Figure 6: Oblique view to the NW of the DEM created from ALS data coloured for elevaton (red higher, green/blue lower). The profile shown intersects the 2 mapped fault segments.

The ALS data also shows clearly that along strike from our sample site, the Fiamignano fault 'faces' in an uphill direction removing any residual doubts that this structure is a normal fault structure and not a landslide (Fig. 6).

FUCINO FAULT

ALS and TLS data from the Fucino – Gioia di Marsi fault have been acquired and show a well developed bedrock scarp at Gioia Di Marsi that continues to the NW below the Fucino plain (Fig. 7).

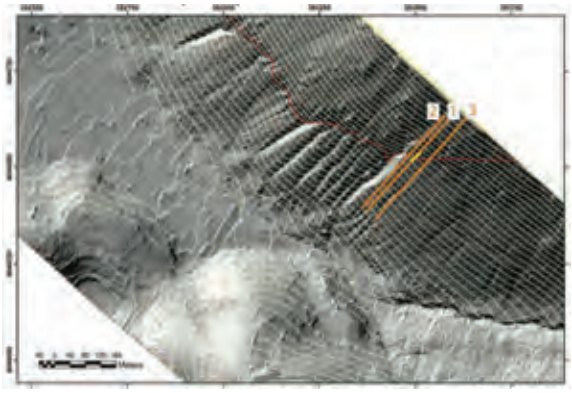

Figure 7: ALS derived hillshade from the Gioia di Marsi fault (vegetation removed) showing trace of the fault scarp. Contours are shown along with 3 profile lines that have been drawn to constrain the fault throw.

DISCUSSION

High resolution topogographic imaging and mapping is a key input to the ^{36}Cl cosmogenic dating of active scarps in Abruzzo. TLS and ALS data have been successfully used to provide geomorphic constraints on the sample sites. These data also provide a permanent record of the sample site that can be examined at any time following the fieldwork campaign. Our recent work has shown that the geomorphology is also a key input for the cosmogenic modelling. Precise control on the slope values for the hangingwall, footwall and the scarp geometry is required in the processing of the raw 36Cl data. A precise measurement of the throw on each fault, the height of scarp and the degree of topographic shielding at each sample site can all be measured precisely using combinations of the ALS and TLS.

Finally the TLS data from the 25 faults that have been scanned to date (see table) provide a baseline dataset that can be used to constrain any surface ruptures or slip increments on bedrock scarps and that might occur as a result of a future earthquake in this region.

Fault Name	Number of Tripod Positions	Number of Scans	Number of points (Millions)
Barete	6	9	48
Campo Felice	14	15	90
Campo Imperatore	4	6	32.6
Caporciano	6	5	21.2
Colforito	3	7	30.6
Costa Corgnetto	4	6	40.5
Fiamignano	10	12	111.5
Frattura	4	13	53.2
Fucino	4	5	17.5
Gioia De Marsi	4	3	34
Leonessa	4	8	44.6
Liri Capistrello	3	6	47.6
Magnola Velino	8	18	64
Maiella	3	4	33.9
Mt Ocre	3	5	22.6
Parasano	10	21	75
Pescasseroli	2	4	16.8
Paganica	7	84	150
Poggio di Roio	6	8	35.7
Roccasale	5	9	30.6
Roccapretura	16	10	47
San Sebastiano	4	8	34
Tre Monte	2	4	19

Acknowledgements: We gratefully acknowledge sponsorship from NERC, Universities of Durham, UCL and Birkbeck and Geospatial Research Ltd.

References

Bubeck, A., M. Wilkinson, G. Roberts, P. Cowie, K. McCaffrey, R. Phillips & P. Sammonds, (2014). The tectonic geomorphology of bedrock scarps on active normal faults in the Italian Apennines mapped using combined ground penetrating radar and terrestrial laser scanning. *Geomorphology*. doi:10.1016/j.geomorph.2014.03.011.

Wilkinson, M., G. Roberts, K. McCaffrey, P. Cowie, J. Faure Walker, I. Papanikolaou, R. Phillips, A. Michetti, E. Vittori, L. Gregory, L. Wedmore & Z. Watson, (2014). Slip distributions on active normal faults measured from LiDAR and field mapping of geomorphic offsets: an example from L'Aquila, Italy, and implications for modelling seismic moment release. *Geomorphology*. http://dx.doi.org/10.1016/j.geomorph.2014.04. 026

INQUA Focus Group on Paleoseismology and Active Tectonics

The slip history of the Pisia fault, Gulf of Corinth, based on bedrock fault scarp analyses

Mechernich, S. (1), Mason, J. (2), Papanikolaou, I. (3), Binnie, S.A. (1), Dunai, T. (1), Reicherter, K. (2)

(1) Institute of Geology and Mineralogy, University of Cologne, Greinstraße 4, 50939 Köln, Germany. Email: s.mechernich@uni-koeln.de
(2) Institute of Neotectonics and Natural Hazards, RWTH Aachen University, Lochnerstr. 4-20, 52064 Aachen, Germany
(3) Laboratory of Mineralogy and Geology, Department of Natural Resources Development and Agricultural Engineering, Agricultural University of Athens, 75 Iera Odos Str., 11855 Athens, Greece

Abstract: *The deformation of the Corinth rift is distributed over numerous normal faults. For instance the ~17-km-long Pisia fault, which experienced up to 150 cm of coseismic displacement during the 1981 Alkyonides earthquake sequence (M_w ~6.7). We investigated a site at the central part of the Pisia fault, which is only affected by minor erosional and depositional processes and not changes by human impact. Based on differences in color and karren termination, we identified five earthquake horizons whose coseismic slip amounts were about 110 cm (1981 AD), 100 cm (EQ2), 75 cm (EQ3), 75 cm (EQ4) and 50 cm (EQ5), respectively. Preliminary ^{36}Cl results suggest that the scarp is ~14-17 kyr old, which is in agreement with the postglacial age assigned to other Mediterranean fault scarps. ^{36}Cl dating of the paleoearthquakes is in progress.*

Key words: *Greece rift, bedrock normal fault, weathering, surface roughness, ^{36}Cl exposure dating.*

INTRODUCTION

The Gulf of Corinth, Greece, is a 110-km-long and 30-km-wide active rift displaying strong seismicity hosted both on north and south dipping normal faults (Moretti et al., 2003; Fig. 1). It is extending ~10-15 mm/yr in its central part and ~4 mm/yr at its eastern termination (e.g. Briole et al., 2000; Reilinger et al., 2010). Most of the numerous onshore faults comprise carbonate bedrock scarps (Fig. 1) and paleoseismic trenching is not possible due to a lack of continuous sediment deposition. In contrast to trenching, cosmogenic nuclide concentrations (e.g. ^{36}Cl in carbonates) on the fault plane can be used to reconstruct slip histories in settings where colluvial deposits are sparse.

Figure 1: Tectonic map of the Gulf of Corinth area (Moretti et al., 2003). Focal mechanisms of the 1981 Alkyonides earthquake sequence are after Hubert et al. (1996).

The latest surface rupturing earthquakes in the Gulf of Corinth occurred at its eastern termination during the 1981 Alkyonides earthquake sequence (Fig. 1). Two segments of the 37-km-long South Alkyonides Fault System (SAFS) were displaced by up to 150 cm (Fig. 2; Jackson et al., 1982). The detailed 1981 slip distribution is shown in Fig. 2. The geomorphic influence of the faults is demonstrated by coastal uplift / subsidence both coseismically using direct measurements, and on long timescales based on notches, marine terraces and elevated beach-rocks (Fig. 2). So far, paleoseismological investigations have only been carried out at the central part of the Skinos fault, and the combined results of three trenches show that the 1981 earthquake and four similar size paleoearthquakes recurred roughly every 330 yrs (Collier et al., 1998). For the highly capable Pisia fault, the recurrence interval of 1981-like (M_s~6.7) earthquakes is unknown.

SITE SELECTION AT THE PISIA FAULT

The ~17-km-long Pisia fault is the westernmost fault of the SAFS and it had the highest coseismic displacements during the 1981 earthquake sequence (Fig. 2). It runs through a valley containing several villages and farms and ends near a Heraion archaeological site (Fig. 2a). The continuous fault scarp along the 1981 rupturing trace highlights preceding surface-rupturing earthquakes.

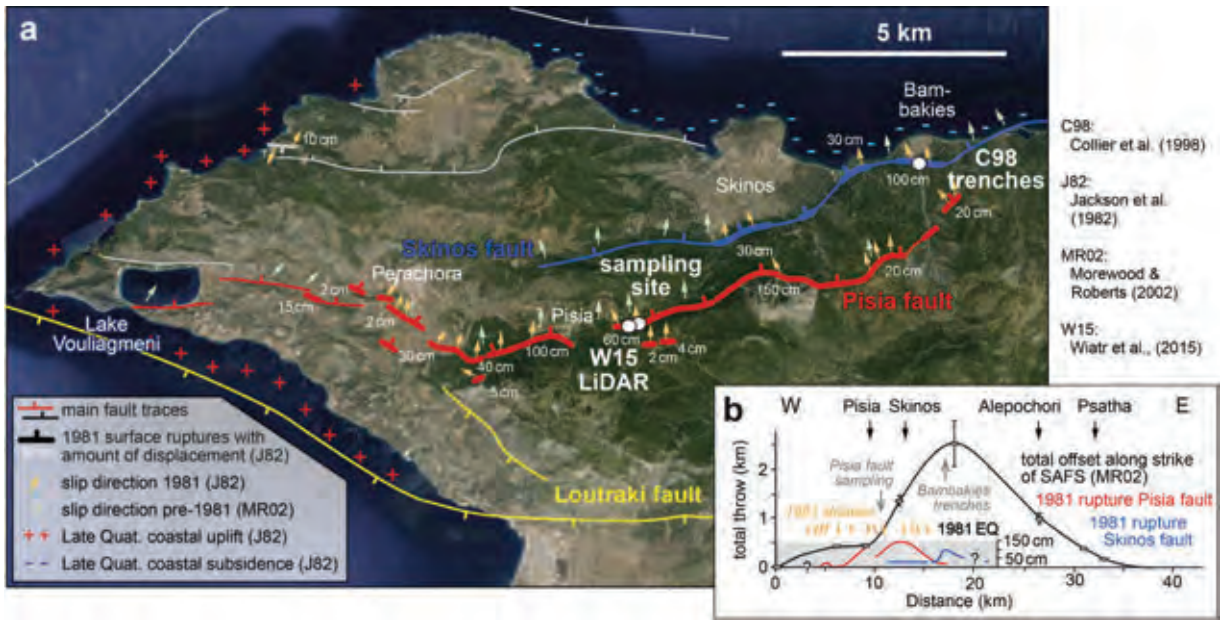

Figure 2: (a) The Peninsula of Perachora with the main faults. The 1981 rupture with its traces and slip amounts is indicated. (b) W-E cross-section showing (i) the displacement during the 1981 earthquakes (compiled from Jackson et al., 1982), and (ii) the total throw of the South Alkyonides Fault System (SAFS) based on geologic cross sections.

The investigation of bedrock fault scarps to reconstruct the Holocene earthquake history requires a careful selection of sites with a focus on erosional and depositional features as well as the slip distribution. The fault plane should have only been exhumed by earthquakes and it should have remained exposed since. Thus, suitable sites must not be affected by denudation processes (e.g. river incision, landsliding events), depositional processes (e.g. alluvial or scree deposits), or anthropogenic processes (e.g. agriculture, road construction, quarries) (Fig. 3). In the Mediterranean region, cemented colluvium is often attached to the fault plane, which excludes many possible sampling sites (Fig. 3).

We selected a location at the central part of the Pisia fault. The site is located on a north-facing slope in a natural forest without anthropogenic landscape changes or indurated colluvium. The slope gradient is 35° on the footwall and 31° on the hanging wall except for three meters at the base of the fault scarp which are flatter (23°) due to the overly of some colluvial deposits. The closest river is located 230 m to the west and we avoided any site where small gullies had incised into the scarp.

METHODS AND RESULTS OF SURFACE ANALYSES

The incremental exhumation of the fault plane due to coseismic slip leads to differential weathering and related changes in the surface roughness of the fault plane. Thereby, the highest part of the fault scarp is exposed to weathering processes the longest. To estimate the relative exposure duration of different horizontal segments of the fault scarp, i.e. to distinguish individual slip events (earthquakes), we used several indicators like the termination of karren, roughness differences, color contrast, lichen growth, and (cosmogenic) ^{36}Cl concentrations. Thereby, we identified 5 possible earthquake events in the lower 4.5 m of the fault scarp (Fig. 4b, c). The higher part was more difficult to analyze due to quarrying of joints by roots and/or solution weathering of the fault plane.

At the sampling site, as well as 1300 m farther east and 100 m farther west, the lowermost 1.1 ± 0.1 m of the fault scarp appears lighter in **color** (Fig. 4a). This lighter color correlates well with the 1981 coseismic total displacement reported by Jackson et al. (1982) and it is probably caused by micro-soil remnants and lack of vegetation (lichen, moss).

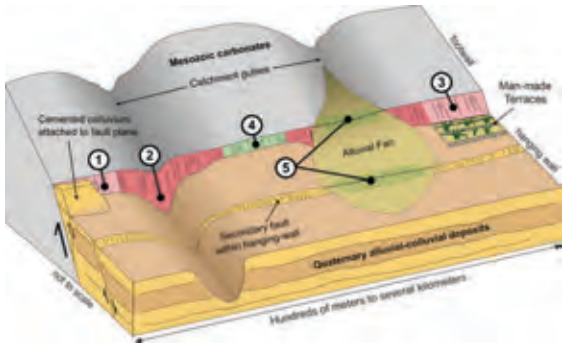

Figure 3: Features of a typical Mediterranean normal fault. Sites (1) to (3) should be avoided for paleoseismic analyses. Fault scarp dating should be undertaken at site (4), and trenching investigations should be carried out at sites with continuous sedimentation (5).

INQUA Focus Group on Paleoseismology and Active Tectonics

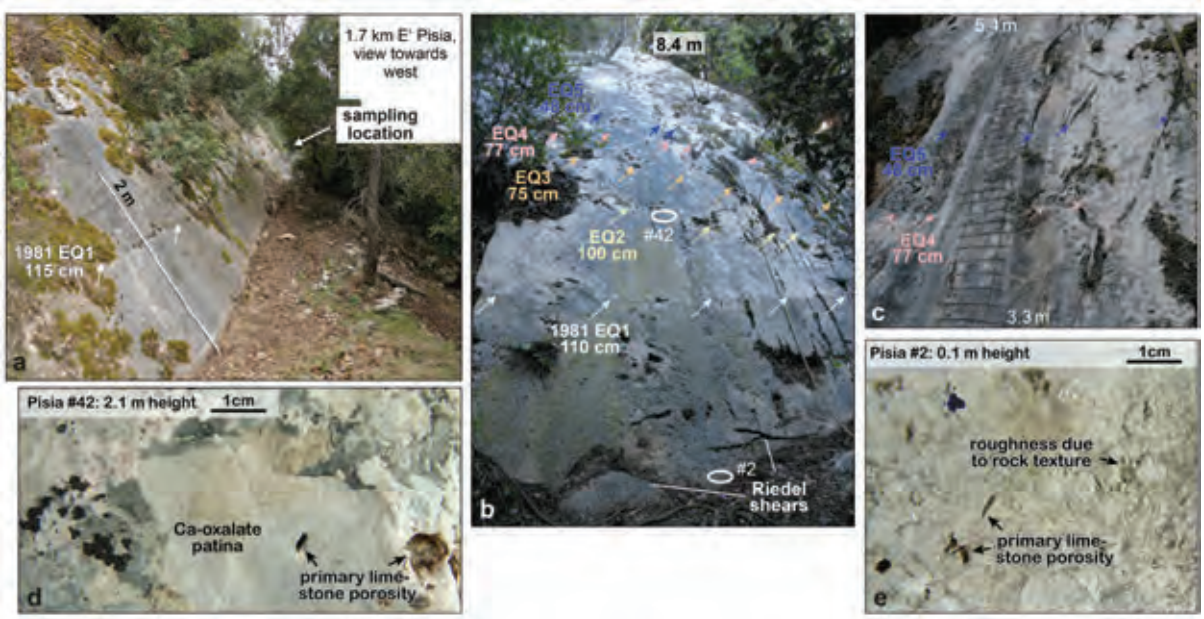

Figure 4: Impressions from the Pisia fault. (a) 15 m east of the sampling location. Note the stripe at 1.1-1.2 m height indicating the exhumation due to the 1981 earthquake. (b, c) Identification of the event horizons based on ending karst features, colour contrast and lichen growth. (d, e) Photographs of two cleaned samples used for roughness analysis. Note the lower micro-roughness of the sample #42 that is longer exposed to weathering than sample #2.

Terminating **karst features** (e.g. karren, naturally small quarried parts) (Fig. 4b, c) can indicate the location of the ancient base of the fault plane. The quarried parts are most prominent at the penultimate earthquake (EQ2) and several karren decrease in depth and extent at EQ5 (Fig. 4b, c).

No vegetation is visible in the lower 1.1 m, which has been exposed for the last 33 years. Above this height, the amount of different **lichen** species and their respective sizes increase upwards. Various kinds of lichens reach 15 cm in diameter at >4 m scarp height (Fig. 4d).

The analyses of differences in the micro-**roughness** of the fault plane surface are in preparation. To reveal the earthquake history of the complete 8.4 m of the fault scarp, we cleaned the samples from dirt, moss and lichens since, particularly in the upper part of the scarp, they have an influence on the roughness. However, after removal of the living part of lichens, an oxalate "patina" composed mainly of biogenetic calcium oxalate remains (Chen et al., 2000), and flattens the rock surface (Fig. 4d). Furthermore, the roughness is also controlled by the texture of the bedrock. The limestone breccia at this site has a high porosity and variable amounts and sizes of clasts. Large clasts jut out (Fig. 4e) and the porosity at the surface builds holes, thus the roughness signal increases together with the percentage of clasts and porosity. We think that the lichen effect and texture are the reason why our calculations of the Terrain Ruggedness Index (TRI, Riley et al., 1999) suggest an overall decreasing roughness with scarp height from 0 to 8.4 m. The decreasing roughness is in contrast to the expectation based on weathering and in contrast to the TRI analysis on the lower 2.2 m of the Pisia fault scarp 180 m farther west (Wiatr et al., 2015).

To get a weathering-independent proxy for the duration of exposure we measure *in-situ* produced cosmogenic **^{36}Cl concentrations**. During the sample preparation, weathered parts and pores are removed with a rotary tool and we selected the clast fraction (without the matrix) to avoid effects from the higher natural chlorine concentration in the matrix. To date, we have only one ^{36}Cl concentration, which is ~2.9*10^{5} at/g rock at 4.4 m scarp height (Fig. 5). Despite this limited data, we modeled distinct earthquakes at the horizons based on the identified weathering horizons (Fig. 4b, c) using the MatLab procedure of Schlagenhauf et al. (2010). They would suggest that the five recent earthquakes were generated in the last ~8 ± 1 kyr and that the 8.4 m of free-face were exhumed in the last ~14-17 kyr (Fig. 5). The ages are preliminary since they depend on only one ^{5}Cl concentration and factors that are therefore still unknown (e.g. pre-exposure time and earthquake recurrence interval). Nevertheless, the results show that the scarps were buried during the last glacial period and exposed together with the post-LGM warming and decrease in denudation rates as suggested already by Armijo et al. (1992).

DISCUSSION, CONCLUSIONS AND OUTLOOK

In addition to the selection of a suitable site, the determination of event horizons is the controlling factor to interpret the earthquake history on bedrock fault scarps. Their detection is most complete and reliable when using multiple methods for their identification. At our site, the distance between the event horizons indicates 50 – 110 cm of coseismic slip during the last

five earthquakes (Fig. 5). In contrast, Wiatr et al. (2015) revealed 4 possible paleoearthquakes 180 m west of our sampling site, with throws of ~30-60 cm, respectively. These lower coseismic displacements compared to our site could be related to the termination of the fault segment about 250 m farther to the west (Fig. 2a).

The discrimination of multiple smaller sized earthquake events in short time periods (temporal clustering) is problematic in all applied methods. Thus the amount of detected events represents the minimum amount of earthquakes while the estimated displacements are maximum bounds and thus refer to maximum earthquake magnitudes. Assuming that the slip values represent the average displacements along the strike of the Pisia fault, the expected maximum magnitudes after Wells and Coppersmith (1994) are M_w 6.7 (1981 EQ), M_w 6.7 (EQ2), M_w 6.6 (EQ3), M_w 6.6 (EQ4), M_w 6.5 (EQ5) ± 0.4, respectively (Fig. 5).

The pattern of roughness with scarp height depends strongly on the local rates of lichen growth and bedrock texture. The possibility to detect earthquake horizons based on the micro-roughness will be tested by a continuous analysis of the Terrain Ruggedness Index in intervals of 5 cm.

Further ^{36}Cl analyses will date the earthquake events and reveal the continuous slip rate. Due to the low ^{36}Cl production rate and the rather low coseismic displacement at our site, a verification of the earthquake horizons locations using cusp modeling is challenging. Even in the case of minimal uncertainties, a recurrence interval of at least 2.5 kyr (determined visually based on own modeling, Fig. 5) would be required to allow reliably detectable cusps. However, the scarp age suggests that five earthquakes were generated in the past 8 ± 1 kyr, thus the recurrence interval would is rather in the order of 1-2 kyr. This emphasizes the need for the aforementioned surface analyses to detect the earthquake horizons in addition to the ^{36}Cl concentrations.

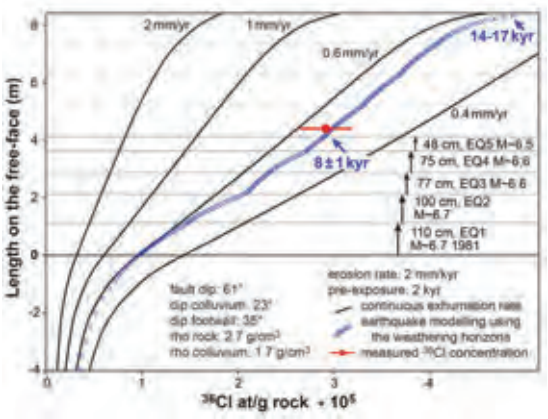

Figure 5: Modelled evolution of ^{36}Cl concentrations at the Pisia fault sampling location for (i) quasi-continuous slip (black curves), and (ii) earthquakes at identified horizons and four earthquakes above (blue curve). So far, only one ^{36}Cl concentration (red) is available.

Acknowledgements: We thank Niels Noack, Jakub Surma, Thomas Wiatr, Sascha Schneiderwind and Aggelos Pallikarakis for several discussions and help during the fieldwork, and René Paillard for his help with the sample analyses. Thanks also to Stefan Heinze for the ^{36}Cl measurements at CologneAMS. The financial support of the German Research Foundation (DFG, ME-4212/3-1) is gratefully acknowledged.

References

Armijo, R., H. Lyon-Caen & D. Papanastassiou, (1992). East-west extension and Holocene normal fault-scarps in the Hellenic arc. *Geology*. *20*, 492-494.

Briole, P., A. Rigo, H. Lyon-Caen, J.C. Ruegg, K. Papazissi, C. Mitsakaki, A. Balodimou, G. Veis, D. Hatzfeld & A. Deschamps, (2000). Active deformation of the Corinth rift, Greece: Results from repeated Global Positioning System surveys between 1990 and 1995. *Journal of Geophysical Research*. *105*, 25605-25625.

Chen, J., H.P. Blume & L. Beyer, (2000). Weathering of rocks induced by lichen colonization - a review. *Catena*. *39*, 121-146.

Collier, R.E.L., D. Pantosti, G. D'Addezio, P.M. De Martini, E. Masana & D. Sakellariou, (1998). Paleoseismicity of the 1981 Corinth earthquake fault: Seismic contribution to extensional strain in central Greece and implications for seismic hazard. *Journal of Geophysical Research*. *103*, 30001-30019.

Hubert, A., G. King, R. Armijo, B. Meyer & D. Papanastasiou, (1996). Fault re-activation, stress interaction and rupture propagation of the 1981 Corinth earthquake sequence. *Earth and Planetary Science Letters*. *142*, 573-585.

Jackson, J.A., J. Gagnepain, G. Houseman, G.C.P. King, P. Papadimitriou, C. Soufleris & J. Virieux, (1982). Seismicity, normal faulting, and the geomorphological development of the Gulf of Corinth (Greece)" the Corinth earthquakes of February and March 1981. *Earth and Planetary Science Letters*. *57*, 377-397.

Moretti, I., D. Sakellarioub, V. Lykousisb & L. Micarellia, (2003). The Gulf of Corinth: an active half graben? *Journal of Geodynamics*. *36*, 323-340.

Morewood, N.C. & G.P. Roberts, (2002). Surface observations of active normal fault propagation: implications for growth. *Journal of the Geological Society, London*. Vol. 159, 263-272.

Reilinger, R., S. McClusky, D. Paradissis, S. Ergintav & P. Vernant, (2010). Geodetic constraints on the tectonic evolution of the Aegean region and strain accumulation along the Hellenic subduction zone. *Tectonophysics*. *488*, 22-30.

Riley, S., S.D. De Gloria & R. Elliot, (1999). A Terrain Ruggedness Index that quantified topographic heterogeneity. *Intermountain Journal of Sciences*. *5*, 23-27.

Schlagenhauf, A., Y. Gaudemer, L. Benedetti, I. Manighetti, L. Palumbo, I. Schimmelpfennig, R. Finkel & K. Pou, (2010). Using in situ Chlorine-36 cosmonuclide to recover past earthquake histories on limestone normal fault scarps: a reappraisal of methodology and interpretations. *Geophysical Journal International*. *182*, 36–72.

Wells, D.L. & K.J. Coppersmith, (1994). New Empirical Relationships among Magnitude, Rupture Length, Rupture Width, Rupture Area, and Surface Displacement. *Bulletin of the Seismological Society of America*. *84*, 974-1002.

Wiatr, T., I. Papanikolaou, T. Fernández-Steeger & K. Reicherter, (2015). Bedrock fault scarp history: Insight from t-LiDAR backscatter behaviour and analysis of structure changes. *Geomorphology*. *228*, 421-431.

6th International INQUA Meeting on Paleoseismology, Active Tectonics and Archaeoseismology,
19-24 April 2015, Pescina, Fucino Basin, Italy

INQUA Focus Group on Paleoseismology and Active Tectonics

Deriving uplift and crustal deformation rates in the upper plate of subduction zones from tectonically deformed sequences of marine palaeoshorelines; tectonic and seismic hazard implications in Calabria (Southern Italy)

Meschis, M. (1), Roberts, G.P. (1), Houghton, S. (1), Underwood, C. (1), Briant, R.M. (2)

(1) Department of Earth and Planetary Sciences, Birkbeck, University of London, WC1E 7HX, UK. Email: marco.meschis.14@ucl.ac.uk
(2) Department of Geography, Environment and Development Studies, Birkbeck, University of London, WC1E 7HX, UK

Abstract: *We test interactions between sea-level change, climate and tectonic activity using a synchronous correlation method to refine and define ages of dated and undated Quaternary marine terraces sequences and their chronology. We mapped and measured the inner edge elevations of marine terraces, tectonically deformed by a Quaternary active normal fault, correlating them with global sea-level curves. The uplift process affecting Calabria is rapid enough to raise parts the hangingwall of the investigated active Vibo Fault above sea-level, so we can correlate terraces across the fault. We suggest that the uplift rates at individual locations along the fault are (a) either enhanced by footwall uplift locations or counteracted by hangingwall subsidence with values decreasing towards the SW fault tip, and (b) are constant through time. We stress that our synchronous correlation method should produce a review of marine terraces investigations worldwide, and that uplift rate perturbations are a key condition to map active faults locations, their deformation rates and the associated seismic hazard above subduction zones.*

Key words: *Marine terraces, Quaternary sea-level, Active faults, Synchronous correlations.*

INTRODUCTION

Seismic hazard analysis requires knowledge of seismicity rates that are stable over long time periods to avoid transient strain-rates associated with single earthquake events or temporal earthquakes clusters (Roberts et al. 2013). For regions above subduction zones, raised sequences of Quaternary marine terraces provide key data to derive long-term crustal deformation rates over multiple seismic cycles (Roberts et al., 2013). Unfortunately, it is common for age constraints to exist for only a few paleoshorelines within a marine terrace sequences. To deal with this it has become common to use a sequential approach where the next higher or lower paleoshoreline from a dated horizon is assumed to belong to the next older or younger sea-level highstand (e.g. Armijo et al., 1996; Giunta et al., 2011 for a review). However, this method is inclined to fail in active tectonically regions affected by low uplift rate values where marine terraces from sea-level highstands that were lower than present-day are overprinted and possibly destroyed by younger sea levels (Roberts et al., 2013). Also, when assuming an uplift rate to use this technique, correlations between expected and measured palaeoshoreline elevations are also produced sequentially so the overall fit of measured to expected values is not commonly examined.

In this study we adopt a synchronous correlation method (Roberts et al., 2009 and 2013). To overcome the "overprinting" problem, this method takes into account the well-known fact that sea-level highstands in the Quaternary period are not evenly-spaced in time, so flights of palaeoshorelines resulting from constant uplift rates will not be evenly-spaced in elevation (Roberts et al. 2013). Correlations between expected and measured palaeoshoreline elevations are carried out synchronously for all values whilst iterating the uplift rate, with the certainty of the results tested by regression analysis.

We investigate a set of well-exposed, but only partially-dated Quaternary marine palaeoshoreline sequence in Calabria (Southern Italy). Palaeoshorelines exist both in the hangingwall and footwall of the Vibo fault and beyond its SW tip close to highly-populated areas such as Vibo Valentia town. This allows us to examine the competing roles of subduction and active normal faulting in controlling uplift, and to derive the slip-rates on this active fault that poses a threat to human life and infrastructure to close town such as Briatico, Cessaniti, Pizzo Calabro.

Previous authors (Monaco & Tortorici, 2000; Jacques et al., 2001; Galli & Bosi, 2002; Catalano et al., 2008; Roberts et al., 2013) studied active faults and their slip rates along the Apenninnes and Calabrian Arc estimating values for fault slip-rates here in the range of 0.2-2.0 mm/yrs, but certainty on slip-rates is hindered by the lack of well-exposed fault scarps outcropping on fault-controlled landscape and the lack of multiple absolute dates for palaeoshorelines. In some of these studies a sequential correlation technique is used to suggest multiple changes in uplift-rate through time in the Late Quaternary that we investigate further herein. In order to (i) constrain the slip-rate on active normal faults and their temporal steadiness and (ii) differentiate "regional" uplift rate and local fault-controlled uplift rate, we combine a synchronous correlation of palaeoshorelines with sea-level highstands and new U/Th dates from fossil corals. We discuss this in terms of seismic hazard and the tectonics of the Calabrian subduction zone.

INQUA Focus Group on Paleoseismology and Active Tectonics

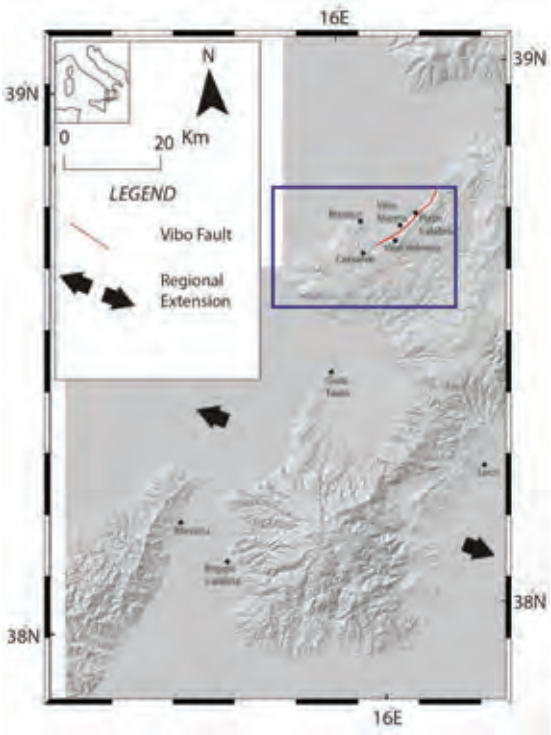

Figure 1: Digital Elevation Model of South of Italy within the geological domain of Calabrian Arc. The blue square shows the investigated area with the Vibo Fault.

Background

The Calabrian Arc links the NW – SE orientated Southern Apennines thrust belt and the E – W orientated Maghrebide thrust belt of Northern Sicily (Tortorici et al., 1995). Furthermore, the oceanic crust of the Ionian Sea is subducting beneath the Calabrian Arc itself, associated with the northward progression of the African plate and progressive Calabrian Arc migration and the opening of the Tyrrenian Extensional Basin (Rehault et al., 1984; Malinverno and Ryan, 1986; Dewey et al., 1989). During the last 3.6 My, the Calabrian Arc has been characterized by active normal faulting on the Tyrrenian side; the regional active extension is WNW – ESE oriented (Monaco and Tortorici, 2000) which is consistent with GPS investigations suggesting a ~2mm/yr extension rate in this orientation (Serpelloni et al., 2005). Historical earthqukes confirm this active extension, rupturing faults including Vibo Fault (e.g. Jacques et al., 2001; Loreto et al., 2013). Additionally, the Calabrian Arc has been affected by prominent uplift confirmed, at different timescales, by (i) GPS investigations (Serpelloni et al. 2013) and (ii) the presence of raised Quaternary and Holocene sequence of paleoshorelines studied by several authors in the past (Malinverno and Ryan, 1986; Dumas et al., 1987; Patacca et al., 1990; Westaway, 1992; Miyauchi et al., 1994; Balescu et al., 1997; Bianca et al., 1999; Bonardi et al., 2001; Doglioni et al., 2001; Tortorici et al., 2003; Faccenna et al., 2004; Cucci and Tertulliani, 2006; Bianca et al., 2011; Giunta et al., 2011; Roberts et al., 2013). The Capo Vaticano peninsula, within the Calabrian Arc, is the focus of our investigations and excellently displays the relationship between ongoing active extension and uplifting processes. Here a dramatic sequence of marine terraces is deformed by the Quaternary active Vibo Fault (Ghisetti, 1981; Dumas et al., 1987; Westaway, 1992; Miyauchi et al., 1994; Bianca et al., 1999; Catalano and De Guidi, 2003; Tortorici et al., 2003; Bianca et al., 2011; Roberts et al., 2013). We performed detailed fieldwork and GIS analysis using a DEM with ~10 m resolution (Tarquini et al. 2007) on palaeoshoreline locations, allowing us to differentiate "regional" uplift-rates and local tectonic-controlled uplift rates.

RESULTS

Our study shows that spatial changes in uplift can be explained (Figs. 2, 3, 4, 5 and 6) by local tectonic subsidence derived by active normal fault activity which counteracts the "regional" uplift, probably associated with the Ionian subduction.

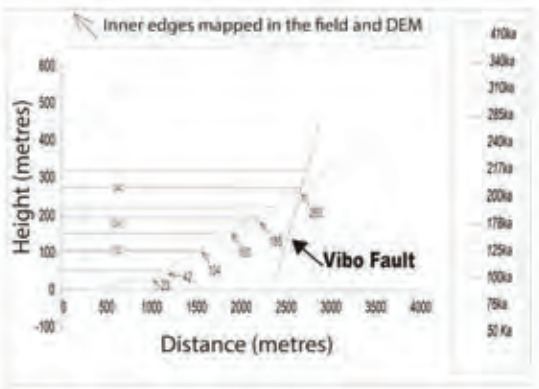

Figure 2: Example of a topographic profile across the 10m DEM, with the synchronous correlation between multiple sea-level highstands and multiple paleoshorelines, from the hangingwall of the Vibo Fault.

Use of synchronous correlations demonstrates a clear relationship between measured elevations of marine terraces inner edges and predicted elevations of sea-level highstands iteratively calculated given an uplift rate value (R^2= 0.9974, as shown in Fig. 3). It also constrains activity rates on the Vibo Fault. Furthermore, mapped inner edges elevations in the field using hand-held GPS compared to DEM-derived elevations resulted in a very robust relationship (R^2 = 0.99 as shown in Fig.4) confirming our consistent DEM analysis. The above is demonstrated by the following:

1) We have achieved correlations between measured and predicted palaeoshoreline elevations with R^2 value >0.9 for 29 transects across the 10m DEM. These interpretations are supported by new coral dates from Stage 5e (~125 ka).

2) The uplift rate of sites in hangingwall locations increases along strike from ~0.4 mm/yr close to the centre of Vibo fault to ~1.75 mm/yr beyond its tip. These uplift rates are associated with classic deformed

palaeoshoreline geometries such as an increase in the number of preserved palaeoshorelines where uplift rates are higher, and an increase in the along-strike tilt angle for progressively older palaeoshorelines.

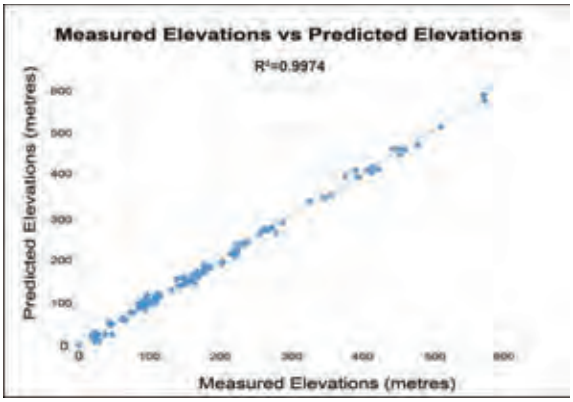

Figure 3: Linear regression showing robust correlation for 29 topographic profiles between predicted inner edges elevations and our measured inner edges elevations. The predicted elevations have been calculated by iteratively defining an uplift rate over the Late Quaternary repeating this value to yield a best fit to the measured palaeoshorelines.

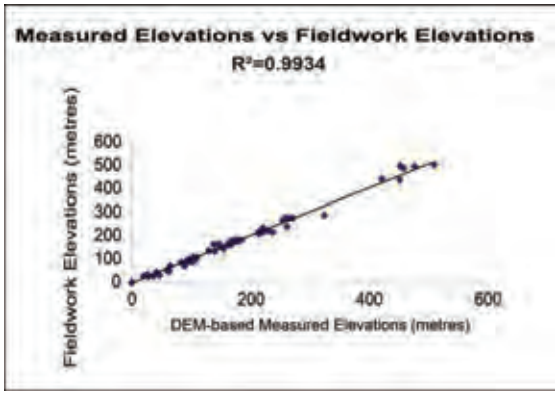

Figure 4: Linear regression showing robust correlation for 29 topographic profiles between field-based and our DEM-based inner edges elevations confirming a consistent relationship between DEM and field analysis.

3) The uplift rates derived from the synchronous correlation produce excellent fits to the data ($R^2 > 0.9$) using constant uplift rate values; temporally varying uplift rates are un-necessary to explain the observations.
4) Mapping of palaeoshorelines around the fault tip and onto the footwall of the Vibo fault allows us to extract the vertical component of the slip-rate across the fault. The palaeoshoreline interpreted to have formed at 340 ka is offset by ~360 m close to the centre of the fault with values decreasing towards the fault tip, implying maximum vertical slip-rate averaged since 340 ka of 1.06 mm/yr. The rates of deformation described herein and in Roberts et al. (2013) are comparable with other fault slip-rate values on faults already studied in the central Apennines (see Roberts & Michetti 2004 for a review) and in the Southern Apennines and Calabria also studied by Jacques et al., (2001) and Galli & Bosi, (2002). Moreover, deriving fault slip-rate allows us to roughly calculate the Earthquake Recurrence Interval (ERI) which is a crucial parameter to approach to the long-term seismic hazard analysis.

Figure 5: Field-mapped inner edges in Vibo Marina town.

Finally, we emphasise that studying tectonically deformed paleoshorelines is a key step (i) to average strain-rates measurements over long-term timescales (1000000 yrs) and (ii) these measurements are crucial for comparison with strain-rates values derived from palaeoseismology and GPS investigations which span shorter timescales, providing a baseline to study seismic hazards. This is facilitated by using a "synchronous" correlation instead of "sequential" for multiple paleoshorelines and multiple Quaternary sea-level highstands.

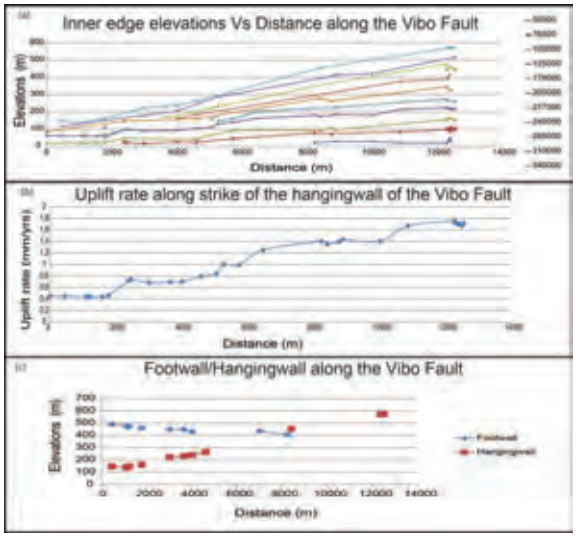

Figure 6: (a) Uplift rate field changing along strike and over the tip of the Vibo fault confirming that regional uplift has been affected by local active normal fault. (b) Inner edges elevations variations along strike the Vibo Fault confirming the faulting activity over the Late Quaternary. (c) Elevation gradients of the HG and FW cutting-offs the palaeoshoreface surface associated with the 340 ka palaeoshoreline.

INQUA Focus Group on Paleoseismology and Active Tectonics

Acknowledgements: This study was funded by NERC grants NE/I024127/1, NE/H003266/1, NE/E01545X/1, NE/B504165/1 and GR9/02995, and a University of Palermo Student Scholarship. We thank S. Tarquini for helping us to access the DEM. Patience Cowie, Ioannis Papanikolaou, Alessandro Michetti, Joanna Faure Walker, Francesco Visini and Bruno Pace are thanked for her discussions on the activity rates of faults and seismic hazards.

References

Armijo, R., B. Meyer, G.C.P. King, A. Rigo & D. Papanastassiou, (1996). Quaternary evolution of the Corinth Rift and its implications for the Late Cenzoic evolution of the Aegean. *Geophysical Journal International*. 126, 11-53.

Balescu, S., B. Dumas, P. Guérémy, M. Lamothe, R. Lhenaff & J. Raffy, (1997). Thermoluminescence dating tests of Pleistocene sediments from uplifted marine shorelines along the southwest coastline of the Calabrian Peninsula (southern Italy). *Palaeogeography, Palaeoclimatology, Palaeoecology*. 130 (1), 25-41.

Bianca, M., C. Monaco, L. Tortorici & L. Cernobori, (1999). Quaternary normal faulting in southeastern Sicily (Italy): a seismic source for the 1693 large earthquake. *Geophysical Journal International.* 139 (2), 370-394.

Bianca, M., S. Catalano, G. De Guidi, A.M. Gueli, C. Monaco, G.M. Ristuccia, G. Stella, G. Tortorici, L. Tortorici & S.O. Troja, (2011). Luminescence chronology of Pleistocene marine terraces of Capo Vaticano peninsula (Calabria, Southern Italy). *Quaternary International,* 232 (1), 114-121.

Bonardi, G., W. Cavazza, V. Perrone & S. Rossi, (2001). Calabria-Peloritani terrane and northern Ionian Sea. In: *Anatomy of an orogen: The Apennines and adjacent Mediterranean basins*. 287-306. Springer Netherlands. doi: 10.1007/978-94-015-9829-3_17.

Catalano, S. & G. De Guidi, (2003). Late Quaternary uplift of northeastern Sicily: relation with the active normal faulting deformation. *Journal of Geodynamics*. 36 (4), 445-467.

Catalano, S., G. De Guidi, C. Monaco, G. Tortorici & L. Tortorici (2008). Active faulting and seismicity along the Siculo-Calabrian Rift Zone (southern Italy). *Tectonophysics*. 453, 177-192.

Cucci, L. & A. Tertulliani, (2006). I terrazzi marini nell'area di Capo Vaticano (Arco Calabro): solo un record di sollevamento regionale o anche di deformazione cosismica? *Il Quaternario.* 19, 89-101.

Dewey, J.F., M.L. Helman, S.D. Knott, E. Turco & D.H.W. Hutton, (1989). Kinematics of the western Mediterranean. *Geological Society, London, Special Publications.* 45 (1), 265-283.

Doglioni, C., F. Innocenti & G. Mariotti, (2001). Why Mt Etna? *Terra Nova,* 13 (1), 25-31.

Dumas, B., P. Gueremy, R. Lhenaff & J. Raffy, (1987). Rates of uplift as shown by raised Quaternary shorelines in Southern Calabria (Italy). *Z. Geomorph. NF* 63, 119-132.

Faccenna, C., C. Piromallo, A. Crespo Blanc, L. Jolivet & F. Rossetti, (2004). Lateral slab deformation and the origin of the arcs of the western Mediterranean. *Tectonics*. 23, TC1012.

Galli, P. & V. Bosi, (2002). Paleoseismology along the Cittanova fault: implications for seismotectonics and earthquake recurrence in Calabria (southern Italy). *Journal of Geophysical Research: Solid Earth. (1978–2012).* 107 (B3), ETG-1.

Ghisetti, F., (1981). Upper Pliocene-Pleistocene uplift rates as indicators of neotectonic pattern: an example from southern Calabria (Italy). *Z. Geomorphol*. 40, 93-118.

Giunta, G., A.M. Gueli, C. Monaco, S. Orioli, G.M. Ristuccia, G. Stella, S.O. Troja, (2011). Middle-Late Pleistocene marine terraces and fault activity in the Sant'Agata di Militello coastal area (north-eastern Sicily). *Journal of Geodynamics*. 55, 32-40.

Jacques, E., C. Monaco, P. Tapponnier, L. Tortorici & T. Winter, (2001). Faulting and earthquake triggering during the 1783 Calabria seismic sequence. *Geophysical Journal International.* 147, 499-516.

Loreto, M.F., U. Fracassi, A. Franzo, P. Del Negro, F. Zgur & L. Facchin, (2013). Approaching the seismogenic source of the Calabria 8 September 1905 earthquake: New geophysical, geological and biochemical data from the S. Eufemia Gulf (S. Italy). *Marine Geology*. 343, 62-75.

Malinverno, A. & W.B.F. Ryan, (1986). Extension in the Tyrrhenian Sea and shortening in the Apennines as result of arc migration driven by sinking of the lithosphere. *Tectonics*. 5 (2), 227-245.

Miyauchi, T., G. Dai Para & S. Sylos Labini, (1994). Geochronology of Pleistocene marine terraces and regional tectonics in the Tyrrhenian coast of South Calabria, Italy. *Il Quaternario.* 7 (1), 17-34.

Monaco, C. & L. Tortorici, (2000). Active faulting in the Calabrian arc and eastern Sicily. *Journal of Geodynamics*. 29, 407-424.

Patacca, E., R. Sartori & P. Scandone, (1990). Tyrrhenian basin and Apenninic arcs: kinematic relations since late Tortonian times. *Mem. Soc. Geol. It.* 45 (1992), 425-451.

Rehault, J.P., G. Boillot & A. Mauffret, (1984). The western Mediterranean basin geological evolution. *Marine Geology*. 55 (3), 447-477.

Roberts, G.P. & A.M. Michetti, (2004). Spatial and temporal variations in growth rates along active normal fault systems: an example from The Lazio-Abruzzo Apennines, central Italy. *Journal of Structural Geology*. 26 (2), 339-376.

Roberts, G.P., S.L. Houghton, C. Underwood, I. Papanikolaou, P.A. Cowie, P. Van Calsteren, T. Wigley, F.J. Cooper & J.M. McArthur, (2009). Localization of Quaternary slip rates in an active rift in 10^5 years: an example from central Greece constrained by ^{234}U-^{230}Th coral dates from uplifted paleoshorelines. *Journal of Geophysical Research*. 114, B10406.

Roberts, G.P., M. Meschis, S.L. Houghton, C. Underwood & R.M. Briant, (2013). The implications of revised Quaternary palaeoshoreline chronologies for the rates of active extension and uplift in the upper plate of subduction zones. *Quaternary Science Reviews*. 78, 169-187.

Serpelloni, E., M. Anzidei, P. Baldi, G. Casula & A. Galvani, (2005). Crustal velocity and strain-rate fields in Italy and surrounding regions: new results from the analysis of permanent and non-permanent GPS networks. *Geophysical Journal International*. 161 (3), 861-880.

Serpelloni, E., C. Faccenna, G. Spada, D. Dong & S.D.P. Williams, (2013). Vertical GPS ground motion rates in the Euro-Mediterranean region: New evidence of velocity gradients at different spatial scales along the Nubia-Eurasia plate boundary. *Journal of Geophysical Research: Solid Earth.* 118 (11), 6003-6024. doi: 10.1002/2013JB010102.

Tarquini, S., S. Vinci, M. Favalli, F. Doumaz, A. Fornaciai & L. Nannipieri, (2012). Release of a 10-m-resolution DEM for the Italian territory: Comparison with global-coverage DEMs and anaglyph-mode exploration via the web. *Computers & geosciences*. 38 (1), 168-170.

Tortorici, G., M. Bianca, G. De Guidi, C. Monaco & and L. Tortorici, (2003). Fault activity and marine terracing in the Capo Vaticano area (southern Calabria) during the Middle-Late Quaternary. *Quaternary International.* 101, 269-278.

Tortorici, L., C. Monaco, C. Tansi & O. Cocina, (1995). Recent and active tectonics in the Calabrian arc (Southern Italy). *Tectonophysics*. 243, 37-55.

Westaway, R., (1992). Seismic moment summation for historical earthquakes in Italy: tectonic implications. *Journal of Geophysical Research: Solid Earth*. *(1978-2012).* 97 (B11), 15437-15464.

INQUA Focus Group on Paleoseismology and Active Tectonics

paleoseismicity.org

Neogene-Quaternary evolution of the Eastern Marsica region (Central Italy)

Miccadei, E. (1), Piacentini, T. (1), Berti, C. (2)

(1) Department of Engineering and Geology, Università degli Studi "G. d'Annunzio" Chieti-Pescara, Via dei Vestini, 31, 66100 Chieti Scalo (CH) Italy. Email: Miccadei@unich.it
(2) Department of Geological Science, University of Delaware, Newark, DE 19716, USA

Abstract: *The relief features of the Apennine chain have been developed in a complex geomorphological and geological setting from Neogene to Quaternary. Growth of topography has been driven by active polyphasic tectonics (thrust-related crustal shortening, strike-slip faulting and high-angle normal faulting related to crustal extension), regional rock uplift, and surface processes, in a complex interrelation, since Upper Miocene(?) – Lower Pliocene. In the last years, geological and geomorphological studies in Central Italy are leading to a new and more complex definition of the geological-structural setting and landscape evolution of the Apennine orogen, resulting from the overprinting of subsequent tectonic phases and surface processes. Finally, the surface data is to be linked to the data of deep geophysical investigations of this area of the Apennines chain.*

Key words: *Geological setting, landscape evolution, Marsica, Central Italy.*

INTRODUCTION

The present landscape of the eastern Marsica, along the axial part and the main drainage divide of the Central Apennines chain, is a high-elevation and high relief landscape dominated by several morphostructures including: high-standing, resistant, Mesozoic and early Tertiary carbonates ridges (i.e. thrust ridges, faulted homocline ridges) and intervening, erodible Tertiary siliciclastics valleys (i.e. fault line valleys) and Quaternary continental deposits filled basins (i.e. tectonic valleys, tectonic basins; Fig. 1; Cavinato et al., 2002; D'Alessandro et al., 2003; Ascione et al., 2008; Piacentini & Miccadei, 2014 and references therein).

Geological and geomorphological studies carried out in Central Italy are outlining to a new and more complex geological-structural setting, faults' hierarchy and landscape evolution of the axial part of the Apennine orogen, related to Neogene-Quaternary polyphasic tectonics and Pleistocene regional uplift (Ascione et al., 2008; Bonini et al., 2014; Piacentini & Miccadei, 2014 and references therein).

Geological mapping and morphostructural analysis in the eastern Marsica area have permitted to identify, and

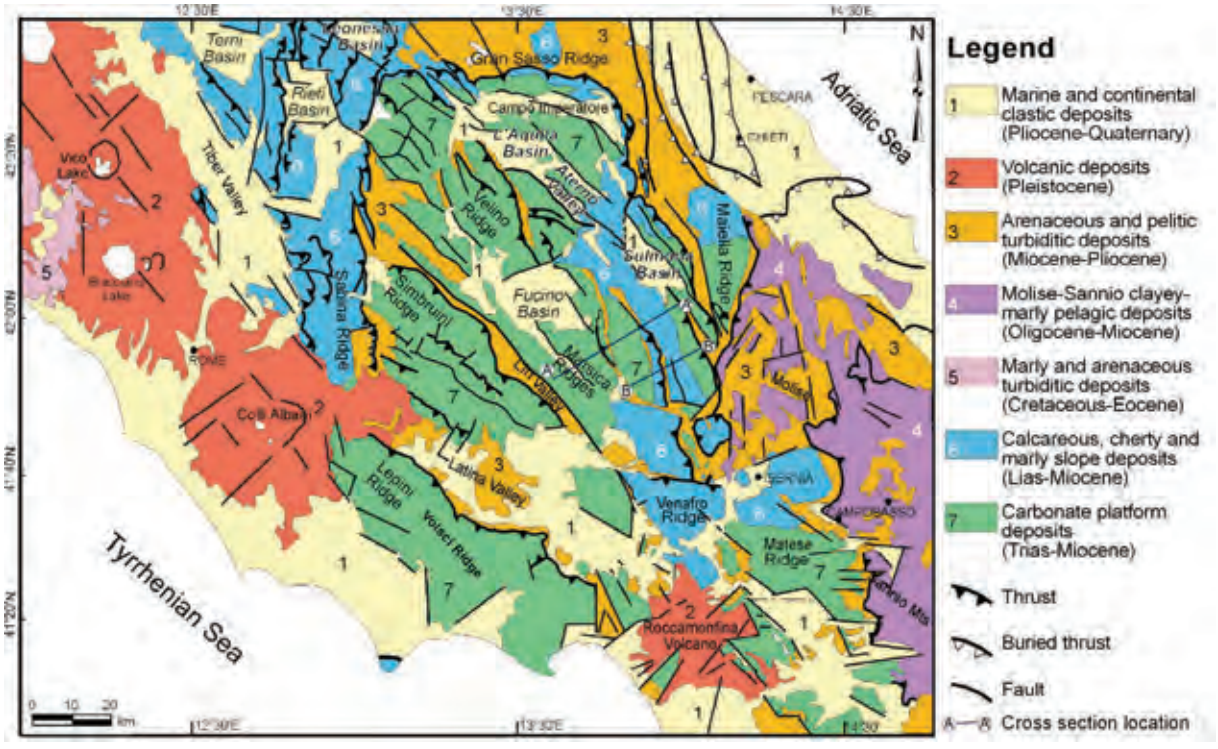

Figure 1: Geological scheme of Central Italy (modified after Parotto et al., 2004).

cinematically characterize, tectonic elements supposed to have a regional significance. These elements are to be added to an already complex geological setting resulting from the interference between a well articulated Meso-Cenozoic paleogeographic evolution and a polyphasic tectonics (Miccadei, 1993; ISPRA, 2010; Miccadei et al., 2012 and references therein).
This work aims to outline the Neogene-Quaternary geological evolution of the eastern Marsica area and the landscape evolution that followed the incipient phases of morphogenesis after the emersion of the Apennines area. Finally, it analyzes the role of tectonics and surface processes in the long term landscape evolution (i.e. Mio?-Pliocene to Quaternary).

METHODS

This work is the results of several studies in the Marsica area incorporating geologic and geomorphologic field mapping of morphostructures and Quaternary continental deposits, and plano-altimetric analysis and morphometry of orography and drainage network.
Field mapping give clues on the definition of geological setting and paleo-landscapes related to different paleo-morpho-climatic environments. Geomorphological evidence of tectonics and their cross-cutting relationships with morphostructures, continental deposits and faults, provide clues on the deciphering of the reciprocal antecedence relationship of the paleo-landscapes and on the timing of tectonics and landscape evolution. Geomorphic evidence of faults is provided also by morphometry of orography and drainage network. Surface data is also compared to the results of deep geophysical investigations, such as the Crop11 Project (Civitavecchia–Vasto) still under study.
Correlation of tectonic elements, paleosurfaces, Quaternary continental deposits, lead to the identification of areas in which tectonics has the main role in the morphogenesis of the landscape and areas where surface processes are predominant.

RESULTS

Trying to read in time the main geological events involving the eastern Marsica area, it is possible to outline the complexity of all the tectonic phases.
The sin-orogenic tectonics induced the overthrusting of tectonic-stratigraphic units along main thrusts (calcareous units over terrigenous ones). As result, the main units seem to be arranged in two different structural levels. It is possible to define "upper units", including carbonate platform and margin facies, and "lower units" including slope and basin facies and more external margin and carbonate platform facies (Fig. 2). Moreover, some small units could belong to a deeper structural level (Fig. 2), whose interpretation is to be connected to the complex tectonic and stratigraphic setting of the southern areas (Monti della Meta). The thrusting of tectonic-stratigraphic units is to be ascribed to Late Miocene (i.e. Late Messinian) and Early Pliocene (Cipollari et al., 1999; Miccadei et al., 2012 and references therein).
During late-orogenic stages, the tectonic-stratigraphic units appear to be displaced along three main transpressional deformation belt, comprising several fault planes mostly NNW-striking. Several superimposed kinematic indicators provide evidence of different transport trends both towards eastern sides and northern sides. The activation time of these elements is still poorly constrained, but should anyway be developed between the last compressional events (Early Pliocene) and the first evidence of post-orogenic extensional tectonics (Early Pleistocene - Gelasian).
Post-orogenic continental deposits are composed of complex sequences of glacial, slope, alluvial fan, fluvial and lacustrine Quaternary deposits, which unconformably overlie the deformed pre-Quaternary bedrock (sealing thrusts and strike-slip faults) and are displaced and tilted by extensional faults. Continental deposits provide a record of long term (Quaternary) and short term (Late Pleistocene – Holocene) spatial and temporal variation of morphotectonic features and faults activity (see also Roberts & Michetti, 2004). Post-orogenic extensional tectonics, developed since Early Pleistocene - Gelasian, together with large scale uplift (mostly since Middle Pleistocene), outlining a complex hierarchy in the relationship with previous, syn- and late-orogenic, tectonic features (Bonini et al., 2014). A more complex structural setting is defined, with the progressive formation of tectonic valleys and basins, widely represented in the Fucino intermontane basin (Fig. 3) (as well as in surrounding intermontane basins; Giaccio et al., 2012; Santo et al., 2014; Piacentini & Miccadei, 2014 and references therein).
From a geomorphological point of view, the area is characterised by glacial and karst landscapes hanging at the highest elevations, and by slope landforms, alluvial fans and fluvial landforms on the flanks and bottom of valleys and Fucino basin, related to the stages of landscape incision and to the alternating warm-cold Pleistocene climate stages. Lacustrine landforms are locally preserved along the slopes of the Fucino basin.
The present day drainage system is characterised by the main drainage divide of Central Apennines (separating Adriatic slope and Fucino endorheic area) and it is mostly composed of longitudinal tectonic valleys and fault line valleys, incised by longitudinal gorges; the longitudinal drainage is linked by transversal gorges/valleys incising the main compressive ridges and composing an overall rectangular drainage pattern.
Morphotectonic features are related to Neogene thrusts, reactivated or displaced by complex kinematic strike slip elements and followed by extensional tectonic features (present surface evidence given by fault line scarps, fault line valleys, fault scarps, fault slopes, wind gaps, etc.). However, neotectonic evidence along Late Pleistocene and Holocene faults is well differentiated. It is quite poor in the eastern Marsica, where recent deposits are poorly displaced by faults, while it is well evident in the Fucino intermontane basin and the surrounding ones, with several Late Pleistocene – Holocene fault scarps and paleoseismological evidences (i.e. Subequan Basin,

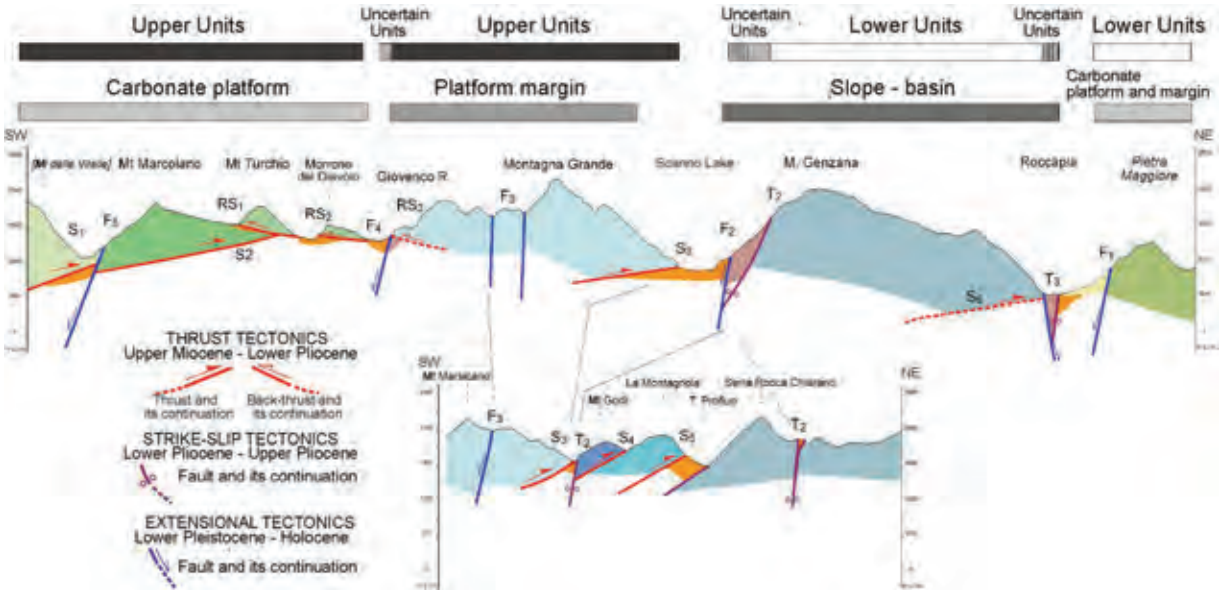

Figure 2: Schematic cross section of the eastern Marsica area. The units are summarized as "upper units" and "lower units". Some small units are still uncertain and could belong to a more deep structural level, whose interpretation is to be connected to the complex tectonic and stratigraphic setting of the southern areas (after Miccadei et al., 2012).

Sulmona Basin, Cinque Miglia Plain, etc.; Roberts & Michetti, 2004; Piacentini & Miccadei 2014 and references therein).

Since Early Pleistocene, extensional tectonics defines a ridges and valleys gentle landscape as suggested by the morpho-lithostratigraphic setting of the older deposits of the post-orogenic continental succession (Fig. 3). However, the present landscape is mostly outlined during the Middle Pleistocene interval. The superimposition of local extensional tectonics and increasing regional uplift (Ascione et al., 2008) induces the development of the large Lake Fucino within a fault-bounded internally draining basin (as well in all the main basins of Central Apennines). On the main ridges' flanks, slope and alluvial fan deposits are terraced and hanging on erosional landscapes, and remnants of karst landscapes are preserved and progressively uplifted on the ridges' top. Pleistocene glacial stages change the spatial-temporal distribution of surface processes and continental deposits.

During the late Middle Pleistocene, while the surrounding areas experience an abrupt change from an endorheic drainage system to an open through-going drainage system (dominated by rivers connecting intermontane basins), the Marsica area is preserved as endorheic, including the persistent Fucino lake.

Up to the whole Holocene, the Fucino area is deeply affected by extensional tectonics (outlined by fault scarps and fault slopes surrounding the large tectonic basin) while the eastern Marsica is mostly affected by surface selective erosion processes (outlined by fault line scarps, deep-narrow fault line valleys and fluvial-karst gorges).

CONCLUSION

The geological and geomorphological analysis of the eastern Marsica region (central Abruzzo) has outlined a structural setting more complex than already known in literature. The identified compressional tectonics, the strike slip tectonics, and the extensional one provide new contributions to the definition of the Neogene-Quaternary evolution. Geometry and kinematics of tectonic elements allowed for defining new constraints concerning regional interpretations and faults hierarchy. Overthrusting of different Mesozoic paleogeographic domains and large displacements that affected the major tectonic elements, make this area a key area for the comprehension of the relationship among the different tectonic-stratigraphic units. In summary, the structural setting shows a tectonics activated since Miocene and still active up to the whole Holocene, although with a heterogeneous spatial-temporal distribution (Fig. 2, 3).

The outlining of a new geological setting defined by the superimposition of lower and upper units and the interposed uncertain units pertaining to the southern Meta domain, the recognition of different morphotectonic features, the identification of paleo-landscapes, and the reconstruction of their history, contribute to define the main phases of syn- and post-orogenic landscape evolution of the Marsica region: it results from the link of alternating morphotectonics and surface processes, due to fault activity, rock uplift processes and alternating karst, glacial, slope, fluvial processes, related to warm-cold climate stages. In this context the Marsica area has been preserved all along the Quaternary as a large endorheic area including the Fucino Lake unlike the other major intermontane basins in Central Italy.

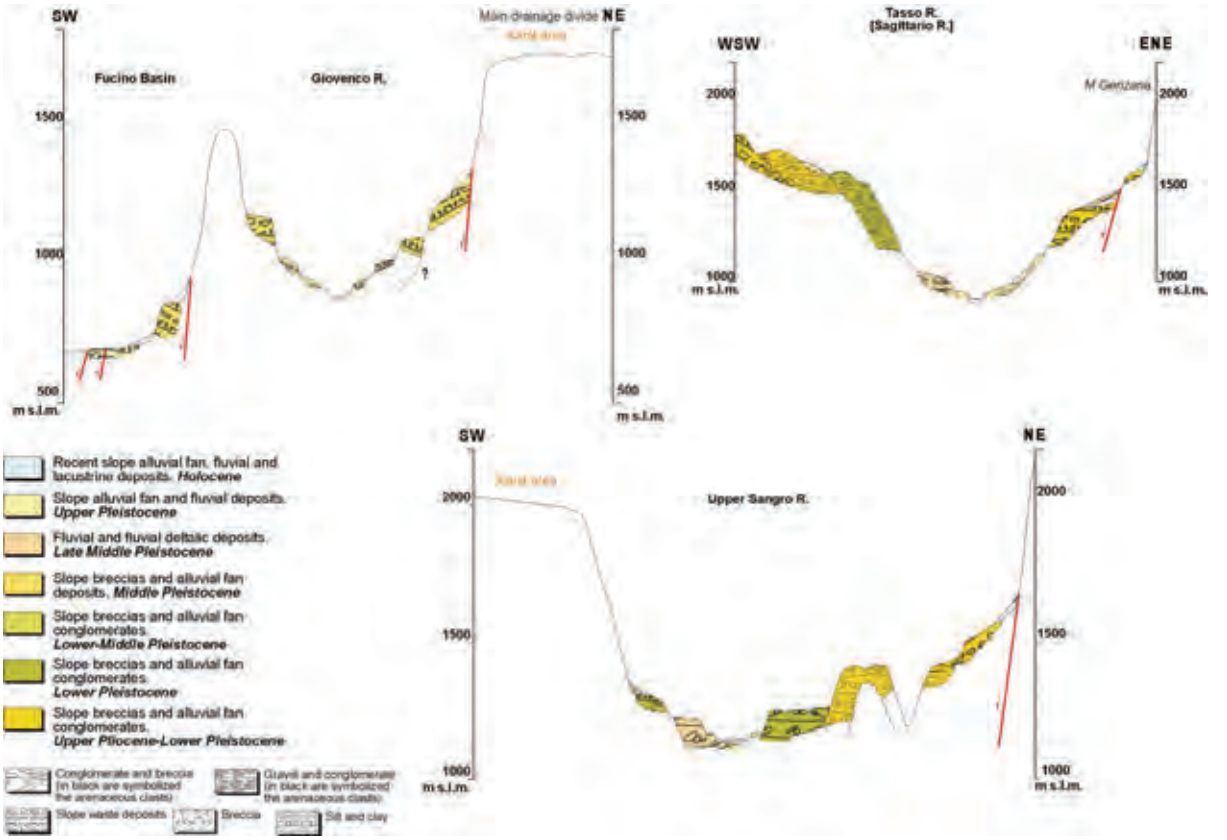

Figure 3: Morpho-litostratigraphic scheme of the Quaternary continental deposits of the eastern Marsica Area (modified after Miccadei et al., 2012; Piacentini and Miccadei, 2014).

References

Ascione, A., A. Cinque, E. Miccadei, F. Villani, C. Berti (2008). The Plio-Quaternary uplift of the Apennine chain: new data from the analysis of topography and river valleys in Central Italy. *Geomorphology*. 102, 105-118.

Bonini, L., D. Di Bucci, G. Toscani, S. Seno, G. Valensise (2014). On the complexity of surface ruptures during normal faulting earthquakes: Excerpts from the 6 April 2009 L'Aquila (central Italy) earthquake (M w 6.3). *Solid Earth*. 5, (1), 389-408.

Cavinato, G. P., C. Carusi, M. Dall'Asta, E. Miccadei, T. Piacentini (2002). Sedimentary and tectonic evolution of Plio-Pleistocene alluvial and lacustrine deposits of Fucino Basin (central Italy). *Sedimentary Geology*. 148, (1-2), 29-59.

Cipollari, P., D. Cosentino, E. Gliozzi (1999). Extension- and compression-related basins in central Italy during the Messinian Lago-Mare event. *Tectonophysics*. 315, 163-185.

D'Alessandro, L., E. Miccadei, T. Piacentini (2003). Morphostructural elements of central–eastern Abruzzi: contributions to the study of the role of tectonics on the morphogenesis of the Apennine chain. *Quaternary International*. 101-102, 115-124.

Giaccio, B., P. Galli, P. Messina, E. Peronace, G. Scardia, G. Sottili, A. Sposato, E. Chiarini, B. Jicha, S. Silvestri (2012). Fault and basin depocentre migration over the last 2 Ma in the L'Aquila 2009 earthquake region, Central Italian Apennines. *Quaternary Science Reviews*. 56, 69-88.

ISPRA (2010). *Carta Geologica d'Italia alla scala 1:50.000, Foglio 378 "Scanno"*. Servizio Geologico d'Italia, ISPRA.

Miccadei, E. (1993). Geologia dell'area Alto Sagittario-Alto Sangro (Abruzzo, Appennino centrale). *Geologica Romana*. 29, 463-481.

Miccadei, E., L. D'Alessandro, M. Parotto, T. Piacentini, A. Praturlon (Eds.) (2012). *Note illustrative della Carta Geologica d'Italia (scala 1:50.000), Foglio 378 "Scanno"*. Servizio Geologico d'Italia, ISPRA. 212 p.

Parotto, M., G.P. Cavinato, E. Miccadei, M. Tozzi (2004). Line CROP 11: Central Apennines. In: Scrocca D., Doglioni C., Innocenti F., Manetti P., Mazzotti A., Bertelli L., Burbi L. & D'Offizi S. (Eds.): *"CROP Atlas: seismic reflection profiles of the Italian crust"*. *Memorie Descrittive Carta Geologica d'Italia*. 62, 145-153.

Piacentini, T., E. Miccadei (2014).The role of drainage systems and intermontane basins in the Quaternary landscape of the Central Apennines chain (Italy). *Rendiconti Lincei - Scienze Fisiche e Naturali*. 25, (2), 139-150.

Roberts, G.P., A.M. Michetti (2004). Spatial and temporal variations in growth rates along active normal fault systems: An example from The Lazio-Abruzzo Apennines, central Italy. *Journal of Structural Geology*. 26, (2), 339-376.

Santo, A., A. Ascione, G. Di Crescenzo, E. Miccadei, T. Piacentini, E. Valente (2014). Tectonic-geomorphological map of the middle Aterno River valley (Abruzzo, Central Italy). *Journal of Maps*. 10, (3), 365–378.

INQUA Focus Group on Paleoseismology and Active Tectonics

paleoseismicity.org

Use of quantitative geomorphological methods in the segmentation of Sperchios active fault zone, central Greece

Michail, M. (1), Chatzipetros, A. (2)

(1) Department of Physics and Earth Sciences, University of Ferrara, Ferrara 44122, Italy. Email: mchmra@unife.it
(2) Department of Geology, Aristotle University of Thessaloniki, 54124, Greece

Abstract: *This paper aims to study the Sperchios Basin, one of the major neotectonic, fault-controlled, features of the Hellenides, with the application of specific morphotectonic indices. The study area includes well exposed fault-bounded mountain fronts with dominant footwall relief. The most prominent structures of this WNW-ESE trending neotectonic basin are WNW-ESE to NW-SE trending faults, the most prominent of which is the Sperchios Fault System (SFS) causing mainly subsidence toward the NNE. The antithetic Coastal Fault System (CFS) also forms a distinct, yet gentler relief at the NE basin boundary. The segmentation of these neotectonic faults allowed detailed measurements, based on morphotectonic characteristics, of each segment separately. Mountain-front sinuosity (Smf) as well as the ratio of valley floor width to valley height (Vf) were among the indices used in this study and contributed to the identification of the potential fault activity. The results show that there is a strong correlation between uplift rates and the morphotectonic signature of faulting, as well as a clear morphotectonic differentiation of fault segments.*

Key words: *Segmentation, morphotectonic indices, Sperchios basin, central Greece, active tectonics.*

INTRODUCTION

The quantitative measurement of an active tectonic landscape, as well as landform evaluation, could provide us with basic information necessary for estimating long-term deformation. Sperchios Basin is one of the most important neotectonic features of Greece, within an area where active tectonics have drastically controlled and formed the landscape. Sperchios basin is located in the Fthiotis area, East Central Greece (Fig. 1). It has a mean WNW-ESE axis, and it extends from Mt. Tymfristos to the west, to Maliakos Gulf to the east (Kranis, 1999). The basin is defined by the mountainous areas of Timfristos to the west, Othris to the east and Kallidromo to the south. Extension has dominated the deformation of the region in the Quaternary period, starting at Late Pliocene - Early Pleistocene, continuing until today. The most important structures are the WNW-ESE to NW-SE trending, NNE-dipping faults that control the margins of this neotectonic basin. However, faults with ENE-WSW and/or NE-SW strike are also present. In this paper we focus on the tectonically young southern margin of Sperchios Basin, which is dominated by large normal faults of E-W to WNW-ESE strike, like most of the neotectonic structures of central Greece (Psomiadis, 2010; Tzanis et al., 2010). The southern part of Sperchios basin is comprised by the Sperchios Fault System (SFS), which consists of two major fault segments, Sperchiada and Kompotades faults, at its western and eastern part, respectively, and the Coastal Fault System (CFS), the western part of the south coast of the North Gulf of Evia, comprising three main faults, the Arkitsa-Longos fault to the east, the Agios Konstantinos fault in the middle and the Kamena Vourla fault to the west (Ganas, 1997; Kranis, 1999).

Figure 1: Indication of the major neotectonic structures of the studied area (modified map after Kranis, 1999).

The basin includes pre-rift formations such as limestones, flysch, radiolarites, ophiolites and a volcaniclastic sequence, Neogene deposits and synrift formations of Tertiary and Quaternary age (alluvial fans). Eliet & Gawthorpe (1995) studied the sedimentary supply of Sperchios basin in relation to active tectonics and footwall uplift, as recorded mainly in the Quaternary sedimentary sequences.

Geomorphic indices have been applied to mountain ranges worldwide in order to determine the relative tectonic activity (e.g. Bull & McFadden, 1977; Keller & Pinter, 1996; Gawthorpe & Leeder, 2000; Bull 2007, 2009). In this paper the faults that have been studied are the Sperchiada fault that bounds the southern part of the basin, Kompotades fault, which controls the central part of the basin, Molos and Kamena Vourla faults on the east-southern part and the North Faults, which are smaller scale faults at the northern part of the basin. The selection of those faults was based on the idea of collecting information from several parts of the basin (north, south, south-east, south-west), with the aim to make a general estimation of the current morphogenetic processes acting on the study area, thus to compare the tectonic activity between the different fault segments, in both southern and northern margins of the basin. The first stage was to separate the fault zones into smaller segments, based on published studies and field data (e.g. changes in the mountain front orientation, overstepping of fault strands, etc.). The second stage included the application of geomorphic indices along the segments of those neotectonic faults. The fault segmentation contributed to the general morphometric analysis of the area and the estimation of the degree of activity for each segment.

DISCUSSION

Fault segmentation is applied to different long faults around the world. The theories imply that faults initiate as separate faults, propagate, and ultimately link to form a long fault (e.g. Ganas & Papoulia, 2000). In order to achieve a better result in our study, we segmented the following faults into smaller sections, taking into consideration the changes in the mountain front orientation and the morphology along the faults.

• Sperchiada Fault (Fig. 2a) and Kompotades Fault (Fig. 2b)
Sperchiada fault to the west and Kompotades fault to the east are the two major segments of Sperchios Fault System, which control the southern margin of the Sperchios basin and have a total length of almost 80 km. We have distinguished two segments for the Sperchiada fault and four segments for the Kompotades Fault. The strike of those faults is E-W to WNW-ESE, while they dip to the NNE. The main criterion for distinguishing smaller segments is the small change in their orientation. This does not necessarily reflect their actual structural segmentation, but there is definitely a geomorphic segmentation that corresponds to different geomorphic quantification.

• Molos Fault (Fig. 2c) and Kamena Vourla Fault (Fig. 2c)
Molos and Kamena Vourla Faults are dipping to the NNW. Molos is a probable westward extension of the Coastal Fault System which controls the western part of southern coast of the North Gulf of Evia (Ganas, 1997). It is characterised by NW-SE strike and we have segmented it into two parts. Kamena Vourla fault, at the west part of the Coastal Fault System, is a high angle structure with an E-W strike.

• North Fault zone (Fig. 2d)
The last fault zone tested in this paper is the North Fault zone. In contrast with the previously mentioned faults, North Fault zone controls the northern margin of Sperchios basin. It is approximately 10 km long with fault striking NE-SW and dipping to the SE. Four segments are proposed for the North Fault zone.

The morphometric analysis in this paper is based on the application of geomorphic indices derived from a Digital Elevation Model (DEM) of the broader area. The work comprised of collection of published geological maps (IGME 1967, 1970), information based on publications, processing and evaluation of data and finally implementing the principal morphotectonic indicators on the fault segments by using Global Mapper 12 software. The data source was Aster GDEM, Worldwide Elevation Data (1.5 arc-second resolution) and the projection used was Greek Grid (GGRS87).

Two indices have been applied in order to evaluate the Sperchios Basin asymmetry: Transverse Topographic Symmetry, T and Drainage Basin Asymmetry, AF. In order to calculate the T index, the basin midline of Sperchios

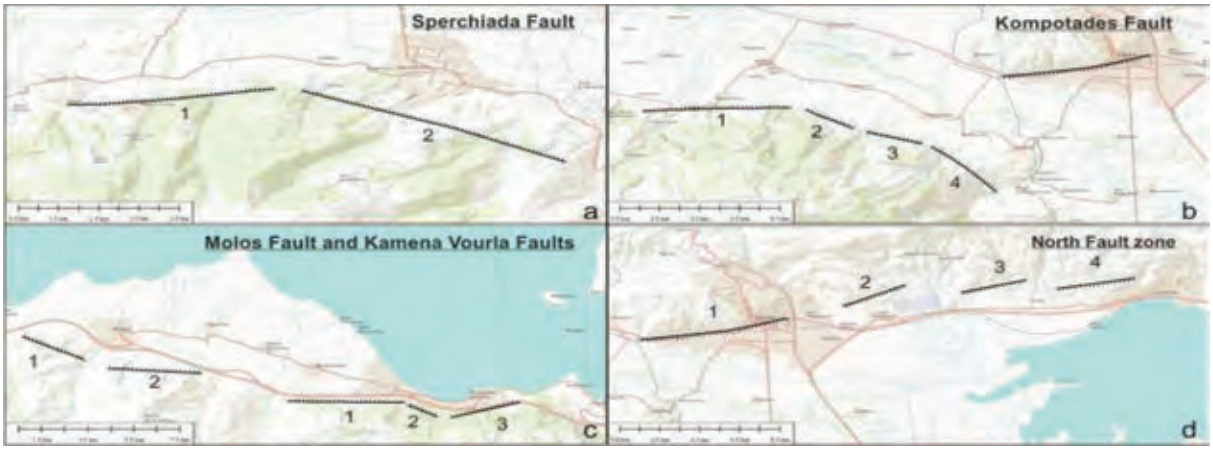

Figure 2: Segmentation of individual faults of the broader Sperchios fault zone.

River was determined in the middle with a red line. Along this midline we have separated 13 equal 4-km long segments (Fig. 3). Based on the results, it is evident that T factor at the first segment as well as between sites p8 and p10, has the highest values, ranging from 0,35 to 0,45, suggesting that the asymmetry at the beginning and in the centre of the basin increases, in comparison to the other segments. The asymmetry factor in Sperchios Basin has a value of 55, showing that the basin has a tectonic rotation (tilting) to the North. One would expect that the basin would show tilt towards the South, where the main fault zone is. However this is not the case for this basin. Our interpretation is that Sperchios fault zone produced a great footwall uplift, causing extensive erosion and hence formation of very big alluvial fans, e.g. the huge Vamvakia alluvial fan at the central part of the basin. These fans have shifted the position of Sperchios River towards the North, overprinting the tectonic signature of Sperchios fault.

The application of S_{mf} and V_f geomorphic indices along the segments of this zone's faults can contribute towards a comprehensive overview of the neotectonic activity. The V_f values are plotted with the S_{mf} values on a same diagram. This combination provides quantitative information of the relative degree of tectonic activity classes of the segmented faults and allows individual mountain fronts to be assigned in different tectonic activity classes (Bull & McFadden, 1977; Keller & Pinter, 1996). The S_{mf} and the mean V_f values of all the segmented faults in our study, are shown in the S_{mf} vs. V_f diagrams (Fig. 4 a, b, c).

According to the active tectonic classification suggested by Keller & Pinter (1996), each fault segment appears to have a different activity, regardless their position or the fact that some of them even belong to the same Fault. The first (A) tectonic class comprises values of S_{mf} lower than 1.5 and V_f values lower than 1.2. The second class consists of S_{mf} lower than 2.5 and V_f lower than 1.5 and the third class is characterized by S_{mf} higher than 2.6.

The two segments of Sperchiada Fault are of tectonic class A and B, for the western and eastern part respectively. In addition, for the Kompotades fault case its eastern part has lower S_{mf} values related to its western part, however all of the segments belong to the A class, which characterizes the more active faults. Moreover, Molos fault, is separated into two different segments which show a different activity, with the western part (Molos_1) less active than the eastern. Three segments have been distinguished for Kamena Vourla fault. All of them reveal an active behaviour with the eastern segment (K. Vourla_3) showing higher activity (class A). Finally, North faults seem to have a lower activity in comparison with the southern marginal large faults.

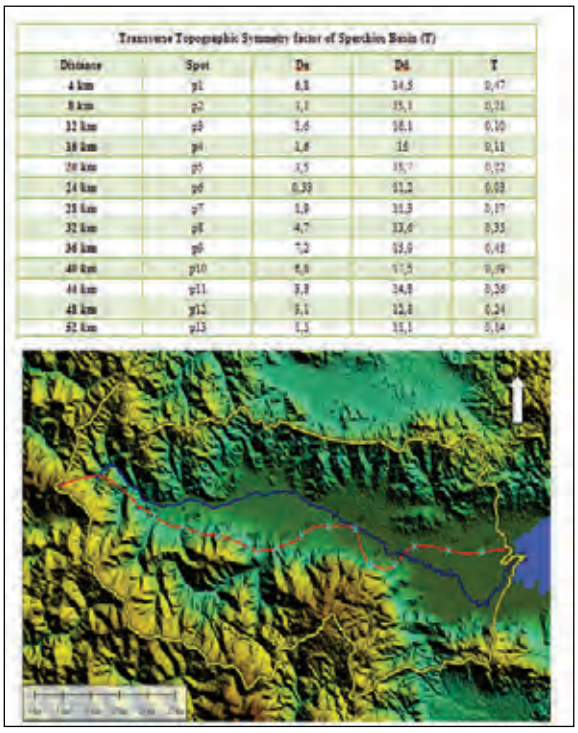

Distance	Spot	Da	Dd	T
4 km	p1	6,8	14,5	0,47
8 km	p2	5,1	15,1	0,34
12 km	p3	2,6	16,1	0,16
16 km	p4	1,8	16	0,11
20 km	p5	3,5	15,7	0,22
24 km	p6	0,38	11,2	0,03
28 km	p7	1,9	10,3	0,17
32 km	p8	4,7	13,6	0,35
36 km	p9	7,2	15,9	0,45
40 km	p10	6,8	17,5	0,39
44 km	p11	3,8	14,9	0,26
48 km	p12	3,1	12,8	0,24
52 km	p13	1,3	11,1	0,12

Figure 3: (a) Transverse Topographic Symmetry (T) results along the whole Sperchios Basin. (b) DEM of the area, showing the 4-km long segments (p1, p2,…, p13) separated by a light blue x symbol, along basin midline, blue line: main river, red line: basin midline, yellow line: Sperchios basin watershed.

Based on the combination of the derived geomorphic indices, Sperchios Basin appears to have a tectonic tilting (high T values in the centre of the basin) to the North (AF=55). After having all the above faults classified based on their S_{mf} and V_F values, we suggest that North Faults appear to be less active (B to C class) in comparison with all the others (A to B class). In addition we observed that even along the same fault the segments seem to have a different tectonic activity.

In respect to segmentation, quantitative morphotectonic analysis can provide valuable information, complementary to structural criteria in order to segment a fault zone. In Sperchios basin the morphotectonic segmentation is in good agreement with the segmentation derived from mapping and structural analysis.

It has to be noted however that quantitative morphotectonic analysis can only provide indications, not evidence of recent tectonic activity. It is therefore important to extend the deformation record of Sperchios fault zone by geological methods (i.e. paleoseismology), in order to enhance the morphotectonic observations.

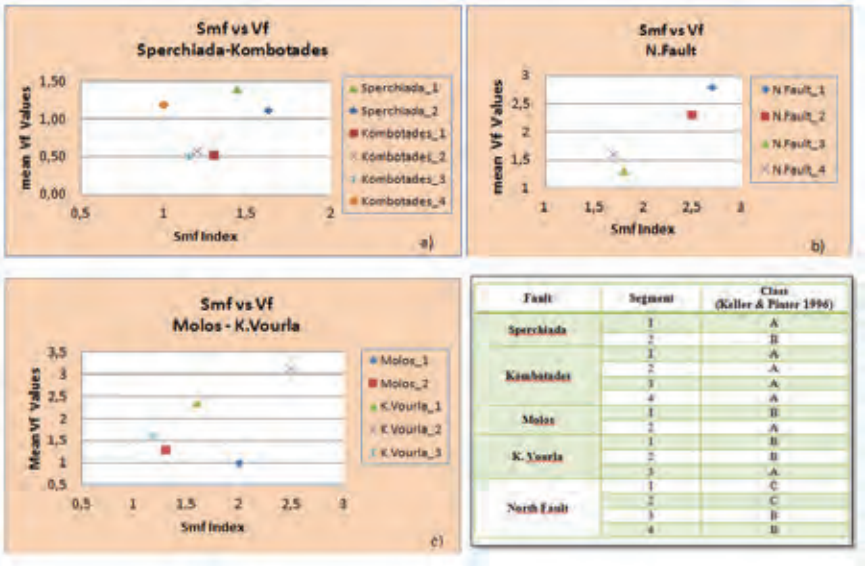

Fault	Segment	Class (Keller & Pinter 1996)
Sperchiada	1	A
	2	B
Kombotades	1	A
	2	A
	3	A
	4	A
Molos	1	B
	2	A
K. Vourla	1	B
	2	B
	3	A
North Fault	1	C
	2	C
	3	B
	4	B

Figure 4: Plot of mean Smf and Vf values of all the segmented faults of this study (a) Sperchiada and Kompotades faults, (b) North faults, (c) Molos and Kamena Vourla faults. Table: Classification of segments of each fault separately, according to the tectonic class division by Keller & Pinter (1996).

Acknowledgements: MM has carried out the current project during her master studies at the Department of Geology, Aristotle University of Thessaloniki, Greece. AC has been partly supported by the project "Characterization of site conditions in Greece for realistic seismic ground motion simulations: pilot application in urban areas", a THALES programme project, funded by the General Secretariat for Research and Technology of Greece.

References

Bull, W., L. McFadden, (1977). Tectonic geomorphology north and south of the Garlock Fault, California, Geomorphology in Arid regions. D.O., Doehring, ed., *Publications in Geomorphology*. State University of New York at Bingamton. p115-138.

Bull, W., (2007). *Tectonic geomorphology of mountains: a new approach to paleoseismology*. Wiley-Blackwell; 1 edition.

Bull, W., (2009). *Tectonically Active Landscapes*. Wiley-Blackwell. 1 edition.

Eliet, P.P., R.L. Gawthorpe, (1995). Drainage development and sediment supply within rifts, examples from the Sperchios Basin, central Greece. *Journal of the Geological Society of London*. 152, Part 5, 883-893.

Ganas, A., (1997). Fault segmentation and seismic hazard assessment in the Gulf of Evia Rift, central Greece. *Unpublished PhD thesis. University of Reading*. 369 pp.

Ganas, A., I. Papoulia, (2000). High-resolution, digital mapping of the seismic hazard within the Gulf of Evia Rift, Central Greece using normal fault segments as line sources. *Nat. Hazards*. 22 (3), 203-223.

Gawthorpe, R.L., M.R. Leeder, (2000). Tectono-sedimentary evolution of active extensional basins. *Basin Research*. 12, 195–218.

IGME, Institute of Geology and Mineral Exploration, (1967). *Geological map of Greece*, scale 1:50,000, Lamia sheet, Athens.

IGME, Institute of Geology and Mineral Exploration, (1970). Geological map of Greece, 1:50,000, Sperchias sheet, Athens.

Keller, A.E., N. Pinter, (1996). *Active Tectonics: Earthquakes, Uplift and Landscape*. Prentice Hall. 338 p.

Kilias, A., M. Tranos, E. Papadimitriou, V. Karakostas, (2008). The recent crustal deformation of the Hellenic orogen in Central Greece; the Kremasta and Sperchios Fault Systems and their relationship with the adjacent large structural features. *Z. dt. Ges. Geowiss*. 159/3, 533-547.

Kranis, H.D., (1999). Neotectonic activity of fault zones in central-eastern mainland Greece (Lokris). *Ph.D. Thesis*.

Psomiadis, E., (2010). Research of geomorphological and environmental changes in the Sperchios River Basin utilizing new technologies. *Ph.D. Thesis*.

Tzanis, E., H. Kranis, & S. Chailas, (2010). An investigation of the active tectonics in central Greece with imaging and decomposition of topographic data. *Journal of Geodynamics*. 49, 55-67.

A large-magnitude, continental, normal-faulting earthquake: the 1739 Yinchuan event in northern China

Middleton, T.A. (1), Walker, R. (1), Parsons, B. (1), Lei, Q. (2), Zhou, Y. (1) and Ren, Z. (3)

(1) COMET+, Department of Earth Sciences, University of Oxford, South Parks Road, Oxford, UK. Email: tim.middleton@earth.ox.ac.uk.
(2) Ningxia Seismological Bureau, Yinchuan, China
(3) Institute of Geology, China Earthquake Administration, Beijing, China

Abstract: *We know of very few continental, normal-faulting earthquakes of magnitude greater than 7.0 from the instrumental period. There are, however, a number of examples from both the historic and prehistoric records. One such earthquake is the supposedly magnitude 8.0 1739 event, which occurred in the Yinchuan Graben in northern China. Here, we use high-resolution, stereo, Pleiades imagery along with field investigations to map, and characterise, this rupture in detail. We confirm that the East Helanshan Fault, on the western side of the graben, was the causative fault and we provide a re-assessment of the magnitude of the earthquake. We suggest that the magnitudes of these large, historic earthquakes, which are typically obtained from isoseismal maps, are commonly overestimates. Nonetheless, our results indicate that an abnormally thick seismogenic layer and a shallow fault dip both contributed to the unusually large size of the 1739 event.*

Key words: *Large-magnitude earthquakes, normal fault, high-resolution DEMs, China.*

INTRODUCTION

Continental, normal-faulting earthquakes greater than magnitude 7.0 are relatively rare. This is in part because they often occur in slowly deforming regions and consequently have long repeat times. Recent examples include: the M7.6 1915 Pleasant Valley (Nevada) event, the M7.9 1957 Muya (Siberia) event, the M7.3 1959 Hebgen Lake (Montana) event, and the M7.0 2006 Mozambique event (Jackson & White, 1989; Copley et al., 2012). However, to find further examples of these large events we have to delve into the historic and prehistoric records. The 1556 Huaxian earthquake, for example, which occurred in Shaanxi Province in central China, is believed to have been greater than magnitude 8.0 and involved a vertical throw of 8 m (Zhou et al., 2014). Similarly, the M7.8 Egiin Davaa event in central Mongolia shows a rupture scarp up to 4.5 m high (Walker et al., in prep). These additional case studies aid our understanding of typical rupture styles and the controls on the maximum magnitude of such events.

Here, we examine in detail another Chinese example: the Yinchuan earthquake. This event occurred in the Yinchuan Graben on the western margin of the Ordos Plateau in northern China on the 3rd January 1739. Ground shaking in the centre of the graben, particularly around the major cities of Yinchuan and Pingluo, reached intensity X on the *new Chinese intensity scale* and lasted for up to two hours after the earthquake (see Figure 1). In the zone of greatest shaking temples, pagodas, offices, houses and city walls all collapsed and more than 50,000 people are thought to have been killed. Ground cracking and surface fissures up to 100 m long are also described in historical records from the time. Here, we aim to map and characterise the rupture in detail by means of remote sensing data and field investigations.

The Yinchuan Graben is bounded by clear north-south trending normal faults: on the western side of the graben lies the East Helanshan Fault, whilst the eastern side is bordered by the Huang He (Yellow River) Fault (Zhang et al., 1986). Further, parallel, normal faults exist within the basin itself including the Luhuatai and Yinchuan-Pingluo Faults (Zhang et al., 1986). These faults remain largely buried beneath Quaternary sediments but are inferred from seismic reflection profiles across the graben (Fang et al., 2009). Given the number of faults in the Yinchuan Graben, the causative fault for the 1739 Yinchuan earthquake has been the subject of much debate in the literature. Some authors attribute it to the Yellow River Fault (Li & Wan, 1984). Others believe that the Yinchuan-Pingluo Fault was responsible because it runs NNE-SSW directly under the city of Yinchuan and coincides with the zone of maximum shaking from the historical records (Chai et al., 2006; Lin et al., 2013).

In 1965 a series of fresh earthquake scarps were discovered along the East Helanshan Fault on the western side of the Yinchuan Graben by the Northwest Seismic Expedition of the Chinese Academy of Science (Liao and Pan, 1982). These scarps were then the focus of a collaborative US-China study in June 1984 (Zhang et al., 1986). Deng and Liao (1996) subsequently identified four locations along the range-front of the Helanshan where scarps could be seen. From north to south these locations are: Hongguozigou, Jianquan, Xiashigou, and Suyukou (see Figure 2). In total, 88 km of discontinuous surface ruptures have been discovered.

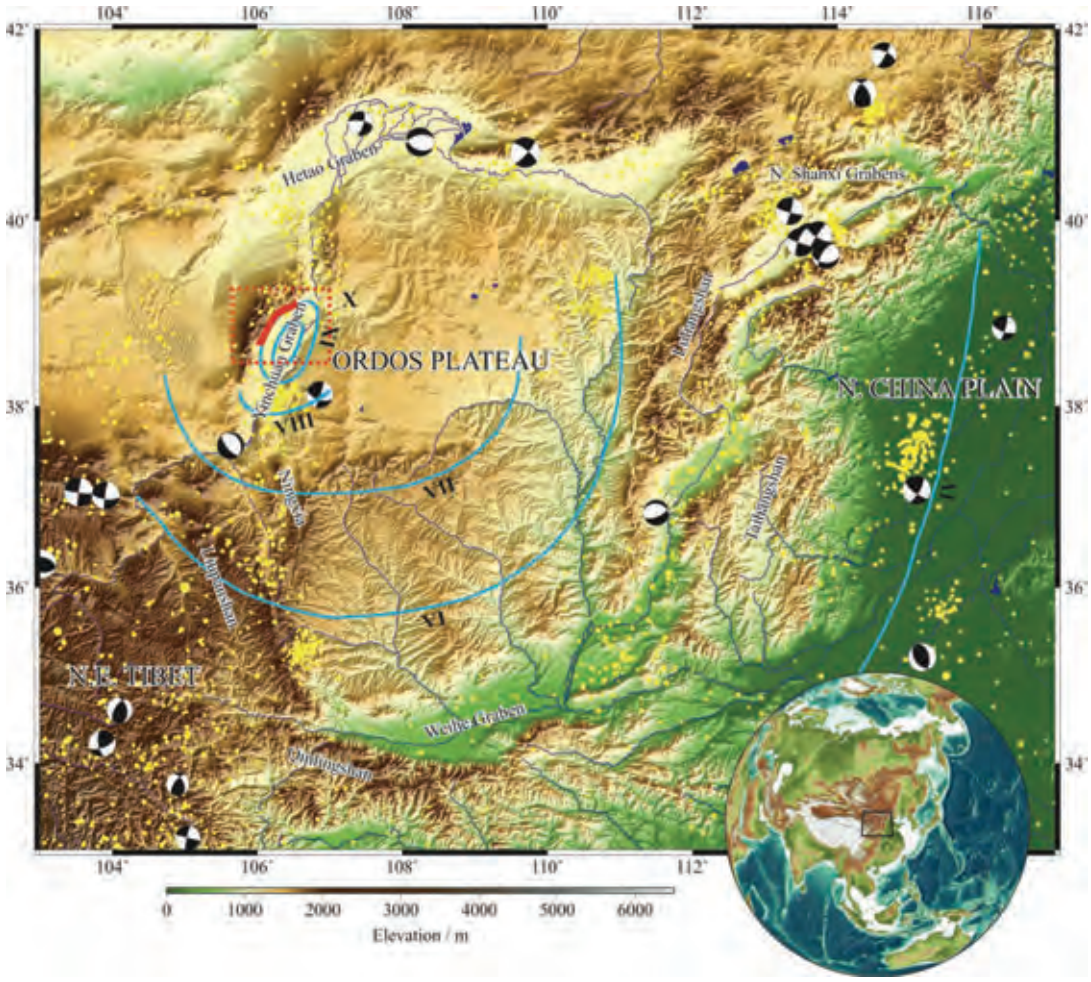

Figure 1: SRTM topography of the Ordos Plateau in north-eastern China. Earthquakes >M5 from Global CMT catalogue (beach balls) and >M2 from ISC catalogue (yellow dots). Red line shows scarps along East Helanshan Fault and red box shows location of Figure 2. Blue lines are isoseismals for 1739 event according to the new Chinese intensity scale (Institute of Geophysics, 1990).

At Hongguozigou (see Figure 2 for location) three parallel fault strands intersect part of the Great Wall of China, which dates from 1531 during the Ming Dynasty (Ding, 1981) Zhang et al. (1986) record total offsets at the Great Wall site of 2.7 m vertically and 3 m right-laterally. However, the offset on the north-westernmost fault strand is hard to determine because the wall here was rebuilt in the 1980s including an offset in the new stonework. The only reliable evidence for an offset on this strand is from a photograph in 1973. However, recent work by Lin et al. (2013) argues that the Great Wall at Hongguozigou was built on pre-existing fault scarps and that the apparent offsets are unrelated to the 1739 earthquake. However, the fact that the wall is broken precisely at the scarp suggests that at least some motion occurred here in 1739.

The Suyukou scarps total around 16.5 km in length and lie 3 to 4 km southeast of the East Helanshan Fault where they cut through four, large, coalesced, alluvial fans (Deng and Liao, 1996). These scarps were produced primarily by normal-faulting earthquakes, though Zhang et al. (1986) claim that some evidence of right-lateral motion can be seen. In this study we did not find any convincing evidence of lateral offsets at Suyukou. The scarps vary in height up to a maximum of approximately 11 m, suggesting that they are compound scarps recording a history of multiple earthquakes. It is the lowest of these scarps (the T1 terrace) that is of primary interest here.

DISCUSSION

In this study we have acquired high-resolution stereo imagery from the Pleiades satellites. This has allowed us to construct a nominally 1 m resolution digital elevation model (DEM) for the entire length of the scarps along the east Helanshan and, in combination with the imagery, to produce geomorphological maps of the range-front and alluvial fans.

At one location, at the southernmost end of the map in Figure 2, a newly-built road provides a cross-section of the T1 scarp at Suyukou (see Figure 3). The exceptional preservation of a free face on this scarp - and soil development up against the scarp - suggest that it was

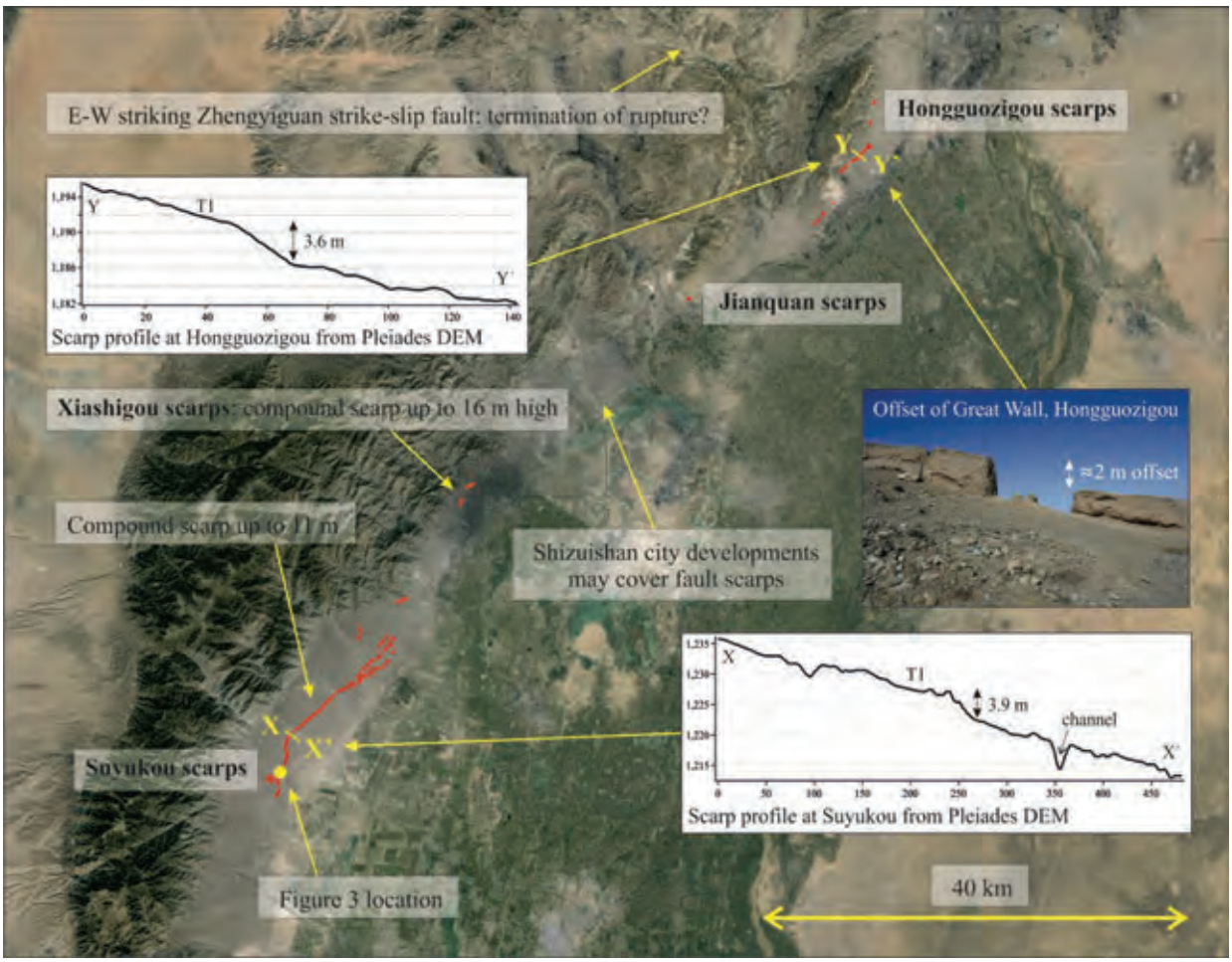

Figure 2: Google Earth image of the Yinchuan Graben. Scarps mapped from the Pleiades-derived DEM are shown in red. Insets show topographic profiles across the scarp at two locations and a field photograph of the Great Wall at Hongguozigou.

produced recently. Further field investigations of the scarps along the rest of the East Helanshan Fault confirm that this free face is ubiquitously present. The free face, along with the following other lines of evidence, lead us to conclude that the East Helanshan Fault was the causative fault for the 1739 event:

1) The elongate isoseismals (shown in Figure 1) are parallel to the East Helanshan Fault (as well as the Yinchuan-Pingluo Fault). Furthermore, the East Helanshan Fault dips shallowly to the southeast. Therefore an earthquake on this fault would be expected to have its hypocentre, and therefore maximum shaking, towards the centre of the graben.
2) The Yinchuan Graben is filled with up to 9 km of sediments (Fang et al., 2009). This sediment is likely to amplify seismic waves during an earthquake, leading to greatest ground motion in the centre of the basin, as shown in the isoseismal map.
3) The isoseismal map is most likely to reflect population density, with greatest shaking recorded in the major cities of Yinchuan and Pingluo, rather than being indicative of the location of the causative fault.
4) Two composite drilling profiles in Yinchuan city, combined with radiocarbon and OSL age constraints, indicate that the last motion on the Yinchuan-Pingluo Fault was between 7.6 and 10.7 ka ago (Lei et al., 2008).
5) Similarly, OSL ages from a trench on the southern portion of the Yellow River Fault indicate that the most recent event was 17.8 to 29.4 ka ago (Wang et al., 2011).

Previous studies on the 1739 Yinchuan earthquake list it as a magnitude 8.0 event (e.g. Deng & Liao, 1996). If this were true, it would be one of the biggest continental, normal-faulting events ever - and it would certainly be larger than anything we have recorded in the instrumental period. From the seismic reflection profile published by Fang et al. (2009) we note that the dip of the East Helanshan Fault (at depth) is roughly 36° and that it extends, at absolute most, to a depth of 28 km. This seismogenic thickness would give a maximum down-dip width of 48 km. Combined with a total rupture length of 88 km and a maximum average slip estimate of

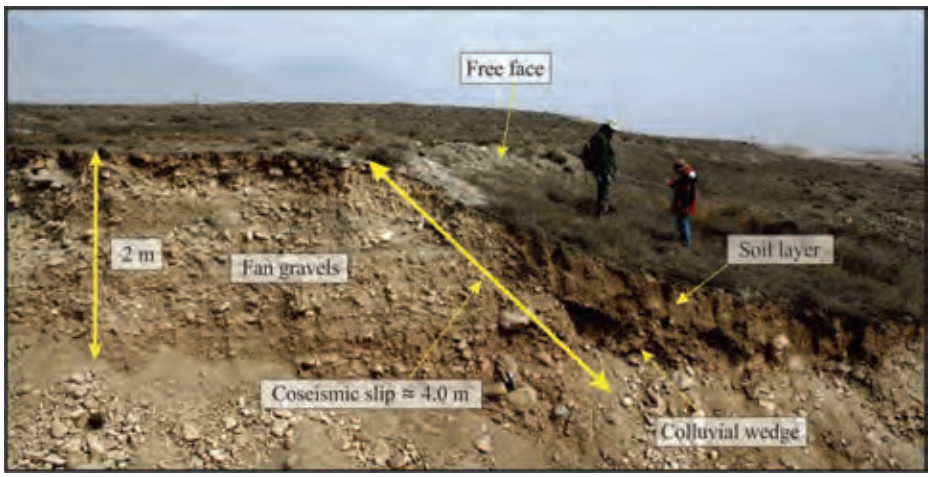

Figure 3: Annotated field photograph showing a cross-section through T1 at the southern end of the Suyukou scarps.

4 m. simple scaling laws suggest that the maximum possible magnitude for the 1739 event is M 7.8. A more conservative down-dip width of 36 km and average slip of 2.5 m yield a magnitude of 7.6. Nonetheless, the unusually large seismogenic thickness and shallow fault dip (for a normal fault) both contribute to the 1739 event being larger than would otherwise be expected. The previously cited value of M8.0, which derives from the isoseismal map, is likely to be an overestimate because it does not take account of wave amplification in the basin sediments. Furthermore, the thickness of sediments in the graben is notably large (up to 9 km), which will have also contributed to the high-magnitude shaking.

It is evident from this study that seismogenic thickness and fault dip are two key parameters that control the maximum size of a normal-faulting earthquake - but it is only in locations with thick seismogenic layers and shallow-dipping normal faults that these large events are possible. An interesting question, therefore, is: how many of our other historic and prehistoric examples overestimate the earthquake magnitude?

Acknowledgements: We are grateful to COMET, LiCS, Earthquakes without Frontiers and the Natural Environment Research Council (UK) for funding and to colleagues at the China Earthquake Administration for making this work possible.

References

Chai, C., G. Meng, P. Du, Y. Wang, B. Liu, W. Shen, X. Xie, (2006). Comprehensive multi-level exploration of buried active fault: an example of Yinchuan buried active fault. *Seismology and Geology*. *28* (4), 536-546 (in Chinese).

Copley, A., J. Hollingsworth, & E. Bergman, (2012). Constraints on fault and lithosphere rheology from the coseismic slip and postseismic afterslip of the 2006 M w 7.0 Mozambique earthquake. *Journal of Geophysical Research*. *117* (B3), B03404. doi:10.1029/2011JB008580.

Deng, Q., & Y. Liao, (1996). Paleoseismology along the range-front fault of Helan Mountains, north central China. *Journal of Geophysical Research*. *101*, 5873-5893.

Ding, M., (1981). Some paleoseismic evidence in the north China region. *Seismology and Geology*. *3*(1), 67-74 (in Chinese).

Fang, S.M., C.B. Zhao, C.Z., Chai, B.J. Liu, S.Y. Feng, Liu, M.J., H. Liu, (2009). Seismological Evidences of the Crustal Structures and Tectonics in the Yinchuan Downfaulted Basin. *Chinese Journal of Geophysics*. *52* (5), 1101–1110. doi:10.1002/cjg2.1435.

Institute of Geophysics, S. S. B. & Institute of Chinese Historical Geography, F. U. (1990). *Atlas of the historical earthquakes in China (the Qing Dynasty period).* China Cartographic Publishing House (in Chinese). p. 244.

Jackson, J.A. & N.J. White, (1989). Normal faulting in the upper continental crust: observations from regions of active extension. *Journal of Structural Geology*. *11*(1/2), 15-36.

Lei, Q., C. Chai, G. Meng, P. Du, Y. Wang, X. Xie, & X. Zhang, (2008). Composite drilling section exploration of Yinchuan Buried Fault. *Seismology and Geology*. *30* (1), 250-263 (in Chinese).

Li, M., & Z. Wan, (1984). Characteristics of the earthquake-generating structures for magnitude 8.0 Pingluo earthquake of 1739 and the process of its preparation. *Seismology and Geology*. *6* (3), 23-28 (in Chinese).

Lin, A., G. Rao, J. Hu & W. Gong, (2013). Reevaluation of the offset of the Great Wall associated with the ca. M 8.0 Pingluo earthquake of 1739, Yinchuan graben, China. *Journal of Seismology*. *17* (4), 1281-1294. doi:10.1007/s10950-013-9391-2.

Walker, R.T., K.W. Wegmann, A. Bayasgalan, R.J. Carson, J. Elliott, M. Fox, R.A. Sloan. The Egiin Davaa rupture, central Mongolia: a large-magnitude prehistoric normal faulting earthquake from a slowly-deforming continental interior. *In preparation*.

Wang, X., C. Chai, P. Du, Q. Lei, G. Yin & Y. Lu, (2011). Luminescence age constraints on palaeo-earthquake events along the Lingwu fault in the Yinchuan Basin, China. *Geochronometria*. *39* (1), 57-61. doi:10.2478/s13386-011-0051-4.

Zhang, B., Y. Liao, S. Guo, R.E. Wallace, R.C. Bucknam & T.C. Hanks, (1986). Fault scarps related to the 1739 earthquake and seismicity of the Yinchuan Graben, Ningxia Huizu Zizhiqu, China. *Bulletin of the Seismological Society of America*. *76* (5), 1253-1287.

Zhang, W., Y. Liao & Z. Pan, (1982). On the piedmont scarp in diluvial fan of Mt. Helanshan. *Seismology and Geology*. *4* (2), 32-34 (in Chinese).

Zhou, Y., J. Ma, R. Walker, X. Feng, X. Song & B. Parsons, (2014). *Are we missing earthquakes? A new insight into the M 8 1556 Huaxian earthquake.* Abstract from the American Geophysical Union Fall Meeting 2014.

6th International INQUA Meeting on Paleoseismology, Active Tectonics and Archaeoseismology,
19-24 April 2015, Pescina, Fucino Basin, Italy

INQUA Focus Group on Paleoseismology and Active Tectonics

The history of faulting in the Yinchuan Graben, northern China

Middleton, T.A. (1), Walker, R. (1), Parsons, B. (1), Lei, Q. (2), Zhou, Y. (1), Ren, Z. (3) and Rood, D.H. (4)

(1) COMET+, Department of Earth Sciences, University of Oxford, South Parks Road, Oxford, UK. Email: tim.middleton@earth.ox.ac.uk
(2) Ningxia Seismological Bureau, Yinchuan, China
(3) Institute of Geology, China Earthquake Administration, Beijing, China
(4) AMS Laboratory, SUERC, Rankine Avenue, East Kilbride, Scotland, UK. Now at: Imperial College, London, UK

Abstract: *The Yinchuan Graben lies on the western margin of the Ordos Plateau, bounded to the west by the Helan Mountains and to the east by the Yellow River (which flows around three sides of the Ordos). There are four, major, sub-parallel, normal faults in the graben, namely (from west to east): the East Helanshan Fault, the Luhuatai Fault, the Yinchuan-Pingluo Fault, and the Huang He (Yellow River) Fault. The southern end of the East Helanshan Fault crosses a series of alluvial fans some 3 km from the Helanshan range-front. In this study we use ^{10}Be exposure dating to show that the range-front here has been inactive for at least 8 ka and that, over the last few hundred thousand years, motion has been transferred from the range-front to the fault in the fans. During this time, the vertical throw rate on the East Helanshan Fault has remained approximately constant at 0.2-0.3 mm/a.*

Key words: *Normal faulting, Yinchuan Graben, ^{10}Be exposure dating, Ningxia Province, China.*

INTRODUCTION

The Yinchuan Graben is approximately 50 km wide and 160 km long and lies at the northern end of Ningxia Province on the western side of the Ordos Plateau. The tectonics of this part of China is complex: Ningxia straddles the transition from compression in the north-eastern corner of the Tibetan Plateau to extension occurring in the graben systems around the Ordos Plateau.

In the Yinchuan Graben, though, clear north-south trending normal faults are indicative of east-west crustal extension (see Figure 1). The East Helanshan Fault borders the western side of the graben, whilst the Huang He (Yellow River) Fault forms the eastern boundary (Zhang et al., 1986). The sub-parallel, Luhuatai and Yinchuan-Pingluo faults both lie within the graben. They have no surface expression, but their presence is deduced from seismic reflection profiles across the basin (Liu et al., 2008; Fang et al., 2009). Figure 2 shows a sketch cross-section across the graben along the line A-A' in Figure 1 after Lei et al. (in press).

Fang et al. (2009) propose that the Yellow River Fault is the dominant structure within the basin. However, their seismic reflection profile shows westward tilting of sediments within the graben. Along with the presence of the Helan Mountains on the western side of the basin, this asymmetry would suggest that it is actually the East Helanshan Fault that is dominant. This being the case, it remains puzzling as to why the Yellow River is on the eastern side of the graben. One possibility is that the high sediment load of the Yellow River leads to such extensive deposition that it flattens out any tilting in the basin, allowing the river to freely meander across the entire width of the graben.

To the south the Sanguankou and Niushoushan Faults strike northwest-southeast, and form the south-western boundary of the graben (Zhang et al., 1986). To the north, the east-west Zhengyiguan Fault cuts basement rocks in the Helanshan and provides a structural termination at this end of the graben (Zhang et al., 1986). The Yinchuan Graben is thought to have extended at 2.9±1 mm/a since the Pliocene (Zhang et al., 1998) and contains up to 9 km of sediments that have accumulated since the late Eocene (Fang et al., 2009; Zhang et al., 1990). Zhang et al. (1990) also estimate an uplift rate of 0.5 to 0.8 mm/a on the East Helanshan Fault based on the thickness of the Quaternary sediments in the basin. The record of historical earthquakes in the graben includes the supposedly M8.0 1739 Yinchuan event and a number of smaller events (Lee et al., 1976, 1978; Liu et al., 2011). In particular, magnitude 6.5 events occurred in 1143 and 1477.

Our purpose here is to investigate the history of faulting on the East Helanshan Fault (see Figure 1). When were the previous earthquakes? When was the range-front at the southern end of the fault last active? And what is the long-term slip rate on the fault? This will then contribute to our understanding of the development of the graben.

A series of fresh scarps were discovered along the East Helanshan Fault in 1965. The southernmost of these scarps, called the Suyukou scarps, are preserved in a series of alluvial fans some 3 km from the range-front. Here, the scarps vary in height up to a maximum of approximately 11 m, suggesting that they are compound scarps recording a history of multiple earthquakes. Deng and Liao (1996) identified four separate terrace levels in the scarp footwalls, T1 to T4, which they correlate with four previous earthquakes (see Figure 3). They also note that the oldest terraces, T3 and T4, have undergone footwall rotation such that they now dip away from the fault, whilst the younger terraces, T1 and T2, follow the regional dip of the fan surfaces and dip towards the fault.

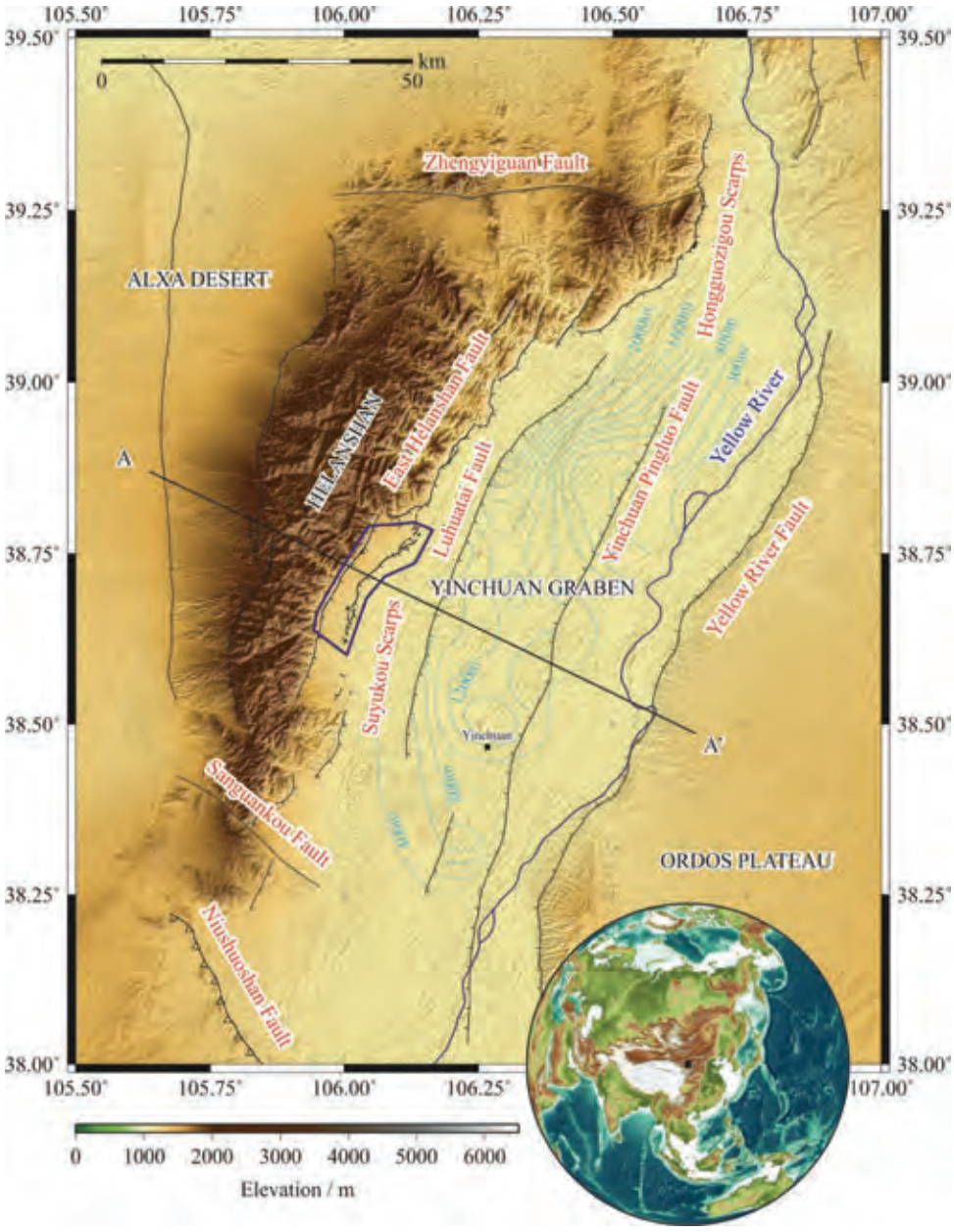

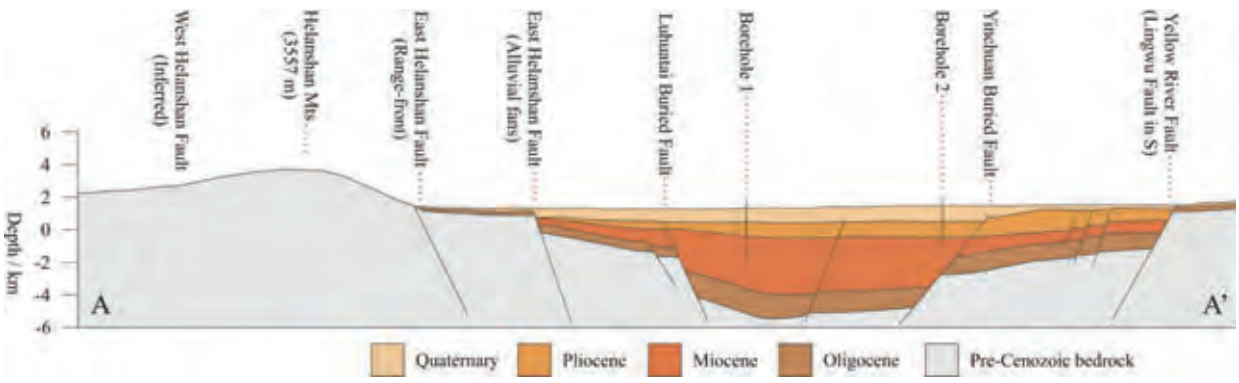

Figure 1 (top): ASTER GDEM topography of the Yinchuan Graben. Faults mapped from satellite imagery and earlier fault maps by Tapponnier and Molnar (1977), Zhang et al. (1986), and Deng and Liao (1996). Quaternary sediment isopachs from Lei et al. (2011). The location of Figure 3 is shown by the dark blue outline.
Figure 2 (bottom): Sketch cross-section along the line A-A' in Figure 1 after Lei et al. (in press).

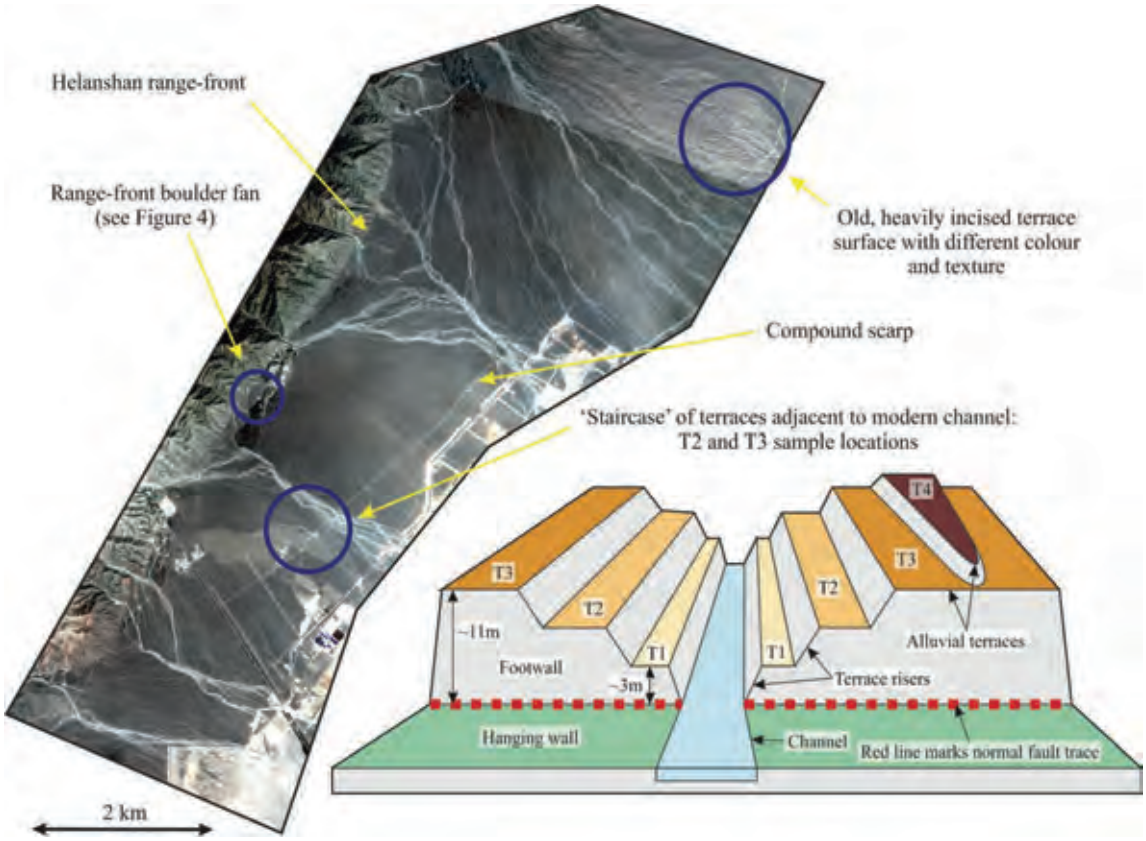

Figure 3: Pleiades satellite imagery of the Suyukou scarps. ^{10}Be sampling locations mentioned in the text are highlighted by blue circles. Inset figure is block diagram showing preservation of aggradational terraces T1 to T4 after Deng and Liao (1996).

Previous work indicates potential earthquakes on the East Helanshan Fault immediately prior to 2630±90 years, 6330±80 years, and 8420±170 years on the basis of radiocarbon ages of colluvial wedges in a palaeoseismic trench (Deng & Liao, 1996). A second trench yielded earthquakes prior to 2720±60 years and 4760±80 years (Deng & Liao, 1996).

DISCUSSION

A new geomorphological map has been made for the area shown in Figure 3 that indicates the location and extent of the terraces T1 to T4 in the footwall of the Suyukou scarps. The inset block diagram in Figure 3 after Deng and Liao (1996) illustrates the expected preservation of aggradational terraces either side of an active channel over multiple earthquake cycles. An example of this 'staircase' pattern is observed at the location marked on the imagery.

In order to determine when the range-front was last active we took ^{10}Be samples from a boulder fan that straddles the range-front (see Figure 3 for location and Figure 4 for a field photograph). Results from a set of 6 boulder tops indicate that the inheritance varies significantly but that a minimum abandonment age for the fan is around 8 ka, suggesting that there have been no earthquakes on the range-front since this time. Further ^{10}Be samples from a high terrace at the range-front yield a vertical throw rate of around 0.2 mm/a. However, this terrace does not correlate with any of those shown in Figure 3.

At the northern end of the Suyukou scarps there is a noticeably older, heavily incised, alluvial terrace surface that pre-dates at least T3 and probably T4 (see Figure 3). An amalgamated sample of quartz pebbles for ^{10}Be dating was collected and the resulting age for this surface was in agreement with ages obtained from individual clasts. These ages give a vertical throw rate of less than 0.1 mm/a.

^{10}Be samples were also taken from the T2 and T3 terrace surfaces (see Figure 3). Aggregate samples of quartz pebbles from these surfaces yielded plausible ages. In particular, the T2 age fits well with the Deng and Liao (1996) trench ages. However, individual clasts from these fan surfaces showed significant variability in their Inherited components (up to around 60 ka), suggesting that these results are not sufficiently reliable to determine the precise timing of previous earthquakes.

Figure 4: Annotated field photograph of the boulder fan that post-dates the most recent event at the range-front.

Nonetheless, interesting conclusions can be drawn. The vertical throw rate based on the age of the T3 scarp is about 0.3 mm/a, and this is judged to be a minimum rate. This is noticeably larger than the vertical throw rate obtained for the old terrace, which is just along strike to the north. Any earthquakes uplifting the T3 scarp must also have uplifted the old terrace. This suggests that most of the uplift of this old terrace occurred comparatively recently and implies an increase in the vertical uplift rate at this location over time. Meanwhile, no movement has taken place at the range-front for at least the last 8 ka. The implication is that motion is being transferred from the range-front fault to the Suyukou scarps in the alluvial fans. Furthermore, the vertical throw rate has so far not changed significantly during this transition, remaining at around 0.2 to 0.3 mm/a. We suggest that the overall rate of movement on the East Helanshan Fault has not changed but that motion is being transferred in order to cut off a corner in the range-front and straighten the fault (see Figure 1).

Acknowledgements: We are grateful to COMET, LiCS, Earthquakes without Frontiers and the Natural Environment Research Council (UK) for funding and to colleagues at the China Earthquake Administration for making this work possible.

References

Deng, Q. & Y. Liao, (1996). Paleoseismology along the range-front fault of Helan Mountains, north central China. *Journal of Geophysical Research*. *101*, 5873-5893.

Deng, Q., Y. Wang, Y. Liao, W. Zhang & M. Li, (1984). Colluvial wedges and Holocene activity along the range-front fault of Helan Shan. *Chinese Science Bulletin*. 557-560.

Fang, S.M., C.B. Zhao, C.Z. Chai, B.J. Liu, S.Y. Feng, M.J. Liu, H. Liu, (2009). Seismological Evidences of the Crustal Structures and Tectonics in the Yinchuan Downfaulted Basin. *Chinese Journal of Geophysics*. *52* (5), 1101-1110. doi:10.1002/cjg2.1435.

Lee, W.H.K., F.T. Wu & C. Jacobsen, (1976). A catalog of historical earthquakes in China compiled from recent Chinese publications. *Bulletin of the Seismological Society of America*. 66 (6), 2003-2016.

Lee, W.H.K., F.T. Wu & S.C. Wang, (1978). A catalog of instrumentally determined earthquakes in China (magnitude greater than 6) compiled from various sources. *Bulletin of the Seismological Society of America*. *68* (2), 383-398.

Lei, Q., C. Chai, P. Du, Y. Wang & G. Meng, (2011). Activity characteristics of Luhuatai Buried Fault since Late Quaternary revealed by drilling. *Seismology and Geology*. *33* (3), 602-614 (in Chinese).

Lei, Q., C. Chai, P. Du, J. Yu, X. Xie & Y. Wang. Re-discussion of the seismogenic structure of the M8.0 Pingluo earthquake in 1739. *Seismology and Geology*. (in press).

Liu, B., C. Chai, S. Feng, C. Zhao & H. Yuan, (2008). Seismic exploration method for buried fault and its up-breakpoint in Quaternary sediment area - an example of Yinchuan buried active fault. *Chinese Journal of Geophysics*. 51 (5), 1475-1483 (in Chinese).

Liu, M., S. Stein & H. Wang, (2011). 2000 years of migrating earthquakes in North China: How earthquakes in midcontinents differ from those at plate boundaries. *Lithosphere*. 3 (2), 128–132. doi:10.1130/L129.1.

Tapponnier, P. & P. Molnar, (1977). Active faulting and tectonics in China. *Journal of Geophysical Research*. 82 (20), 2905-2930.

Zhang, B., Y. Liao, S. Guo, R.E. Wallace, R.C. Bucknam & T.C. Hanks, (1986). Fault scarps related to the 1739 earthquake and seismicity of the Yinchuan Graben, Ningxia Huizu Zizhiqu, China. *Bulletin of the Seismological Society of America*. 76 (5), 1253-1287.

Zhang, P., B.C. Burchfiel, P. Molnar, W. Zhang, D. Jiao, Q. Deng, F. Song, (1990). Late Cenozoic tectonic evolution of the Ningxia-Hui Autonomous Region, China. *Geological Society of America Bulletin*. 102 (11), 1484-1498. doi:10.1130/0016-7606(1990)102<1484.

Zhang, Y., J.L. Mercier & P. Vergely, (1998). Extension in the graben systems around the Ordos (China), and its contribution to the extrusion tectonics of south China with respect to Gobi-Mongolia. *Tectonophysics*. 285, 41-75.

INQUA Focus Group on Paleoseismology and Active Tectonics

Earthquake Archaeological Effects (EAEs) from the archaeological site of Ancient Corinth, Greece and their correlation to seismic events

Minos-Minopoulos, D. (1,2), Pavlopoulos, K. (1,3), Lekkas, E. (4), Dominey-Howes, D. (5)

(1) Harokopio University, Department of Geography, 70 El. Venizelou Str., Kallithea, 176 71, Athens, Greece. Email: dminou@hua.gr
(2) Ministry of Culture and Sports, Ephorate of Paleoanthropology & Speleology, Arditou 34B, 116 36, Athens, Greece
(3) Paris Sorbonne University Abu Dhabi, P.O. 38044 Abu Dhabi, UAE
(4) National and Kapodistrian University of Athens, Faculty of Geology and Geoenvironment, Department of Dynamic, Tectonic and Applied Geology, Panepistimioupolis Zografou, 157 84, Athens, Greece
(5) The University of Sydney, Asia – Pacific Natural Hazards Research Group, School of Geosciences, Sydney NSW 2050, Australia

Abstract: *The archaeological site of Ancient Corinth preserves potential Earthquake Archaeological Effects (EAEs) that according to their classification in relation to intensity intervals are indicative of minimum EMS-98 intensities that range from VII to IX. Historical and instrumental seismicity records, historical archives of drawings and photographs and damage records from the earthquakes of 1858 and 1928 were investigated in an attempt to correlate recorded potential EAEs and relative minimum intensities with seismic events. The study gave the opportunity to verify the applicability of the EAEs classification in relation to the proposed intensity intervals for the earthquake of 1858, to suggest candidate EAEs for rock-hewn monuments and to suggest that the site suffered repeatedly from earthquakes of EMS-98 intensities of VII to VIII and potentially from more than one seismic events of minimum EMS -98 intensity of IX.*

Key words: *Temple of Apollo, Glauke Fountain, rock-hewn monuments, macroseismic intensity.*

INTRODUCTION

The archaeological site of Ancient Corinth is located on an uplifted Pleistocene marine terrace at 75 m altitude on the northern foothills of the Acrocorinth hill, a region characterised by active tectonics and intense seismicity (Fig. 1). Archaeological studies suggest that the site was first inhabited during the Neolithic period (6000 B.C.), its use continued during the Bronze Age and advanced in the late 8th cent. B.C. with intense landscape modification and monumental architecture serving religious, civic and market activities (Fig. 2). Ancient Corinth was razed in 146 B.C. by the Romans and was re-founded as a Roman colony that flourished till the end of 3rd c. A.D., (Crouch 2003).

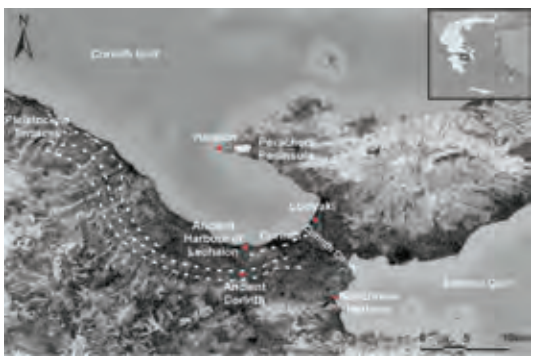

Figure 1: Location map of the study area and surrounding archaeological sites.

The proposed archaeoseismological classification of Earthquake Archaeological Effects (EAEs) and their relation to intensity intervals of EMS-98 macroseismic scale (Rodríguez-Pascua et al., 2011, 2013) was applied on the site of Ancient Corinth in order to investigate potential damage from ground deformation and transient shaking, correlate proposed minimum intensity values with existing seismic records and identify potential seismic events and their effects on the site.

Figure 2: The archaeological site of Ancient Corinth. Monuments studied marked with red line.

METHODS

Each monument of the archaeological site was examined for its geological substratum, typology, state of preservation and potential EAEs. Monuments in a total collapsed state preserving either questionable or even no effects, were not included in the study. The potential EAEs identified on each monument were recorded following a qualitative approach, i.e. each monument

was investigated for the types of effects and not for the number of each effect preserved. The EAEs records were correlated with potential EMS-98 intensity scale values as suggested by Rodríguez-Pascua et al., 2013, and minimum macroseismic intensities were constrained. The results were compared with historical and instrumental seismicity of the region and available regional historical archives and records.

RESULTS

The potential EAEs from the archaeological site of Ancient Corinth were mainly recorded on the monuments of the Peirene Fountain(6th c. B.C.), the Temple of Apollo (550 B.C.), the NW shops, the W shops, the Odeion (1st c. A.D.) and the Theatre (Roman period). Variable building fabric effects were identified summarised to penetrative fractures, rotated and displaced masonry blocks, dropped key stones, folded steps and kerbs, collapsed vaults and dipping broken corners (Fig. 3). The South Stoa, the North Agora and the Bema are mainly characterised by effects of dipping broken corners and penetrative fractures.

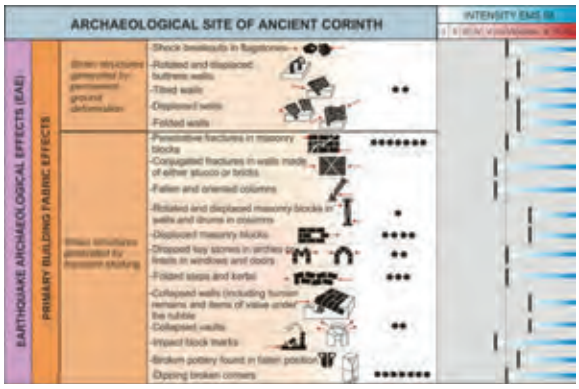

Figure 3: Potential EAEs distribution (black dots) as recorded on monuments of the archaeological site of Ancient Corinth (modified after Rodríguez-Pascua et al., 2013).

The majority of the effects recorded on the monuments of the site relate to EMS-98 minimum intensities of VII (Fig. 3). Three effects summarised to rotated and displaced masonry blocks in walls (Temple of Apollo, NW Shops, Peirene Fountain, Theatre) a displaced column (Temple of Apollo) and collapsed vaults (W shops, Odeion) relate to EMS-98 intensity of IX. Therefore, it can be suggested that the site of Ancient Corinth suffered considerable damage from earthquakes of minimum EMS-98 intensities ranging from VII to IX.

Two rock-hewn monuments of the site preserve extensive fracturing. The Glauke Fountain (Roman period), a rock-hewn monolithic monument carved on sandstone, preserves a set of V-shaped corner cracks in the upper parts of the construction (Fig 4). Peirene Fountain that is partly rock-hewn on the contact between conglomerate and marl deposits preserves extensive crashing and spalling in one of its rock-hewn underground reservoir walls (Fig. 5). Although these effects require geotechnical investigations in order to assess their origin and strain-field and examine potential non-seismic nature, they could be suggested as candidate Earthquake Archaeological Effects for rock-hewn monuments.

Figure 4: The Glauke Fountain with partial collapse that preserves V-shaped corner cracks at its SSE façade.

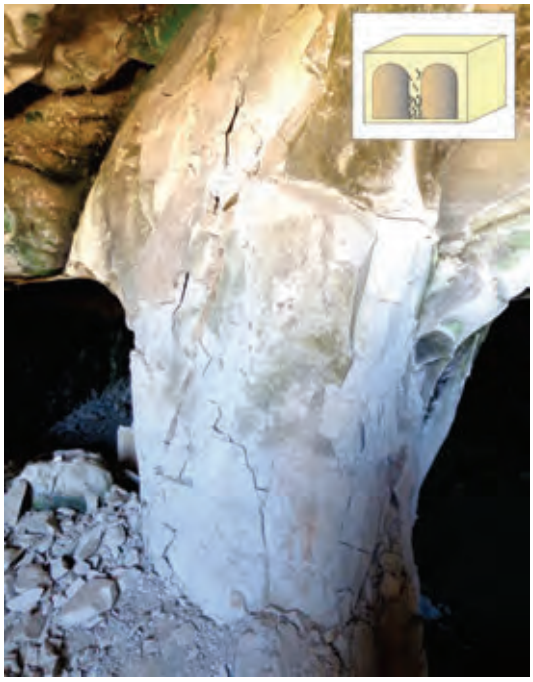

Figure 5: The NE tunnels of Peirene Fountain that preserve crashing/spalling effects on their rock-hewned tunnel wall.

Regional earthquakes with intensities that have caused extensive damage in the vicinity of Ancient Corinth according to the earthquake catalogue by Papazachos & Papazachou (1989) were examined and a number of events were identified. However, damage records for the archaeological site under investigation come mainly from two events, the earthquakes of 1858 and 1928.

The 1858 Earthquake

The 1858 earthquake represents a milestone event of the regional history since it destroyed the city of Old Corinth,

caused its abandonment and the foundation of the modern city of Corinth next to the Corinth canal. The disaster is described in detail by G. Koustas, the prefectural doctor of Corinth in his report published by Pandora journal on the 15th of August 1958. His report provides valuable information on damage distribution, fatalities, injuries and regional environmental effects, allowing a reliable assessment of the macroseismic intensity (MMI X), the magnitude (M=6.7) and epicentre (a few km to the east of Ancient Corinth), (Papazachos & Papazachou, 1989).

For the archaeological site of Ancient Corinth, Koustas (1958), reports that the temple of Apollo suffered extensive damage. One column that was lacking the capital was fractured and displaced. The corner outer epistyle was also fractured and displaced from its position while parts from the rest of the epistyle and capitals were fractured and/or collapsed. The state of Apollo temple before and after the earthquake was investigated and the damage was confirmed through available archives of drawings and photos of the period (Fig. 6).

Figure 6: (a): The Temple of Apollo in 1901. Note the two metal rings that support the single fractured column without a capital, and the displaced outer corner epistyle. This figure is also indicative of the poor state of preservation of the temple base, (ASCSA Corinth Excavations). (b): The Temple of Apollo in our days with rescue restoration measures taken on the epistyle, the base and the fractured column).

During the site survey, it was observed that the middle column in the SSE façade presents horizontal displacement of approximately 10 cm towards the SSE (Fig. 7). Although it is not clear if, and to what extent, this displacement pre-dates the 1858 event, it is considered likely that this effect directly associates with the epistyle displacement. Since the historical archive does not indicate previous displacement of the epistyle, the column displacement could be considered as an additional seismic effect of the 1858 event.

Figure 7: The capital of the column under the restored epistyle that preserves a displacement of ~ 10 cm towards the SSE.

As reported by Koustas (1858), the environmental effects of the earthquake involved rockfalls around Acrocorinth where a section of the fortress walls collapsed while at the northern foothills of Acrocorinth hill, a cave collapsed. In the city of Old Corinth, extensive damage in aqueducts and reservoirs was recorded and the springs of the town dried up. Ground ruptures were dense and extensive especially in slopes. In Kenhreae 200 m inland from the coastline, water spurt in the fields through vents indicative of earthquake induced ground liquefaction. According to the ESI-07 intensity scale (Michetti et al., 2007), the earthquake environmental effects of the 1958 earthquake suggest intensities that range from VII to IX.

The 1928 Earthquake

The 1928 event is one of the first instrumental events with magnitude M=6.3, epicentre near the SE end of the Corinth canal, very shallow depth and MMI intensity of IX (Papazachos & Papazachou 1989). The event destroyed the modern city of Corinth where 3000 buildings suffered irreparable damage and 15.000 people were left homeless, (Drakopoulos et al., 1978). In Ancient Corinth according to the official governmental reports, out of the 380 inspected buildings, 300 were damaged, out of which 250 were considered as repairable and 50 either collapsed or were severely damaged (beyond repair), (Drakopoulos et al., 1978). The macroseismic intensity of the 1928 earthquake for Ancient Corinth is not known. However it can be assumed that it cannot be lower than

VIII due to its proximity to the epicentre and the extent of the damage. Environmental effects of this event were limited to ground cracks and extensive fissures mainly concentrated in the coastal regions near the Corinth canal while small scale landslides and rock falls were observed at the Gerania mountain slopes near Loutraki (Drakopoulos et al., 1978), suggesting ESI-07 intensity of VII-VIII (Michetti et al., 2007).

Figure 8: The NNW facade of the Glauke Fountain. With dashed line the section of the monument that collapsed during the earthquake of 1928.

In search of potential records of damage in the archaeological site, a repor retrieved from the archives of the American School of Classical Studies mentions the extensive damage sustained in Old Corinth and that *"part of Glauke collapsed"*, (Lord, 1947). Through the available photographic archives (E.L.I.A. Catalogue 2015), images dated in 1924 and 1930 were retrieved and compared confirming the partial collapse of the Glauke Fountain (Fig. 8). The damage sustained by the monument can be considered as quite extensive since approximately one third of the Glauke Fountain collapsed. It is notable that although the observed V-shaped corner cracks (Fig. 4) associate directly with the partial collapse of the monument, according to available photographic archives (ASCSA, 2015) they pre-date the 1928 earthquake. These fractures could relate to an earlier seismic event (e.g. 1858) but further studies are necessary in order to assess their nature and origin.

DISCUSSION

The investigations in the archaeological site of Ancient Corinth gave the opportunity to identify potential EAEs that relate to minimum EMS-98 intensities of VII to IX. It also allowed the suggestion of two candidate EAEs for rock-hewn monuments although further geotechnical studies are required. Through the study of historical and instrumental seismicity of the region and available records and archives, the EAEs recorded on the Temple of Apollo were correlated with the earthquake of 1858 (EMS-98 X) and the effects on the Glauke Fountain were partly correlated with the event of 1928 (EMS-98 IX).
It is interesting to note that the Temple of Apollo although it suffered serious damage from the 1858 event it was not affected significantly by the earthquake of 1928. Furthermore, the archaeological site appears to have suffered minimal damage during the earthquakes of 1930 (intensity VII in Ancient Corinth), 1962 (intensity VIII+ in Ancient Corinth) and in 1981 (intensity VIII in Ancient Corinth) regardless the poor state of preservation of the monuments. These observations allow us to suggest that the majority of the EAEs recorded represent a cumulation of seismic effects from numerous historical and modern earthquakes with intensities that range from VII-VIII. The partial correlation of the effects relating to minimum EMS-98 intensities of IX with the 1858 earthquake, indicates that the site potentially has suffered extensive damage from more than one earthquakes of minimum EMS-98 intensity of IX.
Further study of the potential EAEs recorded on the site's monuments and their correlation with the regional historical seismicity is a challenging task due to existing uncertainties. However, it will allow a better understanding of the relationship between site effects and macroseismic intensity, contributing to an archaeoseismological seismic hazard assessment approach for the archaeological site.

Acknowledgements: Many thanks to the LZ' Ephorate of Prehistoric and Classic Antiquities for permitting us to carry out the study on the site. The work was conducted as part of D. Minos-Minopoulos PhD thesis in the Department of Geography, Harokopio University, Athens, Greece.

References

ASCSA. Corinth Excavations Digital Resources. Available from: <http://www.ascsa.edu.gr>. (January 2015).

EL.I.A.. Catalogue of Archives. Available from: <http://www.elia.org.gr>. (January 2015).

Crouch, D.P., (2003) (ed). *Geology and Settlement, Greco-Roman Patterns*. Oxford University Press. New York. 2003, p. 385.

Drakopoulos, J., G. Leventakis, A. Roussopoulos, (1978). Microzonation in the seismic area of Corinth-Loutraki. *Annals of Geophysics*. 31, (1), 51-95.

Koustas, G., (1958). Corinth Earthquake. *Pandora*. 9, (202), 225-229. (in Greek).

Lord, L.E. 1947 (eds). *A History of the American School of Classical Studies at Athens, 1882-1942, an Intercollegiate Project*. Harvard University Press. Cambridge Massachusetts. 1947, p. 494.

Michetti, A.M., E. Esposito, L. Guerrieri, S. Porfido, L. Serva, R. Tatevossian, E. Vittori, F. Audermard, T. Azuma, J. Clague, V. Comerci, A. Gurpinar, J. McCaplin, B. Mohammadioun, N.A. Mörner, Y. Ota & E. Roghozin, (2007). Intensity Scale ESI 2007. In: (Guerrieri, L. & E. Vittori, eds.) *Mem. Descr. Carta Geol. d'Italia., vol. 74, Servizio Geologico d'Italia - Dipartimento Difesa del Suolo, APAT, Rome, Italy.*

Rodríguez-Pascua, M.A., R. Pérez-López, J.L. Giner-Robles, P.G. Silva, V.H. Garduño-Monroy, K. Reicherter, (2011). A comprehensive classification of Earthquake Archaeological Effects (EAE) in archaeoseismology: Application to ancient remains of Roman and Mesoamerical cultures. *Quaternary International.* 242, 20-30.

Rodríguez-Pascua, M.A., P.G. Silva, R. Pérez-López, J.L. Giner-Robles, F. Martín-González, M.A. Perucha, (2013). Preliminary intensity correlation between macroseismic scales (ESI07 and EMS98) and Earthquake archaeological effects (EAEs). In: *Proceedings of the 4th International INQUA Meeting on Paleoseismology, Active Tectonics and Archeoseismology (PATA), 9-14 October 2013, Aachen, Germany.*

Papazachos, B. & K. Papazachou, (1989) (eds). *The Earthquakes of Greece.* Ziti Publications. Thessaloniki. 1999, p. 356.

INQUA Focus Group on Paleoseismology and Active Tectonics

Archaeoseismological investigation of earthquake induced ground liquefaction events at the Early Christian Basilica, Ancient Lechaion harbour, Corinth, Greece

Minos-Minopoulos, D. (1,2), Pavlopoulos, K. (1,3), Apostolopoulos, G. (4), Lekkas, E. (5), Dominey-Howes, D. (6)

(1) Harokopio University, Department of Geography, 70 El. Venizelou Str., Kallithea, 176 71, Athens, Greece Email: dminou@hua.gr
(2) Ministry of Culture and Sports, Ephorate of Paleoanthropology & Speleology, Arditou 34B, 116 36, Athens, Greece
(3) Paris Sorbonne University Abu Dhabi, P.O. 38044 Abu Dhabi, UAE
(4) National Technical University of Athens, School of Mining and Metallurgical Engineering, Applied Geophysics Laboratory, 9 Iroon Polytechniou Str., Zografou, 157 80, Athens, Greece
(5) National and Kapodistrian University of Athens, Faculty of Geology and Geoenvironment, Department of Dynamic, Tectonic and Applied Geology, Panepistimioupolis Zografou, 157 84, Athens, Greece
(6) The University of Sydney, Asia – Pacific Natural Hazards Research Group, School of Geosciences, Sydney NSW 2050, Australia

Abstract: *Ground deformation structures preserved on the decorated floor of the Early Christian Basilica located in the vicinity of the ancient Lechaion Harbour, Corinth, are indicative of reccurent eathquake induced ground liquefaction events. Through the study of archaeological, geophysical and stratigraphical data, the surface structures were correlated with substratum features and three potential ground liquefaction events are suggested. The results are indicative of at least one seismic event before the construction of the Early Christian Basilica that has caused considerable damages to the ancient harbour installations, a second event (524 A.D.) that caused considerable but repairable damages to the temple and a third event that relates to irreparable damages and thus the destruction of the Basilica in A.D. 551.*

Key words*: Archaeoseismology, near surface geophysics, earthquake geology, lateral spreading, sand vents.*

INTRODUCTION

The Gulf of Corinth, represents an active continental rift system in a subduction zone setting, with extensional tectonics expressed through intense seismicity and marginal uplift. The Ancient Harbour of Lechaion is located in the southern coast of the Lechaion Gulf, the southeastern sub-basin of the Corinth Gulf in an estuary enivironment (Fig. 1). It is characterised by an outer harbour edged by moles and an inner artificially excavated harbour representing one of the most important harbours of Greece during antiquity. According to archaeological surveys its construction dates back to the 6th - 7th c. B.C., its use continued during the Roman period and an Early Christian Basilica was constructed at its western part during the late 5th c. A.D., (Pallas, 1959). Geomorphological, sedimentological and geoarchaeological studies suggest episodic uplift (Stiros et al., 1996, Morhange et al., 2012), sea level changes (Mourtzas et al., 2014) and tsunamigenic impact events (Hadler et al., 2013), indicative of neotectonic and geomorphological processes expressed through seismic activity. Archaeological excavations performed by Pallas during the late 1950s to early 1960s suggest that the Early Christian Basilica was destroyed by the A.D. 551 earthquake. Recent restoration works carried out in the Basilica revealed the decorated floor of the temple preserving deformation structures indicative of earthquake induced ground liquefaction. The aim of this work is to present the results of the investigations carried out on the site in order to study and identify the triggering mechanisms of the surface deformation structures and propose a sequence of potential seismic events.

Figure 1: (a) Location map of the study area, (b) Plan of the ancient Harbour of Lechaion.

METHODS

The methods employed in this study involve the combination of field observations and established

geophysical surveys through EM, GPR and ERT methods employed as a reconnaisance survey, with lithostratigraphic data obtained from four drill cores with vibracore equipment and existing archaeological records (Fig. 2). Fieldwork included mapping and cataloguing of distinct ground deformation structures in places where the floor was preserved in a good condition. The EM and GPR survey were carried out along ten ENE-WSW trending lines within the Basilica while the ERT survey included two profiles at right angles to each other along a ENE-SWS and a NNW-SSE trend. The lithostratigraphy was examined by four short depth drill cores in the central part of the southern aisle. Cores 2 and 4 were drilled in circular depressions while 1 and 3 in surrounding locations.

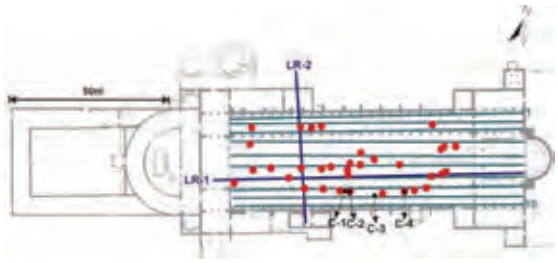

Figure 2: Location of the ten EM and GPR profiles (dashed green lines), the two ERT profiles (purple lines), the distinct deformation structures (red dots) and the drill cores (black dots) in the Early Christian Basilica.

RESULTS

The surface structures represent a cluster of linear and circular depressions and buckling structures with a primary ENE-WSW and secondary NNW-SSE trends (Fig.3). These structures correlate well with the surface expression of earthquake induced ground liquefaction (Obermeier, 2009).

Archaeological stratigraphy

The archaeological subsurface stratigraphy of the Basilica as described by Pallas during his original site excavations (1956 to 1965) includes an artificial fill composed mainly of sand and pebbles with occasional intercalations of clay, lithic and ceramic tiles fragments and mortar. This fill extends to a depth of a least 1 m below the Basilica floor and its lower layer is considered as the preparation ground for the construction of the Basilica (Pallas, 1965). The foundations of the temple are located at a depth of 1.45 m and 1.70 m in sand deposits that date to the 3rd c. B.C. As suggested by a layer of boulders at a depth of 3 m located to the SW of the Basilica, the artificial nature of the subsurface stratigraphy possibly extends to a depth of 3 m (Pallas, 1959).

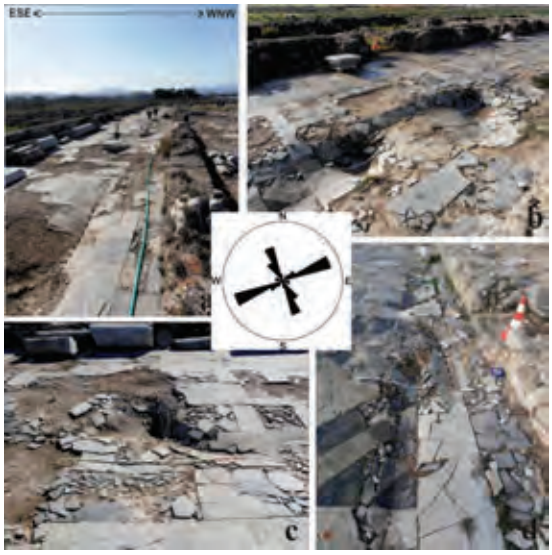

Figure 3: Surface deformation structures on the decorated floor of the southern aisle of the Basilica and corresponding rose diagram with the primary and secondary trends. (a,b) Circular and linear depressions with an ENE-WSW trend. (c) a circular depression in contact with a linear structure of NNW-SSE trend, (d) linear depressions of ENE-WSW trend.

Core drilling

The sedimentary analysis suggests a mixing of high energy fluvial sediments reworked by shallow water marine processes, typical of an estuarine depositional environment. The deposits are characterised by intercalations of coarse silty-sand to very coarse-grained sand and gravel with pebbles up to 2-3 cm diameter. Three sedimentary units were identified, the artificial unit A and the sedimentary units B and C here characterised with caution as "natural" since they could represent artificial fill layers of the ancient harbour installations (Fig. 4).

The artificial nature of the upper 1 m, is confirmed by the stratigraphy in cores 1 and 2 with layers that contain up to 10% clay and bear strong analogies to the archaeological stratigraphy. The absence of artificial fill deposits from cores 3 and 4 suggests that the artificial fill was arranged mainly in the central and WSW part of the temple indicating the presence of a "paleosurface", before the construction of the Basilica, dipping gently towards the WSW.

All four cores above the "paleosurface" contain a packed layer of dark grey colour containing fragments of ceramic tiles and agglomerates that correlates well with the archaeological layer of the preparation ground. This layer appears as a base layer of the artificial fill in cores 1 and 2, while it appears as the surface layer in cores 3 and 4.

The stratigraphy below the "paleosurface" (units B and C) is again characterised by coarse to very coarse sand and gravel with pebbles with a minimal content of fines. The grain size analysis of the four vibracore sedimentary samples suggests potentially liquefiable deposits (Tsuchida & Hayashi, 1971).

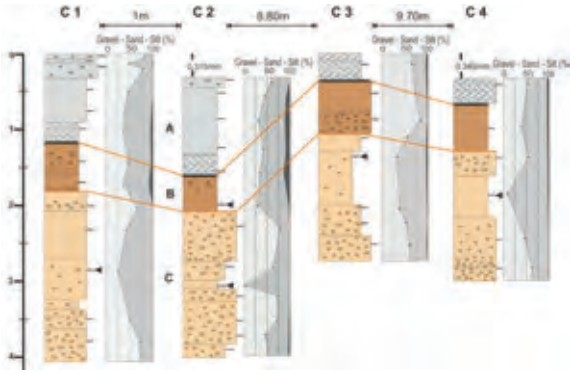

Figure 4: Lithostratigraphic columns of the four boreholes with grain size content and stratigraphic correlation. Horizontal distance between boreholes is indicated at the top of the figure. Bold black line in the logs represents the "paleosurface, black arrows indicate layers with high liquefaction potential.

Sand layers exhibiting high liquefaction potential were identified in both units B and C in cores 2 and 4 that were located in circular depressions (Fig. 4) The lack of high potential liquefaction sand layers in Unit A may be attributed to sediment mixing (Obermeier, 2009). The location and distribution of the high liquefaction potential layers, is indicative of a liquefaction source horizon below 4 m.

Geophysical survey

Substratum structures indicative of earthquake induced ground liquefaction were identified with all three geophysical methods suggesting extensive lateral spreading zones that develop along directions consistent with the two trends recorded on the Basilica floor. The survey suggests primary extensional displacement towards the free face of the inner harbour basin along at least three near vertical fissures with an ENE-WSW strike. These zones are represented in the EM second derivative of apparent conductivity map at 3 m effective depth range as high permeability zones; while in the ERT LR-2 profile they result as near vertical low resistivity zones, (Abu Zeid et al., 2012) (Fig. 5). It is interesting to note that the higher conductivity zones in the EM map are parallel to two linear relatively lower conductivity zones, possibly representing deposits related to harbour constructions pre-dating the Basilica construction.

Potential secondary substratum zones with relative moderate conductivity values oriented NNW-SSE are also indicated in the EM second derivative of the conductivity map at 3 m effective depth range, mostly in the central and southern aisle of the temple. Again, these potential zones correlate well with the upper 5 m of the LR-1 ERT profile, indicating nearly vertical discontinuities up to 2-3m wide in the WSW part of the profile, and with the surface deformation structures. Finally, the GPR profiles indicate 3 m water table depth; vertical zones of low signal amplitude in the upper 3 m that coincide with the near vertical lower resistivity zones of the ERT LR-1 profile and good correlation with the surface structures.

The lateral spreading as indicated by the ERT profiles, has been triggered along a shear zone located at approximately 4 to 5 m depth. This shear zone may represent the liquefied horizon that caused the overlying extensional fissures, allowing rapid ascent through the overlying strata, (Youd, 1984a).

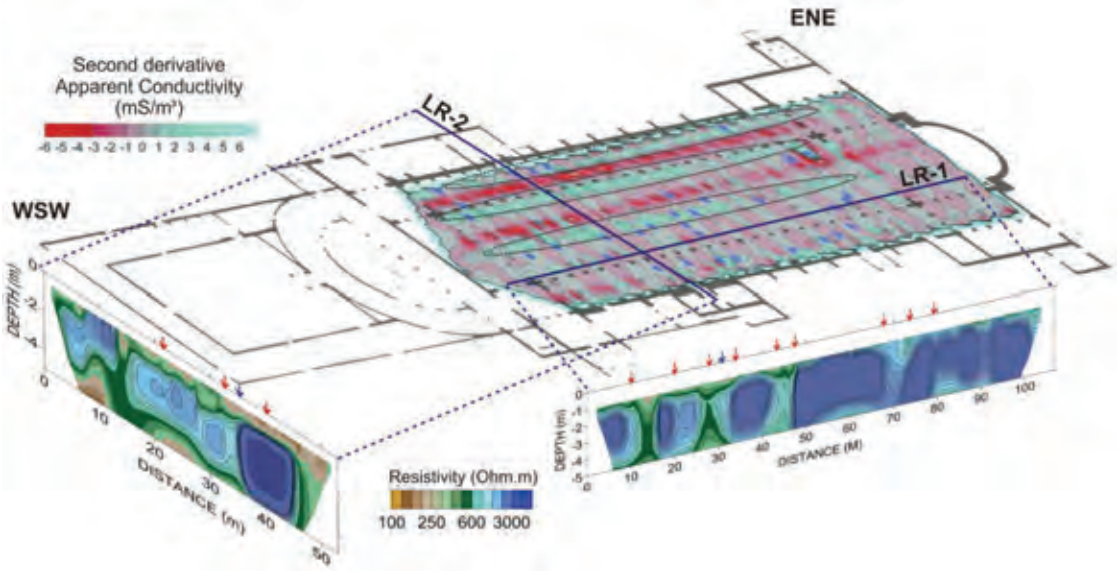

Figure 5: The Early Christian Basilica plan with the EM map of 3 m effective depth range and projections of the two detailed ERT profiles of the upper 5m (LR-1 and LR-2). The three principal high conductivity zones are circled with black dashed lines. Blue dots and red arrows indicate ground deformation structures recorded on the surface. Blue arrows indicate the intersection of the two ERT profiles.

The good correlation between the widespread surface deformation structures and the lateral spreading zones allows to establish a cause-effect relation among the earthquake induced damages of the Basilica and the archaeological findings suggesting the A.D. 551 earthquake as responsible for its destruction. Since the region is characterised by intense seismic activity and ground liquefaction is a phenomenon that generally presents reccurence (Youd, 1984b), the available data were further examined for possible indications and the following observations were made:

1. Although the preserved deformation structures correlate satisfactorily with the substratum structures,they do not present horizontal and vertical displacements of the extent suggested by the geophysical survey. This observation combined with the location of the liquefied sand samples in units B and C, that is, under the artificial fill and the "paleosurface", indicates that liquefaction and initial opening of fissures pre-dates the construction of the Basilica. Therefore, at least one seismic event can be suggested that occured on the site before the construction of the temple (late 5th c. A.D.), potentially during the operation of the ancient harbour.

2. One circular depression in the northern aisle preserves at its margins some remains of a second floor surface, including tiles and mortar, located 0.20 m under the surface of the Basilica floor. The observation is indicative that the floor of the northern aisle at some point underwent restoration. The location of the second floor remains at the margins of the depression suggest that both floors were damaged sequentially by the same process, i.e. the reactivation of a pre-existing sand vent.

The archaeological record suggests supplementary constructive works during the reign of Ioustin A' (518 - 527 A.D.) (Pallas, 1965). During the reign of Ioustin A' the earthquake of A.D. 524 destroyed Ancient Corinth and surrounding region and reconstructions were carried out under the order of the Emperor (Papazachos & Papazachou, 1989). Thus, we might infer that one liquefaction recurrence event was manifested during the earthquake of A.D. 524 causing repairable damages to the Early Christian Basilica.

Considering the recurrence of the liquefaction phenomena, the preserved deformation structures on the floor of the Basilica potentially represent a number of earthquake events and not just the damages resulting from A.D. 551 earthquake. The vicinity of the ancient harbour of Lechaion can be considered as a site valuable for earthquake science studies since it is indicative of a variety of earthquake environmental effects. Further multi-disciplinary studies would contribute to the comprehension of the regional historical seismicity and consequently to regional seismic hazard assessment.

Acknowledgements: We would like to thank the 25th Ephorate of Byzantine Antiquities for the permission to carry out the study at the site and for their warm support during our fieldwork. Additionally, many thanks go to Fanis Chatoupis, fellow geologist, for his direct geotechnical support when needed. The research was conducted as part of Despina Minos-Minopoulos PhD thesis in the Department of Geography, Harokopio University, Athens, Greece.

References

Abu Zeid, N., S. Bignardi, R. Caputo, G. Santarato, M. Stefani, (2012). Electrical resistivity tomography of cosismic liquefaction and fracturing at San Carlo, Ferrara Province, Italy. *Annals of Geophysics*. 55, 4, 713 - 716.

Hadler, H., A. Vött, B. Koster, M. Mathes-Schmidt, T. Mattern, K. Ntageretzis, K. Reicherter, T. Willershäuser, (2013). Multiple late-Holocene Tsunami Landfall in the Eastern Gulf of Corinth Recorded in the Palaeotsunami Geo-archive at Lechaion, Harbour of Ancient Corinth (Peloponnese, Greece). *Zeitschrift für Geomorphologie*. 57, (4), 139 - 180.

Morhange, C., P.A. Pirazzoli, N. Evelpidou and N. Marriner, (2012). Late Holocene Tectonic Uplift and the Silting up of Lechaion, the Western Harbor of Ancient Corinth, Greece. *Geoarchaeology: An International Journal*. Short Communication, 27, 278-283.

Mourtzas, N.D., C. Kissas, E. Kolaiti, (2014). Archaeological and geomorphological indicators of the historical sea level changes and the related palaeogeographical reconstruction of the ancient foreharbour of Lechaion, East Corinth Gulf (Greece). *Quaternary International*. 332, 151-171.

Obermeier, S.F., (2009). Using Liquefaction-Induced and other soft-sediment features for paleoseismic analysis. In: (McCaplin, J., eds), *Paleoseismology, International Geophysics*. 95. doi: 10.1016/S0074-6142(09)95007-0.

Pallas, D.I., (1959). Lechaion Basilica Excavation. *Proceedings of the Archaeological Society at Athens*. (1965), 126-140, (in Greek).

Pallas, D.I., (1965). Lechaion Basilica Excavation. *Proceedings of the Archaeological Society at Athens*. (1967), 137-166, (in Greek).

Papazachos, B., & K. Papazachou, (eds.), (1989). *The Earthquakes of Greece*. Ziti Publications. Thessaloniki. 1999, p. 356, (in Greek).

Stiros, S., P. Pirazzoli, R. Rothaus, S. Papageorgiou, J. Laborel, M. Arnold, (1996). On the Date of Construction of Lechaion, Western Harbour of Ancient Corinth, Greece, *Geoarchaeology: An International Journal*, 11, (3), 251-263.

Tsuchida, H., S. Hayashi, (1971). Estimation of liquefaction potential of sandy soils. *Proceedings of the 3rd Joint Meeting, U.S. - Japan, Panel on Wind and Seismic Effects,* Tokyo. U.S. - Japan Cooperation Program (UNJR). p. 91-101.

Youd, T.L., (1984a). Geologic effects - Liquefaction and associated ground failure. *Proceedings of the Geologic and Hydrologic hazards training program*. Open-File Report. 84, 760. (U.S. Geological Survey), 210-232.

Youd, T.L., (1984b). Recurrence of liquefaction at the same site. *Proceedings of the Eighth World Conference on Earthquake Engineering*. Earthquake Engineering Research Institute, San Francisco, California. 3, 231-238.

INQUA Focus Group on Paleoseismology and Active Tectonics

paleoseismicity.org

A contribution to seismic hazard assessment of the Salento Peninsula (Apulia, Southern Italy)

Nappi, R. (1), Gaudiosi, G. (1), Alessio, G. (1), De Lucia, M. (1), Porfido, S. (2)

(1) Istituto Nazionale di Geofisica e Vulcanologia, Sezione di Napoli - Osservatorio Vesuviano, Napoli, Italy. Email: rosa.nappi@ingv.it
(2) CNR-IAMC Napoli, Italy

Abstract: *The aim of this study is a critical revision of historical and recent seismicity of the Salento peninsula (Apulia, Southern Italy), offering an updated evaluation of its seismic hazard currently underestimated. This area is actually included in the least dangerous IV category of the Italian seismic classification. The Salento Peninsula was struck by the February 20, 1743 earthquake, considered as the strongest seismic event of this area. The reassessment of both the macroseismic effects on man-made structures, and the triggered effects in the natural environment has been carried out on the basis of archival documents and recent literature, according to the MCS and the ESI 2007 scale. The main result of our study has been the re-evaluation of the maximum intensity (Imax=XMCS) of the 1743 earthquake, besides new intensity values for some localities along the Apulian coasts.*

Key words: *Salento, 1743 earthquake, ESI 2007 scale, historical seismicity, seismically-induced effects, instrumental seismicity.*

INTRODUCTION

The geodynamic framework of the Apulian area is characterized by the subduction of the Ionian slab beneath the Calabrian Arc; such compressive regime is still active (Caputo et al., 1970; Castello et al., 2006).
The Salento peninsula (Apulia, Southern Italy) is considered the stable foreland of the Southern Apennines chain (Cinque et al., 1993, Gambini & Tozzi, 1996), although it has been epicentral area of several earthquakes over the last centuries with magnitude $3 \leq M_w \leq 5$, apart from the February 20, 1743 earthquake with M_w =7.1 (CPTI11, Rovida et al., 2011).
This area is also affected by significant seismicity of the surrounded regions: to the east the coast of Albania and the Ionian Islands (western Greece); to the west the Calabrian arc and the Southern Apennines chain (Fig. 1).
The Salento area is actually included in the least dangerous IV category of the Italian seismic classification (http://www.protezionecivile.gov.it/resources/cms/documents/A3_class20140605.pdf).
The main goal of this paper is to provide a contribution to the Salento seismic hazard evaluation through the following investigations:

- Analysis of historical and recent seismicity from available catalogues of the Apulia region and particularly of the Salento peninsula;
- Analysis of historical and recent seismicity of the Salento surrounding regions (Adriatic and Ionian sea, Albania and Greece) in order to identify the seismoinduced effects in the Salento area;
- Identification and evaluation of earthquake environmental effects of the February 20, 1743 earthquake from archival documents and scientific papers;
- Macroseismic revision of the February 20, 1743 earthquake according to the Mercalli-Cancani-Sieberg scale (MCS) and to the Environmental Seismic Intensity scale (ESI 2007) (Michetti et al., 2007; Guerrieri et al., 2012).

DATA ANALYSIS

The historical and recent seismicity in the Apulia region is characterized by a greater frequency of earthquakes in the northern sector compared to the southern one (Fig. 1).

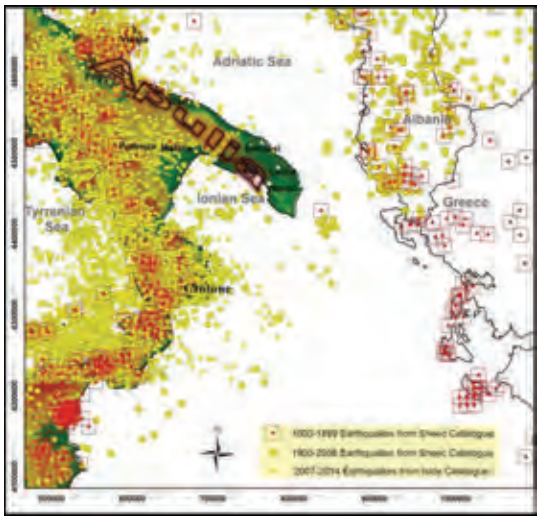

Figure 1: The map shows the spatial distribution of historical and recent seismicity extracted from: CPTI11 (Rovida et al, 2011) and SHEEC, (Stucchi et al., 2013; Grünthal et al., 2013).

Over the last centuries, the Apulia region from Gargano to Salento has been affected by significant earthquakes (Fig. 2), the most important of which have been extracted from the seismic catalogues CPTI11 (Rovida et al., 2011) and SHEEC (Stucchi et al. 2013; Grünthal et al., 2013), and occurred in:

- 1087 (I=VI-VII MCS, Bari);
- 1560 (I=VIII MCS, Barletta-Bisceglie);
- 1627 (I=X MCS, Gargano);
- 1731 (I=IX MCS, Foggia);
- 1743, (I=IX MCS, Ionian sea);
- 1826 (I=VI-VII MCS, Manduria);
- 1889 (I=VII MCS, Gargano);
- 1909 (I=VI MCS, Nardò).

According to the above mentioned catalogues, the 1743 earthquake epicenter is located in the Ionian sea, but the maximum intensity refers to some localities on land.
The instrumental recent seismicity of the Salento peninsula is mainly concentrated around the Strait of Otranto, with the strongest events recorded on October 20, 1974 (Mw = 5.0), (CPTI11, Rovida et al., 2011) and May 7, 1983 (Ml = 5.3) (CSI 1.1, Castello et al., 2006).
The 1627, 1731, 1743 and 1889 earthquakes also generated considerable seismo-induced environmental effects such as tsunami deposits along the Apulian coasts, landslides, liquefaction phenomena and hydrological changes (Margottini, 1982; De Simone, 1993; De Martini et al., 2003; Mastronuzzi et al., 2007; Maramai et al., 2014).
The whole Apulia region has also been struck by strong earthquakes of neighbouring seismogenetic areas located in the Southern Apennines, Adriatic and Ionian Sea, Albania and Greece. Several ground effects, mostly hydrological variations, have been triggered in Northern Apulia by the July 23, 1930 Irpinia earthquake (Imax=X MCS) and the November 23, 1980 Irpinia-Basilicata earthquake (Imax=X MCS) (Porfido et al. 2002, Porfido et al. 2007).
The strongest historical seismic events of the Campania-Lucania Apennines that produced intensity values of I ≥ VI MCS in the Salento area, are the following:

- the 1456 Molise earthquake, Imax = XI MCS;
- the 1694 Irpinia-Basilicata earthquake, Imax=XI MCS;
- the 1857 Basilicata earthquake, Imax = XI MCS.

In addition, well documented examples of Greek earthquakes strongly felt in Salento and in the whole Apulia region were:

– the August 27, 1886 earthquake (epicenter in Peloponnesus, Greece) which was felt in the Salento area with very high values of intensity (I=VII MCS) (Margottini, 1982; Papazachos & Papazachou, 2003; Serva & Michetti, 2010; Grünthal et al., 2013);
– the May 28, 1897 earthquake (epicenter in Tripole, Greece) with intensity I=VI MCS in the Salento area (Margottini, 1982; Papazachos & Papazachou, 2003; Serva & Michetti, 2010, Grünthal et al., 2013);
– the August 11, 1903 earthquake (epicenter in Peloponnesus area) with I=IV-V MCS in the Salento area (Margottini 1982; Serva & Michetti, 2010);
– the June 26, 1926 earthquake (epicenter between Creta and Cipro, Imax=X MCS) which was severely felt all over the Southern Italy. The intensity in the town of Taranto (western Salento) was IV-V MCS (Castenetto et al., 1986);
– the August 28, 1962 earthquake (epicenter in Peloponnesus area) with I=IV-V MCS in the Salento area (Margottini 1982; Serva & Michetti, 2010).

The Salento peninsula was severely hit by the February 20, 1743 earthquake (I=IX MCS, M_w=7.1; CPTI11, Rovida et al., 2011), considered the strongest seismic event of the area, which also generated a large tsunami (Fig. 3) according to the Euro-Mediterranean Tsunami Catalogue (Maramai et al., 2014; NGDC/WDS, 2014). The 1743 epicenter is still very controversial due to the different locations ascribed respectively on land, near the town of Nardò (CFTIMED04, Guidoboni et al., 2007) and offshore, in the Ionian sea (CPTI11, Rovida et al., 2011). This earthquake caused mostly severe damage in Salento, killing about 180 people, 150 of which in the town of Nardò (Lecce), and inflicted heavy damage also in Francavilla Fontana (Brindisi) (Margottini, 1981, 1985). The seismic event was extensively felt on the

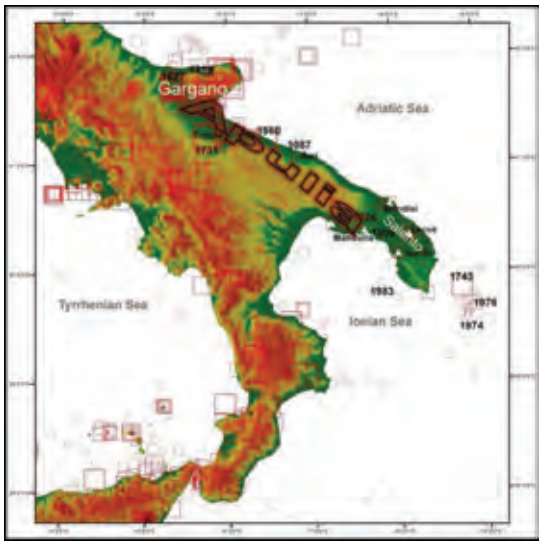

Figure 2: The map shows the spatial distribution of historical earthquakes occurred in the Apulian region, from Gargano to Salento, and in the Southern Italy extracted from CPTI11 (Rovida et al., 2011).

Figure 3: Boulders attributed to the 1743 seismo-induced tsunami on the Salento eastern coast (Torre S. Emiliano near Otranto (Lecce). (Photo by S. Porfido).

western coast of Greece, on the Malta island, in Southern Italy and in some localities of Central and Northern Italy.

DISCUSSION AND CONCLUSIONS

On the basis of recent scientific papers, (Margottini, 1981; Margottini, 1985; Ferrari, 1987; De Simone, 1993; Boschi et al., 1995; Galli & Naso, 2008, Nappi et al., 2014) and historical documents revision (De Giorgi, 1898; Baratta, 1901), a new estimation of the 1743 MCS intensity values of some localities, has been carried out. Furthermore, a critical review of archival documents coeval to the 1743 earthquake, found in the National Archives and church archives, has been performed. For obtaining a more accurate seismic hazard evaluation of the Salento area we have taken into account also geomorphologic data relative to environmental earthquake effects (Mastronuzzi et al., 2007; Nappi et al., 2014; De Lucia et al., 2014,) and architectural elements (De Lucia et al., 2013). The revision of the MCS intensity values and the assessment of the intensity according to the ESI scale, for some localities of the Salento area, have been performed on the basis of all the collected data and the seismoinduced environmental effects.
On the basis of the MCS scale, our re-evaluation has assigned the value of X MCS intensity to the town of Nardò, whose previous intensity value was IX MCS (Margottini, 1981, 1985; Boschi et al., 1995; Guidoboni et al., 2007) and the value of IX - X MCS (Galli & Naso, 2008); the value of IX MCS to Francavilla Fontana, VIII MCS to Castrignano del Capo, Leverano, Mesagne, Tuturano, Manduria, Racale, Salve, and VII MCS to the localities of Calimera, Copertino, Lecce, Oria, Ostuni, Seclì (Fig. 4).
For our re-evaluation of the 1743 earthquake on the basis of ESI scale, the tsunami phenomenon along the southern Adriatic coastline of Salento has been the most

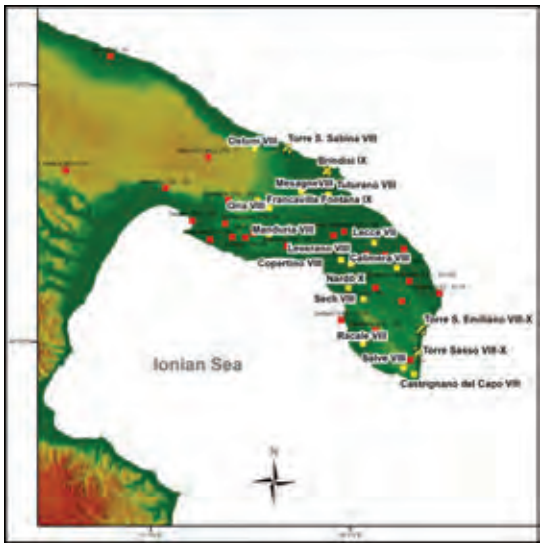

Figure 4: Map of the intensity values of the 1743 Salento earthquake: CFTIMED, 2007 MCS intensity values (red squares); re-evaluated MCS Intensity values in this study (yellow squares); re-evaluated ESI Intensity values in this study (yellow striped squares).

important environmental effect (Mastronuzzi et al., 2007; Mastronuzzi et al., 2011). Accordingly, for the town of Brindisi the ESI intensity value has been raised up from VIII to IX, due to the damage of the harbour mole caused by the tsunami.
Moreover, it has been possible to assess the ESI intensity values of VIII≥ I ≥ X for the localities of Torre Sasso (Tricase) and Torre Sant' Emiliano (Otranto), along the coastline of the Salento peninsula, on the basis of the tsunami blocks dimensions consisting of large boulders with a maximum weight of about 70 tons (Mastronuzzi et al., 2007). Ground effect phenomena triggered by the 1743 earthquake also occurred in the town of Nardò where variations of the water flow rate of wells together with variations of chemical-physical properties of water were observed.
A wide area that includes Albania, Greece and Malta island (Ambraseys, 2009; Galea, 2007) suffered also significant ground seismo-induced effects. Indeed, in the northern area of the island of Kefalonia (Greece) changes of chemical-physical properties of water occurred, in Castel Sant'Angelo (Corfù, Greece) and Malta island landslides took place, and in Butrinto fortress (Albania) ruptures and probably liquefaction phenomena were observed.
In conclusion, a new macroseismic scenario for the 1743 earthquake has been hypothesized (Imax=X MCS), taking into account both the archival and geomorphological data. The earthquake triggered environmental effects that should be taken into account for the seismic intensity assessment, especially considering the destructive tsunami impact on the coastline of the Salento, currently crowded with tourists.
Consequently, the seismic hazard of the Salento peninsula must be re-evaluated and further study should be dedicated to this area, considering also a possible revision of the seismic classification.

Acknowledgements: We thank Prof. G. De Natale, Director of the Osservatorio Vesuviano, INGV (Napoli, Italy) that encouraged and supported this research; Prof. M.O. Spedicato and Prof. L. Ruggiero of the University of Salento; Prof. E. De Simone of the Liceo Scientifico Banzi Bazzoli of Lecce, for the useful discussion about the historical data of the Salento seismicity.

References

Ambraseys, N., (2009). *Earthquakes in the Mediterranean and Middle East.* Press. Cambridge University. 901 p.
Baratta, M., (1901). *I terremoti d'Italia.* Torino. 951 p.
Boschi, E., G. Ferrari, P. Gasperini, E. Guidoboni, G. Smriglio, G. Valensise, (1995*). Catalogo dei forti terremoti in Italia dal 461 a.C. al 1980.* INGV-SGA. 974 p.
Caputo, M., G.F. Panza, D. Postpischl, (1970). Deep structure of the Mediterranean Basin. *Journal of Geophysical Research*, 75, 4919-4923.
Castello, B., G. Selvaggi, C. Chiarabba, A. Amato, (2006). *CSI Catalogo della sismicità italiana 1981-2002, versione 1.1.* INGV-CNT. Roma. http://csi.rm.ingv.it/.
Castenetto, S., E. Di Loreto, L. Liberi, C. Margottini, (1986). Studio macrosismico e risentimento in Italia dei terremoti del Mediterraneo centro-orientale del 26 giugno 1926 e del

17 gennaio 1983. In: *Atti del 4° Convegno del Gruppo Nazionale di Geofisica della Terra Solida*. 439-456.

Cinque, A., E. Patacca, P. Scandone, M. Tozzi, (1993). Quaternary kinematic evolution of the Southern Apennines. Relationship between surface geological features and deep lithospheric structures. *Annali di Geofisica*. 36 (2), 249-260.

De Giorgi, C., (1898). Ricerche su i terremoti avvenuti in Terra d'Otranto. *Mem. Pont. Acc. N. Lincei*. 15, 96-154.

De Lucia, M., R. Nappi, G. Gaudiosi, G. Alessio, (2013). *Sulle tracce del terremoto del 20 febbraio 1743 nei comuni danneggiati del Salento (Puglia meridionale).* Associazione Italiana di Geologia & Turismo. Atti del 5° Congresso Nazionale, 6-7 giugno 2013, Bologna. 141-142.

De Lucia, M., G. Alessio, G. Gaudiosi, R. Nappi, S. Porfido, (2014). A review of the Intensity values for the 1743 Salento earthquake. *Rendiconti Online Società Geololica Italiana*. Suppl. n.1, 31, 608 p. doi: 10.3301/ROL.2014.140.

De Martini, P.M., P. Burrato, D. Pantosti, A. Maramai, L. Graziani and H. Abramson, (2003). Identification of tsunami deposits and liquefaction features in the Gargano area (Italy): paleoseismological implications. *Annals of Geophysics*. 46, 883-902.

De Simone, E., (1993). *Vicende sismiche salentine*. Edizioni del Grifo. 152 p.

Ferrari, G., (1987). Some aspects of the seismological interpretation of information on historical earthquakes. In: *Proceeding, Workshop on historical seismicity*. (Margottini, C. and Serva, L., eds).

Galea, P., (2007). Seismic history of the Maltese islands and considerations on seismic risk. *Annals of Geophysics*. 50, 725-740.

Galli, P., G. Naso, (2008). The "taranta" effect of the 1743 earthquake in Salento (Apulia, Southern Italy). *Bollettino di Geofisica Teorica Applicata*. 49, (2), 177-204.

Gambini, R., M. Tozzi, (1996). Tertiary geodynamic evolution of the Southern Adria microplate. *Terra Nova*. 8, 593-602.

Grünthal, G., R. Wahlström, D. Stromeyer, (2013). The SHARE European Earthquake Catalogue (SHEEC) for the time period 1900-2006 and its comparison to the European Mediterranean Earthquake Catalogue (EMEC). *Journal of Seismology*. 17, (4), 1339-1344 doi: 10.1007/s10950-013-9379 y.

Guerrieri, L., E. Esposito, S. Porfido, A.M. Michetti, E. Vittori, (2012). La scala di intensità sismica ESI 2007 (Italian). *Memorie descrittive della carta geologica d'Italia*. 20-30 p. http://www.isprambiente.gov.it/files/progetti/inqua/esi-eee-volume-april-2012.pdf

Guidoboni, E., G. Ferrari, D. Mariotti, A. Comastri, G. Tarabusi, G. Valensise, (2007). CFTI4Med, Catalogue of Strong Earthquakes in Italy (461 B.C.-1997) and Mediterranean Area (760 B.C.-1500). Istituto Nazionale di Geofisica e Vulcanologia -SGA, Available from http://storing.ingv.it/cfti4med/

Maramai, A., B. Brizuela, L. Graziani, (2014). The Euro-Mediterranean Tsunami Catalogue. Annals of Geophysics, 57 (4) S0435; doi 10.4401/ag-6437.

Margottini, C., (1981). *Il terremoto del 1743 nella penisola salentina*. CNEL-ENEL, Congresso annuale del P.F.G. Udine. 12-14 maggio 1981.

Margottini, C., (1982). *Osservazioni su alcuni terremoti con epicentro in Oriente. Campo macrosismico in Italia del terremoto Greco del 1903*. CNEN-RT/AMB. 82 (3).

Margottini, C., (1985). The earthquake of february 20,1743, in the Ionian Sea. In: *Atlas of isoseismal maps of Italian earthquakes*. CNR-PFG. 114, 2A, 62 p.

Mastronuzzi, G., C. Pignatelli, P. Sansò, G. Selleri, (2007). Boulder accumulations produced by the 20th of February, 1743 tsunami along the coast of southeastern Salento (Apulia region, Italy). *Marine Geology*. 242, 191-205.

Mastronuzzi, G., R. Caputo, D. Di Bucci, U. Fracassi, V. Iurilli, M. Milella, C. Pignatelli, P. Sansò, G. Selleri, (2011). Middle-Late Pleistocene Evolution of the Adriatic Coastline of Southern Apulia (Italy). In: *Response to Relative Sea-Level Changes. Geografia Fisica e Dinamica del Quaternario*. 34, 207-221. doi: 1O.4461/GFDQ.2011.34.19.

Michetti, A.M., E. Esposito, L. Guerrieri, S. Porfido, L. Serva, R. Tatevossian, E. Vittori, F. Audemard, T. Azuma, J. Clague, V. Comerci, A. Gurpinar, J. Mc Calpin, B. Mohammadioun, N.A. Mörner, Y. Ota, E. Roghozin, (2007). Intensity Scale ESI 2007. *Memorie Descrittive della Carta Geologica d'Italia*. 74, 53 p.

Nappi, R., G. Gaudiosi, M. De Lucia, G. Alessio, S. Porfido, (2014). A critical revision of the Salento Peninsula seismicity: the case of the February 20, 1743 earthquake and related environmental effects. *Proceedings GNGTS,* Bologna, 25-27 Novembre 2014, (1) 101-107.

NGDC/WDS, National Geophysical Data Center / World Data Service (NGDC/WDS): Global Historical Tsunami Database. National Geophysical Data Center, NOAA. doi:10.7289/V5PN93H7 (2014 access date).

Papazachos, B.C., C. Papazachou, (2003). *The earthquakes of Greece.* Ziti publications. Thessaloniki. Greece. 286 p. (in Greek).

Porfido, S., E. Esposito, E. Vittori, G. Tranfaglia, A. M. Michetti, M. Blumetti, L. Ferreli, L. Guerrieri, L. Serva, (2002). Areal distribution of ground effects induced by strong earthquakes in the Southern Apennines (Italy). *Surveys in Geophysics*. 23 (6), 529-562.

Porfido, S., E. Esposito, E. Vittori, G. Tranfaglia, L. Guerrieri, R. Pece, (2007). Seismically induced ground effects of the 1805, 1930 and 1980 earthquakes in the Southern Apennines (Italy). *Bollettino della Società Geologica Italiana (Italian Jounal of Geoscience)*. 126, (2), 333-346.

Rovida, A., R. Camassi, P. Gasperini, M. Stucchi, (2011). *CPTI11, la versione 2011 del Catalogo Parametrico dei Terremoti Italiani*. Milano, Bologna, http://emidius.mi.ingv.it/CPTI. doi: 10.6092/INGV.IT-CPTI11.

Serva, L., A. M. Michetti, (2010). *Shakeistics: l'eredità degli studi nucleari in Italia per la valutazione del terremoto di riferimento per la progettazione degli impianti.* Insubria University Press. Fotoincisione Varesina. Varese. 48 p.

Stucchi, M., A. Rovida, A.A. Gomez Capera, P. Alexandre, T. Camelbeeck, M.B. Demircioglu, V. Kouskouna, P. Gasperini, R.M.W. Musson, M. Radulian, K. Sesetyan, S. Vilanova, D. Baumont, D. Fäh, W. Lenhardt, J.M. Martinez Solares, O. Scotti, M. Zivcic, P. Albini, J. Battlo, C. Papaioannou, R. Tatevossian, M. Locati, C. Meletti, D. Vigano, D. Giardini, (2013). The European Earthquake Catalogue (SHEEC) 1000-1899. *Journal of Seismology*. doi:10.1007/s10950-012-9335-2.

INQUA Focus Group on Paleoseismology and Active Tectonics

paleoseismicity.org

Tsunami hazard in the Eastern Mediterranean: Geological evidence from the Anatolian coastal area (Silifke, southern Turkey)

Öğretmen, N. (1,2), Cosentino, D. (1,3), Gliozzi, E. (1,3), Cipollari, P. (1,3), Iadanza, A. (4), Yıldırım, C. (2)

(1) Dipartimento di Scienze, Università degli Studi Roma Tre, Largo San Leonardo Murialdo, 1, I-00146 Roma, Italy. Email: nazik.ogretmen@uniroma3.it
(2) Istanbul Technical University, Eurasia Institute of Earth Sciences, Maslak, 34469 Istanbul, Turkey
(3) Istituto di Geologia Ambientale e Geoingegneria, Consiglio Nazionale delle Ricerche, Area della Ricerca Roma 1 Montelibretti, Via Salaria Monterotondo Scalo, 00016 Roma, Italy
(4) Istituto per l'Ambiente Marino Costiero, Consiglio Nazionale delle Ricerche, Calata Porta di Massa, I-80133 Napoli, Italy

Abstract: *This work is based on out-of-place boulders that have been found along the Mediterranean coasts of Turkey. We interpret these boulders as being transported by tsunami waves impacting the Silifke district. They represent the first geological evidence of tsunami in the southern coast of Anatolia. AMS ^{14}C datings on vermetids and* Petricola lithophaga *fossils found on those boulders point to a tsunami event younger than 1950 AD. According to the very recent tsunami and earthquake catalogues of Eastern Mediterranean area, the only tsunamigenic event younger than 1950 that impacted Anatolian coasts is supposed to be the 10 September 1953 earthquake, which was related to the activity of the SW-Cyprean subduction zone and Paphos transform fault. Linking out-of-place boulders found in Silifke district to this earthquake could be useful to validate tsunami numerical model for reviewing the tsunami hazards in Eastern Mediterranean and to estimate the possible tsunami intensity along the southern Anatolian coast.*

Key words: *Southern Turkey, tsunami, active tectonics, natural hazards, earthquakes.*

INTRODUCTION

This paper is based on a study of out-of-place boulders found in the Silifke district, along the southern Anatolia coast in Eastern Mediterranean, which is a tectonically complex region where the interplay between African, Eurasian, Anatolian and Arabian plates still continue (Fig. 1). This area recently underwent various geodynamic processes such as continental collision (Şengör and Yılmaz 1981, Jolivet and Faccenna 2000, Keskin 2003), plateau uplift (Şengör et al. 2003, Şengör et al. 2008, Cosentino et al. 2012, Schildgen et al., 2012), oceanic subduction (Şengör and Yılmaz 1981) and escape tectonics (Dewey and Şengör 1979, Faccenna et al. 2006). Some of these geodynamical processes are still active in the area and due to this activity Eastern Mediterranean is a highly seismogenic region (Jenkins et al., 2013; Geological Survey of Cyprus, 2014) (Fig. 2).

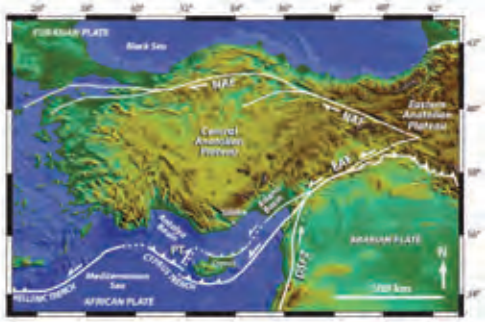

Figure 1: Tectonic setting of Eastern Mediterranean, Anatolia and surrounding regions. EAF: East Anatolian Fault; NAF: North Anatolian Fault; DSFZ: Dead Sea Fault Zone; PT: Paphos Transform.

Seismicity and tsunamis in Eastern Mediterranean

As reported in chronicles by people living the Eastern Mediterranean coasts, the region has been affected by destructive and tsunamigenic earthquakes since at least 1410±100 BC (Yolsal et al. 2007, Altınok et al. 2011, Papadopoulos 2014), which is the first historical record of earthquakes and tsunamis. In southern Turkey, the most important seismogenic zones with a high capability of generating M>6.0 earthquakes are: (1) the East Anatolian Fault (Antakya, İskenderun, Misis) and (2) the Kozan Fault (Kozan, Adana), with low tsunamigenic potential, and (3) the Cyprean Subduction Zone, with high tsunamigenic potential (Noller et al. 2011) (Fig. 1,2). In the surrounding region important tsunamigenic zones are: (1) the eastern Hellenic Arc and (2) the Dead Sea Fault zone.

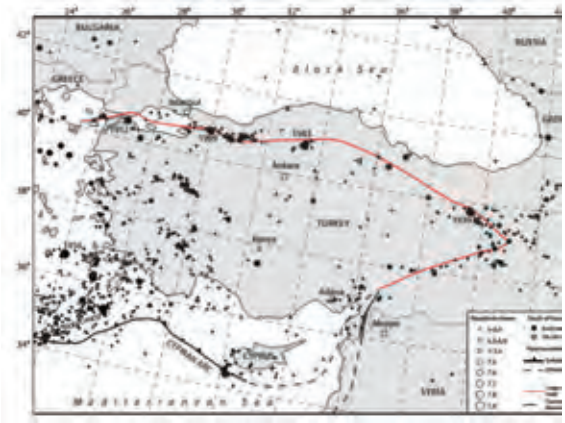

Figure 2: Seismicity from 1900 to 2010 of the Eastern Mediterranean area and vicinity showing epicenter of earthquakes with magnitude more than 6 (redrawn from Jenkins et al., 2013).

In the tsunami catalogues (Altınok and Ersoy 2007, Yolsal et al. 2007, Altınok et al. 2011, Papadopoulos 2014) there are only a few records of tsunamis that have affected the southern Anatolian coasts. The most ancient records of tsunamis are from 140 BC and 524-525 BC. However, after those tsunamis, there are no other tsunamis recorded in the chronicles from southern Anatolia until medieval period. The subsequent events recorded in local chronicles occurred on 16 November 1403, in 1489, and on 10 September 1953, which is the youngest tsunami that hit the southern Anatolian coast (Altınok and Ersoy 2007, Altınok et al. 2011).

To evaluate tsunami wave propagation in Eastern Mediterranean, Yolsal et al. (2007) simulated the tsunamis generated by major historical earthquakes that affected Eastern Mediterranean in 1222 AD and 1303 AD. The 11 May 1222 earthquake (M ~7.5) is related to the activity of the SW Cyprus Arc. Macroseismic observations related to this earthquake have been reported from the coastal area all around the Eastern Mediterranean, including the southern coast of Anatolia (Guidoboni and Comastri, 2005). The propagation of the tsunami wave generated by this earthquake, simulated by using nonlinear shallow-water theory, indicates the arrival of water surface perturbations along the southern Anatolian coast 60 minutes after the earthquake (Yolsal et al., 2007).

Geological evidence of possible tsunami from the southern Anatolian coast

Our field observations for geological evidence of possible tsunami occurring along the southern Anatolian coast are from the Silifke district (Fig. 1). The first place where we found out-of-place boulders is from the coast south of Yeşilovacık, in the proximity of the new harbour under construction (36° 11′ 1.68″N, 33° 39′ 36.32″E). In that area, the rocky coast is characterized by highly deformed Triassic shallow-water limestones and Upper Pleistocene breccias from base slope detrital-fan, which unconformably lies onto the Mesozoic carbonates. Some of the out-of-place boulders show biomarkers from marine environment, and lie above some remnants of marine abrasion platforms, which points to onshore transport by wave-storms and/or tsunami events. The boulders are characterized by Triassic limestones and Upper Pleistocene breccias with biomarkers such as lithophaga borings and vermetids, indicating a provenance from an intertidal marine environment. In particular, we consider that the location of YEŞ 5 boulder, a block of ca. 3 tons of Upper Pleistocene breccia encrusted by vermetids, which lies above an abrasion platform at 2.6 m a.s.l. (Fig. 3), would be consistent with a tsunami wave that hit the Yeşilovacık coast with a minimum run-up of 3 m. AMS ^{14}C dating of vermetids from YEŞ 5 yielded an age younger than 1950 AD.

A second place where we found an onshore transported boulder is in the vicinity of Narlıkuyu (36° 26′ 53.77″N, 34° 7′ 25.43″E). In this area, the rocky coast is mainly characterized by outcrops of deeper-water marls and marly limestones, possibly Pliocene in age.

In this area, a ca. 1.3-ton boulder of Miocene limestone shows lithophaga borings containing *Petricola lithophaga*. The boulder lies 6 m inland from the platform cut at 0.8 m a.s.l. within the Pliocene marls and marly limestones.

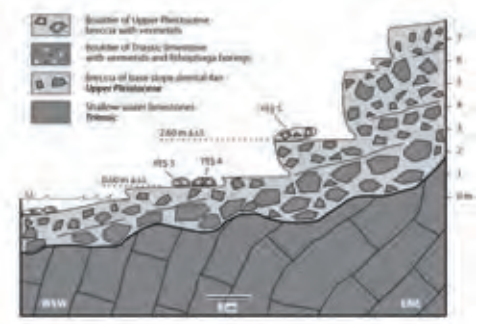

Figure 3: Geological cross-section of the Yeşilovacık outcrop, where some out-of-place boulders were found. YEŞ 3, YEŞ 4, and YEŞ 5 are the boulders that were sampled for ^{14}C dating.

DISCUSSION

The interpretation of out-of-place boulders is the most controversial issue of tsunami geology. How to distinguish onshore tsunami deposits from onshore storm deposits is still a matter of debate (Bourgeois, 2009; Nandasena et al., 2011). However, given that on more exposed coasts of both Yeşilovacık and Narlıkuyu areas the only deposits that could be related to high-energy events are cm-sized mollusk remains and pebbles, which lie on top of marine abrasion platforms at 2 and 5.7 m a.s.l., we consider the energy of storm surge events that periodically could affect those exposed coasts of southern Turkey not enough to transport the coastal boulders we found in Yeşilovacık and Narlıkuyu areas. Accordingly, we interpret the out-of-place boulders along the coast of southern Anatolia, in the Silifke district, to have been transported by tsunami waves, as suggested in several other places along the Mediterranean coasts (Vella et al. 2011; Scicchitano et al. 2007; Barbano et al. 2011; Mastronuzzi and Sansò 2004; Mastronuzzi et al. 2007; Maouche et al. 2009; Noller et al. 2011; Scheffers et al. 2008). Furthermore, the hosting coasts where we found the boulders are in semi-protected embayments capable to attenuate the energy of storm waves coming from open sea.

Considering the location of the coast where we found out-of-place boulders is faced on W-SW direction, we can exclude the tsunami events linked to the seismicity of the Dead Sea Fault Zone and the Levantine Basin as responsible for this boulder transportation onshore the Yeşilovacık area.

In addition, based on the simulations of tsunami wave propagation by Yolsal et al. (2007), tsunami waves generated by the seismicity along the SW Cyprean subduction zone, including the Paphos Transform Fault, and the Hellenic subduction zone are able to impact the southern Anatolian coasts and the Silifke district with the right direction of wave propagation.

For the out-of-place boulders along the coast of the Silifke area, the AMS ^{14}C dating point to a tsunamigenic event younger than 1950 AD. According to the updated Eastern Mediterranean tsunami catalogue compiled by Altinok et al. (2011) and taking into account the simulations by Yolsal et al. (2007), only two tsunamigenic events after 1950 AD could have potentially struck the southern Anatolian coast: 10 September 1953 (SW-Cyprus) and 9 July 1956 (Southern Aegean Sea). The latter event is one of the largest tsunamigenic earthquakes in the Aegean Sea during the 20th century. Anyway, the rapid decrease of the water level rise during the tsunami wave propagation, from 30 m (Amorgos) to 3 m (Crete), and even to 1 m (Fethiye), points to exclude this event as responsible for the onshore transport of out-of-place boulders along the coast of southern Anatolia, in the Silifke district.

Accordingly, based on the updated Eastern Mediterranean tsunami catalogue compiled by Altinok et al. (2011), the only tsunamigenic event that is supposed to have impacted southern Anatolia after 1950 AD is the 10 September 1953 earthquake, with an epicenter offshore of SW Cyprus. For this tsunamigenic event, Altinok et al. (2011) provided detailed information on the tsunamigenic source, noting that the earthquake (M = 6.2) was triggered by 0.35 cm of displacement along a right-lateral transpressional fault, which is consistent with the kinematics of the Paphos Transform Fault (Fig. 1).

Considering the historical maximum magnitude for earthquakes from both the SW Cyprian subduction zone and the eastern Hellenic Arc are larger than M = 6.2, tsunami waves with run-ups higher than 3.0 m could be expected to have struck the southern Anatolian coast in the past, and will likely strike in the future.

The geological evidence of tsunami from the study area contribute to evaluate the reliability of the estimated frequency and magnitude of past tsunami activity leading to a better definition of the tsunami hazard of the region. The evidence for past tsunamis that affected the Mediterranean coast of southern Turkey have to be taken into account for risk assessment of coastal hazards particularly in areas where strategic infrastructures (Akkuyu Nuclear Power Plant) and major expansions of residence complexes have been planned.

Acknowledgements: This study is part of the Anatolian Plateau Climate and Tectonic Hazards (ALERT) project, funded by the European Union Marie Curie Actions "Initial Training Networks" program (FP7-PEOPLE-2013-ITN)" (grant agreement number 607996).

References

Altinok, Y., Ş. Ersoy, (2000). Tsunamis observed on and near the Turkish coast. *Natural Hazards,* 21, 185-205.

Altinok, Y., B. Alpar, N. Özer, H. Aykurt, (2011). Revision of the tsunami catalogue affecting Turkish coasts and surrounding regions. *Natural Hazards and Earth System Sciences,* 11, 273–291.

Barbano, M.S, F. Gerardi, C. Pirrotta, (2011). Differentiation between boulders deposited by tsunamis and storm waves along the south-eastern Ionian coast of Sicily (Italy). *Bollettino di Geofisica Teorica ed Applicata.* 52 (4), 707-728.

Bourgeois, J., (2009). Geologic effects and records of tsunamis. In: (Robinson, A.R. and Bernard, E.N. eds.), *The Sea. vol. 15 – Tsunamis*. pp. 53-91. Harvard University Press.

Cosentino, D., T.F. Schildgen, P. Cipollari, C. Faranda, E. Gliozzi, N. Hudáčková, S. Lucifora, M.R. Strecker, (2012). Late Miocene surface uplift of the southern margin of the Central Anatolian plateau, Central Taurides, Turkey. *Geol. Soc. Am. Bull.* 124, 133-145.

Dewey, J.F., A.M.C. Şengör, (1979). Aegean and surrounding region: complex multiplate and continuum tectonics in a convergent zone. *Geological Society of America Bulletin*. 90, 84-92.

Faccenna, C., O. Bellier, J. Martinod, C. Piromallo, V. Regard, (2006). Slab detachment beneath eastern Anatolia: a possible cause for the formation of the North Anatolian fault. *Earth Planet. Sci. Lett*. 242, 85-97.

Geological Survey Department of Cyprus. In: *Hist. Eartquakes.* http://www.moa.gov.cy/moa/gsd/gsd.nsf/dmlHistEarthquakes_en/dmlHistEarthquakes_en?OpenDocument. Accessed: 9 Oct 2014.

Guidoboni, E., A. Comastri, (2005). *Catalogue of earthquakes and tsunamis in the Mediterranean area from the 11th to the 15th century*. INGV-SGA. Bologna.

Jenkins, J., B. Turner, R. Turner, G.V. Hayes, et al., (2013). Seismicity of the Earth 1900-2010 Middle East and Vicinity (ver. 1.1, Jan. 28, 2014). *U.S. Geological Survey Open File Report*. 2010-1083-K, scale 1:7,000,000.

Jolivet, L., C. Faccenna, (2000). Mediterranean extension and the Africa-Eurasia collision. *Tectonics.* 19, 1095-1106.

Keskin, M., (2003). Magma generation by slab steepening and breakoff beneath a subduction accretion complex: an alternative model for collision-related volcanism in Eastern Anatolia, Turkey. *Geophys. Res. Lett.* 30, (24), p. 8046.

Mastronuzzi, G., P. Sansò, (2004). Large boulder accumulations by extreme waves along the Adriatic coast of Southern Apulia (Italy). *Quaternary International*. 120, 173-184.

Mastronuzzi, G., C. Pignatelli, P. Sansò, G. Selleri, (2007). Boulder accumulations produced by the 20th February 1743 tsunami along the coast of SouthEastern Salento (Apulia region, Italy). *Marine Geology*. 242,191-205.

Maouche, S., C. Morhange, M. Meghraoui, (2009). Large boulder accumulation on the Algerian coast evidence tsunami events in the Western Mediterranean. *Marine Geology*. 262, 96-104.

Nandasena, N.A.K., R. Paris, N. Tanaka, (2011). Reassessment of hydrodynamic equations: Minimum flow velocity to initiate boulder tran sport by high energy events (storms, tsunamis). *Marine Geology*. 281, 70-84.

Noller, S., Z. Zomeni, I. Panayides, (2011). Preliminary field and GIS-based assessment of tsunami hazard on Cyprus. *CIESM workshop monographs,* 42, 49-58.

Papadopoulos, G.A., E. Gràcia, R. Urgeles, V. Sallares, et al., (2014). Historical and pre-historical tsunamis in the Mediterranean and its connected seas: Geological signatures, generation mechanisms and coastal impacts. *Marine Geology.* 354, 81-109.

Scheffers, A., D. Kelletat, A. Vött, S.M. May, S. Scheffers, (2008). Late Holocene tsunami traces on the western and southern coastlines of the Peloponnesus (Greece). *Earth and Planetary Science Letters.* 269, 271-279.

Schildgen, T.F., D. Cosentino, B. Bookhagen, S.Niedermann, C. Yıldırım, H.P. Echtler, M.R. Strecker, (2012). Multi-phased uplift of the southern margin of the Central Anatolian plateau, Turkey: a record of tectonic and upper mantle processes. *Earth Planet. Sci. Lett.* 317-318, 85-95.

Scicchitano, G., C. Monaco, L. Tortorici, (2007). Large boulder deposits by tsunami waves along the Ionian coast of South-Eastern Sicily (Italy). *Marine Geology*. 238 (1-4), 75-91.

Şengör, A.M.C., Y. Yılmaz, (1981). Tethyan evolution of Turkey: a plate tectonic approach. *Tectonophysics*. 75, 181-241.

Şengör, A.M.C., S. Özeren, T. Genç, E. Zor, (2003). East Anatolian high plateau as a mantle supported, north–south shortened domal structure. *Geophys. Res. Lett.* 30, (24), p. 8045.

Şengör, A.M.C., S. Özeren, M. Keskin, M. Sakınç, A.D. Özbakır, I. Kayan, (2008). Eastern Turkish high plateau as a small Turkic-type orogen: implications for post-collisional crust-forming processes in Turkic-type orogens. *Earth Sci. Rev*. 90 (1-2), 1-48.

Vella, C., F. Demory, V. Canut, P. Dussouillez, T.J. Fleury, (2011). First evidence of accumulation of mega boulders on the Mediterranean rocky coast of Provence (southern France). *Natural Hazards and Earth System Sciences*. 11, 905-914.

Yolsal, S., T. Taymaz, A.C. Yalçıner, (2007). Understanding tsunamis, potential source regions and tsunami-prone mechanisms in the Eastern Mediterranean. *Geological Society London. Special Publications*. 291, 201-230.

INQUA Focus Group on Paleoseismology and Active Tectonics

paleoseismicity.org

Holocene extensional faulting at the southeastern margin of the Central Anatolian Plateau: Implications for the kinematics of the Ecemiş Fault Zone (Mersin, southern Turkey)

Öğretmen, N. (1,2), Cosentino, D. (1,3), Gliozzi, E. (1,3), Cipollari, P. (1,3), Yıldırım, C. (2)

(1) Dipartimento di Scienze, Università degli Studi Roma Tre, Largo San Leonardo Murialdo, 1, I-00146 Roma, Italy. Email: nazik.ogretmen@uniroma3.it
(2) Istanbul Technical University, Eurasia Institute of Earth Sciences, Maslak, 34469 Istanbul, Turkey
(3) Istituto di Geologia Ambientale e Geoingegneria, Consiglio Nazionale delle Ricerche, Area della Ricerca Roma 1 Montelibretti, Via Salaria Monterotondo Scalo, 00016 Roma, Italy

Abstract: *This work is based on fault planes developed along the Mediterranean coasts of Turkey. The measured fault planes affect the coastal area of the Silifke district with Holocene offsets. Since the Active Fault Map of Turkey doesn't show any active faults in the study area, they represent the first evidence of active tectonics at the southern margin of the Central Anatolian Plateau. Similar fault planes, with Holocene offsets, have been recently recognized offshore the Silifke area by using high-resolution seismic reflection profiles. Both onshore and offshore Holocene fault systems show extensional kinematics along NE-SW and NNE-SSW E-dipping fault planes. These Holocene fault systems have the same fault plane attitude of the Ecemiş Fault Zone, suggesting a southwestern extension of this fault zone as far as the Silifke region. The high-frequency low-magnitude seismicity with NNE-SSW direction along the southeastern margin of the Central Anatolian Plateau seems to be related to a continuous slip along this active fault system.*

Key words: *Southern Turkey, active tectonics, seismicity, Ecemiş Fault, natural hazards, Holocene.*

INTRODUCTION

Eastern Mediterranean is a tectonically complex region where the interplay between African, Eurasian, Anatolian and Arabian plates still continue (Fig 1). This area recently underwent various geodynamic processes such as continental collision (Şengör and Yılmaz 1981, Jolivet and Faccenna 2000, Keskin 2003), plateau uplift (Şengör et al 2003, Şengör et al 2008, Cosentino et al 2012, Schildgen et al, 2012), oceanic subduction (Şengör and Yılmaz 1981) and escape tectonics (Dewey and Şengör 1979, Faccenna et al 2006). Some of these geodynamical processes are still active in the area and due to this activity Eastern Mediterranean is a highly seismogenic region (Jenkins et al., 2013; Geological Survey of Cyprus, 2014) (Fig 2).

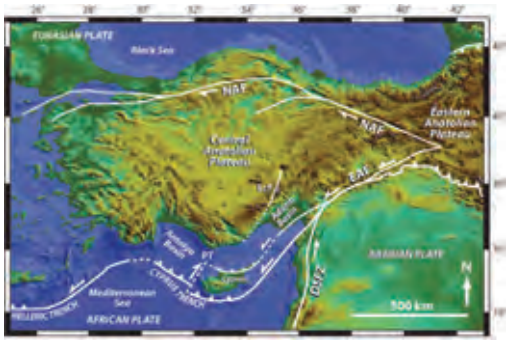

Figure1: Tectonic setting of Eastern Mediterranean, Anatolia and surrounding regions. EAF: East Anatolian Fault; NAF: North Anatolian Fault; DSFZ: Dead Sea Fault Zone; PT: Paphos Transform; EcF: Ecemiş Fault. From Schildgen et al. (2014).

Seismicity in southern Turkey

In southern Turkey, the most important seismogenic zones with a high capability of generating M>6.0 earthquakes are: (1) the East Anatolian Fault (Antakya, İskenderun, Misis), (2) the Kozan Fault (Kozan, Adana), and (3) the Cyprean Subduction Zone, (Fig 1,2).

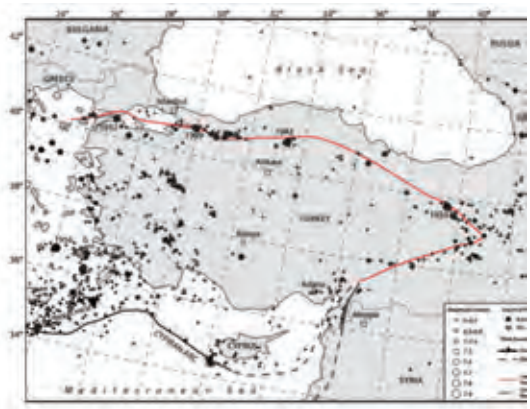

Figure 2: Seismicity from 1900 to 2010 of the Eastern Mediterranean area and vicinity showing epicenter of earthquakes with magnitude more than 6 (redrawn from Jenkins et al., 2013).

In the seismicity map of southern Turkey (Fig. 2), there is only a single earthquake with magnitude more than 6 that has affected the coastal area SW of Adana (Mersin-Silifke area). This result could bring to consider the SE margin of the Central Anatolian Plateau as characterized by low seismicity.

On the contrary, if we would take into account earthquakes with magnitude more than 2 (Fig. 3) we

could figure out an intense seismicity along a NE-SW structure, which corresponds to the present day coastal area and possibly to the SW prolongation of the Ecemiş Fault Zone (Aksu et al., 2014).

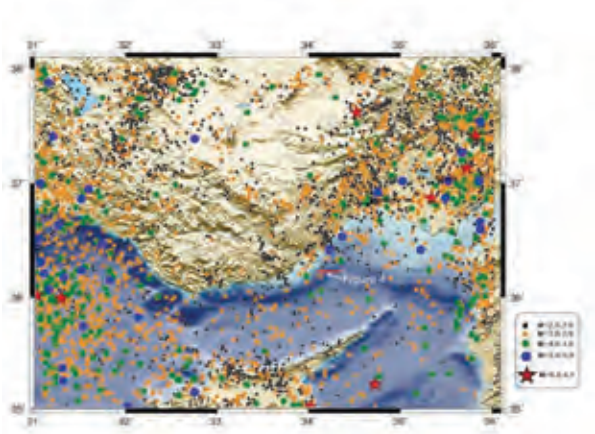

Figure 3: Seismicity of southern Turkey from 1900 to 2014. (from Boğaziçi University, Kandilli Observatory and Earthquake Research Institute).

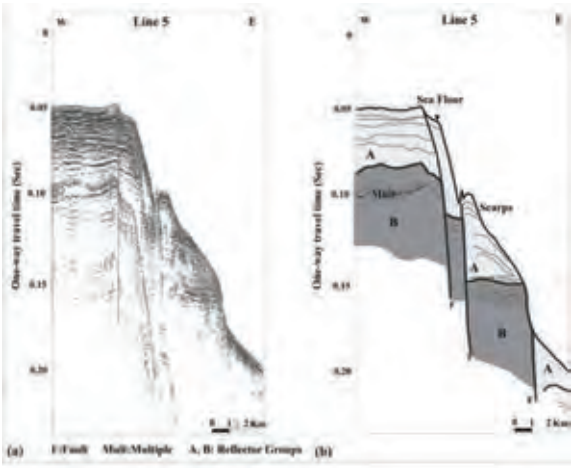

Figure 4: (a) Single channel seismic reflection profile offshore the Silifke coast (see location in Fig. 3). (b) Interpretation of the seismic profile in (a): A – Upper Quaternary seismic unit; B – Plio-Quaternary seismic unit. From Ozel et al. (2007).

Active tectonics in southern Turkey

According to the Active Fault Map of Turkey (Emre et al., 2013) no active faults are affecting the coastal area SW of Adana (Mersin –Silifke region). However, considering the activity along the Ecemiş Fault Zone and the intense seismicity of the region from its SW termination and the Mersin-Silifke area, an additional strand of the Ecemiş active fault could be expected SW of Adana.

Offshore the Silifke area, active tectonics affecting all the Quaternary succession was recognized by Ozel et al. (2007) by interpreting single channel seismic reflection profiles. These authors evidenced a NE-SW major fault system that was considered to be an offshore extension of the Ecemiş Fault Zone. This fault system is mainly characterized by high angle faults, dipping to the SE, which show normal offsets even affecting the youngest seismic reflectors within the Quaternary sequence.

Geological evidence of active tectonics from onshore the southern Anatolian coast

In the study area, late Quaternary uplift rate of 0.7 mm/yr has been recently estimated along the Goksu River valley by surface exposure ages (^{10}Be, ^{26}Al, and ^{21}Ne) of gravels capping fluvial strath terraces (Schildgen et al., 2012). This high uplift rate is consistent with the position of the southern Anatolian coast close to active plate boundaries.

In different places along the coastal area SW of Adana, between Mersin and Yeşilovacık, there are evidence of recent coastal uplift. In the area, Holocene marine notches and wave-cut platform remains, which rest at different elevations above the present sea level, testify for Holocene uplifts of the coastal area.

The Narlıkuyu coastal area is mainly characterized by the outcrop of Middle Miocene shallow-water limestones, subordinately Plio-Quaternary deeper-marine marls and marly limestones that unconformably overlie the Miocene carbonates. In the area, several markers of past sea-level, such as marine notches and abrasion platforms with tidal-pools, are affected by tectonics (Fig. 5).

Figure 5: Extensional fault plane affecting a Holocene abrasion platform with tidal pools and the relative tidal notch.

In a small portion of the study area (Narlıkuyu village), 39 fault planes have been measured. Offsets of the sea-level markers (both marine notches and abrasion platforms with tidal pools) reach values between a few centimetres to 70 cm. Meter-scale structural analyses carried out along the coastal area of Narlıkuyu revealed the presence of two different fault systems affecting the Holocene sea-level markers.

The main fault system is represented by conjugate fault planes striking NNE-SSW, which shows normal offsets of the Holocene marine notches and tidal abrasion platforms. In the same measurement station, a secondary fault system shows deformation along WNW-ESE direction. A preliminary interpretation of those fault systems points to consider this latter to be represented by transfer faults kinematically related to extensional tectonics along NNE-SSW faults.

This conclusion is corroborated by the crystal growth of a syn-kinematic fibrous aragonite observed on one of the major WNW-ESE fault plane measured in the area. The c-axes of those syn-kinematic crystals, which is the growth axes of aragonite, is parallel to the strike of the fault plane, suggesting a strike-slip movement along the WNW-ESE fault during the aragonite growth.

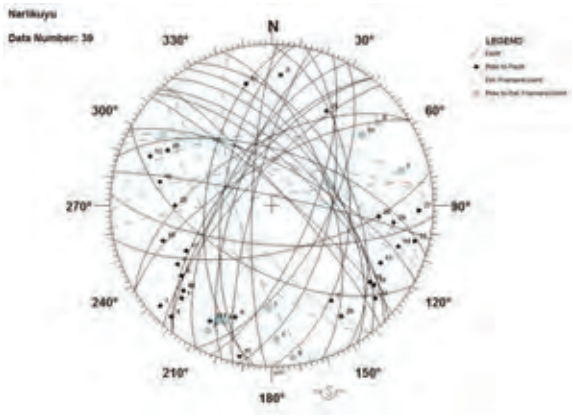

Figure 6: Stereoplot (Schmidt net lower hemisphere) of the fault planes and fractures affecting the Holocene sea-level markers at Narlıkuyu (southern Turkey).

DISCUSSION

In the active fault map of Turkey (Emre et al., 2013) no active faults are reported along the coastal area SW of Adana. In contrast, geological field work carried out along the coast between Mersin and Silifke recognized the occurrence of a NNE-SSW extensional fault system, which affects the Narlıkuyu coastal area with faults showing up to 70 cm of late Holocene offsets.

Deformations characterized by similar geometries and kinematics were recognized by Ozel et al. (2007) in the Silifke offshore. These authors, by using high-resolution seismic reflection profiles, recognized NE-SW fault planes affecting the uppermost Quaternary seismic unit.

Ozel et al. (2007) interpreted the fault planes offshore the Silifke area as the southwestern extension of the Ecemiş Fault Zone. The Ecemiş Fault is one of the most important active fault zones of southeastern Turkey, which contributes together with the Eastern Anatolian Fault and the Cyprean Subduction Zone to accommodate the relative motion among African, Arabian, and Anatolian plates.

The activity of the Ecemiş Fault was recently a matter of debate among many authors. Whereas Jaffey and Robertson (2001) interpreted the Ecemiş Fault as an important active fault zone, Westaway (1999) inferred that its activity predates Oligocene times.

According to Westaway (1999) any Neogene-Quaternary strike-slip motion along the Ecemiş Fault is kinematically inconsistent with the major young strike-slip faults in Turkey, and their kinematic consistency, as reconstructed by Westaway (1994) and Westaway and Arger (1996; 2001), would be broken by introducing extra slip along the Ecemiş Fault or elsewhere.

In contrast, according to Jaffrey and Robertson (2001) there are evidence that the Ecemiş Fault experienced major tectonic activity, dominated by left-lateral strike-slip, during the Oligocene-Early Pliocene. Subsequently, the Ecemiş Fault was dominated by east-west extension, with a very small component of strike-slip (Jaffey and Robertson, 2001).

Our data from the Narlıkuyu area, which show NNE-SSW extensional conjugate fault system with late Holocene offsets, suggest the occurrence of active faulting with extensional behaviour at the southeastern margin of the Central Anatolian Plateau. Measurements of Holocene faults in the Narlıkuyu area show the same fault plane attitude of the Ecemiş Fault Zone, suggesting a southwestern extension of this fault zone as far as the Silifke region, as already discussed by Ozel et al. (2007).

The high-frequency low-magnitude seismicity with NNE-SSW direction along the southeastern margin of the Central Anatolian Plateau (Fig. 3) seems to be related to a continuous slip along this active fault system. In this framework, the extension of the Ecemiş Fault Zone accommodates the differential uplift of the southeastern margin of the Central Anatolian Plateau with respect to the subsiding Adana-Cilicia Basin.

Acknowledgements: This study is part of the Anatolian Plateau Climate and Tectonic Hazards (ALERT) project, funded by the European Union Marie Curie Actions "Initial Training Networks" program (FP7-PEOPLE-2013-ITN) (grant agreement number 607996).

References

Aksu, A.E., T. Calon, J. Hall, B. Kurtboğan, S. Gürçay, G. Çifçi, (2014). Complex interactions fault fans developed in a strike-slip system: Kozan Fault Zone, Eastern Mediterranean Sea. *Marine Geology*. 351, 91-107.

Boğaziçi University, Kandilli Observatory and Earthquake Research Institute. http://udim.koeri.boun.edu.tr/

Cosentino, D., T.F. Schildgen, P. Cipollari, C. Faranda, E. Gliozzi, N. Hudáčková, S. Lucifora, M.R. Strecker, (2012). Late Miocene surface uplift of the southern margin of the Central Anatolian plateau, Central Taurides, Turkey. *Geol. Soc. Am. Bull.* 124, 133-145.

Dewey, J.F., A.M.C. Şengör, (1979). Aegean and surrounding region: complex multiplate and continuum tectonics in a convergent zone. *Geological Society of America Bulletin*. 90, 84-92.

Faccenna, C., O. Bellier, J. Martinod, C. Piromallo, V. Regard, (2006). Slab detachment beneath eastern Anatolia: a possible cause for the formation of the North Anatolian fault. *Earth Planet. Sci. Lett*. 242, 85-97.

Geological Survey Department of Cyprus. In: *Hist. Eartquakes*. http://www.moa.gov.cy/moa/gsd/gsd.nsf/dmlHistEarthquakes_en/dmlHistEarthquakes_en?OpenDocument. Accessed: 9 Oct 2014.

Jenkins, J., B. Turner, R. Turner, G.V. Hayes, et al., (2013). Seismicity of the Earth 1900-2010 Middle East and Vicinity (ver. 1.1, Jan. 28, 2014). *U.S. Geological Survey Open File Report*. 2010-1083-K, scale 1:7,000,000.

Jaffey, N., A.H.F. Robertson, (2001). New sedimentological and structural data from the Ecemis Fault Zone, southern Turkey: implications for its timing and offset and Cenozoic tectonic escape of Anatolia. *Journal of the Geological Society. London*. 158, 367-378.

Jolivet, L., C. Faccenna, (2000). Mediterranean extension and the Africa–Eurasia collision. *Tectonics*. 19, 1095-1106.

Keskin, M., (2003). Magma generation by slab steepening and breakoff beneath a subduction accretion complex: an alternative model for collision-related volcanism in Eastern Anatolia, Turkey. *Geophys. Res. Lett.*,30, (24), p. 8046.

Emre, Ö., T.Y. Duman, S. Özalp, H. Elmacı, S. Olgun, F. Saroglu, (2013). *Active Fault Map of Turkey with explanatory Text*. 1:1,250,000 Scale. MTA. General Directorate of Mineral Research and Exploration. Special Publication Series-30.

Ozel, E., A. Ulug, B. Pekcetinoz, (2007). Neotectonic aspects of the northern margin of the Adana-Cilicia submarine basin, NE Mediterranean. *J. Earth Syst. Sci.* 116, 113-124.

Schildgen, T.F., D. Cosentino, B. Bookhagen, S. Niedermann, C. Yıldırım, H.P. Echtler, M.R. Strecker, (2012). Multi-phased uplift of the southern margin of the Central Anatolian plateau, Turkey: a record of tectonic and upper mantle processes. *Earth Planet. Sci. Lett.* 317-318, 85-95.

Schildgen, T.F., C. Yıldırım, D. Cosentino, M.R. Strecker, (2014). Linking slab break-off, Hellenic trench retreat, and uplift of the Central and Eastern Anatolian plateaus. *Earth-Science Reviews*. 128, 147-168.

Şengör, A.M.C., Y. Yilmaz, (1981). Tethyan evolution of Turkey: a plate tectonic approach. *Tectonophysics*. 75, 181-241.

Şengör, A.M.C., S. Özeren, T. Genç, E. Zor, (2003). East Anatolian high plateau as a mantle supported, north-south shortened domal structure. *Geophys. Res. Lett.* 30, (24), p. 8045.

Şengör AMC, S. Özeren, M. Keskin, M. Sakınç, A.D. Özbakır, I. Kayan, (2008). Eastern Turkish high plateau as a small Turkic-type orogen: implications for post-collisional crust-forming processes in Turkic-type orogens. *Earth-Science Reviews*. 90 (1-2), 1-48.

Westaway, R., (1994). Present-day kinematics of the Middle-East and Eastern Mediterranean. *Journal of Geophysical Research*. 99, 12071-12090.

Westaway, R., (1999). Comment on "A new intracontinental transcurrent structure: The Central Anatolian Fault Zone, Turkey" by A. Koçyiğit and A. Beyhan. *Tectonophysics*. 314, 469-479.

Westaway, R., J. Arger, (1996). The Gölbaşı basin, southeastern Turkey: a complex discontinuity in a major strike-slip fault zone. *Journal of the Geological Society. London*. 153, 729-744.

Westaway, R., J. Arger, (2001). Kinematics of the Malatya-Ovacik fault zone. *Geodinamica Acta*. 14, 103-131.

INQUA Focus Group on Paleoseismology and Active Tectonics

New potential sedimentary evidences of paleotsunamis on coastal lagoons of Chacopata, State of Sucre, Venezuela

Oropeza, J. (1), Audemard, F.A. (1), Beck, C. (2), Vallée, M. (1)

(1) Dpto. de Ciencias de la Tierra, Fundación Venezolana de Investigaciones Sismológicas - FUNVISIS - Apdo. Postal 76880, Caracas 1070-A, Venezuela. Email: joropeza@funvisis.gob.ve
(2) ISTerre, UMR CNRS 5275, Université de Savoie/Grenoble-Alpes, F-73376 Le Bourget du Lac, France

Abstract: *New potential sedimentary evidences of paleotsunami have been found in sedimentary record of coastal lagoons in Chacopata, State of Sucre, Venezuela, located next to El Pilar Fault System. Here, three active coastal lagoons have been explored by small hand-excavated pits, sediment samples and sediment cores to detail sedimentological studies. Preliminary outcomes state the possible occurrence of tsunamis in recent times.*

Key words: *Paleotsunami, Chacopata, coastal lagoons, sedimentary record.*

INTRODUCTION

The Venezuelan coast has been affected by tsunami waves in last 500 years, as documented by many historical reports of different seismic catalogs (Grases, 1976; Singer *et al.*, 1983; Grases *et al.*, 1999, O'Loughlin and Lander 2003) as well as by sedimentary geological investigations carried out in the last years to provide *in situ* geological support to these historical observations (Audemard *et al.*, 2011; Leal & Scremin, 2011; Oropeza *et al.*, 2013). These investigations were initiated in the northeastern coasts, due to the concentration of these reports in this region.

As part of these investigations, in the region of Chacopata, the northernmost end of the Península de Araya, state of Sucre, susceptible to be affected by tsunami waves due to their topographically low plains and particularly low coastal barriers on the west (<1 m), and located within 20-linear-km of the active trace of the El Pilar fault of recognized seismic activity (Schubert, 1977; Vierbuchen, 1984; Audemard, 1997, 1998, 1999, 2000, 2006, 2007; Audemard, *et al.*, 2000; among others); three active coastal lagoons were identified and explored: Bocaripo and Chacopata lagoons (split apart by coastal barriers) and the smallest of the three to the north, unnamed but identified for purposes of this investigation as Laguna del Morro Chacopata (*Figure 1*).

ìPotential sites of sampling on coastal lagoons were identified using satellite images. Fieldwork was performed by acquiring sediment samples and cores, prior opening of hand-excavated-pits on dry lagoon bottom using picks and shovels, and its preliminary lithological description. Furthermore, it took into account geomorphic parameters such as height of coastal barrier and the distance to the sea mouth.

RESULTS

A total of five samples and four undisturbed sediment cores (20 to 75-cm-long) were taken in the study area for radiocarbon dating and further detailed sedimentological analysis. Preliminary results show geological and sedimentological characteristics that might be associated with tsunamigenic or climatic events preserved in the sedimentary record of these coastal lagoons, which are described below.

Figure 1: Lagoons distribution and relative locations of sampling sites in the study area.

Bocaripo lagoon

It shows a very-fine grained sediment profile typical of lagoonal environment. However, behind the lagoon (to the southeast), at least two other ancient lagoon floodplains were observed (*Figure 2*). The first one, fairly narrow and separated by a coastal barrier from the active Bocaripo lagoon, shows a clay overlying a sandy bed, apparently an ancient spit, which represents a typical normal sequence of lagoonal environment. The second one, separated by three coastal barriers and topographically in higher position than the rest (± 1 m), shows under 10-cm-thick of reddish sand, a 30-cm-thick sequence of alternating reddish sand of <2 cm-thick with beige sandy-silt of varying thickness (3-12 cm), which could suggest the occurrence of successive tsunami events in the Holocene. Under these levels, typical clay sediments of lagoonal environments were

identified (*Figure 3*). According to ^{14}C dating, these events occurred after 960 ± 30 BC.

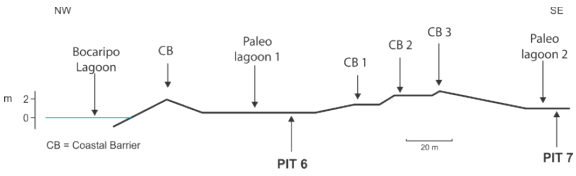

Figure 2: Schematic profile of Bocaripo lagoon and its paleolagoons, showing sampling sites.

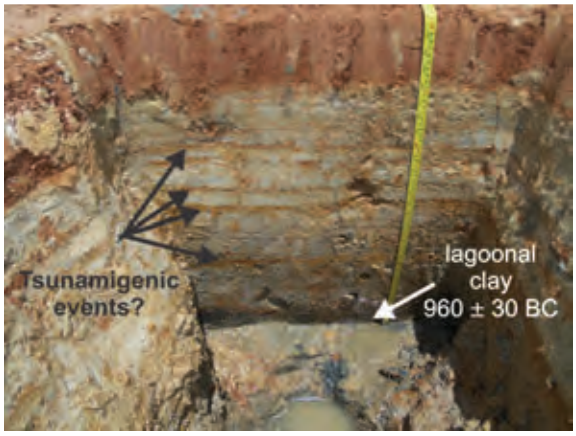

Figure 3: Wall of pit of paleolagoon 2 (Figure 2), showing potential tsunamigenic sands levels.

Chacopata lagoon

Two hand-excavated pits show basically clayey sequences, one of them shows under a 4-cm-thick dark brown sandy-clay, a 36-cm-thick layer mainly composed of molluscs Tivela mactroides and Melongena sp., suggesting a typical sequence of coastal lagoon environment.

Morro de Chacopata lagoon

Two hand-excavated pits show located 85 m from the coastline, show discontinuous 3-cm-thick blackish organic-matter-rich sandy layer is erosionally overlain by a sandy level exhibiting south-directed ripples and scattered small salt lenses (*Figure 4*), which might suggest a marine incursion.

These first results seem very promising to pursue further and more detailed research in the region, keeping all coastal lowlands, and particularly lagoons and saltflats, as potential natural environmental recorders of tsunamites.

PRELIMINARY CONCLUSIONS

Some sedimentological characteristics observed in Chacopata region may correspond to tsunami deposits (tsunamites) but more sampling lateral sites to find these layers are necessary to support this hypothesis.

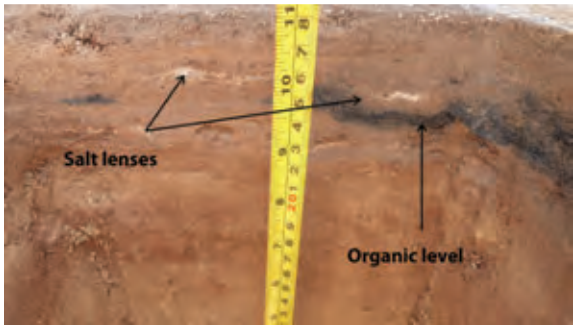

Figure 4: Wall of pit at Morro de Chacopata Lagoon, showing the irregular organic level and salt lenses.

According to the first dating, potentially tsunamigenic sediments could be or not could be associated with seismic events of seismic catalogs of Venezuela, due to its relatively short history seismic (500 years).

Acknowledgements: Authors wish to thank the Earth Sciences Department of FUNVISIS and Earth Sciences Institute (Institut des Sciences de la Terre –ISTerre-) of the Université de Savoie for logistic support and FONACIT-ECOS-Nord Project PI-2009000818 for finantial support.

References

Audemard, F., (1997). *Preliminary Geological Report on the Cariaco July 09th, 1997 Earthquake.* Sucre State. Northeastern Venezuela. Caracas. FUNVISIS. 2 pp.

Audemard, F., (1998). El sismo de Cariaco del 09 de Julio de 1997, Estado Sucre, Venezuela: Nucleación y Progresión de la Ruptura a partir de Observaciones Geológicas. *Congreso Latinoamericano de Geología*. *Memorias* (IX Congreso. Caracas, 1998).

Audemard, F., (1999). Nueva percepción de la sismicidad histórica del segmento en tierra de la falla de El Pilar, Venezuela nororiental, a partir de primeros resultados paleosísmicos. *VI Congreso Venezolano de Sismología e Ingeniería Sísmica*. Mérida. Venezuela. 10 pp (en CD).

Audemard, F., (2000). Major Active Faults of Venezuela. *31st International Geological Congress*. Rio de Janeiro. Brazil (extended abstract).

Audemard, F., M. Machete, J. Cox, R. Dart & K. Haller, (2000). Map and Database of Quaternary Faults in Venezuela and its Offshore Regions. *US Geological Survey Open-File Report.* 00-0018. Include map at scale 1:2.000.000 and 78-page report.

Audemard, F. (2006). Surface rupture of the Cariaco July 09, 1997 earthquake on the El Pilar fault, northeastern Venezuela. *Tectonophysics.* (424), pp. 19-39.

Audemard, F., (2007). Revised seismic history of the El Pilar Fault, Northeastern Venezuela, from the Cariaco 1997 earthquake and recent preliminary paleoseismic results. *Journal Seismology*. 11, Issue 3, pp 311-326.

Audemard, F., C. Beck, K. Leal, L. Scremín, J. Oropeza, E. Carrillo, I. Aguilar, A. Leal, C. Zorrilla & J.A. Rodríguez, (2011). Primeras evidencias geológicas de paleotsunami en el oriente venezolano, producto de sismos históricos locales, entre Cabo Codera y Cumaná. Resumen. *XIV Congreso Latinoamericano de Geología* y *XIII Congreso Colombiano de Geología*. Memorias. Medellín, Colombia. Pp. 163-164.

Grases, J., (1976). Tsunamis en el oriente venezolano. *Boletín Técnico Instituto de Materiales y Modernos Estructurales – IMME*. Facultad de Ingeniería. Universidad Central de Venezuela. Vol. 53. 1976.

Grases, J., R. Altez & M. Lugo, (1999). *Catálogo de sismos sentidos o destructores Venezuela 1530/1998.* Editorial Innovación Tecnológica, 1999. Serie: Facultad de Ingeniería, Universidad Central de Venezuela. Academia de Ciencias Físicas, Matemáticas y Naturales. pp. 654.

Leal, K. & L. Scremin, (2011). *Paleotsunamis en el registro geológico de Cumaná, estado Sucre, Venezuela oriental.* Trabajo especial de grado: Facultad de Ingeniería. Universidad Central de Venezuela. pp 204.

O'Loughlin, K. & J. Lander, (2003). *Caribbean Tsunamis. A 500-Year History from 1498-1998.* Kluwer Academic Publishers. Netherlands, pp. 263.

Oropeza, J., F. Audemard & C. Beck, (2013). Sedimentary record of paleotsunami on the coastal lagoons of northeastern Venezuela. *14eme Congres Francais de Sedimentologie.* Paris. France.

Schubert, C., (1977). La zona de falla de El Pilar: revisión y proyecto. *Boletín Técnico del Instituto de Materiales y Modelos Estructurales – IMME*. UCV. Caracas. pp. 11-23.

Singer, A., C. Rojas & M. Lugo, (1983). *Inventario nacional de riesgos geológicos.* Caracas. FUNVISIS. pp 128. Mapa; tablas.

Vierbuchen, R., (1984). The geology of the El Pilar fault and adjacent areas in northeastern Venezuela. *Geological Society of America*. Memoir 162. pp. 189-212.

INQUA Focus Group on Paleoseismology and Active Tectonics

paleoseismicity.org

Correlating magnetic susceptibility with *facies* changes within borehole cores on either sides of an active fault in Corinth Canal

Pallikarakis, A. (1), Grützner, C. (2), Mason, J. (3), Schneiderwind, S. (3), Papanikolaou, I. (1), Triantaphyllou, M. (4), Migiros, G. (1)

(1) Laboratory Mineralogy - Geology, Agricultural University of Athens, Iera Odos 75, Athina 118 55, Greece. Email: pallikarakisagg@yahoo.gr
(2) Department of Earth Sciences, University of Cambridge, Madingley Rise, Madingley Road, CB3 0EZ Cambridge, UK
(3) Institute of Neotectonics and Natural Hazards, RWTH Aachen University, Lochnerstr. 4-20, 52064 Aachen, Germany
(4) Hist. Geology-Paleontology Department, Faculty of Geology and Geoenvironment, National and Kapodistrian University of Athens, Panepistimiopolis 15784, Athens, Greece

Abstract: *Corinth Gulf is one of the fastest expanding regions worldwide, influenced by several major normal faults. We measured the magnetic susceptibility within boreholes, drilled at the footwall and hanging-wall of the Kalamaki fault, a secondary structure that intersects the Corinth Canal. We correlate magnetic susceptibility (MS) measurements with paleoenvironmental and lithological alternations within the boreholes. We have ascribed low MS values to marine highstand deposits and high MS values to lowstand terrestrial deposits. Glacioeustatic sea level changes and tectonic movements have led to a very complicated* lithosedimentary *pattern, and magnetic susceptibility (MS) measurements can help us interpret the fault's activity.*

Key words: *Corinth Gulf, magnetic susceptibility, paleoenvironment, active fault.*

INTRODUCTION

The Corinth region is influenced by active normal faults up to 20 km length, such as the Kechriaie, South Alkyonides Fault System (SAFS) and Loutraki Faults (Fig. 1); the area is also affected by more distal structures such as the Xylokastro and Agios Vasillios faults (e.g. Roberts et al., 2009).

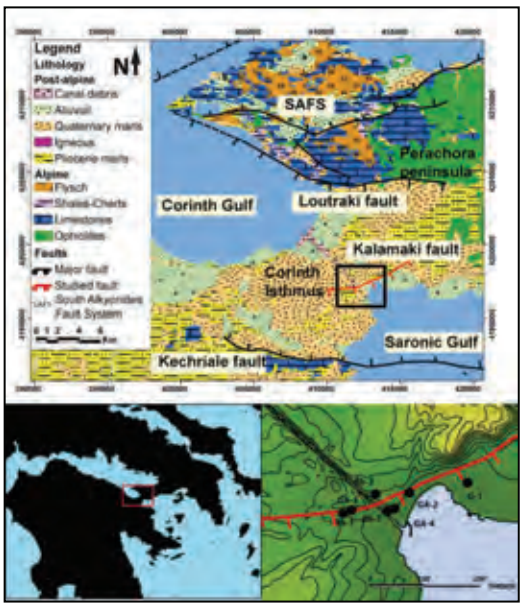

Figure 1: a) Simplified geological map showing the major faults; the studied active fault is highlighted in red (modified from Papanikolaou et al., (In press)). b) Boreholes location at the footwall and hanging-wall of the Kalamaki fault.

Shorter normal faults located at the Canal have also affected the topography displacing Plio-Pleistocene sediments. Currently, the entire Isthmus undergoes uplift controlled by the major faults north of the Perachora peninsula (Fig. 1). The easternmost Corinth Gulf mostly consists of alluvial sequences, Plio-Pleistocene sediments, Flysch, Mesozoic limestone and Ophiolites. Glacioeustatic sea level changes and/or tectonic movements have led to a complicated lithosedimentary pattern with alternating marls, sands and gravels (Collier & Thomson, 1991; Collier & Dart, 1991). Collier et al. (1992) identified six marine transgressive cycles in the Corinth Canal section up to 90 m above present day sea level. The sediments forming the Isthmus are of Pleistocene age (e.g. Freyberg, 1973). The Corinth Canal offers a unique opportunity to study the faults in the area. Most of these faults do not displace the topography and are of limited length; therefore they are considered as secondary structures with low slip-rates. Towards the eastern tip of the Canal we traced a significant structure, the Kalamaki Fault (Papanikolaou et al., 2014). The Kalamaki Fault is ENE-WSW trending, dips towards the SSE and displaces the modern ground surface. Our aim is to compare the magnetic susceptibility of the cores with the changes in the paleoenvironment and identify if and how they are corellated.

METHODOLOGY

The magnetic susceptibility (MS) of sediments depends mostly on mineral composition and grain size (e.g., Mullins 1997, Oldfield, 1991, Da Silva et al., 2009, Reicherter et al., 2010). In general, iron bearing minerals

lead to high values of MS (dimensionless SI units). Terrestrial deposits are often characterized by higher amounts of such minerals compared to marine sediments; therefore MS measurements can help to distinguish between different sedimentary environments. For our study we used the Bartington MS2 system with the MS2K sensor (see also Reicherter et al., 2010).Pallikarakis et al. (2013, 2014) and Papanikolaou et al. (In press) described and analyzed ten borehole cores focusing on the micropaleontological content. Alternations of clay, sand, and gravels were encountered and the paleoenvironmental conditions varied from fluvial-terrestrial to marine. No lacustrine deposits were found. The paleoenvironment was grouped into six categories:

- Fluvial-terrestrial deposits (F) representing torrential events consisting mostly of well-rounded gravels and to a lesser degree sand;
- Coastal (Co) rounded sands and fine gravels representing foreshore paleoenvironment;
- Shallow (less than 30 m depth) marine (M) shoreface deposits of fine sands and clays;
- Shallow marine gravels and sands with mesohaline features (SM) influenced by freshwater input. This suggests that the paleoenvironment was probably closer to the coast and shallower than (c);
- Lagoonal (L) clays, fine sands and rare gravels indicating a very shallow and closed marine paleoenvironment;
- Brackish-Oligohaline (Br), which consists of clay and fine sand and is similar to a lacustrine environment.

Based on these descriptions, we correlated the lithology and the paleoenvironment within the boreholes with the MS measurements. The MS measurements were taken in the laboratory every 2 cm along each core or by calculating the average value if the sample was in a sample bag. In total, approximately 1000 MS measurements were carried out on 8 different borehole cores.

RESULTS

Our data show a clear difference between marine and terrestrial sediments. Higher values are measured at gravely layers, while clayey and sandy layers have less magnetic susceptibility.

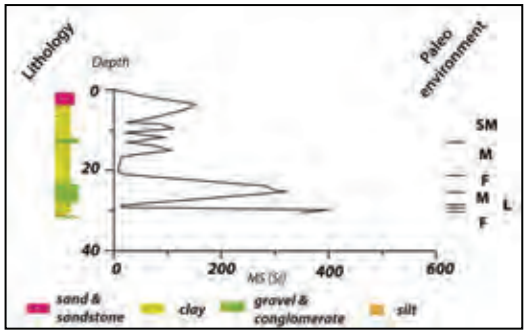

Figure 2: Borehole Bh-1. Two MS peaks values are traced on two gravely layers at the lower part of the borehole. These layers are described as fluvial-terrestrial.

Ophiolite clasts within the sediments are responsible for higher values, since they contain magnetic minerals. In the following paragraph, we describe the lithology and the MS for each drill core (Figs. 2-9). Bh-1 core is characterized as shallow marine with mesohaline features, apart from a layer at 23 to 27 m depth. MS measurements range from 5 - 267 SI. The lower part of the core is characterized by higher MS values. In Bh-3 three distinctive alternations of marine to terrestrial environment are described. MS values range from 1 to 207 SI and follow the changes of the described environment. In Bh-7 we found two distinctive alternations of marine to terrestrial environment, where MS values range from 1 to 227 SI.

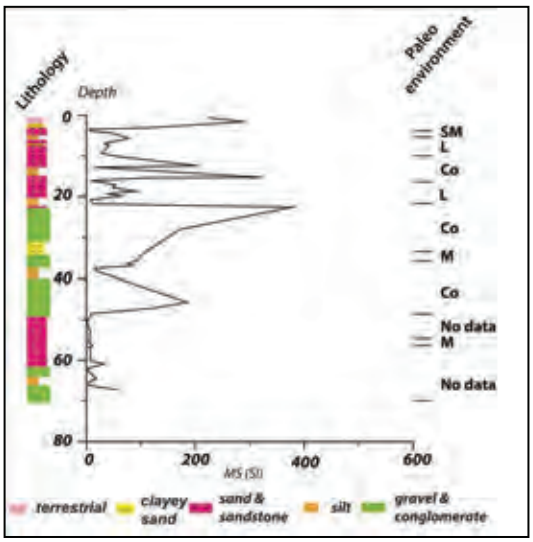

Figure 3: In Bh-3 four MS peak values were traced. These four peaks involve the top-soil consisting terra rosa, a sandy layer and two gravelly layers described as coastal.

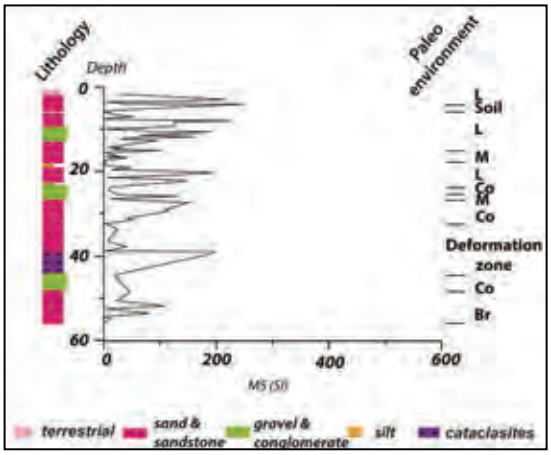

Figure 4: In borehole Bh-7 measurements MS values range from 1 to 227 SI. The highest MS values were measured in coastal environments and at the fault's deformation zone.

The lower section of GA-2 core is characterized by a brackish oligohaline environment, while the upper part represents a shallow marine depositional environment. MS measurements in the upper part range from 1 to 97 SI, while the brackish layer has values of 7 to 9 SI.

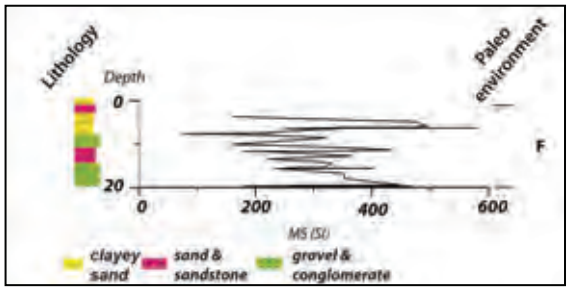

Figure 5: In G-1 the entire core is described as fluvial terrestrial with MS measurements ranging from 75 to 582 SI.

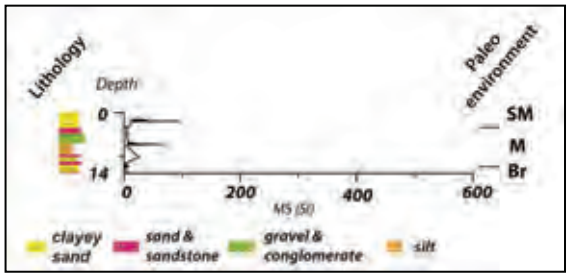

Figure 6: Borehole GA-2. Low MS values are ascribed to a marine and brackish environment.

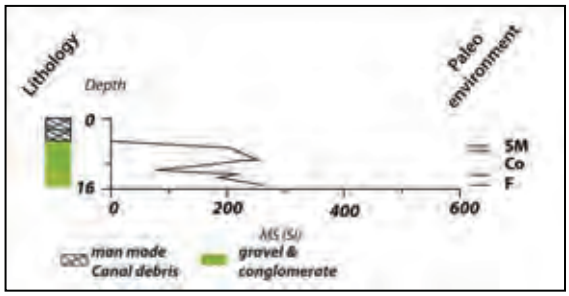

Figure 7: In shallow marine environment we have described generally low MS values (1 -70 SI). However, in borehole GA-3 we can have high MS values (up to 230 SI).

The lower part of GA-3 core is characterized by a fluvial environment which changes upward to coastal and then to shallow marine. MS measurements at the lower fluvial part range from 184.5 to 262; then from 75.5 to 253.5 for the coastal part; while the upper shallow marine part ranges from 97 to 312. The high values in the shallow marine part are GA-4 is characterized by sedimentary environments of lagoonal, shallow marine, shallow marine with mesohaline features, and also coastal and fluvial environments. MS measurements in lagoonal sediments range from 3 to 70 SI, in coastal sediments from 50 to 162 SI, in shallow marine sediments from 1 to 62 SI, in fluvial from 126 to 442 SI and in shallow marine with mesohaline features from 2 to 343 SI. In GA-5 the environment is characterized by coastal, shallow marine to shallow marine with mesohaline features and lagoonal. MS values in the lagoonal environment range from 8 to 12 SI, in shallow marine from 3 to 20 SI, in coastal from 19 to 322.5 and in shallow marine with mesohaline features from 21 to 424 SI.

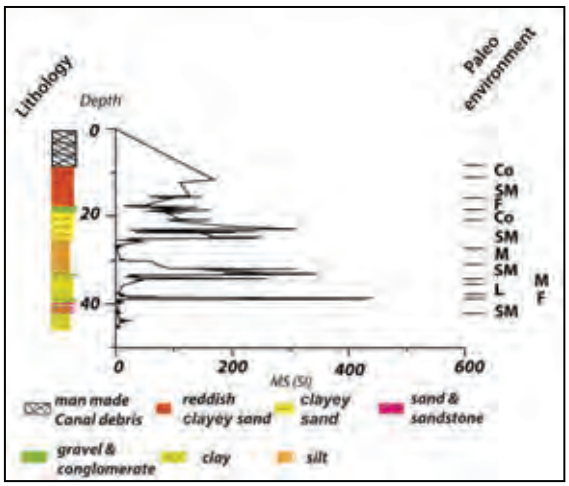

Figure 8: In borehole GA-4 three MS peak values were traced in horizons, characterized as fluvial or coastal.

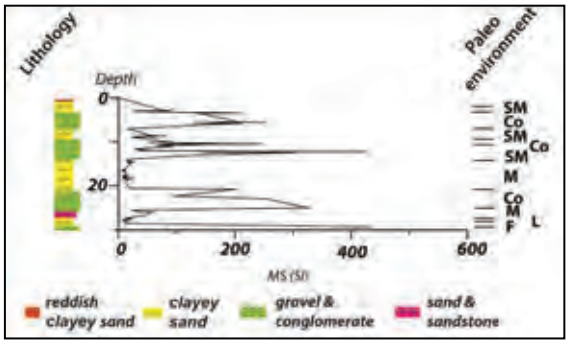

Figure 9: In borehole GA-5 three MS peak values were traced, characterized as fluvial or coastal.

DISCUSSION AND CONCLUSIONS

MS measurements exhibit a clear difference between marine and terrestrial sediments. Shallow marine layers with mesohaline features were influenced by fresh water. High diversity within these layers is due to the fact that gravels were transported by torrential rainfall events. Shallow marine sediments have clearly less MS ranging from 1 to 70 SI. Lagoonal sediments have a unique imprint as well. In lagoonal sediments, MS signal range from 3 to 70 SI and mostly less than 30 SI. However in Bh-7, lagoonal sediments contain clasts which affect the MS signal and higher MS values were measured. Coastal layers range from 4 to 253 SI, as they mostly consist of transported

rounded clasts and grains. Gravely sediments have a distinct imprint with values ranging from 12 to 164 when the clasts consist of limestone or 75 to 582 when the clasts consist of Ophiolites.

Ophiolite clasts within the fluvial terrestrial deposits lead to higher MS measurements. These clasts most likely originate from the Gerania Ophiolite nappes (Fig. 2) and could indicate higher erosional rates and transfer capacity. Therefore we suggest that these fluvial terrestrial sediments should have been transferred and deposited during the Glacioeustatic lowstand, when the area was emerged. During emergence we have higher erosion rates and thus high mobility and re-sedimentation of lowstand clasts of predominately ophiolitic origin. We suggest that there is a relationship between Ophiolite gravely layers with high MS and with glacioeustatic lowstand fluvial deposits.

By correlating marine sediments with glacioeustatic sea level highstands and terrestrial sediments with glacioeustatic lowstands, it is clear that we have alternations of highstand and lowstand deposits within the boreholes. The highly complicated paleoenvironment described within the boreholes characterizes the interrelationship of glacioeustatic sea level changes and tectonic movements. Although the Kalamaki Fault has a relatively limited length of only 5,5 km, it has undoubtedly influenced the lithological processes in the Pleistocene. As the fault controls the topography of the eastern part of the Canal with an elevation of up to 150 m, it can affect the local drainage system and its sediment supply. We suggest that the presence of the fluvial Ophiolite clasts layer, which is traceable in most of the boreholes, is partially affected by the fault's activity. Questions rise though concerning the influence of the fault. In which extend has Kalamaki fault influence the sedimentation procedures? Further analysis will help us distinguish fault's input.

Papanikolaou et al. (in press) correlated lagoonal horizons from boreholes Bh-3 and Bh-7 to estimate the fault's mean slip rate at this site. By correlating the known uplift rate of the area as estimated by Collier et al. (1992) and the glacioeustatic sea level curve by Siddall et al. (2003), the age of these sediments is approximately at 175 ka or older if major erosional processes have occurred. The authors implied a 0.04 ±0.02 mm/yr mean slip rate for this period since the offset between these layers is 4.5±0.4 m. MS measurements confirmed the connection between these two layers. Borehole Bh-7 has poor correlation, however the transition from marine to terrestrial is pretty evident. The transition from low MS values to high MS values in boreholes Bh-3 and Bh-7 located on fault's footwall and hangingwall respectively, has an offset of 6.1±0.4 m. According to this offset the fault's mean slip rate for the same period is higher, at 0.05±0.02 mm/yr. Papanikolaou et al. (in press), is based on foraminiferal assemblages to estimate fault's slip rate, while this paper is based on MS values. Each methodology is independent with each other and either through paleoenvironmental analysis or MS values, Kalamaki fault is an active but low slip rate fault. MS measurements refine the interpretation of the drill cores, thus leading to a better understanding of the tectonic movements relative to sea level. MS is a useful tool for future studies in similar environments, when drill cores are available or other kinds of outcrops allow for MS measurements.

Acknowledgements: The Academy of Athens scholarship fund is thanked for support.

References

Collier, R.E.L., C.J. Dart, (1991). Neogene to Quaternary rifting, sedimentation and uplift in the Corinth Basin, Greece. *Journal of the Geological Society*. 148, 1049-563 1065, doi:10.1144/gsjgs.148.6.1049.

Collier, R.E.L., J. Thompson, (1991). Transverse and linear dunes in an upper Pleistocene marine sequence, Corinth Basin, Greece. *Sedimentology*. 38, 1021-1040.

Collier, R.E.L., R.M. Leeder, P. Rowe, T. Atkinson, (1992). Rates of tectonic uplift in the Corinth and Megara basins, Central Greece. *Tectonics*. 11, 1159-1167.

Da Silva, A.C., K. Potma, J.A.W. Weissenberger, M.T. Whalen, M. Humblet, C. Mabille, & F. Boulvain, (2009). Magnetic susceptibility evolution and sedimentary environments on carbonate platform sediments and atolls, comparison of the Frasnian from Belgium and Alberta, Canada. *Sed. Geol*. 214, 3-18.

Freyberg, V., (1973). *Geologie des Isthmus von Korinth*. Erlanger Geologische Abhandlungen. Heft 95. Junge und Sohn. Universitätsbuchdruckerei Erlangen. 183 pp (in German).

Mullins, C.E., (1977). Magnetic susceptibility of the soil and ist significance in soil science - a review. *Journal of soil science*. 28 (2), 223-246.

Oldfield, F., (1991). Environmental magnetism - a personal perspective. *Quaternary Science Reviews*. 10 (1), 73-85.

Pallikarakis, A., I. Papanikolaou, M. Triantaphyllou, (2013). Paleoenvironmental analysis and active faults in the area between the Corinth and Saronikos Gulfs. *Seismic hazard, critical facilities and slow active faults. Proceedings of the 4th International INQUA meeting on Paleoseismology, Active Tectonics and Archeoseismology (PATA Days*). 10/2013; 4 (1), 177-180.

Pallikarakis, A., I. Papanikolaou, M. Triantaphyllou, K. Reicherter, (2014). Paleoenvironmental & Paleomorphological interpretations, through foraminiferal assemblages in an active tectonic environment. *European Geosciences Union General Assembly 2014*. Vienna, Austria.

Papanikolaou I.D., M. Triantaphyllou, A. Pallikarakis G. Migiros, (In press). Active faulting at the Corinth Canal based on surface observations, borehole data and paleoenvironmental interpretations. Passive rupture during the 1981 earthquake sequence? *Geomorphology*. doi: 10.1016/j.geomorph.2014.10.036.

Reicherter, K., D. Vonberg, B. Koster, T. Fernández-Steeger, C. Grützner, M. Mathes-Schmidt, (2010). The sedimentary inventory of tsunamis along the southern Gulf of Cádiz (southwestern Spain). *Zeitschrift für Geomorphologie*. Supplementbände Volume 54. Supplementary Issue 3, p. 147 -173.

Roberts, G.P., S.L. Houghton, C. Underwood, I. Papanikolaou, P.A. Cowie, P. van Calsteren, T. Wigley, F.J. Cooper, and J.M. McArthur, (2009). Localization of Quaternary slip rates in an active rift in 105 years: An example from central Greece constrained by 234U-230Th coral dates from uplifted paleoshorelines. *Journal of Geophysical Research*. 114, B10406, doi:10.1029/2008JB00058.

Siddall, M., E.J. Rohling, A. Almogi-Labin, C. Hemleben, D. Meischner, I. Schmelzer and D.A. Smeed, (2003). Sea-level fluctuations during the last glacial cycle. *Nature*. 423, 853 - 858.

INQUA Focus Group on Paleoseismology and Active Tectonics

paleoseismicity.org

Study of an active fault at the eastern tip of the Corinth Canal, through surface and borehole data

Pallikarakis, A. (1), Papanikolaou, I. (1), Triantaphyllou, M. (2), Reicherter, K. (3), Migiros, G. (1)

(1) Laboratory Mineralogy - Geology, Agricultural University of Athens, Iera Odos 75, Athina 118 55, Greece.
Email: pallikarakisagg@yahoo.gr
(2) Hist. Geology-Paleontology Department, Faculty of Geology and Geoenvironment, National and Kapodistrian University of Athens, Panepistimiopolis 15784, Athens, Greece
(3) Institute of Neotectonics and Natural Hazards, RWTH Aachen University, Lochnerstr. 4-20, 52064 Aachen, Germany

Abstract: *Kalamaki fault is a secondary structure that intersects the eastern tip of Corinth Canal but is the most important active fault that crosses it. Our aim is to study the fault in detail, involving detailed mapping, borehole data analysis and paleoenvironmental interpretations. Samples taken both from boreholes and surface outcrops were analysed and described regarding their micropaleontological content and paleoenvironmental changes in the sequence. Data show a very complex sedimentological and paleoenvironmental pattern that involves subaerial exposure, fluvial-terrestrial, lagoonal, shallow marine environments and possibly even some lake sediments. Even though that our analysis shows that it is a slow slip-rate fault it has affected the geomorphology of the area.*

Key words: *Corinth Gulf, Paleoenvironment, Boreholes, Foraminifera.*

INTRODUCTION

Northern Peloponnese is uplifting up to 1.5-2 mm/year towards its center that diminishes to 0.3 mm/year towards its eastern end (e.g. Armijo et al., 1996; Collier et al., 1992). This is caused by regional uplift and by the activity of major fault structures. The eastern tip of the Gulf is controlled by faults such as the Kechriaie, the South Alkyonides Fault System (SAFS), the Loutraki, and the Agios Vasillios faults (Fig 1). Our study area lies towards the eastern tip of the Corinth Canal, a 6.3 km long infrastructure which offers a unique opportunity to study the sediments and the faults that offset them. Most of them are normal faults but do not intersect the late Pleistocene strata, do not displace the topography and are of limited length, therefore are considered as active secondary structures with low slip-rate (e.g. Freyberg, 1973). However, towards the eastern tip of the Canal we traced a significant ENE–WSW trending fault, dipping at 60°–65° towards the SSE, it offsets Middle and Upper Pleistocene sediments and bounds alluvial deposits that are located on its hangingwall (Papanikolaou et al. in press). This fault is studied in detail through surface observations and borehole cores.

STUDY AREA

Detailed mapping & Surface Observations

Our detail mapping (1:5000) shows that the Kalamaki fault has limited length of approximately 5.5 km. It controls the topography of the area, producing up to 150 m offset towards its center (Figs 2,3). The Kalamaki fault offsets Upper to Middle Pleistocene sediments. We identified and described a complicated lithology at fault's footwall. The upper part consists mainly of alternations of sandstones, marls and gravely layers. The lower part consists mainly of marls and mudstones. The central part of the footwall's fault is covered by talus cones. The drainage system has partially eroded the sediment and has re-sediment gravel and sand.

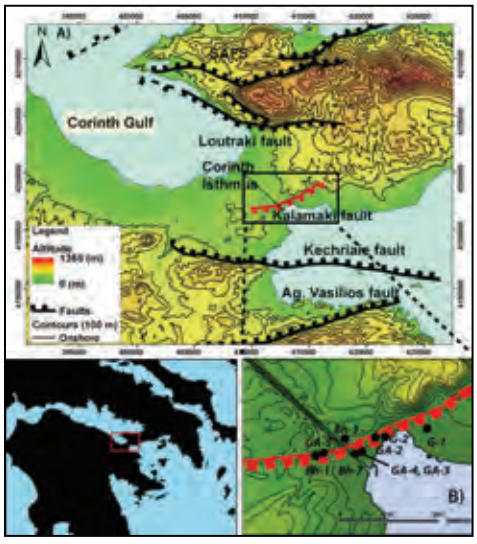

Figure 1: A) DEM of the eastern part of Corinth Gulf showing the major faults; the studied active fault is highlighted in red. B) The area where the boreholes are located.

Fault's hangingwall is covered by an alluvial fan. More than 100 measurements were taken, in order to study the inclination of the strata. Towards its central part the upper layers dip at 5° to 10° towards NNW, while the lower layers at 20° to 35° towards NNW. Layers towards the center of the fault dip at 35° while these closer to its tip at 5° to 15° to the NNW. Approximately 70 samples were taken for micropaleontological analysis.

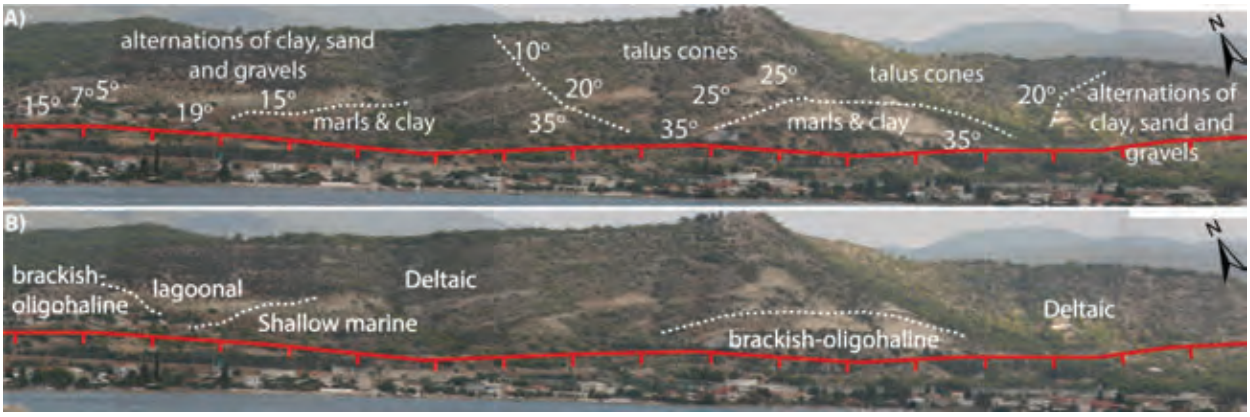

Figure 2: Photomosaic of the study area showing the central part of the fault's footwall. A) Sedimentological description and strata inclination, dipping towards NNW. B) Paleoenvironmental interpretation through foraminiferal assemblages.

Several tectonic structures were identified. More than 50 measurements were extracted from fractures and the fault's plane. The main fault strikes at ~075° and dips approximately at 60° to 70° towards the SSE.

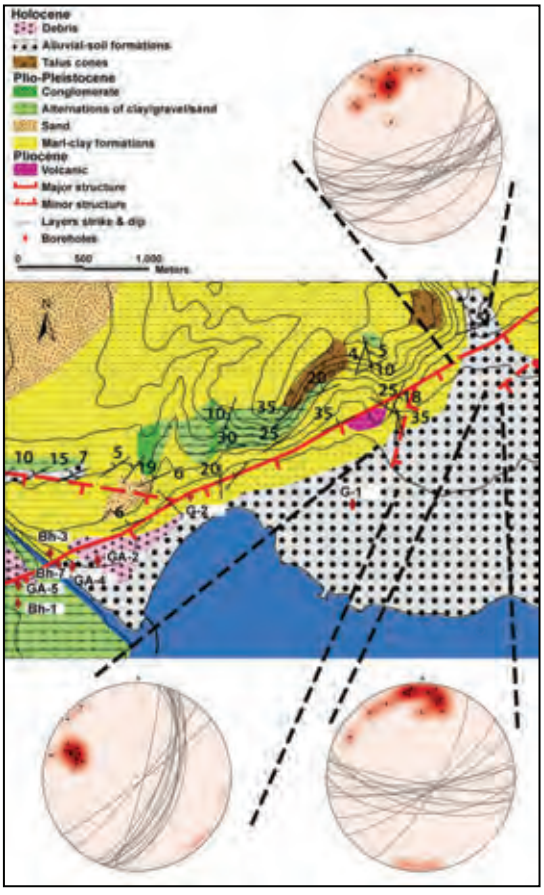

Figure 3: Geological map showing the Kalamaki and neighboring faults, while the stereonets showing faults' dip and strike. (modified from Bornovas et al., 1972, 1984, Collier, 1990, Gaitanakis et al., 1985, Papanikolaou et al., 1989, 1996, in press).

Southwards of the Canal the fault plane trends at ~070° and dips at 70° towards SSE. A minor structure (Fig. 3) is traced north of the main fault plane (Collier, 1990). It strikes at approx. 100° and dips at 60° to 70° towards SSE. Unfortunately, human infrastructures have heavily disturbed the natural terrain and it was not possible to identify a clear fault plane northwards the Canal, apart from several fractures, striking at 60° - 80° and dipping at 50° - 80° towards SSE. A minor structure was described to the northern part of the fault (Fig. 3). It strikes approx. at. 040° and dips towards SE. It has affected the inclination of the sediments which dip towards SE.

Borehole data

Samples from 9 boreholes which were drilled on either side of the Kalamaki fault, were examined for the micropaleontological content. Approximately 290 m of cores were examined and 250 samples were taken Fig. 4).

Figure 4: Samples from the drilled cores. (A) Borehole GA-4 from 18.30 m till 19.20 m, showing the transition from fluvial (gravels) to marine (silt). (B) Borehole GA-4 from 33.00 m to 33.90 m, showing the transition from gravels to sitly sand. (C) Borehole GA-5 from 28.60 m to 29.70 m, showing the transition from marine (clayey sand) to fluvial gravels.

We described alternations of sand, clay, clayey sand, conglomerate, marl, fractions of limestone, even topsoil within the borehole cores. We encountered the same complicated lithological pattern within the boreholes and through surface mapping. There is a poor correlation among these layers. The latter indicates that there are major lateral alternations and stratigraphic variations (Figs. 5, 6).

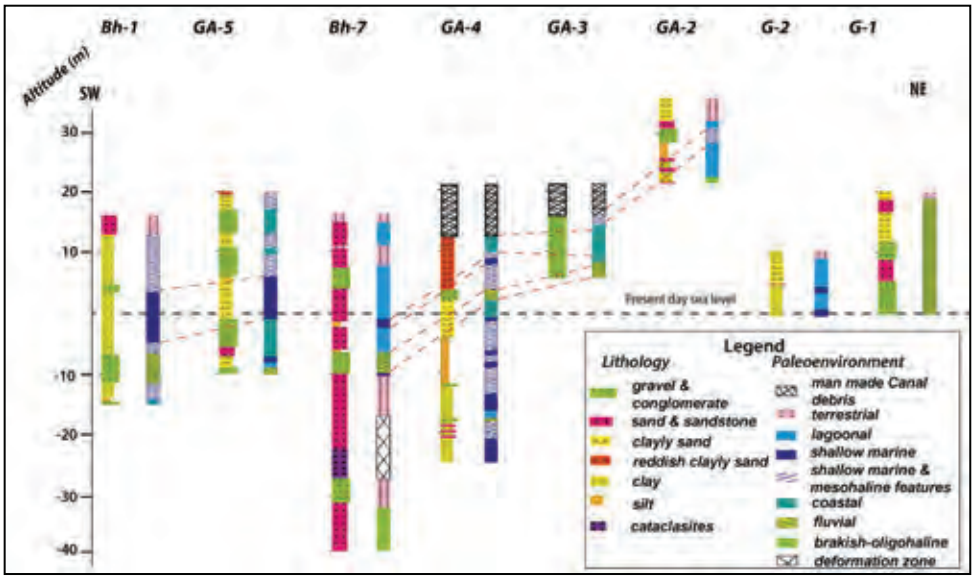

Figure 5: Most of the boreholes were drilled at the immediate hangingwall of the fault. Even to neighboring boreholes, there is a poor correlation showing the complexity of the sedimentological and paleoenvironmetal pattern.

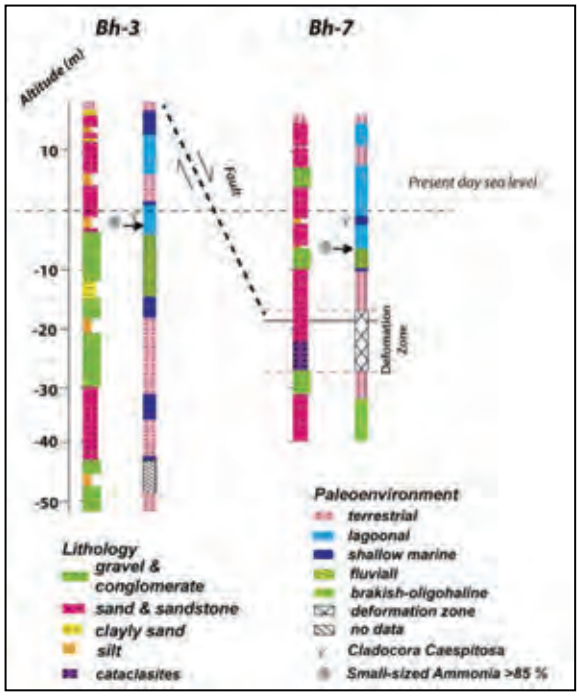

Figure 6: Borehole Bh-3 was the longest one and the only core which was drilled at fault's footwall.

A series of different depositional environments were recognized through micropaleontological analysis of the benthic foraminiferal fauna (e.g. Triantaphyllou et al., 2003). Samples taken from the fault's footwall were also examined for their micropaleontological content. We have identified mainly lagoonal, brackish-oligohaline and fluvial terrestrial paleoenvironments.

Within borehole Bh-1 we identified mainly alternations of lagoonal with shallow marine sediments, interrupted by a fluvial-terrestrial layer. Paleoenvironment in borehole Bh-3 is more complicated. We identified several alternations of shallow marine to lagoonal sediments, interrupted by terrestrial or fluvial terrestrial sediments. It is important to mention that approximately at 21 m depth we found a *Cladocora Caespitosa* corals colony in *situ* and at 22 m depth a lagoonal layer with abundant small size *Ammonia*. Within borehole Bh-7, we identified the same complicated paleoenvironmental pattern as in Bh-3. We described several alternations of shallow marine to lagoonal sediments, interrupted by terrestrial or fluvial sediments. Likewise with borehole Bh-3, we found at 18 m depth a *Cladocora Caespitosa* corals colony in *situ* and at 24 m depth a lagoonal layer abundant at small size Ammonia. From 33 to 45 m depth we found fault's deformation zone with alternations of cataclastites and fragments of limestones. The end of Bh-7 was described as a brackish-oligohaline paleoenvironment due to the presence of ostracods (*Cyprideis* spp.). The entire borehole G-1 was described as terrestrial - fluvial environment. Borehole G-2 was characterized mainly as lagoonal paleoenvironment interrupted by thin layers of shallow marine paleoenvironment. Borehole GA-2 was described as lagoonal to shallow marine with mesohaline features. At the end of the borehole we identified a brackish-oligohaline paleoenvironment, containing ostracods. In borehole GA-3 we identified a shallow marine with mesohaline features to coastal environment.

The end of the borehole is characterized as fluvial terrestrial environment.

Borehole GA-4 was characterized as shallow marine to lagoonal or coastal, interrupted by fluvial sediments at 18 to 21 m depth and at 34 to 37 m depth. In borehole

GA-5 we identified alternations of coastal to shallow marine with mesohaline features and shallow marine environments. At the end of borehole we described a fluvial environment.

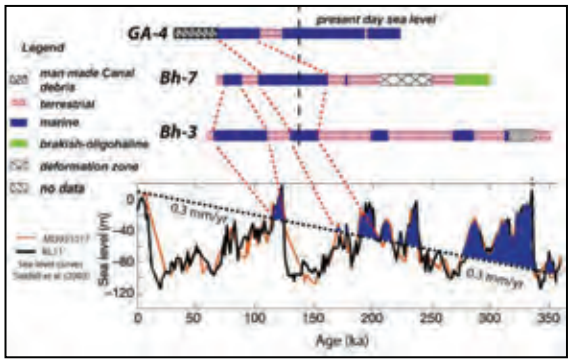

Figure 7: Simplified paleoenvironment in boreholes Bh-3, Bh-7 and GA-4, sea level curve from Siddall et al. 2003 and the expected depositional environment based on the 0.3mm/yr uplift rate from the neighboring dated corals of Collier et al. (1992). Expected marine environments are highlighted with blue.

DISCUSSION

- By correlating marine sediments with glacioeustatic sea level highstands and terrestrial sediments with glacioeustatic lowstands, we imply that we have alternations of highstand and lowstand deposits within the boreholes. If we correlate the known uplift rate of the area (0.3 mm/yr according to Collier et al., (1992)), with global sea level change from Siddall et al., (2003), we can imply the relative dates of the sediments (Fig 7). We expect that age of the marine sediments of the boreholes are probably at 125 ka, at 175 ka, 200 ka, while within the deepest boreholes (Bh-3 and Bh-7) probably even at 240 ka and 300 ka).
- Samples from fault's footwall, indicated that the lower layers (marl formation) were brackish oligohaline. Above these layers we identified marine sediments ranging from lagoonal to shallow marine sediments, while the upper layers were described as deltaic.
- Correlating these results with the paleoenvironments within the boreholes is a difficult process considering all complexities involved. We can suggest though that the lower brackish-oligohaline (lacustrine) sediments are the "Corinth Marl" formation, which is also lacustrine paleoenvironment (e.g. Westaway, 1996). Fault's activity has uplift and has revealed this formation towards its center, where the slip rate is higher.
- Kalamaki fault is an active syn-sedimentary structure that offsets Pleistocene sediments and controls the morphology of the eastern part of the Canal with an elevation of up to 150 m. Detailed mapping has shown that the upper layers towards fault's center dip at lower angle than the lower part. The latter indicates that this fault was highly active during sedimentation. The same occur among the layers of the central part of the fault and its tip, which indicates that the backtilting is controlled by the slip-rate variability from the center to the fault tip (Papanikolaou et al. in press).
- The complicated paleoenvironmetal pattern is the result of the interplay between the glacioeustatic sea level changes and the tectonic movements. However, distinguishing among these two factors is a difficult task. Surface observations combined with the borehole cores have shown major lateral sedimentological and paleoenvironmetal variations not only along strike the fault, but also across strike.

Acknowledgements: The Academy of Athens scholarship fund is thanked for support.

References

Armijo, R., B. Meyer, G.C.P. King, A. Rigo, D. Papanastassiou, (1996). Quaternary evolution of the Corinth Rift and its implications for the Late Cenozoic evolution of the Aegean. *Geophys. J. Int*. 126, 11-53.

Bornovas, J., N. Lalechos, and N. Filipakis, (1972). *1:50.000-scale geological map, Sheet-Korinthos*. Institute of Geology and Mineral Exploration.

Bornovas, J., P. Gaitanakis, A. Spiridopoulos, (1984). *1:50.000-scale geological map, Sheet-Perachora*. Institute of Geology and Mineral Exploration. Athens.

Collier, R.E.L., (1990). Eustatic and tectonic controls upon Quaternary coastal sedimentation in the Corinth Basin, Greece. *J. geol. Soc. London*. 147, 301-314.

Collier, R.E.L., R.M. Leeder, P. Rowe, and T. Atkinson, (1992). Rates of tectonic uplift in the Corinth and Megara basins, Central Greece. *Tectonics*. 1159-1167.

Freyberg, V., (1973). *Geologie des Isthmus von Korinth*, Erlanger Geologische Abhandlungen. Heft 95. Junge und Sohn. Universitätsbuchdruckerei Erlangen. 183 pp (in German).

Gaitanakis, P., A. Mettos, and M. Fytikas, (1985). 1:*50.000 scale geological map, Sheet "Sofikon"*. Institute of Geology and Mineral Exploration.

Papanikolaou, D., G. Chronis, V. Lykousis, P. Pavlakis, G. Roussakis, and D. Syskakis, (1989). *1:100.000 scale, Offshore Neotectonic Map the Saronic Gulf*. Earthquake Planning and Protection Organization. National Centre for Marine Research. University of Athens.

Papanikolaou, D., E. Logos, S. Lozios, and Ch. Sideris, (1996). *1:100.000 scale Neotectonic Map of Korinthos Sheet*. Earthquake Planning and Protection Organization. Athens.

Papanikolaou I.D., M. Triantaphyllou, A. Pallikarakis G. Migiros, (in press). Active faulting at the Corinth Canal based on surface observations, borehole data and paleoenvironmental interpretations. Passive rupture during the 1981 earthquake sequence? *Geomorphology*. doi:10.1016/j.geomorph.2014.10.036.

Triantaphyllou, M.V., K. Pavlopoulos, Th. Tsourou, & M.D. Dermitzakis, (2003). Brackish marsh benthic microfauna and paleoenvironmental changes during the last 6.000 years on the coastal plain of Marathon (SE Greece). *Rivista Italiana Paleontologia et Stratigafia*. 109 (3), 539-547.

Siddall, M., E.J. Rohling, A. Almogi-Labin, Ch. Hemleben, D. Meischner, I. Schmelzer, and D.A. Smeed, (2003). Sea-level fluctuations during the last glacial cycle. *Nature*. 423, 853 - 858.

Westaway, R., (1996). Quaternary elevation change in the Gulf of Corinth of central Greece. *Philos. Trans. R. Soc. London*. Ser. A 354, 1125-1164.

INQUA Focus Group on Paleoseismology and Active Tectonics

paleoseismicity.org

A contribution to environmental studies of the Fucino area from the historical archive of the Geological Survey of Italy

Pantaloni, M., Console, F., Perini, P.

ISPRA, Via V. Brancati, 48, 00144 Rome, Italy. Email: marco.pantaloni@isprambiente.it

Abstract: *The Fucino Plain is one of the most important Central Apennines intermountain basins; originated by tectonic subsidence, the plain is filled by fluvial, lacustrine and glacial continental sediments settled from Pliocene to the recent. Until the second half of 1800 the plain hosted the Fucino lake, which was subject to a long and complex land reclamation activity. The analysis of historic data, realized by Lotti, Montanari and Olivieri that have been found in the archives of the Geological Survey of Italy, and the comparison of these data with topographic measurements performed immediately after the January 1915 earthquake, could allow to obtain new insights about the topographical variations induced by the seismic event. In addition, the analysis of ground effects highlighted by scientists in 1915, shows a good agreement with the observations made by Lotti and co-authors and the geological characterization of the Fucino plain territory.*

Key words: *Fucino Plain, Lake Fucino, land reclamation, topography, coseismic effects.*

HISTORY OF THE FUCINO LAND RECLAMATION

The Fucino plain is a subsiding endoreic area of tectonic origin. The sedimentation process in the plain, despite the difficulty in chronological attributions, began during the Pliocene?-Pleistocene (Centamore et al., 2006; Zarlenga, 1987) and reaches a maximum deposition thickness of 1000 m (Cavinato et al., 2002). The plain is surrounded by the Velino-Sirente Massif and by Marsica Mountains.

The Fucino plain was occupied by a lake related to a karst system that collected waters of the Giovenco river, its main tributary. Before the land reclamation, the regulation of the hydrological regime was held by the intermittent activity of karst channels mainly located in the western sector; the lack of natural outflowing streams caused a high variability in water level that was linked, above all, to the precipitation and insolation regime related to the orbital parameters of the Earth (Giraudi, 1988; 1989). Brisse & De Rotrou (1876) show lake level fluctuation starting from the end of 18th century: it's worth of note that in the period 1783-1835 took place an increase about 10 m and a decrease of about 13 m due to natural causes. During flood episodes the water invaded part of the flat areas, in particular between Ortucchio and Venere dei Marsi.

Figure 1: Hydraulic drain system for the Fucino land reclamation (Lotti et al., , 1915-1916).

In Roman times, owing to these fluctuations in the lake level, hydraulic interventions aimed to regulate the water level were carried out. The Emperor Claudio, in 52 AD, built a system of channels and tunnels that drained water towards the Liri river; the lack of maintenance of drainage tunnels and some landslides on Salviano Mount slopes made no more effective the drainage system (Castenetto & Galadini, 1999).

In 1800, following a period of extreme fluctuations in the lake level (Brisse & De Rotrou, 1876), dredging or reclamation projects of the Fucino basin has been re-proposed. In 1854 the Prince Alessandro Torlonia financed the radical reclamation of the Fucino lake entrusting the task to an Italian-French company, initially coordinated by eng. De Montricher, then by eng. Bermont and, at his death, by eng. Brisse, who completed the work in 1878.

Currently, the water is drained by a complex network of channels that pipe to the main drainage gallery (Fig. 1), located under Salviano Mount and flowing into the Liri river.

COSEISMIC ENVIRONMENTAL EFFECTS IN THE RECLAIMED AREA

The historical archives of the Geological Survey of Italy, collected at the ISPRA Library, contains a large amount of documents consisting of scientific publications from the early decades of the 1800's, a vaste collection of geological and geothematic maps, and a wide collection of documentary material made up of letters, scientific and technical reports. The inspection of these documents allowed the discovery of a collection of scientific and technical reports related to the hydraulics of the Fucino plain. These manuscripts, consisting of six volumes, were written in the period 1915-1916 by engineers Lotti (chief geologist of the Geological Survey of Italy), Montanari and Olivieri. The study,

commissioned by the Prince Alessandro Torlonia, contains an hydraulic analysis of the reclaimed land and technical suggestions to improve the drainage of the area, highlighting the presence of problems related to ground subsidence.
Along with geological considerations, many topographic data from technical projects drawn up by the various companies involved in the reclamation work of 1870 and 1876, have been analyzed together with new measurements carried out in 1915. The analysis of these data highlights a migration of the deepest point of the lake which proceeded, in time, from SE to NW; this phenomenon, taking into account the measurements error, could be attributed to progressive consolidation phenomena of the reclaimed land.

Figure 2: Ground fractures near San Benedetto dei Marsi (Oddone, 1915).

In addition, the comparison of the maps contained in the Lotti and co-authors reports with those related to the damage caused by the Fucino earthquake, published by Oddone (1915), highlights a correspondence between the area of the "small basin" (Fig. 1), the last sector of the Fucino lake dried up, and the place where the most significant effects on the ground has been registered. In this area widespread subsidence phenomena and opening of trenches in not fully consolidated silty-sandy soils have been registered (Fig. 2). As reported by Oddone (1915) and Serva et al. (1986), this area was affected by liquefaction phenomena and spills of water and clayey material from soil fractures, a clear sign of a substrate still saturated with water and the presence of sediments not completely consolidated, contrary to the findings from Lotti and co-authors.

CONCLUSIONS

The analysis of the unpublished original reports of Lotti, Montanari and Olivieri (1915-1916), found in the archive of the Geological Survey of Italy, opens new perspectives in the study and research about topographic changes measured after the 1915 Fucino earthquake. The comparison of these data with those reported by Loperfido (1919) and Oddone (1915) (widely studied by D'Addezio & Valensise, 1998) could allow a refinement of the analysis of the topographical effects induced by the earthquake.

References

Brisse A., & L. De Rotrou, (1876). *Desséchement du lac Fucino*. Edizione bilingue francese e inglese corredata da un Atlante (1883).

Castenetto, S., & F. Galadini (a cura di), (1999). 13 gennaio 1915. Il terremoto nella Marsica. *Agenzia di Protezione Civile. Servizio Sismico Nazionale. Istituto Poligrafico e Zecca dello Stato. Roma*. 789 pp.

Cavinato, G.P., C. Carusi, M. Dall'Asta, E. Miccadei & T. Piacentini, (2002). Sedimentary and tectonic evolution of Plio-Pleistocene alluvial and lacustrine deposits of Fucino basin (Central Italy). *Sediment. Geol.* 148, 29-59.

Centamore E., U. Crescenti, & F. Dramis (a cura di), (2006). *Note illustrative della Carta Geologica d'Italia alla scala 1:50.000.* Foglio 368. Avezzano. S.EL.CA., Firenze.

D'Addezio, G. & G. Valensise, (1998). Il terremoto di Avezzano. Guida alla scoperta degli effetti del terremoto sull'ambiente naturale. *Quaderni di Geofisica*. 1, 1-19.

Giraudi, C., (1988). Evoluzione geologica della Piana del Fucino (Abruzzo) negli ultimi 30.000 anni. *Il Quaternario*. 1 (2), 131-159.

Giraudi, C., (1989). Lake levels and climate for the last 30,000 years in the Fucino area (Abruzzo – Central Italy) – a review. *Palaeogeography, Palaeoclimatology, Palaeoecology*. 70, 249-260.

Loperfido, A., (1919). Indagini astronomiche e geodetiche relative al fenomeno sismico nella Marsica. *Atti Lavori Pubblici*. pp. 95.

Lotti B., T. Montanari & G. Olivieri, (1915-1916). Relazione sulle condizioni idrauliche del Fucino. 6 voll., *Archivio del Servizio geologico d'Italia. Biblioteca ISPRA. inedito*.

Oddone, E., (1915). Gli elementi fisici del grande terremoto marsicano-fucense. *Bollettino della Società Sismologica Italiana*. 19, 71-291.

Serva, L., A.M., Blumetti, & A.M., Michetti, (1986). Gli effetti sul terreno del terremoto del Fucino (13 gennaio 1915); tentativo di interpretazione della evoluzione tettonica recente di alcune strutture. *Memorie della Società Geologica Italiana.* 35, 893-907.

Zarlenga, F., (1987). I depositi continentali del Bacino del Fucino (L'Aquila, Italia Centrale). *Geol. Romana*. 26, 223-253.

INQUA Focus Group on Paleoseismology and Active Tectonics

paleoseismicity.org

The Environmental Seismic Intensity Scale (ESI 2007) for the 1995 Ms=6.6 Kozani-Grevena Earthquake and the 1894 (M=6.4, M=6.8) Atalanti sequence in Greece; Preliminary relationships between Magnitude and the ESI 2007 for Greece and the Mediterranean area

Papanikolaou, I. (1) and Melaki, M. (2)

(1) Laboratory Mineralogy - Geology, Agricultural University of Athens, Iera Odos 75, 118 55, Athens, Greece. Email: i.pap@aua.gr
(2) Laboratory of Natural hazards, Faculty of Geology and Geoenvironment, National and Kapodistrian University of Athens, Panepistimiopolis 157 84, Athens, Greece

Abstract: *This study has two main goals. Firstly, to enrich and compile an ESI 2007 database from earthquakes in Greece. Thus, the ESI 2007 scale was applied in two events, the 1995 Ms=6.6 Kozani-Grevena earthquake (western Macedonia region) and the 1894 Atalanti earthquake sequence (M=6.4 and M=6.8) (Central Greece). These events were selected because they have well documented and extensive co-seismic effects, including primary and secondary surface ruptures, rock falls, landslides and liquefaction phenomena. For the Kozani earthquake, the extracted results were correlated with SAR interferograms, in order to provide a complete and high spatial resolution of the ground deformation. The Kozani-Grevena earthquake produced a maximum intensity IX on the ESI2007 scale and the Atalanti earthquake produced a maximum intensity X. The second goal is to compile a preliminary table correlating earthquake magnitude and the ESI 2007 for Greece and the Mediterranean area.*

Key words: *Kozani-Grevena earthquake, Atalanti, earthquake sequence, Earthquake Environmental Effects, ESI 2007 scale, Intensity.*

INTRODUCTION

The Environmental Seismic Intensity (ESI2007) scale, introduced by INQUA, is a twelve-degree structured scale, which takes into account solely the Earthquake Environmental Effects (EEE), both primary and secondary ones, caused by a seismic event (Michetti et al. 2007). This intensity scale is a reliable tool for the seismic hazard assessment, because EEE are not influenced by human parameters, such as manmade structures and economic development. Among the other advantages, this scale allows: (i) the comparison among recent earthquakes and historical ones, (ii) the assessment of the seismic intensity in sparsely populated or inhabited areas and (iii) the intensity evaluation, where traditional scales saturate (i.e. for intensity X to XII) and only the coseismic environmental effects consider as diagnostics. (Michetti, et al., 2004). The use of many different intensity scales worldwide (e.g. MM, MCS, MSK, JMA), which are also constantly updated (e.g. EMS 1992, EMS 1998, etc.) indirectly demonstrates the inefficiency of current earthquake intensity scales in describing the macroseismic earthquake effects (Papanikolaou, 2011). The ESI 2007 scale offers higher objectivity in the process of assessing macroseismic intensities, particularly in the epicentral area, than traditional intensity scales (Michetti et al. 2004, Serva et al. 2007, Papanikolaou, et al., 2009).
The ESI 2007 scale has been applied in several events in Greece and worldwide. Following the above, the goal is to expand the existing ESI2007 database for Greece and compile a preliminary table correlating earthquake magnitude and the ESI 2007. Therefore, two destructive events have been studied in detail. These events are the 1995 Kozani-Grevena earthquake and the 1894, Atalanti earthquake sequence.

THE MAY 13, 1995, KOZANI-GREVENA EARTHQUAKE

An Ms=6.6 (Mw=6.5) earthquake occurred on May 13, 1995 in north-central Greece (western Macedonia region). The epicentre was at 40.13 N, 21.67 E and originated at a depth of approximately 10 km (Papazachos et al., 1998). The seismic fault is a normal fault trending ENE-WSW and dipping to NNW, with high angle at the surface and lower angle at depth (Mountrakis, et al., 1998). The affected area comprise a wide zone trending E-W, from the northwest boundary of the molassic formation of the "Meso-Hellenic Trench", through the ophiolitic complex of Vourinos Mt and the carbonates of "Almopia", to the neotectonic basin of Kozani (Papanikolaou, 1986). This event caused severe damages on human infrastructure. More than 15 villages and cities suffered significant damage (Carydis et al., 1995). Hundreds of buildings collapsed, including houses, schools, churches and hospitals. In addition, extensive co-seismic environmental effects were recorded including primary surface ruptures and numerous secondary effects (Fig. 1).

Primary Effects
Significant surface ruptures were recorded, implying a maximum intensity IX on the ESI2007 scale. Two main fracture lines, the Paleochori-Sarakina-Nisi line and the Chromio-Varis-Mirsina line, associated with the main and the antithetic fault respectively were observed in the field (Pavlides et al., 1995). The most impressive ruptures were formed along the Paleochori-Sarakina fault that was the main activated structure approximately 15km long (Mountrakis et al., 1998). Detailed data concerning the ruptures were collected from Mountrakis et al., (1998), Pavlides et al., (1995) and Stamatis, (1995) (Fig.1).

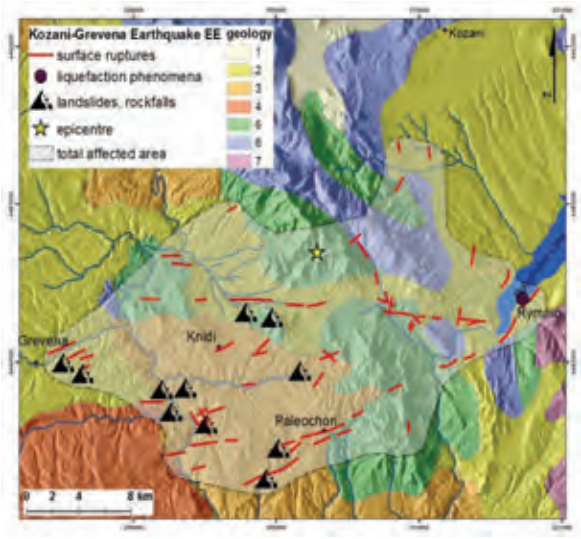

Figure 2: The spatial distribution of the Kozani-Grevena EEE (Mountrakis et al., 1998, Lekkas et al., 1996, Pavlides et al., 1995, Stamatis 1995) and a simplified geological map. 1: Alluvial and Scree, 2: Plio-Pleistocene sediments, 3: "Tsotylion" molassic formation, 4: "Pendalofo" molassic formation, 5: "Vourinos" ophiolitic complex, 6: "Eastern Greece" carbonates, 7: Flambouron" gneisses and schists (after Lekkas et al., 1996).

Secondary Effects

Liquefaction phenomena were observed along a wide zone 4 km long and more than 2 km wide at the southern shore of the Polyfytos artificial lake, responsible for the >80 cm subsidence of the Eani-Rymnio bridge paving (Pavlides et al., 1995). Major landslides occurred near the villages Knidi, Rymnion, Kentron and Kalamitsi and rock falls occurred towards the steep slopes of the Aliakmon river banks (Lekkas et al., 1996). These data were imported and processed into a GIS and EEE (Fig. 1) and intensity maps were produced (Fig.2).

Taking into account the effects and the local geological setting, a maximum intensity IX on the ESI2007 scale was extracted. The estimated affected area of the EEE is about 900 km^2 and in agreement with the expected total area according to ESI2007 scale for Intensity IX. In addition to ground observations the existence of SAR data for this event offered a detailed and high spatial resolution of the deformation field (Rigo et al. 2004). As a result, for the assignment and mapping of the ESI2007 intensity values, field observations were combined with SAR data (Fig. 2).

THE APRIL, 1894 ATALANTI EARTHQUAKE SEQUENCE

The region of Lokris (along the southern coast of the Gulf of Evia) was struck by two pre-instrumental large seismic events that occurred one week apart, on 20 and 27 April 1894 respectively. There are some uncertainties regarding the Magnitudes and both epicentres, however, recent reanalyses, estimate the magnitudes as M=6.4 and M=6.8 respectively (Pantosti et al., 2001).

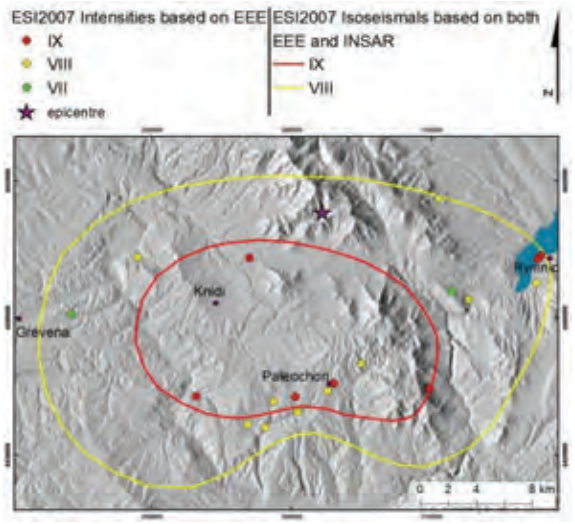

Figure 3: The ESI2007 isoseismal map of the 1995, Kozani-Grevena earthquake.

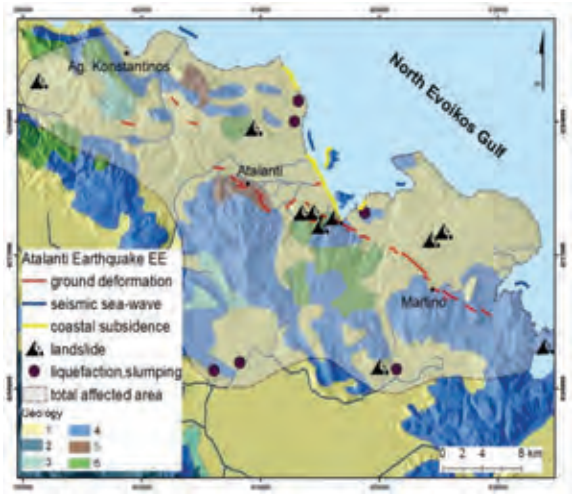

Figure 4: The spatial distribution of the Atalanti Earthquake sequence EE (Ambraseys & Jackson, 1990, Lemeille 1977, Pantosti et al., 2001, Ganas et al., 1997, Skouphos 1894) and a simplified geological map. 1: Post tectonic and late tectonic sediments, 2: "Parnasos-Gkiona" zone formations (mainly limestones), 3: Beotian flysch, 4: "Pelagone" zone formations (mainly limestones), 5: Pre-alpine series formations, 6: Ophiolitic nappe rocks (after IGME, 1993).

Description of Earthquake Environmental Effects

The earthquakes produced extensive damages and significant EEE (Fig. 3). During the first shock, all the villages between Megaplatanos and Martino were devastated and 223 people were killed. The second event destroyed the villages between Megaplatanos and Agios Konstantinos, an area not affected by the first shock, killing 30 people (Ambraseys & Jackson, 1990). However, it is difficult to separate the damages caused by each shock, because they were closely spaced in time.

Primary Effects

Extensive surface ruptures and tectonic subsidence were observed. The most severe effects were observed towards the coastline, where the shore subsided and the peninsula of Gaidouronisi was transformed into an island, with an estimated elevation change of 30-80 cm during the second shock (Cundy et al., 2000). Extensive surface faulting occured, extending from Martino to Atalanti, for about 25 km (Ambraseys & Jackson, 1990). Several researchers (Skouphos 1894, Mitsopoulos 1895, Lemeille 1977, Ambraseys & Jackson, 1990, Ganas, et al., 1997, Pantosti et al., 2001,) have described the ruptures caused by these events, still visible today. The maximum estimated slip is assumed up to 1m (Cundy et al., 2000). These effects imply a maximum ESI2007 intensity X.

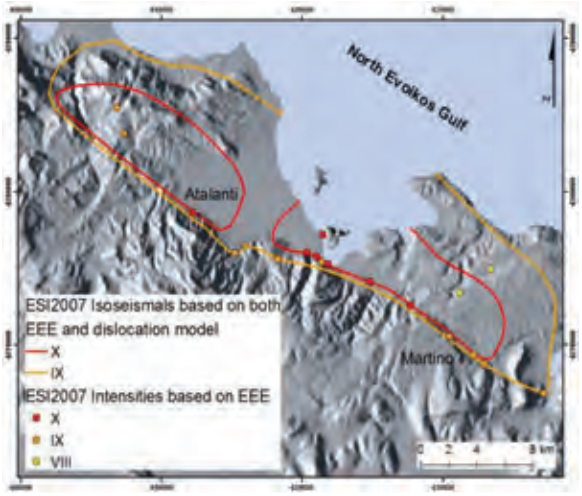

Figure 5: The ESI 2007 isoseismal map of the 1894 Atalanti earthquake sequence.

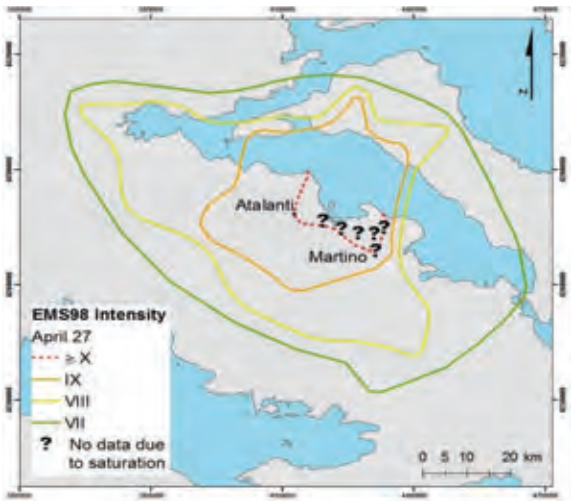

Figure 6: The EMS 1998 scale distribution of the April 27, 1894 Atalanti event. Intensity points from (Albini & Pantosti, 2004). Question marks indicate sites where intensity values could not be evaluated due to saturation effects.

Secondary Effects

During the first shock, the coastal plain from Almyra to Livanates liquefied. However, liquefaction phenomena during the 27, April earthquake occurred in sites distant up to 40km from the epicentral area (Ambraseys & Jackson, 1990). This shock triggered major landslides and seismic sea-waves, flooding a wide area between Agios Konstantinos and Almyra, but the estimates regarding the extend of the inundation vary significantly among authors (Skouphos 1894, Mitsopoulos 1895, Cundy et al., 2000). However, the coastal zone between Almyra and Kato Peli, remained flooded (Cundy et al., 2000). In order to create a complete and accurate ESI2007 intensity map (Fig. 4), EEE intensity values were correlated with the pattern of deformation produced by Cundy et al., (2000), based on an elastic half-space dislocation model. Fig. 5 depicts the EMS98 isoseismals for the 27, April earthquake. The question marks indicate 6 sites that were already destroyed by the first event; therefore, no data regarding the intensity was gathered following the second event. This example, illustrates the saturation problems that traditional intensities face for high intensity >IX values and emphasize once again the importance of the EEE effects for high intensity values.

RELATIONSHIPS BETWEEN THE EARTHQUAKE MAGNITUDE AND THE ESI 2007 SCALE FOR GREECE

The attenuation relationships of traditional intensities form a major source of uncertainty in seismic hazard assessment and in several cases they overshadow all the other factors of uncertainty, even fault slip-rates, which govern the earthquake occurrence (Papanikolaou 2011). The ESI 2007 scale may prove beneficial for the seismic hazard assessment by reducing the present day large uncertainty implied in the attenuation laws. Herein, a preliminary relationship between earthquake Magnitudes and the ESI 2007 is offered. All the earthquake magnitudes were converted to moment magnitude (Mw), using the relations suggested by Scordilis (2006) (Ms to Mw) and Okal & Talandier (1989) (Mm to Mw). Table 1 and Table 2 show the relationship between the Ms and Mw with the ESI 2007 for 11 well documented events in Greece including the Kozani-Grevena and the Atalanti sequence that were described previously (Papathanassiou & Pavlides, 2007, Papathanassiou et al. 2007, Fokaefs & Papadopoulos, 2007, Papanikolaou et al., 2009, Fountoulis & Mavroulis 2013, Mavroulis et al. 2013).

Table 1: Relationship between Ms and ESI 2007 for Greece.

Ms	N	MAGNITUDE			INTENSITY (ESI 2007)		
		min	max	median	min	max	median
5.6-6.0	4	5,5	6	**5,80**	VII-VIII	IX	**VIII+**
6.1-6.5	3	6,3	6,4	**6,36**	VIII-IX	X	**IX+**
6.6-7.0	4	6,6	6,8	**6,70**	IX	X	**X-**

Table 2: Relationship between Mw and ESI 2007 for Greece.

Mw	N	MAGNITUDE			INTENSITY (ESI 2007)		
		min	max	median	min	max	median
5.6-6.0	3	5,7	6	**5,90**	VII-VIII	VIII-IX	**VIII**
6.1-6.5	5	6,1	6,5	**6,30**	VIII-IX	X	**IX+**
6.6-7.0	3	6,6	6,8	**6,70**	IX-X	X	**X-**

Table 3 includes 29 well documented events from the Mediterranean region (Serva et al., 2007, Guerrieri et al., 2009, Gosar, 2012, Di Manna et al., 2012, Silva et al., 2014, ISPRA - INQUA TERPRO), including Table 1.

Table 3: Preliminary table showing the relationship between Mw and ESI 2007 for selected Mediterranean events.

Mw	N	MAGNITUDE			INTENSITY (ESI 2007)		
		min	max	median	min	max	median
4.0-5.5	3	4,2	5,2	**4,70**	VI-VII	VIII	**VII+**
5.6-6.0	6	5,6	6	**5,85**	VII-VIII	IX	**VIII+**
6.1-6.5	7	6,1	6,5	**6,30**	VIII-IX	X	**IX+**
6.6-7.0	10	6,6	7	**6,82**	IX	XI	**X-**
7.1-7.5	3	7.2	7.2	**7,20**	IX	X	**X-**

References

Albini, P. & D. Pantosti, (2004). The 20 and 27 April 1894 (Locris, Central Greece) Earthquake Sources through Coeval Records on Macroseismic Effects. *Bulletin of the Seismological Society of America*. 94, 1305-1306.

Ambraseys, N. & J. Jackson, (1990). Seismicity and associated strain of central Greece between. *Geophysical J. International*. 101, 663-708.

Carydis, P., K. Holeva, E. Lekkas & T. Papadopoulos, (1995). The Grevena (Central-North Greece) Earthquake Series of May 13, 1995. *EERI Special Earthquake Report*. Vol. 29, Number 6.

Cundy, A., et al., (2000). Coastal wetlands as recorders of earthquake subsidence in the Aegean: a case study of the 1894 Gulf of Atalanti earthquakes, central Greece. *Marine Geology*. 170, 3-26.

Di Manna, P., et al., (2012). Ground effects induced by the 2012 seismic sequence in Emilia: implications for seismic hazard assessment in the Po Plain. *Annals of Geophysics*. 55, 697-703.

Fokaefs, A. & G. Papadopoulos, (2007). Testing the new INQUA intensity scale in Greek earthquakes. *Quaternary International*. 173-174, 15-22.

Fountoulis, I. & S. Mavroulis, (2013). Application of the ESI 2007 and the EMS-98 to the Kalamata (SW Peloponnese, Greece) earthquake (Ms=6.2, September 13, 1986) and correlation with neotectonic structures and active faults. *Annals of Geophysics*. 56, S0675.

Ganas, A., G. Roberts, & T. Memou, (1997). Segment boundaries, the 1894 ruptures and strain patterns along the Atalanti fault, Central Greece. *J. Geodynamics*. 26, 461-486.

Gosar, A., (2012). Application of Environmental Seismic Intensity scale (ESI 2007) to Krn Mountains 1998 Mw = 5.6 earthquake (NW Slovenia) with emphasis on rockfalls. *Natural Hazards and Earth System Science*. 12, 1659-1670.

Guerrieri, L. et al., (2009). Capable faulting, environmental effects and seismic landscape in the area affected by the 1997 Umbria-Marche (Central Italy) seismic sequence. *Tectonophysics*. 476, 269-281.

IGME, 1993. *Geological map of Greece (Scale 1:500.000)*. Athens: IGME.

ISPRA - INQUA TERPRO. EEE Catalogue. INQUA TERPRO Project #0811, ISPRA - Geological Survey of Italy Working Group. http://www.eeecatalog.sinanet.apat.it/terremoti/index.php

Lekkas, E., et al., (1996). *Neotectonic implications of Grevena-Kozani earthquake (May 13, 1995, W. Macedonia, Greece)*. International meeting on results of the May 13 1995 earthquake of West Macedonia: One year after. 76-80.

Lemeille, F., (1977). Etudes neotectoniques en Grece centrale nord-orientale (Eubee centrale, Attique, Beotie, Locride) et dans les Sporades du Nord (ıle de Skiros). Centre Orsay: These de Troisieme Cycle Universite Paris. XI, 173 pp (in French).

Mavroulis, S., et al., (2013). Seismic intensity assignments for the 2008 Andravida (NW Peloponnese, Greece) strike-slip event (June 8, Mw=6.4) based on the application of the ESI 2007 and the EMS-98. Geological structure, active tectonics, earthquake environmental effects and damage pattern. *Annals of Geophysics*. 56, S0681.

Michetti, A.M., et al., (2004). The INQUA Scale. An innovative approach for assessing earthquake intensities based on seismically-induced ground effects in natural environment. *Special paper APAT*. Mem. Descr. Carta geol. d'Italia. Vol LXVII. (Vittori, E. & Comerci, V. eds.), p. 115.

Michetti, A.M., et al., (2007). Intensity scale ESI 2007. In: (Guerrieri, L., Vittori, E. Eds.), *Memorie Descrittive Carta Geologica d'Italia. Servizio Geologico d'Italia*. vol. 74. Dipartimento Difesa del Suolo. APAT. Roma. p. 53.

Mitsopoulos, K., (1895). *The Mega-earthquake of Lokris in April 1894*. Ethnikon Typografeion. Athens. p. 40 (in Greek).

Mountrakis, D., et al., 1998. Seismic fault geometry and kinematics of the 13 May 1995 Western Macedonia (Greece) earthquake. *J. Geodynamics*. 26, 175-196.

Okal, E. & J. Talandier, (1989). Mm: a variable period mantle magnitude. *Journal of Geophysical Research*. 94, 4169-4193.

Pantosti, D., et al., (2001). A Reappraisal of the 1894 Atalanti Earthquake Surface Ruptures, Central Greece. *Bulletin of the Seismological Society of America*. 91, 760-780.

Papanikolaou, D., (1986). *Geology of Greece*, p.240. Athens: s.n.

Papanikolaou, I., (2011). Uncertainty in intensity assignment and attenuation relationships: How seismic hazard maps can benefit from the implementation of the ESI 2007. *Quaternary International*, 242, 42-51.

Papanikolaou, I., D. Papanikolaou, & E. Lekkas, (2009). Advances and limitations of the Environmental Seismic Intensity scale (ESI 2007) regarding near-field and far-field effects from recent earthquakes in Greece: implications for the seismic hazard assessment. *Geological Society London. Special Publications*. 316, 11-30.

Papathanassiou, G., & S. Pavlides, (2007). Using the INQUA scale for the assessment of intensity: Case study of the 2003 Lefkada (Ionian Islands), Greece earthquake. *Quaternary International*,173–174, 4-14.

Papathanassiou, G., S. Valkaniotis, & S. Pavlides, (2007). Applying the INQUA scale to the Sofades 1954, Central Greece, earthquake. *Bull. Geol. Soc. Greece*. vol. XXXVII, 1226-1233.

Papazachos, B., (1990). Seismicity of the Aegean and surrounding area. *Tectonophysics*. 178, 287-308.

Papazachos, B., et al., (1998). A model for the1995 Kozani-Grevena Seismic sequence. *J. Geodynamics*. 26, 217-231.

Pavlides, S. et al., (1995). The 13 May 1995 western Macedonia, Greece (Kozanai-Grevena) earthquake; preliminary results. *Terra Nova*. 7, 544-549.

Rigo, A., J. De Chabalier, B. Meyer, & R. Armijo, (2004). The 1995 Kozani–Grevena (northern Greece) earthquake revisited: an improved faulting model from synthetic aperture radar interferometry. *Geophysical J. International*. 157, 727-736.

Scordilis, E., (2006). Empirical global relations converting MS and mb to moment magnitude. *J. Seismology*. 10, 225-236.

Serva, L., et al., (2007). Environmental effects from five historical earthquakes in southern Apennines (Italy) and macroseismic intensity assessment: Contribution to INQUA EEE Scale Project. *Quaternary International*. 173-174, 30-44.

Silva, P., et al., (2014). *Catálogo de los efectos geológicos de los terremotos en España* (in spanish). Riesgos Geológicos/Geotecnia. N.° 4 ed. Madrid. Instituto Geológico y Minero de España.

Skouphos, T., (1894). *Die swei grossen Erdbeben in Lokris am 8/20 und 15/27 April 1894*. Zeitschrift Ges. Erdkunde zu Berlin. 24, 409-474 (in German).

Stamatis, A., (1995). *Essay on the May 13, 1995 Kozani-Grevena Earthquake and on the observations according to the local geological setting*. (in Greek), s.l.: IGME, Kozani.

INQUA Focus Group on Paleoseismology and Active Tectonics

Active Tectonics and Seismic Hazard in Skyros Basin, North Aegean Sea, Greece

Papanikolaou, D. (1), Nomikou, P. (1), Rousakis G. (2), Livanos, I. (1), Papanikolaou, I. (3)

(1) Laboratory of Natural hazards, Faculty of Geology and Geoenvironment, National and Kapodistrian University of Athens, Panepistimiopolis 157 84, Athens, Greece. Email: dpapan@geol.uoa.gr
(2) Inst. of Oceanography, Hellenic Centre for Marine Research, Anavyssos, Greece
(3) Laboratory Mineralogy - Geology, Agricultural University of Athens, Iera Odos 75, 118 55, Athens, Greece

Abstract: *Oceanographic research including swath bathymetry and single channel air-gun lithoseismic profiles was carried out in Skyros Basin, North Aegean Sea. Morphotectonic analysis and the interpretation of the lithoseismic profiles have resulted in the compilation of the tectonic map of the Skyros Basin. The map shows all active faults, both the major marginal faults as well as the secondary faults that accommodate deformation within the internal part of the basin. Important throws of several hundred meters up to more than 1km are extracted as well as considerable strike-slip components since Middle Pleistocene time. The length of the faults range between a few tens of km up to 111km, indicating that these seismic sources have the potential to generate strong earthquakes up to 7.5 magnitude. The vast majority of the mapped seismic sources have not been ruptured or recorded in the historical data, implying that the seismic hazard of the area might be underestimated.*

Key words: *Swath Bathymetry, Lithoseismic profiles, Skyros, active faults.*

INTRODUCTION

Skyros Basin trends E-W and is located in the North Aegean Sea, developed southwards and subparallel to the North Aegean Basin (Fig.1). It is smaller compared to the North Aegean basin, but both accommodate extension and shear due to the extension of the North Anatolian Fault westwards that breaks into several strands (McKenzie 1970, Papadimitriou and Sykes 2001, Kreemer et al. 2004). The latter is also observed by both the bathymetry (e.g. Papanikolaou et al. 2002) and the GPS measurements that show at least 20mm/yr deformation occurring between the Chalkidiki peninsula and the Evia island (McClusky et al. 2000). The creation and development of the two basins of the North Aegean Sea are considered to be the result of westward propagation and opening of the North Anatolian fault since Late Pliocene (Sengor, 1979; Taymaz et al, 1991; Armijo et al, 1999). More recently, the role of the retreating plate boundary and roll back of the Hellenic subduction zone in the Ionian Sea has been emphasized, with a considerable part of the upper plate deformation thought to be driven by the difference of the small European – Africa plate convergence rate with regards to the high Hellenic subduction rate (Royden and Papanikolaou, 2011). In contrast to the well studied North Aegean Basin (Papanikolaou et al, 2002; 2006; Papanikolaou and Papanikolaou, 2007a), the morphology and tectonic structure of the Skyros Basin are poorly known (e.g. Mascle and Martin, 1990). The goal of this study is to map in detail the bathymetry, the active faults and assess the seismic sources of the Skyros Basin.

GEOLOGICAL SETTING

The geological structure of the Skyros Basin in the central Aegean comprises an Alpine basement, mainly made of Mesozoic carbonate rocks tectonically overlain by a Jurassic ophiolite nappe and Cretaceous transgressive sediments and post-orogenic Late Miocene to Quaternary marine sediments (Grekkof et al, 1967, Keraudren, 1970). The dominant structure of the Skyros Basin is a ENE-WSW predominantly strike slip fault towards the SW. This fault separates the geological structure of the Skyros Island in two blocks (Papanikolaou and Royden 2007) and continues further to the SW separating the non metamorphic areas of Central Evia and NW Attica from the metamorphic areas of Southern Evia and SE Attica (Papanikolaou and Papanikolaou, 2007b).

METHODOLOGY

Systematic survey of the Skyros Basin has been carried out in September of 2013 using the R/V «Aegaeo» of the Hellenic Centre of Marine Research (HCMR). The multi-beam bathymetric survey was carried out on the research vessel Aegaeo of the HCMR using the 'SEABEAM 2120' swath system, which is a fully mounted system operating at 20 kHz at water depths not exceeding 6000 m. It has an angular coverage sector of 150‡ with 149 beams, covering a swath width from 7.5 to 11.5 times the water depth for depths of 1000^5000 m, respectively. The maximum swath coverage can reach 9km at maximum depth and provides a satisfactory data quality with vessel speed up to 11 knots. The air gun was operated in 10 in3 at an average speed of 5 knots. The penetration depth of the air gun was several hundred meters with a maximum of 700- 800m (Fig.2 Fig.3, Fig.4, Fig. 5). Coring at selected sites has been also taken into account aiming to determine the sedimentation rate at various environmental conditions that would help the chronological determination of the upper lithoseismic horizons of the basin and especially the Pleistocene

sediments, which were deposited during the successive stages of the climatic fluctuation (e.g. Lykousis, 2009).

RESULTS AND DISCUSSION

The bathymetric map of Skyros Basin, (Fig.1) shows a rather geometric triangular basin with a general trend in the ENE-WSW direction and depths varying from 600 to1200 m.

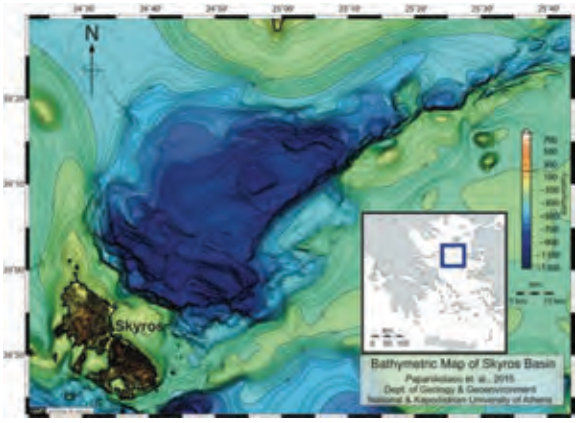

Figure 1: High resolution bathymetric map of the Skyros Basin based on swath bathymetry.

The overall geometry of the basin is shaped by a major slope discontinuity, separating the continental platform from the continental slope at depths between 200-400m. The basin forms an equilateral triangle. Its base is 50km long NW-SE trending at the southwest, parallel to the Skyros Island, whereas its pic is located at the northeast, north of Lesvos Island. The basin comprises 9 sub-basins at depths varying from 1200m at the southwest to 600m to the northeast and is structurally divided into three parts (Fig.6):

i) the eastern part forms a longitudinal semi-graben with one sub-basin trending ENE-WSW of 45km length, but only 5-8 Km width at depths varying between 600-700m (Fig.6). This sub-basin is bounded to the south by a marginal fault of >1.5km of vertical displacement, but with unknown horizontal displacement (Fig.2).

ii) the central part that forms the predominant part of the triangle with 45 Km long NW-SE trending base and 70km long axis at the NE-SW direction. The central part corresponds to an asymmetric graben with a 70km long major marginal fault with >1500m of vertical displacement along its southern slopes and a 70 km long antithetic fault with >400m of vertical displacement along its northern slopes although both marginal faults show important strike-slip component (Fig.3). The internal structure of the tectonic graben comprises 5 sub-basins with depths ranging between 950-700m, bounded by important E-W trending strike-slip fault zones, characterized by flower structures, with minor vertical components ranging from a few meters up to 200m.

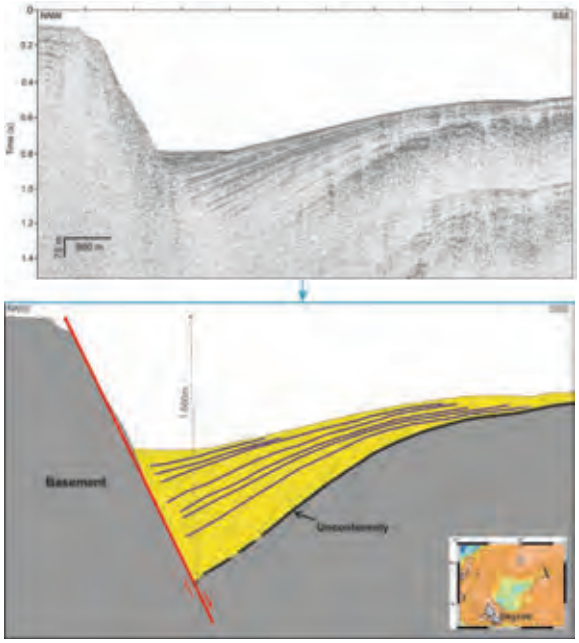

Figure 2: Lithoseismic profile and its interpretation, showing the active growth fault of the eastern part of the Skyros basin. In grey, the alpine basement, in yellow, post alpine sediments (Middle? Pleistocene to present).

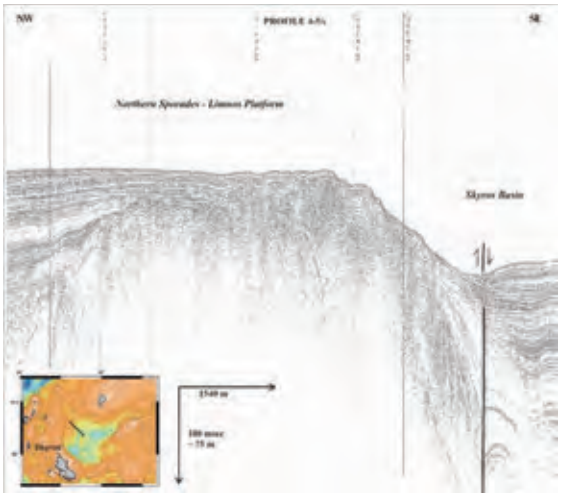

Figure 3: Lithoseismic profile across the northern margin of Skyros basin. The major marginal fault is a subvertical strike slip fault, with more than 400m of vertical displacement.

iii) the western part of the basin trends NW-SE, is 55 km long and 25 km wide, revealing a NW-SE tectonic graben. It comprises two sub-basins, oriented NW-SE separated by an intermediate transverse fault zone. The vertical displacement of the western marginal faults offshore Skyros Island exceeds 1200m (Fig.4), whereas the vertical displacements of the parallel faults creating the tilted western margin of the NW-SE tectonic graben is limited to a few hundred meters (Fig. 5).

It should be emphasized that the Alpine basement was not detected in the lithoseismic profiles of the western

and central parts of the basin, where the postAlpine sedimentary sequences exceed 700m of thickness, contrary to the eastern part, where the maximum thickness was determined at 600m. Seismotectonic and GPS data (e.g. McClusky et al. 2000, Muller et al, 2013) can be correlated to the morphotectonic analysis of the basin, indicating an overall oblique extension towards the SW at a rate of ~10mm/yr. In particular, between the GPS stations on the islands of Limnos and Skyros McClusky et al. (2000) calculate a motion of ~ 11mm/yr towards the SSW during the period 1989-1996, whereas Muller et al. (2013) show ~ 8mm/yr during 1993 – 2009.

The seismic hazard of the basin is controlled by the dominant structure, which is a 111km long ENE–WSW south marginal fault, comprising two major segments (Fig. 6). These two segments have vertical displacements that differ significantly and slightly different directions, indicating that they are probably activated independently. As a result, the main and most probable seismic scenario involves the independent rupture of each of the two segments that are 66 and 45 km long, implying a M=7.20±0.27 and M=6.95±0.22 respectively (based on Wells and Coppersmith 1994 empirical relationships that are widely used and the only available for strike-slip faults in the Aegean setting). However, a multi-segment rupture that could break the entire 111km long structure can not be ruled out. Such a worst-case scenario can generate a Max=7.45±0.25 magnitude earthquake. Additionally, 18 other active faults can generate earthquakes above magnitude 6, with earthquake mechanisms ranging from pure dextral strike-slip to normal faulting. It is noteworthy that the normal faulting character prevails at the southwestern part of the basin whereas the strike-slip component prevails at the northeastern edge of the basin, similarly to the North Aegean Basin northwards (Papanikolaou et al. 2006).

No major historical events have been reported for the Skyros island or the neighboring Skyros basin in the North Aegean (e.g. Papazachos and Papazachou 1997). However, the historical record is expected to be incomplete due to the offshore setting and the lack of important cultural sites in the vicinity. Earthquakes that probably occurred within the Skyros basin and its surrounding structures concern the 2001 M=6.4 and early instrumental era events. In particular, the March 9, 1965 M=6.1 event with significant damage in Alonisos and Skopelos islands, the March 4, 1967 M=6.6 in the Skyros Basin and the destructive 19th February 1968 M=7.1 with its epicenter near the island of Agios Eufstratios. It is interesting to note that all three earthquakes occurred in less than 4 years, thus closely in space and time indicating possible stress transfer and triggering. The 1967 M=6.6 event with its epicenter offshore north of Skyros was strongly felt in Skyros, Aghios Eustratios and Lesbos, but caused no damages (Papazachos and Papazachou 1997). The M=7.1 1968 event created severe damage to the small island of Agios Eufstratios (IX intensity) and 20 fatalities and generated a small tsunami wave that was recorded in Limnos island. Focal mechanism and macroseismic data based on the elongated isoseismals demonstrated that the earthquake occurred on a dextral NE-SW trending strike slip fault (Kiratzi et al. 1991). A major NE-SW trending fault has been mapped in Agios Eusftratios and several Earthquake Environmental effects have been recorded (Pavlides and Tranos 1991). This is similar to the direction of the major south marginal fault of the Skyros basin.

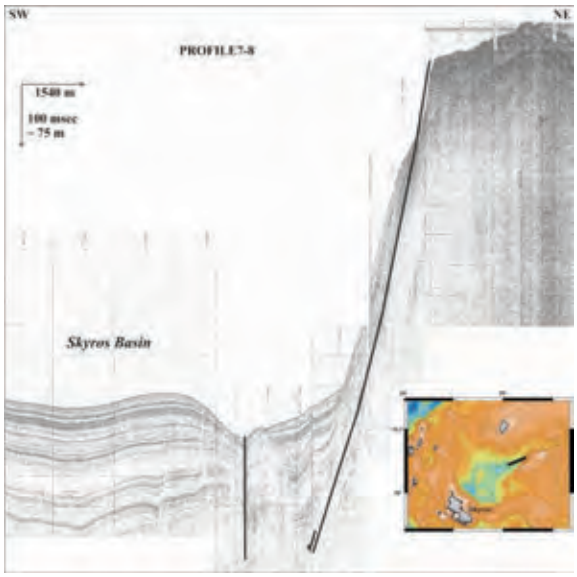

Figure 4: Lithoseismic profile of the SE margin of the Skyros basin, showing a normal and a strike slip fault of ENE-WSW direction.

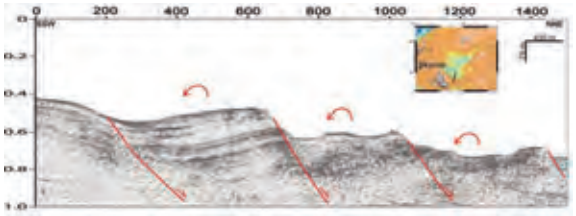

Figure 5: Lithoseismic profile of the SW margin of the Skyros basin, showing titled blocks by NW-SE normal faults

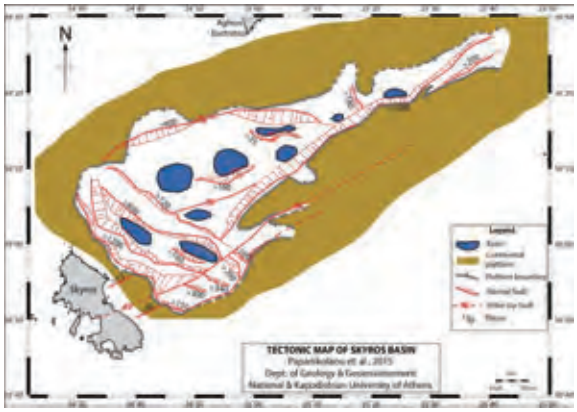

Figure 6: Tectonic map of the Skyros basin, showing the continental platform (in brown), the basinal areas (in blue) and the major normal and strike slip active faults (in red).

On the 26th of July in 2001 an offshore M=6.4 earthquake was recorded at 13km depth, a few km NW of the Skyros island. The earthquake occurred on a sinistral NW-SE trending fault located parallel to the Skyros shoreline (Karakostas et al. 2003, Roumelioti et al. 2004, Ganas et al. 2005). It is the first such focal mechanism recorded in this area that is dominated by dextral strike slip faults trending NE-SW. It is interesting to note that the current study traced at least four major structures (NW-SE trending) parallel to the 2001 activated fault. These four faults are 45 to 55 km long, implying that they are capable of hosting earthquakes of M~7.0.

It is clear that the events reported in the historical and instrumental catalogs did not rupture the entire length of the southern marginal fault at least over the last 5 centuries during which the catalogues are considered complete for M>7.3 (Papazachos et al. 2000). In addition, the vast majority of the seismic sources traced within this study have also not been ruptured, implying that the hazard potential of the area is underestimated based on traditional seismic hazard maps that are based on the historical data.

Acknowledgements: This research was financed by the Earthquake Planning and Protection Organization of Greece. The officers and crew of the oceanographic vessel «Aegaeo» are thankfully acknowledged for their collaboration and help during the cruises. The post-graduate students of Oceanography and Tectonics of the University of Athens G. Papantoniou, M. Alexandri and D. Labridou are thanked for their assistance in the cruises and the elaboration of data.

References

Angelier, J., (1979). *Neotectonique de l'arc Egeen*. These Doct., Univ. Paris VI.

Armijo, R., B. Meyer, A. Hubert, A. Barka, (1999). Westward propagation of the North Anatolian fault into the northern Aegean: timing and kinematics. *Geology*. 27, 267-270.

Ganas, A., G. Drakatos, S.B. Pavlides, G.N. Stavrakakis, M. Ziazia, E. Sokos, V.K. Karastathis, (2005). The 2001 Mw = 6.4 Skyros earthquake, conjugate strike-slip faulting and spatial variation in stress within the central Aegean Sea. *Journal of Geodynamics*. 39, 61-77.

Grekoff, N., G. Guernet, C. Lorenz, (1967). Existence Miocene marin, ancentre de la merEgee, dans l'ile de Skyros (Grece). *C. R. Acad. Sc.* 265, 1276 - 1277.

Karakostas, V.G., E.E. Papadimitriou, G.F. Karakaisis, C.B. Papazachos, E.M. Scordilis, G. Vargemezis, E. Aidona, (2003). The 2001 Skyros, Northern Aegean, Greece, earthquake sequence: off-fault aftershocks, tectonic implications, and seismicity triggering. *Geophys. Res. Lett.* 30 (1), doi: 10.1029/2002GL015814.

Keraudren, B., (1970). Les Formations Quaternaires marines de la Grece (I). *Bull. Muse d Anthropol. Prehistorique de Monaco*. Fas. No 16 (Skyros p.124).

Kiratzi, A., G. Wagner and C. Langston, (1991). Source parameters of some large earthquakes in Northern Aegean determined by body waveform modelling. *Pageoph*. 135, 515-527.

Kreemer, C., N. Chamot-Rooke, X. Le Pichon, (2004). Constraints on the evolution and vertical coherency of deformation in the Northern Aegean from a comparison of geodetic, geologic and seismologic data. *Earth and Planetary Science Letters*. 225, 329-346.

Lykousis, V., (2009). Sea-level changes and shelf break prograding sequences during the last 400 ka in the Aegean margins: subsidence rates and palaeogeographic implications. *Continental Shelf Research.* 29, 2037-2044.

Mascle, J. and L. Martin (1990). Shallow structure and recent evolution of the Aegean Sea: A synthesis based on continuous reflection profiles. *Marine Geology*. 94, 271-299.

McKenzie, D., (1970). Plate tectonics of the Mediterranean region. *Nature*. 226, 239-243.

McClusky, S., et al., (2000). Global Positioning System constraints on plate kinematics and dynamics in the eastern Mediterranean and Caucasus. *Journal of Geophysical Research*. 105, 5695-5719.

Müller, M.D., A. Geiger, H.G. Kahle, G. Veis, H. Biliris, D. Paradissis, S. Felekis, (2013). Velocity and deformation fields in the North Aegean domain, Greece, and implications for fault kinematics, derived from GPS data 1993-2009. *Tectonophysics*. 597-598, 34-49.

Papadimitriou, E.E., L.R. Sykes, (2001). Evolution of the stress field in the northern Aegean Sea (Greece). *Geophysical Journal International*. 146, 747-759.

Papanikolaou D., M. Alexandri, P. Nomikou, D. Ballas (2002). Morphotectonic structure of the western part of the North Aegean Basin based on swath bathymetry, *Marine Geology*. 190, 465-492.

Papanikolaou, D., M. Alexandri, P. Nomikou, (2006). Active faulting in the north Aegean basin. *Geol. Soc. America*. Sp. Paper, 409, 189-209, doi: 10.1130/2006.2409(11).

Papanikolaou, D.J., L.H. Royden, (2007). Disruption of the Hellenic arc: Late Miocene extensional detachment faults and steep Pliocene-Quaternary normal faults - Or what happened at Corinth? *Tectonics*. 26, TC5003, doi: 10.1029/2006tc002007.

Papanikolaou, I.D., D.I. Papanikolaou, (2007a). Seismic hazard scenarios from the longest geologically constrained active fault of the Aegean. *Quaternary*. 171-172, 31-44.

Papanikolaou, D. and I. Papanikolaou, (2007b). Geological, geomorphological and tectonic structure of NE Attica and seismic hazard. Implications for the northern edge of the Athens plain. *Bulletin Geological Society of Greece*, 40/1, 425-438.

Papazachos, B.C. & C.B. Papazachou, (1997). *The earthquakes of Greece*. Ziti Editions, Thessaloniki, p. 304.

Papazachos, B.C., P.E. Comninakis, G.F. Karakaisis, B.G. Karakostas, C.A. Papaioannou, C.B. Papazachos and E.M. Scordilis (2000). *A catalogue of earthquakes in Greece and surrounding area for the period 550 BC-1999*. Publ. Geophysical Laboratory. University of Thessaloniki.

Pavlides, S. and M. Tranos, (1991). Structural characteristics of two strong earthquakes in the North Aegean: Ierissos (1932) and Agios Efstratios (1968). *Journal of Structural Geology*. 13, 205-214.

Roumelioti, Z., A. Kiratzi, D. Dreger, (2004). The source process of the 2001 July 26 Skyros Island (Greece) earthquake. *Geophysical Journal International*. 156, 541–548.

Royden, L.H., and D.J. Papanikolaou, (2011). Slab segmentation and late Cenozoic disruption of the Hellenic arc. *Geochem. Geophys. Geosyst.* 12, Q03010, doi: 10.1029/2010GC003280.

Sengor, A.M.C., (1979). The North Anatolian transform fault: its age, offset and tectonic significance. *J. Geol. Soc. Lond*. 136, 269-282.

Taymaz, T., J.A. Jackson, and D. McKenzie, (1991). Active tectonics of the north and central Aegean Sea. *Geophysical Journal International*. 106, 433-490.

Wells, D.L. and K.J. Coppersmith (1994). New empirical relationships among magnitude, rupture length, rupture width and surface displacement. *Bulletin of the Seismological Society of America*. 84, 974-1002.

INQUA Focus Group on Paleoseismology and Active Tectonics

Evaluation of the macroseismic intensities triggered by the February 3, 2014 Cephalonia, Greece earthquake based on ESI-07 scale

Papathanassiou, G. (1), Valkaniotis, S. (2), Ganas, A. (3) and Papanikolaou, M. (3)

(1) Dept. of Geology, Aristotle University of Thessaloniki, Greece. Email: gpapatha@geo.auth.gr
(2) 9 Koronidos Str., 42100 Trikala, Greece
(3) Institute of Geodynamics, National Observatory of Athens, 11810 Athens, Greece

Abstract: *On January 26 and February 3, 2014, two earthquakes occurred onshore the island of Cephalonia inducing severe environmental effects. The main types of earthquake-induced failures were liquefaction and slope failures and were widespread at the western part of the island and mainly at Paliki peninsula. Although the fact that the generated strong motion by the second event was the highest ever recorded in Greece the structural damages were not significant. In addition, similar environmental failures were triggered by historical earthquakes as it is pointed out in seismic catalogues and reports; liquefaction phenomena at coastal areas and large scale rockfalls. By taking into account the low level of structural damages and the existence of accurate field observations, it was decided to apply the ESI-07 in order to evaluate at this stage the macorseismic intentisty of the 2014 earthquake and compare it with the historical ones in near future. The former was achieved by taking into consideration data provided by field surveys conducted immediately after the two events.*

Key words: *Cephalonia, earthquake, intensity, ESI-07, liquefaction.*

INTRODUCTION

Two strong earthquake events, ML (NOA) 5.8 and ML (NOA) 5.7 occurred on Jan. 26, 2014 13:55 UTC and Feb. 3, 2014 03:08 UTC, respectively, onshore the island of Cephalonia inducing extensive structural damages and geo-environmental effects, mainly in the western and central part. According to the National Observatory of Athens, Institute of Geodynamics (NOA; www.gein.noa.gr) the epicentre of the first event (NOA web report) was located at 38.2089ºN 20.4590ºE, near the town of Argostoli (the capital), while the second one was located at 38.2774ºN 20.4263ºE to the north of village Livadi (Paliki Peninsula). According to the Department of Geophysics, Aristotle University of Thessaloniki (AUTh), the focus of the first event located at 38.16ºN 20.34ºE and the second one at 38.27ºN 20.32ºE. Both earthquakes occurred on near-vertical, strike-slip faults with dextral sense of motion, in response to ENE-WSW horizontal strain in central Ionian Sea (Ganas et al., 2013).

The generated strong ground motions that were recorded on the installed accelerographs in the island are considered as ones of the highest ever recorded in Greece. In particular, regarding the Jan 26 event, the accelerographs installed in Argostoli by EPPO-ITSAK recorded a peak ground acceleration (PGA) value (horizontal component) equal to 383.4 cm/sec^2 (EPPO-ITSAK, 2014a; http://www.itsak.gr/news/news/64) while the accelerograph installed in Lixouri by NOA recorded a PGA value equal to 531 cm/sec^2 (Kalogeras, 2014). The PGA values generated by the Feb 3 event were recorded on the accelerographs installed by EPPO-ITSAK in Chavriata (CHV1), Lixouri (LXR1) and ARG2 (Argostoli) the and were equal to 752 cm/sec^2, 667 cm/sec^2 and 264 cm/sec^2, respectively (EPPO-ITSAK, 2014b).

The goal of this study is to evaluate the macroseismic intensity of the second event, Feb. 3, by applying the Environmental Seismic Intensity scale ESI-07. The evaluation of the intensity is based on the macroseismic observations provided by field surveys that took place immediately after the occurrence of earthquake (Feb. 4–6, 2014 & Feb. 6–9, 2014) and thus, we were able to timely report the triggered geo-environmental effects (liquefaction, slope failures etc.). The documentation of the earthquake-induced environmental effects was realized using the recently released Earthquake Geo Survey App, which is available from Play Store for Android OS devices.

Historical seismicity at the island of Cephalonia

The island of Cephalonia is considered as one of the most active tectonic areas in Europe and the eastern Mediterranean region. More than 10 damaging earthquakes occurred since 17th century and their consequences have been reported in detail by the authorities and locals. Information regarding the generated macroseismic effects has been collected from seismic catalogues (Papazachos and Papazachou, 1989; Galanopoulos, 1955) and from reports published by local authorities, agencies and researchers (Barbiani and Barbiani, 1864; Vergotis, 1867; Partsch, 1892; Moshopoulos, 1994; Albini et al., 1994; Makropoulos and Kouskouna, 1994; Papathanassiou et al., 2005).

Taking into account the collected information, it is concluded that at least 4 earthquakes triggered similar geological failures and structural damages in the peninsula of Paliki as the ones generated by the last two earthquakes. In particular, the 14 June 1759 event caused severe damages in the district of Paliki peninsula and in Lixouri where most of the houses collapsed and a few lives were lost. In Argostoli the shock was strongly felt but caused no damage (Albini et al. 1994). The 24 July 1766 earthquake induced structural damages at the western part of the island and particularly in the area of Paliki peninsula where most of the houses were destroyed. Earthquake damage extended to Assos, Lixouri and Argostoli (Albini et al. 1994). The 22 July 1767 was a destructive earthquake, with casualties (253 deaths). Severe structural damages in Lixouri and in the villages located at Paliki peninsula were reported. In particular, in Lixouri many deaths (50) were reported and almost the whole town suffered great damage. In Assos, houses were completely destroyed and rockfalls were reported. In the town of Argostoli very few houses were left inhabitable (Makropoulos and Kouskouna, 1994). The 4 February 1867 event triggered rockfalls and liquefaction phenomena almost at the same sites as the last one. In particular, a subsidence of 1 m width and 100 m length was observed along the shore of the river in Lixouri, sand crater and ejection of material was reported in a field at the area of Kouvalata while in the village of Agios Dimitrios, a sand crater with 1 m diameter and 0.5 m high was reported (Partsch, 1892). Large-scale landslides were documented in the area of Ag. Stefanos and rockfalls in the area of Anogi.

Evaluating the macroseismic intensity based on ESI-07 scale

During both events, earthquake-related phenomena such as liquefaction, road-fill failures, rock falls, small landslides and stonewall failures were widespread all over the island. No primary, surface ruptures were observed (Valkaniotis et al., 2014). Liquefaction phenomena were mainly triggered in reclaimed lands in the waterfront areas of Argostoli and Lixouri inducing structural damages to quays, sidewalks and piers (Fig.1). In particular, sandy material was ejected from cracks opened on paved roads of an average width 3 cm in Argostoli and 7 cm in Lixouri, respectively. The documented vertical subsidence was larger in Lixouri, up to 15 cm, in comparison to an average of 5 cm in the waterfront area of Argostoli.

Furthermore, scattered small-scale liquefaction phenomena were also reported at several locations of Paliki peninsula. In the northern and eastern part of the island only few isolated rock falls and landslides in loose materials were observed. The most remarkable slope failure was reported in Soullari where a large scale landslide activated on homogenous silt/clay Pliocene-Pleistocene sediments, in a small field on top of a hill.

Taking into account the field observations during the post-earthquake reconnaissance surveys, we estimated the macroseismic intensity based on the definitions of the ESI-07 scale (Michetti et al., 2007). The ESI-07 scale was initially introduced as INQUA scale and the estimation of the degrees is achieved by taking into account the characteristics of the earthquake-induced environmental deformation including primary and secondary effects. The Feb. 3 earthquake was classified as a reliable case study for the application of the ESI scale due to the fact that the environmental effects were widespread and well documented.

Figure 1: Geoenvironmental effects triggered by the 2014 Cephalonia earthquakes. Ejection of sandy material in Argostoli (up), large-scale landslide in Soullari (down). Photos were taken on 9/02/2014.

The locations where the macroseismic intensity was assessed based on ESI-07 scale are classified in three groups depending on the type of the dominant environmental effect. In the first group are included sites where liquefaction phenomena have been documented and the value of intensity was assessed based on the length and width of the ground cracks and sand boils while in the second one are classified sites where landslides and rockfalls are the dominant type of failures and thus, the evaluation of intensity was achieved by taking into account the dimensions of slope failures. The third category of environmental effects concern the documentation of ground cracks and the evaluation of intensity was based on their width and length.

In particular, the macroseismic intensity was evaluated as V in the sites Akrotiri and Livadi coastal plain, since the observed effects are well described by the definition of this degree (ESI-07); "…extremely rare cases are reported of liquefaction, small in size and in areas most prone to this phenomenon…" and "…thin cracks are locally seen where lithology are most prone to this phenomenon…". In the area of Argostoli, the macroseismic intensity was evaluated as VI by taking into account the ESI-07 scale degrees's definition "…rare cases are reported of

liquefaction, small in size and in areas most prone to this phenomenon…" and "…a few minor cracks are common in paved roads…" while a value of VII was assessed in the area of Lixouri following the ESI-07 scale definition "…sand boils up to 50 cm in diameter, in areas most prone to this phenomenon…" and "…centimeter-wide cracks are common in paved roads…".

Regarding the sites where slope failures were reported, the evaluated intensities range between IV and VII. In particular the highest macroseismic intensity was evaluated at the site of Soullari, where a large scale landslide of up to 103 m3 generated by the earthquake and the lowest intensity value was assessed at the sites of Koulourata and Neochori where small scale rock fall phenomena were reported. In addition, intensity value V was assessed for the sites Atheras, Petani beach, Myrtos beach, Agkonas, Kourouklata, Vlachata and Chavdata where rock falls were documented in steep slopes where equilibrium is near the limit state.

Finally, the macroseismic intensity was evaluated as VI at two sites and as VII at one site (table) where ground cracks have been generated by the event and observed during our field survey. These ground cracks are well described by ESI-07 definition degrees of VI as "…millimeter-centimeter wide and up to several meters long fractures are observed… a few minor cracks developed in paved roads…" and of VII as "…centimetric-wide cracks are common in paved roads…".

The evaluated intensities for all the locations are listed in the Table 1 while their distribution is shown in figure 2.

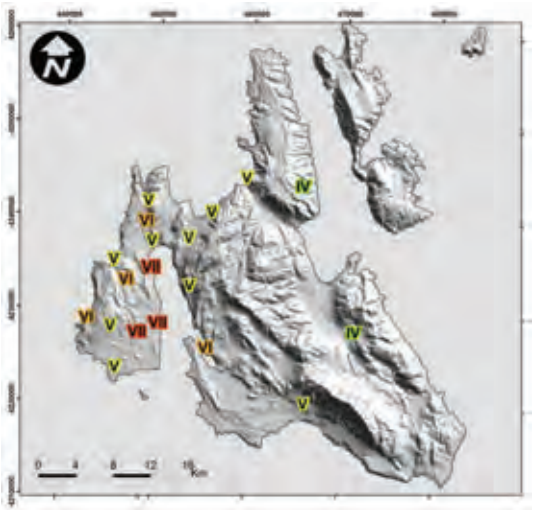

Figure 2: Spatial distribution of macroseismic intensities (ESI-07 scale) of the Feb. 3 event.

CONCLUSIONS

The 2014 Cephalonia earthquakes triggered widespread environmental effects including slope failures and liquefaction. Similar earthquake-induced failures were documented on historical seismicity reports indicating the importance of the environmental effects to the evaluation of macroseismic intensity. Based on our field observations, the macroseismic intensities of the Feb 3, 2014 event were evaluated by applying the ESI-07 scale. It should be pointed out that in some areas the generated environmental effects are the result of site effects and do not represent the macroseismic intensity for the locality. In particular, the degree of liquefaction-induced failures and accordingly the evaluated intensities at the coastal area of Lixouri and Argostoli cannot be considered as representative for the whole town since they were strongly influenced by site effects. However, by taking into account the fact that the historical reports also focused on these coastal areas, describing similar earthquake-induced failures, it was decided to follow the same procedure for the 2014 earthquakes in order to maintain the consistency with the historical seismicity reports.

Site	Long	Lat	ESI-07	EMS
Argostoli	20.49	38.17	VI	V-VI
Argostoli (Marina)	20.49	38.17	VI	
Lixouri	20.43	38.19	VII	VIII
Soulari	20.41	38.19	VII	VII
Livadi coastal plain	20.42	38.27	V	
Akrotiri	20.38	38.15	V	
Road Atheras to Livadi	20.41	38.29	VI	V
Atheras	20.41	38.31	V	VI
Petani Beach	20.37	38.26	V	
Myrtos Beach	20.53	38.34	V	
Livadi delta	20.42	38.25	VII	VII
Near Koulourata	20.67	38.19	IV	
Neochori	20.60	38.33	IV	
Road near Agkonas	20.49	38.30	V	IV
Kourouklata	20.47	38.23	V	VI
Skineas	20.39	38.24	VI	
Moni Kipoureon	20.34	38.20	VI	
	20.46	38.28	V	
Vlachata	20.61	38.1	V	
Chavdata	20.37	38.19	V	VII

Table 1: Spatial distribution of macroseismic intensities (ESI-07 and EMS scale) of the Feb. 3 event. The latter intensities values were obtained by Papadopoulos et al. (2014).

Acknowledgements: Field work was funded by the GSRT project INDES-MUSA http://www.indes-musa.gr/ and the FP7 project RASOR http://www.rasor-project.eu/. We thank Spiros Pavlides, Efthimios Lekkas, Alexis Chatzipetros, Gerassimos Papadopoulos, Ioannis Koukouvelas, Vassilios Karastathis, Alexandra Moshou, Christina Tsimi and Maria Sachpazi for discussions. We also thank the local authorities for permits and assistance.

References

Albini, P., N. Ambraseys, G. Monachesi, (1994). *Material for the investigation of the seismicity of the Ionian Islands between 1704 and 1766*. Materials of the CEC Project "review of historical seismicity in Europe". vol. 2, pp 11-26.

Barbiani, D.G., B.A. Barbiani, (1864). *Memoires sur les tremblements de terre dans l'ile de Zante*. 112 p (in French).

Ganas, A., A.I. Oikonomou, and C. Tsimi, (2013). NOAFAULTS: a digital database for active faults in Greece. *Bulletin of the*

Geological Society of Greece. vol. XLVII and *Proceedings of the 13th International Congress*. Chania, Sept. 2013.

EPPO-ITSAK, (2014a). *The January 26th, 2014 Earthquake in Cephalonia, Preliminary Report*, by EPPO-ITSAK (in Greek). (http://www.slideshare.net/itsak-eppo/20140127 kefaloniaeqpreliminaryreporta).

EPPO-ITSAK, (2014b). *Strong Ground Motion of the February 3, 2014 Cephalonia Earthquake: Effect on Soil and Built Environment in Combination with the January 26, 2014 Event*. (http://www.slideshare.net/itsak-eppo/20140203-kefaloniaeq-report-en).

Kalogeras, I., (2014). *Preliminary Analysis of the Recorded Strong Ground Motion Triggered by the January 26, 2014 Cephalonia Earthquake*. (in Greek) (Available on-line at http://www.gein.noa.gr/Documents/pdf/Cefalonia_20140126_preliminary_web.pdf).

Louvari, E., A.A. Kiratzi, and B.C. Papazachos, (1999). The CTF and its extension to western Lefkada Island. *Tectonophysics*. 308, 223-236.

Makropoulos, K., V. Kouskouna, (1994). *Material for the investigation of the seismicity of the Ionian Islands between 1704 and 1766.* Materials of the CEC Project "review of historical seismicity in Europe". vol. 2, pp 27-36.

Michetti, A.M., E. Esposito, L. Guerrieri, S. Porfido, L. Serva, R. Tatevossian, E. Vittori, F. Audemard, T. Azuma, J. Clague, V. Comerci, A. Gurpinar, J. McCalpin, B. Mohammadioun, N.A. Mörner, Y. Ota, and E. Roghozin, (2007). Intensity Scale ESI 2007. In: (Guerrieri, L. and Vittori, E. Eds.). *Mem. Descr. Carta Geol. d'Italia*. 74, pp. 53, Rome.

Moshopoulos, G., (1994). Inventory of dmages induced by the earthquakes during 1626-1638 in the island of Cephalonia. *Bizantina Simicta.* 9, pp 83-94.

NOA web report (2014). http://www.gein.noa.gr/Documents/pdf/Kefalonia2014_ekthesi_G_I.pdf

Papadopoulos, G., V. Karastathis, I. Koukouvelas, M. Sachpazi, I. Baskoutas, G. Chouliaras, A. Agalos, E. Daskalaki, G. Minadakis, A. Moshou, A. Mouzakiotis, K. Orfanogiannaki, A. Papageorgiou, D. Spanos, I. Triantafyllou, (2014). The Cephalonia, Ionian Sea (Greece), sequence of strong earthquakes of January-February 2014: a first report. *Research in Geophysics*. V4: 5441.

Papathanassiou, G., S. Pavlides, B. Christaras, K. Pitilakis, (2005). Liquefaction case histories and empirical relations of earthquake magnitude versus distance from the broader Aegean region. *Journal of Geodynamics*. Volume 40, Issues 2-3, pp. 257-278.

Papazachos, B.C., (1985). Evidence for transform faulting in the Ionian Sea: the Cephalonia Island earthquake sequence of 1983. *Pure Appl. Geophys*. 123, 387-397.

Papazachos V., K. Papazachou, (1989). *The earthquakes of Greece*. Zitis Publ. Thessaloniki. 356 p (in Greek).

Papazachos, B.C., P.E. Comninakis, G.F. Karakaisis, B.G. Karakostas, Ch.A. Papaioannou, C.B. Papazachos, E.M. Scordilis, (2000). *A catalogue of earthquakes in Greece and surrounding area for the period 550BC-1999*. Publ. Geoph. Lab. Univ. of Thessaloniki. 1, 333 pp.

Partsch, J., (1892). *Cephalonia and Ithaki*. pp. 69-77 (in Greek).

Sachpazi, M., et al., (2000). Western Hellenic subduction and Cephalonia Transform: local earthquakes and plate transport and strain. *Tectonophysics*. 319, 301-319.

Scordilis, E.M., G.F. Karakaisis, B.C. Karakostas, D.G. Panagiotopoulos, S. Valkaniotis, A. Ganas, G. Papathanassiou, M. Papanikolaou, (2014). Field observations of geological effects triggered by the January-February 2014 Cephalonia (Ionian Sea, Greece) earthquakes. *Tectonophysics*. 630 (2014) 150-157.

Vergotis, P., (1867). *The January 23, 1867 Cephalonia earthquake*. 15 p. (in Greek).

INQUA Focus Group on Paleoseismology and Active Tectonics

paleoseismicity.org

Positive correlation between CO2 daily peaks and micro-earthquakes occurrence in deep fault-caves: an empirical model

Pérez-López, R. (1), Bañón, E. (2), López-Gutiérrez, J. (1), Lario, J. (3), Rodríguez-Pascua, M.A. (1), Martín-Velázquez, S. (4), Giner-Robles, J.L. (5), Silva, P.G. (6), del Moral., B. (1), Pueyo-Morer, E.L. (1)

(1) IGME – Instituto Geológico y Minero de España. Geological Hazard Division. GSS-Geological Survey of Spain. C/ Ríos Rosas 23, Madrid, 28003, Spain. Email: r.perez@igme.es
(2) Espeleoclub RESALTES, Molina del Segura Division, Murcia, Spain
(3) Facultad de Ciencias. UNED. Senda del Rey, 9, Madrid 28040, Spain
(4) Universidad Rey Juan Carlos, Madrid, Spain
(5) Dept. Geología y Geoquímica. Universidad Autónoma de Madrid, Spain
(6) Departamento de Geología. Universidad de Salamanca, Spain

Abstract: *The south-eastern part of Spain is determined by different active faults affecting limestone terrains. These terrains have been affected by endokarstic processes. The Benis Cave is the deepest explored cave in the region and it was related to an active fault. Evidence of recent paleoseismic activity and the peculiar topography of the cave, encouraged us to monitor the daily CO_2 content in the air composition at depth (-280m), and for a time period of four months. Our results show a preliminary positive correlation between micro-seismic activity in the surroundings (up to 60 km away), and the CO_2 concentration (daily increasing of 40ppm for the closest microearthquakes). Moreover, there is an empirical relationship between the daily increment value and the distance to the epicentre. Therefore, we propose an increase in the CO_2 concentration into the air karst related to the micro-seismic activity. Despite this preliminary worthy results, more data are needed to establish an accurate model for earthquake forecasting.*

Key words: *CO2 concentration, earthquake, time series, fault-cave, Spain.*

INTRODUCTION

Normally the gas emission related to earthquake occurrence has been analysed in surface rupturing associated to strong earthquakes (M<7) (Bonfanti et al., 2012, Zheng et al., 2013). Besides, the searching of earthquake-induced gas emission is mainly focused in radon (e.g. Birchard & Libby, 1980). In this work, we have monitored atmospheric CO_2 values within a deep cave, which was developed in relation to an active fault.

This cave was developed along the Benis Fault, in the south east part of Spain. We have introduced a CO_2 meter device into the Benis Cave at 280m in depth. Bearing in mind that the air in caves, deeper than 50m, exhibits a positive correlation to the daily barometric variations and there is some delayed response, we can correlate the CO2 sharp changes of the air concentration with other instantaneous processes like earthquakes. Hence, we have obtained a CO_2 time series for four months between the year 2012 and 2013.

The main objective of this work is to correlate the atmospheric CO_2 concentrations in a deep cave with the micro-seismicity. These events were spatially located up to 60 sqkm from the fault-cave. In conclusion, seven events could be related with an increasing of CO_2 emission and for the period of the preceding hours.

GEOLOGICAL SETTING

The Benis Cave is the deepest explored cave of the Murcia Region, south-eastward of Spain. This cave has been developed from the Early-Quaternary along an active fault striking N-S and dipping 75º towards the E (Pérez-López et al., 2009, 2010, 2012, 2013). This fault belongs to the Betic Range, and the movement affects the Prebetic units and the Subbetic ones (Fig. 1).

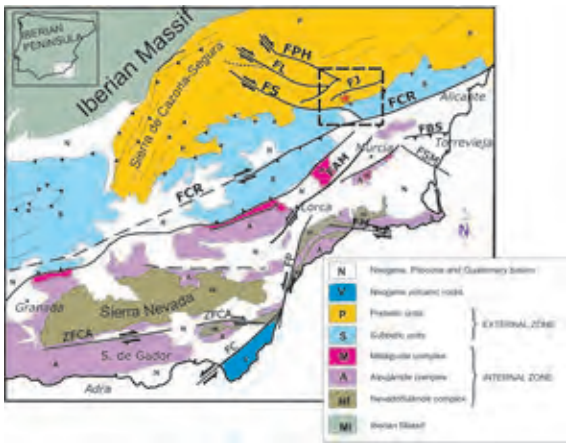

Figure 1: Geographical location and geological setting of the Benis cave (red star). All faults are actives, being the FS: Socovos Calasparra Fault, the FAM: Alhama de Murcia fault and FCR: Crevillente Fault.

The topography of the cave is divided mainly in two parts (Fig. 2). (1) Parallel vertical phreatic tubes developed along an E-trending calcite vein, and with

metric section and evidence of slow flows of water and hydrothermal process (scallops). At 150 metres depth, the phreatic tubes connect with the fault plane and the cave develops a new section (2) fault-cave s.s. The karst affects the fault plane until the deepest zone (-350 m) of the cave, appearing endokarstic decoration due to dripstones (small stalactites and stalagmites), mantle flow of calcite and pop-corns. Pérez-López et al.(2009) described different paleoearthquakes affecting the cave and a ceiling collapse related to a seismic crisis in 1999, with earthquakes of magnitude M4.9.

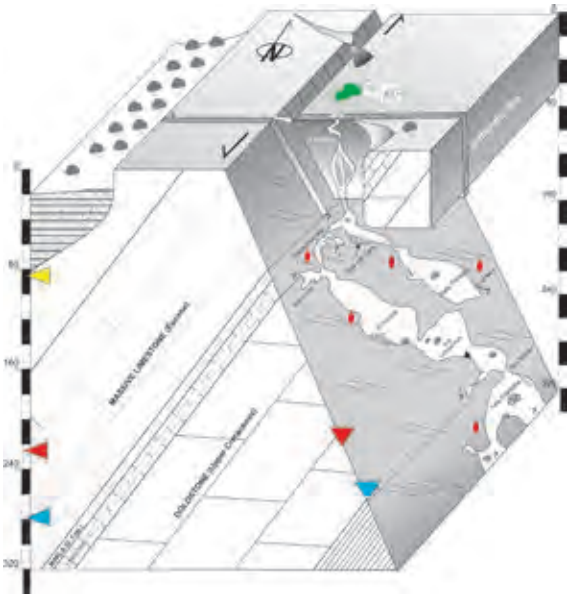

Figure 2: Diagram of the cave development and the fault plane. Yellow triangle is the infilling of the Quaternary deposits, red triangle is the depth where the cave were developed underwater (phreatic endokarstic zone) and the blue one is the last phreatic level into the cave. Beach balls indicate sites of paleoseismic evidence and kinematics grove marks.

CO2 DATA LOGGING: RESULTS

In December of 2012, we have installed a CO_2 data logger, CO_2METER ©, with a non-dispersive infrared (NDIR) sensor with automatic background calibration algorithm, and placed at 280m in depth. This sensor has accuracy of 30 ppm and it works for a CO_2 range of 1% (0-10.000 ppm). The resolution is 1 ppm and the temperature interval is -40 to 60ºC, for a relative humidity of 99%. The data logger recorded a data each 2 hours in an ongoing register during this time interval. We have also compiled the seismic events that have occurred in the vicinity of the cave during the same time interval. Moreover, we have used a hydrophobic device for avoiding condensation on the CO_2 sensor.

We have obtained daily time-series of CO_2 concentration (Fig. 3), from the 22nd of December, 2012 to the 3rd of May, 2013. The CO_2 emission daily values increase along the measurement time with a constant slope, related to the humidity saturation of the sensor. However, this sensor was working during 5 months with no failure. The bias of the CO_2 signal is a long-term trend (Fig. 3) related to the increasing of humidity at the sensor. Accordingly, we have used the difference between two correlative days instead of the daily absolute value of CO_2 into the cave.

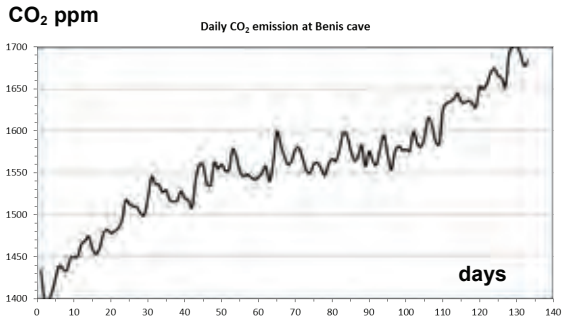

Figure 3: Daily CO_2 emission (ppm, Y-axis) at 290 m. depth within the Benis Cave. The time-series was built with the daily arithmetic mean during 133 days.

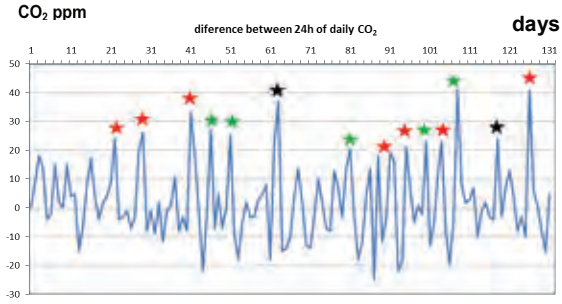

Figure 4: Daily CO_2 variation (Day_{n+1}-Day_n) (Y-axis, ppm). Red stars indicate earthquakes in the same day. Green stars are peaks related to earthquakes in 24h and black stars are days with no earthquake record.

EARTHQUAKES WITHIN THE AREA

We have used the earthquakes recorded by the seismic network of the *Instituto Geográfico Nacional*, from the online catalogue (National Geographical Service of Spain, http://www.ign.es/ign/layoutIn/sismoFormularioCatalogo.do). The earthquakes were recorded from the 22th of December, 2012 to the 3th of May, 2013. The radio of searching was 70 km, because of the main active faulting in the Betic Range are 60 km away from the measurement point.

The IGN catalogue has recorded 89 earthquakes with a maximum magnitude of M3.7 during this time interval. One of these earthquakes was located 5 km away of the pit-cave (with positive correlation), four are located 10 km away (three with positive correlation, located southward of the pit-cave, the negative is located northward) and seven were located 20 km away, with positive correlation. Finally, there are three earthquakes with positive correlation 60 km away to the pit cave and

also, southward of the pit cave. The horizontal error is 1 km (IGN catalogue description, www.ign.es).

DISCUSSION

Figure 4 shows the difference between two correlative CO_2 values (CO_2 day2-CO_2day1). The idea behind this graph is to obtain abrupt changes in 24 hour interval, to be correlated with the earthquake occurrence in the surroundings. Furthermore, we have included the earthquakes recorded in this area related to daily increasing (coloured stars) for searching temporal correlations. Other earthquakes within the search zone did not vary the air content of the cave. These earthquakes are located east and northward of the cave.
As worthy result, we have found a relationship between the atmospheric CO_2 value and the seismic weak events (M<2.5) 20 km away and southward of the pit-cave. The daily coincidence between earthquake and sharp CO_2 increase is represented in the Fig.4 by red stars. In these cases, the daily variation is greater than 20 ppm. This is important because the accuracy is 30 ppm for a punctual measurement and 10 ppm for the daily measurement. Green stars are earthquakes which occurred within 24 hours of the CO_2 peak and black stars are the two uncorrelated cases.
Moreover, we have plotted the maximum CO_2 daily difference and the distance of the epicentre (Fig. 5). There are only six points because there are two equal points. We have not weighed each point with the seismic energy released due to the earthquake size are very small 1.1 <M<2 in relation to the distance of the epicentre. The greater earthquake of M3.7 did not affect the cave air composition apparently.

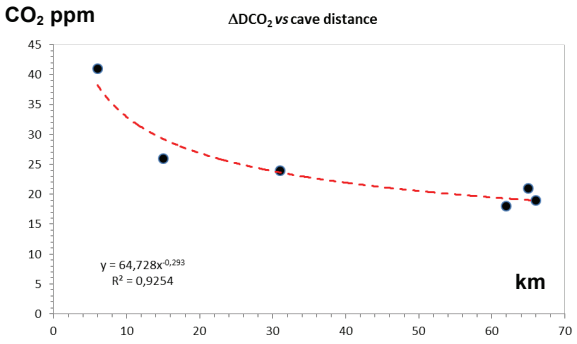

Figure 5: Function of the CO_2 daily variation (in ppm) of the cave atmosphere at 280m depth with the distance of the epicentre.

There is an empirical relationship between the CO_2 anomaly and the earthquake distance of the epicentre according to the following expression:

$$\Delta CO_2(24h) = 64.73 \cdot X^{(-0,29)} \quad \text{[eq. 1]}$$

Where ΔCO_2 is the daily increasing of CO_2 (ppm) with and error of ± 6 ppm, and X is the distance between Benis Cave and the epicentre of the earthquake. Of course, more data are required and stronger earthquake.
In this area, there are no reports about a sharp daily increasing of CO_2 in deep caves related with non-seismic activity, as atmospheric CO_2 sink, dramatic increasing of organic activity and/or massive dissolution of waters. There is no underground aquifer human irrigation from the middle of the XXth century in this zone.
The CO_2 inorganic sources (i.e. not-related to organism breathing) in caves are related to the diffusion into the external atmosphere, diffusion into the voids in underlying rocks, and to dissolution in percolating waters. However, we will have to analyse the isotopic CO_2 data in the air, the soil of the cave at this depth and the pit cave in future research. In this work, we propose that the micro-seismic activity increases the CO_2 gas flux-rate across the karst, independently of the gas source.

CONCLUSIONS

1. There is a positive correlation between micro-earthquakes (M<2.5) and atmospheric anomalies within the Benis fault-cave. Seismic events are related to sharp daily increase in atmospheric CO_2 (>20 ppm).
2. The area of influence for this gas mobilisation is up to 60 km and southward of the pit cave.
3. Furthermore, there is an empirical relationship between the concentration of CO_2 emission and the distance of the epicentre, for the geological units of the Betic Range.

These preliminary results have to be completed with more data, CO_2 devices in other caves related with more active faulting and accurate models of CO_2 sinking and diffusion in karst. Also, isotopic analyses of atmospheric CO_2 into the Benis cave are required. Finally, autocorrelation analysis and the Fourier transform could help to find similarities between both time series.

Acknowledgements: Thanks are given the SpeleoClub RESALTES and all the members who collaborated in this project. This work is a contribution of the Spanish projects SISMOSIMA CGL2013-47412-C2-2-P, and QTECTBÉTICA CGL2012-37281-C02.01.

References

Bonfanti, P., Genzano, N., Heinicke, J., Italiano, F., Martinelli, G., Pergola, N., Telesca L., Tramutoli, V., (2012). Evidence of CO2-gas emission variations in the central Apennines (Italy) during the L'Aquila seismic sequence (March-April 2009). *Bollettino di Geofisica Teorica ed Applicata* , 53, 1, 147-168.

Birchard, G. F. and Libby, W. F. (1980) Soil radon concentration changes preceding and following four magnitude 4.2–4.7 earthquakes on the San Jacinto fault in Southern California. *J. Geophys. Res.* 83(B6), 3100–3106.

Pérez-López, R., Rodríguez-Pascua, M.A., Giner-Robles, J.L., Martínez-Díaz, J.J., Marcos, A., Bejar, M. and Silva, P., (2009). Spelaeoseismology and palaeoseismicity of the "Benis Cave" (Murcia, SE of Spain): coseismic effects of the 1999 Mula earthquake (mb 4.8). *Geological Society of London Special Publications*, 316: 207-216.

Pérez-López, R., E. Bañón, M. Rentero, J.L. Giner-Robles, M.A. Rodríguez-Pascua1, P.G. Silva, J.C. García López-Davalillo y

García-López M., (2010). Análisis Térmico Preliminar de la Sima De Benis (-350m), Murcia. In: *Avances de la Geomorfología en España. XI Reunión Nacional de Geomorfología. Comunicaciones*, 1:1-5.Solsona.Spain

Pérez-López R., E. Bañón, J. Lario, P.G. Silva, M.A. Rodríguez-Pascua, J. García-Mayordomo, E. Pueyo, A. Marcos-Nuez., (2012). Shallow Vertical Geothermal Gradient and Heat Flow within the Benis Cave (-320m, Cieza): Quaternary slip-rate for active fault-caves. *Geotemas*,13, 463-466.

Pérez-López, Raúl, Enrique Bañón, Emilio L. Pueyo, J. Lario, M.A. Rodríguez-Pascua, P.G. Silva, (2013). Weak signal of CO2 emission in deep caves related with weak earthquakes (M<2.5) in tectonically active areas. In: *Reunión Anual de la Unión Geofísica Mexicana*, *GEOS, VOL 33*, nº1. Puerto Vallarta. México.

Zheng, G., S. Xu, S. Liang, P. Shi, J. Zhao, (2013). Gas emission from the Qingzhu River after the 2008 Wenchuan Earthquake, Southwest China. Chemical Geology 339, 187–193.

INQUA Focus Group on Paleoseismology and Active Tectonics

Environmental effects, building collapse and S-wave ground-shaking during the Orihuela earthquake (1048 CE Muslim Period, SE of Spain)

Pérez-López, R. (1), Martín-González, F. (2), Silva, P.G. (3), Béjar-Pizarro, M. (1), Martínez-Díaz, J.J. (4), Rodríguez-Pascua, M.A. (1), Giner-Robles, J.L. (5)

(1) IGME – Instituto Geológico y Minero de España. Geological Hazard Division. GSS-Geological Survey of Spain. C/ Ríos Rosas 23, Madrid, 28003, Spain. Email: r.perez@igme.es
(2) Universidad Rey Juan Carlos. Madrid, Spain
(3) Universidad de Salamanca. Avila, Spain
(4) Dept. Geodinámica. Faculta de Ciencias Geológicas. Universidad Complutense de Madrid, Spain
(5) Dept. Geología y Geoquímica. Universidad Autónoma de Madrid, Spain

Abstract: *Ancient historic earthquakes in different cultural periods are hard to describe according to the present guidelines for paleoseismic records. In this context, the determination of the potential seismic source for hazard analysis comes from different disciplines: geology, archaeology and geophysics. In this work, we have applied this multi approach to the earthquake of Orihuela, which took place in the southeast city of Spain in the year 1048 CE (Muslim period). Firstly, we have estimated the ESI07 environmental macroseismic scale and we have studied the collapse of the major buildings. Secondly, we have carried out a lichenometry timing of the rock-falls nearby of the historical epicentre (50 km away). Finally, we have determined the theoretical radiation pattern of the S-waves from the active faults of the database of Spain within the area. Therefore, three faults could be the potential source for this historical event, The Carrascoy Fault close to the connection to the Hurchillo Fault, and the Alhama de Murcia Fault.*

Key words: *Environmental earthquake effects, historical earthquake, lichenometry, s-wave pattern, Muslim Period Spain.*

INTRODUCTION

The most of the historical seismicity of Spain is mainly located at the southeast part of the country and the catalogue of historical seismicity is complete from the XVIth century onwards. However, several destructive and large earthquakes, affected this zone during the Muslim period of Spain (VIII-XIVth centuries), but then again they have been vaguely described.

One of the most destructive earthquakes during this period of Spain was in the XIth century, the so called Orihuela earthquake. This earthquake was described by the epoch muslim geographer al'Udhri, who was the person in charge to the written description of the geography and social events in the Tudmir kingdom during the XIth century (al Udhri, 1967, Espinar-Moreno, 1994, Bretón González & Espinar Moreno, 1996, Martínez-Solares & Mezcua, 2002, Sánchez-Pérez & Alonso de la Cruz, 2004, Silva et al., 2014 and 2015).

Unfortunately, this is the only evidence of this large historic earthquake that collapsed one of the most important cities in the Muslim Period of Spain, the Orihuela city. Thus, the relevance to determine the parametrization of this earthquake is crucial for realistic hazardous studies of earthquakes in this zone.

Therefore, in this work we have applied a multidisciplinary approach for analysing the potential seismic source of the Orihuela earthquake throughout: (a) an estimation of the ESI07 macroseismic environmental scale (Michetti et al., 2007) according to the historical writings, (b) lichenometric analysis of surroundings rock-falls and volumetric estimation and (c) a theoretical approach of the S-wave radiation pattern from the online active faulting data base of the IGME (*Instituto Geológico y Minero de España*, García-Mayordomo et al., 2012). As preliminary conclusion, either the Carrascoy Fault in the linking area with the Hurchillo or the Alhama de Murcia Fault (Alcantarilla segment), are the best candidates as the seismic source of this earthquake (Fig. 1).

HISTORICAL DATA

A few sentences of the Muslim geographer al-Udhri described a destructive earthquake that collapsed the cities of Mursiya (Murcia) and Uryula (Orihuela) (al Udhri, 1967, Espinar-Moreno, 1994, Bretón-González & Espinar Moreno, 1996): "After the year 440 of the Hijra (1048 CE), earthquakes followed one another in the region of Tudmir, especially in the cities of Uryula and Mursiya and in the area between them. Tremors repeated continuously for about a year, occurring daily several times, by night and by day time. Houses were destroyed and minarets and all high buildings fell down. The major mosque in Orihuela and its minaret were destroyed. In-between the entire region the earth was cracked; many springs dried up and in some of them a foul smell could be felt". Here we can divide the main effects in two types:

Environmental effects

The geological effects described in the historical text of al-Udhri include ground cracks and hydrological anomalies (dried springs and liquefaction Silva et al.,

2015). These effects are located between the cities of Murcia and Orihuela (present names) (Fig. 1). The spatial length between both cities is ca 18 km. Hence, bearing in mind that both localities are within a valley of 8 km width, the potential affected zone for the maximum ESI intensity could be close to 150 km^2. Also, the hydrological anomalies are related to spring drying, liquefaction and gas emission. No reported data on the liquefied grain size. The gas emission probably was methane, according to the bad odour described by the geographer. Therefore, the recommended ESI07 intensity is VIII-IX for this zone (Silva et al, 2014 and 2015). This intensity value is greater than the intensity VIII EMS 98 proposed by Martínez-Solares & Mezcua (2002).

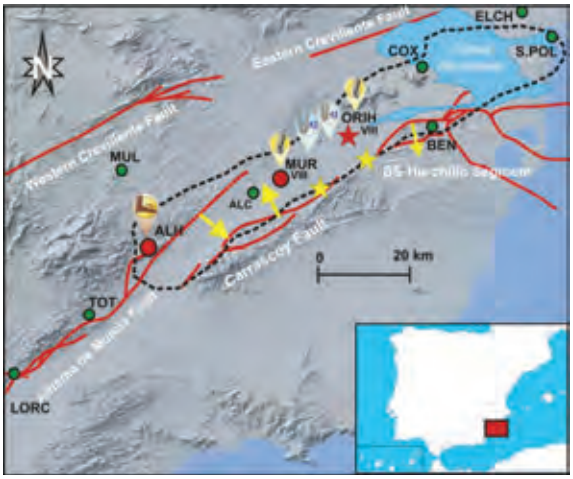

Figure 1: Geographical location of the studied area. The red star corresponds to the macroseismic epicentre of the Orihuela earthquake. Red dots are cities with building damage and environmental effects (ALH Alhama de Murcia, MUR Murcia, ORIH Orihuela. Green dost are cities with no reporting effects MUL Mula, LORC Lorca, TOT Totana, ALC alcantarilla, BEN Benejúzar, COX Cox, GUAD, ELCH Elche, S.POL Santa Pola. Red lines are active faults of the IGME database. Symbols are the environmental effects described in the main text. The dashed line encircles the estimated affected zone. Yellow arrows point to the main SH-wave propagation. Yellow stars are the proposed epicentres. See text for further explanation.

Building damage

The building collapse related to this earthquake is vaguely described as well. However, there are some relevant clues related to the destruction of the minaret of Orihuela. In those days, the Syrian influence in this region and ancient description suggest a minaret of square section (Marrakesh type) and as higher as 30 m and 10x10 m^2 of square length. The entire destruction of this building suggests a strong-motion (Levy and Salvadori, 2002). This implicates long- period of vibration (greater than 1 sec.) and probably far effect (hypocentre located between 10 and 50 km). The geographer pointed out that all the higher edifices were destroyed and a lot of houses also.

The earthquake also triggered aftershocks during one year, with a high frequency of number of small events per day (felt during the daylight and the night). It is relevant that there is no strong aftershock although the elapsed time between the main shock and the aftershocks one year) suggest an earthquake of strong magnitude (probably >= M6).

Figure 2: Snapshot of the largest conglomerate boulder mobilised during the 1048 CE earthquake. The white patch corresponds to a calcicolous lichen "Aspicilia calcarea" affecting the carbonate matrix of the conglomerate. The age of this lichen is 1049 CE and the volume larger than 400 m^3.

Block	age CE	vol m^3
1	1049	432
3	1121	55
2	1164	54
6	1249	70
8	1313	13
5	1424	96
7	1582	12
4	1622	64

Table 1: Lichen ages of the blocks measured in the north part of Alhama de Murcia city. Blocks 7 and 4 are related to the 1579CE earthquake. The age corresponds to the maximum measured lichen ("ante quem"). See fig.1 for the geographical location of Alhama (ALH).

LICHENOMETRY OF ROCK-FALLS

We have carried out a lichen age estimation of the rock-falls in the surrounding of Orihuela. There are a lot of sites with rock-falls although only one of them exhibits boulders as older as 1049 CE (Table 1.). This site is located north to the Alhama de Murcia (see fig.1 for location, ALH) in the south side of the Alhama Range.

We have used the calcicolous lichen "Aspicilia calcarea" as the clock-lichen for dating the boulder. This lichen colonizes the carbonate matrix of the boulder (puddingstone), with small clasts of quartz and allochtoon clasts from metamorphic rocks. We assumed the annual

growth rate of 0.26 mm per year (Pérez-López et al., 2012). The table 1 shows the lichen ages of the lichens measured into the zone. The oldest boulder is 1049 CE and corresponds to the largest boulder into the area, 400 m^3 (Fig. 2). The error of the calibration formula is 4 years.
The area of the rock-falls is located south-westward of the Orihuela city, and 49 km away (Fig. 1). The total volume mobilised by this earthquake in this site was 700 m^3.

city name (ancient name in 1048)	distance to Orihuela	orientation	damage	EEE
Orihuela (Medina Uryula)	0	..	IX	yes
Benejuzar (Beneyucef?)	10	E		
Cox (Benimancoj?)	10	NE		
Murcia (Medina Mursiya)	19	SW	IX	yes
Alcantarilla (Qantara Askaba)	27	SW		
Elche ('Ils)	29	NNE		
Santa Pola (al-Aljub)	36	NE		
Mula (Mulá)	47	W		
Alhama de Murcia (al-Hamma)	49	SW		yes
Cartagena (al-Qayrawan)	50	S		
Jumilla (Coimbra)	54	NE		

Table 2: Geographical parameters of the main cities during the Muslim period of the SE of Spain. The origin point is the epicentre, Orihuela.

S-WAVE RADIATION PATTERN

The S-wave is the responsible of the ground shaking vibration during the earthquake; they have high amplitude and produce vertical and horizontal motion of the ground surface. Hence, we have modelled the seismic S-wave radiation pattern and their congruence with the observed deformation. The Fig. 3 shows the radiation pattern for the Hurchillo segment of the Bajo Segura fault, the Carrascoy fault and the Alhama de Murcia fault (Alcantarilla segment). We have used the online code of http://demonstrations.wolfram.com/RadiationPatternForDoubleCoupleEarthquakeSources/, last access 3th of January, 2015. The Hurchillo fault exhibits a main propagation direction towards SE, similar to the Alhama de Murcia fault. However, the Carrascoy fault shows a double sense although NE is the dominant one.

POTENTIAL SEISMIC SOURCE DISCUSSION

The table 2 shows the cities during the Muslim period in the nearby of the affected zone. Cities affected by the earthquake are showed as red dots in the Fig.1. The affected area appears as an elongated zone about 300 km^2 and with NE-trending.
We have included into the Fig.1 the active faults of the IGME data base (http://info.igme.es/qafi/ last access 8th of January, 2015) and the Lower segment of the Bajo Segura fault (Silva et al., 2015). The closest fault to the epicentre is the Hurchillo segment of the Bajo Segura fault (Table 3), barely a few kilometres southward. However, the Carrascoy fault and the Alhama de Murcia fault (Alcantarilla segment) are both close enough to be considered as potential ones as well.
The location of rock-falls related to this earthquake suggests that the Carrascoy and the Alhama de Murcia could be a good candidate as the seismic source. They are well oriented for the S-wave pattern and close enough of the site.

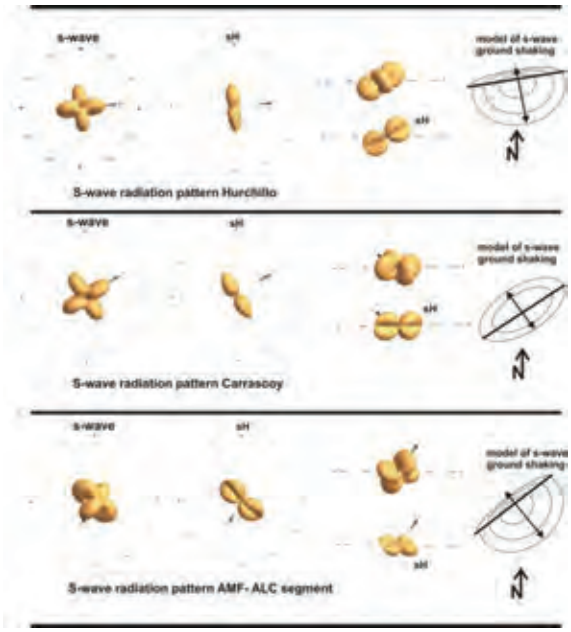

Figure 3: Theoretical model of the S-wave radiation pattern, according to the code online in the web site http://demonstrations.wolfram.com/RadiationPatternForDoubleCoupleEarthquakeSources/, last access 3th of January, 2015. Arrows suggest the main direction of the S-wave propagation. The left and central wave-patterns are views in plan, whereas the right one is a vertical cross section of the wave. The model is a qualitative approximation for the wave propagation.

fault name	strike	dip	type	length km	area km2	youngest deposits	slip rate mm/yr	Max. Mag.	RI (yrs)
BS-Hurchillo	83	60SE	reverse	9,2	117	Upper-Pleist.-Ho	0,35	6,3	1300
Carrascoy	90	90	Rev-SS	32	384	Upper-Pleist.-Ho	0,54	6,8	6000
AMF-Alc	45	90	Rev-SS	25	300	Middle-Pleist.	0,07	6,5	21000

Table 3: Parameterization of the potential faults as seismic source for the Orihuela earthquake. BS-Hurchillo is the Bajo Segura Fault, Hurchillo segment.AMF Alhama de Murcia Fault, Alc-Alcantarilla segment. Rev reverse faulting and SS strike-slip. Pleist.-Pleistocene. Ho-Holocene. RI-recurrence interval. All of these parameters were obtained from the IGME 2011 database. http://info.igme.es/qafi/ last access 8th of January, 2015.

CONCLUSIONS

(1) The Orihuela earthquake is a historic earthquake which occurred in the year 1048 CE (440 Hegira) with associated environmental effects including rock falling, ground cracks and hydrological anomalies. Therefore the estimated ESI07 scale is VIII.
(2) The affected area probably was about more than 500 km^2, in agreement with the VIII-IX ESI scale.

(3) The magnitude was probably greater than M6, although no strong aftershocks were reported.
(4) The potential sources are the Carrascoy Fault, the Alhama de Murcia Fault (north segment) and the Bajo Segura fault (Hurchillo and Lower segments).
(5) According to the results, the area in-between the Carrascoy and Hurchillo faults, could be the best choice as the responsible of the Orihuela earthquake.

Acknowledgements: This work is a contribution of the Spanish projects SISMOSIMA CGL2013-47412-C2-2-P, QTECTBÉTICA CGL2012-37281-C02.01 and CGL2011-14925-E, RESCATELO.

References

Al-`Udhri, A., (1965). *Nusus `an al Andalus min Kitab Tarsi al-akhbar*. ed. 'Abd Al-'Aziz Al-Ahwani, Madrid.

Bretón González, M., & M. Espinar Moreno, (1996). Fenómenos sísmicos que afectaron a las tierras andaluzas en los siglos IX al XII según las crónicas musulmanas. *Homenaje en honor al profesor Fernando de Miguel Martínez*. Granada. pp47-76.

Espinar-Moreno, M., (1994). Los estudios de sismicidad histórica en Andalucía: Los terremotos históricos de la provincia de Almería. In: *El estudio de los terremotos en Almería*. Inst. de Estudios Almerienses. pp. 115-180.

García-Mayordomo J., J.M. Insua-Arévalo, J.J. Martínez-Díaz, A. Jiménez-Díaz, R. Martín-Banda, S. Martín-Alfageme, J.A. Álvarez-Gómez, M. Rodríguez-Peces, R. Pérez-López, M.A. Rodríguez-Pascua, E. Masana, H. Perea, F. Martín-González, J. Giner-Robles, E.S. Nemser, J. Cabral, and QAFI Compilers (2012). The Quaternary Active Faults Database of Iberia (QAFI v.2.0). *Journal of Iberian Geology*. 38 (1), 285-302.

Levy, M., and M. Salvadori, (2002*). Why Buildings Fall Down.* W.W. Norton and Company, New York. 346 p.

Martínez-Solares J.M. & J. Mezcua, (2002). *Catálogo Sísmico de la Península Ibérica (880 aC-1900)*. Monografía, 18. IGN Ediciones. Ministerio de Fomento. Madrid. 253 p.

Michetti A.M., E. Esposito, L. Guerrieri, S. Porfido, L. Serva, R. Tatevossian, E. Vittori, F. Audemard, T. Azuma, J. Clague, V. Comerci, A. Gurpinar, J. Mc Calpin, B. Mohammadioun, N.A. Morner, Y. Ota, and E. Roghozin, (2007). Intensity Scale ESI. In: (Guerrieri, L. & Vittori, E. Eds.): *Memorie Descrittive Carta Geologica d'Italia*, 74, Servizio Geologico d'Italia. Dipartimento Difesa del Suolo. APAT, Roma, 53 pp.

Pérez-López R., F. Martín-González, J.J. Martínez-Díaz, M.A. Rodríguez-Pascua, (2012). Lichenometric age measured on rock-falls related to historic seismicity affecting Lorca and its surroundings (Murcia, SE Spain). *Boletín Geológico y Minero*. 123 (4), 473-485.

Poirier, J.P. and M.A. Taher, (1980). Historical seismicity in the near and middle east, North Africa, and Spain from Arabic documents (VIIth-XVIIIth Century). *Bulletin of the Seismological Society of* America. 70, (6), 2185-2201.

Sánchez Pérez, A.J. & R. del Carmen Alonso de la Cruz, (2004). El territorio alicantino en las fuentes geográficas árabes medievales (SIGLOS IX-XV). *Miscelánea Medieval Murciana.* XXVII-XXVIII, 103-124.

Silva, P.G., M.A. Rodríguez-Pascua, J.L. Giner-Robles, R. Pérez-López, J. Lario-Gómez, M.A. Perucha-Atienza, T. Bardají-Azcárate, P. Huerta-Hurtado, E. Roquero, M.B. Bautista Davila, (2014). *Catálogo de los efectos geológicos de los terremotos de España*. PG Silva y M.A. Rodríguez-Pascua (eds). IGME-AEQUA. Riesgos Geologicos/Geotecnia. nº 4. 352 pp. Madrid.

Silva, P.G., J. Lario, J.L. Giner-Robles, T. Bardají, R. Pérez-López, M.A. Rodríguez-Pascua, M.A. Perucha, E. Roquero, C. Zazo, J.L. Goy, (2015). Seismic paleogeography of coastal zones in the Iberian Peninsula: Understanding ancient and historic earthquakes in Spain. *Cuaternario y Geomorfología*. 29, (1-2).

INQUA Focus Group on Paleoseismology and Active Tectonics

Paleoseismology, Quaternary slip-rate and heat flow of the Benis Fault (SE of Spain)

Pérez-López, R. (1), Martín-Velázquez, S. (2), López-Gutiérrez, J. (1), Lario, J. (3), Silva, P.G. (4), Rodríguez-Pascua, M.A. (1), Giner-Robles, J.L. (5)

(1) IGME – Instituto Geológico y Minero de España. Geological Hazard Division. GSS-Geological Survey of Spain. C/ Ríos Rosas 23, Madrid, 28003, Spain. Email: r.perez@igme.es
(2) Universidad Rey Juan Carlos, Madrid, Spain
(3) Facultad de Ciencias. UNED, Senda del Rey, 9. Madrid 28040, Spain
(4) Dpt. Geología y Geoquímica, Universidad Autónoma de Madrid, Spain
(5) Departamento de Geología, Universidad de Salamanca, Spain

Abstract: *We have carried out a paleoseismic analysis of the Benis Fault, located at the southeast part of Spain. We have estimated the last earthquake size-magnitude and time, from evidence of celling collapse and displaced broken carbonate blocks (M6 and 65 ± 18 ka BP). Our analysis suggests that the tectonic slip-rate of the Benis Fault is lesser than 0.01 mm/yr. Additionally we have measured the deep thermal profile of the Benis Cave (-350 m of vertical development, Cieza, SE of Spain), from single rock point temperature measurements in different field campaigns and for a period of 2 years. The temperature increases with depth, being in consequence a reverse thermal profile in comparison with normal gradients in deep caves. Furthermore, we have estimated the Vertical Geothermal Gradient with a value of 1.85ºC/100 m for the deepest zone (-150-290 m). Finally, we have calculated the heat flux of 0,46 mWm^2.*

Key words: *Paleoseismology, Benis fault, slip rate, heat flux, Spain.*

INTRODUCTION

Endogenous processes are commonly the cause for thermal anomalies into the lithosphere, mainly active tectonics and volcanism. There are a lot of thermal springs and roman baths (*thermaes*) within the Murcia province, i.e. Fortuna Basin, Alhama de Murcia (Muslim word for Arabian bath, al-hamma). Moreover, this area is one of the more active in seismicity of Spain, recording the earthquake of Lorca in 2011 (Mw= 5.1, Martínez-Díaz et al., 2011).

The study of the vertical geothermal gradient is useful for the geomechanical analysis of the upper part of the lithosphere, properties which can be used for the estimation of the deformation tectonic rates (i.e. Luetscher & Jeannin, 2004, García-Mayordomo & Giner-Robles, 2006, Doan & Cornet, 2007). Bearing in mind the presence of thermal zones and active faulting within the Murcia province (Spain), in this work we have calculated the vertical geothermal gradient for the first 350 m of the lithosphere, by using a punctual measurement of the rock temperature into the cave of Benis (Fig.1). The Benis cave is a cave developed throughout the Benis fault (Pérez-López et al., 2009, 2010), reaching 350 metres of depth in the deepest explored zone.

Figure 1 shows the relationship between caves and active faults in the zone. This is because the geological units are mainly carbonates, dolostones and detritic calcareous sandstones. The most of these caves have geothermal gradients related to high temperatures in the air cave: *Sima del Vapor* (-85 m, 43ºC), *Sima de la Higuera* (-105 m, 18ºC), *Sima del Pulpo* (-114 m, 21ºC), and *Sima de Benis* (-350 m, 25ºC), among others. We have chosen the Benis cave (Sima de Benis).

In this work, we have carried out a paleoseismic analysis of the Benis fault and we have described the thermal zonation, calculated the vertical geothermal gradient (VGG) and estimated the heat flow for the Benis cave.

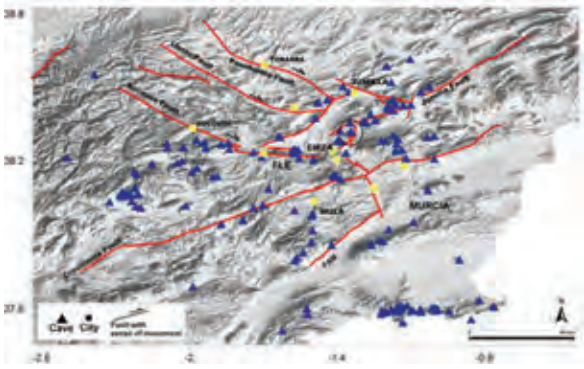

Figure 1: Active faults (red lines) and caves (blue triangles) in the Betic Cordillera. FAM: Alhama de Murcia Fault. The encircled central zone is the Benis fault with N-trending, close to the village of Cieza. Yellow squares are cities.

GEOLOGY OF THE BENIS FAULT

The Benis fault is located in the Betic geological units, in the southeast part of Spain (Jerez-Mir et al, 1972). Regarding the geometry of the fault, it is oriented N-S and dipping 75ºE (Pérez-López et al., 2009). The surface fault trace reaches 6 km, affecting upper Cretaceous limestone, Eocene carbonate units and Quaternary alluvial deposits (Fig. 2). The fault plane shows slickensides inside the cave, compatible with a normal faulting with left-handed strike slip component (Pérez-López et al., 2009).

Pérez-López et al. (2010) have excavated and studied the complete skeleton of a *Lynx pardinus spelaeus*, which was found in the Benis cave (175m depth) in a normal position of death (Fig. 3). These authors suggested that the extinguished feline died by inanition from the bones and teeth analysis, probably related with a past earthquake which obstructed the exit of the cave by ceiling collapse. They dated the time of the death in 64.,4 ± 17.6 ka BP by racemization of amino acids of the teeth (Pérez-López et al., 2012).

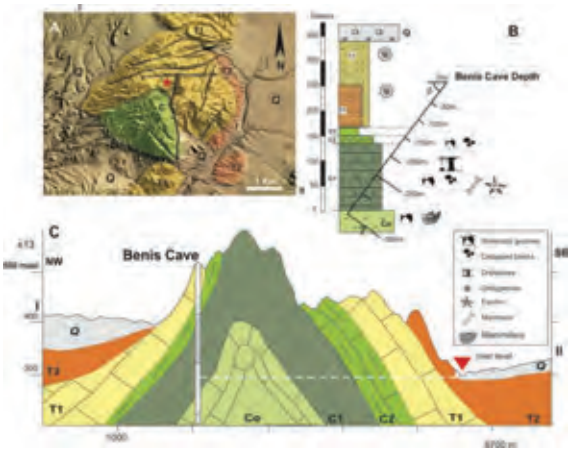

Figure 2: Geological cross section and vertical development of the Benis Cave. The cave affects Cretaceous limestone and dolostone and Tertiary carbonate. The Benis fault affects Quaternary alluvial fans. No dating available for the cave decoration.

Furthermore, this fault shows evidence of oblique movement affecting a glued block on both sides of the fault, with a net slip of ca 60 cm. Assuming this displacement as coseismic offset, the magnitude associated by using the Wells and Coppersmith (1994) empirical relationship is 6.4<M<6.5. This value is lightly greater that using the length trace of the Benis fault and assuming a total surface rupture (6 km), with an earthquake of magnitude 6.3.

THERMAL PROFILE

We have measured punctual values of temperature in the rock of the Benis Cave and at different depth. We have used a THERMOCOUPLE device DELTA-OHM with a K-type sensor, 2 minutes of measurement time, 0.2ºC of accuracy and 0.1ºC of resolution. Besides, we have used a TELAIRE 7001 device for atmospheric CO_2 and temperature. Figure 4 shows the temperature profile obtained in different field work for a period of two years (2010-2011).

We have classified the thermal zones into the cave accordingly to the profile: (Z1) Hetero-thermic shallow zone: located between the pit cave and -50m, this is the zone of influence of the outside atmospheric conditions of temperature (seasonal variations) and CO_2 content. (Z2) Homo-thermic zone: located between 50 and 200 m of depth.

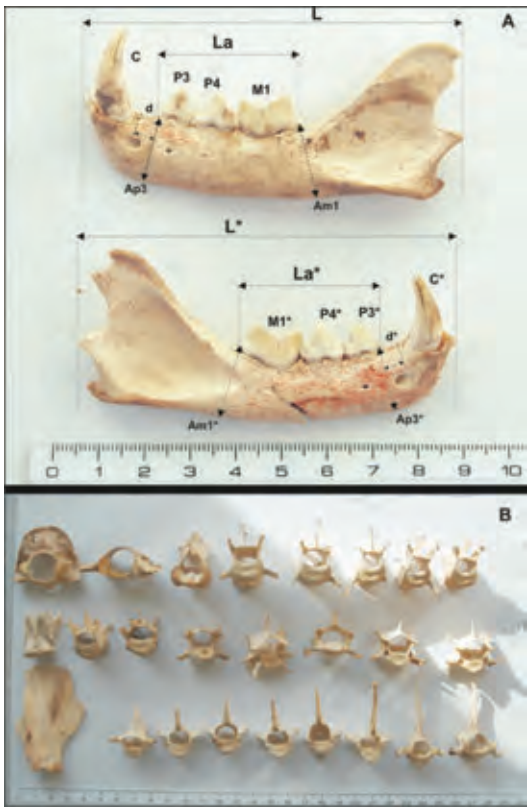

Figure 3: Paleontological record of the "Lynx pardinus spelaeus" excavated into the Benis cave. The racemization analysis was performed on the fangs of the feline.

The temperature is almost constant, ranging between 23ºand 24ºC. (Z3) Hetero-thermic deep zone: between 200 and 320 m of depth, there is an increase of temperature. These zones are similar in depth to those defined by Luetscher & Jeannin (2004) for different deep karst around the world, suggesting the thermal conduction as the main driving process for the rock temperature.

GEOTHERMAL GRADIENT AND HEAT-FLUX

We have fitted a curve for the values of temperature in the hetero-thermal deep zone (200-320 m depth) (Fig.4), since this is the zone with inner heat input. Hence, we have obtained:

$$P= 1091-54*T \qquad [1]$$

Where P is the depth in metres and T is the temperature in ºC. The coefficient of correlation is close to 0.61. According to the equation [1], the vertical Geothermal Gradient is 1.85ºC/100m.

We have used the equation [2] for the estimation of the heat flux:

$$Q= ke*dT/dz \qquad [2]$$

Where "ke", is the thermal conductivity for limestone (k/100m), and in 100m depth of carbonates. We have assumed the k value for limestone of 2.5 $Wm^{-1}K^{-1}$ (Beardsmore & Cull, 2001). Therefore, we obtain a heat flux of Q= 0,46 mW/m^2. This value is very similar to the value obtained by García-Mayordomo and Giner (2006) (45 mW/m^2) into the Betic Range for the Prebetic units.

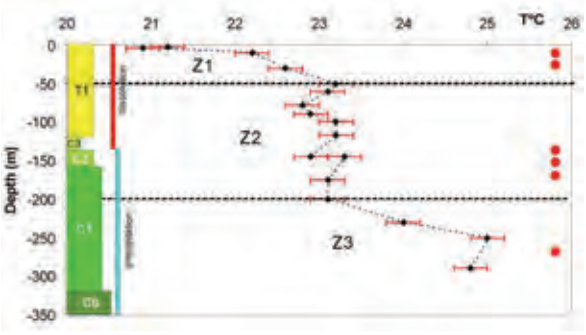

Figure 4: Thermal profile of Benis cave. The profile intersects the fault plane between 150m and 200 m. The upper part, 0-50m is the shallow hetero-metric zone, where there is influence of the outside, atmosphere and seasonal temperature are Cretaceous limestone (C0-C3) and T1 carbonate Tertiary deposits.

DISCUSSION

Firstly, assuming the size-magnitude of the last earthquake of the Benis Fault as M6.5, and dated at 64.4 ka BP, the tectonic slip-rate (SR) can be estimated by using the Slemmons (1982) empirical relationship. Therefore, the SR of the Benis fault ranges between 0.01 and 0.008 mm/yr.
Secondly, we have estimated the heat flux from the geothermal gradient associated to the fault plane. The expression defined by Lachenbruch & Sass, (1980) is:

$$Q= SR*\tau \quad [3]$$

Where Q is the heat flux, SR the tectonic slip-rate of an active fault and τ is the tangential stress. Assuming the minimum value for the tangential stress as the gravity load, then:

$$\tau= \rho*g*z*\sin(\theta) \quad [4]$$

Where ρ is the averaged density of the limestone (2800 kg/m^3), g is the acceleration of the gravity (9.8 m/s^2), z is the fault width where the thermal gradient is estimated (320m) and θ is the dip of the fault (75º).

Finally, resolving the equation [3] and [4] shows that the heat flow of the Benis Fault is close to $1.345 \cdot 10^{-3}$ mWm^{-2}. This value is smaller than the value calculated from the thermal profile.

CONCLUSIONS

(1) The Benis Fault is a sinistral oblique active fault located northward of the Betic Range (Prebetic Unit). It is 6 km long, trending N-S and dipping 75ºE.

(2) The last earthquake was of 6.3<M<6.5 size, from the empirical relationship of surface rupture long and the coseismic off-set (60 cm of net slip), and it took place 64.4 ± 17.6 ka BP, dated by racemization of amino-acids.

(3) The tectonic slip rate of the Benis Fault ranges between 0.008 and 0.01 mm/yr.

(4) The vertical Geothermal Gradient into the area is 1.85º/100m, defining a geothermal zone.

(5) The heat flux derived of the vertical geothermal gradient is 46 mWm^{-2}, being this value similar to others obtained by other authors. However, the heat flux for the Benis Fault is notably lesser, $1.34 \cdot 10\text{-}3$ mWm^{-2}. Therefore, the thermal anomaly within the area is related to karst convection instead of advection of heat by water flow across the fault plane or heat conduction from the fault activity.

Acknowledgements: Thanks to the SpeleoClub RESALTES and all the members who collaborated in this project. This work is a contribution of the Spanish projects SISMOSIMA CGL2013-47412-C2-2-P, and QTECTBÉTICA CGL2012-37281-C02.01.

References

Beardsmore, G.R. & J.P. Cull, (2001). *Crustal Heat Flow: A Guide to Measurement and Modelling*. Cambridge University Press. 344 pp. Cambridge.

Doan, M.L. & F.H. Cornet, (2007). Thermal anomaly near the Aigio fault, Gulf of Corinth, Greece, maybe due to convection below the fault. *Geophysical Research Letters*. 34, L06314, doi: 10.1029/2006GL028931.

García-Mayordomo, J. & J.L. Giner-Robles, (2006). Definición de zonas sismogenéticas en base al gradiente geotérmico, resistencia y profundidad del límite frágil-dúctil en la corteza superior. Aplicación metodológica para el cálculo de la peligrosidad sísmica en el Sureste de España. *Geogaceta*. 39, 55-58.

Jerez-Mir, L., J. Jerez-Mir, G. García-Monzón, (1972). *Mapa geológico de España* E. 1:50.000. Hoja de Mula. nº: 912. IGME. Madrid.

Lachenbruch, A.H. & J.H. Sass, (1980). Heat flow and energetic of the San Andreas Fault zone. *Journal Geophysical Research*. 85 (B11), 6185-6222.

Luetscher, M. & P.Y. Jeannin, (2004). Temperature distribution in karst systems: the role of air and water fluxes. *Terranova*. 16 (6), 344-350.

Martínez-Díaz, J.J., M.Á. Rodríguez-Pascua, R. Pérez-López, J. García-Mayordomo, J.L. Giner-Robles, F. Martín-González, M. Rodríguez-Peces, J.A. Álvarez-Gómez; J.M. Insua-Arévalo, (2011). *Informe geológico preliminar del terremoto de Lorca del 11 de mayo del año 2011, 5.1 Mw*. Informes Técnicos del IGME. 47pp. Madrid.

Pérez-López, R., M.A. Rodríguez-Pascua, J.L. Giner-Robles, J.J. Martínez-Díaz, et al., (2009). Spelaeoseismology and palaeoseismicity of the "Benis Cave" (Murcia, SE of Spain): coseismic effects of the 1999 Mula earthquake (mb 4.8). *Geological Society of London Special Publications*. 316, 207-216.

Pérez-López, R., E. Bañón, M. Rentero, J.L. Giner-Robles, M.A. Rodríguez-Pascua, P.G. Silva, J.C. García López-Davalillo y García-López M., (2010). Análisis Térmico Preliminar de la Sima De Benis (-350m), Murcia. In: *Avances de la Geomorfología en España. XI Reunión Nacional de Geomorfología. Comunicaciones.* 1, 1-5.

Perez-López, R., T. Torres, G. Romero, E. Bañón, M.T. Rentero, J.E. Ortiz y P.G. Silva, (2012). "Lynx pardinus spelaeus" extraction from the Benis Cave -350m (Cieza,): RX and razemization dental analyses. *Geo-Temas*. 13, 265-268.

Slemons, D.B., (1982). Determination of design earthquake magnitudes for microzonation. In: *Proceedings of the 3rd International Earthquake Microzonation Conference*. Seattle. Washington. 119-130.

Wells, D.L., & K.J. Coppersmith, (1994). New empirical relationships among magnitude, rupture length, rupture width, rupture area, and surface displacement. *Bulletin of the Seismological Society of America*. 84, 974-1002.

INQUA Focus Group on Paleoseismology and Active Tectonics

paleoseismicity.org

Interseismic ground velocities of the Central Apennines from GPS and SAR measurements and their contribution to seismic hazard modelling: preliminary results of the ESA CHARMING project

Pezzo, G. (1), Merryman Boncori, J.P. (1), Visini, F. (2), Carafa, M. (3), Devoti, R. (1), Atzori, S. (1), Kastelic, V. (3), Berardino, P. (4), Fornaro, G. (4), Riguzzi, F. (1), Pietrantonio, G. (1), D'Amico, V. (2), Meletti, C. (2) and Salvi, S. (1)

(1) Istituto Nazionale di Geofisica e Vulcanologia (INGV), Centro Nazionale Terremoti, Via di Vigna Murata 605, 00143 Roma, Italy. Email: giuseppe.pezzo@ingv.it
(2) Istituto Nazionale di Geofisica e Vulcanologia (INGV), Sezione di Pisa, Via della Faggiola 32, 56126 Pisa, Italy
(3) Istituto Nazionale di Geofisica e Vulcanologia (INGV), Tettonofisica e Vulcanologia, Via dell'Arcivescovado 8, 67100 L'Aquila, Italy
(4) Istituto per il Rilevamento Elettromagnetico dell'Ambiente (IREA) del Consiglio Nazionale delle Ricerche (CNR), Via Diocleziano 328, 80124 Napoli, Italy

Abstract: *The contribution of space geodetic techniques to interseismic velocity estimation, and thus seismic hazard modelling, has been recognized since two decades and made possible in more recent years by the increased availability and accuracy of geodetic measurements. We present the preliminary results of a feasibility study performed within the CHARMING project (Constraining Seismic Hazard Models with InSAR and GPS), funded by the European Space Agency (ESA). For a 200 km x 200 km study area, covering the Abruzzi region (central Italy) we measure the mean surface deformation rates from Synthetic Aperture Radar and GPS, finding several local to regional deformation gradients consistent with the tectonic context. We then use a kinematic finite element model to derive the long-term strain rates, as well as earthquake recurrence relations. In turn these are input to state-of-the-art probabilistic seismic hazard models, the output of which is validated statistically using data from the Italian national accelerometric and macroseismic intensity databases.*

Key words: *Active Tectonics, Seismic Hazard, SAR, GPS.*

INTRODUCTION

The CHARMING project (Constraining Seismic Hazard Models with InSAR and GPS) is a feasibility study funded by the European Space Agency's (ESA) Support to Science Element (STSE) Pathfinders 2013 programme. The context of CHARMING is Probabilistic Seismic Hazard Assessment (PSHA), i.e. the scientific field which aims to quantify the probability that ground motion at a specified site will exceed some level of a given shaking parameter of engineering interest (e.g. Peak Ground Acceleration, PGA) during a specified future time frame The main aim of the project is to investigate whether surface deformation measurements, derived from GPS and Synthetic Aperture Radar (SAR) data, can be successfully incorporated into PSHA models and improve their quality. In particular, we investigate several aspects related to the marginal benefit provided by the integration of SAR compared to GPS alone, since to our best knowledge this project represents the first attempt worldwide to incorporate SAR measurements into PSHA models.

The areas of interest analyzed within the project include a large portion of central and southern Italy. A restricted development area, comprising the central Abruzzi region, is used for technique developement and validation. At a later stage the developed methods shall be applied to a wider experimental area (larger rectangle in Fig. 1). For these areas we generate interseismic velocity maps, using a combination of ~100 permanent GPS stations (Fig. 1) and measurements derived from coast-to-coast acquisitions of the ERS-1/2 AMI, ENVISAT ASAR and ALOS PALSAR satellite SAR sensors (Fig. 2). The geodetic measurements are screened to exclude contributions of non-tectonic origin (e.g. subsidence). Subsequently, a kinematic finite element model and a tapered Gutenberg-Richter model are applied to the mean velocity measurements to derive long term strain rates and earthquake rates, i.e. the number of earthquakes in a given time period above an established magnitude threshold, Finally, state of the art PSHA modelling techniques are used to generate probabilistic models for PGA and other shaking parameters. A statistical validation of the PSHA model output is carried out, using data from national accelerometric and macroseismic intensity databases.

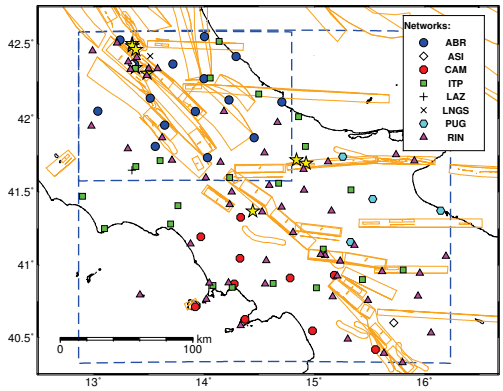

Figure 1: GPS stations and networks within the development (smaller) and experimental (larger) areas (dashed blue rectangles). Orange polygons represent composite and individual seismogenic sources according to the DISS v.3.1.1 catalogue (Working Group, DISS 2010). Yellow stars represent major earthquakes (Mw > 5.0), occurred since 1992.

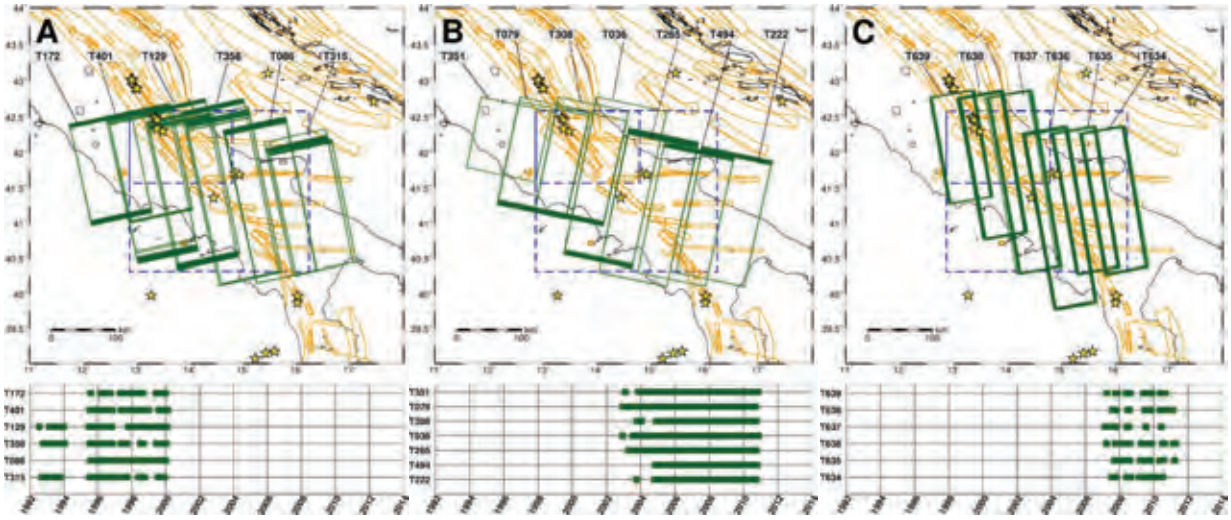

Figure 2: Spatial (top) and temporal (bottom) coverage for (A) ERS-1 and ERS-2 SAR ascending tracks, (B) ENVISAT ASAR descending tracks acquired with Imaging Swath 2 (IS2), and (C) ALOS PALSAR Fine Beam Single and Dual ascending tracks. See the caption of Figure 1 for other plot features.

GEODETIC DATA AND METHODS

GPS data were processed with the method of Devoti et al., (2014) to obtain mean deformation rates. Only stations with >3 years of observations were retained. For the stations in the epicentral area of the the Mw 6.3 2009 L'Aquila earthquake, measurements were truncated to Dec. 31. 2008.

SAR image processing was performed with the combined Persistent Scatterer and Small Baseline approach of (Hooper et al., 2008), implemented in the StaMPS (Stanford Method for Persistent Scatterers) software. One of the tracks (ENVISAT 308 descending) was independently processed with the Small Baseline Subset (SBAS) technique of (Berardino et al., 2002). Ascending and descending passes of the ENVISAT and ERS-1/2 satellites and ascending passes of the ALOS PALSAR sensor (Fig. 2) were processed to derive SAR line-of-sight (LoS) deformation rate maps. These were then calibrated with GPS measurements, projected onto the LoS, to ensure a common reference frame and to correct residual long-wavelength errors in the SAR measurements arising from atmospheric propagation, orbital uncertainties and other sources (Marinkovic and Larsen, 2013). East and Up Cartesian deformation components can be derived in regions of overlap between at least one ascending and one descending SAR acquisition.

In the project's development phase, two experimental approaches are also investigated. The first consists in the application of the Intermittent SBAS (ISBAS) approach (Sowter et al., 2013), which can potentially provide a significant increase in the coverage of the LoS measurements. The second is based on a multi-temporal extension of the Spectral Diversity or Multi Aperture InSAR (MAI) technique (Scheiber and Moreira, 2000; Bechor & Zebker 2006), and could potentially provide a high sensitivity also to the flight-path (~N-S) deformation component.

DISCUSSION

Within the development area, the mean deformation rates from GPS and SAR show in general an excellent level of agreement. An example is shown in Fig. 3, for ENVISAT ASAR descending track 36, for which the differences show a standard deviation of 1.5 mm/year in the SAR LoS (Fig. 4). Our preliminary results also exemplify the complementarity of these two measurement techniques in the Central Apennines. While the GPS is essential to constrain the long-wavelength patterns (>30 km), the SAR can potentially "fill in the gaps" between GPS measurements, thus defining more clearly the spatial extent of features and the location of transition zones.

A preliminary analysis of the GPS data highlights several signals ascribable to the local tectonics. The GPS vertical component (Fig. 5A) shows an overall NW-SE oriented uplift along the central Apennines from 0.5 to more than 2 mm/yr. This long-wavelength velocity pattern could be attributed to the general NE-SW oriented extension of the Apennines chain (D'Agostino et al., 2001). Some local subsiding stations are also recognized, namely SMRA, CHIE, LPEL and VTRA. For the latter three, the subsidence is likely to be very local. However, the SMRA subsidence, possibly associated to the combined action of sediment compaction and ground water pumping, appears to have a larger spatial scale in the SAR measurements (Fig. 3A), so that a tectonic contribution cannot be entirely excluded.

The GPS east and north velocities (Fig. 3A and 3B) show a regional pattern broadly consistent with the NE-SW Apenninic extension. At a more local scale however, we observe interesting velocity gradients between the ALRA, RMI2, CERA and ISER GPS stations, in the area north and east of PBRA and north INGP station. In the first case a > 1 mm/yr extension between the SORA-

BLRA-VVLO-OTRA block, with respect to the ALRA-RNI2-CERA one, can be detected.
The same area shows shortening velocity gradients in the GPS North component (> 1 mm/yr), resulting in a general NE-SW oriented left-lateral deformation zone located between the Matese mountains, to the south, and the Marsica ones, to the north. Although the processed SAR data is not centred on this area, the resulting LoS velocity map (Fig. 3A) seems to show similar deformation patterns.

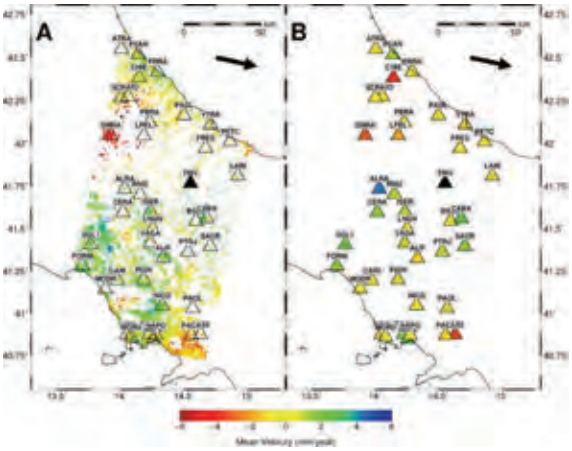

Figure 3: (A) Mean LoS from ENVISAT descending track 36 and (B) from GPS projected onto the SAR LoS. Positive and negative values indicate motion towards and away from the radar respectively. Measurements are referred to the location of the TRIV station. SAR velocities represent an average of measurements in a 1 km radius from the GPS stations.

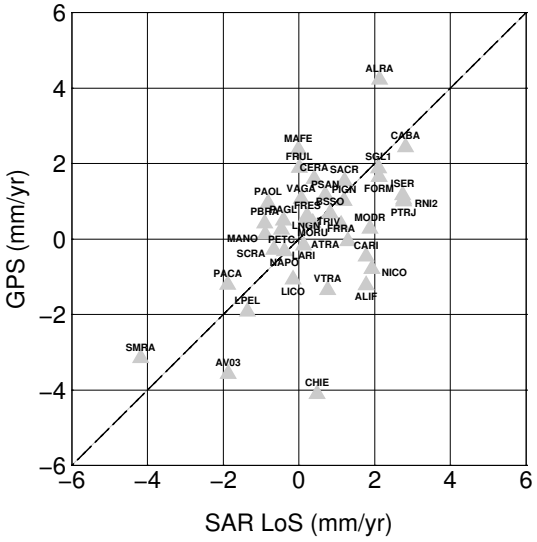

Figure 4: Scatter plot of InSAR (descending ENVISAT track 36) and GPS velocities (projected along the SAR LoS).

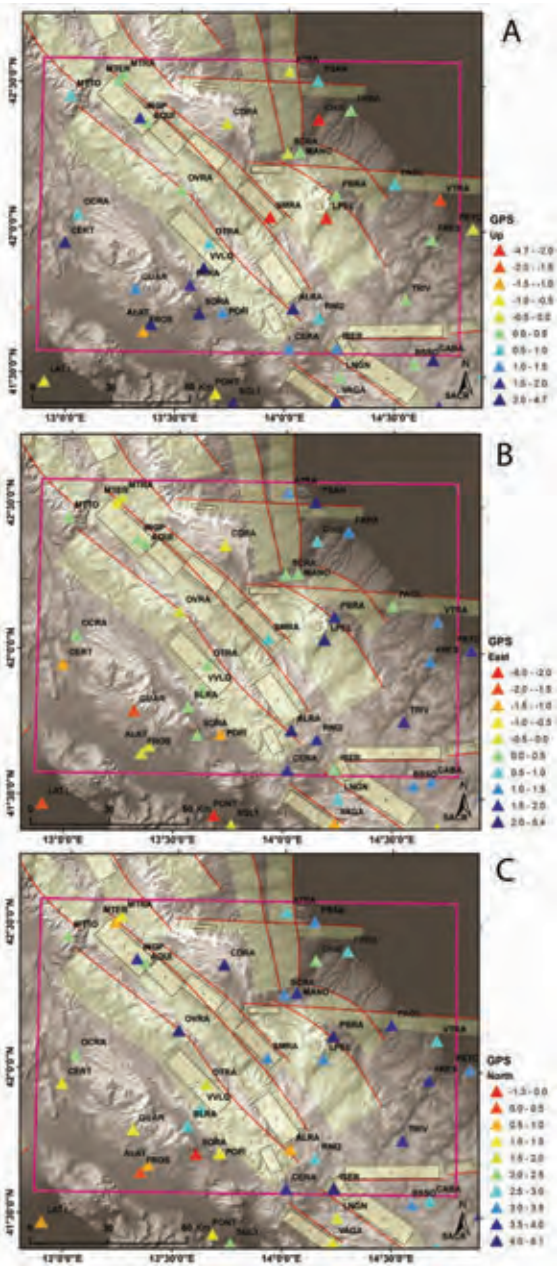

Figure 5: UP (A), East (B) and North components of the GPS velocities from Devoti et al. (2014), development area (purple rectangle) and DISS catalogue seismic sources.

North of PBRA station, we observe two blocks (PBRA-LPEL and ATRA-PSAN) moving eastward more quickly (from 1 to > 2 mm/yr) than CDRA-OVRA, SCRA-MANO and CHIE-FRRA blocks. In the same areas, for the North component, a N-S shortening (~ 1 mm/yr) between the PBRA-MANO-CDRA-OVRA block and the CHIE-FRRA-PSAN-ATRA one can be detected. Thus, the resulting deformation pattern is a NE movement of the Maiella mountain zone (PBRA-LPEL) with respect to the Chieti (CHIE) one (i.e. a shortening) and a northward movement of the Gran Sasso zone (CDRA) with respect to the Chieti one, resulting in a general NE-SW oriented extension. SAR velocities seem compatible with these

patterns, even though further processing of all adjacent tracks from all sensors is needed to confirm these trends. Another interesting velocity gradient concerns the NE part of the development area, in which the MTER-MTRA block is moving westward (~1 mm/yr) and southward (~2 mm/yr) with respect the MTTO-INGP-AQUI block, which shows eastward and northward movements. These velocities result in a left-lateral deformation zone located north of L'Aquila (AQUI), where some seismic sources give place to others to the north. This structural setting is very similar to that of the southern side of the development area, near the CERA station, where we also observe a southward interruption of the main seismic sources, which give place to other structures. Moreover, comparing the GPS data distribution with historical data (Rovida et al., 2011) and seismological data (http://iside.rm.ingv.it) in the timespan of the geodetic measurements (1992-2008 period), it is apparent that in both time intervals these two deforming areas are characterized by an intense seismic activity with respect to adjacent ones, thus strengthening a possible tectonic interpretation (Fig. 6).

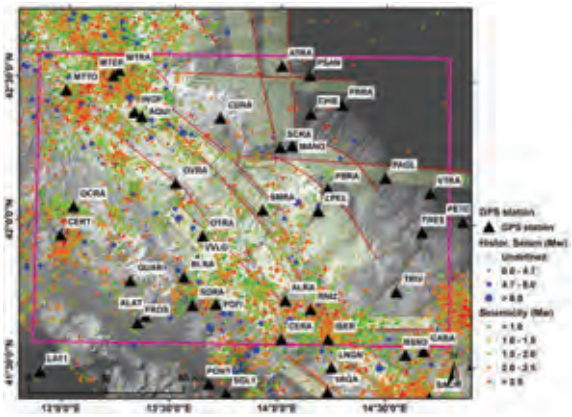

Figure 6: Historical (Rovida et al., 2011) and instrumental seismicity (1992-2008 period) (http://iside.rm.ingv.it), development area (purple rectangle) and DISS catalogue seismic sources.

A preliminary model run was carried out on the GPS data alone, within the development area of interest. We built a finite element model to derive long term average velocity fields accounting for the main tectonic features of the study area. From this model, we then calculated the earthquake rates, i.e. the number of earthquakes in a given time period above an established magnitude threshold, following the Seismic Hazard Inferred From Tectonics (SHIFT) approach (Bird and Liu, 2007; Carafa and Kastelic 2014). Finally, state of the art PSHA modelling techniques were used to generate probabilistic models for horizontal peak ground acceleration (PGA) and other shaking parameters. Our preliminary results, in terms of PGA with 10% probability of exceedance in 50 years on hard ground (Fig. 7), show that expected PGA exceeding 0.2g characterize large part of Apennines and, in particular, two areas have the highest level of hazard with values exceeding 0.4g.

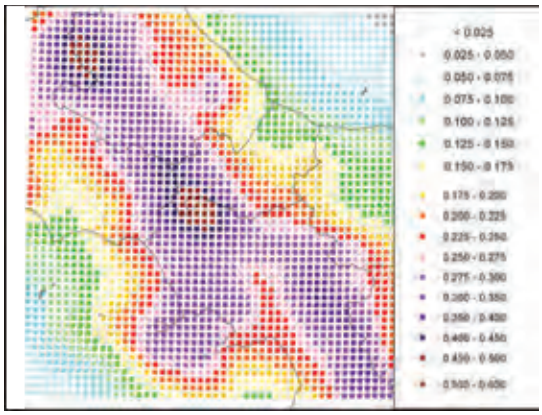

Figure 7: Seismic hazard map showing the PGA distribution with 10% probability of exceedance in 50 years, computed on hard ground (VS30 > 800 m/s) and using the Akkar et al. (2014) ground motion model.

A statistical validation of the PSHA model output was carried out using data from the national accelerometric and macroseismic intensity databases. Our first results suggest that our model is not rejected by the observations, thus supporting the viability of our approach for seismic hazard purposes.

Acknowledgements: GP and JPMB were funded by the European Space Agency - INGV CHARMING project. FV, MMCC, VK were funded by the Abruzzo Project, code: RBAP10ZC8K_003, funded by the Italian Ministry of University and Research (MIUR). Some of the figures were prepared using the public domain GMT software (Wessel & Smith, 1998).

References

Akkar, S., M.A. Sandıkkaya, & J.J. Bommer, (2014). Empirical ground-motion models for point- and extended-source crustal earthquake scenarios in Europe and the Middle East. *Bull. Earthq. Eng*. 12 (1), 359-387, doi: 0.1007/s10518-013-9461-4.

Bechor, N.B.D. & H.A. Zebker, (2006). Measuring two-dimensional movements using a single InSAR pair. *Geophys. Res. Lett.* 33, L16311, doi: 10.1029/2006GL026883.

Berardino, P., G. Fornaro, R. Lanari & E. Sansosti, (2002). A new algorithm for surface deformation monitoring based on small baseline differential SAR interferograms. *IEEE Trans. Geosci. Remote Sens*. 40 (11), 2375-2383. 2002.

Bird, P., & Z. Liu, (2007). Seismic hazard inferred from tectonics: California. *Seismological Research Letters*. 78,1, 37-48. doi: 10.1785/gssrl.78.1.37.

Carafa, M.M.C., & V. Kastelic, (2014). Earthquake rates inferred from active faults and geodynamics: the case of the External Dinarides. *Bollettino di Geofisica Teorica ed Applicata*. 55,1, 69-83.

D'Agostino, N., R. Giuliani, M. Mattone & L. Bonci, (2001). Active crustal extension in the Central Apennines (Italy) inferred from GPS measurements in the interval 1994-1999. *Geophysical Research Letters*. Volume 28, Issue 10, pages 2121-2124

Devoti, R., G. Pietrantonio & F. Riguzzi, (2014). GNSS networks for geodynamics in Italy. *Fisica de la tierra*. Vol. 26, 11-24.

Hooper, A., (2008). A multi-temporal InSAR method incorporating both persistent scatterer and small baseline approaches. *Geophys. Res. Lett.* Vol. 35, L16302, doi: 10.1029/2008GL034654.

Marinkovic, P., and Y. Larsen, (2013). Consequences of long-term ASAR local oscillator frequency decay - an empirical study of 10 years of data, European Space Agency. In: *Proc. of the Living Planet Symposium (abstract)*. Edinburgh. U.K.

Rovida, A., R. Camassi, P. Gasperini & M. Stucchi (eds.), (2011). *CPTI11, the 2011 version of the Parametric Catalogue of Italian Earthquakes*. Milano, Bologna. http://emidius.mi.ingv.it/CPTI, doi: 10.6092/INGV.IT-CPTI11

Scheiber, R. & A. Moreria, (2000). Coregistration of interferometric SAR images using spectral diversity. *IEEE Trans. Geosc. Rem. Sens.* 38 (5), 2179-2191, doi: 10.1109/36.868876.

Sowter A., L. Bateson, P. Strange, K. Ambrose & M. Syafiudin, (2013). DInSAR estimation of land motion using intermittent coherence with application to the South Derbyshire and Leicestershire coalfields, *Rem. Sens. Lett.* 4 (10), 979-987, doi: 10.1080/2150704X.2013.823673.

Wessel, P & W.H.F Smith, (1998). New improved version of the generic mapping tools released. *EOS Trans. Am. Geophys. Union*. 79, 579.

Working Group, DISS, (2010). *Database of Individual Seismogenic Sources (DISS), Version 3.1.1: a compilation of potential sources for earthquakes larger than M 5.5 in Italy and surrounding areas*. (http://diss.rm.ingv.it/diss/).

INQUA Focus Group on Paleoseismology and Active Tectonics

Mapping capable faulting hazard in a moderate-seismicity, high heat-flow environment: the Southern Tuscany-Tuscia province

Piccardi, L. (1), Vittori, E. (2), Blumetti, A.M. (2), Comerci, V. (2), Di Manna, P. (2), Guerrieri, L. (2)

(1) CNR, Institute of Geosciences and Earth Resources, via La Pira 4, 50121 Florence, Italy. Email: piccardi@geo.unifi.it
(2) ISPRA, via Vitaliano Brancati, 48 00144 Rome, Italy

Abstract: *We propose here a survey, still in progress, of active faults affecting the topographic surface in the Southern Tuscany-Northern Latium, a region of high heat flow and moderate to low seismicity. Faults are mapped combining analysis of digital terrain models with local geological information deriving from Carg 1:10,000 maps and other bibliographic data on Quaternary faults.*

Key words: *Active tectonics, capable faulting, Tuscany, geothermal systems.*

INTRODUCTION

A fault is *capable* if it is expected to rupture/deform the ground surface in the near future. In fact, surface faulting represents a serious hazard for infrastructures and buildings and therefore it is one of the most relevant geohazards to be considered in the seismic microzonation process. It must be remarked that fault capability is not restricted to strong magnitude events, being observed also aseismically (creep) or in shallow small magnitude events, as typical in volcanic zones (e.g., the Etna region, Ferreli et al., 2002; Blumetti et al., 2007). Although still far from complete, a working database of capable faults covers most of the Italian territory (ITHACA, http://sgi.isprambiente.it/geoportal/catalog/content/project/ithaca.page), largely overlapping with the most seismic regions. However, there are areas where no information on capable faults is available, although seismicity suggests ongoing tectonic activity.

One of such areas is the Southern Tuscany and Northern Latium (Figure 1), where high heat flow, presumed extinction of the volcanic processes and absence of mapped evidence of Late Quaternary faulting have been often advocated to justify a low seismic hazard. The latter has made this region, especially the coast area away from the Quaternary volcanic apparatuses, a preferred possible site for nuclear installations.

The studies in the 70' for the Montalto NPP and the exploitation of the local geothermal systems has led to a large number of geophysical and geological studies that, despite generally not focused on this specific issue, contribute to detail the fault network. The hydrothermal circulation takes advantage of the rock permeability enhanced by active faulting and fracturing, which also allow high CO_2 degassing of deep provenance. Thus, these studies and the distribution of historical/instrumental seismicity help to locate a number of faults, whose actual surface rupture and seismic potential need to be assessed. This is important also in light of the perturbation of the stress field and seismicity induced by the exploitation process itself, which is particularly evident in the Larderello area, where seismicity is enhanced compared to its surroundings and subsidence locally exceeds 1 cm/y (Persistent Scatters data: http://www.pcn.minambiente.it/GN/).

Aim of this short note is to present a preliminary grid of known/suspected capable faults in the Southern Tuscany-Northern Latium region, derived from integration of morphological, geological and seismic data, as well as information from available literature, as a first step toward field verification.

Geology

The structural setting of the inner zone of the Northern Apennines (e.g. southern Tuscany, Northern Latium and Northern Tyrrhenian Sea) originated from the convergence and collision (Cretaceous-Early Miocene) of the Adria microplate and the European plate, represented by the Sardinia-Corsica Massif (Molli, 2008, for a review).

The collisional and post-collisional processes are responsible for the stacking of several tectonic units derived from oceanic and epicontinental palaeogeographical domains: Ligurian, Sub-Ligurian, Tuscan (internal and external), Umbria-Marche domains, also involving the Triassic-Palaeozoic substratum of the sedimentary cover.

After the emplacement of the tectonic units, extensional tectonics determined the lateral segmentation of the Tuscan succession and of the basal Verrucano Group mainly by east-dipping low-angle normal faults, developing along two main detachment levels located in the Upper Triassic evaporites, underneath the sedimentary cover, and within the Palaeozoic phyllite, underneath the Verrucano Group (Brogi & Liotta, 2008).

This extension migrated eastwards, affecting the inner sectors of the Northern Apennines since the Early-Middle Miocene, coeval with the compression in the external Northern Apennines (e.g., Jolivet et al., 1990). Extensional basins 10-40 km long, 15-20 km wide developed, for the most part now bounded by an array of prevalently high angle normal faults, many of Plio-Pleistocene formation or reactivated. They are separated

longitudinally by transverse structural lineaments and are filled with up to 3 km of upper Miocene to Quaternary deposits. The basins west of the Chianti-Cetona Ridge developed on a thin (20-25 km) continental crust, whereas those to the east are on thicker crust (about 35 km; Giese, 1981; Nicolich, 1987).

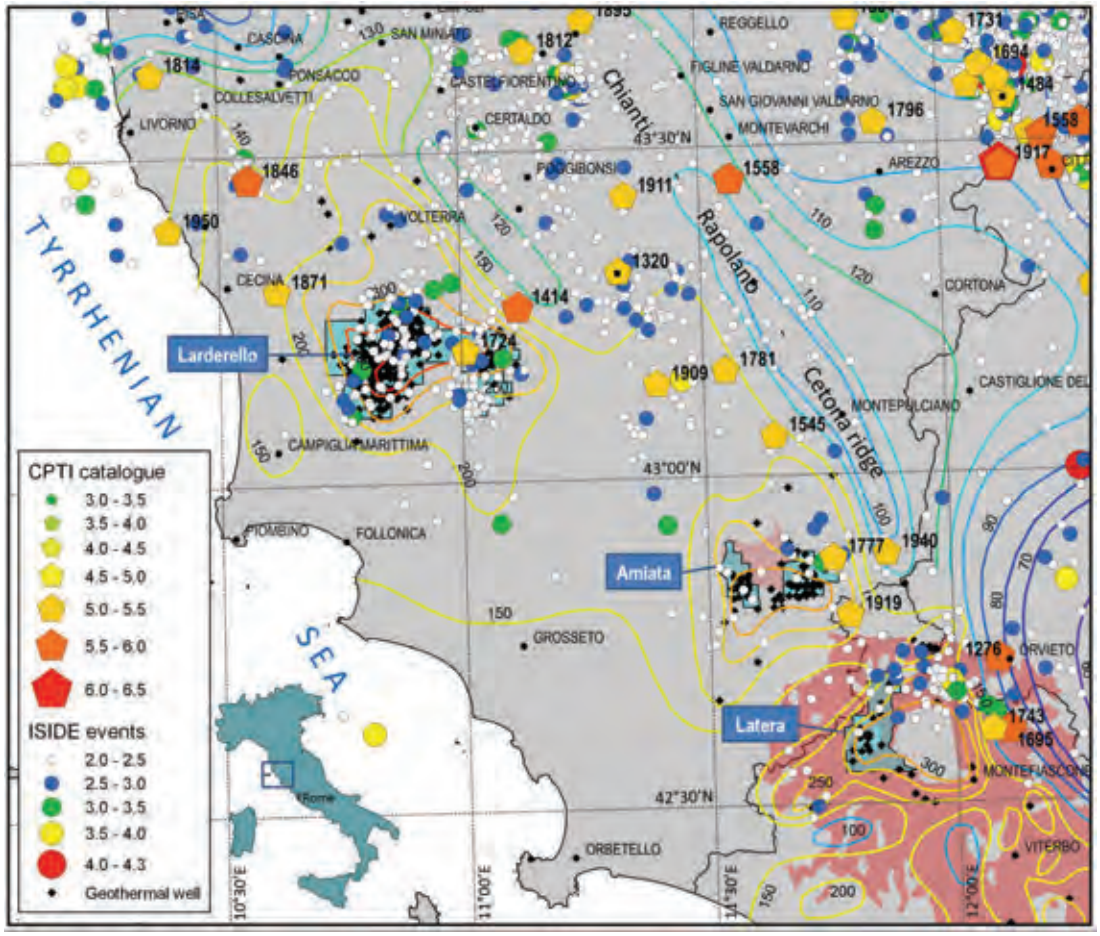

Figure 1: Seismicity, geothermal wells and Isotherms (°C) at 3000 m depth in Central-Southern Tuscany and Northern Latium. The three main geothermal fields (Larderello, Amiata and Latera) are also shown. CPTI: Parametric Catalogue of Italian Earthquakes (Rovida et al., 2011). ISIDE: Italian Seismic Instrumental and parametric Data-basE (http://iside.rm.ingv.it/iside/standard/index.jsp).

The basin-bounding structures cross-cut the pre-existing compressional and extensional structures. The eastern margin of the Radicofani Basin (western side of the Monte Cetona ridge) is bounded by a regional structure, known as the Cetona Fault, exposed for many kilometres (Liotta and Salvatorini, 1994; Piccardi et al., 1997; Sani et al., 2001). This fault system, NNW-SSE striking, consists of west-dipping normal faults characterised by about 1.5-2 km of cumulative displacement (Brogi & Fabbrini, 2009). The Chianti-Cetona ridge seems to separate a high heat flow area in the hanging wall (western side) from a low heat flow area in the footwall (eastern side), as evidenced in Figure 1.

Extensional processes are responsible for the lithospheric thinning (present crustal and lithospheric thicknesses range between 20-24 km and 30-40 km respectively: e.g. Nicolich, 1987; Finetti et al., 2001; Finetti, 2005), magmatic activities and high heat flow.

Since the Late Miocene, magmatic intrusion, younger eastwards, accompanied extension. Magmas with both crustal and mantle geochemical signatures intruded mostly at mid-crustal depths (Serri et al., 1993). Presently, Southern Tuscany is characterized by heat flow of 120 mW/m^2 on average (e.g., Pasquale et al., 2010), with local peaks up to 1000 mW/m^2 in the Larderello geothermal area.

Seismicity

In this sector of the Apennines, most seismicity is concentrated in the axial and external zones, while the internal zone (Southern Tuscany, Northern Latium and Northern Tyrrhenian Sea) shows low-magnitude and shallow seismicity, usually confined between 3 and 10 km (Selvaggi and Amato, 1992). Widespread low-magnitude seismicity (Batini et al., 1985; Albarello et al., 2005) is concentrated in the geothermal areas of Tuscany (Larderello-Travale and Monte Amiata) and

Northern Latium (Bolsena-Latera). GPS data indicate small motion towards NNW (Devoti et al., 2008).
Low seismicity is expected due to the very high local heat flow, which makes ductile creep more likely than brittle friction at depth. In fact, more than 95% of the instrumental events in the ISIDE catalogue of INGV are shallower than 10 km, 65% between 5 and 10 km.
Apart from the seismicity induced and likely triggered by geothermal exploitation, earthquakes are linked either to normal or strike-slip active faults (Brogi & Fabbrini, 2009; Brogi et al., 2014, with references therein). Historically, ca. ten events in seven centuries are known (Rovida et al., 2011) that have caused damage and have estimated magnitude > 5, three of them (1558 Val d'Ambra, 1695 Bagnoregio, and 1846 Orciano Pisano) with epicentral intensities MCS 8-9 to 9. Intensities 8 have been attributed to the 1414 Colline Metallifere and 1276 Orvieto events. Geological effects are known only for the events of 1695 (rise of 4 m of the lake level and flooding for over 4 km around the Bolsena lake) and 1846: liquefaction, landslides and ground fractures, the latter near Volterra, Guardistallo and Rosignano.

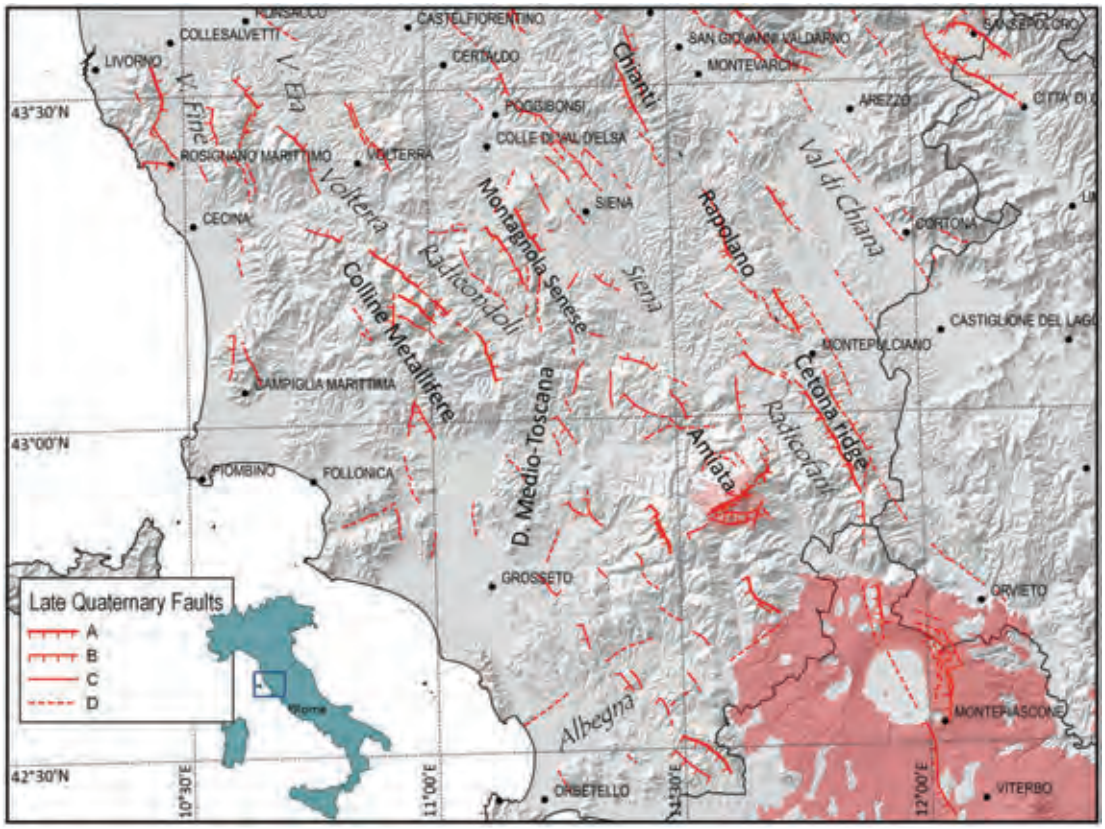

Figure 2: Faults with some evidence from literature data and morphological analysis to be capable. A to D refer to decreasing evidence and reliability of the mapped element.

DISCUSSION

Late Quaternary faulting

We propose here a map, still in progress, of active faults affecting the topographic surface in the Southern Tuscany-Northern Latium region (Fig. 2). The fault grid results from the compilation of fault data represented in many published and unpublished sources, including the Tuscany's high resolution regional geological maps, and geomorphological evidence from digital terrain models. It also takes into account the distribution of the instrumental and historical seismicity (Fig. 1). Although preliminary, our study aims at improving our understanding of geohazards, such as local surface faulting. Furthermore, it allows us to better know the active deformation of the area, as the following examples will help to clarify.
The western side of the Chianti-Rapolano-Cetona ridge appears to be the major tectonic feature of the area. The abrupt change in seismic behaviour visible here also corresponds to a sharp change in thermal gradient. In fact, this is the main fault alignment where capable faulting can be expected. This fault system is likely to continue southward across the Bolsena caldera, which appears downfaulted to the west.
To the west of it, the next major tectonic feature is the NW-SE oriented east-dipping fault system that bounds the Val d'Era-Volterra-Radicondoli depression to the west. This element appears in close relation with the extent of the Larderello-Travale geothermal area. It also

represents the major anthithetic structure of the formerly cited western side of the Chianti-Rapolano-Cetona ridge. Our mapping of active faults confirms also local components of horizontal slip. An example of this can be seen in the Mount Amiata area.

Here, Brogi & Fabbrini (2009) suggest a very recent, late Quaternary tectonic activity, with left oblique faulting responsible for the volcanic eruption, the widespread hydrothermal circulation, the dissection of recent volcanic deposits (300–190 ka). Instead, Borgia et al. (2014) attribute most of the deformation of the volcano edifice to deep-seated gravitational spreading, and do not find evidence of left-lateral slip on the Amiata fault, while right lateral evidence was detected in east-west faults south of the main Amiata fault. The active fault pattern we mapped on the M. Amiata reveals in fact that the architecture of this system is not compatible with a left-lateral slip, but it is coherent with a general oblique-right lateral motion, consistent with the model proposed by Borgia et al. (2014).

Similarly, the architecture of the faults forming the Chianti-Rapolano-Cetona fault system is consistent with a left-lateral component of horizontal motion, in agreement with the results of previous studies (e.g., Piccardi et al., 1997; Piccardi et al., 2006; Sani et al., 2001; Brogi & Fabbrini, 2009, and references therein).

In conclusion, we may argue that, despite the relatively scarce seismicity, the heated crust and its reduced thickness, also in this area active faulting is far from negligible, and responds to the regional tectonic regime. The study of active faults provides therefore an important tool for geohazard assessment, as well as a relevant kinematic indicator of ongoing regional geodynamics.

References

Albarello, D., F. Batini, P. Bianciardi, B. Ciulli, E. Spinelli & M. Viti, (2005). Stress field assessment from ill-defined fault plane solutions: an example from the Larderello Geothermal Field (western Tuscany, Italy). *Bollettino della Società Geologica Italiana*. 3, 187-193.

Batini, F., R. Console & G. Luongo, (1985). Seismological study of Larderello-Travale geothermal area. *Geothermics.* 14, 255-272.

Blumetti, A.M., P. Di Manna, L. Ferreli, D. Fiorenza & E. Vittori, (2007). Reduction of environmental risk from capable faults: The case of the Eastern Etna region (eastern Sicily, Italy). *Quaternary International*. 173-174, 45-56

Borgia, A., A. Mazzoldi, C.A. Brunori, C. Allocca, C. Delcroix, L. Micheli, A. Vercellino & G. Grieco, (2014). Volcanic spreading 1 forcing and feedback in geothermal reservoir development, Amiata Volcano, Italia. *Journal of Volcanology and Geothermal Research*. 84, 16-31.

Brogi, A., D. Liotta, (2008). Highly extended terrains, lateral segmentation of the substratum, and basin development: the Middle-Late Miocene Radicondoli Basin (inner Northern Apennines, Italy). *Tectonics*. 27, TC5002.

Brogi, A., L. Fabbrini, (2009). Extensional and strike-slip tectonics across the Monte Amiata-Monte Cetona transect (Northern Apennines, Italy) and seismotectonic implications. *Tectonophysics*. 476, 195-209.

Brogi A., E. Capezzuoli, I. Martini, M. Picozzi & F. Sandrelli, (2014). Late Quaternary tectonics in the inner Northern Apennines (Siena Basin, southern Tuscany, Italy) and their seismotectonic implication. *Journal of Geodynamics*. 76, 25-45.

Devoti, R., F. Riguzzi, M. Cuffaro & C. Doglioni, (2008). New GPS constraints on the kinematics of the Apennines subduction. *Earth Planet. Sci. Lett.* 273, 163-174.

Ferreli, L., A.M. Michetti, L. Serva & E. Vittori, (2002). Stratigraphic evidence of coseismic faulting and aseismic fault creep from exploratory trenches at Mt. Etna volcano (Sicily, Italy). In: *Ancient Seismites* (Ettensohn, F.R., Rast, N., Brett, C.E. eds.). *Geological Society of America*. Boulder, CO, Special Paper. 359, 49-62.

Finetti I., M. Boccaletti, M. Bonini, A. Del Ben, R. Geletti, M. Pipan & F. Sani, (2001). Crustal section based on CROP seismic data across the North Tyrrhenian-northern Apennines-Adriatic Sea. *Tectonophysics*. 343, 135-163.

Finetti, I.R., (editor) (2005). *CROP Project: Deep Seismic Exploration of the Central Mediterranean and Italy*. Atlases in geosciences. 1. Elsevier.

Giese, P., (1981). Intramontane basins and crustal structure. In: *Sedimentary Basins of Mediterranean Margins* (Wezel, F.C. ed.). CNR Italian Project of Oceanography. Technoprint. Bologna. pp. 55-61.

Jolivet L., R. Dubois, R. Fournier, B. Goffè, A. Michard & C. Jourdan, (1990). Ductile extension in alpine Corsica. *Geology*. 18, 1007-1010.

Liotta, D., G. Salvatorini, (1994). Evoluzione sedimentaria e tettonica della parte centromeridionale del bacino pliocenico di Radicofani. *Studi Geologici Camerti.* 1994/1, 65-77.

Molli, G., (2008). Northern Apennine-Corsica orogenic system: an updated review. *Geol. Soc. London Spec. Publ.* 298, 413-442.

Nicolich, R., (1987) Crustal structures from seismic studie in the frame f the European geotraverse (southern segment) and CROP Projects. In: *The Lithosphere in Italy* (Boriani, A., Bonafede, M., Piccardo, G.B., Vai G.B. eds.). Advances in Earth Science Research. Atti Conveg. Lincei. 80, 41-60.

Pasquale, V., P. Chiozzi, & M. Verdoya, (2010). Tectonothermal processes and mechanical strength in a recent orogenic belt: Northern Apennines. *J. Geophys. Res.* 115, doi: 10.1029/2009JB006631.

Rovida, A., R. Camassi, P. Gasperini, & M. Stucchi, (eds.) (2011). *CPTI11, the 2011 version of the Parametric Catalogue of Italian Earthquakes*, Milano, Bologna. Accessible at http://emidius.mi.ingv.it/CPTI DOI: 10.6092/INGV.IT-CPTI11

Selvaggi, G., A. Amato, (1992). Subcrustal earthquakes in the Northern Apennines (Italy): evidence for a still active subduction? *Geophysical Research Letters.* 19, 2127-2130.

Serri G., F. Innocenti, & P. Manetti (1993). Geochemical and petrological evidence of the subduction of delaminated Adriatic continental lithosphere in the genesis of the Neogene-Quaternary magmatism of central Italy. *Tectonophysics*. 223, 117-147.

INQUA Focus Group on Paleoseismology and Active Tectonics

Comparison among some seismotectonic characteristics of the main historical earthquakes in the Central Apennines (Italy)

Pierantoni, P.P. (1), Centamore, E. (2), Costa, M. (3)

(1) School of Science and Technology - Geology Division, University of Camerino, Via Gentile III da Varano, 62032 – Camerino, Italy. Email: pietropaolo.pierantoni@unicam.it
(2) Via Muzio Clementi, 58 - 00193 Rome, Italy
(3) Via P. Selvelli, 6 - 61032 Fano (PU), Italy

Abstract: *In this work we analyzed three main earthquakes (M>6) in the Central Apennines for which sufficient documentation allows analysis: the 1703 Umbria-Marche-Abruzzo (Norcia-Cascia), the 1915 Fucino and the 2009 L'Aquila earthquakes. The 2009 earthquake is obviously the best documented, and allows for the most detailed analyses, which can serve as a reference for the other events. The three events analyzed show similarities with regard to the development of seismic sequence and kinematics. First of all, it can be assumed that they derived by the activation of the same seismogenic structure, the CCFS. The quaternary left-transtensive Celano-Cittareale fault system (CCFS) consists of several sub-parallel high-angle main branches, trending NW-SE to NNW-SSE, and extends for more than 75 km along the axial zone of the Central Apennines, at least from Fucino Plain to Cittareale-Norcia. Secondly, the structure was clearly activated by contiguous segments and was scaled over time.*

Key words: *Seismicity pattern, Active faults, Seismic profile, Central Apennines.*

INTRODUCTION

Along the axial zone of the Umbria-Marche and Lazio-Abruzzo Apennines lies a system of Quaternary NW-SE trending extensional faults, generically defined by Cello et alii (1997) as the Central Apennines Fault System (CAFS). According to Cello and other authors, this fault system is the surface expression of a deep seismogenic structure dipping to the SW, responsible for the frequent earthquakes of great energy that occur in this sector of the Apennine chain. In a previous work regarding the 2009 L'Aquila earthquake, Pierantoni et alii (submitted, 2015) identified and defined an high-angle NE-dipping active structure, the Celano-Cittareale fault system (CCFS), on the surface and in the depth (Fig. 1). This complex structure consists of several sub-parallel main branches, sometimes anastomosed, trending NW-SE to NNW-SSE, and extends for more than 75 km along the axial zone of the Central Apennines, at least from Fucino Plain (most likely further south) to Cittareale. The CCFS is therefore part of the CAFS and probably is its main structure; the Celano-L'Aquila Fault identified by Salvi & Nardi (1995) is part of CCFS. The curved shape of this structure (snake geometry according to Krauss et alii (2009) is mostly due to transversal faults (approximately NE-SW) which have determined the snake development without causing significant interruption, at least on the surface. These transversal faults are in fact segments, in some cases reactivated, in others exhumed, of structures formed during the previous compressive tectonic phase in the Apennines as tear faults or transfer faults or other faults of regional significance, such as the the Celano-Bussi Fault (CBF; Centamore et alii, 2002 or Avezzano-Bussi line, Vezzani & Ghisetti, 1997 and Ghisetti & Vezzani, 1999 a.r.t.).

In addition to the latter, the main transversal faults from south to north are: the Torrita Fault (TF), the Montereale Fault System (MFS), the S. Vittorino Fault (SF); the Rocca di Mezzo Fault (RMF) (Fig 1).

By means of available seismic lines (www.videpi.com), the CCFS geometry was reconstructed in depth; it was identified as a flower structure in which the branches join or approach at about 6-7 km of depth (deeper below the Fucino Plain). In the Aquilan area, the flower branches are mostly NE-dipping, low to high angle (approximately 40°- 60°), while the deeper plane is high angle, NE-dipping at least up to about 18-19 km of depth (Fig. 2). Below the eastern part of the Fucino Plain, the flower branches are all high-angle, some of them NE-dipping and others SW-dipping, as those on the surface. The CCFS deep plane is not directly identified on seismic lines of the Fucino area, but some of its elements give reason to believe that it is NE-dipping. However, it cannot be excluded that the CCFS deep plane, which is of a very high angle, may also have opposite dipping due to local structural or inherited situations, as indeed is indicated by the "snake" trend and some structural remarks on the surface (Pierantoni et alii, 2015). Based on surface geological and structural knowledge, during the Quaternary this structure had a polyphasic activity with left transtension episodes up to the middle Pleistocene, and mainly extensional afterwards. The seismic activity of some CCFS segments was highlighted by numerous Authors (Saroli et alii, 2008 a.r.t.; Galli et alii, 2008 a.r.t.). The CCFS was thus identified as a regional seismogenic structure (deeply rooted, high-angle, NE-dipping left shear zone), and the main one responsible for the 2009 L'Aquila earthquake. During the Aquilan seismic sequence, both left transtensional and extensional earthquakes were recorded at the CCFS. In particular, extensional and transtensional earthquakes alternate

near the flower branches, while only left transtensional ones occur below.

Figure 1: Simplified tectonic map of the Central Apennine (key box A, location of the area in fig. 3).

The distribution of aftershock hypocenters along a high-angle and NE-dipping plane, almost continuous up to 18-19 km depth, suggests the role of main seismogenetic structure for CCFS. The CCFS activation caused the subsequent seismogenic involvement through accommodation of antithetic faults adjacent to it (Barisciano fault system-BFS / Stabiata fault-STF to the south and Mt. Gorzano fault-GF to the north) and one of the transversal faults (San Vittorino fault-SF). In fact the earthquakes associated to these structures occur slightly later; moreover they are shallower and distributed along a low-angle SW-dipping plane.

The three main earthquakes (M> 6) in the area for which sufficient documentation allows analysis were those of 1703, 1915 and 2009. The 2009 earthquake is obviously the best documented, and allows for the most detailed analyses, which can serve as a reference for the other events.

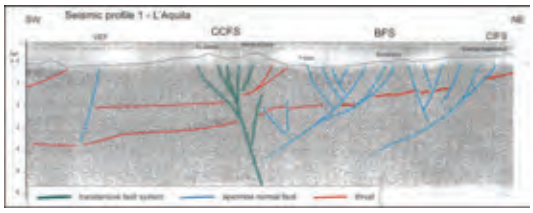

Figure 2: Seismic profile 1 (IT 89-01).

Thus the 2009 earthquake will be used as the reference element for the discussion. The new interpretation of the seismogenic sources obtained by careful review of the abundant documentation for this event can be compared against the interpretations of the other two events. The 2009 Aquilan seismic sequence was characterized by a main shock of MW=6.1 (6/4/2009) preceded and followed by numerous events of lesser energy (foreshocks and aftershocks). The space-time arrangement of these events featured clusters of epicenters separated from each other or delimited by some transversal faults, and staggered over time from south to north. Three transversal faults correlated to three clearly separate clusters of earthquakes during the Aquilan seismic sequence. These were the Rocca di Mezzo fault (RMF) to the south, the San Vittorino fault (SF) and the Marana fault (MF) in the center and the Torrita fault (TF) to the north. The RMF, MF and TF had a passive role because they simply separated the areas of some clusters, while the SF initially acted as a passive fault, but soon activated as a right transfer fault, becoming seismogenic. As previously stated, the main seismogenic structure of the 2009 L'Aquila earthquake was the CCFS. The foreshocks, the main shock and the deeper aftershocks were located inside it, and only later through accommodation did the antithetic faults BFS/STF, GF become seismogenic. The clusters of earthquakes scaled over time along this structure indicate that it was activated by segments from the south and gradually propagated northward involving progressively contiguous faults by accommodation, first the BFS/STF, then the SF and finally the GF (Fig. 3). The BFS/STF and GF are local SW-dipping faults, more superficial and therefore antithetical to the CCFS. The transversal faults including SF are sub-vertical and confined each of these segments. The initial rupture of

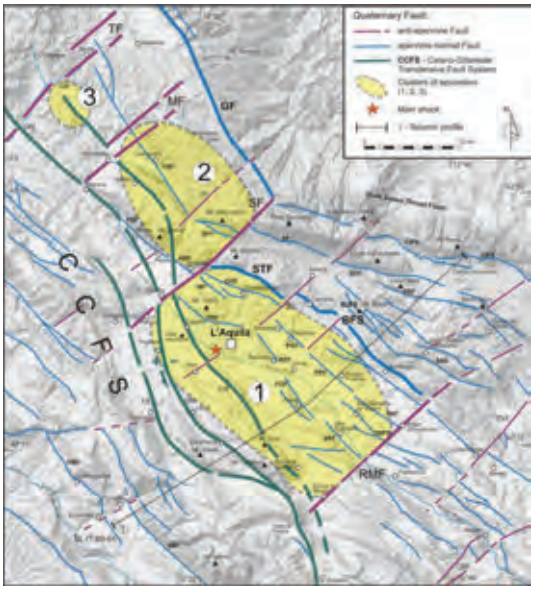

Figure 3: Structural scheme of 2009 L'Aquila seismic sequence.

about 10/12 km that occurred in the southern segment of the CCFS caused the main shock of MW= 6.1.

Figure 4: Structural scheme of 1915 earthquake. Isosisma of the greatest intensity (XII grade MCS, yellow area; by Oddone, 1915, modified).

The Fucino 1915 earthquake data are somewhat fewer and less precise. The epicentre of this approximately M=7 earthquake was in the eastern sector of the Plain, which was the site of widespread superficial coseismic effects (Oddone, 1915; Serva et alii, 1986; Galli et alii, 2008 a.r.t.). The focal mechanism was left transtensional. The isosisma of the greatest intensity (XII) (Oddone, 1915) had two trends, approximately orthogonal to each other (Fig. 4). The main branch developed in a NNW-SSE direction for about 20 km in the eastern sector of the Plain, while the other moved in a ENE-WSW direction between Paterno and Avezzano for about 10 km along the northern edge of the Plain. In this sector, the isosismes were very close together, indicating rapid energy attenuation to the north. In fact, E and N of Celano there was not a high intensity isosime. The greater and more frequent coseismic effects shown by Oddone (1915) were located at the NNW-SSE trending branch; this branch corresponds with the segment of the CCFS below the Fucino Plain, marked by strong quaternary activity and a complex flower structure (Fig. 5), and with the faults outcropping along the eastern edge of the Plain. The ENE-WSW trending branch coincided with the Tre Monti fault, in the western part of the Avezzano-Bussi structure, which is also characterized by strong quaternary activity.

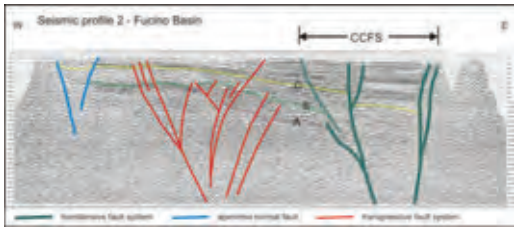

Figure 5: Seismic profile 2.

According to the Oddone (1915), Serva et alii (1986) and Galli et alii (2008) reconstructions, the western part of this structure (Avezzano-Celano or Tre Monti) was strongly involved in this seismic event, while the eastern part (Celano-Bussi) confined the effects of the earthquake to the north.

The M=7 earthquake epicenter was in the eastern Fucino Plain (CNR, 1985; Guidoboni et al., 2007), and then fell on the buried segment of the CCFS. According to Gasperini et al. (1985) and Basili & Valensise (1991) the focal mechanism of this earthquake was mainly strike-slip with high-angle to subvertical plane. The Basili & Valensise (1991) reconstruction seems more consistent with the NW-SE trend of the more eastern structures of the Fucino Plain. The left transtensional focal mechanism is perfectly consistent with the quaternary kinematics of the CCFS, which in this area moved the Tre Monti branch about 3 km south of Celano-Bussi one (Pierantoni et al., 2015). It is plausible that this CCFS segment was activated for an initial length of about 20 km, roughly corresponding to isosima XII, compatible with the M=7 estimated by seismologists. The serious damage recorded in Avezzano and surrounding areas may have been caused by local amplification, and/or more likely by activation of the south-western branch (Tre Monti fault) of the Avezzano-Bussi structure, which thus would have had a dual role, with the western side (TMF) as a transfer fault and the eastern side (CBF) as a confinement fault. In fact, the Avezzano-Bussi fault is divided into two segments because it is dislocated by the CCFS.

Figure 6: Structural scheme of 1703 earthquake (Baratta, 1936 and Blumetti, 1995, modified).

There is less information about the 1703 earthquake. Baratta (1936) and Blumetti (1995) indicate that the area affected by the quake as a whole trended NW-SE and was in the axial Apennines sector (Fig. 6). This is confirmed also by the CFTI catalog. The seismic sequence developed in three phases with a shift of the mesosismic area from Norcia towards L'Aquila, that is, from northwest to southeast, in about 20 days, and further south it involved many of the areas hit by the 2009 L'Aquila earthquake. Blumetti (1995) asserts that

the seismic sequence is characterized by 3 main high-intensity earthquakes (VIII-IX grade MCS) and the propagation from N/NW to S/SE developed "probably along a single segmented fault". Probably, the three Baratta mesosimic areas were distinctly separated from each other by transversal faults (Figs. 1, 3, 6). All this leads to the hypothesis that during this seismic sequence, there was a stepwise activation from north to south of three seismic sources, clearly separated spatially and over time, following the progressive activation of segments of the same structure (CCFS), as in the 2009 L'Aquila earthquake. Compared to the 2009 event, the 1703 event had an opposite shift in polarity and greater amplitude of different areas of resentment. These differences were not substantial, since the shift in polarity does not depend on the kinematic mechanism of structure activation, but on other unknown causes. The increased width of the area affected may be attributable to an event of greater magnitude or to errors in assessment and comparison of macroseismic effects.

DISCUSSION

The three events analyzed show obvious similarities with regard to the development of seismic sequence and kinematics. Therefore, it can be assumed that the three seismic sequences (1703, 1915 and 2009) derived by the activation of the same seismogenic structure, the CCFS. There may be some uncertainty for the earthquake of 1703, given the limited data available, but the reconstructions of Baratta (1936) and Blumetti (1995) suggest that the correlation is somewhat likely. Moreover, it is assumed that the activated segments were bounded (in a clear manner for the Fucino and Aquila earthquakes and presumably for the 1703 earthquake) by NE-SW transversal structures that at times acted as transfer faults and at other times functioned simply as confinement faults (Figs. 1, 3, 4, 6). The segments activated from time to time were more or less long, and this resulted in the greater or lesser magnitude of earthquakes connected to them. The Aquila and Fucino earthquakes occurred as a result of the left transtensional movement of a CCFS segment, consistent with its flower geometry and kinematics. During the 1703 earthquake, the Umbria-Marche (Norcia / Cascia) sector of this structure was also activated, but this was not the case in the 1915 and 2009 earthquakes. In recent times (1979, 1997), this sector was itself affected by other important seismic events that were slightly less powerful than those taken into account (a more detailed analysis of these recent earthquakes will be presented in the extended version of this paper). During the 1915 Fucino earthquake, neither the L'Aquila sector nor the Umbria-Marche sector were involved directly. All this confirms that the CCFS structure activates from time to time by segments, with some segments seeming to be activated more frequently than others. In fact, in the last three centuries, major earthquakes have occurred at almost all the sectors affected by the CCFS from Norcia to Fucino; only in the intermediate sector between Rocca di Mezzo and Celano there were no large earthquakes.

Acknowledgements: This work was supported by grants from the University of Camerino (FAR – Fondo di Ricerca d'Ateneo).

References

Baratta, M., (1936). *I terremoti d'Italia*. R. Acc. Naz. Lincei. vol. VI. Firenze.

Basili, A. & G. Valensise, (1991). Contributo alla caratterizzazione della sismicità dell'area marsicano-fucense. In: *Aree Sismogernetiche e Rischio sismico in Italia*. pp 197-214. (Boschi, E. & Dragoni, M. eds.). Atti del II° Convegno. Roma.

Blumetti, A.M., (1995). Neotectonic investigation and evidence of paleoseismicity in the epicentral area of the January-February 1703 Central Italy. In: (Serva, L. and Slemmons, D.B. eds.). *Perspectives in Paleoseismology*. Bull. Assoc. Eng. G. 6, 83-100.

Cello, G., S. Mazzoli, E. Tondi & E. Turco, (1997). Active tectonics in the Central Apennines and possible implications for seismic hazard analysis in Peninsular Italy. *Tectonophysics*. 277, 43-68.

Centamore, E., F. Fumanti, S. Nisio, (2002). The Central Northern Apennines geological evolution from Triassic to Neogene time. *Boll. Soc. Geol. It.* Spec. Vol. 1, 181-197.

CNR, (1985). Catalogo dei terremoti italiani dal 1000 al 1980. *Quaderni della ricerca scientifica*. 114, 2b.

Galli P., F. Galadini, D. Pantosti, (2008). Twenty years of paleoseismology in Italy. *Eart. Sci. Rev*. 88, 89-117.

Guidoboni, E., G. Ferrari, D. Mariotti, A. Comastri, G. Tarabusi and G. Valensise, (2007). *Catalogue of strong Earthquakes in Italy 461 B.C. -1997 and Mediterranean Area 760 B.C. - 1500.* CFTI http://storing.ingv.it/cfti4med.

Gasparini, C., G. Iannaccone and R. Scarpa, (1985). Fault plane solutions and seismicity of the italian peninsula. *Tectonophysics*. 117, 59-78.

Ghisetti, F. & L. Vezzani, (1999). Geometrie deformative ed evoluzione cinematica dell'Appennino Centrale. *Studi Geol. Camerti.* (1996-1997). 14, 127-154.

Kraus, R.K., F.M. Elter, C. Eva, E. Eva, M. Padovano & S. Solarino, (2009). An alternative interpretation for the seismic sequence of the L'Aquila earthquake: a combination between imposed strike-slip system and strain ellipse frame. *Proceedings of 28° GNGTS National Conference*. Trieste 16-19/11/2009. 172-173.

Oddone, E., (1915). Gli elementi fisici del grande terremoto marsicano-fucense del 13 Gennaio 1915. *Boll. Soc. Sism. It.* 19, 71-215.

Pierantoni, P.P., E. Centamore & M. Costa, (2015). Structural setting and deep seismogenic structures of the 2009 l'Aquila earthquake and surrounding areas (Central Apennine, Italy). (*IJG, submitted*).

Salvi, S., & A. Nardi, (1995). The Ovindoli fault: a segment of a longer, active fault-zone in central Abruzzi (Italy). In: (Serva, L. and D.B. Slemmons eds.). *Perspectives in Paleoseismology*. Bull. Assoc. Eng. Geol. 6, 101-113.

Saroli, M., M. Moro, H. Borghesi, D. Dell'Acqua, F. Galadini, P. Galli, (2008). Nuovi dati paleosismologici dal settore orientale del bacino del Fucino (Italia centrale). *Il Quaternario*. 21, 383-394.

Serva, L., A.M. Blumetti, and A.M. Michetti, (1986). Gli effetti sul terreno del terremoto del Fucino (13 Gennaio 1915); tentativo di interpretazione della evoluzione tettonica recente di alcune strutture. *Mem. Soc. Geol. It*. 35, 893-907.

Vezzani, L. & F. Ghisetti, (1997). *Carta Geologica dell'Abruzzo*. Scala 1:100.000. S.EL.CA. Firenze.

INQUA Focus Group on Paleoseismology and Active Tectonics

paleoseismicity.org

Seismites recording glacio-isostatic rebound after melting of the Scandinavian Ice Sheet in Latvia

Pisarska-Jamroży, M. (1), Van Loon, A.J. (1), Nartišs, M. (2), Krievâns, M. (2)

(1) Institute of Geology, Adam Mickiewicz University, Maków Polnych 16, 61-606 Poznań, Poland. Email: pisanka@amu.edu.pl
(2) Faculty of Geography and Earth Sciences, University of Latvia, Rainis Blvd. 19, 1576 Riga, Latvia

Abstract: *The cycles of loading and unloading of the earth crust as a result of growing and retreating land-ice masses during the Pleistocene resulted in numerous phases of glacio-isostatic rebound. Rebound was commonly stepwise, which resulted in successive earthquakes. These earthquakes are, if their magnitude was sufficiently large, reflected in layers (seismites) that are characterised by soft-sediment deformation structures that give the affected layer (or sets of layers) a deformed – sometimes even chaotic – appearance over long distances. Here we describe for the first time a series of seismites in Latvia, a Baltic country that was partially covered by the Pleistocene ice sheets. The seismites under study here were detected at Valmiera in NE Latvia along the Gauja River.*

Key words: *Soft-sediment deformation structures, Glacio-isostatic rebound, Neotectonics, Seismites, Pleistocene.*

Seismites related to glacio-isostatic rebound are known from numerous places, particularly on the northern hemisphere (Mörner, 1990, 1991; Muir-Wood, 2000; Kaufmann et al., 2005, Hampel et al., 2009, Brandes et al., 2012; Van Loon & Pisarska-Jamroży, 2013). The northern part of Latvia was not affected by strong endogenic tectonic activity during the Quaternary; this implies that the Pleistocene seismites must be attributed to glacio-isostatic rebound, in this case glacio-isostatic uplift when the Weichselian ice sheet retreated. Such isostatic rebound may induce earthquakes that leave traces in the form of soft-sediment deformation structures (SSDS; Van Loon, 2009; Van Loon & Maulik, 2011; Brandes et al., 2012; Brandes & Winsemann, 2013) if sediments susceptible to plastic deformation and, particularly, liquefaction and/or fluidisation are present. If layers are deformed over long distances due to the shock waves produced by earthquakes, these layers (in contrast to the usage by some authors not the SSDS!) are called 'seismites' (Seilacher, 1969; Van Loon, 2014).

The seismites under study were detected at Valmiera in NE Latvia (Fig. 1) and extend over some hundreds of metres, though not all seismites could be traced far because of coverage by thick vegetation or a thick talus burying the sediments that are locally exposed in steep cliffs in the Gauja river banks (Fig. 2). The seismites with their abundant SSDS occur between undeformed sediments (Fig. 2), which show similar grain sizes (fine-grained sand, very fine-grained sand and admixtures of silt and clay). Well-sorted sands like these are prone to deformation, particularly liquefaction and fluidisation, whereas silt is prone to plastic deformation (Montenat et al., 2007). This makes the individual layers in the section under study highly susceptible to earthquake-induced deformation over laterally extensive distances, thus becoming seismites. Most of the SSDS in the seismites at Valmiera are, as far as plastic deformation is concerned, loadcasts, pseudonodules and flames; fluidisation and liquefaction resulted mainly in fluid-escape structures (Fig. 3).

Figure 1: Location of the study area.

Figure 2: The Valmiera exposure along the Gauja river.

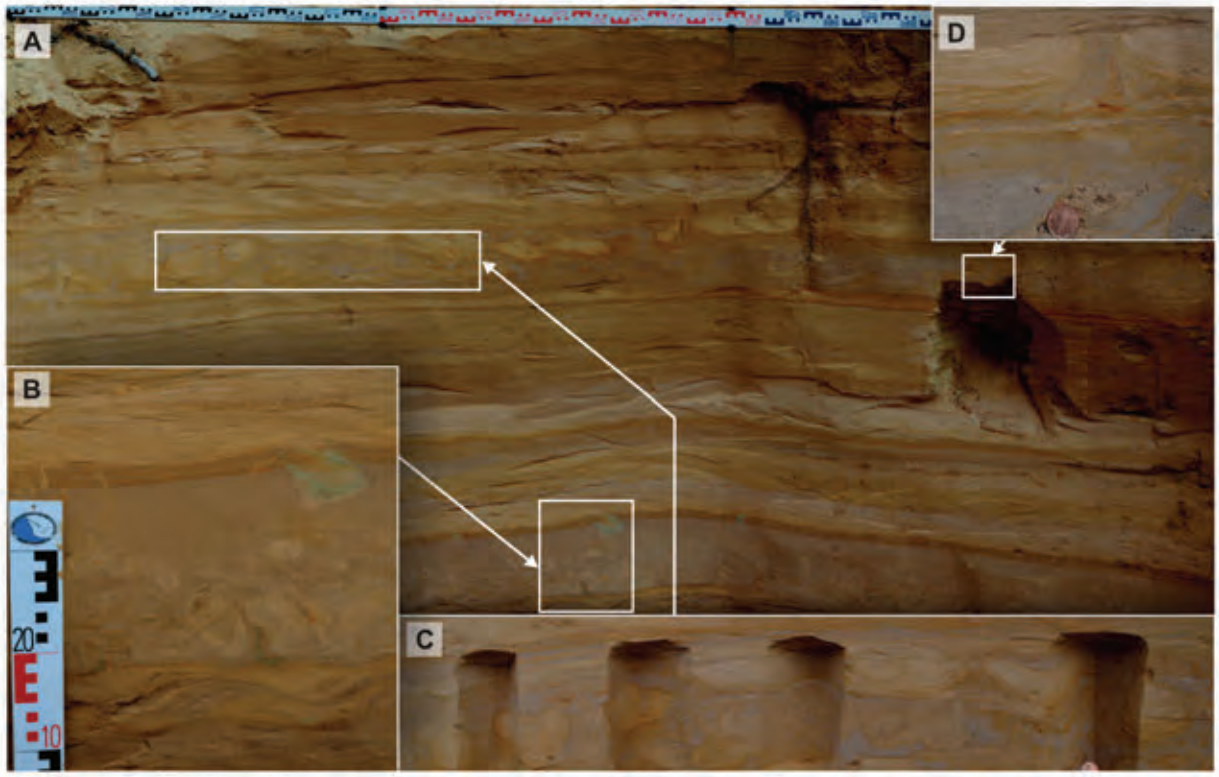

Figure 3: The Valmiera exposure showing lateral continuity of soft-sediment deformation structures in some seismites. A: Superposition of deformed levels. B-C: Loadcasts, ball-and-pillow structures and flame structures. D: Fluid-escape structure.

The best section occurs at Valmiera, where the cliff along the river is some 7 m high. This section contains seven layers that we interpret as seismites; they are all present in glaciofluvial sands that form part of a Weichselian (Würm; OIS 2) distal sandur that has locally be reworked and now forms part of a river terrace. Considering the fact that the terrace is covered only by material that is reworked by tree roots and human activity, it must be deduced that this terrace dates from the last Weichselian glaciofluvial sedimentation phase; this implies, in turn, that the earthquakes that led to the origination of the seismites must have taken place during the late Weichselian or later. Consequently, the oldest of these seismites cannot be older than maximally a few tens of thousands of years. As seven seismites formed in this time-span, their average occurrence was at most once within a few thousands of years. This seems consistent with the field data: sufficient time elapsed between successive earthquakes of sufficient magnitude for inducing seismites to result in the deposition of an (undeformed) layer or set of layers between the earthquake-affected layers. Thus a succession could build up of mostly undisturbed sediments, with some seismites as intercalations.

The Baltic region and adjacent areas are recognized as areas of low seismic activity, but there have been registered moderate earthquakes. Latvian sources indicate that the magnitudes of historical seismic events do not exceed 4.4. The earthquake with magnitude 4.4 on December 19, 1908 in Latvia was related to the Liepaja-Saldus fault zone, which was shown as a neotectonically active area by Šliaupa et al. (2006). Historical sources report on some moderate earthquakes in southern Latvia, but no earthquakes have been documented in northern Latvia, where the Valmiera outcrop is located. This might be explained by an 'inter-isostatic rebound' phase, but it might also well be that the post-glacial isostatic uplift has diminished so much during the past few millennia that earthquakes with a sufficiently high magnitude to produce seismites did no more occur.

Acknowledgements: The work has been financially supported by a grant from the Polish Ministry of Science and Higher Education (research project No. N N307 057540) and by a grant from the National Science Centre Poland (decision No. DEC-2013/09/B/ST10/00031).

References

Brandes, Ch., J. Winsemann, J. Roskosch, J. Meinsen, D.C. Tanner, M. Frechen, H. Steffen, & P. Wu, (2012). Activity along the Osning Thrust in Central Europe during the Lateglacial: ice-sheet and lithosphere interactions. *Quaternary Science Reviews.* 38, 49-62.

Brandes, C. & J. Winsemann, (2013). Soft-sediment deformation structures in NW Germany caused by Late Pleistocene seismicity. *International Journal of Earth Sciences.* 102, 2255-2274.

Hampel, A., R. Hetzel, G. Maniatis & T. Karow, (2009). Three-dimensional numerical modeling of slip rate variations on

normal and thrust fault arrays during ice cap growth and melting. *Journal of Geophysical Research.* 114, 8406-8420.

Kaufmann, G., P. Wu & E.R. Ivins, (2005). Lateral viscosity variations beneath Antarctica and their implications on regional rebound motions and seismotectonics. *Journal of Geodynamics*. 39, 165-181.

Montenat, C., P. Barrier, P. Ott d'Estevou, C. Hibsch, (2007). Seismites: an attempt at critical analysis and classification. *Sedimentary Geology*. 196, 5-309.

Mörner, N.A., (1990). Glacioisostatic and long term crustal movements in Fennoscandia with respect to lithospheric and atmospheric processes and properties. *Tectonophysics*. 176, 13-24.

Mörner, N.A., (1991). Intense earthquakes and seismotectonics as a function of glacial isostasy. *Tectonophysics*. 188, 407-410.

Muir-Wood, R., (2000). Deglaciation seismotectonics: a principal influence on intraplate seismogenesis at high latitudes? *Quaternary Science Reviews*. 19, 1399-1411.

Seilacher, A., (1969). Fault-graded beds interpreted as seismites. *Sedimentology*. 13, 15-19.

Šliaupa, S., R. Kačianauskas, D. Markauskas, G. Dundulis & E. Ušpuras, (2006). Design Basis Earthquake of the Ignalina Nuclear Power Plant. *Geologija*. 54, 9-30.

Van Loon, A.J., (2009). Soft-sediment deformation structures in siliciclastic sediments: an overview. *Geologos*. 15, 3-55.

Van Loon, A.J., (2014). The life cycle of seismite research. *Geologos*. 20, 61-66.

Van Loon, A.J. & P. Maulik, (2011). Abraded sand volcanoes as a tool for recognizing paleoearthquakes, with examples from the Cisuralian Talchir Formation near Angul (Orissa, eastern India). *Sedimentary Geology*. 238, 145-155.

Van Loon, A.J. & M. Pisarska-Jamroży, (2014). Sedimentological evidence of Pleistocene earthquakes in NW Poland induced by glacioisostatic rebound. *Sedimentary Geology*. 300, 1-10.

INQUA Focus Group on Paleoseismology and Active Tectonics

Geological investigation along the Sulmona active normal fault (central Italy) and its effects on the seismic microzoning of the area

Pizzi, A. (1), Di Domenica, A. (1), Di Federico, P. (1), Faure Walker, J.P. (2), Roberts, G. (3)

(1) Dept. of Engineering and Geology, University "G. D'Annunzio" of Chieti-Pescara, Chieti, Italy. Email: pizzi@unich.it
(2) Institute for Risk and Disaster Reduction, University College London, UK
(3) Dept. of Earth and Planetary Sciences, Birkbeck, University of London, Malet St., London, UK

Abstract: *Due to its ~2 kyr "silent state", the active Sulmona normal fault represents one of the most hazardous faults in central Italy, and the associated seismic risk is increased by the occurrence of important cities and several historical buildings and critical facilities. We investigated the central sector of the Sulmona fault through geological-geomorphological, geophysical and paleoseismological studies. The complex fault architecture has been analyzed along some gully exposures between Sulmona and Roccacasale villages. Here, two major fault zones have been mapped. The eastern one extends for 50 m from the rock fault scarp which marks the contact between the carbonate bedrock and the Quaternary deposits. Major evidence of late Quaternary faulting are observed along the further to the west (300-500 m basin-ward) fault zone. Our observations confirm that a multidisciplinary approach is useful to better assess the paleoseismic behaviour of complex fault zones and to define the areas of fault-rupture hazard during standard seismic microzonation work.*

Key words: *Sulmona active normal fault, central Apennines, geological and geophysical investigations, paleoseismology, seismic microzoning.*

INTRODUCTION

The Sulmona basin (Abruzzi, Italy) is an intramontane half-graben, developing in the outer Central Apennines carbonate chain (Fig. 1a), filled by a thick sequence of Quaternary fluvio-lacustrine deposits. It extends in a NW-SE direction for about 23 km, it is 4 to 7 km wide and it is limited to the east by the Sulmona active normal faults system (Miccadei et al., 1999; Vittori et al., 1995; Gori et al., 2011; 2014; Galli et al., 2015). Two main sub-parallel NW-SE Quaternary normal faults affect the western slope of Mt. Morrone (Fig. 1b). The Western Sulmona Fault (WSF) marks the contact between Quaternary slope, alluvial and lacustrine deposits and the Meso-Cenozoic carbonate bedrock along the Mt. Morrone range front (Fig. 1 b-c). It shows well-developed free faces on the carbonate bedrock and displaces Middle-Late Pleistocene alluvial fans and Late Pleistocene slope deposits, whereas minor sub-parallel and oblique splays offset Holocene deposits (Sylos Labini et al., 1993; Vittori et al., 1995; Galadini and Galli, 2000; APAT, 2005; Galli et al., 2015). The Eastern Sulmona Fault (ESF, Fig. 1b) affects the western slope of Mt. Morrone at higher elevation, where the fault scarps are locally covered by Late Pleistocene slope derived breccias. Our study is focused on the WSZ and its sub-parallel western splay, hereafter defined as the Western Sulmona Splay (WSSp) (Fig. 1b).
The measurement of the exposed bedrock fault planes indicate N110-140 striking segments, several kilometers long, with a right-stepping en-échelon geometry, although also E-W and N-S-trending segments can be recognized. In particular, step-over zones are connected by minor fault segments striking ca. N-S and represent the areas where major alluvial fans develop (Fig. 1b). Fault striae measured on the bedrock fault planes indicate a normal dip-slip to slightly oblique kinematics (Pizzi and Pugliese, 2004).
Before the recent work of Galli et al. (2015), no paleoseismological studies were available and no historical earthquakes were clearly associated with the activation of the Sulmona fault system. Its seismic potential was estimated based on empiric criteria (e.g., fault length and finite displacement), suggesting a potential magnitude of M 6.5-6.7 (Barchi et al., 2000; Valensise and Pantosti, 2001; Pizzi et al., 2002; Gori et al., 2011). This rank of maximum expected magnitude for the Sulmona fault has been recently confirmed by paleoseismological studies (Galli et al., 2015).
The most recent earthquake related to the Sulmona fault system occurred ca. 2ky B.P., as documented by archaeoseismic and paleoseismological studies (Ceccaroni et al., 2009; Galli et al., 2015), hence, there is a great chance of a magnitude 6.5-6.7 earthquake striking the area within the next few centuries. Therefore, in the ongoing microzonation studies of the area, it is crucial to accurately determine fault parameters such as slip rates, recurrence intervals and slip per event, as well as, to map in detail the fault trace. An accurate mapping of active and capable faults, indeed, can be very important in order to define future land use planning and to set retrofit priorities on existing buildings.

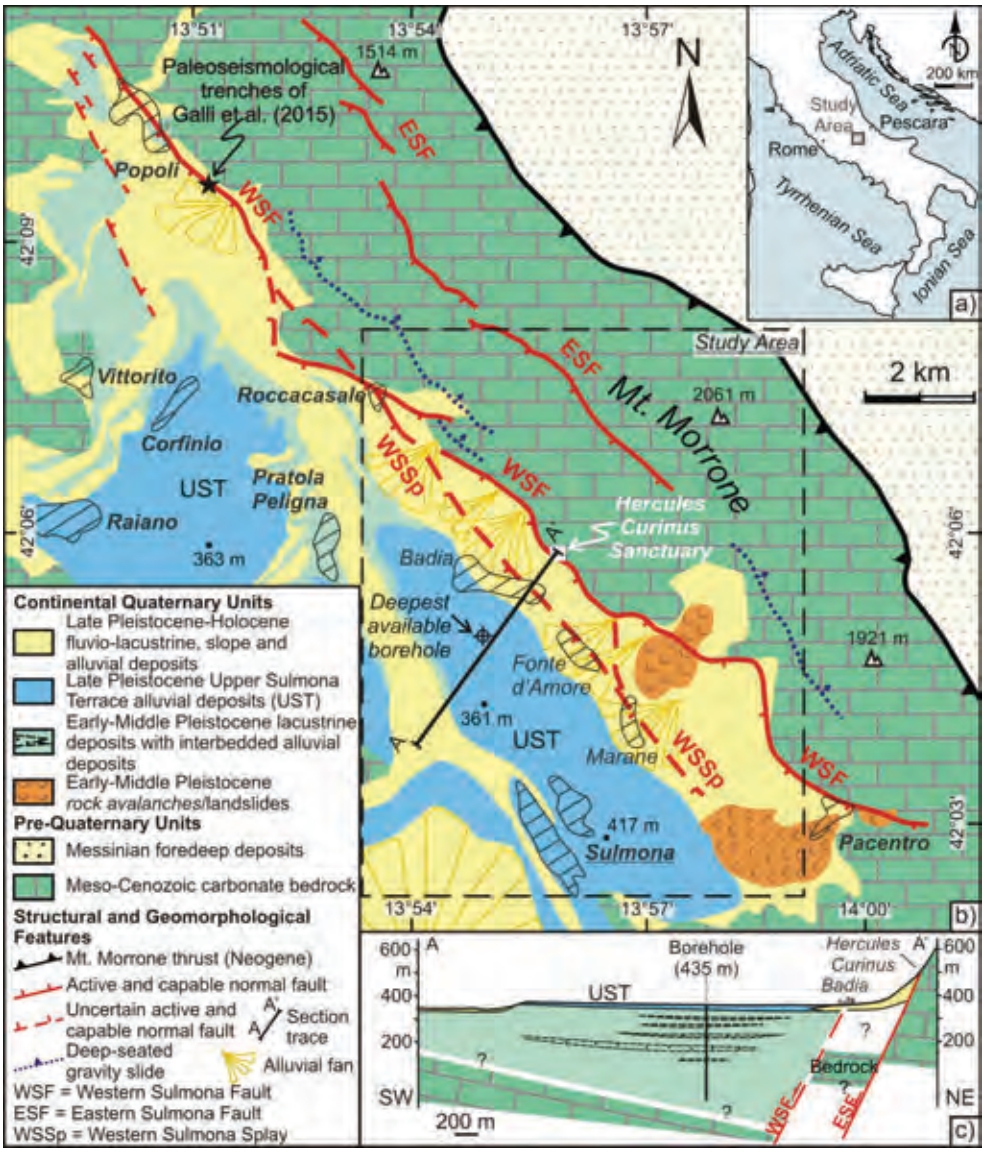

Figure 1: a) Location map. b) Simplified geological map of the Sulmona basin (modified from Galli et al., 2015). Two main NW-SE-trending active normal faults affect the western slope of Mt. Morrone. The Western Sulmona Fault (WSF) marks the contact between the Meso-Cenozoic carbonate bedrock and the Quaternary basin infilling. Minor splays are associated to the WSF and displace Late Quaternary alluvial fan deposits where many built-up areas rise up. c) Simplified geological cross-section through the Sulmona basin. The activiy of the Quaternary normal faults guided the development of a deep basin filled by a thick Pleistocene fluvio-lacustrine succession. The deepest borehole available in the area investigated the subsurface up to 435 m at depth without reaching the pre-Quaternary carbonate bedrock.

Although Galli et al. (2015) provided new insight about the recent history of events along the Sulmona fault, such studies have been exclusively performed in the northwestern sector of the 23 km-long Sulmona fault, near the town of Popoli (Fig. 1b). Therefore the evaluation of the seismic potential of the fault should be corroborated by detailed studies in the central portion of the fault (Sulmona-Roccacasale sector, Fig. 1b), where maximum slips and slip-rates should be expected. Moreover, in the area of Popoli evidence of Holocene displacements have been recorded basically in proximity of the bedrock fault scarp (eg., Gori et al., 2011; Galli et al., 2015), while in the central and southern sectors (between Roccacasale and Pacentro villages, Fig. 1b) recent deformations seem to localize away from the bedrock fault scarp, in correspondence of basin-ward fault splays which are still poorly known. The study of these splays are of major considerable importance due to town expansion plans.

Following the above, geological-geomorphological, geophysical and paleoseismological studies have been performed in order to investigate the central sector of the Sulmona fault, between the Sulmona town and the Roccacasale village.

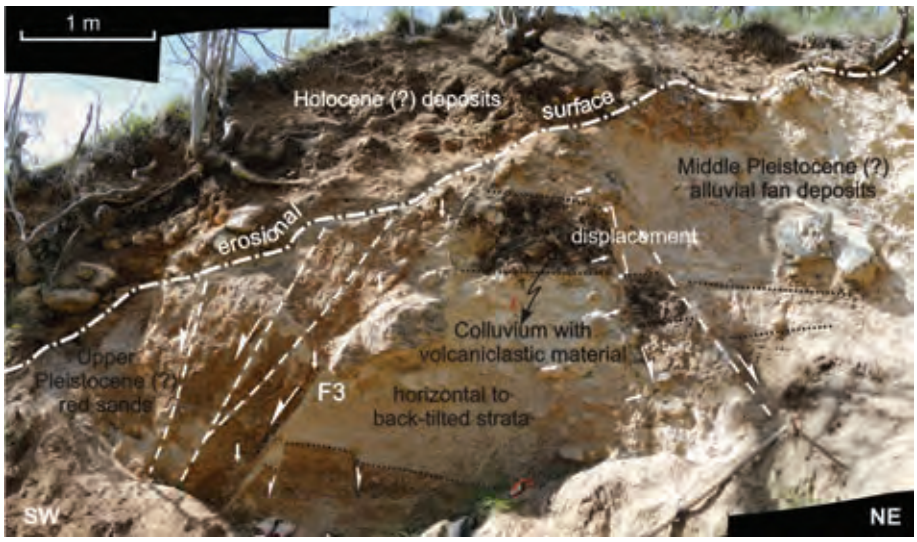

Figure 2: Particular of the F3 fault strands and related secondary structures observed in the WSF zone (see text for explanation).

Our study aims to define the surface and subsurface geometry of the master fault and related splays, to reconstruct their recent paleoseismic history and to establish both seismic potential and surface rupture hazard of the Sulmona active fault system.

THE SULMONA ACTIVE NORMAL FAULT: AREA BETWEEN ROCCACASALE AND SULMONA

A detailed geological-structural mapping, with a paleoseismological approach, has been performed along natural trenches represented by two sharply incised gullies. These gullies are up to 20-30 m deep and extend for several hundreds of meters (from the bedrock fault plane toward the basin) across strike the Sulmona Fault (see Fig. 1). The gully walls offer an almost continuous exposure of the fault zone architecture in the hangingwall of the major fault plane (WSF), hardly observable in classical paleoseismological investigations. In particular, two major fault zones have been distinguished. The eastern one is a complex fault zone which extends from the bedrock fault plane (WSF, master fault which marks the contact between the carbonate bedrock and the Quaternary deposits) towards the basin for about 40-50 m. The comparison between the trench section obtained along the gully walls and the results from a Ground Penetrating Radar (GPR) survey, acquired parallel to the gully (5-10 m to the north), shows a good correlation both in terms of fault strands distribution and geometry of the Quaternary deposits (Fig. 3). GPR data, moreover, provided a more reliable evaluation of the minimum down-throws associated to the main fault strands that are generally hard to evaluate in the gully exposures due to the lack of correlative layers across the fault.
Several minor synthetic and antithetic fault strands have been mapped. Two synthetic splays are likely characterized by cumulative displacements of several meters. In particular, the F3 fault strand (Fig. 2) determines the contact between cemented alluvial fan gravel deposits, probably of Middle Pleistocene age, and the unit made of red sands and gravel in abundant sandy matrix in the hangingwall, probably of Late Pleistocene age (radiocarbon dating are ongoing). Figure 2, moreover, shows back-tilted alluvial deposits strata in the footwall block of the F3 and the presence of several subordinated antithetic and synthetic structures both in the hangingwall and footwall of the fault. The upper portion of the fault strand is sealed by an erosional surface which is followed by the youngest unit of the sequence, probably of Holocene age, laying with a bedding conformable with the present slope angle (Fig. 2). Both geologic and GPR data do not provide evidence of recent faulting, i.e. faults reaching the ground surface or that at least may have affected the uppermost Holocene layers.
More evidence of late Quaternary faulting (dating is in process), instead, are observed in gully exposures, 300-500 m to the west (i.e. basin-ward) of the aforementioned rock fault scarp. Near the cemetery of the village of Roccacasale, in fact, Late Pleistocene alluvial fan deposits are faulted by a secondary splay (WSSp) that branches off the master fault. This fault puts in contact cemented conglomerates in its footwall with sandy-gravel alluvial deposits in the hangingwall. A tephra layer interbedded within the alluvial fan deposits in the hangingwall (Vittori et al., 1995) indicates at least 3-4 m of minimum down-throw associated to this fault. The peculiar foiditic composition of this tephra layer, which extensively outcrops ~3-4 m below the original top surface of others corresponding alluvial fans in the Sulmona area, allowed its correlation with the Albano-7 tephra dated by different authors at ~36 ka B.P. (Galli et al., 2015 with references).

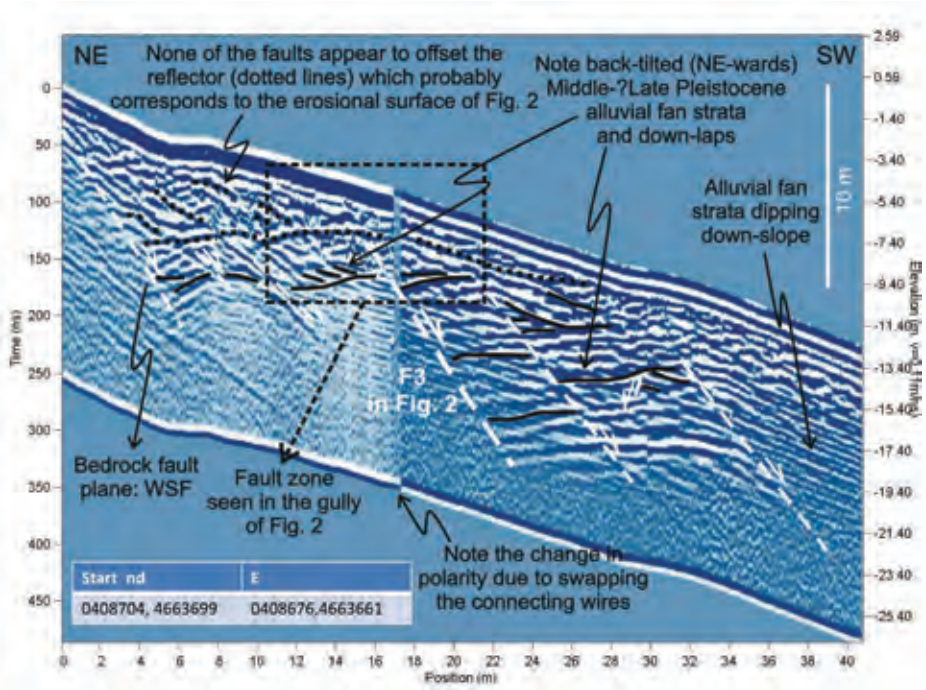

Figure 3: Results from a GPR survey in the hangingwall of the WSF. The GPR profile runs parallel to the gully at a distance of 5 m NW-wards from the fault zone showed in Fig. 2. The GPR profile interpretation shows good correlations with the geological data observed in the gully, both in terms of the fault zone architecture and geometry of the Pleistocene-Holocene stratigraphic units and erosional surfaces. None of the faults of the c. 40 m wide fault zone seem to offset the erosional surface at the base of the ?Holocene colluvium (dotted line). GPR parameters: frequency 200 MHz; antenna separation 0.5 m; step size 0.1 m; stacks 256; time window 300 ns; sampling interval 800 ps; assumed ground velocity 0.11 m/ns.

DISCUSSION AND CONCLUSIONS

The present study provided a better understanding of the central-southern sector of the Sulmona fault system, both along the WSF and the sub-parallel, more to the west, WSSp between the village of Roccacasale and the municipality of Sulmona. Although in the Roccacasale area, field data suggest that the WSSp has been active in very recent times, a Holocene activity of the WSF cannot be ruled out. In fact, because of the occurrence of erosional surfaces, the top of the stratigraphic sequence in the WSF zone generally results incomplete. In this view, surface rupturing along both the WSSp and WSF can not be excluded during major earthquakes, and they even may have alternated during distinct paleoseismic events.

Despite WSF and WSSp are the surface expression of the same deep seismogenic fault, spaced 300-500 m apart, we point out that they represent two distinct fault zones in terms of fault-rupture hazard. Therefore, following the criteria of Boncio et al. (2012) for delineating zones of surface fault-rupture hazard along active normal faults, we suggest that, at present, different areas of fault setback can be delineated for the WSF and WSSp fault zones. However, detailed studies can better constrain the fault setback areas and define the seismic hazard related to the Sulmona fault system.

Acknowledgements: We are grateful to Ioannis Papanikolaou for his help during the GPR survey.

References

APAT (2005). *Carta Geologica d'Italia alla scala 1:50.000.* Foglio 369 "Sulmona". APAT. S.EL.CA. Firenze.

Barchi, M., F. Galadini, G. Lavecchia, P. Messina, A.M. Michetti, L. Peruzza, A. Pizzi, E. Tondi & E. Vittori, (2000). *Sintesi delle Conoscenze sulle Faglie Attive in Italia Centrale: Parametrizzazione ai Fini della Caratterizzazione della Pericolosità Sismica*. CNR. Gruppo Nazionale per la Difesa dai Terremoti. Roma. p. 62.

Boncio, P., P. Galli, G. Naso & A. Pizzi, (2012). Zoning Surface Rupture Hazard along normal faults: insight from the 2009 Mw 6.3 L'Aquila, Central Italy, earthquake and other global earthquakes. *Bulletin of the Seismological Society of America*. 102, 918-935.

Ceccaroni, E., G. Ameri, A.A. Gomez Capera & F. Galadini, (2009). The 2nd century AD earthquake in central Italy: archaeoseismological data and seismotectonic implications. *Natural Hazards*. 50, 335-359.

Galadini, F. & P. Galli (2000). Active tectonics in the Central Apennines (Italy) - Input data for seismic hazard assessment. *Natural Hazards*. 22, 225-270.

Galli, P., B. Giaccio, E. Peronace & P. Messina, (2015). Holocene paleoearthquakes and early-late Pleistocene slip rate on the Sulmona fault (central Apennines, Italy). *Bulletin of the Seismological Society of America*. 105, (1).

Gori, S., B. Giaccio, F. Galadini, E. Falcucci, P. Messina, A. Sposato, & F. Dramis, (2011). Active normal faulting along the Mt. Morrone south-western slopes (central Apennines, Italy). *International Journal of Earth Science*. 100, 157-171.

Gori, S., E. Falcucci, F. Dramis, F. Galadini, P. Galli, B. Giaccio, P. Messina, A. Pizzi, A. Sposato, & D. Cosentino, (2014). Deepseated gravitational slope deformation, large-scale rock failure, and active normal faulting along Mt. Morrone

(Sulmona basin, Central Italy): Geomorphological and paleoseismological analyses. *Geomorphology*. 208, 88-101.

Miccadei, E., R. Barberi & G.P. Cavinato, (1999). La geologia quaternaria della Conca di Sulmona (Abruzzo, Italia centrale). *Geologica Romana*. 34, 58-86.

Pizzi, A. & G. Pugliese, (2004). InSAR-DEM analyses integrated with geologic field methods for the study of long-term seismogenic fault behavior: Applications in the axial zone of the central Apennines (Italy). *Journal of Seismology*. 8, 313-329.

Pizzi, A., F. Calamita, M. Coltorti & P. Pieruccini, (2002). Quaternary normal faults, intramontane basins and seismicity in the Umbria-Marche-Abruzzi Apennine Ridge (Italy): contribution of neotectonic analysis to seismic hazard assessment. *Boll. Soc. Geol. It.* spec.vol. 1, 923-929.

Sylos Labini, S., R. Bagnaia & A. D'Epifanio, (1993). Studi sulla neotettonica della Conca di Sulmona. *Quaternaria Nova*. 3, 343-360.

Valensise, G. & D. Pantosti, (2001). The investigation of potential earthquake sources in peninsular Italy: A review. *Journal of Seismology*. 5, 287-306.

Vittori, E., G.P. Cavinato, & E. Miccadei, (1995). Active faulting along the northeastern edge of the Sulmona basin, Central Apennines, Italy, In: *Perspectives in Paleoseismology* (Serva, L., Slemmons, D.B. eds.). Ass. of Eng. Geol. 6, 115-126.

INQUA Focus Group on Paleoseismology and Active Tectonics

Geomorphological slip rate and preliminary paleoseismological study along the Boconó Fault, Venezuela

Pousse, L. (1), Vassallo, R. (2), Jouanne, F. (3), Audemard, F. (4), Pathier, E. (5), Carcaillet, J. (5), Garambois, S. (5), Oropeza, J. (4), Aray, J. (4)

(1) ISTerre, Université de Savoie Mont-Blanc, Campus Scientifique 73376 Le Bourget du Lac cedex, France.
Email: poussele@univ-savoie.fr
(2) ISTerre, Université de Savoie Mont-Blanc, France
(3) ISTerre, Université de Savoie Mont-Blanc, France
(4) FUNVISIS (Fundación Venezolana de Investigaciones Sismológicas), Av. Guaicaipuro con calle Tiuna, prolongación calle Mara, Qta Funvisis El Llanito, Caracas, Venezuela
(5) ISTerre, OSUG-C, 1381, rue de la Piscine 38400 Saint-Martin d'Hères, France

Abstract: *Boconó Fault is a major active fault which triggered many Mw>7 historical earthquakes in Venezuela. It is part of a tectonic system constituted by internal minor blocks and numerous faults that accommodates relative movements between Caribbean and South America Plates. In the Yaracuy Valley despite the potential of big earthquake on the Boconó Fault (Mw=7 in 1812), the fault behavior and the seismic hazard remains poorly known. ^{10}Be dating of alluvial fans offset by the fault were carried out and allowed to obtain a slip rate of 8.2-16.3 mm/yr. This geomorphological rate, consistent with the regional geodetic rate of 12 ± 2 mm/yr according to Reinoza (2014), indicates that most of the deformation between South America plate and minor blocks such as the Triangular Maracaibo block is localized on the Boconó Fault. To complete this study a trenching site was chosen through the fault combining neotectonic study and georadar analysis.*

Key words: *Boconó Fault, paleoseismology, slip rate, ^{10}Be dating, Venezuela.*

INTRODUCTION

Northern Venezuela is crosscut by a plate boundary between the Caribbean and South America, (Figures 1 and 2). Considering the South American plate fixed, the Caribbean plate moves 2 cm/yr to the east (De Mets et al., 2010).

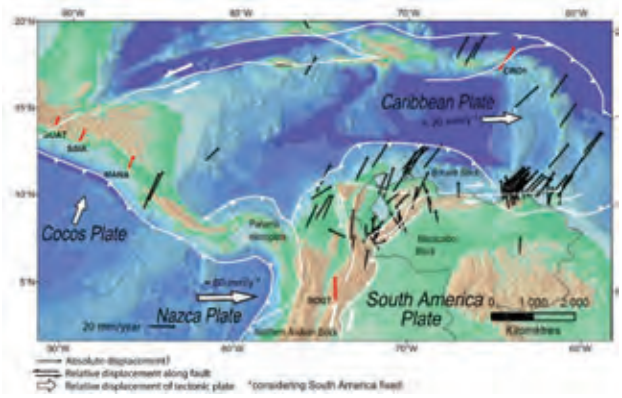

Figure 1: Caribbean geodynamic, black arrows are velocity field obtained from processing expressed in the IGb08 reference frame, red arrows showing IGS reference sites, white arrows represent relative displacement considering South-America fixed. Based on Reinoza, 2014; DeMets et al., 2010; Monod et al., 2010.

One of the major faults of this area is the Boconó fault. The Boconó fault accommodates the NE-SW component of the oblique convergence between the Maracaibo block and the South America Plate (Figures 1 and 2), (Audemard and Audemard, 2002; Monod et al., 2010). This NE-SW large strike-slip fault continues offshore to the East, where it is connected with the San Sebastian - El Pilar system fault. This system accommodates the Caribbean - South America relative displacement. Along the Pilar Fault an aseismic slip of 10 mm/yr is observed at surface and with geodetic measurement (Reinoza, 2014; Jouanne et al., 2010) while for Boconó F. the aseismic behavior is not proven from available data.

The Boconó Fault is tectonically active and threaten populated regions. The oldest historical event known occurred in 1531 (Audemard et al. 2000). Each fault segment ruptured once or, at most, twice in the last five centuries (Audemard, 2014). To estimate the average recurrence of destructive earthquakes - like the one that devastated several cities located along the fault in 1812 - we propose to jointly apply the analysis of long-term (10^4-10^5 years) displacement rates along major strike-slip faults, and the characterization of the return time for the last 3-4 most recent seismic ruptures. In particular, we will focus these studies on the westernmost segment of Boconó Fault, in the Yaracuy valley (Figure 3) where the 1812 event was the deadliest (Altez, 2006; Choy et al., 2010). In this valley the width of fault zone, distribution and segmentation of deformation are poorly known and paleoseismologic calendar is up today very incomplete. To address these issues, our approach combines morphotectonic/paleoseismologic analysis using data on complementary time scales.

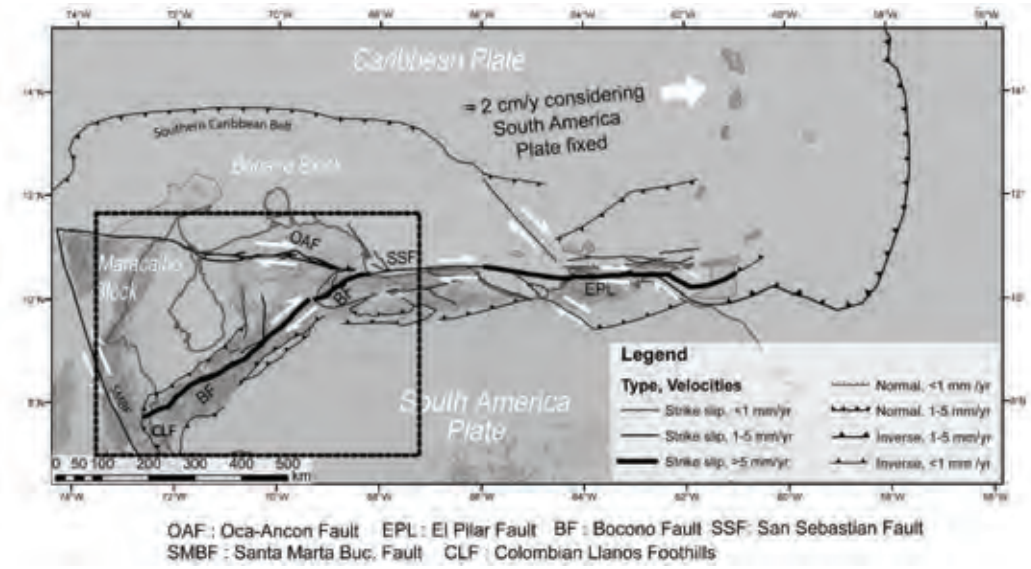

Figure 2: Major faults in Venezuela, black square is the location of the Figure 3. Fault mapping is based on Audemard et al. (2000) and velocities are based on DeMets et al. (2010).

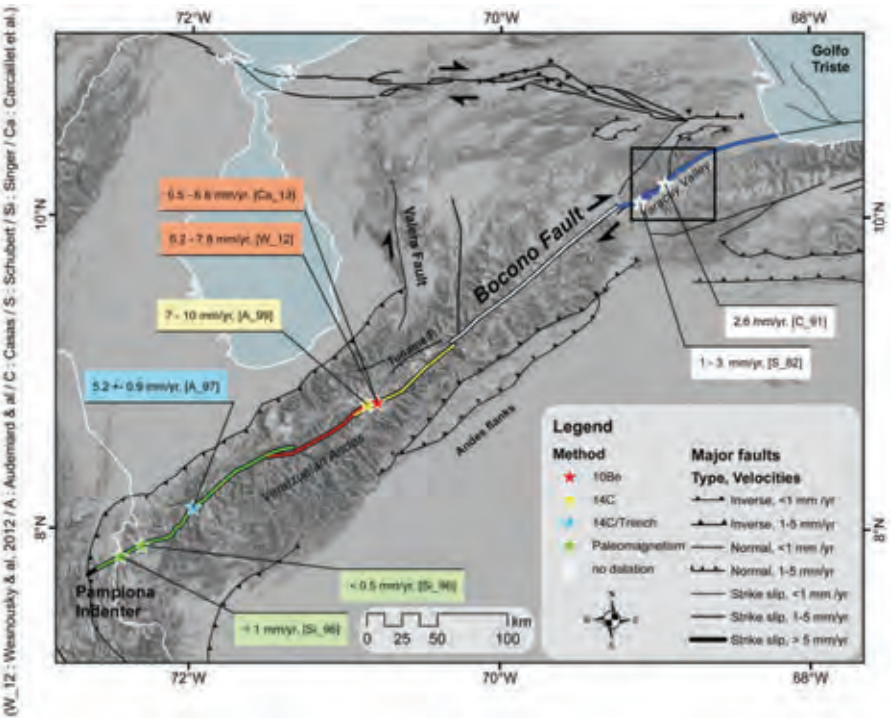

Figure 3: Published geomorphological slip rates along the Boconó Fault, in labels are displayed quaternary slip rates, estimation methods and references, black square is the approximate location of Figures 4 and 6 (Audemard et al., 1999, 2000; Audemard, 2014, 1997; Carcaillet et al., 2013; Casas-Sainz, 1992; Schubert, 1983; Singer and Beltran, 1996; Wesnousky et al., 2012).

Long term displacement rates

There are three quantified rates concerning Central Venezuelan Andes based on dated markers displaced by the fault. The first marker is a moraine in Apartaderos dated by radiocarbon method, which yields a slip rate of 7-10 mm/yr (Audemard et al., 1999). The second markers are Los Zerpa and La Victoria moraine crests (Mucubají) (Audemard, 2009), dated by ^{10}Be which yields a fault slip rate of 6.2-7.8 mm/yr (Wesnousky et al. (2012) ages modified by Carcaillet et al. (2013)). The third estimation was in Los Zerpas moraine dated by ^{10}Be (Carcaillet et al., 2013), it give a slip rate of 6.5-6.8 mm/yr.

Other investigations have proposed slip rate estimations along the fault without absolute dating method. We summarize it in Figure 3. Among these estimations, in our area of interest, investigators correlated shifted old alluvial fans by the fault with dated alluvial fans in Colombia. Schubert (1983) assesses a slip rate of 1-3 mm/yr, Giraldo (1985) of 5 mm/yr and Casas-Sainz (1992) of 1.3-2.6 mm/yr. To perform an accurate determination of slip rate along this segment of the Boconó Fault we mapped, measured and sampled the alluvial fans offset by the fault, in order to date them by in-situ ^{10}Be.

We thus sampled three alluvial fans, where we have collected quartz pebbles/sand in depth profiles, or boulders at the surface. The most relevant result in terms of displacement rebuilding analysis and dating is at the Yaritagua alluvial fan, which is shifted by 1.4-1.8 km (Figures 4 and 5). The model issued of inversion of data yields an exposure age between 110.000 and 170.000 yrs. It allows to estimate a fault slip rate of 8.2-16.3 mm/yr.

Concerning the other alluvial fans, the data are more complicated to interpret because the neotectonic context is more complex, yet they do not contradict the estimate at Yaritagua.

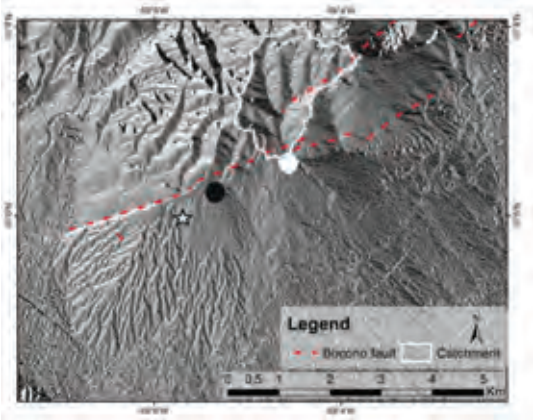

Figure 4: Shaded 12m-DEM showing Yaritagua alluvial fan displaced by the Boconó Fault. White star is the sampling site, black circle is the alluvial fan apex, and white circle is the basin outlet. Offset is the distance between the two circles. DEM was acquired with DLR's TanDEM-X satellite © DLR 2014.

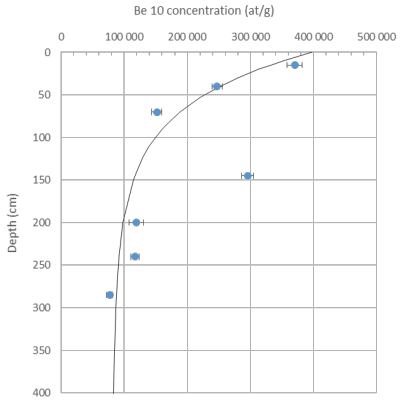

Figure 5: Plot of the ^{10}Be concentrations versus depth. The solid curve represents the best-fit exponential model of data inversion by least squares assuming 3m/Ma of erosion, density 2.4 g/cm3. The sample at 1.50 meters deep was not considered in the inversion.

DISCUSSION

Concerning present deformation GPS studies, Perez et al. (2011) reported an 80 km wide zone of right lateral shear centered along Boconó fault. Their modeling in the Andes shows that it may be related to 12 ± 2 mm/yr with a locking depth of 14 ± 4 km. This geodetic rate is slightly higher than the geomorphological rate found in the Andes (6.2-10 mm/yr for "accurate" rates). In the westernmost segment Reinoza (2014) assess a velocity of 11.28 ± 0.5 mm/yr (azimuth 60°, Quibor site). To compare with geological rate we use a regional geodetic rate of 12 ±2 mm/yr (Maracaibo area).

Our slip rate in Yaritagua (8.2-16.3 mm/yr) is higher than those previously published and it is closer to the geodetic rate, indicating that most of the deformation between South America plate and the Maracaibo block is localized along the Boconó Fault. This result increases the seismic hazard along the fault zone. However, this preliminary result is to be confirmed by other datings, and estimation of hazard requires a better knowledge of paleoseismologic calendar.

Paleoseismological characterization of the last 3-4 seismic rupture return time

In Yaracuy Valley, two trenches were carried out (Audemard in prep; Audemard, 2014) following a neotectonic study (Bueno et al., 2006) but no return time could be estimated. Therefore three new trenching sites have been preselected using spatial images and fieldwork observations. On these three sites ground-penetrating radar (GPR) profiles were established. This prior imagery to trenching is useful to define the width of the damaged area and to obtain information on the nature and geometry of sedimentary markers, which is sine qua non condition for the success of excavations that will be realized. It allowed us to focus on a trenching site where ruptures are best imaged: La Mata site (Figures 6 and 7).

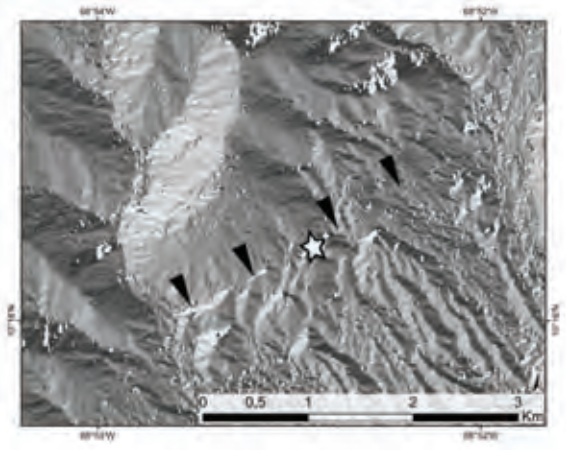

Figure 6: Shaded 12m-DEM showing La Mata site, white star is the location of trenching site, black arrow highlights the fault trace. DEM was acquired with DLR's TanDEM-X satellite © DLR 2014.

La Mata trenching site is a 2 meters high shutter ridge which deflects a small stream creating a shallow pond. This configuration is ideal because it determines the retention of fine materials in thin sedimentary horizons, limits the erosion of this fault zone portion, and thus allows a good record of the deformation. This trench should allow estimating a return period of the last few co-seismic events.

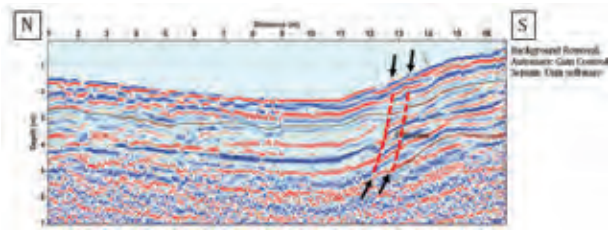

Figure7: Ground Penetrating Radar profile collected with 80 MHz antenna in La Mata trenching site. This profile was processed using Seismic Unix. Red dashed lines represent discontinuities in the profile and may be fault ruptures.

CONCLUSION

^{10}Be dating on an alluvial fan offset by the Boconó fault provides a Quaternary slip rate of 8.2 16.3 mm/yr. This value is comparable to the regional geodetic rate, this indicates that most of the deformation between South America plate and the Maracaibo block is localized on the Boconó Fault. However, this preliminary result is to be confirmed by other datings. To determine the seismic hazard it is necessary in addition to characterize the latest seismic cycles. For this purpose a trenching site was chosen and we expect to obtain paleoseismologic data that will complement the few existing ones. In the future we expect, in the same area, to establish quantification of the instantaneous deformation through interferometric data. The confrontation of these data will allow (1) to clarify the deformation regime of this strike-slip fault forming the plate boundary Caribbean / South America (2) to assess the importance of the creep on these accidents and to locate any roughness, and (3) to provide an estimation of earthquake magnitudes and return time periods.

Acknowledgements: The authors thank FUNVISIS for yielding aerial photos, topographic maps, archives of the study area, and the logistical support given during the field work. We acknowledge GIAME, Fondo Nacional de Ciencia Tecnología e Innovacíon (FONACIT) and Evaluation - Orientation de la COoperation Scientifique (ECOS) (project: FONACIT-ECOS Nord PI 2009000818, FONACIT 2012002202 2013000361), Isterre-Sud, Labex@OSUG2020 and UDSM (University of Savoie) for economical support during the field trip. We would like to thank the Laboratorio de Procesamiento Avanzado de Imagenes Satelitales LPAIS, German Aerospace Centre (DLR), and ISIS-CNES for providing satellite images. We thank M. Arnold, G. Aumaître and K. Keddadouche for assistance during AMS measurements for Beryllium 10.

References

Altez, R., (2006). E*l desastre de 1812 en Venezuela: sismos, vulnerabilidades y una patria no tan boba*. Univ. Catolica Andres.

Audemard, F., D. Pantosti, M. Machette, C. Costa, K. Okumura, H. Cowan, H. Diederix, C. Ferrer, L. Acosta, A. Alvarado, A. Arzola, L. Drake, C. Gardini, I.C. Gomez, J. Laffaille, A.M. Perez, M. Rengifo, A. Saadi, H. Vergara, (1999). Trench investigation along the Merida section of the Boconó fault (Central Venezuelan Andes), Venezuela. *Tectono*. 308, 1-21.

Audemard, F.A., (1997). Holocene and historical earthquakes on the Boconó fault system, southern Venezuelan Andes: Trench confirmation. Paleoseismology Underst. Past Earthq. Using. *Quat. Geol*. 24, 155-167.

Audemard, F.A., (2009). *5.3.8 Falla de Boconó (VE-06b y VE-06c)*. Atlas Deform. Cuaternarias Los Andes.

Audemard, F.A., (2014). Segmentación sismogenética de la falla de Boconó a partir de investigaciones paleosísmicas por trincheras, Venezuela occidental: ¿migración de la ruptura hacia el noreste en tiempos históricos? *Rev. Asoc. Geológica Argent*. 71, 247-259.

Audemard, F.A., M. Machette, J. Cox, R. Dart, K. Haller, (2000). *Map and Database of Quaternary Faults in Venezuela and its Offshore Regions*. U.S. Geological Survey.

Audemard, F.E., F.A. Audemard, (2002). Structure of Merida Andes, Venezuela: relations with South America-Caribbean geodynamic interaction. *Tectono*. 345, 299-327.

Bueno, M.L., R. Ollarves, F. Audemard, L. Rodríguez, (2006). *Cartografía morfotectónica de la falla de Boconó en el tramo San Felipe - Barquisimeto.* Presented at the VIII Congreso Venezolano de Sismología e Ingeniería Sísmica. VIII CONVESIS. Volume 1.

Carcaillet, J., I. Angel, E. Carrillo, F.A. Audemard, C. Beck, (2013). Timing of the last deglaciation in the Sierra Nevada of the Mérida Andes, Venezuela. *Quat. Res*. 80, 482-494.

Casas-Sainz, A., (1992). *A Neotectonic model for the Northern sector of the Boconó Fault (Southern of the Caribbean plate, Venezuela)*. Presented at the 13 Caribb. Geol. Conf. Pinar del Rio. Cuba. pp. 1-19.

Choy, J.E., C. Palme, C. Guada, M. Morandi, S. Klarica, (2010). Macroseismic Interpretation of the 1812 Earthquakes in Venezuela Using Intensity Uncertainties and A Priori Fault-Strike Information. *Bull. Seismol. Soc. Am*. 100, 241-255.

DeMets, C., R.G. Gordon, D.F. Argus, 2010. Geologically current plate motions. *Geophys. J. Int*. 181, 1-80.

Giraldo, C., (1985). *Neotectonique et sismotectonique de la region d'El Tocuyo San Felipe (Venezuela centro Occidental).* USTL. France.

Jouanne, F., F.A. Audemard, C. Beck, A. Van Welden, R. Ollarves, (2010). Present-day deformation along the El Pilar Fault in eastern Venezuela : evidence of creep along a major transform boundary. *J. of Geodyna*. 51, 398-410.

Monod, B., D. Dhont, Y. Hervouët, (2010). Orogenic float of the Venezuelan Andes. *Tectono*. 490, 123-135.

Perez, O.J., R. Bilham, M. Sequera, (2011). GPS derived velocity field in Western Venezuela: dextral shear component associated to the Boconó fault and convergent component normal to the Andes. *Interciencia*. 26, 69-74.

Reinoza, C.E., (2014). *Application de la géodésie satellitaire GNSS à haute résolution à la déformation de la marge Sud-Caraïbe. Implication pour l'aléa sismique dans l'Ouest et le Nord-Est du Venezuela.* UJF USMB. France.

Schubert, C., (1983). La cuenca de Yaracuy: una estructura neotectonica en la region centro occidental de Venezuela. *Geol. Norandina*. 194-202.

Singer, A., C. Beltran, (1996). *Active faulting in the Southern Venezuelan Andes and Colombian borderland.* Presented at the 3rd Inter. Symp. on Andean Geodyn. Saint - Malo. pp. 243-246.

Wesnousky, S.G., R. Aranguren, M. Rengifo, L.A. Owen, M.W. Caffee, M.K. Murari, O.J. Pérez, (2012). Toward quantifying geomorphic rates of crustal displacement, landscape development, and the age of glaciation in the Venezuelan Andes. *Geomorpho*. 141-142, 99-113.

INQUA Focus Group on Paleoseismology and Active Tectonics

Paleoseismicity on the northern part of the Yangsan Fault, S-E Korea

Rezaei, S. (1), Lee, J.H. (1), Hong, Y. (1), Gwon, S.H. (1), Kim, Y.S. (1), Rockwell, T.K. (2)

(1) Dept. of Earth & Environmental Sciences, Pukyong National University, Busan 608-737, South Korea. Email: rsoureh@yahoo.com
(2) Dept. of Geological Sciences, San Diego State University, San Diego, CA 92182, USA

Abstract: *Excavations on two parallel E-W trending trenches in the northern part of the Yangsan Fault indicate Quaternary faulting events. The fault strikes NNE-SSW and dips to the SE, which contacts Cretaceous intrusions and Quaternary deposits in both of our trenches. The fault gouges and their cross-cutting relations with different Quaternary layers, especially along the northern walls of our trenches, indicates at least two paleoseismic events. The last event seems to be very young and the fault penetrated up to the Quaternary layers located at the 10 cm below the surface. This kind of detailed studies on Quaternary faults of Korean peninsula are important due to the safety of nuclear power plants near the study area.*

Key words: *Yangsan Fault, Quaternary faulting, Paleoseismic events, Nuclear power plant.*

INTRODUCTION

The Korean peninsula is located between earthquake-prone countries of China and Japan (Kyung & Lee, 2006). It is considered to be a relatively stable margin compare to the other parts of the Asian continent (e.g. Kim et al., 2004). However several Quaternary faults are known in the south-eastern part of this peninsula (Fig. 1). Based on previous research (Lee and Na 1983; Lee 1998), several historical earthquakes occurred in this peninsula, of which 10 large events; are recorded in the Gyeongju area. Two well-known main faults in Korea are: the NNE-SSW trending Yangsan Fault and the NNW-SSE trending Ulsan Fault, which are located in the Gyeongsang Basin (Fig.1a). The Yangsan Fault is dominantly a right-lateral strike-slip system whereas the Ulsan Fault is dominantly a reverse fault (Kyung & Lee, 2006).
In this research we excavated two parallel E-W trenches across the northern part of the Yangsan Fault to study the activity of the fault in this area because this is an important issue related with the safety of the Weolsung nuclear power plant which is located about 23 km to the fault trace (Kim et al, 2004).

TECTONIC SETTING AND TRENCH SITE SELECTION

The south-eastern part of the Korean Peninsula is a relatively well-studied area for Quaternary faults (e.g., Ryoo *et al*. 2000). The most important structural features in this area are the Yangsan Fault and the Ulsan Fault, which intersect with an acute angle in the Gyeongju area (Fig.1b) (Choi et al., 2015).
The area is affected by several deformation events, which originated from interaction between several adjacent tectonic plates including the Eurasian Plate, the Pacific Plate, the Philippine Sea plate and the Indian plate (e.g. Yoon & Chough, 1955; Kim and Park, 2006). Present day deformation in the area is caused by the compression resulting from the subduction of the Pacific Plate and/or extrusion due to the collision of the Indian and Eurasian plates (Jun and Jeon, 2010). The closure of the East Sea causes a compressional stress regime in the area with the trend of ENE-WSW and different faults with Quaternary activity have been reported. Moreover, the most of them are reverse faults (Kyung, 2003; Ree et al., 2003).
For this research, we analyzed satellite imagery of the area to select the best sites for potential paleoseismic trenches. Based on geomorphological studies and lineament analysis of the area (Fig.1c), we selected the trench site, one of the best potential sites for Quaternary deposits and channel sediments developed along a small drainage.

DESCRIPTION OF THE TRENCH SECTIONS

We excavated two parallel E-W trenches across the northern part of the Yangsan Fault at the coordinate of 36° 3' 35.96" N and 129° 15' 14.66" E. The trench site is named the Danguri site, so in this paper we refer to the first trench as D1 and the second trench as D2. The D1 is an L-shape trench that is 10m in length and 2~4m in width. The depth of trench D1 is variable from about 1 m in the shallower parts to 4 m in the deepest parts. Because the exact contact of the fault and younger deposits was disturbed in the D1, we decided to excavate trench D2 to the north of trench D1. Trench D2 is a single-slot with 10m length and 1m width, and the depth varies from 1~5m. In this paper we discuss the well-exposed northern sections of both trenches.

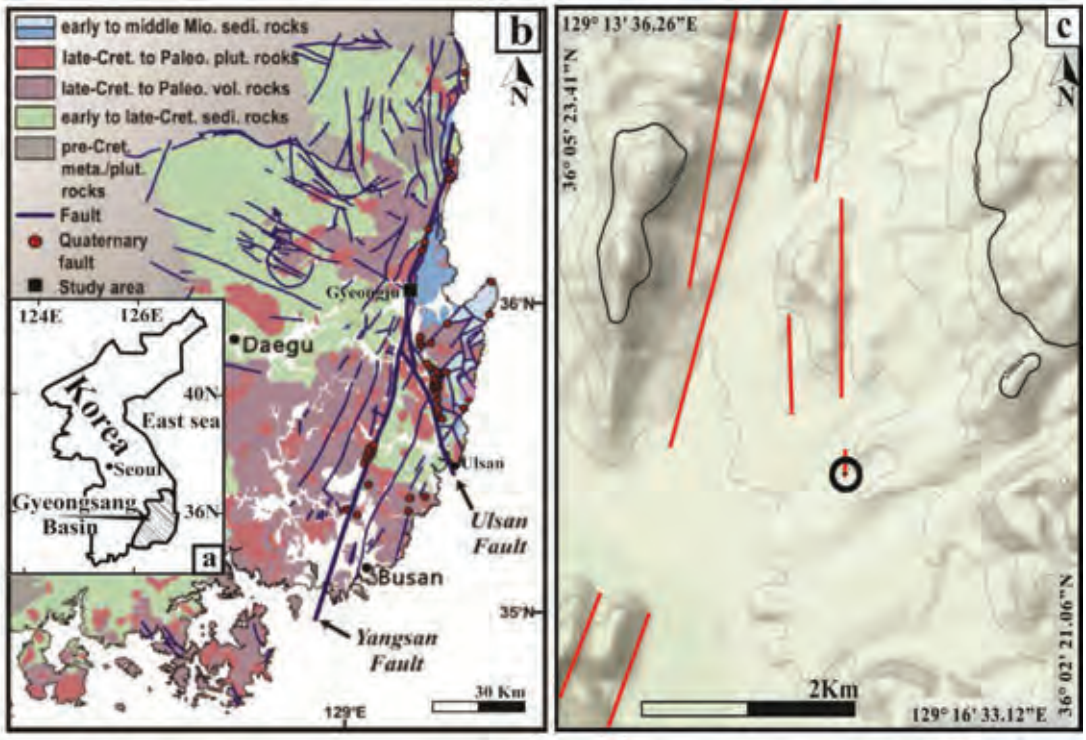

Figure 1: a General map of Korean Peninsula and the location of Gyeongsan basin. b: Geological map of Gyeongsan basin; Yangsan Fault and Ulsan Fault are the main fault system in the south-eastern part of Korea (modified after Choi et al., 2015) (the black square indicates the location of study area). c: Topographic map of the study area. Fault lineaments are shown by red lines (the black circle shows the trenching site).

SECTION D1-N (NORTHERN WALL OF THE FIRST TRENCH)

In the northern wall of trench D1, the fault juxtaposes Cretaceous intrusive rocks in the hanging wall and Quaternary deposits in the footwall (Fig.2). Based on special characteristics of sedimentary layers, such as the amount of matrix or amount of grains, grain size, roundness or angularity of grains and colour of layers, we divided the Quaternary deposits of this section into four unites. We marked the sedimentary units as D, F, G and H from top to bottom. Unit H is partly yellowish in colour and the sand and gravel content is higher than the percentage of matrix and the pebbles are not well-rounded indicating a local source. The pebbles in unit H show dragging by the fault. Unit G is a dark bluish very fine-grained layer, and it has been deformed into a clear drag structure in the footwall of the fault. Unit F is a gray layer with a high percentage of subangular grains. In Unit F, some weak evidences of dragging is also detectable. Unit E is composed of very angular channel deposits with a low percentage of matrix. On the top of the granitic host rock, some clear channels deposits are developed by erosion and fill deposits of the unit D.
The fault strikes N10°-20° E/75°-80°SE and the trend and the plunge of slickenlines on the fault plane is 15° /019 ° with the pitch angle of 15°N. Fault plane characteristics and dragging in the layers of footwall indicate a right lateral strike-slip sense of motion with a reverse component. Two clear zones of fault gouge with different colour are distinguishable; a black gouge of 5-7cm width affected unites H, G and F and didn't affect Unit D whereas a sky blue-coloured 7-10cm thick gouge layer affected all four units of H, G, F and D. These two different gouges indicate the occurrence of at least two different faulting events.

SECTION D2-N (NORTHERN WALL OF THE SECOND TRENCH)

There are some similarities and some differences between trenches D1-N and D2-N (Fig.3). The orientation of the fault in trench face D2-N is almost the same as that in trench face D1-N (N15°E/75°SE). We divided the sedimentary layers into units A, B, C, D, E, F, and G from top to the bottom. Unit E is located between units D and F and is composed of well-rounded boulders. The apparent displacement of unit E along the fault indicates a reverse component of slip across the fault. Along this trench face there is no evidence of dragging in units G or F. The fault gouge can be divided into two different layers based on their black versus blue colour. However, there is no exact delineation for the black gouge as we observed in trench face D1-N. However, the fault with sky blue gouge penetrates into unit D and the pebbles of the unit D show preferred orientation parallel to the fault surface. We could distinguish another layer which is composed of very condensed, very fine-grained soil, which we designated as unit C.

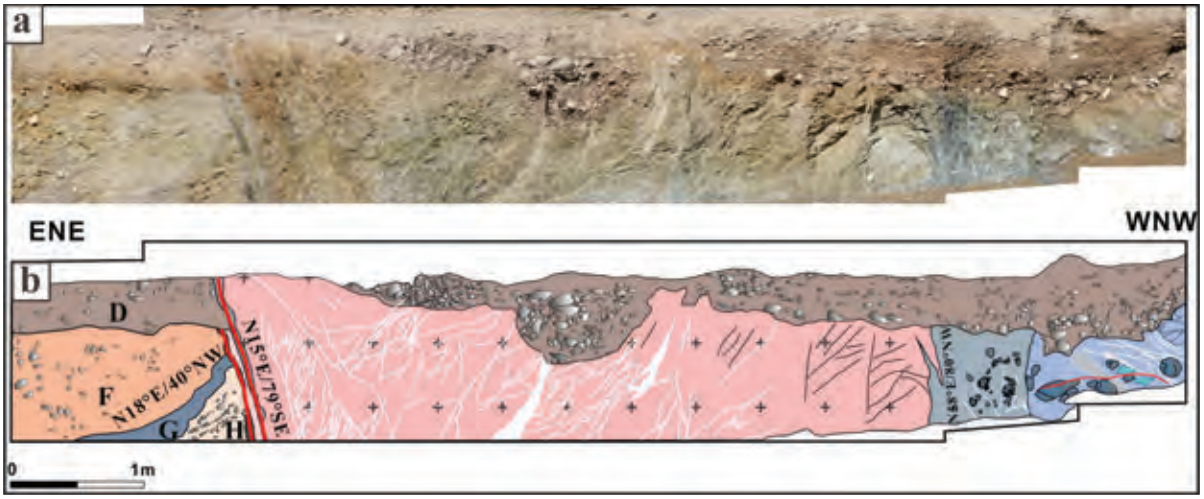

Figure 2: Northern wall of the first trench (D1-N). The different sediments are named by the D, F, G, and H from top to the bottom. The layers H and G show dragging along the fault. Note that the D layer has filled the small channels on the host rock.

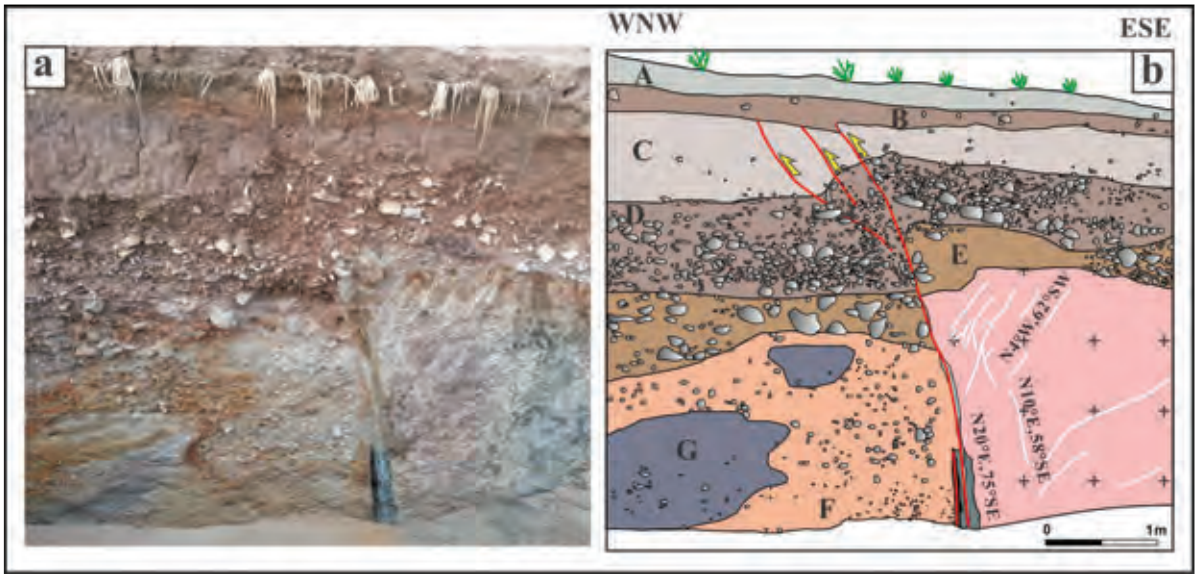

Figure 3: Northern wall of the second trench. Field observations indicate that the fault affected very young sediments (Layer C) and it formed positive flower structure near the surface. It is not clear that the fault affected the layer B or not.

The orientation of small grains, along several branches of the fault inside of unit C, exhibits a positive flower structure indicating strike-slip faulting with a reverse component. Unit B layer in this exposure is very thin and it is not clear whether the layer was affected by the fault. Unit A layer is the rice farm soil of anthropic origin and is not affected by the fault. On this section, the vertical distance from the tip of the fault to the surface; is just about 10cm, indicating a recent faulting event. For numerical ages for the last faulting event, OSL and C14 age dating is being carried out.

DISCUSSION

Formation of two fault gouge seams with different colours in trench D1-N, with each one cutting different horizons, indicates at least two seismic events (Fig. 2).
Fault plane characteristics, including slicken-lines, rake angle of the fault, layer displacement and positive flower structures, indicate right-lateral movement with a reverse component along this fault.
Based on our field investigations, we suggest a simple structural model for the study area as shown in figure 4.

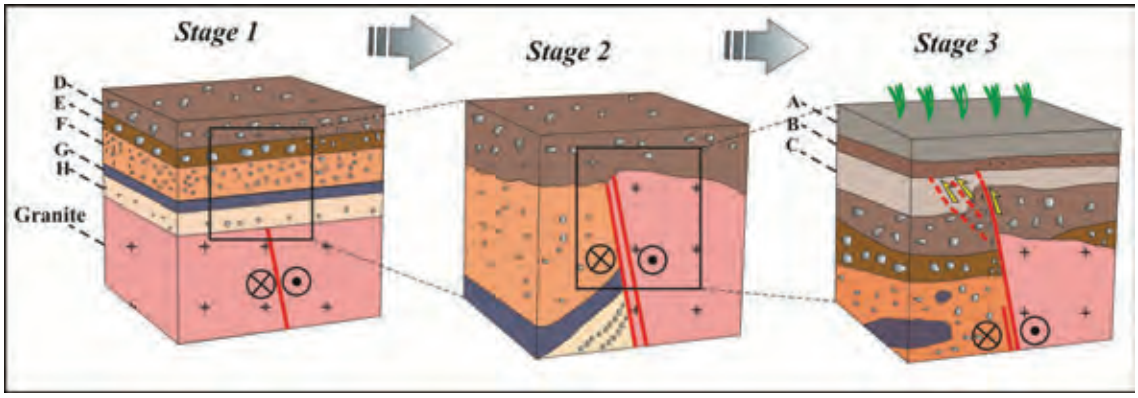

Figure 4: Structural model for the Danguri trench site. Field evidences show that at least two faulting events are recorded on these trench sections.

We summarize the deformation history of the area in the three main stages. In the first stage, faulting deformed the older sedimentary layers which were deposited over the granitic host rock. The fault movement caused dragging of unit G and H as it is shown in stage 2 of fig. 4. Probably there was at least one other faulting event in the area. Some of the units, such as unit E, are affected by this other faulting event but we cannot observe them in trench face D1-N. However, some younger units such as unit D, are affected, indicating erosion by surface waters in the area. In stage 3, as is distinguishable in trench face D2-N (fig. 3), the latest seismic event clearly cut units D and C. Finally, younger deposits as unit B were deposited across the fault, followed by development of the rice patties at the surface.

CONCLUSIONS

Field investigations based on trench excavations, lineament analysis and geomorphologic research in the northern part of the Yangsan Fault; indicate late Quaternary faulting in the area.

Fault gouge characteristics and cross-cutting relationships indicate at least two late Quaternary faulting events in the area.

In trench face D2-N, the fault is traceable up to within 10cm below the ground surface probably indicating a very recent faulting event. However, age dating data are necessary to determine the exact age of the faulting.

Acknowledgements: We thank to all GSGR members for their helps for the trench work. Useful discussions with 5th PATA attendants were very helpful.

References

Choi, J.H., S.J. Yang, S.R. Han, Y.S. Kim, (2015). Fault zone evolution during Cenozoic tectonic inversion in SE Korea. *Journal of Asian Earth Sciences*. v. 98, pp. 167-177.

Jun, M.S., J.S. Jeon, (2010). Focal mechanism in and around the Korean Peninsula. *Jigu-Mulli-wa-Mulli-Tamsa.* 13, 198-202 (in Korean with English abstract).

Kim, Y.S., J.Y. Park, J.H. Kim, H.C. Shin & D.J. Sanderson, (2004). Thrust geometries in unconsolidated Quaternary sediments and evolution of the Eupcheon Fault, southeast Korea. *Island Arc*. 13, 403-415.

Kim, Y.S., H.C. Kim, et al., (2004). Detail geological survey of Eupcheon Fault. Unpublished report, KOPEC. Yongin.

Kim, Y.S., J. Park, (2006). Cenozoic deformation history of the area around Yangnam-Yangbuk, SE Korea and its tectonic significance. *J. Asian Earth Sci*. 26, 503-517.

Kyung, J.B. & K. Lee, (2006). Active fault study of the Yangsan Fault System and Ulsan Fault System, south-eastern part of Korean Peninsula. *Journal of Korean Geophysical Society*. vol. 9, No. 3, pp.219-230.

Kyung, J.B., (2003). Paleoseismology of the Yangsan fault, southeastern part of Korean peninsula. *Ann. Geophys*. 46, 983-996.

Lee, K. & S.H. Na, (1983). A study of micro- earthquake activity of the Yangsan fault, *Journal of the Geological Society of Korea*. v. 19, pp. 127-135.

Lee, K., (1998). Historicall earthquake data of Korea. *Journal of the Geological Society of Korea*. v. 1, pp. 3-22.

Ree, J.H., Y.J. Lee, E.J. Rhodes, Y. Park, S.T. Kwon, U. Chwae, J.S. Jeon, B. Lee, (2003). Quaternary reactivation of Tertiary faults in the southeastern Korean Peninsula: age constrain by optically stimulated luminescence dating. *Island Arc.* v.12, pp. 1-12.

Ryoo, C.R., B.J. Lee, & U. Chwae, (2000). Quaternary fault and its remote sensing image in the southeastern Korea. *CCOP Technical Bulletin.* 29, 5-28.

Yoon, S.H., S.K. Chough, (1995). Regional strike slip in the eastern continental margin of Korea and its tectonic implications for the evolution of Ulleung Basin, East Sea (Sea of Japan). *Geol. Soc. Am. Bull*. 107, 83.97.

INQUA Focus Group on Paleoseismology and Active Tectonics

New insights on the occurrence of ancient earthquakes in Central Spain: Archaeoseismology of the Complutum area (4th century AD, Madrid)

Rodríguez-Pascua, M.A. (1), Heras, C. (2), Bastida, A.B. (2), Giner-Robles, J.L. (3), Silva, P.G. (4), Perucha, M.A. (1), Roquero, E. (5), Carrasco, P. (4), Pérez-López, R. (1), Lario, J. (6), Bardaji, T. (7)

(1) Instituto Geológico y Minero de España, Madrid, Spain. Email: ma.rodriguez@igme.es
(2) Trébede, Patrimonio Cultural, S.L. Torres de la Alameda, Madrid, Spain
(3) Facultad de Ciencias, Universidad Autónoma de Madrid, Madrid, Spain
(4) Dpto. Geología, Escuela Politécnica Superior de Ávila, Universidad Salamanca, Ávila, Spain
(5) Dpto. Edafología, E.T.S.I. Agrónomos, Universidad Politécnica de Madrid, Madrid, Spain
(6) Facultad de Ciencias. UNED, Madrid, Spain
(7) Dpto. Geología. Fac. Ciencias, Universidad de Alcalá de Henares, Madrid, Spain

Abstract: *The ancient Roman city of Complutum (Alcalá de Henares, Madrid) was founded in the first century AD and it was one of the most important cities of Hispania. The old Roman city was destroyed, abruptly abandoned, relocated in a close place and rebuilt in the 4th century AD. The destruction of the city and its new location is not still explained by the archaeology. In this paper we show different earthquake archaeological effects (EAEs) affecting the La Magdalena site (an agricultural holding located 4 km away from the core of Complutum). We used a multidisciplinary approach in order to identify and characterize apparent EAEs affecting the archaeological site. The most important earthquake geological effect identified in the site is the occurrence of liquefaction (sand dikes and ground settlement) affecting roman structures, such as water tanks, houses and graves. Ground liquefaction generated significant ground cracks and folds in the foundations of the buildings. Several Roman sites along the valley were also abruptly abandoned during the 4th century AD, in some cases with EAEs of similar origin. This suggests the occurrence of a 5.5 – 6.0 Mw seismic event in the zone according the empirical limit of seismically-induced liquefaction.*

Key words: *Complutum, earthquake, Earthquake Archaeological Effects (EAEs), Liquefaction, 4th century AD.*

INTRODUCTION

The archaeological site of "La Magdalena" is located in the Henares Valley (Madrid, Central Spain; Fig. 1) adjacent to the present town of Alcala de Henares, the old Roman City of "*Complutum*" (II-IV Century AD). This site has six occupational phases, from the Chalcolithic period (Campanian pottery; c. BC 2500), two roman industrial stages during the Early Imperial period (1st BC – 2nd centuries AD) finally transformed in a necropolis during the Late Imperial period (3rd to 5th centuries AD). Eventually the site record several post-roman periods of occupation during the centuries VI, VII and VIII, mainly corresponding to Visigoth graveyards. During the middle 4th century AD an earthquake affected the site as evidenced by ground disruptions and clear anomalies in the archaeological record. Several sites along the valley, including the main city of Complutum were abruptly abandoned or relocated during the same period, most of them also displaying apparent earthquake archaeological effects (EAEs).

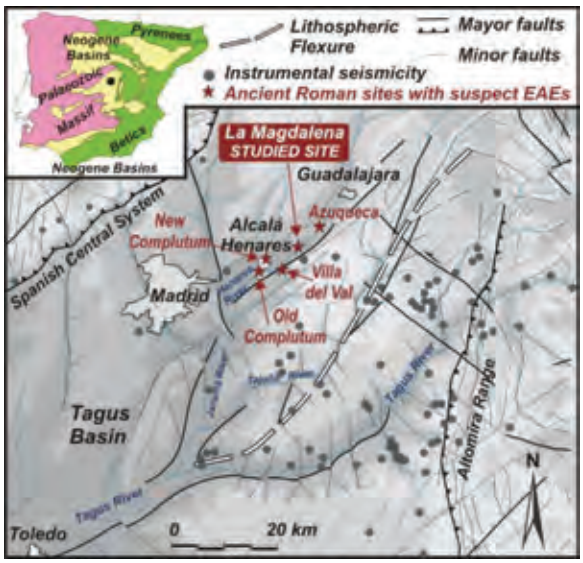

Figure 1: Geographical location of the archaeological Site of La Magdalena, ancient roman city of Complutum (Alcalá de Henares, Madrid).

GEOLOGICAL SETTING

The archaeological site of La Magdalena is located in the Madrid Basin, founded on the floodplain of the Henares River 5 m above the present river thalweg (Fig. 1). In detail, the site is placed in the internal edge of a large meander and the sedimentary record display the occurrence of offlaped sand-gravel point bars and channels, topped by fine-grained (clayey - silts) floodplain deposits. This fluvial stack (5 - 10 m thick) has an Holocene age probably older than 4,900-4,500 years according to the Calcolithic findings in the archaeological site. The fluvial sediments overlay the thick clayey Miocene substratum of this area of the Neogene Basin. This zone of the Henares valley is featured by the occurrence of a nearly-linear scarp (40-

60 m high) along the southern margin of the river, probably developed along a NE-SW km-scale normal fault as proposed by several authors (i.e. Pérez-González & Portero, 2004; Giner et al., 2012). This fault will work as northern boundary of a lithospheric-scale flexure, parallel to the Spanish Central System, responsible for the historical and instrumental seismicity recorded in the area (Fig. 1; Giner et al., 2012).

Figure 2: Fractured Cistern, ground cracks affecting the floor and impact block marks.

EARTHQUAKE ARCHAEOLOGICAL EFFECTS

The remains of the Late Imperial Roman period excavated at the site show evidences of EAEs in both factory buildings and in the necropolis remains. Below are listed and briefly described the different type of deformations recorded in the site:

Open Ground cracks and related liquefaction

Ground cracks are metric in length with openings up to 30 cm. In one of the cases, the ground cracks directly affect a cistern built in 1 m thick hydraulic "*opus caementicium*" (Fig. 2) generating fractures and displacements in the archaeological remains. The ground cracks propagated from the foundations cutting the thick floor of the cistern and displaying a clear continuity with the ground cracks affecting the substratum (presently filled by sands). Consequently, the fracturing of such type of resistant roman hydraulic concrete can be clearly linked to ground failure, and destruction due to building ruin and degradation can be rejected. The cracked floor of the cistern displays two significant impact marks overprinted to the cracks, which can be interpreted as local collapses of the side walls or roof materials soon after or during the abrupt destruction of the cistern.

In order to check the relationship between ground cracks and the fractures affecting the cistern, a prospective trench (1.5 m deep) was open at the base of the cistern. This water-facility is directly founded on a 50 cm thick clayey anthrophic level with archaeological remains overlying a 20 cm thick clayey silt level. The underlying sediments are constituted by gravelly sands (50 cm) and at least a 40 cm thick gravel bed of quartzite pebbles embedded in medium-coarse sized sand (Fig. 3). The contacts between the different units are wavy and irregular displaying cm-scale vertical sand dikes of the lower sandy units intruded in the overlying confining layer of finer sediments (Fig. 3). In detail, the basal gravel bed is intruded in the whole overlying sedimentary sequence, with the apparent vertical mobilization of smaller gravels (3-5 cm), which prove the occurrence of significant liquefaction processes around the destroyed building. In fact, the sand dikes extruded at surface through the ground cracks and open fractures affecting the floor of the cistern, since during the archaeological excavation of the building, the remains were nearly filled by sands.

The liquefaction processes involved in the destruction of the cistern triggered differential ground settlement and "lateral spreading" resulting in the severe rotation, tilting and collapse of one of the sides of the cistern structure (Fig. 2). The liquefaction of near-surface (< 1m) sand and gravel levels underlying the site generate apparent NE-SW ground folding all over the entire site affecting different types of structures (Fig. 4). The foundations of some buildings (made by rows of fluvial quartzite pebbles) display a clear bending coherent with surface folding. The foundations of basilica-pattern build adjacent to the damaged cistern display a monoclonal folding and height differences between its eastern and western zone (c. 50 m apart) is about 1 m. Foundations in the SW corner of this building are missed, suspect of local sagging as a consequence of surface liquefaction. In this sense, the unique structure of the site built with heavy masonry blocks (NE sector) sunken about 3 m down the average level of the archaeological site (Fig. 4). Exploratory trenches in one of the sides of the sunk building exposed a N055E vertical sand dike 1 m wide sub parallel to the main folds affecting the site.

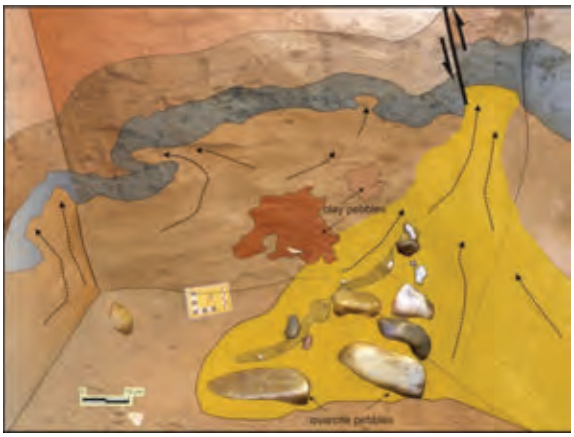

Figure 3: Photography and interpretational sketch of the liquefaction structures located under the cistern made of hydraulic mortar.

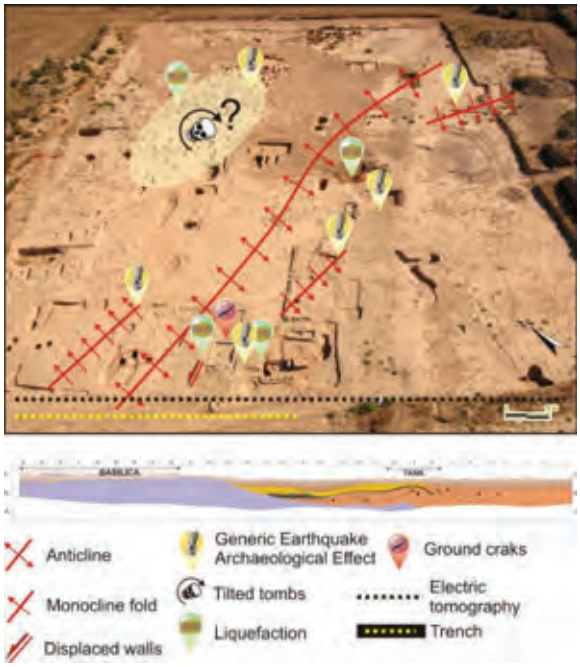

Figure 4: Aerial view of the La Magdalena archaeological site displaying ground surface deformations and recorded EAEs (up). Simplified stratigraphic-log of the exploratory trench showing paleo-liquefaction features associated to the recorded EAEs and surface ground deformations of the site(up).

Anomalies in the Necropolis (Forensic EAEs):

The main area of the necropolis located in the northern part of the site is altered (Fig. 4) containing several phases of burials. The early phase belongs to the early imperial period (≤ 3rd century AD) and the second one to the late one (4th centuries AD). In this last burial level, deceased persons were buried in wood coffins. Wood remains and iron spikes of the coffins were found in many of the graves. In most of these cases skeletons were found tilted and disturbed, with the pelvis displaced towards the thorax position, crania displaced from the necks, or a mixture of jumbled bones. It is interpreted that this particular burial level suffered the effects of ground shaking and liquefaction, stirring and tumbling the skeletons (after the lost of muscular bone cohesion) within the coffins. It is to note that previous (without coffins) and subsequent burials (Visigoth graves) in the zone do not display such post-mortem disturbances. Common cases of severe disturbance of burials are documented for seismically-induced landslides and liquefaction in historical earthquakes in Spain from intensity levels up to VIII MSK (i.e. 1884 AD Arenas del Rey event), even triggering the ejection of burial coffins. This particular *post-mortem* forensic EAE will be subject of further detailed analyses in order to identify bone-displacement vectors for reconstructs dominant directions of ground movement.

GEOPHYSICAL PROSPECTING & TRENCHING

Electric resistivity tomography profiles (ERT Schlumberger array) were done parallel to the southern wall of the basilica building and the cistern (N150ºE; Fig 4). The preliminary interpretation indicates the presence of an important deformed and sunken paleochannel replaced by a new smaller one by avulsion processes. The main zone of deformation is located beneath the western zone of the basilica and the cistern, where the ancient channel is apparently busted upwards as shown by the ERT profile (Fig. 5). Additionally a 30 m length exploratory trench (2.5 m deep) was open to explore the suspect deformation displayed by the ERT profile (Fig. 4). Data from the trench indicate that the deformed fluvial deposits are buried by a clayey floodplain level, on which the first settlements in the site occur (Calcolithic silos and graves, BC 2900 - 2500) and on which are founded the deformed buildings explored in this work. Underlying this top level a sandy channel (c. 10 x 1.2 m) display an anticline-like upwards bending just under the destroyed cistern. The orientation of the anticline observed at both walls of the trench is congruent with the main directions of ground flexures recorded at the surface. The deformation of the fluvial sediments is triggered by the complete liquefaction of an underlying thick sandy level (c. 1.5-2.8 m thick) in which the sedimentary structures (nicely preserved in adjacent units) were completely blurred by the full fluidization of the sands, which extruded over the deformed channel. The fluidization process also affected sandy gravels outcropping at the base of the trench, which record

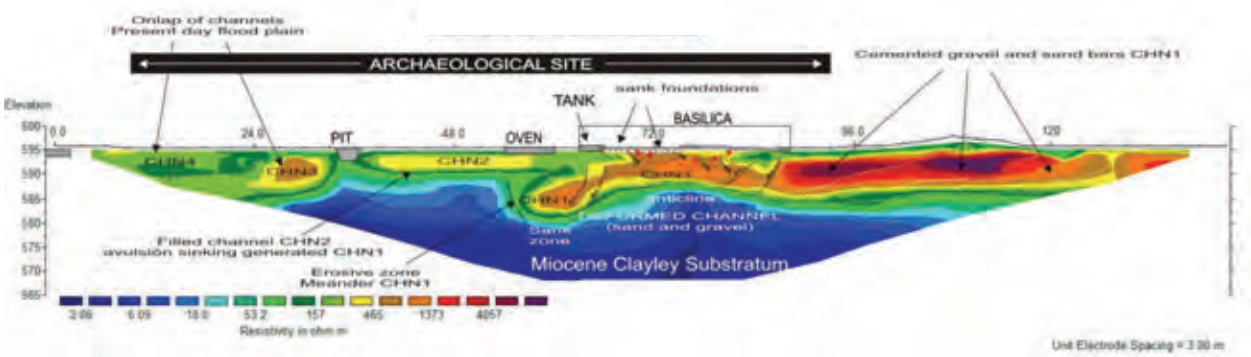

Figure 5: ERT 2D Pseudosection displaying deep deformations printed in the point bar- channel sequence underlying the archaeological site.

apparent injection features. In any case, the large deformations observed in the ERT profiles seems to be previous to the Calcolithic period, but the near-surface paleo-liquefaction features recorded in the exploratory trench can be linked to the deformations recorded in the roman remains. Therefore, these latter processes seems to be a discrete reactivation of large deformation structures acting in the zone before c. 5,000 yr BP.

DISCUSSION AND CONCLUSIONS

The deformation structures affecting the archaeolo-gical site of "La Magdalena" can be categorized according the EAE classification of Rodriguez-Pascua et al. (2011). There are two outstanding geological coseismic effects: (1) Sand ejections affecting the buildings and the necropolis; (2) Open ground cracks and folded substratum. Both are caused by ground liquefaction and differential settlement, and also considered in the ESI-07 scale (Michetti et al., 2007) from intensity levels ≥VIII according to the observed dimensions.

The archaeological remains record three noticeable primary coseismic effects in the building fabric: (1) Tilted and folded walls throughout the entire site; (2) Broken and displaced walls (cistern); and (3) Impact block marks (cistern). To these common archaeological effects the necropolis records a new type of forensic EAE witnessed by the disturbed skeletons in the burials of the 4th century AD.

During the 4th Century the industrial buildings of the site are abandoned and the zone is only used as a graveyard during late-Roman and Visigoth times (≤ 8th Century AD). In spite of no clear signals of abrupt abandonment being present at the investigated site, many Roman settlements around the area record sudden abandonments or related-anomalies during the 4th century AD (Fig. 1; Gómez-Pantoja, 2013). Fires and subsequent abandonements, unexpected changes in building patterns and land-use are recorded in the in the houses of *"Hippolytus"* and *"Los Grifos"* located in *Complutum* 7 km SE from the site (Rascón Marqués, 2007), *"Villa de El Val"* rural settlement of the Henares Valley about 4 km away (Rascón Marqués et al., 1991), and Azuqueca de Henares 8 km NE (Cardín y Cuadrado, 2013). Additionally the zone records the abrupt abandonment of the main city of *Complutum* soon after (c. 350 AD) its main period of Monumental development (275 - 300 AD). The city was abandoned and re-located about 2 km away in the present-day location of Alcalá de Henares (Gómez-Pantoja, 2013). At least an area of about 50 km^2 along the Henares Valley shows archaeological anomalies during the middle 4th century AD closely related to the deformation period identified in La Magdalena archaeological site.

The observed deformations can be certainly related to abrupt extensive liquefaction of near-surface sandy levels triggering ground differential settlement damaging roman buildings, disturbing burial sites and leaving permanent deformations in the ancient ground surface. Such extensive liquefaction, in sand-grain size materials, needs of at least an earthquake 5.5 - 6.0 Mw according to empirical approaches for seismically-induced liquefaction by near-field seismic sources (i.e. Obermeier, 1996). If this is the case, this recovered ancient earthquake exceeds the intensity and magnitude levels of the instrumental and historical records for central Spain. In fact, this densely populated zone (2.800 habitant/km^2), close to the Madrid urban area (30 km away), is actually outside the area of application of the Spanish Seismic Building Code (IGN, 2013). Therefore the unearthing of such "lost earthquakes" in these populated areas is critical to update seismic hazard assessments in Central Spain.

Acknowledgements: This work is a contribution of the Spanish projects CATESI-07 (IGME-MINECO), CGL2012-37281-C02.01 (QTECTBETICA-USAL), CGL2013-47412-C2-2-P (SISMOSIMA-IGME).

References

Cardín, I., M.A Cuadrado, (2013). Yacimiento del Polígono UG XVI de Azuqueca de Henares. En: *La romanización en Guadalajara, arqueología e historia.* (Cerdeño, M.L., Gamo, E. y Sagardoy, T., eds.). Ed. La Ergástula. Madrid. España. 137-144.

Giner-Robles, J.L., R. Perez-Lopez, P.G. Silva, A. Jiménez Díaz, M.A. Rodriguez-Pascua, (2012). Recent tectonic model for the Upper Tagus Basin (central Spain). *Journal of Iberian Geology*. 38, 113-126.

Gómez-Pantoja, J., (2013). Complutum y su territorio. En: *La romanización en Guadalajara, arqueología e historia.* (Cerdeño, M.L., Gamo, E. y Sagardoy, T., eds.). Ed. La Ergástula. Madrid. España. 63-72.

IGN (2013). *Actualización de Mapas de Peligrosidad Sísmica en España 2012*. IGN. Madrid. 267 pp.

Michetti, A.M., E. Esposito, L. Guerrieri, et al., (2007). Environmental Seismic Intensity scale – ESI 2007. Intensity Scale ESI-07 (Guerrieri, L., Vittori, E. Eds.). *Mem. Descr. Carta Geologica d'Italia 74*. APAT. Rome. Italy. 41 pp.

Obermeier, S.F., (1996). Use of liquefaction - induced features for paleoseismic analysis. *Engineering Geology*. 44, 1 - 76.

Pérez-González, A., J.M. Portero, (2004). *Mapa Geológico de España 1.50.000*. Alcalá de Henares (560). MAGNA 2ª Serie. IGME. Madrid. 52 pp.

Rascón Marqués, S., A. Méndez Madariaga y P.D. del Río Español, (1991). La Reocupación del mosaico del Auriga Victorioso en la villa romana del Val (Alcalá de Henares). Un estudio de microespacio. *Arqueología, paleontología y etnografía*. 1, 181-200.

Rascón Marqués, S., (2007). La así llamada casa de Hippolytus: la fundación de los anios y la schola de una agrupación colegial de la ciudad romana de Complutum. *Archivo Español de Arqueología*. 80, 119-152.

Rodríguez-Pascua, M.A., R. Pérez-López, P.G. Silva, J.L. Giner-Robles, V.H., Garduño-Monroy y K. Reicherter, (2011). A Comprehensive Classification of Earthquake Archaeological Effects (EAE) for Archaeoseismology. *Quaternary International*. 242, 20-30.

INQUA Focus Group on Paleoseismology and Active Tectonics

Overview of combining regional strain-rate, slip-rate variability and stress transfer during fault interaction for seismic hazard assessment and understanding of continental deformation

Roberts, G.P. (1), Cowie, P.A. (2), McCaffrey, K. (3), Gregory, L.C. (4), Phillips, R.J. (4), Faure Walker, J. (5), Wedmore, L. (5), Watson, Z. (5), Sammonds, P. (5), Papanikolaou, I. (6), Zijerveld, L.J.J. (1), Dunai, T.J. (7), Binnie, S.A. (7), Freeman, S. (8), Wilcken, K. (8), Shanks, R. (8), Vittori, E. (9), Michetti, A.M. (10)

(1) Birkbeck, University of London, London, United Kingdom. Email: g.roberts@bbk.ac.uk
(2) University of Bergen, Bergen, Norway
(3) University of Durham, United Kingdom
(4) University of Leeds, Leeds, United Kingdom
(5) University College London, London, United Kingdom
(6) Agricultural University of Athens, Athens, Greece
(7) University of Cologne, Cologne, Germany
(8) Scottish Universities Environmental Research Centre, AMS Laboratory, East Kilbride, United Kingdom
(9) ISPRA - Istituto Superiore per la Protezione e la Ricerca Ambientale, Roma, Italy
(10) Dipartimento di Scienza e Alta Tecnologia Università dell'Insubria, Como, Italy

***Abstract**: Active faults experience earthquake rupture due to stress transfer from neighbouring earthquakes only if the fault in question is close to its failure stress. We lack knowledge of which faults are close to their failure stress and thus cannot interpret calculations of Coulomb stress transfer in terms of the probability of impending earthquakes. This presentation suggests that for active normal faults in central Italy whose geometry and slip-rates are well known, it is possible measure slip-rate variability and perhaps the elapsed time since the last earthquake(s), normalised to the fault slip-rates averaged over many earthquakes, using ^{36}Cl cosmogenic exposure dating, because these are proxies for how close a fault is to its failure stress. We will combine this with calculations of stress transfer from historical and palaeoseismic earthquakes to reveal which faults are late in the cycle of loading and stress release, allowing end-users to prepare and increase social/economic resilience to earthquakes.*

***Key words:** Cosmogenic dating, elapsed time, slip-rate variability, Coulomb stress transfer, interseismic loading.*

INTRODUCTION

The seismic hazard represented by a fault, averaged over numerous seismic cycles (10^2-10^4yrs), is controlled primarily by the fault slip-rate because earthquake recurrence intervals, for a given magnitude of damaging earthquake on a specific fault, are shorter for higher slip-rates (Roberts and Michetti 2004, Faure Walker et al. 2010). However, following a damaging earthquake, the seismic hazard represented by a neighbouring fault is altered by Coulomb stress transfer, with subsequent rupture either brought forward in time or delayed, depending on the geometry of the faults in question. It is common practice to attempt to re-calculate the probability of a damaging earthquake on the fault that received the stress by using rupture-time advance/delay to refine the probability implied by the long-term slip rate (e.g. Stein 2003, Pace et al. 2014). However, key elements in such calculations are knowledge of the elapsed time since the last damaging earthquake, and whether recent slip has kept pace with longer term slip-rates, because the stress renewal process, whereby ruptured faults are re-loaded by regional stress, takes time to prepare a fault for subsequent rupture. Unfortunately, data on elapsed times and slip-deficits are generally lacking, especially for faults whose recurrence intervals for damaging earthquakes are hundreds to thousands of years, that is, a time period longer than the historical record (Peruzza et al. 2010). In summary, a fault will only experience earthquake rupture due to stress transfer in the days/years after a neighbouring earthquake if that fault was already loaded to an extent that it was ready to fail, but whether it is ready to fail or not is usually unknown. Thus, despite the commonly held view that it is possible to calculate rupture-time advance/delay and hence short-term changes in probability, we emphasise that this is not the case unless the elapsed time and presence, or not, of late Holocene slip-deficits is known. We are trying to measure elapsed times and slip-rate variability (including late Holocene slip deficits and surpluses) on the major active normal faults in central Italy whose 15 ±3 ka –averaged slip-rates and geometries are known (Figure 1; Roberts and Michetti 2004). We utilise *in situ* ^{36}Cl cosmogenic exposure dating, following, but modifying to an extent the approach of recent pioneering work (e.g. Benedetti et al. 2002, 2013; Schlagenhauf et al. 2010, 2011), to assess rupture-time advance/delay across an entire intra-plate fault system. With a background knowledge that earthquakes may cluster in time due to elastic interactions between neighbouring faults (e.g. Cowie et al. 2012, and this issue), we emphasise the need for knowledge of late Holocene slip-deficits or surpluses as well as a single value for elapsed time (compare with Peruzza et al. 2010 and Pace et al. 2014). We do not know for how long and by how much a fault can be behind or ahead of its multi-seismic-cycle slip-rate due to temporal earthquake clustering. This is important because,

presumably, a long elapsed time since the last earthquake is even more significant in terms of imminent rupture if the fault, and faults sharing the tectonic process across strike, have been behind their multi-seismic-cycle slip-rates for a time period that approaches that for several seismic cycles and/or by an amount of slip that approaches that for several seismic cycles. We will show that it is precisely these kinds of features that our results from ^{36}Cl dating can reveal (see Gregory et al. and Cowie et al. this issue). This is important because natural variability in earthquake recurrence intervals (temporal earthquake clustering), although known from only a small number of high quality palaeoseismic investigations worldwide, is thought to be common due to results from numerical models of fault growth (Cowie et al. 2012). These models show that it is not just the elapsed time since the last earthquake that is important. Rather, in the models, temporal clustering exhibits spatial variations in cluster characteristics (duration, slip amplitude during the cluster) across variable fault geometries, with greater irregularity in the timing and magnitude of earthquake slip-event sequences where faults overlap in complex geometries to share the regional load (Cowie et al. 2012). This implies that values for elapsed time normalised to the multi-seismic cycle loading rate will vary both through time and spatially across a fault system, as will cluster duration and slip amplitude during that cluster; we lack measurements of these variables.

APPROACH

We are trying to measure, using *in situ* ^{36}Cl cosmogenic dating, the spatial distribution of (a) elapsed time and slip deficits/surpluses, (b) cluster duration, and (c) slip amplitude during the most recent cluster, across a fault system where we expect imminent earthquakes, showing how (a), (b) and (c) relate to fault geometries, fault-specific slip/loading rates, stress transfer and earthquake probabilities. The hypothesis we investigate is that the stress baseline [controlled by (a), (b) and (c) above] for refining multi-seismic cycle earthquake probabilities with data on Coulomb stress transfer will be spatially-rough. By "stress baseline" we mean the stress-levels on each fault in a system: if the stress is the same on each fault, the baseline is smooth; if temporal earthquake clustering and its associated history of stress transfer and interseismic loading have produced different stress-levels on each fault, the baseline is rough. A partial example of this is shown in Figure 1 where we present stress heterogeneity solely from coseismic stress transfer, omitting interseismic loading that Roberts and Michetti (2004) have shown must occur at different rates (see Wedmore et al. this issue). As we cannot measure stress directly from faults at depths of 12-15 km where intra-plate, damaging earthquakes nucleate, we need a proxy measure. The proxy measure we propose is provided by (a) elapsed time and slip deficits/surpluses, (b) duration of the most recent cluster, and (c) slip amplitude during the most recent cluster, and we show that this can be measured with *in situ* ^{36}Cl cosmogenic exposure dating at enough sites in central Italy to map this proxy for the spatial-roughness of the stress baseline across an entire fault system (see Gregory et al. this issue). Moreover, we can place this knowledge of stress roughness in the context of 8 key constraints of the fault system that can be achieved in central Italy (see Figure 1, which shows the faults are well-characterised in terms of their structural geology and earthquake history). These 8 constraints are in place (Cowie et al. 2013) and consist of knowledge of: (i) the fault geometry; (ii) the kinematics of faulting at multiple sites; (iii) the far-field regional loading rate implied by geodesy and geologically-constrained motions; (iv) how the regional stress-loading rate has contributed to multi-seismic cycle slip-rates at multiple locations along each active fault and hence regional, but fault-specific strain-rate fields; (v) how overlapping faults interact to share the regional loading rate; (vi) the historical record of past earthquakes; (vii) the palaeoseismological record of past earthquakes; (viii) fault-specific strain-rates from GPS geodesy at the length-scale of individual active faults. Overall, we are trying to understand the mechanism of deformation to help constrain seismic hazard (see Cowie et al. this issue).

METHOD

Specifically, we combine observations of structural geology, geomorphology and Coulomb stress transfer with sampling for ^{36}Cl on fault planes exhumed during slip. We sample portions of the faults exhumed by past coseismic slip, and dig trenches at the bases of fault scarps to collect sub-surface fault-plane samples. This combination of measurements will constrain the residence-time of the samples beneath the ground surface relative to what this residence-time should be given independent knowledge of the multi-seismic cycle slip-rate, providing constraints on (a), (b) and (c). Multiple study sites will allow us to measure the spatial distribution of (a), (b) and (c). We also sample upper slopes above scarps to help constrain the scarp age and long-term slip-rate. We will test the hypothesis that the baseline controlled by (a), (b) and (c) normalised to the slip-rate field (see Faure Walker et al. this issue and Figure 1) is rough, quantifying the extent of this. We will use these quantifications to refine multi-seismic cycle earthquake probabilities with knowledge of Coulomb stress transfer from historical/palaeoseismic earthquakes. For some examples we will calibrate our ^{36}Cl measurements of elapsed time and cluster duration/intensity with knowledge of known elapsed times since historical earthquakes, like the 1915 Fucino event. However, for most locations, there are no existing measurements of elapsed time. For faults that have (1) long elapsed times, and/or (2) are behind their long-term slip-rate in the late Holocene, we will calculate if they have had their stresses raised by neighbouring earthquakes – such faults are candidates for imminent rupture if the slip deficit has not been filled by slip in the same time period on faults across strike. This will establish a proxy for a stress baseline from which

Coulomb stress increases from historical and palaeoseismic earthquakes can be viewed. At present, Coulomb stress transfer calculations assume the stress baseline is spatially smooth (e.g. Stein 2003), and our measurements will quantify the effect of this assumption, changing the way the earthquake community views and uses Coulomb stress transfer calculations.

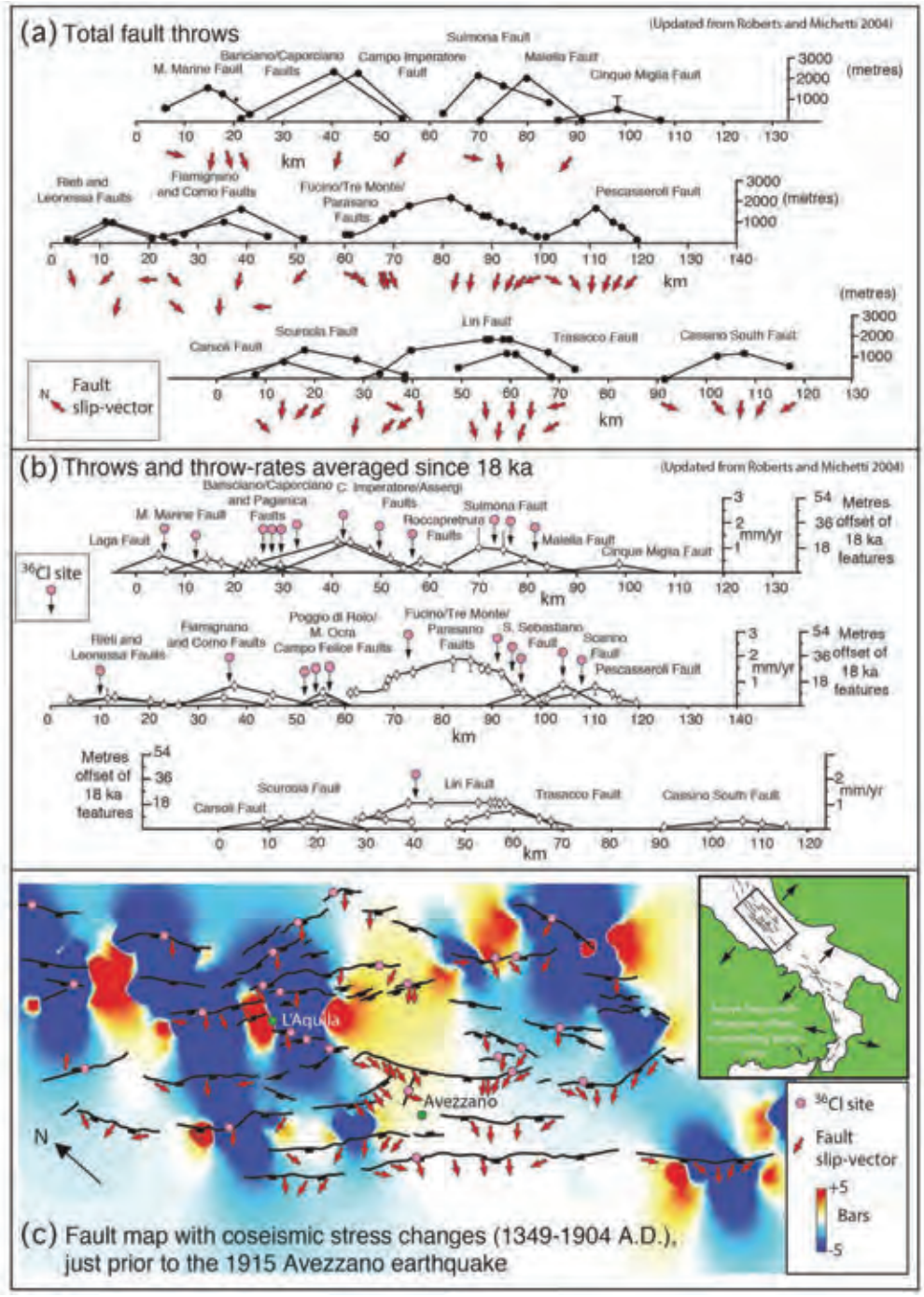

Figure 1: Overview of the structural geology (throw, throw-rate and kinematics) and earthquake-induced coseismic stress changes for active normal faults central Italy. Throws correlate with throw-rate, suggesting the latter are representative of longer time periods. Sites have been selected for ^{36}Cl in situ cosmogenic dating principally due to considerations of the geomorphology and structural geology (see McCaffrey et al. and Watson et al. this issue) so that we can be sure exhumation of fault planes form the ground is solely due to coseismic slip. Sites have also been selected to allow tests of along strike and across strike fault interaction. We assume scarps date from 18 ka in this figure, but consider a wider range (15 ±3 ka and larger in our modeling of ^{36}Cl accumulation).

RESULTS

The slip-rates on faults averaged over 15 ±3 ka from geomorphic offsets constrain strain-rates that, when summed across strike over multiple faults, correlate with topography that has developed over 2-3 Ma (Cowie et al. 2013). This suggest slip-rates over 15 ±3 ka (Figure 1) are a good measure of the multi-seismic-cycle deformation rates. We can use these as a baseline from which we can assess slip-rates measured over shorter timescales from ^{36}Cl cosmogenic dating. Our results from ^{36}Cl cosmogenic dating show that few of the faults we have measured exhibit constant slip-rates over a <15 ±3 kyrs timescale, instead exhibiting pulses of activity that we interpret as temporal earthquake clusters (see Cowie et al. this issue for the implications of this). Periods of activity last several thousand years, separated by periods of inactivity of similar duration. We have several examples where when one fault exhibits a period of activity, whilst another, across strike, has a period of inactivity. This suggests that faults share the work involved in maintaining regional, across-strike strain-rates on a <15 ± 3ka timescale. We emphasise this additional complication to the concept of elapsed time, because it is clear that slip-deficits on individual faults may only be significant when viewed in terms of the overall budget of slip summed across strike. This is because partitioning of deformation between faults across strike suggests they are interacting. Our Coulomb stress transfer work is designed to test whether simple elastic interaction can explain the partitioning of deformation. We show that cumulative interseismic loading and cumulative coseismic stress changes from all the earthquakes since 1349 A.D. can be summed to produce a regional stress map for comparison with ^{36}Cl cosmogenic results (see Wedmore et al., this issue). One interpretation, following combined analysis of Coulomb stress transfer and slip deficits/surpluses from ^{36}Cl, suggests the ruptured portion of 1915 Mw 6.9 Avezzano earthquake fault had a significant slip-deficit compared to slip expected from its 15 ±3 kyrs slip-rate. To this extent, and with hindsight, the 1915 earthquake should have been expected.

Overall, this work impacts on how we view T_{mean}, T_{elap} and α in probabilistic seismic hazard assessments that include faults as seismic sources (T_{mean} = mean earthquake recurrence interval; T_{elap} = elapsed time since the last earthquake; α = the variation in earthquake recurrence intervals compared to the mean interval; see Peruzza et al. 2010). T_{mean} can only be defined if measured over multiple seismic cycles. T_{elap} and α are important, but must be considered taking into account the existence (or not) of slip deficits/surpluses summed across strike that last for several seismic cycles due to elastic interaction between faults.

CONCLUSIONS

We suggest that a combination of knowing how slip-rates are shared across strike using ^{36}Cl cosmogenic dating and Coulomb stress transfer studies is an under-utilised approach to studying seismic hazard. We have much to learn about both techniques, but suggest that initial results are consistent with the idea that faults located along and across strike from each other share the job of maintaining regional strain-rates because they interact, with implications for how we perceive seismic hazard.

Acknowledgements: This work was supported by NERC grants: NER/S/A/2006/14042, NE/E01545X/1 and NE/I024127/1, and the IRDR at UCL. Financial support was also provided by the Statoil-University of Bergen Akademia agreement (P.A.C.).

References

Benedetti, L., R. Finkel, D. Papanastassiou, G. King, R. Armijo, F. Ryerson, D. Farber, F. Flerit, (2002). Post-glacial slip history of the Sparta fault (Greece) determined by ^{36}Cl cosmogenic dating: Evidence for non-periodic earthquakes. *Geophysical Research Letters*. 29, 8. doi: 10.1029/2001GL014510.

Benedetti, L., I. Manighetti, Y. Gaudemer, R. Finkel, J. Malavieille, K. Pou, M. Arnold, G. Aumeitre, D. Bourles, K. Keddadouche, (2013). Earthquake synchrony and clustering on Fucino faults (central Italy) as revealed from in situ ^{36}Cl exposure dating. *Journal of Geophysical Research*, *Solid Earth*. doi: 10.1002/jgrb.50299.

Cowie, P.A., G.P. Roberts, J. Bull, F. Visini, (2012). Relationships between fault geometry, slip rate variability and earthquake recurrence in extensional settings. *Geophysical Journal International*. doi: 10.1111/j.1365-246X.2012.05378.x.

Cowie, P.A., C.H. Scholz, G.P. Roberts, J.P. Faure Walker, P. Steer, (2013). Viscous roots of active seismogenic faults revealed by geologic slip rate variations. *Nature Geoscience*. 6, 1036-1040 2013. doi:10.1038/ngeo1991.

Faure Walker, J.P., G.P. Roberts, P. Sammonds, P.A. Cowie, (2010). Comparison of earthquakes strains over 10^2 and 10^4 year timescales: insights into variability in the seismic cycle in the central Apennines, Italy. *Journal of Geophysical Research*. vol.115, B10418. doi: 10.1029/2009JB006462.

Pace, B., G.M. Bocchini, P. Boncio, (2014). Do static stress changes of a moderate-magnitude earthquake significantly modify the regional seismic hazard? Hints from the L'Aquila 2009 normal-faulting earthquake (Mw 6.3, central Italy). *Terra Nova*. doi: 10.1111/ter.12117, 26, 6, 430-439.

Peruzza, L., B. Pace, F. Cavallini, (2010). Error propagation in time-dependent probability of occurrence for characteristic earthquakes in Italy. *J. Seismol*. doi: 10.1007/s10950-008-9131-1.

Roberts, G.P., A.M. Michetti, (2004). Spatial and temporal variations in growth rates along active normal fault Systems: an example from Lazio-Abruzzo, central Italy. *Journal of Structural Geology*. 26, 339-376.

Schlagenhauf, A., Y. Gaudemer, L. Benedetti, I. Manighetti, L. Palumbo, I. Schimmelpfennig, R. Finkel, K. Pou, (2010). Using in situ Chlorine-36 cosmonuclide to recover past earthquake histories on limestone normal fault scarps: a reappraisal of methodology and interpretations. *Geophysical Journal International*. 182, 36-72.

Schlagenhauf, A., I. Manighetti, L. Benedetti, Y. Gaudemer, R. Finkel, J. Malavieille, K. Pou, (2011). Earthquake Supercycles in Central Italy, Inferred from ^{36}Cl Exposure Dating. *Earth and Planetary Science Letters*. 307, 487-500.

Stein, R., (2003). Earthquake conversations. *Scientific American*. 288, No. 1, 72-79.

INQUA Focus Group on Paleoseismology and Active Tectonics

Preliminary imaging of active faults in the Montello-Collalto area (Southeastern Alps, Italy) by a high-sensitivity seismometric network

Romano, M.A. (1), Peruzza, L. (1), Priolo, E. (1), Garbin, M. (1), Picotti, V. (2), Guido, F.L. (3) and Ponza, A. (3)

(1) OGS (Istituto Nazionale di Oceanografia e di Geofisica Sperimentale), CRS (Centro Ricerche Sismologiche), Borgo Grotta Gigante, 42/C – 34010 Sgonico (TS) and Via Treviso, 55 - 33100 Cussignacco (UD), Italy. Email: aromano@inogs.it
(2) ETH Zürich, Earth Science Department, Sonneggstrasse 5, 8092 Zürich, Switzerland
(3) GEOPHI S.r.L., Via Cristoni, 80 - 40033 Casalecchio di Reno (BO), Italy

Abstract: *The Montello-Collalto (MC) area, located at the front of Southeastern Alps, is very interesting for the high convergence rates documented by geodetic measurements; geological and geophysical surveys provide evidence of active compressive structures. Historically this area has been struck by at least one event with M>6; during the last decades the seismicity has been moderate, with one M_D=4.0 earthquake, and only few events with M_D>3.*
At the end of 2011, a high-quality seismometric network has been deployed in the MC area for monitoring the seismicity potentially induced by gas storage activities in an underground natural reservoir, depleted in the 90'ies. The network allows to record background microseismicity with a completeness magnitude that reaches M_L=0.0 locally. None of the 518 events of our catalogue (January, 1st, 2012 till October, 31st, 2014) is located in proximity of the reservoir; instead the imaging at depth of the main tectonic structures can be clearly depicted.

Key words: *Montello (Italy), Collalto seismometric network, microseismicity, fault geometry imaging.*

INTRODUCTION

We do not know all the tectonic structures dissecting the Earth's crust. Active faults, especially if not outcropping, are often revealed only by the imaging of earthquakes that occur on them, sometimes clustered in space and time. During the last years, however, the analysis of the background seismicity has demonstrated to be effective in recognizing and characterizing geometry and kinematics of active faults (e.g. De Matteis et al., 2012; Romano et al., 2013). With this aim, the deployment of local high-sensitivity seismometric networks is of crucial interest, as the networks operating for seismic alarm purposes at national or continental scale are not usually adequate for detecting and locating microseismicity (M<2) with sufficient accuracy.

The high-sensitivity Collalto Seismic Network

Since the beginning of 2012, a local seismometric network named Rete Sismica di Collalto (RSC) is operating in the Montello area (Veneto region, Northeastern Italy; Fig. 1). It has been realized and is being managed by OGS on the behalf of Edison Stoccaggio S.p.A. with the aim of monitoring the natural and induced seismicity of the natural gas storage concession known as 'Collalto Stoccaggio' (Priolo et al., 2015).

The RSC consists of ten seismometric stations and one Global Navigation Satellite System permanent geodetic station with the following features:

- 1 very broad-band and high-dynamics station (ED06);
- 3 extended short-period and high-dynamics stations (ED05, ED07 and ED08);
- 5 extended short-period stations (ED02, ED03, ED04, ED09 and ED10);
- 1 extended short-period station located in a deep well (ED01).

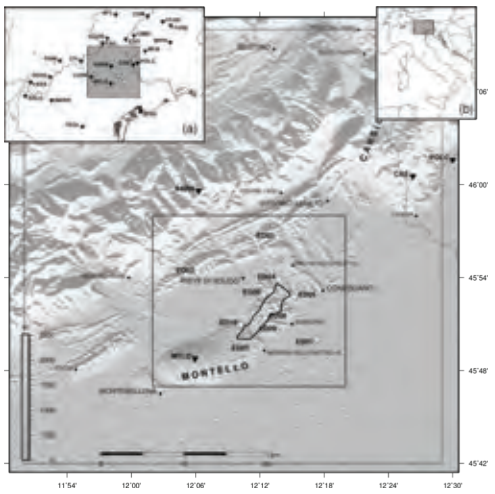

Figure 1: Location map of the study area, also at (a) regional and (b) national scales. Black and white triangles represent the stations belonging to the Northeastern Italy (NEI) Integrated Seismic Network, and those belonging to RSC, respectively. Both networks are managed by OGS. In the main panel, the solid irregular line indicates the gas storage reservoir; the thin rectangle shows the area where RSC has its maximum detection capability (hereinafter Area A). Modified by Priolo et al., 2015.

The double feature of high dynamics and high sensitivity of the instrumentation ensures high quality registrations of medium-strong earthquakes as well as micro-seismic events. Moreover, the deployment of the seismic stations with a spacing of 2-4 km above the reservoir guarantees an adequate resolution power at the reservoir depth (about 1.5 km). In order to improve the signal-to-noise ratio, all the seismological sensors are installed in boreholes with variable depth, depending on the local soil and instrument type.

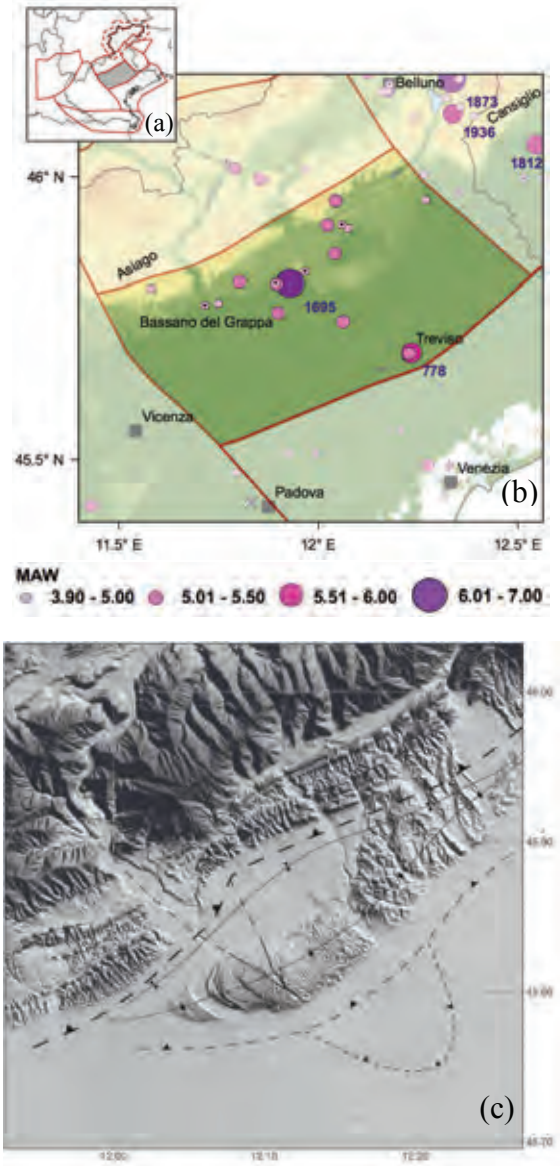

Figure 2: Historical earthquakes and preliminary structural sketch of the investigated area: (a, b) the compilation of historical seismicity data is as reported in Sugan and Peruzza (2011); they refer to the PS (Pedemontana Sud) district. The biggest symbol at the centre represents the macroseismic location of the 1695 Asolo earthquake (MW 6.5, Rovida et al., 2011). (c) main thrusts and folds identified by seismic profiles.

The study area

The MC area and surrounding regions of the Venetian piedmont are located at the outer margin of Southeastern Alps, in the so-called PS district (Sugan and Peruzza, 2011). This is characterized by a fold-and-thrust system trending ENE-WSW, verging mainly S-SE (Poli et al., 2008) and buried under alluvial deposits. The compressive deformation, started in Messinian-Pliocene age, continues today with a deformation rate of 2-3 mm/yr (e.g. Castellarin et al., 1992; Benedetti et al., 2000; Serpelloni et al., 2005). The seismogenic potential in such a district is linked to the existence of faults capable of generating earthquakes with M > 6 (Galadini et al., 2005). According to the historical seismicity catalogue (CPTI11; Rovida et al., 2011) at least one event with M>6 occurred in this area (i.e. the 1695 Asolo earthquake; Fig. 2).

The instrumental seismicity recorded by the OGS in the PS district since 1977 (http://rts.crs.inogs.it) is moderate. The biggest event has M_D=4.0, while only few events exceed magnitude 3. Some other microseismic studies based on dense temporary networks (Lovisa et al., 2008; Anselmi et al., 2011; OMBRA Project Group, 2011) have been carried on in the Montello area, but they have not yet sketched out convincing images of the hypothetical "silent" sources.

In this paper, we describe the most recent and detailed picture of the natural microseismicity obtained by analysing the data acquired by RSC from 1 January 2012 to 31 October 2014.

DATA, ANALYSIS AND DISCUSSIONS

Data collection

RSC stations acquire and transmit raw data in continuous. Signals are sampled at 200 Hz, coherently with the aim of recording microseismicity with the adopted network geometry. At the OGS acquisition centers, the data are at first converted in MiniSEED format, and then saved in two independent storage systems, i.e. OASIS (http://oasis.crs.inogs.it, which is the OGS archiving infrastructure of instrumental seismological data), and a network archive unit for further processing.

Data are processed both in real-time and off-line modes. The first one is used for displaying the signals on dedicated monitors as they are acquired, performing some basic analysis on the fly, and for sending alert messages to the seismological team; the second one performs all the final standard processing (e.g.: detection, location, and magnitude estimation) with the maximum possible sensitivity and accuracy (see Priolo et al., 2015, for details).

Off-line processing works on the integrated dataset of both RSC and NEI data. It is tuned to detect and locate very weak events, thus it is not fully automatic, and it needs the control of a seismologist. Indeed, false events are unavoidable when high sensitivity is required and their removal by visual inspection is necessary. Once true earthquakes are identified, they are manually picked and re-located in a standard way.

Standard analysis

The standard level of the RSC processing is designed in order to preserve an adequate level of coherency with that one performed by the NEI network. Therefore, the location is performed by using the same code and regional velocity model (see details in Priolo et al., 2015).

The local magnitude (M_L) of all events is estimated from the signal amplitude by using the attenuation relationship proposed by Bragato and Tento (2005), as for the NEI. In our case, however, the systematic station residuals are iteratively minimized.

The completeness magnitude (M_c) is about 0.6 if the whole dataset (from 1 January 2012 to 31 October 2014) is taken into account, and it reduces to 0.0 (Fig. 3) considering only the earthquakes belonging to the area A (Fig. 1), where the capability detection of the local network is at best. Estimates of the seismicity rate (a-value) and of the b-value for the area A, obtained with ZMAP (Wiemer, 2001), are also given in Figure 3.

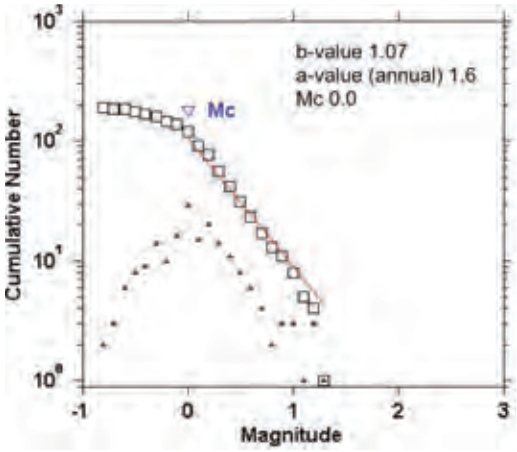

Figure 3: Magnitude–frequency distribution and completeness magnitude (Mc) for earthquakes located in area A in the period 1 January 2012-31 October 2014.

The M_c obtained from our catalogue conveys the noticeable performances of our local network, especially close to the gas storage reservoir.

DISCUSSION

From 1 January 2012 to 31 October 2014, 518 events have been located in the MC area and surrounding regions, with M_L ranging from -0.8 and 2.9; a main earthquake of M 4.6 occurred during this period falls outside the study area represented in Fig. 4. The full list of events and their location parameters are monthly released on the RSC web site (http://rete-collalto.crs.inogs.it).

In most of cases, the hypocentral depths are between 7 and 15 km, although shallower and deeper events have been located. The statistical horizontal and vertical errors exceed 3 km only in few cases, being of about 1 km outside the area A and of hundreds of meters inside it.

From the map and section represented in Fig. 4, it can be observed that seismicity is not homogeneously distributed in the space, but the seismic events located by RSC tend to align themselves along a surface, which deepens from south-east to north-west. This spatial distribution depicts a trend in accordance to the main structural features reconstructed by integrating surface geology and seismic profiles. This observation, together with the absence of seismicity within 3 km from reservoir edges, might suggest a fully tectonic origin of recorded microearthquakes; it reasonably excludes a connection between actual seismicity and the gas storage activities (Priolo et al., 2014).

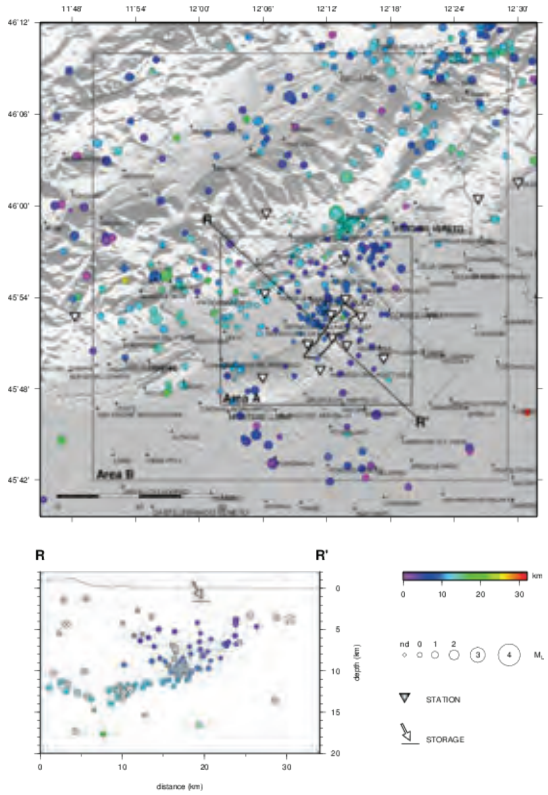

Figure 4: Map and section view of earthquakes located by RSC in the period 1 January 2012 - 31 October 2014. The thin dashed line encloses earthquakes plotted on section RR'. The horizontal and vertical bars represent the location errors. White circles with an internal cross represent events for which the horizontal or the vertical errors are larger than 3 and 5 km, respectively. (Modified by Priolo et al., 2015).

Acknowledgements: We thank Edison Stoccaggio S.p.A and all the OGS colleagues Seismological Section for their collaborative work.

References

Anselmi, M., A. Govoni, P. De Gori & C. Chiarabba, (2011). Seismicity and velocity structures along the south-Alpine thrust front of the Venetian Alps (NE-Italy). *Tectonophysics*. 513, 37-48.

Benedetti, L., P. Tapponier, G.C.P. King, B. Meyer, & I. Manighetti, (2000). Growth folding and active thrusting in the Montello

region, Veneto, northern Italy. *Journal of Geophysical Research*. 105, B1, 739-766.

Bragato, P.L., A. Tento, (2005). Local magnitude in northeastern Italy. *Bulletin of the Seismological Society of America*. 95, (2), 579-591.

Castellarin, A., L. Cantelli, A.M. Fesce, J. Mercier, V. Picotti, G.A. Pini, G. Prosser & L. Selli, (1992). Alpine compression tectonics in the Southern Alps. Relations with the N-Apennines. Ann. *Tecton*. 6, 62-94.

De Matteis, R., E. Matrullo, L. Rivera, T.A. Stabile, G. Pasquale & A. Zollo, (2012). Fault Delineation and Regional Stress Direction from the Analysis of Background Microseismicity in the southern Apennines, Italy. *Bull. Seismol. Soc. Am*. 102, (4), 1899-1907.

Galadini, F., M.E. Poli & A. Zanferrari, (2005). Seismogenic sources potentially responsible for earthquakes with M≥ 6 in the eastern Southern Alps (Thiene-Udine sector, NE Italy). *Geophys. J. Int.* 161, 739–762.

Lovisa, L., M. Garbin & L. Peruzza, (2008). Distribuzione spazio-temporale dei terremoto registrati nel Vallone Bellunese. Atti XXVII GNGTS. Sessione 2.1. 158-159.

OMBRA Project Group, (2011). OMBRA: Observing Montello Broad Activity-Deployment of a temporary seismic network to study the deformation process across Montello fault (Eastern Alps). *Rapporti Tecnici INGV*. n. 180. http://istituto.ingv.it/l-ingv/produzione-scientifica/rapporti-tecnici-ingv/rapporti-tecnici-2011.

Poli, M.E., P. Burrato, F. Galadini & A. Zanferrari, (2008). Seismogenic sources responsible for destructive earthquakes in north-eastern Italy. *Boll. Geof. Teor. Appl*. 49, 301-313.

Priolo, E., M.A. Romano, M. Romanelli, M.P. Plasencia Linares, M. Garbin, P. Bernardi, D. Zuliani, P. Fabris & L. Peruzza, (2014). *Rete di rilevamento sismico finalizzata al monitoraggio della sismicità naturale e microsismicità indotta presso la concessione di stoccaggio gas metano denominate "Collalto Stoccaggio" (TV)*. Anno di esercizio 2014 – Seconda relazione annuale. Prescr. min. di cui alla nota DVA-2013-0005150 dd. 27/03/2013. Relazione OGS n. 2014/79, Sez. CRS 26, 11 dicembre 2014. Available at http://rete-collalto.crs.inogs.it

Priolo, E., M. Romanelli, M.P. Plasencia Linares, M. Garbin, L. Peruzza, M.A. Romano, P. Marotta, P. Bernardi, L. Moratto, D. Zuliani & P. Fabris, (2015). Seismic Monitoring of an Underground Natural Gas Storage Facility: The Collalto Seismic Network. *Seism. Res. Lett*. 86,(1), 109-123.

Romano, M.A., R. de Nardis, G. Lavecchia, M. Garbin, L. Peruzza, E. Priolo, M. Romanelli & F. Ferrarini, (2013). Preliminary analysis of the microearthquakes-faults association in the Sulmona basin (central Apennines, Italy). *Rend. Online Soc. Geol. It.* 29, 150-153.

Rovida, A., R. Camassi, P. Gasperini & M. Stucchi (Editors), (2011). *CPTI11, la versione 2011 del Catalogo Parametrico dei Terremoti Italiani*. Milano. Bologna. http://emidius.mi.ingv.it/CPTI

Serpelloni, E., M. Anzidei, P. Baldi, G. Casula & A. Galvani, (2005). Crustal velocity and strain-rate fields in Italy and surrounding regions: new results from the analysis of permanent and non-permanent GPS networks. *Geophysical Journal International*. 161, (3), 861-880. doi: 10.1111/j.1365-246X.2005.02618.x.

Sugan, M., L. Peruzza, (2011). Distretti sismici del Veneto. *Boll. Geofis. Teor. Appl.* Supplement Dec 2011. s3-s90. ISSN 0006-6729. http://www2.ogs.trieste.it/bgta/.

Wiemer, S., (2001). A Software Package to Analyze Seismicity: ZMAP. *Seismol. Res. Lett*. 72, 373-382.

INQUA Focus Group on Paleoseismology and Active Tectonics

Fault displacement hazard assessment: perspectives from the siting of the Italian National Repository of Low and Intermediate Level radioactive Waste Short Lived (LILW-SL)

Roncoroni, M. (1,2), Ripamonti, L. (1,2), Ventura, G. (1), Lombardo M. (1), Rosati, M. (1), Chiaravalli, F. (1), Michetti, A.M. (2)

(1) Sogin S.p.A., via Torino 6, 00184 Roma, Italy
(2) Università degli Studi dell'Insubria, Dip. Scienza e Alta Tecnologia, via Valleggio 11, 22100 Como, Italy

Abstract: *On June 2014 the process of Italian National Repository of Low and Intermediate Level radioactive Waste siting started. The aim is to perform an ad hoc methodology for the seismotectonic characterization and fault displacement hazard assessment in Italy, one of the main issue in the maintenance of LILW-SL isolation from the biosphere for a long time scale.*

Key words: *Siting, capable fault, surface displacement.*

INTRODUCTION

Decree law 31/2010 has established roles, responsibilities and procedures for identifying the site for the facilities of disposal of LILW –SL and for temporary storage of higher activity waste in Italy. On June 2014 ISPRA (Italian nuclear safety authority) has issued Technical Guide GT n. 29 "Technical criteria for a near surface disposal facility for low and intermediate level radioactive waste", and, consequently, the process of localization of the national repository was started. The first step was the delivering by SOGIN (the Italian company for the Nuclear Installations management) to ISPRA, on January 2015, of a proposal of National Map of Potentially Suitable Areas for the localization of the LILW-SL repository, i.e. a map indicating areas, even vast, which have characteristics suitable for the localization of the LILW repository.
The Repository will be an environmental surface structure to provide final disposal of approximately 75,000 m^3 of Low and Intermediate activity waste (LILW-SL), as well as temporary safe storage of about 15,000 m^3 of higher activity waste pending the availability of a geologic repository.
This structure will be built within a Technology Park, i.e. a research center, open to international collaboration, aimed at research and development in the field of decommissioning and radioactive waste management.
Sogin has been assigned by law the task of locating, building and operating the Technology Park, that will include the National radioactive waste repository.
The siting process aims to find a site where radioactive substances isolation from the biosphere will assure until the completely decay (i.e. natural reduction) of the activity to non-harmful level for man and environment.
Assured isolation of LILW-SL for a long time scale (in order of centuries) means employing several artificial and natural barriers between waste and environment:

* the waste form itself, duly conditioned with cement;
* modules and cells qualified for a design life of 350 years;
* a final multi-layer impermeable cover over the filled cells;
* active monitoring and if needed maintenance activities (institutional control);
* the natural characteristics of the site.

Fault displacement is one of the main issue in siting process mainly because it could be a strongly limiting factor in the isolation assurance, the primary requirement of safety. An exhaustive tectonic analysis in the previous steps of the process and a detailed seismotectonic characterization and qualification of the final site are fundamental tools to address this issue.

ITALIAN LILW-SL REPOSITORY SITING PROCESS

ISPRA, in the GT n. 29, has defined "Exclusion Criteria" and "Investigation Criteria" that must be considered consistently with the level of detail of the investigation proper of each phase of siting.
On the basis of GT n. 29 and IAEA criteria, and according to decree n. 31/2010, Sogin S.p.A realized a proposal of a "national map of potentially suitable areas" (CNAPI), that will be publicly discussed before its final publication. Sogin S.p.A., in collaboration with several research institutions, acquired at national scale all relevant public data to perform the application of exclusion criteria through thematic maps concerning geology, hydrology, hydrogeology, meteorology and climate, seismology, volcanology, geomorphology, subsoil natural resources and nature and, at sub-regional scale, data concerning the cultural heritage, planning and legal constraints of the territory. In addition, studies have been developed to fill data gaps and to improve the confidence level on applying the exclusion criteria in relation to land modification due to slow and fast natural processes.

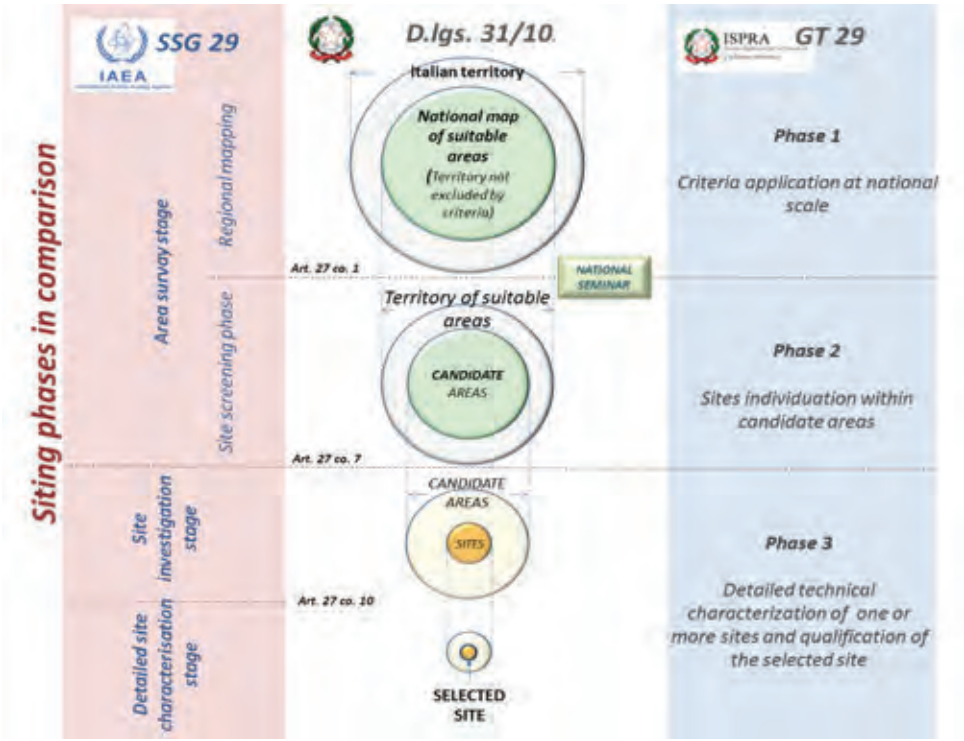

Figure 1: Schematic representation of siting process.

In the near future, in the site screening, site investigation and detailed site characterization stages of the siting process, these studies will have to be deepened in order to necessarily guarantee the suitability of the selected site (figure 1).

FAULT DISPLACEMENT RISK ASSESSMENT IN THE LILW-SL REPOSITORY SITING PROCESS

In GT n.29 fault displacement hazard is considered in the exclusion criterion "CE3" where it is stated that areas in which fault displacement was verified are unsuitable for the localization of the LILW repository. Moreover, ISPRA has indicated databases ITHACA (Italy Hazard from Capable faults) and DISS (Database of Individual Seismogenic Sources) as data sources.
Obviously, these databases are not complete, and are continuously enhanced by data from new studies. Nevertheless they were considered useful means for the uniform and complete application of criterion CE3 at national scale in the first phase of regional mapping.
Subsequent phases would be performed with increasing detail starting from site screening phase for the individuation of the more suitable sites within the areas previously identified, to the last phase of detailed site characterization.
Fault displacement assessment starts from a conceptual model of environment focused on the main issues and characteristics of the particular area considered.
This kind of model is based on the regional seismotectonic model in which all probably active and potentially capable faults are identified and characterized and the likely maximum earthquake defined for all of the seismogenic sources. Such model has to include also coseismic effects that modified or could modify the environment, like ground displacement, liquefactions, landslides, re-activation of other structures, etc., fundamental issue in the assessment of the territory vulnerability (Porfido et al., 2007).
Moreover, capable fault movements not related to seismic event or non-tectonic phenomena able to modify geomorphology, like aseismic creep, volcanic tectonic, sackung, salt tectonics (McCalpin, 2014) or underground anthropic activities will also be evaluated (figure 2).
This level of analysis strongly depends on the understanding of local geologic and tectonic setting and on the correct identification of the time window to consider, because the definition of such parameters influences every following steps in feature characterization and interpretation.
Every recognized tectonic or non-tectonic, seismogenic or non-seismogenic features should be represented by an interpretative internally consistent model that consider all geologic, structural, stratigraphic, kinematic, seismic, and other relevant data.

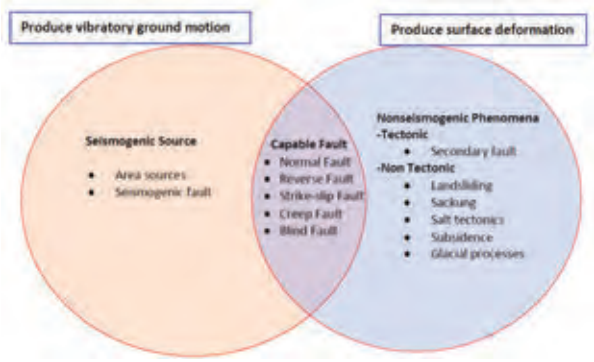

Figure 2: Relationship among seismogenic sources, capable faults and nonseismogenic or non-tectonic phenomena (modified by Hanson et al., 1999).

Developing of reliable models is fundamental for the final fault displacement hazard evaluation. Such models require also an explicit and exhaustive treatment of uncertainties; if the feature characterization process included the choice of different interpretations, all of these competing alternatives should be explicitly acknowledged and the relative degree of confidence that each alternative correctly explains the fault origins should be provided, e.g. following the logic tree building methodology.

Depending on fault origin, final hazard evaluation shall be performed in different ways (figure 3).
For example, in case of tectonic or non tectonic seismogenic faults and if no sufficient basis is available to decide conclusively that the feature is not capable, in SSG-9 (2010), IAEA suggests the use of PFDHA (Probabilistic Fault Displacement Hazard Analysis) (e.g. Youngs et al, 2003; Moss and Ross, 2011; Petersen et al., 2011, Takao et al., 2013). In this case, uncertainties treatment assumes a prominent role, above all in the choice of best fitting model of displacement attenuation based on geological context and tectonic setting (Stirling et al., 2013).

CONCLUSION

Fault displacement could be one of the main issue affecting the maintenance of LILW-SL isolation from the biosphere, both during the operative phase and after the closure of the repository and the characterization of the seismotectonic setting and its likely evolution is a needful step in the siting process. The aim is to consider the siting process of Italian LILW-SL repository as a "case study" to define and verify a procedure useful to perform a complete site specific analysis for the fault displacement hazard assessment at different scales using modern tools (i.e. to improve mapping and mesaurements) and methodologies.

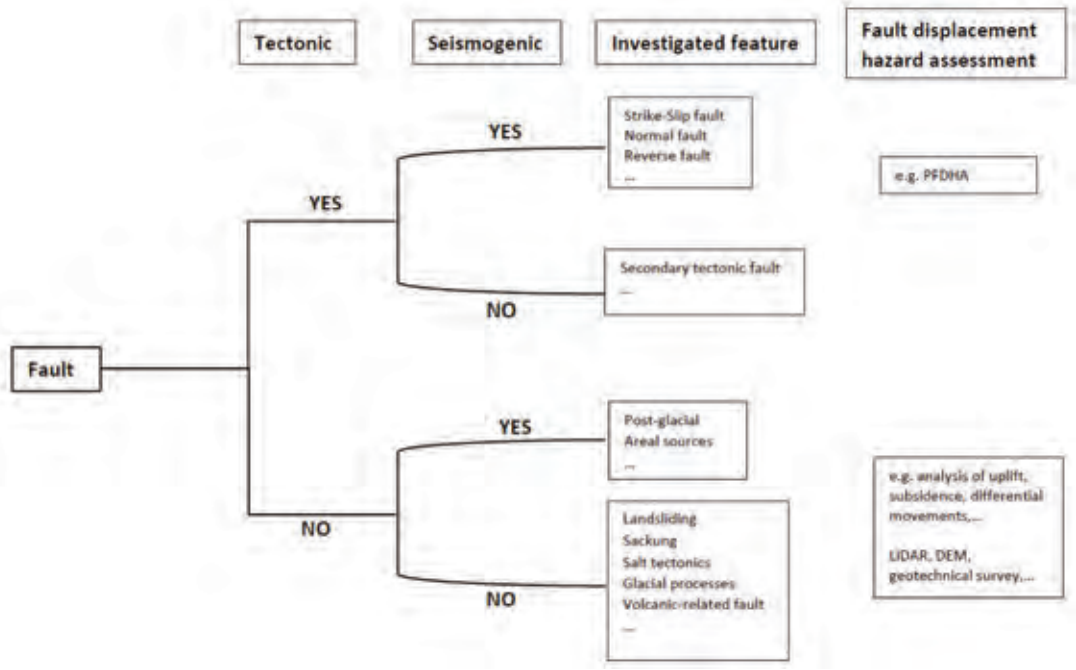

Figure 3: Synthetic fault classification and relative fault displacement hazard assessment methodology (modified by Hanson et al., 1999).

Acknowledgements: We thank the "DNPT Siting Group" for the great work done and the University of Insubria geologic research Group.

References

Hanson, K.L., K.I. Kelson, M.A. Angell and W.R. Lettis, (1999). *Techniques for identifying faults and determining their origins*. NUREG/CR-5503. U.S. Nuclear Regulatory Commission. Washington DC. 504 pp.

International Atomic Energy Agency, (2010). Seismic Hazards in Site Evaluation for Nuclear Installations. *IAEA Safety Standard Series. No. SSG-9*. Vienna.

McCalpin, J., (2014). *Surface faulting without earthquakes; sackung and salt tectonics*. 5th International INQUA Meeting on Paleosismology, Active Tectonics and Archeoseismology (PATA). 21 -27 September 2014. Busan. Korea.

Moss, R.E.S. and Z.E. Ross, (2011). Probabilistic Fault Displacement Hazard analysis for reverse faults. *Bull. Seism. Soc. Am*. 101, no. 4, 1542-1553.

Petersen, M.D., T.E. Dawson, R. Chen, T. Cao, C.J. Wills, D.P. Schwartz and A.D. Frankel, (2011). Fault Displacement Hazard for Strike-Slip Faults. *Bull. Seism. Soc. Am*. 101, no. 2 805-825.

Porfido, S., E. Esposito, G. Tranfaglia, R. Pece, L. Serva e E. Vittori, (2007). Effetti geomorfologici indotti nell'appennino meridionale dagli eventi sismici del 1805, 1930 e 1980. *Atti del 23° convegno Nazionale GNGTS.*

Stirling, M.W., T. Goded, K. Berryman and N. Litchfield, (2013). Selection of Earthquake Scaling Relationships for Seismic-Hazard Analysis. *Bull. Seismol. Soc. Am*. 103, 2993-3011.

Takao, M., J. Tsuchiyama, T. Annaka and T. Kurita, (2013). Application of Probabilistic Fault Displacement Hazard Analysis. in Japan. *Japan Association for Earthquake Engineering Proceedings.* 13, no. 1, 17-36.

Youngs, R.R., et al., (2003). A Methodology for Probabilistic Fault Displacement Hazard Analysis (PFDHA). *Earthquake Spectra*. 19, 1, 191-219.

INQUA Focus Group on Paleoseismology and Active Tectonics

The *Baelo Claudia* tsunami hypothesis - results from a multi-method sediment analysis of late-Roman deposits (Gibraltar Strait, Southern Spain)

Röth, J. (1), Mathes-Schmidt, M. (1), García Jiménez, I. (2), Rojas Pichardo, F.J. (2), Grützner, C. (3), Silva, P.G. (4), Reicherter, K. (1)

(1) Neotectonics and Natural Hazards group, RWTH Aachen University, Lochnerstr. 4-20, 52056 Aachen, Germany.
Email: joschka.roeth@rwth-aachen.de
(2) Conjunto Arqueológico de Baelo Claudia, Área de Investigación y Conservation, Ensenada de Bolonia, s/n, 11391 Tarifa (Cádiz), Spain
(3) Department of Earth Sciences, University of Cambridge, Madingley Rise, Madingley Road, CB3 0EZ Cambridge, United Kingdom
(4) Departamento de Geología, Universidad de Salamanca, Escuela Politécnica Superior de Ávila, C/Sto Tomas, s/n, 05003 Ávila, Spain

Abstract: *In order to determine the cause for the burial of the ruined Roman harbor zone of Baelo Claudia, nine vertical sediment profiles from the lower city sector (Decumanus Maximus, Bolonia Beach and Therma outside the city walls) were investigated. Using a multi-method approach, including particle size analysis by sieving and laser diffraction, magnetic susceptibility measurements and micro-paleontological examination, we found fining upward sequences, fluvial channels, chaotic sedimentary layers, intensely varying magnetic susceptibility and well preserved exotic marine micro-fauna assemblages (Ammonia sp., Cibicides sp., Elphidium sp., Globigerina sp. and Miliolida). Selective subsamples were subjected to radiocarbon dating. Based on field observations and resulting data it can be concluded that a destructive tsunami hit the littoral area in late-Roman times (ca. AD 400-450). A tsunami run-up of minimum 8 m and landward inundation of about 200 m are estimated.*

Key words: *Tsunami, Extreme Wave Event (EWE), Particle Size Analysis, Magnetic Susceptibility, Foraminifera.*

INTRODUCTION

The *Conjunto Arqueológico de Baelo Claudia* ("site of *Baelo Claudia*") is located at Bolonia Bay at the northern coast of the Gibraltar Strait right between the vicinities of Barbate and Tarifa (Figure 1). The regional geology is characterized by the Betic-Rif orogenic arc, the African-European plate boundary and the passive Southwest Iberian Margin. Offshore the Gulf of Cádiz a subduction process has been going on since the Quaternary, featuring overthrusting oceanic crust and a rather aseismic accretionary complex (Purdy, 1975; Gutscher et al., 2002).

Recent studies contributed to a remarkable database of destructive historic earthquakes and tsunami events, which affected the Gulf of Cádiz (Lario et al., 2011; Silva & Rodríguez-Pascua, 2014). However, apart from two devastating seismic events in the 1st and 3rd century (AD 40-60 and AD 260-290, MSK ≥ VIII) *Baelo Claudia* apparently has been spared (Grützner, 2011; Silva et al., 2005, 2009). Thus, tsunamigenic deposits within the site of *Baelo Claudia* were often assumed, but never confirmed. However, washover deposits of Roman age (2150-1825 cal. BP) postulated by Alonso Villalobos et al. (2003) probably link to the 1st century earthquake event (AD 40-60).

Dark cohesive sandy layers including shell debris, isolated clasts and rounded pottery parts were found along the E-W trending *Decumanus Maximus* (*DM*, main Roman trading road). These layers from the 5th to 6th century AD (García Jiménez, 2013) usually mimic the local morphology, begin with a gravelly base and are often covered by silty caps. We focused on these deposits and examined additional samples from the beach cliff and the maritime thermal complex, both located adjacent to the old roman shoreline (Bernal et al., 2013).

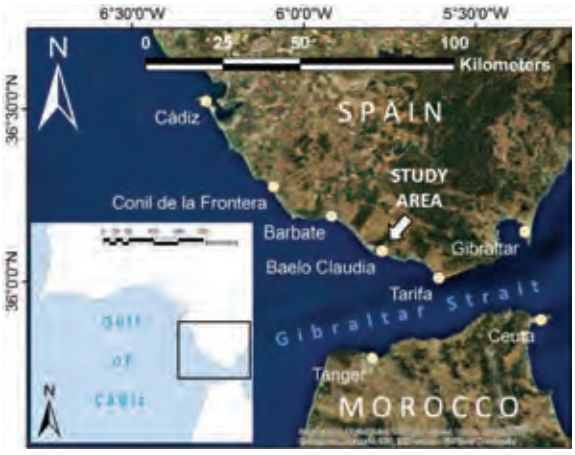

Figure 1: Geographic setting of the study area at the northern coast of the Gibraltar Strait (created with ArcGIS; copyright: 2014 ESRI, DeLorme, NAVTEQ).

METHODS

Nine vertical sediment profiles (50-140 cm) were analyzed and classified based on magnetic susceptibility (MagSus) measurements (*Bartington MS2 Magnetic Susceptibility Meter*), particle size analysis (wet sieving via *Retsch AS 200*; laser diffraction per *Beckmann Coulter LS 12 320*) and by the paleontological examination taking into account especially the micropaleontological content and in particular the Foraminifera. This multi-

method approach enables a reliable paleo-environmental reconstruction. The resulting data are partly supported by radiocarbon dating while youngest archaeological discoveries were used for the preliminary determination of age and historical significance.

OBSERVATION & RESULTS

In the following the main output of the first author's unpublished bachelor thesis (2014) is presented. Figure 2 displays the representative DMW1 sediment profile. It shows most of the features which can also be found in the other profiles. The results of the milieu interpretation after particle size analysis are shown in Figure 3 and the locations of selected sampling sites are presented within the proposed inundation map (Figure 4).

Within the site of *Baelo Claudia* a wide range of anthropogenic (Roman) objects or waste material like shell debris, pottery, construction material, animal bones, charcoal, metal and glass can be found. Incorporated metal and ceramic fragments are often responsible for medium to high values and peaks in MagSus, while lower values indicate a marine origin. Furthermore minimum values often correspond to higher amounts of marine micro-fauna, a finer matrix and poor sorting quality. The beach sand (BOLBEACH; average grain size: 300 µm), the fluvial and aeolian deposits of the beach cliff (BOL1) and single sand-rich layers within the other profiles show medium sorting quality and good permeability. However, most of the samples (DMW1 (Figure 2), DME1-DME5, DMC1, THE1c) contain dark yellowish brown, poorly sorted, silty to gravelly sand with undulating (bi- and even trimodal) grain size distribution curves, usually have corresponding low permeability, a median grain size of around 200 µm and coarsest percentiles (largest grains) commonly between 3 and 10 cm in diameter.

Chaotic sedimentary successions (high energy transportation & sudden deposition) as well as fining upward sequences and also low energy deposits (middle DMW1) were determined through particle size analysis. DMW1 exhibits continuously finer (low k) material with flat grain distribution curves and low quartile deviations.

Chaotic layers (e.g. bottom and top of DMW1) often contain well rounded pottery fragments, indicating aquatic transportation or prolonged wave erosion within the site of *Baelo Claudia*. Based on the approach of Passega (1964) the granulometric features of most of the samples indicate a tsunamigenic origin (Figure 3).

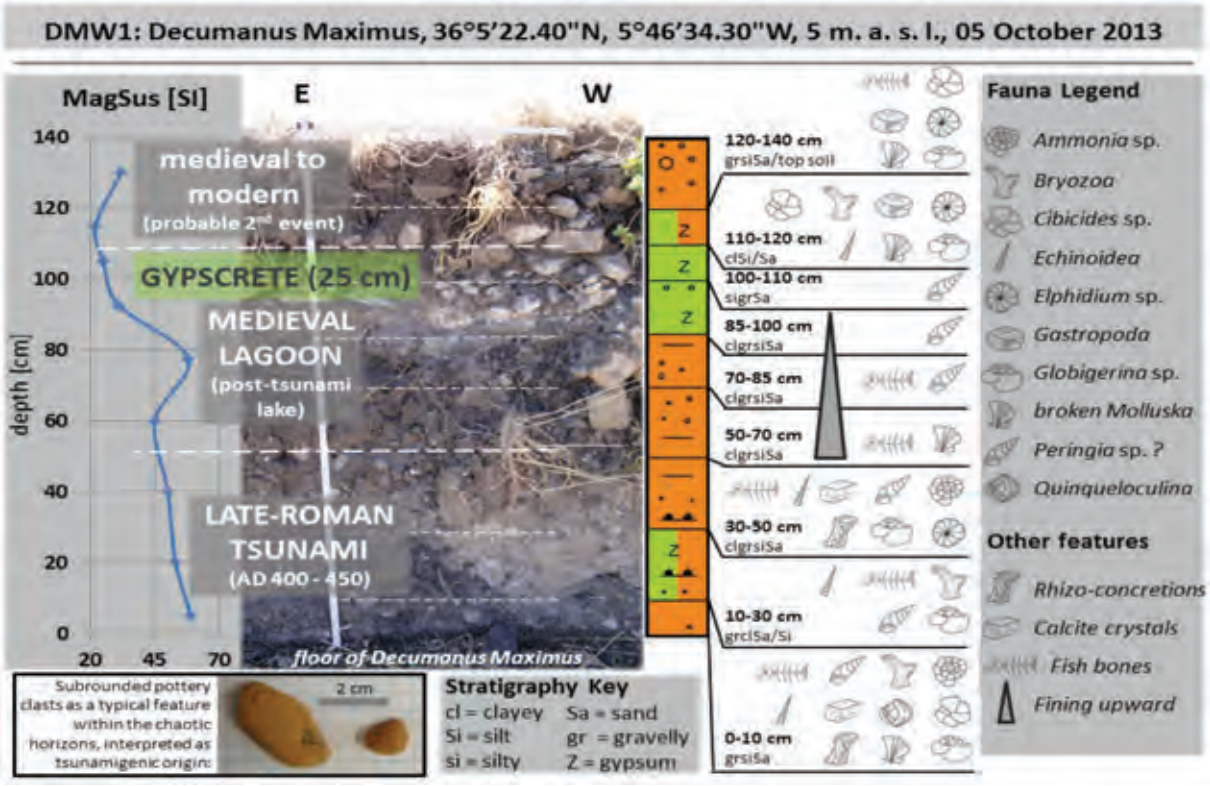

Figure 2: The DMW1 sampling site (western Decumanus Maximus) serves as an example sediment profile. While other examined profiles partly provide different results, many typical features are presented here. The probable 2nd medieval to modern event remains undetermined.

Assemblages of poorly preserved *Ammonia* sp., *Cibicides* sp., *Elphidium* sp., *Globigerina* sp., sea urchin spines (*Echinoidea*), fish bones and broken Mollusks are common throughout the whole area. While some samples do not contain much material, other single layers display a significant amount and large diversity of marine micro-fossils (middle DME2; upper DMW1). Samples from the present beach display a high diversity of poorly preserved marine micro-fauna (BOLBEACH, BOL1). Better preservation is provided by suspected energetic wave-event-like deposits (middle DME2, upper DMW1) and the lagoonal layers (middle DMW1) burying the *Decumanus Maximus*. A large amount of well to moderately preserved species can be observed in the lower part of DMW1 and throughout the DME3 profile.
High quantities of remarkably well preserved specimens of *Elphidium crispum* and *Ammonia becarii* in their original shape were found in lower DME2. Abrasion and recrystallization is relatively low and all specimens contain mud in their still open chambers, while most of the outlets are broken. These adult foraminifera were certainly buried after a short and deadly marine flooding process.

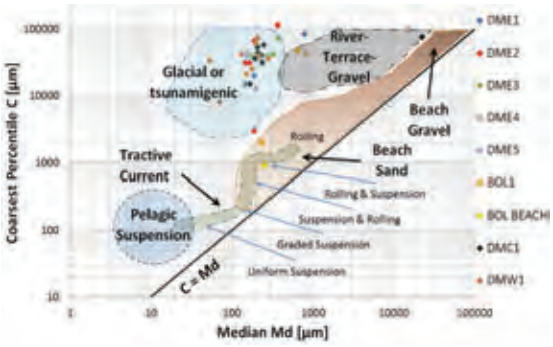

Figure 3: C-Md diagram for milieu interpretation after Passega (1964). Littoral samples are located in the beach sand field as expected. However, the majority of the samples plot in the glacial/tsunamigenic deposits field or at the transition to river terrace gravel, indicating poor sorting and sudden deposition.

Within the middle of the DMW1 profile a lagoonal to palustrine/peritidal gypscrete layer with a thickness of ca. 25 cm clearly separates the reworked post-Roman colluvium from overlying flood deposits. This most likely indicates two distinct intense flooding and reworking processes (Figure 2). Small grain size, the thickness of the gypsum and the solitary presence of *Peringia* sp. indicates a lagoonal (brackish) environment, which in turn implies a relative long time period between the deposition of the lower and the upper portion of the DMW1 profile. Within the more chaotic beds with finer matrix material and low MagSus values rhizo-concretions occur representing calcite precipitation from near surface waters. Even euhedral calcite crystals were found in these particular layers.

A first approach of layer correlation based on our observations is presented in Figure 5. The city streets perpendicular to the coast (*Cardini*) therefore served as predefined features to form back-wash channels. Lagoonal deposits in the western city sector represent the formation of a post-tsunami lake in the Early Middle Ages.
Curiously northward (upslope) dipping layers were found in the pool of the maritime thermal complex (THE1c, Figure 6). A dark, fine grained interlayer between a basal collapse horizon (column drums, large blocks) and overlying sandy layers also indicates a marine influence. Minimum MagSus values correspond to the presence of rhizo-concretions and marine micro-fossils.

CHRONOLOGICAL CONSTRAINS

While charcoal from BOL1 indicates a modern (20th century AD) fluvial outlet at the beach cliff, the charcoal from the layers in the thermal pool (THE1c) is of Roman age (>255 cal. AD)and sharply overlaps the date of the second earthquake event recorded in the city (AD 260-290; Grützner, 2011; Silva et al., 2009). Consequently the northward dipping pool deposits can be interpreted as: (a) tsunami deposits trapped in the pool incorporating material from the ruin of the city matching with the AD 260-290 event; (b) a tsunami deposit which recycled the early Roman colluvium more than 100 years after the aforementioned earthquake. This second scenario matches with the proposals of Bernal et al. (2013), who indicate that the pool fill relates to the second half of the 5th century AD, when the building was abandoned. This model also explains the occurrence of pottery fragments of the 4th century AD within the pool fill.
Indeed, the preliminary dating presented here does not allow to definitively relating the tsunami deposits with the 3rd century earthquake, but to the eventual abandonment of the Roman city in AD 395 (Silva et al., 2009). Data collected from the *Decumanus Maximus* seem to point to a similar interpretation (Figure 6). There, two apparent event levels (Figure 3) suggest the occurrence of old tsunami deposits burying the *DM* (early 5th century AD) and a younger undetermined flooding event topping the sedimentary sequence.

CONCLUSION

The output and interpretation of the combined data strongly indicates tsunamigenic sedimentation processes within the site of *Baelo Claudia*. A minimum of one tsunami event of late-Roman age (> 255 cal. AD) affected the lower city sector. This date matches with both; (a) the second earthquake recorded in the city in AD 260-290; (b) the younger age of the late numismatic evidence of the Roman occupation of the city (AD 395; Sillières, 1997). In fact the dated charcoals within the filling of the pool could be drafted (reworked) from the early post roman colluvium, resulting in a younger (maximum) age between ca. AD 400-450.

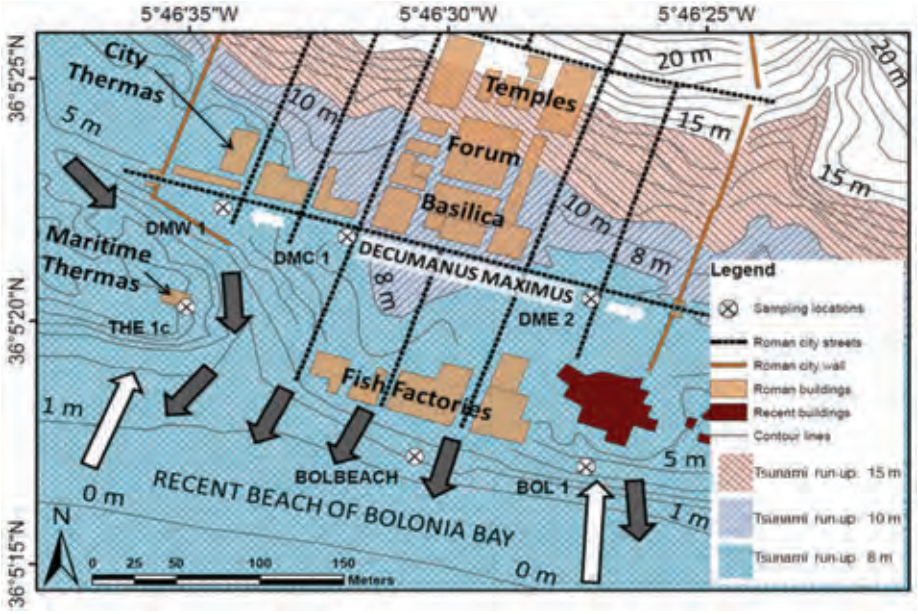

Figure 4: Map of the lower sector of Baelo Claudia. Based on the recent morphology the possible extent of three tsunami run-up heights is marked (8 m, 10 m and 15 m). Large white arrows indicate the most probable run-up direction. Dark grey arrows show the preferred orientation of possible back wash deposits and channels. Not indicated sampling sites (DME1, DME3, DME4 and DME5) are located next to DME2 on top of the eastern Decumanus Maximus.

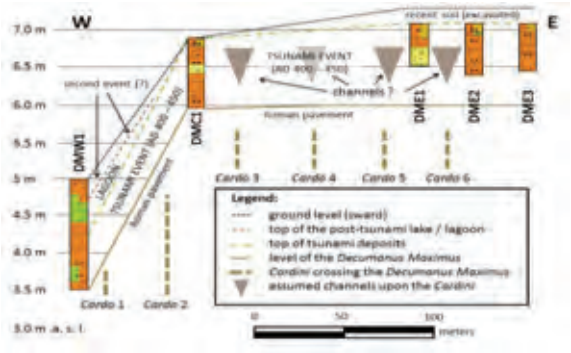

Figure 5: Approach for layer correlation with selected profiles (ca. 50x vertical exaggeration). The illustration shows the tsunami deposits on top of the Decumanus Maximus overlain by lagoonal deposits of a post-tsunami lake in the west. The Cardini are indicating preferred flow paths for possible back wash channels.

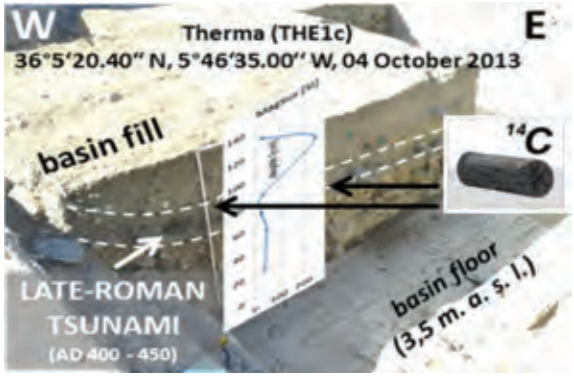

Figure 6: Pool filling of the Therma outside the city walls (THE1c) with the approximate locations where the charcoal pieces for age calibration (>255 cal. AD) were taken. While the dark, silty northward dipping layer corresponds with minimum MagSus values, low values in the basal collapse horizon and high values in the upper section were measured. Though, the Therma is believed to have been abandoned at least in the 5th century.

This event (AD 400-450) adds new data to the Holocene record of tsunamis in southern Spain and perfectly matches the catalogue of Lario et al. (2011), who listed similar and simultaneous observations at the Punta Umbria and Doñana spit-bars. Based on the level of deposition of the DME samples an energetic wave event with 8 m in height and a minimum landward inundation of 200 m are estimated, but could have been easily exceeded (Figure 4). The extreme wave event (EWE) deposits (minimum thickness: 30-60 cm) burying the *DM* and within the *Therma* are most likely of the same age and originate from the same tsunami event. This event possibly contributed to the eventual ruin of *Baelo Claudia* and may also have influenced the sudden economic downturn of the Western Roman Empire.

Lagoonal deposits of a post-tsunami lake are topped by a second event recorded at the *Decumanus Maximus* (Figure 2), which probably represents a medieval flooding horizon from either terrestrial or even marine origin.

Acknowledgements: The authors are grateful to the staff of the *Conjunto Arqueológico de Baelo Claudia*, who supported and collaborated in the research. We are also very grateful for the priceless support of Dr. Marianne Dohms (Institute for Geography of the RWTH Aachen University), Janet Rethemeyer (Cologne AMS Team, Cologne University), Benjamin Koster, Alexander Rösner, Sebastian Grohmann and Tabea Schröder. This is a contribution of the Spanish research project CGL2012-37581-C02-01 (QTECBETICA-USAL).

References

Alonso Villalobos, C., F.-J. Gracia-Prieto, L. Ménanteau, R. Ojeda-Calvo, J. Benavente-González & J.-A. Martínez del Pozo (2003). Paléogéographie de l'anse de Bolonia (Tarifa, Espagne) à l'époque romaine. *The Mediterranean World Environnement and History*, 407-417.

Bernal, D., A. Arévalo, J.A. Expósito, J. Díaz, J. Lagóstena, J.M. Vargas, M. Lara, et al. (2013). Las termas y el suburbium marítimo de Baelo Claudia, Avance de un reciente descubrimiento. *Revista Onoba*, 1, 115-152.

García Jiménez, I. (2013). *Informe Preliminar Intervención Arqueológica Puntual Decumanus Maximus Baelo Claudia*. Bolonia: Conjunto Arqueológico de Baelo Claudia, Junta de Andalucia, 199 pages.

Grützner, C. (2011). *The Baelo Claudia earthquake problem*. Doctoral thesis. RWTH Aachen University, 168 pages.

Gutscher, M.-A., J. Malod, J.-P. Rehault, I. Contrucci, F. Klingelhoefer, L. Mendes-Victor & W. Spakman (2002). Evidence for active subduction beneath Gibraltar. *Geology*, 30(12), 1071-1074.

Lario, J, C. Zazo, J.L. Goy & P.G. Silva (2011). Holocene palaeotsunami catalogue of SW Iberia. *Quaternary International*, 242(1), 196-200.

Passega, R. (1964). Grain size representation by CM patterns as geologic tool. *Journal of Sedimentological Petrology*. 34 (4), 830-847.

Purdy, G.M. (1975). The Eastern End of the Azores-Gibraltar Plate Boundary. *Geophysical Journal of the Royal Astronomical Society*, 43(3), 973-1000.

Sillières, P. (1997). *Baelo Claudia, una ciudad romana de la Bética*. Madrid: Casa de Velázquez, 240 pages.

Silva, P.G., F. Borja, C. Zazo, J.L. Goy, T. Bardají, L. De Luque, J. Lario, et al. (2005). Archaeoseismic record at the ancient Roman city of Baelo Claudia (Cádiz, south Spain). *Tectonophysics*, 408(1-4), 129-146.

Silva, P.G., K. Reicherter, C. Grützner, T. Bardají, J. Lario, J.L. Goy, C. Zazo, et al. (2009). Surface and subsurface palaeoseismic records at the ancient Roman city of Baelo Claudia and the Bolonia Bay area, Cádiz (south Spain). *Geological Society, London, Special Publications*, 316, 93-121.

Silva, P.G. & M.A. Rodríguez-Pascua (Eds.). (2014). Catálogo de los Efectos Geológicos de los Terremotos en España. *Serie Riesgos Geológicos/Geotécnia, 4*. Instituto Geológico y Minero de España (IGME), Madrid, 358 pp.

INQUA Focus Group on Paleoseismology and Active Tectonics

Paleoseismic evidence of the Vodice fault capability (Ljubljana Basin, Slovenia)

Jamšek Rupnik, P. (1), Atanackov, J. (1), Skaberne, D. (1), Jež, J. (1), Milanič, B. (1), Novak, M. (1), Lowick, S. (2), Bavec, M. (1)

(1) Geological Survey of Slovenia. Dimičeva ul. 14. SI-1000 Ljubljana, Slovenia. Email: petra.jamsek@geo-zs.si
(2) Institute of Geological Sciences, University of Bern, Baltzerstrasse 1+3. 3012, Bern, Switzerland

Abstract: *We performed a paleoseismologic study of the active Vodice reverse fault, located in the centre of the Ljubljana Basin in Slovenia to investigate its past seismic activity. Trench at location Hraše revealed tectonically tilted and coseismically offset sediment layers. Using ^{14}C and OSL dating the latest event observed in the trench was constrained to Late Pleistocene to Holocene. Our results confirm the Vodice fault being a seismic source and a capable fault.*

Key words: *Paleoseismology, reverse fault, Vodice fault, Ljubljana Basin.*

INTRODUCTION

The Vodice fault is located in the Ljubljana Basin at the transition between the Southern Alps and the Dinarides (*Figure 1*). The basin is bounded by two NW-SE-striking dextral strike-slip faults, the Sava fault to the north and the Žužemberk fault to the south, interpreted as master faults that controlled the subsidence of the Ljubljana Basin in a releasing overstep between them (Vrabec and Fodor, 2006). Smaller ~E-W oriented reverse faults that displace Quaternary sediments in the basin (Verbič, 2006) indicate a change in the deformational regime from transtensional subsidence to transpression (Jamšek Rupnik, 2013). Geological and geomorphological observations, earthquake focal mechanisms, and geodetic measurements suggest that the NW-SE-striking dextral faults and ~E-W-striking reverse faults are active in the current regional stress regime with ~N-S oriented

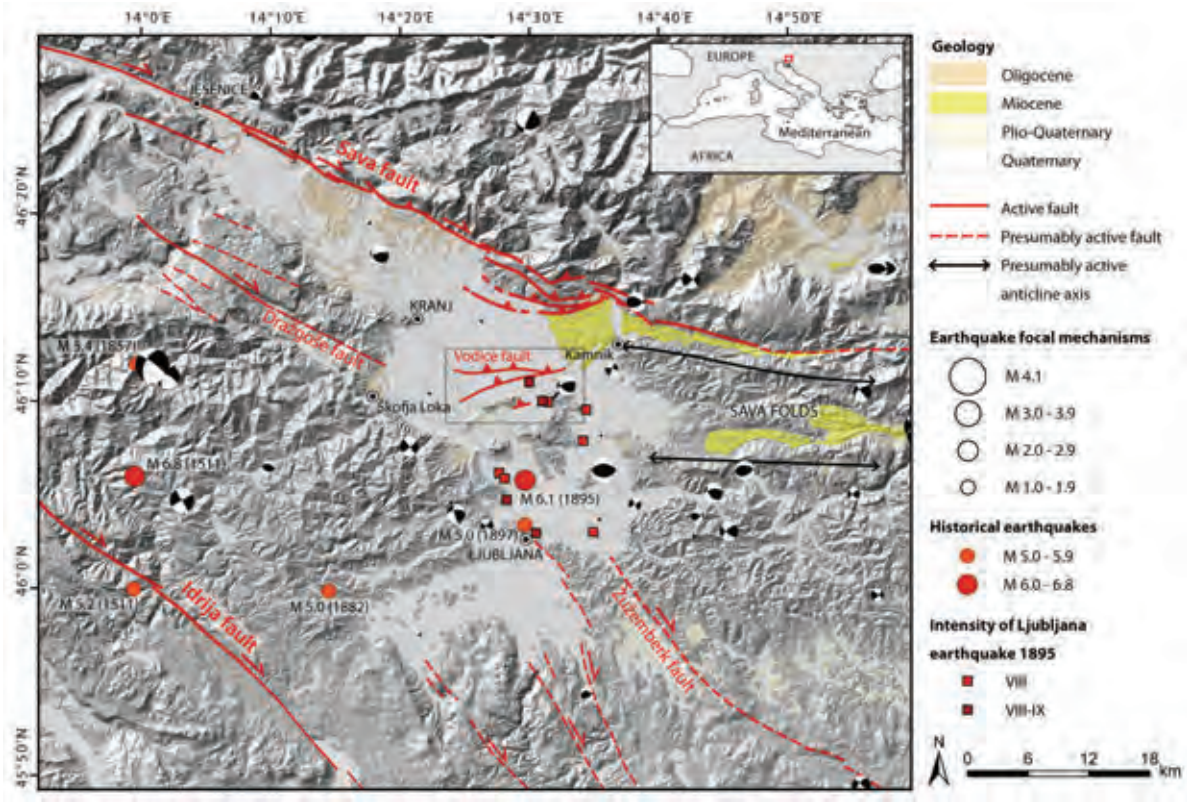

Figure 1: Seismotectonic map of the Ljubljana Basin showing main active structures (Jamšek Rupnik, 2013), Oligocene to Quaternary geological units (Buser, 2009), historical earthquake epicenters with magnitude above 5.0 (Živčić, 2009), maximum intensities of the Ljubljana 1895 M=6.1 earthquake (Ribarič, 1982; Cecić, 2011) and focal mechanisms (Ložar Stopar and Živčić, 2007, 2008, 2011, 2012; Čarman et al., 2010). Square indicates position of Figure 2.

axis of maximum horizontal compression (Poljak et al., 2000; Vrabec and Fodor, 2006; Verbič, 2006; Bavec et al., 2012; Jamšek Rupnik et al., 2012, 2013; Moulin et al., 2014).

The Ljubljana Basin is the most densely populated and a highly urbanized region of Slovenia, experiencing continuous seismic activity with earthquake magnitudes frequently reaching 3-4 (Živčić, 2009). The largest recorded event in the basin was the destructive 1895 Ljubljana earthquake with macroseismic magnitude 6.1 (Ribarič, 1982) and maximum intensities of VIII-IX EMS-98 (Cecić, 2011). The fault responsible for this earthquake is still unknown. The seismic hazard is further increased by the unconsolidated Quaternary sedimentary infill of the basin, reaching up to 280 m of thickness, which may significantly enhance site effects during earthquakes (Gosar et al., 2010).

The Vodice fault presents one of the active and possibly seismogenic reverse faults in the Ljubljana Basin (Verbič, 2006; Jamšek Rupnik et al., 2013). In the area of Vodice, 15 km north of Ljubljana, two prominent fault scarps, oriented WSW-ENE, are clearly visible (*Figure 2*). Detailed geomorphological analysis was carried out to investigate tectonic vs. erosional origin of the scarps, which together with structural observations of Quaternary sediments revealed that the scarps are the surface expression of an active emergent reverse fault, dipping 35°NNW near the surface (Jamšek Rupnik et al., 2013; Jamšek Rupnik, 2013). The slip-rate of the fault was estimated at 0.3 ± 0.2 mm a^{-1} over the last 134 ka and a theoretical seismogenic potential for an earthquake with M 5.9 to 6.5 every several thousand years (Jamšek Rupnik, 2013), which is within the range of values documented in similar tectonic settings, for example thrust faults in the Po Plain, Italy (e.g. Benedetti et al., 2000, 2003; Burrato et al., 2008). In this paper we present the results of paleoseismological investigation confirming the Vodice fault as a capable seismic source that ruptured the surface during the Late Pleistocene to Holocene.

PALEOSEISMOLOGICAL TRENCH

Two locations for paleoseismological trenches were identified on the southern, more pronounced Vodice fault scarp, both in the western part of the scarp where this is not forested or urbanized (*Figure 2*). Location Hraše was chosen after a GPR survey showed the fault in the subsurface of the fault scarp. The other location (Valburga) was chosen within the dry valley crossing the fault aiming at exposing younger sediments with the trench. Two trenches were excavated, one at location Hraše and another at location Valburga. Only the trench in Hraše was successful in revealing the Vodice fault displacements.

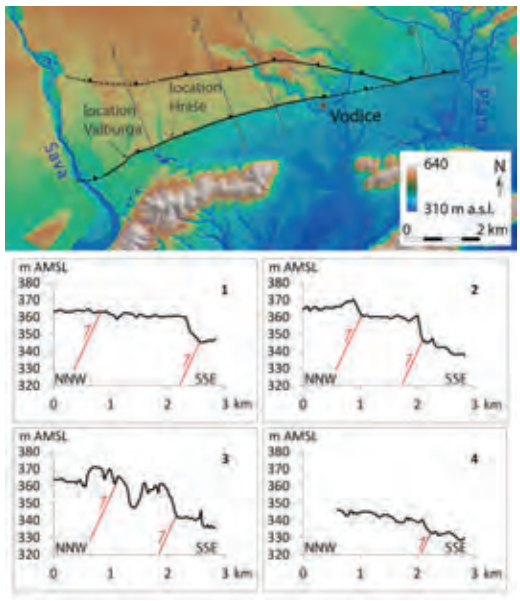

Figure 2: DEM of the Vodice area showing fault scarps and locations of two paleoseismological trenches. Profiles across the scarps derived from 5 m resolution DEM (from Jamšek Rupnik et al., 2013) are vertically exaggerated.

The trench in Hraše was 55 m long and 2-3 m deep, exposing soil horizons and mostly fine to medium grained sediments on top of karstified conglomerate (*Figure 3*). Well cemented, but shattered and karstified Pleistocene conglomerate prevailed in the upper part of the trench (N part) and prevented deeper trench excavation. Sediments on top of the conglomerate consisted mostly of gravelly mud to sandy mud, with fewer layers of muddy to sandy gravel and one layer of sand. In the lower part of the trench/fault scarp, these sediments were well layered (*Figures 3, 4*). Layers of sediments were about 0.1 to 2.0 m thick and apparently dipping 10-60°S with progressively lesser dip from N to S. Since these layers were interpreted as being deposited in a fluvial environment their observed dip suggests systematic and progressive tectonic tilting. Additionally, the succession is dissected by several joints and faults dipping 45-60°N (*Figure 4*). Displacements along faults D, E, F and G are of centimetre scale, along fault C the displacement is 50 cm and along fault B it is 130 cm. A particular phenomenon was observed in between faults E and D, where the content is a mixture of layers found on both sides of faults. For example, the thin sand layer (marked in orange, *Figure 4*) ends at the fault E but its fragments are found also within the mixture package (between E and D) as a series of scattered sand lenses continuing where the sand layer should be. We interpret this perturbation as earthquake-induced.

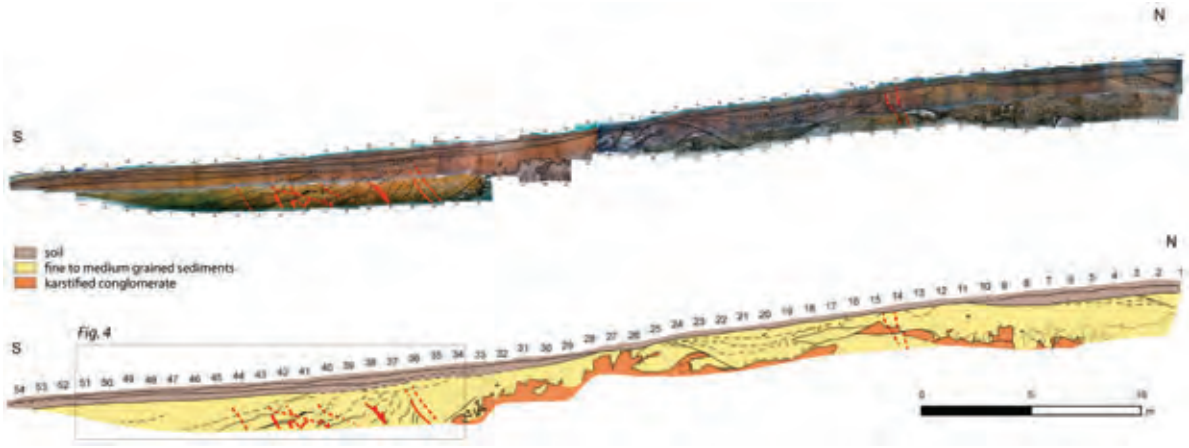

Figure 3: Photomosaic and interpretation of main stratigraphic units in the paleoseismological trench across the Vodice fault at location Hraše.

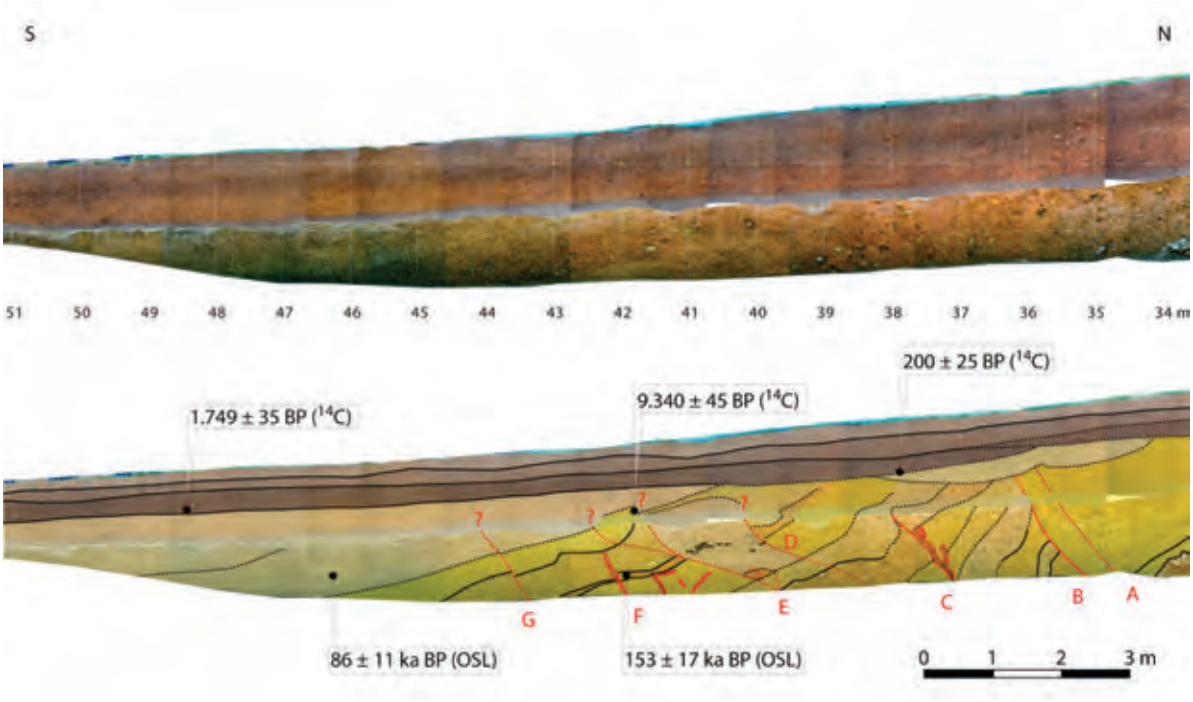

Figure 4: Photomosaic and trench log in the lower part of the Vodice fault scarp at location Hraše. Note the bench separating surficial from lower section of the trench.

The chronology in the trench was established with ^{14}C, and OSL dating (*Figure 4*). Two samples of charcoal found in the lowermost soil horizon were dated at 200 ± 25 a BP and 1.749 ± 35 a BP. Charcoal found on the upper portion of the mixture package yielded an age of 9.340 ± 45 years. Two samples were dated with OSL and IRSL using both quartz and polymineral fine grains respectively. For the sample taken from the layer that stratigraphically tops the majority of the disturbed layers (VD1/2) the quartz and polymineral ages were in very good agreement with a combined age of 86 ± 10 ka. This good agreement suggests that the polymineral signal does not suffer from significant anomalous fading. For the lowermost sample taken from disturbed sand layer, the quartz signal was considered to be in saturation. However, for the polymineral fraction, burial doses remained well below saturation of the signal and the age of 153 ± 17 ka is considered reliable.

DISCUSSION

The progressive southward tilting of sediment layers observed in the trench is in agreement with reverse faulting along the Vodice fault. Reverse offset was also observed along the faults in the trench. The offsets confirm the seismic activity of the Vodice fault and

capability to rupture the surface. The 50 cm offset could theoretically be created during a magnitude 6.4 ± 0.5 earthquake and the 130 cm offset during a magnitude 6.6 ± 0.5 earthquake (Wells and Coppersmith, 1994). The age estimations suggest the majority of tilting and faulting of older sediment layers occurred before 86 ± 11 ka BP and the latest observed faulting happened after 86 ± 11 ka BP, but not later than 1.749 ± 35 a BP. The age of the latest event is thus not well constrained. However, the presence of the 9.340 ± 45 a old charcoal within the package of mixture found in between the layers that are more than 86 ± 11 ka old may be explained by an earthquake opening the crack to capture the charcoal dated at about 9 ka PB. In this case, the age of the last event observed in the trench Hraše would be about 9 ka. Our study confirms the occurrence of past earthquakes on the Vodice fault, however, the stratigraphic record at surveyed sites did not allow for better interpretation of the fault's seismic history. Other locations with appropriate stratigraphic record will need to be considered for further investigation.

Acknowledgements: This work was funded by the Slovenian Research Agency, through the project L1–2383 Seismotectonic model of the Ljubljana Basin (cofounded by the Slovenian Environment Agency), the project J6–4016 The adaptation patterns of human activities to the environmental changes after Last Glacial Maximum in Slovenia, the programme P1 – 0011 Regional geology and the Young Researcher Grant (contract 1000-09-310068).

References

Bavec, M., T. Ambrožič, J. Atanackov, I. Cecić, B. Celarc, A. Gosar, P. Jamšek Rupnik, J. Jež, D. Kogoj, B. Koler, M. Kuhar, B. Milanič, M. Novak, P. Pavlovič Prešeren, S. Savšek, O. Sterle, B. Stopar, M. Vrabec, M. Zajc & M. Živčić, (2012). Some seismotectonic characteristics of the Ljubljana Basin, Slovenia. *Geophysical research abstracts.* 14, 9370.

Benedetti, L., P. Tapponnier, G.C.P. King, B. Meyer & I. Manighetti, (2000). Growth folding and active thrusting in the Montello region, Veneto, northern Italy. *J. Geophys. R. Solid Earth*. 105, (B1), 739-766.

Benedetti, L., P. Tapponnier, Y. Gaudemer, I. Manighetti & J. Van der Woerd, (2003). Geomorphic evidence for an emergent active thrust along the edge of the Po Plain: The Broni-Stradella fault. *J. Geophys. Res*. 108, (B5), 2238.

Burrato, P., M. E. Poli, P. Vannoli, A. Zanferrari, R. Basili & F. Galadini, (2008). Sources of M(w) 5+ earthquakes in northeastern Italy and western Slovenia: An updated view based on geological and seismological evidence. *Tectonophysics*. 453, (1-4), 157-176.

Buser, S., (2009). *Geological map of Slovenia 1:250.000.* Geological Survey of Slovenia. Ljubljana.

Cecić, I., (2011). *The macroseismic intensity dataset of the Ljubljana 1895 earthquake.* Unpublished dataset. Ministry of Agriculture and Environment, Slovenian Environment Agency, Seismology and Geology Office. Ljubljana.

Čarman, M., M. Živčić & M. Ložar Stopar, (2010). Earthquakes in the Gorenja vas region in January and February 2009. In: *Earthquakes in 2009* (Gosar, A. ed.). Ministry of Agriculture and Environment, Slovenian Environment Agency, Seismology and Geology Office, Ljubljana, 65-71.

Gosar, A., J. Rošer, B. Šket Motnikar & P. Zupančič, (2010). Microtremor study of site effects and soil-structure resonance in the city of Ljubljana (central Slovenia). *Bulletin of earthquake engineering.* 8, (3), 571-592.

Jamšek Rupnik, P., (2013). *Geomorphological evidence of active tectonics in the Ljubljana Basin: doctoral dissertation*. Ljubljana. 214 p.

Jamšek Rupnik, P., L. Benedetti, M. Bavec & M. Vrabec, (2012). Geomorphic indicators of Quaternary activity of the Sava fault between Golnik and Preddvor. *RMZ – Material and Geoenvironment.* 59,(2/3), 299-314.

Jamšek Rupnik, P., L. Benedetti, F. Preusser, M. Bavec & M. Vrabec, (2013). Geomorphic evidence of recent activity along the Vodice thrust fault in the Ljubljana Basin (Slovenia) – a preliminary study. *Annals of Geophysics*. 56, (6), S0680.

Ložar Stopar, M. & M. Živčić, (2007). Fault plane solutions of some stronger earthquakes in Slovenia in 2005. In: *Earthquakes in 2005* (Vidrih, R. ed.). Ministry of Agriculture and Environment, Slovenian Environment Agency, Seismology and Geology Office, Ljubljana, 57-62.

Ložar Stopar, M. & M. Živčić, (2008). Fault plane solutions of some stronger earthquakes in Slovenia in 2006 and 2007. In: *Earthquakes in 2007* (Vidrih, R. ed.). Ministry of Agriculture and Environment, Slovenian Environment Agency, Seismology and Geology Office, Ljubljana, 48-53.

Ložar Stopar, M. & M. Živčić, (2011). Fault plane solutions of some stronger earthquakes in Slovenia in 2008 and 2009. In: *Earthquakes in 2010* (Gosar, A. ed.). Ministry of Agriculture and Environment, Slovenian Environment Agency, Seismology and Geology Office, Ljubljana, 71-75.

Ložar Stopar, M. & M. Živčić, (2012). Fault plane solutions of some stronger earthquakes in Slovenia in 2010 and 2011. In: *Earthquakes in 2011* (Gosar, A. ed.). Ministry of Agriculture and Environment, Slovenian Environment Agency, Seismology and Geology Office, Ljubljana, 58-62.

Moulin, A., L. Benedetti, A. Gosar, P. Jamšek Rupnik, M. Rizza, D. Bourlès, J.F. Ritz, (2014). Determining the present-day kinematics of the Idrija fault (Slovenia) from airbone LiDAR topography. *Tectonophysics*. 628, 188-205.

Poljak, M., M. Živčić & P. Zupančič, (2000). The seismotectonic characteristics of Slovenia. *Pure Appl. Geophys.* 157, 37-55.

Ribarič, V., (1982). *Seismicity of Slovenia. Catalogue of earthquakes (792 A.D.-1981).* Seismological Survey of Slovenia. Ljubljana. 649 p.

Verbič, T., (2006). Quaternary-active reverse faults between Ljubljana and Kranj, central Slovenia. *Razprave IV. razreda SAZU*. 47, (2), 101-142.

Vrabec, M. & L. Fodor, (2006). Late Cenozoic tectonics of Slovenia: structural styles at the Northeastern corner of the Adriatic microplate. In: *The Adria microplate: GPS geodesy, tectonics and hazards* (Pinter, N. ed.). Springer, Dordrecht, 151-168.

Wells, D. L. & K. J. Coppersmith, (1994). New Empirical Relationships among Magnitude, Rupture Length, Rupture Width, Rupture Area, and Surface Displacement. *Bulletin of the Seismological Society of America.* 84, (4), 974-1002.

Živčić, M., (2009). *Catalogue of earthquakes in Slovenia.* Internal documentation. Ministry of Agriculture and Environment, Slovenian Environment Agency, Seismology and Geology Office. Ljubljana.

INQUA Focus Group on Paleoseismology and Active Tectonics

Qualitative evaluation of earthquake hazards for archaeological and historical sites in Israel

Salamon, A. (1), Netzer-Cohen, C. (1), Zilberman, E. (1), Amit, R. (1), Cohen, M. (2)

(1) Geological Survey, 30 Malkhe Israel, Jerusalem 95501, Israel. Email: Salamon@gsi.gov.il
(2) Israel Antiquities Authority, Conservation Department, Rockefeller Museum, POB 586, Jerusalem, 91004, Israel

Abstract: *Commonly, there are numerous vulnerable buildings in earthquake countries but limited resources for retrofitting. Thus it is essential to prioritize the highest risk ones for reinforcement. Here we focus on evaluating the earthquake related hazards for archaeological and historical heritage sites in Israel. Many of them tend to be in poor condition, hosting many visitors and hence in urgent need of anti-seismic strengthening. First we graded qualitatively the severity of the relevant hazards, namely surface rupture, peak ground acceleration and amplification, slope failure, liquefaction and tsunami. However, the outcomes did not accord with the historical experience. We then calibrated the grading because the hazards are not uniform in time and damaging potential, and this time the results appear more balanced. Our approach is also applicable for preliminary hazard evaluation of public structures such as schools etc. Nonetheless, for any engineering and physical intervention, a complementary site specific investigation is still needed to derive the proper geotechnical parameters.*

Key words: *Earthquake hazards, damage severity, qualitative evaluation.*

INTRODUCTION

Commonly, there are numerous vulnerable buildings in earthquake countries but limited budget and resources for retrofitting, and therefore there is a need to prioritize the highest risk ones for reinforcement. The risk in this case is the product of the earthquake related hazards, and the vulnerability of the given building which rests upon various aspects such as its use and function, social, moral and economical values, and of course its structural conditions.

There are many invaluable archaeological and historical sites in Israel, typically hosting numerous visitors simultaneously. Yet while Israel is vulnerable to strong shaking, the majority of these structures are in poor condition and in urgent need of anti-seismic strengthening. The Conservation Department of the Israel Antiquities Authority (IAA) initiated a project entitled 'Disaster Risk Reduction of Cultural Heritage Sites in Israel' in order to define the earthquake related hazards that threaten these heritage structures, evaluate their vulnerability and determine the risk they face (Cohen et al., 2012). Grading the level of the risk across that inventory is expected to enable the IAA to make preferences in proper retrofitting.

Here we describe the methodology used for evaluating the earthquake related hazards for the given inventory of the heritage sites. In parallel, the IAA conducted a comprehensive field work in order to describe and evaluate the vulnerability of these structures, relating to factors such as state of preservation, presence of structural elements, etc. The product of the hazard as was determined in our study (Salamon et al., 2014) with the vulnerability assessed by the IAA is expected to yield the overall risk.

METHODOLOGY

Since the original inventory consists of about 750 different structures, we concentrated on conducting qualitative evaluation. First we graded automatically, with the aid of a GIS platform, the severity of each of the listed heritage structures, in relation with the relevant earthquake hazard factors. The factors are surface rupture (see Figure 1, as a demonstrative example), peak ground acceleration (PGA) and the associated site amplification (Figure 2), dynamic slope failure, liquefaction and tsunami. During this stage we constructed for each of the hazard factors an ad-hoc scale of severity that is consisted of 4 qualitative degrees. The degrees were determined according to the classifications that were defined in the original thematic hazard maps. During the pilot stage we assigned the same scale of relative severity - 4 degrees, for each of the hazards. Figure 1 demonstrates the location of the given sites in relation with the map of 'Active' and 'Potentially active' faults in northern Israel, and Table 1 exemplifies the severity scale formulated for the PGA factor.

Severity	Relative severity	Conditions
Highest	**4**	PGA > 0.2g
High	**3**	0.2g > PGA > 0.15g
Moderate	**2**	0.15g > PGA > 0.1g
Lowest	**1**	PGA < 0.1g

Table 1: Relative severities proposed for the Peak Ground Acceleration factor.

Evaluating the preliminary results and comparing it with the historical record (Zohar et al., 2013), we realized that the overall grading methodology is biased. Sites that

have already been severely damaged several times in history (e.g. Tiberias, Bet She'an) appeared less vulnerable than others that were partially harmed only (e.g. Caesarea). WE noted that sites along the Mediterranean coast were graded high due to exposure to liquefaction and tsunami hazards, while there is little past evidence for such damage. At the same time sites closer to the Dead Sea Transform are not sensitive to liquefaction and tsunami but were actually hit again and again due to strong shaking.

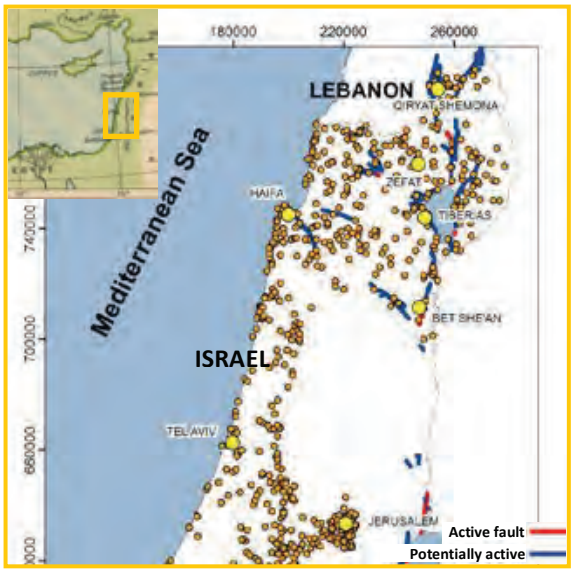

Figure 1: The inventory of heritage sites (orange dots) in northern Israel in relation with the 'Active' and 'Suspected Active' faults (after Sagy et al., 2013). The orange square on the upper left inset shows the location in respect with the Levantine region (nineteenth century historical map of the Ottoman area, modified from Miller, 1913).

We realized that this was because we used equal scales to each of the various hazards, while in fact they are not uniform. In Israel, seismic shaking is calculated for 10% probability of experiencing an earthquake of a given size or greater over a 50-year period (i.e. an event per 475 years, SI 413), while surface rupture is based mainly on an event per 13,000 years (Sagy et al., 2013). Liquefaction is based on the evaluation of the threshold geological conditions necessary for failure (Frydman et al., 2007; Salamon et al., 2008), maps of dynamic slope instability show the relative sensitivities according to the critical acceleration needed to generate failure during an earthquake (Katz and Almog, 2006; Katz et al., 2008; Katz, 2012), and tsunami hazard relates to the worst case scenarios (Salamon, 2009). Moreover, the damaging potential of each of these factors also differs: seismic shaking can destroy a building completely while surface rupture may only fracture it. Although a comprehensive evaluation has not yet been done, it appears that in Israel the seismic shaking was the dominant damaging factor in the past and then slope failure (Zohar et al., 2013). The other three were secondary and less 'effective'.

We thus reduced to a half all the relative grading of the severity scales (see the example in Table 2 in regard with surface rupture), except the grading attributed to the seismic shaking (Table 1).

Severity	Relative severity	Conditions
Highest	2	0 - 15 m from an active fault
High	1.5	0 - 15 m from a suspected active fault
Moderate	1	15 – 200 m from active or suspected active fault
Low	0.5	0 – 15 m from any other fault
Negligible	0	200 m < from any type of fault

Table 2: Relative severities of Surface Rupture after calibration.

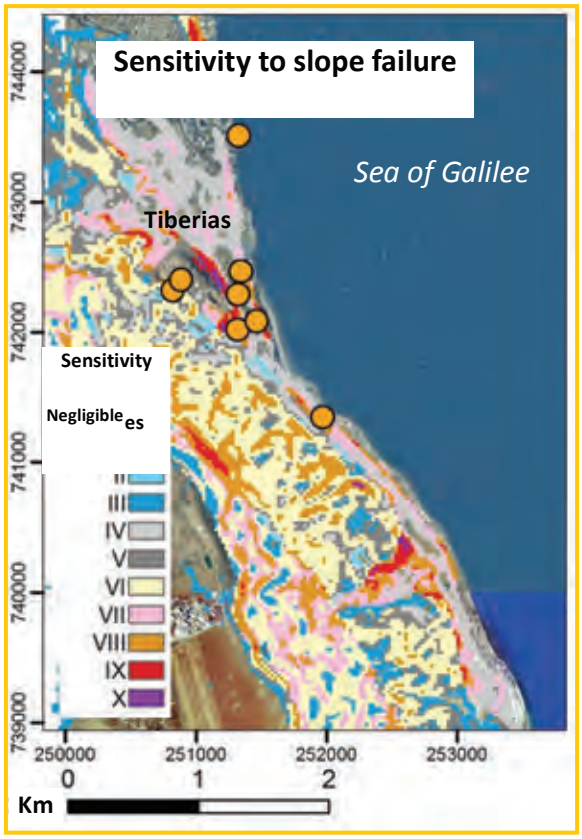

Figure 2: Location of the heritage sites in and around the city of Tiberias, along the coast of the Sea of Galilee (see location of the city in Fig. 1), in respect with the map of sensitivity to slope failure (after Katz and Almog, 2006).

In the second round we dropped about two thirds of the inventory buildings that were anyhow graded low

during the preliminary stage and concentrated on the heritage structures that were found most threatened. We then constructed a map for each one or a close group of the heritage sites and examined its exposure to the relevant hazards that threaten it. Figure 2 shows an example of that process in respect to the heritage sites in and around the city of Tiberias, northern Israel, in relation with sensitivity to slope failure. In the following stage we graded systematically the severity for each of the structures in respect with each of the relevant hazards and then summed the overall severities.

EVALUATION AND DISCUSSION

All in all, in the second stage we graded the severity of about 250 heritage structures located in about a hundred different sites (see the example of Tiberias in Figure 2). We then summed the grades and determined the overall severity of each of the structures. It was now possible to compare the results from the two stages and see that the calibration process balanced the grading and produced results that accord better with the actual historical experience (see the example in Table 3).

Site Working stage	Caesarea 1st	 2nd	Bet She'an 1st	 2nd
Surface Rupture	0	0	0	0
PGA	1	1	4	4
Amplification	3	1.5	4	2
Slope failure	0	0	0	0
Liquefaction	2	1	0	0
Tsunami	4	2	0	0
SUM	**10**	**5.5**	**8**	**6**

Table 3: Comparison between two representative sites, Caesarea along the Mediterranean coast and Bet She'an near to the Dead Sea Transform. In the 1st stage Caesarea got higher points then Bet She'an, contrary to the historical experience, but in the 2nd stage (in red) the calibration reversed the grading and balanced the picture.

Being now on a less shaky ground with the results, to use a relevant metaphor, we listed the buildings in order of severity, from the highest to the lowest. The relative grading of the severity of the heritage structures in northern Israel is presented in Fig. 3. The findings show that the sites exposed to the highest severities are located along the Jordan Rift Valley, close to the Dead Sea Transform where the peak ground accelerations and the exceptional seismic amplification are the strongest in Israel (Figure 3). High severities, though not so extreme, appear also along the Mediterranean coast which is exposed to tsunami inundation as well as liquefaction in places. The Central Galilee and the Inner Plane of Israel however, are less threatened, although seismic accelerations and ground amplifications, respectively, might still be significant.

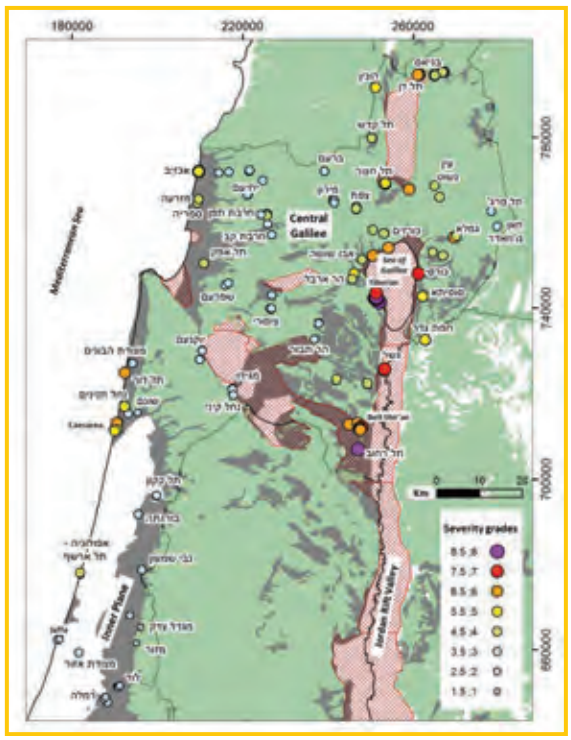

Figure 3: The overall relative severity grading of the heritage sites in northern Israel as was conducted during the 2nd stage, projected on the map of areas vulnerable to exceptional amplification. This map (after Gvirtzman and Zaslavsky, 2009) is now part of the Israeli Building Code, SI – 413.

CONCLUSIONS

The methodological approach presented here is applicable for a qualitative, preliminary earthquake hazard evaluation of any group of structures or buildings such as residential apartments, schools and infrastructure facilities, in order to prioritize retrofit and reinforcement. Evidently, the first stage of evaluation produced grading that did not reflect the historical experience and thus needed adjustment. In the second stage however, we re-graded the severity scales according to our intuitive judgment and achieved better results. Certainly, further established? calibration and fine tuning of the different severity scales is needed in order to achieve consistent and homogenized scales. Still, for any engineering and physical intervention, a site specific investigation is still needed in order to derive the proper geotechnical parameters for appropriate planning.

Acknowledgements: Thanks are due to the anonymous reviewer for constructive and focused comments. The project

was funded by the Inter-Ministerial Steering Committee for Earthquake Preparedness in Israel.

References

Cohen, M., et al., A. Salamon, R. Amit, E. Zilberman, & O. Baruch. (2012). Risk map for Culture Heritage sites in Israel, Stage A: Earthquake hazard pilot map for archaeological sites, methodology. Israel Antiquities Authority, Conservation Department. Geological Survey of Israel, Report GSI/14/2012 (in Hebrew). Submitted to the Inter-Ministerial Steering Committee for Earthquake Preparedness in Israel.

Frydman, S., A. Salamon, D. Zviely, R. Biton & O. Katz, (2007). Geotechnical assessment of the liquefaction potential in the western Zevulun Plain, Israel. *Geological Survey of Israel*, Report GSI/09/2007, and the *National Building Research Institute. Technion Israel Institute of Technology. Haifa.* Prepared for the Inter-Ministerial Steering Committee for Earthquake Preparedness in Israel (in Hebrew, English abstract).

Gvirtzman, Z. & Y. Zaslavsky, (2009). *Map of areas suspected on exceptional amplification. Explanation remarks*. GII and GSI joint report GSI/15/2009.

Katz, O., (2012). *National hazard map for earthquake induced landslides in Israel; Southern Sheet, Scale 1: 200,000*. Geological Survey of Israel. Report GSI/18/2012 (in Hebrew).

Katz, O. & E. Almog, (2006). *National hazard map for earthquake induced landslides in Israel; Northern Sheet, Scale 1: 200,000*. Geological Survey of Israel. Report GSI/38/2006 (in Hebrew).

Katz, O., H. Hecht & E. Almog, (2008). *National hazard map for earthquake induced landslides in Israel; Central Sheet, Scale 1: 200,000.* Geological Survey of Israel. Report GSI/07/2008 (in Hebrew).

Miller, W., (1913). *The Ottoman Empire, 1801-1913*. Cambridge University Press, 1913. Perry-Castañeda Library, Map Collection. The University of Texas at Austin. http://www.lib.utexas.edu/maps/historical/ottoman_empire_1801.jpg

Sagy, A., A. Sneh, M. Rosensaft, & Y. Bartov, (2013). *Map of 'Active' and 'Potentially Active' Faults that Rupture the Surface in Israel. Updates 2013 for Israel Standard 413*: *Definitions, comments and clarifications*. Report No. GSI/02/2013 (in Hebrew).

Salamon, A., (2009). *Areal maps of potential tsunami inundation along the Mediterranean coast of Israel, in Haifa Bay, the Tel-Aviv area Ashdod and Ashqelon*. Geological Survey of Israel. Report GSI/24/2009. Prepared for the Inter-Ministerial Steering Committee for Earthquake Preparedness in Israel (in Hebrew, English abstract).

Salamon, A., D. Zviely, M. Rosensaft, T. Lehmann, A. Heimann & R. Avramov, (2008). *Zones of required investigation for liquefaction hazard in the coastal plain of Israel*. Geological Survey of Israel. Report TR-GSI/34/2008. Prepared for the Inter-Ministerial Steering Committee for Earthquake Preparedness in Israel (in Hebrew, English Abstract).

Salamon, A., C., Netzer-Cohen, E., Zilberma & R. Amit, (2014). *Qualitative evaluation of earthquake hazards for archaeological and historical sites in Israel*. Prepared for the Conservation Department, Israel Antiquity Authority, Geological Survey of Israel. Report GSI/28/2014.

SI (Standards Institute) 413, (2013). *Design provisions for earthquake resistance of structures*. Amendment No. 3. The Standards Institution of Israel.

Zohar, M., A. Salamon & R. Rubin, (2013). Damage patterns of past earthquakes in Israel – Preliminary Evaluation of historical sources. *Geological Survey of Israel. Final report GSI/17/2013, contract 210-17-006.*

INQUA Focus Group on Paleoseismology and Active Tectonics

paleoseismicity.org

The May 24, 2014 North Aegean Trough earthquake: stress change and displacement patterns

Sboras, S. (1,2), Chatzipetros, A. (1), Pavlides, S. (1), Fotiou, A. (3), Pikridas, C. (3) and Bitharis, S. (3)

(1) Department of Geology, Aristotle University, 54124, Thessaloniki, Greece. Email: ac@geo.auth.gr and pavlides@geo.auth.gr
(2) Institute of Geology and Mineral Exploration, 13677, Athens, Greece
(3) Department of Rural and Surveying Engineering, 54124, Thessaloniki, Greece

Abstract: *The May 24, 2014 North Aegean earthquake was caused by the activation of a segment of North Aegean Trough, the western extension of the North Anatolian Fault Zone. Based on the physical properties of the main shock and the corresponding focal mechanism, a stress change analysis has been performed using the best fit fault model for this case. Several neighbouring active faults have been taken into account and stress change has been examined for all of them. Furthermore, a comparison between modelled surface displacements and the actual ones, as recorded by GPS stations in the broader area, showed an adequately good correlation. GPS time series show a quasi-elastic behaviour of the upper crust, as the deformation evolved for two days after the earthquake.*

Key words: *Coulomb stress change, coseismic deformation, fault modelling, GPS.*

INTRODUCTION

The May 24, 2014 event occurred at 09:25:03 (UTC) in the offshore area between the islands of Lemnos and Samothrace (Figure 1) and caused light damages and injuries in the surrounding area; however, damages and injuries were more intense and spread in Turkey. The magnitude varies from M_W6.3 (AUTh) up to M_W6.9, which was suggested by the majority of institutes.

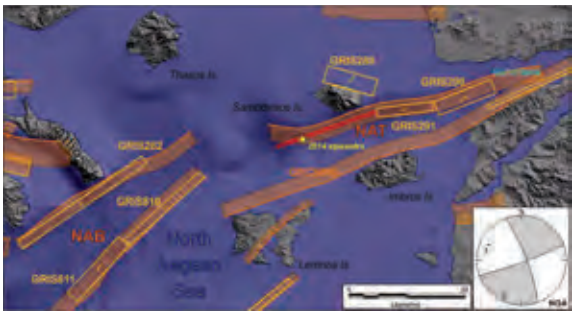

Figure 1: The main active tectonic structures in the North Aegean Sea taken from GreDaSS (yellow and orange coloured are ISSs and CSSs, respectively). The red ISS-type fault is responsible for the May 24, 2014 earthquake (epicentre marked by a yellow star).

The recent evolution of the northern Aegean is characterised by the westward motion of the Anatolian plate along the North Anatolian Fault (e.g. Jolivet, 2001) which in turn pushes the Aegean plate southwards (e.g. McKenzie, 1978). The North Aegean Sea is dominated by two major tectonic structures: the North Aegean Trough (NAT), which is considered as the continuation of the North Anatolian Fault (NAF), and the North Aegean Basin (NAB). These structures are mainly dextral ones, accompanied by large normal faults, indicating a transtensional geotectonic regime (Pavlides & Caputo, 1994). NAT consists of two large, roughly parallel and opposite fault zones that cross and affect the sea-floor of the eastern part of the North Aegean Sea (Caputo *et al.*, 2013), while NAB is directly connected with the NAT, although there is a slight geometric, behavioural and morphological change that can be observed N-NNW from Lemnos Island. The main active tectonic structures in the study area are described by Chatzipetros et al. (2013) and can be found in the Greek Database of Seismogenic Sources (GreDaSS; Figure 1; Caputo et al., 2013). The main types of seismogenic sources included in GreDaSS are (according to Basili et al. 2008, and Sboras 2012):

- Individual Seismogenic Sources (ISS): they are obtained from geological and geophysical data and are characterized by a full set of geometric (strike, dip, length, width and depth), kinematic (rake, average displacement per event) and seismological (magnitude, slip rate, return period) parameters. ISSs are assumed to exhibit "characteristic" behaviour with respect to rupture length/width and expected mean and maximum magnitude. The ISSs favour accuracy of the information supplied over the completeness of the sources themselves. As such, they can be used for deterministic assessment of seismic hazard.
- Composite Seismogenic Sources (CSS): they are obtained from geological and geophysical data and characterized by geometric (strike, dip, width, min/max depth) and kinematic (rake) parameters, but their sliding surface geometry is more loosely defined. CSSs can represent large fault zones which can contain an unspecified number of ISSs. They are not assumed to be capable of a characteristic earthquake but their potential can derive from existing earthquake catalogues or other geological considerations. A CSS is essentially inferred on the

basis of regional surface and subsurface geological data that are exploited well beyond the simple identification of active faults or youthful tectonic features. Opposite to the ISSs, this category of sources favours completeness of the record of potential earthquake sources over accuracy of source description. CSSs can be used for regional probabilistic Seismic Hazard Assessment and for investigating large-scale geodynamic processes.

The aftershock horizontal distribution, according to NOA, lies along a WSW-ENE-trending axis and can be divided into three clusters: one located near to the epicentre of the mainshock and two others that are bilaterally distanced along the WSW-ENE axis, immediately south of the Athos peninsula and inside the Gulf of Saros respectively. This pattern implies stress accumulation bilaterally from the two tips of the causative fault. The depth range of the aftershock distribution shows that seismicity was concentrated at the first ca. 16 km of the crust for the central and eastern clusters and 20 km respectively for the western cluster.

The N. Aegean Sea shows a characteristic bathymetric relief due to the multitude and variety of faults (Koukouvelas & Aydin, 2002; Papanikolaou et al., 2002) and it exhibits a rich historical and instrumental seismicity, in both terms of frequency and magnitudes. Nevertheless, historical events are hard to be associated with specific faults due to the large errors in the epicentral locations, especially of the offshore earthquakes, and the large number of active faults that exist in the broader area. Moreover, the recent earthquake showed that rupture directivity diversely affected urban areas situated on both extensions of the fault tips, a fact that could give wrong estimations on macroseismic epicentres. Thus, few are the reliable events that can be directly associated with specific faults. These, according to GreDaSS, are:

1. The "Saros Gulf" ISS (GRIS290), associated with the March 27, 1975 (M_W6.6) earthquake.
2. The "Samothrace SE" ISS (GRIS291), associated with the July 6, 2003 (M_W5.7) earthquake sequence.
3. The "North Samothrace" ISS (GRIS288), associated with the February 9, 1893 (M_W6.8) earthquake.
4. The "NAB segment A" ISS (GRIS810), associated with the August 6, 1983 (M_W6.6) earthquake.
5. The "NAB segment B" ISS (GRIS811), associated with the January 18, 1982 (M_W6.6) earthquake, and
6. The "Athos" ISS (GRIS282), associated with the November 8, 1905 (M7.5) earthquake.
7. The western part of the "South NAT" CSS (GRCS800), not associated with any specific event.

Coulomb static stress change

In the present work we study the fault interaction after the May 24, 2014 earthquake in the North Aegean Sea, using the Coulomb failure criterion: $\Delta C_{ff} = \Delta\tau_s + \mu'\Delta\sigma_n$, where $[\Delta\tau_s]$ is the shear stress change on the failure plane, $[\mu']$ is the friction coefficient and $[\Delta\sigma_n]$ is the normal stress change. In order to visualize the areas where stress is increased or decreased for the types of faulting in the study area, we used the Coulomb v3.3 application (Toda et al., 2005) which resolves the shear and normal components of the stress change on a grid or on specified 'receiver' fault planes, of a homogeneous, elastic and isotropic half-space. For this reason, we used the focal parameters of NOA (strike = 70°, dip = 85°, rake = -167°, depth = 14 km, M_0 = 1.693E+19 Nm) and a fault plane with the following dimensions (according to the focal depth and the depth range of the aftershocks distribution): 45 km length and 12 km width, minimum depth of 3 km and maximum depth of 15 km. respectively and we calculated the stress change for each fault in the surrounding area at the depth of 12 km.

The results (Figure 2) show that the remotest faults, GRIS290, GRIS810, GRIS811 and GRIS282, are not affected by the May 24, 2014 rupture. The adjacent "Samothrace SE" ISS (GRIS291) shows stress rise, while the "North Samothrace" ISS (GRIS288) to the north and the western part of the "South NAT" CSS (GRCS800) to the south are located in the stress drop areas. This is probably the reason why the aftershock distribution was constrained along the 2014 fault's strike axis.

Displacement pattern

The displacement pattern of the May 24, 2014 earthquake at zero depth (surface) is also modelled using the Coulomb v3.3 application (Toda et al., 2005), which is based on the Okada (1992) dislocation solution formulae (Figure 3). As a source fault we used the same fault model of the Coulomb stress change calculations.

The most significant displacements are observed on the three surrounding islands (Samothrace, Imbros and Lemnos). In fact, the horizontal displacement pattern (FIG) indicates that the highest displacement took place on Samothrace Is. (ca. 0.18 m towards NE). Imbros Is. exhibits ca. 0.08 m displacement in a WNW direction and Lemnos Is. shows a much lower displacement in a SSW direction. Accordingly, uplift is observed on Samothrace Is., whereas subsidence is observed on Imbros and Lemnos Islands.

The May 24, 2014 rupture was recorded by GPS stations in the surrounding area. The horizontal and vertical components of the recordings are compared with the modelled displacement pattern, resolved into its horizontal and vertical components at each GPS station. Preliminary results show that there is a quite good agreement between the modelled and the actual rupture components (Table 1).

The highest displacements have been recorded in Samothrace, Lemnos and Alexandroupolis, as expected from the nature and location of the causative fault. Dextral displacement was prominent, while vertical offset was low, indicating a strike-slip fault with small normal component. The effect of the earthquake on remote stations was negligible and below the error threshold, therefore the respective measurements were not taken into account.

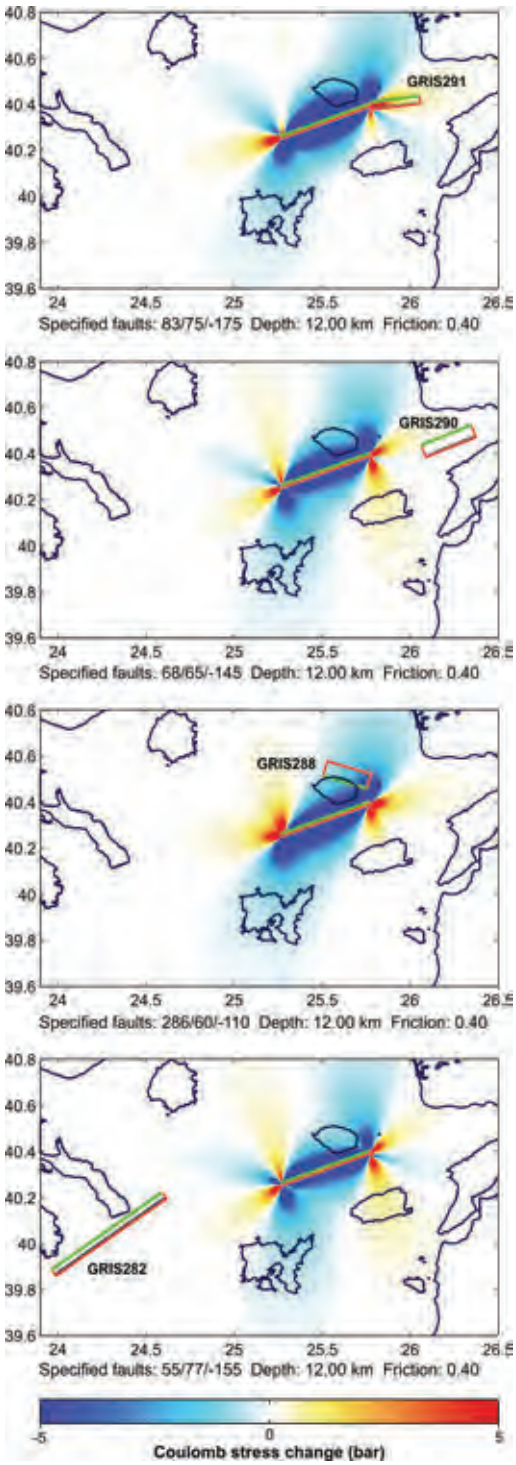

Figure 2: Coulomb stress changes after the May 24, 2014 earthquake calculated each time for different faults.

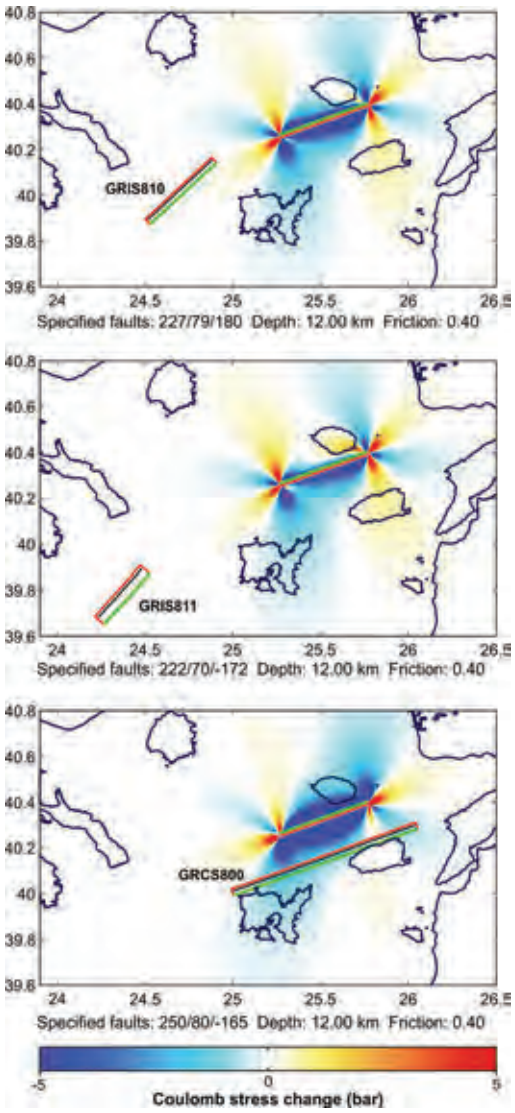

Figure 2 (continued).

The data presented in Table 1 are the final displacements, after taking into account readings from various stations, and their comparison to the modelled ones. However, based on the time series of the closest GPS stations, it seems that the displacement was not instantaneous during the earthquake, but it was stabilized after approximately two days. This gradual evolution of the deformation can result from a combination of the physical properties of the upper crust and a triggered creep on secondary conjugate strike-slip faults. The observed deformations in stations located far from the epicentre have to be attributed to random causes and are not been taken into account.

INQUA Focus Group on Paleoseismology and Active Tectonics

Location	Long	Lat	E	E'	N	N'	U	U'
Nicosia (CY)	33.396	35.141	-0.12	-0.01	0.05	0.01	-0.15	0.00
Ankara (TR)	32.758	39.887	0.10	-0.02	0.02	0.01	-0.26	0.01
Gebze (TR)	29.451	40.787	0.06	-0.05	-0.06	0.03	0.00	0.01
Maslak (TR)	29.019	41.104	0.07	-0.03	-0.16	0.04	0.07	0.01
Sofiko (GR)	26.546	41.414	0.22	0.24	0.47	0.47	0.16	-0.14
Lesvos (GR)	26.265	39.246	-0.23	-0.26	0.02	0.03	0.09	0.04
Chios (GR)	26.127	38.368	-0.03	-0.07	-0.09	-0.08	-0.32	-0.02
Bucharest (RO)	26.126	44.464	0.43	0.02	0.30	0.04	0.39	-0.02
Alexandroupolis (GR)	25.853	40.849	1.20	1.15	1.84	2.74	-0.20	-0.39
Samothrace (GR)	25.524	40.474	8.71	8.22	3.50	8.27	1.53	1.97
Komotini (GR)	25.406	41.120	0.82	0.35	0.31	0.74	0.89	-0.12
Lemnos (GR)	25.181	39.897	-2.01	-1.56	-4.77	-3.26	-0.66	-0.42
Kavala (GR)	24.387	40.934	0.52	0.65	0.11	-0.33	-1.04	0.20
Chania (GR)	24.071	35.533	0.05	-0.01	0.08	-0.03	0.18	-0.01
Stratoni (GR)	23.791	40.520	0.34	0.42	-0.33	-0.16	0.60	0.13
Sofia (BG)	23.395	42.556	-0.06	0.07	-0.13	-0.02	0.39	0.02
Thessaloniki (GR)	23.004	40.567	0.30	0.19	-0.01	-0.08	-0.98	0.07
Ohrid (FYROM)	20.794	41.127	0.25	0.06	-0.11	-0.02	-0.05	0.02
ASI (IT)	16.704	40.649	0.02	0.01	0.06	-0.01	0.21	0.01
Graz (AT)	15.493	47.067	-0.05	0.01	0.01	0.00	-0.12	0.00
Sicily (IT)	14.990	36.876	-0.06	0.00	-0.07	0.00	0.03	0.00

Table 1. Summary comparative table of GPS data recorded in stations located in the broader area and modelled displacements (E-N-U and E'-N'-U' respectively).Values are in cm, rounded to the second decimal digit. The location of Lemnos and Samothraki Islands are shown in Figure 1.

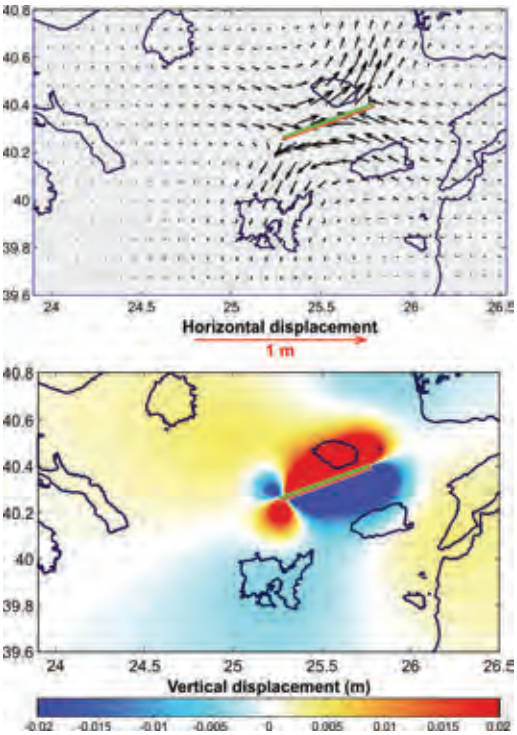

Figure 3. The horizontal (up) and vertical (down) displacements, as modelled using the Okada (1992) formulae.

Acknowledgements: AC has been partly supported by the project "Characterization of site conditions in Greece for realistic seismic ground motion simulations: pilot application in urban areas", a THALES programme project, funded by the General Secretariat for Research and Technology of Greece. SS would like to thank the Research Committee of AUTh for the 1-year postdoctoral fellowship (2013-2014) under of which part of this work was carried out. Finally, the authors would like to thank SmartNet, NOANET and HEPOS networks for providing GPS data used in this paper.

References

Basili, R., Valensise, G., Vannoli, P., Burrato, P., Fracassi, U., Mariano, S., Tiberti, M.M., Boschi, E. (2008). The database of individual seismogenic sources (DISS), version 3: summarizing 20 years of research on Italy's Earthquake Geology. Tectonophysics, 453(1-4), 20-43.

Caputo, R., A. Chatzipetros, S. Pavlides & S. Sboras, (2013). The Greek Database of Seismogenic Sources (GreDaSS): state-of-the-art for northern Greece. *Ann. Geophys.*, 55, (5), 859-894.

Chatzipetros, A., A. Kiratzi, S. Sboras, N. Zouros & S. Pavlides (2013). Active faulting in the north-eastern Aegean Sea Islands. *Tectonphysics,* 591-598, 106-122.

Jolivet, L., (2001). A comparison of geodetic and finite strain in the Aegean, geodynamic implications. *Earth Planetary Science Letters.* 187, 95-104.

Koukouvelas, I.K. & A. Aydin (2002). Fault structure and related basins of the North Aegean Sea and its surroundings. *Tectonics,* 21, 10.1-10.17.

McKenzie, D., (1978). Active tectonics of the Alpine-Himalayan belt: the Aegean Sea and surrounding regions. *Geophys. J. R. Astr. Soc.*, 55, 217-254.

Okada, Y., (1992). Internal deformation due to shear and tensile faults in a half-space. *Bull. Seismol. Soc. Am.*, 82, (2), 1018-1040.

Papanikolaou, D., M. Alexandri, P. Nomikou & D. Ballas (2002). Morphotectonic structure of the western part of the North Aegean Basin based on swath bathymetry. *Marine Geology,* 190, 465-492.

Pavlides, S. & R. Caputo (1994). The North Aegean region: a tectonic paradox? *Terra Nova,* 6, 37-44.

Sboras, S. (2012). The Greek Database of Seismogenic Sources: seismotectonic implications for North Greece. PhD thesis, University of Ferrara, Ferrara, Italy, 252 pp.

Toda, S., R. S. Stein, K. Richards-Dinger & S. Bozkurt, (2005). Forecasting the evolution of seismicity in southern California: Animations built on earthquake stress transfer. *J. Geophys. Res.*, 110, B05S16.

INQUA Focus Group on Paleoseismology and Active Tectonics

Innovative trenching investigations on active normal faults: A combination of experience, remote sensing applications and geophysics

Schneiderwind, S. (1), Mason, J. (1), Wiatr, T. (1), Grützner, C. (2), Pallikarakis, A. (3), Reicherter, K. (1)

(1) RWTH Aachen University, Institute of Neotectonics and Natural Hazards, Lochnerstr. 4-20, 52064 Aachen, Germany. Email: s.schneiderwind@nug.rwth-aachen.de
(2) Dept. of Earth Sciences, University of Cambridge, Madingley Rise, Madingley Road, CB 3 0EZ Cambridge, UK
(3) Laboratory Mineralogy – Geology, Agricultural University of Athens, Iera Odos 75, Athina 118 55, Greece

Abstract: *The majority of normal faults on Crete comprise Mesozoic carbonate bedrock fault scarps juxtaposed against Quaternary alluvial-colluvial sediments. An outcrop at the west dipping Sfaka fault in the east of the island was studied by combining classical paleoseismic trenching techniques and multispectral approaches. A conventional trench log was compared to results of iso cluster analyses of both a true color photomosaic representing the spectrum of visible light and a near-infrared backscatter signal image from t-LiDAR measurements. The disadvantages of passive data collection (e.g. illumination) were thus negated by complementing the dataset with active t-LiDAR measurements. The multispectral analysis of distinct layers corresponds well with the experience-based conventional trench logging. Based on this, a 3D-interpretation of GPR data collected on the vertical trench wall was possible. This allows layer thicknesses and subsurface geometries to be estimated.*

Key words: *Paleoseismology, Normal Faulting, Trenching, GPR, t-LiDAR.*

INTRODUCTION

Paleoseismological studies often aim to identify earthquake recurrence intervals and maximum credible magnitudes of prehistoric earthquakes (McCalpin, 2009), as these are input parameters for estimating the seismic hazard potential of active fault zones (Michetti et al., 2005; Reicherter et al., 2009). The Mediterranean is a tectonically active region where normal faulting has led to the development of bedrock fault scarps which mainly consist of Mesozoic carbonates. The post-glacial stable climatic conditions with erosion rates lower than slip rates allow these scarps to be preserved in the landscape, and the hanging-wall sediments may have record primary and secondary ground effects of past earthquakes (Benedetti et al., 2002; Papanikolaou et al., 2005; Reicherter et al., 2011). Modern investigation techniques include fault scarp dating (e.g. Benedetti et al., 2002, 2003; Carcaillet et al., 2008), t-LiDAR (terrestrial Light Detection and Ranging) applications (e.g. Wilkinson et al., 2010; Wiatr et al., 2013, 2015; Bubeck et al., 2014), and techniques that focus on the hanging-wall deposits of bedrock normal faults like paleoseismic trenching (e.g. Galli et al., 2008; Grützner et al., 2010). Paleoseismic trenching is often accompanied by geophysical prospection surveys prior to the trenching phase to identify optimum locations (e.g. Demanet et al., 2001; Alasset and Meghraoui, 2005; Grützner et al., 2012); many studies have shown that earthquake related sedimentary structures can be identified in the shallow subsurface with geophysics (e.g. Chow et al., 2001; Reiss et al., 2003; Bubeck et al., 2014).
In this study we show that t-LiDAR is not limited to morphological approaches on the surface, and high-resolution 3D subsurface models from ground-penetrating radar (GPR) help to make experience-based trenching investigations more objective.

STUDY SITE

The island of Crete (southern Greece) comprises normal bedrock fault scarps juxtaposed against Quaternary alluvial-colluvial or marine sediments (Fig. 1). Features such as colluvial wedges (a consequence of degradation of the scarp), fissure fills and displaced strata commonly occur and may contain datable material such as paleosols or gastropods (McCalpin, 2009). The faults on the island are orientated in two principal directions (WNW-ESE and NNE-SSW). They are 5-15 km in length with annual slip-rates of 0.3-1.3 mm/a (Caputo et al., 2010).

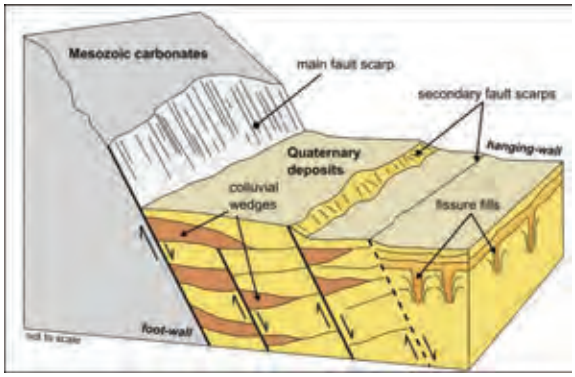

Figure 1: Sketch of a typical postglacial normal fault showing bedrock juxtaposed against Quaternary sediments which contain structures caused by recurrent earthquakes (modified after Reicherter et al., 2003).

Sfaka Fault

The Sfaka fault in eastern Crete is a west dipping normal fault situated in the Ierapetra Fault Zone. Caputo et al. (2010) recorded a maximum scarp height of 12 m measured along the 9 km long fault scarp. An outcrop in the form of a road cut at 35° 7'58.97"N and 25°54'26.01"E exhibits the fault zone as a contact between footwall Mesozoic carbonates and hanging-wall colluvium (Fig. 2). The outcrop cuts the fault at an angle of approximately 75°.

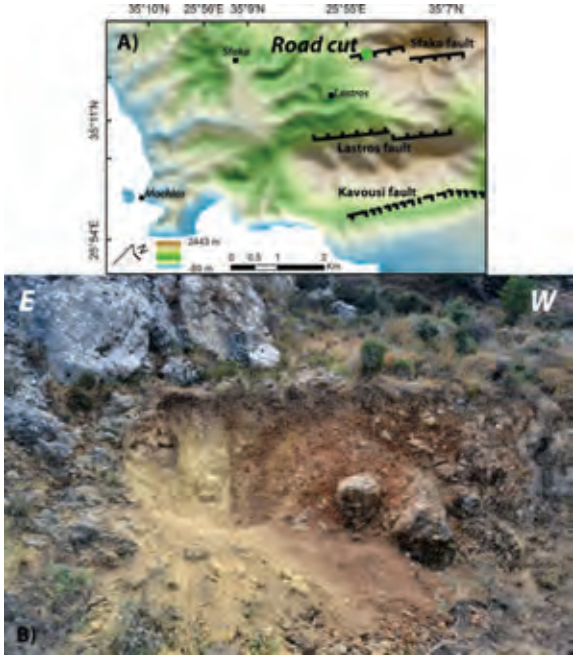

Figure 2: A) Overview map of the Lastros-Sfaka-Graben system. Note the location of the road cut along strike (green dot). B) Outcrop at the Sfaka fault comprising the degraded bedrock scarp (upper left) and a variety of coseismic sedimentology. Grid width is 1 m.

METHODOLOGY

The road cut in figure 2 is comparable to a paleoseismic trench and was further excavated, cleaned and gridded. Conventional paleoseismic trenching techniques were used as well as t-LiDAR measurements in order to improve the accuracy of paleoearthquake reconstruction. A multispectral analysis of t-LiDAR backscatter data and the luminescence of true color photographs were compared to the trench log. A GPR survey was conducted to obtain 3D information of layer continuation and thickness variation at depth (Fig. 3).

Paleoseismic trenching

In the conventional manner the trench wall was gridded, flagged, logged and photographed. The photomosaic of true color images (RGB; red, green, blue) was converted into a gray-level image to eliminate hue and saturation information while retaining the luminance (0-255). The image was georeferenced in order to make it comparable to other datasets.

t-LiDAR measurements

The t-LiDAR scanning was undertaken at both close range and long-mid range to determine geometrical relationships between the footwall, hanging-wall, the prolongation of the scarp, and the trench wall. High-resolution DEMs with a resolution of 0.1 m were produced.

The backscatter signal of the t-LiDAR results from the reflection of transmitted waves of near-infrared light. Intensity values were stored as grayscale values from 0-255. Thus, the backscattered signal was also used for the multispectral analysis.

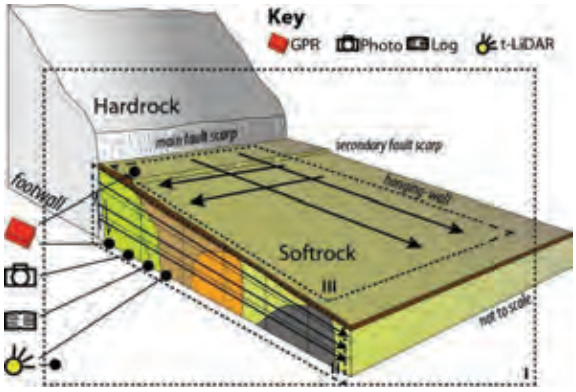

Figure 3: A simplified model of a typical hardrock-softrock fault and related subsurface features. Dashed lines show the different workspaces: I) Overall workspace for a long-mid range t-LiDAR scan to retrieve the geometric relation of footwall, hanging-wall, scarp, and trench; II) area of operations (log, photo, t-LiDAR, GPR) on the trench wall; III) workspace for GPR measurements (black arrows) on top of the colluvium.

Multispectral analysis

Iso clustering is based on the minimum Euclidean distance of cell values within a certain cluster. This was applied to both the gray-level photomosaic and the t-LiDAR backscatter signal datasets. The most significant parts of the spectra represent either one layer on their own or a certain spectral composition. These were highlighted to reproduce discrete deposits shown in the log (see Fig. 4).

Ground-Penetrating Radar

GPR was carried out on the vertical trench wall and on the slope surface above the trench (Fig. 3). Therefore, we used a GSSI 400 MHz antenna which provides a resolution of around 0.1 m. Based on distinct layers in the trench log and taking into account the results of the multispectral analysis, GPR-data were interpreted to determine the 3D architecture of outcropping strata.

RESULTS

The classified reproduction of the grayscale photomosaic results in six classes of spectral similarities. Of these, three classes are representative for log reproduction. This is done by filling the majority of a mapped layer by one class or by a certain composition of two or three classes (Fig. 4a). The remaining classes either represent shadows generated by the surface's curvature (lowermost values ranging from 0 - 98), or areas where the contained pixel values are evenly and widely spread and do not show any lithological significance.

The backscatter signal values range from 52-255. Four out of six calculated classes were quantified to describe lithofacies from the reproduction of the t-LiDAR backscatter signal. The lightest grayscale values from 220 to 255 cover approximately 75 % of the trench wall. Borders between mapped layers were identified by recognizing patterns of cluster compositions. An additional layer which is not included in the trench log is identified in the center of the trench wall (Fig. 4b).

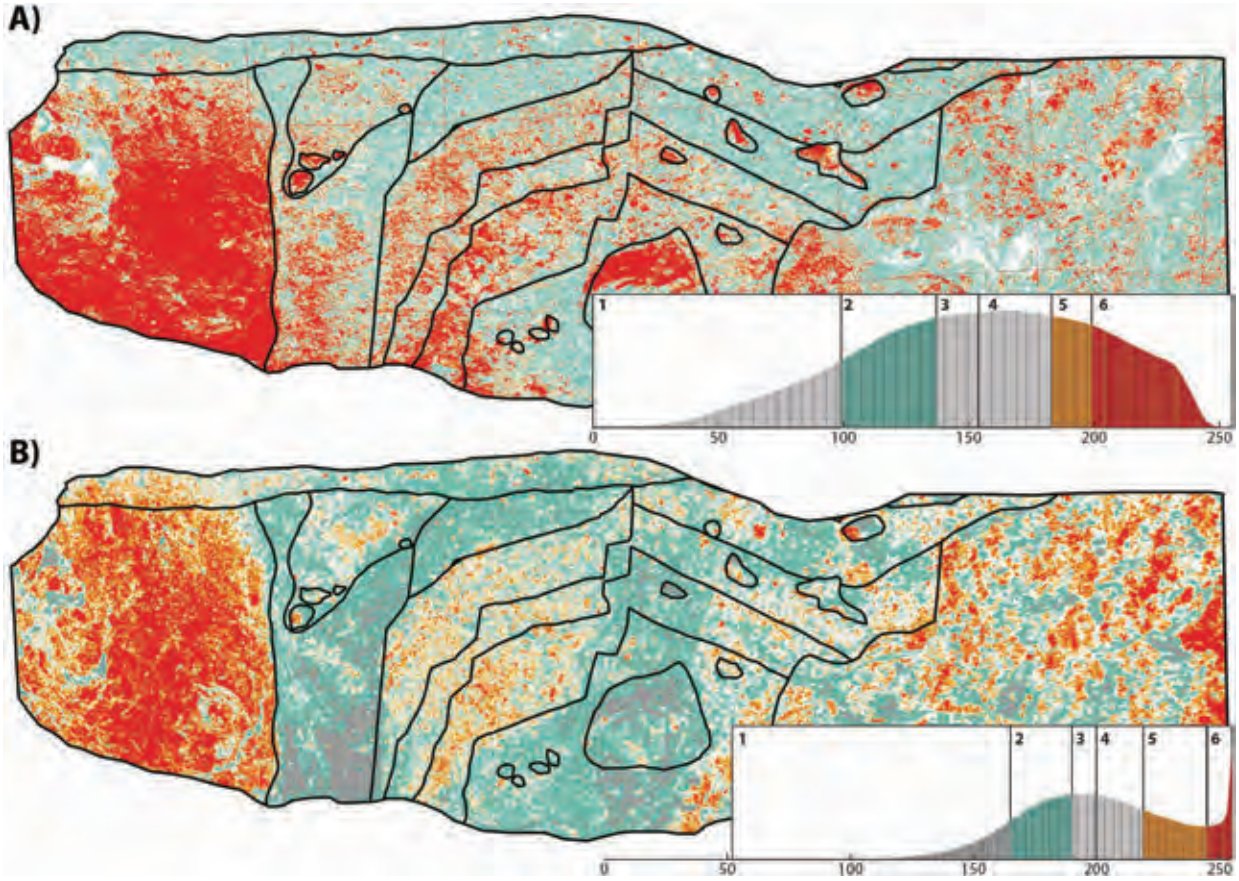

Figure 4: Iso clustering of visible light and near-infrared spectra. Black lines indicate mapped borders and transitions between different units. Histograms show signal intensity coded from 0-255 and calculated classes. A) Classified reproduction of the grayscale photomosaic. Classes 2, 5 and 6 are either representative for a mapped layer by one class or by a certain composition of two or three classes. B) Classified reproduction of the t-LiDAR backscatter signal. Specific compositions of classes 2, 5, and 6 allow delineating varying strata.

Using the trench log and multispectral information enables radar facies to be distinguished. This then leads to a 3D model of coseismic features within the hanging-wall. 8 out of 10 previously mapped units can be traced at depth using GPR (Fig. 5).

DISCUSSION

For decades now, trenching investigations have been one of the established methods for paleoseismic research. However, the outcome is highly dependent on the ability of the trench logger to define mappable units. Passive data collection done by imaging techniques includes significant disadvantages mainly due to differing angles of illumination since the outcrop is not a perfectly even wall. Thus, the lightest parts in the photomosaic, visualized here with values from 183-255, mainly represent a high matrix luminance and also the bright (top) sides of boulders and clasts. Rectification and parallax effects yield an additional error in the order of a few centimeters. t-LiDAR measurements require expensive equipment and software solutions. High-

resolution 3D images as well as the backscatter signal within the spectrum of near-infrared enable access to complementary information on the physical properties of materials. A multispectral approach, using unsupervised clustering on both spectra supports the results from the trench log and complements the findings. The resulting verified lithology of the trench wall serves as a calibration factor for GPR measurements. Due to a resolution of about 0.1 m the calibration is necessary to recognize and interpret minor differences in sedimentological compositions. This method allows more accurate statements to be made about geometric layer thicknesses. These are needed to correlate the amount of vertical offset caused by a specific surface rupturing event (e.g. Reiss et al., 2003).

CONCLUSION

Our results show that based on distinct layers in the trench log and obvious structures in both the photomosaic and t-LiDAR images, a 3D-interpretation of GPR-data is possible. Furthermore, lithological interpretations are more reliable because distinct layers can be traced with depth into the trench wall, and a more accurate statement on layer thickness is possible. The presented workflow enhances the objectivity of paleoseismic interpretations which will improve the accuracy of seismic hazard assessments.

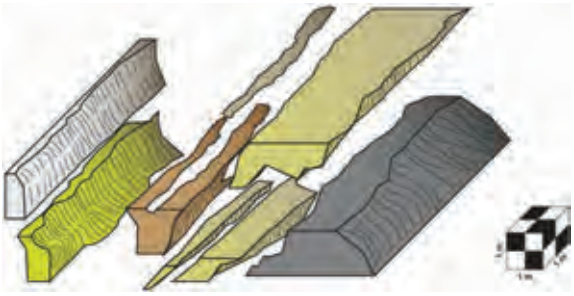

Figure 5: A model of coseismic features and their geometrical variance within the hanging-wall estimated from GPR images. Using this technique it is possible to estimate layer thicknesses.

Acknowledgements: We would like to thank Ioannis Papanikolaou for his cooperation and support on Crete and mainland Greece. Furthermore, thanks to Silke Mechernich and Alexander Woywode who supported us in the field. We are grateful for the loan of equipment and excellent food from the Zorbas Taverna in Pachia Ammos.

References

Alasset, P.J. & M. Meghraoui, (2005). Active faulting in the western Pyrenees (France): Paleoseismic evidence for late Holocene ruptures. *Tectonophysics*. 409, 39-54.

Benedetti, L., R. Finkel, G. King, R. Armijo, F. Ryerson, D. Farber & F. Flerit, (2002). Application of geomorphic analysis and gorund-penetrating radar to characterization of paleoseismic sites in dynamic alluvial environments: an example from southern California. *Tectonophysics*. 368, 25-32.

Benedetti, L., R. Finkel, G. King, R. Armijo, D. Papanastassiou, F.J. Ryerson, F. Flerit, D. Farber & G. Stavrakakis, (2003). Motion on the Kaparelli fault (Greece) prior to the 1981 earthquake sequence determined from 36Cl cosmogenic dating. *Terra Nova*. 15, 118-124.

Bubeck, A., M. Wilkinson, G.P. Roberts, P.A. Cowie, K.J.W. McCaffrey, R. Phillips & P. Sammonds, (2014). The tectonic geomorphology of bedrock scarps on active normal faults in the Italian Apennines mapped using combined ground penetrating radar and terrestrial laser scanning. *Geomorphology*. dx.doi.org/10.1016/j.geomorph.2014.03.011 (in press).

Caputo, R., S. Catalano, C. Monaco, G. Romagnoli, G. Tortorici & L. Tortorici, (2010). Active faulting in the island of Crete (Greece). *Geophysical Journal International*. 183, 111-126.

Carcaillet, J., I. Manighetti, C. Chauvel, A. Schlagenhauf & J.M. Nicole, (2008). Identifying past earthquakes on an active normal fault (Magnola, Italy) from the chemical analysis of its exhumed carbonate fault plane, *Earth and Planetary Science Lett*ers. 271, 145-158.

Chow, J., J. Angelier, J. Hua, J. Lee & R. Sun, (2001). Paleoseismic event and active faulting: from ground penetrating radar and high-resolution seismics reflection profiles across the Chihshang Fault, eastern Tiawan. *Tectonophysics*. 333, 241-259.

Demanet, D., F. Renardy, K. Vanneste, D. Jongmans, T. Camelbeeck & M. Meghraoui, (2001). The use of geophysical prospecting for imaging active faults in the Roer Graben, Belgium. *Geophysiscs*. 66, 78-89.

Galli, P., F. Galadini & D. Pantosti, (2008). Twenty years of paleoseismology in Italy. *Earth-Science Reviews*. 88, 89-117.

Grützner, C., K. Reicherter & P. Silva, (2010). Comparing semiquantitative logic trees for archaeoseismology and paleoseismology: The Baelo Claudia (southern Spain) case study. *The Geological Society of America*. Special Paper. 471, 129-143.

Grützner, C., K. Reicherter, C. Hübscher P. & Silva, (2012). Active faulting and neotectonics in the Baelo Claudia area, Campo de Gibraltar (southern Spain). *Tectonophysics*. 554-557, 241-259.

McCalpin, J., (2009). Paleoseismology. 2nd edition. *International Geophysics Series*. Vol. 95. Academic Press.

Meghraoui, M., T. Camelbeeck, K. Vanneste, M. Brondeel, & D. Jongmans, (2000). Active faulting and paleoseismology along the Bree fault, lower Rhine graben, Belgium. *J. Geophys. Res*. 105 (B6), 13809 - 13841.

Michetti, A.M., F.A. Audemard & S. Marco, (2005). Future trends in paleoseismology: Integrated study of the seismic landscape as a vital tool in seismic hazard analyses. *Tectonophysics*. 408, 3-21.

Papanikolaou, I., G. Robert & A.M. Michetti, (2005). Fault scarps and deformation rates in Lazio-Abruzzo, Central Italy: comparison between geological fault slip-rate and GPS data. *Tectonophysics*. 408, 147-176.

Reicherter, K., A. Jabaloy, J. Galindo-Zaldivar, P. Ruano, P. Becker-Heidmann, J. Morales, S. Reiss & F. Gonzalez-Lodeiro, (2003). Repeated palaeoseismic activity of the Ventas de Zafarraya fault (S Spain) and its relation with the 1884 Andalusian earthquake. *Int. J. Earth Sci*. 92, 912-922.

Reicherter. K., A.M. Michetti & P.G. Silva, (2009). Introduction. In: *Paleoseismology: Historical and Prehistorical Records of Earthquake Ground Efffects for Seismic Hazard Assessment, Vol., 316* (Reicherter, K., Michetti, A. M., Silva, P. G. eds.). Geological Society of London. 1-10 (Special Publication).

Reicherter, K., N. Hoffman, K. Lindhorst, S. Krastel, T. Fernández-Steeger, C. Grützner & T. Wiatr, (2011). Active basins and neotectonics: morphotectonics of the Lake Ohrid basin (FYROM and Albania). *Z. dt. Geowiss*. 162/2, 217-234.

Reiss, S., K. Reicherter & C.D. Reuther, (2003). Visualization and characterization of active normal faults and associated sedimentary structures by high-resolution ground penetrating radar (GPR). *Geol. Soc. London*. Spec. Publ. 211, 247-255.

Wiatr, T., K. Reicherter, I. Papanikolaou, T. Fernández-Steeger & J. Mason, (2013). Slip vector analysis with high resolution t-LiDAR scanning. *Tectonophysics*. 608, 947-957.

Wiatr, T., I. Papanikolaou, T. Fernández-Steeger & K. Reicherter, (2015). Bedrock fault scarp history: Insight from t-LiDAR backscatter behaviour and analysis of structure changes. *Geomorphology*. 228, 421-431.

Wilkinson, M., G.P. Roberts, K. McCaffrey, P.A. Cowie, J.P. Faure Walker, I. Papanikolaou, R.J. Phillips, A.M. Michetti, E. Vittori, L. Gregory, L. Wedmoree and J. Watson, (2014). Slip distributions on active normal faults measured from LiDAR and field mapping of geomorphic offsets: an example from L'Aquila, Italy, and implications for modelling seismic moment release. *Geomorphology*. doi: /10.1016/j.geomorph.2014.04.026 (in press).

INQUA Focus Group on Paleoseismology and Active Tectonics

Surface Faulting from the August 24, 2014 Mw 6.0 South Napa, CA, Earthquake

Schwartz, D.P. (1), Ponti, D.J. (1), Dawson, T.E. (2), Brooks, B.A. (1), DeLong, S.B. (1), Hecker, S. (1), Hudnut, K.W. (3), Kelson, K.I. (4), Lienkaemper, J.J. (1), Prentice, C.S. (1), Rosa, C.M. (1), Rubin, R.S. (2), Seitz, G.G. (2), Sickler, R.R. (1), Wesling, J.R. (5)

(1) US Geological Survey, Menlo Park, CA, USA. E-mail: dschwartz@usgs.gov
(2) California Geological Survey, Menlo Park, CA, USA
(3) US Geological Survey, Pasadena, CA, USA
(4) U.S. Army Corps of Engineers, Sacramento, CA, USA
(5) California Office of Mine Reclamation, Sacramento, CA, USA

Abstract: *Surface rupture associated with August 24, 2014 Mw 6.0 South Napa earthquake is the most extensive for a Calfiornia earthquake of similar magnitude. We used traditional field techniques, airborne and satellite interferometry, post-event airborne LiDAR, and Terrestrial Laser Scanning (TLS), including mobile, truck-mounted TLS to map the rupture. It extends at least at least 12.5 km northwest of the epicenter and locally is distributed across multiple traces in a zone ~ 2 km across. Maximum right-lateral coseismic slip along the primary rupture was 46 cm and the cumulative surface offset across multiple traces was 60 cm. Rapid afterslip occurred along the southern half of the main fault trace and the amount appears to be approximating the coseismic offset. The South Napa earthquake is a reminder that even moderate magnitude earthquakes will continue to be important sources of damage when they occur in urbanized areas.*

Key words: *Surface faulting, afterslip, Napa, mapping techniques.*

INTRODUCTION

The August 24, 2014 Mw 6.0 South Napa earthquake was only the fourth M≥6 earthquake to occur in the San Francisco Bay Region (SFBR) since 1906. The SFBR is within the boundary between the Pacific and North American plates. Slip across this plate boundary occurs primarily on moderate (3mm/yr) to high (24 mm/yr) slip rate strike-slip faults including the San Gregorio, San Andreas, Hayward, Rodgers Creek, Calaveras, Greenville, and Concord-Green Valley faults (*Figure 1*).

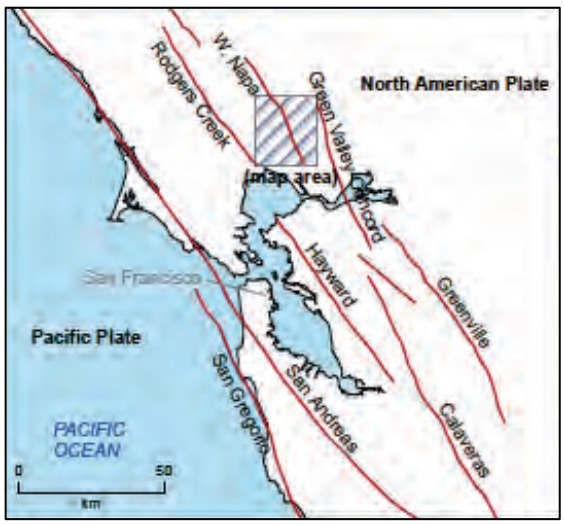

Figure 1. Major faults int the San Francisco Bay Region plate boundary (from Brocher et al., 2015).

The West Napa fault zone (WNFZ) is the northerly structural continuation of the Calaveras fault system and extends northwest through the Napa Valley. It is poorly characterized with regard to slip rate (estimated at 1-2 mm/yr), recurrence interval, timing of past earthquakes, and even location of Holocene-active fault traces. Only an 8 km –long section of the WNFZ, located east and south of the of the primary surface rupture, had been identified by the State of California as Holocene and zoned as a surface fault rupture hazard. The Napa Valley of California has historically been a region of low seismicity. The largest earthquake since about 1850 to occur directly in the Napa Valley, and likely on the WNFZ, was the September 2000 Mw 4.9 Yountville earthquake, which caused damage in the city of Napa but was not associated with surface faulting.

SURFACE RUPTURE

The South Napa Earthquake of August 24, 2014 nucleated at a depth of 9.7 km and ruptured unilaterally to the northwest rupture. An overview of the event including geologic, geodetic, seismologic, strong motion, and damage observations can be found in Brocher et al., 2015. The surface faulting, which included both coseismic offset and afterslip, was the most extensive of any documented California earthquake of similar magnitude (*Table 1*). The surface ruptures were mapped over a period of weeks using traditional field techniques, airborne and satellite interferometry, post-event airborne LiDAR, and Terrestrial Laser Scanning (TLS), including mobile, truck-mounted TLS. Roads, rows of grapevines, and other cultural features offset by the surface faulting provided piercing points. The collection of field observations on cell phone apps that converted data to KMZ files that could be viewed in Google Earth

aided rapid communication and dissemination of findings. Over 900 field observations document that right-lateral surface faulting occurred NW of the epicenter along five NW-trending sub-parallel fault traces within a zone ~2- km-wide and at least 12.5 -km - long (A-E, *Figure 2*); a short zone of left-stepping en echelon cracks also occurred 2.5 km east of the epicenter (F, *Figure 2*). The maximum cumulative coseismic surface slip, distributed across traces A-E, was 60 cm.

Figure 2. Map of surface ruptures A-F (yellow lines. White numbers are offset values (cm). Red star is earthquake epicenter.

The primary faulting occurred on rupture trace A along the west edge of the zone, and extended for at least 12.5 km from the Napa River at Cuttings Wharf northwest to beyond Alston Park in the city of Napa. UAVSAR interferograms produced by NASA suggest that faulting may have extended an additional 2.3 km to the SE and an additional 0.7 km to the NW, but tectonic displacements along these trends could not be verified in the field. Initial coseismic surface offset was small close to the epicenter, if it occurred at all, and reached a maximum of 46 cm approximately 10 km to the NW on fault trace A (*Figure 3*). Slip on fault trace A occurred both coseismically and as afterslip, with most of the total displacement along the southern half of this rupture trace occurring as afterslip (*Figure 4*).

Afterslip was most rapid on the central section of trace A, increasing initial slip by ≥20 cm 1 day after the mainshock. Measurements to date suggest that the afterslip along this section of the rupture will approximate the coseismic slip on the northern half of fault trace A (*Figure 5*). Afterslip is not a common characteristic of California earthquakes of moderate magnitude, having been only documented following four of eleven events (*Table 1*).

Figure 3. En-echelon surface rupture through vineyard near location of maximum coseismic offset on fault trace A. Photo by Daniel Ponti, USGS.

Figure 4. Afterslip across CA Highway 12 on the day of the earthquake (8/24/14) and on the day following (8/25/14). Afterslip was rapid and will approximate the amount of coseismic slip on the northern half of fault trace A. Photos by Tim Dawson, California Geological Survey.

The longest secondary rupture, trace C, extends ~7 km SSE from the northern end of the rupture zone, where trace A appears to merge with it. Fault trace C passes through residential areas resulting in faulting damage to homes. Dextral offsets of ≤8 cm were observed along C with no evidence for afterslip. The four other traces are each <1.5 km in length and display minor, discontinuous right lateral offsets of ≤6 cm. Local geomorphic expression of prior faulting, and post-earthquake trenching investigations on some of these ruptures, suggest that they may be part of a broad, active shear zone within which the amount of displacement and extent of rupture along the 2014 traces may vary from earthquake to earthquake. However, the down-dip structural connections between these ruptures and

primary trace A are not known. The short lengths of fault traces B, D, E, and F suggest that these ruptures, at least in this event, may have been dynamically triggered.

Event (year)	Magnitude (M)	Focal Depth D (km)	Coseismic Surface Rupture Length (km)	Coseismic Dmax at Surface (cm)	Creep prior to event	Surface afterslip (cm)
1. Desert Hot Springs (1948)	6.0	8.0	0	0	no	nr
2. Galway Lake (1975)	5.0 ML	5.8	6.8	1.5	no	nr
3. Parkfield (1966)	6.0	8.6	0 (SA) 10(SWFZ)	0(SA) 6.6(SWFZ)	yes	31 (SA)
4. Homestead Valley (1979)	4.8 ML 5.5 4.5 ML 4.8 ML	8.3 9.3 8.9 2.0	3.25(HV) 1.5 (JV)	11 1	no	nr
5. Coyote Lake (1979)	5.9	6.96	0	0	yes	0.5
6. Greenville (1980)	5.8	14.79	4-6	≥1	yes	≥1
7. Morgan Hill (1984)	6.2	8.42	0	0	yes	nr
8. North Palm Springs (1986)	6.02	10.4	9	<0.1	no	nr
9. Elmore Ranch (1987)	6.04	10.8	10	20	no	nr
10. Joshua Tree (1992)	6.16	12.3	0	0	no	nr
11. Parkfield (2004)	6.0	7.9	0 (SA) 8 (SWFZ)	<0.2(SA) 6.6(SWFZ)	yes	13-35 SA
12. South Napa (2014)	6.0	10.7	≥12.5	≥40	no	≥35

Magnitude (M): Magnitudes are Mw unless noted as ML. Source is UCERF 3 seismicity catalog (Felzer, 2013) unless otherwise noted.
Focal Depth D (km): Source is UCERF 3 seismicity catalog (Felzer, 2013) unless otherwise noted.
Coseismic surface rupture length (km): Reported length of rupture at the surface at time of event, distinct from afterslip. Where multiple fault traces occurred length listed is for the longest trace.
Coseismic Dmax: Reported maximum coseismic surface displacement. Does not include afterslip. nr_ Not reported.

Notes

1. M and D (Felzer, 2013). Richter et al (1958) report no surface rupture; 18 km aftershock zone
2. M and D ([illegible]). Surface offset data from Hill and Beeby (1977)
3. M and D (Ellsworth, 1990). San Andreas creeping at 20 mm/yr. Afterslip along 44 km of main San Andreas (SA) Coseismic slip on Southwest Fracture Zone (SWFZ). Surface offset data from Lienkaemper and Prescott (1989)
4. M and D (Felzer (2013). Earthquake swarm with ruptures along Homestead Valley (HV) and Johnson Valley (JV) faults, both re-ruptured during 1992 M7.2 Landers event. Surface offset data from Hill et al. (1980)
5. M and D (Oppenheimer et al., 1990); 14 km rupture length at depth. Discontinuous surface cracking for 14.4 km is likely afterslip. Surface observations from Armstrong (1979)
6. M and D (Ellsworth, 1990). Pre-event creep at 1-2 mm/yr (Lienkaemper et al.,2013). Total surface slip (coseismic + afterslip) was 2.5 cm (Bonilla et al., 1980). Concurrent rupture of conjugate Las Positas fault.
7. M and D (Oppenheimer et al., 1990). 25km rupture length at depth (between 4-10km). No unequivocal coseismic surface rupture (Harms et al.,1987)
8. M and D (Felzer, 2013). Discontinuous, en echelon, left-stepping fractures for 9 km along surface trace Banning strand of SA. Offset data from Sharp et al. (1986) who refer to these as "trace fractures" and interpret them as incipient faulting.
9. M and D (Felzer, 2013). Slip distributed on 6 traces across across 8.5 km-wide zone. Longest is 10 km (Elmore Ranch fault). Cumulative surface Dmax for all traces is 20 cm, average ~10 cm Surface offset data from Hudnut et al. (1989).
10. M and D (Felzer, 2013). 1.5 km discontinuous, triggered slip on East Wide Canyon fault (Rymer, 2002)

Table 1. Comparison of Seismological and Surface Faulting Parameters for ~M6 Strike-Slip Earthquakes in California since 1948 (modified from Brocher et al., 2015).

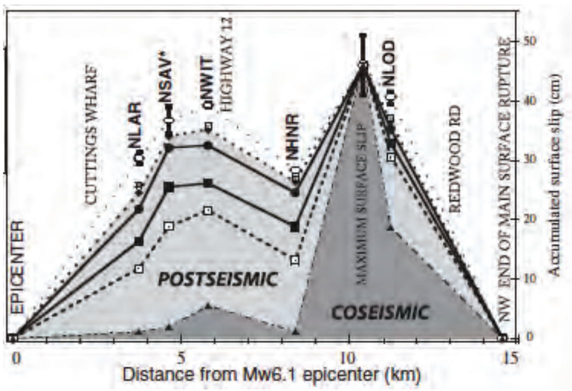

Figure 5. Surface slip profile showing distribution of coseismic slip and after and afterslip (postseismic) (from Wei et al., 2015).

CONCLUSIONS

The South Napa surface rupture raises several intriguing and important issues:

- Most of the rupture occurred on previously unmapped faults or along parts of mapped faults that were not recognized as Holocene-active. What are the implications for characterization of potential earthquake sources, not only in California but also in other seismically active regions? What is the temporal definition of an active seismic source?
- Why was the rupture so extensive for this magnitude? What crustal properties controlled the length and amount of surface offset? Do all of the 2014 ruptures represent seismogenic slip along faults that merge into the main fault trace A or were they shallow, dynamically triggered sections of other longer faults?
- Afterslip only occurred along about half of the principal trace. What physical properties control the occurrence and rate of afterslip, a process with implications for post-earthquake response and recovery?
- The South Napa earthquake is a reminder that although long, large-magnitude ruptures capture the attention of the public, the media, and hazard modelers, moderate magnitude earthquakes such as this will continue to be important sources of damage when they occur in urbanized areas.

References

Brocher, T.A., A. Baltay, J.L. Hardebeck, J. Polet, E. Langenheim, A. L., Llenos, J.J. Lienkaemper, D.P. Schwartz, J.L. Blair, T. Dawson, et al., (2015). The M 6.0 24 August 2014 South Napa earthquake. *Seismological Research Letters.* 86, no. 2A, 309-325, doi: 10.1785/0220150004.

Wei, S., S. Barbot, R. Graves, J.J. Lienkeemper. T. Wang, K. Hudnut, Y. Fu, and D. Helmberger, (2015). The 2014 Mw 6.1 South Napa earthquake: a unilateral rupture with shallow asperity and rapid afterslip. *Seismological Research Letters.* 86, no. 2A, 344-354, doi: 10.1785/0220140249.

6th International INQUA Meeting on Paleoseismology, Active Tectonics and Archaeoseismology,
19-24 April 2015, Pescina, Fucino Basin, Italy

INQUA Focus Group on Paleoseismology and Active Tectonics

Challenges facing Fault-Based PSHA for 6≤M≤7 earthquakes: An example from the west Corinth rift, Greece

Scotti, O. (1), Boiselet A. (1,2), Lyon-Caen, H. (2), Albini, P. (3), Bernard, P. (4), Briole, P. (2), Ford, M. (5), Lambotte, S. (6), Matrullo, E. (2), Rovida, A. (3), Satriano, C. (4) and ANR-SISCOR Team

(1) Institut de Radioprotection et Sûreté Nucléaire, BP 17, 92 262 Fontenay-aux-Roses, France. Email : Oona.scotti@irsn.fr
(2) Ecole Normale Supérieure Paris, Laboratoire de géologie, CNRS, Paris, France
(3) Istituto Nazionale di Geofisica e Vulcanologia, Milano, Italy
(4) nstitut de Physique du Globe, Paris, France
(5) Centre de Recherches Pétrographiques et Géochimiques, Vandoeuvre-Les-Nancy, France
(6) Institut de Physique du Globe Strasbourg, CNRS, Strasbourg Cedex, France

Abstract: *Fault-Based probabilistic seismic hazard assessment requires forecasting earthquakes along each fault. The robustness of such earthquake forecasts for faults producing M6-6.5 earthquakes depends first of all on the completeness of the geological information on the faults. For such magnitude levels the probability of identifying surface rupturing events is between 30 and 80 %. Thus chances of missing blind or poorly exposed faults are not negligible. Furthermore robustness depends on available measurement qualities along each fault, knowledge of 3D fault geometries, criteria for multi-fault rupture possibilities, estimates of seismic and aseismic slip rates, assumptions on magnitude-area relationships and magnitude-frequency distributions as well as on earthquake probability models. The purpose of this presentation is to discuss challenges and pitfalls that accompany such an endeavour and propose ways forward.*

Key words: *Fault-PSHA, slip rate, 3D fault geometry, aseismic deformation.*

INTRODUCTION

Computing the expected ground motion at a nuclear power plant following deterministic or probabilistic methodologies has been traditionally performed on the basis of historical and instrumental seismicity catalogues only. The need to consider geological data(information coming from paleo-seismological and morphological studies of faults) has long been recognized in the United States (see Diablo Canyon Nuclear Power Plant, for example) and is today clearly stated in reference seismic design guidelines such as IAEA (2010). Use of faults for seismic hazard assessment (SHA) is however still a subject of continuous development and debate in the community. The debate is of particular concern in low to moderate seismicity countries when simplified models are used. Such models consider all magnitudes greater than a given threshold M_t to be located on identified faults (proposed M_t range from 5 to 6,5). Not only are the chances of missing blind or poorly exposed faults not negligible but once identified collecting, collecting relevant fault data in the field is not always possible. Often, availability of fault databases is actually lacking (not many countries have the means to develop and maintain such databases). So the first challenge is to create a database reflecting the available level of knowledge. Assuming the database exists, many other challenges wait ahead such as:

1. Which faults should be considered (slip rate criteria, maximum magnitude criteria?).
2. How should faults be represented? Discrete Planes, Fault Zones, Fault sections, Fault polygons.
3. What are the spatial and temporal constraints for attributing slip rates to faults?
4. How to allow for multi fault ruptures?
5. Which magnitude-frequency distributions (MFD) of earthquakes for which fault?
6. Which fraction of on-fault versus off-fault seismicity?
7. Last but not least, how to constrain the amount of aseismic deformation (on and off faults)?

This paper discusses some of these issues based on the dataset available for parameterizing the faults in the western part of the Corinth Rift (WCR) in Greece. Possible ways forward are then proposed aiming towards (i) representations of fault-based PSHA calculations that reflect the actual level of knowledge available in any given region and (ii) motivating next-generation fault-based PSHA that incorporate not only seismicity and geological information but also deformation models.

CONTEXT AND DATA

The WCR is one of the most active tectonic structures of the euro-mediterranean area. Its NNE-SSW opening rate is 1.5 cm/yr (strain rate of 10-6/yr) results into a high microseismicity level and a few destructive, $6 \leq M \leq 7$ earthquakes per century, activating a system of mostly north dipping normal faults (Figure 1). Since 2001, monitoring arrays of the European Corinth Rift Laboratory (CRL, www.crlab.eu) allowed to better track the mechanical processes at work, with short period and broad band seismometers, continuous GPS, borehole strainmeters, …). The recent (300 kyr) tectonic history

has been revealed by on-land (uplifted fan deltas and terraces) and offshore geological studies (mapping, shallow seismic, coring, e.g. see Beckers et al., 2015), showing a fast evolution of the normal fault system.
Relocated microseismicity, outlines a north-dipping 1 to 3 km thick structure between 6 and 9 km in depth on which most faults appear to root (Lambotte et al., 2014). The diffusion of the microseismicity suggests its triggering by pore pressure transients, with no or barely detected strain (Bernard et al. 2014). Paleoseismological (trenching, paleo-shorelines, turbidites), archeological and historical studies completed the catalogues of instrumental seismicity, and provided the basis for discussing the earthquake rupture forecasts (ERF) of M>=6 in the WCR within the SISCOR group (Boiselet, 2014).

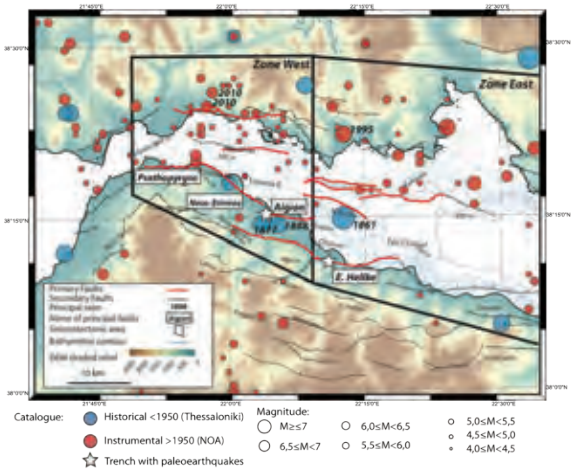

Figure 1: M≥5 earthquakes based on revised instrumental (red) and historical (blue) earthquake catalogues of the Corinth Rift. Black boxes represent the two fault-zone polygons (Zone West = WCR and Zone East). (Boiselet, 2014).

METHOD

An important contribution of the work presented in Boiselet (2014), beyond the synthesis and critical assessment of existing data, is the development of a "community-based" ERF fault model reflecting the level of knowledge gathered thus far by the WCR-SISCOR working group. A logic tree methodology was used to explore uncertainties and diversity of opinions in available and updated seismological and geological information concerning fault geometries, seismic slip rates, magnitude-area relationships, MFD and probability models. For each fault, geometries and slip rates are discussed and relevant uncertainties are explored.

SOME OF THE ISSUES AT STAKE

Which faults should be considered in the ERF?
The WCR is composed of a complex network of faults displaying a great range of slip rates. For this study, only faults with estimated slip rates greater than 0.5 mm/yr are modeled (red faults in Figure 1).

Seismic History of faults
A revision of historical sources and intensity evaluations has allowed improving the location and magnitude of some important events in the WCR. This notwithstanding, uncertainty in location poses still some challenges, even for the best geologically known fault in the region (e.g. Aigion fault).

Presence of blind faults
The 1995 M6.2 "Aigion" earthquake highlighted the presence of low-angle, blind structures in the WCR fault-system. How many such structures exist in the WCR? What is their exact geometry? What is the slip rate that is been released seismically along such faults? Which data can constraint such information?

Uncertainty in the 3D geometries
If most faults were considered planar with a small uncertainty in their dips and their down-dip extent, for the Psathopyrgos and the East Helike faults it appeared necessary to envisage a possible link (low weight equal to 0.2) with the shallow dipping blind structures identified at depth by recent earthquakes (i.e., 1995) (Figure 2).

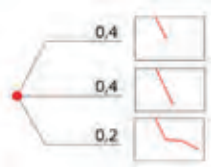

Figure 2: Example of complex down-dip geometries envisaged for the Psathopyrgos and the East Helike faults.

From throws to slip rates on dipping faults
The main source of information available to estimate the slip rates along these dip-slip faults is the throw, which is the vertical separation of originally continuous geological layers. In the WCR context, the complete information including submerged hanging wall data is seldom available and it is necessary to make assumptions about the ratio between footwall uplift (FU) and hanging wall subsidence (HS) on both sides. This ratio is a subject of debate. Values proposed, for the East Helike fault vary from 1:1 to 1:3.2, and for the Aigion fault from 1:1.3 to 1:1.6. The choice of the ratio has a major impact on the estimates of slip rates. In this paper, a single ratio of FU/HS of 1:1.5 was assumed for the entire fault dataset, based on the AIG10 borehole data and the argument that 1:1 is less likely, as subsidence is expected to be more important than uplift, and that 1:2 seems too high according to the WCR working group. Estimated slip rates for the 13 faults range then between [4.5 -6.9] mm/yr for the fastest slipping Psathopyrgos fault to [0.5 – 1.45] mm/yr estimated for the Marathias and Helike West Faults. The age of the markers considered for slip rate estimates range from 2 up to 1500 kyr for the Psathopyrgos and East Channel fault, for example.

Considering the fast-dynamics of the region, this heterogeneity in the time-period considered introduces an additional uncertainty as slip rates may have varied over such time scales in this region.

Multi-fault ruptures

Most large multi-fault ruptures are probably extremely unlikely, but experience has shown that such ruptures may occur and including them in the model will allow for evaluation of the consequences of large, rare events. Which criteria should be used, however, is still a matter of debate. In the case of the WCR, for example, considering a 5 km critical distance, as suggested in the recently published model for California, would lead to linking up all the faults of the WCR (Figure 3, a). The threshold of 1.5 km considered in this study is leads to rupture scenarios capable of generating 6.5<M<6.75 earthquakes. This is consistent with estimates proposed for some historical and paleo-seismological events. In the ERF calculations, 60% of the rupture scenarios are provided by single fault ruptures, 30% by two-fault ruptures and only 10% by 3 fault ruptures (M> 6.75).

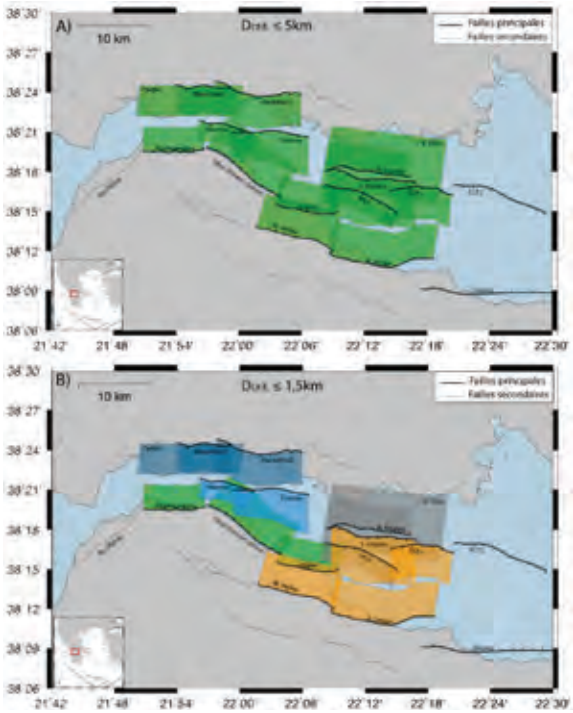

Figure 3: Multi-fault rupture scenarios for the WCR-fault system considering a critical distance of 5 km (a) and 1,5 km (b) (from Boiselet, 2014).

Consistency of geologic/geodetic earthquake rates

Figure 4 compares earthquake rates estimated from the earthquake catalogue for the WCR zone with those estimated from geodesy (opening rate is 1.5 cm/yr in a roughly N-S direction) and those estimated from the proposed fault models (so-called geologic).

Geodetic earthquake rates modeled with a characteristic MFD-YC (e.g. a higher occurrence rate of high-magnitude events compared to a Gutenberg-Richter prediction) reproduce reasonably well observed seismic rates in the 5<M<6 range. However, geologic rates under-predict seismic rates. Most importantly, for M>6.0, earthquake rates predicted from geodetic considerations are much higher than those inferred from geologic considerations. Thus, it appears that at the scale of the WCR polygon, the fault model is incomplete. Either faults are missing, or fault-slip rates are underestimated, or/and there is aseismic deformation taking place in the volume between the faults.

Probability models of earthquakes

Both time-independent and time-dependent probability models are considered. For time-dependent models it is necessary to estimate the coefficient of aperiodicity, $\alpha = \sigma/\mu$ (where μ is the mean recurrence time and σ the standard deviation of the mean recurrence time between earthquakes.

When α is close to 1, the time series exhibits clustering properties. Values <1 indicate the possible presence of periodicity of recurrence times, ($\alpha=0$, completely periodic). In the WCR, only the Aigion fault (3 events in two different sites, Pantosti el al., 2004) and the East Helike fault (6 events; Koukouvelas et al. 2005) have some information for an estimate of α. Depending on the hypothesis (dating uncertainties and association of historical earthquakes) the seismic and paleoseismic history of these faults suggest an aperiodicity factor of:

$0{,}7 < \alpha < 1{,}4$ for Aigion
$0{,}6 < \alpha < 1{,}0$ for East Helike

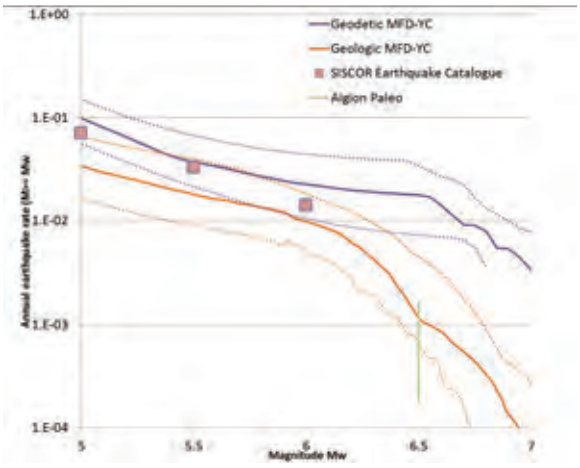

Figure 4: Mean and standard deviations (logic tree: geometry/ slip rates/ Mmax) of the earthquake rates estimated for the faults of the WCR based on the characteristic MFD-YC compared to estimates based on geodetic extension rate across the WCR polygon and Siscor Earthquake Catalogue.

These estimates have to be considered with caution, as the corresponding magnitudes, inferred from offsets observed in the trench based on Wells and Coppersmith (1994) are between 6.2 and 6.5 and slightly higher if Leonard (2010) is used instead. In this magnitude range, not all faults rupture the surface (the probability of observing surface ruptures for these events is between 30 and 80 %, e.g. Youngs et al., 2003 and references therein). For all faults, only two aperiodicity values were tested (0.5 and 0.7). When no information is available on the date of the last event on any given fault, the date of completeness of M≥6.0 was assumed (Tcomp = 1725). In general, differences in ERF between Poisson and time-dependent probability models differ at most by 3%. Irrespective of the probability model, the highest ERF for the next 30 years for M≥ 6.0 are for the Psathopyrgos and Neo-Erineos faults: 11% and 14 % respectively.

RESULTS

Figure 5 shows a synthetic summary of the results. ERF for each fault are affected by a high degree of uncertainty due mainly to the poorly constrained 3D geometry of the faults and lack of accurate slip rates along them. Results are also shown for the WCR-polygon (Figure 1) based only on the earthquake catalogue and the uncertainties therein.

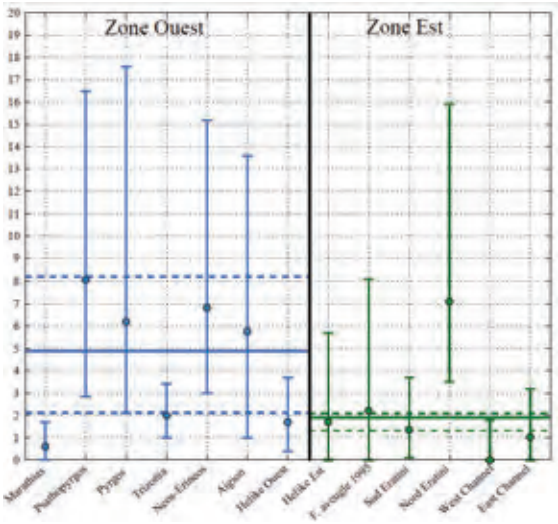

Figure 5: ERF and uncertainties for M≥6 in the next 30 years uncertainties (normalized by 100 km^2) for each fault (dots) and for each polygon (lines). (From Boiselet, 2014).

DISCUSSION AND PERSPECTIVES

The WCR is a young and fast deforming rift partly buried under the Gulf. It is composed of a complex network of short fault segments, releasing deformation with relatively moderate *6≤M≤7* earthquakes every century. Imaging of the 3D geometries of each fault and characterizing their seismic behavior has proven quite challenging. Moreover, an important component of aseismic deformation appears to be taking place.

Considering the complex WCR fault-system as a single WCR-polygon, with ERF based on the seismic catalogue alone, appears to provide a regional vision which is consistent but much simpler than the fault approach developed here, and at the same time it captures most of the fault-ERF epistemic uncertainty. The polygon approach reflects the actual level of knowledge and modelling capabilities available in the WCR to this day. It provides also a clear message to the end-users: inside this polygon strong earthquakes (estimated at ≤~M7) may be expected to occur anywhere therein. Surprisingly, as suggested by the comparative analysis between observed seismic and expected geologic and geodetic earthquake rates inside the WCR- polygon, it appears that a "characteristic-MFD" hypothesis best describes the expected earthquakes rates of M>=6.

For site specific PSHA, however, the fault- PSHA approach needs to be pursued, fault slip rates and off-fault deformation need to be better assessed by improved geologic information, such as datable offset markers that can be tied across a fault, and from modeling-space geodetic measurements. To address the issue of aseismic deformation, it is necessary to move towards the next generation of seismic fault-PSHA models. One possibility is to incorporate deformation models (i.e. Bird, 2009) such as recently proposed by Field et al. (2013).

A COMMUNITY PROJECT

Improving fault-databases and striving for completeness of fault-records for M>6.0 is an enormous challenge (see some recent European Projects). However, keeping this effort alive, evolving toward a tool integrating the community concerned and developing a network of Fault-PSHA practitioners and earthquake geologists in Europe is also critical for a common understanding and sharing of this relatively new discipline in Europe where maximum magnitudes rarely exceed M7.

Acknowledgements: This work was supported by French CNRS, ENS and IRSN in the framework of the ANR-SISCOR (2010-2014).

References

IAEA 2010 Specific Safety Guide NO. SSG-9. Seismic Hazards in Site Evaluation for Nuclear Installations.

Bernard, P. et al., (2014). The Corinth Rift Laboratory, Greece (CRL): A Multidisciplinary Near Fault Observatory (NFO) on a Fast Rifting System. *AGU*.

Beckers, A. et al., (2015). Testing the sedimentary impacts of recent moderate earthquakes in different settings in the Western Gulf of Corinth. *6th International INQUA Meeting on Paleoseismology*. This volume.

Bird, P., (2009). Long-term fault slip rates, distributed deformation rates, and forecast of seismicity in the western United States from joint fitting of community geologic, geodetic, and stress direction data sets. *J. Geophys. Res*. 114 (B11), B11403.

Boiselet, A., (2014). Cycle sismique et aléa sismique d'un réseu de failles actives: le cas du rift de Corinthe (Grèce). *PhD Thesis*. ENS, IRSN. France.

Field, E.H., et al., (2013). Uniform California earthquake rupture forecast, version 3 (UCERF3) - The time-independent model. *U.S. Geological Survey. Open-File Report.* 2013-1165, p. 97. California Geological Survey Special Report 228, and Southern California Earthquake Center Publication 1792.

Lambotte, S. et al., (2014). Reassessment of the rifting process in the Western Corinth Rift from relocated seismicity. *Geophys. J. Int.* 197 (3). 1822-1844.

Leonard, M., (2010). Earthquake fault scaling: Self-consistent relating of rupture length, width, average displacement, and moment release. *Bull. Seismol. Soc. Am.* 100, no. 5A, 1971-1988.

Pantosti, D. et al., (2004). Palaeoseismological investigations of the Aigion Fault (Gulf of Corinth, Greece). *Comptes Rendus Geoscience*. 336 (4), 335-342.

Koukouvelas, I. et al. (2005). Slip rates on the Helike Fault, Gulf of Corinth, Greece: new evidence from geoarchaeology. *Terra Nova*. 17 (2), 158-164.

Wells, D.L., & K.J. Coppersmith, (1994). New empirical relationships among magnitude, rupture length, rupture width, rupture area and surface displacement. *Bull. Seism. Soc. America*. 84, 974-1002.

Youngs, R.R. & K.J. Coppersmith, (1985). Implications of fault slip rates and earthquake recurrence models to probabilistic seismic hazard estimates. *Bulletin of the Seismological Society of America.* 75 (4), 939-964.

Youngs, R.R. et al., (2003) A methodology for Probabilistic Fault Displacement Hazard Analysis (PFDHA). *Earthquake Spectra.* 19 (1), 191.

INQUA Focus Group on Paleoseismology and Active Tectonics

paleoseismicity.org

Probabilistic Fault Displacement Hazard Analysis (PFDHA): database that needs to be considered

Serva, L. (1), Livio, F. (2), Gurpinar, A. (1)

(1) Independent consultant
(2) Dipartimento di Scienza ed Alta Tecnologia – Università dell'Insubria, Via Valleggio, 11 22100 Como (CO), Italy.
Email: franz.livio@uninsubria.it

Abstract: *Available interferometric data from recent earthquakes clearly show that major earthquakes produce relatively large crustal deformation over wide areas around the fault. As a consequence, these large areas undergo significant strain and stress that need to be considered in the analysis of seismic and fault displacement hazards for an NPP. Here, we consider probability of surface displacement due to faulting.*

Key words: *PFDHA, InSAR, capable faults.*

INTRODUCTION

It is well-known that only earthquakes above a certain magnitude typically produce surface faulting while all earthquakes produce crustal deformation. When considerable, such crustal (ground) deformation (subsidence and or uplift) is clearly shown by satellite interferometric (InSAR) data. The size and shape of the area affected by deformation depends on the earthquake focal depth, type of faulting, Magnitude and, therefore, on the size of the rupture at the hypocenter. Fig. 1 shows the correlation between Mw and the area of coseismic deformation as shown by interferometric data indicated in Table 1.
For this dataset we checked length and width of the deformed areas located both in the hangingwall and the footwall sectors. For simplicity, the generally elliptical

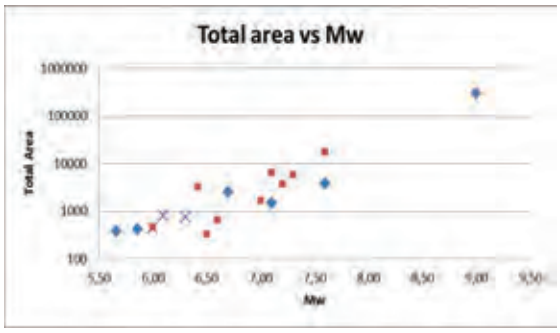

Figure 1: correlation between Mw and total area of deformation (Km^2). Symbols group different fault kinematics: ◊ = thrust; □ = strike slip; X = normal faulting.

Date	Earthquake	Mw	depht	Kin.	HW length (km)	HW width (km)	HW area (kmq)	FW length (km)	FW width (km)	FW area (kmq)	Total area (kmq)	Ref.
06/04/09	L'Aquila	6,30	8,8	N	31,9	16,9	539	25,2	8,6	217	756	Walters et al. (2009)
17/05/93	Eureka	6,10	13	N	32,9	12,7	418	26,9	14,3	384	802	Peltzer & Rosen (1995)
06/06/00	Orta–Cankırı	6,00	8	NL	26,8	16,9	453	0,0	0,0	0	452	Taymaz et al. (2007)
08/11/97	Mainji	7,60	22	SL	166,9	48,1	8035	170,0	56,8	9654	17688	Funning et al. (1997)
12/01/10	Haiti	7,00	13	SL	52,6	14,3	753	45,3	20,6	935	1688	Lepinay et al. (2010)
24/02/04	Al Hoceima	6,50	13	SL	16,5	8,3	137	19,8	9,6	190	327	Cakir et al. (2006)
26/12/03	Bam	6,60	10	SR	24,1	11,3	271	31,7	12,0	379	650	Fialko et al. (2005)
16/10/99	Hector Mine	7,10	0,1	SR	81,0	36,3	2941	131,6	26,2	3444	6385	Simons et al. (2002)
28/06/92	Landers	7,30	1,09	SR	69,5	26,4	1836	86,1	45,5	3911	5746	Massonnet et al. (1993)
24/08/14	Napa Valley	6,00	10	SR	25,4	10,2	258	20,1	10,2	204	462	http://aria.jpl.nasa.gov/node/39
22/02/11	Christchurch	6,42	5	SR	64,0	31,4	2009	55,8	21,9	1220	3229	Elliott et al. (2012)
17/08/99	Izmit	7,40	17	SR	224,4	107,2	24055	236,7	100,8	23864	47919	Delouis et al. (2002)
12/11/99	Duzce	7,20	14	SRN	61,6	27,6	1703	78,5	25,6	2011	3714	Burgmann et al. (2002)
20/05/12	Emilia 1	5,86	5	TH	32,8	12,5	410	0,0	0,0	0	409	Bignami et al. (2012)
29/05/12	Emilia 2	5,66	9,6	TH	32,9	11,3	370	0,0	0,0	0	369	Bignami et al. (2012)
23/10/11	Van	7,10	7,2	TH	33,4	18,1	603	36,9	24,6	909	1511	Dogan & Karakas (2013)
11/03/11	Tohoku	9,00	30	TH	764,0	396,0	302544	0,0	0,0	0	302544	Kobayashi et al. (2011)
08/10/05	Kashmir	7,60	10	TH	69,3	37,4	2589	62,1	20,4	1266	3855	Pathier et al. (2006)

Table 1: Table 1: Earthquake dataset used for the correlation in Fig, 2. Legend: Date, date of the event; Event, name of the event; Mw, Magnitude; Depth, depth of the event; K, kinematics of the fault movement (N= normal, NL = normal left, SL = left-lateral, SR = right-lateral, SRN = right transtensive, TH = thrusting), etc); HW length/width/area: length/width/area of the deformed hangingwall sector; area; FW length/width/area: length/width/area of the deformed footwall sector; Ref:reference used to measurements.

areas have been approximated as rectangles which result in a systematic error of about 20% which do not, however, impact the conclusions.
It is also quite clear that the total area affected by coseismic deformation can be considered a good proxy for earthquake Magnitude even if focal depth remains an important parameter.

DISCUSSION

Considering these earthquake-induced deformation fields we now give a brief summary of the present knowledge about the faults located in these areas. This summary is given in regard to the currently available databases on the primary and secondary (distributed) surface faulting produced by strong earthquakes.
Regarding primary faulting: Fig. 2 represents the state of the art of the correlation between Mw and probability of primary surface faulting after Youngs (2003). A variable threshold Mw value for surface faulting can be assessed, depending on different regression datasets and fault kinematics, however it is clearly visible that the probability of primary surface faulting starts to be significant for values of Mw>5.5-6.0.

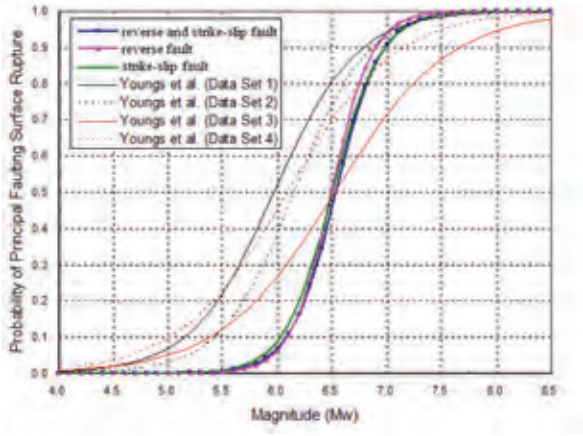

Figure 2: probability curves for primary surface faulting in relation to different earthquake Magnitude (after Youngs et al. 2003).

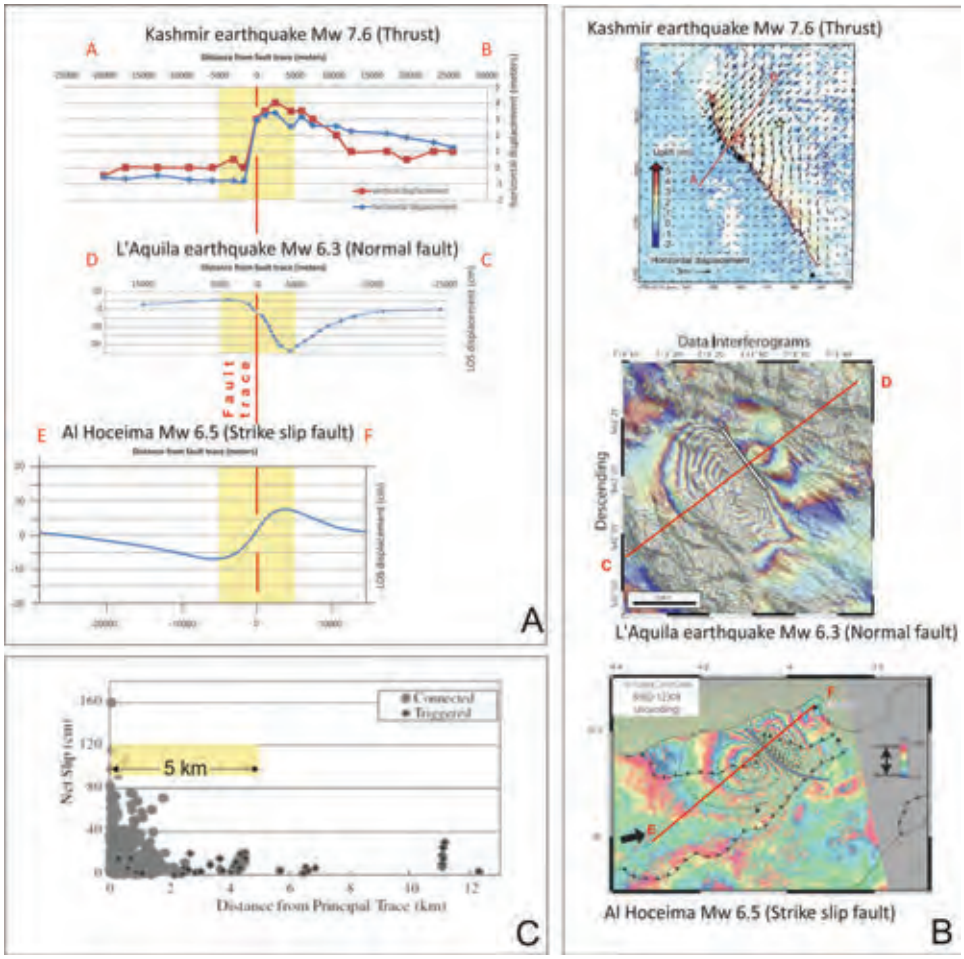

Figure 3: example of coseismic surface deformation across three considered faults of different kinematics. A) surface displacement or InSAR derived LOS displacement profiles; B) section traces; C) distributed secondary-faulting slip against distance from the main fault (after Petersen et al., 2011); note that faulting distribution is considered symmetric on both sides of the fault. Maps are from Pathier et al. (2006), Walters et al. (2009) and Cakir et al. (2006) for the Kashmir, L'Aquila and Al Hoceima earthquakes respectively.

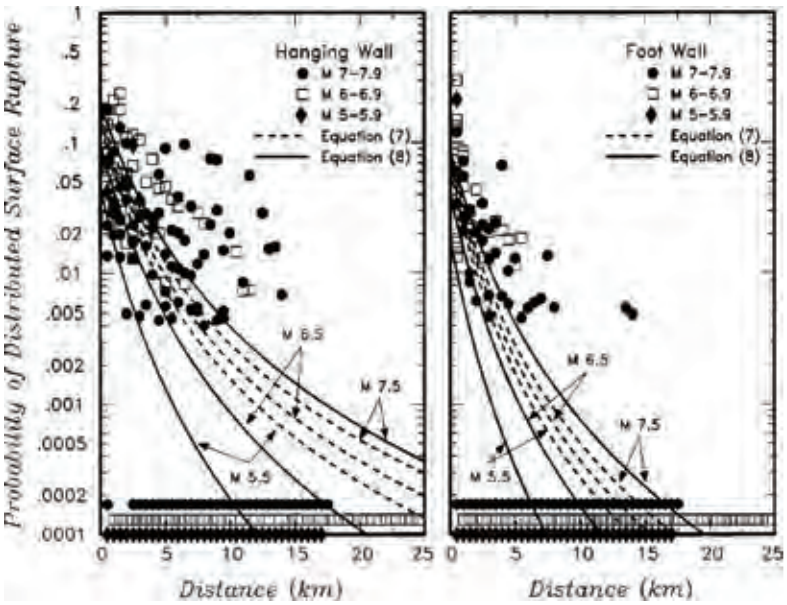

Figure 4: Conditional probability of slip for distributed faulting. Symbols show the rate of occurrence of distributed faulting for individual earthquakes (after Youngs et al., 2003); two different distribution are proposed for hangingweall ans footwall sectors respectively.

The assessment of displacement for distributed faulting is somewhat more complicated. In Fig. 3c the relationship given in Petersen et al (2011) about slip on distributed faulting is reported. This diagram shows the distributed-fault displacement data (labeled as connected) through the net slip as a function of distance from the mapped primary fault. In order to have a better idea of what can happen in the deformed area and, specifically, for the distributed faulting, we have drawn 3 sections showing InSAR-derived coseismic surface displacement (or Line of Sight displacement LOS) and crosscutting a thrust, normal and strike slip fault (Fig. 3a-b). We have highlighted the 5 km buffer distance from the primary fault. This has been done in order to schematically show where, along a transect orthogonal to fault trend, the crust has been more deformed and therefore where, in turn, the probability of surface rupture could be higher.

As clearly visible the trend of the deformation is significantly different from those discussed in Petersen et al (2011) and in Youngs et al (2003), Fig. 4. In particular, we consider that the latter could be significantly different because of the used dataset, derived from the field surveys conducted after strong earthquakes in the last tens of years. These data, although very valuable, are not able to reflect the real

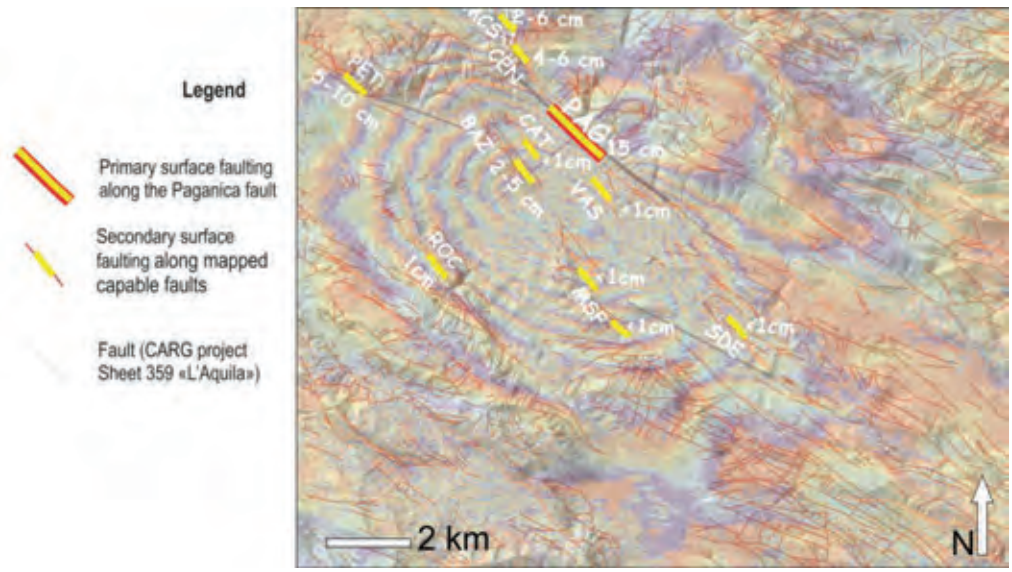

Figure 5: Coseismic reactivation along capable faults induced by the 2009 L'Aquila earthquake (modified, after Guerrieri et al., 2010).

field of distributed faulting mainly because field surveys were done focusing on the primary fault strand and only sporadically on the area affected by distributed faulting. In order to better explain this point, two case studies (L'Aquila eq, 2009; Mw. 6.3 and Niigataken Chuetsu-oki eq. Mw 6.8.) are provided. A synthesis of the L'Aquila earthquake is given here, which, we believe, is one of the best studied recent cases for surface faulting since a careful survey on several well known faults was done after the earthquake by different groups considering also the InSAR data (Guerrieri et al.2010). In Fig. 5 the L'Aquila sheet of the Italian official geological map is presented at scale 1:50000. It is clear that the number of faults that were not surveyed is significant and we believe that this is a common case for most of the areas from where the distributed fault database has been retrieved.

CONCLUSIONS

We believe that the above data and comments should be taken into account in PFDHA. This, in order to give to it a more complete view of what can happen to the distributed faults that are located in the area affected by significant deformation due to strong earthquakes The probability graphs on distributed faulting used at present (Fig.4), may need to be modified on the basis of a more complete dataset as described above.

Acknowledgements: We want to thank Dr. Fiorenzo Fumanti and Dr. Luca Guerrieri for the fruitful discussions and the significant work they did in the preparation of the figures. A special thanks is also for Dr. Antonio Godoy for part of the data regarding the levelling at Kashiwasaki NPP.

References

Bignami, C., P. Burrato, V. Cannelli, M. Chini, E. Falcucci, A. Ferretti, S. Gori, C. Kyriakopoulos, D. Melini, M. Moro, F. Novali, F. Saroli, S. Stramondo, G. Valensise & P. Vannoli, (2012). Coseismic deformation pattern of the Emilia 2012 seismic sequence imaged by Radarsat-1 interferometry. *Annals of Geophysics*. 55 (4).

Bürgmann, R., M.E. Ayhan, E.J. Fielding, T.J. Wright, S. McClusky, B. Aktug, C. Demir, O. Lenk & A. Türkezer, (2002). Deformation during the 12 November 1999 Düzce, Turkey, earthquake, from GPS and InSAR data. *Bulletin of the Seismological Society of America*. 92 (1), 161-171.

Cakir, Z., M. Meghraoui, A.M. Akoglu, N. Jabour, S. Belabbes & L. Ait-Brahim, (2006). Surface deformation associated with the Mw 6.4, 24 February 2004 Al Hoceima, Morocco, earthquake deduced from InSAR: implications for the active tectonics along North Africa. *Bulletin of the Seismological Society of America*. 96 (1), 59-68.

Delouis, B., D. Giardini, P. Lundgren & J. Salichon, (2002). Joint inversion of InSAR, GPS, teleseismic, and strong-motion data for the spatial and temporal distribution of earthquake slip: Application to the 1999 Izmit mainshock. *Bulletin of the Seismological Society of America*. 92 (1), 278-299.

Doğan, B. & A. Karakaş, (2013). Geometry of co-seismic surface ruptures and tectonic meaning of the 23 October 2011, Mw 7.1 Van earthquake (East Anatolian Region, Turkey). *Journal of Structural Geology* 46, 99-114.

Elliott, J.R., E.K. Nissen, P.C. England, J.A. Jackson, S. Lamb, Z. Li, M. Oehlers & B. Parsons, (2012). Slip in the 2010–2011 Canterbury earthquakes, New Zealand. *Journal of Geophysical Research: Solid Earth*. (1978-2012), 117(B3).

Fialko, Y., D. Sandwell, M. Simons & P. Rosen, (2005). Three-dimensional deformation caused by the Bam, Iran, earthquake and the origin of shallow slip deficit. *Nature*. 435 (7040), 295-299.

Funning, G.J., B. Parsons, & T.J. Wright, (2007). Fault slip in the 1997 Manyi, Tibet earthquake from linear elastic modelling of InSAR displacements. *Geophysical Journal International*. 169 (3), 988-1008.

Guerrieri L., G. Baer, Y. Hamiel, R. Amit, A.M. Blumetti, V. Comerci, P. Di Manna, A.M. Michetti, A. Salamon, A. Mushkin, G. Sileo & E. Vittori, (2010). InSAR data as a field guide for mapping minor earthquake surface ruptures: Ground displacements along the Paganica Fault during the 6 April 2009 L'Aquila earthquake. Journal of Geophysical Research. Vol. 115. doi:10.1029/2010JB007579.

Kobayashi, T., M. Tobita, T. Nishimura, A. Suzuki, Y. Noguchi & M. Yamanaka, (2011). Crustal deformation map for the 2011 off the Pacific coast of Tohoku Earthquake, detected by InSAR analysis combined with GEONET data. *Earth Planets and Space*. 63 (7), 621.

Massonnet, D., M. Rossi, C. Carmona, F. Adragna, G. Peltzer, K. Feigl & T. Rabaute, (1993). The displacement field of the Landers earthquake mapped by radar interferometry. *Nature*. 364 (6433), 138-142.

Mercier de Lépinay, B., A. Deschamps, F. Klingelhoefer, Y. Mazabraud, B. Delouis, V. Clouard, Y. Hello, Y. Crozon, B. Marcaillou, D. Graindorge, M. Vallée, J. Perrot, M.P. Bouin, J.M. Saurel, Charvis P. & M. St-Louis, (2011). The 2010 Haiti earthquake: A complex fault pattern constrained by seismologic and tectonic observations. *Geophysical Research Letters*. 38 (22).

Pathier, E., E.J. Fielding, T.J. Wright, R. Walker, B.E. Parsons & S. Hensley, (2006). Displacement field and slip distribution of the 2005 Kashmir earthquake from SAR imagery. *Geophysical Research Letters*. 33 (20).

Peltzer, G. & P. Rosen, (1995). Surface displacement of the 17 May 1993 Eureka Valley, California, earthquake observed by SAR interferometry. *Science*. 268 (5215), 1333-1336.

Petersen M.D., T.E. Dawson, R. Chen, T. Cao, C.J. Wills, D.P. Schwartz & A.D. Frankel, (2011). Fault Displacement Hazard for Strike-Slip Faults. *Bulletin of the Seismological Society of America*. Vol. 101, No. 2, pp. 805-825, April 2011.

Simons, M., Y. Fialko & L. Rivera, (2002). Coseismic deformation from the 1999 Mw 7.1 Hector Mine, California, earthquake as inferred from InSAR and GPS observations. *Bulletin of the Seismological Society of America*. 92 (4), 1390-1402.

Taymaz, T., T.J. Wright, S. Yolsal, O. Tan, E. Fielding & G. Seyitoğlu, (2007). Source characteristics of the 6 June 2000 Orta-Çankırı (central Turkey) earthquake: a synthesis of seismological, geological and geodetic (InSAR) observations, and internal deformation of the Anatolian plate. *Geological Society, London*. Special Publications. 291(1), 259-290.

Youngs, R.R., W.J. Arabasz, R.E. Anderson, A.E. Ramelli, J.P. Ake, D.B. Slemmons, J.P. McCalpin, D.I. Doser, C.J. Fridrich, F.H. SwanIII, A.M. Rogers, J.C. Yount, L.W. Anderson, K.D. Smith, R.L. Bruhn, L.K. Knuepfer, R.B. Smith, C.M. de Polo, K.W. O'Leary, K.J. Coppersmith, S.K. Pezzopane, D.P. Schwartz, J.W. Whitney, S.S. Olig & G.R. Toro, (2003). A methodology for probabilistic fault displacement hazard analysis (PFDHA). *Earth. Spectra*. 19,191-219

Walters, R.J., J.R. Elliott, N. D'Agostino, P.C. England, I. Hunstad, J.A. Jackson, B. Parsons, R.J. Phillips & G. Roberts, (2009). The 2009 L'Aquila earthquake (central Italy): A source mechanism and implications for seismic hazard. *Geophysical Research Letters*. 36 (17).

INQUA Focus Group on Paleoseismology and Active Tectonics

Tectonic deformation study of the Great Sumatera Active Fault (Semangko Segment)

Setiawan, J.H., Sopian, Y., Soehaimi, A.

Geological Agency, Ministry of Energy and Mineral Resources Indonesia, 57 Diponegoro Street, Bandung, Indonesia.
Email: jhsetia@gmail.com

Abstract: *The subduction thrust between oceanic Indian-Australia (IA) and continent Euroasian (EA) plates is the major dynamic agent of the tectonic deformation in the Sumatera Island, especially along the Great Sumatera Fault Zone (GSFZ). Some results of the geodetic monitoring on the Semangko fault segment, West Lampung Province, along the GSFZ are shown here. The effect of subduction-related deformation is represented by the KNAT benchmark that relatively moves toward NE, at a velocity of 30 mm/y. Between the towns of Liwa and Kotaagung, the SALW benchmark shows that the western block of the fault relatively moves toward NW at a velocity of 26 mm/y. The eastern block relatively moves southwards, as shown by AGNG benchmark at a velocity of 15 mm/y. The PDNG benchmark, which is located north of AGNG, relatively moves toward NW at a velocity of 13 mm/y. The different directions and velocities of the benchmarks between the west and east blocks across the Semangko Fault Segment confirm the Great Sumatera Fault move right-laterally at a rate of ca. 4 cm/y. Also the focal mechanisms of the 1933 and 1994 earthquakes confirm this dominant kinematics.*

Key words: *Geotectonic Deformations, GPS Monitoring.*

INTRODUCTION

The Sumatera fault is the most active and hazardous seismic source zone in the Sumatera Island, after the subduction zone, whose earthquakes can reach extreme magnitudes, as occurred in 2004 (e.g., Lay et al., 2005). Therefore, the seismogenetic studies along this fault are of great relevance for seismic hazard assessment. The deformation study by GPS monitoring introduced here is an important contribution to the aim above, since it provides a quantitative estimate of slip movement. This quantitative value contributes to evaluate the maximum potential magnitude and possibly point out particularities in the strain field.

REGIONAL TECTONICS

The tectonic deformation process in Sumatera Island is caused by the subduction of the oceanic Indian-Australian (IA) plate beneath the continental Euroasian plate (EA).

The subduction thrust along the EA-IA boundary is mainly controlled by the 5000 km long Andaman-Sunda-Java trench (Fig. 1). As a response to the arc-shaped trench, the EA-IA plate convergence becomes increasingly oblique from south (Java) to north (Andaman Islands). Offshore Java, the direction of convergence is perpendicular to the trench strike; offshore Sumatra, the subduction of IA plate beneath the EA plate is more complex; the direction of convergence becomes progressively oblique to the trench strike; relative movements of the two plates are partitioned into nearly arc-perpendicular thrusting at the trench and arc-parallel, right-lateral slip on the GSFZ (Figure 2) (Fitch, 1972; McCaffrey, 1991, McCaffrey et al., 2000). North of Sumatra, the GSFZ transitions into the Andaman back-arc spreading center complex (McCaffrey et al., 2000). This marks the eastern extent of the developing Andaman/Burma microplate (DeShon et al., 2005).

The major subduction systems that extend through this region have been modeled by Gudmundsson and Sambridge (1998). Major changes in slab-dip occur and define kink zones that range in plunge from oblique to nearly orthogonal to the local strike direction of each slab. The subducting slab beneath the Sunda-Banda arc indicates a pronounced curve from Sumatra, where it dips ~30° to 45° NE, through Java and Nusa Tenggara, where it dips ~50° to 70° N, to the Banda Islands, where it forms a concave spoon-shaped structure with an axis that plunges ~40° toward the west.

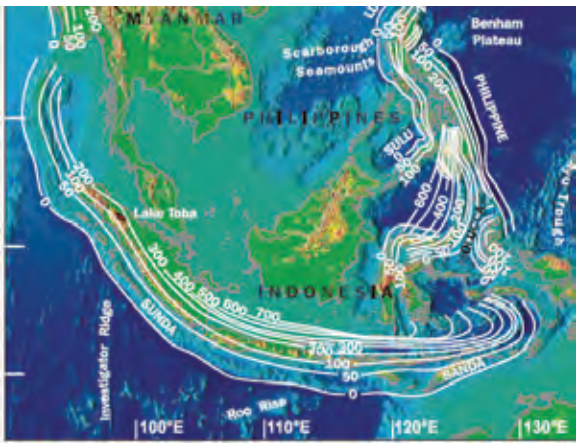

Figure1: Subduction slab topology model for Southeast Asia and the west Pacific. (Compiled from Gudmundsson and Sambridge (1998), with minor modification in Japan from Baba et al. (2002). Digital topography and bathymetry models are from the U.S. National Geophysical Data Center (http://www.ngdc.noaa.gov). (After Garwin et al., 2005, modified).

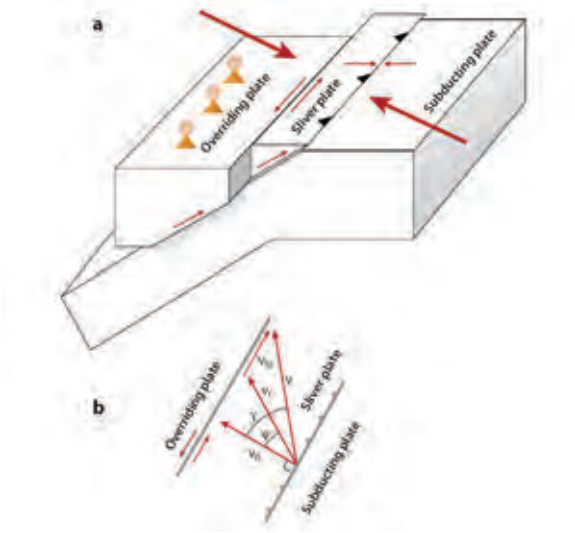

Figure 2. Block diagram showing the geometry of the sliver plate and its motion under conditions of oblique subduction (The nonorthogonal (oblique) motion of the subducting plate under the overriding plate imparts along-strike shear stress at its base, which can detach the leading edge of the overriding plate forming the so-called sliver plate. The sliver plate slides laterally relative to the upper plate along a strike-slip fault (e.g., Sumatran fault) and thrusts over the subducting plate. (b) The vector geometry of such a system. Total relative motion vector V, direction of Vss (the strike-slip vector) from fault orientation, and azimuth of Vt (the thrust vector) from earthquake slip vectors allow a unique solution to the triangle formed by V, Vt, and Vss, providing estimates of the magnitudes of Vt and Vss. ψ is the slip vector obliquity, γ is the convergence obliquity, and Vn is the velocity normal to the trench (After McCaffrey 2009).

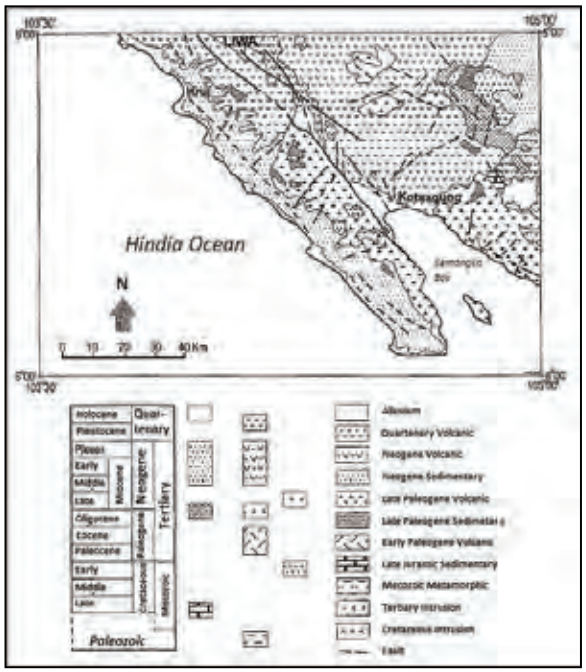

Figure 3: Geological Map of West Lampung District (Amin, et al., 1993).

Geology of Sumatera Active Fault (Semangko Segment)

The geology along the GSFZ (Semangko Segment), based on Amin et al. (1993), consists of volcanic, intrusive, metamorphic and sedimentary rocks. The oldest formations belong to Paleozoic and Mesozoic (metamorphic, intrusive and sedimentary rocks). The Neogene formations are made of volcanic, intrusive and sedimentary rocks. The youngest deposits are Quaternary volcanic products and continental sediments (Figure 3).

The Great Sumatera fault in this region is marked by typical strike-slip morphostructures (fault scarps, elongated valleys and ridges, right lateral displacement of ridges and valleys, small to big sagponds, pull-apart lakes). Fault kinematic indicators (shear and tension joints, gash/shear fractures, slickensides) confirm the fault kinematics with a maximum compression axis running SW - NE.

GEODETIC MEASUREMENT

The GPS data used in this research result from episodic monitoring. Figure 4 shows the distribution of the GPS benchmarks. The duration of each GPS episodic monitoring is 2 doy (day of year), for a minimum of 8 hour per day as shown in Table 1. The vector displacements for each GPS benchmark have been calculated using the software Garmit 10.4. For some stations, the registration time was insufficient to obtain robust solutions. The present vector displacements have been combined with previous vector displacements. The resulting vector displacement estimations are shown in Figure 5 and listed in Table 2.

The Semangko Segment of the GSFZ slips right-laterally, with a relative motion of the western block toward NW with average velocity of 26 mm/y, while the eastern block moves toward SE by 15 mm/y.

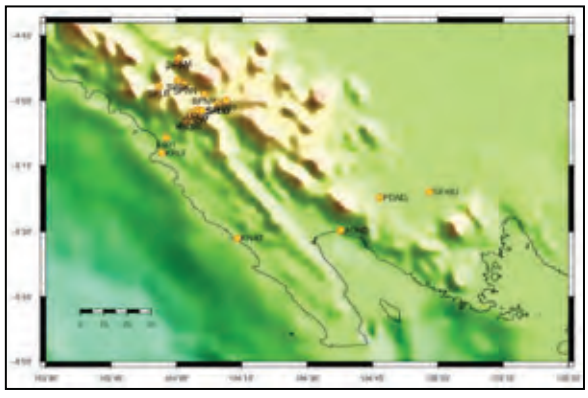

Figure 4: Distribution of benchmarks for episodic GPS monitoring in the West Lampung Province.

INQUA Focus Group on Paleoseismology and Active Tectonics

Table 1: Coordinates and duration of GPS monitoring.

GPS Station	DOY	Longitude (° east)	Latitude (° south)	Time started	Time ended	Duration of record	Location of GPS Station
BPNP	119	104.1051	-4.9757	7:21:15	23:59:55	16:38:40	BPN Padang Dalam
	120			0:00:00	6:33:50	6:33:50	BPN Padang Dalam
	187			7:27:15	23:59:55	16:32:40	BPN Padang Dalam
	188			0:00:00	3:00:45	3:00:45	BPN Padang Dalam
HTPS	119	104.0049	-4.8456	3:15:10	23:59:55	20:44:45	Hotel Pusri
	120			0:00:00	1:55:05	1:55:05	Hotel Pusri
K601	112	103.9607	-5.1430	3:42:20	23:59:55	20:17:35	K601
	113			0:00:00	2:25:00	2:25:00	K601
	186			6:06:15	23:59:55	17:53:40	K601
	187			0:00:00	4:46:30	4:46:30	K601
K602	112	104.0378	-5.0758	4:42:45	23:59:55	19:17:10	K602
	113			0:00:00	3:09:40	3:09:40	K602
	186			7:48:40	23:59:55	16:11:15	K602
	187			0:00:00	6:09:35	6:09:35	K602
KRLW	121	104.0699	-5.0467	1:15:30	9:35:55	8:20:25	Kolam Renang Liwa
	122			0:56:40	9:24:00	8:27:20	Kolam Renang Liwa
KRUI	112	103.9435	-5.2016	2:44:50	23:59:50	21:15:00	SMA Krui
	113			0:00:00	1:49:40	1:49:40	SMA Krui
	186			5:09:20	23:59:50	18:50:30	SMA Krui
	187			0:00:00	4:17:20	4:17:20	SMA Krui
LPLW	121	104.0814	-5.0356	3:24:15	10:44:45	7:20:30	Lapang Liwa
	122			1:21:45	9:37:40	8:15:55	Lapang Liwa
PTNB	108	104.0519	-5.0711	2:09:25	23:59:55	21:50:30	Pos TNBBS
	109			0:00:00	1:28:10	1:28:10	Pos TNBBS
SALW	108	104.0988	-5.0389	1:30:50	23:59:50	22:29:00	SMA Liwa
	109			0:00:00	1:45:00	1:45:00	SMA Liwa
	187			6:50:30	23:59:55	17:09:25	SMA Liwa
	188			0:00:00	2:29:15	2:29:15	SMA Liwa
SDSM	106	104.0090	-4.8342	4:12:20	23:59:50	19:47:30	SD Sukamarga
	107			0:00:00	2:58:40	2:58:40	SD Sukamarga
SPB1	119	104.1894	-4.9998	5:09:20	23:59:50	18:50:30	SMP Belalau0
	120			0:00:00	4:32:00	4:32:00	SMP Belalau0
SPBL	108	104.1571	-5.0132	1:01:00	23:53:55	22:52:55	SMP Belalau
	109			0:00:40	1:16:50	1:16:10	SMP Belalau
SPLB	106	103.9328	-4.9467	2:23:20	23:59:55	21:36:35	SMP N Lombok
	107			0:00:00	1:24:20	1:24:20	SMP N Lombok
SPRN	106	104.0329	-4.9373	3:13:20	23:59:55	20:46:35	SMP Ranau
	107			0:00:00	2:13:10	2:13:10	SMP Ranau
	187			8:29:50	23:59:50	15:30:00	SMP Ranau
	188			0:00:00	3:56:30	3:56:30	SMP Ranau
SPSK	121	104.0049	-4.9225	2:17:10	23:59:50	21:42:40	SMP N 4 Sukau
	122			0:00:00	2:09:30	2:09:30	SMP N 4 Sukau
APRO	106	107.9488	-6.4294	12:17:00	23:59:30	11:42:30	
	107			0:00:30	10:28:00	10:27:30	

Table 2: Results of vector displacement estimate of each GPS monitoring station.

Name of GPS Station	Longitude (°)	Latitude (°)	Vel.East(m/y)	Vel.North (m/y)	Sd.Vel.East (m/y)	Sd.Vel.North (m/y)
KRUI	103.9435	-5.2016	-0.0229	0.0122	0.0015	0.0013
SALW	104.0988	-5.0389	-0.0252	0.007	0.0016	0.0014
AGNG	104.6279	-5.4954	0.0115	-0.0157	0.0013	0.001
PDNG	104.7778	-5.3728	-0.0126	0.0052	0.0017	0.0015
SEWU	104.9686	-5.3511	0.043	-0.0017	0.0019	0.0016
KNAT	104.2332	-5.5259	0.0021	0.0303	0.0016	0.0012

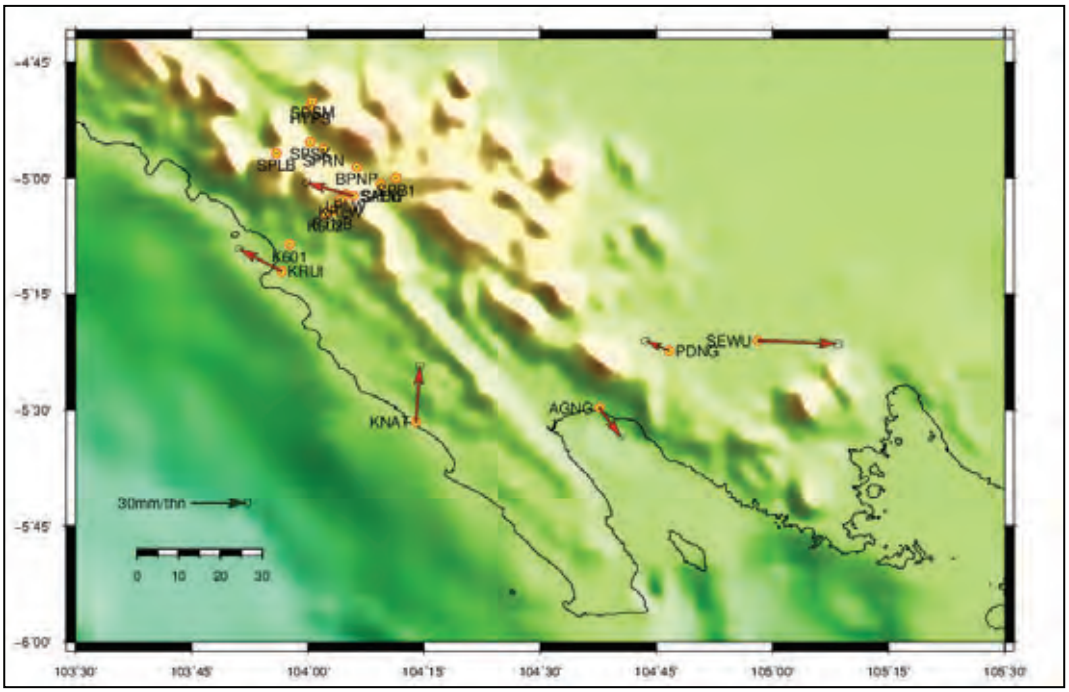

Figure 5: Displacement vectors from GPS monitoring in Lampung. Scale of vector is 30 mm/y, ellipse scale of standard deviation is 1.5 mm.

CONCLUSIONS

The GPS benchmarks in southeastern Sumatera island show two main directions of movement. The displacement shown by station KNAT toward NE is in agreement with the subduction of the oceanic Indian-Australian (IA) plate beneath the continental Euroasian plate (EA). The other deformation is controlled by the slip along the Great Sumatera Fault. The GPS benchmark stations KRUI and SALW, located on the west block of the fault move toward NW, while the GPS stations AGNG and SEWU, located on the eastern block, move toward SE. However, PDNG appears to move slowly north-westerly. Based on the average velocity rate from all the benchmarks, the right lateral slip along the investigated section of the GSFZ is about 4 cm/y.

Acknowledgements: The authors wish to thank the Preparatory Committee of the 6th International INQUA Meeting on Paleoseismology, Active Tectonics and Archeoseismology (PATA-Days) in Fucino, Italy, and all their colleagues in the Quaternary Working Group of the Geological Survey Institute, Geological Agency, Ministry of Energy and Mineral Resources for their contributions on seismotectonics and active fault research in South Sumatera.

References

Amin, T.C., Sidarto, S. Santosa and W. Gunawan, (2010). *Geological Map of West Lampung District Scale 1:250.000*. Geological Research and Development Centre of Indonesia.

Baba, T., Y. Tanioka, P.R. Cummins, and K. Uhira, (2002). The slip distribution of the 1946 Nankai earthquake estimated from tsunami inversion using a new plate model. *Physics of the Earth and Planetary Interiors*. 132, 59-73.

DeShon H.R., E.R. Engdahl, C.H. Thurber, M. Brudzinski, (2005). Constraining the boundary between the Sunda and Andaman subduction systems: Evidence from the 2002 Mw 7.3 Northern Sumatra earthquake and aftershock relocations of the 2004 and 2005 great earthquakes. *Geophys. Res. Lett.* 32 (24). doi: 10.1029/2005GL024188.

Department of Earth Atmospheric and Planetary Sciences, MIT (2010). GAMIT and GLOBK home page.

Fitch, T.J., (1972). Plate convergence, transcurrent faults, and internal deformation adjacent to Southeast Asia and the western Pacific. *J. Geophys. Res.* 77, 4432-4460.

Gudmundsson, O., M. Sambridge, (1998). A regionalized upper mantle (RUM) seismic model. *J. Geophys. Res.* 103, B, 7121-7136.

Garwin S., R. Hall, Y. Watanabe, (2005). Tectonic Setting, Geology, and Gold and Copper Mineralization in Cenozoic Magmatic Arcs of Southeast Asia and the West Pacific. *Economic Geology 100th Anniversary Volume.* 891-930.

Lay, T., H. Kanamori, C. Ammon, M. Nettles, S. Ward, R. Aster, S. Beck, S. Bilek, M. Brudzinski, R. Butler, H. DeShon, G. Ekström, K. Satake, S. Sipkin, (2005). The Great Sumatra-Andaman Earthquake of 26 December 2004. *Science*. 308, 1127-1133.

McCaffrey, R., (1991). Slip vectors and stretching of the Sumatran fore arc. *Geology*. 19, 881-884.

McCaffrey, R., P.C. Zwick, Y. Bock, L. Prawirodirdjo, J.F. Genrich, C.W. Stevens, S.S.O. Puntodewo & C. Surabaya, (2000). Strain partitioning during oblique plate convergence in northern Sumatra: geodetic and seismologic constraints and numerical modeling. *J. Geophys. Res.* 105 (B12), 28, 363-28, 376.

McCaffrey, R., (2009). The Tectonic Framework of the Sumatran Subduction Zone. *Annu. Rev. Earth Planet. Sci.* 37, 345-66.

INQUA Focus Group on Paleoseismology and Active Tectonics

Analysis of faulted paleosol sequences in the Palomares Fault Zone (Betic Cordillera, SE Spain): Paleoseismological and Climatic implications

Silva, P.G. (1), Roquero, E. (2), Rodríguez-Pascua, M.A. (3), Bardají, T. (4), Carrasco-García, P. (5), Huerta, P. (1), J.L. Giner-Robles (6), Zazo, C. (6), Goy, J.L. (1)

(1) Dpto. Geología, Universidad de Salamanca, Escuela Politécnica Superior, Ávila, Spain. Email: pgsilva@usal.es
(2) Dpto. Edafología. E.T.S.I. Agrónomos. Universidad Politécnica de Madrid, Madrid, Spain
(3) Instituto Geológico y Minero de España, IGME, Madrid, Spain
(4) U.D. Geología. Universidad de Alcalá. Alcalá de Henares (Madrid), Spain
(5) Dpto. Ingeniería del Terreno, Universidad de Salamanca, Escuela Politécnica Superior, Ávila, Spain
(6) Dpto. Geología y Geoquímica, Universidad Autónoma de Madrid, Cantoblanco, Madrid, Spain
(7) Dpto. Geología, Museo Nacional de Ciencias Naturales (CSIC), Madrid, Spain

Abstract: *We use offset paleosols as earthquake horizon events and soil development as a relative timing-clock tool in the natural exposures of the strike-slip Palomares Fault (PLF) located at La Escarihuela (Murcia, SE Spain). The section records eight paleosols on overlapped Pleistocene alluvial-colluvial deposits vertically displaced 21 and 12 cm (33 cm) by the fault, evidencing two recurrent surface faulting events with net slip rates of c. 1 m (6 Mw). Comparing soil features (soil thickness, spacing, Bt thickness, clay and carbonate contents) with the conventional Oxygen Isotopic Stages (OIS) establishes paleoclimatic relationships and a relative time-scale for soil development and faulting on the basis of regional geochronological proposals on alluvial fan development.*

Key words: *Paleosols, Soil development, Surface faulting, Palomares fault, Betic Cordillera, Spain.*

INTRODUCTION

Natural fault exposures and fault-trench analyses are devoted to unravel the paleoseismic history of surveyed faults by means of the identification of discrete earthquake event horizons. In this work, a well-preserved sequence of offset paleosols in the natural exposures of the strike-slip Palomares Fault (PLF; SE Spain) are used as earthquake horizon events. Soil analyses help to determine soil development throughout time, by means of soil granulometry, clay and $CaCO_3$ contents and soil morphological properties (genetic horizon, thickness, Munsell color, etc.). These pedological parameters help to establish soil development, used as a relative time tool to compare soil development with the Middle-Late Pleistocene climatic cycles (Oxygen isotopic Stages: OIS) to unravel relative time-horizons for the recorded surface faulting events. The studied site is located on the trace of the PLF fault-zone bounding the eastern boundary of the Eastern Betics Shear Zone (EBSZ; Silva et al., 1997). Together with the well-known Lorca-Alhama de Murcia Fault (LAF), the PLF works as the second master fault-zone, of this crustal-scale structure in the Murcia Region (Silva et al., 1993, SE Spain). The PLF is credited with being the first fault within the Betic Cordillera to be scientifically recognized, with Quaternary activity by Bousquet (1976) at the site of Palomares (Almería Region; Fig. 1).

Figure 1: Location of the Palomares Fault (PLF) and surveyed sites (black circles) in relation with the Eastern Betics strike-slip faults and main localities. White dotted line indicate cross-section of figure 2.

THE PALOMARES FAULT

The Palomares fault in the Murcia region bound the eastern margin of the Guadalentín Depression SE Lorca, constituting the Almenara Mountain Front about 12 km east of the Las Estancias range-front fault controlled by the LAF (Silva et al., 2003). In this sector the PLF fault zone, 29 km long and 2 km wide displays three main fault traces stepping the Almenara front piedmont (Fig.

1). In this zone, these three main fault strands generate linear surface faulting of consistent N10-20 E orientation displaying transtensional and transpressional features in relation to the dominant left-lateral strike slip kinematics displayed by the PLF (Silva et al., 2003). These kinematics give place to the generation of intervening lineal tectonic reliefs and fault scarps with metric offsets (Silva et al., 1997).

The studied zone, located 12 km east of Pto. Lumbreras (Fig. 1), display tree main sites in which offset of alluvial fan sedimentary sequences and/or surfaces occur. These presently are visible as degraded normal fault scarps along the N012 PLF2 trace. This fault strand displays a visible rupture length of 12.8 km from the Locality of Pulpí (south) to the Aljibejo zone (north), distributed in small "en echelon" segments, 3.8 to 2.3 km long (Figs. 1, 2). In the northern zone, east-facing fault scarps are nearly buried by a colluvial wedge which contributes to the gentle slope of the present topographic step and indicates the old age of the surface rupture features (Fig. 2). These east-facing fault scarps cut Late (ABJ1 Site) to Middle Pleistocene (ABJ2 Site) fan surfaces, which show a mature and weak calcrete development respectively, of Km massive petrocalcic horizons 0.6 (ABJ1) to 1.2 m thick (ABJ2).

Recent dating of fan surfaces in the zone of Goñar, about 15 km west in the LAF Mountain front (Shobatti et al., 2011; Ortuño et al., 2012), establishes relationships between age and existing models of calcrete and alluvial fan development for the zone (Alonso-Zarza et al., 1999; Silva, 2014). These relationships indicate that old mature calcretes in the ABJ2 site hold a minimum age of c. 300 ka (OIS 9; Middle Pleistocene). Calcrete fan surfaces at the ABJ1 site are less developed, displaying only massive Ck petrocalcic horizons, presumably formed during onset of the Late Pleistocene, c. 120 - 110 ka BP (OIS 5), according to geochronological data provided by Ortuño et al., (2012).

A third site is La Escarihuela (Figs. 1, 2) located in the western strand of the fault (PLF3). This site displays nice exposures of faulted alluvial-soil sequences sealed by a thick undisturbed calcrete (Fig. 3), similar to that faulted by the PLF2 at the ABJ2 site. Therefore the underlying faulted sequence (c. 4 m thick) is older than c. 300 ka (OIS 9). The sequence is composed by repeated colluvial and alluvial deposits mainly derived from the adjacent Linear tectonic relief of Cabezo del Muro (Figs. 1, 2). This is important since this tectonic relief linked to the PLF2 strand, shuttered the drainage from the main mountain front developed along the PLF1 strand (Silva et al., 1997; Fig. 2).

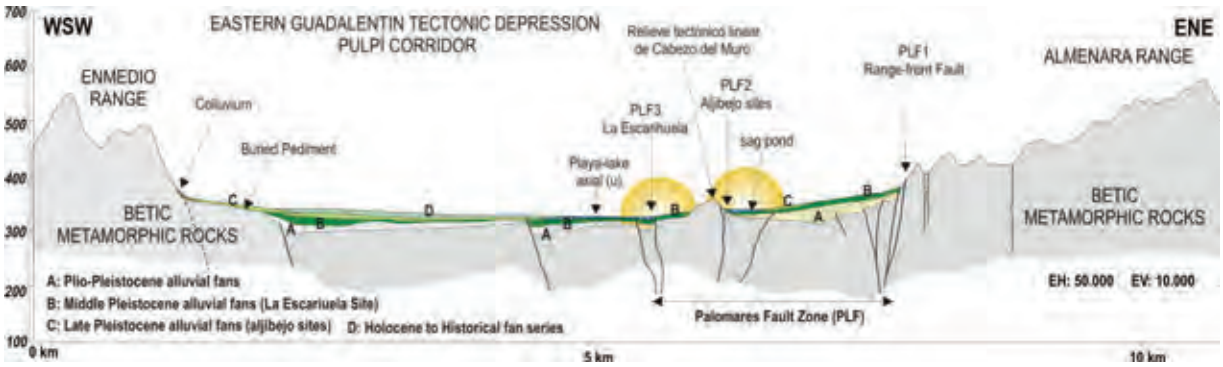

Figure 2: Synthetic cross-section displaying the main topographic features and sedimentary units affected by the various fault strands of the Palomares Fault Zone (PLF) around the site studied in this work. Note different fault strands PLF1 to PLF3.

Consequently, the lower portion of sedimentary sequence at La Escarihuela only was sourced from a really limited narrow catchment, 55 m high, 300 m wide and 2.3 km long (c. 0.7 km^2). Therefore the faulted paleosoil sequence analyzed in this study, represents a time-condensed alluvial sequence recording Middle Pleistocene climatic conditions and changes in SE Spain. In addition, the soil sequence provides a relative chronological framework to explore the timing of past surface faulting events.

SOIL-DEVELOPMENT AND FAULTING EVENTS (LA ESCARIHUELA SITE)

La Escarihuela site records eight paleosols (top Ps1 to basal Ps8) on alluvial-colluvial deposits (Fig.3). They are affected by at least three near vertical N10-20E faults with accumulated vertical offsets of 12 and 33 cm (Fig. 3). Comparing these different fault offsets it is possible to discern two paleoseismic events with a vertical displacement per event of 21 cm (Event 1) and 12 cm (Event 2). Event 1 affects the lower paleosols Ps8 to Ps5, recording true surface faulting. Event 2 affects nearly the entire sequence up to paleosol Ps2 (ground flexure), produced by blind reverse faulting (Ps4 to Ps2; Fig. 3).

In both events dominant left-lateral oblique-reverse kinematics dominated as evidenced by sub-horizontal fault plane striae (10-11º) orientations and nice positive flower structures. The last, produced during the second event affecting the indurate Ck horizon in Ps3 and the whole Ps2 soil profile (Fig. 3). 10-11º N172E pitch striae, indicate net left-lateral oblique slips of 234 ± 5 cm (Event 1) to 162 ± 6 cm (Event 2). These fault slip values suggest the record of two recurrent events with

estimated magnitudes of c. 5.9 Mw ± 0.2 and 6.4 Mw ± 0.3 respectively. As above-mentioned, the PLF3 fault trace at La Escarihuela is sealed by a massive clacrete (BKm) about 300 ka old.

The paleosol sequence develops on overlapped sedimentary units, 50 to 20 cm thick, indicating alternating stages of soil formation and sedimentation (Fig. 3).

Two great soil-units can be observed in the section, related to soil evolution and environmental conditions: (a) the upper calcrete profile Ps1; and (b) a lower unit formed by superposition of several similar paleosols featuring by argillic reddish to brown Bt horizons (5YR5/4d, 5YR4/4m) overlying calcic Bk to Ck horizons ($CaCO_3$. 20 - 30%) consisting of the Paleosols Ps2 to Ps8. In the three upper soils of the lower unit (Ps2 to Ps4), Bk/Btk calcic horizons originated with the recalcification of existing argillic horizons, giving place to a colour lightening (5YR 6/3d, 5/4m) associated with significant $CaCO_3$ content about 8-12% (Fig. 3). To a minor extent, Ps5 is also affected by these recalcification processes. In any case, the entire soil sequence evolves upwards to more arid conditions evidenced by increasing accumulation of carbonate on the original argillic horizons. Increasing aridification promoted the superposition of different pedogenetic cycles responsible for the recalcification of underlying paleosols, specially from the Ps3, a prominent Ck horizon marking the clear onset of more arid conditions in the area (Fig. 3).

Clay content is variable throughout the sequence, but soil colours are similar, since they are mainly inherited from previous well-developed red soils (2,5YR 4/6d, 3/6m) on the adjacent metamorphic source area. In fact, the basal red soil (Ps8), developed on breccias-like colluvial deposits, display the highest soil-clay (< 0,002 mm) percentages for the sequence (c. 40%) and a high degree of rubefaction. Ps8 incorporates a large amount of deep-weathered phyllites coming from the source area (Cabezo del Muro) favouring clay particle formation subject to subsequent illuviation over a long pedogenetic period. Ps7 is a well-defined Bt horizon, overlying and maybe reworking the first 5-8 cm Ps8. In any case the clay content of Ps7 declines to a value of 10% (Fig.3), and clay contents are not recovered through the whole series, with values generally down to 10%.

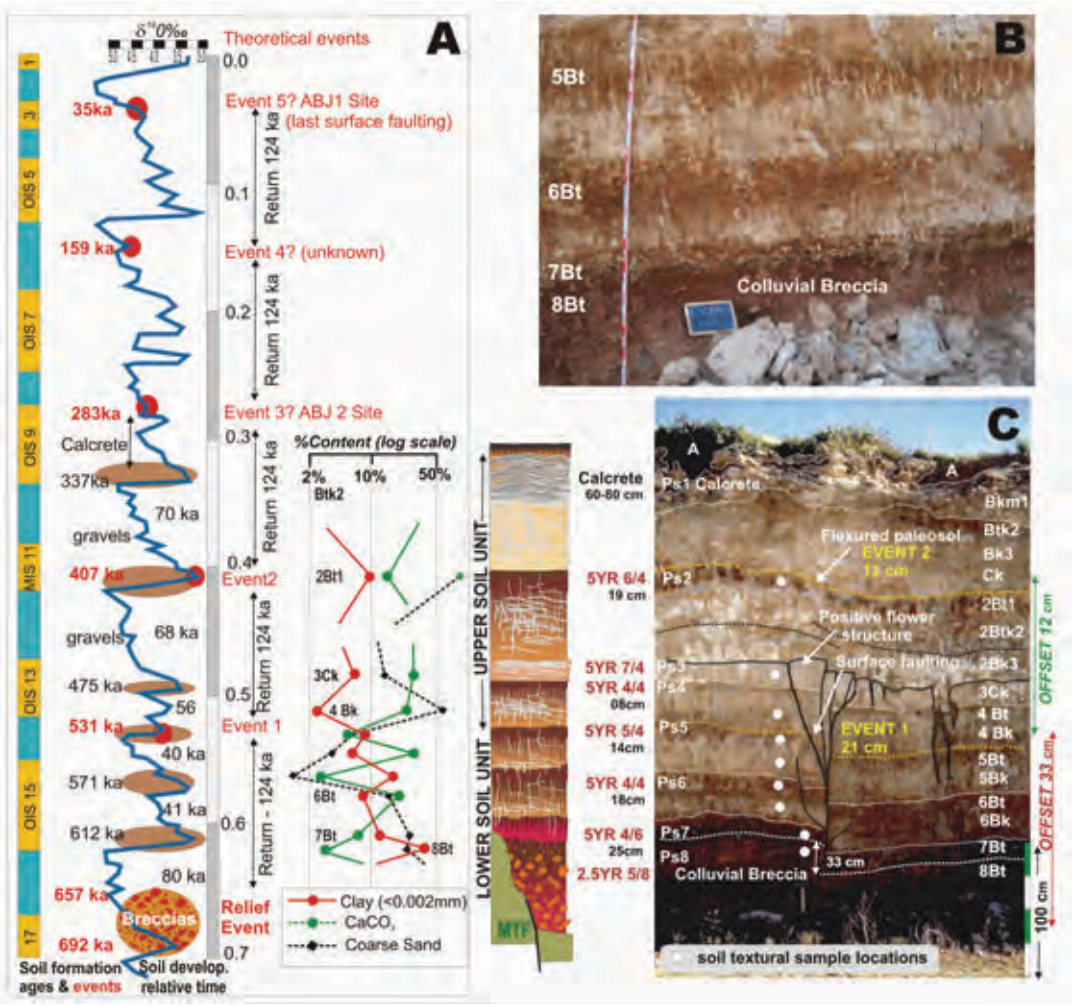

Figure 3: A: OIS Conventional climatic curve compared with stages of soil development, textural soil data-sequence (logarithmic scale) and recorded paleoseismic events at La Escarihuela Site. B: Detail of reddish-brown alluvial soils of the lower unit. C: Recurrent reverse faulting of the entire soil sequence discussed in the text (Palomares Fault Zone, Murcia Region).

This means, that in spite of the noticeable reddish colours of the Bt horizons (mainly inherited), pedogenic clay illuviation didn`t last for long periods as evidenced by low clay contents. In any case, the increasing pedogenic accumulation of carbonate troughout time is encompassed by a decreasing trend on clay illuviation linked to progressive aridification.

The last reddish alluvial soil of the sequence is Ps2, developed on gravel-channel deposits coming from the main Mountain Front (Fig. 2). This soil has a variable thickness, but displays a well-developed Bt horizon (2Bt1 in Fig.3) of similar features than those displayed by Ps5 and Ps6. All the alluvial reddish soils developed in the sequence are linked to typical Mediterranean climatic condition, but showing a progressive aridification throughout time. In fact the soil sequence is topped by Ps1 featuring the development of a thick mature calcrete horizon (Bkm), indicating the onset of extreme arid conditions (Fig. 3). Younger, alluvial fan surfaces feature the absence of reddish-soils and development of petrocalcic horizons with different stages of development. Recent dating in the region (Ortuño et al., 2012), indicate that calcrete development on alluvial sediments lasted till the Last Interglacial Period (OIS 5; Silva, 2014).

CONCLUSIONS

Soil textural analyses from the various units (Fig.3) clearly indicate altering stages of clay illuvation (Bt horizons; wet periods) and carbonate leaching and precipitation (Btk, Bk, Ck; dry periods). Comparing soil features with the conventional OIS scale establishs relative paleoclimatic relationships and a relative time-scale for soil development. Considering an age of c. 330 ka (OIS 9) for the top calcrete horizon, peaks of clay illuviation have been adjusted to OIS warm stages. The results indicate that the complete sequence of paleosols developed between c. 612 ka (MIS 15) and c.337 ka (MIS 9), with peaks of soil formation during warmer isotopic stages: OIS 15, 13 and 11 (lower unit), and eventually OIS 9 (Upper unit). The Btk2 horizon of Ps1 is the last reddish soil developed in the zone, after which calcrete formation dominates. Calcrete developed at least during all this warm isotopic stage between c. 337 – 280 ka (Fig. 3).

These relative time-climatic correlations date the paleoseismic events in c. 531 ka (Event1) and 407 ka (Event 2) with a recurrence period of c. 124 ka. This suggest that surface faulting events recorded at the Aljibejo sites (Figs1, 2) occurred after 283 ka (ABJ2 Site) and about 35 Ka (ABJ1 Site). An intervening (unknown) event probably occurred around c. 159 ka (Fig.3). Taking into account that vertical offset of ABJ2 (2.1m) is twice that of the ABJ2 (1.1 m), very probably the unknown event accumulated in the ABJ2 fault scarp.

Research is ongoing in the zone. Geophysical prospecting and fault trenching analyses will be developed in the Aljibejo sites during 2015. These future data will hopefully help to the completion and dating of a detailed, more recent fault-rupture history. Preliminary 2D Electric Tomography profiles in the Aljibejo sites indicate apparent faulting on calcrete surfaces of the OIS 5 presently buried by the most recent playa–lake sediments in the Aljibejo area.

Acknowledgements: Work funded by the Spanish Research Projects CGL2012-37581-C02-01 (QTECT BETICA - USAL), CGL2012-33430 (CSIC). This work is a contribution of the Spanish Working Group of the INQUA TERPRO Project 1299 (EEE Metrics).

References

Alonso Zarza, A.M., P.G. Silva, J.L. Goy, C. Zazo, (1998). Fan-surface dynamics, plant-activity and calcrete development: Interactions during ultimate phases of fan evolution in the semiarid SE Spain (Murcia). *Geomorphology*. 24, 147-167.

Bousquet, J.C., (1979). Quaternary strike-slip faults in southern Spain. *Tectonophysics*. 52, 277-286.

Ortuño, M., E. Masana, E. García-Meléndez, J.J. Martínez-Díaz, C. Canora, P. Štepancíková, P. Cunha, R. Sohbati, J.P. Buylaert, A.S. Murray, (2012). Paleoseismic study of a slow-moving and silent fault termination: the Alhama de Murcia-Góñar system (Eastern Betics, Spain). *Geological Society of America Bulletin*. 124 (9/10), 1474-1494.

Shobati, R., A.S. Murray, J.P. Buylaert, M. Ortuño, P. Cunha, E. Masana, (2011). Luminescence dating of Pleistocene alluvial sediments affected by the Alhama de Murcia fault (eastern Betics, Spain) – a comparison between OSL, IRSL and post-IR IRSL ages. *Boreas*. 10, 2-13.

Silva, P.G., (2014). The Guadalentín Tectonic Depression (Betic Cordillera, Murcia). In: *Landscapes and Landforms of Spain* (Gutiérrez, F. and Gutiérrez, M. eds.). World Geomorphological Landscapes Series. Springer Science. Dordrecht. Germany. pp. 25 - 35.

Silva, P.G., J.L. Goy, C. Zazo, T. Bardají, (2003). Fault generated mountain fronts in southeast Spain: geomorphologic assessment of tectonic and seismic activity. *Geomorphology*. 250, 203-226.

Silva, P.G,, J.L. Goy, C. Zazo, J. Lario, T. Bardají (1997). Palaeoseismic indications along "aseismic" fault segments in the Guadalentín Depression (SE Spain). *J. Geodynamics*. 24, 105-115.

INQUA Focus Group on Paleoseismology and Active Tectonics

Looking for seismites in the Fucino basin: preliminary results from an combined geological-geophysical approach

Smedile, A. (1), Civico, R. (2), Del Carlo, P. (3), Sapia, V. (2), De Martini, P.M. (2), Pantosti, D. (2), Brunori, C. (2), Orefice, S. (2), Pinzi, S. (2), Pucci, S. (2)

(1) Istituto Nazionale di Geofisica e Vulcanologia, via dell'Arcivescovado 8, 67100 L'Aquila, Italy. Email: alessandra.smedile@ingv.it
(2) Istituto Nazionale di Geofisica e Vulcanologia, via di Vigna Murata 605, 00143 Roma, Italy
(3) Istituto Nazionale di Geofisica e Vulcanologia, via della Faggiola 32, 56126 Pisa, Italy

Abstract: *We present a combined geological-geophysical study on the lacustrine sequence of the Fucino Plain (central Italy). New acquired data on liquefaction features and the recovery of a seismite in the lacustrine sequence are shown. Our preliminary results suggest the occurrence of three seismic events in the last ca. 45 kyr. Moreover, a first attempt to find out the source deposit responsible of the widespread liquefaction phenomena has been performed by means of shallow engine boreholes and ERT profiles.*

Key words: *Fucino Plain, lacustrine deposits, liquefaction features, seismites.*

INTRODUCTION

The 1915 Avezzano earthquake (Ms=7.0), which struck the Fucino Plain (central Italy), is one of the major seismic events occurred in Italy over the last few centuries. Due to its relatively recent occurrence, the coseismic effects were extensively illustrated by Oddone (1915) in terms of intensity distribution and detailed description. Extensive paleoseismological research has been performed during '90 years to better understand the seismogenic behaviour of the structure responsible for the 1915 earthquake (see Galadini & Galli, 1999 and references therein). Paleoseismological analysis outlined the occurrence of ten surface faulting events in the past 33.000 years (Galadini & Galli, 1999).

The Fucino Plain is an extensional intramountain basin filled by Pliocene to Quaternary continental alluvial and lacustrine deposits (Cavinato et al., 2002). It was the site of Lake Fucino, a large endorheic lake drained at the end of the 19th century.

Most of the published paleoseismic data on the Fucino Plain derived from on-fault paleoseismic trenching. In our study we investigated the lacustrine sequences to detect the off-fault record of several paleoseismic events by means of methodologies applied in different tectonic settings (e.g. Monecke et al., 2006; Beck, 2009; Kagan et al., 2011; Avsar et al., 2014).

Compared to other terrestrial environments, lacustrine environments may contain relatively well preserved, continuous, and long sedimentary archives. However, unlike the clear seismic origin of coseismic deformations detected by on-fault trenching, sedimentary events in lacustrine sequences may have several triggering mechanisms other than seismic activity, usually of climatic origin. Therefore, temporal correlation with historical seismicity and/or on-fault trenching data is crucial in order to assign a seismic triggering mechanism to lacustrine sedimentary anomalies (Avsar et al., 2014).

Here we present an integrated geological-geophysical study on the most recent lacustrine sequence of the Fucino Plain retrieved by Electrical Resistivity Profiles (ERT), shallow boreholes and the exceptional recovery of a cleaned ditch affected by liquefaction features. Being aware of the fact that several lake level fluctuations occurred in the past due to global climatic variations (Giraudi, 1989),

we focused our research close to the area that apparently displays the longer lacustrine sedimentary sequence and where several coseismic effects of the 1915 Avezzano earthquake where reported and studied (Oddone, 1915; Galadini et al., 1997, Galadini & Galli, 1999).

DATA COLLECTION AND METHODS

Since 1875, when the lake was finally drained, the Fucino Plain became a flat area, intensively cultivated and crossed by many E-W and N-S trending ditches (*Figure 1*). In spring 2014 a field survey was performed on the Fucino Plain looking for new liquefaction features along many ditches.

Up to now, evidence for liquefaction was found along a single, E-W trending, 1.5 m deep dry ditch. The exposed sequence, properly cleaned and rectified, was photographed, described using coloured nails to separate the main layers/unit, and sampled for radiocarbon and sedimentological analyses. Moreover, several 5m long engine cores were performed both in the present-day depocenter of the Fucino Plain (named "Bacinetto") and close to that area where the longest lacustrine sedimentation record exists (*Figure 1*). On each PVC core a Computed Axial Tomography (CAT) was performed in order to identify peculiar intervals or sudden changes in the sedimentation otherwise not easily identifiable through a normal visual inspection. After the CAT inspection only the core performed next to the studied ditch was opened, photographed, logged and sampled for sedimentological, paleonvironmental, tephrostratigraphical and radiocarbon analyses. Apart from C14 dating, the other analyses are still in progress.

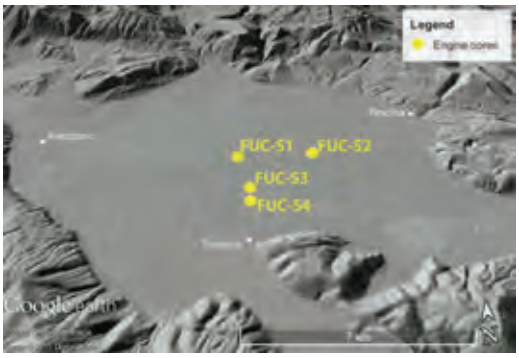

Figure 1: Five meters Digital Elevation Model (DEM) draped over a Google Earth bird's eye view of the Fucino Plain. Yellow pins locate all the engine cores. The investigated ditch and the ERT profile are located in correspondence of FUC-S4.

An Electrical Resistivity Tomography (ERT) profile along the W–E trending ditch was acquired *(Figure 1)*. We deployed a 64 electrodes and 126 m long array with both Wenner and dipole-dipole quadrupoles configuration using a Syscal R2 resistivimeter (IRIS Instrument). A non-linear smoothness-constrained least-squares optimization technique is used to calculate the resistivity of the model blocks from the apparent resistivity data (de Groot-Hedlin & Constable, 1990; Loke & Dahlin, 2002).

STRATIGRAPHY

From the selected FUC-S4 core a sequence of ca. 5 m was analysed and subdivided in three main units.
Starting from the bottom ca. 3 m thick of laminated gray to green-gray, organic rich silty clay is found (unit A). Furthermore, three different well distinguishable tephra layers (*Figure 2*) related to the Colli Albani eruptions, basing on morphoscophical and petrographycal features, are present in the lowermost 0.5 m (*sensu* Giaccio et al., 2007). Additional chemical analyses on these tephra are still in progress to better discriminate the different eruptions.
In unit A, at about -4.5 m of depth, a peculiar interval, few centimetres thick with several small laminae forming a chevron-fold type shape at small scale, is detected (*Figure 2*). The acquired CAT images confirmed the presence of this disturbed layer sampled in the PVC tube and enabled us to exclude that a deformation would have occurred during opening and cleaning operations of PVC tube. This feature can be interpreted as the result of seismic shaking (seismite). Moving up along the core, the following unit B, represented by a gray to hazel oxidized clayey silt rich in manganese nodules, is present between -2.65 and -1.40 m of depth.
The uppermost 20 cm of unit B shows an infill of gray silt that continues also in the uppermost third unit. In fact, the latter unit C composed mainly by silt and clayey silt shows in the lower 0.50 m both lithologies upside down and with vertical contacts. This unit, that represents the most recent in time, is not well distinguishable in the core and on the ditch walls. Moreover, the CAT analyses showed that unit C is a structureless sediment full of empty spaces and characterized by a reduced cohesion, similar to that of Galadini et al. (1995) defined as "de-structured silty deposits".
Thus, the 1.80 m thick sequence shown on both sides of the ditch walls, likely correlates with the first 1.50 m of the FUC-S4 engine core (unit C and upper part of unit B).
On both sides of the ditch a ca 0.80 m thick, pale gray clayey silt, highly oxidized in the lower portion is exposed at ca. –1.80 m below the ditch top soil. Similarly to the core log, this clayey interval is cut by several filled fissures of sandy-silty material that can be likely interpreted as dikes related to liquefaction (*Figure 2*). This interval is overlaid by an alternation of gray massive and whitish laminated silts with a total thickness of ca. 0.70 m. The top of the ditch sedimentary sequence ends with 0.30 m of agricultural soil (ploughed horizon) whose surface represents likely the lake bottom in 1875 (year of the lake drainage). In fact, due to the superficial drainage system inception, the sedimentation rate in the Fucino Plain can be considered negligible.

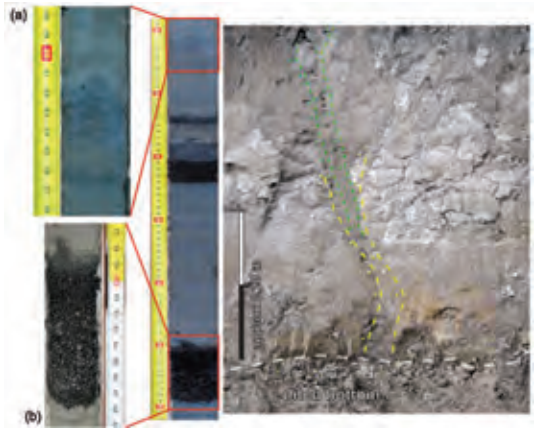

Figure 2: Pictures of the unit A from FUC-S4 core and the ditch wall. On the left side (a) detail of the chevron-fold type shape (seismite) and (b) the lower tephra layer; on the right a zoom of the N ditch wall showing the two filled fissures related to a double liquefaction phenomenon.

Differently from the core log, the ditch clearly shows how filled fissures developed. In fact, on the same dikes two open vent and fissure generations are present. One older fissuration event likely occurred during the sedimentation of the oxidized gray clayey silt, because of the occurrence of a sill of sandy silt within these fine sediments. Within the same dykes a new filled fissure of sandy-silty material developed and cut only part of the upper silty alternation. This second fissure does not seem to reach the ploughed layer but stops within the upper whitish laminated silty interval.
The stratigraphy retrieved using engine cores and field data seems to be confirmed in first approximation by the interpretation of the ERT profile. In fact, the 2D section (*Figure 3*) shows a thin resistive layer (ranging from 5 Ωm

to about 50 Ωm) throughout the profile with an average thickness of about 2.0 m (the sequence in the ditch). This superficial interval overlay a low resistive layer, showing resistivity of about 10 Ωm, down to a depth of 5 m. The lower part of the 2D electro-resistivity section indicates a change in the stratigraphy due to the presence of an intermediate, moderately resistive, ca. 5.0 m thin layer with resistivity values ranging from 15 to 19 Ωm, respectively. Therefore, we interpreted this layer to be the response of coarser materials with respect to the uppermost low resistive clayey sediments (unit A).

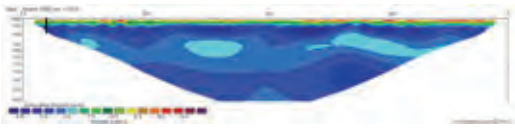

Figure 3: Electrical resistivity tomography result. A logarithmic colour scale for the resistivity model accentuates discrimination of low-to-mid-range resistivities. Solid black line shows the location of the FUC-S4 borehole.

CHRONOLOGY

The age of the investigated deposits can be estimated by 5 AMS C14 dating (*Table 1*) and tephrochronology.
All the ages retrieved from C14 resulted in stratigraphical order and no overlaps or inversion were recognized. Consequently, the lowermost unit A seems to be Upper Pleistocene in age as suggested by the combination of C14 dating and tephrochronology (see samples from FUC-S4 at 2.67 and 4.11 m, respectively in *Table 1*). In fact, the recognized tephra can be related to the Colli Albani eruptions and dated back to ca. 30-45 kyr (Giaccio et al., 2007).

Unit	Site/ depth (m)	Sample	Conventional age (BP)	Calibrated age (2 sigma)
B	Ditch/ 1.6	FUC 1	4510±30 BP	BP 5305-5045
B	Ditch/ 1.7	FUC 2bis	4700±30 BP	BP 5580-5320
B	FUC-S4/1.66	FUCS4 (164-166)	8270±40 BP	BP 9415-9125
A	FUC-S4/2.67	FUCS4 (265-267)	22490±80 BP	BP 27060-26555
A	FUC-S4/4.11	FUCS4 (408-411)	27030±130 BP	BP 31190-30950

Table 1: Measured and calibrated ages (according to Calib REV7.0, Stuiver & Reimer, 1993; IntCal13, Reimer et al.,2013) of the samples collected. Measurements were performed at the Beta Analytics Inc. (Florida).

On the contrary, the intermediate unit B resulted to be younger of ca. 27.000 yr and older of ca. 5580 BP. Because of the lack of any dating material in the sediments no direct age constrains are available for the uppermost unit C. Nevertheless we can say that it was deposited between 5580 yr BP and the 1875 AD. Furthermore, it corresponds to a period were many changes in lake levels took place due to both previously mentioned climatic events as well as to preliminary attempts in controlling the lake water level made at the time of the Ancient Roman period by means of three draining tunnels dug at different elevations (Giraudi, 1989).

RESULTS AND INTERPRETATION

Our geological-geophysical study provided new preliminary results in terms of liquefaction features and seismites as well as for the reconstruction of the lacustrine sequence of the Fucino Plain.
Despite any paleosoil or physical stratigraphical discontinuities were detected, we cannot exclude the presence of depositional gaps in the studied sequence. In fact, during the sedimentation of the oxidized gray clay (unit B), indicating a low lake level, or during the sedimentation occurred after the Ancient Roman period, several discontinuities were reported in the western portion of the plain by Galadini & Galli (1999).
Moreover, in the deepest unit A, an important change in the sedimentation rate occurred, as testified by the ages of tephra layers related to the Colli Albani eruption (ca. 15 kyr in 0.30 m).
The changes in the sedimentation rate occurred in the study sequence, related to climatic oscillation as suggested by Giraudi (1989), are likely responsible for the lack of evidence of some of the seismic events reported by Galadini & Galli (1999) on the basis of on-fault paleoseismological investigations.
Nevertheless, in the ditch two paleo-liquefaction events were identified. The path used by the liquefied sandy silt to reach the surface at the time of the seismic events seems to be the same and, even if sedimentological analysis has not confirmed it yet, the material found in the filled fissures apparently seems to share the same grain size.
Moreover, the ERT profile highlighted a change in the stratigraphy just below the end of the engine core. This lowermost layer can be likely the source of the liquefied sandy-silty material (*Figure 3*).
Taking into account the radiocarbon dating, the lower paleo-liquefaction event, generated during the sedimentation of the oxidized gray clayey silt (unit B), likely occurred after 5305BP (upper sample FUC1 collected in unit B). Because of the lack of any datable organic material in the youngest unit C, we cannot assign an age to the upper paleo-liquefaction. Nevertheless, it occurred most probably before the 1875 lake draining because the upper fracture termination does not reach the ploughed soil.
Regarding the only one disturbed layer reported at ca. 4.5 m, we may suggest its relationship to a seismic event occurred before ca. 31 kyr BP. In fact, this event occurred before the age of the deepest C14 sample (see FUCS4 at -4.11 m in *Table 1*).

Comparing our results with those published by Galadini & Galli (1999), we can suggest that the liquefaction phenomena discovered in this study may have been triggered by the same events reported as E4 (3944-3618 BC) and E2 after 426-782 AD, respectively. Moreover, in the same age interval of our unique evidence of seismite, Galadini & Galli (1999) reports an old surface displacement event (or group of events, E10) occurred between 32.520±500 yr BP and about. 20.000 yr BP.
Because liquefaction occurrence and location is strongly related to local conditions at the time of the earthquake that may vary substantially in time, more extensive investigations of the lake area are needed to produce a complete liquefaction history of this area.

Acknowledgements: This work was conducted in the framework of a national project focused on the seismic risk of the Abruzzo region (FIRB Abruzzo project, "High-resolution analyses for assessing the seismic hazard and risk of the areas affected by the 6 April 2009 earthquake"; http://progettoabruzzo.rm.ingv.it/en).
Many thanks to Dr. A. Genovese and R. Traini who permitted us to performe the Computed Axial Tomography on our cores at the G.B Grassi Hospital in Ostia (Rome).

References

Avsar, U., A. Hubert-Ferrari, M. De Batist, G. Lepoint, S. Schmidt & N. Fagel, (2014). Seismically-triggered organic-rich layers in recent sediments from Gollükoy Lake (North Anatolian Fault, Turkey). *Quaternary Science Review*. 103, 67-80.

Beck, C., (2009). Late Quaternary lacustrine paleoseismic archives in north-western Alps: examples of earthquake-origin assessment of sedimentary disturbances. *Earth-Science Review*. 96, 327-344.

Cavinato, G.P., C. Carusi, M. Dall'Asta, E. Miccadei & T. Piacentini, (2002). Sedimentary and tectonic evolution of Plio-Pleistocene alluvial lacustrine deposits of Fucino basin (central-Italy*). Sedimentary Geology*. 148, 29-59.

Galadini, F., P. Galli, (1999). The Holocene paleoearthquaqkes on the 1915 Avezzano earthquake faults (central Italy): implications for active tectonics in the central Italy. *Tectonophysics*. 308,143-170.

Galadini, F., P. Galli & C. Giraudi, (1995). Individuazione ed analisi di deformazione geologiche associate a liquefazoni indotte da terremoti. *Geologia Applicata e Idrogeologia*. 30 (1).

Galadini, F., P. Galli & C. Giraudi, (1997). Paleosismologia della Piana del Fucino (Italia centrale). *Il Quaternario.* 10, 27-64.

Giaccio, B., A. Sposato, M. Gaeta, F. Marra, D.M. Palladino, J. Taddeucci, M. Barbieri, P. Messina & M.F. Rolfo, (2007). Mid-distal occurrences of the Albano Maar pyroclastic deposits and their relevance for reassessing the eruptive scenarios of the most recent activity at the Colli Albani Volcanic District, Central Italy. *Quaternary International*. 171-172, 160.

Giraudi, C., (1989). Lake levels and climate for the last 30000 years in the Fucino area (Abruzzo, central Italy): A review. *Palaeogeography, Palaeoclimatololgy, Palaeoecology*. 70, 249-260.

de Groot-Hedlin, C., S. Constable, (1990). Occam's inversion to generate smooth, two-dimensional models form magnetotelluric data. *Geophysics*. 55, 1613-1624.

Kagan, E., M. Stein, A. Agnon & F. Neumann, (2011). Intrabasin paleoearthquake and quiescence correlation of the late Holocene Dead Sea. *Journal of Geophysical. Research.* 116, B04311. http://dx.doi.org/10.1029/2010JB007452.

Loke, M.H., T. Dahlin, (2002). A comparison of the Gauss-Newton and quasi-Newton methods in resistivity imagingin version. *Journal of Applied Geophysics*. 49, 149-162.

Monecke, K., F.S Anselmetti, A. Becker, M. Schnellmann, M. Sturm & D. Giardini, (2006). Earthquake-induced deformation structures in lake deposits: a late Pleistocene to Holocene paleoseismic record for Central Switzerland. *Eclogae Geologie Helvetica.* 99, 343-362.

Oddone, G., (1915). Gli elementi fisici del grande terremoto marsicano-fucense del 13 gennaio 1915. *Bollettino Società Sismologica Italiana*. 19, 71- 215.

Reimer, P.J., E. Bard, A. Bayliss, J.W Beck, P.G. Blackwell, C. Bronk Ramsey, P.M. Grootes, T.P. Guilderson, H. Haflidason, I. Hajdas, C. HattŽ, T.J. Heaton, D.L. Hoffmann, A.G. Hogg, K.A. Hughen, K.F. Kaiser, B. Kromer, S.W. Manning, M. Niu, R.W. Reimer, D.A. Richards, E.M. Scott, J.R. Southon, R.A. Staff, C.S. Turney & J. van der Plicht, (2013). IntCal13 and Marine13 Radiocarbon Age Calibration Curves 0-50,000 Years cal BP. *Radiocarbon*. 55 (4).

Stuiver, M., P.J. Reimer, (1993). Extended 14C database and revised CALIB radiocarbon calibration program. *Radiocarbon.* 35, 215-230.

INQUA Focus Group on Paleoseismology and Active Tectonics

Architecture and deformation mechanisms within a carbonate-hosted fault zone (Fucino basin)

Smeraglia, L. (1), Carminati, E. (1), Billi, A. (2), Doglioni, C. (1)

(1) Dipartimento di Scienze della Terra, Sapienza Università di Roma, Roma, Italy. Email: luca.smeraglia@uniroma1.it
(2) IGAG, Consiglio Nazionale delle Ricerche, Roma, Italy

***Abstract**: The Central Apennine are one of the most seismically active regions in the Mediterranean area and is affected by moderate to large shallow earthquakes that enucleate in and propagate through carbonate rocks. In this work we present a detailed fieldwork and microstructural analysis to define the architecture and deformation mechanisms of an exhumed fault zone in carbonates, the Tre Monti fault, at the northern boundary of the Fucino Basin. Fault rocks assemblages show differences in deformation mechanisms between the main and external fault planes, and subsidiary fault planes developed within the damage zone. We infer that this variety of fault rocks represents different deformation processes acting during different stages of fault development and fluid circulation. The multidisciplinary but field-based study of fault surfaces and fault rocks is fundamental to reveal the geological record of past earthquakes and seismic cycles and is strongly complementary to the seismological-based one.*

***Key words:** Seismic cycle, fault rocks, calcite cements, fluid circulation.*

INTRODUCTION

Many seismically active regions on Earth, including the Mediterranean area, contain thick sequences (up to 4-10 km) of sedimentary carbonates (mainly limestones and dolostones) in the brittle upper crust. In the central Mediterranean area, Italy, the Balkans and the Aegean region are affected by moderate to large shallow crustal earthquakes and seismic sequences (i.e. hypocenters of the main shocks at 7-15 km depth). Although the mainshocks of some of these earthquakes are likely to have initiated within the crystalline basement, rupture propagation in to the shallow crust occurred within the overlying carbonate rocks. Within this framework fault zones hosted in carbonates represent significant seismogenic sources and their investigation in terms of fault zone structure and fault-related deformation processes is fundamental to improve our knowledge of earthquake mechanics and fluid circulation during the seismic cycles. In recent years many authors described fault zone architecture and deformation mechanisms (Micarelli et al., 2003; Agosta and Aydin, 2006; Fondriest et al., 2012 and references therein) and the role of fluids within the seismic cycle in carbonate fault zones (Benedicto et al., 2008; Nuriel et al. 2011; Doglioni et al., 2013 and reference therein). Nevertheless the Central Apennine are still an excellent natural laboratory for the field-based and microstructural study of fault zones.

In this work we studied a well-exposed, 3D outcrop in an abandoned quarry near the town of Celano, of the WSW–trending and 8 km long Tre Monti fault zone, the northern boundary of the Fucino Basin, an intramontane half-graben filled by Plio–Quaternary alluvial and lacustrine deposits, which was formed in Upper Pliocene and Quaternary time in the Apennines by extensional tectonic activity. Kinematic indicators along the fault zone record mainly dextral transtensional movement, suggesting that the Tre Monti fault acted as a dextral transfer zone between two left-stepping major normal faults: the Venere-Serrone fault and the Velino fault.

In order to define the internal architecture of the fault zone we integrate classical structural analysis with

Figure 1: Panoramic view of the studied quarry. A) External fault plane that juxtapose middle Pleistocene continental deposits in the hangingwall and lower to middle Cretaceous oolithic limestone in the footwall; B) Subsidiary fault plane developed within the damage zone. The white line highlights the 100 m thick damage zone. Geographical coordinates of the outcrop from Google Earth: 42° 04'36.92" N 13°29'59.87" E.

microstructural studies of oriented thin sections of fault rocks using both optical and electron microscopy (SEM). Moreover cathodoluminescence was used to distinguish the different phases of fluid circulation and the crosscutting relationships between different generations of fault fractures and veins.

Figure 2: External fault plane (see Figure 1, A). A) Detailed of the contact (red line) between the brownish ultracataclastic layer and the microbreccia.

DISCUSSION

The 3D exposure allowed us to distinguish three main domains within the overall architecture of the fault zone (*Figure 1*). The external fault plane, dipping towards the Fucino Basin, juxtaposes lower to middle Cretaceous oolithic limestone in the footwall and upper Pliocene to middle Pleistocene continental deposits in the hangingwall (*Figure 1, A*). The deformation is highly localized in a fault core consisting of a layer of ultracataclasite (up to 10 cm in width) above a layer a fault microbreccia (up to 50 cm in width) (*Figure 2, A*). The ultracataclasite formed by fracturing and smearing of the carbonates of the footwall and it records slip localization within very fine and distinctive layers, whereas diffuse pressure solution seams highlight interseismic phases (*Figure 3*). Beneath this layer the fault microbreccia records a diffuse and intense deformation accommodated mostly by dilatant and minor shear microfracture. In this zone the cataclastic process is poorly developed or totally absent. Within the fault core cathodoluminescence (CL) revealed almost three phases of fluid circulation. A dull red luminescence (medium Mn^{2+}/Fe^{3+} ratio) characterizes the fractures of the microbreccia and the cement within the ultracataclasite, these features are crosscut by fractures with bright and red luminescence (elevated Mn^{2+}/Fe^{3+} ratio), whereas a non luminescent calcite (low Mn^{2+}/Fe^{3+} ratio) precipitated within a fracture network that postdate all previous structures (*Figure 4*).

The damage zone (up to 100 m width, *Figure 1*) is characterized by an intense network of subsidiary and fault-related fractures, mostly unmineralised or filled with small crystals of elongated-blocky calcite. Plagues of cemented fault breccias (up to 50 cm thick) with numerous large voids and reworked fragments from the damage zone are attached to a huge and highly undulated subsidiary fault plane which developed within the damage zone, 100 m far from the external fault plane (*Figure1, B*). The fault itself cuts cemented fault breccias and does not show the characteristic ultracataclastic layer of the external fault plane. All the veins and cements within the damage zone and fault breccias show no luminescent calcite (low Mn^{2+}/Fe^{3+} ratio).

Fault rock assemblage and microstructural studies allowed us to recognise different fault rocks that pertain to different conditions of deformation that operated during different stages of fault development. We infer that deformation is initially accommodated within a narrow and localized fault core that developed a cataclastic fabric and localization features in a fluid-confined and poorly-oxygenate environment, as indicated by dull and bright red luminescence (high content of Mn in the reduced state). With progressive exhumation, the fault damage zone become characterized by fault rocks developed in a less confined environment (e.g. fault breccias) with significant fluid interaction in a oxygenate environment (no luminescence, high content of Fe in the oxided state), probably related to meteoric water infiltration. Future isotopic analysis will be performed to validate this interpretation.

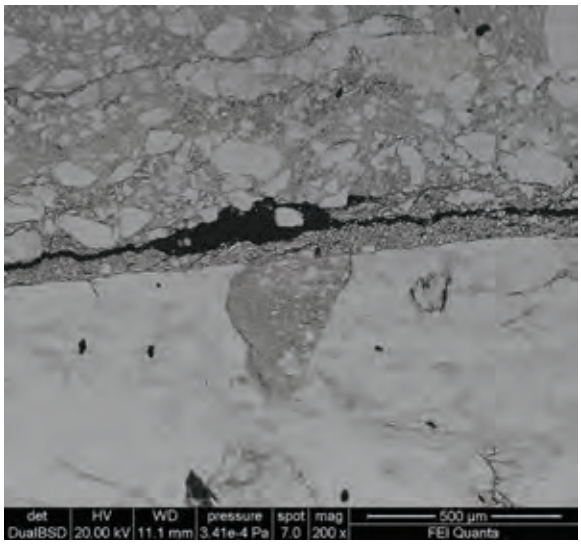

Figure 3: SEM image of the distinct localization features between the ultracataclasite and the microbreccia.

CONCLUSION

Our study shows the complex relationship between the different microstructures and fluid circulations that develops during fault evolution and seismic cycle. The interaction between fracture and fluid circulation is

testified by the presence of mutually crosscutting calcite-filled veins related to seismic rupture or propagation. Although these calcite precipitates could originate from near surface and oversaturated fluids, the presence of these veins can record complex interaction between fault zone and aquifers. In the future the in situ monitoring of aquifers near fault zones can play a key role in understanding fluid pathways related to seismic cycle (interseismic, coseismic and post-seismic phases). Moreover the study of exhumed fault zone and fault rocks is complementary to the seismological-based one. In fact seismology, geophysics and geodesy furnish key parameters related to the earthquake source (e.g. seismic moment, static stress drop, radiated energy) but lack sufficient resolution to constrain detailed three-dimensional fault zone geometry and coseismic on- and off-fault deformation processes at scales relevant to earthquake physics. Seismological studies and field-based studies should run together and interact to increase our knowledge of earthquake mechanics.

Acknowledgements: Financial support from Progetti di Ateneo (Sapienza) 2012, led by Doglioni Carlo is acknowledged. M. Albano is thanked for his help with SEM. F. Berra is thanked for his help with cathodoluminescence (CL) microscopy. Domenico Mannetta is thanked for thin sections preparation.

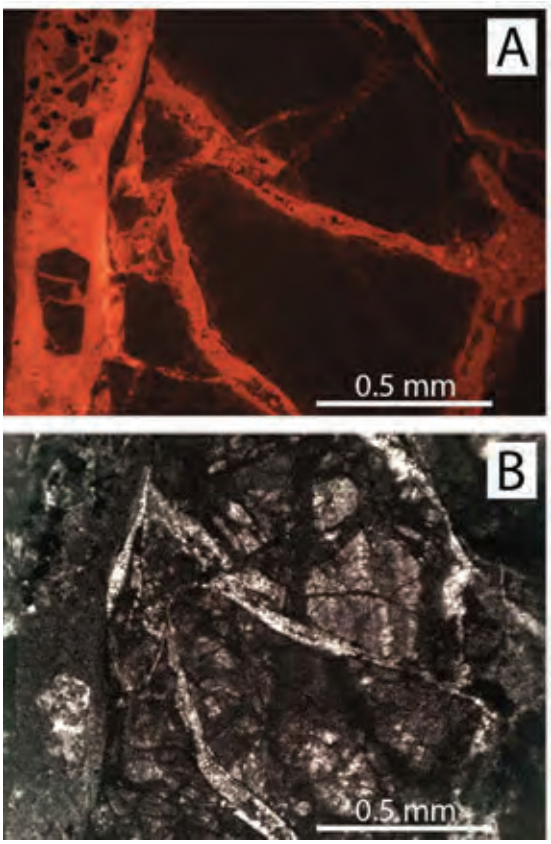

Figure 4: Microstructures of fault-related calcite precipitates. A) Sample of microbreccia under CL light. Dull red luminescence within small fractures that permeate the background; calcite filled veins showing bright red luminescence; non luminescent calcite in fractures postdates all structures; B) The same sample under plane-polarized light.

References

Agosta, F. & A. Aydin, (2006). Architecture and deformation mechanism of a basin-bounding normal fault in Mesozoic platform carbonates, central Italy. *Journal of Structural Geology*. 28, 1445-1467.

Benedicto, A., V. Plagnes, P. Vergely, N. Flottè & R.A. Schultz, (2008). Fault and fluid interaction in a rifted margin: integrated study of calcite-sealed fault-related structures (southern Corinth margin). In: (Wibberley, C.A.J., Kurz, W., Imber, J., Holdsworth, R. E. & Collettini, C. eds.). *The Internal Structure of Fault Zones: Implications for Mechanical and Fluid-Flow Properties*. 299, 257-275. The Geological Society of London. (2008).

Doglioni, C., S. Barba, E. Carminati & F. Riguzzi, (2013). Fault on-off versus coseismic fluids reaction. *Geoscience Frontiers*. 5, 767-780.

Fondriest, M., S.A.F. Smith, G. Di Toro, D. Zampieri & S. Mittempergher, (2012). Fault Zone Structure and Seismic Slip Localization Dolostones, an example from the Southern Alps, Italy. *Journal of Structural Geology*. 45, 52-67.

Micarelli, L., I. Moretti & J.M. Daniel, (2003). Structural properties of rift-related normal faults: the case study of the Gulf of Corinth, Greece. *Journal of Geodynamics*. 36, 275-303.

Nuriel, P., G. Rosenbaum, T.I. Uysal, J. Zhao, S.D. Golding, R. Weinberger, V. Karabacak & Y. Avni, (2011). Formation of fault-related calcite precipitates and their implications for dating fault activity in the East Anatolian and Dead Sea fault zones. *Geological Society of London*. Special Publications. 359, 229-2.

INQUA Focus Group on Paleoseismology and Active Tectonics

paleoseismicity.org

Satellite geodetic data in the analysis of the seismic hazard on faults in an intracratonic setting of the SE South America

Sobrero, F.S. (1), Brunetto, E. (2)

(1) Faculty of Engineering and Hydric Sciences, Littoral National University, Santa Fe, Argentina. Email: francosobrero@gmail.com
(2) ClCyTTP-CONICET (National Council of Science and Technology), Entre Ríos, Argentina

Abstract: *The precision that satellite geodetic data offer, allows us to monitor intraplate areas where the movements of the lithosphere are otherwise imperceptible. In the case of Argentina, most of the neotectonic studies are focused on the Andes, considering the Pampa Region as a stable region and without seismogenic capability. This great plain region is located in the foreland basin eastward from the Pampean Ranges and the cratonic area of the Mesopotamia, in the latitudinal segment of the Nazca Plate sub-horizontal subduction. In this work, the Velocity Model for South America and the Caribbean (VEMOS09) was analyzed as well as the data from 5 GNSS Permanent Stations (PS) with data series longer than 3 years, in order to observe the regional tendency of the velocity field in the Rio de la Plata Craton (RPC).*

Key words: *Rio de la Plata Craton, GNSS Data, Active Intraplate Deformation, Faulting Kinematics, Seismic Hazard.*

INTRODUCTION

Satellite geodetic data is currently used in studies of different fields of the Earth Sciences, especially to determine or estimate the rates of crustal deformation in the surroundings of "active" faults. These studies have been carried out more frequently in areas of active tectonics, such as subduction zones and interplate settings. However, the precision that satellite geodetic data offers, allows us to monitor intraplate areas where the movements of the lithosphere are milder.

In the case of Argentina, most of the neotectonic studies are focused on the Andes, considering the Pampa and the Mesopotamia as stable regions, without seismogenic capability. This great plain region is located in the foreland basin eastward from the Pampean Ranges and the neighbour cratonic area, in the latitudinal segment of the Nazca Plate sub-horizontal subduction (*Fig*. 1). Two main fault systems with Quaternary activity were defined in the Argentinean area of the Rio de la Plata Craton (RPC): 1) the Tostado-Selva Fault System (Pasotti & Castellanos, 1963; Iriondo, 1989; Brunetto, 2008), 2) the Río Paraná Fault System (Iriondo 1989; Brunetto et al., 2014).

The main examples of satellite geodetic data applied to real time geodynamics in low-activity regions can be found in the Mississippi alluvial lowland (Smalley et al., 2005; Stein, 2007) as well as the Brazilian portion of the South American plate (Alves et al. 2003). Given that those regions, as well as other intraplate areas have reported high magnitude earthquakes, it is considered also necessary to monitor the southeastern region of the South American plate.

The purpose of this work was to analyze and interpret the velocity field in the RPC, aiming to determine the kind of stress that structures are undergoing, as well as their order of magnitude.

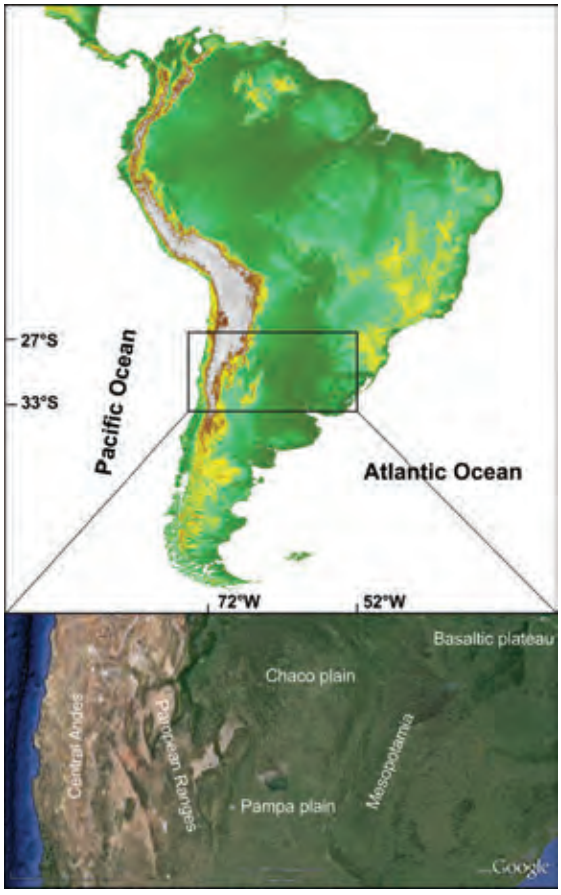

Figure 1: Map of location.

An interpretation of the geodetic data was carried out based on the geological and geomorphological evidence available that suggests faulting and recent deformation.

METHODOLOGY

First of all, the Velocity Model for South America and the Caribbean (VEMOS09) (Drewes & Heidbach, 2012) was run, in order to have an approach of the velocity field in the intracratonic area of study. This analysis was only qualitative, given that the Model has an average precision of 1,5 mm/yr. Aiming to have better local velocity values for the region, more data were analyzed (*Fig. 2)*.

In South America, the international organization responsible for providing reliable and precise GNSS data is SIRGAS (Sistema de Referencia Geocéntrico para las Américas). It operates coordinated with the DGFI (Deutsches Geodätisches Forschungsinstitut), who delivers cumulative (multi-year) coordinate solutions aligned to the ITRF, and velocity solutions for many permanent stations (PS) of the network, with a sub-millimeter precision.

Here it was used the multi-year solution SIR10P01 of the SIRGAS-CON network (Seemüller et al., 2010), which encompasses the weekly solutions provided by SIRGAS from January 2, 2000 (GPS week 1043) to June 5, 2010 (GPS week 1586). The PS which were taken into account were TUCU and UCOR (western cratonic area) and MECO, UNRO and LPGS (eastern cratonic area). All five PS have been functioning for at least 3 years (*Table 1*).

Permanent Station	VN (mm/yr)	±	VE (mm/yr)	±	Start	End
TUCU	11,6	0,2	1,7	0,2	01/01/2001	23/01/2006
UCOR	11,4	0,4	1,6	0,4	05/04/2004	26/02/2010
UNRO	11,9	0,1	0,6	0,1	02/04/2004	26/02/2010
LPGS	12,1	0,1	-0,7	0,1	02/01/2000	26/02/2010
MECO	11,9	0,4	-0,7	0,5	19/10/2006	17/02/2010

Table 1: North and East velocity components of the Permanent Stations.

Using the baseline methodology between two PS (Mukul et al., 2010) the residual velocities between both groups of stations were calculated, in order to estimate the relative movement between them. At first, it was calculated the vector sum on the baselines considering the absolute velocities of the PS, so as to find the magnitude of the convergence/divergence vector over each baseline. Secondly, a resultant regional velocity vector was obtained for the whole set of PS (*Fig*. 3)

The resultant regional velocity vector was projected onto the modal orientations (azimuths) of morphological lineaments that suggest structural control over the relief in the area. These orientations were obtained from satellite images mapping rectilinear drainage segments and axes of linear hill ridges and they were processed by means of circular statistics.

The kinematics in the region was interpreted from the modal trends of the faults and the normal and tangential components obtained from the projection of the residual velocity regional vector onto the dominant orientations.

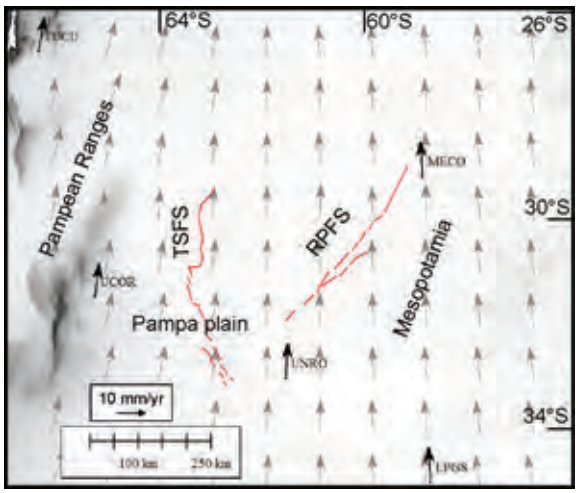

Figure 2: Permanent Stations velocity vectors in black and VEMOS09 vectors in grey. TSFS: Tostado Selva Fault System (Brunetto, 2008); RPFS: Rio Paraná Fault System (Brunetto et al., 2014).

Finally, high definition satellite images were analyzed in order to find evidence of paleoseismic activity in the region.

RESULTS

Regional kinematic indicators measured using geodetic data suggest that the region of the RPC is undergoing compressional and transpressional stress.

The converging tendency in this cratonic area shown by VEMOS09 was confirmed by the absolute velocities of the PS delivered by SIRGAS. Even though all of the PS show a main North component, the western group of stations is moving towards the East, opposite to the eastern group (*Fig 2*). The error ellipses associated to each PS were also plotted, displaying that the velocity values are significant (*Table 1*, *Fig. 3*)

The residual velocity vectors evidences shortening on each baseline. The magnitude of shortening is around 2 mm/yr in three of the four baselines. They represent the stress field in the whole RPC. The UCOR-UNRO baseline was analyzed separately; there, the shortening value is 1,11 mm/yr. This is a measure of the western portion of the RPC located in the foreland setting of the Pampean ranges.

The resultant regional velocity vector (*Fig*. 3) has a magnitude of 2,39 mm/yr and SE direction. The kinematics analysis suggests that reverse faulting occurs on NNW-SSE faults and lateral strike-slip with reverse component on NW-SE and ENE-WSW faults.

Based on these data, in the western dominion, the shortening component on NNO-SSE lineaments is around 1 mm/yr, faster than the strike-slip component (aprox. 0,5 mm/yr).

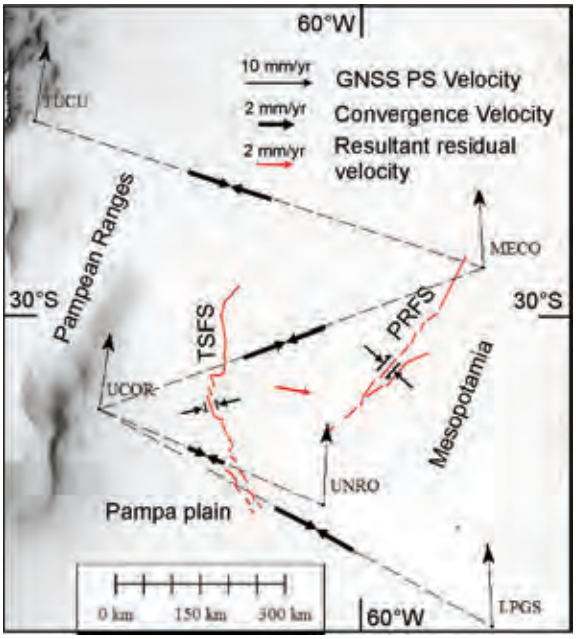

Figure 3: PS absolute velocities and convergence velocities on baselines between PS. Regional residual velocity is also shown.

Additionally, a series of oddly circular ponds were found aligned parallel to the main lineament of the Tostado-Selva Fault System (*Fig. 4*).

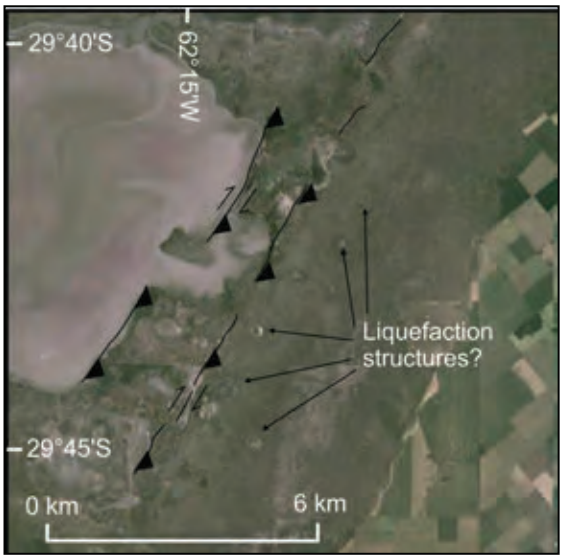

Figure 4: Scarp of the Tostado-Selva Fault System where possible evidence of liquefaction associated to paleoseismicity can be observed.

The genesis of these ponds is still unknown, but their aspect and location would suggest liquefaction caused by seismicity.

DISCUSSION

The results of this work show that the intracratonic area of study is undergoing differential stress probably caused by the interaction between the tangential forces transmitted from both the Mid-Pacific and the Mid-Atlantic Ocean Ridges. This interaction seems to be located mainly in the central region of the RPC. The general shortening in the area is approximately 2 mm/yr. Given that the considered stations are distant, probably the deformation is distributed among various structures. GNSS data proxy provides information to characterize the present regional field of deformation in the SE cratonic area of the South American plate. Therefore, the kinematics interpretation cannot unequivocally be attributed to a particular fault or segments of fault.

However, recent deformation might mainly be being distributed in the two major fault systems in the region, the Tostado Selva and Río Paraná Fault Systems (TSFS and RPFS).

Quaternary stratigraphic record displays shallow lake and pond facies in anomalous topographic positions. They were used as geomorphic markers of subsequent tectonic deformation (Brunetto et al, 2010; Brunetto et al., 2012). Gravimetric data enabled to identify old faults matching surface structural features, which suggested that the mechanisms of the active faulting is the reactivation of pre-existing faults without generating surface ruptures (Brunetto & Gimenez, 2012). The style of deformation would be characterized by dominant reverse displacements on blind faults that generates mild flexures in surface (Brunetto & Gimenez, 2012).

It is not yet well established if this dynamics have seismogenic capability in the area which could represent a seismic hazard. Nevertheless, 4 historical earthquakes of approximately 5M (less than 150 years ago) have been reported in the region, and the presence of circular ponds aligned with the main lineaments of faulting might be evidence of paleoearthquakes.

The geodesic data are not conclusive evidence of seismic hazard in the region. However, confluence of geomorphologic, stratigraphic and geological information allow to suspect that the main faults accumulate energy of deformation., Late Quaternary deformation detected in the region could be released: a) slowly through low magnitude earthquakes and/or b) by means of intermediate magnitudes earthquakes with very long recurrence periods. More detailed paleoseismological studies and the acquisition of high-resolution records using a network of local stations in order to detect low-seismicity will be required to answer these questions.

Acknowledgements: This work is framed in the research project CAI+D PI 2011 funded by the Littoral National University (Argentina)

References

Alves, M.C.S., M.C. Santos & C. Gemael, (2003). A velocity field estimation of the Brazilian portion of the SOAM plate. *GPS Solutions*. 7 (3), 186-193.

Brunetto, E., (2008). *Actividad neotectónica en el sector oriental de la cuenca inferior del río Dulce, laguna Mar Chiquita y bloque*

San Guillermo. Doctoral Thesis. Facultad de Ciencias Exactas, Físicas y Naturales, Universidad Nacional de Córdoba, (unpublished), 306 p.

Brunetto, E., M. Iriondo, L. Zamboni & M.G. Gottardi, (2010). Quaternary Deformation around the Palo Negro area, Pampa Norte, Argentina. *Journal of South American Earth Sciences*, 29: 627–641.

Brunetto, E., B.S. Ferrero, J. Marino, F. Tentor, M. Sturtz, L. Zamboni & L. Casanave, (2012). *Evolución geológica del Pleistoceno del centro de Entre Ríos*. V Congreso Argentino de Cuaternario y Geomorfología; Río Cuarto, Argentina, 132 p.

Brunetto, E., M.E. Gimenez, (2012). Características de la deformación cuaternaria en el centro de la llanura pampeana. *XV Reunión de Tectónica*. San Juan, Argentina, 36-37.

Brunetto, E., D. Kröhling, C. Francisconi, (2014). *La geomorfología de una región representativa de Pampa Norte y sur de la Mesopotamia en el contexto de los procesos endógenos. Aportes para el mapeo de áreas de llanura*. XIX Congreso Geológico Argentino; Cordoba, Argentina. S13.

Drewes, H., O. Heidbach, (2012). The 2009 Horizontal Velocity Field for South America and the Caribbean. In: *Geodesy for Planet Earth (*Kenyon S., M.C. Pacino, U. Marti eds.), IAG Symposia, 136: 657-664.

Iriondo, M., (1989). Major fractures of the Chaco-Pampa plain. In: *Bulletin of the INQUA Neotectonics Comission (*Mörner N. ed), N.A. 12, 42.

Mukul, M., S. Jadei, A.K. Bhattacharyya & K. Bushan, (2010). Crustal Shortening in Convergent Orogens: Insights from Global Positioning System (GPS) Measurements in Northeast India. *Journal Geological Society of India*. 75: 302-312.

Pasotti, P. & A. Castellanos, (1963). El relieve de la llanura santafesino-cordobesa comprendida entre los paralelos 32º y 32º 30´S desde 62º 45´W hasta el río Paraná. *Publicaciones del Instituto de Fisiografía y Geología de la Universidad Nacional de Rosario*. 47: 1-79.

Seemüller, W., L. Sánchez, M. Seitz, H. Drewes, (2010). The Position and Velocity Solution SIR10P01 of the IGS Regional Network Associate Analysis Centre for SIRGAS (IGS RNAAC SIR). *DGFI Report*. 86.

Smalley, R. Jr, M.A. Ellis, J. Paul & R.B. Van Arsdale, (2005). Space geodetic evidence for rapid strain rates in the New Madrid seismic zone of central USA. *Nature Letters*. 435: 1088-1090.

Stein, S., (2007). New Madrid GPS: Much ado about nothing? *Eos (Trans actions, American Geophysical Union*). 88: 58–60.

INQUA Focus Group on Paleoseismology and Active Tectonics

Active Fault Study in the Eastern Coast of Bali Island, Indonesia

Soehaimi, A., Setianegara, R.

Geological Agency, Ministry of Energy and Mineral Resources Indonesia, 57 Diponegoro Street, Bandung, Indonesia.
Email: s.asdani@yahoo.com

Abstract: *This note gives a first account of a capable right-lateral fault running NW-SE, found as a rectilinear scarp up to 6 m high, on the southeastern coast of Bali Island. Geomorphological, geophysical and geodetic data have allowed a first appraisal of this tectonic lineament. This fault might substantially contribute to the seismic hazard of the region and therefore needs be analyzed in detail and considered in a revision of the present SHA model for Bali.*

Key Words: *Geotectonics, Active Fault, capable fault.*

INTRODUCTION AND GEOLOGICAL SETTING

The Bali Island is a preferred international touristic destination, for its beautiful panorama and the Hindu Bali culture. This island is located between two mayor tectonic boundaries. Its western side, along the Bali Strait, is bounded by a right lateral strike slip fault (after Garwin, 2000). On the eastern part, along the Lombok Strait, there is the so-called Wallace Line, a biogeographic lineament that makes the boundary of Sunda Sheraton (west) and Australia Sheraton (east). In the southern part of this island, subduction along the Java trench of the oceanic Indo-Australia plate under the continental Sunda plate (7.5 cm/y) is source of strong seismicity, defining a typical Benioff zone (Fitch, 1972). The most recent destructive Bali earthquakes occurred in1976, 1977 and 2011. The strongest subduction event in this zone (Sumbawa earthquake, Mw 8.3) occurred in 1977. It caused a tsunami that hit also the east and south coasts of Bali, reaching a runup of 8 m. Historically, the most destructive event in Bali was recorded in 1917 (MMI IX, M 6.6); it caused at least 1,500 casualties, especially because of the numerous triggered landslides. North of Bali, in the Flores Sea, there is a system of active back-arc thrusts and back-thrusts, which are also source of relevant seismic hazard.

Several old and active volcanoes lie in the median part of Bali, the most active being Buyan - Baratan, Batur (Pleistocene - Holocene) and Agung (Holocene - Recent). At the top of Buyan - Bratan and Batur volcanoes there are big craters and lakes, with steep slopes. Several faults with clear signs of Holocene activity are located in the surroundings of this volcano range. The highest elevation in this region is reached by the volcanic cone and crater valley of Seraya, at 1058 m above sea level.

Apart from the median zone of volcano apparatuses, the rest of the island has a gentle morphology, with flat or gently undulated areas. The stratigraphy is mainly made of volcanic products, with Quaternary alluvial and slope deposits made of reworked volcanic material. Coral reef limestones are found in the southern edge of the island. Thrust and strike-slip faulting is found cutting the Ulakan volcanic products and the coral reef limestones. Faulting affects also the recent (Late Pleistocene-Holocene) Buyan - Bratan, Batur and Agung volcanic deposits. In particular, on the eastern coast of the island between Klungkung and Sanur areas, an active fault has been recognized marked by elongated fault scarps (N 50°E/80°) parallel to the NE-SW-trending coastal zone (Fig. 1). Average height of this scarp is 6 m above sea level, with northwest block up. Based on fault kinematic analyses, this right lateral fault has also a normal component. In this short note, we give a first account of this feature, which potentially has a great relevance for the seismic hazard of the island.

The Sumatera fault is the most active and hazardous seismic source zone in the Sumatera Island, after the subduction zone, whose earthquakes can reach extreme magnitudes, as occurred in 2004 (e.g., Lay et al., 2005). Therefore, the seismogenetic studies along this fault are of great relevance for seismic hazard assessment. The deformation study by GPS monitoring introduced here is an important contribution to the aim above, since it provides a quantitative estimate of slip movement. This quantitative value contributes to evaluate the maximum potential magnitude and possibly point out particularities in the strain field.

Figure 1: Elongated fault scarp of Eastern coast Bali Island active fault.

NEOTECTONIC ANALYSIS

The lithostratigraphy study has shown three facies of deposits: volcanic facies (in land area), transition facies (between in land and coastal area) and fluvial facies (in land area). The transition facies is shown by old beach sand, located 6 m above present sea level, which consists of coarse grains of pumice, medium grains of femic crystals and light minerals as feldspar and quartz. Its elevation is indicative of the uplift processes in this area. Indications of main fault reactivation is found in the fluvial facies where a shear zone with reverse fault mechanism can be seen N345°E/83°. This fault is a secondary fault of main fault (normal right-lateral fault). Lithology variation and fault indication are shown in Figure 2.

Morphostructural indications of active faulting are the intensive head-ward erosion process along river channels that cut across the fault scarp and fans deposits in front of it. The presence of this fault underground has been also imaged by means of geoelectrical and GPR soundings across the main scarp. Geoelectrical resistivity and electromagnetic wave soundings have revealed a typical anomaly of fault displacement. Near surface ruptures are also expressed by the Ground Penetration Radar (GPR). Vertical cross-section of geo electrical and GPR soundings on the same trace are shown in Figure 3.

GPS monitoring in Bali Island, period March 2013 – April 2014 (PVMBG, Geological Agency, 2014), shows that the GPS benchmarks mainly move relatively toward NE, with horizontal velocity rates of 17.6 to 48.7 mm/y. Several GPS benchmarks along the fault cited above (BMKG, Sukowati/SKWT, Kelungkung/KLKG), show a different rate of horizontal and vertical movements between the NW block (KLKG benchmark: H = 48.7 mm/y, V = 1293.56 mm/y, influenced by local landslide) and the SE block (BMKG benchmark: H = 42.6 mm/y, V = - 51.6 mm/y). The different benchmark velocities point to a normal right-lateral fault movement between the two fault blocks. Figure 4 shows a map of the Eastern Bali Island active fault.

POTENTIAL EARTHQUAKE HAZARD

Potential earthquake hazard in Bali Island expressed by Indonesia Seismic Hazard Map, Ministry of Public Work (2012). In this map Bali island located in a high- seismic hazard zone which is shown the bedrock acceleration at short period S_S = 0.8 to 0.9 g and bedrock acceleration at 1 second period S_1 = 0.3 to 0.4 g. The maximum intensity of destructive earthquakes in Bali Island shown by the Seririt Earthquake (1976) and the Culik Earthquake (1979), both earthquakes were felt at VIII MMI (Soehaimi, et al., 2014). The Composite Intensity of destructive earthquakes in Bali Island is given in Fig. 5 (Soehaimi et al., 1993).

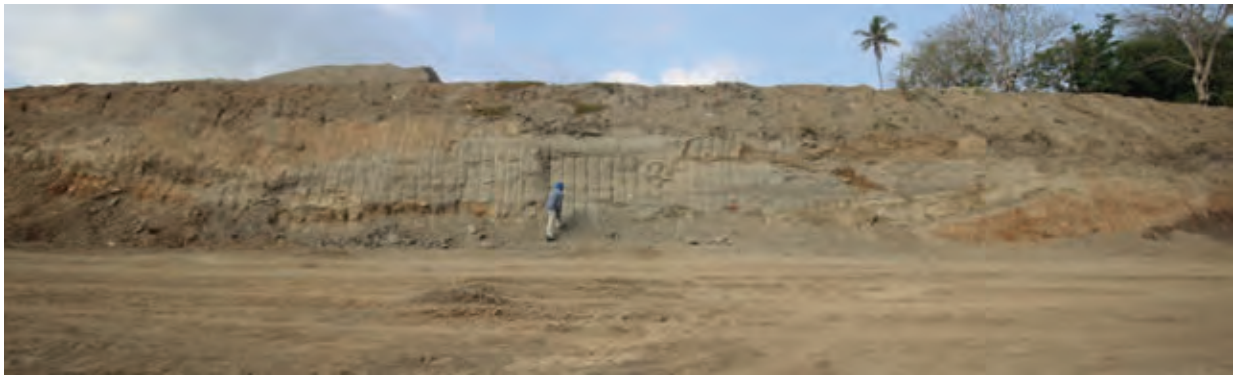

Figure 2: Outcrop showing lithology change and reactivation fault of N345°E/83° (secondary fault), main fault located at right figure.

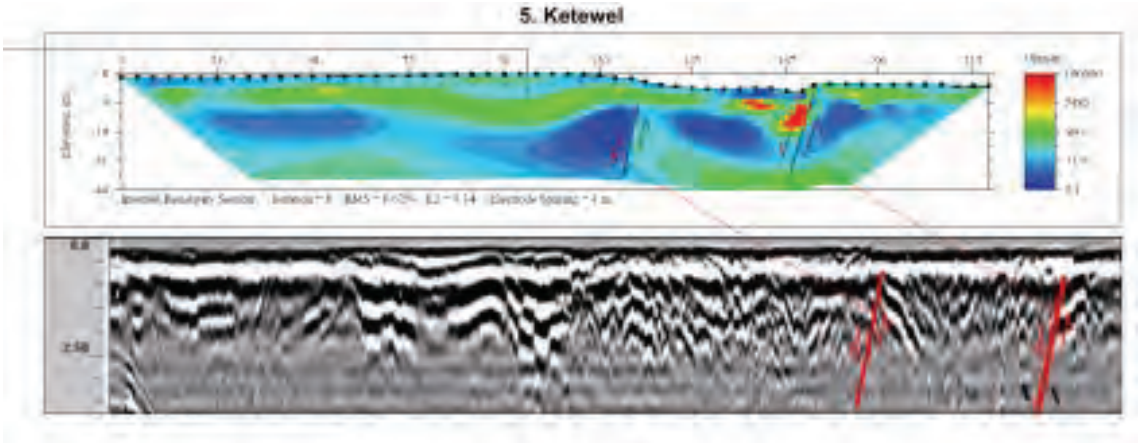

Figure 3: Profiles of near surface geo electrical and GPR soundings, with anomalies indicating the N 50°E fault.

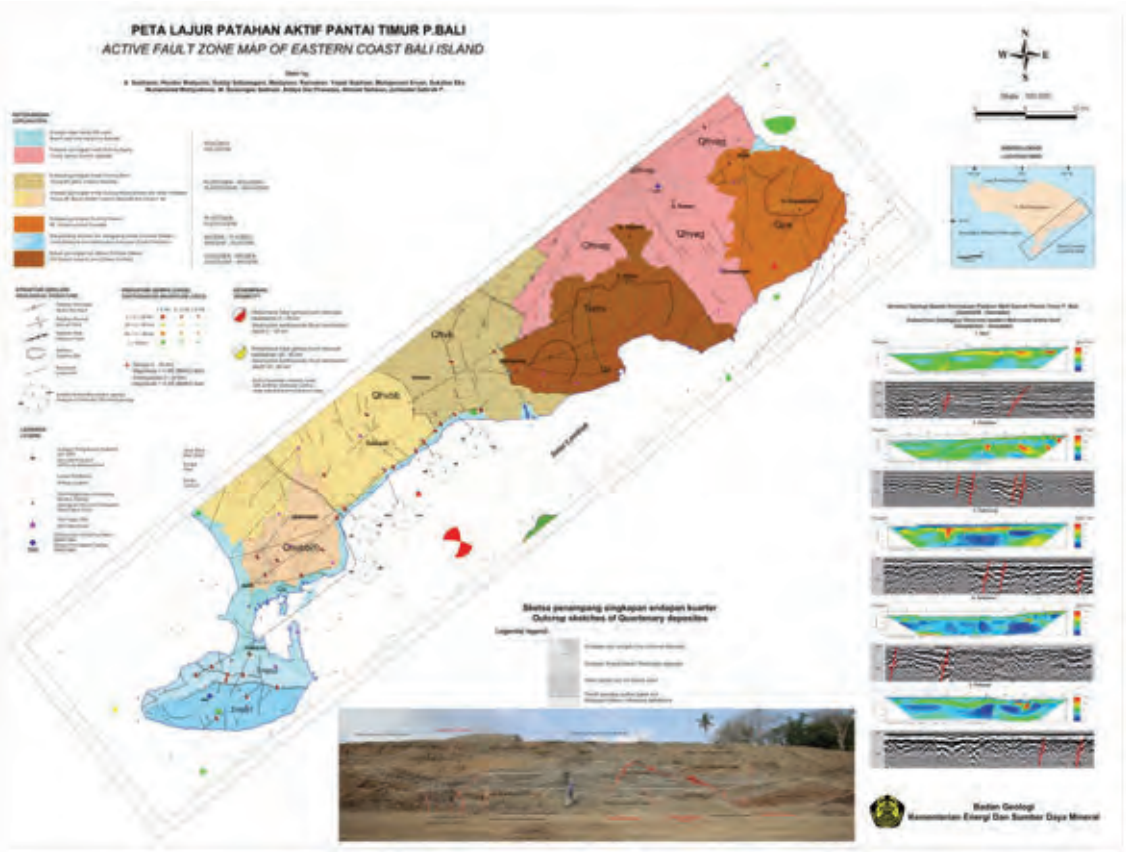

Figure 4: Active fault zone map of Eastern Bali Island.

CONCLUSIONS

Figure 5: Composite Intensity of destructive earthquakes in Bali island (Soehaimi et al., 1993).

The eastern coast of Bali Island is marked by an active fault that represent one of the seismic source zones to be considered in SHA. Based on the Global Relations between Seismic Fault Parameters and Moment Magnitude of Earthquakes equations by Papazachos B.C et all (2004), the maximum earthquake magnitude (Mw) of this faults is estimated to be 6.5. In order to mitigate the consequent earthquake risk in this region, the current seismic hazard assessment (either PSHA or DSHA) should be updated taking into account this fault and the basic characters for site response analysis (microzonation) should be assessed.

Acknowledgements: The authors wish to thank the Preparatory Committee of the 6th International INQUA Meeting on Paleoseismology, Active Tectonics and Archeoseismology (PATA-Days) in Fucino, Italy, and all their colleagues in the Quaternary Working Group of the Geological Survey Institute, Geological Agency, Ministry of Energy and Mineral Resources for their contributions on seismotectonics and active fault research in South Sumatera.

References

Fitch, T.J., (1972). Plate convergence, transcurrent faults, and internal deformation adjacent to Southeast Asia and the western Pacific. *J. Geophys. Res.* 77, 4432-4460.

Bali Governor Office, (1976). Information of destructive earthquake of Seririt 1976. *Internal report of Bali governor office.*

Bali Pos July 20, (1976). The losses caused by destructive earthquake of Seririt 1976.

Garwin, S., (2000). *The setting, geometry and timing of intrusion-related hydrothermal systems in the vicinity of the Batu Hijau porphyry copper-gold deposit, Sumbawa, Indonesia*. Unpublished Ph.D. thesis, Nedlands, Western Australia, University of Western Australia, 320 p.

Kertapati, E., E. Putranto, I. Bahar, (1991). The destructive earthquakes catalog of Indonesia. *Geological Research and Development Centre*.

Ministry Public Work of Indonesia, (2012). Peta gempa Indonesia NEIC, USGS. (2014). Seismicity of Bali island in years 1973 – 2014.

Purbo Hadiwidjoyo, M.M., H Samodra, and T.C. Amin, (1998). *Geological Map of Bali Island, Scale 1:250,000.*

Papazachos, B.C., E.M. Scordillis, D.G. Panagiotopoulos, C.B. Papazachos and G.F. Krakaisis, (2004). Global relations between seismic fault parameters and momento magnitude of earthquake. *Bull of Geological Society of Greece*. Vol. XXXVI, 2004.

Soehaimi, A., E. Kertapati, (1993). Seismotectonic of Bali Island. *CCOP Technical Workshop*. Bali 1993.

Soehaimi, A., J.H. Setiawan, and Marjiyono (2014). Seismotectonics and active faults of Bali Island. *5th International INQUA meeting on Paleoseismology, Active Tectonics and Archeoseismology (PATA).* Busan Korea, 153-156.

INQUA Focus Group on Paleoseismology and Active Tectonics

paleoseismicity.org

Digging for records of slow fault slip in the region with strong Pleistocene periglacial mass wasting: experience from the Bohemian Massif (Alpine-Carpathian foreland)

Špaček, P. (1), Ambrož, V. (1), Táborík, P. (2), Štěpančíková, P. (2)

(1) Inst. of Physics of the Earth, Masaryk University, Brno, Czech Republic. Email: spacek@ipe.muni.cz
(2) Inst. of Rock Structure and Mechanics, Academy of Science of the CR, Prague, Czech Republic

INTRODUCTION

The Bohemian Massif forms a part of the Alpine-Carpathian foreland (Fig. 1) which was affected in Tertiary by considerable faulting related to alpine collision. Local Pleistocene subsidence in Neogene basins, weak present-day seismicity and some other features indicate that slow faulting continues to Quaternary in some parts of the massif. The general uplift of the massif throughout Cenozoic has lead to its long-term regional-scale denudation, resulting in differential erosion and local formation of relatively high scarps often resembling those of large active faults. In Pleistocene, the continental ice sheet repeatedly proceeded to within 0-300 km off the northern limits of the Bohemian Massif (Fig. 1) and the topography of the slopes was often rejuvenated by periglacial mass wasting. While the non-tectonically rejuvenated scarps associated with older faults are often misinterpreted as a signature of active tectonic slip, the periglacial process

Figure 1: Schematic map showing the junction region of the Bohemian Massif (green) and the Alpine-Carpathian orogeny (orange). The Upper Morava basin (blue) is superposed onto their tectonic contact. Vertical hatching shows the maximum extent of Pleistocene ice-sheet.

of slope degradation is the most serious obstacle to correct fault slip analysis since it largely overprints the possible record of tectonic faulting. Here, example is given of a fault scarp where multiple trenching allowed to distinguish the tectonic deformation of sediments from the superposed slope-related faulting. Some other examples are briefly noted to illustrate the variety of slope deformation structures which may be ambiguous and therefore incorrectly interpreted.

TECTONIC NORMAL FAULTING OR LANDSLIDING? (CASE STUDY)

Extensive research is being carried out of the faults of the Upper Morava Basin - a Plio-Pleistocene structure superposed onto the Carpathian front (Špaček et al., 2014). We selected a prominent, NW-SE trending Kosir fault with the length of 30 km and pronounced morphology to perform a detailed study of its SW scarp evolution in Upper Pleistocene to Holocene. Shallow structure of the foot slope was studied by electric resistivity tomography (ERT) on several profiles (2 examples in Fig. 2). In most profiles a moderately to steeply dipping (50-80°) fault terminating the Tertiary basin against the Devonian to Late Carboniferous shales and limestones is clearly seen. The fault is covered with variably thick (up to >10m) deposits interpreted as coarse- to fine-grained colluvium and loess. Two sites for trenching were selected in the fault segment with relatively high scarp, each exhibiting different morphology and diferent relative position of the fault trace and slope foot.

First trench (trench A, 30 m long and 4-6 m deep, locality Starechovice; Fig. 2) was located in a relatively steeper slope (~15°) with >17 m thick sediment accumulation verified by a shallow drill. It exposed the succession of several generations of loess with paleosol and colluvia on top of the bedrock disrupted by numerous moderately to steeply (60-80°) dipping synthetic faults and minor antithetic faults, both exhibiting prevailing normal slip ranging from <1 cm to 1.6 m (Fig. 3). These faults form a splay-like system resulting in the stepwise shape of the basin margin revealed by electric resistivity tomographic profiles. Both syn- and post-sedimentary faults are present and clear basinward increase of their age is indicated.

The succession exposed in the trench and reached by the drill was dated at 12-75 ka by one ^{14}C and six OSL ages (all internaly consistent) allowing a detailed, time-constrained reconstruction of sedimentary and deformational processes. At the main fault, relatively large slip rate of 0.2-0.3 mm/a is indicated for Late Weichselian to Early Holocene (17-11 ka).

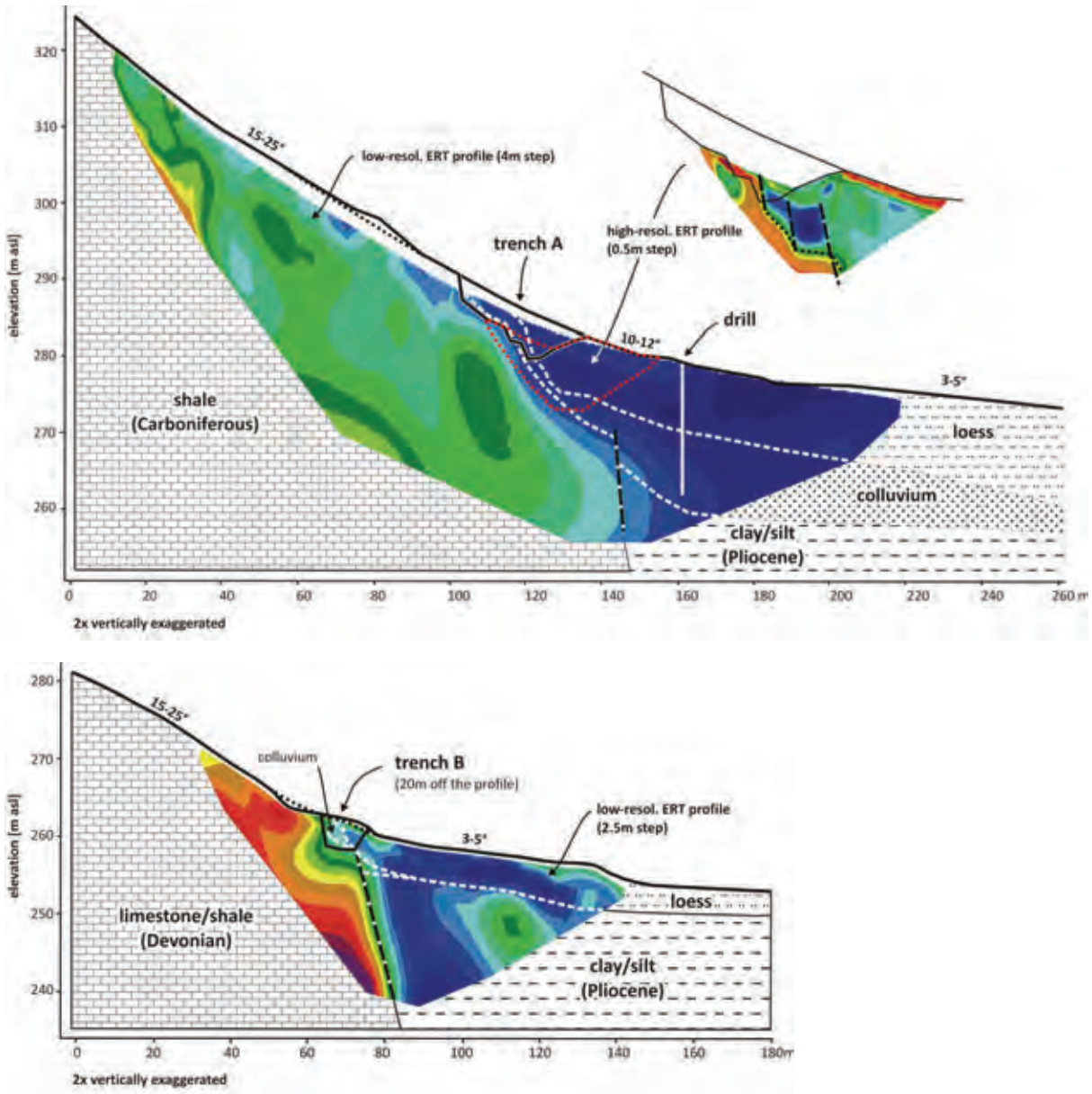

Figure 2: Elevation profiles and interpreted electric resistivity tomographic profiles (ERT) at the trenching sites A and B.

Although the repeated activity localized in a relatively narrow zone with only meter-scale migration towards the slope may support the tectonic origin of the faults, many features (blind faults, significant back-rotation of the hanging-wall blocks) suggest that the general architecture was formed by near-surface, creep-like slope-related slip. Slope-related origin is also supported by ERT-indicated moderately dipping boundary between bedrock and colluvium (Fig. 2). The whole structure may be interpreted as a slow landslide, the exposed faulted zone representing its headwall and accomodation zone above the basal shear plane with uneven, bedrock controlled, topography. The development (and the relaxation rate) of the slope instability may have been partly controlled by tectonic slip on the main burried fault, nevertheless, these relations could not have been determined at this site alone.

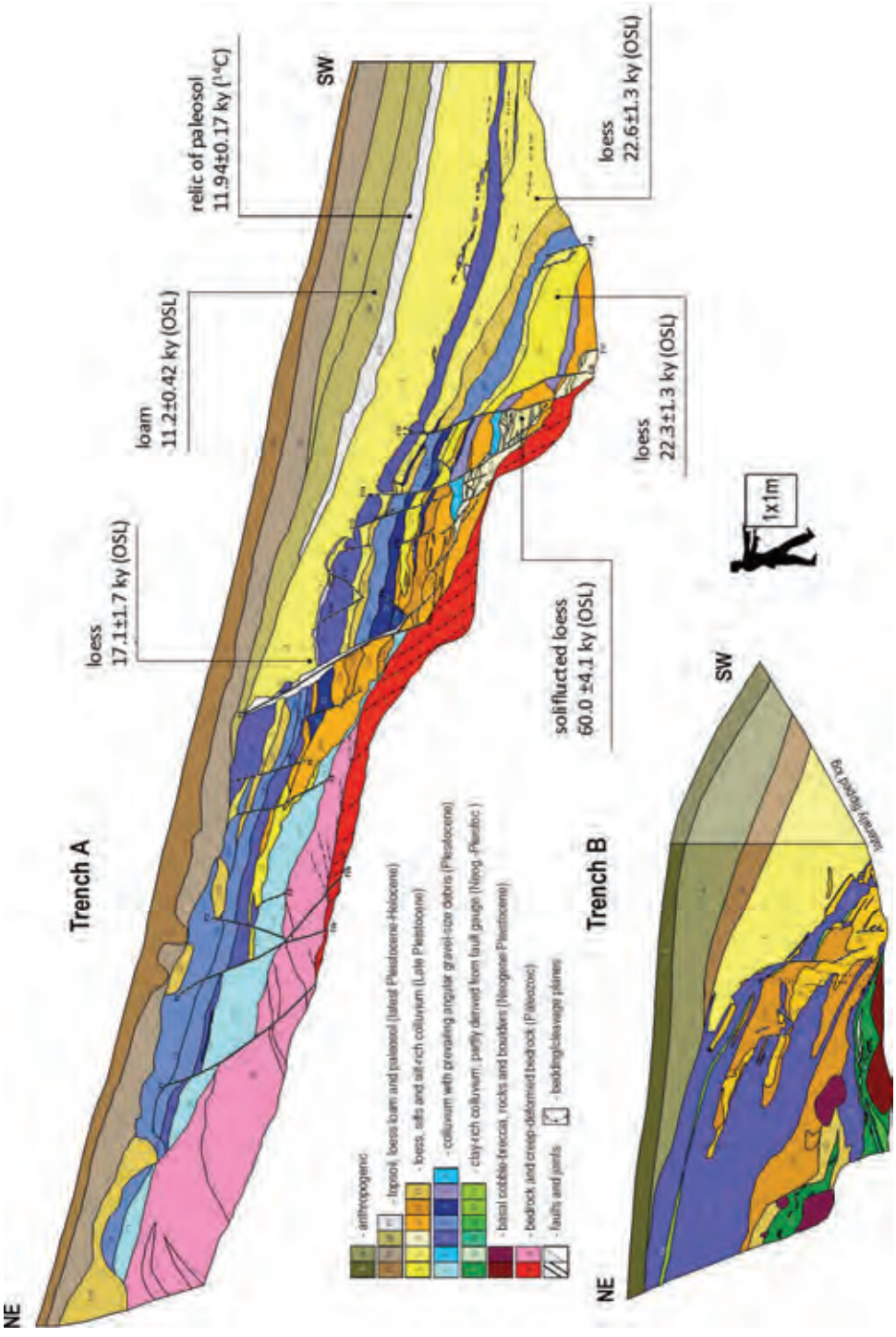

Figure 3: Schematic logs of trenches A and B. The contrasting intensity of faulting is explained by different dominant mechanisms of deformation - landsliding (trench A) and slow tectonic slip (trench B).

To help solving this problem we trenched another site on the same fault (trench B, 13m long and >4.5m deep; locality Čelechovice, 1.5km from trench A; Fig. 2) at the foot of scarp with flat (5° slope) relief beneath. Slight anthropogenic modifications to shallow depth were indicated. Here, no suitable conditions for the formation of a landslide with deep-reaching base are expected, although solifluction in the active layer of permafrost is likely to have occurred. Similar to trench A, top loess layer is in a rather steep contact (35-40°) with a narrow

wedge of colluvium formed by alternating gravelly debris, silt-rich debris and silt beds (Fig. 2). The lower part of the colluvium contains large limestone boulders, sheared clays and basal cobbly breccia likely representing an older fault scarp deposit. In contrast to trench A, clear discrete faults or shear bands are very rarely observed. However, steeply cut beds within the colluvial succession above the geophysically indicated fault suggest a small active slip in Pleistocene. A more detailed geophysical survey and redeepening of the trench is planned to rule out the possible role of the loess-covered paleorelief or deeper reaching solifluction zone on the slope instability.

When comparing the two excavated profiles we clearly see distinct contrasts in the style of the faulting which can be attributed to significantly different mechanisms of deformation. The inferred slope instability-related faulting (trench A) is much better developed than the assumed small tectonic slip on the same fault (trench B). If bedrock was not reached in the trench A, the observed structures could have been easily mistaken for normal faulting of purely tectonic origin.

THE CHALLENGING GELIFLUCTION

Permafrost reaching to minimum depths in order of 50-100 m formed repeatedly in the Bohemian Massif since Lower Pleistocene (e.g., Czudek, 1997). The thickness of active layer is mostly less than 2 m, however, in periods of climate warming we must assume general deepening of permafrost surface topped by water-saturated layer forming a deeper seated zone of mechanical weakness. When clay-rich lithologies prevail at the footslope, the effects of gelifluction may reach far from the scarp, causing deeper reaching (>3 m) deformation even in a flat topography with <5° slope. This may be explained as a forced deformation by large volumes of mass derived from the scarp rather than driven by the in-situ slope instability. Gelifluction taking place on fault scarps not only leads to destruction of the records of older faulting but sometimes produces small-scale deformation structures closely resembling the tectonic ones.

In addition to flat shear zones often observed in geliflucted colluvium (variable thickness, dip angle ranging between that of the present surface and subhorizontal), steeply dipping zones with preferred orientation of clasts were observed in silt-rich colluvium near its steep (~75°) contact with bedrock. This can be explained, apart from the tectonic origin, as a result of strain localization at the fixed leading boundary between the rocks with contrasting rheological properties during the ductile flow of water-saturated loose colluvium.

Small scale faults with slip of cm-dm order are sometimes observed in soft sediments affected by solifluction. These are common in clay-rich sediments where perfect slickensides are developed and may also bear striations, sometimes significantly deflected from dip direction. Less comonly, well developed steep faults of non-tectonic origin were observed in sands, possibly formed by solifluction-driven reactivation of older tectonic faults.

CONCLUSION

General instability of slopes in periglacial zone puts considerable limitations to active fault slip studies. Processes of mass wasting often bias the records of older faulting and obliterate the information on the age of faulting, often leaving us with the only option to date it merely as „pre-solifluction". After critical assessment of profiles excavated in footslope deposits we often come to conclusion that structures strongly resembling tectonic deformation were likely produced by slope-related deformation or that we are simply not able to distinguish between the two. Trenching to larger depths often reveals a non-tectonic origin of near-surface steep faults by showing their linkage with flat detachment zones. It must be kept in mind that in case of deeper reaching landslides these cryptic relations may not be revealed by trenching within <10 m below surface. We emphasize here a need of caution when interpreting structures on slow faults with assumed normal kinematics in regions with strong regional Pleistocene mass wasting.

Acknowledgement: This research was supported by Czech Science Foundation Project P210/12/0573.

References

Czudek, T., (1997). Relief of Moravia and Silesia in Quaternary. *Sursum. Tišnov*. 213 p. (in Czech).

Špaček P., O. Bábek, P. Štěpančíková, J. Švancara, J. Pazdírková, J. Sedláček, (2014). The Nysa-Morava Zone: an active tectonic domain with Late Cenozoic sedimentary grabens in the Western Carpathians' foreland (NE Bohemian Massif). *International Journal of Earth Sciences*. doi: 10.1007/s00531-014-1121-7.

INQUA Focus Group on Paleoseismology and Active Tectonics

paleoseismicity.org

Sedimentary and tectonic evolution of the San Nicandro lacustrine depositional system (Pliocene-Pleistocene, southern L'Aquila Basin, central Italy)

Spadi, M. (1), Cosentino, D. (1,2), Nocentini, M. (1), Gliozzi, E. (1,2)

(1) Dipartimento di Scienze, Università degli Studi Roma Tre, Rome, Italy. Email: marco.spadi@uniroma3.it
(2) Istituto di Geologia Ambientale e Geoingegneria-CNR, Rome, Italy

Abstract: *L'Aquila Basin, like many other intermontane basins in central Italy, developed due to an extensional tectonic regime, still active, which controlled its sedimentation. In the south-eastern branch of the L'Aquila Basin, the Paganica-S. Demetrio-Castelnuovo (PSC) sub-basin, the tectono-sedimentary processes lead the deposition of three main synthems: San Demetrio Synthem (upper Piacenzian-Gelasian), San Mauro Synthem (Middle Pleistocene), and Late PSC Synthem (Upper Pleistocene-Holocene). The San Demetrio Synthem includes a deep-lacustrine depositional system and its marginal deposits. Within this synthem, a peculiar ostracod fauna made of six new species referable to genera Caspiocypris, Cypria and Ilyocypris was found, which suggested the correlation with the Late Piacenzian-Gelasian ostracod assemblages of the Tiberino Basin, dating the setting of the PSC sub-basin to the Late Pliocene-Early Pleistocene.*

Key words: *Quaternary Geology, L'Aquila Basin, Lacustrine environment, Ostracods palaeontology.*

INTRODUCTION

The L'Aquila Basin is an intermontane basin correlated to the extensional tectonics that affected the Apennine chain in its post-orogenic phase. Most of the central Apennine intermontane basins (Tiberino, Rieti and Fucino basins) developed as morpho-structural depressions with a west-dipping master fault on the eastern margin and antithetical minor faults delimiting the western margin (Fig. 1).

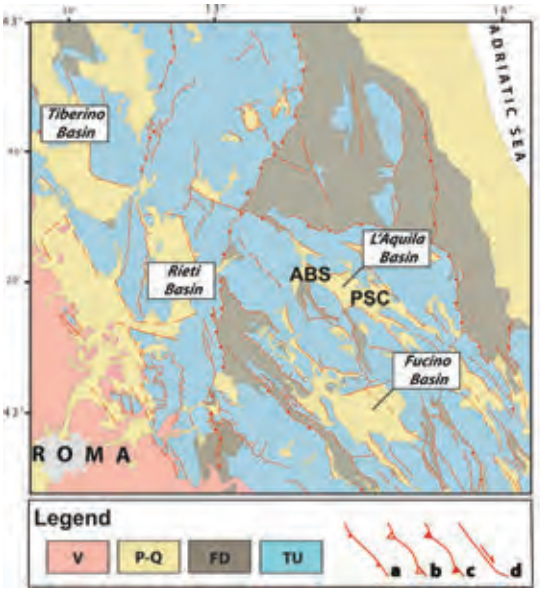

Figure 1: Structural sketch of the central Apennines. V: Quaternary Volcanics; P-Q: Plio-Quaternary marine and continental deposits; FD: Apennine Foredeep Deposits; TU: Apennine Tectonic Units; a) normal fault; b) minor thrust; c) major thrust; d) strike-slip fault; (modified from Cosentino et al., submitted).

Those extensional tectonic elements played an important role on the sedimentary evolution of the Plio-Quaternary deposits of the L'Aquila Basin. The entire L'Aquila Basin is a complex system formed by the coalescence of smaller basins. Its sedimentary filling is made of continental deposits that unconformably overlay the Meso-Cenozoic bedrock, which crops out along the margins of the basin. The basin is divided by L'Aquila-Hill into two major sub-basins: the L'Aquila-Scoppito sub-basin (ASB) to the west, and the Paganica-S. Demetrio-Castelnuovo sub-basin (PSC), to the southeast. Many recent studies carried out after the L'Aquila earthquake (April 6, 2009), focalized their attention mainly on the recent deposits. Very few papers have been recently focused on the long-term tectono-sedimentary evolution of the basin. In this paper, we want to stress our attention on the early stage of evolution of the PSC sub-basin, showing new data on its stratigraphical setting and fossil content.

Geological setting of the PSC sub-basin

In the PSC sub-basin, three main filling phases, related to the Pliocene-Quaternary interval, were recognised. The oldest deposits pertain to the San Demetrio Synthem that includes different formations deposited in a lacustrine environment (Cosentino et al., submitted). This synthem is unconformably overlain by the San Mauro Synthem (Bertini & Bosi, 1993) (= Upper fluvial PSC Synthem in Giaccio et al., 2012), formed by fluvial and alluvial fan coarse grain deposits. In the upper part of the San Mauro Synthem, a tephra layer was $^{39}Ar/^{40}Ar$ dated to an age of 367±2 kyr. The PSC filling ends with terraced alluvial deposits, Late PSC Synthem (Giaccio et al., 2012) (Late Pleistocene-Holocene) related to the erosional and depositional processes still active in the L'Aquila intermontane basin (Fig. 2).

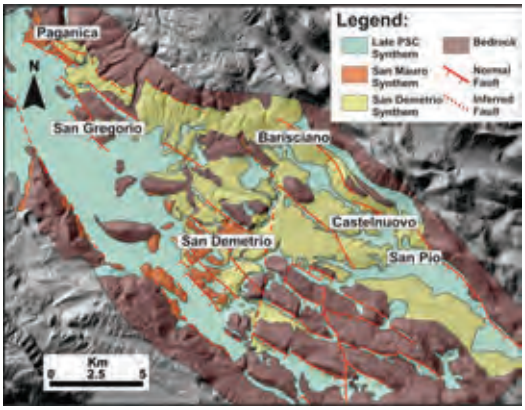

Figure 2: Simplified geological map of the Paganica-San Demetrio-Castelnuovo (PSC) sub-basin.

The last two synthems are at the hanging wall of the Paganica-S. Demetrio fault system in the western part of the sub-basin, indicating the activity of this fault system since at least the Middle Pleistocene (Giaccio et al., 2012). On the contrary, the San Demetrio Synthem occupies a larger portion of the basin, indicating a different impact on the paleogeography of the PSC-sub-basin (Fig. 3).

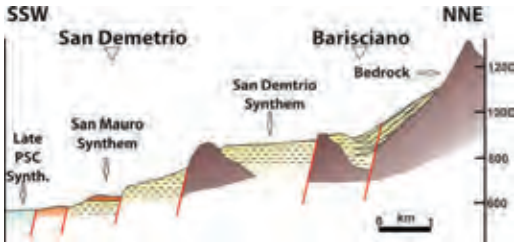

Figure 3: Geological sections across the PSC sub-basin, modified from Giaccio et al., 2012.

The San Demetrio Synthem includes several formations deposited in different environments related to a lacustrine system. The first formation (San Nicandro Fm.) consists of laminated to massive whitish calcareous silts bearing freshwater ostracods, sponges spicules (*Spongilla lacustris*) and mollusc fragments. Those fossil assemblages point to a relatively deep-water and low energy lacustrine environment (Fig. 4). Above or heteropical to it, a Gilbert-type delta system gradually formed, depositing bottomset beds (Prata d'Ansidonia Fm.), marked inclined foresets beds (about 30° dipping) arranged to form a delta slope (Valle Orsa Fm.), and topset beds with sub-parallel horizontal stratification related to a floodplain (Valle dell'Inferno Fm.). Bedding and paleocurrent analyses reveal that Gilbert-type delta prograded into the lake (San Nicandro Fm.) from N or NW. Its coarse sediments are made of well-rounded calcareous gravels, while silts and silty-sands represent the fine-grained deposits.

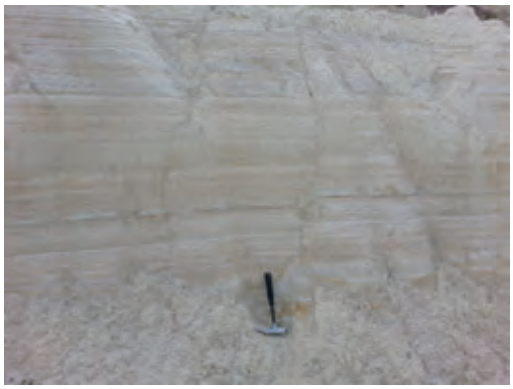

Figure 4: Laminated deep-lacustrine silts of San Nicandro Fm. crop out near Castelnuovo village.

Along the northeastern margin of the lake, alluvial fan and slope deposits developed with conglomerates (Valle Valiano Fm.), breccia deposits (Fonte Vedice Fm.), and intercalations of silts and fan conglomerates (Madonna della Neve Fm.) (Giaccio et al., 2012).

Chronological constrain

The ostracod assemblages recovered in the San Nicandro, Prata d'Ansidonia and Valle Orsa formations. are characterized by a *Caspiocypris* species flock, with the dominance of four new species of *Caspiocypris* and with the presence of two new species related, respectively, to *Cypria* and *Ilyocypris* genera (Fig. 5) (Spadi et al., submitted). The peculiar ostracod assemblage of the San Nicandro Fm. can be compared with the ostracod assemblages of the Fosso Bianco Fm. in the Tiberino Basin, which bears a similar *Caspiocypris* species flock (Medici and Gliozzi, 2008). As far as we know, the San Demetrio Synthem and the Fosso Bianco Fm. are the only post-Messinian Italian deposits that bear this genus. Then, we suggest a correlation between the lake deposits of the San Demetrio Synthem (L'Aquila Basin) and the upper Piacenzian-Gelasian lacustrine succession of the Fosso Bianco Fm. (Tiberino Basin). Further correlations on the morpho-stratigraphical evolution of both the ASB and the PSC sub-basins with respect to other central Apennine intermontane basins (Tiberino and Rieti), and the tectono-stratigraphic evolution of the Tyrrhenian margin of the central Apennines, further constrain the L'Aquila Basin set up during the late Piacenzian (Cosentino et al., submitted).

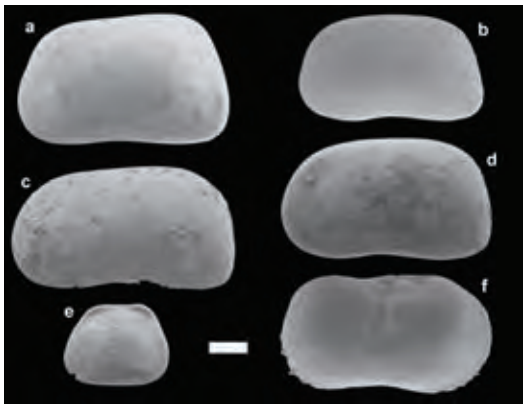

Figure 5: Ostracod assemblage from San Demetrio Synthem. a: Caspiocypris 1 sp. nov.; b: Caspiocypris 2 sp. nov.; c: Caspiocypris 3 sp. nov.; d: Caspiocypris 4 sp. nov.; e: Cypria sp. nov.; f: Ilyocypris sp. nov. (Spadi et al., submitted). White bar corresponds to 0.2 mm.

DISCUSSION

According to the paleoenvironmental reconstruction based on the location of the deep lacustrine sediments, the San Nicandro Lake had an elongated shape oriented NW-SE with a length of at least 15 km and a maximum width of 7 km. The lake extended on a surface about 70 km2 from San Gregorio village (to the north) to San Pio delle Camere (to the south) (Fig. 6). It is possible to state that during the late Piacenzian-Gelasian the PSC sub-basin was largely occupied by lake. The lake margins were characterized by steep coastlines, as demonstrated by the coarse and disorganized slope-related sediments at the basin margin. The Gilbert-type delta with 30-40 m thick foresets developed on equally high-submerged escarpments (Basilici, 1997).

This indicates that nearby the margins the lake was at least 40 m deep. However, it is possible to suppose that distally the lake was deeper, as suggested by the dominance of *Caspiocypris*.

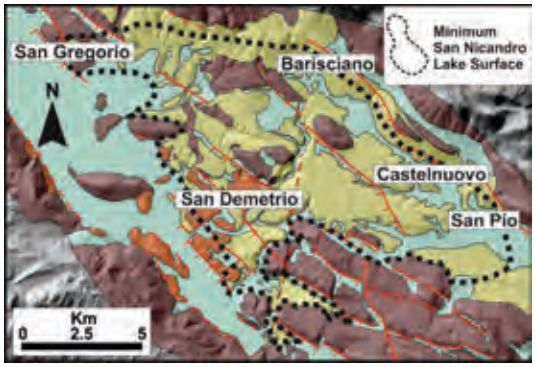

Figure 6: Probable minimum surface of the San Nicandro Lake based on the outcrops of deep lacustrine silts (San Nicandro Fm.). See Fig. 2 for the legend of geological map.

The paleomorphological characteristics inferred for the San Nicandro Lake suggest that its origin and evolutive history was strongly controlled by tectonics in a rapid subsiding basin. The extensional tectonics responsible for the evolution of the basin acted along NW-SE normal faults at the NE margin of the PSC sub-basin. In fact, the present day distribution of the sediments related to the San Demetrio Synthem generally reflects the geometry of the main tectonic structures that occur within the sub-basin, with the marginal deposits (alluvial fan sediments) arranged along these tectonic features.

CONCLUSION

1) According to the ostracod assemblages found within the San Demetrio Synthem, the opening, and subsequent evolution, of the south-eastern sector of the L'Aquila Basin (PSC sub-basin) occurred in the late Piacenzian-Gelasian with the deposition of the lacustrine depositional system of the San Demetrio Synthem. Three main different depositional environments have been recognized: (1) a distal deep lake, where mainly fine-grained deposits occur (San Nicandro Fm.); (2) the proximal areas at the lake margins, with Gilbert-type delta deposits; and (3) steep coasts at the NE margin.
2) The San Nicandro Lake was a large and deep lake, at least 15 km long, 7 km wide and $\geq$ 40 m deep, elongated NW-SE. Its size, shape, depth, and facies distribution were mainly controlled by NE-SW extension.

References

Basilici, G., (1997). Sedimentary facies in an extensional and deep-lacustrine depositional system: the Pliocene Tiberino Basin, Central Italy. *Sedimentary geology*. 109, 73-94.

Bertini, T., C. Bosi, (1993). La Tettonica Quaternaria nella Conca di Fossa (L'Aquila). *Il Quaternario*. 6 (2), 293-314.

Cosentino, D., R. Asti, M. Nocentini, E. Gliozzi, T. Kotsakis, M. Mattei, D. Esu, M. Spadi, M. Tallini, F. Cifelli, M. Pennacchioni, G. Cavuoto, V. Di Fiore, (submitted). Onset and subsequent evolution of the central Apennine extensional intermontane basins: New insights from the tectonically active L'Aquila Basin (central Italy). *Quaternary Science Reviews*. (submitted).

Giaccio, B., P. Galli, P. Messina, E. Peronace, G. Scardia, G. Sottili, A. Sposato, E. Chiarini, B. Jicha, S. Silvestri, (2012). Fault and basin depocentre migration over the last 2 Ma in the L'Aquila 2009 earthquake region, central Italian Apennines. *Quaternary Science Reviews*. 56, 69-88.

Medici, M.C., E. Gliozzi, (2008). Preliminary data on freshwater ostracods from the Middle-Late Pliocene Tiberino "palaeo-ancient lake" (Umbria, Central Italy). *Atti del Museo Civico di Storia Naturale di Trieste*. supplement vol. 53, 49-66.

Spadi, M., E. Gliozzi, D. Cosentino, M. Nocentini, (submitted). Late Piacenzian-Gelasian freshwater ostracods (Crustacea) from L'Aquila Basin (central Apennines, Italy). *Journal of Systematic Palaeontology*. (submitted).

INQUA Focus Group on Paleoseismology and Active Tectonics

Holocene activity of the Mariánské Lázně Fault (Cheb basin, Bohemian Massif): youngest proved surface faulting in central Europe?

Štěpančíková, P. (1), Táborík, P. (1,2), Fischer, T. (2), Hartvich, F. (1), Karousová, M. (2), Stemberk, J. (1,2), Nováková, L. (1)

(1) Institute of Rock Structure and Mechanics, Czech Academy of Sciences, V Holešovičkách 41, 18209 Prague 8, Czech Republic. Email: stepancikova@irsm.cas.cz
(2) Charles University in Prague, Faculty of Science, Albertov 6. Prague 2, 128 43, Czech Republic

Abstract: *The NNW-SSE trending Mariánské Lázně Fault (MLF) zone is situated in the western part of the Bohemian Massif (Czech Republic). It is morphologically very pronounced and limits the Tertiary Cheb basin on the SE. A trenching survey was combined with shallow geophysics to study the late Quaternary activity of the MLF. Trenching revealed repeated movements along the several faults of various ages within the MLF on the Cheb basin limit. The youngest fault cuts and deformes young Holocene deposits of the age interval 5.3 - 1.1 ka BP, which is the youngest proved surface faulting in central Europe reported so far.*

Key words: *Paleoseismology, shallow geophysics, Holocene faulting, Mariánské Lázně Fault, Cheb basin.*

The NNW-SSE trending Mariánské Lázně Fault (MLF) zone is one of the morphologically most pronounced features in the western part of the Bohemian Massif (Fig. 1). The northern segment limits the Tertiary Cheb Basin, which is typical of present-day earthquake swarms, abundant occurrences of mantle-derived carbon-dioxide emanations, and Quaternary volcanism. The MLF intersects the N-S main seismoactive zone of Nový Kostel, the most active zone of the West Bohemia/Vogtland region (Fischer et al. 2012).

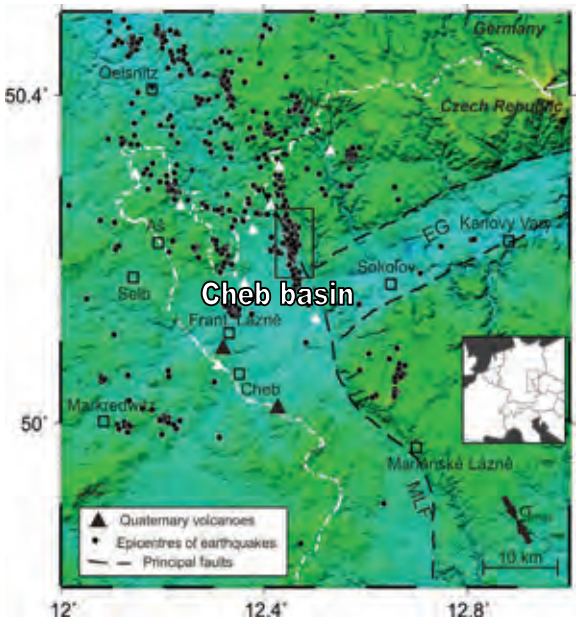

Figure 1: Cheb basin in West-Bohemia/Vogtland seismoactive area. The central rectangle indicates the area of interest; Mariánské Lázně Fault (MLF) and Eger Rift (EG) are indicated by dashed lines.

The study locality is situated at the northeastern limit of the Cheb basin, which is controlled by the northern termination of the MLF. In order to study the Quaternary activity of the fault, a trenching was combined with ground penetration radar (GPR) and electric resistivity tomography (ERT) to extrapolate the traces of the exposed faults and distribution of the offset sedimentary bodies.

The trenching site is situated between Nový Kostel and Kopanina villages and it was chosen based on the most recent morphology, where the marginal slope is expressed by a gentle convex fault scarp and by a linear arrangement of points where series of sub-parallel valleys become deeply incised into an apparently uplifted blocks. The 100 m long trench exposed a succession of sedimentary units, whose lithologies are briefly described downhill southwestwards as follows (Fig. 2): in the upper part of the trench clayey-sandy colluvium cover a completely disintegrated, chemically weathered mica-schists basement. The following Miocene Cheb basin fill consists of inclined beds of various formations, whose ages in the trench decrease donwhill towards the basin centre as well as the ages of the faults which cut them. Thus, the weathered basement is covered by probably Lower Clay and Sand Formation (A-B) comprising of basal conglomerates with ferric cement and reworked gravely sands with ferricretes. This formation is terminated by the fault striking at 162° (F4) towards the following Plio-Pleistocene Vildstein Formation (C) which is formed by diagonally stratified fine gravels and sands. These sediments are disturbed by minor sub-parallel 137°-142° striking normal faults (F3) with offsets of 10 cm.

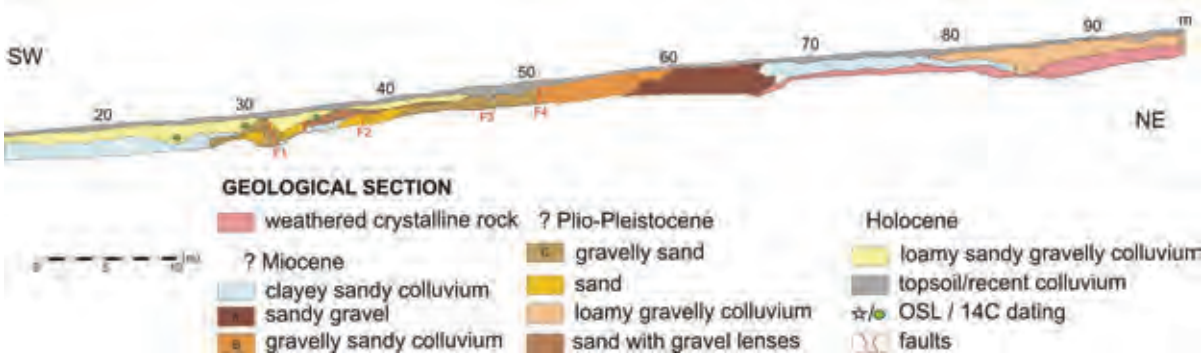

Figure 2: Simplified lithological section of the SE-facing wall of the trench Kopanina.

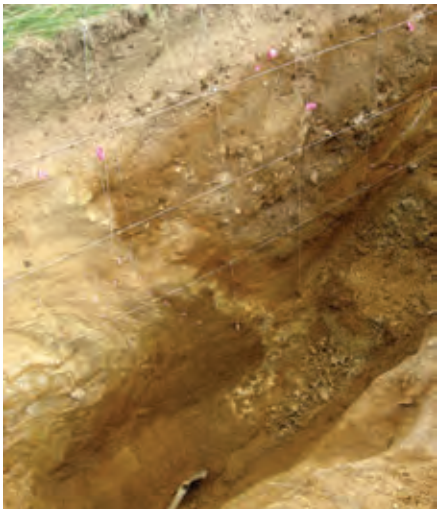

Figure 3: The youngest fault in the SE-facing trench wall cutting the Holocene colluvium and warping the Plio-Pleistocene fluvial sandy gravels and clayes; 0.5 m grid.

Further downhill, up to 45° tilted heterogeneous layers of overlying fine gravels and sands are cut by the sub-vertical fault with strike of 132° (F2), which is filled with white clay and accompanied by distinctive iron mineralization. The OSL dating methods yielded age of 418±34 ka for the inclined sediments. The following layers of clayey sand to clay (495±37 ka OSL) are downwarped and deformed by the youngest 134° (F1) striking fault (Fig. 3), which separates them from deformed stratified coarse sands (485±36 ka OSL) to the southwest. This youngest fault coincides with the slightly convex morphology of the fault scarp on the foot of the slope. The age of the youngest loamy sandy gravelly colluvium downwarped by this fault was constrained by the charcoals dated by radiocarbon dating method as 5.3 - 1.1 ka BP. The further details and discussion on discrete events will be a subject of the conference presentation.

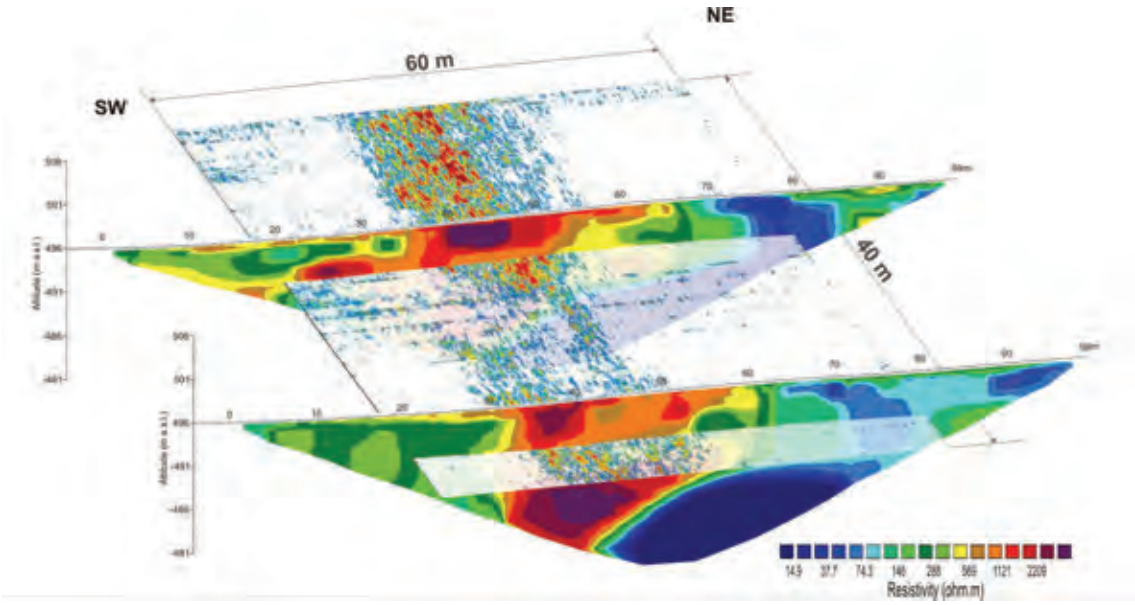

Figure 4: Intersection of the two ERT profiles and the GPR time slice corresponding to the depth of 5 m. Note the striking correlation between the high resistivity and high reflectivity of the material in the centre of the profiles.

The method of electric resistivity tomography (ERT) along two profiles parallel to the trench identified a strong resistivity contrast between the high resistive bodies of sandy gravels and high conductive clayey sands and weathered crystalline basement. The 2-D ground penetration radar (GPR) sections show direct correlation of reflections with lithological boundaries identified in the trench. The correspondence of reflections and resistivity contrasts is shown in Figure 4.

Our results suggest a complex fault pattern in the studied area. The deformation character of the disturbed sediments implies that several identified faults had significant horizontal component. The documented vertical offsets suggest possible moment magnitude M_w = 6.3 for some of the movements, based on combination of empirical relationships "magnitude versus maximum displacement" and "magnitude versus surface rupture length" (Wells and Coppersmith, 1994). The study evidences the so far youngest clearly proved surface faulting rupture reported from central Europe.

Acknowledgements: The research was supported by Grant Agency of Czech Academy of Sciences, project No. IAA300120905 and Czech Science Foundation No. P210/12/0573.

References

Fischer, T., Štěpančíková, P., Karousová, M., Táborík, P., Flechsig, Ch., M. Gaballah, (2012): Imaging the Mariánské Lázně Fault (Czech Republic) by 3-D ground-penetrating radar and electric resistivity tomography. *Studia Geophysica et Geodaetica*. 56 (4): 1019-1036.

Wells, D.L., Coppersmith, K.J., 1994. Empirical relationships among magnitude, rupture length, rupture area, and surface displacement. *Bulletin of the Seismological Society of America*. 82, 974–1002.

6th International INQUA Meeting on Paleoseismology, Active Tectonics and Archaeoseismology,
19-24 April 2015, Pescina, Fucino Basin, Italy

INQUA Focus Group on Paleoseismology and Active Tectonics

Tracing geological records of recent tsunamis - insights into their regional variability and new research approaches

Szczuciński, W.

Institute of Geology, Adam Mickiewicz University in Poznan, Maków Polnych 16, 61-606 Poznań, Poland. Email: witek@amu.edu.pl

Abstract: *During the last decade tsunami research has received unprecedented attention from the scientific community, as well as from the public and decision makers, largely in a response to a series of tsunamis including the disastrous Indian Ocean Tsunami (2004) and Tohoku-oki tsunami (2011). One of the key emerging issues is the common understanding of the role of identification of paleotsunami deposits as part of efforts to improve tsunami hazard assessment. However, recent studies on tsunami deposits have revealed that their identification is far from easy. This paper presents some outcomes from studies conducted in various geographical regions, ranging from tropics (Thailand) through the temperate zone (Japan, Poland) to polar regions (Greenland). It is focused on presentation of new methods applied in the studies of tsunami deposits; some have been already proven to be useful (geochemistry) while others (dendrochronology, paleogenetics) are still being tested.*

Key words: *Tsunami deposits, saltwater indicators, aDNA, dendrochronology, hazard assessment.*

INTRODUCTION

During the last dozen years tsunamis have appeared to be the most disastrous natural process worldwide. The dramatic, large tsunamis on Boxing Day, 2004 in the Indian Ocean and on March 11, 2011 offshore Japan caused natural catastrophes that are recognised as the worst recorded in terms of the number of victims and economic losses, respectively. In the aftermath, they have become a topic of high public and scientific interest, the latter expressed by a large increase in a number of peer-reviewed publications following 2004. They are related to a number of subdisciplines of tsunami science, however, one of them is particularly important, namely studies on the geological record of tsunamis.

The record of past tsunamis, mainly in form of tsunami deposits, is often the only way to identify tsunami risk at a particular coast due to relatively low frequency of their occurrence. There are many examples proving the importance of geological record and need for its more and more detail studies. For instance, before 2004 the Andaman Sea coast of Thailand was not considered as being at risk from tsunamis. However, the studies of paleotsunami records following the disaster confirmed that tsunamis have already hit that coast (e.g., Jankaew et al., 2008; Yawsangratt et al., 2009; Fujino et al., 2009). Another example comes from east coast of Japan, where predecessors of the 2011 Tohoku-oki tsunami were already known prior to the event (e.g., Minoura et al., 2001), whilst recent observations have indicated that the magnitude of these older events was probably underestimated (e.g., Goto et al., 2011, 2014). These examples point to the importance of the correct identification and interpretation of tsunami and palaeotsunami deposits to provide a better understanding of event magnitudes for tsunami hazard assessment.

The identification of paleotsunami deposits is often difficult mainly because the tsunami deposits are made up of various sediment types, that may be similar to storm deposits or have been altered by post-depositional processes. There is no simple universal diagnostic set of criteria that can be applied to interpret tsunami deposits with absolute certainty (Goff et al., 2012). Thus, there is a need to develop new methods, which can enhance 'classical', mainly sedimentological and stratigraphic approaches. Moreover, since the tsunami hazard is currently recognised for most of the coastlines worldwide it appears that the geological effects of tsunamis and their preservation may vary with depositional environment and climatic zone.

The objective of the present contribution is to show the application of several new approaches (geochemistry, dendrochronology, paleogenetics) employed in the study of the geological impacts of recent tsunamis from various geographical regions, namely in the monsoonal-tropics, and on temperate and polar regions. It is mainly based on my own studies of coastal zones affected by the 2004 Indian Ocean Tsunami in Thailand, the 2011 Tohoku-oki tsunami and older paleotsunamis in Japan, catastrophic saltwater inundations at the coasts of Baltic Sea and the 2000 landslide-generated tsunami in Vaigat Strait (west Greenland), as well as on a review of published studies.

CASE STUDIES

This paper reviews the key findings from studies of several tsunami and paleotsunami deposits in order to provide a wide geographical range. The onshore deposits from 2004 Indian Ocean tsunami were studied along circa 100 km of the coast of Thailand (Szczuciński et al., 2006, 2012b). Many of the investigated sites were monitored after the tsunami to assess post-depositional changes (Szczuciński, 2012).

The tsunami deposits originating from the 11 March 2011 Tohoku-oki tsunami were investigated in detail along a circa 5 km-long shore perpendicular transect nearby Sendai (e.g., Goto et al., 2011; Szczuciński et al., 2012a). The paleotsunami deposits discussed here were investigated on the Sendai Plain (Chagué-Goff et al., 2012a), as well as on the eastern coast of Hokkaido Island.

The southern coast of Baltic Sea was investigated in search of potential paleotsunami events (Szczuciński et al., in review). The documented paleoevents from coastal plain deposits were investigated using sedimentological, geochemical and micropaleontological methods.

Finally, the effects of the AD 2000 large rock avalanche and tsunami (with runup height up to 50 m a.s.l.) in Vaigat Strait (Greenland) were studied along several tens of km of the coastline (Szczuciński et al., 2012c). The study included also application of tree ring analyses of polar shrubs (Buchwał et al., 2015).

RESULTS AND DISCUSSION

Salinity indicators

For tsunami deposits left on land their geochemical composition, indicating deposition from seawater, is one of the most important 'proxies'. There are several potential seawater indicators. Chagué-Goff (2010) in her review of chemical signatures of paleotsunamis discussed for instance: chlorine, sodium, sulphur, boron, bromine, iodine, germanium and uranium. Among them the most abundant indicators are Na and Cl. However, they are also the most mobile in the environment.

In Thailand, fresh 2004 tsunami deposits were found to be composed mainly of fine to medium sand, significantly enriched in 'salts' (Na, K, Ca, Mg, Cl and SO4) and some trace elements (Cd, Cu, Zn, Pb, As) (Szczuciński et al., 2005). However, only one year after the tsunami the concentrations of the 'salts' were close to local background levels (Szczuciński et al., 2007), mainly due to very high rainfall during rainy season (over 3000 mm of precipitation per year).

The tsunami deposits left by Tohoku-oki tsunami on the Sendai plain (Chagué-Goff et al., 2012a, 2012b) were enriched particularly in chlorine, sodium, sulphur, strontium and bromine. The concentrations of these elements were monitored during the year following the tsunami (Chagué-Goff et al., 2014). Although the concentrations in general decreased, the chloride concentrations one year after the tsunami were still above the guideline limits for rice seedlings. The slower reduction of the salinity observed here is partly due to lower precipitation, but probably the major factor is the site topography. The Sendai Plain is flat and divided by numerous dikes, so the surface water drainage is very limited. The analyses of over 1000 year old sandy paleotsunami deposits from the same area (Chagué-Goff et al., 2012a) revealed, however, that most of potentially indicatory elements were near the detection limits (e.g. chlorine). The only elements with higher concentrations were Sr and Rb. This may be partly due to sandy nature of the deposits, as fine-grained and organic-rich deposits are characterised by much better sorption properties.

However, in some cases also sandy sediments may reveal clear chemical signal of salinity even after long periods. On the southern cost of Baltic Sea a ca 500 years old paleoevent sandy layer is enriched in Na and Cl. A similar situation is observed in an arctic setting (Greenland), where 12 years after the event, tsunami deposits still contained much more 'salt'-related elements than the local soils.

These examples show show that, especially in the case of sandy deposits, salinity indicators must be treated with caution. The interpretation should also take into account local conditions like topography, climate, groundwater etc. More new geochemical approaches are appearing including stable isotope ratios and organic geochemistry and it is likely that the geochemistry of tsunami deposits will be an increasingly important tool in their identification.

Dendrochronology

Dendrochronological analyses provide a potentially valuable means to date and identify tsunami events and coastal processes. They have been used for instance for dating of 1700 Cascadia earthquake and tsunami (Jacoby et al., 1997). However, the potential usefulness of growth rings analyses for event identification, dating and for assessment of natural recovery of ecosystems after tsunami have not been yet fully explored.

This method was applied in coastal zone of Thailand, several years after the 2004 tsunami. The objective was to assess if the tsunami was recorded in growth tree rings - their thickness and structure. However, most of the trees in the coastal zone were *Casuarina* trees, which are very difficult for sampling due to their extreme hardness. The second most common plant are palm trees, which are not suitable for dendrochronology as they do not produce growth rings. In single specimen of a local fruit tree the ca 2004 tree ring was found to be weaker.

In the polar zone, trees are present in a dwarf form as tundra shrubs, e.g. willow (*Salix* spp.), which form annual growth rings that can be used for dating purposes. Buchwał et al. (2015) provided an example of the first application of dendrochronological analysis for tsunami research in the Arctic. They used *Salix glauca*, a common tundra shrub, collected from a coastal plain that was inundated by a landslide-generated tsunami in November 2000 AD, which occurred in Vaigat Strait, west Greenland. They found that *Salix glauca* shrubs occupied the tsunami deposits surface during the first growth season after the event and characterised by high growth resistance. The results of this study suggest that they may be precise dating tool, help in identification of an event (a large number of the shrubs of the same age and lack of older plants), and can provide insight into the post-even recovery of the ecosystem.

Paleogenetics

Among the most commonly used approaches to identify paleotsunami is the study of microfossils (e.g.

foraminifera, diatoms). They are most commonly used to show marine origin of sediments, although there are some examples where almost no marine microfossils are found in the recent tsunami deposits (e.g., on Sendai Plain in Japan - Szczuciński et al., 2012a). The common problem with microfossils in coastal settings (eg. marshes, peat bogs) is that they may not be preserved. For instance, it was found during studies on post-depositional changes of 2004 tsunami deposits and in paleotsunami deposits in Thailand (Jankaew et al., 2008; Szczuciński, 2012; Yawsangratt et al., 2012) that the tests composed of calcium carbonate as well as from silica have been largely dissolved with time.

The rapid progress in paleogenetic studies suggests that analyses of remnants of DNA of marine organisms may be a new research direction. A recent successful application of the method to the deep sea and fjord sediments, greater than 30,000 years old (e.g. Lejzerowicz et al., 2013; Pawłowska et al., 2014) proved that it is possible to extract DNA and identify it from sediments that are affected by oxygenated waters and bioturbating organisms. Thus hypothetically, ancient DNA of marine organisms could be deposited with tsunami deposits and may be preserved in geological record, even in absence of their micropaleontological evidence. An attempt was made to apply the paleogenetic studies for well dated paleotsunami deposits from eastern Hokkaido Island, Japan. The study is in progress.

CONCLUSIONS

The identification and precise dating of paleotsunami deposits is a key to improve tsunami hazard assessment. However, tsunami deposits are highly variable and their identification remains difficult in many cases. It is important also to take into account postdepositional changes, which varies among environments and climatic zones. Development of new research methods is necessary to improve the identification and dating precision of tsunami deposits. None of the new methods is expected to be a single, perfect one. However, a combination of them may provide valuable insights. Among the developing methods are these related to geochemistry, biology and genetics. The applications of geochemistry has already been proven to be useful and certainly will develop further in the near future. The remaining methods, although promising, need to be tested first.

Acknowledgements: This contribution results from review of several co-authored works (listed in references) and fruitful discussions with co-authors to whom I express my sincere thanks. This paper particularly benefited from discussions with Agata Buchwał, Catherine Chagué-Goff, James Goff, Kazuhisa Goto, Bruce Jaffe, Antony Long, Stanisław Lorenc, Wojciech Majewski, Przemysław Niedzielski, Yuichi Nishimura, Jan Pawłowski, Andrzej Piotrowski, Grzegorz Rachlewicz, Bruce Richmond, Matt Strzelecki, Daisuke Sugawara and Supawit Yawsangratt. The study was partly funded by Polish National Science Centre grants No. 2011/01/B/ST10/01553 and 2011/01/B/ST10/07220, as well as Polish Ministry of Science and Higher Education grant No. N N523 3768 33.

References

Buchwał, A., W. Szczuciński, M. Strzelecki & A.J. Long, (2015). New insights into 2000 AD tsunami in west Greenland from analyses of tree-ring structure of *Salix glauca*. *Polish Polar Research*. 36 (1), in press.

Chagué-Goff, C., (2010). Chemical signatures of palaeotsunamis: a forgotten proxy? *Marine Geology*. 271, 67-71.

Chagué-Goff, C., A. Andrew, W. Szczucinski, J. Goff & Y. Nishimura, (2012a). Geochemical signatures up to the maximum inundation of the 2011 Tohoku-oki tsunami - implications for the 869 AD Jogan and other palaeotsunamis. *Sedimentary Geology*. 282, 65-77.

Chagué-Goff, C., P. Niedzielski, H.K.Y. Wong, W. Szczuciński, D. Sugawara & J. Goff, (2012b). Environmental impact assessment of the 2011 Tohoku-oki tsunami on the Sendai Plain. *Sedimentary Geology*. 282, 175-187.

Chagué-Goff C., H.K.Y. Wong, D. Sugawara, J. Goff, Y. Nishimura, J. Beer, W. Szczuciński & K. Goto, (2014). Impact of Tsunami Inundation on Soil Salinisation: Up to One Year After the 2011 Tohoku-Oki Tsunami. In: *Tsunami Events and Lessons Learned - Environmental and Societal Significance. Advances in Natural and Technological Hazards Research*, *Vol. 35*, (Kontar Y., Santiago-Fandino V., Takahashi T. eds.), Springer Science+Business Media B.V., Dordrecht. 193-214.

Fujino S., H. Naruse, D. Matsumoto, T. Jarupongsakul, A. Sphawajruksakul & N. Sakakura, (2009). Stratigraphic evidence for pre-2004 tsunamis in southwestern Thailand. *Marine Geology*. 262, 25-28.

Goff, J., C. Chagué-Goff, S. Nichol, B. Jaffe & D. Dominey-Howes, (2012). Progress in palaeotsunami research. *Sedimentary Geology*. 243-244, 70-88.

Goto, K., C. Chagué-Goff, S. Fujino, J. Goff, B. Jaffe, Y. Nishimura, B. Richmond, D. Sugawara, W. Szczuciński, D.R. Tappin, R.C. Witter & E. Yulianto, (2011). New insights of tsunami hazard from the 2011 Tohoku-oki event. *Marine Geology*. 290, 46-50.

Goto, K., S. Fujino, D. Sugawara & Y. Nishimura, (2014). The current situation of tsunami geology under new policies for disaster countermeasures in Japan. *Episodes*. 37(4), 258-264.

Jacoby, G.C., D.E. Bunker & B.E. Benson, (1997). Tree-ring evidence for an A.D. 1700 Cascadia earthquake in Washington and northern Oregon. *Geology*. 25, 99-102

Jankaew, K., B.F. Atwater, Y. Sawai, M. Choowong, T. Charoentitirat, M.E. Martin & A. Prendergast, (2008). Medieval forewarning of the 2004 Indian Ocean tsunami in Thailand. *Nature*. 455, 1228-1231.

Lejzerowicz, F., P. Esling, W. Majewski, W. Szczuciński, J. Decelle, C. Obadia, P.M. Arbizu & J. Pawlowski J., (2013). Ancient DNA complements microfossil record in deep-sea subsurface sediments. *Biology Letters*. 9 (4): 20130283.

Minoura, K., F. Imamura, D. Sugawara, Y. Kono & T. Iwashita, (2001). The 869 Jogan tsunami deposit and recurrence interval of large-scale tsunami on the Pacific coast of northeast Japan. *Journal of Natural Disaster Science*. 23, 83-88.

Pawłowska, J., F. Lejzerowicz, P. Esling, W. Szczuciński, M. Zajączkowski & J. Pawłowski, (2014). Ancient DNA sheds new light on the Svalbard foraminiferal fossil record of the last millennium. *Geobiology*. 12, 277-288.

Szczuciński, W., (2012). The post-depositional changes of the onshore 2004 tsunami deposits on the Andaman Sea coast of Thailand. *Natural Hazards*. 60 (1), 115-133.

Szczuciński, W., P. Niedzielski, G. Rachlewicz, T. Sobczyński, A. Zioła, A. Kowalski, S. Lorenc & J. Siepak, (2005). Contamination of tsunami sediments in a coastal zone inundated by the 26 December 2004 tsunami in Thailand. *Environmental Geology*. 49 (2), 321-331.

Szczuciński, W., N. Chaimanee, P. Niedzielski, G. Rachlewicz, D. Saisuttichai, T. Tepsuwan, S. Lorenc & J. Siepak, (2006). Environmental and geological impacts of the 26 December 2004 tsunami in coastal zone of Thailand - overview of short

and long-term effects. *Polish Journal of Environmental Studies*. 15 (5), 793-810.

Szczuciński, W., P. Niedzielski, L. Kozak, M. Frankowski, A. Zioła & S. Lorenc, (2007). Effects of rainy season on mobilization of contaminants from tsunami deposits left in a coastal zone of Thailand by the 26 December 2004 tsunami. *Environmental Geology*. 53, 253-264.

Szczuciński, W., M. Kokociński, M. Rzeszewski, C. Chagué-Goff, M. Cachao, K. Goto & D. Sugawara, (2012a). Sediment sources and sedimentation processes of 2011 Tohoku-oki tsunami deposits on the Sendai Plain, Japan - insights from diatoms, nannoliths and grain size distribution. *Sedimentary Geology*. 282, 40-56.

Szczuciński, W., A. Piotrowski, P. Sydor & J. Krzymińska, (in review). Sedimentary record of extreme catastrophic saltwater floodings of storm and/or tsunami origin on the southern Baltic Sea coast, Rogowo, Poland. *Sedimentary Geology*.

Szczuciński, W., G. Rachlewicz, N. Chaimanee, D. Saisuttichai, T. Tepsuwan & S. Lorenc, (2012b). 26 December 2004 tsunami deposits left in areas of various tsunami runup in coastal zone of Thailand. *Earth, Planets and Space*. 64, 843-858.

Szczuciński, W., N.J. Rosser, M.C. Strzelecki, A.J. Long, T. Lawrence, A. Buchwal, C. Chague-Goff & S. Woodroffe, (2012c). Sedimentary Record and Morphological Effects of a Landslide-Generated Tsunami in a Polar Region: The 2000 AD Tsunami in Vaigat Strait, West Greenland. *American Geophysical Union (AGU) Fall Meeting. San Francis*co. ID: 1479941.

Yawsangratt, S., W. Szczuciński, N. Chaimanee, S. Chatprasert, W. Majewski & S. Lorenc (2012). Evidence of probable paleotsunami deposits on Kho Khao Island, Phang Nga Province, Thailand. *Natural Hazards*. 63, 151-163.

Yawsangratt S., W. Szczuciński, N. Chaimanee, R. Jagodziński, S. Lorenc, S. Chatprasert, D. Saisuttichai & T. Tepsuwan (2009). Depositional effects of 2004 tsunami and hypothetical paleotsunami near Thap Lamu Navy Base in Phang Nga Province, Thailand. *Polish Journal of Environmental Studies*. 18, 17-23.

INQUA Focus Group on Paleoseismology and Active Tectonics

Coseismic hydrological changes in response to the 1915 Fucino (Central Italy) earthquake

Tertulliani, A., Cucci, L.

Istituto Nazionale di Geofisica e Vulcanologia, via di Vigna Murata 605, 00143 Roma, Italy. Email: luigi.cucci@ingv.it

Abstract: *The M~7 1915 Fucino (Central Italy) produced a remarkable dataset of 73 coseismic hydrological changes in the near and intermediate field that consist in variation of the flow of streams and springs, liquefaction, rise of water temperature and turbidity. We study the coseismic water level changes induced by the earthquake in the near field through the modelling of the coseismic strain field induced by seventeen individual faults proposed through different approachs. We find i) best fits between modelled deformation and observed data are displayed by sources (derived by geological or seismological data) located along the eastern side of the Fucino basin. Also, we infer a possible active involvement in a 1915-like seismogenic process for fault splays (located in the central-western part of the basin) synthetic and antithetic to the main seismogenic structures. ii) evidence against a number of seismogenic structures (uniquely derived by macroseismic or geodetic data, or characterized by reverse faulting and/or by right-lateral strike-slip) that prove to be inconsistent with the polarities of the hydrological signatures.*

Key words: *Hydrology, Seismicity and tectonics, Fractures and faults.*

INTRODUCTION

Hydrological changes following earthquakes have been reported for centuries because they are among the most outstanding coseismic phenomena and can be observed over great distances. Examples include liquefaction, formation and/or disappearance of springs, changes in the streamflow and in groundwater level, and variations in the chemical characteristics of waters.

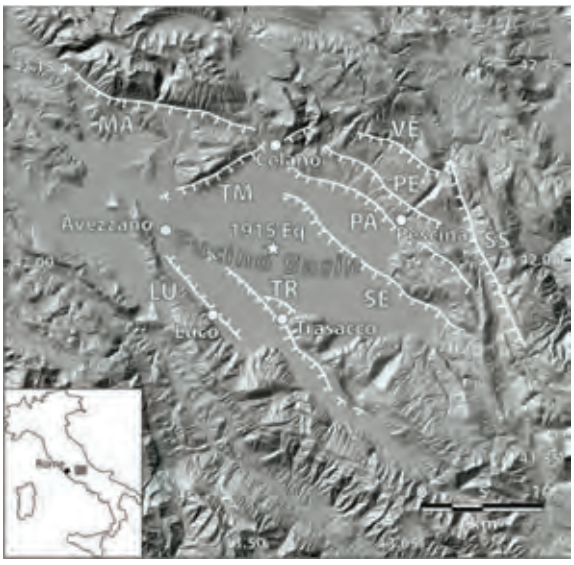

Figure 1: Map of the study area. A white star indicates the epicentral location of the 1915 earthquake. Faults abbreviation: LU, Luco Fault; MA, Magnola Fault; PA, Parasano Fault; PE, Pescina Fault; SE, Serrone Fault; SS, San Sebastiano Fault; TM, Tre Monti Fault; TR, Trasacco Fault; VE, Ventrino Fault.

In the last decades the character of the hydrological changes that follow major earthquakes has often been found to be dependent on the style of faulting, with the most significant response firstly observed to accompany major normal fault earthquakes (Muir-Wood & King, 1993). Thus, being potentially associated with the seismogenesis, such hydrological changes can represent a footmark of the earthquake, and can be investigated to better characterize those seismic events for which we lack enough accuracy on the epicentral location or on the source, or for which these parameters are still debated. Investigating the hydrological changes can be particularly helpful in the study of those earthquakes for which we have poor or contradictory observations, such as historical earthquakes (e.g. Tertulliani and Cucci, 2009).

The 13 January 1915 Fucino (Abruzzi, central Italy) M~7 earthquake (Figure 1) is a perfect candidate for this kind of studies. Though ranked among the most powerful earthquakes in the whole seismic history of the Italian Peninsula, uncertainties still exist on the role played by the plethora of tectonic structures that have been indicated from time to time by geological, seismological, geodetic and macroseismic data as the source responsible of the earthquake.

HYDROLOGICAL CHANGES INDUCED BY THE 1915 EARTHQUAKE

Our reference documents, both coeval and subsequent to the 1915 Fucino earthquake, describe widespread environmental effects observed throughout the affected area. In particular, most of the data were provided by the report of the field work of Oddone (1915), and by the so-called macroseismic postcards (short, standard descriptions of the effects of noticeable earthquakes written by members of the official Italian network of seismic Observatories).

We stored a collection of 73 reviewed observations of hydrological changes that occurred following the earthquake at about 68 different localities (Figures 2 and 3). The dataset presents different types of hydrological

changes, most of the data concerning excess flow in streams and springs. Less frequently, a flow decrease or spring disappearance was reported; in some cases, we had notices from localities where the coeval accounts reported unspecific flow variations. The hydrological variations were sometimes accompanied by changes in the physical characteristics of the waters such as turbidity and rise of the temperature. Liquefaction was observed in several localities, mostly located less that 10 kilometers from the epicenter within the Fucino basin (filled with deposits prone to liquefaction). Most of the phenomenon observed tended to peak between some this process we assume that the observed streamflow variations are the hydrological response to coseismic strain changes (Muir-Wood and King, 1993), so that we expect to find observations of streamflow increase in hours to a few days after the earthquake, some of them lasting for several months up to one year following the event.

DISCUSSION

We calculated the coseismic field of deformation produced by seventeen individual seismic sources potentially associated with the event, and compare it to the observations of hydrological changes. Our aim is to identify a preferred source, or alternatively to rule out some of the faults proposed by previous investigators. In areas that undergo compressional strain, and data of streamflow decrease in areas of dilational strain.

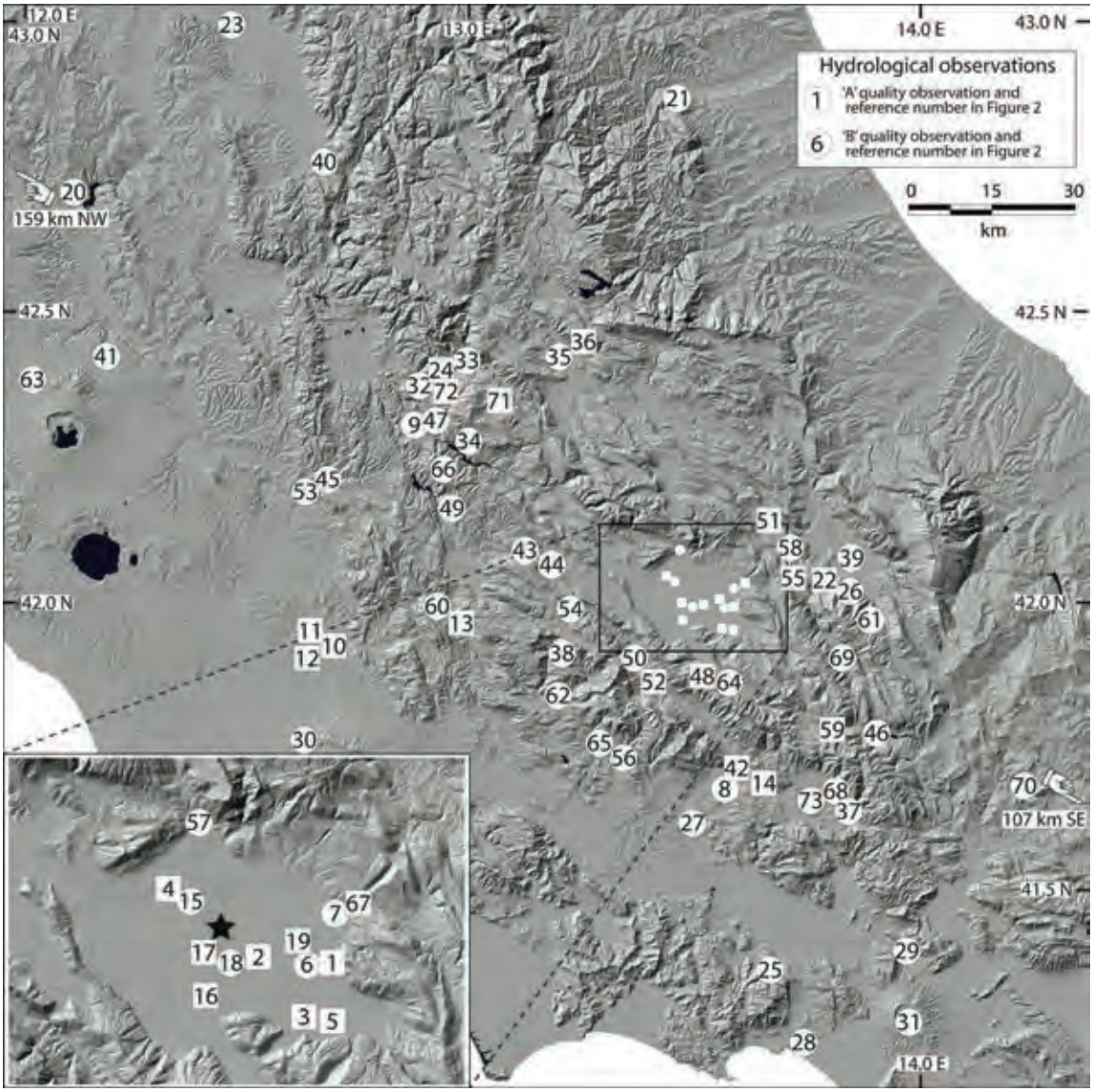

Figure 2: General map of the hydrological effects produced by the 1915 earthquake. In the inset we show a blow-up of the Fucino Basin and the epicentral location of the event (black star).

Calculations of the strain were made in an elastic halfspace with uniform isotropic elastic properties. The output of our calculations are plots of volumetric strain at the free surface on the 17 individual sources; an example of these plots is shown in Figure 4. To find out which of the above cited sources better matches the observed streamflow changes we selected only the solutions that showed more than 50% of points with polarities of the observed hydrological effects in agreement with the expected deformation. Only four individual faults out of seventeen display satisfactory percentages of agreement between observed and expected strain. A comparison between the four preferred faults and the other solutions provided some interesting insights:

i) The four candidate sources that display the best fits between calculated coseismic strain and observed hydrological signatures share several distinctive features. Indeed they share the same kinematics, as they are all normal faults (two of them with an important component of left-lateral slip), the same geometry, as they are all ~135°-striking, SW-dipping, ~35 km-long structures, and almost the same location, as they border the eastern side of the Fucino basin. The Serrone Fault and the Parasano Fault are the two individual structures that better fit with these characteristics, and thus we consider that these two faults generated the main coseismic field of deformation during the 1915 earthquake. This piece of evidence also supports the hypothesis that the coseismic ruptures observed in the field represented primary surface faulting. Also, the contribution to the total strain field of other single faults such as the Pescina Fault and the Ventrino Fault does not significantly enhance the fit between coseismic deformation and observed data. Therefore we suggest that these structures are secondary faults from the perspective of the hydrological response. Finally, one of the best scoring potential sources (derived from geological data) is a multi-faulting system that considers the presence, in the middle of the Plain and close to the western side of the basin, of fault splays synthetic (Trasacco Fault) and antithetic (Luco Fault) to the main seismogenic structures. Though the role played by these splays is debated, their imprint on the general pattern of strain provides a remarkable fit with the hydrological signatures and allows us to infer a possible active involvement in a 1915-like seismogenic process.

ii) All the plots of volumetric strain associated with earthquake sources derived exclusively from the inversion of geodetic or of intensity data proved to be inconsistent with the polarities of the hydrological signatures observed in the field. Both the geodetic candidate sources showed a deformation pattern poorly consistent with the observed data. Furthermore, the sources derived from macroseismic data displayed very low values of percentage, and no significant difference in their performance was observed depending on the different sense of movement imposed to the fault; we suggest that the strike (~120°) and the location (slightly shifted respect to the Fucino basin) of this family of sources, rather than their rake, played a preminent role in the resulting pattern of coseismic deformation. As regards the rake, we finally remark that even the sources characterized by a significant right-lateral component or by reverse faulting are discarded because of their insufficient number of consistent polarities. The plots of coseismic strain clearly indicate that the sense of slip is critical to discriminate between the performance of sources that otherwise share comparable fault parameters.

NO.	LOCALITY	LAT	LON	CODE	EVIDENCE	EPIC. DIST.	REFERENCE	NOTES
1	Molino di Venere	41,9915	13,6361	A	Natural spring disappeared	9.1	Oddone (1915); Galli (2000)	Field survey 16-19 Jan; lasted four days
2	Bacinetto	41,9979	13,5776	A	Flooding	4.3	Oddone (1915)	Field survey 16-19 Jan; lasted four days
3	Ortucchio road 28/31	41,9573	13,6146	A	Flooding	9.4	Oddone (1915); Seismic postcard	Field survey 16-19 Jan; lasted four days
4	Road 11 near Paterno	42,0462	13,5041	A	Pond dried up	4.2	Oddone (1915)	Field survey 16-19 Jan
5	Road 28	41,9533	13,639	A	Water discharge	11.3	Oddone (1915); Galadini et al., (1999)	Field survey 16-19 Jan
6	Road 24	41,991	13,6341	B	"Craterlets" (sand venting-mud volcanoes)	9.0	Oddone (1915); Galli (2000)	Visited in Aug 1915
7	Pescina	42,0239	13,6514	B	"Craterlets" (sand venting-mud volcanoes)	10.1	Oddone (1915); Galli (2000); Galadini et al., (1999)	Coeval report not directly surveyed

Figure 3: Except from the list of the hydrological effects observed following the 1915 Fucino earthquake.

iii) The scanty results shown by the earthquake sources derived from the inversion of intensity data appear not unexpected. Because the algorithms that use intensity observations provide an estimation of the barycenter of strong shaking rather than the location where the quake actually starts, seismogenic sources inferred from macroseismic data can turn out unsatisfactory when included in the seismotectonic frame of an area.

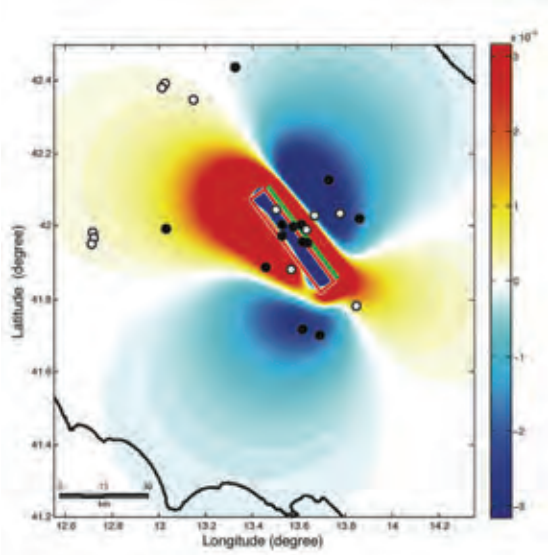

Figure 4: Example of plot of calculated volumetric strain along one of the potential sources and observed hydrological effects produced by the 1915 earthquake.

Finally, we suggest that comparing the predicted strain fields of fault earthquakes with their hydrological effects can be an alternative and effective methodology capable of being used to estimate the focal mechanism of a major earthquake, especially of an historical earthquake. Infact, models of coseismic strain can readily explain the differences between the hydrological signatures of fault earthquakes, as well as the geographical extent of the hydrological response. The date of the 1915 earthquake in the 'dark ages' of modern seismology places it at an ideal time at which this method could be appropriate.

References

Muir-Wood, R. & G.P. King, (1993). Hydrological signatures of earthquake strain. *J. Geophys. Res*. 98, 22035-22068.

Oddone, E., (1915). Gli elementi fisici del grande terremoto Marsicano- Fucense del 13 Gennaio 1915. *Boll. Soc. Sism. Ital.* 19, 71-216.

Tertulliani, A. & L. Cucci, (2009). Clues to the identification of a seismogenic source from environmental effects: the case of the 1905 Calabria (Southern Italy) earthquake. *Nat. Hazards Earth Syst. Sci.* 9, 1787-1803.

6th International INQUA Meeting on Paleoseismology, Active Tectonics and Archaeoseismology,
19-24 April 2015, Pescina, Fucino Basin, Italy

INQUA Focus Group on Paleoseismology and Active Tectonics

paleoseismicity.org

Palaeoseismological investigation across the Gyrtoni Fault, Tyrnavos Basin, Central Greece

Tsodoulos, I. (1), Pavlides, S. (2), Caputo, R. (3,4), Chatzipetros, A. (2), Koukouvelas, I. (5), Stamoulis, K. (1), Ioannides, K. (1)

(1) Dept. of Physics, Nuclear Physics Laboratory, University of Ioannina, GR-45110 Ioannina, Greece. Email: itsodoul@cc.uoi.gr
(2) Dept. of Geology, Aristotle University of Thessaloniki, GR-54124 Thessaloniki, Greece
(3) Dept. of Physics & Earth Sciences, University of Ferrara, I-44122 Ferrara, Italy
(4) Research and Teching Center for Earthquake Geology, Tyrnavos, Greece
(5) Dept. of Geology, Division of Marine Geology and Geodynamics, University of Patras, Patras-26500, Greece

Abstract: *We present the preliminary results of a palaeoseismological investigation carried out along the Gyrtoni Fault, Tyrnavos Basin (Central Greece), of which the occurrence and recent tectonic activity was previously based only on non invasive techniques, like mapping, remote sensing analyses and electrical resistivity tomographies. Two palaeoseismological trenches emphasize the occurrence of 2 palaeoearthquake displacements in the past ~4.0 ka. An ongoing dating of the collected samples, using the Optically Stimulated Luminescence (OSL) and ^{14}C methodologies, is expected to permit us to constrain the timing of the* linear morphogenic earthquakes observed in the trenches and thus reconstruct the recent seismotectonic behaviour of the fault.

Key words: *Gyrtoni Fault, palaeoseismology, trench, OSL dating, Greece.*

INTRODUCTION

The Middle-Late Quaternary Tyrnavos Basin (Fig. 1) has a general E(SE)–W(NW) orientation and it is bordered by two antithetic sets of normal faults, both showing a partial overlapping right-stepping geometry. To the north, are the south-dipping Rodia and the Gyrtoni faults, while to the south are the antithetic Tyrnavos and Larissa faults (Caputo et al., 1994). The ESE-WNW trending Gyrtoni Fault (GF) is a 12-13 km-long, south dipping normal fault and is located at a distance of ~10 km north from the Larissa city (Caputo et al., 2012).

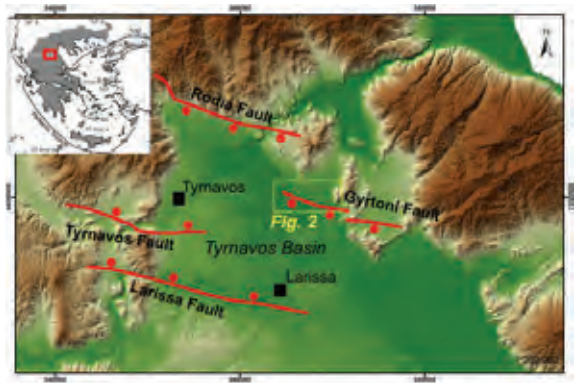

Figure 1: Simplified tectonic map of the Tyrnavos Basin (faults adapted from Caputo et al., 1994).

The fault controls an approximately 10 m-high and 50-110 m-wide degraded composite fault scarp. As the fault scarp is developed in poorly cemented lacustrine deposits it is largely, but irregularly eroded, and the precise location of its trace is not evident in the field (Fig. 2). The possible maximum magnitude associated with this fault is Mw 6.1 (Caputo et al., 2012). The occurrence and recent tectonic activity of the fault, was previously based only on mapping, remote sensing analyses and electrical resistivity tomographies (Caputo et al., 2003).
In this work we present the preliminary results of a palaeoseismological investigation carried out along the GF, aimed at documenting the recent activity and the seismogenic behaviour of this tectonic structure.

PALAEOSEISMOLOGICAL TRENCHES

Two single-slot (California-style) trenches were excavated across a 10 m-high south facing fault scarp at the central section of the west fault segment of the GF (Fig. 2). The first trench (Gyrtoni 1) was dug, in 2012, as an exploratory trench. The trench was 27 m-long, 2 m-wide and up to 4 m-deep (Fig. 2). The second trench (Gyrtoni 2) was 9 m-long, 2 m-wide and up to 3 m-deep, and was dug during 2014 at about 1 km to the west from the first trench (Fig. 2).

Figure 2: Location of the two palaeoseismological trenches. The dash line marks the trace of the Gyrtoni Fault.

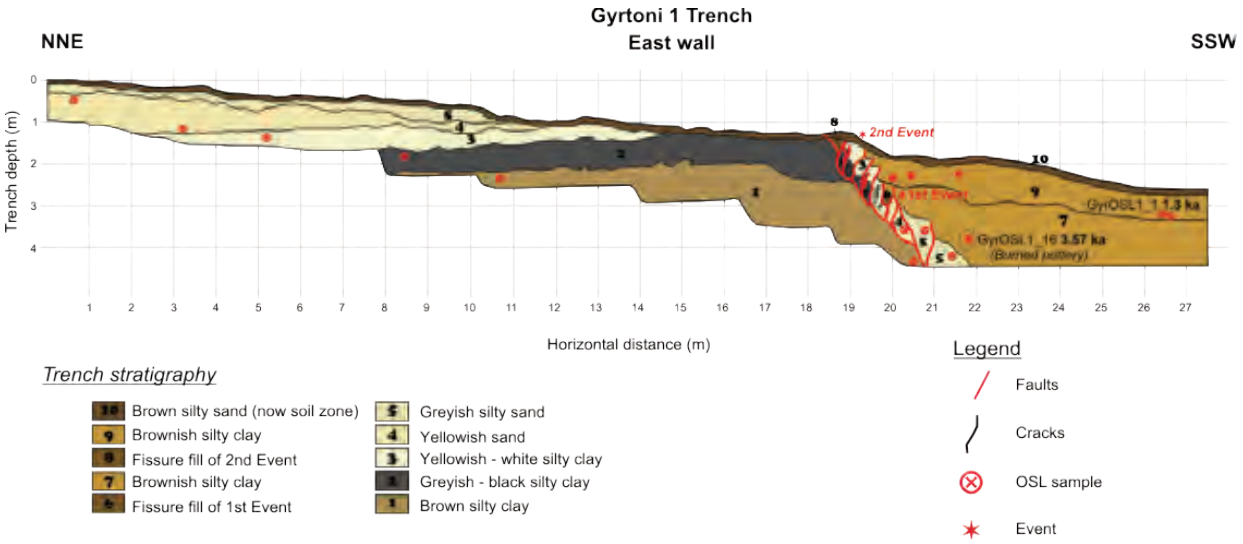

Figure 3: Simplified log of the east wall of the Gyrtoni 1 palaeoseismological trench.

The walls of the trenches were cleaned, gridded with a 1 m x 1 m string grid, sedimentary boundaries and structural features were mapped in detail and photographed and finally samples were collected for age determination. The east wall of the first trench is presented in Fig. 3, while the east wall of the second trench is shown in Fig. 4.

Both trenches intersect the fault zone which separates a series of well stratified, thick to very thick beds of fluvial-lacustrine deposits exposed on the upthrown block from colluvial deposits of the downthrown block.

In both the excavated trenches the fault zone was exposed as a complex, 2-m-wide zone of stepped normal fault strands. The fault strands are merged toward the base of the trenches into a single shear zone dipping 60-70° to the south (Figs. 3 and 4). The fault zone is composed of displaced blocks, relatively intact and occasionally rotated (e.g. subunits 2a, 2b and 2c in Fig. 4), of sedimentary units from the upthrown block.

LUMINESCENCE DATING

Twenty six samples were collected for Optically Stimulated Luminescence (OSL) dating from the sedimentary units exposed on the walls of the two trenches. Sediment samples, one for each lithologic unit, were collected from the upthrown fault block in order to establish a reliable chronological framework; sediment and pottery samples were collected from the downthrown fault block of the trenches to constrain the timing of the displacements observed in the trench and thus reconstruct the recent seismotectonic behaviour.

Sample preparation and luminescence measurements were carried out at the luminescence dating laboratory of the Archaeometry Center of the University of Ioannina.

The grain-size fraction of 63-100 μm, for samples from Gyrtoni 2 trench, and 125-250 μm, for samples from Gyrtoni 1 trench, were extracted by wet-sieving. The extracted grains were treated with HCl, H_2O_2, HF and concentrated HCl to separate quartz subsamples. The purity of the quartz extract was checked using the OSL-IR depletion ratio (Duller, 2003). Following sample preparation, luminescence measurements were performed on a Risø TL/OSL-DA-20 reader (Bøtter-Jensen et al., 2003) and signals were detected using a 7 mm Hoya U-340 optical filter in front of an EMI 9235QA photomultiplier tube. Measurements of OSL were made on the chemically purified coarse-grained quartz, using the Single-Aliquot Regenerative-dose (SAR) protocol of Murray & Wintle (2000; 2003).

The environmental dose rates were calculated from radionuclide concentrations, measured by high-resolution gamma spectrometry (Murray et al., 1987), at the Nuclear Physics Laboratory of the University of Ioannina, using the conversion factors of Adamiec & Aitken (1998).

PRELIMINARY RESULTS

The detailed analysis of the trench walls allowed as the identification of at least two faulting events. The minimum age of the two faulting events were derived by samples GyrOSL1_1 (Fig. 3) and GyrOSL2_5E (Fig. 4), and GyrOSL1_16 (Fig. 3) and GyrOSL2_2E (Fig. 4), respectively. The preliminary results of the 4 OSL ages are in stratigraphic order and indicate that unit 9 (Fig. 3) was deposited before about 1.3 ka. The colluvial deposits unit 7 (Fig. 3) and unit 6 (Fig. 4) were deposited before ca. 3.7 ka. The two identified palaeoearthquakes produced a total displacement of about 1.6 m with an average displacement of about 0.8 m each. According to our preliminary interpretation, the first event occurred

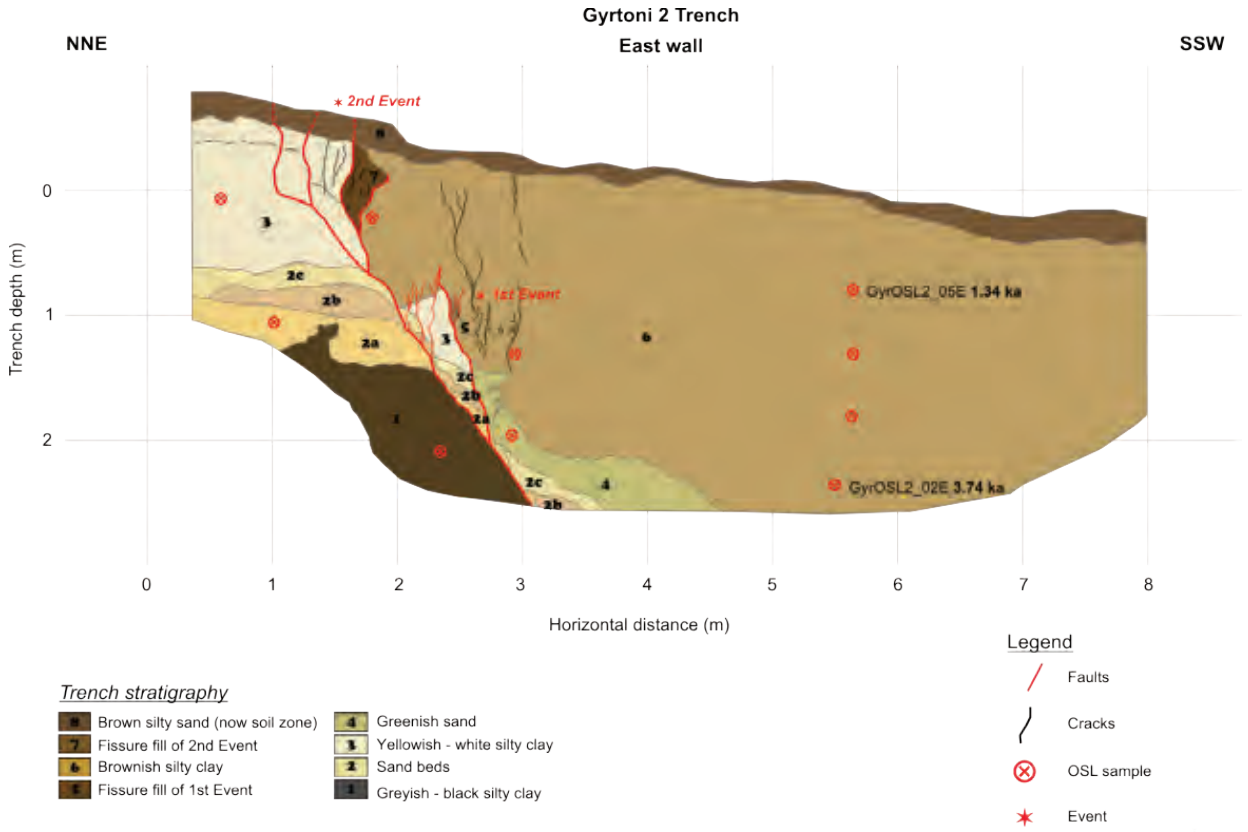

Figure 4: Simplified log of the east wall of the Gyrtoni 2 palaeoseismological trench.

before 3.7 ka, while the most recent event (2nd Event) occurred before 1.3 ka. As a first approximation and assuming a characteristic earthquake behavior (Schwarz & Coppersmith, 1984), these OSL ages suggest a recurrence interval in the order of few thousands of years, say between ca. 1.9 ka and 5 ka. From the available dating results and following the above assumptions, the slip rate could be tentatively estimated between ca. 0.1 and 0.6 mm/a therefore slightly higher than previously suggested (Caputo, 1995).

The seismic history of the Gyrtoni Fault was completely unknown and thus these data offer new results for improving our knowledge on the Holocene tectono-stratigraphy of this structure and for better evaluation of the seismic hazard potential of Larissa.

Acknowledgements: The research project is implemented within the framework of the Action «Supporting Postdoctoral Researchers» of the Operational Program "Education and Lifelong Learning" and is co-financed by the European Social Fund (ESF) and the Greek State. We would like to thank an anonymous reviewer for reading and improving earlier version of the manuscript.

References

Adamiec, G., M.J. Aitken, (1998). Dose-rate conversion factors: update. *Ancient TL*. 16,37-50.

Bøtter-Jensen, L., C.E. Andersen, G.A.T. Duller, A.S. Murray, (2003). Developments in radiation, stimulation and observation facilities in luminescence measurements. *Radiation Measurements*. 37, 535-541.

Caputo, R., (1995). Inference of a seismic gap from geological data: Thessaly (Central Greece) as a case study, *Ann. Geofisica*. 38, (1), 1-19.

Caputo, R., J.P. Bravard & B. Helly, (1994). The Pliocene Quaternary tecto-sedimentary evolution of the Larissa Plain (eastern Thessaly, Greece). *Geodinamica Acta*. 7, (4), 219-231.

Caputo, R., S. Piscitelli, A. Oliveto, E. Rizzo & V. Lapenna, (2003). The use of electrical resistivity tomography in active tectonics. Examples from the Tyrnavos Basin. Greece. *J. Geodyn.* 36, (1-2), 19-35.

Caputo, R., A. Chatzipetros, S. Pavlides & S. Sboras, (2012). The Greek Database of Seismogenic Sources (GreDaSS): state-of-the-art for northern Greece. *Annals of Geophysics*. 55, (5), 859-894.

Duller, G.A.T., (2003). Distinguishing quartz and feldspar in single grain luminescence measurements. *Radiation Measurements*. 37, 161-165.

Murray, A.S., R. Marten, A. Johnston, P. Martin, (1987). Analysis for naturally occurring radionuclides at environmental concentrations by gamma spectrometry. *Journal of Radioanalytical and Nuclear Chemistry*. 115, 263-288.

Murray, A.S., A.G. Wintle, (2000). Luminescence dating of quartz using an improved single-aliquot regenerative-dose protocol. *Radiation Measurements*. 32, 57-73.

Murray, A.S., A.G. Wintle, (2003). The single aliquot regenerative dose protocol: potential for improvements in reliability. *Radiation Measurements*. 37, 377-381.

Schwartz, D.P., & J. Coppersmith, (1984). Fault behaviour and characteristic earthquakes: examples from Wasatch and San Andreas faults. *J. Geophys. Res.* 89, 5681-5698.

INQUA Focus Group on Paleoseismology and Active Tectonics

The Mw 5, 2013 Matese earthquake epicentral area (southern Italy): new data on the earthquake ground effects and active tectonics framework

Valente, E. (1), Ascione, A. (2), Bigi, S. (3), Buscher, J. (2), Ciotoli, G. (4,5), Porfido, S. (6)

(1) Dipartimento di Scienze Umanistiche, Sociali e della Formazione, Università del Molise, Campobasso, Italy
(2) Dipartimento di Scienze della Terra, dell'Ambiente e delle Risorse, Università Federico II, Napoli, Italy. Email: alessandra.ascione@unina.it
(3) Dipartimento di Scienze della Terra, Università La Sapienza, Roma, Italy
(4) Istituto di Geologia Ambientale e Geoingegneria – Consiglio Nazionale delle Ricerche, Roma, Italy
(5) Istituto Nazionale di Geofisica e Vulcanologia, Sezione Roma 2, Roma, Italy
(6) Istituto per l'Ambiente Marino Costiero - Consiglio Nazionale delle Ricerche, Napoli, Italy

Abstract: *The Matese ridge area (southern Apennines) is located in one of the most seismically active sectors in Italy. On 29th December 2013, it was affected by a Mw=5 earthquake. In the Matese area, we are carrying out a study aimed at identifying and characterizing active faults at the surface through the integration of geomorphological, structural and soil gas data, and at outlining the ground effects of the 2013 earthquake. The new data indicate that the active fault system is more complex than previously assessed. In addition, our estimation of the epicentral intensity of the 2013 earthquake according to the ESI scale (Michetti et al., 2007) indicates that earthquakes of relatively low energy may trigger noticeable environmental hazards.*

Key words: *Active faults, seismically induced ground effects, geomorphology, soil gas, southern Apennines.*

INTRODUCTION

The Matese area (southern Apennines), which falls in one of the most seismically active sectors of Italy, has recorded in historical times a number of earthquakes with a magnitude of around 7 (e.g., Esposito et al., 1987; Gasperini et al., 1999; Galli & Galadini, 2003; Fracassi and Valensise, 2007; Serva et al., 2007; Locati et al., 2011; Rovida et al., 2011; Fig. 1) and frequent moderate earthquakes. From December 2013 to January 2014, the Matese ridge area was affected by a seismic sequence. The main event, which occurred on December 29th 2013, was characterised by a moderate magnitude (17:08 UTC, Mw 5.0, according to ISIDE; http://iside.rm.ingv.it) and caused damage corresponding to a maximum intensity of VII MCS in the Piedimonte Matese and Faicchio villages (Convertito et al., 2014). The earthquake, the epicentre of which has been localized in the southeastern part of the Matese ridge, at a hypocentral depth of 12 km (Fig. 2; D'Amico et al., 2014; Milano, 2014), was also felt in the towns of Isernia, Caserta, Benevento, Napoli, Avellino and Salerno (location in Fig. 1).

In the 2013 earthquake epicentral area, and in the surrounding Matese ridge - Alife alluvial plain area, we are carrying out a study aimed at outlining the active tectonic framework by identifying and characterizing active faults at the surface based on the integration of geomorphological, structural and soil gas data. The field surveys and the collection of reports and information from local people have also allowed recognition of several ground effects that may have been directly related to the 2013 earthquake.

The ~2000 m high Matese ridge is located in the Campania-Molise sector of the southern Apennines. The southern Apennines is a NE-directed fold and thrust belt that formed from the Miocene to Quaternary.

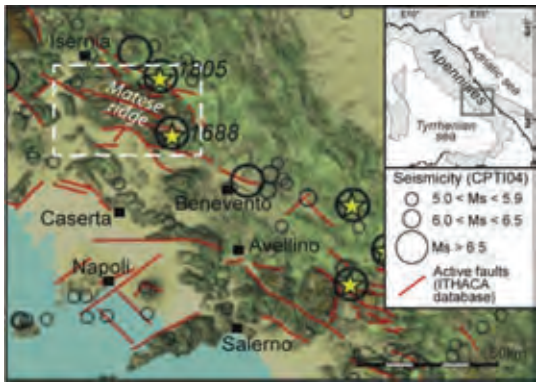

Figure 1: Historical earthquakes (Ms>5.0) in the southern Apennines according to CPTI (2004). The withe box indicates location of map in Fig. 3. (After Serva et al., 2007 modified).

Ceasing of thrusting occurred in the early part of the Middle Pleistocene, and was followed by the onset of a new tectonic regime with NE-SW oriented maximum extension (e.g., Cello et al., 1982; Cinque et al., 1993; Montone et al., 1999; Patacca et al., 2008). The structures related to this regime include extensional faults that dissect the thrust belt (e.g., Cello et al. 1982; Ascione et al., 2013). Based on fault-plane solutions, normal faults also control seismicity in the mountain belt, which is affected by low to moderate events punctuated by strong earthquakes, mostly following the chain axis and originating on NW-SE trending faults (e.g., DISS Working Group, 2010).

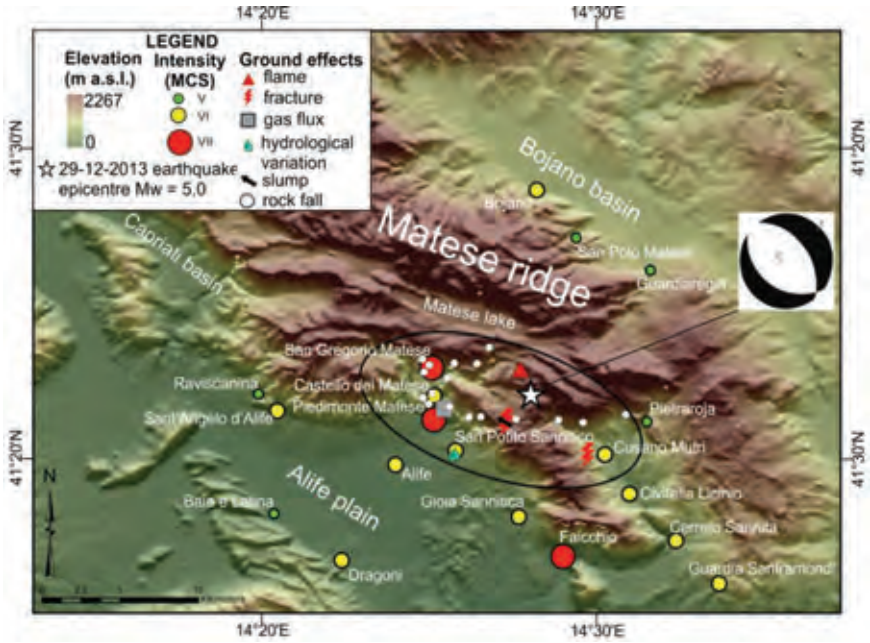

Figure 2: Epicentre location (http://iside.rm.ingv.it) of the M=5, December 29th 2013 Matese earthquake, MCS intensity recorded in the main villages of the Matese area (from Convertito et al., 2014) and main ground effects associated with the earthquake.

In the Matese area, tectonic units of the fold and thrust belt are composed of Mesozoic-Tertiary successions overlain by Neogene foredeep basin deposits. From top to bottom, these units consist of carbonate successions (Apennine Platform, outcropping in the Matese ridge), pelagic basin successions (Molise-Sannio Basin, outcropping to the N and E of the ridge), and the buried Apulian platform carbonates (Mazzoli et al., 2000). The thrust pile is dissected by NW-SE and E-W trending high-angle faults reactivated by the Middle Pleistocene to Present extensional regime (Mazzoli et al., 2000, and references therein). The main Quaternary extensional faults bound the Matese ridge towards the NE and SW, with the latter ones lowering the top of the carbonates below the sea level in the Alife alluvial basin (Corniello & Russo, 1990). Late Quaternary activity of mainly NW-SE, WNW-ESE and E-W trending faults in the Matese ridge and adjoining alluvial basins has also been recognised (Cinque et al., 2000; Galli & Naso, 2009).

In the Matese area, strong historical earthquakes with a high level of damage (I>X MCS) occurred in 1456, 1688 and 1805 (Fig. 1). The December 1456 earthquakes were probably the most powerful in Italy, with different epicentral areas spanning from the Abruzzo to the Campania regions (Figliuolo, 1988), Imax=XI MCS, M=7.2 (Rovida et al., 2011). The M=7, I=XI MCS June 5th 1688 earthquake hit the southeastern area of the Matese ridge causing the destruction of Cerreto Sannita and Civitella Licinio and heavy damage in 130 localities in the districts of Benevento, Avellino and Caserta. About 10,000 casualties have been estimated (Serva, 1985; Rovida et al., 2011). In 14 localities, including Cerreto Sannita and the town of Benevento, seismically induced effects mainly consisted of slope movements, however ground cracks and hydrological variations were also observed (Porfido et al., 2007; Serva et al., 2007). On July 26th, 1805, a destructive earthquake with a maximum intensity of I=XI MCS and an estimated magnitude of 6.7 (Fig. 1; Esposito et al., 1987) hit the Molise Region and part of Campania. This earthquake damaged over 200 localities and claimed more than 5,000 lives. Based on the review of historical documents, and consistent with geological investigations (Guerrieri et al., 2000; Michetti et al., 2000b; Porfido et al., 2002), a large number of effects on the natural environment were identified in 50 municipalities located both in the near and far field areas. Primary effects such as surface faulting, and secondary effects including hydrological anomalies, ground cracks, slope movements, ground settlements were recorded (Porfido et al., 2002; Porfido et al., 2007; Serva et al., 2007). Along the Campania coast tsunami waves were observed (Mallet, 1852-1854; Baratta, 1901), classified with Intensity 2 in the Euro-Mediterranean Tsunami Catalogue (Maramai et al., 2014).

In the last few decades, the Matese area has been affected by low-magnitude background seismicity characterised by both sparse earthquakes and seismic sequences (Milano et al., 2005; Chiarabba et al., 2011). The M=5 earthquake which struck the Matese area on December 29th 2013 was characterised by a normal faulting focal mechanism and a NE oriented T axis (http://cnt.rm.ingv.it/tdmt.html), consistent with moment tensor solutions for 31 small to moderate events of the entire December 2013-January 2014 seismic sequence (e.g., D'Amico et al., 2014).

DISCUSSION

The study we have carried out has allowed the detection of a dense net of faults showing geomorphological-stratigraphical evidence of late Quaternary activity in the Matese area. Such evidence, coupled with the analysis of longitudinal profiles of more than 40 streams, has also provided information on the spatial distribution of large-scale vertical motions.

Faults showing evidence of activity in the late Quaternary include few major structures with WNW-ESE and NW-SE trends and lengths around 10 km. These occur at the boundary of subsiding alluvial basins, e.g., the Capriati basin (e.g., Cinque et al., 2000; Galli & Naso, 2009), the Alife plain and the Matese Lake. In addition, several strands, characterised by mainly N-S and E-W trends, relatively small offsets and a small size (few km long) are identified within both major topographic highs and lows. Such minor structures probably represent the response to local variations in the regional stress field (Ascione et al., 2014). In the southeastern part of the Matese ridge, recent vertical motions are suggested by the presence, in the top surface, of small-size dammed basins and by features of the active/relic fluvial network (wind gaps, water gaps).

Important information on the features of the southern Matese active fault system has been obtained through the detection of anomalous emissions of several gas species (CO_2, CH_4, Rn and He) along fault strands in the western part of the study area (Fig. 3; Ascione et al., 2014). Such emissions, pointing to strong gas leakage along active fault strands, suggest that the southern Matese active fault system is composed of a complex fracture network linking surface faults to deeply rooted structures.

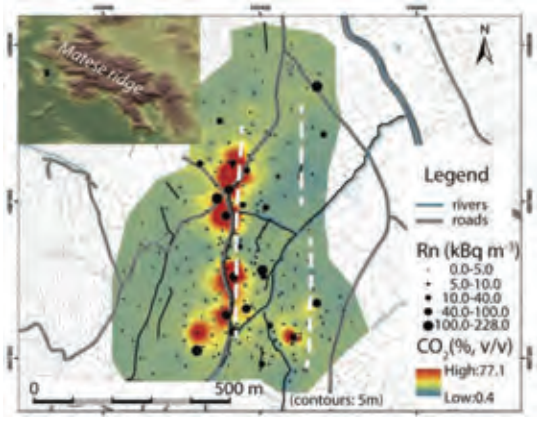

Figure 3: Soil gas (CO_2 and Rn) emission detected in the Colle Sponeta area (location in inset map). The main soil gas anomalies are aligned along active fault traces (dashed white lines).

The December 29th 2013 earthquake has induced a series of ground effects, which include small size landslides (mostly rock falls) and hydrological variations. Several rock falls have affected the roadcuts in the area between Piedimonte Matese and San Gregorio Matese. In the latter site, damages to the aqueduct have also been reported. Associated with the seismic sequence, variations in the spring discharge, and an increase in the turbidity of spring water at one of the major springs have also been recorded (Fig. 2). Local people described the occurrence of a flame in an area very close to the instrumental earthquake epicentre (Fig. 2) at the very beginning of the main shock. This localised effect, commonly observed during earthquakes (Oddone, 1915), is frequent in those areas in which strong gas (methane and/or hydrogen) emissions are detected (Ascione et al., 2014). Following this phenomenon, a further soil gas investigation in the epicentre area is presently being carried out. A coseismic scarp up to around 40 cm high, around 50 m long, striking N120 and facing NE (Fig. 4) has been identified in the Matese ridge top surface, at a distance of about 2.5 km to the SW of the earthquake epicentre (Fig. 2). The scarp follows a WNW-ESE trending fault damming a small size, internally drained basin. In particular, it affects the northeastern slope of a subdued carbonate ridge, which bounds the basin to the SW. Such a scenario allows hypothesising that the scarp results from coseismic fault reactivation. However, further investigations are being carried out with the aim of assessing whether such scarp represents a primary or secondary earthquake effect. In fact, taking into account the scarp features (height and length) and those of the 2013 earthquake (magnitude and hypocentral depth), an origin of the scarp as local effect (e.g., compaction of fault breccia) cannot be ruled out.

Figure 4: The around 40cm high, N120 trending, NE-facing coesismic scarp in the Piano d'Amore area (Matese ridge).

The spatial distribution of the ground effects (which cover an area of around 90 km^2; Fig. 2) allows for the estimation of the epicentral intensity according to the ESI Scale (Michetti et al., 2007). The resulting evaluation is I_0 = VIII ESI, a value exceeding by one degree the former MCS scale intensity evaluation by Convertito et al. (2014).

The new data on the 2013 earthquake ground effects, and on the spatial distribution, geometry and gas-bearing properties of active faults provide information

crucial to the assessment and mitigation of seismic hazards in the Matese area. Our data point to the occurrence, in the Matese area, of a deformation pattern at the surface more complex than previously assessed. In addition, the M=5, 29th December 2013 earthquake ground effects indicate that earthquakes of relatively low energy and intensity barely exceeding the damage threshold of man made structures, may trigger noticeable environmental hazards. Such information provides a more complete perspective on an earthquake scenario, which should be seriously considered in the framework of both seismic hazard prevention and mitigation, and, on a local scale, civil planning.

Acknowledgements: This work was financially supported by the Dipartimento della Protezione Civile (DPC) - Istituto Nazionale di Geofisica e Vulcanologia (INGV) 2014-15 research project "Active faults and fluid circulation in the Matese area", responsible A. Ascione.

References

Ascione, A., S. Bigi, G. Ciotoli, A. Corradetti, G. Etiope, L. Ruggiero, P. Sacco, C. Tartarello, S. Tavani & E. Valente, (2014). The southern Matese active fault system: New geochemical and geomorphological evidence. *Atti 33° Convegno Nazionale GNGTS, Tema 1: Geodinamica*. 11-19.

Ascione, A., S. Mazzoli, P. Petrosino & E. Valente, (2013). A decoupled kinematic model for active normal faults: Insights from the 1980, MS = 6.9 Irpinia earthquake, southern Italy. *Bulletin of the Geological Society of America*. 125, (7-8), 1239-1259.

Baratta, M., (1910). I terremoti d'Italia. Bocca, Torino.

Chiarabba, C., P. De Gori & A. Amato, (2011). Do earthquake storms repeat in the Apennines of Italy? *Terra Nova*. 23, (5), 300-306.

Cinque, A., A. Ascione & C. Caiazzo, (2000). Distribuzione spazio-temporale e caratterizzazione della fagliazione quaternaria in Appennino meridionale. In: *Le ricerche del GNDT nel campo della pericolosità sismica* (Galadini F., Meletti, C., Rebez, A. eds). CNR – Gruppo Nazionale per la Difesa dai Terremoti, Roma, 203-218.

Ciotoli, G., S. Bigi, C. Tartarello, P. Sacco, S. Lombardi, A. Ascione & S. Mazzoli, (2014). Soil gas distribution in the main coseismic surface rupture zone of the 1980, Ms=6.9, Irpinia Earthquake (southern Italy). *Geophysical Research Letters*: *Solid Earth*. 119, (3), 2440-2461.

Convertito, V., E. Cubellis, A. Marturano, F. Obrizzo & S.M. Petrazzuoli, (2014). Terremoto del 29 dicembre 2013 nel Matese (M_W = 5.0). Indagine speditiva degli effetti nell'area epicentrale e analisi preliminare della sequenza sismica. *Rapporti Tecnici INGV* n. 290. ISSN 2039-7941.

Corniello, A. & D. Russo, (1990). La piana del medio corso del F. Volturno (Campania) idrogeologia e vulnerabilità all'inquinamento delle falde. *Atti I Convegno sulla gestione e protezione delle acque sotterranee*. Modena, September 1990, 131-148.

CPTI, (2004). Catalogo Parametrico dei Terremoti Italiani. ING, GNDT, SGA, Servizio Sismico Nazionale (vers. 2004), http://emidius.mi.ingv.it/CPTIS

D'Amico, S., L. Cammarata, M. Cangemi, D. Cavallaro, R.M. Di Martino & M. Firetto Carlino, (2014). Seismic moment tensors and regional stress in the area of the December 2013–January 2014, Matese earthquake sequence (Italy). *Journal of Geodynamics*. 82, 118-124.

DISS Working Group, (2010). Database of Individual Seismogenic Sources (DISS), Version 3.1.1: A compilation of potential sources for earthquakes larger than M 5.5 in Italy and surrounding areas. http://diss.rm.ingv.it/diss, INGV 2010.

Esposito, E., G. Luongo, A. Marturano & S. Porfido, (1987). Il terremoto di S. Anna del 26 luglio 1805. *Memorie Società Geologica Italiana*. 37, 171-191.

Figliuolo, B., (1988). Il terremoto del 1456. 2 vol. Altavilla Silentina (SA).

Fracassi, U. & G. Valensise, (2007). Unveiling the sources of the catastrophic 1456 multiple earthquake: hints to an unexplored tectonic mechanism in southern Italy. *Bulletin of the Seismological Society of America*. 97, (3), 725-748.

Galli, P. & F. Galadini, (2003). Disruptive earthquakes revealed by faulted archaeological relics in Samnium (Molise, southern Italy). *Geophysical Research Letters*. 30, (5), 1266.

Galli, P. & G.A. Naso, (2009). Unmasking the 1349 earthquake source (southern Italy): paleoseismological and archaeoseismological indications from the Aquae Iuliae fault. *Journal of Structural Geology*. 31, 128–149.

Gasperini, P., F. Bernardini, G. Valensise & E. Boschi, (1999). Defining seismogenic sources from historical earthquake felt reports. *Bulletin of the Seismological Society of America*. 89, 94–110.

Guerrieri, L., G. Scarascia Mugnozza & E. Vittori, (2000). Analisi stratigrafica e geomorfologica della conoide tardoquaternaria di Campochiaro ed implicazioni per la conca di Bojano in Molise. *Il Quaternario*. 12 (2), 119–129.

Locati, M., R. Camassi R. & M. Stucchi (eds), (2011). DBMI11, the 2011 version of the Italian Macroseismic Database. Milano, Bologna, http://emidius.mi.ingv.it/DBMI11.

Mallet, R., (1852-1854). Catalogue of recorded earthquakes 1600 B.C.-1850 A.D. Report on state of Science. Third report on the Facts of Earthquake Phenomena.

Maramai, A., B. Brizuela & L. Graziani, (2014). The Euro-Mediterranean Tsunami Catalogue. *Annals of Geophysics. 57,* (4), S0435; doi:10.4401/ag-6437.

Mazzoli, S., S. Corrado, M. De Donatis, D. Scrocca, R.W.H. Butler, D. Di Bucci, G. Naso, C. Nicolai & V. Zucconi, (2000). Time and space variability of «thin-skinned» and «thick-skinned» thrust tectonics in the Apennines (Italy). *Rendiconti Lincei: Scienze Fisiche e Naturali*. s. 9, 11, 5-39.

Michetti, A.M., E. Esposito, L. Guerrieri, S. Porfido, L. Serva, R. Tatevossian, E. Vittori, F. Audemard, T. Azuma, J. Clague, V. Comerci, A. Gurpinar, J. McCalpin, B. Mohammadioun, N.A. Mörner, Y. Ota & E. Roghozin, (2007). Intensity Scale ESI 2007. *Memorie Descrittive della Carta Geologica d'Italia*. Roma. 74, 53 p.

Michetti, A.M., L. Serva & E. Vittori, (2000a). ITHACA-Italy Hazard from Capable faults. In: The 31st International Geological Congress, Rio de Janeiro, Brasil, July 2000, abstract + CD. http://www.apat.gov.it/site/it-IT/Progetti/ITHACA_-_catalogo_delle_faglie_capaci

Michetti, A.M., A.M. Blumetti, E. Esposito, L. Ferreli, L. Guerrieri, S. Porfido, L. Serva & E. Vittori, (2000b). Earthquake Ground Effects and Seismic Hazard Assessment in Italy examples from the Matese and Irpinia areas, Southern Apennines. In: *Active Fault Research for the New Millennium*, Proceedings of the Hokudan Symposium and School on Active Faulting. Hokudan, Japan, pp. 279–284.

Milano, G., R. Di Giovambattista & G. Ventura, (2005). The 2001 seismic activity near Isernia (Italy): implications for the seismotectonics of the Central–Southern Apennines. *Tectonophysics*. 401, (3), 167-178.

Milano, G., (2014). Seismological investigation of the 2013-2014 seismic sequence of the Matese massif (Southern Apennines, Italy). *Atti 33° Convegno Nazionale GNGTS, Tema 1: Geodinamica*. 11-19.

Montone, P., A. Amato & S. Pondrelli, (1999). Active stress map of Italy. *Journal of Geophysical Research*. 104, (B11), 25,595–25, 610.

Patacca, E., P. Scandone, E. Di Luzio, G.P Cavinato & M. Parotto, (2008). Structural architecture of the Central Apennines. Interpretation of the CROP 11 seismic profile from the Adriatic coast to the orographic divide. *Tectonics*. 27, TC3007.

Porfido, S., E. Esposito, E. Vittori, G. Tranfaglia, A.M. Michetti, M. Blumetti, L. Ferreli, L. Guerrieri & L. Serva, (2002). Areal distribution of ground effects induced by strong earthquakes in the Southern Apennines (Italy). *Surveys in Geophysics*. 23, (6), 529-562.

Porfido, S., E. Esposito, E. Vittori, G. Tranfaglia, L. Guerrieri & R. Pece, (2007). Seismically induced ground effects of the 1805, 1930 and 1980 earthquakes in the Southern Apennines (Italy). *Italian Journal of Geosciences*. 126, (2), 333-346.

Rovida, A., R. Camassi, P. Gasperini & M. Stucchi (2011). CPTI11, la versione 2011 del Catalogo Parametrico dei Terremoti Italiani. Milano, Bologna, http://emidius.mi.ingv.it/CPTI.

Serva, L., (1985). The earthquake of June 5, 1688 in Campania. In: *Atlas of Isoseismal Maps of Italian Earthquakes* (Postpischl D. ed), vol. 114(2A). CNR - Progetto Finalizzato Geodinamica, Roma. 44–45.

Serva, L., E. Esposito, L. Guerrieri, S. Porfido, E. Vittori & V. Comerci, (2007). Environmental effects from five hystorical earthquakes in Southern Apennines (Italy) and macroseismic intensity assessment: contribution to INQUA EEE Scale project. *Quaternary International*. 173, (17), 30–44.

INQUA Focus Group on Paleoseismology and Active Tectonics

Frequent earthquakes recorded in a section with twelve seismites at Rakuti (SE Latvia)

Van Loon, A.J. (1), Pisarska-Jamroży, M. (1), Nartišs, M. (2), Krievâns, M. (2), Soms, J. (3)

(1) Institute of Geology, Adam Mickiewicz University, Maków Polnych 16, 61-606 Poznań, Poland. Email: tvanloon@amu.edu.pl
(2) Faculty of Geography and Earth Sciences, University of Latvia, Rainis Blvd. 19, 1576 Riga, Latvia
(3) Department of Geography, Daugavpils University, Parades 1, LV 5401, Daugavpils, Latvia

Abstract: *A glaciolacustrine-glaciofluvial succession of some 7 m thick near Rakuti (SE Latvia) contains twelve layers that must be interpreted as seismites. The succession dates from the late Weichselian and probably represents a time-span of the order of a few thousand years. This implies that at least twelve high-magnitude earthquakes occurred with an average frequency of 1 per 100-200 years. Although it is known that tectonic activity affects the area also in historical times, it must be assumed that at least part of the twelve layers with continuous lateral deformations resulted from earthquakes, and thus should be considered as seismites. The earthquakes must have been induced by glacio-isostatic rebound as a consequence of the retreat of the south-eastern flank of the last Scandinavian Ice Sheet.*

Key words: *Seismites, Latvia, Glacio-isostatic rebound, Pleistocene, Soft-sediment deformation structures.*

Large earthquakes tend to be followed by aftershocks, which also may have magnitudes that are sufficient to change undisturbed sedimentary layers into strongly deformed ones: seismites. It is commonly not known how long a specific tectonic phase lasts, and what is the (average) time interval between two successive large shocks. Historical data indicate that a few high-magnitude aftershocks may occur within a relatively short time-span (Matsuda et al., 1978, for instance, mention 800-1500 years for the Kanto District in Japan), but the aftershocks are rarely sufficiently strong to induce shock waves that are capable of deforming layers at or near the sedimentary layers over such large lateral distances that these layers may be considered as seismites. It is worthwhile to mention here that the term 'seismites' was introduced by Seilacher (1969) to indicate layers that were more or less entirely deformed by earthquake-induced processes. Insufficient knowledge of the original literature has, unfortunately, resulted in several publications in which the term 'seismite' is used for the deformation structures in earthquake-affected layers, but this is a misconception (Van Loon, 2014) that should become obsolete as soon as possible, if only to avoid confusion between layers and soft-sediment deformation structures (SSDS).

Figure 1: Location of the study area.

The geological record of series of successive seismites reflecting repeated earthquakes is fairly scarce. Most publications about successive hard-rock layers with deformations induced by an earthquake while the sediment was still unlithified, estimate the recurrence time as several thousands (e.g. Pantosti et al., 2012: 2150 years) to tens of thousands of years (e.g. Ezquerro et al., in press: 45,000 years).

Hardly any data are available about series of earthquakes with an average recurrence time of only a few hundred years are known from the Pleistocene, even though the numerous advances and retreats of the large continental ice caps must have resulted in a huge number of rebound-related earthquakes. Reasons for this may be (1) rather gradual rebound instead of rebound in the form of earthquake-inducing faulting; (2) rebound in the form of frequent faulting that induced earthquakes of insufficient magnitude to produce seismites; (3) lack of sufficient exposures in Pleistocene sediments, leaving seismites undetected; and (4) earthquake-affected sediments with a granulometry that is insufficiently susceptible to deformations. Considering all these restrictive conditions, it is not surprising that sections in areas without endogenic tectonic activity with Pleistocene sediments showing a series of seismites are rare.

Figure 2: Lateral extent of twelve seismites levels in the section in Rakuti. Numbers indicate levels of seismites.

A section near Rakuti (SE Latvia) (Fig. 1) represents such a rare feature, as it contains at least twelve seismites in a section (Fig. 2) of about 7 m thick, dating from the late Weichselian. The exposed section (55°53'51"N, 27°05'30"E) is some 7 m high and consists mainly of fine-grained glaciolacustrine sediments and some more silty/sandy sediments of glaciofluvial origin; both the sedimentary and the geomorphological setting suggest that the section forms part of a kame terrace (cf. Zelčs et al., 2014).

The section under study forms part of a large quarry, in which the exploited sediments represent partly different stratigraphic levels. Yet, it seems that the two lowermost seismites in the section under study can be correlated with seismites some 150 m to the West in a section that is truncated by a boulder-rich gravel. This suggests that the layers considered to represent seismites extend over considerable distances.

The seismites are strongly deformed layers, sometimes intercalated between undeformed layers, sometimes stacked on top of each other (Fig. 3). This indicates that sometimes sufficient time elapsed between successive earthquakes of sufficient magnitude to build up a recognisable sedimentary succession of which only the uppermost layer(s) became disturbed by the seismic shock, whereas other earthquakes apparently occurred to quickly after each other. In some cases it seems that the same layer has been affected by more than one seismic shock, indicating that the successive shocks occurred soon after each other.

One of the questions posed by the frequent occurrence of seismites at Rakuti is where the epicentre of the triggering fault was located. As a magnitude of about 4.5 is required for the formation of seismites with liquefaction features, and because the power of the shock waves diminishes with distance from the epicentre, it seems that the faults cannot have had their epicentre in Scandinavia: the faulting must have been more nearby. In 1908 an earthquake occurred near Daugavpils (SE Latvia), but this was most probably due to neotectonics (Šliaupa et al., 2006), so this fault seems not responsible for the Rakuti seismites. If the epicentre would have been truly close to Rakuti, it could be expected that some brecciation would have taken place (cf. Gruszka et al., 2007), but no brecciation has been noted at Rakuti. This would imply that the faulting took place probably more than a few kilometres from Rakuti. It should be taken into account, however, that lateral changes in lithology affect the properties of the passing shock waves and thus the nature of the deformations in a seismite (Rodríguez-Lopez et al., 2007; Moretti & Van Loon, 2014). Moreover, earthquake-induced shock waves cannot propagate across shear planes (Schwab and Lee, 1988; Mazumder et al., 2006). In principle, one might reconstruct the direction in which the epicentre was situated by analysing lateral changes in the nature of the SSDS; by lack of other outcrops with seismites in the vicinity, this is, however, impossible for the Rakuti seismites. The fault (or faults) responsible for the origination of these seismites therefore remains a problem that might be solved by more focused future fieldwork.

Anyway, the frequency of the seismites near Rakuti suggests that glacio-isostatic rebound was the trigger, as was also deduced for several other places around the Baltic (Mörner, 1990, 1991; Brandes et al., 2012; Hoffman & Reicherter, 2012; Brandes & Winsemann, 2013; Van Loon & Pisarska-Jamroży, 2014).

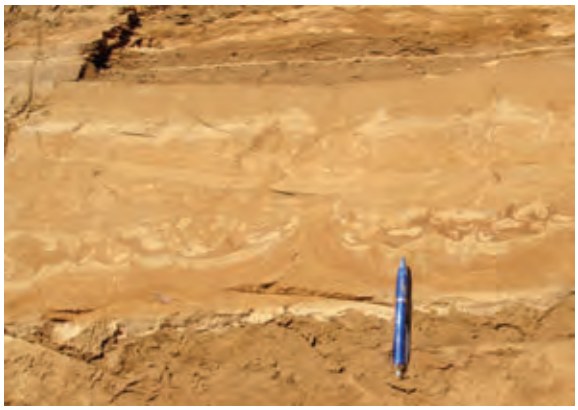

Figure 3: Detail of the section at Rakuti. Successive seismites are separated by undeformed sediments, sometimes stacked on top of each other.

INQUA Focus Group on Paleoseismology and Active Tectonics

Acknowledgements: The work has been financially supported by a grant from the Polish Ministry of Science and Higher Education (research project No. N N307 057540) and by a grant from the National Science Centre Poland (decision No. DEC-2013/09/B/ST10/00031).

References

Brandes, Ch., J. Winsemann, J. Roskosch, J. Meinsen, D.C. Tanner, M. Frechen, H. Steffen & P. Wu, (2012). Activity along the Osning Thrust in Central Europe during the Lateglacial: ice-sheet and lithosphere interactions. *Quaternary Science Reviews*. 38, 49-62.

Brandes, C. & J. Winsemann, (2013). Soft-sediment deformation structures in NW Germany caused by Late Pleistocene seismicity. *International Journal of Earth Sciences*. 102, 2255-2274.

Ezquerro, L., M. Moretti, C.L. Liesa, A. Luzón & J.L. Simón. Seismites from a well core of palustrine deposits as a tool for reconstructing the palaeoseismic history of a fault. *Tectonophysics*. (in press).

Gruszka, B. & A.J. Van Loon, (2007). Pleistocene glaciolacustrine breccias of seismic origin in an active graben (central Poland). *Sedimentary Geology*. 193, 93-104.

Hoffman, G. & K. Reicherter, (2012). Soft-sediment deformation of Late Pleistocene sediments along the southwestern coast of the Baltic Sea (NE Germany). *International Journal of Earth Sciences*. 101, 351-363.

Matsuda, T., Y. Ota, M. Ando & N. Yonekura, (1978). Fault mechanism and recurrence time of major earthquakes in southern Kanto district, Japan, as deduced from coastal terrace data. *Geological Society of America Bulletin*. 89, 1610-1618.

Mazumder, R., A.J. Van Loon, & M. Arima, (2006). Soft-sediment deformation structures in the Earth's oldest seismites. *Sedimentary Geology*. *186*, 19-26.

Moretti, M., A.J. Van Loon, (2014). Restrictions to the application of 'diagnostic' criteria for recognizing ancient seismites. *Journal of Palaeogeography*. 3, 162-173.

Mörner, N.A., (1990). Glacioisostatic and long term crustal movements in Fennoscandia with respect to lithospheric and atmospheric processes and properties. *Tectonophysics*. 176, 13-24.

Mörner, N.A., (1991). Intense earthquakes and seismotectonics as a function of glacial isostasy. *Tectonophysics*. 188, 407-410.

Pantosti, D., D.P. Schwartz, & G. Valensise, (2012). Paleoseismology along the 1980 surface rupture of the Irpinia Fault: implications for earthquake recurrence in the southern Apennines, Italy. *Journal of Geophysical Research, Solid Earth*. doi: 10.1029/92JB02277.

Pisarska-Jamroży, M., A.J. Van Loon, M. Nartišs, & M. Krievâns, (this volume). Seismites recording glacio-isostatic rebound after melting of the Scandinavian Ice Sheet in Latvia.

Rodríguez-Lopez, J.P., N. Merléndez, A.R. Soria, C.L. Liesa, & A.J. Van Loon, (2007). Lateral variability of ancient seismites related to differences in sedimentary facies (the syn-rift Escucha Formation, mid-Cretaceous, Spain). *Sedimentary Geology*. 201, 461-484.

Schwab, W.C. & H.J. Lee, (1988). Causes of two slope-failure types in continental-slope sediment, northeastern Gulf of Alaska. *Journal of Sedimentary Petrology*. 58, 1-11.

Seilacher, A., (1969). Fault-graded beds interpreted as seismites. *Sedimentology*. 13, 15-19.

Šliaupa, S., R. Kačianauskas, D. Markauskas, G. Dundulis & E. Uškuras, (2006). Design Basis Earthquake of the Ignalina Nuclear Power Plant. *Geologija*. 54, 9-30.

Van Loon, A.J., (2014). The life cycle of seismite research. *Geologos*. 20, 61-66.

Van Loon, A.J. & M. Pisarska-Jamroży, (2014). Sedimentological evidence of Pleistocene earthquakes in NW Poland induced by glacioisostatic rebound. *Sedimentary Geology*. 300, 1-10.

Zelčs, Soms, J. & E. Greiškalns, (2014). Stop 10: Kame terrace in the Upper Daugava depression at Rakuti, near Krāslava. In: *Late Quaternary terrestrial processes, sediments and history: from glacial to postglacial environments – excursion guide and abstracts* (Zelčs, S. & Nartišs, M., eds). University of Latvia (Riga). 61-66.

INQUA Focus Group on Paleoseismology and Active Tectonics

paleoseismicity.org

In sequence/out-of sequence Late-Quaternary deformation in Northwestern Himalaya

Vassallo, R. (1), Mugnier, J.L. (1), Vignon, V. (1), Malik, M.A. (2), Jouanne, F. (1), Jayangondaperumal, R. (3), Buoncristiani, J.F. (4), Carcaillet, J. (1), Jomard, H. (5)

(1) Institut des Sciences de la Terre, Université de Savoie et Université Joseph Fourier, Chambéry et Grenoble, France. Email: riccardo.vassallo@univ-savoie.fr
(2) Jammu University, Jammu, India
(3) Wadia Institute of Himalayan Geology, Dehradun, India
(4) Laboratoire Biogéosciences, Université de Bourgogne, Dijon, France
(5) Institut de Radioprotection et de Sûreté Nucléaire, Fontenay-aux-Roses, France

Abstract: *Three main thrusts (Main Boundary Thrust, Medlicot-Wadia Thrust and Main Frontal Thrust) at the front of Northwestern Himalaya, in the Jammu and Kashmir region, have accommodated most of the India–Eurasia convergence across the belt over the last million years. Within a 200-km-long seismic gap zone, the last main earthquake occurred in 1555. Using geomorphic markers and combining 10Be, OSL and 14C dating, we quantified the activity of each fault to better constrain the seismic hazard. While the Main Boundary Thrust is inactive since at least 30 ka, the Medlicot-Wadia Thrust and the Main Frontal Thrust accommodate a large part of the India-Eurasia convergence. Geomorphic shortening rates across these faults are 11.2±3.8 mm/yr and 9.0±3.2 mm/yr, respectively, implying a minimum 6 m slip deficit since last event. Deformation, both at the Quaternary and at the historical time-scale, follows an in-sequence/out-of-sequence pattern.*

Key words: *Active tectonics, Himalaya, geomorphic markers, Quaternary geochronology, seismic hazard.*

INTRODUCTION

Quaternary deformation due to the collision between India and Eurasia in the Northwestern Himalayan belt has been accommodated by a series of sub-parallel South-verging thrusts (Figure 1). These thrusts merge at depth on a sub-flat detachment plane, the Main Himalayan Thrust (Srinivasan and Khar, 1996; Yin, 2006; Jouanne et al., 2011; Mugnier et al., 2013). Stress accumulating on these faults is partly released seismically, with historical events M >7.5 (Ambraseys and Jackson, 2003; Ambraseys and Douglas, 2004; Hussain et al., 2009). The last two main regional seismic events were the 1905 Kangra Mw 7.8 earthquake and the 2005 Muzaffarabad Mw 7.6 earthquake (Figure 1).

The former occurred either beneath the frontal part of the belt or on a more internal thrust (Bilham, 2001; Ambraseys and Douglas, 2004; Wallace et al., 2005) while the latter was clearly triggered on an internal thrust (Avouac et al., 2006; Kumahara and Nakata, 2006; Yeats et al., 2006; Kaneda et al., 2008). In between these two ruptures, a 200-km-long zone has experienced a period with no major events since 1555 AD, when the Kashmir earthquake estimated to be larger than Mw 7.5 caused damages over a vast region extending from the front of the range to the Kashmir basin (Ambraseys and Douglas, 2004). The localization of its epicenter remains unknown and so its origin cannot be assigned to any given structure.

This lack of information and the occurrence of earthquakes on internal and external structures in the region at the historical time-scale rise two fundamental questions about the localization of the seismogenic structures over the millennial time-scale in this part of the belt. Does deformation follow an in-sequence or an out-of-sequence pattern? And which are the most active tectonic faults capable of producing destructive earthquakes?

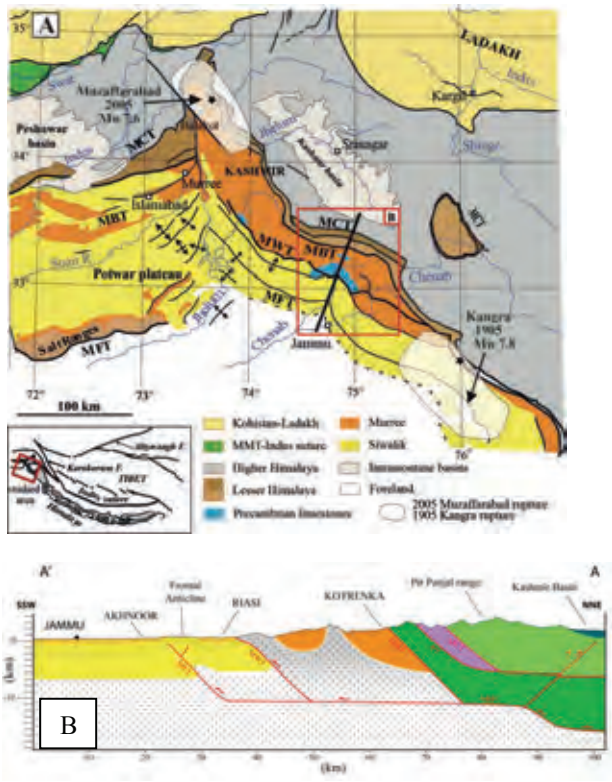

Figure 1: A) Simplified structural map of the Northwestern Himalayan front. Modified from Pêcher et al. (2008); B) Crustal cross-section of the transect indicated in A.

To answer these questions we determine the chronology of the tectonic activity of these thrusts and quantify their present contribution to the accommodation of convergence. Our approach consists in studying the alluvial morphotectonic markers that cross the potentially active structures by mapping them, measuring their cumulated deformation and dating them coupling 10Be, OSL and 14C geochronometers.

RESULTS

Our results show that active deformation in Northwestern Himalaya is localized on the two more external structures: the Medlicott-Wadia Thrust and the Main Frontal Thrust. Tectonic activity on the Main Boundary Thrust ceased more than ~30 ka ago, since an alluvial fan deposited at that time above the fault zone shows a constant-sloping undeformed tread (Figure 2). We therefore consider that this fault is no longer seismogenic in the region, since the contrary would imply very long recurrence period.

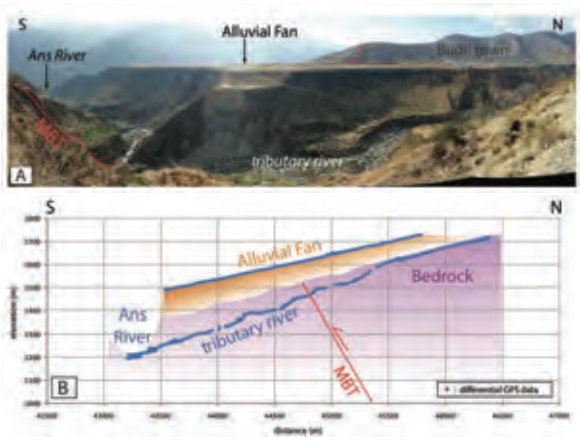

Figure 2: A) Photograph of the Budil fan crossing the Main Boundary Thrust in a tributary valley of the Ans river; B) Topographic profiles obtained by differential GPS of the alluvial deposits and of the tributary river showing no tectonic deformation of these geomorphic markers.

The Medlicott-Wadia Thrust, in the Riasi region, has a completely different impact on the landscape. The alluvial fan built by the Nodda river, a tributary of Chenab river, presents a complex tectonic scarp across a fault zone 1.2 km thick and 250 m high (Figure 3). This scarp is associated with gouge zones in the bedrock, where Precambian limestones overthrust Late-Quaternary alluvia (Figure 4). This deformation corresponds to the cumulated reverse displacement on several fault splays of a hectometer-scale folding. The vertical displacement of the fan surface is 150 ± 30 m since 14 ± 2 ka (fan age). Considering a mean dip of the thrust of 45°, it yields a geomorphic shortening rate of 11.2 ± 3.8 mm/yr accommodated by this fault over this period. This rate is consistent with another geomorphic observation on an older marker: in the hanging-wall, we dated the highest preserved strath terrace of the Chenab river by 10Be and OSL at 36 ± 5 ka. This age correlates with the OSL dating of Chenab deposits in the footwall, suggesting an initial continuity of this alluvial marker. Taking into account the river vertical incision rate in the hanging-wall and in the footwall, we calculate a shortening rate of 10.6 ± 2.0 mm/yr over this period, indistinguishable from the rate calculated over 14 ka.
Two 25-m-long paleoseismological trenches realized within the fan across the two most external splays of the fault show that the great 1555 earthquake ruptured one of them. Several co-seismic ruptures observed are consistent with single displacements of >4-5 meters.

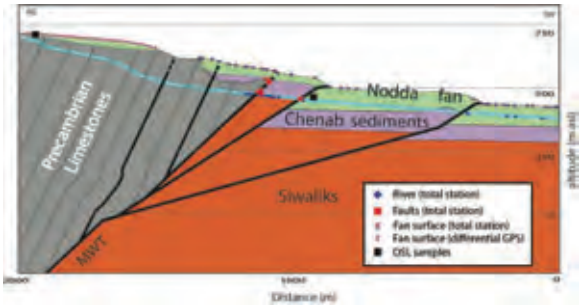

Figure 3: Cross-section of the hectometric-scale scarp produced by the cumulated reverse movement of the different splays of the Medlicott-Wadia Thrust in the alluvial fan of the Nodda river.

Figure 4: Emergence at surface of the Medlicott-Wadia Thrust revealed by river incision, where old formations (Precambrian limestones) overthrust much younger detrital formations (Quaternary fluvial deposits). This implies cumulated movement of several kilometers along the thrust.

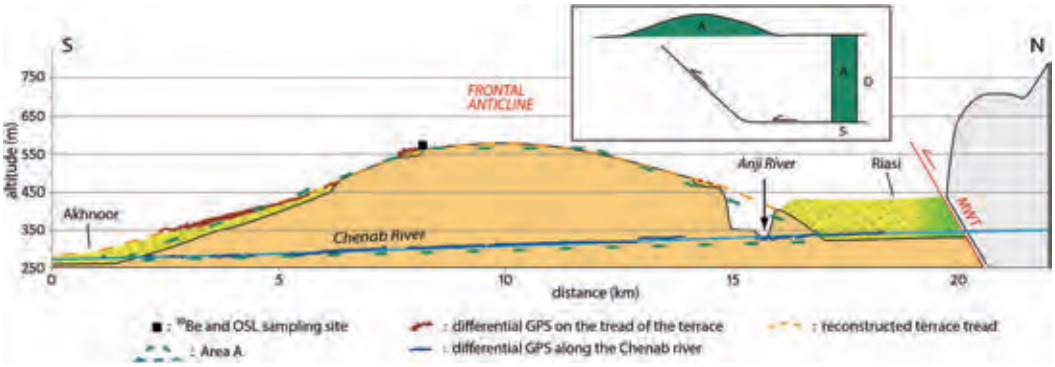

Figure 5: Cross-section of the Frontal Anticline above the Main Frontal Thrust bounded at the top by a folded strath terrace. In the box: sketch of the method used to calculate the horizontal shortening.

The Main Frontal Thrust is a blind structure that produced a ~20 km wide anticline over the last 2 Ma. The Chenab river incises the anticline perpendicularly to its axis as a response of the uplift associated with the shortening along the Main Frontal Thrust. We correlated the remnants of a fluvial strath terrace abandoned by the Chenab to quantify the shortening rate along this structure. In absence of a well-constrained geometry of the blind ramp at depth, we used the excess area method (Hossack, 1979) and estimated the area of the anticline section under the terrace en-velope (A) and the depth of the detachment plane (D) in order to determine a horizontal shortening (S) across this structure since the abandonment of the terrace (Figure 5). We calculated the area A of 2.3 ± 0.5 km2 and estimated the depth D of the flat detachment from the seismic profile of Srinivasan and Khar (1996) at 9 ± 1 km. This yields a horizontal shortening S across the anticline of 212 ± 68 m. We determined the geomorphic shortening rate on the Main Frontal Thrust dividing this value by the age of the abandonment of the terrace. A combined 10Be-OSL age of 24 ± 1 ka yields a shortening rate of 9.0 ± 3.2 mm/yr.

DISCUSSION

Shortening rates on the Medlicott-Wadia Thrust (since ~ 14ka) and the Main Frontal Thrust (since ~24ka) are 11.2 ± 3.8 mm/yr and 9.0 ± 3.2 mm/yr, respectively. Consequently, at the Late-Quaternary scale, these two thrusts are the main active tectonic structures accommodating a large part of the total India–Eurasia convergence. Part of these rates may be due to the particular geometry of the Chenab re-entrant that could locally add an oblique component (Figure 1). However, if we consider the lower bound of these rates, it is within the same range as the instantaneous rate (12.5–14 mm/yr) obtained by geodesy in Northwestern Himalaya (Schiffman et al., 2013; Jade et al., 2014; Jouanne et al., 2014).

The regional deformation pattern at the Late-Quaternary time scale is partly in-sequence (slip along the Medlicott-Wadia Thrust) and partly out-of-sequence (slip along the Main Frontal Thrust). Earthquakes associated with this deformation may be either localized on one of the two ramps or on the main common basal detachment. In the first case, seismogenic ruptures propagate along structures a few kilometers long lying between the base of the ramp and the surface, as observed for the 2005 Muzaffarabad Mw 7.6 earthquake (Yan et al., 2013). In the second case, large seismogenic ruptures may propagate over several tens of kilometers of the sub-flat detachment before reaching one or both ramps. For a total release of the slip deficit accumulated in the gap zone since 1555 at ~13mm/yr, the co-seismic slip would be ~6 m and would produce a Mw 8.2–8.3 earthquake.

This scenario is consistent with the ruptures that we observed in the paleoseismological trenches on the Medlicott-Wadia Thrust.

Acknowledgments: This study is a synthesis of the recent papers published by our team in EPSL (Vassallo et al., 2015) and in Geomorphology (Vignon et al., in press) and ongoing work in Jammu and Kashmir. This research was funded by the PAKSIS program of the ANR Catel, INSU TS-ALEAS, Université de Savoie and Labex@OSUG 2020.

References

Ambraseys, N.N., D. Jackson, (2003). A Note on Early Earthquakes in Northern India and Southern Tibet. Bangalore. *INDE. Current Science Association*. 13 p.

Ambraseys, N.N., J. Douglas, (2004). Magnitude calibration of north Indian earth-quakes. *Geophys. J. Int.*159, 165-206.

Avouac, J.P., F. Ayoub, S. Leprince, O. Konca, D.V. Helmberger, (2006). The 2005, Mw 7.6 Kashmir earthquake: sub-pixel correlation of ASTER images and seismic waveforms analysis. *Earth Planet. Sci. Lett.* 249, 514-528.

Bilham, R., (2001). Slow tilt reversal of the Lesser Himalaya between 1862 and 1992 at 78◦E, and bounds to the southeast rupture of the 1905 Kangra earthquake. *Geophys. J. Int.* 144, 713-728.

Hossack, J.R., (1979). The use of balanced cross-sections in the calculation of orogenic contraction: a review. *J. Geol. Soc.* 136, 705-711. http://dx.doi.org/10.1144/gsjgs.136.6.0705.

Hussain, A., R. Yeats, MonaLisa (2009). Geological setting of the 8 October 2005 Kashmir earthquake. *J. Seismol.* 13, 315-325.

Jade, S., M. Mukul, V.K. Gaur, K. Kumar, T.S. Shrungeshwar, G.S. Satyal, R.K. Dumka, S. Jagannathan, M.B. Ananda, P.D. Kumar, S., Banerjee, (2014). Contempo-rary deformation in the

Kashmir-Himachal, Garhwal and Kumaon Himalaya: significant insights from 1995-2008 GPS time series. *J. Geod.* 88, 539-557. http://dx.doi.org/10.1007/s00190-014-0702-3.

Jouanne, F., A. Awan, A. Madji, A. Pêcher, M. Latif, A. Kausar, J.L. Mugnier, I. Khan, N.A. Khan, (2011). Postseismic deformation in Pakistan after the 8 October 2005 earthquake: evidence of afterslip along a flat north of the Balakot-Bagh thrust. J. *Geophys. Res.* 116, B07401.

Jouanne, F., A. Awan, A. Pêcher, A. Kausar, J.L. Mugnier, I. Khan, N.A. Khan, J. Van Melle, (2014). Present-day deformation of northern Pakistan from Salt Ranges to Karakorum Ranges. *J. Geophys. Res., Solid Earth*. http://dx.doi.org/10.1002/2013JB010776.

Kaneda, H., T. Nakata, H. Tsutsumi, H. Kondo, N. Sugito, Y. Awata, S.S. Akhtar, A. Ma-jid, W. Khattak, A.A. Awan, R.S. Yeats, A. Hussain, M. Ashraf, S.G. Wesnousky, A.B. Kausar, (2008). Surface rupture of the 2005 Kashmir, Pakistan, earth-quake and its active tectonic implications. Bull. Seismol. Soc. Am. 98, 521-557.

Kumahara, Y., T. Nakata, (2006). Active Faults in the Epicentral Area of the 2005 Pak-istan Earthquake. In: *Spec. Publ., vol.41. Res. Cent. Reg. Geogr*. Hiroshima Univ. p. 54.

Mugnier, J.L., A. Gajurel, P. Huyghe, R. Jayangondaperumal, F. Jouanne, B. Upreti, (2013). Structural interpretation of the great earthquakes of the last millennium in Central Himalaya. *Earth-Sci. Rev.*127, 30-47.

Pêcher, A., L. Seeber, S. Guillot, F. Jouanne, A. Kausar, M. Latif, A. Majid, G. Mahéo, J.L. Mugnier, Y. Rolland, P. van der Beek, J. Van Melle, (2008). Stress field evolution in the northwest Himalayan syntaxis, northern Pakistan. *Tectonics*. 27, TC6005.

Schiffman, C., B.S. Bali, W. Szeliga, R. Bilham, (2013). Seismic slip deficit in the Kashmir Himalaya from GPS observations. *Geophys. Res. Lett.* 40, 5642-5645. http://dx.doi.org/10.1002/2013GL057700.

Srinivasan, S., B.M. Khar, (1996). Status of hydrocarbon exploration in Northwest Himalaya and foredeep - contribution to stratigraphy and structure. In: *Geol. Surv. India Spec. Publ*. vol.21, pp.295-405.

Yan, Y., V. Pinel, E. Trouvé, E. Pathier, J. Perrin, P. Bascou, F. Jouanne, (2013). Coseismic slip distribution of the 2005 Kashmir earthquake from SAR am-plitude image correlation and differential interferometry. *Geophys. J. Int*. http://dx.doi.org/10.1093/gji/ggs102.

Yeats, R.S., A. Kausar, T. Nakata, (2006). Conferees examine deadly 2005 Kashmir Earthquake. *Eos.* 87, 115.

Yin, A., (2006). Cenozoic tectonic evolution of the Himalayan orogen as constrained by along-strike variation of structural geometry, exhumation history, and foreland sedimentation. *Earth Sci. Rev.* 76, 1-131.

Wallace, K., R. Bilham, F. Blume, V.K. Gaur, V. Gahalaut, (2005). Surface de-formation in the region of the 1905 Kangra Mw =7.8 earthquake in the period 1846–2001. *Geophys. Res. Lett*. 32, L15307. http://dx.doi.org/10.1029/2005GL022906.

INQUA Focus Group on Paleoseismology and Active Tectonics

Evidence of seismogenic activity of Perales fault in the Ixtlahuaca basin, Mexico

Velázquez-Bucio, M.M. (1), Benente, L. (2), Garduño-Monroy, V.H. (3), Michetti, A.M. (4), Groppelli, G. (5)

(1) CIGA, Universidad Nacional Autónoma de México. Antigua Carretera a Pátzcuaro No. 8701, Col. Ex-Hacienda de San José de la Huerta. 58190. Morelia, Michoacán, Mexico. Email: magda_vb@yahoo.com.mx
(2) Piedra-consulting / enterprise services. http://www.piedra-consulting.com/
(3) Instituto de Investigaciones en Ciencias de la Tierra, Edificio U. Ciudad Universitaria. Universidad Michoacana de San Nicolás de Hidalgo. 58060, Mexico
(4) Dipartimento di Scienza e Alta Tecnologia, Università dell'Insubria, Via Valleggio 11, 22100 Como, Italy
(5) C.N.R. Istituto per la Dinamica dei Processi Ambientali, sez. di Milano, Via Mangiagalli 34, 20133 Milano, Italy

Abstract: *The study area is located in central Mexico, in the Trans-Mexican Volcanic Belt (TMVB) one of the areas with highest geological activity. The structural framework that controls the kinematics of the studied area is linked to the Acambay graben, characterized by structures mainly oriented E-W, where the November 19, 1912, Ms 6.9 earthquake took place. The lacustrine and fluvial sequences of Ixtlahuaca basin are currently affected by faults and uplift of Perales fault footwall, which has migrated into the basin during the Late Quaternary. The Ixtlahuaca-basin has been considered as aseismic zone, however, soft sediment deformations and paleoliquefaction features are clearly genetically related with synsedimentary faulting of the lake basin floor. The identified structures and the application of the ESI 2007 scale (Michetti et al, 2007) suggests a seismically induced origin; the deformational structures are similar and the intensity in the two areas is from VII to IX.*

Key words: *Perales fault, Ixtlahuaca basin, Acambay graben, soft sediment deformation, ESI 2007 scale.*

INTRODUCTION

The center of Mexico, one of the most populated areas of the country, is characterized by large E-W trending tectonic basins, controlled by a set of Quaternary normal faults. Ixtlahuaca and Acambay are two of the largest intra-arc basins of such region. Within the Acambay basin, recent lake sediments (Pleistocene to Present) are highly deformed because of faults and/or deformation structures (Garduño and Israde, 2006; Langridge et al., 2000, 2013; Suter et al, 2001; Rodriguez-Pascua et al. 2010), related to Quaternary and historical surface ruptures, and particularly, to the November 19th, 1912 earthquake. Conversely, the Ixtlahuaca basin 51 km South of Acambay graben, and 69 km West of the Mexico City, is controlled by the Quaternary evolution of Perales fault (fig. 1), and does not report any historical seismic record, so it has been considered as aseismic zone. However, the application of the ESI 2007 scale (Michetti et al, 2007) to deformational structures generated by the paleo-seismic events in physical environment of Tierras Blancas-San Bartolo Lanzados (Filonzi, 2005; Rodriguez-Pascua et al., 2010; 2012) and San Pedro El Alto basins (Velázquez, in prep.), within the graben, and their comparison with those found in the Ixtlahuaca basin (Benente, 2005), shows that ancient earthquakes similar to those produced by the main faults of the Acambay graben, occurred also in the Ixtlahuaca area (Velázquez-Bucio et al., 2012).
The aim of this work is the analysis of deformation structures in the stratigraphic sequence of Ixtlahuaca basin, as indicators of seismic activity of the Perales fault, which is important to consider for the seismic hazard assessment in the central Mexico.

STUDY AREA

The Ixtlahuaca basin is located between 19°30' to 19°34'N and 99°50' to 99°44'W at 2540 to 2600 m a.s.l (fig. 1). The lacustrine and fluvial sequence has settled during the Middle Pleistocene and is mainly constituted of terrigenous and biogenic sediments interbedded with epiclastic and pyroclastic deposits that indicate a synchronous intense volcanic activity. The sequence is currently affected by faults and uplift of the footwall of the NNW-SSE Perales Fault, which during the Late Quaternary has migrated into the basin.
The length of the Perales fault is about 45 km; the structure controlled the subsidence enabling the sedimentation of the lacustrine facies and subsequently, controlled the uplift and the closure of the basin; toward inside the basin, the faults are intersected by E-W structures developed during the lifting.
According to Israde-Alcántara and Garduño-Monroy, (1999) it is possible to subdivide the history of the Ixtlahuaca in three evolutionary phases (Israde-Alcántara, Garduño-Monroy, 1999). The first two represent maximum depth phases allowing terrigenous alluvial and deep-basin (diatomite) sediments deposition. The third phase belongs to the basin closure and its faulting and uplift to the current level and the start of an intense erosional phase.
The stratigraphic sequence of the Ixtlahuaca de Rayon basin is made of terrigenous and biogenic facies interbedded with pyroclastic and epiclastic deposits, where a series of deformational structures, (e.g. liquefaction, plastic and brittle sediments deformation) have been registered.

The basin consists of lacustrine and alluvial-lacustrine sediments deposited between Miocene and Quaternary.

Miocene – Lower Pleistocene: extensional tectonics determined the normal fault systems activation with E-W and NW-SE orientation.

Pleistocene: continuous active extensional tectonics with NE-SW fault system activation, set up of the subsidence of the basin allowing at the same time the deposition of deep basin sediments.

Late Pleistocene - Holocene: the uplift of sedimentary successions caused the closure of the basin and intense erosion, asserted by the presence of erosional channels also inside the diatomite. Northward migration of the Perales Fault causes the emergence of the footwall sector of the basin and the stratigraphic succession ends with deposits of paleosols, lahars and debris flows.

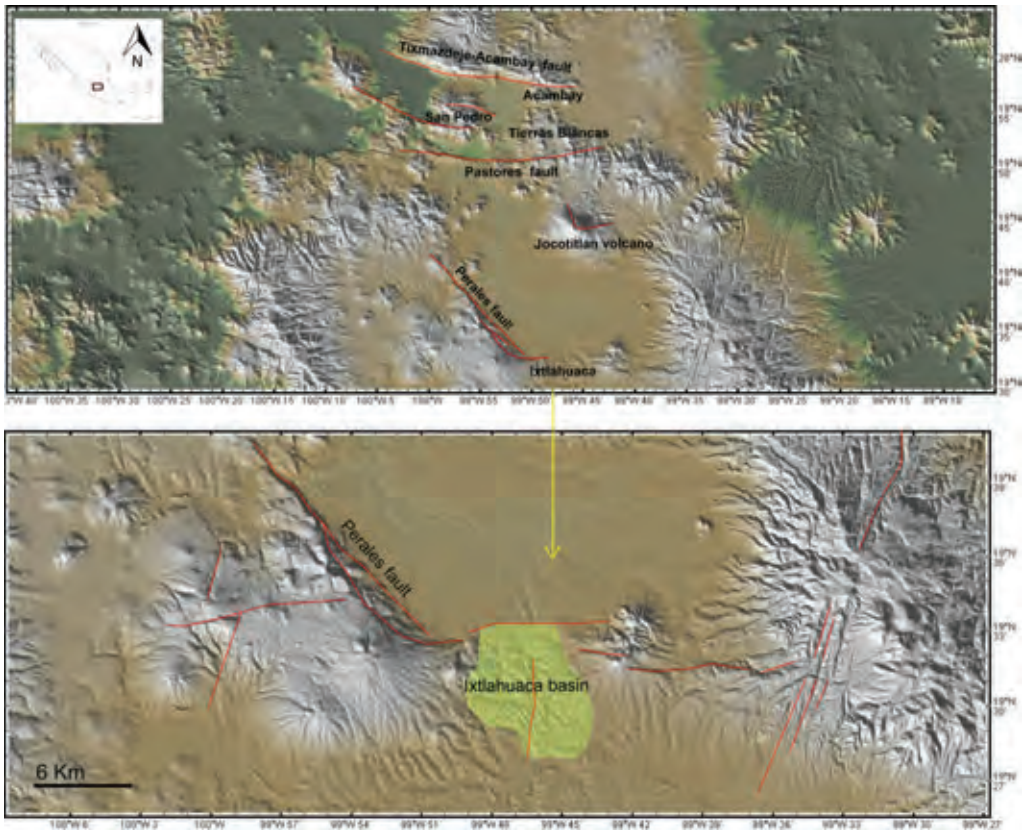

Figure 1: Study area; Ixtlahuaca basin and the Perales fault linked to the Acambay graben. In green the Ixtlahuaca basin, where deformation structures of five earthquakes were identified.

The basin evolution has been affected by lacustrine transgression and regression events related to the activity of the faults present in the area. We can recognize three members representing different depositional environments:

El Salto member: characterized by pyroclasts (ash and pumice), silt and sand levels.

Río Lerma member: located in the central part of the study area and characterized by the presence of layers of up to 16 m of massive diatomite.

El Junco member: characterized by sand and silt-sandy deposits, with sedimentary structures. Finally at the top there are recent sediments (debris flow, coverage tepetates, silts and soils) covering in unconformity the sequence: deposited on the uplifted and eroded succession.

SEISMIC EVENTS AND COSEISMIC DEFORMATIONAL STRUCTURES

Considering the stratigraphic chronology, it is possible to correlate stratigraphically the seismic events with the three stages of evolution of the basin. The three members constituting the formation belong to different independent facies, besides the paleoseismic events identified in each member cannot be summed but, using the megaslump layer as a marker horizon, Benente (2005) concluded that there have been at least 5 events, two earthquakes preceding the event creating the slump and two later events:

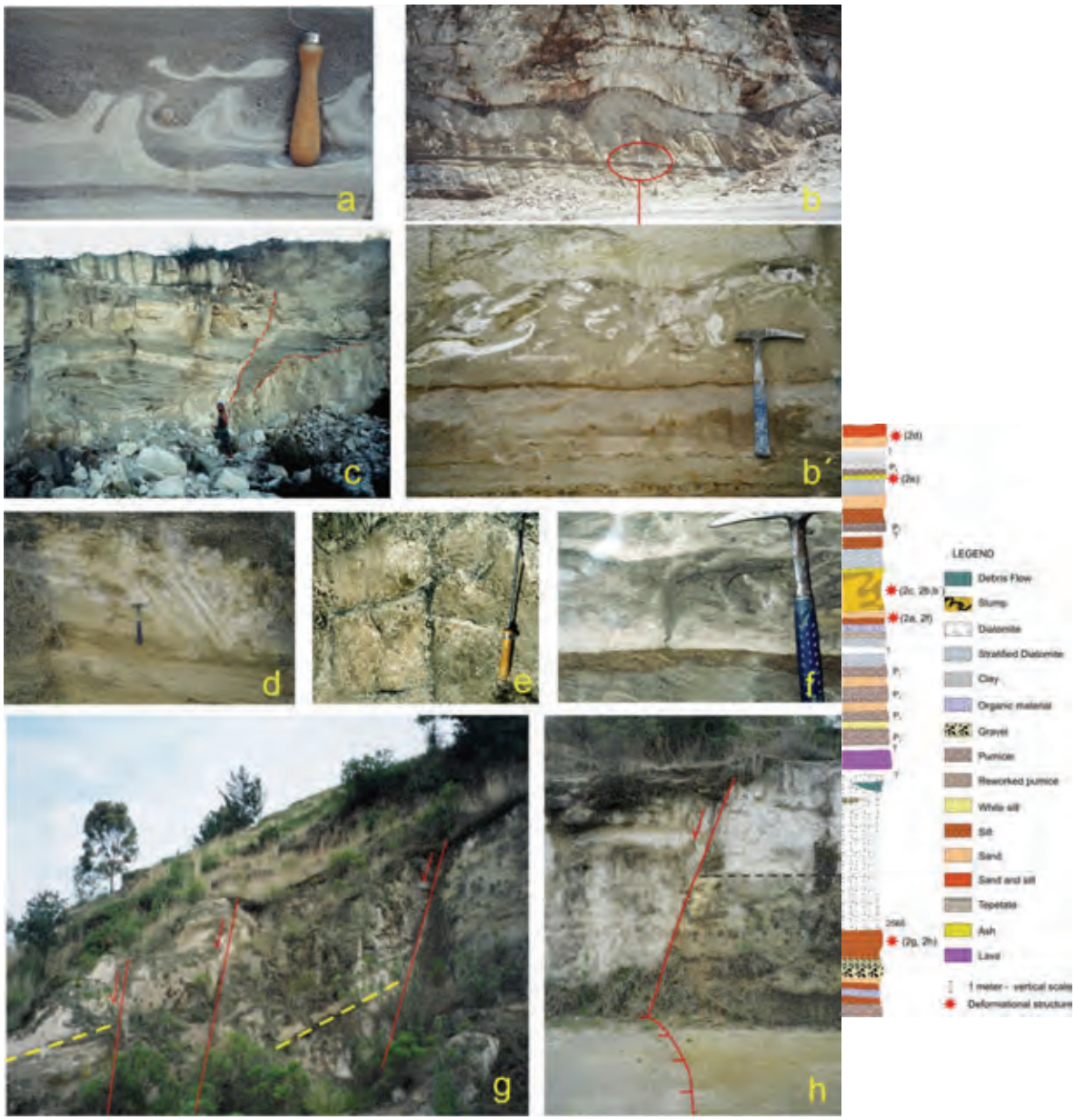

Figure 2: Structures identified in the Ixtlahuaca basin: a) flame structure in silt-sandy sediment, (ESI2007-VII); b,b') Seismically-induced megaslump, consisting of sand and silt, (ESI2007-VIII); c) Isoclinal fold within a diatomite horizon, affected by synsedimentary faulting (ESI2007-IX);d) Brittle collapse of a level of silts and sands within the sands, Member El Salto; e) Dykes cross inside a sandy sediment, (ESI2007-VII); f) Structures to collapse or load, alternating of silty sand and silty sand gray white (ESI2007-VII);g), h) Surficial faults, NW-SE orientation (ESI2007-VIII-IX). To the right, stratigraphic column with earthquakes.

Earthquake 1

Faults constitute a system of normal faults trending NW-SE bordering the basin east (Figure 2g and h). The length of the faults is about 1.5 km and the scarp less than 1 m. The earthquake is pointed out by a stratigraphic unconformity. A sudden change in the layers attitude could be explained with a fast tilting, correlated to a strong earthquake.

Earthquake 2

Flame structures in a succession of dark sands and white silts with thicknesses between 1 to 5 cm (Fig. 2 a). It can be explained by assuming that at the instant when the earthquake occurred, the sediments had a different susceptibility to liquefaction and the parameter that has controlled this change was probably a different level of saturation of alternating silty-sandy.

Collapse structures are present in littoral facies as well as in the central and western part of the basin. They consist of alternation of white and gray silty sands. Figure 2 f, represents a load structure characterized by fracturing of white sands and a collapse of the overlying gray silty sands. The white sand bed tends to rise, because the water present in the pores has been brought under pressure during the earthquake.

Eartquake 3

Faults intersect most of study area; some of them are associated to seismic events and represents the brittle response of sediments, in addition to the liquefaction and deformation structures in ductile material. Inside the basin, there are fault systems that make horst and graben morphology without exceed 30 centimeters and affecting the same levels of collapse structures identified in the eastern sector (littoral).

Fold by slip seismically induced is located within a deposit of 10 m diatomite not stratified, belonging to the member Rio Lerma (Fig.2 c); is a fold isoclinal of sandy sediment, plastically deformed during the sliding induced by an earthquake. The sliding surface has an inclination of about 5°. The earthquake has caused slippage, by decoupling the sands from diatomite.

Marker bed - slump is present in the whole area (fig. 2 b,b', cuts the three members of Ixtlahuaca formation, constituted by ash, silt, clay and diatomite layers. It has a thickness between 3-5 m, and their top and bottom comprises sediments undeformed. Possibly this is the most important seismic event and contemporary to megaslump identified within sediments of Acambay graben. The detailed observation of the slump allows to identify elements that may characterize a greater development of structures according to the intensity of the earthquake; in this case the presence of structures of white-pink silt collapsed inside the silty-sandy sediment indicates a complete liquefaction (fig. 2 b').

Earthquake 4

Cross dikes are present in the western sector on an ash layer. They appear as cracks in the ash level with injection of silty material (fig. 2e). Developed within a sediment consisting of sands at the top, and gray silts at the bottom; the thickness of the layers is about 30 cm for the sands and 50-60 cm to silts gray. The dikes are of two different sizes: the larger, up to 2 cm, orthogonal to each other, while the thinner (less than 1 cm), grow chaotically within the sediment.

Earthquake 5

Fragile collapse structures are on the top of the member El Salto and affect a thickness of about 1 m of sediments; at the bottom of the stratigraphic sequence lies a brown sand layer and at the top there is an alternation of white silt and gray sand (Fig. 2d).

INTERPRETATION

The areal diffusion of deformational structures identified near Ixtlahuaca (Fig. 2) is basinwide, at precise stratigraphic levels between undeformed depositional horizons, and is similar to the seismically-induced structures described in the literature. Soft sediment deformations and paleoliquefaction features are genetically related with synsedimentary faulting of the lake basin floor. For these reasons, it has been suggested that their origin is due to ancient earthquakes. The observation of surface faulting within the lake basin also indicates that at least some of these paleoearthquakes have been generated by a local seismic source.

The stratigraphic analysis allowed identifying facies related with the events. However, only an earthquake is certainly correlated throughout the area and it is the slump, which has affected the whole study area. Such structure could be possibly contemporary to the slump identified into Acambay graben, suggesting an earthquake with a wide regional spread ($M \geq 6$). In any case, the paleoseismic structures are evidence of seismic events of magnitudes great than 5. The comparison of published data from the Acambay 1912 earthquake with new analysis of paleoseismic evidence on the same graben (San Bartolo Lanzados y San Pedro El Alto), and the identified structures in the Ixtlahuaca basin, using the ESI 2007 scale, suggest for this a) a seismically induced origin, b) a local seismic source, which represents a significant seismic hazard in the central part of Mexico, and must be considered in the assessment of this kind of natural events to which the population is exposed.

References

Benente, L., (2005). *Analisi stratigrafica e strutturale del bacino lacustre di Ixtlahuaca de Rayon-Arco Vulcanico Messicano, e implicazioni paleosismologiche*. Corso di Laurea in Scienze Geologiche. Facoltà di Scienze Matematiche, Fisiche e Naturali. Università degli Studi di Milano. Italia. pp.181

Filonzi, S., (2005). *Analisi paleosismologica del bacino lacustre di San Bartolo Lanzados - Arco Vulcanico Messicano*. Università degli Studi di Milano. Facoltà di Scienze MM.FF.NN. Italia.

Garduño-Monroy, V.H., I. Israde-Alcántara, (2006). *Field guide for the excursion of Central Mexico basins from Acambay to Patzcuaro Basins*. D.pto de Geologia y Mineralogía. IIM–UMSNH. Mexico. 1-10.

Israde-Alcántara, I., (1995). *Bacini Lacustri dal Settore Centrale dall'arco vulcanico messicano. Stratigrafia ed evoluzione vulcanotettonica basata sulle diatomee*. Università degli Studi di Milano, Tesis doctoral, Italia: 254

Langridge, R.M., R. J. Weldon II, J.C. Moya, G. Suárez, (2000). Paleoseismology of the 1912 Acambay earthquake and the Acambay-Tixmadejé fault, Trans-Mexican Volcanic Belt. *Journal of Geophysical Research*. Vol. 105. No. B2: 3019-3037.

Langridge, R.M., M. Persaud, F.R. Zúñiga, G.J. Aguirre Diaz, P. Villamor, P. Lacan (2013). Preliminary paleoseismic results from the Pastores fault and its role in the seismic hazard of the Acambay graben, Trans-Mexican Volcanic Belt, Mexico. *Revista Mexicana de Ciencias Geológicas. v. 30, núm. 3, 463-481*

Michetti, A.M., E. Esposito, L. Guerrieri, S. Porfido, L. Serva, R. Tatevossian, E. Vittori, F. Audemard, T. Azuma, J. Clague, V. Comerci, A. Gürpinar, J. McCalpin, B. Mohammadioun, N.A. Mörner, Y. Ota, E. Roghozin, 2007. *Environmental Seismic Intensity Scale 2007 - ESI 2007. Memorie Descrittive della Carta Geologica d'Italia*. 74, 7-54, Servizio Geologico d'Italia. Dipartimento Difesa del Suolo. APAT. Roma. Italy.

Rodríguez-Pascua, M.A., V.H. Garduño-Monroy, I. Israde-Alcántara, R. Pérez-Lopéz, (2010). Estimation of the paleoepicentral area from the spatial gradient of deformation

in lacustrine seismites (Tierras Blancas Basin, Mexico). *Quaternary International.* 219 (1): 66-78.

Rodríguez-Pascua, M.A., V.H. Garduño-Monroy, R. Pérez-Lopéz, M.A. Perucha-Atienza, I. Israde-Alcantara, (2012). The Acambay Earthquake of 1912, revisited 100 Years After. *3rd INQUA-IGCP-567 International Workshop on Active Tectonics, Paleoseismology and Archaeoseismology*. Morelia. Mexico (2012), Abstract Volume: 157-159.

Suter, M., M. López Martínez, O. Quintero Legorreta, M. Carrillo Martínez, (2001). Quaternary intra-arc in the central Trans-Mexican volcanic belt. *Bulletin, Geological Society of America*. 113, 693-703.

Velázquez Bucio, M.M., A.M. Michetti, L. Benente, G. Gropelli, V.H. Garduño Monroy, S. Filonzi, M.A. Rodríguez Pascua, R. Pérez Lopéz, K. Chunga, (2013). *Proceedings of the 4th International INQUA Meeting on Paleoseismology, Active Tectonics and Archeoseismology (PATA)*. Germany. 285-289.

Velázquez Bucio, M.M., *Estratigrafía cosísmica en secuencias lacustres del Holoceno en el graben de Acambay, Estado de México y evaluación del peligro sísmico*. Tesis de doctorado en Geografía. CIGA, UNAM. México. (In prep.).

INQUA Focus Group on Paleoseismology and Active Tectonics

Historical sources and Geology: earthquakes documented in the memoirs of Giovanni Maria Mastai and Francesco Pesaresi (Senigallia, central Italy, AD 1727 – 1760)

Venturati, A.

Centro di Ricerca di Micropaleontologia Ambientale, 61122 Pesaro, Italy. Email: crma_ps@libero.it

Abstract: *The motivation for this research was the update and enrichment of the Parametric Catalogue of Italian Earthquakes (CPTI11) with two authoritative primary historical sources. The two historical chronicles were written and compiled by Giovanni Maria Mastai and Francesco Pesaresi from AD 1727 to 1760. The authors narrate with numerous details, several historical events of political-economic character of the town of Senigallia. Particular emphasis is placed on natural phenomena, as remarkable environmental perturbations or earthquakes and seismic events, and their effects that struck the inhabitants and the town of Senigallia and surrounding areas during the eighteenth-century.*

Key words: *Historical source, earthquake, Parametric Catalogue of Italian Earthquakes, Senigallia, central Italy.*

INTRODUCTION

Knowledge of the past is a determining factor for identifying the geographical areas characterized by a high seismic risk, their evolution over time and therefore be able to build, if possible, adequate defences.
One of the tools used by the scientific community is the "historical source", otherwise any written document that contains information about a specific seismic event and allows us, to add a step to knowledge on the effects that this event caused.
The aim of this research was to bring to the attention of the Italian scientific community, two authoritative primary historical sources identified as chronicles, written during AD 1727 and 1760 by Giovanni Maria Mastai and Francesco Pesaresi that covered the eighteenth-century of the town of Senigallia (central Italy).
The authors were contemporaries and fellow-citizens chroniclers.
The authors describe political events, economic life of the town, action of armies, development of epidemics, climate trends as extreme drought periods or very rainy or snowy periods, major flooding of the rivers.
The chronicles report with special emphasis on natural phenomena as earthquakes and seismic events that struck the inhabitants and the town of Senigallia and surrounding areas during the eighteenth-century.
These primary historical sources could be used for an enrichment and updating the Parametric Catalogue of Italian Earthquakes (Rovida et al., 2011).

DISCUSSION

In this research are reported every single earthquake or seismic event mentioned and documented in the chronicles of Giovanni Maria Mastai and Francesco Pesaresi from AD 1727 to 1760.

The distinguished chroniclers, belonging to two noble families of Senigallia, showed mostly attentive not only to the political events of their city, but also the weather, famine, epidemics and natural phenomena in general.
Even with different ability, these historical eyewitnesses have fortunately passed valuable information about earthquakes recorded in the town of Senigallia and surrounding areas.
The chronicles of Mastai G.M. were recently published and edited by Anselmi (1987, 1989), the chronicles of Pesaresi F. were instead treated by Morici (2013).
However, the studied historical sources do not define with precision the magnitude and how was devastating each seismic event for the town of Senigallia.
The chronicles reported that some earthquakes were often associated with rumbles with epicenter located in the Adriatic Sea, close to the city of Senigallia.
As described by Mastai G.M. in reference to the seismic event of the 20 june 1744:
"*Pareva che il tremor della terra, cioè de teremoti fosse cessato, conforme infatti si era da giorni dieci non si era inteso, almeno da molti generalmente, quando ad 20 detto giugno di sabato ad ore 22 ¾ incirca si fe ben risentire con precedere imprima per la via del mare verso levante, come un tuono soteraneo, come ogni volta ordinariamente, che si faceva sentire il teremoto detto tuono precedeva*".

Here is reported the list of single seismic event recorded in the town of Senigallia, as mentioned and documented in the chronicles of Giovanni Maria Mastai and Francesco Pesaresi from AD 1727 to 1760:
1727, 12, 14 - Event recorded in the chronicles of Pesaresi F., also reported in CPTI04 and CPTI11.
1728, 01, 01 - chronicles of Pesaresi F.
1728, 05, 14 - chronicles of Pesaresi F.
1741, 04, 24 - chronicles of Mastai G.M., also reported in CPTI04 and CPTI11.
1744, 05, 27 - chronicles of Mastai G.M. and Pesaresi F., also recorded in CPTI04 and CPTI11.

1744, 05, 28 - chronicles of Pesaresi F.
1744, 05, 29 - chronicles of Pesaresi F.
1744, 05, 30 - chronicles of Pesaresi F.
1744, 05, 31 - chronicles of Pesaresi F.
1744, 06, 03 - chronicles of Mastai G.M.
1744, 06, 09 - chronicles of Pesaresi F.
1744, 06, 20 - chronicles of Mastai G.M. and Pesaresi F.
1744, 06, 21 - chronicles of Mastai G.M. and Pesaresi F.
1744, 06, 24 - chronicles of Mastai G.M. and Pesaresi F.
1744, 06, 25 - chronicles of Mastai G.M. and Pesaresi F.
1744, 06, 28 - chronicles of Mastai G.M. and Pesaresi F.
1744, 06, 29 - chronicles of Mastai G.M. and Pesaresi F.
1744, 07, 18 - chronicles of Mastai G.M.
1744, 08, 15 - chronicles of Mastai G.M. and Pesaresi F.
1745, 01, 09 - chronicles of Mastai G.M. and Pesaresi F.
1745, 07, 06 - chronicles of Mastai G.M.
1745, 08, 22 - chronicles of Mastai G.M.
1751, 07, 27 - chronicles of Pesaresi F., also reported in CPTI04 and CPTI11.
1755, 06, 20 - chronicles of Pesaresi F.
1756, 01, 05 - chronicles of Mastai G.M.
1756, 01, 20 - chronicles of Pesaresi F.
1756, 10, 06 - chronicles of Pesaresi F., also reported in Camassi et al., (2011).
1756, 11, 20 - chronicles of Pesaresi F.
1760, 01, 12 - chronicles of Pesaresi F.

Acknowledgements: This is publication no. 24 of the Centro di Ricerca di Micropaleontologia Ambientale.

References

Anselmi, S., (1987). *Soldati, epidemie, edilizia nella Senigallia del Settecento, 1739-1746*. Comune di Senigallia Editore. 125 p.

Anselmi, S., (1989). *L'ampliazione di Senigallia, 1747-1762*. Comune di Senigallia Editore. 145 p.

Camassi, R., V. Castelli, D. Molin, F. Bernardini, C.H. Caracciolo, E. Ercolani & L. Postpischl, (2011). Materiali per un catalogo dei terremoti italiani: eventi sconosciuti, rivalutati o riscoperti. *Quaderni di Geofisica*. 96, 391 p.

Gruppo di lavoro CPTI, (2004). *Catalogo Parametrico dei Terremoti Italiani, versione 2004 (CPTI04)*. INGV, Bologna, http://emidius.mi.ingv.it/CPTI04//

Morici, R., (2013). *Il clima raccontato da un cronista senigalliese del Settecento*. Biblioteca Comunale Antonelliana di Senigallia. 69 p.

Rovida, A., R. Camassi, P. Gasperini & M. Stucchi (2011). *CPTI11, the 2011 version of the Parametric Catalogue of Italian Earthquakes*. Milano, Bologna, http://emidius.mi.ingv.it/CPTI, doi: 10.6092/INGV.IT-CPTI11

INQUA Focus Group on Paleoseismology and Active Tectonics

paleoseismicity.org

Shallow subsurface imaging of the Piano di Pezza active normal fault (central Italy) using high-resolution refraction and electrical resistivity tomography coupled with time-domain electromagnetic data

Villani, F. (1), Tulliani, V. (2), Sapia, V. (3), Fierro, E. (4), Civico, R. (3), Baccheschi, P. (1), Di Giulio, G. (1), Vassallo, M. (1), Pantosti, D. (3)

(1) Istituto Nazionale di Geofisica e Vulcanologia, via dell'Arcivescovado 8, 67100 L'Aquila, Italy. Email: fabio.villani@ingv.it
(2) Anglia Cathodic Protection Services Ltd, Meadow View Industrial Estate, Reach Road, Burwell, Cambridgeshire, CB25 0GH, U.K.
(3) Istituto Nazionale di Geofisica e Vulcanologia, via di Vigna Murata 605, 00143 Roma, Italy
(4) Dipartimento di Scienze e Tecnologie, Università degli Studi di Camerino, Via Gentile III da Varano, 62032 Camerino, Italy

Abstract: *The Piano di Pezza fault (PPF) is the north-westernmost segment of the >20 km long Ovindoli-Pezza active normal fault-system (central Italy). Although existing paleoseismic data document high vertical Holocene slip rates (~1 mm/yr) and a remarkable seismogenic potential of this fault, its subsurface setting and Pleistocene cumulative displacement are still unknown. We investigated the shallow subsurface of a key section of the PPF using seismic and electrical resistivity tomography coupled with time-domain electromagnetic measurements (TDEM). We provide 2-D Vp and resistivity images showing details of the fault structure and the geometry of the shallow basin infill down to 35-40 m depth. We can estimate the dip and the Holocene vertical displacement of the master fault. TDEM measurements in the fault hangingwall indicate that the pre-Quaternary carbonate basement may be found at ~90-100 m depth.*

Key words: *Central Apennines, refraction tomography, electrical resistivity tomography, time-domain electromagnetic measurement, active fault.*

INTRODUCTION

The inner sector of the central Apennines of Italy is characterized by a complex network of Pliocene-Quaternary normal faults (Cavinato & de Celles, 1999; Ghisetti & Vezzani, 1999) that originated several intramontane continental basins (Bosi et al., 2003; Giaccio et al., 2012; Pucci et al., 2014). Under the current NE-directed extensional stress regime, the high crustal seismicity rate is mainly released by normal-faulting earthquakes (Chiarabba et al., 2005; Chiaraluce, 2012 and references). Paleoseismic analyses have unravelled the late Holocene slip-history of many active normal faults in this sector of the chain (Galli et al., 2008 and reference therein; Cinti et al., 2011). Notwithstanding the wealth of geological data constraining the recent evolution of most normal faults, only in few cases detailed subsurface information is available to provide a proper structural model of the basins they originated. Shallow geophysical investigation of active faults may extend the limited investigation depth typical of paleoseismic trenching, moreover it can yield valuable information on long-term fault displacement and unravel minor structures (e.g.: Villani et al., 2014).

As a case-study, we selected the Piano di Pezza fault (hereinafter PPF, Figure 1). The PPF is the north-westernmost segment of the >20 km long active Ovindoli-Pezza normal fault system, and according to paleoseismic data it exhibits one of the highest Holocene vertical slip rates in the Apennines (~1 mm/yr; Pantosti et al., 1996), with large inferred vertical displacement per event (> 2 m). This fault bounds to the north a 5 km long continental basin (Piano di Pezza; Figure 1) filled with glacial, lacustrine and fluvial deposits, and its footwall exposes Mesozoic-Tertiary marine limestones. The subsurface structure and infilling thickness of this basin are unknown, nor the shallow geometry of the bounding fault is well constrained.

Figure 1: geological sketch of the Piano di Pezza basin. The blue lines indicate normal faults, the red lines thrusts.

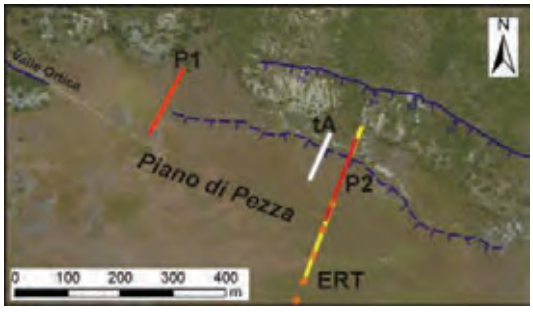

Figure 2: close up view of the survey area showing seismic, electrical resitivity profiles and TDEM measure points (orange); the PPF exhibits two splays: we investigated the shallow subsurface of the lower one, where it displaces late Holocene alluvial fans; tA is trench A after Pantosti et al., 1996.

With the aim of extending information from previous paleoseismic analyses and very shallow GPR investigations (Jewell & Bristow, 2006), we performed an integrated geophysical survey focusing a key section of the PPF (Figure 2). We acquired 2 high-resolution seismic profiles, 1 electrical resistivity profile and 7 time-domain electromagnetic soundings (TDEM) crossing the fault where it displaces some small late Holocene alluvial fans, originating a ~5 m high fault scarp.
We try to infer the subsurface fault geometry and recover the depth of the pre-Quaternary basement.

METHODS AND DATA ACQUISITION

Traveltime tomography proved successful in imaging complex media, such as fault zones (Morey & Schuster, 1999; Sheley et al., 2003), so we conceived our seismic investigations to get tomographic images of the Piano di Pezza fault at depth. The 2 seismic profiles (named P1 and P2) are 142 m long each, and they were acquired using a 72 vertical geophones array (40 Hz eigenfrequency) with 2 m spacing and a sledgehammer as energy source. We handpicked ~20,000 first-arrival traveltimes that were input to a non-linear tomographic code to produce 2-D Vp models of the shallow subsurface (details of the method in: Improta et al., 2002).
Electrical resistivity tomography (ERT) is a powerful tool to investigate shallow faults and complex structures as well (Griffits & Barker, 1993; Storz et al., 2000). We acquired 1 ERT profile paralleling seismic line P2. We deployed a 64 electrodes and 315 m long array with both Wenner-Schlumberger and dipole-dipole configurations of quadrupoles. The apparent resistivity data were inverted through a linearized least-squares algorithm to obtain true resistivity sections (Constable *et al.* 1987; Loke & Dahlin 2002).

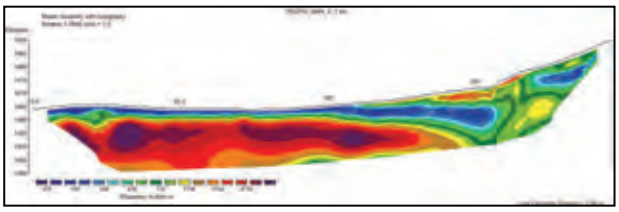

Figure 3: shallow electrical resistivity model across the Piano di Pezza fault.

In order to infer the pre-Quaternary basement depth in the hangingwall of the PPF, we also performed 5 time domain electromagnetic measurements (TDEM). The method is based on the induction of a time-varying secondary magnetic field produced by decay current in the ground. This secondary magnetic field is measured by an induction receiver coil generally placed inside of a transmitter loop. As the current diffuses deeper into the ground (at later time), the signal measurements provide information on the conductivity of the lower layers. Our data were collected using a high frequency 1D receiver coil, placed at the centre and outside a transmitter square loop of 50 m size. We acquired very early time gates data starting from ~ 9 μs (after current turn off) up to 800 μs using a Geonics 47 transmitter. Random electromagnetic noise were also collected and checked against measured voltage data in order to discharge biased late time gates before data inversion. Data from field measurements were processed and inverted using SiTYEM\SEMDI software in order to obtain 1D resistivity models of the subsoil (Hydrogeophysics-Group, 2001)

PRELIMINARY RESULTS AND DISCUSSION

We show some preliminary results of our integrated geophysical surveys. The ERT model (Figure 3) with dipole-dipole configuration across the fault scarp clearly depicts the ~50° SW-dipping fault zone involving alluvial fan deposits with resistivity <500 Ωm and their concurrent thickening in the hangingwall. Moreover, the top-surface of the underlying high-resistivity body (>1000 Ωm) shows an evident dip towards the fault, suggesting back-tilting due to fault activity. We interpret the shallower layers as Holocene alluvial fan gravelly and sandy deposits (recovered in the trenches by Pantosti et al., 1996) laying over a > 20 thick Last Glacial Maximum till (~21-18 ka; Cassoli et al., 1986; Giraudi, 1989). Vp tomograms suggest this alluvial fan is affected by > 10 m vertical displacement (Figure 4). They also help defining the fault-zone down to 35-40 m depth suggesting it has a ~50° dip.

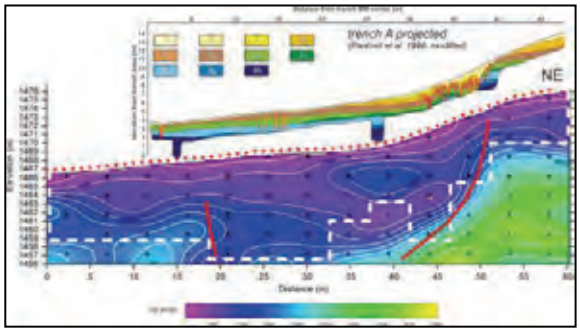

Figure 4: detail of the Vp tomogram of seismic line P2 across the PPF compared with trench A (after Pantosti et al., 1996).

TDEM data inversion yielded 1-D vertical resistivity models (Fig. 5): they indicate that ~200 m far from the surface fault trace the pre-Quaternary carbonate basement is 90-100 m deep, thus giving a robust constraint to the evaluation of the cumulative offset of the PPF (~150 m). Moreover, for the uppermost part of the subsoil, TDEM and ERT model significantly agree in terms of depth and thicknesses of the shallower resistivity layers.

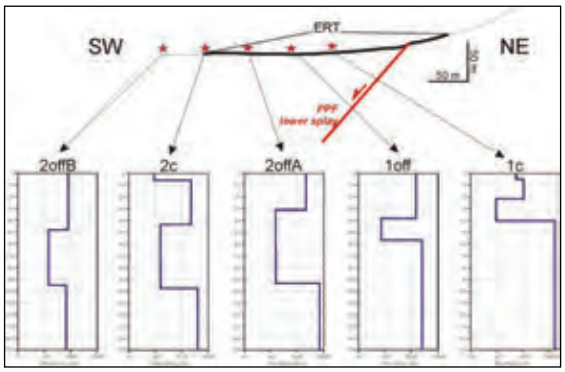

Figure 5: 1-D resistivity models obtained through inversion of TDEM data (position of soundings along the ERT profile is idicated by red stars). A deep resistive layer (>5000 Ωm), interpreted as the carbonate basement, is evidenced at 90-100 m depth (beneath soundings 2offB, 2c and 2offA) in the hangingwall of the PPF. Data from soundings 1off and 1c are less reliable in the deeper part due to strong 3D effects.

Our geophysical data yield for the first time valuable information on the subsurface setting of an important active normal fault exhibiting one of the highest Holocene slip rates in the central Apennines. These data are crucial to understand the middle- to long-term behaviour of this fault, its overall displacement and possibly its inception age.

Acknowledgements: This study was performed in the framework of the FIRB Abruzzo project, "High-resolution analyses for assessing the seismic hazard and risk of the areas affected by the 6 April 2009 earthquake" (http://progettoabruzzo.rm.ingv.it/en; F. Villani, V. Sapia & R. Civico funding code: RBAP10ZC8K_005; P. Baccheschi funding code: RBAP10ZC8K_003; G. Di Giulio & M. Vassallo funding code: RBAP10ZC8K_007).

References

Bedrosian, P.A., M.K. Burgess & T. Nishikawa, (2013). Faulting and groundwater in a desert environment: constraining hydrogeology using time-domain electromagnetic data. *Near Surface Geophysics*. 11, (5), 545-555.

Bosi, C., F. Galadini, B. Giaccio, P. Messina, & A. Sposato, (2003). Plio-Quaternary continental deposits in the Latium-Abruzzi Apennines: the correlation of geological events across different intermontane basins. *Il Quaternario*. 16 (1Bis), 55-76.

Cassoli, A., L. Corda, C. Lodoli, A. Malatesta, M.V. Molaroni, & A. Ruggeri, (1986). Il glacialismo quaternario del gruppo Velino-Ocre-Sirente. *Memorie Società Geologica Italiana*. 35, 855-867.

Cavinato, G.P., & P.G. De Celles, (1999). Extensional basins in the tectonically bimodal central Apennines fold-thrust bel, Italy: response to corner flow above a subducting slab in retrograde motion. *Geology*. 27, 955-958.

Chiarabba, C., L. Jovane & R. Di Stefano, (2005). A new view of Italian seismicity using 20 years of instrumental recordings. *Tectonophysics*. 305, 251-268.

Chiaraluce, L., (2012). Unraveling the complexity of Apenninic extensional fault systems: A review of the 2009 L'Aquila earthquake (Central Apennines, Italy). *Journal of Structural Geology*. 42, 2-18.

Cinti, F.R., D. Pantosti, P.M. De Martini, S. Pucci, R. Civico, S. Pierdominici, L. Cucci, C.A. Brunori, S. Pinzi, & A. Patera, (2011). Evidence for surface faulting events along the Paganica fault prior to the 6 April 2009 L'Aquila earthquake (central Italy). *Journal of Geophysical Research*. 116, 2156-2202.

Constable, S.C., R.L. Parker & C.G. Constable, (1987). Occam's inversion: A practical algorithm for generating smooth models from electromagnetic sounding data. *Geophysics*. 52, (3), 289-300.

Galli, P., F. Galadini & D. Pantosti, (2008). Twenty years of paleoseismology in Italy: *Earth Sciences Review*. 88, 89-117.

Giaccio, B., P. Galli, P. Messina, E. Peronace, G. Scardia, G.Sottili, A. Sposato, E. Chiarini, B. Jicha & S. Silvestri, (2012). Fault and basin depocentre migration over the last 2 Ma in the L'Aquila 2009 earthquake region, central Italian Apennines. *Quaternary Science Review*. 56, 69-88.

Ghisetti, F. & L. Vezzani, (1999). Depths and modes of Pliocene-Pleistocene crustal extension of the Apennines (Italy). *Terra Nova*. 11, 67-72.

Giaccio, B., P. Galli, P. Messina, E. Peronace, G. Scardia, G. Sottili, A. Sposato, E. Chiarini, B. Jicha & S. Silvestri, (2012). Fault and basin depocentre migration over the last 2 Ma in the L'Aquila 2009 earthquake region, central Italian Apennines. *Quaternary Sci. Rev.* 56, 69-88, doi: 10.1016/j.quascirev.2012.08.016.

Giraudi, C., (1989). Datazione con metodi geologici delle scarpate di faglia post-glaciali di Ovindoli - Piano di Pezza (Abruzzo - Italia Centrale): implicazioni. *Memorie Società Geologica Italiana*. 42, 29-39.

Griffiths, D.H. & R.D. Barker, (1993). Two-dimensional resistivity imaging and modelling in areas of complex geology. *J. Appl. Geophys.* 29, 211-226.

Hydrogeophysics Group, (2001). Getting Started with SiTEM and SEMDI. University of Aarhus. Aarhus, Denmark.

Improta, L., A. Zollo, A. Herrero, R. Frattini, J. Virieux, & P. Dell'Aversana, (2002). Seismic imaging of complex structures by non-linear traveltime inversion of dense wide-angle data: Application to a thrust belt. *Geophysical Journal International*. 151, 264-278.

Jewell, C.J., & C. Bristow, (2006). GPR studies in the Piano di Pezza area of the Ovindoli - Pezza fault, central Apennines, Italy: extending paleoseismic trench investigations with high-resolution GPR profiling. *Near Surface Geophysics*, 4, (3), 147-153.

Loke, M.H. & T. Dahlin, (2002). A comparison of the Gauss-Newton and quasi-Newton methods in resistivity imaging inversion. *Journal of Applied Geophysics*. 49, 149-162.

Morey, D. & G.T. Schuster, (1999). Paleoseismicity of the Oquirrh fault, Utah, from shallow seismic tomography. *Geophysical Journal International*, 138, 25-35, doi: 10.1046/j.1365-246x.1999.00814.x.

Pantosti, D., G. D'Addezio & F.R. Cinti, (1996). Paleoseismicity of the Ovindoli-Pezza fault, central Apennines, Italy: a history including a large, previously unrecorded earthquake in the Middle Ages (860-1300 A.D.). *Journal of Geophysical Research*. 101, 5937-5959.

Pucci, S., F. Villani, R. Civico, D. Pantosti, P. Del Carlo, A. Smedile, P.M. De Martini, E. Pons-Branchu & A. Gueli, (2014). Quaternary geology map of the Middle Aterno Valley, 2009 L'Aquila earthquake area (Abruzzi Apennines, Italy). *Journal of Maps*. doi: 10.1080/17445647.2014.927128.

Sheley, D., T. Crosby, M. Zhou, J. Giacoma, J. Yu, R. He, & G.T. Schuster, (2003). 2-D seismic trenching of colluvial wedges and faults. *Tectonophysics*. 368, 51-69.

Storz, H., W. Storz & F. Jacobs, (2000). Electrical resistivity tomography to investigate geological structures of the Earth's upper crust. *Geophysical Prospecting*. 48, 455-471. doi: 10.1046/j.1365-2478.2000.00196.x.

Villani, F., S. Pucci, R. Civico, P.M. De Martini, I. Nicolosi, F. D'Ajello Caracciolo, R. Carluccio. G. Di Giulio, M. Vassallo, A. Smedile & D. Pantosti, (2014). Imaging the structural style of an active normal fault through multi-disciplinary geophysical investigation: a case study from the Mw 6.1, 2009 L'Aquila earthquake region (central Italy). *Geophysical Journal International*. 200 (3), 1676-1691. doi: 10.1093/gji/ggu462.

INQUA Focus Group on Paleoseismology and Active Tectonics

Historic and Prehistoric earthquake ruptures of central Asia

Walker, R.T. (1), Abdrakhmatov, K. (2), Campbell, G. (3), Gruetzner, C. (3), Mackenzie, D. (1), Mukambayev, A. (4)

(1) Department of Earth Sciences, Oxford University, South Parks Road, Oxford, OX1 3AN, U.K. Email: richw@earth.ox.ac.uk
(2) Institute of Seismology, NAS Kyrgyz Republic, Asanbay 52/1, Bishkek, Kyrgyzstan
(3) Bullard Laboratories, Cambridge University, Madingley Road, CB3 0EZ, U.K.
(4) Kazakhstan National Data Center, Institute of Geophysical Research, Chaikinoy str. 4, 050020 Almaty, Kazakhstan

Abstract: *We present an overview of field work results undertaken through the joint NERC-ESRC 'Earthquakes without Frontiers' hazard program. One of the main focus areas for this program is the northern Tien Shan, with an emphasis on the regions around the city of Almaty (population ~ 2 million). We identify several ruptures around SE Kazakhstan, each of which would be destructive were they to repeat at the present-day. In our presentation, we show preliminary results of surveys in the epicentral region of the 1889 Chilik earthquake, and also of ruptures from a magnitude 8 earthquake on the Lepsy fault, which may be related to an historic event in 1716. We will present observations from high-resolution optical satellite imagery and from field-based geodetic and photogrammetric methods, including the production of decimetric digital elevation models from low-altitude aerial photography. Remote-sensing data such as these are useful in determining the slip amount and direction, and also in helping to identify older earthquakes along the recently reactivated faults.*

Key words: *Central Asia, Earthquake, trenching, historic, prehistoric.*

INTRODUCTION

The active faulting and mountain building in central Asia forms an important part of the on-going continental collision between India and Eurasia (e.g. Abdrakhmatov et al., 1996). Faults in the region together accommodate over 1 cm/year of N-S shortening (e.g. Abdrakhmatov et al., 1996) and cause widespread destructive earthquakes, such as the destructive 1889 and 1911 events in Almaty, Kazakhstan. Rapid growth of urban centres across the region has increased the vulnerability to earthquakes, and yet the hazard - in terms of the probable magnitudes of future events, the average intervals between large earthquakes, and even the locations of the faults that are likely to fail - is not uniformly known.

Instrumental catalogues of earthquakes, despite being a vital source of information for understanding active tectonics and seismic hazard, do not fully represent the distribution of seismic sources within slowly straining intra-plate settings – such as the northern Tien Shan - where the interval between destructive earthquakes in a given region might be very long. The cold, relatively arid, environment of central Asia causes surface ruptures from large-magnitude earthquakes to be preserved for periods of > 1000 years (e.g. Baljinnyam et al., 1993; Walker et al., 2006) providing a more appropriate timescale over which to examine distributions of earthquakes.

In our presentation, we focus on the Chilik region of SE Kazakhstan and also on the ruptures of a late prehistoric earthquake rupture on the Lepsy fault of SE Kazakhstan, which had a potential magnitude of 8.3 (Campbell et al., 2015).

Figure 1: rupture of the 1911 Kemin earthquake in the Chon-Aksu valley, Kyrgyzstan (magnitude 8.1). The earthquake caused substantial damage to the city of Almaty in Kazakhstan (see Figure 2 for location).

DISCUSSION

Although it has suffered relatively few damaging earthquakes in the past 100 years Almaty, the largest city in Kazakhstan, was badly damaged by a sequence of earthquakes in 1887 (Mw 7.3), 1889 (Mw 8.3), and 1911 (Mw 8.1). The rupture of the 1911 event was mapped immediately afterwards (Bogdanovitch et al., 1914) and is still well-preserved at present (e.g. Delvaux et al., also see Figure 1). The absence of detailed constraint on the location, size, and slip-direction of the 1889 rupture (which was not mapped in the same detail as the 1911 event) constitutes a fundamental gap in our understanding of the sequence. In the presentation, we shall show initial results from palaeoseismic

investigation of a large and well-preserved rupture SE of Almaty, which is of a size compatible with it forming in a magnitude 8+ earthquake, which may be the source of the 1889 Chilik earthquake.

By exploiting the fact that earthquake ruptures are preserved for long periods in the cold and arid climate of central Asia, we use satellite imagery to analyse the landscape of the northern Tien Shan to identify prehistoric earthquake ruptures, whose source parameters we determine from field-based and remote-sensing survey methods. Several of our field investigations in the region are reported in this volume.

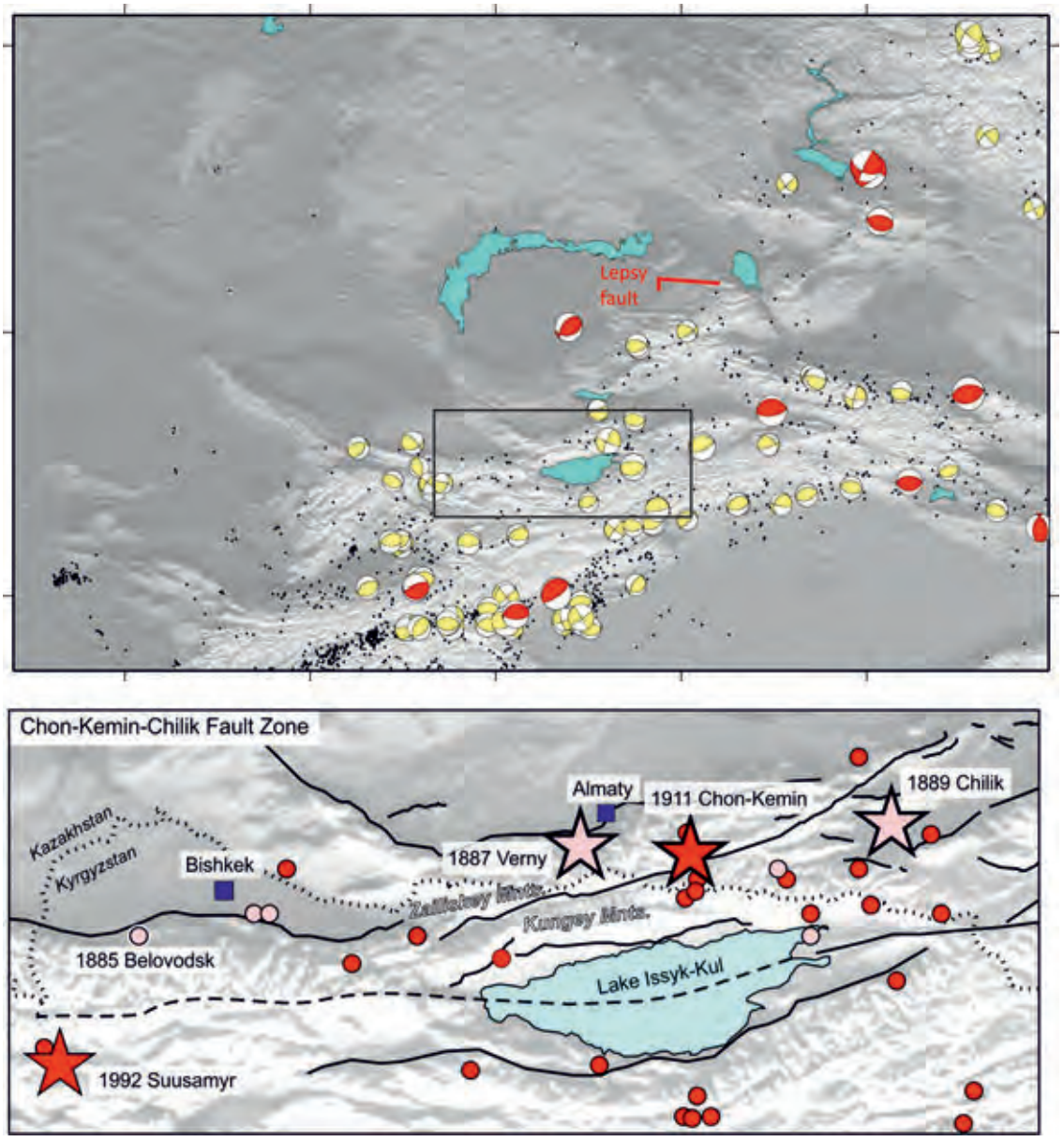

Figure 2: The upper panel is a shaded-relief topographic map of the Tien Shan region, with instrumentally recorded earthquakes from Sloan et al. (2011). Red focal mechanisms are those with centroid depths > 30 km. Those in yellow have depths < 30 km. The location of the Lepsy palaeo-earthquake rupture (Campbell et al. 2015) is shown in red.
In the lower panel is a close-up of the region around Almaty, with 20th century seismicity marked in red, and 19th century seismicity marked in pink. Epicentres of four major destructive events are marked by stars. The rupture of the 1911 Chon-Kemin earthquake occurred south of Almaty, along the Chon-Kemin-Chilik fault zone in Kyrgyzstan.

In another of our studies, published in Campbell et al., (2015), we identify a prehistoric rupture, sited NE of Almaty near the town of Lepsy, which is likely to have formed in a magnitude ~8 event within the last 400 years. This rupture is conspicuous in satellite imagery, digital topography and in the field. The scarp is ~120 km long, and from the displacement of stream channels and risers we characterise its slip as oblique reverse / right-lateral. Vertical displacement in the earthquake was ~7 m, suggesting slip on the fault-plane of 10 m or more.

Close to the western end of the fault, the scarp is uninterrupted as it crosses the bed of a now-abandoned north-flowing river bed. River diversion occurred either during scarp formation, or prior to it. A pre-date on the 7 m scarp comes from reed beds within fluvial sands from this abandoned river channel. Radiocarbon dating of the reeds dates yields an age of 400 years or less. As the geomorphology of the area indicates that river diversion occurred during or prior to the scarp formation, the age control shows that the earthquake occurred in the last 400 years. We speculate that the scarp may have formed in a historic event reported in 1716, whose epicentre has previously been estimated to lie further south, in the Chinese Tien Shan.

A lack of geomorphic evidence for larger cumulative displacements along the Lepsy rupture suggests that the recurrence interval is very long, and further implies that active faults within the Tien Shan region may not show any discernible Holocene features. The Lepsy rupture hence has implications for mapping sources of future seismic hazard.

Acknowledgements: We thank the Natural Environment Research Council (UK) for support through the joint NERC-ESRC 'Increasing Resilience to Natural Hazards' Earthquakes without Frontiers program. We also thank the NERC-funded COMET 'Centre for the Observation and Modelling of Earthquakes, Volcanoes, and Tectonics'. RTW is grateful for support from the Royal Society through its University Research Fellowship program.

References

Abdrakhmatov, K., & fifteen others, (1996). Relatively recent construction of the Tien Shan inferred from GPS measurements of present-day cristal deformation rates. *Nature*. 384, 450-453.

Baljinnyam, I., & ten others, (1993). Ruptures of major earthquakes and active deformation in Mongolia and its surroundings. *Memoirs of the Geological Society of America*. 181, 1-62.

Bogdanovitch, K.I., I.M. Kark, B. Ya. Korolkov, D.I. Mushketov, (1914) Earthquake in northern district of Tien Shan, 22 December 1911. *Geology Committee.* New Series, 89. St. Petersburg.

Campbell, G.E., R.T. Walker, K. Abdrakhmatov, J.L. Schwenninger, J. Jackson, J.R. Elliott & A. Copley, (2013). The Dzhungarian fault: Late Quaternary tectonics and slip rate of a major right-lateral strike-slip fault in the northern Tien Shan region. *Journal of Geophysical Research*. 118, 1-18.

Campbell, G.E., R.T. Walker, K. Abdrakhmatov, J. Jackson, J.R. Elliott, D. Mackenzie, T. Middleton & J.L. Schwenninger, (2015). Great earthquakes in low-strain-rate continental interiors: an example from SE Kazakhstan. *Journal of Geophysical Research*. (in revision).

Delvaux, D., K.E., Abdrakhmatov, I.N., Lemzin & A.L., Strom, (2001). Landslide and Surface breaks of the 1911 M 8.2 Kemin Earthquake. *Landslides*. 42, 1583-1592.

Sloan, R.A., J.A. Jackson, D. McKenzie, K. Priestley, (2011). Earthquake depth distributions in central Asia, and their relations with lithospheric thickness, shortening and extension. *Geophysical Journal International*. 185, 1-29.

Walker, R.T., & ten others, (2006). Geomorphology and structure of the Jid right-lateral strike-slip fault in the Mongolian Altay Mountains. *Journal of Structural Geology*. 28, 1607-1622.

INQUA Focus Group on Paleoseismology and Active Tectonics

paleoseismicity.org

Study of the links between slip at depth and at the surface for the 1997 Colfiorito earthquakes using detailed structural mapping; the role of fault orientations

Watson, Z.K. (1), Roberts, G.P. (2), Faure Walker, J.P. (1), Wedmore, L.N.J. (1)

(1) Institute for Risk and Disaster Reduction, University College London, Gower Street, WC1E 6BT. Email: zoe.watson.13@ucl.ac.uk
(2) Department of Earth and Planetary Sciences, Birkbeck, University of London, Malet Street, London, WC1E 7HX

Abstract: *Detailed structural mapping has been undertaken along fourteen different normal faults scarps throughout the central and northern Italian Apennines, including the Mt. Le Scalette fault near Colfiorito. These maps show that there is variability in the strike and dip due to corrugations and breached relay zones of the exposed scarps over a range of scales (meter to hundreds of meters). For the Mt. Le Scalette fault, the data collected demonstrate a systematic relationship between the coseismic slip (visible on the free face as a pale un-weathered stripe), strike and dip. We interpret this structural link between slip and fault orientation to mean that the un-weathered stripe must have a tectonic origin and that slip at depth in the earthquake propagated to the surface.*

Key words: *Structural maps, Colfiorito, active scarps.*

INTRODUCTION

Since the 1915 Fucino earthquake that claimed the lives of 33,000 people, extensive fieldwork throughout the Apennines has been conducted in order to locate and collect data on active normal faults that have the capability of generating damaging earthquakes. Particular interest is whether slip at depth propagates upwards to produce surface ruptures. Here we show that spatial variations in fault strike, and changes in dip that accompany them, directly affect the magnitude of surface slip allowing a test of whether measured surface slip is primary coseismic slip or produced by compaction. Detailed structural mapping, with a spatial resolution down to 2m, has been undertaken along fourteen different normal faults throughout the Apennines (Fig. 1); here we present one example in detail. Mapping highlights that normal faults exhibit variability in strike and dip due to corrugations and breached relay zones over a range of scales (meter to hundreds of meters). We demonstrate a systematic relationship between fault parameters suggesting that the surface fault scarp is connected to the seismogenic fault at depth.

BACKGROUND

Normal faults in the Apennines have been active since the regional stress field changed from compressive to extensional in the Plio-Pleistocene (~2-3Ma) (*Cavinato et al.*, 2002; *Roberts and Michetti*, 2004). Since the Last Glacial Maximum (15 ±3kyr) throw rates on these normal faults have been higher than the erosion rate. Hence surface fault scarps of Mesozoic limestone are visible throughout the Apennines and are suitable for detailed structural mapping (Fig. 1).
Normal faulting earthquakes with M_w>5.5 are believed by some to rupture to the surface in the Apennines. For example after the 1998 Lauria earthquake (M_w=5.6), a 1cm high free face was observed (*Michetti et al.*, 2000), which the authors attributed to coseismic motion. However other authors argue that observed surface ruptures (such as those seen after the Lauria earthquake and the Colfiorito earthquakes) are due to compaction during seismic shaking (e.g. *Basili et al.*, 1998) rather than coseismic motion (e.g. *Vittori et al.*, 2000). Whether the active faults extend to the surface or not has important implications for the growth of normal faults and their related geomorphology, and for understanding the magnitudes of earthquakes that can be expected in the future. This is important when discussing the seismic hazard of the region. Detailed structural mapping can be used to resolve this debate.

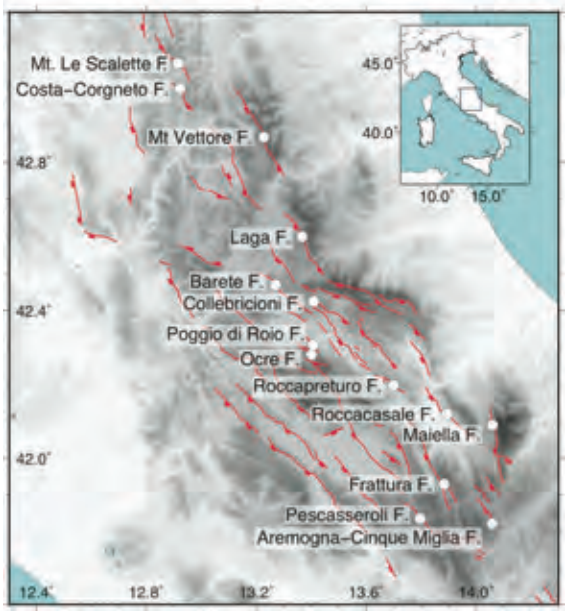

Figure 1: Summary map of normal faults that have been partially mapped in detailed. Red lines indicate active normal faults. White circles show the locations where detailed mapping has been undertaken. Inset shows the location of the main figure (blue box) in Italy.

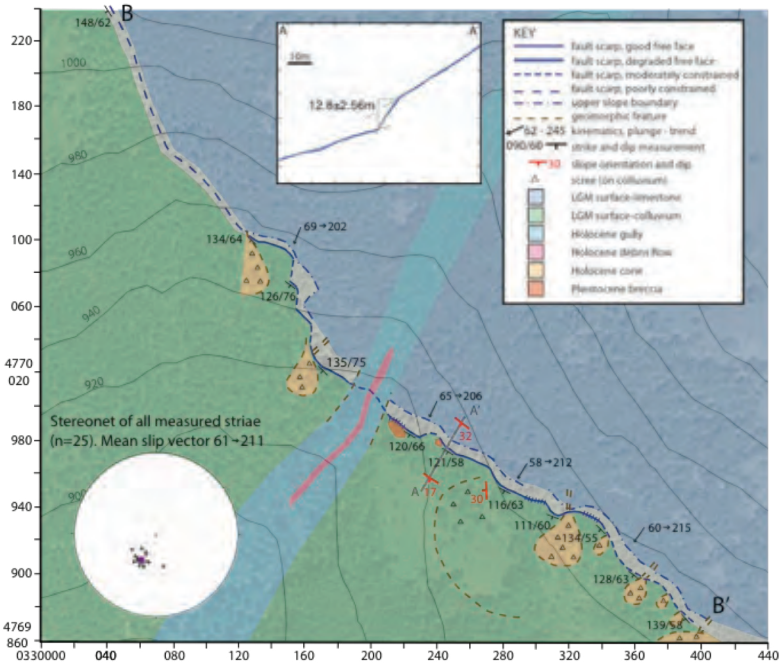

Figure 2: Structural and geomorphological map of a well exposed section of the Mt. Le Scalette fault near Colfiorito (total length ~6km). Kinematic data were collected from frictional wear striae. Inset shows a topographic profile perpendicular to the fault scarp. An offset surface can be seen, most-likely dating from the last glacial maximum; this is now preserved as lower and upper slopes. Contours in pale grey indicate that the bends of the fault scarp are true and not due to the effect of topography. Coordinates used are UTM, zone 33T, WGS84 datum.

Figure 3: Field photographs of the Mt. Le Scalette fault: a.) view onto the fault scarp, the pale un-weathered stripe is evident at the base; b.) view along the fault scarp looking approximately north-west.

One of the faults that have been mapped is the Mt. Le Scalette fault near Colfiorito, Umbria (Figs. 2 and 3). This fault is of particular interest because it is known to have ruptured at depth during a series of normal faulting earthquakes in September 1997 (M_w= 5.7, 6.0). At the base of the surface fault scarp a pale un-weathered stripe is evident (see Fig. 3a); some authors argue that this is due to compaction during shaking, and we investigate this further herein.

METHODS

Detailed structural mapping using a handheld GPS and compass clinometer has been undertaken (Figs. 1 and 2). For the Mt. Le Scalette fault the vertical extent of the pale un-weathered stripe (slip) has been measured along the mapped section of the fault. Relationships between fault parameters, such as strike (orientation of the fault scarp), dip, slip, and slip direction have been investigated.

RESULTS

The structural data collected from the Mt. Le Scalette fault scarp show that the fault dip, strike, kinematics and slip (converted to throw) are inter-related (Fig. 4). Higher dip values and coseismic throw are observed along portions of the scarp where the fault strike is oblique to the mean slip direction (211°, the horizontal line on Fig. 4 shows the strike value representing pure dip-slip motion,

that is, perpendicular to the mean slip direction from Fig. 2). The minimum values for the strike, dip and slip are spatially coincident along the fault. This relationship has been quantified on other faults (Parasano-Pescina fault, Abruzzo, *Faure Walker et al.*, 2009; Campo Felice Fault in Abruzzo, *Wilkinson et al., in press*). In these cases, the total Holocene throw is observed to be higher where the slip is oblique and the dip is higher, and lower where the slip is less oblique and the dip is less (or across a breach fault). *Faure Walker et al.*, (2009) explain these results by showing that sites with oblique slip vectors and a higher dip require a greater throw rate if principal strain-rates are conserved along the strike of a fault.

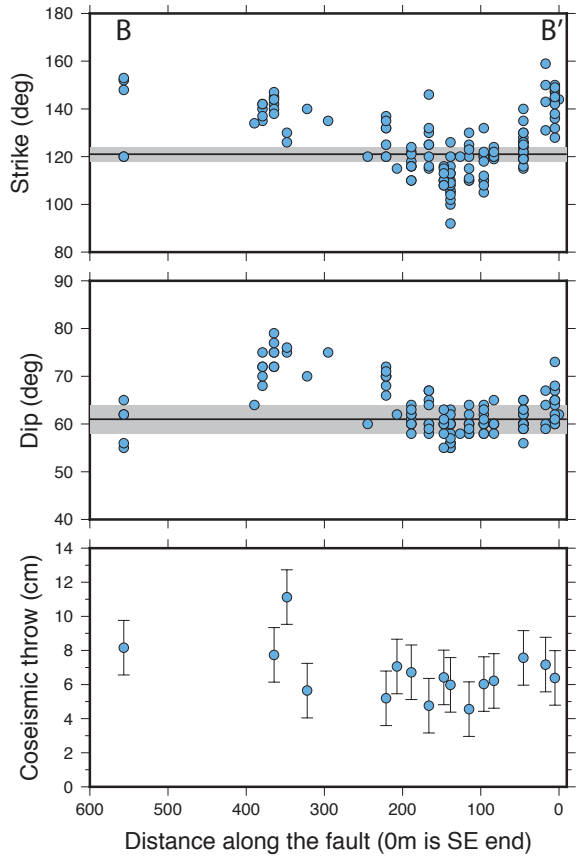

Figure 4: Data collected and plotted against the distance along the Mt. Le Scalette fault. The mean coseismic throw for each locality is plotted. Maximum values in all three parameters are found at ~350m and ~0m along the fault with minimum values at ~150m. The black line in the top figure represents a strike perpendicular to the mean slip vector; the grey represents the 95% confidence interval. The black line in the middle figure represents the plunge of the mean slip vector, with the 95% confidence interval.

CONCLUSIONS

Structural data collected from the Mt. Le Scalette fault show a systematic relationship between strike, dip and slip measured on the fault scarp. Thus, we conclude that the slip is structurally-controlled, primary coseismic slip producing a surface rupture, rather than secondary slip due to compaction during shaking. If the pale un-weathered stripe seen at the base of the free face were solely due to compaction, then it would be expected to vary along the fault in a random way that was un-related to the structure of the fault zone, and by at least two orders of magnitude (as modelled by *Vittori et al.*, 2000 for the nearby Costa-Corgneto fault). However, the systematic relationship between measured structural parameters, suggests that this pale un-weathered stripe must have been tectonically exhumed during the September 1997 earthquake(s).

Acknowledgements: This study was funded by the Natural Environment Research Council (NE/E01545X/1 and NE/I024127/1) and NERC Studentship NE/L501700/1.

References

Basili, R., V. Bosi, F. Galadini, P. Galli, M. Meghraoui, P. Messina, M. Moro and A. Sposato, (1998). The Colfiorito Earthquake Sequence of September–October 1997: Surface Breaks and Seismotectonic Implications for the Central Apennines (Italy). *J. Earthq. Eng.* 2. 291-302.

Cavinato, G.P., C. Carusi, M. Dall'Asta, E. Miccadei and T. Piacentini, (2002). Sedimentary and tectonic evolution of Plio-Pleistocene alluvial and lacustrine deposits of Fucino Basin (central Italy). *Sediment. Geol.* 148, 29-59.

Faure Walker, J.P., G.P. Roberts, P.A. Cowie, I.D. Papanikolaou, P.R. Sammonds, A.M. Michetti and R.J. Phillips (2009). Horizontal strain-rates and throw-rates across breached relay zones, central Italy: Implications for the preservation of throw deficits at points of normal fault linkage. *J. Struct. Geol.* 31 (10), 1145-1160.

Michetti, A. M., L. Ferreli, E. Esposito, S. Porfido, A. M. Blumetti, E. Vittori, L. Serva, and G.P. Roberts, (2000). Ground effects during the 9 September 1998, Mw=5.6, Lauria earthquake and the seismic potential of the "aseismic" Pollino region in Southern Italy. *Seismol. Res. Lett.* 71 (1).

Roberts, G.P. and A.M. Michetti (2004). Spatial and temporal variations in growth rates along active normal fault systems: an example from The Lazio-Abruzzo Apennines, central Italy. *J. Struct. Geol.* 26 (2), 339-376.

Vittori, E., G. Deiana, E. Esposito, L. Ferreli and L. Marchegiani, (2000). Ground effects and surface faulting in the September-October 1997 Umbria-Marche (central Italy) seismic sequence. *J. Geodyn.* 29, 535-564.

Wilkinson, M. et al., (in press). Slip distributions on active normal faults measured from LiDAR and field mapping of geomorphic offsets: an example from L'Aquila, Italy, and implications for modelling seismic moment release. *Geomorphology*.

INQUA Focus Group on Paleoseismology and Active Tectonics

Investigating the cause of earthquake clusters in the central Apennines, Italy by modelling co-seismic and interseismic Coulomb stress change from 1349-2009

Wedmore, L.N.J. (1), Faure Walker, J.P. (2), Roberts, G.P. (3), Sammonds, P. (4), McCaffrey, K. (5)

(1) Institute for Risk and Disaster Reduction, University College London, London, WC1E 6BT, United Kingdom.
Email: l.wedmore.11@ucl.ac.uk
(2) Institute for Risk and Disaster Reduction, University College London, London, WC1E 6BT, United Kingdom
(3) Department of Earth and Planetary Sciences, Birkbeck College, University of London, London, WC1E 6HX, United Kingdom
(4) Institute for Risk and Disaster Reduction, University College London, London, WC1E 6BT, United Kingdom
(5) Department of Earth Sciences, Durham University, Durham, DH1 3LE, United Kingdom

Abstract: *Recent earthquake activity in the central Apennines has been concentrated along the north eastern set of faults whereas long term geologic strain shows a more heterogeneous distribution across the mountain belt. This apparent clustering of earthquakes is a common feature of normal faulting systems. 27 historical earthquakes extending back to 1349 AD are used to assess the role of co-seismic and interseismic stress changes on the earthquake cycle and the production of earthquake clusters. A shear zone rheology at depth is modelled to calculate the interseismic stress loading rates on active faults in the region that produces recurrence intervals that match those found in palaeoseismic trenches. Co-seismic stress changes are modelled for each earthquake and stresses are resolved onto all faults in the region. For 16 out of 17 of the earthquakes from 1703 AD, Coulomb stress was positive immediately prior to rupture with interseismic loading dominant over co-seismic stress changes.*

Key words: *Coulomb Stress, Earthquakes, Clustering, Italy.*

INTRODUCTION

In low strain rate regions, there is evidence for clustering of earthquakes on particular faults over short periods of time and consequently, measurements of slip on different timescales are not always in agreement. In the central Apennines, Italy, historical records of shaking for large magnitude earthquakes (Guidoboni et al., 2007) since 1349 A.D. show that recent earthquake activity has been concentrated on faults in the north-east of the region with faults on the south-west side of the Apennines experiencing relatively low slip rates during this period. In contrast, strain rates averaged since 15 ka show a more heterogeneous distribution across the mountain chain. Elastic stress interactions between faults have been shown to influence seismicity over short timescales following individual earthquakes (King et al., 1994). It has been suggested that these stress interactions can influence earthquake recurrence over longer timescales (Scholz, 2010), but previous studies have been hindered by limited knowledge of earthquake locations or poor knowledge of the geometry and kinematics of the active faults. Here we model both the co-seismic and interseismic Coulomb stress interactions between active faults for 27 earthquakes over 665 years from 1349-2014 in the central Apennines to investigate the relationship between long term slip rates and the location of the most recent earthquakes. We calculate interseismic stress accumulation on faults by modelling deep rooted viscous shear zones beneath the brittle base of each fault; this results in similar earthquake recurrence times to those recovered from palaeoseismic studies. From 1703-2009, after the model has had time to spin up, we show how 23 of the 24 faults were positively stressed prior to their rupture.

BACKGROUND

Geological strain rates measured across a preserved 15 ±3 ka surface show how strain is partitioned between the north eastern and south western set of faults in the central Apennines. In contrast, analysis of macroseismic shaking records from historical earthquakes from 1349-2009 shows how the majority of recent activity has occurred on the north eastern set of faults. Over 15 ±3kyrs, earthquake recurrence, and hence fault slip rates, are controlled by viscous flow in narrow localized shear zones beneath the active faults (Cowie et al., 2013), yet on shorter timescales other processes are influencing earthquake recurrence leading to the clustering of activity.

Many attempts have been made to explain earthquake clustering through elastic stress interactions principally by modelling Coulomb stress changes following large earthquakes (e.g. King et al., 1994; Stein et al 1997; Deng and Sykes, 1997). However, the magnitudes of co-seismic stress changes are often very small in comparison to the long-term accumulation of stress on faults. Therefore it is necessary to know more than simply the co-seismic stress changes in order to build up a picture of the overall stress state of an active fault. Knowing the elapsed time since the last earthquake on a fault can provide vital information as to how many years the interseismic stress has been accumulating since the last earthquake on a fault. However, many previous studies have been limited by the short duration and

incomplete knowledge of historical earthquakes in an area.

In the central Apennines, the historical records of earthquake activity (Guidoboni et al., 2007) reliably extend in detail back to 1349 AD for large (M≥5.8) earthquakes (Michetti et al., 1996). In addition to the historical records, there are extensive palaeoseismic, seismological, geodetic, archaeoseismic and contemporary records of active faulting during this period (Galli et al., 2008; Pace et al., 2006). Furthermore, the strain rate field from geological offsets, derived from the geometry, kinematics and slip rates of the active faults in the central Apennines, have been constrained by >15 yrs of field campaigns (Morewood and Roberts, 2000; Roberts and Michetti, 2004; Papanikolaou et al., 2005; Faure Walker et al., 2010; 2012; Wilkinson et al., 2014)

METHODOLOGY

Stress changes were modelled in an elastic half space, with discontinuities representing the faults mapped in the central Apennines. Interseismic strain accumulation on all faults was modelled by extending the surface expression of the faults into the lower crust, and adopting a model of viscous shear zones that control long term strain accumulation in the area (Cowie et al., 2013). The portions of the faults in the upper crust are locked while the portions in the lower crust slip at the same rate as the slip rates measured over 15 kyrs at the surface. The Coulomb stress loading is then resolved on the locked upper portion of the fault. Faults were modelled as planar linear features discretized into 3 x ~3 km patches. Surface measurements of the kinematics of the faults (Morewood and Roberts, 2000; Roberts and Michetti, 2004; Papanikolaou et al., 2005; Faure Walker et al., 2010; 2012; Wilkinson et al., 2014) were adopted to vary the rake of each fault patch along the length of each fault.

The faults responsible for each of the historical earthquakes were identified from palaeoseismic results, macro seismic shaking records, contemporary reports of surface faulting, geodetic records and seismological results. We iterated earthquake locations to deal with uncertainty on which fault ruptured. The magnitudes of the historical earthquakes were taken from the CFTI catalogue (Guidoboni et al., 2010). Given uncertainty in the magnitudes for some of the early earthquakes, end member models were run, with the magnitudes of earthquakes from 1349-1703 A.D. varied by 0.5 degrees of magnitude and from 1703-1933 A.D. by 0.2 degrees of magnitude. Earthquake magnitudes were used to determine the length of the fault rupture and the average slip of the earthquake using empirical relationships (Wells and Coppersmith, 1994). Simple concentric slip models were used with the average slip from the empirical relationships maintained across the faults that slipped in each event. Coulomb stresses were resolved on individual faults, bypassing any assumptions about optimally orientated faults and regional stress fields. All Coulomb stress calculations were performed in the Coulomb 3.3 code (Lin and Stein, 2004; Toda et al., 2005). To calculate the total stress accumulation, coseismic stresses were added to the interseismic stresses that had accumulated over time, with all faults set at zero stress in 1349 A.D.. We analysed the results only from after 1703 A.D. to allow the model to spin-up for 354 years and produce a stress field that was not artificially uniform as assumed in most previous studies. Stress drop was assumed to be complete following an earthquake on any fault section that slipped during that event.

RESULTS

To assess whether the methodology used to calculate the interseismic stress accumulation results in reliable stress loading rates, we compute approximate recurrence intervals. By calculating the stress drop expected on each fault, given its length, we compare this with the time it would take to accumulate enough stress through interseismic loading to reach this stress drop value to produce an approximate recurrence interval for an earthquake on each fault. Recurrence intervals calculated using this method have a mean of 2800yrs for the 96 faults investigated which is similar to recurrence intervals revealed by palaeoseismic trenching in the area. This suggests that the method used to adopt the shear zone rheology is a reasonable approximation that describes interseismic stress accumulation on faults in the central Apennines.

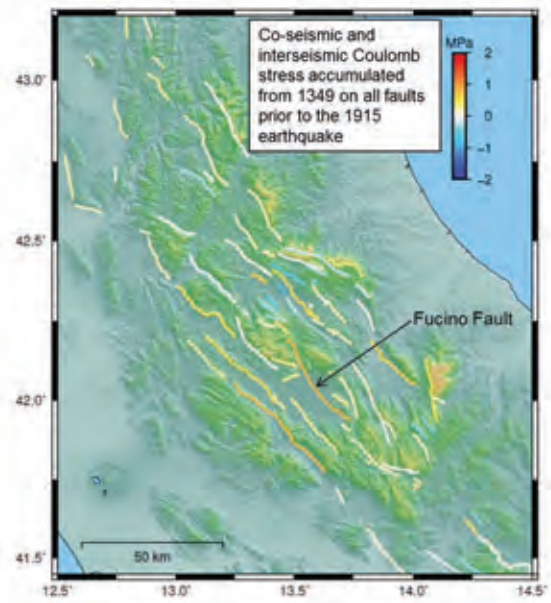

Figure 1: Mean co-seismic and interseismic Coulomb stress on faults in the central Apennines immediately prior to the 1915 A.D. Fucino earthquake from accumulated stress changes from 1349 A.D.

By combining the co-seismic and interseismic stress on faults immediately prior to a rupture we are able to assess the state of stress on a fault prior to an earthquake occurring. Figure 1 shows the mean level of Coulomb stress on all faults in the central Apennines immediately

prior to the 1915 Fucino earthquake. The Fucino Fault had the highest mean level of stress of all 96 faults modelled immediately prior to the earthquake.

DISCUSSION

In contrast to many previous studies, the period of time included in our model is sufficient such that we can analyse the stress on faults prior to the most recent earthquakes where we have knowledge of stress prior to the earthquake of greater than 350 years. This allows us to analyse the role of both interseismic and co-seismic stress changes in accumulating stress on a fault that results in an earthquake. The stress on faults prior to each earthquake in the time period 1703-2009 A.D. following 350 years of stress build-up is shown in *Figure 2*.

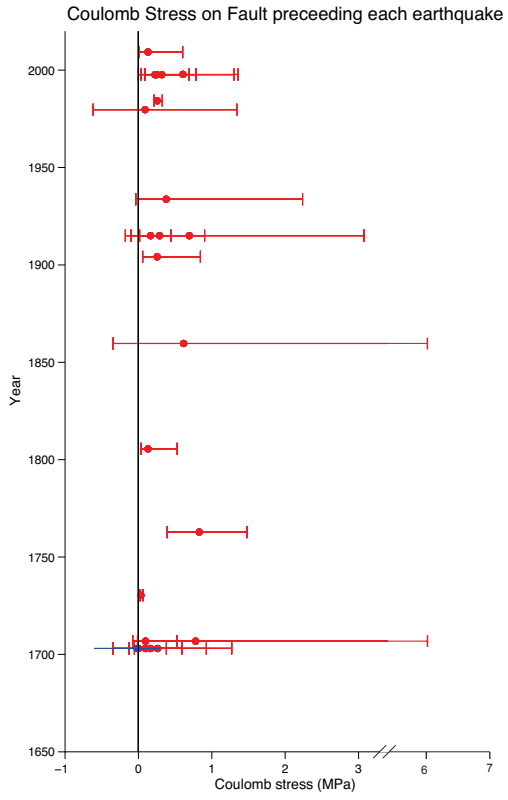

Figure 2: Coulomb stress on faults immediately prior to rupture for 17 earthquakes from 1703-2009 A.D.. The range of stresses on individual fault patches is shown by the bars with the mean stress on the fault indicated by the filled circle.

This shows how for all but one of the 17 earthquakes from 1703-2009 A.D. the stress on the fault prior to rupture was positive. This result is largely controlled by the interseismic stress accumulation. The co-seismic stress changes are on the order of 0.1 MPa, however these are dwarfed by the interseismic stresses when the model is run for hundreds of years.

Without knowledge of the total time elapsed since the last earthquake on each fault, and hence the role of interseismic stress loading, it is difficult to assess whether a fault is close to failure. The length of catalogue modelled here exceeds any previous work and allows us to greater understand the role of stress accumulation. We show that when using Coulomb stress modelling to understand seismic hazard following an earthquake, it is vital to include both the time elapsed since the last earthquake on all faults (for modelling the interseismic loading) in addition to the co-seismic stress changes from earthquakes on neighbouring faults as it is the interseismic loading that contributes most to the state of stress on each fault. Without this knowledge, it becomes difficult to assess the role of co-seismic stress transfer in triggering short (days to weeks) and longer term (tens to hundreds of years) clusters of earthquake activity in the central Apennines.

Acknowledgements: The UCL Institute for Risk and Disaster Reduction (IRDR), Birkbeck College and Geospatial Research Ltd are thanked for providing the funds for this research. In addition, GR, PS and KM are funded by NERC grant NE/I024127/1.

References

Cowie, P.A., C.H. Scholz, G.P. Roberts, J.P. Faure Walker & P. Steer, (2013). Viscous roots of active seismogenic fault revealed by geologic slip rate variations. *Nature Geoscience*. 6 (12) 1036-1040.

Deng, J. & L.R. Sykes, (1997). Evolution of stress field in Southern California and triggering of moderate-size earthquakes: A 200 year perspective. *Journal of Geophysical Research, Solid Earth*. 102 (B5), 9859-9886.

Faure Walker, J.P., G.P. Roberts, P.R. Sammonds & P. Cowie, (2010). Comparison of earthquake strains over 10^2 and 10^4 year timescales: Insights into variability in the seismic cycle in the Central Apennines, Italy. *Journal of Geophysical Research*. 115, doi: 10.1029/2009JB006462.

Faure Walker, J.P., G.P. Roberts, P. Cowie, I. Papanikolaou, A. Michetti, P. Sammonds, M. Wilkinson, K. McCaffrey, & R. Phillips, (2012). Relationship between topography, rates of extensión and mantle dynamics in the actively extending Italian Apennines. *Earth and Planetary Science Letters*. 325-326, 76-84.

Galli, P., F. Galadini, & D. Pantosti, (2008). Twenty years of palaeoseismology in Italy. *Earth-Science Reviews*. 88 (1-2), 89-117.

Guidoboni, E., G. Ferrari, D. Mariotti, A. Comastri, G. Tarabusi & G. Valensise, (2007). CFTI4med, Catalogue of strong earthquakes in Italy (461 B.C.-1997) and mediterranean área (760 B.C.-1500), INGV-SGA.

King, G. C., Stein, R. S. & Lin, J., (1994). Static stress changes and the triggering of earthquakes. *Bulletin of the Seismological Society of America*. 84 (3), 935-953.

Lin, J. & R.S. Stein, (2004). Stress triggering in thrust and subduction earthquakes and stress interaction between the Southern San Andreas and nearby thrust and strike-slip faults. *Journal of Geophysical Research*. 109 (B2). doi: 10.1029/2003JB002607

Michetti, A.M., F. Brunamonte, L. Serva & E. Vittori, (1996). Trench investigations of the 1915 Fucino earthquake fault scarps (Abruzzo, central Italy): Geological evidence of large

historical events. *Journal of Geophysical Research, Solid Earth*. 101 (B3), 5921-5936.

Morewood, N.C. & G.P. Roberts, (2000). The geometry, kinematics and rates of deformation with an en echelon normal fault segment boundary, central Italy. *Journal of Structural Geology*. 22, 1027-1047.

Pace, B., L. Peruzza, G. Lavecchia & P. Boncio, (2006). Layered seismogenic source model and probabilistic seismic-hazard analyses in central Italy. *Bulletin of the Seismological Society of America*. 96 (1), 107-132.

Papanikolaou, I., G.P. Roberts & A.M. Michetti, (2005). Fault scarps and deformation rates in Lazio-Abruzzo, central Italy: Comparison between geological fault slip-rate and GPS data. *Tectonophysics*. 408 (1-4), 147-176.

Roberts, G.P & A.M. Michetti, (2004). Spatial and temporal varaitions in growth rates along active normal fault systems: an example from the Lazio-Abruzzo Apennine, central Italy, *Journal of Structural Geology*. 26 (2), 339-376.

Scholz, C.H., (2010). Large earthquake triggering, clustering, and the synchronization of faults. *Bulletin of the Seismological Society of America*. 100 (3), 901-909.

Stein, R.S., A.A. Barka & J.H. Dieterich, (1997). Progressive failure on the North Anatolian fault since 1939 by earthquake stress triggering. *Geophysical Journal International*. 128 (3), 594-604.

Toda, S., R.S. Stein, K. Richards-Dinger & S.B. Bozkurt, (2005). Forecasting the evolution of seismicity in southern California: Animations built on earthquake stress transfer. *Journal of Geophysical Research*. 110. doi: 10.1029/2004JB003415.

Wells, D.L. & K.J. Coppersmith, (1994). New empirical relationships among magnitude, rupture length, rupture width, rupture area, and surface displacement. *Bulletin of the Seismological Society of America*. 84 (2), 974-1002.

Wilkinson, M., G.P. Roberts, K. McCaffrey, P.A. Cowie, J.P. Faure Walker, I. Papanikolaou, R.J. Phillips, A.M. Michetti, E. Vittori, L. Gregory, L. Wedmore, Z.K. Watson, (2014). Slip Distributions on active normal faults measured from LiDAR and field mapping of geomorphic offsets: an example from L'Aquila, Italy, and implications for modelling seismic momento release. *Geomorphology*. doi: 10.1016/j.geomorph. 2014.04.026

INQUA Focus Group on Paleoseismology and Active Tectonics

Geomorphological and paleoseismological investigations on the Gaenserndorf Terrace in the central Vienna Basin (Austria)

Weissl, M. (1), Hintersberger, E. (1), Lomax, J. (2), Decker, K. (1)

(1) Department of Geodynamics and Sedimentology, University Vienna, Althanstrasse 14, A-1090 Vienna, Austria.
Email: michael.weissl@univie.ac.at
(2) Institut of Geography, Justus-Liebig-University, Senckenbergstraße 1, D-35390 Gießen, Germany

Abstract: *In the central Vienna Basin normal faults define the eastern and western margins of Pleistocene Danube terraces north of Vienna. The terrace body is built up of coarse sandy gravel and sand. The gravels are locally covered with eolian sand and loess of the last glacial revealing OSL/IRSL ages of about 15 ka. High resolution digital terrain models (LIDAR) show relicts of a periglacial landscape in the northern part of the MIS 8 terrace. Large elongated depressions are interpreted as the basins of former thermokarst lakes due to analogies in recent periglacial zones, and presently dry valleys which are interpreted as the outflows of these lakes and drainages of the terrace surface. The periglacial morphology on the terrace is only preserved in the elevated part of the terrace which is located in the footwall of the bounding normal faults. In the hanging wall Quaternary basins are filled with up to 40 m thick Pleistocene and Holocene growth strata.*

Key words: *Vienna Basin, Paleoseismological Trenching, Geomorphology of the Quaternary.*

INTRODUCTION

The Vienna Basin is a SSW-NNE oriented Neogene basin of about 200 km length and 55 km width. It extends from the eastern Alps in Austria to the western Carpathians in the Czech Republic. This noticeable crustal-scale pull-apart basin evolved between two left stepping segments of a major sinistral transform system with basin subsidence starting in the early Middle Miocene. Recent analyses of Miocene and active tectonics show that a number of Miocene faults form offsets or boundaries between Middle and Late Pleistocene deposits. These faults are consequently regarded as active and capable of generating severe earthquakes with magnitudes up to M ~ 7 (Fig. 1).

Active kinematics is characterized by a seismically active sinistral strike-slip fault system, which is located at the SE margin of the Miocene basin. This fault system splits up into a number of normal fault splays crossing the basin. Geological, geophysical and geomorphological mapping reveal seven normal faults of that type in the central part of the Vienna Basin. Even though those splay faults do not show any historical or instrumental seismicity, geological and morphological data proof that they moved at very slow velocities of <0.1mm/a during the Quaternary (Decker et al., 2005).

THE PLEISTOCENE GÄNSERNDORF TERRACE

The central Vienna Basin is covered by wide floodplains of the Danube River and the Morava River. A Pleistocene river terrace extending from Vienna to the Carpathian Mountains in Slovakia is called Gänserndorf Terrace (GDT).

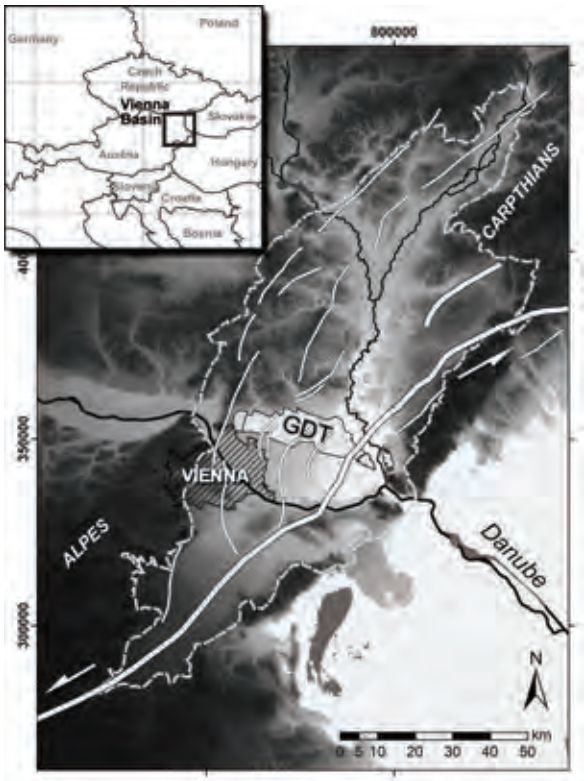

Figure 1: The Vienna Basin Transfer Fault (VBTF) and splay faults dissecting the Gänserndorf Terrace (GDT) in the central basin. Coordinates are Gauss Kruger, MGI M34.

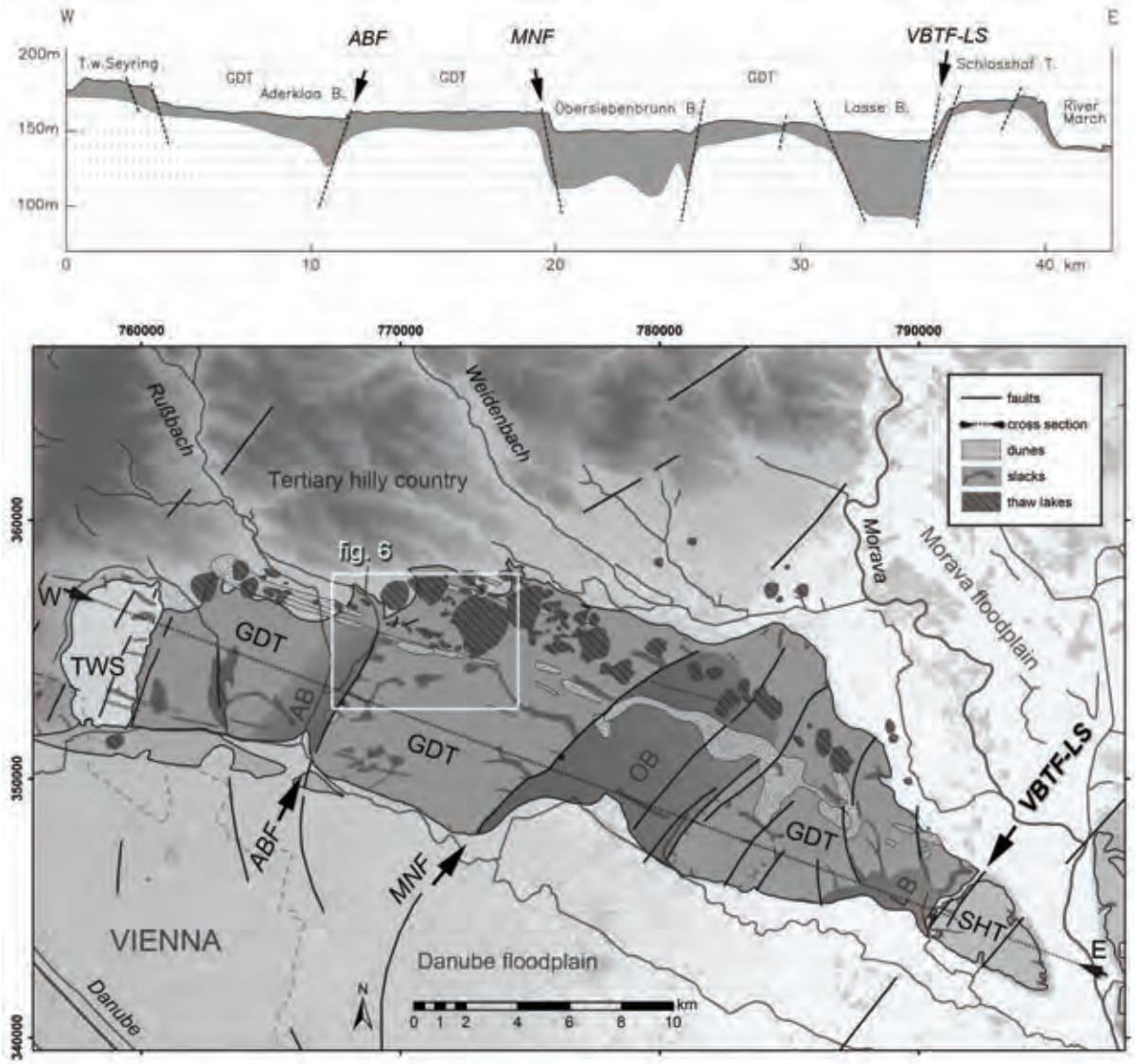

Figure 2: (above): DEM based cross-section of the Vienna Basin and thickness of the Quarternary sediments based on drilling data. Faults: Aderklaa-Bockfliess Fault (ABF); Markgrafneusiedl Fault (MNF); Lassee segment of the Vienna Basin Transfer Fault (VBTF-LS).

Figure 3: (below): Geomorphology of the Central Vienna Basin area: Gänserndorf Terrace (GDT); Terrace west of Seyring (TWS); Schlosshof Terrace (SHT); Basins: Aderklaa Basin (AB); Obersiebenbrunn Basin (OB); Lassee Basin (LB).

The terrace body consists of coarse sandy gravel and sand. Usually, those Quaternary river sediments reach a height of about 10 m on the terrace. Due to tectonic subsidence in the basins the sandy gravels accumulated to a thickness of about 30 m in the Aderklaa Basin, 40 m in the Obersiebenbrunn Basin, and 60 m in the Lassee Basin (Fig. 2).

Infrared Stimulated Luminescence (IRSL) age data reveals ages between about 300 and 200 ka (MIS 8) for the gravel terrace (Fiebig et al., 2011). The gravels are locally covered with loess of the last glacial revealing SL/IRSL ages of about 15 ka.

Several parallelly striking faults cross the the GDT (Fig. 3).

In the western part the NW-dipping Aderklaa-Bockfliess normal fault forms a distinct fault scarp with a height up to 5 m. In the central part, this terrace is offset by the SE-dipping Markgrafneusiedl normal fault which forms an up to 17 m high fault scarp. In the East, the Lassee segment of the Vienna Basin Transfer Fault (VBTF) produced a ~25 m high NW-dipping fault scarp forming the margin of the so called Schlosshof Terrace (SHT). IRSL dating of terrace sediments revealed MIS 8 ages indicating the tectonic subsidence of the GDT relative to the Schlosshof terrace since the Pleistocene.

In the South, the erosional forces of the River Danube form the terrace margins. In the North, the terrace

adjoins to the slopes of the Tertiary hilly country and the erosional force of the Weidenbach river valley.

SURVEYING

Miocene and active tectonics in the Vienna Basin have been analysed since 10 years. It is obvious that the Miocene faults can offset and delimit Middle to Late Pleistocene and Holocene deposits. But the interpretation is not easy in many cases because erosional, glacial and anthropogenic processes can produce similar morphological features as active faults.
During earlier projects, faults were investigated at places in the central parts of the Gaenserndorf terrace and on the western slope of the Schlosshof terrace. The Aderklaa-Bockließ Fault, Markrafneusiedl Fault, and the Lassee segment of the VBTF were investigated at three sites by paleoseismological trenches (Fig. 4. Chwatal et al., 2005; Hintersberger et al., in press). All fault scarps were surveyed by a series of GPR profiles, reflection seismic, and resistivity profiles to localize the fault precisely (measurement and processing by the Technical University of Vienna).
The West-Austria-Gasleitung (WAG-Pipeline) crosses the Gänserndorf terrace in East-West direction in its northern part. During the construction of the pipeline some faults were observed in the trench walls (Posch-Trözmüller & Peresson, 2010).

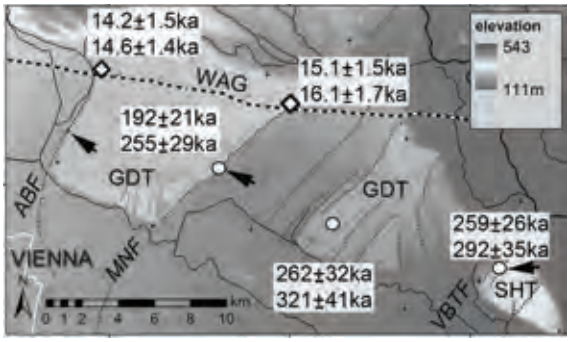

Figure 4: OSL-ages of the Pleistocene river terrace sediments (circles) and of the eolian/alluvial cover (diamonds); trench sites (arrows); course of the WAG pipeline: dashed line; terraces: Gänserndorf terrace (GDT); Schlosshof terrace (SHT); faults: Aderklaa-Bockfliess fault (ABF); Markgrafneusiedl fault (MNF); Vienna Basin Transfer Fault (VBTF). OSL ages (Fiebig et al., 2011).

Especially the normal fault of the Markgrafneusiedl Fault is well documented (Fig. 5). The margin between the hanging wall of the Obersiebenbrunn Basin and the foot wall of the Gänserndorf Terrace is clearly visible. The sandy sediments of the subsided Basin in the East adjoin the gravels of the Terrace in the West.

PERIGLACIAL MORPHOLOGY

DEM, high resolution digital terrain models (LIDAR) and satellite images show relicts of a periglacial landscape (Fig. 6). Large elongated depressions in the northern part of the GDT terrace are interpreted as the basins of former thermokarst lakes due to analogies in recent periglacial zones (Grosse et al, 2013). Presently dry valleys are interpreted as the outflows of these lakes.

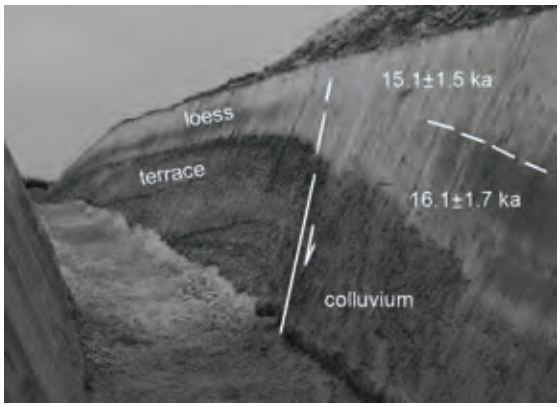

Figure 5: Markgrafneusiedl fault exposed in the pipeline construction pit WAG. The fault cuts off the deposits of the Gänserndorf terrace and also displaces the overlying loess. Numbers refer to sediment ages determined by IRSL/OSL techniques.

The central part of the GDT is characterized of eolian sand cover and wind parallel dunes (Fink, 1955; Wiesbauer et al., 1997). Depressions and dry valleys in this zone are interpreted as slacks drainaging the terrace surface during the glacial. Diverse forms of periglacial phenomena in different areas of the terrace are explained by different substrates and formation conditions.
The periglacial morphology on the terrace is only preserved in the elevated part of the terrace which is located in the footwall of the bounding normal faults. Both, the Markgrafneusiedl and the Aderklaa-Bockfliess faults delimit the terrace from fault-bounded Quaternary basins in the hanging walls of the faults as well the Lassee segment of the VBTF. These basins are filled with up to 40 m thick Pleistocene and Holocene growth strata composed of Danube river sediments and sandy alluvium transported by creeks from the northern tertiary hilly country. The most important creek is the Rußbach which crosses the Gänserndorf Terrace in the western part parallel to the Aderklaa-Bockfließ fault. The youngest sedimentation in these basins is dominated by Holocene high-stage floods of the Danube River and reworked sand and silt which were eroded in the higher areas.
The digital terrain model shows especially in the northern part of the terrace many depressions of different size. Mostly they have rounded rims forming with flat ridge at SE side.
The depressions are very shallow with a flat ground and hardly appreciable in the landscape. It is possible to distinguish different types of rather oval or more fan shape contour. The diameters can vary from hundred meters up to two kilometres. The depressions are

situated in the parts covered by reworked loess whereas the sand covered central parts and the southern margins of the Gänserndorf terrace alike the adjacent higher terrace don´t show comparable morphological features.

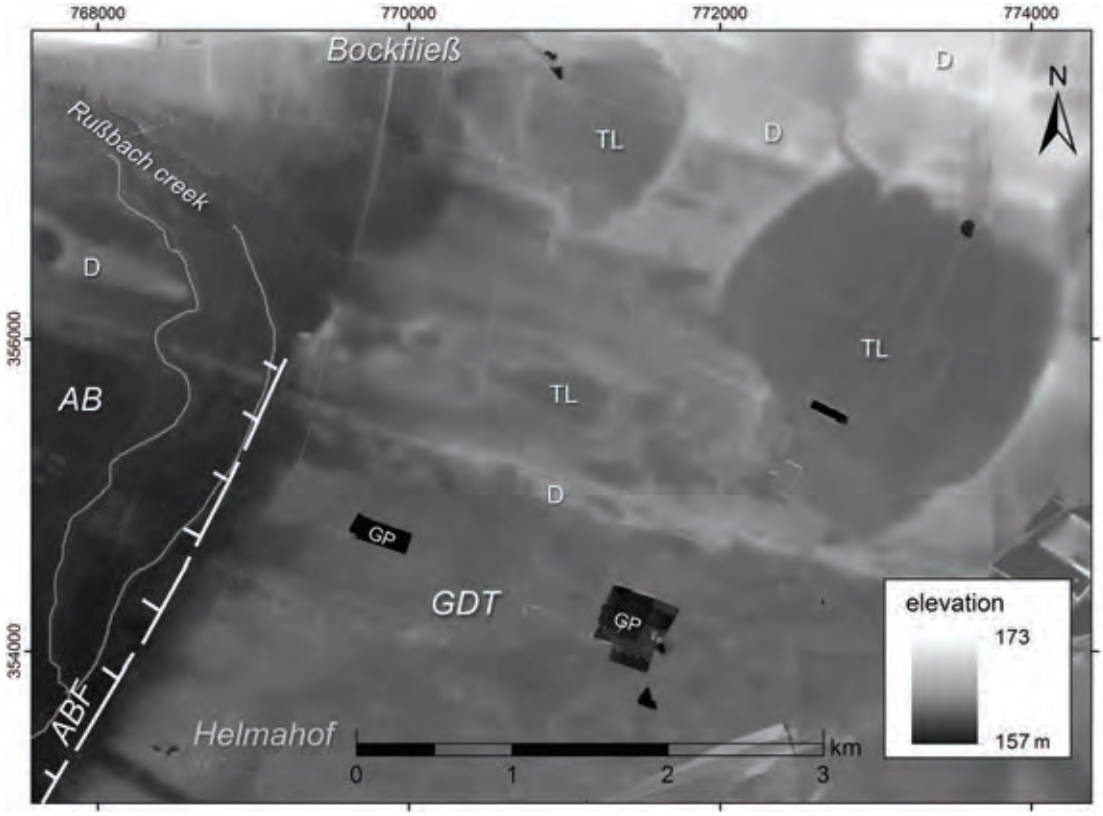

Figure 6: LIDAR (1 m ground resolution) showing the geomorphology of the northern Gänserndorf terrace (GDT); in the W: Aderklaa Basin (AB) with floodplain of the Rußbach creek. This creek runs parallel to the Aderklaa–Bockfliess fault. Former Taw lakes (TL) and wind parallel dunes (D) in the northern part of the Gänserndorf terrace. Dry valleys corrugating the fault scarp indicate advanced subsidence before the last Glacial. Gravel pit (GP).

CONCLUSIONS

Three faults delimit well defined parts of the Pleistocene Gänserndorf Terrace from fault-bounded Quaternary basins in the hanging walls of the faults. Characteristics of the periglacial morphology are preserved in elevated parts of the terrace, in the footwall of the bounding normal faults. Draining valleys corrugating the fault scarps are an indication of the advanced subsidence of the Aderklaa and Obersiebenbrunn Quaternary basins before the last Glacial.

Acknowledgements: The research projects on active faults in the Vienna Basin and the city of Vienna was funded by the OMV.

References

Brauneis, S., A. Hudribusch, (2009). *Geländeaufnahme WAG II - Loop 600 Plus, Km 2.750 - Km 37.600.* Kartierbericht, Aufnahmezeitraum: 29.6. 2009 - 2. 12. 2009. Vienna, Geologische Bundesanstalt.

Chwatal, W., K. Decker & K.H. Roch, (2005). Mapping of active capable faults by high-resolution geophysical methods: examples from the central Vienna Basin. *Austrian Journal of Earth Sciences*. 97, 52-59.

Decker, K., H. Peresson & R. Hinsch, (2005). Active tectonics and Quaternary basin formation along the Vienna Basin Transform fault. *Quaternary Science Reviews*. 24, 307-322.

Fiebig, M., J. Lomax, E. Hintersberger & K., Decker, (2011). Quaternary evolution of the Vienna Basin (Austria) - reconstruction through luminescence dating In: *XVIII INQUA, Conference Abstracts*. ID 2266.

Fink, J., (1955). Das Marchfeld. *Verhandlungen der Geologischen Bundesanstalt*. Spec. Vol. D: 88-116. Vienna.

Grosse, G., B. Jones, & C. Arp (2013). Thermokarst Lakes, Drainage, and Drained Basins. In: *Treatise on Geomorphology, Vol 8, Glacial and Periglacial Geomorphology*. (Shroder, J.F., Giardino, R., Harbor, J. eds.). San Diego. 325-353.

Posch-Trözmüller, G., M. Peresson, (2010). Geologische Bearbeitung kurzfristiger Aufschlüsse in Niederösterreich mit Schwerpunkt auf infrastrukturelle Bauten in schlecht aufgeschlossenen Regionen und auf rohstoff-wissenschaftliche, umweltrelevante und grundlagen-orientierte Auswertungen. Neue Bauaufschlüsse - Neues Geowissen: Niederösterreich, Projekt NC 69/2009-2011, Jahresendbericht 2009. Geologische Bundesanstalt. Vienna.

Wiesbauer, H., K. Mazzucco & L. Schratt-Ehrendorfer, (1997). Dünen in Niederösterreich: Ökologie und Kulturgeschichte eines bemerkenswerten Landschaftselementes, Fachberichte des NÖ Landschaftsfonds Nr. 6. Amt d. NÖ Landesregierung, Naturschutzabteilung. St. Pölten.

INQUA Focus Group on Paleoseismology and Active Tectonics

Accommodation of Strike-Slip by Normal Faults and Block Rotations in the Transtensional Walker Lane of North America

Wesnousky, S., Bormann, J., Kreemer, C., Hammond, W., Brune, J.

Center for Neotectonics, Seismological Laboratory, Geodetic Laboratory, Departments of Geological Sciences and Engineering and Nevada Bureau of Mines and Geology, University of Nevada, Reno, USA. Email: wesnousky@unr.edu

Abstract: *Greater than or equal to 30 km of cumulative right-lateral crustal displacement and 5-6 mm/yr of the ongoing relative right-lateral motion between the Pacific and North American plates are observed along the northwest striking Walker Lane. The right-lateral shear has been accommodated in significant part rotations of crustal blocks bounded by northeast striking left lateral faults as well as discontinuous, en echelon, normal fault-bounded basins that likely accommodate significant vertical axis rotations of the intervening crust. The observations presented here provide an illustrative example of how large amounts of crustal shear may be accommodated in the absence of strike-slip faults and points to difficulties attendant to melding geologic and geodetic observations in the analysis of seismic hazard.*

Key words: *Neotectonics, Active Faults, Seismic Hazard.*

INTRODUCTION

The Walker Lane is a northwest trending zone of discontinuous active faults and disrupted topography that sits between the Sierra Nevada on the west and the north-northeast trending faults and ranges of the Great Basin to the east (Fig. 1). About one fifth of the ongoing ~50 mm/yr of right-lateral transform motion across the Pacific-North American plate boundary is accommodated east of the Sierra Nevada, mostly localized within the Walker Lane. Estimates of cumulative right-slip across the zone range from upwards of 100 km or more in the south to ~30 km in the north. The occurrence of both normal and strike-slip faulting within the Walker Lane indicate transtensional deformation. Here I focus on describing those regions where it seems right-slip is accommodated in large part by either normal faults, block rotations, or both.

Faults of the Walker Lane

The faults of the Walker Lane may for convenience of discussion be divided into those of the southern, central, and northern Walker Lane. These are color coded from north to south in Fig. 1 as magenta (southern), black and red (central), and northern (blue). The colored faults are right-lateral strike-slip whereas those in solid black are left-lateral strike-slip. Also present and a significant part of the discussion here are a set of 7 normal fault bounded basins (the Tahoe, Carson, Smith, Mason, Antelope, Bridgeport, and Walker Lake basins). A primary characteristic of this system of faults is the lack of discontinuity or through-going strike-slip faults. The northern limit of strike-slip faults of the southern Walker Lane (magenta) are interrupted by a set of east-striking left-lateral strke-slip faults. Similarly, there is a gap between strike-slip faults of the central (red) and northern (blue) Walker Walker Lane. Within and east of that gap are located the en-echelon set of normal fault founded basins. Geologic measures of right-offset across

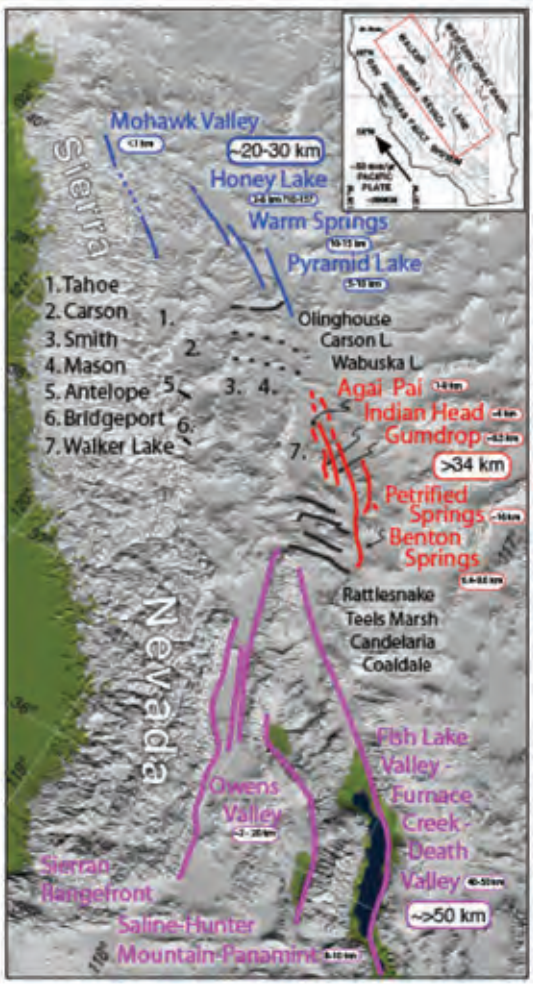

Figure 1: Active Faults and Basins of Walker Lane.

the zone range from >50 km in the southern Walker Lane, > 34 km in the central Walker Lane, and 20-30 km in the northern Walker Lane (Fig. 1).

Crustal Block Rotations between Southern and Central Walker Lane

The Rattlesnake, Teels Marsh, Candelaria, and Coaldale faults (Figs. 1 & 2) sit within a right-step between the northwest striking right-slip faults of the Southern and Central Walker Lane. Each of the faults displays fault morphology indicative of left-slip and the presence of basins on opposite sides and ends of the faults that may most easily explained by the left-slip being accompanied by vertical axis rotations. The idea is illustrated in Fig. 3.

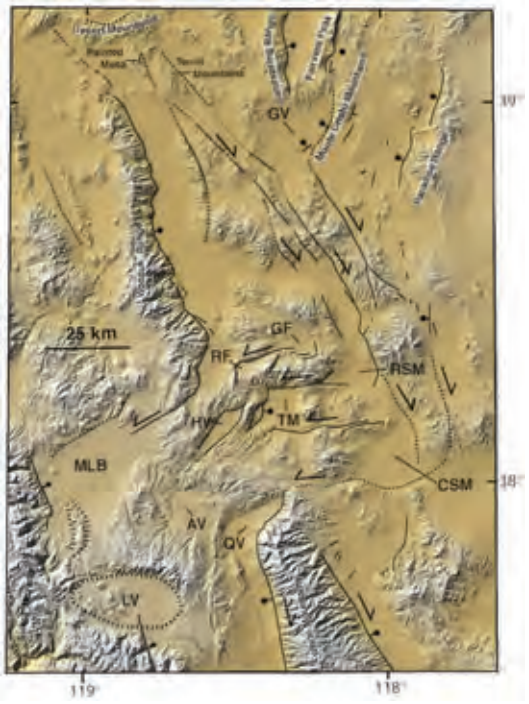

Figure 2: Physiography and Faults between right-slip faults of Southern and Central Walker Lane.

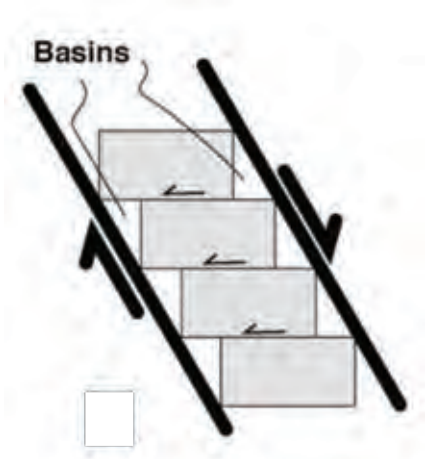

Figure 3: Inferred mode of development of faults and basins between strike-slip faults of Southern and Central Walker Lane.

Accommodation of Strike-Slip by Development of Normal Faults and Vertical Axis Rotations in the northern Walker Lane

The geodetic velocity field, the slip rates of rangebounding normal faults, and physiography of the basins in that portion between and to the west of north trending right-slip faults of the Central (red in Fig. 1) and Northern (blue in Fig. 1) are summarized in Figure 4. Geologic rates of displacement on rangebounding faults may be compared to those determined from geodesy in Figure 4. The azimuth and horizontal rate of extension determined from published geologic studies are annotated and delineated by the two-headed black arrows adjacent to each of the major range-bounding faults in Fig. 4. The points of the two arrowheads span the minimum and maximum bounding estimates of horizontal extension for the respective faults. The vectors of horizontal extension and fault-parallel right-lateral shear determined from the geodetic velocity field are shown by magenta and blue arrows, respectively.

It is observed in Fig. 4 that the geodetic velocity field vectors (red) are oriented southeast and increase in magnitude consistent with about 5-6 mm/yr of right-lateral shear. They also tend to increase in size from northwest to southeast to define about 1-2 mm/yr of extension parallel to the Walker Lane. Together the observations define a zone of transtension. If one traverses along the set of yellow paths drawn on the Fig 4, one does not intersect any major active fault and the other two cross faults but the slip rates of the faults are insufficient to explain the geodetic shear field. Indeed, none but the Walker Lake rangefront fault are documented to shown any strike-slip.

Three major observations arise from the data summarized in Fig. 4: 1) there are no major northwest-trending strike-slip faults traversing the area, 2) geologic and geodetic slip rates on the observed major range-bounding faults are insufficient to explain the entirety of the geodetically observed shear across the region, and 3) geodetic measurements reveal a significant component of NW-SE extension parallel to the Walker Lane. We infer from the observations that the displacement field across the region is taken up by a combination of vertical axis rotations, southeastward translation of crustal blocks approximately parallel to the Walker Lane, and opening of the en echelon set of basins. The idea is visualized in the model shown on the left of Fig. 5. A block of wax is heated and the central portion of the block is subject to a right-lateral shear with a small component of extension. Subsequently, an identical block of wax is heated and ice applied to the surface to create a 'brittle crust' and subjected to the same shear. The result is a broad zone of en echelon crustal blocks and basins. The blocks have generally undergone clockwise vertical axis rotations and the basins record a component of extension and block translation along the axis of principal shear.

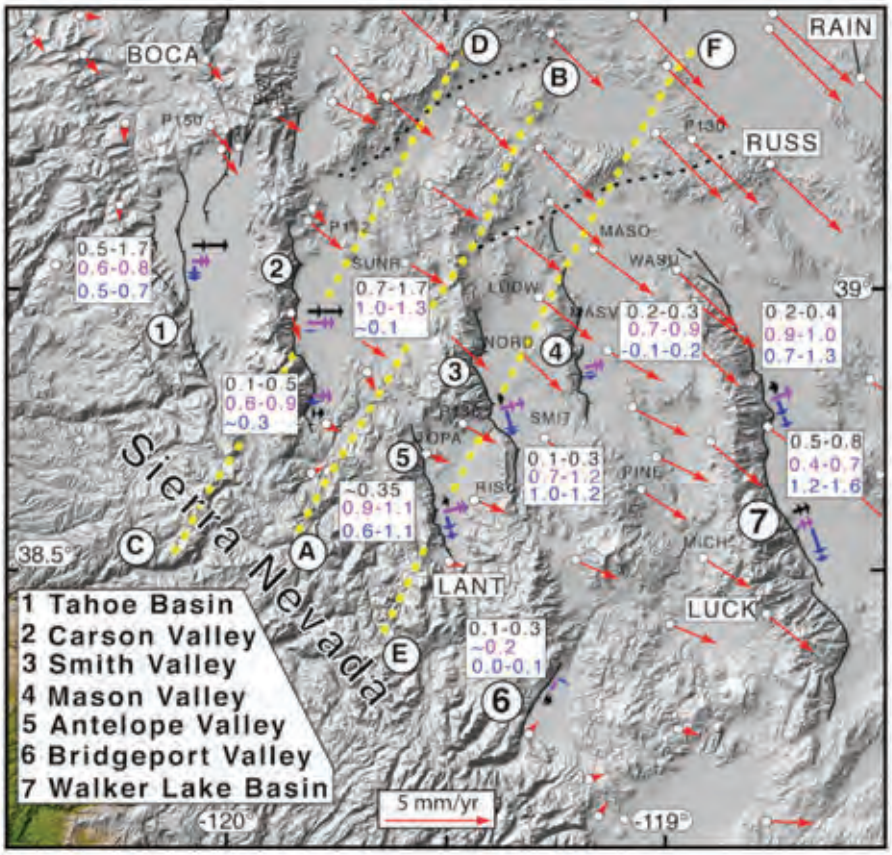

Figure 4: Physiography, geodetic velocity field (red vectors), geologic slip rates (black arrows and text, mm/yr), geodetically determined fault-normal (magenta) and right-shear (blue) fault slip rates of fault bounded basins between strike-slip faults of Central and Northern Walker Lane. Yellow dotted lines are paths across shear zone discussed in text.

Figure 5: Blocks of wax subjected to transtensional shear. Upper is warmed block. Lower is same but ice place on surface to produce a brittle layer. The model produces features such as triangular basins, block rotations, and the possibility of traversing a path across the zone of shear that doesn't intersect any 'faults'.

DISCUSSION AND CONCLUSION

The idea that crustal rotation provides a mechanism to accommodate displacement in a zone of shear is not new. Nonetheless, these two regions provide particularly illustrative examples of how vertical axis rotation can serve to accommodate significant amounts of right shear. Strike-slip faults of the Southern and Central Walker Lane are documented to have accrued >34-50 km of right-slip and so the east-striking left-lateral faults and accompanying vertical axis rotations likely accommodated a significant part of this right shear.

The northern Walker Lane likewise provides an insightful illustration of the complexity that may accompany the accommodation of simple shear. Here, the ~30 km of right-lateral cumulative strike slip has been accommodated in the absence of any well-developed strike-slip faults. Rather, the deformation has been taken up primarily by the development of a set of en echelon normal fault bounded basins and an apparently significant amount of crustal rotation. If the pattern of cumulative strain accommodation remains active today, a component of geodetic deformation recorded across the region is likewise also reflecting block rotations. If so, the assumption that all geodetically observed shear across the region will be accommodated by earthquakes will likely lead to overestimates of the level of seismic hazard in the area. The observation may be pertinent to assessments of seismic hazard in other regions as well.

Acknowledgements: The National Science Foundation provided support for this research.

References

Wesnousky, S.G., J.M. Bormann, C. Kreemer, W.C. Hammond and J.N. Brune, (2012). Neotectonics, Geodesy, Seismic Hazard in the northern Walker Lane of Western North America: Thirty kilometers of crustal shear and no strike-slip? *Earth and Planetary Science Letters*. 329-330, 133-140. doi: 10.1016/j.epsl.2012.02.018.

Wesnousky, S.G., (2005). Active faulting in the Walker Lane, *Tectonics*. 24, TC3009. doi: 10.1029/2004TC001645.

ISSN 1590-2595

Quaderni di Geofisica

http://istituto.ingv.it/l-ingv/produzione-scientifica/quaderni-di-geofisica/

I Quaderni di Geofisica coprono tutti i campi disciplinari sviluppati all'interno dell'INGV, dando particolare risalto alla pubblicazione di dati, misure, osservazioni e loro elaborazioni anche preliminari, che per tipologia e dettaglio necessitano di una rapida diffusione nella comunità scientifica nazionale ed internazionale. La pubblicazione on-line fornisce accesso immediato a tutti i possibili utenti. L'Editorial Board multidisciplinare garantisce i requisiti di qualità per la pubblicazione dei contributi.

ISSN 2039-7941

rapporti tecnici INGV

http://istituto.ingv.it/l-ingv/produzione-scientifica/rapporti-tecnici-ingv/

I Rapporti Tecnici INGV pubblicano contributi, sia in italiano che in inglese, di tipo tecnologico e di rilevante interesse tecnico-scientifico per gli ambiti disciplinari propri dell'INGV. La collana Rapporti Tecnici INGV pubblica esclusivamente on-line per garantire agli autori rapidità di diffusione e agli utenti accesso immediato ai dati pubblicati. L'Editorial Board multidisciplinare garantisce i requisiti di qualità per la pubblicazione dei contributi.

ISSN 2039-6651

Miscellanea INGV

http://istituto.ingv.it/l-ingv/produzione-scientifica/miscellanea-ingv/

La collana Miscellanea INGV nasce con l'intento di favorire la pubblicazione di contributi scientifici riguardanti le attività svolte dall'INGV (sismologia, vulcanologia, geologia, geomagnetismo, geochimica, aeronomia e innovazione tecnologica). In particolare, la collana Miscellanea INGV raccoglie reports di progetti scientifici, proceedings di convegni, manuali, monografie di rilevante interesse, raccolte di articoli ecc..

Coordinamento editoriale e impaginazione
Centro Editoriale Nazionale | INGV

Progetto grafico e redazionale
Laboratorio Grafica e Immagini | INGV Roma

Via di Vigna Murata, 605
00143 Roma
Tel. +39 06518601 Fax +39 065041181

http://www.ingv.it

Istituto Nazionale di Geofisica e Vulcanologia